

# Talanta

The International Journal of Pure and Applied Analytical Chemistry

---

## Editors-in-Chief

**Professor G.D. Christian**, University of Washington, Department of Chemistry, 36 Bagely Hall, P.O. Box 351700, Seattle, WA 98195-1700, U.S.A.

**Professor J.-M. Kauffmann**, Université Libre de Bruxelles, Institut de Pharmacie, Campus de la Plaine, C.P. 205/6, Boulevard du Triomphe, B-1050 Bruxelles, Belgium

## Associate Editors

**Professor J.-H. Wang**, Research Center for Analytical Sciences, Northeastern University, Box 332, Shenyang 110004, China

**Professor J.L. Burguera**, Los Andes University, IVAIQUIM, Faculty of Sciences, P.O. Box 542, 5101-A Mérida, Venezuela.

## Assistant Editors

**Dr R.E. Synovec**, Department of Chemistry, University of Washington, Box 351700, Seattle, WA 98195-1700, U.S.A.

**Professor J.-C. Vire**, Université Libre de Bruxelles, Institut de Pharmacie, Campus de la Plaine, C.P. 205/6, Boulevard du Triomphe, B-1050 Bruxelles, Belgium

## Talanta

R. Apak (Istanbul, Turkey)  
L.G. Bachas (Lexington, KY, U.S.A.)  
E. Bakker (Auburn, AL, U.S.A.)  
D. Barceló (Barcelona, Spain)  
K. Booksh (Tempe, AZ, U.S.A.)  
C.M.A. Brett (Coimbra, Portugal)  
Yi. Chen (Beijing, China)  
R. Compton (Oxford, U.K.)  
S. Cosnier (Grenoble, France)  
P.K. Dasgupta (Lubbock, TX, U.S.A.)  
D. Diamond (Dublin, Ireland)  
G.A. Eiceman (Las Cruces, NM, U.S.A.)  
M.-R. Fuh (Taipei, Taiwan)  
K. Grupdan (Chaing Mai, Thailand)

V.K. Gupta (Roorkee, India)  
A. Gustavo González (Sevilla, Spain)  
I. Gutz (Sao Paulo, Brazil)  
E.H. Hansen (Lyngby, Denmark)  
P. de B. Harrington (OH, U.S.A.)  
W.L. Hinze (Winston-Salem, NC, U.S.A.)  
A. Ivaska (Turku, Finland)  
B. Karlberg (Stockholm, Sweden)  
U. Karst (Enschede, The Netherlands)  
R. Lobinski (Pau, France)  
C.A. Lucy (Edmonton, AB, Canada)  
M.D. Luque de Castro (Cordoba, Spain)  
I.D. McKelvie (Victoria, Australia)  
E. Morosonova (Moscow, Russia)

J.-M. Pingarron (Madrid, Spain)  
E. Pretsch (Zürich, Switzerland)  
W. Schuhmann (Bochum, Germany)  
M. Shamsipur (Kermanshah, Iran)  
K. Suzuki (Yokohama, Japan)  
D.L. Tsalev (Sofia, Bulgaria)  
Y. Umezawa (Tokyo, Japan)  
K. Vytras (Pardubice, Czech Republic)  
B. Walczak (Katowice, Poland)  
R. von Wandruszka (Moscow, U.S.A.)  
J. Wang (Tempe, AZ, U.S.A.)  
J.D. Winefordner (Gainesville, U.S.A.)  
Xiu-Ping Yan (Tianjin, China)  
E.A.G. Zagatto (Piracicaba, SP, Brazil)

---

Copyright © 2006 Elsevier B.V. All rights reserved.

**Publication information:** *Talanta* (ISSN 0039-9140). For 2007, volumes 71–73 are scheduled for publication. Subscription prices are available upon request from the Publisher or from the Regional Sales Office nearest you or from this journal's website (<http://www.elsevier.com/locate/talanta>). Further information is available on this journal and other Elsevier products through Elsevier's website: (<http://www.elsevier.com>). Subscriptions are accepted on a prepaid basis only and are entered on a calendar year basis. Issues are sent by standard mail (surface within Europe, air delivery outside Europe). Priority rates are available upon request. Claims for missing issues should be made within six months of the date of dispatch.

**Orders, claims, and journal enquiries:** please contact the Customer Service Department at the Regional Sales Office nearest you:

**Orlando:** Elsevier, Customer Service Department, 6277 Sea Harbor Drive, Orlando, FL 32887-4800, USA; phone: (+1) (877) 8397126 [toll free number for US customers], or (+1) (407) 3454020 [customers outside US]; fax: (+1) (407) 3631354; e-mail: [usjcs@elsevier.com](mailto:usjcs@elsevier.com)

**Amsterdam:** Elsevier, Customer Service Department, PO Box 211, 1000 AE Amsterdam, The Netherlands; phone: (+31) (20) 4853757; fax: (+31) (20) 4853432; e-mail: [nlinfo-f@elsevier.com](mailto:nlinfo-f@elsevier.com)

**Tokyo:** Elsevier, Customer Service Department, 4F Higashi-Azabu, 1-Chome Bldg, 1-9-15 Higashi-Azabu, Minato-ku, Tokyo 106-0044, Japan; phone: (+81) (3) 5561 5037; fax: (+81) (3) 5561 5047; e-mail: [jp.info@elsevier.com](mailto:jp.info@elsevier.com)

**Singapore:** Elsevier, Customer Service Department, 3 Killiney Road, #08-01 Winsland House I, Singapore 239519; phone: (+65) 63490222; fax: (+65) 67331510; e-mail: [asiainfo@elsevier.com](mailto:asiainfo@elsevier.com)

**USA mailing notice:** *Talanta* (ISSN 0039-9140) is published monthly by Elsevier B.V. (P.O. Box 211, 1000 AE Amsterdam, The Netherlands). Annual subscription price in the USA US\$ 3,818 (valid in North, Central and South America), including air speed delivery. Application to mail at periodical postage rate is paid at Rathway, NJ and additional mailing offices.

**USA POSTMASTER:** Send address changes to *Talanta*, Publications Expediting Inc., 200 Meacham Avenue, Elmont, NY 11003.

**AIRFREIGHT AND MAILING** in the USA by Publications Expediting Inc., 200 Meacham Avenue, Elmont, NY 11003.

# Ion-pair extraction and GC–MS determination of linear alkylbenzene sulphonates in aqueous environmental samples

Mehmet Akyüz\*

Zonguldak Karaelmas University, Faculty of Sciences and Letters, Department of Chemistry, 67100 Zonguldak, Turkey

Received 10 October 2005; received in revised form 24 May 2006; accepted 7 June 2006

Available online 13 July 2006

## Abstract

A GC–MS method was developed for the determination of linear alkylbenzene sulphonates (LAS) and sulphophenylcarboxylic acids (SPC) in aqueous environmental samples. LAS and SPC were isolated from aqueous samples using methylene green (MG) as ion-pair reagent and derivatised with diazomethane for their chromatographic analysis. LAS and SPC were then analysed with GC–MS in EI mode as their methyl esters. The method eliminates positive and negative interferences found by the methylene blue method and considered to be selective and sensitive for the determination of LAS and SPC in aqueous samples. The recovery of LAS was 98% with a relative standard deviation (R.S.D.) of 2.0% and the detection limit obtained from calculations by using GC–MS results based on S/N:3 was lower than 10 ppb. Obtained results revealed that the method can also be employed in the analysis of organic compounds bearing sulphate and sulphonate groups.  
© 2006 Elsevier B.V. All rights reserved.

**Keywords:** GC–MS analysis; Linear alkylbenzene sulphonates; Biodegradation; Ion-pair extraction; River water; Sea water

## 1. Introduction

Linear alkylbenzene sulphonates (LAS) are the most important synthetic anionic surface active agents widely used as the principal constituents of commercial detergents as well as institutional cleaning and industrial purposes [1,2]. Commercially available LAS are mixtures of isomers, with alkyl chain lengths ranging from C<sub>10</sub> to C<sub>14</sub>. LAS are significant environmental pollutants, as their bio-degradation involves the consumption of bio-available oxygen resulting in an increase in chemical oxygen demand [1]. LAS are not only toxic, but also contribute to the permeation of other pollutants into aquatic animals [3]. SPC are biotransformation intermediates formed during biological degradation of LAS and the presence of SPC in water and sediment is important as it may indicate ongoing bio-degradation of LAS [4–7]. The toxicity of LAS has been estimated by determining their effects on the energy-coupled reverse electron transfer (RET) in fishes and invertebrates and expressed as the toxicant concentration decreasing the reduction rate of NAD<sup>+</sup> to an extent of 50% (EC 50). This ranged from 0.61 mg/L for a commercial LAS mixture to 18,000 mg/L for individual SPC, respectively

[8]. Therefore, monitoring the levels of LAS in environmental waters is important for the protection of human health and the environment.

Almost all the spectrophotometric determinations of anionic surfactants are based on the formation of ion-pairs and their subsequent extraction into organic solvents [9–13]. Methylene blue active substances (MBAS) are the most frequently used cationic ion-pair reagents for the determination of LAS [14,15]. Because of its high sensitivity, the methylene blue (MB) method is normally used to determine low levels of surfactants in aqueous samples such as wastewaters and surface waters. However, this procedure has always been known to be subjected to positive and negative interferences [14,15], although it has been used for a long time as the standard method for environmental analysis. As it is possible to quantitatively extract LAS under all reported conditions, as well as the extraction of other compounds with the MBAS method, it is necessary to combine this method with a more specific technique such as GC or GC–MS for precise identification.

MG is a phenothiazine basic cationic dye used for biological stains, pH indicators and is used as a model dye for textile, leather, paper, plastics, ink and printing. Laser-induced fluorescence spectra of MB and MG in a variety of solvents with different polarity and various concentrations of anionic surfactants have been investigated [16]. It has been reported that there

\* Tel.: +90 372 257 40 10x1371; fax: +90 372 257 41 81.

E-mail address: [makyuz2004@yahoo.co.uk](mailto:makyuz2004@yahoo.co.uk).

was no appreciable shift in the emission maxima with the SDS concentrations, however there might be changes in the fluorescence intensities used in the determination of the critical micelle concentration (cmc) of surfactants [16].

Methods for the determination of polar aromatic sulphonates in aquatic environmental samples have been reviewed by Reemtsma [17]. High-performance liquid chromatography (HPLC) [1,18–20], liquid chromatography-electrospray-tandem mass spectrometry [21] and gas chromatography-mass spectrometry (GC–MS) [22–26] methods have been widely used to determine LAS and SPC in environmental samples. Solid phase extraction [1,19,20] has also been used to clean up or extract the compounds of interest prior to HPLC and GC–MS. Capillary zone electrophoresis (CZE) technique has also been reported for the determination of anionic surfactants [27–31].

The aim of this work was to develop analytical techniques that could be applied to a variety of samples including commercial detergent, wastewater, river water and sea water to determine the LAS and their degradation products. Although there are several methods showing lower detection limits using C18 isolation and GC–MS, the method described here compares methylene green with the widely used Methylene blue which has shortcomings [14,15].

The following paper presents an analytical procedure, which was developed to enable the precise determination of LAS, SPC and similar organic molecules bearing sulphate and sulphonate groups by resolving the variability of the results and to eliminate positive and negative interferences reported in the MBAS method. In the proposed method, the isolation of the compounds of interest from aqueous environmental samples was performed using MG as an ion-pair reagent, and then isolated compounds were hydrolysed with HCl and derivatised with diazomethane prior to GC–MS analysis.

## 2. Experimental

### 2.1. Chemicals and reagents

Arylan SE, a commercial mixture containing 14 homologues and isomers of linear alkylbenzene sulphonic acids with C<sub>10–12</sub> chain lengths was used as the LAS standard and supplied by Akros Chemicals, England. Methylene Green was purchased from Fisher Scientific, UK. Diazald (*N*-methyl-*N*-nitroso-*p*-toluenesulphonamide) was purchased from Aldrich.

#### 2.1.1. Preparation of reagent solution

**Methylene Green reagent:** 0.1 g of methylene green was dissolved in 100 mL water. Three millilitre of this solution was transferred to a 100 mL flask and 50 mL water, 4.1 mL 6N H<sub>2</sub>SO<sub>4</sub> and 5 g NaH<sub>2</sub>PO<sub>4</sub>·H<sub>2</sub>O added, respectively. The solution was made up to 100 mL with deionised water after shaking until dissolved.

### 2.2. Sample extraction and derivatisation

The aqueous samples were added to a separatory funnel and the pH of the sample was adjusted to 5 by dropwise addition of 0.1 M HCl after adding 25 mL of methylene green reagent. Then

it was extracted three times with chloroform (3 mL × 4 mL). The chloroform extracts containing MG-LAS and SPC were taken into a vial and then evaporated to dryness under nitrogen stream. Two to four drops of concentrated HCl were added to the residue and the vial was tightly closed. Hydrolysis of compounds was performed in the sealed vial by heating at 80 °C for 20–25 min. Diazomethane prepared from diazald [32] in ether was added to the dry residues which were evaporated to dryness under a stream of nitrogen until a yellow colour persisted. Then, ethereal diazomethane was evaporated under a gentle stream of nitrogen and the esterified compounds were diluted in hexane. The hexane layer is separated and dried over anhydrous sodium sulphate. The solution was then concentrated to a volume of 0.5 mL under a gentle stream of nitrogen and the final solutions (1–1.5 μL) were injected into GC–MS in splitless mode. LAS and SPC were then analysed as their methyl sulphonate derivatives by GC–MS and the overall process is schematically demonstrated in Fig. 1.

### 2.3. Instrumental analysis

A Finnigan MAT 4500 GC/MS instrument operating in the electron impact (EI) mode was used. Column identi-

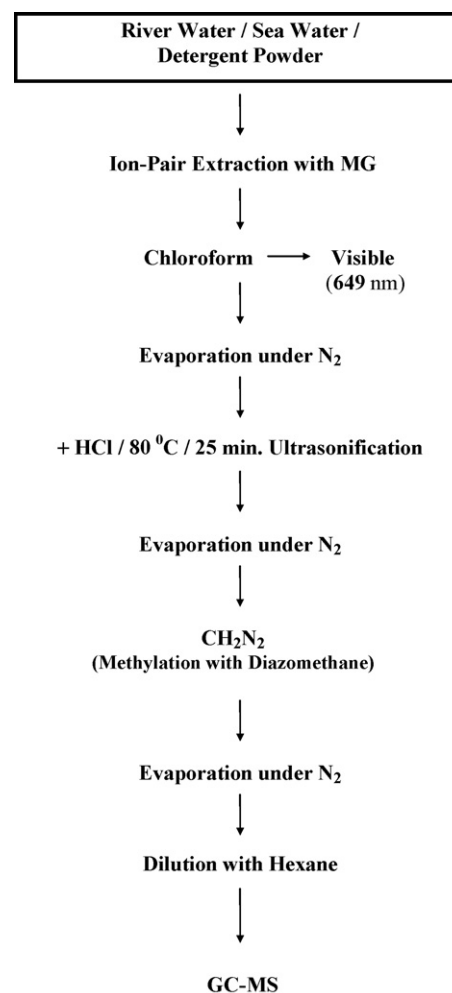


Fig. 1. Flow chart showing the isolation and preparation of the compounds of interest for GC–MS analysis.

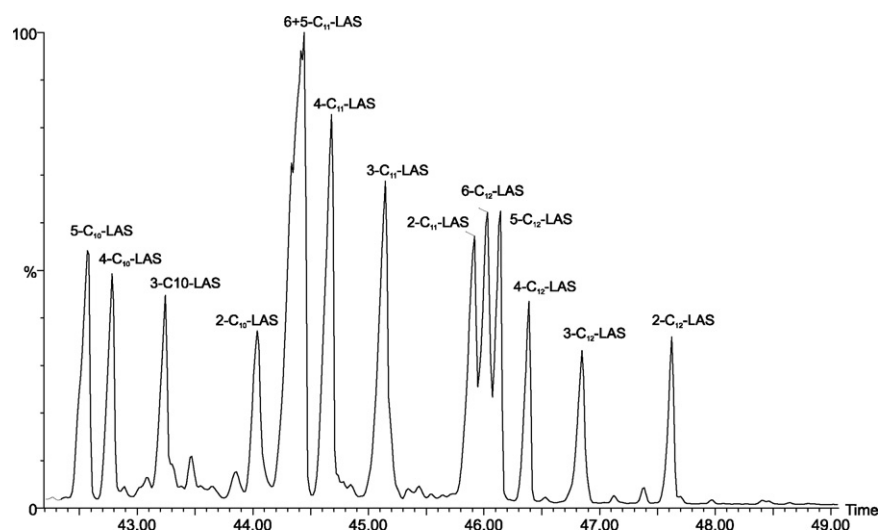


Fig. 2. TIC of methyl derivatives of linear alkylbenzene sulphonate standard (Arylan SE).

fication: DB-5, column length: 50 m, i.d.: 0.25 mm, film thickness: 0.25  $\mu\text{m}$ . Temperature program: initial temperature 40  $^{\circ}\text{C}$  ramped at 5  $^{\circ}\text{C}/\text{min}$  to 300  $^{\circ}\text{C}$  10 min hold. Flow rate: 40  $\text{cm s}^{-1}$  equivalent flow at ambient temperature, head pressure: 0.7  $\text{kg cm}^{-2}$ , ion source temperature: 170  $^{\circ}\text{C}$ , transfer line temperature: 200  $^{\circ}\text{C}$ , scan range: 50–500  $m/z$ , scan rate: 1  $\text{scan s}^{-1}$ , electron energy: 70 eV, electron current: 350  $\mu\text{A}$ .

### 3. Results and discussion

#### 3.1. Interpretation of mass spectra of LAS standard

Firstly, the LAS standards were derivatised with diazomethane and methyl esters of linear alkylbenzene sulphonate acids were analysed by GC-MS. Total ion chromatogram (TIC) of the methylated linear alkylbenzene sulphonate acids standard

(Arylan SE) is shown in Fig. 2. Identification of the components was performed by interpreting their mass spectra. For example, interpretation of mass spectrum of methylated 5-C<sub>10</sub> LAS was carried out as follows; the fragmentation ions of both  $m/z$  241 and 255 come from the expected cleavage on the tertiary carbon atom. Two hundred and forty-one and 255 give the expected  $\beta$  cleavage of the aromatic ring and eventually give  $m/z$  185 a McLafferty re-arrangement which is the characteristic ion for both LAS and SPC in the spectrum called the base peak. Another peak is observed at  $m/z$  199 which comes from  $m/z$  241 and 255 by another rearrangement with H transfer. The ion observed at  $m/z$  145 is formed by the loss of a methyl sulphonate group from the ion observed at  $m/z$  241. The ion observed at  $m/z$  281 is formed by the loss of a methanol ( $M^+ - 32$ ) and peaks at  $m/z$  77 and 91 belong to  $\text{C}_6\text{H}_5^+$  and  $\text{C}_6\text{H}_5\text{CH}_2^+$  (tropylium ion), respec-

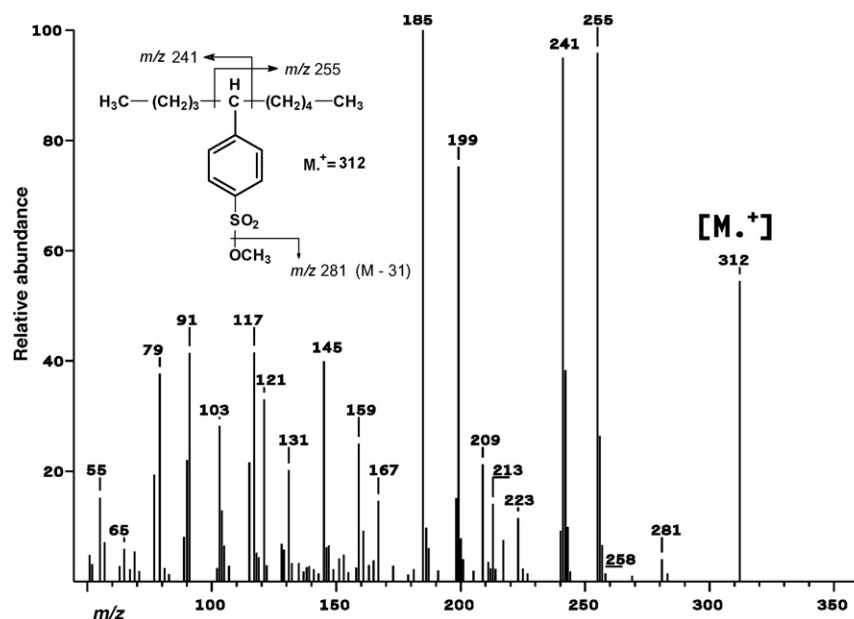


Fig. 3. Mass spectrum of methyl ester of 5-C<sub>10</sub> LAS produced from Arylan SE.



tively. The mass spectrum of methylated 5-C<sub>10</sub> LAS is shown in Fig. 3.

All the other LAS-methyl esters were interpreted in the same manner and the expected fragmentation patterns were obtained. 5-Sulphophenyl valeric acid was also derivatised by the reaction with diazomethane and analysed by GC–MS as a model compound for SPC. The mass spectrum of methylated 5-sulphophenyl valeric acid is shown in Fig. 4 and the interpretation of mass spectrum was carried out in the following way; the compound yields a very low intensity peak for the molecular ion observed at  $m/z$  286. The ion observed at  $m/z$  254 is formed by the loss of a methanol ( $M^+ - 32$ ) and the ion at  $m/z$  226 is formed by the neutral loss of CO. The base peak observed at  $m/z$  131 is formed by the loss of a methyl sulphonates group from the ion observed at  $m/z$  226. The ion observed at  $m/z$  185 is common for LAS and SPC methyl esters. The ion observed at  $m/z$  103 is formed by the loss of a methyl sulphonate group from the ion observed at  $m/z$  199. The ion observed at  $m/z$  74 belongs to the enol ion (C<sub>3</sub>H<sub>6</sub>O<sub>2</sub>) by McLafferty re-arrangement which is common for SPC methyl esters. The ion observed at  $m/z$  87 is also common for SPC methyl esters which belongs to the (C<sub>2</sub>H<sub>4</sub>COOCH<sub>3</sub>)<sup>+</sup>. The different chain lengths were accounted for by the loss of the CH<sub>2</sub> groups. Different isomers of the same homologues were determined by the base peak together with expected cleavage on the C atoms bonded to the benzene ring giving first two more stable fragmentation ions such as peaks at  $m/z$  241 and 255. These peaks are characteristic for both LAS and SPC methyl esters.

### 3.2. Recovery of the compounds of interest from aqueous samples

In a previous work [1,33], the detailed composition of a commercial mixture containing 14 homologues and isomers of linear

Table 1

Composition of Arylan SE linear alkyl benzene sulphonic acid mixture

Ø-Position of isomers	LAS homologues		
	C <sub>10</sub> (%)	C <sub>11</sub> (%)	C <sub>12</sub> (%)
2	3.281	7.657	3.196
3	3.792	10.098	3.089
4	3.877	12.864	5.106
5	5.108	20.766	9.425
6	–	(5+6Ø)	9.426
Total (97.685%)	16.058	51.385	30.242

alkylbenzene sulphonic acids with C<sub>10</sub>–12 chain lengths (Arylan SE) was determined using individual isomers and homologues by peak areas on GC–MS and this mixture was used in this work as the standard and its composition was given in the Table 1.

Firstly, a known amount of this standard (5–10 mg) was derivatised with diazomethane and diluted in hexane. Seven calibration standards with the concentrations in a range from 5 to 100 µg/L were prepared by diluting the derivatised standard hexane solution and used for calibration. Calibration standards of LAS were analysed as their methyl esters by GC–MS in EI mode triplicate. Calibrations were performed by calculating the peak areas of the compounds and the calibration graphs were linear for the concentration ranges stated. The linearity of the proposed method for the analysis of the compounds of interest was calculated in the investigated concentration range, as shown by the determination coefficients ( $R^2$ ).

In order to evaluate the recoveries of LAS, a solution of a known concentration of LAS mixture was prepared and a known volume of this solution was spiked into distilled and previously amine-free water to give final concentrations around 50 µg/L of LAS. Spiking the known volumes (10, 25 and 50 mL) of LAS solution (50 µg/L) with river and sea water samples (250

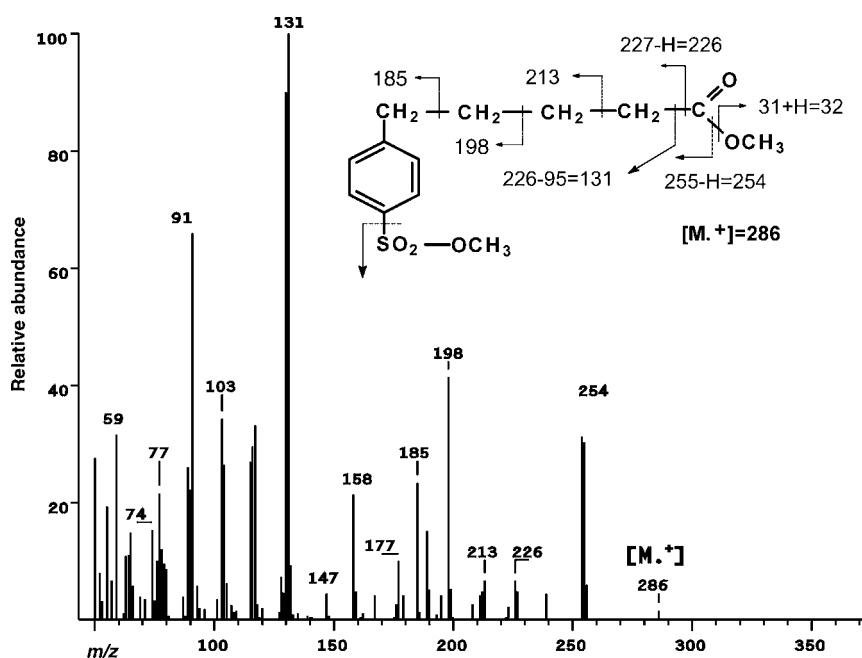


Fig. 4. Mass spectrum of acid methyl ester of 5-sulphophenyl valeric acid.

and 500 mL) which have been analysed for the compounds of interest were also performed (plus the blank value). Quantitative analyses of the LAS in known volumes of these samples were performed in triplicate using GC–MS in EI mode. The concentrations of each of LAS were calculated by peak areas and the peak areas were compared with the calibration graphs of the standards.

The formation of ion-pairs of MG with anionic surfactants was investigated and the results revealed that like MBAS, MG showed the similar ion-pair ability with anionic surfactants in aqueous solutions. Using the proposed method, optimum extraction pH of LAS was investigated and for both LAS and SPC, it was found to be 5. The extraction efficiency of the LAS-MG ion-pair into chloroform was found to be comparable to the LAS-MBAS. The obtained results showed that the method has a similar sensitivity to the MBAS and it is more selective and is free from positive and negative interferences. The percentage recovery of LAS with relative standard deviation (R.S.D.) at pH 5 was also calculated. The different isomers and homologues of LAS behaved in a very similar manner during recovery experiments. The limit for the detection of the combined ion-pair extraction method with MG, derivatisation with diazomethane and analysis by GC–MS technique, was determined using spiked LAS standards in the water sample and the samples were analysed under optimal conditions. The limit of detection (LOD) of each of the LAS was estimated for triplicate runs by comparing the signal-to-noise ratio (S/N) of the lowest detectable concentration to S/N of three.

### 3.3. Determination of LAS as their methyl esters in a commercial detergent powder

In order to confirm the viability of the proposed method, it was applied to an unspecified commercial detergent powder to determine the content of the anionic surfactants (LAS). A solution of known amount of detergent powder was prepared and a known volume of this solution was analysed according

to the procedure described in this work. Identification of the components was performed by interpreting their mass spectra. Quantitative analysis of LAS was performed using GC–MS in EI mode using their peak areas and the peak areas were compared with the calibration graphs. The content of the anionic surfactants as the total concentrations of LAS isomers and homologues LAS were determined to be 6% in dry powder. A number of both liquid and solid commercial detergent samples were analysed in the same way and their anionic surfactant contents found within the range of 4.0 and 15%.

### 3.4. The characterization of LAS and SPC as their methyl esters in the biodegradation medium

In order to observe the degradation of a commercial detergent powder in the natural environment, water collected from the environment which was used as a natural medium were simulated by maintaining the sample, at room temperature, in sunlight with aeration until no compounds of interest could be detected. The samples were then spiked with commercial detergent powder (10 mg/L) and used as a bacterial growth medium and determination of the amount of the spiked compounds as LAS remaining was performed at intervals using the standardised procedure used in this work. Total ion chromatogram (TIC) of the methylated LAS standard isolated from spiked water sample at the start of the experiment (time 0) is identical with the chromatogram shown in Fig. 2.

After 24 h, the SPC and LAS isolated from 250 mL of medium was methylated prior to GC–MS analysis and the total ion chromatogram (TIC) of methyl derivatives of LAS and SPC is shown in Fig. 5. The identification of the methyl esters of LAS and SPC was performed using previously obtained mass spectra from the compounds used as standards and the concentrations of LAS isomers and homologues were calculated by peak areas. For example, interpretation of the mass spectrum of 3-C<sub>7</sub>-SPC methyl ester was carried out in the following way; the fragmentation ions of both  $m/z$  213 and 284 come from the expected

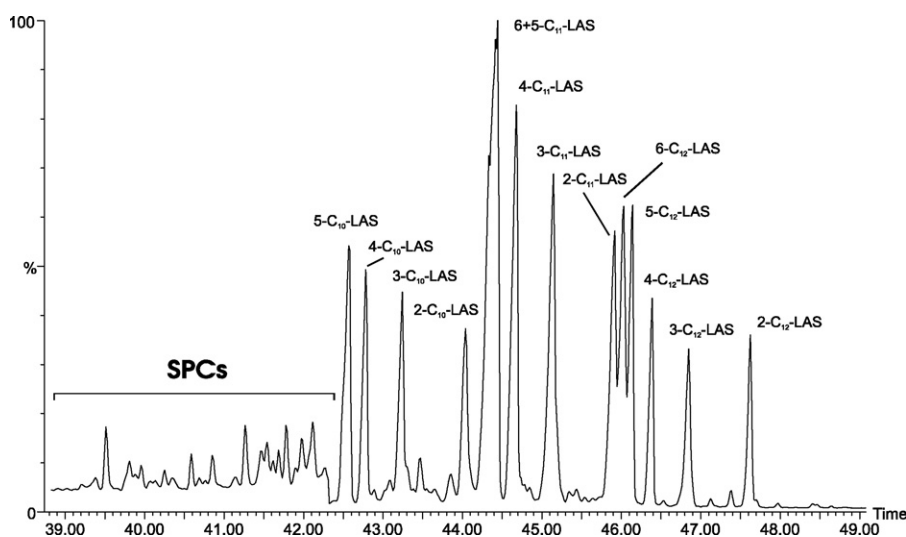


Fig. 5. TIC of methyl derivatives of Arylan SE Standard Spiked Water Sample.

cleavage on the tertiary carbon atom. The peak is observed at  $m/z$  199 which comes from  $m/z$  213 and 284 by another re-arrangement with H transfer. Two hundred and thirteen and 284 give the expected  $\beta$  cleavage of the aromatic ring and eventually give  $m/z$  185 a McLafferty re-arrangement which is the characteristic ion for both LAS and SPC. The ion observed at  $m/z$  118 is formed by the loss of a methyl sulphonate group from the ion observed at  $m/z$  213. The ion observed at  $m/z$  103 is formed by the loss of a methyl sulphonate group from the ion observed at  $m/z$  199. The ion observed at  $m/z$  74 belongs to the enol ion ( $C_3H_6O_2$ ) by McLafferty re-arrangement which is common for SPC methyl esters. The ion observed at  $m/z$  87 is also common for SPC methyl esters which belongs to the  $(C_2H_4COOCH_3)^+$ . The ion observed at  $m/z$  227 is formed by the loss of the ion at  $m/z$  87 from the molecular ion observed at  $m/z$  314.

The results obtained from the degradation experiments indicated that the different isomers and homologues of LAS degrade differently and these results are agree with Swisher distance principal [4–6]. Besides LAS, some sulphophenyl carboxylic acids were identified having alkyl chain lengths between 5 and 9 C atoms and this observation is confirmed that SPC are initial biotransformation products of LAS as much of the literature testifies [4–7]. Through the obtained results from degradation experiments, it can be concluded that, the method was suitable for the observation of degradation kinetics of LAS under both laboratory and natural conditions.

### 3.5. Determination of LAS and SPC as their methyl esters in environmental samples

Environmental samples analysed for the compounds of interest included river water and sea water. River water samples (500 mL) collected from the Zonguldak region, where the river

has highly been polluted with mainly sewage effluent and industrial waste, were analysed by the proposed method at different times of the year in triplicate. The mean concentration of total homologues and isomers of LAS was significant (224 ppb) to estimate their effect on the environment although the proposed method is enable to determine individual homologues and isomers of LAS under the minimum effect concentration limit reported in the literature for environmental samples [8]. The individual homologues and isomers of LAS determined in one of the river water sample are: 5-C<sub>10</sub> LAS (26 ppb), 4-C<sub>10</sub> LAS (17 ppb), 3-C<sub>10</sub> LAS (16 ppb), 2-C<sub>10</sub> LAS (12 ppb), 6+5-C<sub>11</sub> LAS (52 ppb), 4-C<sub>11</sub> LAS (16 ppb), 3-C<sub>11</sub> LAS (11 ppb), 2-C<sub>11</sub> LAS (8 ppb), 6-C<sub>12</sub> LAS (16 ppb), 5-C<sub>12</sub> LAS (16 ppb), 4-C<sub>12</sub> LAS (8 ppb), 3-C<sub>12</sub> LAS (6 ppb) and total level is 204 ppb.

The sea water samples (1 L) collected from the harbour in Zonguldak city where river water taken from were analysed at different times of the year in triplicate and the mean concentration of total homologues and isomers of LAS was found to be 58 ppb. TIC of the methylated anionic surfactants as LAS isolated from (1 L) sea water sample is shown in Fig. 6. The individual homologues and isomers of LAS determined in one of the sea water sample are: 5-C<sub>10</sub> LAS (12 ppb), 4-C<sub>10</sub> LAS (8 ppb), 3-C<sub>10</sub> LAS (8 ppb), 4-C<sub>10</sub> LAS (12 ppb), 6+5-C<sub>11</sub> LAS (24 ppb), 4-C<sub>11</sub> LAS (10 ppb), 3-C<sub>11</sub> LAS (5 ppb), 6-C<sub>12</sub> LAS (6 ppb), 5-C<sub>12</sub> LAS (6 ppb), 4-C<sub>12</sub> LAS (4 ppb) and total level is 83 ppb.

Isolation procedure described in this work, which is sensitive enough for the determination of minimum effect concentration of LAS in aqueous environmental samples and believed to be more selective than SPE, can also be combined with an HPLC [1,34] but it was preferred to combine it with GC–MS due to its higher sensitivity and resolution.

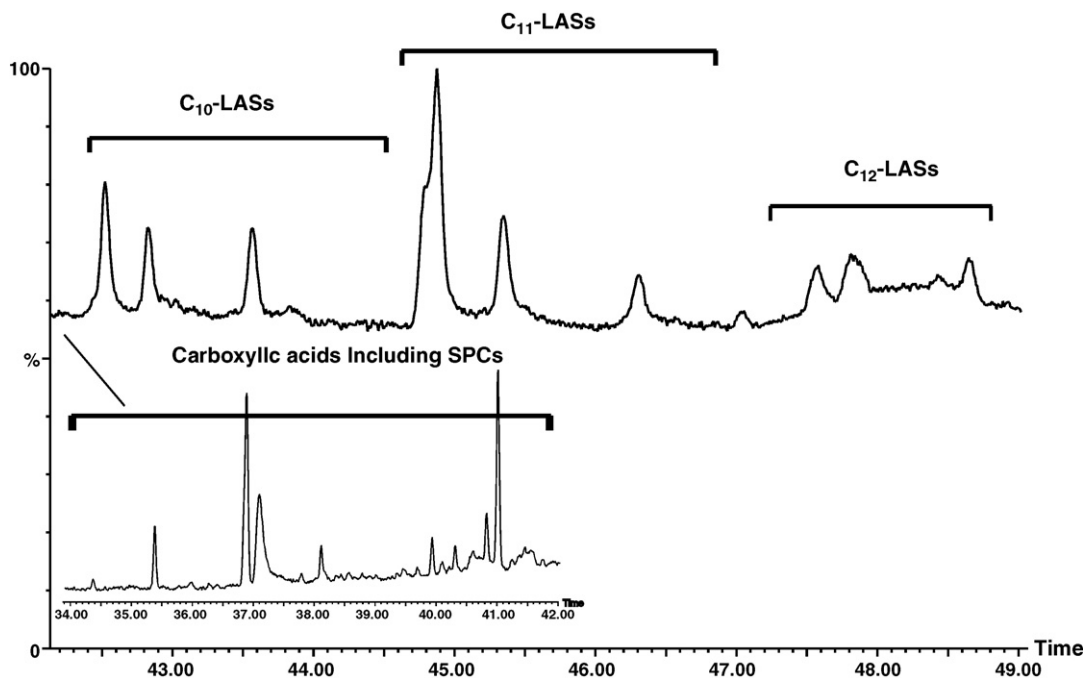


Fig. 6. TIC of methyl derivatives of LAS isolated from Sea Water Sample.

The results revealed that the formed LAS-MG ion-pairs can be hydrolysed at 80 °C for 20–25 min, whereas complete hydrolysis of LAS-MBAS ion-pairs needs over 130 °C for 50–55 min. However, even at low temperatures and a shorter time interval, LAS-MBAS ion-pairs are hydrolysed to some extent which is believed to result in the variabilities in spectrophotometric results; although it has been reported [35] that alkylsulphates could be differentiated from alkylsulphonates by acid hydrolysis. The MG also forms weak ion-pairs with some organic anions, such as carboxylic acids and phenolic compounds and these ion-pairs are easily hydrolysed under the conditions mentioned above.

A number of water samples were analysed by both UV and GC–MS and obtained results were compared. These results indicated that the total concentrations of LAS and SPC in some of the environmental water samples determined by GC–MS may decrease to the level of 10% of the total concentration if determined by UV; the remaining 90% may consist of other compounds, such as carboxylic acids and phenolic compounds that give a positive response to the method. As was seen, these differences can only be sorted out and LAS and SPC can be analysed individually by using the proposed method. The extractibility of LAS over a wide range of pH for the MG method is an advantage which enables the isolation of the organic molecules bearing sulphate and sulphonate groups besides the isolation of LAS. The formation of ion-pairs of MG with organic molecules bearing sulphate and sulphonate groups have also been investigated and the results obtained showed that different types of sulphates and sulphonates form ion-pairs with MG and all isolated compounds are hydrolysed with HCl which makes possible the GC–MS analysis of the compounds of interest after esterification with diazomethane. The developed method eliminates all interferences such as colourless ion-pair compounds and carboxylic acids, phenolic compounds because chloroform extracts are hydrolysed and all isolated compounds are derivatised for GC–MS analysis and identified individually.

The obtained results revealed that the proposed method has been successfully applied to commercial detergent, wastewater, river water and sea water samples for the determination of LAS and their degradation products. The recovery of LAS was 98% with the precision of the method, as indicated by the relative standard deviation (RSD) of 2.0% and the detection limit obtained from calculations by using GC–MS results based on S/N:3 was lower than 10 ppb. Excellent linearity was obtained in the concentration range of 5 and 100 ppb, and the method showed good reproducibility with correlation coefficients higher than 0.9995.

Consequently, the method is believed to be suitable for the qualitative and quantitative determination of most of organic anions having sulphates or sulphonates in aqueous environmental samples.

#### 4. Conclusions

The developed method, consisting of ion-pair extraction with MG and derivatisation with diazomethane proved well suited for the GC–MS determination of LAS and SPC from aqueous environmental samples. Through the obtained results, it may be

concluded that the method developed, besides the analysis of LAS and SPC, can be proposed as a procedure for the determination of organic substances bearing sulphate and sulphonate groups in aqueous environmental samples. Excellent linearity was obtained in the concentration range of 5 and 100 ppb, and the method showed good reproducibility with correlation coefficients higher than 0.9995.

#### Acknowledgement

The author wishes to thank the Zonguldak Karaelmas University for the opportunity and support to carry out this research.

#### References

- [1] M. Akyüz, D.J. Roberts, Turk. J. Chem. 26 (5) (2002) 669–679.
- [2] M. Sáez, V.M. León, A. Gómez-Parra, E. González-Mazo, J. Chromatogr. A 889 (2000) 99–104.
- [3] Y. Nomura, K. Ikebukuro, K. Yokoyama, T. Takeuchi, Y. Arikawa, S. Ohno, I. Karube, Biosens. Bioelectron. 13 (1998) 1047–1053.
- [4] R.D. Swisher, Surfactant Biodegradation, second ed., Marcel Dekker, New York, 1987, Surfactant science series; v. 18, ISBN 0-8247-6938-4.
- [5] P. Schoberl, Tenside. Surfact. Det. 26 (1989) 86–94.
- [6] C. Zhang, K.T. Valsaraj, W.D. Constant, D. Roy, Water Res. 33 (1) (1999) 115–124.
- [7] L. Cavalli, A. Gellera, A. Landone, Environ. Toxicol. Chem. 12 (1993) 1777–1788.
- [8] E. Argese, A. Marcomini, P. Miana, C. Bettiol, G. Perin, Environ. Toxicol. Chem. 13 (5) (1994) 737–742.
- [9] E. Chirilă, I. Carazeanu, S. Dobrinaş, Talanta 53 (2000) 271–275.
- [10] T.V. Vladimirova, E.E. Morgunova, Russ. J. App. Chem. 74 (12) (2001) 2095–2097 (Translated from Zhurnal Prikladnoi Khimii 74 (12) (2001) 2035–2037).
- [11] S. Rubio-Barroso, V. Rodriguez-Gamonal, L.M. Polo-Diez, Anal. Chim. Acta 206 (1988) 351–355.
- [12] M. Kamaya, Y. Tomizawa, K. Nagashima, Anal. Chim. Acta 362 (1998) 157–161.
- [13] T. Sakai, H. Harada, X. Liu, N. Ura, K. Takeyoshi, K. Sugimoto, Talanta 45 (1998) 543–548.
- [14] I. Sanemasa, E. Oota, K. Aoi, J.-Z. Zheng, Anal. Sci. 18 (2002) 347–350.
- [15] M. Koga, Y. Yamamichi, Y. Nomoto, M. Irie, T. Tanimura, T. Yoshinaga, Anal. Sci. 15 (1999) 563–568.
- [16] S.E. Jayaraj, M. Umadevi, V. Ramakrishnan, J. Incl. Phenom. Macro. 40 (2001) 203–206.
- [17] T. Reemtsma, J. Chromatogr. A 733 (1996) 473–489.
- [18] K. Heinig, C. Vogt, G. Werner, J. Chromatogr. A 745 (1996) 281–292.
- [19] A. Di Corcia, R. Samperi, Environ. Sci. Technol. 28 (1994) 850–858.
- [20] A. Marcomini, A. Di Corcia, R. Samperi, J. Chromatogr. 644 (1993) 59–71.
- [21] P. Eichhorn, Ó. López, D. Barceló, J. Chromatogr. A 1067 (2005) 171–179.
- [22] W.-H. Ding, J.C.H. Fann, Anal. Chim. Acta 408 (2000) 291–297.
- [23] W.-H. Ding, C.-T. Chen, J. Chromatogr. A 857 (1999) 359–364.
- [24] W.-H. Ding, J.-H. Lo, S.-H. Tzing, J. Chromatogr. A 818 (1998) 270–279.
- [25] H. Hon-Nami, T. Hanya, J. Chromatogr. 161 (1978) 205–212.
- [26] W.-H. Ding, S.-H. Tzing, J.-H. Lo, Chemosphere 38 (11) (1999) 2597–2606.
- [27] W.-H. Ding, C.-H. Liu, J. Chromatogr. A 929 (2001) 143–150.
- [28] J. Riu, P. Eichhorn, J.A. Guerrero, Th.P. Knepper, D. Barceló, J. Chromatogr. A 889 (2000) 221–229.
- [29] C. Kanz, M. Nölke, T. Fleischmann, H.-P.E. Kohler, W. Giger, Anal. Chem. 70 (1998) 913–917.
- [30] K. Heinig, C. Vogt, G. Werner, Analyst 123 (1998) 349–353.
- [31] J. Riu, D. Barceló, Analyst 126 (2001) 825–828.

- [32] K. Blau, J.M. Halket (Eds.), *Handbook of Derivatives for Chromatography*, second ed., John Wiley and Sons Ltd., 1993.
- [33] M. Akyüz, *HPLC and GC–MS Determination of Surfactants and their Biodegradation Products in the Environment*, Ph.D. Thesis, University of Bristol, UK, 1997.
- [34] S. Wangkarn, P. Soisungnoen, M. Rayanakorn, K. Grudpan, *Talanta* 67 (2005) 686–695.
- [35] T.M. Schmitt, *Analysis of Surfactants*, Marcel Dekker, Inc., New York, 1992, Surfactant Series v. 40, p. 292, ISBN 0-8247-8551.



# Simultaneous determination of aliphatic and aromatic amines in indoor and outdoor air samples by gas chromatography–mass spectrometry

Mehmet Akyüz\*

Zonguldak Karaelmas University, Faculty of Sciences and Letters, Department of Chemistry, 67100 Zonguldak, Turkey

Received 15 June 2006; received in revised form 18 October 2006; accepted 19 October 2006

Available online 27 November 2006

## Abstract

A gas chromatography–mass spectrometry (GC–MS) method has been proposed for the simultaneous determination of aliphatic and aromatic amines in indoor and outdoor air samples. The method includes pre-concentration of the compounds by percolating the air samples through the acidic solution, ion-pair extraction with bis-2-ethylhexylphosphate (BEHPA), derivatisation of compounds with isobutyl chloroformate (IBCF) and their GC–MS analysis. Aliphatic and aromatic amines were isolated from aqueous samples using BEHPA as ion-pair reagent and derivatised with IBCF for their chromatographic analysis. Aliphatic and aromatic amines were then analysed with GC–MS in both electron impact (EI) and positive and negative ion chemical ionisation (PNICI) mode as their isobutyloxycarbonyl (*iso*BOC) derivatives. The obtained recoveries ranged from 75.6 to 96.8% and the precision of this method, as indicated by the relative standard deviations (R.S.D.) was within the range of 1.0–4.4%. The detection limits obtained from calculations by using GC–MS results based on S/N: 3 were within the range of 0.08–0.01 ng/m<sup>3</sup>.

© 2006 Elsevier B.V. All rights reserved.

**Keywords:** Ion-pair extraction; Aliphatic and aromatic amines; GC–MS; Indoor–outdoor air samples

## 1. Introduction

Volatile aliphatic amines like methylamine, dimethylamine, ethylamine, diethylamine, propylamine, dipropylamine, butylamine and dibutylamine are important air pollutants due to their odorous and toxic characteristics and they are found in the air as a result of their industrial commercial applications or their widespread use as intermediates in chemical and pharmaceutical industries [1,2]. In addition to their toxic characteristics most of alkylamines are sensitizers and irritants to the skin, mucous membrane and respiratory tract and it is well known that they can react with nitrite, forming carcinogenic nitrosamines [3,4].

Aromatic amines like morpholine, aniline, phenylethylamine, chloroanilines, piperazine, naphthylamines, aminophenols, toluenediamines and 4-aminobiphenyl are biologically active compounds, well known as environmental pollutants because of their toxicity and carcinogenicity as they are widely used in industry to make dyes, cosmetics, medicines, rubber,

textiles, agrochemicals and as reagents intermediates in many chemical syntheses [5,6]. Therefore, the monitoring of levels of aliphatic and aromatic amines in indoor and outdoor air is important to protect human health and the environment because of human exposure to these compounds through diet and inhalation.

The most widely used techniques for the determination of aliphatic [1,2] and/or aromatic amines [5,6] in air samples are gas chromatography (GC) coupled with different detectors [1,3,5], high-performance liquid chromatography (HPLC) [4,7–10], ion chromatography [11], spectrophotometry [12]. Gas chromatography–mass spectrometry (GC–MS) has been recognized as the method of choice for the analysis of aliphatic and aromatic amines in environmental samples, due to its superiority in selectivity and sensitivity. A pre-concentration step is necessary to obtain good sensitivity and derivatisation step is generally required to improve the gas chromatographic properties because of the polarity of the amines. Liquid–liquid extraction after percolation of the air sample through the acidic solution (LLE) [6,13] and solid-phase extraction (SPE) [1,2,7,12,14] have been widely employed for the isolation of these amines from air samples. The most popular derivatisation techniques employed for gas chromatographic analysis

\* Tel.: +90 372 257 40 10x1371; fax: +90 372 257 41 81.

E-mail address: [makyuz2004@yahoo.co.uk](mailto:makyuz2004@yahoo.co.uk).



of amines are acylation, silylation, carbamate formation, sulphonamide formation and phosphoamide formation [15].

This study focuses on the development of analytical techniques that could be applied to indoor and outdoor air samples to determine various aliphatic and aromatic amines by adapting our previous method for the analysis of amines in water and sediment samples [16].

The following paper presents an analytical procedure, proposed to enable the precise determination of low-level aliphatic and aromatic amines in indoor and outdoor air and rainwater samples. This procedure offers several significant advantages over the other techniques available, such as higher selectivity in isolation, efficient derivatisation and higher sensitivity. In the proposed method, air samples were percolated through the 0.1 M HCl solution using constant flow air pump to trap aliphatic and aromatic amines in the aqueous acidic solution as their hydrochloric salts. The compounds of interest were extracted from aqueous solution with chloroform containing bis-2-ethylhexylphosphate (BEHPA) as ion-pair reagent and derivatised with isobutyl chloroformate. Aliphatic and aromatic amines were then analysed as their isobutyloxycarbonyl (*iso*BOC) derivatives by GC–MS.

## 2. Experimental

### 2.1. Chemicals and reagents

All the reagents were of analytical grade. Bis(2-ethylhexyl)-phosphate, isobutyl chloroformate, methylamine, ethylamine, diethylamine, *n*-propylamine, butylamine, piperidine, morpholine, diphenylamine, aniline, *N*-methylaniline, benzylamine, 4-aminophenol, 4-bromoaniline, piperazine, 2,5-dichloroaniline, 3,5-dichloroaniline, 3,4-dichloroaniline, dibutylamine, pyrrolidine, 3-aminophenol, 3-chloroaniline, 4-chloroaniline, 2-nitroaniline, 3-nitroaniline, *m*-toluidine, 4-methyl-*o*-phenylenediamine, chloroform, toluene, di-sodium hydrogen phosphate, sodium hydrogen carbonate, sodium sulphate, hydrochloric acid and isobutylalcohol were purchased from Merck. Phenylethylamine was supplied by Aldrich. 4-Aminobiphenyl was supplied by Reidel-de Haen. Pyridine was purchased from J.T. Baker. 1-Naphthylamine was supplied by Sigma. Dimethylamine, 4-ethylaniline and 2-ethylaniline were purchased from Fluka. 2,6-Diethylaniline was purchased from Alfa Aesar.

### 2.2. Samples extraction and derivatisation

Air samples (0.5–1.5 m<sup>3</sup>) were percolated through the two Drechsel bottles, containing 100 mL of 0.1 M HCl solution using constant flow air pump to trap aliphatic aromatic amines in the aqueous acidic solution as their hydrochloric salts. The pump was regulated at a rate of 46 mL/s and it would sample 1 m<sup>3</sup> of air in about 6 h, and then, our previous method was applied to the aqueous phase with minor modifications [16]. The aqueous phases were added to a separatory funnel and the pH of the solution was adjusted to 1 by dropwise addition of 0.01 M HCl. Then it was extracted with chloroform (3 × 3 mL) and separated.

The pH of the aqueous phase was adjusted to 8, as it has been selected to be the extraction pH of the method [16], by dropwise addition of 1 M Na<sub>2</sub>HPO<sub>4</sub> and then was extracted three times using 0.1 M BEHPA in chloroform (3 × 3 mL). The chloroform extracts containing the compounds to be analysed were back extracted with 0.1 M HCl solution for 3 min using ultrasonic bath. Then, the pH of the aqueous layer containing these amines was again adjusted to 8 and extracted three times with chloroform containing 0.1 M BEHPA (3 × 3 mL). The chloroform layer was taken into a vial after drying over anhydrous sodium sulfate and then evaporated to dryness under nitrogen stream at room temperature. Acetonitrile, pyridine and isobutyl alcohol (150, 200, 10 μL) and then *iso*BCF (300 μL) were added to the residue and the vial was then closed and kept at room temperature for 10 min. Then, the mixture was evaporated under a gentle stream of nitrogen at room temperature and the derivatised compounds were diluted in toluene. The toluene layer is separated and dried over anhydrous sodium sulphate after shaking with alkaline methanol (1 mL) followed by 1.5 mL of 5 M NaOH for 3–4 min and centrifuging at 4000 × *g* for 2–3 min. The solution was then concentrated to a volume of 100 μL under a gentle stream of nitrogen and the final solutions (1–2 μL) were injected into GC–MS in splitless mode (5 min purge off). Although they were stable when stored at –15 °C, the *iso*BOC derivatives of the compounds of interest were analysed as soon as they were prepared. Aliphatic and aromatic amines are then analysed as their *iso*BOC derivatives by GC–MS in both electron impact (EI) and positive and negative ion chemical ionisation (PNICI) mode and quantitative analysis was performed in SIM mode. The overall process is schematically shown in Fig. 1.

### 2.3. Instrumental analysis

In this study, a Thermo-Finnigan MAT 4500 GC/MS–MS instrument operating in the electron impact and positive and negative ion chemical ionisation mode were used. The specifications of the apparatus are as follows—column identification: ZB–5 ms, column length: 30 m, ID: 0.25 mm, film thickness: 0.25 μm. Temperature program—initial temperature 80 °C<sub>3 min hold</sub> at 3 °C/min to 140 °C<sub>3 min hold</sub> at 5 °C/min to 290 °C<sub>10 min hold</sub>. Flow rate: 1.3 mL/min, ion source temperature: 200 °C, transfer line temperature: 200 °C, scan range: 30–450 *m/z*, scan rate: 1 scan/s, electron energy: 70 eV for EI and 30 eV for PNICI, and electron current: 350 μA.

## 3. Results and discussion

### 3.1. Interpretation of mass spectra of model compounds

Firstly, aliphatic and aromatic amine standards were derivatised with isobutyl chloroformate (IBCF) and their *iso*BOC derivatives were analysed by GC–MS. Total ion chromatogram (TIC) of derivatised amine standards are shown in Fig. 2.

Identification of the components was performed by interpreting their mass spectra obtained in the electron impact mode. All the other *iso*BOC derivatives of aliphatic and aromatic amines were interpreted in the same way and relatively similar

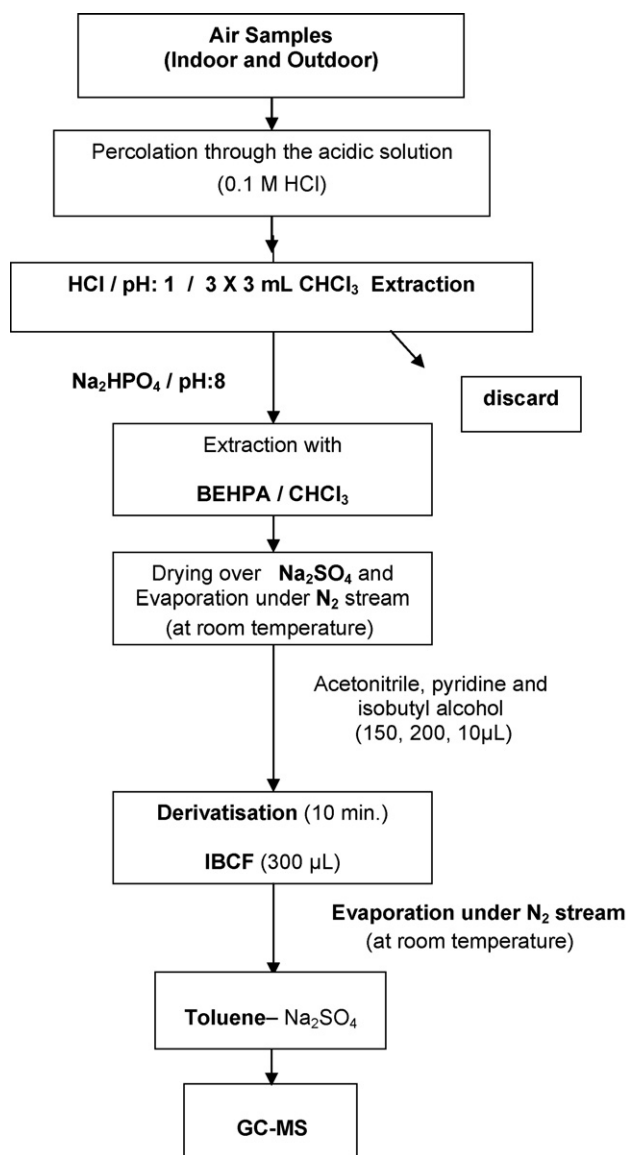


Fig. 1. Flow chart showing the isolation and preparation of the compounds of interest for GC-MS analysis.

fragmentations were obtained. For example, interpretation of mass spectrum of *isoBOC* derivative of aniline was carried out in the following way; the ions observed at  $m/z$  137, 120 and 93 are formed by the loss of  $C(CH_3)_3$ ,  $OC(CH_3)_3$  and  $OCOC(CH_3)_3$  groups from the molecular ion observed at  $m/z$  193. The loss of the butyl groups gives the ion at  $m/z$  57 when using IBCF. These peaks are characteristic for the isobutyloxycarbonyl derivatives. The molecular ion of aniline at  $m/z$  93 observed as the base peak is formed by the loss of isobutyloxycarbonyl group from the molecular ion of *isoBOC* derivatives of aniline observed at  $m/z$  193. Identification of the compounds was also confirmed by GC-MS in PNICI mode using methane as reagent gas.

### 3.2. Recovery of the compounds of interest from samples

Firstly, a standard solution containing 10 mg/L of each of the amines was prepared in acetone and diluted to give a final con-

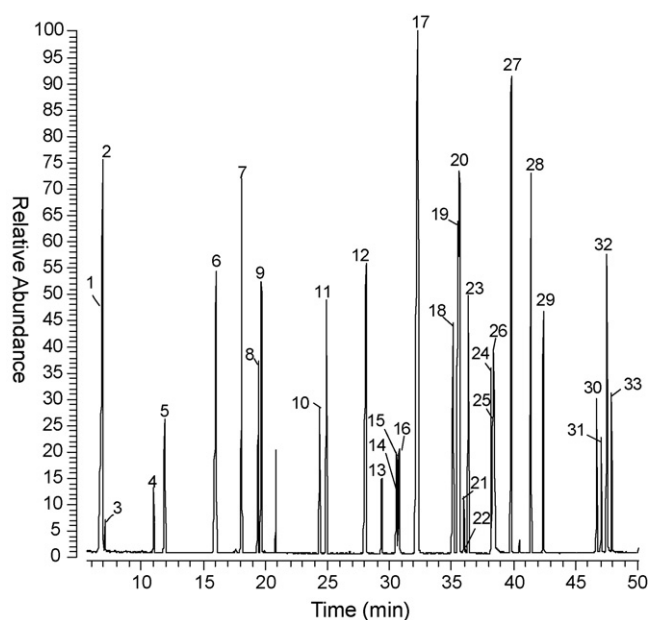


Fig. 2. Total ion chromatogram (TIC) of isobutyloxycarbonyl derivatives of aliphatic and aromatic amine standards. The concentrations of derivatised amines are within the range of 0.01–0.08 ng/ $\mu$ L (1  $\mu$ L injection). (1) Methylamine, (2) dimethylamine, (3) ethylamine, (4) diethylamine, (5) propylamine, (6) butylamine, (7) pyrrolidine, (8) morpholine, (9) piperidine, (10) dibutylamine, (11) *N*-methylaniline, (12) aniline, (13) diphenylamine, (14) *m*-toluidine, (15) benzylamine, (16) phenylethylamine, (17) 2-ethylaniline, (18) 2,6-diethylaniline, (19) 3-chloroaniline, (20) 4-ethylaniline, (21) 4-chloroaniline, (22) 2,5-dichloroaniline, (23) 3,5-dichloroaniline, (24) 4-bromoaniline, (25) 2-nitroaniline, (26) 3-nitroaniline, (27) 3,4-dichloroaniline, (28) piperazine, (29)  $\alpha$ -naphthylamine, (30) 3-aminophenol, (31) 4-aminophenol, (32) 4-methyl-*o*-phenylenediamine and (33) 4-aminobiphenyl.

centration of 100 ng/L and then derivatised with IBCF. Seven calibration standards with the concentrations in the range from 0.01 to 25 ng/L were prepared by diluting the derivatised standard solution (100 ng/L) and used for the calibration. Calibration standards of aliphatic and aromatic amines were analysed as their *isoBOC* derivatives by GC-MS in SIM mode in triplicate. Calibrations were performed by calculating the peak areas of the compounds and the calibration graphs were linear for the concentration ranges stated.

The linearity of the proposed method was calculated in the investigated concentration range, as the determination coefficients,  $R^2$ , shown in Table 1. The limit of detection (LOD) of each of the amines was estimated to be seven replicate runs by comparing the signal-to-noise ratio (S/N) of the lowest detectable concentration to a S/N: 3.

In order to evaluate recoveries of amines from aqueous solution, a solution of a known concentration (50 ng/L) of amines mixture was prepared by diluting the standard solution and known volumes (10, 20 and 50 mL) of this solution was spiked into the distilled water that had previously been shown to contain no amines to give final concentrations around 0.5, 1.0 and 5.0 ng/L of each of the amines, respectively. Spiking the known volumes (25, 50 and 100 mL) of amines solution (50 ng/L) with water samples (250 and 500 mL) which were analysed for the compounds of interest were also performed to evaluate absolute recovery (plus the blank value). Quantitative analyses of the

Table 1  
The absolute recoveries of amines for overall procedure with R.S.D.s at selected pH,  $R^2$ , LOD and QI

Standard amines	Optimum extraction pH	Absolute recoveries (%) with R.S.D.s at selected pH 8	$R^2$	LOD (ng/m <sup>3</sup> )	QI <sub>1,2,3</sub> <i>m/z</i>
Methylamine	8.88	75.6 (2.6)	0.9926	0.08	76, 58, 132
Dimethylamine	7.50	86.0 (2.8)	0.9956	0.07	90, 72, 146
Ethylamine	8.08	89.4 (2.4)	0.9945	0.07	106, 79, 146
Diethylamine	8.15	90.6 (2.2)	0.9922	0.06	118, 102, 72
<i>n</i> -Propylamine	8.18	90.7 (1.8)	0.9928	0.05	104, 130, 160
Butylamine	8.00	89.6 (1.7)	0.9940	0.04	118, 130, 174
Pyrrolidine	7.50	89.8 (2.5)	0.9976	0.03	116, 70, 172
Morpholine	7.92	93.1 (2.3)	0.9979	0.03	116, 88, 188
Piperidine	8.12	94.9 (1.7)	0.9976	0.04	128, 84, 186
Dibutylamine	8.50	92.8 (2.2)	0.9978	0.03	130, 186, 230
<i>N</i> -Methylaniline	7.78	96.4 (1.0)	0.9994	0.01	151, 107, 207
Aniline	8.01	95.5 (1.5)	0.9993	0.01	93, 137, 193
Diphenylamine	8.93	96.8 (2.4)	0.9988	0.01	169, 141, 66
<i>m</i> -Toluidine	8.50	95.3 (1.4)	0.9982	0.01	150, 106, 207
Benzylamine	9.21	92.3 (3.8)	0.9924	0.01	150, 106, 207
Phenylethylamine	9.01	95.7 (2.0)	0.9994	0.01	164, 106, 221
2-Ethylaniline	8.50	95.5 (1.8)	0.9994	0.01	106, 121, 221
2,6-Diethylaniline	8.00	96.5 (1.4)	0.9995	0.01	148, 175, 249
3-Chloroaniline	8.50	94.8 (1.6)	0.9983	0.02	127, 171, 227
4-Ethylaniline	8.00	96.2 (1.7)	0.9996	0.01	165, 106, 221
4-Chloroaniline	8.50	94.9 (1.9)	0.9978	0.02	172, 152, 227
2,4-Dichloroaniline	8.90	94.7 (2.0)	0.9976	0.02	161, 205, 261
2,5-Dichloroaniline	9.00	94.8 (1.8)	0.9976	0.02	161, 205, 261
3,5-Dichloroaniline	9.00	94.8 (1.3)	0.9976	0.02	205, 161, 261
4-Bromoaniline	8.33	93.8 (4.2)	0.9954	0.05	171, 215, 271
2-Nitroaniline	9.00	92.3 (4.4)	0.9920	0.07	135, 106, 235
Piperazine	8.11	95.8 (2.2)	0.9978	0.01	187, 87, 287
$\alpha$ -Naphthylamine	7.90	94.3 (1.8)	0.9989	0.01	143, 187, 243
3-Aminophenol	8.00	93.8 (1.6)	0.9984	0.03	153, 209, 309
4-Aminophenol	8.06	93.9 (1.8)	0.9984	0.03	153, 209, 309
4-Methyl- <i>o</i> -phenylenediamine	8.50	92.6 (2.1)	0.9988	0.01	121, 221, 322
4-Aminobiphenyl	8.21	95.3 (2.3)	0.9982	0.01	213, 169, 269

$n = 7$ ; quantifiers ions: QI<sub>1</sub>, QI<sub>2</sub> and QI<sub>3</sub>.

amines in known volumes of these samples were performed in seven replicates using GC–MS in SIM mode. The concentrations of amines were calculated by peak areas and these areas were compared with the calibration graphs of the standards. The optimum extraction pHs of each amine were investigated and most of them were found to be around 8. The extraction pH of the method was therefore selected to be 8. The recoveries of amines at selected pH were also evaluated. The absolute recoveries of amines from aqueous solution with relative standard deviations (R.S.D.s) at optimum and selected extraction pHs were reported in our previous work [16]. The absolute recoveries of amines for overall procedure described in this work was estimated considering the recoveries of amines from aqueous solution with R.S.D.s at selected extraction pH and the recoveries of amines from air samples.

To evaluate recoveries of the compounds from air samples, two systems each composed of two drechsel bottles containing 100 mL of 0.1 M HCl solution were connected to constant flow air pumps separately. Another drechsel bottle containing 50 mL of standard amine solution at the concentration of 10 ng/L of each of the amines was connected in front of one of these systems and the pumps were regulated at the same flow rate of 46 mL/s. Air samples were then percolated through both systems simulta-

neously. The recovery experiments were performed in triplicate using 10, 20 and 50 mL of standard solution (10 ng/L), respectively, plus the blank value. In order to confirm the absolute recoveries from air, the recovery experiments were also performed in seven replicates using standard amines and clean air. The aqueous phases containing the compounds of interest are analysed in the same way as described in Section 2. Obtained results revealed that water soluble amines were almost 100% with R.S.D.s within the range of 0.3–0.9 trapped into acidic solution and these results are in agreement with the results reported by Skarping et al. [3] and Grönberg et al. [17]. The absolute recoveries of the compounds of interest for overall procedure with R.S.D.s at selected pH, correlation coefficients ( $R^2$ ), limits of detection and quantifier ions (QI) are shown in Table 1.

As it has been reported in our previous work [16], derivatisation of dry residue obtained from the chloroform extract with IBCF was carried out in this work and lower limits of detection were obtained in comparison to the two-phase derivatisation [6,13,18–20]. The obtained results revealed that, the ion-pairs of amines with BEHPA in chloroform may prevent the losses due to volatilization of low-molecular weight aliphatic amines and once derivatised it becomes easier to keep volatile amines as their *iso*BOC derivatives probably due to their higher molecular

mass for the simultaneous determination of low-level aliphatic and aromatic amines in air and rainwater samples.

### 3.3. Determination of aliphatic and aromatic amines as their isoBOC derivatives in air samples

In order to confirm the viability of the proposed method, it was applied to indoor and outdoor air samples to determine various aliphatic and aromatic amines. Indoor and outdoor air samples were collected simultaneously at six points in Zonguldak province during Summer (May–September) times of 2004–2005 and Winter (October–April) times of 2005–2006. The indoor air samples ( $1\text{ m}^3$ ) collected from both smoking and non-smoking areas were analysed for the compounds of interest by the proposed method. Structural identification of isobutyloxycarbonyl derivatives of aliphatic and aromatic amines was carried out by interpretation of the mass spectra and possible match with reagent grade standards' spectra and existing library data obtained in EI mode and also confirmed by PNICI. Quantitative analyses of the identified amines were performed in SIM mode using their peak areas and the peak areas were compared with the calibration graphs. Total ion chromatogram of isobutyloxycarbonyl derivatives of aliphatic and aromatic amines isolated from one of the indoor air samples ( $1\text{ m}^3$ ) collected from smoking area are shown in Fig. 3. The seasonal mean concentrations of amines determined in indoor air samples by using the proposed method during Summer times of 2004–2005 and Winter times of 2005–2006 are shown in Table 2.

In the most of indoor air samples collected from smoking areas in Zonguldak where the number of asthma patients is known as high, piperazine was found at the highest concentrations to be up to 19.98 and 27.68  $\text{ng}/\text{m}^3$  in Summer and Winter times, respectively, which can induce asthma and partly reacts with nitrite forming carcinogenic *N*-mononitrosopiperazine in stomach when transported with saliva after inhalation [3]. Piper-

azine was also found at relatively higher concentrations in indoor air samples collected from non-smoking areas up to 10.15  $\text{ng}/\text{m}^3$  in Summer and 12.88  $\text{ng}/\text{m}^3$  Winter times. Furthermore, *n*-propylamine, butylamine and dibutylamine were found at relatively higher concentrations in indoor air samples collected from smoking areas in Winter times which were up to 11.73, 22.10 and 6.72  $\text{ng}/\text{m}^3$  and in indoor air samples collected from non-smoking areas in Winter times up to 2.05, 6.75 and 2.70  $\text{ng}/\text{m}^3$ , respectively.  $\beta$ -Naphthylamine, known to cause bladder cancer in humans, was found in indoor air samples collected from smoking areas at concentrations up to 4.48  $\text{ng}/\text{m}^3$  in Winter times whereas it was not detected in the air samples collected from non-smoking area and outdoor air samples during Summer times.

In addition, aniline was also found in concentrations in indoor air samples collected from smoking areas up to 25.50  $\text{ng}/\text{m}^3$  and non-smoking areas up to 8.93  $\text{ng}/\text{m}^3$ . Furthermore, aniline was found at relatively higher concentrations in Summer time indoor air samples collected from smoking area at up to 13.02  $\text{ng}/\text{m}^3$  from non-smoking area up to 3.40  $\text{ng}/\text{m}^3$  and outdoor air samples up to 2.50  $\text{ng}/\text{m}^3$ . Aniline and its derivatives were found relatively at higher concentrations in indoor air samples than outdoor air samples. The source of aniline and its derivatives in indoor air is likely due to smoking and widespread usage of these compounds in paints, cleaning products, shoe polishing and cosmetics [5,6].

The outdoor air samples ( $1\text{ m}^3$ ) collected from six different points in Zonguldak province where pollution is very high due to mainly solid coal waste and where coal is also used for central heating between October and April were analysed by the proposed method and the seasonal mean concentrations of amines determined in outdoor air samples in Summer times of 2004–2005 and Winter times of 2005–2006 are shown in Table 2.

Piperazine was found at the highest concentrations in outdoor air samples at up to 9.67  $\text{ng}/\text{m}^3$  in Summer times and 11.86  $\text{ng}/\text{m}^3$  in Winter times. Furthermore, dimethylamine, *n*-propylamine, dibutylamine, aniline and *p*-toluidine were found in outdoor air samples at relatively higher concentrations at up to 2.52, 2.03, 0.45, 2.50 and 2.33  $\text{ng}/\text{m}^3$  Summer times and 3.76, 3.61, 3.80, 6.90 and 5.21  $\text{ng}/\text{m}^3$  in Winter times, respectively.

The results obtained from outdoor air samples in Zonguldak showed that the concentrations of amines measured depend mainly on the air temperature and frequency of rain. To prove that rainwater sample which was taken from the first rain after a few dry days was analysed and similar pattern in the chromatogram was found as in the outdoor air sample taken before the rain. The seasonal mean concentrations of aliphatic and aromatic amines identified in rainwater samples during Summer times of 2004–2005 and Winter times of 2005–2006 are shown in Table 2. The analyses of the air samples after the rain showed that the levels of the amines significantly dropped as a result of removal of the compounds from the atmosphere by rain. These results indicated the fact that there are significant correlations between the levels of amine compounds in outdoor air and rainwater samples as reported by Grönberg et al. [17].

The results revealed that the proposed method, as described in our previous work [16], has been successfully applied to air

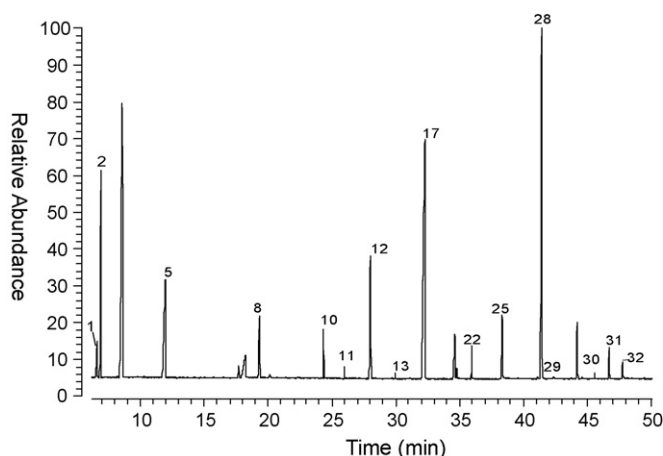


Fig. 3. TIC of isobutyloxycarbonyl derivatives of aliphatic and aromatic amines isolated from one of the indoor air sample. (1) Methylamine, (2) dimethylamine, (5) propylamine, (8) morpholine, (10) dibutylamine, (11) *N*-methylaniline, (12) aniline, (13) diphenylamine, (17) 2-ethylaniline, (22) 2,5-dichloroaniline, (25) 2-nitroaniline, (28) piperazine, (29)  $\alpha$ -naphthylamine, (30) 3-aminophenol, (31) 4-aminophenol and (32) 3,4-toluenediamine.

Table 2

The seasonal mean concentrations of amines determined in air and rainwater samples collected during Summer times of 2004–2005 and Winter times of 2005–2006 in Zonguldak

Compounds	Indoor air (Summer–Winter)		Outdoor air (Summer–Winter)	Rainwater (Summer–Winter)
	Smoking area mean concentrations (ng/m <sup>3</sup> )	Non-smoking area mean concentrations (ng/m <sup>3</sup> )	Mean concentrations (ng/m <sup>3</sup> )	Mean concentrations (ng/L)
Methylamine	1.05–1.76	0.46–0.85	0.26–1.30	0.10–0.12
Dimethylamine	1.11–3.46	1.68–3.41	2.18–2.96	0.47–2.43
Ethylamine	ND–0.12	0.21–1.20	ND–0.35	ND–0.21
Diethylamine	1.35–1.92	0.61–0.80	0.83–0.62	ND–0.36
<i>n</i> -Propylamine	4.16–8.73	0.66–1.33	0.68–3.11	0.43–1.88
Butylamine	7.50–14.10	1.21–2.25	0.05–0.36	0.13–0.33
Morpholine	2.70–4.28	0.60–1.10	0.30–0.43	0.11–0.32
Piperidine	ND–0.34	0.45–1.13	ND–0.04	ND–0.05
Dibutylamine	1.11–4.72	0.79–1.26	0.15–2.60	0.21–0.43
<i>N</i> -Methylaniline	1.34–3.32	1.03–1.75	0.35–0.67	ND–0.11
Aniline	6.12–21.03	1.18–4.42	1.64–4.02	0.98–1.16
Diphenylamine	ND–0.48	0.03–1.30	ND–0.06	ND–ND
<i>m</i> -Toluidine	ND–0.54	ND–0.03	ND–0.21	0.08–0.16
Benzylamine	ND–0.65	ND–0.16	ND–0.36	0.56–1.06
Phenylethylamine	ND–ND	0.50–ND	0.06–0.18	0.12–0.18
2-Ethylaniline	ND–0.45	0.93–ND	ND–ND	ND–ND
<i>p</i> -Toluidine	1.11–16.17	1.08–4.68	0.94–2.85	0.89–1.62
2,6-Diethylaniline	ND–0.20	0.21–ND	0.23–0.27	ND–ND
4-Ethylaniline	ND–0.56	0.08–0.72	0.08–0.49	0.13–0.24
4-Chloroaniline	0.40–0.42	0.49–0.78	0.08–0.23	0.52–1.81
2,4-Dichloroaniline	0.09–0.66	ND–1.00	0.20–0.25	0.12–0.78
2,5-Dichloroaniline	0.12–0.13	0.53–1.05	0.12–0.66	0.34–0.58
3,5-Dichloroaniline	ND–0.47	0.18–0.56	0.08–0.32	0.08–0.25
4-Bromoaniline	ND–ND	0.10–ND	0.24–ND	0.18–0.60
2-Nitroaniline	0.42–1.21	0.32–0.96	0.38–0.62	0.21–0.71
Piperazine	8.30–21.62	4.85–9.58	3.41–9.00	0.18–3.20
$\alpha$ -Naphthylamine	1.32–2.71	0.07–1.66	0.18–0.67	0.07–0.14
$\beta$ -Naphthylamine	1.54–2.38	ND–1.05	ND–0.33	ND–0.16
3-Aminophenol	0.62–ND	0.44–0.51	0.34–0.45	0.22–0.53
4-Aminophenol	1.20–2.23	1.16–1.52	0.41–0.87	0.24–0.59
Methyl- <i>o</i> -phenylenediamine	ND–ND	ND–0.76	0.10–0.34	0.32–1.42
4-Methyl- <i>o</i> -phenylenediamine	0.44–1.03	0.06–0.45	0.06–0.40	0.43–1.52
4-Aminobiphenyl	0.42–0.98	0.38–0.70	ND–0.05	0.07–0.22

$n \geq 6$ ; ND: not detected; Summer: May–September (while central heatings off); Winter: October–April (central heatings on).

and rainwater samples with some suitable modifications for the simultaneous determination of aliphatic and aromatic amines. The obtained recoveries ranged from 75.6 to 96.8% and the precision of this method, as indicated by the relative standard deviations (R.S.D.s) was within the range of 1.0–4.4%. The limits of detection obtained from calculations by using GC–MS results based on S/N: 3 were within the range from 0.08 to 0.01 ng/m<sup>3</sup>. The detection limits differ substantially for the various amines determined, but all were below our stated limits of detection. Excellent linearity was obtained in the concentration range of 0.01–25 ng/L, with correlation coefficients ( $R^2$ ) in the range of 0.9920–0.9996.

#### 4. Conclusions

Consequently, the method described in this study has been shown to be suitable with satisfactory accuracy and good reproducibility for the qualitative and quantitative determination of aliphatic and aromatic amines at the levels of ng/m<sup>3</sup> in air samples.

Through the obtained results, it may be concluded that, the method developed can be proposed as a procedure in the monitoring of trace levels of aliphatic and aromatic amines in a variety of environmental samples including indoor air, outdoor air and rainwater to protect human health and the environment because of human exposure to these compounds through diet and inhalation, due to its effective selectivity in isolation, efficient derivatisation and higher sensitivity in comparison to the most of the other methods available.

#### Acknowledgements

The author wishes to thank the State Planning Organization of Turkey (2003K121120), and the Zonguldak Karaelmas University (2004-13-02-12) for the opportunity and support to carry out this research.

#### References

- [1] J. Namieśnik, A. Jastrzębska, B. Zygmunt, J. Chromatogr. A 1016 (2003) 1.

- [2] L. Pan, J.M. Chong, J. Pawliszyn, *J. Chromatogr. A* 773 (1997) 249.
- [3] G. Skarping, T. Bellander, L. Mathiasson, *J. Chromatogr.* 370 (1986) 245.
- [4] N.A. Santagati, E. Bousquet, A. Spadaro, G. Ronsisvalle, *J. Pharm. Biomed.* 29 (2002) 1105.
- [5] J. Zhu, B. Aikawa, *Environ. Int.* 30 (2004) 135.
- [6] G. Palmiotto, G. Pieraccini, G. Moneti, P. Dolara, *Chemosphere* 43 (2001) 355.
- [7] Y. Moliner-Martínez, P. Campíns-Falcó, R. Herráez-Hernández, J. Verdú Andrés, *Anal. Chim. Acta* 502 (2004) 235.
- [8] A.S. Claeson, A. Östin, L.A. Sunesson, *Anal. Bioanal. Chem.* 378 (2004) 932.
- [9] D. Karlsson, J. Dahlin, G. Skarping, M. Dalene, *J. Environ. Monit.* 4 (2002) 216.
- [10] G. Kallinger, R. Niessner, *Mikrochim. Acta* 130 (1999) 309.
- [11] I.H. Chang, C.G. Lee, D.S. Lee, *Anal. Chem.* 75 (2003) 6141.
- [12] Y. Moliner-Martínez, P. Campíns-Falcó, R. Herráez-Hernández, *J. Chromatogr. A* 1059 (2004) 17.
- [13] T. Weiss, J. Angerer, *J. Chromatogr. B* 778 (2002) 179.
- [14] G. Seeber, M.R. Buchmeiser, G.K. Bonn, T. Bertsch, *J. Chromatogr. A* 809 (1998) 121.
- [15] H. Kataoka, *J. Chromatogr. A* 733 (1996) 19.
- [16] M. Akyüz, Ş. Ata, *J. Chromatogr. A* 1129 (2006) 88.
- [17] L. Grönberg, P. Lövkvist, J.Å. Jönsson, *Chemosphere* 24 (1992) 1533.
- [18] P. Hušek, *J. Chromatogr. B* 717 (1998) 57.
- [19] H.G. Uglund, M. Krogh, K.E. Rasmussen, *J. Chromatogr. B* 701 (1997) 29.
- [20] T. Laundh, B. Åkesson, *J. Chromatogr.* 617 (1993) 191.



# Soft modelling for the resolution of highly overlapped voltammetric peaks: application to some Pb-phytochelatin systems

Arístides Alberich, Cristina Ariño\*, José Manuel Díaz-Cruz, Miquel Esteban

*Departament de Química Analítica, Universitat de Barcelona, Martí i Franquès 1-11, E-08028 Barcelona, Spain*

Received 19 December 2005; received in revised form 31 March 2006; accepted 6 April 2006

Available online 26 May 2006

## Abstract

A differential pulse polarographic (DPP) study of the  $Pb^{2+}/Cys-Gly$ ,  $Pb^{2+}/\gamma-Glu-Cys$ ,  $Pb^{2+}/PC_2$  and  $Pb^{2+}/PC_3$  systems is performed, being  $PC_2$  and  $PC_3$  the phytochelatins of general structure  $(\gamma-Glu-Cys)_n-Gly$ , with  $n = 2$  and  $3$ , respectively. Analysis of DPP data is assisted by multivariate curve resolution with alternating least squares (MCR-ALS) method in order to establish the complexes formation sequence and their final stoichiometries. DPP signals of these systems present, besides overlapping of peaks due to free metal ion and metal complexes, interference of mercury anodic signals. Despite these complications, MCR-ALS allows us to propose a model of complexation for each system, and some tentative structures for the complexes.

© 2006 Elsevier B.V. All rights reserved.

**Keywords:** Heavy metals speciation; Lead; Phytochelatins; Voltammetry; Multivariate curve resolution

## 1. Introduction

Heavy metals can cause serious damages – even at very low doses – by replacing essential elements on biological functions. This makes indispensable the heavy metal detoxification of contaminated soils in order to avoid their entry in the trofic chain. Among the methods to remove/immobilize metals, bioremediation (the process of using organisms to restore damaged areas) presents the advantages of being cheap and non-destructive to ecological systems [1].

In response to an excessive uptake of certain heavy metal ions, plants, algae and many fungi can induce the intracellular synthesis of Cys-rich polypeptides [2,3]. These peptides, named phytochelatins ( $PC_n$ ), have the general structure  $(\gamma-Glu-Cys)_n-Gly$ , where  $n$  can be as high as 11, but is generally in the range of 2–5. In the case of mammals, heavy metal regulation is through metallothioneins (MT) that are also proteins with high content in thiol groups.

The synthesis of  $PC_n$  in plants and algae has been widely demonstrated both in laboratory cultures and in field studies, and the recent advances in the understanding of  $PC_n$  biosynthesis and

its function are derived predominantly from molecular genetic approaches using model organisms [3–6]. However, sequence of formation and final stoichiometry of  $PC_n$ -metal complexes is still not totally known. By this reason, it is of great interest to study these complexation processes to understand and optimize phyto remediation.

Voltammetric techniques have proved to be useful for the study of heavy metal complexation by MT [7,8] and  $PC_n$  [9,10] because they allow working at the cellular concentration and because the strong dependence of voltammetric signals on the metal speciation. In fact, differential pulse polarography (DPP) provides signals for the different species of the system: free peptide, free metal ion and metal bound in different chemical environments. The application of multivariate curve resolution with alternating least squares (MCR-ALS) to DPP data allows the characterization of involved systems taking profit of its great capability to resolve highly overlapped signals [11–13]. Such approach has been satisfactorily applied in the study of Cd- $PC_2$  and Cd/Zn- $PC_3$  systems [14,15], of Cd/Zn with  $\alpha$ - and  $\beta$ -MT domain [16] and of Zn-glutathione-fragment systems [17].

In the present paper, the complexation of  $PC_2$ ,  $PC_3$  and two glutathione-fragments with  $Pb^{2+}$  has been considered. Although Scarano and Morelli [9] induced  $PC_n$  formation in algae and studied their metal complexes (including lead) by DPP or by combination of size-exclusion chromatography with off-line

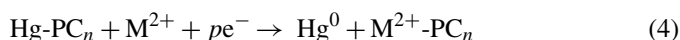
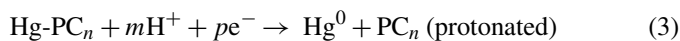
\* Corresponding author. Tel.: +34 93 402 15 45; fax: +34 93 402 12 33.  
E-mail address: [cristina@apolo.qui.ub.es](mailto:cristina@apolo.qui.ub.es) (C. Ariño).

detection of PC by HPLC, and metal ion by atomic absorption spectrometry [18], to the best of our knowledge,  $\text{Pb}^{2+}$  has been not systematically studied in the presence of  $\text{PC}_n$  until now.

In a previous work [19], the complexation of  $\text{Pb}^{2+}$  by glutathione was investigated, obtaining satisfactory results but remarking the experimental and data treatment difficulties due to the interference of the anodic signals of mercury. These signals come from the formation of mercurous thiolate of the pure ligands. Thus, for instance, a cysteine mercurous thiolate  $\text{Hg}_2(\text{SR})_2$  is formed when the potential previous to the DPP pulse is sufficiently positive to produce mercury oxidation [20], what is favored by the presence of a complexing medium:



In a similar way, other mercury thiolates [21–23] can be formed and then, when a reducing potential pulse is applied, two kinds of processes can take place:



coming out the free ligand and the complex signal that are related to the anodic processes. The potentials of these anodic signals depend on the Hg-ligand bond and on the ligand equilibria, but they appear in the  $\text{Pb}^{2+}$  reduction region, thus yielding overlapping signals and hindering the resolution of the systems. Then, from a methodological point of view the resolution of these systems has great interest as examples of particularly complicated cases.

## 2. Experimental

### 2.1. Chemicals and instrumentations

Cys-Gly and  $\gamma$ -Glu-Cys were provided by Sigma with a purity of 85%  $\text{PC}_2$  and  $\text{PC}_3$  by Diver Drugs with a purity of 91.8 and 91.4%, respectively. All other reagents used were Merck analytical grade.  $\text{Pb}^{2+}$  stock solutions were prepared by dissolving  $\text{Pb}(\text{NO}_3)_2$  in water and standardized complexometrically [24].  $0.01 \text{ mol L}^{-1}$  maleic acid/maleate buffer solutions were used for pH regulation and ionic strength control. Maleate forms weak and labile  $\text{Pb}^{2+}$ -complexes [25] that can be easily considered as side reactions using the formalism of conditional stability constants. All solutions were prepared in ultrapure filtered water (Milli-Q plus 185, Millipore).

Differential pulse polarography (DPP) measurements were performed in an Autolab system PGSTAT20 (EcoChemie, The Netherlands) attached to a Metrohm 663 VA stand (Metrohm, Switzerland) and a PC with GPES4 software (EcoChemie). An Orion SA 720 pH-meter was used for pH-monitoring during the experiments. All measurements were carried out in a glass cell at room temperature ( $20^\circ\text{C}$ ) under a purified nitrogen atmosphere (SEO N50). Working, reference and auxiliary electrodes were a static mercury drop electrode (SMDE, drop area of  $0.5 \text{ mm}^2$ ), an  $\text{Ag}|\text{AgCl}|3 \text{ mol L}^{-1} \text{ KCl}$  reference electrode and a glassy carbon

electrode, respectively. Pulse time of 50 ms, pulse amplitude of 50 mV, drop time of 0.8 s and potential step of 4 mV were used.

### 2.2. Procedure

In titrations of peptide with  $\text{Pb}^{2+}$ , 20 mL of  $2 \times 10^{-5} \text{ mol L}^{-1}$  peptide solution in maleic/maleate buffer (pH 6.8) are placed into the cell and purged with nitrogen during 40 min. Then, a DPP curve is recorded. After that, aliquots of a  $5 \times 10^{-4} \text{ mol L}^{-1}$   $\text{Pb}^{2+}$  solution are added and DPP curves recorded. Between additions, solutions are purged and mechanically stirred for 1.5 min. Titrations are also performed in the opposite way: 20 mL of  $1 \times 10^{-5} \text{ mol L}^{-1}$   $\text{Pb}^{2+}$  solution are placed into the cell and, after deaeration and measurement, aliquots of  $2.5 \times 10^{-4} \text{ mol L}^{-1}$  peptide are done, and the corresponding DPP curves recorded.

## 3. Data treatment

Voltammograms are smoothed, baseline-corrected, and converted into data matrices by means of some homemade programs implemented in Matlab [26]. When a non-negligible volume of titrant solution is added, data are also corrected for dilution. Multivariate curve resolution with alternating least squares (MCR-ALS) analysis of data is done by several homemade Matlab programs available at: <http://www.ub.es/gesq/mcr/mcr.htm>.

The main object of MCR-ALS and its different steps have been described elsewhere [11–16,27]. However, it is important to remark for further discussions that in the frame of MCR-ALS application to electrochemical data, the concept of “component” must not be interpreted as a chemical species, as it happens with spectroscopic data, but to an electrochemical process giving a signal (including physical phenomena like, for instance, electroic adsorption of a species [14]).

Relevant constrains used here in MCR-ALS treatment are: selectivity, non-negativity and signal shape (to describe the expected peak-shaped signal by a proper parametric equation [12]). The chemical equilibrium constrains for successive, mononuclear and electroactive complexes is also considered in some cases in the present work. This approach consists of fitting a set of complexation constants  $\beta_1 \cdot \dots \cdot \beta_n$  to the concentration profiles obtained at every ALS iteration. This requires the assumption of a complexation model, i.e., the number and stoichiometry of metal complexes and some initial estimates of the stability constants [28]. The constrain is based on the combination of mass balances and equilibrium constants to yield the polynomial equation:

$$\begin{aligned} &[\text{L}]^{n+1} \beta_n + [\text{L}]^n \{ \beta_n (n c_{\text{TM}} - c_{\text{TL}}) + \beta_{n-1} \} \\ &+ [\text{L}]^{n-1} \{ \beta_{n-1} ((n-1) c_{\text{TM}} - c_{\text{TL}}) + \beta_{n-2} \} \\ &+ \dots - c_{\text{TL}} = 0 \end{aligned} \quad (5)$$

where  $\beta_0 = 1$  and  $c_{\text{TM}}$  and  $c_{\text{TL}}$  are the total concentrations of metal and ligand, respectively. Using the command *roots* of Matlab it is possible to find a numerical solution for the free ligand concentration  $[\text{L}]$ , which, for a set of  $c_{\text{TM}}$  and  $c_{\text{TL}}$  values,

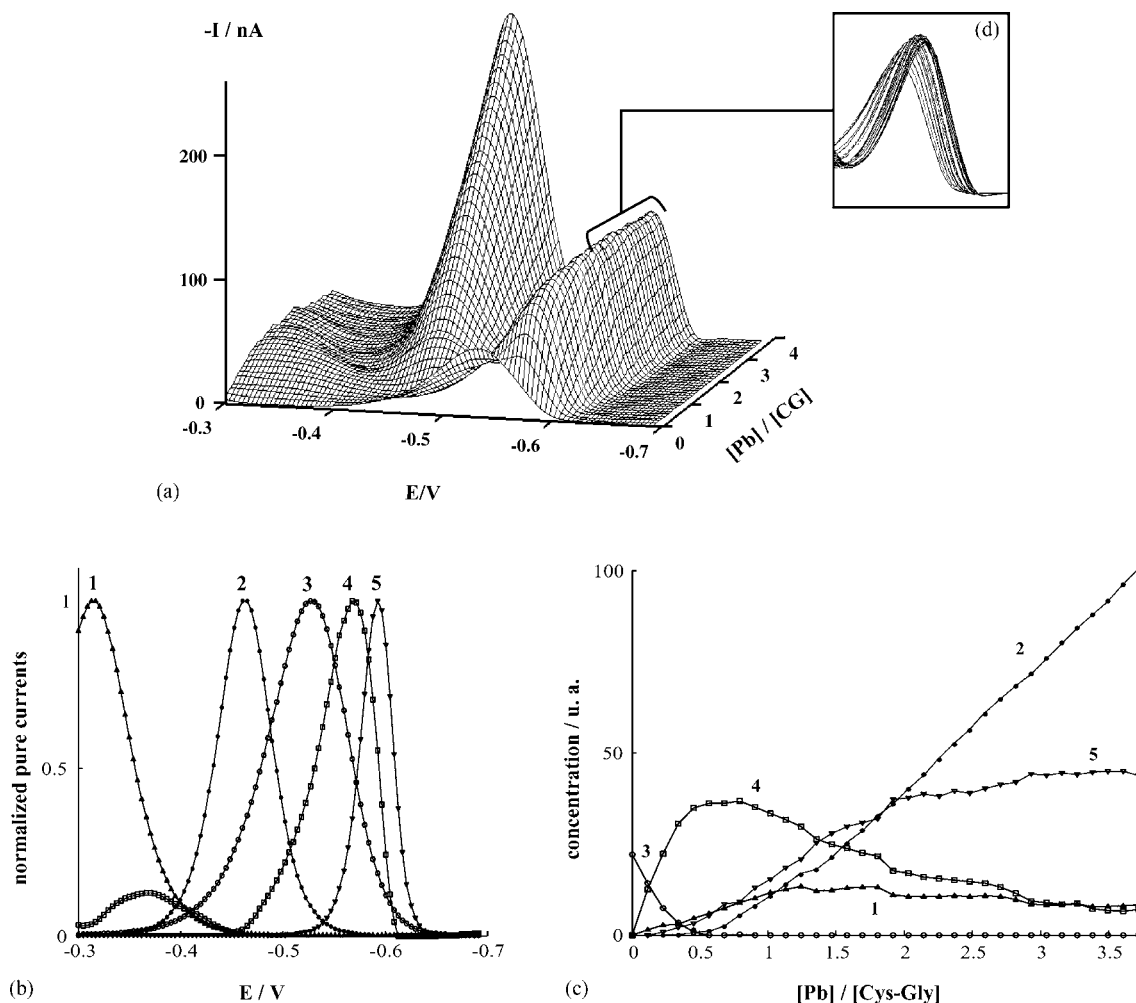


Fig. 1. Current data matrix obtained in the DPP titration of  $2 \times 10^{-5} \text{ mol L}^{-1}$  Cys-Gly with  $\text{Pb}^{2+}$  at pH 6.8 (a), the corresponding normalized unitary voltammograms (b) and concentration profiles (c) obtained in the MCR-ALS analysis of the data, and detail of a part of the matrix (d).

allows one to obtain the equilibrium concentration of all metal species from  $\beta_1 \cdots \beta_n$  (*betacalc* program) and vice versa (*betafit* program).

Once the ALS decomposition has been performed, the resulting matrices must be analyzed: matrix  $\mathbf{V}^T$  gives normalized individual voltammograms for each component (process), while matrix  $\mathbf{C}$  gives their concentration profiles. When the equilibrium constrain is applied, besides the optimized  $\mathbf{C}$  and  $\mathbf{V}^T$  matrices, an optimized set of complexation constants is obtained. The analysis of this information allows us to obtain the possible stoichiometries (provided by the metal–ligand ratios where species appear, disappear or stabilize), some suggestions about the relative stability of metal bindings and, as a consequence, of the complexes (the more negative is the peak potential, the more stable are the bindings of the complex), and, in some cases, some indications about reversibility or presence of adsorption phenomena. The relative error of  $\mathbf{I}$  matrix decomposition is expressed as a percentage of lack of fit (lof).

In the following the components described from MCR-ALS analysis are numbered according to their situation on the potential axis.

## 4. Results and discussion

### 4.1. $\text{Pb}^{2+}$ /Cys-Gly system

Fig. 1a shows the evolution of the DPP curves recorded in the titration of Cys-Gly with  $\text{Pb}^{2+}$ . Singular value decomposition (SVD) of the data matrix suggests the existence of at least four components (results not shown). However SVD does not provide conclusive information but guidance for further steps in MCR-ALS since different electrochemical processes behaving in a similar way could be not resolved by SVD and thus considered as a single component [12]. This can be the present case, where the reduction processes of  $\text{Pb}^{2+}$ -complexes are associated to several anodic processes due to Hg electrode (see further). As discussed later, the application of constrains in MCR-ALS (especially signal-shape), allows one to resolve some of these ambiguities.

The best MCR-ALS results (lof=5.7%) were obtained assuming five components, and applying constrains of non-negativity for both concentrations and signals, selectivity at the beginning of the titration and signal-shape for the voltammo-

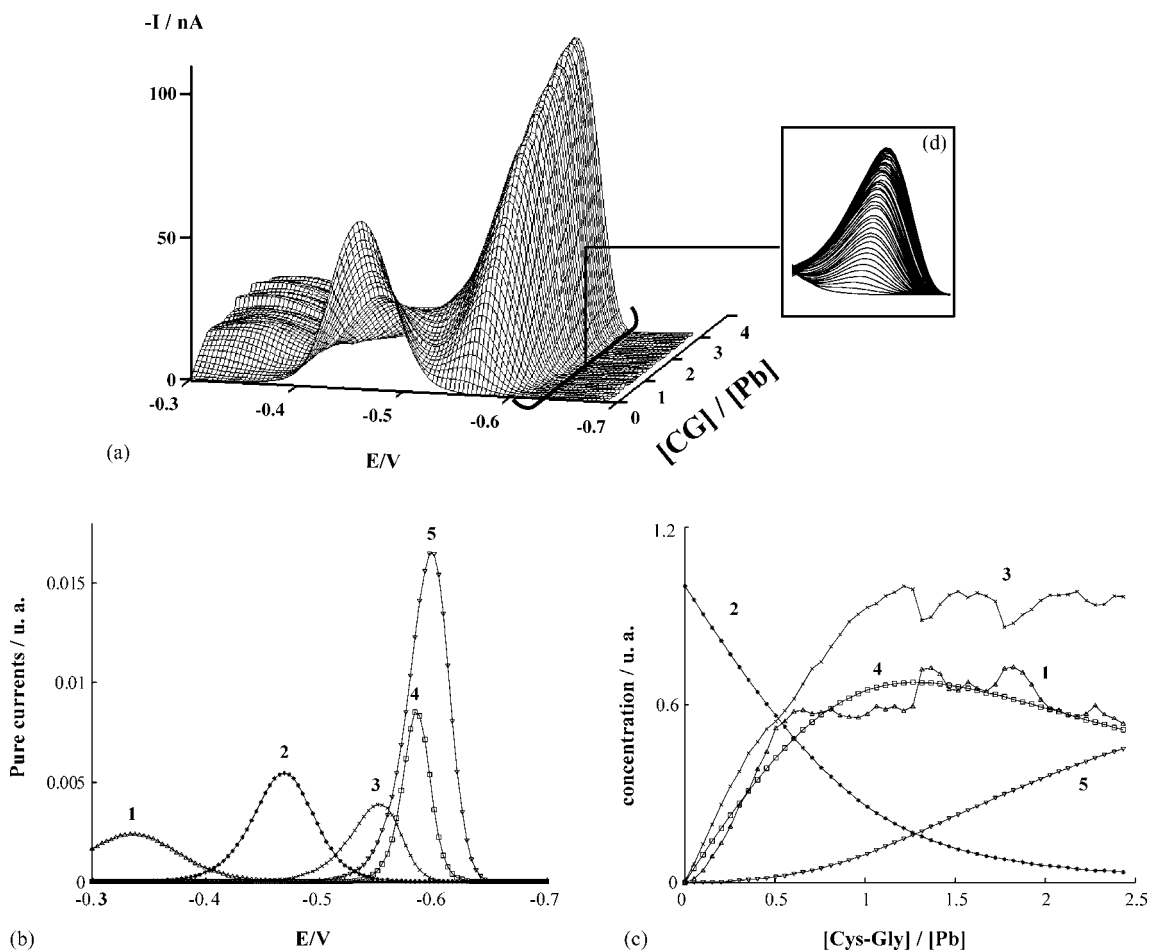


Fig. 2. Current data matrix obtained in the DPP titration of  $1 \times 10^{-5} \text{ mol L}^{-1} \text{ Pb}^{2+}$  with Cys-Gly at pH 6.8 (a), the corresponding unitary voltammograms (b) and concentration profiles (c) obtained in the MCR-ALS analysis of the data, and detail of a part of the matrix (d).

grams of all components except component 4 because, as it can be observed, component 4 shows a peak at ca.  $-0.60 \text{ V}$  and a second minor peak at ca.  $-0.35 \text{ V}$ . In Fig. 1b, component 2 is clearly associated to the reduction of free  $\text{Pb}^{2+}$ , whereas component 3 represents the electrode process of Cys-Gly, i.e., the reduction of the Hg-Cys-Gly complexes formed on the Hg electrode surface, as observed previously [17]. The rest of components are related to the reduction of  $\text{Pb}^{2+}$  bound to Cys-Gly in different ways.

From concentration profiles in Fig. 1c, it can be deduced that component 4 is related to the reduction of a 1:2  $\text{Pb}^{2+}$ :Cys-Gly complex since it reaches a maximum at a ratio close to 0.5, then stabilizes and at ratios greater than 1 begins to decrease. Component 1 shows a qualitatively analogous behavior to component 4; this feature, added to the fact that its peak potential is pH-independent (experiments not shown) and less negative than the reduction potential of free  $\text{Pb}^{2+}$ , suggests that component 1 is related to anodic Hg processes where the Pb complexes are involved [17]. Such processes can be very intricate and sometimes cannot be explained with a single component. In the present case, most of the evolution of the signal is explained with component 1 and it seems that the lower peak of component 4 explains the additional variations of the anodic signal that are produced as the 1:2  $\text{Pb}^{2+}$ :Cys-Gly complex is formed. It must be noted that the use of two components to explain the anodic signal

produced poorer results than the ones here described. The previous assignments of components 2 and 3 to free  $\text{Pb}^{2+}$  and Cys-Gly, respectively, are consistent with the stoichiometry proposed for the complex (component 4) because Cys-Gly disappears at the  $\text{Pb}^{2+}$ :Cys-Gly ratio of 0.5 and then free  $\text{Pb}^{2+}$  appears. The proposal of a fifth component has been necessary to justify the shift of the signal at more negative potentials once it reaches a maximum of intensity (Fig. 1d), and to achieve satisfactory results. This kind of potential shift means a serious problem in the MCR-ALS analysis of voltammetric data because it can be caused by some phenomena (equilibria among different species, loss of reversibility, presence of electrodic adsorption) that generate a loss of linearity on the measured current. The achievement of linearity (required by MCR-ALS) is reflected in voltammetry by a fix potential peak for each electrochemical process. The overall evolution of the concentration profiles of components 4 and 5 is not conclusive and the reverse titration must be considered.

In the titration of  $\text{Pb}^{2+}$  with Cys-Gly (Fig. 2), a first MCR-ALS analysis shows two components (numbers 4 and 5) related to two different complexes, two components associated to anodic Hg processes (components 1 and 3) and the component due to the reduction of free  $\text{Pb}^{2+}$  (component 2). The hypothesis of formation of two complexes (probably with 1:1 and 1:2  $\text{Pb}^{2+}$ :Cys-Gly stoichiometries) is held by the picture of the zone where the

Table 1  
Tentative structures for the proposed complexes of the studied  $Pb^{2+}$ -peptide systems

System	Complexes	Models
Pb-Cys-Gly	ML	
	$ML_2$	
Pb-PC2	ML	
	$M_2L$	
Pb-PC3	ML	
	$M_2L$	

Black balls correspond to thiol groups and grey balls to  $Pb(II)$ .

complexes appear (Fig. 2d), showing the progressive shift of the peak towards more negative potentials since the beginning of the titration, just the opposite to the previous titration. In order to verify this hypothesis, the equilibrium constrain was applied to components 2, 4 and 5 (related to free  $Pb^{2+}$ , 1:1 and 1:2 complexes, respectively) in a new MCR-ALS analysis of the data matrix from the titration of  $Pb^{2+}$  with Cys-Gly. The fitting was quite satisfactory (lof = 9.7%) providing the stability constant values of  $\log \beta_1 = 6.10 \pm 0.02$  and  $\log \beta_2 = 11.19 \pm 0.03$  for the 1:1 and 1:2 complexes, respectively, and both the unitary voltammograms and concentration profiles (Fig. 2). In Fig. 2c it can be seen that the components 2, 4 and 5, related to the species involved in the equilibrium constraint, present smoothed concentration profiles, in the same way as the unit voltammograms constrained to signal shape, whereas the concentration profiles not restricted to the equilibrium constraint (components 1 and 3) accumulate more noise than in previous cases (e.g. Fig. 1c). The goodness of these results confirms the formation of two successive complexes with the tentative structures proposed in Table 1.

#### 4.2. $Pb^{2+}/\gamma$ -Glu-Cys system

The data matrices obtained in the DPP titrations of  $\gamma$ -Glu-Cys with  $Pb^{2+}$  and vice versa are qualitatively comparable to those of

the  $Pb^{2+}$ -Cys-Gly system (Figs. 1a and 2a, respectively), but with the signals due to the anodic Hg processes more strongly overlapped to the signals associated to the reduction of both free and complexed  $Pb^{2+}$ . After several analyses of these data by MCR-ALS, satisfactory results and conclusions were not achieved. However, it seems that, as in the previous system, a 1:2 complex predominates in the titration with  $Pb^{2+}$  (results not shown). No useful information can be drawn from the titration with peptide.

#### 4.3. $Pb^{2+}/PC_3$ system

Because of some additional complications on the  $Pb^{2+}/PC_2$  system as respect to  $Pb^{2+}/PC_3$ , systematic study of  $Pb^{2+}/PC_3$  is firstly described.

The SVD analysis from the data matrix of the titration of  $PC_3$  with  $Pb^{2+}$  (Fig. 3a) suggests the existence of five components. In MCR-ALS analysis, constrains of non-negativity for both concentrations and signals, selectivity for  $PC_3$  at the beginning of the titration and for all those species whose concentrations become zero along the titration and, finally, signal shape for the voltammograms of all species out of component 5 are applied. The reasons for not applying signal shape constrain to component 5 are essentially the same as in the case of component 4 in Pb/Cys-Gly system. Figs. 3b and c summarize the most satisfactory MCR-ALS results achieved (lof = 7.4%).

Component 4 is clearly associated with  $PC_3$  because it is the only that appears before the addition of  $Pb^{2+}$ . The electrochemical process behind this signal is probably the reduction of the Hg- $PC_3$  complex formed due to the previous oxidation of Hg in the presence of  $PC_3$ , as it happens with many sulfur compounds [23]. Free  $PC_3$  disappears at a  $Pb^{2+}$ -to- $PC_3$  ratio close to 1.0. This value is determined from the projection of the initial profile of component 4.

Component 2 is undoubtedly due to the reduction of the free  $Pb^{2+}$  because of its location (Fig. 3b). Moreover, at ratios higher than 2, the added  $Pb^{2+}$  remains free and its concentration increases linearly (Fig. 3c).

Components 3 and 5 seem to correspond to the reduction of  $Pb^{2+}$  bound to  $PC_3$  in different manners. An explanation of the complexation sequence could be as follows: when  $Pb^{2+}$  is added to  $PC_3$ , and until a  $Pb^{2+}$ -to- $PC_3$  ratio of 1.0, a very stable 1:1 complex, with  $Pb^{2+}$  very strongly bound to two thiols of the same  $PC_3$  molecule, is formed (related to component 5). As more  $Pb^{2+}$  is added, the concentration of this 1:1 complex remains constant but another two components appear until  $Pb^{2+}$ -to- $PC_3$  ratios slightly higher than 2. Component 3 seems to be related to the reduction of other  $Pb^{2+}$  bound at quite less negative potential than the other. Thus, the final compound is a 2:1  $Pb^{2+}$ : $PC_3$  complex, and component 3 may be the reduction of the  $Pb^{2+}$  bound to the sulfur atom that remains free in  $PC_3$  after the binding of the first  $Pb^{2+}$ . This description takes into account the evolution of concentration profiles, and the  $Pb^{2+}$ -to- $PC_3$  ratios where components appear, disappear or stabilize. Table 1 shows the proposed tentative structures of these complexes.

As mentioned previously for peptidic fragments, and due to the location of its normalized unitary voltammogram (Fig. 3b),



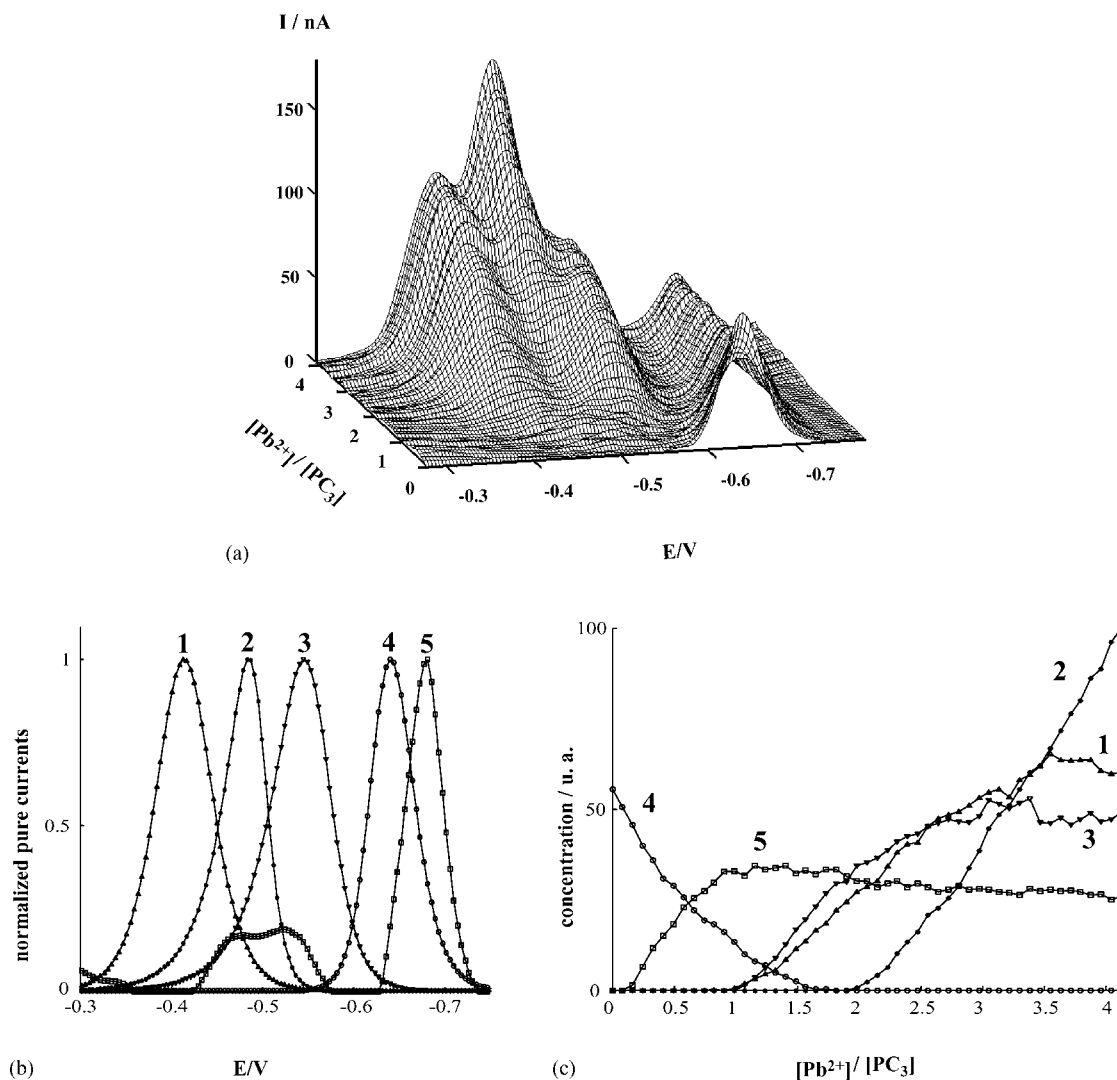


Fig. 3. Current data matrix obtained in the DPP titration of  $2 \times 10^{-5} \text{ mol L}^{-1}$   $(\gamma\text{-Glu-Cys})_3\text{Gly}$  ( $PC_3$ ) with  $Pb^{2+}$  at pH 6.8 (a), and the corresponding normalized unitary voltammograms (b) and concentration profiles (c) obtained in the MCR-ALS analysis of the data.

component 1 may be the anodic signal associated to component 3 because they evolve in parallel (Fig. 3c).

Stabilisation of components 3 and 1 occurs at ratios higher than 2 (Fig. 3c). This is probably due to the adsorption of the complex onto Hg electrode, increasing the signal currents, and consequently, the concentrations profiles.

Concerning the titration of  $Pb^{2+}$  with  $PC_3$  (Fig. 4a), the large background of the data matrix associated to anodic processes is the predominant feature. SVD cannot yield reliable results due to the deficiency of rank of the data, i.e., the number of components that may be linearly interdependent in their contributions to the total current is high. Thus, components 1 and 2 are related to the anodic processes associated with the appearance of free  $PC_3$  (component 4) and of a complex (component 5), respectively. Finally, component 3 corresponds to the reduction of free  $Pb^{2+}$ . Despite the species distribution (Fig. 4c), when MCR-ALS is applied without the signal shape constrain (Fig. 4b), the normalized unitary voltammogram of the complex includes two minor anodic signals. Although this profusion of anodic signals means a limitation in the estimation of stoichiometries, from concen-

trations profiles diagram (Fig. 4c) a 1:1 complex seems to be formed. The greatest ambiguity is in the stoichiometry of the complex because of the almost total overlapping with the signal due to free  $PC_3$  (component 4). It appears from that diagram that the  $M_2L$  complex is not formed, as we expected, even at the beginning of the titration, when the excess of free  $Pb^{2+}$  is high. This fact probably responds to the preference of  $Pb^{2+}$  to be strongly bound by two sulfur groups of the same  $PC_3$ . In spite of all these considerations, the error associated to the MCR-ALS decomposition is considerably low (lof = 5.3%).

#### 4.4. $Pb^{2+}/PC_2$ system

The comparison of matrices for the  $Pb^{2+}/PC_3$  system with these of  $PC_2$  shows similar evolutions. So, in MCR-ALS analysis of data from the titration of  $PC_2$  with  $Pb^{2+}$  (Fig. 5), the number of components considered and constrains applied have been the same than for  $PC_3$  system. The best results (lof = 9.9%) yield the normalized unitary voltammograms and the concentration profiles of Figs. 5b and c.



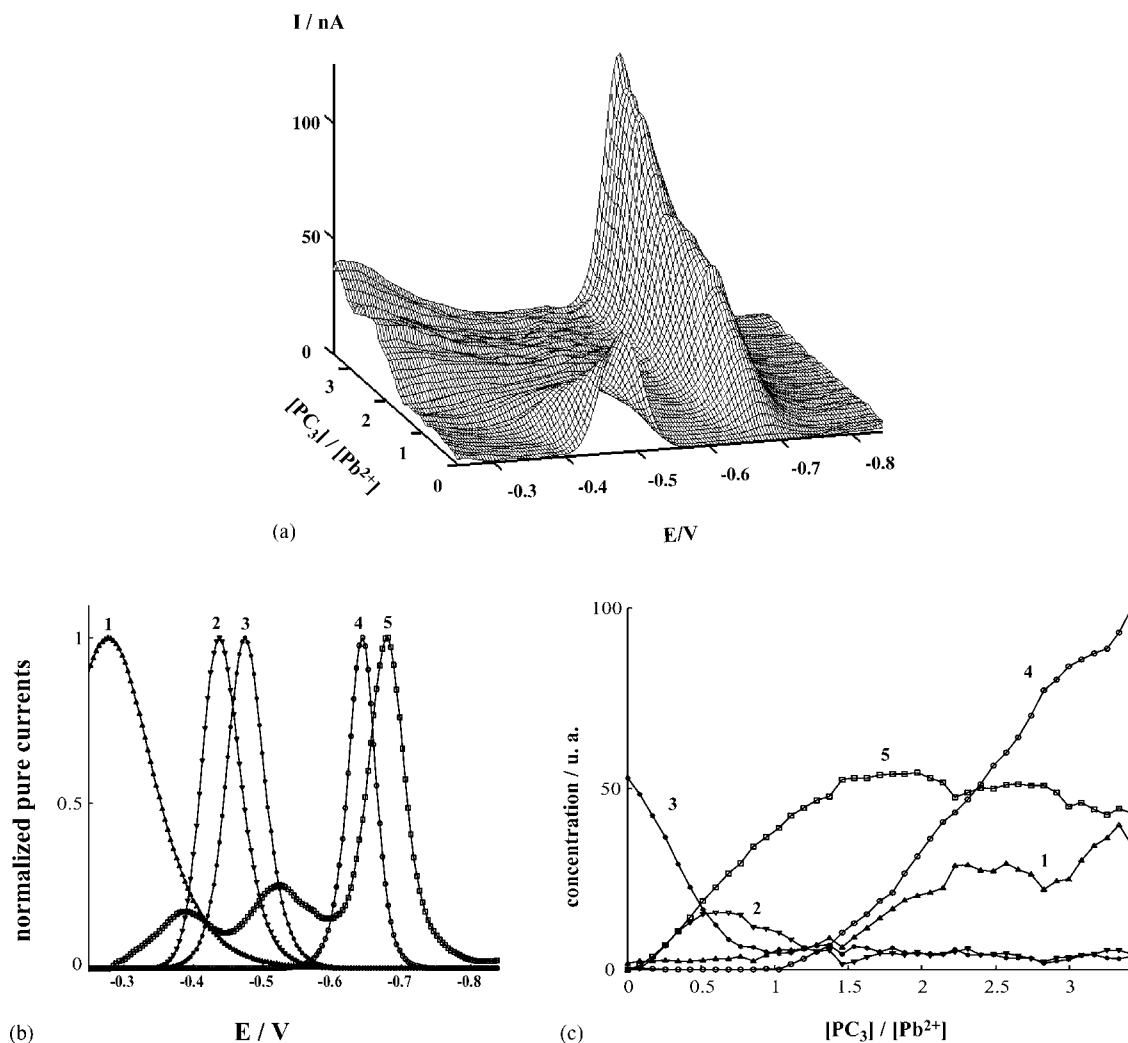


Fig. 4. Current data matrix obtained in the DPP titration of  $1 \times 10^{-5} \text{ mol L}^{-1} \text{ Pb}^{2+}$  with  $(\gamma\text{-Glu-Cys})_3\text{Gly}$  ( $\text{PC}_3$ ) at pH 6.8 (a), and the corresponding normalized unitary voltammograms (b) and concentration profiles (c) obtained in the MCR-ALS analysis of the data.

From MCR-ALS analysis, component 4 is due to the reduction of free  $\text{PC}_2$  (the only species at the beginning of the titration) and component 2 to the reduction of free  $\text{Pb}^{2+}$ . In agreement with  $\text{Pb}^{2+}/\text{PC}_3$  system, components 3 and 5 seem to correspond to the reduction of  $\text{Pb}^{2+}$  bound to one and two sulfur groups of  $\text{PC}_2$ , respectively. Finally, component 1 should correspond to the anodic signal associated to component 3.

Nevertheless, in this system some problems make more difficult to extract a complexation picture from this experiment. At first, occurrence of the second complex (related to component 3) is quite lower, and it comes out from a zone where anodic signals associated to the first complex are significant. This, together with the overlapping of components 4 and 5, hinders the good resolution of characteristic M:L ratios to deduce when the different species appear, disappear or stabilize. At second, when the signal associated to the first complex (component 5) reaches a quasi-plateau, a progressive potential shift to more negative values takes place, as in the  $\text{Pb}^{2+}/\text{Cys-Gly}$  system, but in minor extension. Then, if two different components are considered for this unique signal, the concentration profile of the first complex would be too affected; but, if we consider only one component

for this signal (component 5), its concentration profile does not stabilize until a M:L ratio much higher than the real one.

Despite these considerations, a tentative complexation process can be formulated by comparison with the  $\text{Pb}^{2+}/\text{PC}_3$  system. When  $\text{Pb}^{2+}$  is added to  $\text{PC}_2$ , a very stable 1:1 complex (related to component 5) is formed until a M:L ratio of ca. 1.0 (Fig. 5c), where free  $\text{PC}_2$  decreases significantly (component 4). For such a deduction, a projection of the initial profile must be observed at a ratio of ca. 1. Deviations from that projection are because of the strong overlapping of the signals. As in  $\text{Pb}^{2+}/\text{PC}_3$ ,  $\text{Pb}^{2+}$  is bound to two thiol groups of the same  $\text{PC}_2$  molecule. When more  $\text{Pb}^{2+}$  is added, new components 1 and 3 (with small concentration profiles) appear. Component 3 seems to correspond to the reduction of a  $\text{Pb}^{2+}$  bound to only one thiol group (as its potential at quite less negative value than for component 5 indicates) and component 1 to its anodic process. Since free  $\text{Pb}^{2+}$  (component 2) does not appear until a ratio of ca. 1.2 (determined from the extrapolation of final part of its concentration profile) and free  $\text{PC}_2$  is absent, a small fraction of 1:1  $\text{Pb}^{2+}/\text{PC}_2$  complex could liberate one thiol group to allow the entrance of a new  $\text{Pb}^{2+}$  in the structure (Table 1). The calculated concentra-

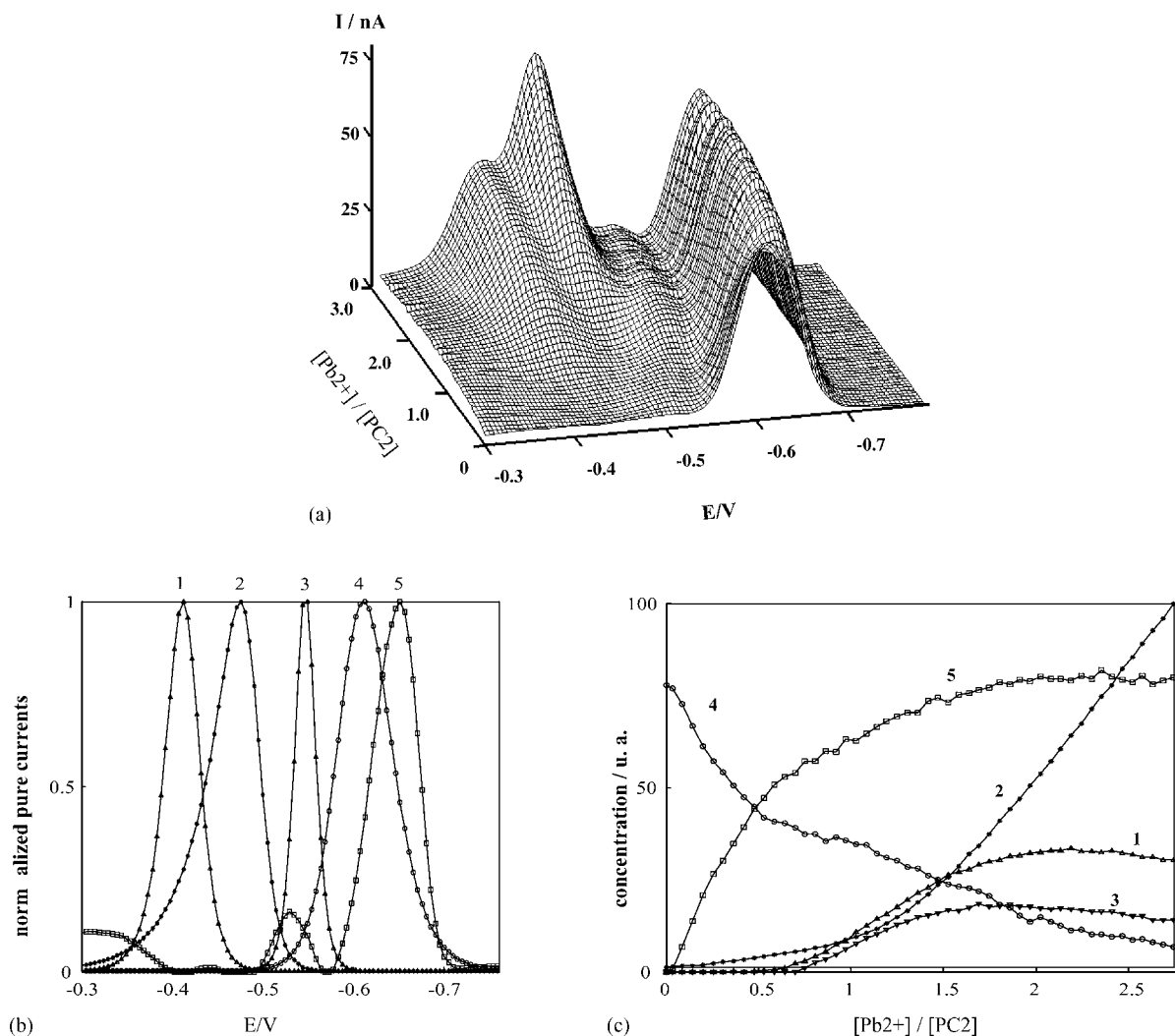


Fig. 5. Current data matrix obtained in the DPP titration of  $2 \times 10^{-5} \text{ mol L}^{-1}$  ( $\gamma$ -Glu-Cys) $_2$ Gly ( $PC_2$ ) with  $Pb^{2+}$  at pH 6.8 (a), and the corresponding normalized unitary voltammograms (b) and concentration profiles (c) obtained in the MCR-ALS analysis of the data.

tion profile of the first (1:1) complex (related to component 5) does not fall due to the signal shift mentioned before, and the resulting ambiguity created in the MCR-ALS analysis. At the end of the experiment, at M:L ratios of 1.5 or higher, it can be concluded that the most important fraction of  $PC_2$  is strongly bound by one Pb atom forming a ML complex, and the rest of  $PC_2$  fraction is more weakly bound by two Pb atoms, forming a  $M_2L$  complex.

The titration of  $PC_2$  with  $Pb^{2+}$  gives similar data than that for  $PC_3$  (Fig. 4a) but, in this case, two highly overlapped anodic signals can be seen at both sides of free  $Pb^{2+}$  signal. These features cause a high ambiguity in MCR-ALS results, thus being impossible to precise a concentration profile for free  $Pb^{2+}$  and, therefore, an acceptable complexation sequence.

## 5. Conclusions

The combined use of DPP and MCR-ALS allows us to detect the presence of differently bound Pb(II) providing information to propose complexation models between lead and different Cys-containing peptides. From the analysis of the concentra-

tion profiles and taking into account the relative position of the DPP peaks, tentative structures for  $Pb^{2+}/\text{Cys-Gly}$ ,  $Pb^{2+}/PC_2$  and  $Pb^{2+}/PC_3$  systems are proposed (Table 1). The results are very satisfactory because of the additional problem due to the interference from the anodic mercury signals in the presence of those ligands that overlap with the peaks of the free metal ion and the metal complexes. Only the  $Pb^{2+}/\gamma$ -Glu-Cys system could not be satisfactorily resolved.

Thus, the valuable information obtained in this study (although requiring further confirmation by structural techniques) suggests that the methodology used can play a key role in the study of metal binding by  $PC_n$ .

## Acknowledgements

The authors gratefully acknowledge financial support from the Spanish Ministerio de Ciencia y Tecnología (Project BQU2003-07587-CO2-01), and thank the Generalitat of Catalonia (Project 2005SGR-00186). Aristides Alberich thanks the Spanish Ministerio de Ciencia y Tecnología for a Ph.D. grant.

## References

- [1] B. Suresh, G. Ravishankar, *Crit. Rev. Biotechnol.* 24 (2004) 97.
- [2] W.E. Rauser, *Cell Biochem. Biophys.* 31 (1999) 19.
- [3] M.H. Zenk, *Gene* 179 (1996) 21.
- [4] C.S. Cobbett, *Plant Physiol. Biochem.* 123 (2000) 825.
- [5] J.A. de Knecht, N. van Baren, W.M. Ten Bookum, F.S. Wong, W. Harro, P.L.M. Koevots, H. Schat, J.A.C. Verkleij, *Plant Sci.* 106 (1995) 9.
- [6] J.F. Souza, W.E. Rauser, *Plant Sci.* 165 (2003) 1009.
- [7] M. Dabrio, A.R. Rodríguez, G. Bordin, M.J. Bebianno, M. De Ley, I. Sestáková, M. Vasak, M. Nordberg, *J. Inorg. Biochem.* 88 (2002) 123.
- [8] G. Bordin, Guest Ed., *Mol. Cell. Biol.* 46 (2000) (special issue on Metallothioneins).
- [9] G. Scarano, E. Morelli, *Electroanalysis* 10 (1998) 39.
- [10] I. Sestáková, H. Vodickova, P. Mader, *Electroanalysis* 10 (1998) 764.
- [11] J.M. Díaz-Cruz, R. Tauler, B.S. Grabaric, M. Esteban, E. Casassas, *J. Electroanal. Chem.* 393 (1995) 7.
- [12] M. Esteban, C. Ariño, J.M. Díaz-Cruz, M.S. Díaz-Cruz, R. Tauler, *Trends Anal. Chem.* 19 (2000) 49 (and references therein).
- [13] M. Esteban, C. Ariño, J.M. Díaz-Cruz, *Trends Anal. Chem.* 25 (2006) 86.
- [14] B.H. Cruz, J.M. Díaz-Cruz, I. Sestáková, J. Velek, C. Ariño, M. Esteban, *J. Electroanal. Chem.* 520 (2002) 111.
- [15] B.H. Cruz, J.M. Díaz-Cruz, C. Ariño, M. Esteban, *Environ. Sci. Technol.* 39 (2005) 778.
- [16] M.J. López, C. Ariño, M.S. Díaz-Cruz, J.M. Díaz-Cruz, R. Tauler, M. Esteban, *Environ. Sci. Technol.* 37 (2003) 5609.
- [17] B.H. Cruz, J.M. Díaz-Cruz, C. Ariño, M. Esteban, *Electroanalysis* 15 (2003) 1177.
- [18] G. Scarano, E. Morelli, *Biometals* 15 (2002) 145.
- [19] B.H. Cruz, J.M. Díaz-Cruz, M.S. Díaz-Cruz, C. Ariño, M. Esteban, R. Tauler, *J. Electroanal. Chem.* 516 (2001) 110.
- [20] M. Heyrovsky, P. Mader, V. Veselá, M. Fedurco, *J. Electroanal. Chem.* 369 (1994) 53.
- [21] W. Stricks, I.M. Kolthoff, *J. Am. Chem. Soc.* 74 (1952) 4646.
- [22] R.A.F. Bullerwell, *J. Polarogr. Soc.* 9 (1963) 7.
- [23] J.M. Séquaris, *Comp. Anal. Chem.* 27 (1992) 115.
- [24] A.I. Vogel, *Textbook of Quantitative Chemical Analysis*, fifth ed., Longman, London, 1989.
- [25] F. Berbel, J.M. Díaz-Cruz, C. Ariño, M. Esteban, *J. Electroanal. Chem.* 432 (1997) 243.
- [26] The Matlab Version 5.3. R. 11, Mathworks Inc., Cochituate Place, MA.
- [27] R. Tauler, B. Kowalski, *J. Chemom.* 9 (1995) 31.
- [28] J.M. Díaz-Cruz, J. Agulló, M.S. Díaz-Cruz, C. Ariño, M. Esteban, R. Tauler, *Analyst* 126 (2001) 371.

## A permeation liquid membrane system for determination of nickel in seawater

A. Aouarram<sup>a</sup>, M.D. Galindo-Riaño<sup>a,\*</sup>, M. García-Vargas<sup>a</sup>,  
M. Stitou<sup>b</sup>, F. El Yousfi<sup>b</sup>

<sup>a</sup> Department of Analytical Chemistry, Faculty of Science, University of Cádiz, Campus Río San Pedro, 11510 Puerto Real, Cádiz, Spain

<sup>b</sup> Département de Chimie, Faculté des Sciences, Université Abdelmalek Essaadi, B.P. 2121 M'hannech II, 93 002 Tétouan, Morocco

Received 9 November 2005; received in revised form 27 February 2006; accepted 20 March 2006

Available online 2 May 2006

### Abstract

The use of a permeation liquid membrane system for the preconcentration and separation of nickel in natural and sea waters and subsequent determination by atomic absorption spectroscopy is presented. 2-Hydroxybenzaldehyde *N*-ethylthiosemi-carbazone (2-HBET) in toluene is used as the active component of the liquid membrane. A study strategy based on a simplex design has been followed. Several chemical and physical parameters were optimized. Maximum permeation coefficient was obtained at a feed solution pH of 9.4, 0.3 mol l<sup>-1</sup> of HNO<sub>3</sub> in the stripping solution and 1.66 mmol l<sup>-1</sup> of 2-HBTE in toluene as carrier. The precision of the method was 4.7% at 95% significance level and a detection limit of 0.012 μg l<sup>-1</sup> of nickel was achieved. The preconcentration procedure showed a linear response within the studied concentration range from 3 to 500 μg l<sup>-1</sup> of Ni in the feed solution. The method was validated with different spiked synthetic seawater and certified reference water samples: TMDA-62 and LGC 6016, without matrix interferences and showing good concordance with the certified values, being the relative errors -5.9% and -2.2%, respectively. Under optimal conditions, the average preconcentration yield for real seawater samples was 98 ± 5%, with a nickel preconcentration factor of 20.83 and metal concentrations ranging between 2.8 and 5.4 μg l<sup>-1</sup>.

© 2006 Elsevier B.V. All rights reserved.

**Keywords:** Bulk liquid membrane; Extraction–reextraction process; Seawater; Determination of nickel; 2-Hydroxybenzaldehyde *N*-ethylthiosemicarbazone

### 1. Introduction

Many heavy metals are toxic and cause environmental damage, such as nickel. This metal is released into the aquatic environment from dissolution of rocks and soil, atmospheric fallout and biological cycles. Also, the high consumption of nickel products in industrial activities and sewage waste-waters inevitably leads to environmental pollution.

Nickel is an essential metal to plants and some animals, being a component of the enzyme urease and of five other important enzymes [1]. It is moderately toxic element but can cause allergic reactions and certain nickel compounds are carcinogenic [2].

Natural water contains low concentration levels (0.5–1.5 μg l<sup>-1</sup>), being background level of 0.3 μg l<sup>-1</sup> in river

water [3] and 0.7 μg l<sup>-1</sup> in surface seawater [4]; but those are increased owing to pollution of water (i.e. nickel concentration in Mersey Estuary (UK) ranged from about 0.59 to 13.5 μg l<sup>-1</sup> (10–230 nmol l<sup>-1</sup>) [5].

Considering the low content of nickel in environmental samples, sensitive analytical techniques are required. Nickel determination in water samples usually could be carried out directly by atomic spectrometry: inductively-coupled plasma optical emission (ICP-OES) or electrothermal and flame atomic absorption spectrometry (ETAAS and FAAS), although the detection limits is not sufficient when the concentrations are too low; moreover, seawater samples with high salinity require simplifying the matrix prior the analysis. So, preconcentration is an effective means for analyzing both complex matrices and samples with low levels of metal.

Many preconcentration techniques have been proposed. Various methods of preconcentration of analytes prior to determination with atomic spectrometry are based on solvent extraction [6–9], but sometimes these procedures cannot be combined with

\* Corresponding author. Tel.: +34 956 016362; fax: +34 956 016460.  
E-mail address: [dolores.galindo@uca.es](mailto:dolores.galindo@uca.es) (M.D. Galindo-Riaño).

ICP-OES, ETAAS or FAAS, because of difficulties of introducing organic solvents into plasma, furnace or flame [10]. So, extraction-stripping methods have been used among others.

Permeation liquid membrane (PLM) techniques offer a potential attractive alternative to these conventional processes in that they combine the process of extraction and stripping in a single unit operation. Two aqueous phases are separated by an immiscible membrane liquid. Preconcentration and separation of analyte occurs automatically as soon as the permeation membrane, containing specific metal ion carrier (extracting agent), is in contact with the feed solution. The flux through the membrane is the key factor of interest [11]. Three basic PLM systems can be used: bulk (BLM), supported (SLM) and emulsion (ELM) liquid membranes; in this paper, a BLM system has been used because of simplicity to use [12].

The applications of PLMs to analysis of natural waters show many potential advantages: high selectivity, reduced sample handling, easy automation and useful in field or in situ analysis. Also, these systems can provide free and other chemical forms of the test metals, being useful for speciation studies of environmental relevance [13]. Different reagents can be employed for sample enrichment and separation in trace analysis of metals in waters. One possibility is to use ion-pairing reagents (counter ion transport extraction) (di-2-ethylhexylphosphoric acid (DEPHA) [14], methyltrioctylammonium chloride (Aliquat 336) [15], laurate anion (LA) [11]). Another possibility is to use complexation equilibria, involving reagents such as crown ethers (1,10-didecyl-diaza-18-crown-6 (Kriptofix 22DD) [16], dibenzo-18-crown-6 [17]), calixarenes (5,11,17,23,29,35-hexa-*tert*-butyl-37,39,41-tri-methoxy calyx[6]arene-38,40,42-triol [18]), organophosphorous compounds (triisobutylphosphine sulphide (Cyanex 471X)[19]; tributylphosphate (TBP)[20]; phosphine oxide (Cyanex 923)[21,19], tri-*n*-octyl-phosphine oxide (TOPO) [18]), benzoylthiourea derivatives (*N*-benzoyl-*N'*,*N'*-diheptadecylthiourea [22]), 8-hydroxyquinoline [23], ... Sometimes, a combination of these possibilities increases the efficacy of the system using synergic reagents. In most cases, the reported methods were applied to industrial waste water, synthetic water, river water or spiked seawater. There were only few applications to real seawater [17,18,24], but usually, the permeation fluxes were lower in seawater because the co-transport of other metals ions (principally, ions of seawater saline matrix) was an interference. So, the efficacies of the processes usually were not of 100% (40–95%). Papantoni et al. [23] have proposed a PLM system for the preconcentration of Ni using a combination of two extraction mechanisms (8-hydroxyquinoline in the donor solution and Aliquat-336 in the membrane liquid) with efficiency of 70%.

The use of ligands with imine group has been proposed previously for us as carrier in BLM [25]. This group of reagents shows interesting properties as complexing agent of transition metal ions: metallic complexes are quickly formed, usually as neutral chelates and the selectivity can be enhanced depending on pH values. A 100% preconcentration of Cu and Cd was obtained using 2-acetylpyridine benzoylhydrazone in real seawater, showing the potential applicability of these reagents [25].

In this paper, the preconcentration and separation of nickel in water using a new BLM system with an imine ligand is presented. A liquid membrane containing 2-hydroxybenzaldehyde *N*-ethylthiosemicarbazone (2-HBET) dissolved in toluene as carrier was used. 2-HBET is a multidentate ligand of transition metals with five potential coordination sites (3N, 1O and 1S atoms) [26]. After enrichment, metal was determined in the receiving acid solution by flame or furnace atomic absorption spectrometry, simple and conventional techniques. The effect of chemical and physical variables on the transport of nickel through the liquid membrane was studied using a modified simplex method [27]. The analysis of nickel in natural waters was possible, even in seawater samples. The method offers important advantages such as simplicity and economy and enables eliminating matrix interferences in waters.

## 2. Experimental

### 2.1. Instrumentation

The cell used for the transport experiments was a cylindrical glass cell (11.34 cm i.d.) with a concentric glass tube (2.56 cm i.d.) which contained separated two aqueous phases (described elsewhere [25]). The feed solution was placed into the external cylinder ( $V_f = 250$  ml) and the stripping solution (receiving solution) was transferred into the inner cylinder ( $V_s = 12$  ml). Liquid organic phase with carrier was added on the top of both aqueous solutions. The membrane area in contact with the two aqueous solutions was 95.85 cm<sup>2</sup>. In these conditions the preconcentration factor was 20.83, provided by the ratio  $V_f/V_s$ . Solutions in the cell were stirred with two Teflon-coated magnetic bars by using a model Agimatic-S magnetic stirrer (Selecta, Spain). Transport experiments were carried out with temperature control using a thermostatic bath (TECTRON-100, 3473100, Selecta, Spain).

An atomic absorption spectrometer (AAS) was used for the measurements of nickel in acid solutions using a Solaar M Series (Unicam, UK) (GFAAS, graphite furnace or FAAS, flame) with a hollow cathode lamp at a wavelength of 232 nm and a 0.1 nm spectral band. GFAAS determinations were performed using pyrolytically coated graphite tubes and Zeeman background corrector. Air-acetylene flame and deuterium background corrector were used for FAAS analysis. The instrumental parameters were those recommended by the manufacturer. A Metrohm model 757 VA Trace Analyzer processor with a Metrohm 747 VA Electrode Stand with automated hanging mercury drop electrode (HMDE) was used for the voltammetric measurements in saline samples, using a reference method for nickel with dimethylglyoxim by adsorptive cathodic stripping voltammetry (AdCSV) (VA Application Note No. V-69, Metrohm) [28]. A Unicam Helios Gamma&Delta (Unicam Limited, UK) spectrophotometer was used for UV-vis spectroscopic measurements with 1 cm quartz glass cells (1 cm × 1 cm × 4.5 cm).

Organic matter was removed for real water samples by UV irradiation with a Metrohm model 705 UV Digester in quartz tubes. A model 2001 pH-meter equipped with 52–02 combined



glass-Ag/AgCl electrode (Crison, Spain) was used for pH measurements.

Sample handling and preparation of solutions were performed using polyethylene gloves and under a class 100 laminar flow hood cabinet Crusair model 9005-FL (Cruma, Spain).

Water used for experiments was purified by reverse osmosis with an Elix 3 system followed by deionization with an 18 M $\Omega$  cm<sup>-1</sup> deionised Milli-Q system (Millipore, USA).

All laboratory materials were acid cleaned (2 mol l<sup>-1</sup> HNO<sub>3</sub>), rinsed with Milli-Q water and stored in a laminar flow cabinet.

## 2.2. Chemicals

2-HBET was synthesized by reaction between 2-hydroxybenzaldehyde (2-HB) and ethylthiosemicarbazone (ET) (Sigma–Aldrich, Steinhein, Germany). Ethanolic solutions of 2-HB (1 ml in 20 ml) and ET (1.12 g in 20 ml) were mixed under reflux heating 15 min. Crystals were filtered off and subsequently crystallized from 1:1 ethanol/water. Actually, Sigma–Aldrich Company (2005 Catalog; CAS number: 76572-70-8) supplies this ligand (C<sub>10</sub>H<sub>13</sub>N<sub>3</sub>OS; formula weight: 223.3). Solutions of 2-HBET (0.2–2.14 mmol l<sup>-1</sup>) in toluene were prepared weekly and kept at 4 °C in darkness when not use. They were used as liquid membrane. Aqueous stock metal standard solutions were prepared by dissolving AAS standard solutions of 1000 mg l<sup>-1</sup> (Merck, Darmstadt, Germany) in 0.05 mol l<sup>-1</sup> HNO<sub>3</sub>.

Britton buffer solutions were used to adjust the pH of feed solutions during the optimization process (pH 8–11) and prepared according to previously reported [29], using sodium hydroxide, o-boric acid, o-phosphoric acid, acetic acid and potassium chloride of Suprapur grade (Merck, Darmstadt, Germany).

The synthetic, certified and real samples were adjusted with 6 mol l<sup>-1</sup> NH<sub>4</sub>Cl/NH<sub>3</sub> buffer solution (pH 9.4), avoiding high dilution of samples.

All reagents were of analytical-reagent or Suprapur grade and all solutions were prepared using Milli-Q deionised water, absolute ethanol or toluene of pro analysis grade (Merck, Darmstadt, Germany).

## 2.3. Preconcentration and separation procedure

Transport experiments were carried out with the cell described above. The aqueous feed solution ( $V_f = 250$  ml) contained ion nickel (500  $\mu$ g l<sup>-1</sup>) and buffered with Britton–Robinson buffer (0.25 mol l<sup>-1</sup> ionic strength in feed solution). The stripping solution ( $V_s = 12$  ml) contained 0.1–1.5 mol l<sup>-1</sup> HNO<sub>3</sub>. The organic liquid membrane ( $V_o = 80$  ml) containing 0.2–2.14 mmol l<sup>-1</sup> 2-HBET in toluene was added over both aqueous solutions. Aqueous solutions were stirred by Teflon-coated magnetic bars at 750 rpm and the system temperature was controlled using a thermostatic bath.

During transport experiment, different 2 ml aliquots of the stripping solution were taken periodically to measure nickel concentration, while 2 ml of nitric acid with the same concentration used and saturated in toluene were added to keep the

volume of the receiving solution constant. The acid extracts were measurement by atomic absorption spectroscopy and the nickel concentrations obtained were corrected taking into account these dilutions. Saline samples were measurement by stripping voltammetry: 10 ml of sample was transferred into the voltammetric cell and the pH adjusted by pH 9.5 ammonium buffer solution (0.5 ml of 6 mol l<sup>-1</sup>); 0.1 ml of 0.053 mol l<sup>-1</sup> DMG in ethanol was added and AdCSV measurements of the Ni-DMG complex were carried out.

UV digestion of real waters with organic matter content was carried out when was necessary, in order to avoid metal organic complexes with high stability to avoid interference in the metal transport experiments or for voltammetric measurements.

The experimental variables were optimized in order to achieve the highest efficiency in the transport of nickel complex across the membrane. Therefore, the permeability  $P$  (cm min<sup>-1</sup>) of nickel across the membrane was used as response variable, using the following linear curve:

$$-\ln[\text{Ni}]_f = \frac{Q}{V_f} Pt - \ln[\text{Ni}]_{f,0}$$

The  $P$ -value was determined from data sets in the form of nickel concentration versus time, where  $A$  was the effective membrane area and  $V_f$  was the volume of feed solution.  $[\text{Ni}]_{f,0}$  and  $[\text{Ni}]_f$  were the nickel concentrations in the feed solution at time 0 and  $t$ , respectively. Also, nickel recovery (%) in the stripping solution was used.

## 3. Results and discussion

2-HBET is a thiosemicarbazone multidentate ligand. Usually, it can be bonded to different transition metals, producing very stable heteropolynuclear complexes [26]. This ligand has been applied in this paper for the first time as carrier of nickel in a liquid membrane, forming an uncharged chelate. This neutral complex is extracted by the organic phase and destroyed by the acid phase, producing the metal transport through the membrane. The pH gradient between feed and stripping solutions is the driving force for this transport. The absence of organic reagent did not produce transport of the metal ion.

The continuous variation method (Job's method) was applied in order to establish the stoichiometry of the complex used in this study. About 8:2 aqueous-ethanolic solutions of nickel chelate buffered at pH 9.4 were prepared and their absorbances were measured at 420 nm with visible spectrophotometer. The nickel/ligand ratio obtained was 1:1.

### 3.1. Optimization of the preconcentration procedure

A set of preliminary experiments was performed to establish the significant variables on the metal transport, which were subsequently analyzed by using a modified simplex design.

The previous physical and chemical parameters studied were pH and components of the feed and strip solutions, type and volume of organic solvent, 2-HBET concentration in organic liquid membrane and stirring rate of solutions. These experiments were carried out with temperature control at  $28 \pm 0.5$  °C.



Table 1  
Simplex design with significant variables and values for the *P* (permeability) response (toluene volume: 80 ml; feed solution: 500  $\mu\text{g l}^{-1}$  of Ni; stirring rate: 750 rpm; temperature:  $28 \pm 0.5$  °C; extraction time: 4.5 h)

Vertex	pH of feed solution	Strip solution: $[\text{HNO}_3]$ ( $\text{mol l}^{-1}$ )	[2-HBET] ( $\text{mmol l}^{-1}$ )	Permeability ( $\times 10^3 \text{ cm min}^{-1}$ )	Type
1	7	1.5	0.20	0.026	I
2	7	0.5	1.00	4.69	I
3	9	0.5	0.20	7.82	I
4	9	1.5	1.00	2.34	I
5	9.7	0.2	1.27	14.61	R
6	11	-0.5	1.80	Not possible	E
7	8.1	-0.7	0.65	Not possible	R
8	8.8	0.9	0.91	6.26	C <sup>-</sup>
9	11.3	0.6	0.59	2.09	R
10	8.1	0.5	0.90	10.17	C <sup>-</sup>
11	9.1	-0.1	0.67	Not possible	R
12	8.9	0.6	0.85	12.78	C <sup>-</sup>
13	8.8	0.4	1.81	10.69	R
14	10.2	0.3	1.72	15.64	R
15	11.2	0.2	2.13	3.65	E
16	10.4	0.3	0.75	15.64	R
5RE1	9.7	0.2	1.27	19.56	R
17	11.3	-0.1	1.64	Not possible	R
18	9.5	0.4	1.05	16.43	C <sup>-</sup>
19	9.2	0.3	1.94	17.21	R
20	8.7	0.3	1.12	12.51	R
21	9.8	0.3	1.57	19.30	C <sup>-</sup>
22	9.6	0.1	2.14	15.91	R
23	9.5	0.3	1.32	21.13	C <sup>-</sup>
24	10.1	0.2	0.83	17.21	R
25	9.4	0.3	1.66	21.38	C <sup>-</sup>

I: initial simplex; R: reflexion; E: expansion; C<sup>+</sup>: positive contraction; C<sup>-</sup>: negative contraction.

The most adequate conditions were found to be basic pH values for feed solution, dilute nitric acid as strip solution, toluene as organic solvent, minimum volume of organic solution that could permit a good contact among the phases ( $V_o = 80$  ml) and maximum stirring rate (750 rpm) avoiding the mix of different phases. Also, the transport was facilitated with an increase of the 2-HBET:Ni concentration ratio. In any cases, the significant variables were pH of the feed and strip solution and 2-HBET concentration as carrier.

Therefore, several variables were kept fixed, whilst a modified simplex with the significant variables was carried out in order to obtain the optimal conditions (Table 1) by using the software Multisimplex 2.0.4 [27]. The response of simplex was the permeability coefficient. The initial simplex with four vertices (three variables) was performed using previous adequate conditions for no significant variables. The simplex was stopped after 26 transport experiments. The criterion selected for stopping the simplex was based on the comparison of the variance of the proposed method (variance of experiment number 5 =  $1.46 \times 10^{-6}$ , for  $n = 4$ ) with the variance of each simplex. This comparison was carried out using the corresponding *F*-values. Optimum conditions were obtained for trial 25 producing a permeability of  $21.38 \times 10^{-3} \text{ cm min}^{-1}$  with the following values of chemical variables: pH 9.4 in the feed solution,  $0.3 \text{ mol l}^{-1} \text{ HNO}_3$  in the stripping solution,  $1.66 \text{ mmol l}^{-1}$  2-HBET in the liquid membrane.

At optimum conditions, the dependence of the transport of metal with the temperature was studied within the range of

25–50 °C. Higher values diminished the permeability probably due to the hydrolysis of 2-HBET. Fig. 1 shows the temporal variation of preconcentration yield of nickel at different temperature. Hundred percent efficiency was possible to achieve from 4 to 5.5 h depending on this parameter.

### 3.2. Effect of saline matrix in the source phase

The effect of saline concentration in the source phase on the efficiency of nickel transport was studied using NaCl addition in the usual range of natural water: 0, 10, 20, 30 and 40  $\text{g l}^{-1}$ , at 50 °C, containing 500  $\mu\text{g l}^{-1}$  of Ni. It was found a low decrease in the percentage of metal transport, being successively the preconcentration yield diminished a value of  $3.3 \pm 0.3\%$  for each studied salinity value. It was necessary to increase the shaking time, from 4 to 6.5–7 h with higher saline samples in order to

Table 2  
Preconcentration of nickel from different concentrations of spiked synthetic seawater (temperature: 50 °C; preconcentration time: 7 h;  $n = 2$ )

Ni spiked ( $\mu\text{g l}^{-1}$ ) <sup>a</sup>	Ni found by proposed method ( $\mu\text{g l}^{-1}$ ) <sup>b</sup>	Error (%)
$50 \pm 2$	$48 \pm 5$	-4.0
$17 \pm 2$	$18 \pm 1$	+5.9
$5.30 \pm 0.01$	$5.45 \pm 0.08$	+2.83

<sup>a</sup> Determination by AdCSV [28].

<sup>b</sup> Proposed preconcentration method + detection by AAS.

Table 3

Determination of nickel in certified reference waters and seawater samples using the proposed new method (temperature: 50 °C; preconcentration time: 7 h)

Sample	Ni concentration ( $\mu\text{g l}^{-1}$ )	Ni found by proposed method ( $\mu\text{g l}^{-1}$ ) <sup>a</sup>	Relative error (%)
LGC 6016	$186 \pm 3^b$	$182 \pm 4$	-2.2
TMDA-62	$98 \pm 9^b$	$92 \pm 1$	-5.9
Seawater 1 <sup>c</sup>	$5.4 \pm 0.5^d$	$5.1 \pm 0.1$	-5.6
Seawater 2 <sup>c</sup>	$3.9 \pm 0.2^d$	$3.81 \pm 0.09$	-2.3
Seawater 3 <sup>c</sup>	$2.8 \pm 0.2^d$	$2.86 \pm 0.06$	+2.1

<sup>a</sup> Proposed preconcentration method + detection by AAS ( $n = 2$ ).<sup>b</sup> Certified value.<sup>c</sup> Seawater samples were collected in different sectors of Huelva Coast, Spain.<sup>d</sup> Determination by AdCSV ( $n = 6$ ) [28].

obtain complete efficient preconcentration ( $100 \pm 3\%$  at 6.5 h and  $10\text{--}40 \text{ g l}^{-1}$  of NaCl).

### 3.3. Analytical performance of the method

In transport experiments, the reproducibility of the preconcentration yield was studied by performing four replicate transport experiments with  $500 \mu\text{g l}^{-1}$  of Ni under the optimized conditions at 50 °C. The precision of the method was 4.7% for significance level at 95% ( $n = 4$ ) with  $500 \mu\text{g l}^{-1}$  of Ni, Ni recovery being  $99 \pm 3\%$  at 4 h.

Four replicates of blank were measured using optimal conditions and deionised water. The obtained value was  $0.036 \pm 0.004 \mu\text{g l}^{-1}$ . The limit of detection, defined as the concentration of analyte giving response equivalent to three times the standard deviation of the blank, were  $0.012 \mu\text{g l}^{-1}$  of Ni. Blank samples were measured by GFAAS, because detection limit of FAAS was not enough.

The preconcentration procedure showed a linear response within the tested concentration range from 3 to  $500 \mu\text{g l}^{-1}$  in the feed solution.

In order to determine the application of the method to seawater, synthetic seawater [30] solutions containing Ni were prepared and analyzed by the proposed method and compared with those obtained by AdCSV [28]. Studies with different con-

centration of metal showed that seawater synthetic matrix did not interference in nickel determination after the preconcentration procedure (Table 2).

### 3.4. Accuracy of the method

The accuracy of the method for nickel was assessed by analyses of two reference certified water: fortified water from Lake Ontario (TMDA-62) and estuarine water (LGC 6016). Two replicates of each reference material were preconcentrated and analyzed after UV digestion with hydrogen peroxide 30% Suprapur (Merck, Darmstadt, Germany), being UV digestion not necessary for TMDA-62. Efficient preconcentration was achieved after 7 h, being the relative errors  $-5.9\%$  and  $-2.2\%$ , respectively (Table 3).

### 3.5. Determination of nickel in seawater samples

The method was applied to different samples of seawater from coast of Huelva (Spain) for the determination of nickel. Samples were filtered through  $0.45 \mu\text{m}$  pore size filters, acidified with  $\text{HNO}_3$  and stored until the application of the method. Nickel was measured after UV digested with  $\text{H}_2\text{O}_2$  using the proposed method. The results in Table 3 were in good agreement with the values obtained using AdCSV method for seawater [28] and no significant differences at 95% confidence interval were found between them. The average preconcentration yield for real samples was  $98 \pm 5\%$ .

## 4. Conclusions

Nickel can be effectively transported, through a liquid membrane of toluene containing 2-HBET. The efficiency of the process is 100% at 4–7 h, depending on the ionic strength of the sample and the temperature of the process. The method has a nickel preconcentration factor of 20.83.

This system permits the separation, preconcentration and quantitative determination of nickel in natural water, where low levels of metal concentration are found. Also, the proposed method can be applied satisfactorily to the analysis of seawater with complex saline matrix, allowing measurements by AAS, a common and simple technique but in which saline ions interfere with analysis direct.

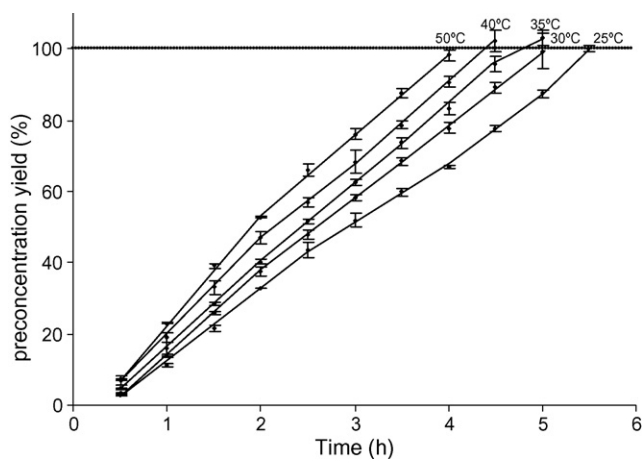


Fig. 1. Temporal variation of preconcentration yield at different temperature (feed solution:  $500 \mu\text{g l}^{-1}$  of Ni at pH 9.4; stripping solution:  $0.3 \text{ mol l}^{-1}$   $\text{HNO}_3$ ; BLM ( $V_0 = 80 \text{ ml}$ ):  $1.66 \text{ mmol l}^{-1}$  2-HBET in toluene; stirring rate: 750 rpm).

## Acknowledgements

This research was supported from funds of the Presidency of the Andalusia Community Government (Spain) (Project: AM7/04) and by Minister of Science and Technology of Spain (Project: REN2003-09361-C03-02/MAR).

## References

- [1] R.K. Thauer, *Science* 293 (5533) (2001) 1264.
- [2] H.A. McKenzie, L.E. Smythe, *Quantitative Trace Analysis of Biological Materials*, Elsevier, Amsterdam, 1988.
- [3] B. Salbu, E. Steinnes, *Trace Elements in Natural Waters*, CRC Press, Boca Raton, 1995.
- [4] U. Forstner, G.T.W. Wittmann, *Metal Pollution in the Aquatic Environment*, 2nd revised ed., Springer-Verlag, Berlin, 1983.
- [5] M. Martino, A. Turner, M. Nimmo, *Mar. Chem.* 88 (2004) 161.
- [6] K.W. Bruland, R.P. Franks, G.A. Knauer, J.H. Martin, *Anal. Chim. Acta* 105 (1979) 233.
- [7] L.G. Danielsson, B. Magnusson, S. Westerlund, K. Zhang, *Anal. Chim. Acta* 144 (1982) 57.
- [8] A.M. De Kersabiec, G. Blanc, M. Pinta, *Fresenius'Z. Anal. Chem.* 322 (1985) 731.
- [9] S. Sachsenberg, T. Klenke, W.E. Kumbein, E. Zeeck, *Fresenius'J. Anal. Chem.* 342 (1992) 163.
- [10] J.W. Olesik, A.W. Moore, *Anal. Chem.* 62 (1990) 840.
- [11] J. Buffle, N. Parthasarathy, N.K. Djane, L. Mathiasson, in: J. Buffle, G. Horvai (Eds.), *In Situ Monitoring of Aquatic Systems: Chemical Analysis and Speciation*. IUPAC Series on Analytical and Physical Chemistry of Environmental Systems, John Wiley and Sons Ltd, Sussex, England, 2000, pp. 408–493.
- [12] R.R. Bartch, J.D. Way, *ACS Symposium Series* 716, Washington, DC, 1996, 422 p.
- [13] N. Parthasarathy, M. Pelletier, J. Buffle, *J. Phys. IV France* 107 (2003) 1021.
- [14] K. Ndungú, N.K. Djane, L. Mathiasson, *J. Chromatogr. A* 826 (1998) 103.
- [15] N. Djane, K. Ndungú, C. Johnsson, H. Sartz, T. Tornstrom, L. Mathiasson, *Talanta* 48 (5) (1999) 1121.
- [16] N. Parthasarathy, M. Pelletier, J. Buffle, *J. Chromatogr. A* 1025 (1) (2004) 33.
- [17] Y.K. Agrawal, S. Sudhakar, *Sep. Pur. Technol.* 27 (2002) 111–119.
- [18] J. Ramkumar, S.K. Nayak, B. Maiti, *J. Membr. Sci.* 196 (2002) 203.
- [19] F.J. Alguacil, H. Tayibi, *Desalination* 180 (2005) 181.
- [20] H.G. Nowier, N. El-said, H.F. Aly, *J. Membr. Sci.* 177 (2000) 41.
- [21] F.J. Alguacil, A.G. Coedo, M.T. Dorado, *Hydrometallurgy* 57 (2000) 51.
- [22] C. Fontás, M. Hidalgo, V. Salvadó, E. Anticó, *Anal. Chim. Acta* 547 (2005) 255.
- [23] M. Papantoni, N. Djane, K. Ndung'u, J.A. Jonson, L. Mathiasson, *Analyst* 120 (1995) 1471.
- [24] C. Mendiguchía, C. Moreno, M. García-Vargas, *Anal. Chim. Acta* 460 (2002) 35.
- [25] M.D. Granado-Castro, M.D. Galindo-Riño, M. García-Vargas, *Spectrochim. Acta Part B* 59 (2004) 577.
- [26] D. Kovala-Demertzi, P.N. Yadav, M.A. Demertzis, J.P. Jasiski, F.J. Andreadaki, I.D. Kostas, *Tetrahedron Lett.* 45 (2004) 2923.
- [27] MultiSimplex, version 2.0.4, MultiSimplex AB (publ), Karlskrona, Sweden, 1998.
- [28] Methrom, Determination of nickel and cobalt in seawater, VA Application Note No. V-69, 2004, <http://www.metrohm.com/infocenter/applications/notes/index.php4>.
- [29] C. Mongay, V. Cerda, *Ann. Chim.* 64 (1974) 409.
- [30] K. Grasshoff, M. Ehrhardt, K. Kremling, *Methods of Seawater Analysis*, 2nd ed., Verlag-Chemie GmbH, Weinheim, Germany, 1983, p. 365.

# Application of matrix solid-phase dispersion to the propham and maleic hydrazide determination in potatoes by differential pulse voltammetry and HPLC

Alberto Sánchez Arribas<sup>a,\*</sup>, Esperanza Bermejo<sup>a</sup>, Manuel Chicharro<sup>a</sup>, Antonio Zapardiel<sup>b</sup>

<sup>a</sup> *Departamento de Química Analítica y Análisis Instrumental, Universidad Autónoma de Madrid, C/ Francisco Tomás y Valiente 7, 28049 Madrid, Spain*

<sup>b</sup> *Departamento de Ciencias Analíticas, Universidad Nacional de Educación a Distancia (UNED), Paseo Senda del Rey 9, 28040 Madrid, Spain*

Received 7 February 2006; received in revised form 10 April 2006; accepted 13 April 2006

Available online 23 May 2006

## Abstract

The application of the matrix solid-phase dispersion (MSPD) process as sample treatment in connection with the electrochemical detection is studied for the first time. For this purpose, a novel methodology is introduced for the extraction of propham and maleic hydrazide herbicides from potatoes samples based in the MSPD process prior to their electrochemical detection. Potato samples disruption was done by blending them with C<sub>8</sub> bonded-phase and selective herbicide extraction was achieved by successive treatment of the blended with 50 mM phosphate buffer pH 7.4 (for maleic hydrazide) and methanol (for propham). The extraction procedure efficiency was estimated using differential pulse voltammetry in potato samples spiked with the herbicides yielding recovery values of 98% and 68% for propham and maleic hydrazide, respectively. No significant adverse effect of the MSPD process was observed on the herbicides electrochemical signals. For comparison, recovery studies using HPLC with UV detection were carried out and a good correlation in the results obtained by using both techniques was observed.

© 2006 Elsevier B.V. All rights reserved.

**Keywords:** Matrix solid-phase dispersion; Electrochemical detection; Propham; Maleic hydrazide; Chlorpropham; Potato

## 1. Introduction

In the present days, agricultural and food industries take advantage of the continuing development of chemicals that increase the yield and lifetime of crops and fruits. For these purposes, different fertilizers, pesticides (mainly insecticides and herbicides) and preservatives are widely used. The massive usage of these compounds and the little knowledge of their secondary effects in humans lead to new disease risks for the consumers and EU directives have established the maximum allowed residual limits (MRL) of these agrochemicals that should be detected in foodstuffs. For these reasons new, fast and effective detecting protocols are demanded for controlling the occurrence of these compounds in food matrixes.

Propham (isopropyl phenylcarbamate) and maleic hydrazide (1,2-dihydropyridazine-3,6-dione) are herbicides that prevent the sprouting of stored potatoes. They work by preventing cell

division, thereby stopping sprouting. These compounds are not proved to be related to cancer disease [1] and they are currently considered innocuous for humans [2] but their actual final effects and hazards have not been accurately determined since it is well known the acetyl cholinesterase inhibition produced by carbamates [3], propham could be degraded into aniline metabolites [4], in fact more dangerous than the former, or maleic hydrazide induces chromosome aberrations in plants [5]. These pesticides have been determined mainly in soil, water and vegetable samples (including potato) by chromatographic techniques. Propham has been analyzed by gas chromatography (GC) [6–8], high-performance liquid chromatography (HPLC) coupled to mass spectrometry [9], UV [10–12] or chemiluminescence [4] detection and thin-layer chromatography (TLC) [13] while maleic hydrazide has been analyzed by gas chromatography (GC) [14], high-performance liquid chromatography (HPLC) coupled to mass spectrometry [15], UV [16] or fluorescence [17] detection and capillary electrophoresis (CE) with UV detection [18]. Fewer antecedents related to the electrochemical detection could be found for propham [19,20] or maleic hydrazide [21–23]. There are some examples regarding the

\* Corresponding author. Fax: +34 91 4974931.

E-mail address: [alberto.sanchez@uam.es](mailto:alberto.sanchez@uam.es) (A.S. Arribas).

independent detection of propham [4,6,7,9] or maleic hydrazide [15–18,21] in potato samples but there is no contribution related to their combined detection in these matrixes.

In this work we study for the first time the use of the matrix solid-phase dispersion (MSDP) process as sample treatment in connection with the electrochemical detection. With this objective, the analytical challenge of the detection of maleic hydrazide and propham in potatoes was chosen for these studies and a novel methodology for the extraction and afterwards electrochemical detection of these herbicides was introduced. MSPD is a new analytical technique which facilitates the preparation, treatment and extraction of solid and viscous samples [24]. MSPD provides homogeneous food sample disruption and dispersion by blending with bonded-phase solid supports ( $C_8$ ,  $C_{18}$ , ...). During the blending process, these supports act as an abrasive and as a bound solvent that break the sample architecture, disperse its components and promote more effective interactions between them and the analytes. The obtained homogeneous mixture presents an additional advantage since the contained supports could act as chromatographic stationary phases in the extraction process, thus allowing the selective elution of the analytes using different solvents. Since extraction and clean-up are carried out in the same step, analysis time and solvent consumption could be reduced. MSPD has been applied to isolate pesticides in fruits and vegetables usually in connection with chromatographic techniques for the pesticides detection [9,25–27]. In this work the pesticide detection was carried out using electrochemical techniques (differential pulse voltammetry), studying the compatibility between this detection mode and MSPD. Such techniques and the voltammetric ones in particular are relatively simple to apply, quite rapid and reasonably cheap providing good sensitivity and selectivity to electroactive analytes. In order to demonstrate the applicability and validity of the proposed extraction methodology in connection with the electrochemical detection, a comparative study was carried out using HPLC with UV detection.

## 2. Experimental

### 2.1. Reagents

Maleic Hydrazide, Propham and Chlorpropham grade Pestanal were purchased from Riedel-de-Haën (Madrid, Spain). The herbicide stock solutions were prepared by dissolving an appropriate amount of the compound in water (maleic hydrazide) and methanol, respectively. All stock solutions were kept away from the light and stored under refrigeration. Diluted solutions were prepared daily from the stock solutions. Methanol, acetone and acetonitrile grade Pestanal purchased from Riedel-de-Haën (Madrid, Spain) were used as solvents. All the other chemicals were analytical-reagent grade and they were used without further purification. Ultrapure water ( $\rho > 18 \text{ M}\Omega$ ) from a Millipore-MilliQ system was used for preparing all solutions.

MFE-Pak  $C_8$  bonded-phase, polypropylene syringe bodies and Isolute ENV+ polymeric cartridges used in the matrix solid-phase dispersion procedure were from Supelco and supplied by Análisis Vínicos (Tomelloso, Spain).

### 2.2. Apparatus

All the electrochemical measurements were carried out using a BAS 100B electrochemical analyzer (BAS, West Lafayette, USA) in a conventional three electrodes configuration. A glassy carbon disk (3 mm diameter, BAS, model MF 2012), a platinum wire and Ag/AgCl, 3 M NaCl (BAS, model RE-5B) were used as working, counter and reference electrode respectively. All potentials are referred to this reference system. Data storage and conversion to a “txt” files were performed with BAS W 2.3 software (BAS, West Lafayette, USA) through a Pentium IV PC computer connected to the electrochemical analyzer.

HPLC experiments were carried out using a Varian Prostar 240 chromatograph equipped with diode array photometric detection.

### 2.3. Procedures

#### 2.3.1. Sample preparation

Raw potatoes were acquired from local markets. The samples were prepared as described in the European Council directive 2002/63/EC, which establishes the sampling methods for the official control of pesticide residues on products from plant or animal origin [28]. Samples were cut in pieces and a representative portion, 500 g, was processed with an electric food chopper mixer and stored in the freezer before being used. Spiked potato samples were prepared by addition of the appropriate amounts of the herbicide stock solution to obtain the desired concentrations.

#### 2.3.2. Matrix solid-phase dispersion procedure

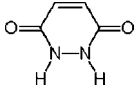
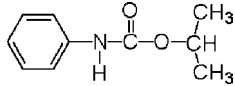
0.5 g portions of potato sample were weighted, mixed and blended for 5 min with 0.5 g of  $C_8$  sorbent in a glass mortar in order to obtain a mixed stationary phase. Then the mixture was introduced into a 10 mL polypropylene syringe body and packed using a syringe plunger. 3.0 mL of 50 mM phosphate buffer pH 7.4 and 10.0 mL of methanol were passed consecutively through the mixture by low vacuum and stored separately. Phosphate fraction containing maleic hydrazide was cleaned by passing through a polymeric ENV+ cartridge, previously activated by passing 2.0 mL of methanol and water, before the electrochemical or HPLC measurements. The methanolic fraction containing propham was introduced directly to the HPLC system or pre-concentrated by  $N_2$  solvent evaporation (from 10.0 to 4.0 mL in order to prevent any analyte loss) and conditioned by addition of 2.0 mL of 0.10 M phosphate buffer pH 1.9 before the electrochemical measurements.

#### 2.3.3. Electrochemical measurements

Initially, the glassy carbon electrode was cleaned by hand polishing using first emery paper (600) for 2 min, then emery paper (BAS) for additional 2 min, followed by fine grades of alumina slurries of 1.0, 0.3 and 0.05  $\mu\text{m}$  (Buehler, Spain) for 2 min in each step with exhaustive water rinsing after that. Between each measurement, the electrode surface was regenerated by polishing with 0.05 alumina slurry for 2 min. Differential pulse voltammetry was employed for all the voltammetric experiments using the default parameters provided by



Table 1

Chemical structure		
Chemical name	1,2-Dihydropyridazine-3,6-dione [123-33-1]	Isopropyl phenylcarbamate [101-21-3]
Molecular weight (g mol <sup>-1</sup> )	112.10	179.22
Solubility in water (g L <sup>-1</sup> )	6 (25 °C) [17]	0.25 (20 °C) [13]
pK <sub>a</sub>	5.65 [17]	15.0 [30]
Half life	2–8 weeks [17]	15 days [13]

the equipment—scan rate: 20 mV s<sup>-1</sup>; pulse amplitude: 50 mV; pulse width: 50 ms; pulse period: 200 ms; sampling time: 17 ms. No further optimization of these operational parameters was attempted. The supporting electrolyte used for propham measurements consisted in 30 mM phosphate buffer containing 66% methanol with an apparent pH of 1.9 while a 50 mM phosphate buffer pH 7.4 was used for maleic hydrazide. These supporting electrolytes were chosen in accordance with the previously reported conditions for the electrochemical detection of these herbicides [19,20,23]. All measurements were done at room temperature.

#### 2.3.4. HPLC measurements

The separations for measuring propham were carried out using a modified procedure based on the one described by Marvin et al. [29] which includes a C<sub>8</sub> Zorbax Lichrosorb RP-8 column (200 mm × 4.6 mm, 10 μm particle size, Ref. 79915 MO-174) with water/acetonitrile gradient elution from 82:12 (from 0 to 15 min) to 35:65 proportions (up to 15 min) in connection with a 2.0 mL min<sup>-1</sup> flow rate, at 35 °C with 50 μL sample volume sample. The wavelength used for detection was 234 nm.

In the case of maleic hydrazide, a separation procedure adapted from Lee et al. [17] was used. This procedure employs a C<sub>18</sub> Microsorb 100-5 column (250 mm × 4.6 mm, 5 μm particle size) in connection with 0.04% phosphoric acid, 5% acetonitrile in water mobile phase in isocratic elution (1.0 mL min<sup>-1</sup>). The sample volume was 20 μL and the temperature was fixed at 25 °C. Maleic hydrazide was detected at 303 nm.

### 3. Results and discussion

The first part of these studies consisted in the optimization of the extraction procedure. Matrix solid-phase dispersion procedures greatly simplify the sample treatment by proper choosing of the bonded-phase, on which the analytes characteristics play a key role. In our case there is a huge difference between maleic hydrazide and propham properties as could be deduced from Table 1. For this reason, the procedure optimization was carried out individually for each compound and then combining compatible conditions in order to obtain the best analytical signals by differential pulse voltammetry. Once the extraction procedure was optimized, the performance of the MSPD and its possible effects on the electrochemical signals were evaluated and a comparative study by HPLC was carried out.

#### 3.1. Optimization of propham extraction conditions

The optimization of the extraction conditions for propham was carried out using potato samples spiked with 100 μg g<sup>-1</sup> and the selected bonded-phase was silica modified with C<sub>8</sub> groups. Under these conditions, propham is dispersed and retained on the sorbent and could be selectively extracted by organic solvents from spiked potato samples. Methanol, acetonitrile and acetone were tested as extractants (results not shown) and the best compromise between analyte recovery, interference elimination and better analytical signals was obtained with methanol. Nevertheless, the voltammetric signals obtained from these extracts (see curves “a” and “b” in Fig. 1) have high background currents and several interfering peaks located at +0.95, +1.15 and +1.30 V that disturb propham signals located at +1.27 V. In order to improve the voltammetric signals, a previous clean-up step was introduced by passing 3.0 mL of water which could eliminate highly polar interferents while propham has more affinity to the non-polar bonded-phase. In this way, a great enhancement in the voltammetric signals is achieved, with well-defined and sharper propham peaks, a significant decrease in the background

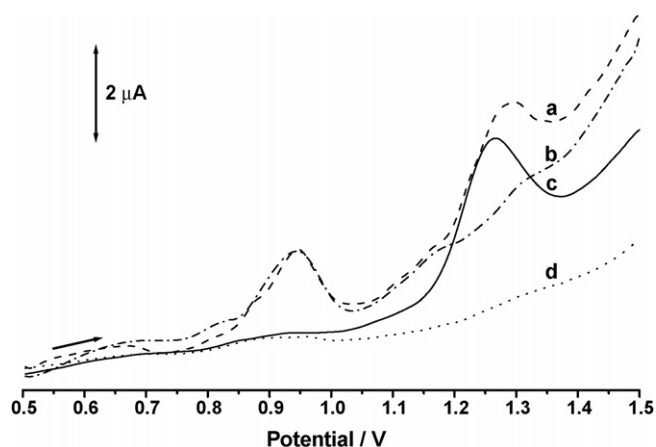


Fig. 1. Effect of the cleaning step on the voltammetric signals of extracts containing propham. (a) Extract from potato sample spiked with propham (100 μg g<sup>-1</sup>) without clean-up step; (b) extract from unspiked potato sample without clean-up step; (c) extract from potato sample spiked with propham (100 μg g<sup>-1</sup>) with clean-up step; (d) extract from unspiked potato sample with clean-up step. Voltammetric parameters—scan rate: 20 mV s<sup>-1</sup>; pulse amplitude: 50 mV; pulse width: 50 ms; pulse period: 200 ms; sampling time: 17 ms. Supporting electrolyte: 30 mM phosphate buffer containing 66% methanol with an apparent pH of 1.9. WE, glassy carbon; AE, platinum wire; RE, Ag/AgCl, 3 M NaCl. All potentials are referred to this reference system.

(about 50%) and the disappearance of the interfering peak, as could be observed in Fig. 1.

### 3.2. Optimization of maleic hydrazide extraction conditions

After these experiments the performance of the extraction procedure was checked in potato samples spiked with maleic hydrazide ( $45 \mu\text{g g}^{-1}$ ). Under these extraction conditions maleic hydrazide is completely extracted in the water fraction and no analytical signals were found in the methanolic fraction. Obviously, the water fraction is enriched in highly polar interferents which do not allow the electrochemical quantification of maleic hydrazide as they are oxidized at a closer potential ( $+0.75 \text{ V}$  measured in fractions previously conditioned with phosphate buffer pH 7.4 to a final concentration of 50 mM). This interfering signal is the same observed previously in the above section (curves “a” and “b” in Fig. 1). Taking into account the high solubility in water and the relatively low oxidation potential, it was assumed that these electroactive interferents were basically phenolic molecules such as phenolic acids (mainly chlorogenic acid), flavonoids (catechin), anthocyanins, carotenoids or vitamins [31–33] present in potatoes. In order to separate these interferents, a new clean-up step was introduced for the water fraction. Firstly, the water fraction pH was conditioned to 7.4 with phosphate buffer in order to keep negatively charged maleic hydrazide and uncharged the phenolic interferents. Under these conditions, the extract was passed through a polymeric ENV+ cartridge which retains the neutral phenolic interferents and the most of the other substances present in potatoes while maleic hydrazide remains in the buffer solution [18]. As a result of this clean-up step, good voltammetric signals of maleic hydrazide without any interference were obtained. These results are summarized in Fig. 2. In order to simplify the process, the first clean-up was done directly with 50 mM phosphate buffer pH 7.4, the same conditions used for the interferent elimination through the polymeric cartridge, and similar results were obtained.

### 3.3. Sequential extraction and electrochemical detection of propham and maleic hydrazide

Finally, the optimized extraction procedure was used to evaluate the compatibility of the MSPD and the electrochemical detection studying the herbicides recovery in potato samples spiked both with maleic hydrazide ( $45 \mu\text{g g}^{-1}$ ) and propham ( $100 \mu\text{g g}^{-1}$ ). The standard addition method was chosen for these recovery studies for four different potato samples. The voltammetric signals registered for one of these potato samples are showed in Fig. 3. The extraction process allows to obtain voltammetric signals with negligible interference (check “U” signals), well defined peak signals of the herbicides and good linearity in the concentration range covered by the additions, as can be seen in the standard addition plots (Fig. 3 insets). The calculated recoveries were  $98 \pm 6\%$  and  $68 \pm 9\%$  for propham and maleic hydrazide, respectively, pointing out the good efficiency of the extraction process. These recoveries values are similar to those reported previously for extractions

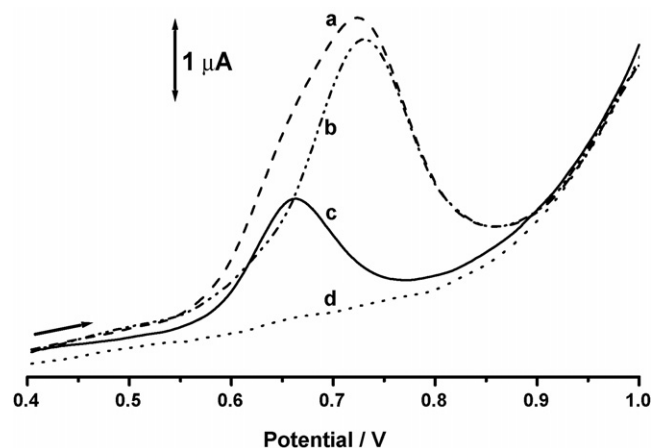


Fig. 2. Effect of the ENV+ cleaning step on the voltammetric signals of extracts containing maleic hydrazide. (a) Extract from potato sample spiked with maleic hydrazide ( $45 \mu\text{g g}^{-1}$ ) without ENV+ clean-up step; (b) extract from unspiked potato sample without ENV+ clean-up step; (c) extract from potato sample spiked with maleic hydrazide ( $45 \mu\text{g g}^{-1}$ ) with ENV+ clean-up step; (d) extract from unspiked potato sample with ENV+ clean-up step. Voltammetric parameters—scan rate:  $20 \text{ mV s}^{-1}$ ; pulse amplitude:  $50 \text{ mV}$ ; pulse width:  $50 \text{ ms}$ ; pulse period:  $200 \text{ ms}$ ; sampling time:  $17 \text{ ms}$ . Supporting electrolyte:  $50 \text{ mM}$  phosphate buffer pH 7.4. WE, glassy carbon; AE, platinum wire; RE, Ag/AgCl,  $3 \text{ M NaCl}$ . All potentials are referred to this reference system.

of propham [4,6,7,9] (ranging from 57 to 100%) and maleic hydrazide [15–18,21] (ranging from 74 to 96%) in potatoes using different extraction and detection methodologies. From the slopes of the standard addition plots the concentration sensitivities in solution were calculated, being  $21 \text{ nA } \mu\text{M}^{-1}$  ( $r = 0.9992$ ,  $n = 5$ ) and  $39 \text{ nA } \mu\text{M}^{-1}$  ( $r = 0.998$ ,  $n = 5$ ) for propham and maleic hydrazide respectively. The detection limits ( $S/N = 3$ ) associated to these measurements were calculated, obtaining  $18 \mu\text{g g}^{-1}$  for propham and  $3.6 \mu\text{g g}^{-1}$  for maleic hydrazide in potatoes. These detection limits are comprised in the micromolar range, result frequently reported for the electrochemical detection of organic compounds using pulse voltammetric techniques without stripping [21,34,35], and allow to use this method for the detection of concentrations of maleic hydrazide below its MRL ( $50 \mu\text{g g}^{-1}$ ) [36] and propham dosages higher than its MRL ( $0.05 \mu\text{g g}^{-1}$ ) [37]. It could be concluded from these studies that there is no significant influence of the MSPD process on the performance and effectivity of the electrochemical detection, demonstrating the suitability and compatibility of this detection mode with the MSPD sample treatment. The combination of the MSPD with the electrochemical techniques present some advantages such as the low organic solvent consumption, compatible with the “green analytical chemistry” trends [38], is quite fast and allows the sequential extraction and detection of analytes with very different chemical properties without complicate or tedious derivatization and clean-up steps. On the other hand, this protocol could be also valid for the analysis of chlorpropham, an anti-sprouting compound closely related with propham [4] with similar chemical and electrochemical properties [19,20], which could be extracted in the methanolic fraction and detected in the same fashion as propham, as could be observed in Fig. 4.

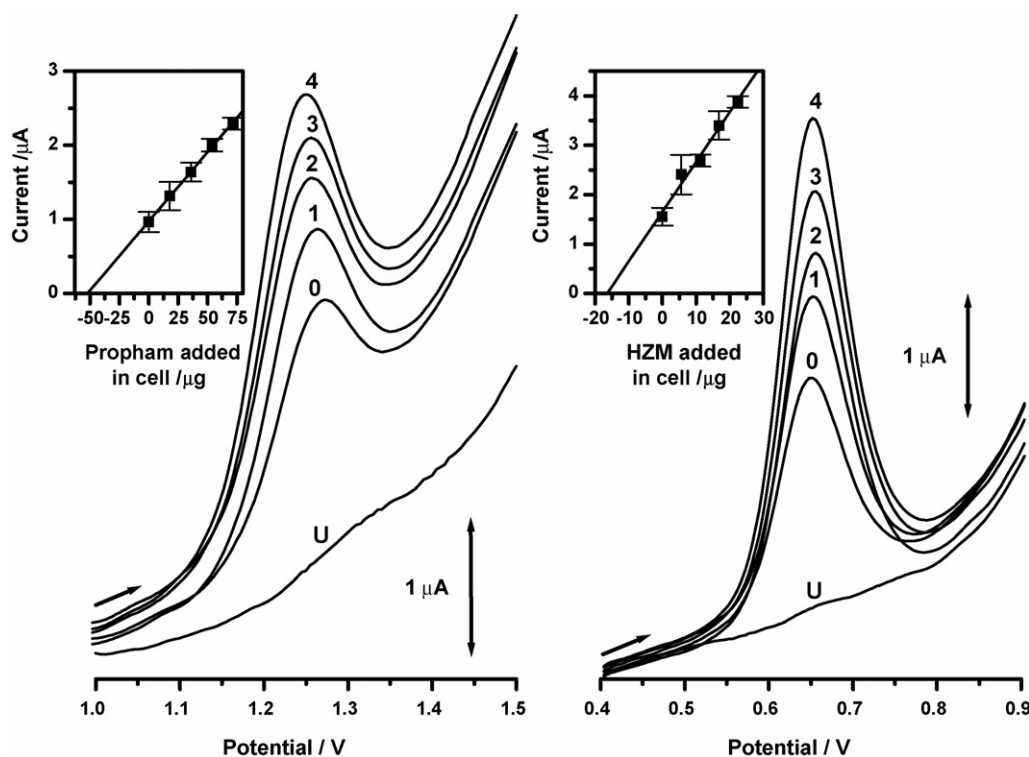


Fig. 3. Recovery studies by DPV from potato samples spiked with protham ( $100 \mu\text{g g}^{-1}$ ) and maleic hydrazide ( $45 \mu\text{g g}^{-1}$ ). (U) Extract from unspiked potato sample. (0) Extract from spiked potato sample. (1–4) Successive additions of 18 and  $5.6 \mu\text{g}$  of protham and maleic hydrazide respectively to solution “0”. The corresponding standard addition plots are shown as insets and each point correspond to the mean value of four measurements. Other conditions as in Figs. 1 and 2.

The difference in the peak potential for protham ( $+1.27 \text{ V}$ , curve “b”) and chlorprotham ( $+1.32 \text{ V}$ , curve “c”) could be used as identification parameter in potatoes treated only with one compound, but their identification and quantification are not possible in the presence of both herbicides (curve “a”) since the analytical signal is the combination of their individual contributions.

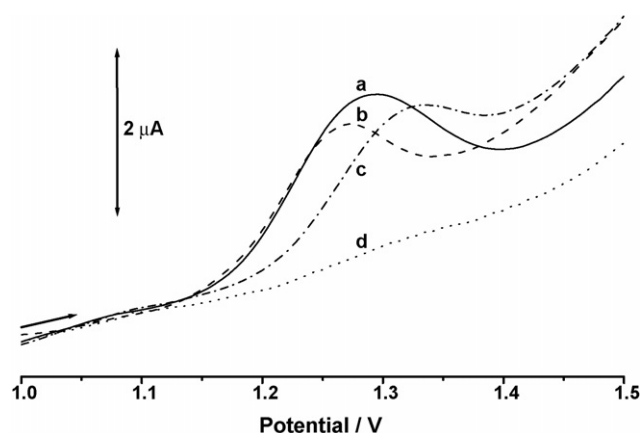


Fig. 4. Effect of the presence of chlorprotham on the voltammetric signals of extracts from potato samples. (a) Extract from potato sample spiked with protham ( $100 \mu\text{g g}^{-1}$ ) and chlorprotham ( $100 \mu\text{g g}^{-1}$ ); (b) extract from potato sample spiked with protham ( $100 \mu\text{g g}^{-1}$ ); (c) extract from potato sample spiked with chlorprotham ( $100 \mu\text{g g}^{-1}$ ); (d) extract from unspiked potato sample. Other conditions as in Fig. 1.

### 3.4. Comparative study with HPLC

In order to compare the recovery results obtained by DPV, the extracts from potato samples spiked both with maleic hydrazide ( $72 \mu\text{g g}^{-1}$ ) and protham ( $50 \mu\text{g g}^{-1}$ ) were analyzed by HPLC with DAD photometric detection. The signals corresponding to the spiked potatoes were compared to those obtained from unspiked potato extracts fortified with the same herbicides amount. The chromatograms registered in these experiments are displayed in Fig. 5. Under these experimental conditions, the extracts used for protham determination contain more interferents when compared to the maleic hydrazide ones, as could be observed in “c” chromatograms, but well defined herbicides peaks with baseline separation from the interfering signals are obtained in both cases. As revealed by the chromatograms, some interfering substances are present in the extracts but it is clear that they have less influence on the electrochemical signals, more selective under these conditions to the herbicides. This information is also promising for future evolution of the proposed concept for herbicide screening and then combined with separation techniques for the resolution of the general analytical monitoring of preservatives such as chlorprotham in potatoes, which can not be distinguished from protham by direct DPV. The recovery values calculated from four different potato samples in these experiments were  $84 \pm 10\%$  and  $67 \pm 4\%$  ( $n=4$ ) for protham and maleic hydrazide, respectively. A good correlation in the recovery results calculated using both techniques was obtained, confirming the applicability and good performance of

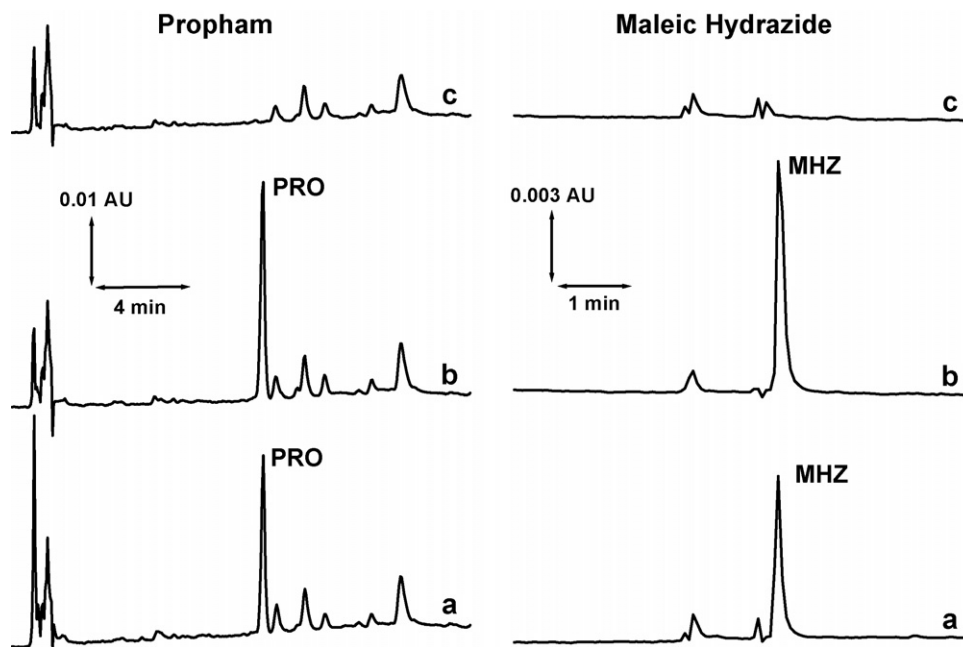


Fig. 5. Recovery studies by HPLC from potato samples spiked with propham and maleic hydrazide. (a) Extract from potato sample spiked with propham ( $50 \mu\text{g g}^{-1}$ ) and maleic hydrazide ( $72 \mu\text{g g}^{-1}$ ); (b) extract from unspiked potato sample fortified after the extraction procedure with the same herbicides amount used in (a); (c) extract from unspiked potato sample. Separation and DAD detection conditions are described in the Section 2.3.4. The propham and maleic hydrazide chromatograms correspond to 234 and 303 nm wavelengths respectively.

the new extraction protocol based on the favorable connection of the MSPD process with the fast, simple and sensitive electrochemical detection.

#### 4. Conclusions

The applicability of the matrix solid-phase dispersion in connection with the electrochemical detection has been demonstrated using a new protocol for the sequential extraction and quantification of propham and maleic hydrazide in potato samples. This new protocol simplifies and reduces the sample treatments and processing before the analytical measurements and the quantification of these pesticides after the extraction could be successfully done by electrochemical techniques with good recoveries. The results obtained open new prospects for the detection of propham and maleic hydrazide in potato samples by combining this protocol with selective separation techniques such as capillary electrophoresis and the simple and sensible electrochemical detection.

#### Acknowledgements

The authors wish to thank Ministerio de Educación y Ciencia de España and Fondo de Desarrollo Regional de la Unión Europea for the financial support of these Projects (CTQ2004-06334-C02-01-02). HPLC experiments were carried out in Servicio Interdepartamental de Investigación (SIdI) facilities within Universidad Autónoma de Madrid. The authors greatly appreciate the SIdI personnel assistance for these experiments.

#### References

- [1] D. Kirkland, M. Aardema, L. Anderson, L. Müller, *Mutat. Res.* 584 (2005) 1–256.
- [2] D. Osindky, J. Mager Stellman, in: *The International Labour Office (Ed.), Encyclopaedia of Occupational Health and Safety*, vol. III, fourth ed., 1998 (Chapter 62).
- [3] K.D. Khalaf, A. Morales-Rubio, M. de la Guardia, *Anal. Chim. Acta* 280 (1993) 231–238.
- [4] E. Orejuela, M. Silva, *Anal. Lett.* 37 (2004) 2531–2543.
- [5] G. Ribas, J. Surrallés, E. Carbonell, N. Xamena, A. Creos, R. Marcos, *Mutagenesis* 11 (1996) 221–227.
- [6] M.J. Santos Delgado, S. Rubio Barroso, G. Toledano Fernández-Tostado, L.M. Polo-Díez, *J. Chromatogr. A* 921 (2001) 287–296.
- [7] E. Conte, G. Imbroglini, P. Bertolini, I. Camoni, *J. Agric. Food Chem.* 43 (1995) 2985–2987.
- [8] H. Beernaert, P. Hucorne, *Z. Lebensm. Unters. Forsch.* 193 (1991) 433–435.
- [9] X. Pous, M.J. Ruiz, Y. Pico, G. Font, *Fresenius J. Anal. Chem.* 371 (2001) 182–189.
- [10] L. Sun, H.K. Lee, *J. Chromatogr. A* 1014 (2003) 165–177.
- [11] M.P. García de Llasera, M. Bernal-González, *Water Res.* 35 (2001) 1933–1940.
- [12] Y. Gou, J. Pawliszyn, *Anal. Chem.* 72 (2000) 2774–2779.
- [13] M. Petrovic, S. Babic, M. Kastelan-Macan, *Croat. Chem. Acta* 73 (2000) 197–207.
- [14] J.M. Renaud, I. Keller, G. Vuillaume, *J. Chromatogr.* 604 (1992) 243–246.
- [15] D.J. Lewis, K.A. Barnes, K. Wilkinson, S.A. Thorpe, S.L. Reynolds, J.R. Startin, *J. Chromatogr. A* 750 (1996) 391–396.
- [16] H. Nagami, *Bull. Environ. Contam. Toxicol.* 58 (1997) 764–768.
- [17] W.-C. Lee, T.-L. Li, P.-C. Chang, S.-S. Chou, *J. Food Drug Anal.* 9 (2001) 167–172.
- [18] D.T. Kubilius, R.J. Bushway, *J. Agric. Food Chem.* 46 (1998) 4224–4227.

- [19] W.J. Albery, B. Fleet, A.M. Oliveira, *J. Appl. Electrochem.* 14 (1984) 550–553.
- [20] W.M. Mayer, M.S. Greenberg, *J. Chromatogr.* 208 (1981) 295–304.
- [21] Y. Ni, P. Qiu, S. Kokot, *Talanta* 63 (2004) 561–565.
- [22] M. Shibata, P. Zuman, *J. Electroanal. Chem.* 420 (1997) 79–87.
- [23] M.S. Lin, B.I. Jan, *J. Chin. Chem. Soc.* 46 (1999) 879–884.
- [24] S.A. Barker, *J. Chromatogr. A* 885 (2000) 115–127.
- [25] C. Soler, J. Manes, Y. Pico, *J. Chromatogr. A* 1088 (2005) 224–233.
- [26] S. Bogialli, R. Curini, A. Di Corcia, M. Nazzari, D. Tamburro, *J. Agric. Food Chem.* 52 (2004) 665–671.
- [27] X.C. Blasco, Y. Pico, G. Font, *J. AOAC Int.* 85 (2002) 704–711.
- [28] Commission Directive 2002/63/EC, *Off. J. Eur. Commun.* L187 (2002) 30.
- [29] C.H. Marvin, I.D. Brindle, C.D. Hall, M. Chiba, *J. Chromatogr.* 503 (1990) 167–176.
- [30] M. Bergon, J.-P. Calmon, *J. Agric. Food Chem.* 31 (1983) 738–743.
- [31] A.J. Blasco, M.C. González, A. Escarpa, *Anal. Chim. Acta* 511 (2004) 71–81.
- [32] S.R. Kanatt, R. Chander, P. Radhakrishna, A. Sharma, *J. Agric. Food Chem.* 53 (2005) 1499–1504.
- [33] C.M. Verde Méndez, M.A. Rodríguez Delgado, E.M. Rodríguez Rodríguez, C. Díaz Romero, *J. Agric. Food Chem.* 52 (2004) 1323–1327.
- [34] E.M. Garrido, C. Delerue-Matos, J.L.F.C. Lima, A.M.O. Brett, *Anal. Lett.* 37 (2004) 1755–1791.
- [35] S.A. Oezkan, B. Uslu, H.Y. Aboul-Enein, *Crit. Rev. Anal. Chem.* 33 (2003) 155–181.
- [36] “Productos Vegetales, Límites Máximos y Control de Residuos de Plaguicidas”, B.O.E. 30 March 2001. No 77, p. 1204. Based on the European Directive 91/414/CEE.
- [37] “Productos Vegetales, Límites Máximos y Control de Residuos de Plaguicidas”, B.O.E. 17 October 2001. No 249, p. 38173. Based on the European Directive 91/414/CEE.
- [38] J. Namiesnik, *J. Sep. Sci.* 24 (2001) 151–153.



# Photolysis-assisted, long-path FT-IR detection of air pollutants in the presence of water and carbon dioxide

Zoltán Bacsik<sup>a</sup>, János Mink<sup>a,b,c,\*</sup>

<sup>a</sup> Chemical Research Centre, Hungarian Academy of Sciences, Pusztaszeri út 59-67, H-1025 Budapest, Hungary

<sup>b</sup> Analytical Chemistry Research Group of the Hungarian Academy of Sciences, University of Veszprém, Egyetem u. 10, H-8200 Veszprém, Hungary

<sup>c</sup> Faculty of Information Technology, Research Institute of Chemical and Process Engineering, University of Veszprém, Egyetem u. 10, H-8200 Veszprém, Hungary

Received 16 November 2005; received in revised form 1 March 2006; accepted 17 March 2006

Available online 27 April 2006

## Abstract

Seven important air pollutants have been investigated by photolysis-assisted FT-IR spectroscopy. This technique renders invisible the spectra of water and carbon dioxide, which are two of the main concerns in long-path infrared spectroscopy. A cell, equipped with a UV lamp, was used to oxidise the analyte in the air sample and the spectrum recorded was used as a new background for the original sample spectrum. The optimum UV irradiation time and correctness of the concentrations were determined for this technique and compared with those from traditional methods. The signal-to-noise (S/N) ratios of the so-called “shadow spectra” were better than, or at least comparable to, the S/N ratios in the absorbance spectra obtained by using as background an air or an evacuated cell reference and subtraction of the spectra of water and carbon dioxide from a spectral library. The detection limits for the volatile organic compounds investigated have been improved by using this new method in which an appropriate background spectrum can be obtained quickly. The limitations of the method are that it cannot be applied to non-UV reactive compounds, such as methane, and the detection limits can be appreciably degraded when bands due to ozone in the shadow spectra overlap with those of the compounds under investigation.

© 2006 Elsevier B.V. All rights reserved.

**Keywords:** Air pollutants; Photolysis-assisted FT-IR spectrometry; Detection limits

## 1. Introduction

The recent extensive developments in the design of infrared spectrometers and the practical advantages of such spectroscopic equipment have led to the increasing use of Fourier transform infrared (FT-IR) spectroscopy for the detection and analysis of atmospheric pollutants [1–5]. Moreover, the newer open-path sampling techniques offer fresh analytical possibilities, such as in situ and continuous monitoring, which can result in on-line measurements without the so-called wall and memory effects of the gas cells. In several cases, the use of a non-continuous extractive method is reasonable [6] because of its simplicity and cost effectiveness when compared to other detection methods

for gaseous pollutants, such as GC-MS. Despite the substantial advantages of FT-IR spectroscopy in gas analysis, however, there are still many experimental difficulties that have to be overcome.

Because of the low concentrations of gaseous samples, a long-path cell is necessary in most cases for environmental gas measurements [7]. In open-path infrared spectroscopy, the path can be increased by lengthening the distance between the source and the interferometer. In the laboratory, long-path gas cells are used to increase the absorbance of the analyte. While the detection limits can be augmented in this way, the concomitant increased absorption of atmospheric water and carbon dioxide can cause significant problems. In most cases, the absorption bands of these two compounds are strongly overlapped with the bands of the air pollutants of environmental interest [8]. Therefore, the spectra of H<sub>2</sub>O and CO<sub>2</sub> should be removed from the sample spectra before any other bands are measured.

The most common method of elimination is to use a library of water and CO<sub>2</sub> spectra of varying concentrations, which

\* Corresponding author at. Chemical Research Centre, Hungarian Academy of Sciences, P.O. Box 17, H-1525, Budapest, Hungary. Tel.: +36 88624487; fax: +36 88624487.

E-mail address: [mink@almos.vein.hu](mailto:mink@almos.vein.hu) (J. Mink).

can then be subtracted from the pollutant spectra so that the bands of the pollutants can be seen clearly. The spectral library must be from the same spectrometer, since each spectrometer has a different spectral response with some variations in band positions, widths and shapes. And, in the concentration ranges of interest, the pollutant absorbances may exhibit deviations from the Lambert–Beer law, which is why the H<sub>2</sub>O and CO<sub>2</sub> absorbances must be comparable to those in the sample spectra. Using this method, sometimes the measurements are simple and take a short time. Often, however, it is difficult to eliminate the H<sub>2</sub>O and CO<sub>2</sub> spectra and selection of the proper spectra takes a long time, especially when higher detection limits are needed. Using a long-path cell, a little change in the concentrations can lead to large effects in the absorbance spectra.

Since open-path measurements present greater difficulties for recording a background spectrum, several methods have been developed and applied for this purpose and many of them can be used in extractive measurements. After selecting, with the aid of the data manipulation software, appropriate points in “empty” regions of the single-beam spectrum of the sample, a smooth curve can be constructed through these points and used as a synthetic background. The EPA’s guidance document [9] advises the spectrometer operator to use a synthetic background whenever possible. Griffith and Jamie [1] have warned, however, that this technique may have many potential pitfalls and should be used only when collection of real background spectra is impractical. The so-called shifting method was introduced for use in OP/FT-IR by Xiao and Levine [10] and has been discussed in detail by Giese-Bogdan et al. [11]. In closed-cell measurements, the shifting method produces about three times higher deviations than does the conventional method. Other effective methods have also been applied to measure the benzene band that is highly overlapped with that of CO<sub>2</sub> [12,13]. To compensate for the atmospheric H<sub>2</sub>O vapour and/or CO<sub>2</sub> absorptions, synthetic reference spectra can be calculated [14] from known line parameters in certain databases, such as HITRAN [15] or GEISA [16], provided the path-length, humidity and temperature are known. Some researchers [17,18] have suggested that very low-resolutions (16–32 cm<sup>-1</sup>) can be employed in order to lower the noise and thus make the spectral quantification easier.

A useful technique has been described by Görög [19] for the spectrophotometric determination of ketosteroids in pharmaceutical preparations in which the “lack of the compound” was determined in the case of interfering compounds: a reagent was added to the solution to eliminate the analyte. A similar approach has been described by Hanst [20] in which the spectra of H<sub>2</sub>O and CO<sub>2</sub> are rendered invisible. A cell, fitted with a UV lamp, is used to oxidise the analyte in the air sample and the spectrum recorded is used as a new background for the original sample spectrum. Benzene, toluene and *o*-xylene have been determined by this so-called photolysis-assisted pollution analysis (PAPA) technique. In the original PAPA paper [20], no experimental details, such as oxidation time, noise levels, detection limits, etc., for the application of the technique were reported. In the present work, seven important environ-

mental polluting compounds have now been investigated by this PAPA technique. Proper UV irradiation time and correctness of the concentration determined by the technique are compared with the values obtained by the traditional spectral subtraction of library H<sub>2</sub>O and CO<sub>2</sub> reference spectra or a “background air” single-beam spectrum with similar H<sub>2</sub>O and CO<sub>2</sub> concentrations to the sample spectra was used.

As part of this work, we will illustrate the differences in the spectra obtained by the various methods. We have coined the term “shadow spectroscopy” for the PAPA method and the spectrum obtained by this technique is known as the “shadow spectrum”. By dividing the sample spectrum after UV irradiation by the original sample spectrum, the bands of the oxidised pollutants appear as negative absorbances (the absence of a particular pollutant can be established).

## 2. Experimental

### 2.1. Instrumentation

Infrared spectra of the gaseous samples were recorded on a Bio-Rad (Digilab) FTS-185 Fourier transform infrared spectrometer equipped with a photolysis-assisted pollution analyser 5-32 type, 25.7-m pathlength multiple-pass gas cell (Infrared Analysis Inc., Anaheim, CA, USA) and a MCT detector. The cell contains a 40-W medium pressure quartz mercury resonance lamp and is designed for use in the sample compartment of the infrared spectrometer. The sample compartment was enclosed by a plastic cover especially designed for this purpose and was purged with dry air.

The UV-lamp of the cell emits 1–2% of its radiation in the 185-nm mercury line and about 90% in the 254-nm line with the remainder being in lines that fall in the near-UV and visible range. Under UV radiation, atomic oxygen can be produced, leading to the formation of ozone and hydroxyl radicals, which can react with the pollutant molecules. Hanst has suggested several possible reactions that could occur under these conditions [20].

### 2.2. Materials

Seven compounds with important environmental interest were chosen to investigate by this method, namely acetone, methane, benzene, toluene and *m*-, *o*- and *p*-xylene, the absorption bands of which are overlapped by H<sub>2</sub>O and/or CO<sub>2</sub> spectra. The calibration concentrations were prepared by a special vacuum system attached to the gas cell. Samples of the single compound liquids (except methane since it is a gas at STP) for spectroscopic purity were connected to the vacuum system in test tubes and then the air over the liquid was removed, while the single compound was frozen by liquid nitrogen. After evacuating the system and reducing the vacuum, a known quantity of single compound was expanded into the gas cell by measuring its vapour pressure in the system by a diaphragm manometer (KJL902058, Kurt J. Lesker Co., Pittsburgh, PA, USA). Five experiments were carried out with each compound with decreasing concentrations, close to the detection limits.

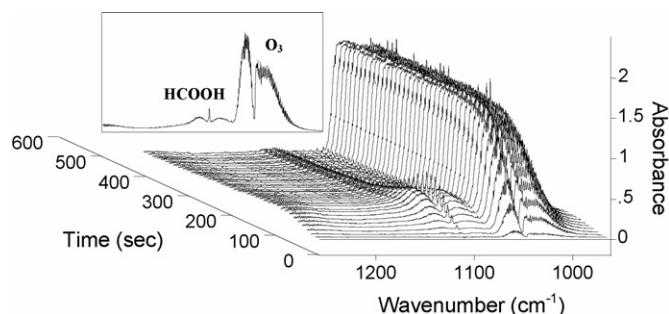


Fig. 1. Change of the O<sub>3</sub> band during the investigation time of benzene oxidation. A weaker spectral feature due to formic acid is observed next to the O<sub>3</sub> band as an intermediate product of the oxidation.

### 3. Results and discussion

#### 3.1. Spectra collection

When the sample compound was introduced to the gas cell, a long-time kinetic study was carried out in order to monitor the appropriate oxidation time. The spectra were recorded in the spectral range of 4000–550 cm<sup>-1</sup> and the spectral resolution was 0.5 cm<sup>-1</sup>. The identification and the quantification were performed with the aid of a spectral library (Infrared Analysis Inc., Anaheim, USA).

As an example, the study of benzene will now be described. Four interferograms were accumulated in every 10 s time period. When the first spectrum had been recorded, the UV lamp was switched on. The change in O<sub>3</sub> concentration is illustrated in Fig. 1. After 1 min of UV exposure, the formation of O<sub>3</sub> slowed down. The O<sub>3</sub> production rate was similar for all the compounds at this low concentration range of pollutant analytes. A minor dependence of O<sub>3</sub> formation on O<sub>2</sub> concentration has been established by Larsen et al. [21].

Using this spectroscopic method to monitor the oxidation of benzene, it was shown that the initial spectral features of this compound had disappeared after 100 s for the highest concentration investigated (4.27 ppm). Therefore, in order to ensure the complete oxidation of benzene, a 3-min exposure time was chosen.

The original sample absorbance spectra were observed in two different ways:

1. Dividing the original sample single-beam spectra by a single-beam spectrum of an evacuated cell. The “background air” reference spectrum was then recorded using the same evacuated cell single-beam spectrum as a background. These two absorbance sample spectra were next subtracted from each other.
2. The absorbance spectra were obtained with an evacuated cell background and then library CO<sub>2</sub> and H<sub>2</sub>O spectra were subtracted.

The so-called shadow spectrum can be produced in two different ways.

1. Single-beam operation

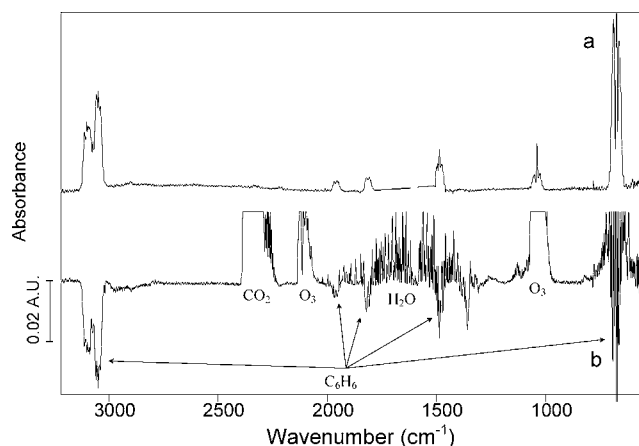


Fig. 2. “Shadow” spectrum of benzene. (a) Reference spectrum of benzene and (b) absorbance spectrum after decomposition of benzene.

After initially recording the single-beam spectrum of the sample, a few minutes of UV radiation exposure led to the decomposition of most of the pollutant molecules (e.g., see the negative bands of benzene in Fig. 2b) and strong bands due to the formation of O<sub>3</sub> appear in the spectrum. Dividing by the original sample spectra (before oxidation), weak negative bands of the decomposition products of C<sub>6</sub>H<sub>6</sub> can be observed alongside of the strong, positive O<sub>3</sub> and weak CO<sub>2</sub> and H<sub>2</sub>O bands (Fig. 2b).

#### 2. Absorbance operation

A single-beam spectrum of the evacuated cell was used as reference for producing an absorbance spectrum of the sample (Fig. 3a). After UV light exposure, another absorbance spectrum (Fig. 3b) was generated using the same single-beam spectrum of the evacuated cell as background. After subtraction of the two absorbance spectra, the bands of H<sub>2</sub>O and CO<sub>2</sub> are compensated to a reasonable extent and, at the same time, the weak positive bands of the oxidised and decomposed air pollutants produce the so-called shadow spectrum (Fig. 3c). This method was chosen in this work.

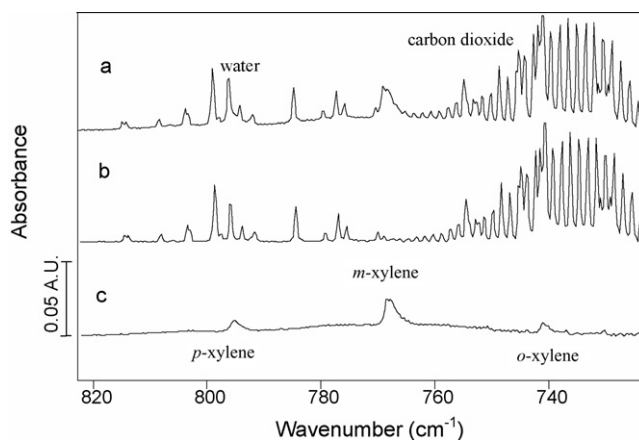


Fig. 3. The production of the “shadow” spectrum. (a) Sample spectrum (2.26 ppm *m*-xylene, 0.22 ppm *o*-xylene and 1.25 ppm *p*-xylene in air). (b) Sample spectrum after 3-min UV-irradiation (with an O<sub>3</sub> reference spectrum added). (c) The so-called shadow spectrum (spectrum b subtracted from spectrum a).

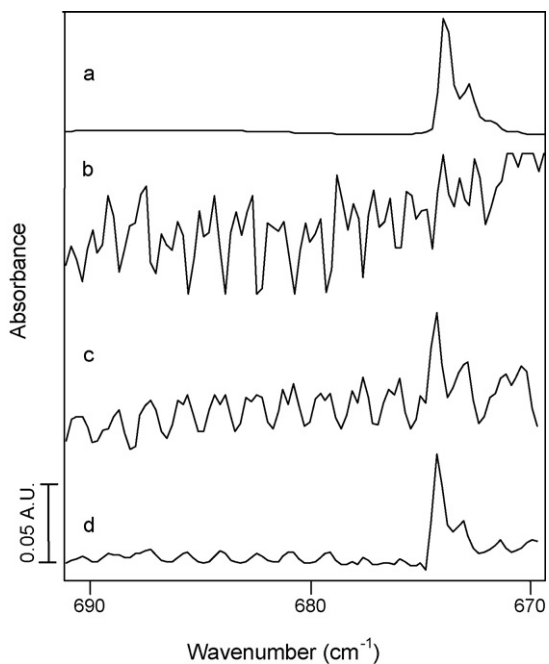


Fig. 4. Visualisation of the  $674\text{ cm}^{-1}$  benzene band (umbrella vibration) in the sample spectrum (3.41 ppm benzene in air) using different backgrounds. (a) Benzene reference. (b) Sample after  $\text{CO}_2$  subtraction (evacuated cell background). (c) Sample with air background. (d) The “shadow” spectrum of benzene.

### 3.2. Advantages of shadow spectroscopy

The spectral subtraction of  $\text{H}_2\text{O}$  and  $\text{CO}_2$  always results in an increase in the noise of the residual spectra due to the differences in the absorbance levels of the two spectra, the noise in the reference spectrum and the frequency shifts between them.

All these problems can be eliminated by using shadow spectroscopy. On comparing the noise level in the three spectra (Fig. 4b–d) obtained by the various techniques, the difference is quite conspicuous. Using an air spectrum as background, rather noisy absorbance spectra were obtained due to the difference in  $\text{CO}_2$  concentration during the sample and the background collection. It can be seen that the residual noise is about 50% of the band intensity (Fig. 4c), while that determined from the shadow spectrum is less than 10% (Fig. 4d).

The increasing noise effect of the subtraction is greater when the concentration difference is higher. Consequently, during the multiplication of the reference spectrum by the subtraction factor, the noise will be increased by the same level. Once the subtraction of the low intensity spectral features of  $\text{CO}_2$  is completed, the strong bands always appear in the negative absorbance range due to the failure of the Lambert–Beer law (Fig. 5). The weaker toluene band at  $695\text{ cm}^{-1}$  cannot be detected at this low concentration range using this path length. Although the shadow spectrum also contains noise, the signal-to-noise ratio is much better and the sharp Q-branch at  $695\text{ cm}^{-1}$  also becomes clearly visible (Fig. 5b).

In order to substantiate the analytical results from shadow spectroscopy, the concentration determinations have also been performed by the more traditional methods (with no manipulation of spectra) at a high concentration level, at which the

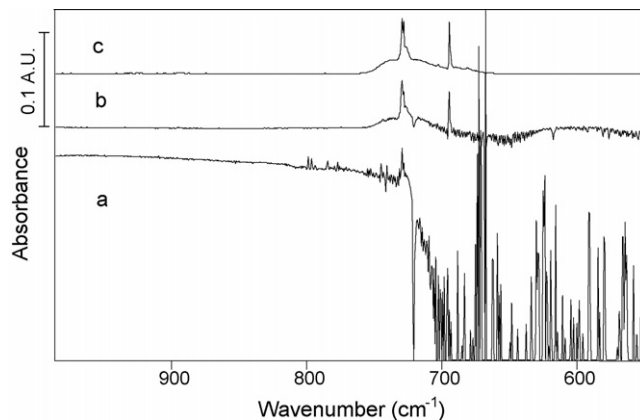


Fig. 5. Carbon dioxide elimination from toluene sample spectrum (3.2 ppm toluene in air) with the aid of spectral subtraction (a) and produced by shadow spectroscopy (b); spectrum (c) refers to the toluene reference spectrum.

Table 1  
Concentrations of benzene with different background spectra

Concentration (ppm)		
Evacuated cell background	Air background	Shadow spectrum
4.27	4.29	4.30
3.40	3.41	3.41
2.88	2.86	2.89
–	1.23	1.18
–	0.39	0.36

benzene band can be safely used for this purpose. The results for benzene are listed in Table 1. It can be concluded that the concentrations, which can be derived from the shadow spectra, are appropriate since the same values are determined at higher concentration levels. That means that the efficiency of oxidation was 100%.

The detection limits of the gases have been determined on basis of noise in the absorbance spectra next to the band used for analysis. The minimal detectable concentration was determined at the  $3\sigma$  level. In most cases, the detection limits (Table 2) have been considerably improved when compared with the results obtained by conventional methods. The most significant improvement is shown for benzene, where the band is heavily interfering with the perpendicular band of  $\text{CO}_2$ .

It must be emphasised that “background air” is not a well-defined situation. The  $\text{H}_2\text{O}$  and  $\text{CO}_2$  content in this spectrum depends on many variables. There was only one common air

Table 2  
Detection limits for the investigated compounds by different methods (ppm)

Compounds	Evacuated cell background	Air background	Shadow spectroscopy
<i>o</i> -Xylene	–	0.020	0.040
<i>p</i> -Xylene	0.220	0.070	0.060
Benzene	2.500	0.350	0.030
Toluene	0.120	0.240	0.030
Acetone	0.250	0.020	0.020
<i>m</i> -Xylene	0.160	0.020	0.010



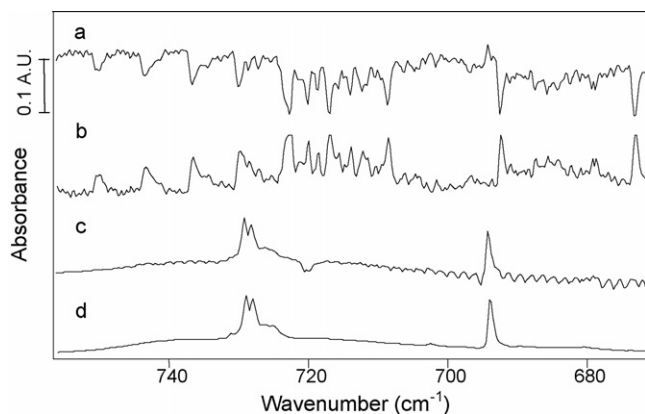


Fig. 6. Subtraction of the own O<sub>3</sub> reference spectrum (b) from the shadow spectrum (a) of the sample (1.62 ppm toluene in air). (c) The shadow spectrum after O<sub>3</sub> subtraction (absorbance scale expanded:  $\times 4$ ). (d) Toluene reference spectrum.

background spectrum used for each sample, which was recorded well before the sample measurements by filling the cell at the same location, where the cell was later filled for the sample measurements.

#### 4. Limitations

If appearing O<sub>3</sub> lines after the UV irradiation of the sample overlap with the bands of the analyte, further improvement of the detection limits of the investigated compounds can be realised by additional subtraction (or addition) of the O<sub>3</sub> reference spectrum. An example is given in Fig. 6 for toluene determination. For this reason, we recorded our own O<sub>3</sub> spectrum in the gas cell containing only background air in the absence of any analyte samples. From Fig. 1, it is apparent that the O<sub>3</sub> level reaches a constant level after several minutes of UV irradiation, so that the amounts of O<sub>3</sub> in the reference spectrum and in the sample spectrum are very close to one another. In this way, O<sub>3</sub> elimination does not affect drastically the noise level in the sample spectra (the scaling factor is very close to 1).

The other main limitation of shadow spectroscopy is that it cannot be used to measure unreactive gases. Methane is one of the permanent compounds in our atmosphere (1.5–2.5 ppm), i.e. there are no air samples without the presence of CH<sub>4</sub>. In contrast with the other hydrocarbons discussed above, it was not possible to achieve complete elimination of CH<sub>4</sub> from the gas cell by UV irradiation. After 30-min exposure, the concentration of CH<sub>4</sub> decreased from 11.29 to 2.02 ppm, a good illustration that the shadow spectroscopy method is not suitable for quantitative analysis of methane.

#### 5. Conclusions

According to the results obtained for volatile organic compounds (*p*-, *m*- and *o*-xylene, benzene, toluene, acetone), it has been demonstrated that the detection limits can be improved considerably by means of shadow spectroscopy, when compared to the results obtained by conventional subtraction of library H<sub>2</sub>O and CO<sub>2</sub> absorbance spectra (using an evacuated cell back-

ground). In the case of an air background, varying efficiencies were achieved, since it is usually rather difficult to obtain a proper air background, but detection limits were significantly reduced when strongest band in the analyte spectrum (benzene and toluene) is overlapped with perpendicular band of CO<sub>2</sub>. The S/N ratio of the shadow spectra is better than, or at least comparable to, the S/N in the spectra produced by air backgrounds. In places where the analyte always exists in the air or the humidity and CO<sub>2</sub> concentration is not permanent, the best choice is shadow spectroscopy, because there is no need for a time-consuming procedure to select a proper background spectrum and to correct for possible frequency shifts. A low-noise absorbance spectrum can be recorded after a brief UV irradiation of the sample.

The basic limitation of this method is that the molecules in air samples under measurement must be decomposed by UV irradiation. In the future, a list must be drawn up for the measurable compounds to apply this method safely in quantitative analysis. Another disadvantage is caused by the strong development of negative ozone bands in the sample spectra. This latter problem practically can be solved by compensation of the O<sub>3</sub> absorption with an O<sub>3</sub> reference spectrum measured under similar conditions as those for the samples.

#### Acknowledgements

We are particularly grateful to Professor I.S. Butler (McGill University, Montreal) for valuable discussions during preparation of the manuscript. Special thanks to Krisztián Horváth (Ráksi, Somogy, Hungary) for continuous support.

#### References

- [1] D.W.T. Griffith, I.M. Jamie, in: R.A. Meyers (Ed.), *Encyclopedia of Analytical Chemistry*, Wiley, Chichester, 2000, pp. 1979–2007.
- [2] G.M. Russwurm, J.W. Childers, in: J.M. Chalmers, P.R. Griffiths (Eds.), *Handbook of Vibrational Spectroscopy: Open-path Fourier Transform Infrared Spectroscopy*, vol. 2, Wiley, New York, 1750.
- [3] R.L. Spellicy, J.D. Webb, in: J.M. Chalmers, P.R. Griffiths (Eds.), *Handbook of Vibrational Spectroscopy: Atmospheric Monitoring Using Extractive Techniques*, vol. 2, Wiley, New York, 1721.
- [4] Z. Bacsik, J. Mink, G. Keresztury, *Appl. Spectrosc. Rev.* 39 (2004) 295.
- [5] Z. Bacsik, J. Mink, G. Keresztury, *Appl. Spectrosc. Rev.* 40 (2005) 327.
- [6] Z. Bacsik, V. Komlósi, T. Ollár, J. Mink, *Appl. Spectrosc. Rev.* 41 (2006) 77.
- [7] P.L. Hanst, in: J.M. Chalmers, P.R. Griffiths (Eds.), *Handbook of Vibrational Spectroscopy: Long Path Gas Cells*, vol. 2, Wiley, New York, 2002, p. 960.
- [8] P.L. Hanst, S.T. Hanst, in: M.W. Sigrist (Ed.), *Air Monitoring by Spectroscopic Techniques: Gas Measurements in Fundamental Infrared Region*, Wiley-Interscience, New York, 1994, pp. 335–466.
- [9] EPA FT-IR Open-path Monitoring Guidance Document, US EPA, Research Triangle Park, 1996.
- [10] H. Xiao, S.P. Levine, *Anal. Chem.* 65 (1993) 2262.
- [11] S. Giese-Bogdan, S.P. Levine, K. Molt, *J. Air Waste Manag. Assoc.* 49 (1999) 114.
- [12] U. Müller, H.M. Heise, H. Mosebach, A.G. Gärtner, T. Häusler, *Field Anal. Chem. Tech.* 3 (1999) 141.
- [13] B. Lechner, P.J. Sturm, *Proc. SPIE* 3493 (1998) 88.
- [14] D.W.T. Griffith, *Appl. Spectrosc.* 50 (1996) 59.



- [15] L.S. Rothman, A. Barbe, D. Chris Benner, L.R. Brown, C. Camy-Peyret, M.R. Carleer, K. Chance, C.V. Clerbaux, Dana, V.M. Devi, A. Fayt, J.-M. Flaud, R.R. Gamache, A. Goldman, D. Jacquemart, K.W. Jucks, W.J. Lafferty, J.-Y. Mandin, S.T. Massie, V. Nemtchinov, D.A. Newnham, A. Perrin, C.P. Rinsland, J. Schroeder, K.M. Smith, M.A.H. Smith, K. Tang, R.A. Toth, J. Vander Auwera, P. Varanasi, K. Yoshino, J. Quant. Spectrosc. Radiat. 82 (2003) 5 (The HITRAN Molecular Spectroscopic Database: Edition of 2000 Including Updates through 2001).
- [16] N. Jacquinet-Husson, E. Arie, J. Ballard, A. Barbe, G. Bjoraker, B. Bonnet, L.R. Brown, C. Camy-Peyret, J.-P. Champion, A. Chedin, A. Chursin, C. Clerbaux, G. Duxbury, J.-M. Flaud, N. Fourrie, A. Fayt, G. Graner, R. Gamache, A. Goldman, V. Golovko, G. Guelachvilli, J.-M. Hartmann, J.C. Hilico, J. Hillman, G. Lefevre, E. Lellouch, S.N. Mikhailenko, O.V. Naumenko, V. Nemtchinov, D.A. Newnham, A. Nikitin, J. Orphal, A. Perrin, D.C. Reuter, C.P. Rinsland, L. Rosenmann, L.S. Rothman, N.A. Scott, J. Selby, L.N. Sinita, J.M. Sirota, A.M. Smith, K.M. Smith, V.I.G. Tyuterev, R.H. Tipping, S. Urban, P. Varanasi, M. Weber, J. Quant. Spectrosc. Radiat. 62 (1999) 205.
- [17] P.R. Griffiths, B.K. Hart, H.S. Yang, R.J. Berry, *Talanta* 53 (2000) 223.
- [18] P. Jaakkola, J.D. Tate, M. Paakkunainen, J. Kauppinen, P. Saarinen, *Appl. Spectrosc.* 51 (1997) 1159.
- [19] S. Görög, *J. Pharmaceut. Sci.* 57 (1968) 1737.
- [20] P.L. Hanst, Proceedings of the US EPA/A&WMA International Symposium: Measurements of Toxic and Related Pollutants, 1994, pp. 576–582.
- [21] E.S. Larsen, W.W. Hong, M.L. Spartz, *Appl. Spectrosc.* 51 (1997) 1656.

# Separation of cobalt(II) from nickel(II) by solid-phase extraction into Aliquat 336 chloride immobilized in poly(vinyl chloride)

Alexandra H. Blitz-Raith<sup>a</sup>, Rohani Paimin<sup>a</sup>, Robert W. Cattrall<sup>b</sup>, Spas D. Kolev<sup>c,\*</sup>

<sup>a</sup> School of Molecular Sciences, Victoria University, Vic. 8001, Australia

<sup>b</sup> Department of Chemistry, La Trobe University, Vic. 3086, Australia

<sup>c</sup> School of Chemistry, The University of Melbourne, Vic. 3010, Australia

Received 18 January 2006; received in revised form 12 April 2006; accepted 13 April 2006

Available online 23 May 2006

## Abstract

A solid-phase absorbent obtained by the immobilization of Aliquat 336 chloride in poly(vinyl chloride) is reported to extract preferentially Co(II) from its 7 M hydrochloric acid solutions containing Ni(II). Under the experimental conditions there was no extraction of Ni(II) which allowed the complete separation of these two ions. Co(II) was rapidly and quantitatively back-extracted with deionised water. A mechanism for the extraction of Co(II) is proposed based on the formation of the ion-pair  $A^+[HCoCl_4]^-$  where  $A^+$  is the Aliquat 336 cation. Fe(III) and Cd(II), usually present in Co(II) and Ni(II) samples, were also extracted into the solid-phase absorbent though at a slower rate than Co(II) and they did not interfere with the separation of Co(II) from Ni(II). It was also demonstrated that this approach allowed the complete separation of Ni(II) from the other metal ions mentioned above.

© 2006 Elsevier B.V. All rights reserved.

**Keywords:** Solid-phase extraction; Polymer inclusion membranes; Aliquat 336 chloride; Separation of cobalt(II) from nickel(II)

## 1. Introduction

A frequently encountered problem with spectrophotometric [1] and graphite furnace atomic absorption spectrometric [2] methods for the determination of cobalt and nickel when present together is their mutual interference. A suitable method for their separation prior to the analytical measurement is solvent extraction.

Conventional solvent extraction for cobalt recovery from acidic solutions uses various systems including extraction from chloride media with basic reagents such as amines and fully substituted quaternary ammonium compounds, e.g. Aliquat 336 dissolved in diluents like kerosene [3,4]. One of the challenging aspects of this technology is to design systems that can separate cobalt from nickel because of the chemical similarities of the two elements.

An early paper by Paimin and Cattrall [5] described the solvent extraction chemistry of Co(II) from 4 M and 7 M HCl solutions using Aliquat 336 chloride dissolved in chloroform

and they reported high extraction constants for this metal ion. The stoichiometry of the extracted complex was determined and evidence that the Co(II) species extracted had the formulation  $[HCoCl_4]^-$  was provided by the same authors.

Studies in the field of ion-selective electrodes have shown that Aliquat 336 chloride acts as an excellent plasticizer for poly(vinyl chloride) (PVC) and that stable membranes [6,7] and beads [8] can easily be formed by dissolving the reagents in tetrahydrofuran (THF) and allowing the THF to evaporate. In addition to the use of such membranes in ion-selective electrodes, there is considerable interest in using PVC-based systems containing appropriate reagents for solid-phase extraction. There are examples in the literature of successful PVC-based solid-phase extraction systems for the separation of metal ions and small organic molecules [9] some of which have emanated from the laboratories of the present authors and their collaborators (i.e., Au(III) [10,11], Pd(II) [12], Cd(II) [13] and Cu(II) [14]). In some of these studies, the ions of interest were transported across an Aliquat 336 chloride/PVC membrane from a feed to a receiver solution.

It was thus of interest in the present work to evaluate such a solid-phase absorbent for the separation of Co(II) from Ni(II)

\* Corresponding author. Tel.: +61 3 8344 7931; fax: +61 3 9347 5180.  
E-mail address: [s.kolev@unimelb.edu.au](mailto:s.kolev@unimelb.edu.au) (S.D. Kolev).

from their hydrochloric acid solutions without having to use the diluent needed in a conventional solvent extraction system reported by Paimin and Cattrall [5]. Fe(III) and Cd(II) are often present in samples containing Co(II) and Ni(II). For this reason it was also of interest to study the influence of Fe(III) and Cd(II) on the separation of Co(II) from Ni(II).

## 2. Experimental

### 2.1. Reagents

Aliquat 336 chloride (Aldrich, USA) and high molecular mass PVC (Selectaphore, Fluka, USA) were used in the preparation of the solid-phase absorbent membranes. THF (BDH, UK) was HPLC grade. It was further purified by passing it through an activated alumina column to remove the stabilizer and peroxides. Standard Co(II), Ni(II), Fe(III) and Cd(II) solutions, used in the membrane extraction experiments and for calibration purposes, were prepared from  $\text{CoCl}_2 \cdot 6\text{H}_2\text{O}$ ,  $\text{NiCl}_2 \cdot 6\text{H}_2\text{O}$ ,  $\text{FeCl}_3 \cdot 6\text{H}_2\text{O}$  and  $\text{CdCl}_2 \cdot 2.5\text{H}_2\text{O}$  (all purchased from Ajax Finechem, Australia) in 1.0–10.0 M HCl (BDH, UK). MilliQ deionised water (MilliQ, USA) was used for all solution preparations.

### 2.2. Solid-phase absorbent membrane preparation

Weighed amounts of Aliquat 336 chloride and PVC with a total mass of 800 mg were dissolved in 10 ml of THF and the solution was poured into a glass ring on a flat glass plate. The THF was allowed to evaporate in air at room temperature over 12 h and a colorless and flexible membrane was obtained that contained 10, 20, 30 or 40% (m/m) Aliquat 336 chloride depending on the amount of reagent used. The membrane was then peeled from the glass plate, and used in the solid-phase extraction experiments. The membranes appeared visibly homogeneous though earlier atomic force microscopy (AFM) studies revealed that the surface in contact with air when the membrane was formed differed to some extent from the surface in contact with the glass plate [13]. With membranes containing 40% Aliquat 336 chloride this difference was found to be insignificant and both surfaces appeared smooth in the AFM images.

### 2.3. Co(II) extraction and back extraction studies

The solid-phase extraction and back extraction experiments were conducted in beakers containing 100 ml of aqueous solution and a membrane cut into four segments of approximately equal size. The solution was thermostated at 25 °C (Ratek water bath equipped with a Ratek TH5 thermal regulator, Australia) and stirred mechanically with a magnetic stirring bar at a constant rate throughout the experiment. The concentration of Co(II) in the solution at various time intervals during the extraction and back extraction experiments was monitored by taking 1.0 ml samples for analysis. Solution removed as a result of each sampling was replaced with an equal volume of the initial solution in the extraction experiments or of the back extraction solution in the back extraction experiments.

The extraction experiments were conducted using concentrations of hydrochloric acid from 1.0 to 10.0 mol l<sup>-1</sup> with the initial Co(II) concentration ranging between 60 and 336 mg l<sup>-1</sup>.

In the back extraction experiments, the 40% Aliquat 336 chloride/PVC absorbent membrane used in the extraction of Co(II) from 7.0 M hydrochloric acid solutions of 60, 100, 152, 175, 211, or 336 mg l<sup>-1</sup> Co(II), was stripped in deionised water or hydrochloric acid (0.5, 1.0, 3.0, and 5.0 mol l<sup>-1</sup>). The concentrations of the Cl<sup>-</sup> and H<sup>+</sup> ions in the back extraction solutions were measured at equilibrium. These results assisted in identifying the Co(II) species extracted into the absorbent.

### 2.4. Separation of Co(II) from Ni(II) in the absence and presence of Fe(III) and Cd(II)

Extraction experiments involving the separation of Co(II) from Ni(II) based on the use of 40% Aliquat 336 chloride/PVC absorbent membranes were conducted both in the absence or presence of Fe(III) and Cd(II). These two ions frequently accompany cobalt and nickel in their samples. These experiments were carried out similarly to the Co(II) extraction experiments outlined above. In the extraction experiments involving Co(II) and Ni(II) only, one 40% Aliquat 336 chloride/PVC absorbent membrane was used. The initial concentrations of both Co(II) and Ni(II) in their 7.0 M HCl feed solutions were 100 mg l<sup>-1</sup> and these concentrations were monitored in time. In the separation of Co(II) from Ni(II) in the presence of Fe(III) and Cd(II), five 40% Aliquat 336 chloride/PVC absorbent membrane were mechanically stirred for 60 min in a 100 ml solution where the initial concentration of each one of the metal ions involved was 25 mg l<sup>-1</sup>. The concentration of each metal ion in the feed solution was measured at the end of the extraction experiment.

### 2.5. Chemical analysis

The concentrations of Co(II), Ni(II), Fe(III) and Cd(II) in the feed and back extraction solutions were determined by flame atomic absorption spectrometry (Varian Model Spectra AA 400 spectrometer, Australia). When deionised water was used as the back extraction solution, the concentration of the H<sup>+</sup> ion was measured potentiometrically (Model B417 pH meter, Hanna Instruments, USA). The determination of the chloride ion concentration in the back extraction solution was based on direct precipitation titration with a standard 0.010 M solution of AgNO<sub>3</sub> and fluorescein indicator (Fluka, USA) [15].

## 3. Results and discussion

### 3.1. Influence of the HCl concentration on Co(II) extraction

The effect of the concentration of hydrochloric acid on the extraction of Co(II) was studied using the 40% Aliquat 336 chloride/PVC membrane composition. Membranes were in contact with 100 ml of the appropriate HCl solution (1.0–10.0 M) containing 100 mg l<sup>-1</sup> Co(II) for 60 min which was found to be an adequate time to reach equilibrium. Table 1 shows the percentage Co(II) extracted as a function of the HCl concentration. It can be

Table 1

Influence of the hydrochloric acid concentration on the percentage of Co(II) extracted into a 40% (m/m) Aliquat 336 chloride/PVC solid absorbent membrane from 100 ml of a solution containing  $100 \text{ mg l}^{-1}$  Co(II)

HCl conc. ( $\text{mol l}^{-1}$ )	1.0	2.0	3.0	4.0	5.0	6.0	7.0	8.0	9.0	10.0
Co(II) extracted (%)	10.5	13.9	17.0	18.2	23.0	29.1	34.1	35.3	35.9	36.5

seen that this percentage increases steadily with increasing HCl concentration from 1.0 to 7.0 M. This behavior is identical to that seen by Paimin and Cattrall [5] in their solvent extraction study of Co(II) into chloroform solutions of Aliquat 336 chloride. Further increase in the HCl concentration resulted in an insignificant increase in the percentage Co(II) extracted and so the optimal concentration of HCl for the extraction of Co(II) was selected as 7.0 M. The Aliquat 336 chloride/PVC membranes were found to be stable at all concentrations of HCl studied.

The relative standard deviation (RSD) for the Co(II) concentration in three replicate feed solutions (initial Co(II) concentration of  $100 \text{ mg l}^{-1}$ ) after 60 min extraction was 0.6% while the RSD for six replicate measurements of the Co(II) concentration in one of these solutions was found to be 0.1%.

### 3.2. Effect of the membrane composition on the extraction of Co(II)

The effect of the membrane composition on the extraction of Co(II) from 7.0 M HCl is shown in Fig. 1. Similarly to the solvent extraction of Co(II) from HCl solutions by Aliquat 336 chloride dissolved in chloroform [5], the amount of Co(II) extracted into the Aliquat 336 chloride/PVC membranes increased with the membrane Aliquat 336 chloride concentration. For this reason, the optimal Aliquat 336 chloride concentration was selected as 40% (m/m) and all further studies were conducted using this membrane composition.

One very interesting and important feature of the extraction curves shown in Fig. 1 is the rapid equilibration time. As can be seen equilibrium was reached in less than 60 min, which was about two orders of magnitude faster than that for comparable

PVC-based solid-phase absorbent systems studied in our laboratory where extraction was conducted from solutions of lower hydrochloric acid concentration [10,11]. We are of the opinion this is related to the species being extracted and possibly to the extraction mechanism and may have important implications in future work we are planning on using these membranes in metal ion transport studies.

### 3.3. Back extraction of Co(II)

Back extraction experiments involving different concentrations of HCl (0–5.0 M) in the back extraction solution revealed that the degree of back extraction increased by decreasing the concentration of HCl. It was established that deionised water was capable of rapid and quantitative back extraction of the Co(II) from the Aliquat 336 chloride/PVC membranes. This is demonstrated in Fig. 2 which shows both the extraction and back extraction curves for the 40% Aliquat 336 chloride/PVC membrane for an initial Co(II) aqueous concentration of  $100 \text{ mg l}^{-1}$  in 7 M HCl and deionised water as the back extraction solution. It can be seen that the total amount of Co(II) extracted was quantitatively stripped by deionised water during back extraction on the same time scale as for the extraction cycle. It should be noted that deionised water was also the back extraction solution of choice used by Paimin and Cattrall [5] in their solvent extraction system. Under these experimental conditions 35% of the Co(II) ion in the initial solution were extracted. A similar experiment conducted with initial Co(II) concentration of  $25 \text{ mg l}^{-1}$  resulted in 92.4% extraction which later was quantitatively back extracted into deionised water. When the number of membranes was increased to five, Co(II) was practically

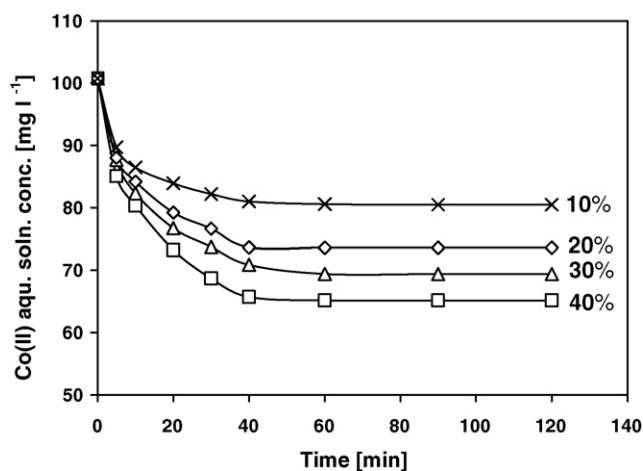


Fig. 1. Extraction vs. time curves for solid absorbent membranes containing 10% (x), 20% (◇), 30% (△) and 40% (□) (m/m) Aliquat 336 chloride/PVC (initial aqueous concentration:  $100 \text{ mg l}^{-1}$  Co(II) in 7.0 M HCl).

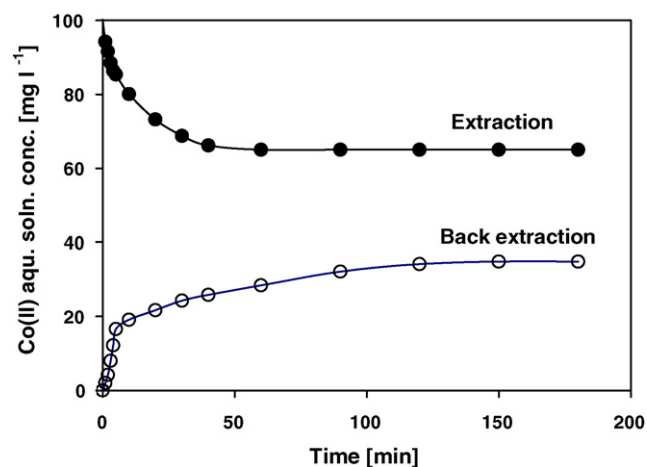


Fig. 2. Extraction and back extraction vs. time curves for Co(II) using the 40% (m/m) Aliquat 336 chloride/PVC membrane (initial aqueous solution (●)  $100 \text{ mg l}^{-1}$  Co(II) in 7.0 M HCl; back extraction solution (○) deionized water).

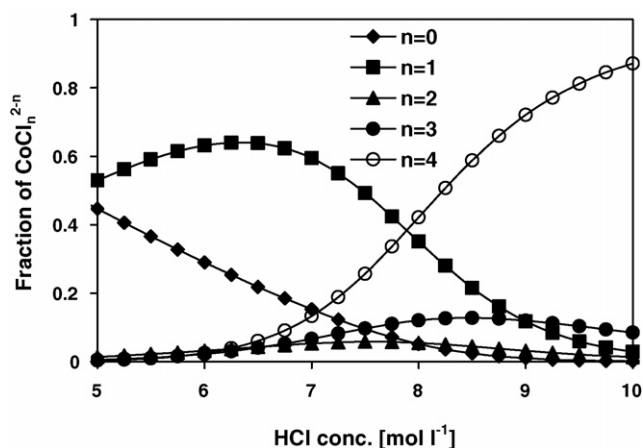


Fig. 3. Speciation diagram for aqueous Co(II) chlorocomplexes at different concentrations of hydrochloric acid.

completely extracted (99.1%). These results show that by increasing the amount of the membrane used Co(II) can be quantitatively extracted from its 7.0 M hydrochloric acid solutions.

The chemical analysis of the solutions used to back extract the membranes that had been used in the extraction of Co(II) from 60, 100, 152, 175, 211, and 336 mg l<sup>-1</sup> solutions in 7.0 M HCl revealed that the ratio between the molar concentrations of H<sup>+</sup>, Co(II) and Cl<sup>-</sup> was [H<sup>+</sup>]:[Co(II)]:[Cl<sup>-</sup>] = 1(±0.03):1(±0.05):3(±0.05). This result agrees with earlier solvent extraction studies by Paimin and Cattrall [5] who proposed that the extracted Co(II) species was [HCoCl<sub>4</sub>]<sup>-</sup> and that the extracted complex had the formula A<sup>+</sup>[HCoCl<sub>4</sub>]<sup>-</sup> where A<sup>+</sup> represents the quaternary ammonium cation of Aliquat 336.

### 3.4. Mechanism of Co(II) extraction from its hydrochloric acid solutions

In HCl solutions, Co(II) can form four chlorocomplexes, CoCl<sub>n</sub><sup>2-n</sup> where n = 1, 2, 3, 4. The distribution of these complexes as a function of the concentration of HCl between 5 and 10 M is shown in Fig. 3. The stability constants of the Co(II) chlorocomplexes (Eq. (1)) at 25 °C and concentrations of HCl higher than 5.0 M, used in the calculations of the fraction of each chloride complex, are log K<sub>1</sub> = -1.05, log K<sub>2</sub> = -2.69, log K<sub>3</sub> = -1.54, and log K<sub>4</sub> = -1.34. These values were experimentally determined by Bjerrum et al. [16].

$$K_n = \frac{[\text{CoCl}_n^{2-n}]}{[\text{CoCl}_{n-1}^{3-n}]\text{a}_{\text{Cl}^-}} \quad (n = 1, 2, 3, 4) \quad (1)$$

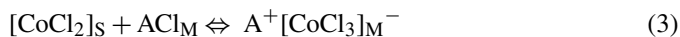
The activity of the chloride ion in Eq. (1) was calculated by the one parameter activity function (Eq. (2)) introduced by the same researchers [16].

$$\text{a}_{\text{Cl}^-} = [\text{Cl}^-]10^{([\text{Cl}^-]-0.5)} \quad (2)$$

Fig. 3 shows that the concentrations of the neutral and two negatively charged Co(II) chlorocomplexes that are capable of forming ion-pairs with the Aliquat 336 cation at the membrane/solution interface, start to increase at HCl concentrations

higher than 5.0 M. This finding agrees with the experimental results showing improved extraction of Co(II) at higher concentrations of HCl (Table 1).

The following stoichiometric equations describe possible extraction processes involving the Co(II) chlorocomplexes mentioned above (i.e., [CoCl<sub>2</sub>], [CoCl<sub>3</sub>]<sup>-</sup> and [CoCl<sub>4</sub>]<sup>2-</sup>):



where A<sup>+</sup> is the Aliquat 336 cation and subscripts S and M refer to the solution and membrane phases, respectively.

It has been established that in the solvent extraction of metal chlorocomplexes with Aliquat 336 chloride, solvents with higher viscosity favor the extraction of the smaller sized ion-pair [5]. Since the viscosity of a PVC-based plasticized membrane is considerably higher compared to the organic phases used in solvent extraction, it can be expected that the trichlorocobaltate(II) complex will be extracted preferentially into Aliquat 336 chloride/PVC membranes (Eqs. (3) and (4)) than the tetrachlorocobaltate(II) complex (Eq. (5)). In addition to the viscosity factor, the extraction of [CoCl<sub>4</sub>]<sup>2-</sup> will be inhibited because the corresponding extraction reaction (Eq. (5)) requires the participation of two adjacent interfacial Aliquat 336 chloride ion-pairs instead of one as in Eqs. (3) and (4).

Depending on the ion-pair formed, back extraction will take place according to one of the following stoichiometric equations:

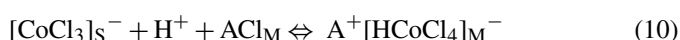


If only the two ion-pairs mentioned above (i.e., A<sup>+</sup>[CoCl<sub>3</sub>]<sup>-</sup> and A<sub>2</sub><sup>+</sup>[CoCl<sub>4</sub>]<sup>2-</sup>) are responsible for the extraction of Co(II) into Aliquat 336/PVC membranes, the [Co(II)]:[Cl<sup>-</sup>] ratio in the back extraction solution should be 1:2. However, the experimentally measured [Co(II)]:[Cl<sup>-</sup>] ratio was found to be 1:3.

This result is similar to that obtained by Paimin and Cattrall [5] in their solvent extraction studies, i.e., Co(II) is extracted into the membrane as the A<sup>+</sup>[HCoCl<sub>4</sub>]<sup>-</sup> ion-pair which upon back extraction (Eq. (8)) releases H<sup>+</sup>, Co(II) and Cl<sup>-</sup> ions in ratio [H<sup>+</sup>]:[Co(II)]:[Cl<sup>-</sup>] = 1:1:3.



The extraction process in this case can be described by Eqs. (9) and (10):



It is also possible that the formation of A<sup>+</sup>[HCoCl<sub>4</sub>]<sup>-</sup> at the membrane/solution interface may involve the aqueous complexes [HCoCl<sub>4</sub>]<sup>-</sup> and [HCoCl<sub>3</sub>] (Eqs. (11) and (12)).





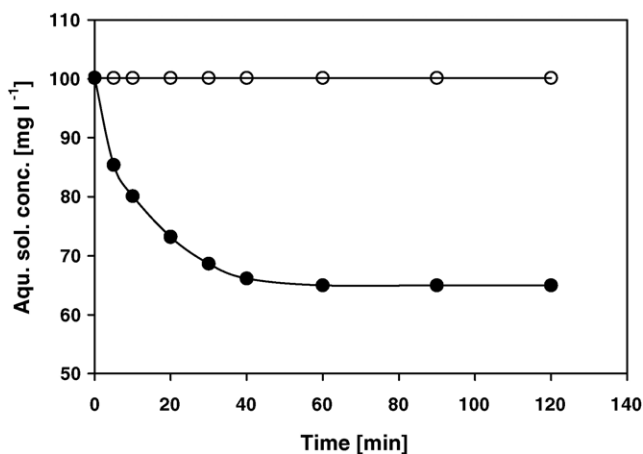


Fig. 4. Extraction vs. time curves for Co(II) (●) and Ni(II) (○) using the 40% (m/m) Aliquat 336 chloride/PVC membrane (initial solution composition: 100 mg l<sup>-1</sup> Co(II) and 100 mg l<sup>-1</sup> Ni(II) in 7.0 M HCl).

The above suggestions are supported by the work of Belousov and Ivanov [17] who confirmed the presence of complex acids of chlorocobaltate(II) species, i.e., [HCoCl<sub>3</sub>] and [H<sub>2</sub>CoCl<sub>4</sub>], in concentrated HCl. The corresponding dissociation constants were determined as  $K_d = 6.60 \times 10^2$  for [HCoCl<sub>3</sub>] and  $K_{d,1} = 6.85 \times 10^3$  and  $K_{d,2} = 3.60 \times 10^1$  for [H<sub>2</sub>CoCl<sub>4</sub>]. It can be calculated that the concentrations of both [HCoCl<sub>4</sub>]<sup>-</sup> and [HCoCl<sub>3</sub>] increase with the concentration of HCl, though their concentrations remain substantially lower (i.e., more than an order of magnitude) than those of the corresponding proton-free chloride complexes (i.e., [CoCl<sub>3</sub>]<sup>-</sup> and [CoCl<sub>4</sub>]<sup>2-</sup>).

### 3.5. Separation of Co(II) from Ni(II) in the absence and presence of Fe(III) and Cd(II)

Extraction experiments using a 7.0 M HCl solution containing 100 mg l<sup>-1</sup> of both Co(II) and Ni(II) were carried out with a 40% Aliquat 336 chloride/PVC absorbent membrane. Under these conditions rapid extraction of Co(II) took place and no extraction of Ni(II) showing that this membrane system was highly selective for Co(II) in the presence of Ni(II) (Fig. 4). The reason for this selectivity is the tendency for Ni(II) to retain its hexa-coordination in high concentrations of chloride and, unlike Co(II), does not form tetrahedral anionic chlorocomplexes.

The separation experiment involving a 100 ml 7.0 M HCl feed solution containing 25 mg l<sup>-1</sup> of Co(II), Ni(II), Fe(III) and Cd(II) and five 40% Aliquat 336 chloride/PVC absorbent membranes resulted in the extraction of 99.1% of Co(II), 99.0% of Fe(III) and 98.9% of Cd(II). Again Ni(II) was not extracted at all.

These results suggest that the 40% Aliquat 336 chloride/PVC solid absorbent offers attractive possibilities not only for the quantitative separation of Co(II) from Ni(II) but also for the efficient separation of Ni(II) from other base metal ions such as Fe(III) and Cd(II).

## 4. Conclusions

On the basis of the results obtained it can be concluded that Aliquat 336 chloride/PVC solid absorbent membranes provide an attractive alternative to conventional solvent extraction methods for the separation of Co(II) from Ni(II). These membranes show high selectivity for Co(II) in the presence of Ni(II) and allow the separation of these two metal ions in the absence and presence of other base metal ions such as Fe(III) and Cd(II) which often accompany Co(II) and Ni(II) in their samples. The back extraction of Co(II) into deionised water was found to be fast and quantitative. Ni(II) does not extract in the Aliquat 336 chloride/PVC membranes studied at all and this can be used for the separation of Ni(II) from other metal ions.

Further studies regarding the possibilities of separating Co(II) from Ni(II) in the presence of a wider range of metal ions are currently in progress. In addition, the application of the solid absorbent in the form of beads is also underway and with the much larger surface area available with beads than for membranes, it is to be expected that extraction and back extraction will be much faster.

## Acknowledgement

S.D. Kolev and R.W. Catrall thank the Australian Research Council for project funding under its Discovery Project scheme.

## References

- [1] R.S.L.C. Ferreira, C.A.C. Spinola, D.S. de Jesus, Talanta 43 (1996) 1649.
- [2] S. Akman, G. Doner, Spectrochim. Acta B 50B (1995) 975.
- [3] M. Cox, in: J. Rydberg, C. Musikas, G.R. Choppin (Eds.), Solvent Extraction in Hydrometallurgy. Principles and Practices of Solvent Extraction, Marcel Dekker, Inc, New York, 1992 (Chapter 10).
- [4] R.-S. Juang, H.-C. Kao, Sep. Purif. Technol. 42 (2005) 65.
- [5] R. Paimin, R.W. Catrall, Aust. J. Chem. 36 (1983) 1017.
- [6] G.J. Moody, R.B. Oke, Analyst 95 (1970) 910.
- [7] R.W. Catrall, Polymer membrane potentiometric chemical sensors, in: R.G. Compton (Ed.), Chemical Sensors, Oxford Chemical Primers no. 52, Oxford University Press, Oxford, 1997 (Chapter 3).
- [8] I. Tsagkatakis, S. Peper, R. Retter, M. Bell, E. Bakker, Anal. Chem. 73 (2001) 6083.
- [9] L.D. Nghiem, P. Mornane, I.D. Potter, J.M. Perera, R.W. Catrall, S.D. Kolev, J. Membr. Sci. (in press).
- [10] G. Argiropoulos, R.W. Catrall, I.C. Hamilton, S.D. Kolev, R. Paimin, J. Membr. Sci. 138 (1998) 279.
- [11] S.D. Kolev, G. Argiropoulos, R.W. Catrall, I.C. Hamilton, R. Paimin, J. Membr. Sci. 137 (1998) 261.
- [12] S.D. Kolev, R.W. Catrall, R. Paimin, I.D. Potter, Y. Sakai, Anal. Chim. Acta 413 (2000) 241.
- [13] L. Wang, R. Paimin, R.W. Catrall, S. Wei, S.D. Kolev, J. Membr. Sci. 176 (2000) 105.
- [14] Y. Baba, K. Hoaki, J.M. Perera, G.W. Stevens, T.J. Cardwell, R.W. Catrall, S.D. Kolev, in: Proceedings of the Sixth World Congress of Chemical Engineering, Melbourne, Australia, 2001 (Conference Media CD).
- [15] W.J. Williams, Handbook of Anion Determination, Butterworths, London, 1979.
- [16] J. Bjerrum, A.S. Halonin, L.H. Skibsted, Acta Chem. Scand. A 29 (1975) 326.
- [17] E.A. Belousov, V.M. Ivanov, Russ. J. Phys. Chem. 51 (1977) 314.

## Potentiometry as a method of antioxidant activity investigation

Kh.Z. Brainina<sup>a,\*</sup>, A.V. Ivanova<sup>a</sup>, E.N. Sharafutdinova<sup>a</sup>, E.L. Lozovskaya<sup>b</sup>, E.I. Shkarina<sup>b</sup>

<sup>a</sup> *Urals State University of Economics, 62, 8 March St., 620219 Ekaterinburg, Russia*

<sup>b</sup> *Biochemical Physics Institute of RAS, Moscow, Russia*

Received 4 August 2005; received in revised form 1 March 2006; accepted 3 March 2006

Available online 18 April 2006

### Abstract

Problems of terminology applied for antioxidant properties of substances are being discussed. Selection of the term ‘Antioxidant Activity’ is being proved. New method of the determination of this index is offered, where electrode potential shift as a result of redox chemical reaction between substance to be determined and oxidized form of mediator system serves as a source of information. Good correlation is fixed between data obtained by potentiometric method and known chemiluminescent, Radox methods, and photometric method with the use of stable radical 2,2-diphenyl-1-picrylhydrazyl. Accuracy and reliability of the results, simplicity of the analysis procedure and its self-descriptiveness make the method offered to become good alternative to the known methods of antioxidant activity determination.

© 2006 Elsevier B.V. All rights reserved.

**Keywords:** Potentiometry; Antioxidant activity; Herbal extracts; Wine

### 1. Introduction

Free radicals participate and are being formed in biochemical reactions providing organism cells’ vital functions. Negative impact of various environmental factors may lead to excess free radicals formation and as a result—to oxidative stress rise. Oxidative stress causes diseases and fastens organism ageing in general [1]. On the other hand activated oxygen metabolites containing no unpaired electron are formed in living organisms. Above-mentioned metabolites are not free radicals but manifest oxidative properties and are able to generate radicals. Concept ‘activated oxygen metabolites’ successfully comprises compounds both of radical and non-radical nature. Complex of compounds of the kind is illustrated by diagram from the above-cited book.

Active oxygen compounds (AOC) are of great interest particularly because of their dual role in living organism, i.e. damage of organism cells and tissues and protection from external health effects. At the same time it should be taken into consideration that not only compounds containing unpaired electron, namely free radicals, are toxic but also other oxygen compounds (see [Diagram 1](#)). Usually AOC are strong oxidizers but in some cases,

depending on environment, some of them ( $O_2^{\bullet-}$ ,  $H_2O_2$ ) perform reductive properties.

System protecting organism from free radical excess comprises enzymes with oxide reductase activity, non-enzyme proteins, polypeptides, water and oil soluble vitamins, SH—containing amino acids, flavonoids, carotinoids, etc. [1]. Most of the compounds listed prevent oxidative stress evolution interrupting chain oxidative reactions. That is why these substances are called both substances with antiradical activity and antioxidants (AO). Foodstuff and nutrients serve as a source of most of antioxidants.

Unfortunately terminology in this sphere is not established yet. It is proposed to distinguish ‘reductant’ (reducing agent in chemical sense of the word) and ‘antioxidant’ or ‘bioantioxidant’. Prior and Cao [2] suggest to call antioxidant ‘substance that, when present at low concentrations compared with those of oxidisable substrate, significantly prevents or delays a prooxidant initiated oxidation of the substrate’. The latter practically coincides with definition given earlier by Gutteridge [3].

Benzie and Strain [4] suggest to consider ‘antioxidant’ as ‘generic form describing a group of compounds which may prevent the generation of oxidizing species, remove such species or inactivate them thus preventing, delaying or minimizing oxidisable changes to important biomolecules’.

Thus from the data given above it is difficult to find difference between meanings of ‘reductive agent’ and ‘antioxidant’,

\* Corresponding author. Tel.: +7 343 257 2415.  
E-mail address: [baz@usue.ru](mailto:baz@usue.ru) (Kh.Z. Brainina).

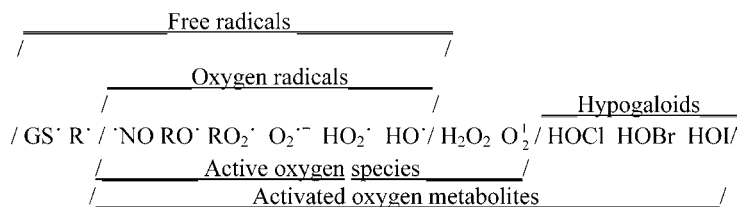


Diagram 1. Free radicals and active oxygen compounds.

‘reductant’ and ‘antioxidant’. When discussing this problem it should be taken into consideration that ‘reductants’ and ‘antioxidants’ are donors of electrons and AOC are acceptors of electrons. Of course, thermodynamic possibility of the reaction between them is determined by the ratio redox potentials of the corresponding systems; reaction rate is determined by kinetics of the components’ interaction. Thus to determine antioxidants concentration, reagents should be selected to provide thermodynamic possibility of chemical reaction with substance to be determined and reaction of the reagents rate should be high enough. By the way, mentioned in [2] FRAP impossibility of reduced glutathione determination is caused obviously by the fact that one or both of above mentioned conditions are not fulfilled.

Problem to be discussed is if it is correct enough to determine AO using oxidation/reduction reactions. From general point of view it seems clear that reaction of radical with antioxidant giving electron away (oxidation) leads to radical removal from oxidation chain. This is equivalent to inhibition reaction which serves the base of the most widely used methods of AO determination [5–8]. On the other hand this conclusion obviously is not unambiguous. Radical compounds are intermediate products of some antioxidants oxidation reactions. They, depending on electron and steric factors, are able either to take part in chain oxidation reactions, i.e. manifest prooxidative properties, or to be oxidized, manifesting essentially antioxidant properties. It is also known that some oxygen radicals manifest reductive properties, i.e. are able to react like antioxidants. The same is characteristic for variable valence ions (Fe<sup>2+</sup>, Cu<sup>+</sup>, etc.) and hydrated electron forming as a result of water radiolysis.

Thus to evaluate biological AO properties of the compound one needs to take into consideration at least some factors:

- Dual role, which some antioxidants can play in mutagenesis and carcinogenesis. For example hydroxyl groups of phenolic antioxidants would undergo autooxidation into quinoid structures followed by redox cycling, which would generate reactive AOC. So phenolic antioxidant some times behave like prooxidants. Nevertheless, usually they react with free radicals produced by other compounds and act as radical ‘traps’ manifest themselves as antioxidants. Thus, these molecules have the potential of acting as both pro- and antioxidants depending on redox state of their biological environment. In the cellular environment, these two opposing effects may be competitive.
- Synergism: it is known that reactions of reciprocal reduction and replenishment of ascorbic acid pool are available due to

glutathione regenerating ascorbate [9] and ascorbate regenerating  $\alpha$ -tocopherole) [10].

Cumulative action of all antioxidants present in plasma and body fluids, providing an integrated parameter, than the simple sum of measurable antioxidants should be taken into consideration. Thus, capacity of known and unknown antioxidants and their synergistic interaction will be assessed [2].

Taking into consideration above discussed problems it is worth concluding that complex parameter antioxidant activity (AOA) is much more informative than data on content of individual AO in the investigated sample.

Unfortunately no method exists to provide total information on state and interactions of such complicated systems in which antioxidants, prooxidants and oxidants react. Also there is no common term to determine antioxidant properties of the compound or compound complex. It is supposed to distinguish [11] “antioxidant capacity” and “antioxidant activity”. The first one means measure of the moles of given free radical scavengers by a test solutions. Rate constant of antioxidant acting against free radicals is considered as antioxidant activity [11]. Such terms as “antioxidant power” [4] and “antioxidant ability” [12] are also used as a measure of AO concentration. Thus mixture of thermodynamic and kinetic comprehensions is fixed. In general term ‘activity’ is used as thermodynamic and it should not be applied as kinetic one.

Further in this work following [12] we will consider terms antioxidant activity, capacity, power, ability as synonyms, in thermodynamic sense, and connecting them with concentration (activity) of substance or group of substances. Radical oxidation chain break registration would provide information on AO effective impact as scavenging agents. But it is still impossible and methods of AO determination (TRAP, TOSC, TEAC, ORAC) are based on reduction reaction.

Trolox equivalent capacity (TEAC) assay is based on antioxidants’ ability to reduce radical cations 2,2’-azinobis(3-ethylbenzotiazoline 6-sulfonat) (ABTS) and thus to inhibit absorption in long wave part of the spectra (600 nm). Water soluble Vitamin E derivation Trolox [5] is applied as a standard in this case.

Oxygen radical absorption capacity (ORAC) [13] method presumes registration of substrate (B—phycoerythrin or fluorescein) fluorescence [2] after reaction with AO in the sample to be investigated in comparison with reference template. To determine peroxy radicals Trolox again is used as a standard, to determine hydroxyl radicals—gallic acid is used.

Total radical trapping parameter (TRAP) assay is rather widely used in investigations and has various modifications

[5,7,8,14]. This method presumes antioxidants' ability to react with peroxy radical 2,2'-azobis(2-amidinopropan)dihydrochloride (AAPH). TRAP modifications differ in analytical signal registration methods. Mostly finishing stage of analysis constitutes peroxy radical AAPH reaction with luminescent (luminol), fluorescent (dichlorofluorescein-diacetate, DCFH-DA) or other optically active substrate. Trolox is also most often used as a standard.

In ferric reducing/antioxidant power (FRAP) assay reaction of Fe(III)-tripiridyltriazine reduction to Fe(II)-tripiridyltriazine is used. The last one is brightly blue and its' absorption band is 593 nm [4,12].

It is easy to notice that all the methods described, despite substrate reacting with antioxidants: either long living radicals (TEAC, TRAP), AOS (ORAC), or iron complex compound (FRAP), are based on reduction reaction.

Radicals stand as electron acceptors and in all above listed methods the ability of antioxidants to reduce radicals is being determined. As a rule, Trolox is used as a standard, i.e. and AO concentration or sum of AO concentrations is determined.

Obviously, it is worth while to agree with Prior and Cao [2] that all methods of AO determination have various disadvantages. EPR spectra registration is direct method. But very short radical life time and a great number of parallel reactions in which they participate do not allow one to follow effect of one or another AO.

Thus, if we agree that electron donors are the main substances scavenging radicals, providing radical reaction chain break, destroying or inactivating oxidizers by means of electron transfer from "antioxidant" to the oxidant, it should be accepted that consumption of correctly selected mediator in redox chemical reaction provides information on 'antioxidant' concentration (activity).

From this point of view it is essential what is meant by 'correctly selected mediator'. Most of oxygen radicals are strong oxidizers, which fact determines high values of redox potentials of the system radical—its reduced form, for example,  $E_{\text{OH}/\text{OH}^-} = 1.55 \text{ V}$  relative to normal hydrogen electrode [15]. Redox potentials of widely used AO vary from  $-0.42$  to  $+0.30$  [16]. Consequently mediator should meet the following condition:

$$E_{\text{Rad}/\text{Rad}(\text{red})}^0 > E_{\text{Ox}/\text{Red}}^0 > E_{\text{AOox}/\text{AOred}}^0$$

where  $E_{\text{Rad}/\text{Rad}(\text{red})}$  is the redox potential of the pair oxidized/reduced AOC;  $E_{\text{Ox}/\text{Red}}^0$  is the redox potential of mediator system;  $E_{\text{AOox}/\text{AOred}}^0$  is the redox potential of the pair oxidized/reduced antioxidant.

By the way, FRAP method [4,12] applies iron complex compounds, not oxidizing SH—which fact causes known disadvantage of the discussed method. It can be considered as an example of "incorrect" selected cyctem.

The second condition of 'correctly selected mediator' is rather high rate of chemical reaction with basic antioxidants.

And in the third place—passing of any signal forming reaction providing chemiluminescence, luminous energy absorption or electrode potential shift. The first two of the approaches men-

tioned demand additive reagent introduction. The last one is free of above disadvantages.

In this work potentiometric method of antioxidant activity determination is proposed. The results obtained with the use of potentiometric method and widely used methods of chemiluminescence, Radox and photometric with the use of stable radical 2,2-diphenyl-1-picrylhydrazyl (DPPG) are compared.

## 2. Materials and methods

### 2.1. Instrumentation

Potentiometric measurements were carried out with the use of tester AOT-1 (IVA, Russia) and voltmeter III-300 (Russia). ORP-electrode "Phoenix" (USA) served as a working electrode.

Photometer KFK-3 (Zagorsk, Russia) with glass cuvette ( $l = 10 \text{ mm}$ ) and spectrophotometer UVIKON 930 (Tegimenta AG Company) were used for optical measurements.

For assessment of AO activity by chemiluminescent (CL) method the device developed by I.I. Sapezhinskiy (Biochemical Physics Institute of RAS) was used [17,18].

### 2.2. Reagents

$\text{K}_4[\text{Fe}(\text{CN}_6)]$  and  $\text{K}_3[\text{Fe}(\text{CN}_6)]$  (Reachim, Russia) qualified as 'pure',  $\text{KHPO}_4$  and  $\text{NaHPO}_4$  (Reachim, Russia) qualified as 'pure for analysis', methanol qualified as 'chemically pure', ascorbic acid (pharmacopeia), 2,2-diphenyl-1-picrylhydrazyl (ICN Biomedical, USA), reagent set by Radox Laboratories Ltd. (UK), glycyl-tryptophane (Gly-Trp) (Reanal, Hungary), riboflavine (Merck), the other reagents were of chemically purity grade.

### 2.3. Investigated substances

Wine, herbs, extracts, infusions and balms were purchased in retail.

Water and water-alcohol extracts of herbs were prepared as follows: 1 g of grinded herb material was poured by distilled water or 50% water-alcohol solution up to volume 10 ml and kept in hermetic test-tubes at  $60^\circ\text{C}$  for 18 h.

### 2.4. Methods

#### 2.4.1. Potentiometry

To determine antioxidant activity chemical interaction of antioxidants with mediator system  $\text{K}_3[\text{Fe}(\text{CN}_6)]/\text{K}_4[\text{Fe}(\text{CN}_6)]$  leading to its' redox potential shift was used. Reaction was carried out in K-Na-phosphate buffer solution pH 7.2. Electrode potentials were measured before (1) and after (2) introduction of the sample investigated:

$$E = E_0 + b \lg \frac{C_{\text{ox}}}{C_{\text{red}}}, \quad (1)$$

$$E_1 = E_0 + b \lg \frac{C_{\text{ox}} - X}{C_{\text{red}} + X}. \quad (2)$$



Antioxidant activity (concentration) in the solution is calculated according to formula:

$$AOA = \pm \frac{C_{ox} - \alpha C_{red}}{1 + \alpha}, \quad (3)$$

where  $E$  and  $E_1$  are the potentials maintaining in the system before and after analyzed antioxidant introduction (V);  $E_0$  is the standard potential of mediator system (V);  $C_{ox}$  is the concentration of mediator oxidized form (M);  $C_{red}$  is the concentration of mediator reduced form (M);  $X$  is the concentration of reacting antioxidant (eq/l); AOA is the antioxidant activity;  $\alpha = 10^{(E_1 - E)/b}$ ;  $b = 2.3RT/nF$ , Eqs. (2) and (3) can be given as it is done above if  $n = 1$ .

Taking into consideration the fact that solution ionic force practically remains constant and the source of information is potential shift, but not its absolute value it is correct enough not to distinguish between activity and concentration. Just the last value is used further for antioxidant activity characterization.

#### 2.4.2. Radox

Radox method represents standardized Trolox equivalent capacity (TEAC) modification. The determination was based on inhibition of 2,2-azinbis(3-ethylbenzothiazine-6-sulfonate) (ABTS) absorption by antioxidants at 600 nm. ABTS radicals were obtained as a result of interaction of methmyoglobin with  $H_2O_2$ . Absorption of solution containing ABTS and methmyoglobin before and after introduction of a substrate (hydrogen peroxide) was measured.

Measurements were held for solutions of:

- (i) ABTS + methmyoglobin +  $H_2O$ , parameter  $D_1$  is determined;
- (ii) ABTS + methmyoglobin +  $H_2O_2$ , parameter  $D_2$  is determined;
- (iii) ABTS + methmyoglobin + Trolox, parameter  $D_3$  is measured;
- (iv) ABTS + methmyoglobin + Trolox +  $H_2O_2$ , parameter  $D_4$  is measured;
- (v) ABTS + methmyoglobin + sample to be investigated, parameter  $D_5$  is measured;
- (vi) ABTS + methmyoglobin + sample +  $H_2O_2$ , parameter  $D_6$  is measured.

Three minutes were allowed to pass after mixing ingredients before parameters  $D$  measurements.

Antioxidant activity was calculated using the formula suggested by analytical set producer:

$$AOA = \frac{1.7}{(D_2 - D_1) - (D_4 - D_3)} [(D_2 - D_1) - (D_6 - D_5)].$$

Antioxidant activity was given in mM/l of Trolox.

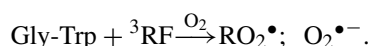
#### 2.4.3. Photochemiluminescent method

The assessment of AO activity was performed by chemiluminescent (CL) method in the model system of photooxidation of peptide Gly-Trp using the riboflavine (RF) as a photosensitizer. The buffer solution containing 0.1 mM Gly-Trp,

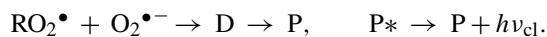
$2 \times 10^{-5}$  M riboflavine and testing sample was irradiated with monochromatic light with  $\lambda = 436$  nm (in the absorption band of riboflavine). Light of this wavelength was isolated from the emission of the mercury lamp using a combination of colour filters. Irradiation performed at the room temperature with stirring. Within 60 s the irradiated solution was pumped in to a cell of a highly sensitive photometric device and the chemiluminescence signal was recorded with the automatic recorder.

The process of CL induction during RF-sensitized photooxidation of Gly-Trp can be demonstrated by the following scheme:

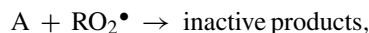
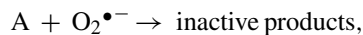
1. Free radicals formation:



2. Registration of CL signal:



3. Antioxidant effect (A is the antioxidant):



where  ${}^3RF$  is riboflavine triplet;  $RO_2^{\bullet}$ —Gly-Trp peroxide radical; D is the dioxetan, intermediate product of Gly-Trp oxidation;  $P^*$  is the product responsible for CL.

As follows from the scheme, CL yield would be decreased upon introduction of substances that scavenge free radicals.

The following parameters of AO activity were used:

- 1)  $C_{1/2}$  is the 50% inhibition concentration—the concentration in testing sample at which the chemiluminescence intensity decreased by 50% (the CL intensity without tested product was taken as a reference). Concentration of tested samples was expressed in volumetric percentage.
- 2) Parameter “A” (mg/ml)—the total content of antioxidants in rutin equivalents:

$$A = \frac{C_{1/2}^R}{C_{1/2}^X} \times 100\%,$$

where  $C_{1/2}^R$  is the 50% inhibition concentration of rutin;  $C_{1/2}^X$  is the 50% inhibition concentration in testing sample.

#### 2.4.4. Photocolorimetry

Interaction of AO and 2,2-diphenyl-1-picrylhydrazyl was held in argon saturated water–alcohol media. DFPG solution maximum optical density is observed at 550 nm. For AOA concentration determination difference of optical density before and after addition of solution containing AO or herbal extract were measured. Ascorbic acid was selected as a standard. Anti-DFPG



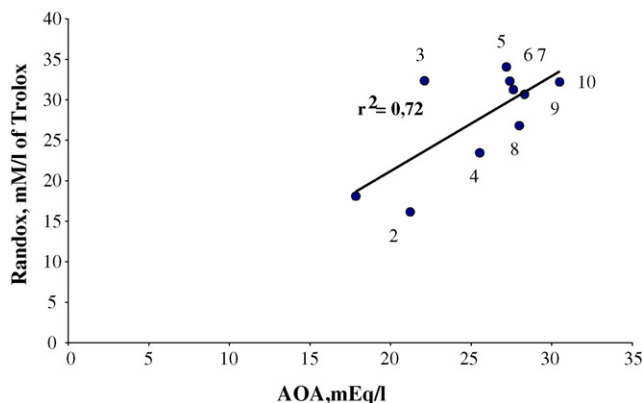


Fig. 1. Comparison of results of AOA determination in various wine samples obtained by Radox and potentiometric methods. Wine samples: (1) Sophia, Merlot, Bulgaria; (2) Vin de Pays d'Oc Jean de Beauvais, Merlot 2002, France; (3) Trivento Bonarda 2003, Argentina; (4) Tsar Assen, Cabernet Sauvignon 2002, Bulgaria; (5) Uina Hermina, Rioja 2002, Spain; (6) Sophia, Cabernet Sauvignon 2001, Bulgaria; (7) Oltina, La revedere, Sweden; (8) Sunny ridge, Cabernet Sauvignon 2002, South Africa; (9) El Condor, Cabernet Sauvignon 2002, Chile; (10) Pravova Valley, Sangiovese 1999, Special reserve, Romania.

activity was calculated using the expression:

$$A = \frac{D}{B},$$

where  $A$  is the anti-DFPG activity (eq/l);  $D$  is the optical density of 2,2-diphenyl-1-picrylhydrazyl solution;  $B$  is the slope of the dependence of 2,2-diphenyl-1-picrylhydrazyl optical density versus ascorbic acid solution concentration.

### 3. Results

Fig. 1 shows the results of AOA determination by potentiometric method and Radox method for analysis of 10 wine samples.

Correlation coefficient is 72%.

Comparison of the results of AOA of herbal extracts and balsams obtained by potentiometric and chemiluminescent methods is shown on Fig. 2.

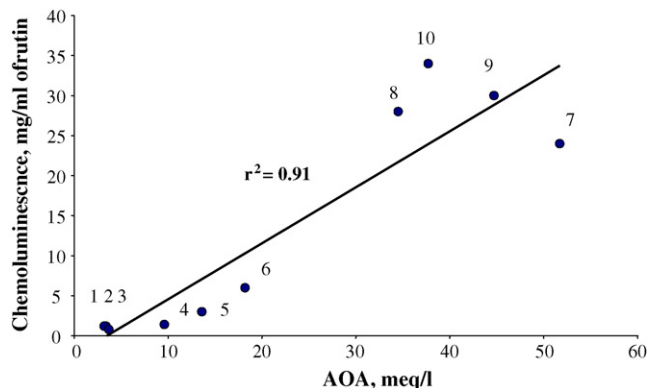
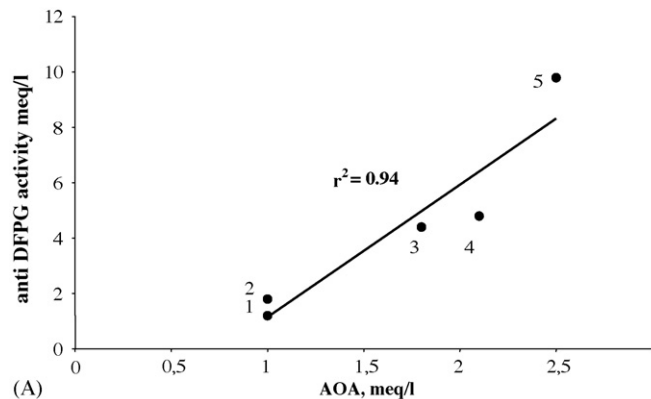
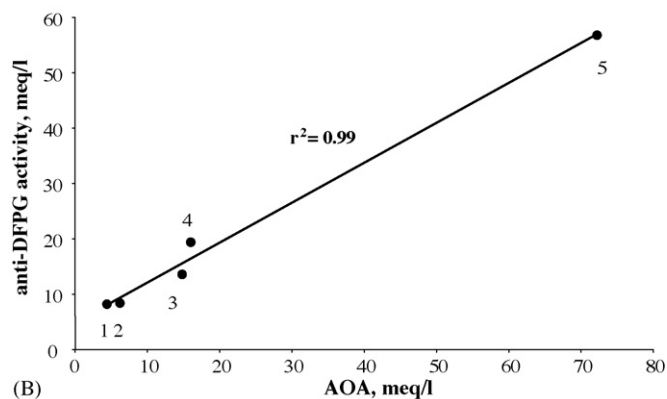


Fig. 2. Comparison of the results of AOA determination in herbal extracts and balsams obtained by potentiometric and chemiluminescent methods. Samples: (1) Vlasov balsam; (2) immunal; (3) Echinopanax elatum extract; (4) Altay balsam; (5) Ochakov balsam; (6) Tincture #9; (7) balsam Pervoprestolny; (8) leusea extract; (9) Rotokan; (10) eleuterocock extract.



(A)



(B)

Fig. 3. Comparison of the results of AOA of (A) and water-herb (B) herb extracts obtained by photometric method with the use of 2,2-diphenyl-1-picrylhydrazyl stable radical and by potentiometric method. Investigated samples: (1) haws; (2) juniper fetus; (3) Acorus calamus rhizome; (4) dandelion roots; (5) oak bark.

Correlation coefficient is 91%.

Fig. 3 shows the results of AOA potentiometric and photometric determination of antioxidant activity of water and alcohol herb extracts with the use of diphenylpicrylhydrazyl stable radical.

Correlation coefficients were 94% for water and 99% for alcohol extracts.

Difference in correlation coefficient obtained for wine and herbal extracts can be determined using methods based on different radical oxidative reactions and different nature of the samples. Taking into account different reactions serving as signal generating in the methods mentioned, correlation should be accepted as very good.

### 4. Conclusion

In the work presented methods for comparison were selected in which long living radicals (ABTS, DFPG) or super-oxid anion (chemiluminescence) served as oxidant-prooxidant model. Antioxidant activity values measured with suggested potentiometric method correlate well with antioxidant activity determined by chemiluminescent, Radox methods and photometric method with the use of stable radical 2,2-diphenyl-1-picrylhydrazyl. Correlations are linear, correlation coefficients approach 1.

Results obtained demonstrate that suggested potentiometric method provides objective and reliable information on antioxidant activity of various samples. Method suggested is express and does not need expensive instrumentation and reagents. These are its' undoubted advantages.

Result validation and reliability, self-descriptiveness, simple way of carrying out analysis make suggested method good alternative to known methods of antioxidant activity determination.

At the same time we realize that information obtained by suggested potentiometric method is fully correct only for assessment of donor–acceptor electron properties of investigated systems. As other widely used methods, it gives no direct information on kinetics and mechanism of radical oxidation chain break by investigated antioxidants.

### Acknowledgements

The financial support of ISTC, project 2132 and INTAS No. 00-273 is acknowledged. The authors thank Dr. Lo Gorton (University of Lund, Lund, Sweden) for provision to make Randox test.

The authors thank Dr. Elena B. Burlakova (Biochemical Physics Institute of RAS, Moscow, Russia) for her valuable comments.

### References

- [1] N.K. Zenkov, V.Z. Lankin, E.B. Menschikova, *Oxidative Stress*, Maik Nauka/Interperiodika, 2001.
- [2] R.L. Prior, G. Cao, *Free Radic. Biol. Med.* 27 (1999) 1173.
- [3] J.M.C. Gutteridge, *NATO ASI Series*, vol. H92, Springer-Verlag, Berlin, Heidelberg, NY, 1995, pp. 157–164.
- [4] I.F.F. Benzie, J.J. Strain, *Methods Enzymol.* 299 (1999) 15.
- [5] C. Rice-Evance, N.J. Miller, *Methods Enzymol.* 234 (1994) 279.
- [6] D.D.M. Wayner, G.W. Burton, K.U. Ingold, S. Locke, *FEBS Lett.* 187 (1985) 33.
- [7] H. Alho, J. Leinonen, *Methods Enzymol.* 299 (1999) 14.
- [8] M. Valkonen, T. Kuusi, *J. Lipid Res.* 38 (1997) 823.
- [9] J.E. Packer, T.F. Slater, R.L. Wilson, *Nature* 278 (1979) 737.
- [10] R. Stoker, M.J. Weidemann, N.H. Hunt, *Biochim. Biophys. Acta* 881 (1986) 391.
- [11] A. Gizelli, M. Serafini, F. Natella, C. Scaccini, *Free Radic. Biol. Med.* 29 (2000) 1106.
- [12] I.F.F. Benzie, J.J. Strain, *US Patent* 6,177,260 (2001).
- [13] G. Gao, C.P. Verdon, A.H. Wu, R.L. Prior, *Clin. Chem.* 41 (1995) 1738.
- [14] A. Gizelli, M. Serafini, G. Maiani, E. Assini, A. Ferro-Luzzi, *Free Radic. Biol. Med.* 27 (1994) 29.
- [15] A.J. Bard (Ed.), *Standard Potentials in Aqueous Solutions*, Marcel Dekker Inc., New York, 1985.
- [16] V.I. Slesarev, *The Principles of Chemistry of Living Being*, Chimizdat, St-Peterburg, 2001.
- [17] E.L. Lozovskaia, E.N. Makareeva, Iu.V. Makedonov, I.I. Sapejinskiy, *Biophysics (Russia)* 43 (1991) 549.
- [18] E.L. Lozovskaia, I.I. Sapejinskiy, *Biophysics (Russia)* 38 (1993) 31.

# A comparative study of chemical modifiers in the determination of total arsenic in marine food by tungsten coil electrothermal atomic absorption spectrometry

Carlos G. Bruhn<sup>a,\*</sup>, Catherine J. Bustos<sup>a</sup>, Katia L. Sáez<sup>b</sup>,  
José Y. Neira<sup>a</sup>, Solange E. Alvarez<sup>a</sup>

<sup>a</sup> Departamento de Análisis Instrumental, Facultad de Farmacia, Universidad de Concepción, P.O. Box 237, Concepción 4039200, Chile

<sup>b</sup> Departamento de Estadística, Facultad de Ciencias Físicas y Matemáticas, Universidad de Concepción, P.O. Box 237, Concepción 4039200, Chile

Received 26 January 2006; received in revised form 8 March 2006; accepted 9 March 2006

Available online 18 April 2006

## Abstract

Three platinum group elements (Pd, Ir and Rh) both in solution and in pre-reduced form, and also combined with  $\text{Mg}(\text{NO}_3)_2$  or ascorbic acid, were assessed as possible chemical modifiers on the atomization of As in digest solutions of seafood matrices (clam and fish tissue) by tungsten coil electrothermal atomic absorption spectrometry (TCA-AAS) and compared without a modifier. Of 28 modifier alternatives in study including single form and binary mixtures, and based on maximum pyrolysis temperature without significant As loss and best As absorbance sensitivity during atomization, three modifiers: Rh (0.5  $\mu\text{g}$ ), Ir (1.0  $\mu\text{g}$ ) and Rh (0.5  $\mu\text{g}$ ) + ascorbic acid (0.5  $\mu\text{g}$ ), at optimum amounts were pre-selected and compared. The definitive modifier (rhodium (0.5  $\mu\text{g}$ )) was selected by variance analysis. The mean within-day repeatability was 3% in consecutive measurements (25–300  $\mu\text{g l}^{-1}$ ) (three cycles, each of  $n=6$ ) and showed good short-term stability of the absorbance measurements. The mean reproducibility was 4% ( $n=18$  in a 3-day period) and the detection limit ( $3\sigma_{\text{blank}}/\text{slope}$ ) was 42 pg ( $n=16$ ). Quantitation was by standard additions to compensate for matrix effects not corrected by the modifier. Three sample digestion procedures were compared in fish and clam tissue samples: microwave acid digestion alone (A) or combined with the addition of 2% (m/v)  $\text{K}_2\text{S}_2\text{O}_8$  solution followed either by UV photo-oxidation (B) or re-digestion in a thermal block (C). The accuracy was established by determination of As in certified reference material of dogfish muscle (DORM-2). Procedures B and C showed good recoveries (102% ( $n=4$ ) and 103% ( $n=7$ ), respectively), whereas procedure A was not quantitative (85%). The methodology is simple, fast, reliable, of low cost and was applied to the determination of total As in lyophilized samples of clam and fish collected in the Chilean coast.

© 2006 Elsevier B.V. All rights reserved.

**Keywords:** Chemical modifiers; Arsenic; Tungsten coil electrothermal atomizer; Sample pretreatment; Lyophilized clam; Lyophilized fish

## 1. Introduction

Arsenic (As) is a worldwide recurring pollutant of natural origin commonly associated with ores of metals like copper, lead, and gold [1]. This metalloid is found in the environment in several chemical forms [2], and is well known as a source of serious health effects by prolonged intake even at low concentrations. In particular, inorganic As (As(III) + As(V)) is extremely toxic and long-term exposure has been associated with cancers of the skin and internal organs (e.g., bladder, lung) as

well as various non-cancerous disorders (e.g., keratoses, hyperpigmentation) [3,4], whereas methylated species such as monomethylarsonic acid (MMA), di-methylarsinic acid (DMA), and tri-methylarsine oxide (TMAO) have a moderate toxic effect on humans and biota, and the cationic species arsenobetaine (AsB) and arsenocholine (AsC) are considered non-toxic [2,5]. The main exposure routes to As in humans are dietary and drinking water ingestion. Among dietary sources, seafood exposures might be of concern because As concentrations can be orders of magnitude higher than those associated with other food groups. Also, naturally occurring As is very broadly distributed in many subsurface drinking water aquifers around the globe [6,7]. In Latin America, particularly in Central and Northern Chile, copper mining and smelting is a major source of contamination by

\* Corresponding author. Tel.: +56 41 203027; fax: +56 41 226382.  
E-mail address: [cbruhn@udec.cl](mailto:cbruhn@udec.cl) (C.G. Bruhn).

As, and a few smelters in this area are responsible of a large fraction of As emissions [8]. Besides, the soils and aquifers in the North of Chile are characterized by high As content due to the geomorphology exceptionally rich in As [9]. Hence, owing to natural and anthropogenic contamination and to the high mobility and bioavailability of As species, diffusion throughout the food chain including water and food for human consumption, is expected.

Actually, there is still a need of reliable and simple analytical methods and procedures for As determination in different food sources, because the determination of total As continues to be highly relevant in order to provide reliable data on the total content of As in seafood and other matrices. Among atomic spectrometric techniques, during the last decade electrothermal atomic absorption spectrometry (ET-AAS) with a tungsten coil atomizer (TCA) has shown noteworthy features as a supplementary atomization source to the flame. For small laboratories and service organizations with restricted instrumental budget the study of alternative atomization means in ET-AAS is suitable and relevant. According to a recent review [10], tungsten devices in analytical atomic spectrometry continue to provide simple and versatile atomizer alternatives. In 1988, Berndt and Schaldach [11] proposed the use of a double-layer coiled tungsten filament (150 W) which offers some advantages to enable the determination of As in solution samples, such as low power supply requirements, fast heating and low cost of the coils [12]. Though, some disadvantages limit its use, for example lack of a TCA commercial system, atomization under non-isothermal conditions, short residence time of the atomic vapor and matrix effects are produced in the solid and gaseous phase. Lately, in this research group our efforts aimed to contribute to the elucidation of these inconveniences.

One of the approaches pursued to minimize matrix effects is the use of chemical modifiers in trace metal determinations by TCA-AAS. Recently, the use of modifiers with metal atomizers was reviewed by Nóbrega et al. [13], pointing out that there is no panacea similar to the Pd + Mg mixture used in graphite furnace AAS because the chemical processes implicated during atomization are different from those occurring in a graphite tube. Both single and combined modifiers were used to thermally stabilize the analyte in a TCA without enclosure [11] operating in a reducing environment, enabling the elimination of the sample matrix and in parallel attaining a sensitivity enhancement [14–16]. It is well known that As is thermally stabilized in pyrolytic graphite surface by using W, Zr, and the platinum group metals (PGMs) as chemical modifiers, considering a thermal pre-reduction of the modifier in this surface. Among the most successful modifiers are Pd, Ir, Rh and Ru applied either (i) singly and directly onto the pyrolytic graphite surface, or (ii) on a pretreated graphite surface coated with W or Zr carbides, or (iii) combining Pd and Ir in these applications [17]. This procedure allows the trapping of hydride-forming elements and also volatile elements in the graphite surface followed by the atomization step, thereby enabling the determination of ultra-traces of metalloids and volatile elements by ET-AAS with high sensitivity, without analyte loss in molecular form and eliminating matrix effects. Regarding metal atomizers, recently Hou et al.

[18] established the feasibility of Ir as a permanent chemical modifier for the TCA, and Barbosa et al. [19] showed that a Rh-coated tungsten coil was useful for selenium hydride collection. More recently, a systematic study was performed by TCA-AAS to establish among three PGMs (Pd, Ir, and Rh) an optimum chemical modifier to enable the determination of As at trace levels in biological materials, and Rh (2.0 µg) in pre-reduced form was found more effective [20]. The aim of this work is to extend the study of chemical modifiers for As determination in digest solutions of seafood samples, in particular of fish and clam tissues, including Pd, Ir, Rh both in solution and in pre-reduced form, and also combined with Mg(NO<sub>3</sub>)<sub>2</sub> and ascorbic acid, well known modifiers used in ET-AAS with the graphite furnace [21], comparing their performance in terms of maximum pyrolysis temperature to eliminate the sample matrix without significant As loss in this step, and best absorbance sensitivity for As in the atomization step. In addition, three sample digestion procedures are considered in this study to provide a complete conversion of As present in various organoarsenicals into As(V), bearing in mind that these species comprise the major fraction of the As content in these seafood matrices (>90%) [22–24]. The employ of microwave acid digestion alone or combined with the addition of K<sub>2</sub>S<sub>2</sub>O<sub>8</sub> followed either by UV photo-oxidation [25,26] or re-digestion in a thermal block are compared in fish and clam tissue samples. Both seafood matrices are significant food items in the Chilean diet and it would be of great utility to have a reliable, simple, fast and inexpensive method that would make it possible to quantify total As therein.

## 2. Experimental

### 2.1. Apparatus

A Perkin-Elmer (PE) Model 1100 atomic absorption spectrometer (Überlingen, Germany) was equipped with a TCA [11]. The limiting time resolution of the spectrometer was 0.02 s and peak height absorbance was measured throughout [15] at the 193.7 nm As resonance line (EDL System 2 lamp, PE). The absorbance was background corrected with a deuterium arc, and time-resolved absorption signals were printed out. The measurement time was 1.0 s. Lamp current and slit-width settings corresponded to manufacturer's recommendations. Sample and reference solution aliquots of 10 µl were manually delivered into the coil through a micropipette (Transferpette, Brand, Wertheim, Germany). The double-layer coiled tungsten filament (150 W, Osram, Munchen, Germany, Part No. 64633 HLX) was heated by a programmable power supply with a voltage feedback circuit (Anacom Equipment and System, Sao Bernardo do Campo, SP, Brazil) and run with a PC computer (Pentium 100 MHz). A purpose-built control interface was used to trigger the read command of the spectrometer. Argon–hydrogen (90:10) (Indura, Santiago, Chile) for TCA-AAS was used as purge gas at an optimum flow rate of 1.5 l min<sup>-1</sup> throughout.

Marine food samples were ground and blended both in a pre-cleaned mixer (Philips HR2810/A) and a pre-cleaned chopper (Sindelen model Silhouette P-123) fitted with stainless steel blades and plastic vessels. The samples were frozen in a Frio

Lux freezer and lyophilized in a Leybold (model Lyovac GT2) freeze dryer supported by a Welch vacuum pump (model W series,  $10^{-1}$  to  $10^{-2}$  Pa). The lyophilized samples were powdered in a micro-dismembrator (B. Braun Biotech, Melsungen, Germany) equipped with PTFE containers with lid and PTFE balls by using a cryogenic approach. Liquid nitrogen (AGA, Concepcion, Chile) was used to freeze the ground mass of the fish samples within the PTFE flasks before comminution in the micro-dismembrator [27]. Microwave sample digestions were carried out in a Milestone MLS-1200 MEGA microwave system (Bergamo, Italy) by using Milestone's digestion HPR-1000/6 rotor with TFM vessels. In the first re-digestion approach assisted by UV photo-oxidation, the digest solution was passed in a continuous flow mode through a Tefzel tubing (i.d. 0.30 mm, 270 cm in length) coiled along a germicidal UV fluorescent tube (15 W). The later was fixed in a wood support under an aluminum shield containing several venting slots to dissipate minor heat produced by the low power radiation. A Ismatec MCP (model ISM 726 (2–200 rpm)) peristaltic pump was used to propel the digest solution through the coil tubing, which was held at 0.5 cm from the UV tube surface affixed throughout by four galvanized wire strips set parallel to the UV tube (equidistant to the wires) to avoid a warm up effect from the radiation. The second re-digestion approach was performed in a laboratory made aluminum thermal block supplied with five cavities drawn therein to lay the digestion tubes, a thermo regulator inserted in the side of the block and a thermometer set in a central orifice on top, and was heated at the required temperature by a portable furnace controlled through a rheostat. An analytical balance AA 200 DS (sensitivity 0.02 mg, Denver Instrument Co.); a vortex shaker, a laboratory oven and several micropipettes (Transferpette and Finnipette) were also used.

## 2.2. Reagents, materials and samples

Most reagents were of analytical-reagent grade (Merck, Darmstadt, Germany), except for  $\text{HNO}_3$  which was further purified in a quartz sub-boiling still (Kürner, Rosenheim, Germany) and stored in quartz,  $\text{Mg}(\text{NO}_3)_2 \cdot 6\text{H}_2\text{O}$ ,  $\text{H}_2\text{O}_2$  (30%, m/m) which was Suprapur grade (Merck), Iridium stock solution (Strem Chemicals, Inc., Newburyport, MA, USA) and Rhodium stock solution (Aldrich, Milwaukee, WI, USA). The modifiers stock solutions were  $10.0 \pm 0.2 \text{ g l}^{-1}$  Pd (as  $\text{Pd}(\text{NO}_3)_2$  in 15%, v/v  $\text{HNO}_3$ ),  $1000 \mu\text{g ml}^{-1}$  Ir (as  $\text{IrCl}_3$  in 10% HCl) and  $1000 \mu\text{g ml}^{-1}$  Rh (Rh in 5% HCl). Modifier solutions of Pd, Ir, Rh, Mg and ascorbic acid were prepared in the concentration range 5–1000  $\mu\text{g ml}^{-1}$  by dilution of the stock solutions (Pd, Ir and Rh) and by dissolving 0.2637 g of  $\text{Mg}(\text{NO}_3)_2 \cdot 6\text{H}_2\text{O}$  in 25 ml ( $1000 \mu\text{g ml}^{-1}$  Mg) and 0.025 g of ascorbic acid in 25 ml ( $1000 \mu\text{g ml}^{-1}$ ), respectively. The pre-selected modifiers and optimized amounts for more in depth studies in sample matrices were Rh ( $50 \mu\text{g ml}^{-1}$ ) in solution (0.5  $\mu\text{g}$ ), Ir ( $100 \mu\text{g ml}^{-1}$ ) in solution (1.0  $\mu\text{g}$ ) and the binary mixture Rh ( $50 \mu\text{g ml}^{-1}$ ) + ascorbic acid ( $50 \mu\text{g ml}^{-1}$ ) in solution (0.5  $\mu\text{g}$  + 0.5  $\mu\text{g}$ , respectively). The re-digestion procedures were performed in 2% (m/v)  $\text{K}_2\text{S}_2\text{O}_8$  solution prepared daily in 0.5% (m/v) NaOH. Ultrapure (u.p.) water

( $18.3 \text{ M}\Omega \text{ cm}$  at  $25^\circ\text{C}$ ) was used throughout. Arsenic (V) stock solutions ( $1000 \mu\text{g ml}^{-1}$ ) were prepared from Titrisol concentrate (Merck), and reference solutions of As(V) were prepared daily by stepwise dilution of a working standard solution ( $20 \mu\text{g ml}^{-1}$ ) prepared weekly. The stock and the later solutions were stored at  $4^\circ\text{C}$  until use. Standard additions (10, 20, 40 and  $60 \mu\text{g l}^{-1}$  As(V)) were applied for As determination in sample solutions.

A certified reference material (CRM) of dogfish muscle (DORM-2, National Research Council of Canada, Canada) and a homogenized, lyophilized, powdered clam sample of *Semella solida* ("almeja") collected in natural banks from the Chilean coast [28] were used in the pyrolysis and atomization studies with all matrix modifiers and their combinations. The CRM was used too in the accuracy study. Also, besides the former clam sample, a powdered sample of clam *Tagelus dombeii* ("navajuela") and five powdered samples of fish muscle (three samples of *Merluccius gayi* ("merluza común") and two samples of *Salmo Salar* ("salmón del Atlántico")) caught in the coastal area of the Eighth Region of Chile were analyzed for total As by the proposed methodology. Both clam samples were prepared as reported elsewhere [28] and the fish samples corresponded to fresh fish obtained directly from a fisherman at the fish market, and were washed carefully with distilled water, dried externally with paper towel, skinned, filleted with a plastic knife, and cut in small slices. These slices were ground first in a pre-cleaned mixer and second, in a pre-cleaned chopper, and the ground mass obtained as a paste was transferred into a pre-weighed glass vessel; the vessel was reweighed, frozen in a freezer at  $-20^\circ\text{C}$  for 24 h, lyophilized in a freeze dryer for 120 h divided in consecutive 8-h periods (with the corresponding freezing periods overnight) to enable redistribution of the ground mass within the glass container, and reweighed to obtain the sample water content. The lyophilized sample divided in small fractions was powdered in a micro-dismembrator using a cryogenic approach with liquid nitrogen [27]. All powdered fractions were mixed together in a closed PTFE container and homogenized in a mechanical shaker. This product was screened through a set of three polyester sieves (16–32–65 mesh, respectively) being the largest particle size of the fine powder between 180 and  $250 \mu\text{m}$ . The later was re-homogenized, weighed, divided in plastic containers and stored in a desiccator at room temperature. The residual humidity was  $<2\%$  in the fish samples and  $<5.5\%$  in the clam samples.

Glass and plastic materials were cleaned as described elsewhere [12].

## 2.3. Sample solutions in study

Samples (500 mg lyophilized clam or fish) were digested in a microwave system; the digestion was performed in a mixture of  $\text{HNO}_3/\text{H}_2\text{O}_2$  (6:1) according to manufacturer's suggested program and to conditions indicated elsewhere [29] without an evaporation step after digestion: step 1, 1 min/250 W; step 2, 1 min/0 W; step 3, 5 min/250 W; step 4, 5 min/400 W; step 5, 5 min/650 W; and step 6, 5 min/0 W. The total digestion time was 22 min. No temperature and pressure measurements were made



due to the lack of automatic temperature or pressure control accessories in the microwave digestion unit. The digest solutions were carefully transferred into 25-ml volumetric flasks and diluted with u.p. water (sample digest solution) (A). Besides this approach, the sample digest solution was re-digested further for a complete conversion and oxidation into inorganic As(V) of the organoarsenicals still present in this solution. Thus, a photo-oxidation (B) and a re-digestion in an aluminum thermal block (C) were applied. In both approaches a 10 ml aliquot of the sample digest solution was mixed with 10 ml of 2% (m/v)  $K_2S_2O_8$  solution (in 0.5%, m/v NaOH), and this solution mixture (M) was prepared in duplicate. In approach B, the M solution was propelled through a Tefzel tubing (described previously), irradiated by a germicidal UV fluorescent tube (15 W) in continuous flow mode at a flow rate of  $1 \text{ ml min}^{-1}$  for 30 min, and was stored at  $4^\circ\text{C}$  until analysis (within 48 h). In approach C, two 6-ml aliquots of M solution were transferred into two silica digestion tubes respectively, re-digested in the aluminum thermal block between 50 and  $60^\circ\text{C}$  for 3 h, and subsequently heated up to  $100^\circ\text{C}$  and held for 1 h at this temperature, for the decomposition of  $K_2S_2O_8$  and partial evaporation of the solution [30]. Both re-digested solutions were transferred quantitatively and combined in a 25-ml volumetric flask, and diluted with u.p. water. Sample and CRM digest solutions were diluted suitably to fit within the third lowest segment of the linear working range and above the limit of quantification for As determination. Blank solutions of the acid digestion and re-digestions were prepared likewise.

#### 2.4. Procedure

A preliminary study was performed on the thermal program of the TCA with a blank and diluted digest solutions (1:25) of lyophilized fish muscle (DORM-2) and clam tissue (*Semelle solida*), all of them spiked with As(V) ( $100 \mu\text{g l}^{-1}$ ), without and with Pd, Ir, Rh, Mg and ascorbic acid (Asc.ac.) as chemical modifiers, both in single form and in binary mixtures, and applied into the tungsten coil both in solution (all of them) and in pre-reduced form (Pd, Ir, Rh and Mg) to establish the optimum pyrolysis conditions based on the highest temperature possible without significant As loss in this step, and high As absorbance sensitivity. An 8-step thermal program of the TCA was used in this study (Table 1); steps 1, 2, 4, 5 and 8 were optimized in previous work [20], and steps 3 and 6 correspond to the pyrolysis and atomization, respectively. The pyrolysis and atomization times (30 and 2.5 s, respectively) were selected based on the corresponding conditions established in previous studies performed in digest solutions of biological matrices [20]. During the pyrolysis study, the maximum atomization temperature (step 6) and the clean temperature (step 7) applied was  $1750^\circ\text{C}$  (11.5 V) in an attempt to extend the modifier effect. In each modifier and application approach was used a new coil to avoid possible memory effects. The first approach was the use of each modifier in solution at set concentration of  $50 \mu\text{g ml}^{-1}$  for Pd, Ir, Rh and Mg, based on our previous experience with elements of the PGMs as modifiers in the TCA [20], and  $100 \mu\text{g ml}^{-1}$  for Asc.ac [29]. Using the optimized pyrolysis and atomization conditions established therein, the concentration of each modifier was studied

Table 1

Thermal program for the determination of As<sup>a</sup> without and with chemical modifier by TCA-AAS

Step	Time (s)	Voltage (V)	Temperature ( $^\circ\text{C}$ )	Effect
1	60	0.50	250	Dry (1)
2	50	0.55	280	Dry (2)
3	30	In study <sup>b</sup>	In study <sup>b</sup>	Pyrolysis
4	10	0	20	Cool
5	0.20	0	20	Read
6	2.5	In study <sup>c</sup>	In study <sup>c</sup>	Atomization
7	3	11.5	1750	Clean
8	10	0	20	Cool

<sup>a</sup> Injection volume, 10  $\mu\text{l}$ .

<sup>b</sup> In the study of pyrolysis step the atomization temperature was  $1750^\circ\text{C}$  (11.5 V). In the selected modifier (Rh (0.5  $\mu\text{g}$ )) the optimum temperature was:  $850^\circ\text{C}$  (2.5 V) (blank digest);  $760^\circ\text{C}$  (2.0 V) (clam and fish tissue digest).

<sup>c</sup> The optimum atomization temperature was:  $1860^\circ\text{C}$  (13.0 V) (blank digest);  $1800^\circ\text{C}$  (12.0 V) (clam and fish tissue digest).

separately in the range between 5 and  $250 \mu\text{g ml}^{-1}$ ; additionally, the modifier concentrations were studied too in some binary mixtures (Rh–Asc.ac.; Rh–Mg; Rh–Ir; Ir–Asc.ac.; Pd–Mg; and Pd–Asc.ac.), based on the pyrolysis curves obtained with As(V) ( $100 \mu\text{g l}^{-1}$ ). Also, the elements of the PGMs (Pd, Ir and Rh) and Mg were used as modifiers in pre-reduced form (p-r), and the optimized conditions for the pre-reduction are shown in Table 2. In this case, 2 modifier approaches were tested on the tungsten coil: (i) 10 consecutive injections of 30  $\mu\text{l}$  (or 20  $\mu\text{l}$ ) of a  $1000 \mu\text{g ml}^{-1}$  modifier solution (Pd, Ir and Rh) equivalent to 300  $\mu\text{g}$  (or 200  $\mu\text{g}$ ), each one pre-reduced as indicated in Table 2 (step 5) in the search of a permanent modifier effect; and (ii) a single injection of 10  $\mu\text{l}$  of  $200 \mu\text{g ml}^{-1}$  solution equivalent to 2.0  $\mu\text{g}$  (Pd, Ir and Rh) pre-reduced likewise, before the injection of the As reference or sample solution in study, to make sure that a modifier effect was obtained in it. The coil temperature was estimated by voltamperometric measurements according to a procedure described elsewhere [12,14] and the mean uncertainty of this temperature estimate is 6.2% [14]. New coils were conditioned as described elsewhere [20] and aligned in the radiation beam before proceeding with the measurements. The modifiers studied included 28 alternatives and were compared without a modifier. Besides the use of a single modifier, some binary combinations were considered as well, based on apparent synergic modifier effects by comparison of the pyrolysis curves with those obtained without a modifier. Since the modifier effect observed

Table 2

Thermal program for the pre-reduction of the modifier on the TCA

Step	Time (s)	Voltage (V)	Temperature ( $^\circ\text{C}$ )	Effect
1	20	0.65	315	Dry (1)
2	25	0.60	300	Dry (2)
3	40	0.55	280	Dry (3)
4	20	0.50	250	Dry (4)
5	10	x <sup>a</sup>	x <sup>a</sup>	Pre-reduction
6	2	11.5	1750	Atomization
7	10	0	20	Cool

<sup>a</sup> 3.0 V/ $950^\circ\text{C}$  (Ir); 6.0 V/ $1330^\circ\text{C}$  (Pd); 3.0 V/ $950^\circ\text{C}$  (Rh); 1.5 V/ $625^\circ\text{C}$  (Mg).

with Pd both in solution and in pre-reduced form was not significant, the binary mixtures Pd–Ir and Pd–Rh were not considered in this study. After establishing the optimum pyrolysis temperatures, the three modifiers and/or mixtures with best performance according to the criteria indicated above were selected for the study on the atomization temperature. The definitive selection of the most appropriate modifier in the aforementioned diluted digest solutions of fish muscle and clam tissue spiked with As(V) ( $100 \mu\text{g l}^{-1}$ ) was by one-way variance analysis (Tukey test) [31], comparing the pyrolysis curves and the As absorbance obtained at the maximum voltage without significant As loss.

Interference effects of the main cations and anions according to the approximate concentrations present in digest solutions of clam and fish muscle, considering both the sample amount digested and the final solution volume were assessed for As(V) ( $200 \mu\text{g l}^{-1}$ ) in aqueous reference solutions with the selected modifier Rh ( $0.5 \mu\text{g}$ ). For cations at two concentration levels were studied the effects of  $\text{Na}^+$  (10 and  $100 \mu\text{g ml}^{-1}$ ),  $\text{K}^+$  (20 and  $200 \mu\text{g ml}^{-1}$ ),  $\text{Ca}^{2+}$  (15 and  $150 \mu\text{g ml}^{-1}$ ),  $\text{Cu}^{2+}$  ( $0.1$  and  $1.0 \mu\text{g ml}^{-1}$ ),  $\text{Mg}^{2+}$  (5 and  $50 \mu\text{g ml}^{-1}$ ),  $\text{Fe}^{3+}$  (1 and  $10 \mu\text{g ml}^{-1}$ ) and  $\text{Zn}^{2+}$  (1 and  $10 \mu\text{g ml}^{-1}$ ) as nitrates. The anions studied likewise corresponded to  $\text{Cl}^-$  (15 and  $150 \mu\text{g ml}^{-1}$ ) (as  $\text{NH}_4\text{Cl}$ ),  $\text{SO}_4^{2-}$  (10 and  $100 \mu\text{g ml}^{-1}$ ) (as  $(\text{NH}_4)_2\text{SO}_4$ ) and P (15 and  $150 \mu\text{g ml}^{-1}$ ) (as  $(\text{NH}_4)_2\text{HPO}_4$ ). Blank solutions were prepared and measured for each concomitant ion at both concentration levels and As absorbance of the corresponding solution was blank corrected. In each instance, the background corrected absorbance, the peak shape and the background absorbance were compared with those obtained for As without interference in Rh ( $0.5 \mu\text{g}$ ) modifier. This study was performed with the optimized thermal program for As(V) in Rh ( $0.5 \mu\text{g}$ ) using  $10 \mu\text{l}$  injections.

The analytical performance was assessed for As by using As(V) without modifier (sensitivity and linear working range) and in the selected modifier (Rh,  $0.5 \mu\text{g}$ ) under optimized conditions by systematic evaluation of the linear working range, characteristic mass ( $m_0$ ), repeatability, reproducibility and detection limit ( $\text{D.L.}, 3\sigma_{\text{blank}}/\text{slope}$ ). The three sample pretreatment procedures (A, B, C) were applied to independent subsamples of a CRM of dogfish muscle tissue (DORM-2) and the results obtained in the determination of total As in Rh ( $0.5 \mu\text{g}$ ) modifier by TCA-AAS in the respective digest solutions – based on dry weight (following the procedures recommended by the CRM producer for establishing the sample humidity) [32] – were compared both with the certified concentration and among them. The accuracy was established by the determination of As in the CRM of fish muscle. Quantitation was performed by standard additions. The methodology including the three sample pretreatment procedures was applied to the determination of total As in typical clam and fish samples.

### 3. Results and discussion

#### 3.1. Study of pyrolysis and atomization for As in seafood samples using chemical modifiers

In previous study on chemical modifiers for As determination by TCA-AAS [20] performed in single form with pre-reduced

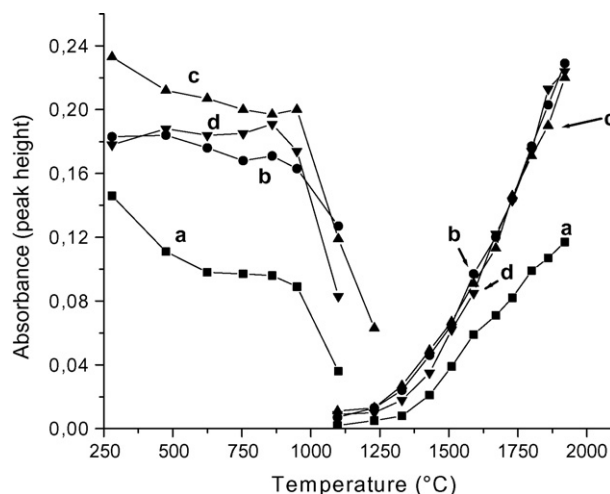


Fig. 1. (a–d) Pyrolysis and atomization temperature curves of  $1.0 \text{ ng As(V)}$  in acid-digested blank solution: (a) without chemical modifier; (b) in  $0.5 \mu\text{g Rh}$ ; (c) in  $0.5 \mu\text{g Rh} + 0.5 \mu\text{g Asc.ac.}$ ; (d) in  $1.0 \mu\text{g Ir}$ . In pyrolysis study the atomization temperature was  $1750^\circ\text{C}$ ; in atomization study the pyrolysis temperatures were  $850^\circ\text{C}$  (no modifier;  $0.5 \mu\text{g Rh}$ ;  $1.0 \mu\text{g Ir}$ ) and  $950^\circ\text{C}$  ( $0.5 \mu\text{g Rh} + 0.5 \mu\text{g Asc.ac.}$ ).

Pd, Ir and Rh, it was shown that Pd was not effective and Rh ( $2.0 \mu\text{g}$ ) was the most satisfactory modifier. Nevertheless, no further modifiers and other treatment alternatives were considered. In the present work, 28 pyrolysis studies were performed as described in Section 2.4. The pyrolysis temperature was varied between  $280^\circ\text{C}$  ( $0.55 \text{ V}$ ) and  $1100^\circ\text{C}$  ( $4.0 \text{ V}$ ) and the outcome of these studies was a pre-selection of three chemical modifiers with the best performance in terms of thermal stabilization of As (maximum pyrolysis temperature without significant As loss) and maximum As absorbance in the three aforementioned digest solutions compared to without a modifier. The pre-selected modifiers applied in solutions were: Rh ( $0.5 \mu\text{g}$ ), Ir ( $1.0 \mu\text{g}$ ) and Rh ( $0.5 \mu\text{g}$ ) + Asc.ac. ( $0.5 \mu\text{g}$ ), and subsequently their atomization temperatures were studied (at optimum pyrolysis temperature) between  $1100^\circ\text{C}$  ( $4.0 \text{ V}$ ) and  $1920^\circ\text{C}$  ( $14.0 \text{ V}$ ). As is shown in Fig. 1, in acid digested blank solution spiked with As ( $100 \mu\text{g l}^{-1}$ ) without modifier (Fig. 1a) clearly the pyrolysis curve differs from the same curves obtained with modifiers (Fig. 1b–d) in absorbance sensitivity (being significantly lower by a factor of 2) and in the profile. Also, this pyrolysis curve illustrates two effects; between 280 and  $625^\circ\text{C}$  a significant decrease in absorbance indicates apparent As loss in one molecular form (not evident in the presence of Rh modifier), whereas between  $625$  and  $850^\circ\text{C}$  a second form more stable thermally became apparent which is lost above  $850^\circ\text{C}$ . Based on these results,  $850^\circ\text{C}$  was selected as the pyrolysis temperature without modifier, which is coincident with the optimum pyrolysis temperature in the presence of Rh ( $0.5 \mu\text{g}$ ) or Ir ( $1.0 \mu\text{g}$ ) modifiers, whereas  $950^\circ\text{C}$  was the optimum pyrolysis temperature in Rh ( $0.5 \mu\text{g}$ ) + Asc.ac. ( $0.5 \mu\text{g}$ ) modifier. In the atomization curves (Fig. 1) (using a pyrolysis temperature of  $850^\circ\text{C}$  ( $2.5 \text{ V}$ ) (no modifier;  $0.5 \mu\text{g Rh}$ ;  $1.0 \mu\text{g Ir}$ ) or  $950^\circ\text{C}$  ( $3.0 \text{ V}$ ) ( $0.5 \mu\text{g Rh} + 0.5 \mu\text{g Asc.ac.}$ )), no plateau was reached in any of them but a significantly higher relative absorbance for As by a factor of 2 was observed between 1850

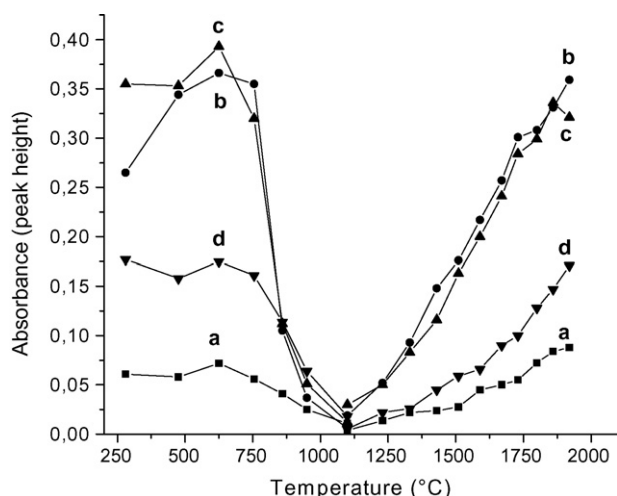


Fig. 2. (a–d) Pyrolysis and atomization temperature curves of 1.0 ng As(V) in diluted (1:25) acid-digested dogfish muscle (DORM-2) solution: (a) without chemical modifier; (b) in 0.5 µg Rh; (c) in 0.5 µg Rh + 0.5 µg Asc.ac.; (d) in 1.0 µg Ir. In pyrolysis study the atomization temperature was 1750 °C; in atomization study the pyrolysis temperatures were 625 °C (no modifier; 0.5 µg Rh + 0.5 µg Asc.ac.; 1.0 µg Ir) and 760 °C (0.5 µg Rh).

and 1950 °C (13.0 and 14.0 V) in the three modifiers, showing along this study a similar trend with steeper curves compared without a modifier. The selected atomization temperature was 1850 °C (13.0 V). The same study was performed in diluted sample digest solutions of clam and fish tissue, and the pyrolysis and atomization curves showed some significant differences compared without a modifier. Since the pyrolysis and atomization curves obtained in both matrices were quite similar, the results obtained in fish tissue will be discussed further.

As is shown in Fig. 2 in diluted acid-digested solutions of fish tissue spiked with As ( $100 \mu\text{g l}^{-1}$ ) without modifier, the optimum pyrolysis temperature was 625 °C (1.5 V) and the maximum absorbance obtained is significantly smaller (at least by a factor of 4.9–5.2 times in the pyrolysis study) compared with the maximum absorbance obtained for As in Rh (0.5 µg) and in Rh (0.5 µg) + Asc.ac. (0.5 µg), and smaller (by a factor of 3.2) compared with the maximum absorbance obtained for As in Ir (1.0 µg) modifier. Without modifier the interference effect of concomitants was similar in fish digest as in clam, causing similar loss of arsenic in both matrices. Apparently in the presence of the pre-selected modifiers the higher relative absorbance of As obtained in both sample digests compared to the case without modifier could be explained by a reduction of analyte loss due to concomitants effect [20]. The optimum pyrolysis temperature was 760 °C (2.0 V) in Rh (0.5 µg) providing some thermal stabilization of As, and was 625 °C (1.5 V) both in Rh (0.5 µg) + Asc.ac. (0.5 µg) and in Ir (1.0 µg), showing no difference with the optimum temperature obtained without modifier. In the atomization curves a significantly higher relative absorbance for As by a factor of 4.1 in Rh (0.5 µg) + Asc.ac. (0.5 µg) and 3.9 in Rh (0.5 µg), was shown up compared to the no use of modifier. Iridium (1.0 µg) modifier was somewhat less effective, and As absorbance was higher by a factor of 1.9 respect to the no use of modifier. An incipient plateau is noticed in the atomization curves obtained without

modifier and in Rh (0.5 µg) + Asc.ac. (0.5 µg) modifier. In the fish digest study like in the clam study the selected atomization temperature was 1800 °C (12.0 V), to extend the useful coil lifetime. A difference found comparing the atomization curves obtained in both sample digests and in the blank digest was the relative sensitivity for As between 1330 and 1950 °C (6.0 and 14.0 V, respectively). In the blank digest study the relative sensitivity was quite comparable between the three pre-selected modifiers and higher than without modifier, whereas in clam and fish digests the relative sensitivity was much higher and comparable between Rh (0.5 µg) and Rh (0.5 µg) + Asc.ac. (0.5 µg), being lower in Ir (1.0 µg) and much lower without modifier.

Hitherto, in both sample digests Rh modifier without or with Asc.ac. was more effective than Ir in thermally stabilizing As, and although there was a slight thermal stabilization effect in particular with Rh compared to the no use of modifier, the main effect observed in the three pre-selected modifiers was a significant increase in relative absorbance, being more favorable in Rh (0.5 µg) and in Rh (0.5 µg) + Asc.ac. (0.5 µg).

### 3.2. Selection of the modifier by variance analysis

An attempt was made to establish a systematic approach using a statistical tool to compare the pyrolysis curves obtained for As among the three pre-selected modifiers with similar performance in terms of thermal stabilization. The pyrolysis curves, the optimum pyrolysis temperature without significant As loss and the corresponding As absorbances obtained therein in the blank digest and in the diluted digest solutions of clam and fish tissue spiked with As ( $100 \mu\text{g l}^{-1}$ ) were compared by variance analysis (ANOVA). Since first order interactions in the three digest solutions were significant, comparisons between modifiers were performed in each study voltage. In blank digest the optimum pyrolysis temperature was 950 °C (3.0 V) and the mean As absorbance obtained in Rh (0.5 µg) + Asc.Ac. (0.5 µg) (0.200) was significantly higher than in the other modifiers. In this digest without sample matrix, Rh (0.5 µg) + Asc.Ac. (0.5 µg) appears as most suitable among the studied modifiers. In clam and fish digests the optimum pyrolysis temperature obtained for As in Rh (0.5 µg) was 760 °C (2.0 V) and the mean As absorbance was 0.306 and 0.355, respectively, being significantly higher compared with the other modifiers. Using Rh (0.5 µg) + Asc.ac. (0.5 µg) modifier and the same pyrolysis temperature, the mean As absorbance obtained in clam (0.306) and fish tissue (0.320) corresponded to the next alternative modifier. In fish tissue digest another alternative modifier was Rh (0.5 µg) + Asc.ac. (0.5 µg). Both in clam and fish digest solution the pyrolysis curves obtained in Rh (0.5 µg) and Rh (0.5 µg) + Asc.ac. (0.5 µg) were the most satisfactory and concurrently similar. Based on these comparisons, the definitive selected modifier for further analytical studies was Rh (0.5 µg), since the mixture Rh (0.5 µg) + Asc.ac. (0.5 µg) did not show any additional feature to persuade on this decision.

### 3.3. Analytical figures of merit

After the selection and optimization of Rh modifier (0.5 µg), the calibration curves and linear working ranges for As were

Table 3  
Calibration graphs<sup>a</sup> for As(V) obtained by TCA-AAS<sup>b</sup> without and with Rh (0.5 µg)

Modifier	Calibration range (µg l <sup>-1</sup> )	Slope ± S.D. <sup>c</sup>	Intercept ± S.D.	Standard error <sup>d</sup>	Correlation coefficient
None	10–250	0.0014 ± 0.00001	-0.0017 ± 0.0016	0.0027 (7)	0.9998
Rh (0.5 µg)	10–300	0.00186 ± 0.00002	0.0007 ± 0.0037	0.0054 (8)	0.9997

<sup>a</sup> Linear regression ( $A = mC + b$ ) representative of  $n = 6$  for each data point.

<sup>b</sup> Obtained with eight-steps thermal program.

<sup>c</sup> Standard deviation.

<sup>d</sup> Number of data points in parentheses.

Table 4  
Analytical figures of merits obtained for As in Rh (0.5 µg) by TCA-AAS

Reciprocal sensitivity (µg l <sup>-1</sup> )	Characteristic mass (pg)	Linear working range (µg l <sup>-1</sup> )	Within-day repeatability CV%	Reproducibility CV%	Detection limit (pg)
2.3	23	10–300	3	4	42

established with and without modifier for comparison, and are reported in Table 3. In Rh modifier the slope sensitivity for As was higher by 33% and the linear working range was more extensive compared without a modifier; the correlation coefficients were quite satisfactory in both conditions. In Table 4 are shown the analytical figures of merit obtained in Rh (0.5 µg) modifier; the characteristic mass was 23 pg obtained with 10-µl injections of As solutions, and was somewhat higher than in previous study with pre-reduced Rh (2.0 µg) [20] mainly due to a lower atomization temperature selected in the present work which enables a more extended linear working range and convenient coil lifetime. The mean within-day repeatability obtained in three cycles, each of six consecutive measurements and each cycle performed with new independent coil, turning off and on the spectrophotometer and EDL lamp between cycles was 3% (1% (300 µg l<sup>-1</sup>) to 8% (25 µg l<sup>-1</sup>)). The mean reproducibility obtained in 18 measurements performed per day in 3 different days with newly prepared solutions of the same concentrations was 4% (2% (300 µg l<sup>-1</sup>)–8% (25 µg l<sup>-1</sup>)), which indicates that the intralaboratory variability was small for As reference solutions in Rh modifier. The detection limit (D.L.,  $3\sigma_{\text{blank}}/\text{slope}$ ) of As in the presence of Rh (0.5 µg) was established in consecutive measurements with 10-µl injections of two As(V) reference solutions (10 and 20 µg l<sup>-1</sup>) alternated with a blank solution and

was 4.2 µg l<sup>-1</sup> (42 pg) ( $n = 16$ ). The CV% obtained in these consecutive measurements was 13% and 8% for 10 and 20 µg l<sup>-1</sup> As(V), respectively. This detection limit is comparable with the detection limit obtained in previous work for As in pre-reduced Rh (2.0 µg) [20]. Compared to the detection limit obtained by ET-AAS with the graphite furnace and integrated platform using longitudinal Zeeman background correction is higher by a factor of 4 [33]. Nevertheless, the detection limit obtained for As with Rh (0.5 µg) modifier by TCA-AAS is suitable for its direct determination in diluted digest solutions of the seafood matrices in study. The method detection limit by TCA-AAS was assessed for As in acid digested fish sample matrix with Rh modifier and was 0.2 µg g<sup>-1</sup> dry weight (dw) and the quantification limit was 0.7 µg g<sup>-1</sup> (dw). This figure of merit is satisfactory to determine total As in fish and clam samples according to the total As levels reported in the literature [34,35].

The effect of concomitants on As (200 µg l<sup>-1</sup>) in Rh modifier was assessed at two different concentration levels for the main cations and anions present in the study matrices, and was expressed with respect to As absorbance normalized to 100% (Table 5) measured without interferent. In the presence of Na<sup>+</sup>, K<sup>+</sup>, Cu<sup>2+</sup>, Zn<sup>2+</sup>, Cl<sup>-</sup> and SO<sub>4</sub><sup>2-</sup> there were no significant interference effects on As (>91%) in both concomitant concentration levels. As is shown in Table 5 the main effects

Table 5  
Interference effects<sup>a</sup> on As (200 µg l<sup>-1</sup>) in Rh (0.5 µg) modifier by various concomitant ions by TCA-AAS

Interferent	C <sub>1</sub> (µg ml <sup>-1</sup> )	% Absorbance <sup>b</sup>	C <sub>2</sub> (µg ml <sup>-1</sup> )	% Absorbance <sup>b</sup>
Na <sup>+</sup>	10	92	100	94
K <sup>+</sup>	20	97	200	96
Ca <sup>2+</sup>	15	122	150	79
Mg <sup>2+</sup>	5	92	50	148
Fe <sup>3+</sup>	1	81	10	44
Zn <sup>2+</sup>	1	96	10	93
Cu <sup>2+</sup>	0.1	95	1	91
SO <sub>4</sub> <sup>2-</sup>	10	99	100	94
HPO <sub>4</sub> <sup>2-</sup>	15	21	150	1
Cl <sup>-</sup>	15	95	150	92

<sup>a</sup> C<sub>1</sub> and C<sub>2</sub> are concentration levels.

<sup>b</sup> Respect to As absorbance without interferent.



corresponded to great signal depressions produced by P (as  $\text{HPO}_4^{2-}$ ) at  $15 \mu\text{g ml}^{-1}$  (21%) and  $150 \mu\text{g ml}^{-1}$  (1%), followed in strength by  $\text{Fe}^{3+}$  at  $1 \mu\text{g ml}^{-1}$  (81%) and  $10 \mu\text{g ml}^{-1}$  (44%), and by  $\text{Ca}^{2+}$  at  $150 \mu\text{g ml}^{-1}$  (79%), whereas the main opposite effects with enhancement on As absorbance were observed in the presence of  $\text{Mg}^{2+}$  at  $50 \mu\text{g ml}^{-1}$  (148%) followed in strength by  $\text{Ca}^{2+}$  at  $15 \mu\text{g ml}^{-1}$  (122%). In the presence of Mg (0.5  $\mu\text{g}$ ) as modifier it is possible to observe full compensation of the interferences by  $\text{Ca}^{2+}$  and  $\text{Fe}^{3+}$ , however not for the effect by P as phosphate. The effect of  $\text{H}_2\text{PO}_4^-$  and  $\text{HPO}_4^{2-}$  on As absorbance (As  $200 \mu\text{g l}^{-1}$ ) without Rh modifier was studied at two concentrations (15 and  $150 \text{ mg l}^{-1}$  as P). The results showed drastic signal depressions in As absorbance: with  $\text{H}_2\text{PO}_4^-$ , 88% and 96% drop, respectively; and with  $\text{HPO}_4^{2-}$ , 92% and 99% drop, respectively. Thus, the depression effect of both phosphate species is similar. In the presence of Rh modifier as shown in Table 5, the depression effect with  $\text{HPO}_4^{2-}$  is still quite significant, suggesting that Rh at the used concentration was too low to overcome this effect.

Simulating a sample matrix solution by mixing all cations and anions at the high concentration level considered in this study, As absorbance was 48% respect to the normalized signal. In order to reduce these interference effects not corrected by Rh modifier with the thermal program in use, the sample digest solutions were diluted properly and quantitation was performed by the standard addition method.

### 3.4. Study of sample pretreatment and evaluation of accuracy

In order to select and evaluate an appropriate sample pretreatment approach, independent subsamples of a CRM of dogfish muscle tissue (DORM-2) (certified total As =  $18.0 \pm 1.1$  ( $\mu\text{g As g}^{-1}$ )) were processed by the three procedures described before, and the results obtained in the determination of As ( $n$  = number of independent determinations) are:  $15.3 \pm 0.69$  ( $\mu\text{g g}^{-1}$ ) ( $n=5$ ) (procedure A);  $18.3 \pm 1.34$  ( $\mu\text{g g}^{-1}$ ) ( $n=4$ ) (procedure B); and  $18.6 \pm 0.74$  ( $\mu\text{g g}^{-1}$ ) ( $n=7$ ) (procedure C). Compared with the certified As concentration, the result obtained by procedure A was poor with a recovery of 85% of total As present in this material, and statistically significant difference

was established by Student's  $t$ -test at a 95% confidence level ( $p=0.0002$ ). By procedures B and C the recoveries in CRM were quite satisfactory (102% and 103%, respectively), and no statistically significant differences became evident by  $t$ -test compared with the certified value ( $p=0.6344$  (B);  $p=0.2296$  (C)). Also, the results obtained in this CRM by procedure A compared with procedures B and C showed statistically significant differences: A versus B,  $p=0.0032$ ; A versus C,  $p=0.00001$ ; whereas the comparison between procedures B and C revealed no statistical difference at a 95% confidence level ( $p=0.6375$ ). Most probably, the microwave acid digestion procedure in  $\text{HNO}_3\text{--H}_2\text{O}_2$  was not effective in full conversion of As present in organoarsenicals into As(V), and these species could be lost during the pyrolysis step of the thermal program in the TCA. The re-digestion of the sample digest solution in  $\text{K}_2\text{S}_2\text{O}_8$ , assisted either by UV photo-oxidation (B) or by heating in a thermal block (C), was effective to the complete conversion purpose to As(V). Hence, procedures B and C were selected for the analytical applications of this determination of total As in seafood by TCA-AAS. The accuracy expressed by the mean relative percent error ( $E_{\text{rel}}\%$ ) for total As determination in the CRM DORM-2 was 2% in procedure B and 3% in procedure C, and precision expressed by the relative standard deviation (R.S.D.) was 7% by procedure B and 4% by procedure C. Both figures are satisfactory and provide confidence on the feasibility of this methodology with sample pretreatment by procedures B and C.

### 3.5. Analytical application in seafood samples

The TCA was applied to the determination of total As in samples of lyophilized clam (*Semelle solida* and *Tagelus dombeii*) and fish tissue (*Merluccius gayi* and *Salmo Salar*) by the three sample pretreatment procedures and the results are shown in Table 6. Procedure A was included to verify if As recoveries in samples of clam and fish tissue denote similar figures as those observed in the CRM. In general, the concentration (dw) of As was in the range  $3.2\text{--}6.8 \mu\text{g g}^{-1}$  by procedure A,  $3.7\text{--}8.6 \mu\text{g g}^{-1}$  by procedure B and  $3.8\text{--}8.5 \mu\text{g g}^{-1}$  by procedure C, and assuming a mean water content of 85% in the original samples, the highest As concentration (fresh mass, fm) would be  $1.3 \mu\text{g g}^{-1}$  which can be considered relatively low by comparison with

Table 6  
Determination of total As concentration ( $\mu\text{g g}^{-1}$ ) (dry weight) in clam and fish muscle samples by TCA-AAS in Rh (0.5  $\mu\text{g}$ ) modifier after three sample pretreatment procedures<sup>a</sup>

Sample	Procedure A		Procedure B		Procedure C	
	Mean	S.D. <sup>b</sup>	Mean	S.D.	Mean	S.D.
<i>Semelle solida</i>	6.8	0.19 ( $n=6$ ) <sup>c</sup>	8.6	0.70 ( $n=3$ )	8.4	0.50 ( $n=4$ )
<i>Tagelus dombeii</i>	5.8	0.37 ( $n=3$ )	7.4	0.35 ( $n=3$ )	7.0	0.10 ( $n=3$ )
<i>Merluccius gayi</i> I	5.8	0.30 ( $n=3$ )	6.6	0.10 ( $n=3$ )	7.2	0.40 ( $n=3$ )
<i>Merluccius gayi</i> II	5.6	0.10 ( $n=3$ )	6.5	0.34 ( $n=6$ )	6.9	0.35 ( $n=3$ )
<i>Merluccius gayi</i> III	5.7	0.18 ( $n=3$ )	6.8	0.11 ( $n=3$ )	6.8	0.26 ( $n=3$ )
<i>Salmo Salar</i> I	3.2	0.10 ( $n=5$ )	3.8	0.10 ( $n=5$ )	3.9	0.10 ( $n=5$ )
<i>Salmo Salar</i> II	3.3	0.21 ( $n=5$ )	3.7	0.10 ( $n=5$ )	3.8	0.13 ( $n=5$ )

<sup>a</sup> A = microwave digestion (M.D.); B = M.D. +  $\text{K}_2\text{S}_2\text{O}_8$  + UV photo-oxidation; C = M.D. +  $\text{K}_2\text{S}_2\text{O}_8$  + re-digestion in thermal block at controlled temperature.

<sup>b</sup> Standard deviation.

<sup>c</sup>  $n$  = number of independent determinations.



As levels (fm) reported by the USFDA in bivalve mussels and crustacean ( $1.1\text{--}30\ \mu\text{g g}^{-1}$ ) [36]. Hence, the As levels found in seafood samples within this work are safe and do not represent any sanitary risk to consumers by exposure through the diet. In the clam samples, as a mean the recovery of As by procedure A is 75% and 82% with respect to the As content determined by procedures B and C correspondingly, and it correlates well with the recovery (85%) obtained by procedure A in the CRM (DORM-2). In the three samples of *Merluccius gayi* tissue, the results obtained by procedure A are quite similar ( $5.6\text{--}5.7\ \mu\text{g g}^{-1}$ ), and consistently lower with respect to the results by procedures B ( $6.5\text{--}6.8\ \mu\text{g g}^{-1}$ ) and C ( $6.7\text{--}7.1\ \mu\text{g g}^{-1}$ ). As a mean the As content determined by procedure A was 85% and 82% with respect to procedures B and C correspondingly, and it correlates well with the recovery obtained by procedure A in DORM-2. Also, in the two samples of *Salmo Salar* tissue, the results obtained by procedure A are quite similar ( $3.2\text{--}3.3\ \mu\text{g g}^{-1}$ ), and consistently lower with respect to the results by procedures B ( $3.7\text{--}3.8\ \mu\text{g g}^{-1}$ ) and C ( $3.8\text{--}3.9\ \mu\text{g g}^{-1}$ ). As a mean the As content determined by procedure A was 87% and 84% with respect to procedures B and C correspondingly, and also it correlates well with the recovery obtained by procedure A in DORM-2. Thus, these results confirm that procedure A does not render quantitative recovery of As; however, by procedures B and C the As content provides quantitative recovery.

The proposed methodology is simple and reliable, the sample readout frequency is  $21\ \text{h}^{-1}$ , and by keeping the nitric acid concentration low (<1%) the coil performance is unaffected (no absorption signal degradation) at least in 300 heating cycles. The tungsten coil atomizer is a good alternative for laboratories with limited funds and the use of chemical modifiers could expand the analytical applications by TCA-AAS.

## Acknowledgement

The authors are grateful for the financial support of Grant No. 1030693 by the Fondo Nacional de Desarrollo Científico y Tecnológico (FONDECYT) of Chile.

## References

- [1] J.O. Nriagu, in: W.T. Frankenberger Jr. (Ed.), Environmental Chemistry of Arsenic, Marcel Dekker, New York, 2002, pp. 1–26.
- [2] W.R. Cullen, K.J. Reimer, Chem. Rev. 89 (1989) 713.
- [3] W.A. Pott, S.A. Benjamin, R.S.H. Yang, Rev. Environ. Contam. Toxicol. 169 (2001) 165.
- [4] C.O. Abernathy, D.J. Thomas, R.I. Calderon, J. Nutr. 133 (Suppl. 1) (2003) 1536S.
- [5] M.B. Amran, M.J.F. Leroy, A. Lamotte, C. Demesmay, M. Ollé, M. Albert, G. Rauret, F. López-Sánchez, in: Ph. Quevauviller, E.A. Maier, B. Griepink (Eds.), Quality Assurance for Environmental Analysis, Elsevier, Brussels, 1995, pp. 285–304.
- [6] A.H. Welch, D.B. Westjohn, D.R. Helsel, R.B. Wanty, Groundwater 38 (2000) 589.
- [7] D.K. Nordstrom, Science 296 (2002) 2143.
- [8] L. Gidhagen, H. Kahelin, P. Schmidt-Thomé, C. Johansson, Atmos. Environ. 36 (2002) 3803.
- [9] J. Pastenes, M. Salgado, A. Illanes, J. López, E. Olmos, Segunda Jornada sobre Arsenicismo Laboral y Ambiental, Servicio de Salud de Antofagasta, Departamento de Programas sobre el Ambiente, Antofagasta, 1984 (Chapter 23).
- [10] X. Hou, B.T. Jones, Spectrochim. Acta Part B 57 (2002) 659.
- [11] H. Berndt, G. Schaldach, J. Anal. Atom. Spectrom. 3 (1988) 709.
- [12] C.G. Bruhn, F.E. Ambiado, H.J. Cid, R. Woerner, J. Tapia, R. Garcia, Anal. Chim. Acta 306 (1995) 183.
- [13] J.A. Nóbrega, J. Rust, C.P. Callaway, B.T. Jones, Spectrochim. Acta Part B 59 (2004) 1337.
- [14] C.G. Bruhn, J.Y. Neira, G.D. Valenzuela, J.A. Nóbrega, J. Anal. Atom. Spectrom. 13 (1998) 29.
- [15] C.G. Bruhn, J.Y. Neira, G.D. Valenzuela, J.A. Nóbrega, Talanta 48 (1999) 537.
- [16] C.G. Bruhn, J.Y. Neira, M.L. Guzmán, M.M. Darder, J.A. Nóbrega, Fresenius J. Anal. Chem. 364 (1999) 273.
- [17] I.L. Shuttler, M. Feuerstein, G. Schlemmer, J. Anal. Atom. Spectrom. 7 (1992) 1299.
- [18] X. Hou, K.E. Levine, A. Salido, B.T. Jones, M. Ezer, S. Elwood, J.B. Simeonsson, Anal. Sci. 17 (2001) 175.
- [19] F. Barbosa Jr., S.S. Souza, F.J. Krug, J. Anal. Atom. Spectrom. 17 (2002) 382.
- [20] C.G. Bruhn, V.N. Huerta, J.Y. Neira, Anal. Bioanal. Chem. 378 (2004) 447.
- [21] D.L. Styris, in: K.W. Jackson (Ed.), Electrothermal Atomization for Analytical Atomic Spectrometry, Wiley, Chichester, 1999, pp. 311–358.
- [22] P.J. Brooke, W.H. Evans, Analyst 106 (1981) 514.
- [23] O. Muñoz, D. Vélez, R. Montoro, Analyst 124 (1999) 601.
- [24] O. Muñoz, D. Vélez, M.L. Cervera, R. Montoro, J. Anal. Atom. Spectrom. 14 (1999) 1607.
- [25] R.H. Atallah, D.A. Kalman, Talanta 38 (1991) 167.
- [26] M.G. Lobos, Especiación de Arsénico Mediante Acoplamiento de Cromatografía Líquida, Fotooxidación UV, Generación de Hidruros, Fluorescencia Atómica (HPLC-UV-HG-AFS) y su Aplicación a Muestras Ambientales de Ecosistemas Marinos y Terrestres, Ph.D. Thesis, Pontificia Universidad Católica de Valparaíso, Chile, 2003.
- [27] C.G. Bruhn, A.A. Rodríguez, C. Barrios, V.H. Jaramillo, J. Becerra, U. González, N.T. Gras, O. Reyes, SEREMI-Salud, J. Anal. Atom. Spectrom. 9 (1994) 535.
- [28] I. De Gregori, D. Delgado, H. Pinochet, N. Gras, M. Thieck, L. Muñoz, C. Bruhn, G. Navarrete, Sci. Tot. Environ. 111 (1992) 201.
- [29] C.G. Bruhn, N.A. San Francisco, J.Y. Neira, J.A. Nóbrega, Talanta 50 (1999) 967.
- [30] C.J. Bustos, Selection of chemical modifiers by variance analysis for the determination of total arsenic in seafood by atomic absorption spectrophotometry with tungsten coil atomizer, Professional title Dissertation, Universidad Técnica Federico Santa María, Chile, 2004.
- [31] J.N. Miller, J.C. Miller, Statistics and Chemometrics for Analytical Chemistry, 4th ed., Prentice Hall, New Jersey, 2001.
- [32] National Research Council Canada, Dogfish muscle certified reference material for trace metals (DORM-2), Ottawa, 1999.
- [33] The Perkin-Elmer Corporation, Recommended Conditions for THGA Furnaces, Publication B31 10.06, Überlingen, 1991.
- [34] M.L. Cervera, A. Navarro, R. Montoro, J. Gomez, Fresenius J. Anal. Chem. 347 (1993) 58.
- [35] O. Muñoz, D. Vélez, M.L. Cervera, R. Montoro, J. Anal. Atom. Spectrom. 14 (1999) 1607.
- [36] M.A. Adams, M. Bolger, C.D. Carrington, C.E. Coker, G.M. Cramer, M.J. Di Novi, S. Dolan, Guidance Document for Arsenic in Shellfish, U.S. Food and Drug Administration, Washington, DC, 1993, pp. 1–24.

# Coelectroosmotic capillary electrophoresis of phenolic acids and derivatized amino acids using *N,N*-dimethylacrylamide-ethylpyrrolidine methacrylate physically coated capillaries

Alegría Carrasco-Pancorbo<sup>a</sup>, Alejandro Cifuentes<sup>b</sup>, Sonia Cortacero-Ramírez<sup>a</sup>,  
Antonio Segura-Carretero<sup>a,\*</sup>, Alberto Fernández-Gutiérrez<sup>a</sup>

<sup>a</sup> Department of Analytical Chemistry, Faculty of Sciences, University of Granada, C/Fuentenueva s/n, 18071 Granada, Spain

<sup>b</sup> Institute of Industrial Fermentations, CSIC, Juan de la Cierva 3, 28006 Madrid, Spain

Received 7 December 2005; received in revised form 4 April 2006; accepted 13 April 2006

Available online 24 May 2006

## Abstract

Two different families of compounds, i.e., phenolic and amino acids have been separated by capillary electrophoresis using a physically adsorbed polymer as capillary coating. The polymer used was *N,N*-dimethylacrylamide-ethylpyrrolidine methacrylate (DMA-EpyM) and it provided an stable coating by only flushing the capillary with a DMA-EpyM aqueous solution for 2 min between runs. The usefulness of this procedure has been demonstrated through the fast analysis of different families of solutes. Two different detection systems, diode-array detector and laser-induced fluorescence, have been used to determine phenolic acids and derivatized amino acids with fluorescein isothiocyanate, respectively. The main factors affecting reversal of electroosmotic flow (EOF) such as pH, type and concentration of buffer, and concentration and influence of organic solvents, as well as all the instrumental conditions were studied and optimized for both families of compounds.

© 2006 Elsevier B.V. All rights reserved.

**Keywords:** Phenolic acids; Amino acids; Coelectroosmotic capillary electrophoresis; Coating; Laser-induced fluorescence; DMA-EpyM

## 1. Introduction

Capillary electrophoresis (CE) is a rapidly growing, powerful separation technique that is being used for the separation and characterization of a wide variety of analytes. Because of a good suitability, CE methods have been often used for the separation of small molecules and ions [1–4]. The application of an electric field when using capillary electrophoresis induces a flow of the bulk solution towards the cathode called electroosmotic flow (EOF). Control of the EOF is of major importance for the optimization of separations [5,6]. Different strategies have been adopted to control the EOF including changes in the physicochemical buffer properties, modifications of the capillary surface or application of an external radial voltage to the capillary [7–11].

Concerning to the second approach, there are other reasons for chemical modification of the capillary wall in electrophoresis. Goals may also include reduction or elimination of analyte–wall interactions, improved reproducibility, or resolution of particularly difficult separation problems [12]. The general modification of the capillary wall can be classified into the following categories [13]: to perform dynamic coating by adding the cationic or neutral modifier to the electrolytes [14–16], to adsorb the cationic modifier to the capillary wall permanently by physical adsorption [17,18], and to fix the hydrophilic layer permanently by covalent bonding and/or cross-linking [19,20]. An ideal capillary wall coating is stable under conditions required for separation, preferably over a broad range of buffer pH. Nowadays, another factor to bear in mind to evaluate the suitability of a coating is if its use is compatible with CE–MS applications.

The dynamic coating can cause severe problems when CE is combined with MS because the presence of the non-volatile buffer constituents may deteriorate the ionization of the analytes. Hence, permanent modification would be preferable. Some of the covalent bondings and/or cross-linkings require a relatively

\* Corresponding author. Tel.: +34 958243296; fax: +34 958249510.  
E-mail address: [ansegura@ugr.es](mailto:ansegura@ugr.es) (A. Segura-Carretero).

complicated coating procedure, although their advantage is that they have a long lifetime [13]. On the other hand, the physical adsorption has a shorter lifetime, but it has a simple coating procedure and good reproducibility [21].

Phenolic acids and amino acids are two families of compound very important for health. One vast area of interest has been in food quality [22–24]. Phenolic acids have been associated with color, sensory qualities, and nutritional and antioxidant properties of foods [25]. One impetus for analytical investigations has been the role these phenolics have in organoleptic properties (flavor, astringency, and hardness) of foods [26,27]. Additionally, the food industry has investigated the content and profile of phenolic acids, their effect on fruit maturation, prevention of enzymatic browning, and their roles as food preservatives [28]. Recent interest in phenolic acids stems from their potential protective role, through ingestion of fruit and vegetables, against oxidative damage diseases (coronary heart disease, stroke, and cancers) [29–31].

Amino acids are also very important in many fields [32]. Their compositional analysis in proteins and peptides is essential for the study of the primary structure in biochemistry [33]. Determination of amino acids in body fluids such as urine and blood can help in the diagnosis and treatment of diseases [33]. While in food science, amino acids are measured to correlate flavor trends, monitor fermentation and assess the quality of the final product [34–37].

Different CE methods with reversal EOF have already been applied for the separations of phenolic compounds [38–43] and amino acids [44,45] using different non-permanent coatings. The *N,N*-dimethylacrylamide-ethylpyrrolidine methacrylate (DMA-EpyM) proposed in this work is a simple and reproducible physically adsorbed coating that was synthesized by reaction of *N*-(2-hydroxyethyl)-2-pyrrolidine with methacryloyl chloride and purified by a column chromatography [46]. The use of other physically adsorbed polymers has been proved as an interesting strategy to reduce the adsorption phenomena in several previous papers [18,47,48]; however, because the attachment of the coating to the wall is based on adsorption, a small amount of coating agent is frequently added to the separation medium to keep the coating on the capillary wall surface, fact that as we have commented before could be a problem in CE–MS.

Using DMA-EpyM, adding coating agent in the buffer is not necessary, its regeneration is achieved just only flushing the capillary with a polymer solution between injections and for this reason its use is compatible with CE–MS methods. The usefulness of this polymer coating has been demonstrated in the analysis of proteins in food [46,49] and, recently in the analysis of amino acids by chiral capillary electrophoresis-mass spectrometry [50].

The main goal of this research is the development of new CE procedures based on coelectroosmotic capillary electrophoresis using the mentioned DMA-EpyM copolymer as coating for demonstrating that it is useful for the analysis of two families of compounds (phenolic acids and amino acids, using DAD-detector and LIF, respectively), which are very interesting from a medical and industrial point of view. We have also proved that its use permits the addition of organic modifiers to the buffer without losing repeatability or reproducibility.

## 2. Materials and methods

### 2.1. Instrumentation

CE determination of phenolic acids was performed with a Beckman P/ACE™ MDQ capillary electrophoresis instrument. A diode-array detector was used to detect the individual compounds at their optimum wavelengths and to identify them by comparing their UV spectra with those of the reference compounds, comparing migration times, and by spiking the mixture of all the phenolic acids with standard compounds. UV detection was performed at 210 and 275 nm simultaneously in all the analyses. Data acquisition and processing were carried out with GOLD software installed in a personal computer.

The detection of amino acids was carried out using a Beckman 5500 capillary electrophoresis equipped with a laser-induced fluorescence detector, using an argon ion laser as excitation source (488 nm) and the electropherograms were recorded by monitoring the emission intensity at 520 nm.

All capillaries (fused silica) used were obtained from Beckman instrument, Inc. (Fullerton, CA, USA) and had an inner diameter of 75  $\mu\text{m}$ , a total length of 57 cm and an effective separation length of 50 cm. The temperature was controlled in both instruments using a fluorocarbon based cooling fluid.

### 2.2. Chemicals

The phenolic acids: 4-hydroxyphenylacetic acid, gallic acid (3,4,5-trihydroxybenzoic acid), vanillic acid (4-hydroxy-3-methoxybenzoic acid), protocatechuic acid (3,4-dihydroxybenzoic acid), caffeic acid (3,4-dihydroxycinnamic acid), dopac (3,4-dihydroxyphenylacetic acid), *p*-coumaric acid (4-hydroxycinnamic acid), sinapinic acid (3,5-dimethoxy-4-hydroxycinnamic acid), *trans*-cinnamic acid, *o*-coumaric acid (2-hydroxycinnamic acid), ferulic acid (4-hydroxy-3-methoxycinnamic acid) and gentisic acid (2,5-dihydroxybenzoic acid) standard were obtained from Sigma–Aldrich (St. Louis, MO). 4-Hydroxybenzoic acid was acquired from Fluka. The stock solutions containing all the 13 compounds were prepared in methanol/water (50:50, v/v) at a concentration of 200  $\text{mg L}^{-1}$  for each analyte.

The family of amino acids was made with three non-essential (glutamic acid, aspartic acid and glycine) and two essential amino acids (threonine and tryptophan), all of them were obtained from Sigma (St. Louis, MO, USA). Stock standard solutions of a mixture of these five compounds were prepared in doubly deionized water containing different concentrations of the analytes under study (5  $\text{mg L}^{-1}$  for glycine and threonine; 10  $\text{mg L}^{-1}$  in the case of aspartic acid and glutamic acid; and 15  $\text{mg L}^{-1}$  for tryptophan). For the first four mentioned compounds we used these concentrations to obtain the same signal height (approx.); in the case of tryptophan the detection and quantification limits were lower, for this reason we used a bigger concentration of this compound in the mixture of five amino acids.

The solutions used for the derivatization procedure of the amino acids were: FITC ( $1.0 \times 10^{-2}$  M) in acetone (obtained

from Scharlau), and a 0.2 M sodium carbonate/bicarbonate buffer (pH 9).

Sodium hydroxide was purchased from Merck (Darmstadt, Germany); sodium tetraborate (borax) and di-sodium hydrogen phosphate were obtained from Sigma, and sodium acetate and potassium hydrogen phthalate from Panreac (Montcada I Reixac; Barcelona (Spain)), which were all used as running buffers at different concentrations and pHs. Methanol was acquired from Panreac (Montcada I Reixac, Barcelona, Spain) and 2-propanol was obtained from Merck (Germany); they were HPLC grade.

### 2.3. Coating procedure

The synthesis of the DMA-EpyM polymer used as coating has been described elsewhere [46]. A very simple coating strategy was used flushing the capillary prior to each run with a diluted polymer solution ( $0.1 \text{ mg mL}^{-1}$  in water) for 2 min and then flushing the capillary with the separation buffer for 2 min.

### 2.4. CE conditions for phenolic acids

Separation of phenolic acids was performed in a coated fused silica capillary with  $75 \mu\text{m}$  internal diameter (i.d.) and a total length of 57 cm (50 cm to the detector).

A buffer solution of 50 mM  $\text{Na}_2\text{HPO}_4$  at pH 6 with 10% of 2-propanol (v/v) was selected as optimum for CE separations after appropriate optimization (see Section 3.1). In these conditions a mixture of 13 phenolic acids was injected hydrodynamically in the cathodic end at 3450 Pa (0.0345 bar or 0.5 psi) for 8 s. Each electrophoretic run was carried out at  $-25 \text{ kV}$  (resulting in a current of  $-125 \mu\text{A}$  approx.) maintaining the capillary temperature at  $22^\circ\text{C}$ . UV detection was performed at 210 and 275 nm simultaneously. Diode-array detection was used over the range of 190–600 nm to achieve spectral data.

All solutions were filtered through a  $0.45 \mu\text{m}$  Millipore (Bedford, MA, USA) membrane filters before injection into the capillary.

Every time a new capillary was used it was preconditioned by rinsing with 0.5 M NaOH for 20 min, followed by a 5 min rinse with Milli-Q water. Between injections, capillaries were rinsed with water for 1 min, 2 min of polymer solution ( $0.1 \text{ mg mL}^{-1}$ ) and 2 min of buffer solution.

The running buffer was changed after four runs.

### 2.5. Derivatization of amino acids and CE conditions

The derivatization reaction for the amino acids consisted in  $495 \mu\text{L}$  of 0.2 M carbonate buffer (pH 9),  $1000 \mu\text{L}$  of FITC solution ( $1.0 \times 10^{-2} \text{ M}$ ) and  $1000 \mu\text{L}$  of acetone mixed with  $600 \mu\text{L}$  of a mixture of amino acids at different concentrations, adding doubly deionized water to a final volume of 5 mL in a test tube, using very similar conditions to those described elsewhere [51]. This solution was introduced in a thermostatic bath for 2 h at  $50^\circ\text{C}$ , and 2 mL of the resulting solution were diluted to a final volume of 10 mL with doubly deionized water before the analysis.

This solution was injected in the CE–LIF for the analysis.

Separation of the derivatized amino acids was performed in a coated fused silica capillary with  $75 \mu\text{m}$  internal diameter (i.d.) and a total length of 57 cm (50 cm to the detector).

As above, the CE buffer for amino acids analysis was carefully selected obtaining the best results using a solution of 25 mM  $\text{Na}_2\text{HPO}_4$  at pH 6 and 20% propanol (v/v).

The derivatized mixture was injected hydrodynamically at 0.5 psi for 12 s and detection was carried out by on-column measurement of 488 nm wavelength excitation and 520 nm emission. The voltage applied was  $-25 \text{ kV}$  and the current achieved was  $-59 \mu\text{A}$  maintaining the capillary temperature at  $22^\circ\text{C}$ .

All solutions were filtered through a  $0.20 \mu\text{m}$  Millipore (Bedford, MA, USA) membrane filters before injection into the capillary.

The capillary conditioning was the same that the protocol described in Section 2.4. The running buffer was changed after four runs.

## 3. Results and discussion

### 3.1. Separation of phenolic acids using DMA-EPyM coated capillaries

This family of phenolic acids was made to obtain a representative phenolic acid mixture to propose a potent analytical method for the analysis of these compounds in a wide variety of samples. Caffeic, *p*-coumaric, vanillic, ferulic and protocatechuic are acids present in nearly all plants [52]. Furthermore, several of the compounds we have included in the standard mixture are present in grape and berry extracts, orange, apple and other juices, bread, carrots, dried lentils, white, red and rose whines, olive fruits, olive oils, beer, etc.

The instrumental and experimental conditions were carefully studied to obtain the best sensitivity and resolution among the analytes under study. The effect of pH was studied between 5.0 and 9.5 using different buffers depending on the range of pH. The DMA-EPyM coated capillaries show an anodal EOF at low pH values, a nearly zero EOF at pHs around 6 and a low cathodal EOF at pHs higher than 8 [46].

After the preliminary studies, we decided to compare the different buffer solutions at a concentration of 50 mM. Sodium acetate/acetic acid was used in the range of pH from 4.5 to 5.5, observing that the migration times of the analytes decreased with an increase of the pH value. Potassium hydrogen phthalate/sodium hydroxide was used between 4.5 and 6, but using this buffer the current was not very stable. Best results were obtained with di-sodium hydrogen phosphate/monobasic sodium phosphate buffer; it was checked in the range of pH 6–8. Finally, to study higher pH values, sodium tetraborate with HCl or NaOH was used (between 8 and 10). When sodium tetraborate was used, the time of analysis in all the range of pH was longer than that obtained with other buffers; this fact could be explained for the cathodal EOF generated, and also obviously for the different separation power of each buffer. In Fig. 1, the behaviour of three of the used buffers is shown. A more detailed study between pH 6 and 8 was carried out (in steps of 0.2) after choosing di-sodium



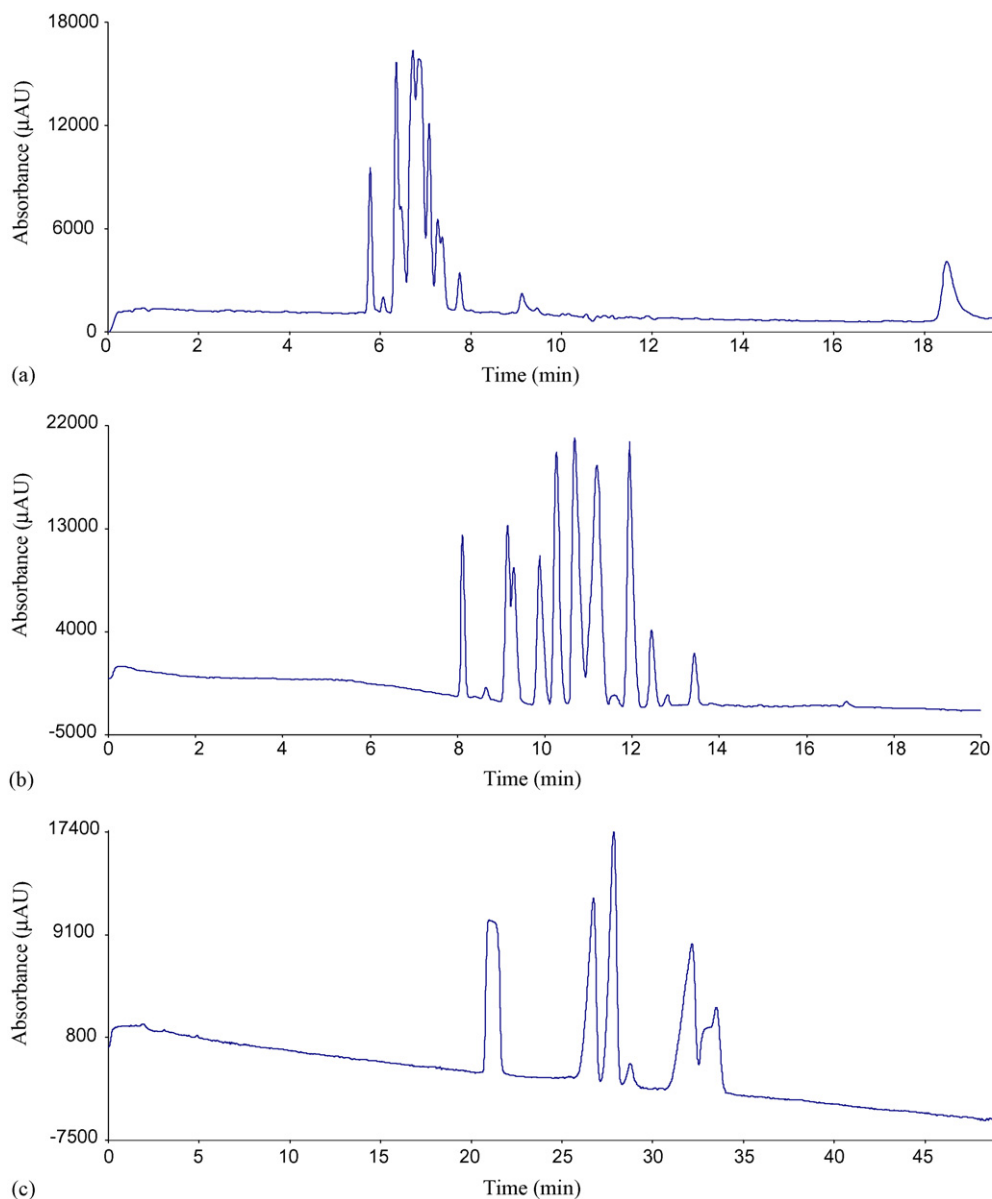


Fig. 1. Electropherograms of a sample containing the 13 phenolic acids under study (in methanol/water (50:50, v/v) at a concentration of  $40 \text{ mg L}^{-1}$  of each compound) using different buffer systems: (a) sodium acetate/acetic acid at a pH value of 5.5; (b) di-sodium hydrogen phosphate/monobasic sodium phosphate buffer at a pH value of 6; and (c) sodium tetraborate at a pH of 9.6. Other separation conditions: capillary,  $57 \text{ cm} \times 75 \text{ }\mu\text{m}$  (effective separation length of 50 cm); applied voltage,  $-25 \text{ kV}$ ; buffer concentration, 50 mM; hydrodynamic injection, 0.5 psi for 8 s. Detection was performed at 210 nm.

hydrogen phosphate solution as buffer and the optimum value was pH 6.

The buffer concentration was investigated in a range between 25 and 75 mM (in steps of 5). We found that 50 mM of di-sodium hydrogen phosphate buffer at pH 6 represented a good compromise for the resolution of the compounds studied and a reasonable analysis time, since higher buffer concentrations improved the separation but provided longer analysis time.

In order to achieve the total separation of phenolic acids the addition of different organic solvents to the separation buffer was studied. Namely methanol, acetonitrile, 1-propanol and 2-propanol were tested, obtaining the best results with 2-propanol. It could be observed that the resolution of all the analytes after

study was sufficient with 10% of 2-propanol (v/v); with higher percentages of 2-propanol, the resolution was not improved, but rather it was even worse (see Fig. 2). The percentage of 2-propanol was studied between 0 and 30% (v/v). The addition of organic modifiers to the buffer could also permit us to prove the repeatability and reproducibility of DMA-EPyM in presence of organic solvents.

The effect of the applied voltage on resolution of the 13 compounds was studied using the previously mentioned buffer composition, and the optimum value was  $-25 \text{ kV}$ . As we were working with compounds which have negative charge at the optimum pH of the buffer, changing the polarity of the electrodes (reversed) makes sense to reduce the analysis time. The



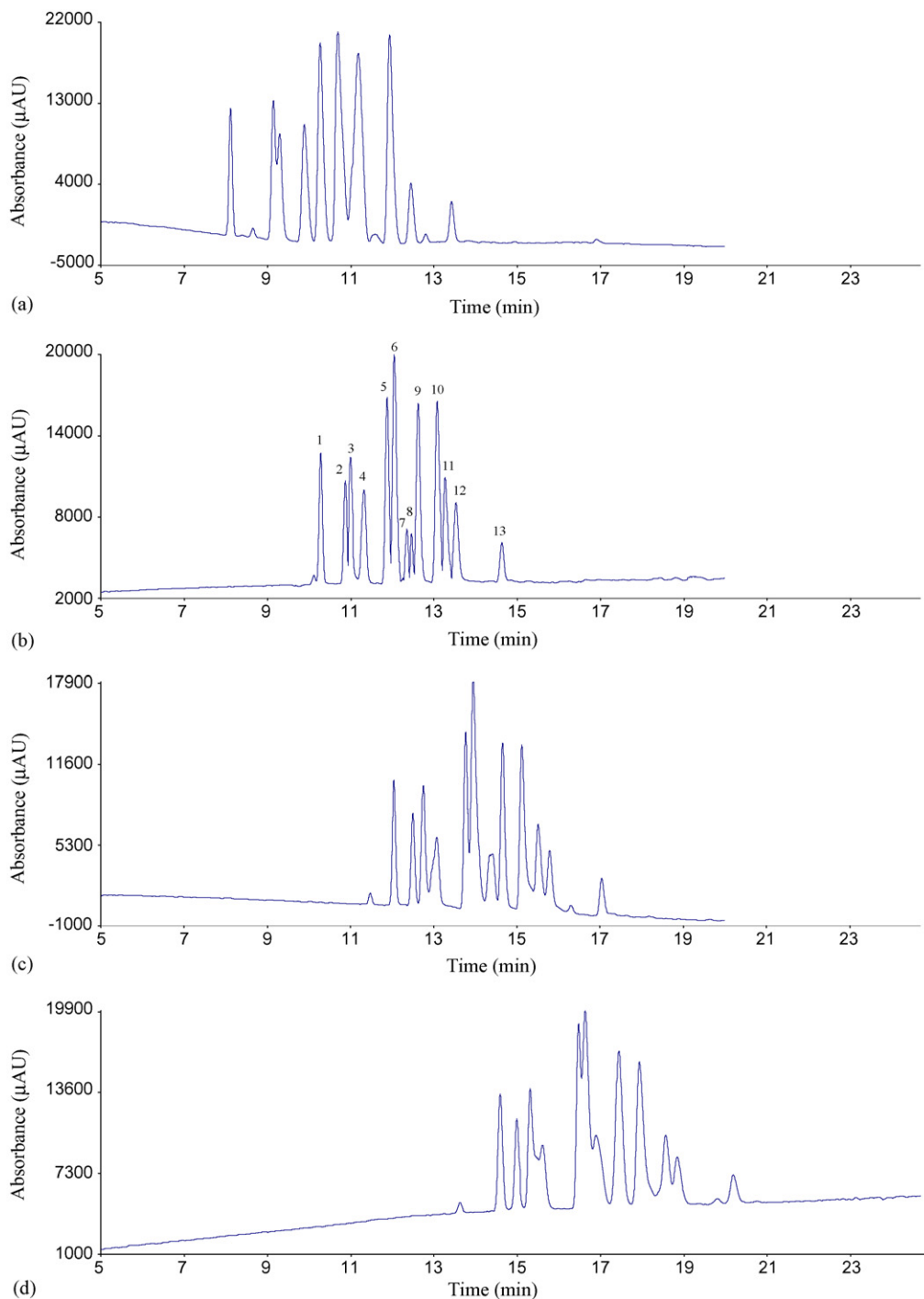


Fig. 2. Study of the influence of the addition of organic modifier (2-propanol) at different concentrations to the buffer solution: (a) 0% of 2-propanol; (b) 10% of 2-propanol; (c) 15% of 2-propanol; and (d) 20% of 2-propanol. Other separation conditions: capillary, 57 cm  $\times$  75  $\mu$ m (effective separation length of 50 cm); applied voltage,  $-25$  kV; di-sodium hydrogen phosphate/monobasic sodium phosphate buffer at a pH value of 6 and 50mM; hydrodynamic injection, 0.5 psi for 8 s. Sample containing all the 13 phenolic acids at 40 mg L $^{-1}$ . Detection was performed at 210 nm. Peak identification numbers: 1, 4-hydroxybenzoic acid; 2, gentisic acid; 3, protocatechuic acid; 4, vanillic acid; 5, gallic acid; 6, *trans*-cinnamic acid; 7, 4-hydroxyphenylacetic acid; 8, *o*-coumaric acid; 9, *p*-coumaric acid; 10, dopac; 11, caffeic acid; 12, ferulic acid; and 13, sinapinic acid.

samples were injected at the negative end (hydrodynamic injection during 8 s) and detection was performed at the positive end.

The temperature during washing and analysis was 22 °C.

The optimum electropherogram obtained from a standard mixture of these 13 phenolic acids can be seen in Fig. 2b.

### 3.2. Separation of amino acids using DMA-EPyM coated capillaries

Glutamic acid, aspartic acid and glycine (non-essential), and threonine and tryptophan (essential) were selected for their separation using coelectroosmotic capillary electrophoresis using

DMA-EPyM. We chose these compounds because of their importance from a medical and nutritional point of view, and their presence in a lot of foods (fish, meat, beans, dairy products, cottage cheese, bananas, etc.). Furthermore, if we consider their side chains, working with these five compounds, we analyze the simplest amino acid (glycine) since it has the smallest possible side chain ( $-H$ ), one which contains an aromatic side chain (tryptophan), one amino acid that contains an extra hydroxyl group (threonine), and two with acidic side chains. This family permitted to demonstrate that the separation of these compounds can be carried out using LIF as detection system and adding organic modifiers in the separation buffer using DMA-EpyM as stationary polymer in the capillary.

For the development of this method the steps carried out in the optimization were the same than those described in the Section 3.1.

In this case, three different salts were tested as buffers (disodium hydrogen phosphate, sodium borate and sodium acetate), and again, di-sodium hydrogen phosphate provided the best electropherograms. The effect of pH was studied between 5.7 and 8.0 using 25 mM di-sodium hydrogen phosphate buffer solution (concentration value selected in the preliminary studies) and a value of pH 6 gave rise to the best resolution plus a satisfactory analysis time.

The effect of ionic strength on resolution for the mixture of five amino acids was also checked varying the concentration of di-sodium hydrogen phosphate between 20 and 50 mM at optimum pH value, obtaining the best resolution with a concentration of 25 mM.

Then, the percentage of 2-propanol was studied between 0 and 25% (v/v) (using a 25 mM di-sodium hydrogen phosphate at pH 6). The increase of this percentage improved the resolution between peaks, and finally we decided to select 20% as optimum value.

The instrumental variables were carefully studied as well. The optimum voltage value was  $-25$  kV and hydrodynamic injection time (0.5 psi) was used selecting as optimum time 12 s.

Fig. 3 shows the electropherogram of the separation of these five derivatized amino acids in the optima conditions. The elution order is easily understood observing the structure of the molecules under study: firstly, aspartic and glutamic acids which contain in their chemical structure two  $-COOH$  groups. These two compounds only differ in one  $-CH_2-$  group in their side chains. The other three compounds have the same charge at the optimum pH, so the elution order will depend on the size of the molecules and will be glycine, threonine and tryptophan.

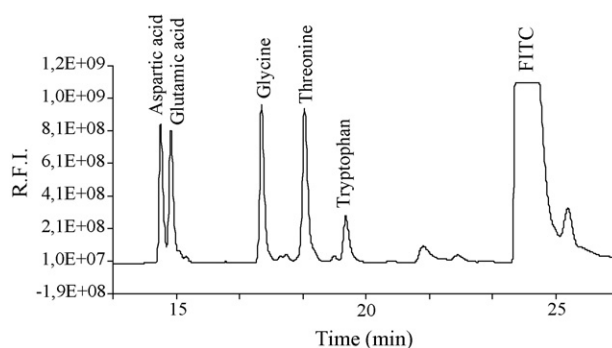


Fig. 3. Electropherogram obtained for a sample of five amino acids under optimized conditions using laser-induced fluorescence as detector. Optima separation conditions: capillary,  $57 \text{ cm} \times 75 \mu\text{m}$  (effective separation length of 50 cm); applied voltage,  $-25$  kV; buffer, 25 mM  $\text{Na}_2\text{HPO}_4$  at pH 6 and 20% propanol; hydrodynamic injection, 0.5 psi for 12 s. Conditions of detection: 488 nm wavelength excitation and 520 nm emission. Sample containing the five analytes under study in these concentrations:  $120 \mu\text{g L}^{-1}$  for glycine and threonine;  $240 \mu\text{g L}^{-1}$  in the case of aspartic acid and glutamic acid; and  $360 \mu\text{g L}^{-1}$  for tryptophan.

### 3.3. Repeatability and reproducibility study

#### 3.3.1. Study of the repeatability and reproducibility of the CE-UV method for phenolic acids

Repeatability was studied by performing series of separations using the optimized method on one of the samples containing all the standards ( $40 \text{ mg L}^{-1}$  of each phenolic acid) on the same day (intraday precision,  $n=8$ ) and on three consecutive days (interday precision,  $n=12$ ). The relative standard deviations (R.S.D.s) of peak areas and migration times were determined considering five of the phenolic compounds under study (4-hydroxybenzoic acid, protocatechuic acid, *o*-coumaric acid, caffeic acid and sinapinic acid). We chose these compounds to check the repeatability and reproducibility in all the zones of the electropherogram, with analytes with short, medium and long migration time.

The intraday repeatabilities on the migration time for these five analytes (expressed as R.S.D.) were found inside the range between 0.49 and 0.94%, whereas the interday repeatabilities on the migration time were between 0.89 and 1.64%.

The intraday repeatabilities on the total peak area (expressed as R.S.D.) were between 1.24 and 2.32%, whereas the interday repeatabilities on total peak area were found in the range from 2.14 to 3.22%. These data are summarized in Table 1.

In practice, batch-to-batch reproducibility is a key issue. The reproducibility was studied by performing eight separations

Table 1  
R.S.D. values of the peak area and migration time obtained in the study of repeatability of the CE-UV method for the phenolic acids

Compound	Intraday ( $n=8$ )		Interday ( $n=12$ )	
	Peak area	Migration time	Peak area	Migration time
4-Hydroxybenzoic acid	1.24	0.54	2.14	0.89
Protocatechuic acid	2.32	0.49	2.35	1.23
<i>o</i> -Coumaric acid	1.76	0.67	2.16	0.91
Caffeic acid	1.87	0.89	3.22	0.98
Sinapinic acid	2.01	0.94	2.28	1.64

Table 2

R.S.D. values of the peak area and migration time obtained with different columns, different sample and different operator of the CE–UV method for the phenolic acids

Compound	Reproducibility ( $n = 8$ )	
	Peak area	Migration time
4-Hydroxybenzoic acid	2.32	1.23
Protocatechuic acid	3.01	1.54
<i>o</i> -Coumaric acid	2.89	2.54
Caffeic acid	2.03	2.67
Sinapinic acid	2.77	2.33

of other sample containing all the standards of phenolic acids ( $40 \text{ mg L}^{-1}$  of each phenolic acid under study) 24 h later than the analysis of the first, under the same conditions but different operator and different capillary. The results obtained, as shown in Table 2, were between 1.23 and 2.67% for the migration times and between 2.03 and 3.01% for total peak area (expressed as R.S.D.) considering the five analytes previously mentioned.

### 3.3.2. Repeatability and reproducibility study of the CE–LIF method for amino acids

This study was carried out performing series of separations using the optimized method, as we have described in the previous section. The repeatability of the DMA–EpyM coating was evaluated by measuring the relative standard deviations (R.S.D.s) of migration times of all the five amino acids under study (glutamic acid, aspartic acid, glycine, threonine and tryptophan). Eight replicates of migration time measurement for the five amino acids at the same day were used to examine the short-term stability of the coated capillary. These data can be seen in Fig. 4, the migration time data indicate that the short-term stability of the coated capillary is reasonably good (with R.S.D.s in the range of 0.39–0.65%). Similarly, eight replicates of migration time measurement for the five amino acids on different days in one week were also used to test the long-term stability of the stationary polymer coated capillary. As shown in Fig. 5, the migration time data indicate that the long-stability of the coated capillary is also reasonably good (with R.S.D.s in the range of 0.33–1.03%).

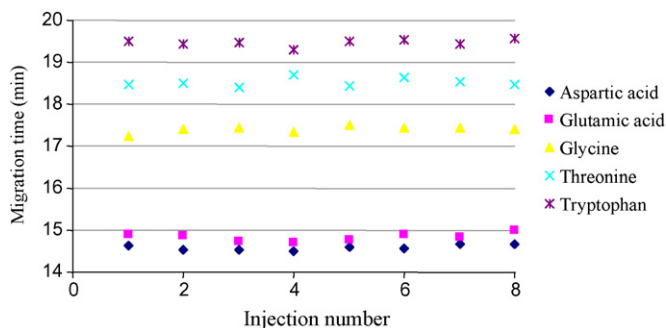


Fig. 4. Study of intraday repeatability for the CE–LIF method. Eight replicates of migration time measurement for the five amino acids at the same day were used to examine the short-term stability of the coated capillary. Sample containing the five analytes under study in these concentrations:  $120 \text{ } \mu\text{g L}^{-1}$  for glycine and threonine;  $240 \text{ } \mu\text{g L}^{-1}$  in the case of aspartic acid and glutamic acid; and  $360 \text{ } \mu\text{g L}^{-1}$  for tryptophan.

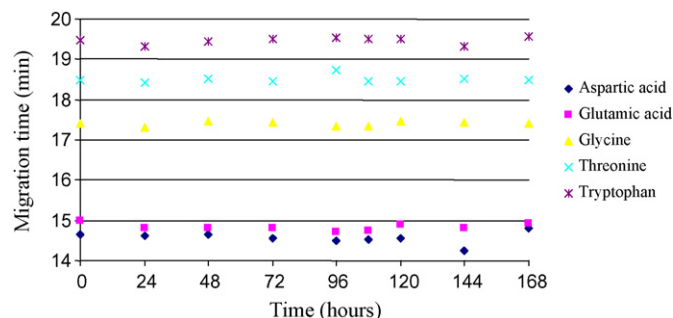


Fig. 5. Study of interday repeatability for the CE–LIF method. Eight replicates of migration time measurement for the five amino acids on different days in one week were also used to examine the long-term stability of the stationary polymer coated capillary. Sample containing the five analytes under study in these concentrations:  $120 \text{ } \mu\text{g L}^{-1}$  for glycine and threonine;  $240 \text{ } \mu\text{g L}^{-1}$  in the case of aspartic acid and glutamic acid; and  $360 \text{ } \mu\text{g L}^{-1}$  for tryptophan.

As commented before, reproducibility is a very important issue. The reproducibility was studied by performing 24 separations of other sample containing all the standards of amino acids 24 h later than the analysis of the first, under the same conditions but different operator and different capillary. The results obtained were between 1.02 and 2.98% for the migration times (expressed as R.S.D.) considering the five analytes previously mentioned (2.98% for glutamic acid, 2.32% for aspartic acid, 1.54% for glycine, 1.23% for threonine and 1.02% for tryptophan), suggesting that this physically adsorbed copolymer gives a good batch-to-batch reproducibility using this CE–LIF method for amino acids.

### 3.4. Calibration, linearity and detection limits

#### 3.4.1. Calibration curves, linearity and detection limits for phenolic acids

The detection limits ( $\text{LOD} = 3\sigma_b/b$ ) and quantitation limits ( $\text{LOQ} = 10\sigma_b/b$ ) of the method were tested for the studied analytes using the IUPAC method, where  $\sigma_b$  is the white standard deviation and  $b$  the slope of the calibration curves [53]. Standard calibration graphs were prepared for each analyte and all calibration curves showed good linearity between LOQ depending on the analytes studied and  $200 \text{ mg L}^{-1}$ . Each point of the calibration plot was repeated three times in the same way. The calibration plots indicate good correlation between peak areas and analyte concentrations; regression coefficients were higher than 0.996 for all the compounds quantified. The results obtained for the phenolic acids are summarized in Table 3.

#### 3.4.2. Calibration curves, linearity and detection limits for amino acids

Standard calibration graphs were prepared for each analyte in the range of  $\text{LOQ}–1200 \text{ } \mu\text{g L}^{-1}$  for glycine and threonine, from  $\text{LOQ}$  to  $2400 \text{ } \mu\text{g L}^{-1}$  in the case of aspartic and glutamic acid, and from  $\text{LOQ}$  to  $3600 \text{ } \mu\text{g L}^{-1}$  for tryptophan and three replicates of each point of the calibration curve were made to set up the calibration. The detection (LOD) and quantification limit (LOQ) were calculated for the studied analytes using the method proposed by Curie [53]. The calibration plots indicate

Table 3  
Limit of detection (LOD) and quantification (LOQ) for each phenolic acid under study

Compound	LOD (mg L <sup>-1</sup> )	LOQ (mg L <sup>-1</sup> )
4-Hydroxybenzoic acid	1.23	4.10
Gentisic acid	1.87	6.23
Protocatechuic acid	1.34	4.47
Vanillic acid	1.92	6.40
Gallic acid	0.98	3.28
<i>Trans</i> -cinnamic acid	0.46	1.53
4-Hydroxyphenylacetic acid	3.23	10.77
<i>o</i> -Coumaric acid	3.47	11.57
<i>p</i> -Coumaric acid	0.96	3.20
Dopac	1.11	3.70
Caffeic acid	1.46	4.87
Ferulic acid	1.59	5.30
Sinapinic acid	1.79	5.98

Table 4  
Limit of detection (LOD) and quantification (LOQ) for each amino acid under study

Compound	LOD (μg L <sup>-1</sup> )	LOQ (μg L <sup>-1</sup> )
Aspartic acid	45	150
Glutamic acid	51	170
Glycine	18	61
Threonine	14	46
Tryptophan	134	446

good correlation between peak areas and analyte concentrations; regression coefficients were higher than 0.995 for all the compounds quantified. The results obtained for the amino acids are summarized in Table 4.

#### 4. Conclusions

The aim of this study has been to demonstrate that coelectroosmotic capillary electrophoresis using DMA-EpyM as stationary polymer can be used for the analysis of phenolic acids and amino acids. Two methods have been developed; in the case of phenolic acids, we used a CE–UV, and for the amino acids, a CE–LIF method was chosen. Both of them could be used for the analysis of the extracts of a plenty of products which contain these compounds of great interest.

The relative standard deviations (R.S.D.) obtained in the study of repeatability were lower than 0.94% (intraday results) and 1.64% (interday) for the migration times in the case of CE–UV for phenolic acids, and lower than 0.65% (intraday) and 1.03% (interday) for the CE–LIF method to study amino acids.

Detection limits in the CE–UV method for the phenolic acids were between 0.46 mg L<sup>-1</sup> for *trans*-cinnamic acid and 3.47 mg L<sup>-1</sup> for *o*-coumaric acid, and in the CE–LIF method were between 14 μg L<sup>-1</sup> for threonine and 134 μg L<sup>-1</sup> for tryptophan.

It is important to highlight that these values demonstrate that DMA-EpyM provides a stable coating even when the separation buffer contains organic modifiers. All these facts make broader the usefulness of this coating.

#### Acknowledgements

The authors are very grateful to the research group FQM 297 of the Junta de Andalucía and the Ministry of Science and Technology (Projects BQU 2002-03418 and PETRI No. 95-809.OP). The authors thank to the Institute of Science and Technology of Polymers (CSIC) for their valuable contribution carrying out the synthesis of the polymer coating used.

#### References

- [1] P. Jandik, G.K. Bonn, Capillary Electrophoresis of Small Molecules and Ions, VCH Publishers, New York, 1993.
- [2] A. Fernández-Gutiérrez, C. Cruces-Blanco, S. Cortacero-Ramírez, A. Segura-Carretero, Chromatographia 52 (2000) 413.
- [3] J. Hagberg, J. Chromatogr. A 988 (2002) 127.
- [4] H. Sawada, C. Nogami, Anal. Chim. Acta 507 (2004) 191.
- [5] E. Kenndler, J. Capillary Electroph. 3 (4) (1996) 191.
- [6] E. Kenndler, J. Microcolumn Sep. 10 (3) (1998) 273.
- [7] N.A. Poldin, M.A. Hayes, Anal. Chem. 72 (5) (2000) 1088.
- [8] V. Kasicka, Z. Prusik, P. Sazelova, M. Chiari, I. Miksik, Z. Deyl, J. Chromatogr. B 741 (1) (2000) 43.
- [9] C.S. Lee, W.C. Blanchard, C.T. Wu, Anal. Chem. 62 (1990) 1550.
- [10] C.S. Lee, D.C. McManigill, C.T. Wu, Anal. Chem. 63 (1991) 1519.
- [11] M.A. Hayes, A.G. Ewing, Anal. Chem. 64 (1992) 512.
- [12] J. Horvath, V. Dolnik, Electrophoresis 22 (2001) 644.
- [13] H. Katayama, Y. Ishihama, N. Asakawa, Anal. Chem. 70 (1998) 5272.
- [14] Y.J. Yao, S.F.Y. Li, J. Chromatogr. A 663 (1994) 97.
- [15] M. Gilges, M.H. Kleemiss, G. Schomburg, Anal. Chem. 66 (1994) 2038.
- [16] P.G. Righetti, C. Gelfi, B. Verzola, L. Castelletti, Electrophoresis 22 (2001) 603.
- [17] K.A. Assi, K.D. Altria, B.J. Clark, J. Pharm. Biomed. Anal. 15 (1997) 1041.
- [18] F.B. Erim, A. Cifuentes, H.J. Poppe, C. Kraak, J. Chromatogr. A 708 (1995) 356.
- [19] S. Hjerten, J. Chromatogr. 347 (1985) 191.
- [20] D. Schmalzing, C.A. Piggee, F. Foret, E. Carrilho, B.L. Karger, J. Chromatogr. 480 (1993) 149.
- [21] E. Cordova, J. Gao, G.M. Whitesides, Anal. Chem. 69 (1997) 1370.
- [22] L. Barthelmebs, C. Divies, J.F. Cavin, Appl. Environ. Microbiol. 66 (2000) 3368.
- [23] S. Hakkinen, M. Heinonen, S. Karenlampi, H. Mykkanen, J. Ruuskanen, R. Torronen, Food Res. Int. 32 (1999) 345.
- [24] L. Xu, L.L. Diosady, Food Res. Int. 30 (1997) 571.
- [25] J.A. Maga, Crit. Rev. Food Sci. Nutr. 10 (1978) 323.
- [26] J.B. Harborne, The Flavonoids: Advances in Research Since 1986, Chapman & Hall, London, UK, 1994.
- [27] H. Peleg, M. Naim, R.L. Rouseff, U. Zehavi, J. Sci. Food Agric. 57 (1991) 417.
- [28] F. Shahidi, M. Nacsk, Food Phenolic: Sources, Chemistry, Effects, and Application, Technomic Publishing Company, Inc., Lancaster, PA, 1995.
- [29] R.J. Robbins, J. Agric. Food Chem. 51 (10) (2003) 2866.
- [30] C.A. Gomes, T. Girao da Cruz, J.L. Andrade, N. Milhazes, F. Borges, M.P.M. Marques, J. Med. Chem. 46 (2003) 5395.
- [31] H. Masaki, N. Okamoto, S. Sakaki, H. Sakurai, Biol. Pharm. Bull. 20 (1997) 304.
- [32] V. Poinso, C. Bayle, F. Courderc, Electrophoresis 24 (2003) 4047.
- [33] T. Soga, D.N. Heiger, Anal. Chem. 72 (2000) 1236.
- [34] T.C. Liao, C.M. Jiang, M.C. Wu, J.Y. Hwang, H.M. Chang, Electrophoresis 22 (2001) 1484.
- [35] E. Chiavaro, S. Bonardi, E. Maggi, Ind. Aliment. 37 (1998) 1397.
- [36] K.H. Steinkraus, Food Res. Int. 27 (1994) 259.
- [37] M. Villamiel, N. Corzo, I. Martínez-Castro, A. Olano, Food Chem. 56 (1996) 385.
- [38] S.M. Masselter, A.J. Zemmann, O. Bobleter, Electrophoresis 14 (1993) 36.
- [39] N.J. Benz, J.S. Fritz, J. High Resol. Chromatogr. 18 (1995) 175.

- [40] S.M. Masselter, A.J. Zemann, J. Chromatogr. A 693 (1995) 359.
- [41] S.M. Masselter, A.J. Zemann, J. Anal. Chem. 67 (1995) 1047.
- [42] A.J. Zemann, J. Capillary Electroph. 2 (1995) 131.
- [43] A. Carrasco-Pancorbo, A. Segura-Carretero, A. Fernández-Gutiérrez, J. Sep. Sci. 28 (2005) 925.
- [44] H.Y. Zhai, P.X. Cai, Z.G. Chen, G.H. Li, X. Ye, J.Y. Mo, Chem. J. Chinese U 25 (2004) 1037.
- [45] M.S. Chun, D.S. Chung, Anal. Chim. Acta 491 (2003) 173.
- [46] N. González, C. Elvira, J. San Román, A. Cifuentes, J. Chromatogr. A 1012 (2003) 95.
- [47] J.K. Towns, F.E. Regnier, J. Chromatogr. 516 (1990) 69.
- [48] M. Chiari, M.F. Cretich, L. Damin, R. Ceriotti, Electrophoresis 21 (2000) 909.
- [49] C. Simó, C. Elvira, N. González, J. San Román, C. Barbas, A. Cifuentes, Electrophoresis 25 (2004) 2056.
- [50] C. Simó, A. Rizzi, C. Barbas, A. Cifuentes, Electrophoresis 26 (2005) 1432.
- [51] S. Cortacero-Ramírez, D. Árraez-Román, A. Segura-Carretero, A. Fernández-Gutiérrez, Food Chem. 100 (2007) 383–389.
- [52] F. Shahidi, P.K. Wanasundara, Crit. Rev. Food Sci. Nutr. 32 (1992) 67.
- [53] L.A. Curie, Pure Appl. Chem. 67 (1995) 1699.



# Photolytic oxidation of As species for determination of total As (including the ‘hidden’ As fraction) in coastal seawater by hydride generation-atomic fluorescence spectrometry

E. Castro, I. Lavilla, C. Bendicho\*

*Departamento de Química Analítica y Alimentaria, Área de Química Analítica, Facultad de Química, Universidad de Vigo, As Lagoas-Marcosende s/n, 36200 Vigo, Spain*

Received 10 November 2005; received in revised form 25 February 2006; accepted 3 March 2006  
Available online 18 April 2006

## Abstract

Ultraviolet irradiation (photolysis) in alkaline medium was applied for pretreatment of seawater samples so as to accurately determine total As by continuous-flow hydride generation-atomic fluorescence spectrometry. This sample pretreatment is meant to convert non-reducible As forms into inorganic As, which easily forms arsine. The optimised parameters were the treatment time and the pH of the medium. The behaviour of four hydride-reactive As species [As(III), As(V), MMA, DMA], and AsB, i.e. a typical non-hydride-reactive As species, when subjected to UV irradiation was studied. UV irradiation at pH 1 lead to conversion of all species into As(V) with the exception of AsB and DMA. Conversions of DMA and AsB into As(V) at pH 11 in less than 30 min were observed under UV irradiation. The limit of detection of As (measured as As(V)) by hydride generation-atomic fluorescence spectrometry was 0.1  $\mu\text{g/L}$  and the repeatability of the oxidation procedure was about 10%. The method was applied to determination of total and directly reducible As at 11 sampling points of the Galician Coast (Atlantic Ocean, Spain). Total As concentrations were in the range 1.4–4.8  $\mu\text{g/L}$ . A significant As fraction, between 20 and 44%, depending on the sampling point, corresponded to non-reducible As which was converted by UV irradiation into hydride-reactive As. This fraction should represent the sum of DMA, which yields a low sensitivity in the continuous flow-AFS system, and the hidden As fraction.

© 2006 Elsevier B.V. All rights reserved.

**Keywords:** Total As; Hidden As; Seawater; Photolysis; Atomic fluorescence spectrometry

## 1. Introduction

As is present in seawater at extremely low levels (around 1  $\mu\text{g/L}$ ) being distributed among As(III), As(V), MMA, DMA and unknown organic forms [1]. Hydride generation-atomic absorption spectrometry (HG-AAS) has been the technique of choice for determination of As in seawater due to its simplicity and sensitivity [2]. However, the extremely low As contents in seawater requires a prior preconcentration step using cold traps [3], graphite tubes [4] or sorbents [5]. A further drawback is that total As concentrations cannot be determined when the hydride generation technique is directly applied to the sample owing to the occurrence of non-reactive species. The conversion of non-hydride reactive organic As (also named as refractory

or hidden As) into reducible As forms has been demonstrated using alkaline digestion [6] or UV irradiation [7,8] prior to HG-AAS determination. This suggests that a gross underestimate may be made when using the hydride generation technique for the direct determination of As in estuarine and coastal seawater.

The use of a more sensitive detection technique than AAS such as atomic fluorescence spectrometry (AFS), can avoid preconcentration steps prior to detection. Only a few works have dealt with the determination of As in seawater by HG-AFS. Moreda-Pineiro et al. [9] reported the use of HG-AFS for determination of total As in seawater. However, the method did not have into account the presence of methylated and refractory As species. Featherstone et al. [10] carried out the determination of As(III), As(V), MMA and DMA in seawater by hydride generation, cold trapping of the hydrides and AFS detection. This work did not tackle the determination of total As including the ‘hidden’ As.

\* Corresponding author. Tel.: +34 986 812281; fax: +34 986 812556.  
E-mail address: [bendicho@uvigo.es](mailto:bendicho@uvigo.es) (C. Bendicho).

The aim of this work is to develop a method for the accurate determination of the total As content in coastal seawater with minimum sample pretreatment and without any preconcentration step. Seawater samples were collected along the Galician Coast (Atlantic Ocean, Spain) and total As was determined by HG-AFS after conversion of all As species into As(V) by UV irradiation. The method provides information about the hydride-reactive and the non-hydride reactive As fraction and could be used for screening purposes prior to more sophisticated analytical techniques for speciation.

## 2. Experimental

### 2.1. Apparatus

A PS Analytical Model Excalibur atomic fluorescence detector (UK), equipped with an integrated continuous hydride generation system and a As boosted discharge lamp (Photron) was used. Conditions for arsine generation in the continuous-flow system were as follows: the NaBH<sub>4</sub> flow-rate was 4 mL/min; carrier flow-rate (HCl) was 8 mL/min; reducing agent concentration was 0.7% m/v; carrier concentration (HCl) was 30% v/v; drying gas flow-rate (N<sub>2</sub>) was 2.5 L/min. The As atomic fluorescence line at 193.7 nm was employed for quantification. Instrumental parameters are shown in Table 1. A 705 UV-digester (Hg high pressure lamp, 500 W) (Metrohm) was used for UV-irradiation of seawater samples.

### 2.2. Reagents

All chemicals were of analytical-reagent grade. Deionized water from a Milli-Q water purifier (Millipore, Mosheim, France) was used throughout. As standards were prepared from the following reagents: Na<sub>2</sub>HAsO<sub>4</sub>·7H<sub>2</sub>O (Panreac, Spain); [(CH<sub>3</sub>)<sub>2</sub>HAsO<sub>2</sub>] (DMA) (Riedel-de Haën, Germany) and CH<sub>3</sub>AsO(ONa)<sub>2</sub>·6H<sub>2</sub>O (MMA) (Carlo Erba, Italy); As<sub>2</sub>O<sub>3</sub> (Merck, Germany). Arsenobetaine (AsB) [BCR CRM 626, 1031 ± 6 µg/g] (European Commission, Community Bureau of

Table 1  
Instrumental parameters

Atomic fluorescence detector	
Wavelength (nm)	193.7
Bandpass (nm)	0.5
Primary current (mA)	27.5
Boost current (mA)	35
Range	10
Continuous hydride generation	
[NaBH <sub>4</sub> ] (% m/v)	0.7
[HCl] (% v/v)	30
N <sub>2</sub> flow-rate (L/min)	2.5
NaBH <sub>4</sub> flow-rate (mL/min)	4
HCl flow-rate (mL/min)	8
Signal acquisition	
Delay (s)	10
Analysis (s)	30
Memory (s)	50



Fig. 1. Map of the study area with sampling points (S1–S9).

Reference) (now, the standards, measurement and testing programme). NaBH<sub>4</sub> and HCl (Merck) were employed as reducing and carrier agent, respectively, for the continuous-flow hydride generation system. 0.1 M NaOH was employed for stabilisation of the reducing agent. Acid pH was adjusted with HCl whilst alkaline pH was adjusted with NaOH.

### 2.3. Procedure

Seawater samples were collected at different points along the Galician Coast (Atlantic Ocean, Spain) (Fig. 1). Polyethylene bottles were used for sampling. These bottles were kept in a 20% (v/v) HNO<sub>3</sub> solution and rinsed with ultrapure water before use. Once in the laboratory, samples were subjected to the following pretreatment: filtration through 0.45 µm filter, adjustment to pH 2 with HCl and storage at 4 °C until analysis. For determination of total As, a 10 mL sample was placed into a quartz tube, pH was adjusted to 11 with NaOH and the sample subjected to UV irradiation for 1 h. Samples were acidified with HCl prior to arsine generation. This measurement gives an estimation of the sum As(III) + As(V) + MMA + DMA + ‘hidden As’. For determination of hydride-reactive As, samples were injected into the continuous-flow hydride generation system without any pretreatment. This measurement should give an estimation of the sum As(III) + As(V) + MMA. The procedure is depicted in Fig. 2. Procedural blanks were run using the same procedure as for samples.

Conditions for the continuous-flow hydride generation system were as follows: a 30% (v/v) HCl concentration solution as carrier; a 0.7% (m/v) NaBH<sub>4</sub> solution stabilized with 0.1 mol/L NaOH was used as reducing agent; the flow rates for the carrier and reducing agent solutions were 8 and 4 mL/min, respectively.

## 3. Results and discussion

### 3.1. Effect of UV irradiation on As species

Apart from organoarsenic species that cannot be detected by the hydride generation technique, methylarsenicals such as DMA and MMA can yield volatile methylated arsines when they react with NaBH<sub>4</sub>. Nevertheless, these methyl-As hydrides can

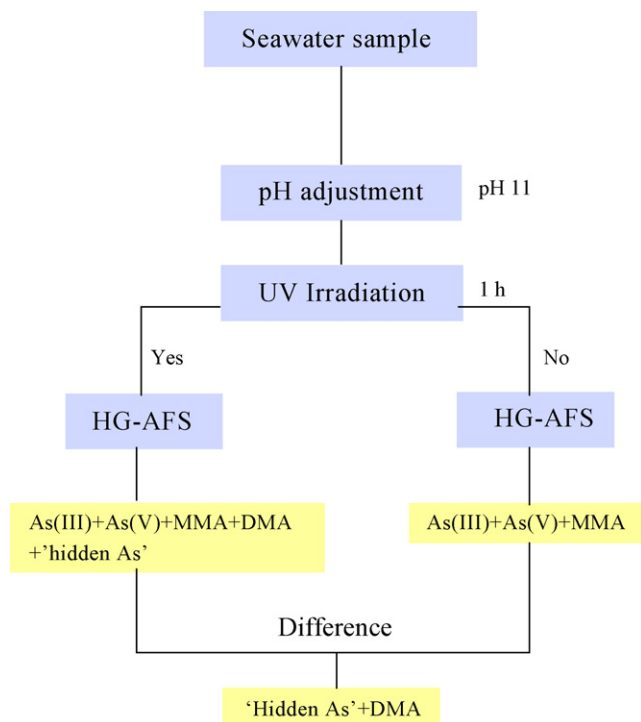


Fig. 2. Schematic diagram showing the protocol for determination of total and hydride-reactive As by HG-AFS following UV irradiation of seawater samples.

provide a significantly different sensitivity as compared to inorganic As when on-line hydride generation is employed rather than batch systems. The presence of non-reactive hydride As species such as AsB, trimethylated As compounds, etc. makes a prior oxidative treatment necessary. AsB has not been found in seawater at a detectable level but can be useful as a model compound in order to study the conversion of non-reactive As species into As(V) by UV irradiation. The effect of pH on UV oxidation of As(III) (50  $\mu\text{g/L}$ ), MMA (20  $\mu\text{g/L}$ ), DMA (10  $\mu\text{g/L}$ ) and AsB (10  $\mu\text{g/L}$ ) was investigated (Fig. 3). As(V) (50  $\mu\text{g/L}$ ) was also included in the study in order to ascertain the stability of

this species upon UV irradiation. The UV treatment time was fixed at 30 min. Results are the average value of three separate UV oxidation experiments. As can be observed, As(III) was oxidised to As(V) at any pH in the range 1–11. Stability of As(V) upon UV irradiation is confirmed by the graph corresponding to this As species. On the other hand, MMA was easily converted into As(V) in a pH range of 1–11 but DMA required a pH in the range 5–11. While MMA gave a fluorescence intensity signal similar to that of As(V) without UV irradiation pretreatment, DMA gave only a 10–15% signal compared to the As(V) signal. Decomposition of AsB into As(V) has been typically performed in alkaline medium often in the presence of a strong oxidant such as  $\text{K}_2\text{S}_2\text{O}_8$  [6]. When AsB solutions containing 20  $\mu\text{g/L}$  of As were UV irradiated at acid pH no conversion was observed. However, decomposition of AsB in alkaline medium even in the absence of a chemical oxidant was efficient (Fig. 3).

The effect of the UV irradiation time on solutions containing As(III) (50  $\mu\text{g/L}$ ), As(V) (50  $\mu\text{g/L}$ ), MMA (20  $\mu\text{g/L}$ ), DMA (20  $\mu\text{g/L}$ ) and AsB (20  $\mu\text{g/L}$ ) was investigated (Fig. 4). The study for As(III) and As(V) was carried out at acid pH (pH 1). Under these conditions, As(III) (50  $\mu\text{g/L}$ ) was converted into As(V) within 10 min. The As(V) formed remained unchanged for a period of at least 60 min. When a As(V) solution of 50  $\mu\text{g/L}$  was UV irradiated, reduction of As(V) to As(III) was observed at the beginning of the treatment. After 20 min, all As(III) present was transformed into As(V). Conversion of As(III) into As(V) at alkaline pH was equally effective. As indicated above, no oxidation of AsB and DMA upon UV irradiation took place at acid pH. Consequently, the effect of the UV irradiation time for AsB, MMA and DMA was studied in alkaline medium (pH 11). As can be observed in Fig. 4, MMA was likely converted into As(V) within a short UV irradiation time but DMA required UV irradiation for at least 30 min.

At pH 13, conversions of AsB into As(V) could be performed in less than 10 min, whereas at pH 11, the UV treatment needed to be prolonged for at least 30 min. Blank contamination due to NaOH added for pH 13 adjustment was suspected, so pH 11

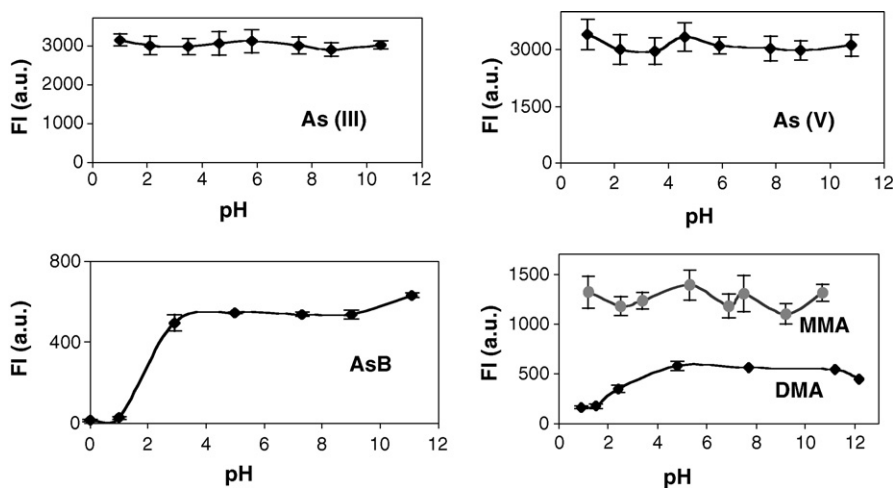


Fig. 3. Effect of pH on conversion of As(III), AsB and DMA into As(V). A graph showing the stability of As(V) upon UV irradiation is also included. The UV irradiation time was fixed at 30 min. FI (a.u.) is fluorescence intensity expressed as arbitrary units. Results are the average value of three separate UV oxidation experiments.

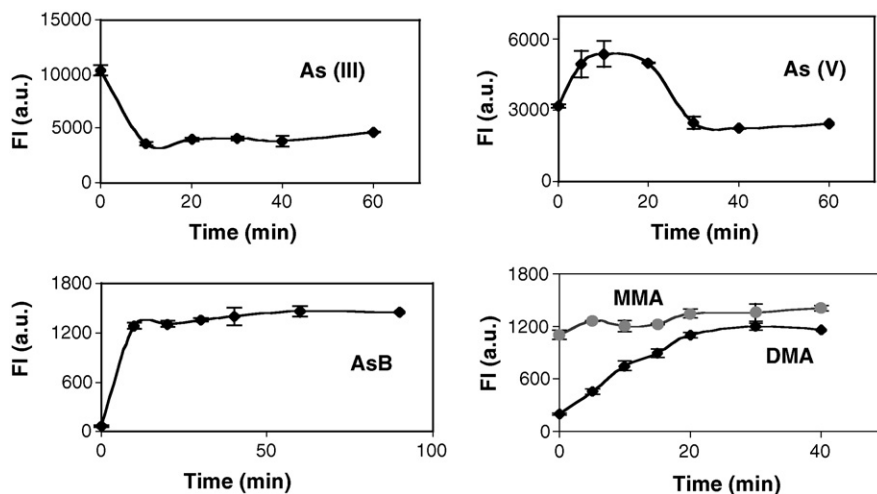


Fig. 4. Effect of the UV irradiation time on conversion of As(III), AsB and DMA into As(V). A graph showing the stability of As(V) upon UV irradiation is also included. Experiments were performed at acid pH (pH 1) for As(III) and As(V) and alkaline pH (pH 11) for AsB, DMA and MMA. FI (a.u.) is fluorescence intensity expressed as arbitrary units. Results are the average value of three separate UV oxidation experiments.

is recommended. For efficient conversion of all As species into As(V), UV irradiation at pH 11 for at least 30 min is needed.

In order to assess the influence of the saline matrix on conversions of As species into As(V), UV irradiation of solutions containing each As species at pH 11 was performed for 30 min. The composition of the model saline solution was the following: 3% (m/v) NaCl; 0.5% MgCl<sub>2</sub> and 0.15% CaSO<sub>4</sub>. The conversion percentages for this solution were  $97 \pm 3$ ,  $92 \pm 1$ ,  $82 \pm 3$  and  $58 \pm 1$  for As(III), DMA, MMA and AsB, respectively. The low conversion efficiency obtained for AsB in this matrix indicates that UV irradiation needs to be extended for longer times so that improved conversion efficiencies are reached. With a treatment time of 1 h, conversions of AsB into As(V) in the model saline solution were above 90%.

### 3.2. Analytical characteristics

The equation for the calibration curve of As(V) was:  $FI = 62.313 [As] + 8.34$ , where the As concentration is expressed in  $\mu\text{g/L}$  and FI is the fluorescence intensity. The regression coefficient was  $R^2 = 0.996$ . The calibration graph was linear at least up to  $80 \mu\text{g/L}$  As. The limit of detection (LOD) ( $3\sigma$  criterion) of As in seawater using hydride generation from As(V) was  $0.1 \mu\text{g/L}$ . The repeatability of the oxidation procedure, expressed as relative standard deviation (R.S.D.), was better than 10% ( $N = 8$ ). Repeatability was studied with the model saline solution containing As(III), As(V), MMA, DMA and AsB ( $20 \mu\text{g/L}$  of As from each species) subjected to UV

irradiation under optimal conditions (pH 11; 1 h UV irradiation time).

### 3.3. Method validation

Given that the method provides a suitable limit of detection for determination of total As in seawater, no reduction of As(V) into As(III) was performed prior to hydride generation, despite the higher sensitivity displayed by As(III).

The method was validated against CRM BCR 403 seawater, with a certified content of  $1.461 \pm 0.218 \mu\text{g/kg}$ , which can be transformed to  $\mu\text{g/L}$  units taken into account the seawater density. The concentration value is  $1.5 \pm 0.2 \mu\text{g/L}$ . Determination of As in this CRM by the proposed method yielded a concentration value of  $1.8 \pm 0.3 \mu\text{g/L}$  ( $N = 4$ ). When applying a *t*-test, no significant differences occurred between the experimental and the certified value for  $p = 0.05$ .

A recovery study was also carried out to establish the validity of the method (Table 2). For this purpose, a seawater sample corresponding to sampling point S6, which had already been subjected to UV irradiation, was spiked at three concentration levels with As(III), As(V), DMA, MMA and AsB. The total As content for this sample as determined by HG-AFS was  $2.6 \pm 0.2 \mu\text{g/L}$ . Recovery of the spiked As with and without UV irradiation was 93 and 42%, respectively. It means that total As contents can be accurately measured in seawater even in the presence of very stable species such as AsB when a prior UV treatment is performed.

Table 2  
Recovery study for spiked seawater

Sample concentration ( $\mu\text{g/L}$ )	Spiked content ( $\mu\text{g/L}$ )	Measured content ( $\mu\text{g/L}$ )		Average recovery (%)	
		With UV	Without UV	With UV	Without UV
$2.6 \pm 0.2$	As(III) + As(V) + MMA + DMA + AsB (0.5 ng/mL of each)	$4.9 \pm 0.3$	$3.7 \pm 0.3$	92	44
	As(III) + As(V) + MMA + DMA + AsB (1 ng/mL of each)	$7.3 \pm 0.5$	$4.6 \pm 0.2$	94	40
	As(III) + As(V) + MMA + DMA + AsB (1.5 ng/mL of each)	$9.6 \pm 0.6$	$5.7 \pm 0.4$	93	41

Average value  $\pm$  standard deviation ( $N = 3$ ).

Table 3

Analytical results for the determination of As in coastal seawater by HG-AFS with and without UV pre-treatment

Sampling point	Description	Total As found ( $\mu\text{g/L}$ ) <sup>a</sup>		$t_{\text{exp}}$	$t_{\text{crit}}$
		With UV treatment	Without UV treatment		
S1	Bayona beach	1.6 ± 0.1	0.9 ± 0.1	10.2	2.45
S2	America beach	1.7 ± 0.2	1.4 ± 0.1	3.3	2.45
S3	Patos beach	1.7 ± 0.2	1.2 ± 0.2	2.96	2.45
S4	Canido beach	2.5 ± 0.3	2.0 ± 0.3	2.04	2.45
S5	Lagares River mouth	4.8 ± 0.1	5.4 ± 0.3	3.81	2.45
S6	Vigo harbour	2.6 ± 0.2	2.5 ± 0.1	0.97	2.45
S7	Teis beach	2.9 ± 0.2	1.9 ± 0.3	2.85	2.45
S8	Arealonga beach	2.3 ± 0.4	1.7 ± 0.3	2.66	2.45
S9	Cesantes beach	2.3 ± 0.4	1.7 ± 0.4	2.18	2.45
S10	Placeres beach	1.4 ± 0.2	1.1 ± 0.1	3.71	2.45
S11	Marin harbour	2.0 ± 0.2	1.5 ± 0.2	4.3	2.45

<sup>a</sup> Average value ± standard deviation ( $N=8$ ).

### 3.4. Hydride-reactive and hidden As in coastal seawater

Analytical results for total and hydride-reactive As in 11 sampling points of coastal seawater are shown in Table 3. As can be observed, inaccurate total As concentration in coastal seawater are obtained unless a prior conversion of As species into inorganic As is performed. Higher As contents in the range 0.3–1  $\mu\text{g/L}$  can be noted, meaning an increase of up to 78% in relation to the total As found without UV treatment. When comparing both set of results using a  $t$ -test, significant differences ( $p=0.05$ ) arise with exception of sample points S4, S6 and S9. This means that contribution of the ‘hidden As’ and DMA in those sample points is negligible. This fact could be related to the occurrence of intensive urban and industrial activity nearby to those sampling sites, mainly to S6 (harbour). Therefore, biological productivity, which is the responsible for the methylation of inorganic As is clearly diminished in polluted sites. The sample point S5 is the only one in which the total As found without UV treatment is significantly higher than that found with UV treatment. An explanation for this behaviour could be the presence of an enhanced As(III) concentration and the absence of non-hydride reactive As at this sampling point, which would cause a higher fluorescence signal for the sample not subjected to UV oxidation. It should be stressed that the analytical approach shown in Fig. 2 gives an accurate total As concentration in seawater but determination of non-reactive As may suffer from bias when As(III) is present at a significant concentration as compared to those of As(V) and MMA. In this case, an overestimation of the non-reactive fraction should occur when As(V) is used as a calibrant. This bias should be minimum in oxic seawater, where As(V) predominates over As(III).

## 4. Conclusions

Arsine generation from UV-irradiated seawater samples in alkaline medium allows an accurate determination of total As by

continuous-flow hydride generation-atomic fluorescence spectrometry, including the ‘hidden As’ fraction. The sum of DMA and the ‘hidden As’ represents a significant percentage (up to 44%) of the total As present in some sampling points. Detection by atomic fluorescence avoids the need for a prior preconcentration stage. Determination of the reactive and non-reactive As fractions in seawater is accomplished in both a simple and fast way. No chemical oxidants are employed to destroy non-hydride reactive organoarsenic, thus minimizing any errors that could arise from sample contamination or losses. Likewise, pre-reduction of As(V) formed upon UV treatment to As(III) for maximum sensitivity is not required and hence, a simplification of the method is achieved.

## Acknowledgement

Financial support by the Galician government (Xunta de Galicia) (project PGIDIT05PXIB31401PR) is gratefully acknowledged.

## References

- [1] J.M. Neff, Bioaccumulation in Marine Organisms, Elsevier, Oxford, 2002, pp. 57–78.
- [2] B. Welz, M. Sperling, Atomic Absorption Spectrometry, Wiley-VCH, Weinheim, 1999, p. 672.
- [3] M.O. Andreae, Anal. Chem. 49 (1977) 820.
- [4] J.Y. Cabon, N. Cabon, Anal. Chim. Acta 418 (2000) 19.
- [5] S. Karthikeyan, T. Prasada, C.S.P. Iyer, Talanta 49 (1999) 523.
- [6] A.M.M. de Bettencourt, M.O. Andreae, Appl. Organomet. Chem. 5 (1991) 111.
- [7] A.G. Howard, S.D.W. Comber, Appl. Organomet. Chem. 3 (1989) 509.
- [8] A.G. Howard, S.D.W. Comber, Mikrochim. Acta 109 (1992) 27.
- [9] J. Moreda-Pineiro, M.L. Cervera, M. de La Guardia, J. Anal. At. Spectrom. 12 (1997) 1377.
- [10] A.M. Featherstone, E.C.V. Butler, B.V. O’Grady, P. Michel, J. Anal. At. Spectrom. 13 (1998) 1355.



# Solid-phase extraction of iron(III) with an ion-imprinted functionalized silica gel sorbent prepared by a surface imprinting technique

Xijun Chang<sup>a,\*</sup>, Na Jiang<sup>a</sup>, Hong Zheng<sup>a,b</sup>, Qun He<sup>a</sup>, Zheng Hu<sup>a</sup>, Yunhui Zhai<sup>a</sup>, Yuemei Cui<sup>a</sup>

<sup>a</sup> School of Chemistry and Chemical Engineering, Lanzhou University, Lanzhou 730000, PR China

<sup>b</sup> Qinghai Normal University, Xining 810008, PR China

Received 19 October 2005; received in revised form 25 February 2006; accepted 3 March 2006

Available online 18 April 2006

## Abstract

A new Fe(III)-imprinted amino-functionalized silica gel sorbent was prepared by a surface imprinting technique for selective solid-phase extraction (SPE) of Fe(III) prior to its determination by inductively coupled plasma atomic emission spectrometry (ICP-AES). Compared with non-imprinted polymer particles, the ion-imprinted polymers (IIPs) had higher selectivity and adsorption capacity for Fe(III). The maximum static adsorption capacity of the ion-imprinted and non-imprinted sorbent for Fe(III) was 25.21 and 5.10 mg g<sup>-1</sup>, respectively. The largest selectivity coefficient of the Fe(III)-imprinted sorbent for Fe(III) in the presence of Cr(III) was over 450. The relatively selective factor ( $\alpha_r$ ) values of Fe(III)/Cr(III) were 49.9 and 42.4, which were greater than 1. The distribution ratio ( $D$ ) values of Fe(III)-imprinted polymers for Fe(III) were greatly larger than that for Cr(III). The detection limit ( $3\sigma$ ) was 0.34  $\mu\text{g L}^{-1}$ . The relative standard deviation of the method was 1.50% for eight replicate determinations. The method was validated by analyzing two certified reference materials (GBW 08301 and GBW 08303), the results obtained is in good agreement with standard values. The developed method was also successfully applied to the determination of trace iron in plants and water samples with satisfactory results.

© 2006 Elsevier B.V. All rights reserved.

**Keywords:** Fe(III)-imprinted amino-functionalized silica gel sorbent; Preparation; Surface imprinting technique; Solid-phase extraction (SPE); ICP-AES

## 1. Introduction

The traditional preconcentration and separation methods for metal ions are liquid–liquid extraction, coprecipitation, and ion-exchange, etc. These methods often require large amounts of high purity organic solvents, some of which are harmful to health and cause environmental problems [1]. Nowadays, the solid-phase extraction (SPE) is being widely utilized for preconcentration or separation of metals due to the following advantages. These include [2–5]: (1) higher enrichment factors; (2) absence of emulsion; (3) safety with respect to hazardous samples; (4) minimal costs due to low consumption of reagents; (5) flexibility; (6) easy of automation. An efficient adsorbing material should possess a stable and insoluble porous matrix having suitable active groups (typically organic groups) that interact with metal ions. Silica gel is an ideal support for organic groups

because it is a stable under acidic conditions and non-swelling inorganic material, and has high mass exchange characteristics and very high thermal resistance [6]. Immobilization and cross-linking of organic compounds with certain functional groups on the surface of silica gel has gained important application in different research and industrial fields [7–11]. The effectiveness of such materials in binding metal ions has been attributed to the complexation chemistry between the ligand and the metal. However, the basic disadvantage of these solid sorbents is the lack of metal selectivity, which leads to other species interfering with the target metal ion(s) [12]. But molecular imprinting technique can exactly change this problem.

Molecular imprinting is a technique for preparing polymeric materials that are capable of high molecular recognition. In molecular imprinting, a molecular “memory” is imprinted on the polymer. Molecular imprinting polymers (MIPs) are capable of recognizing and binding the desired molecular target with a high affinity and selectivity [13]. Because of the highly crosslinked polymeric nature of MIP materials, they are intrinsically stable and robust. Moreover, MIP materials are low cost

\* Corresponding author. Tel.: +86 931 8912582; fax: +86 931 8912582.

E-mail address: [jiangn04@st.lzu.edu.cn](mailto:jiangn04@st.lzu.edu.cn) (X. Chang).

to produce and can be stored in a dry state at room temperature for long periods of time [14]. Ion-imprinted polymers (IIPs) are similar to MIPs, but they can recognize metal ions after imprinting and retain all the virtues of MIPs [15–18]. IIPs have outstanding advantages such as predetermined selectivity in addition to being simple and convenient to prepare. A particularly promising application of IIPs is the solid-phase extractive preconcentration of analytes present in low concentration or the separation from other coexisting ions or complex matrix. Thus, ion-imprinted polymers for solid-phase extraction is a fast developing area for the application of ion imprinting technology [19]. One of the first ionic template effects in the synthesis of chelating polymers was reported by Nishide and Tsuchida [20] in the mid-1970s. Recently, Takagi and co-workers [21] introduced a novel imprinting technique called surface template polymerization. Surface molecular imprinting is one of the important types of molecular imprinting. Surface molecularly imprinted polymer not only possesses high selectivity but also avoids problems with mass transfer [22].

For metal ions, molecular imprinting can be interpreted as ionic imprinting exactly. So far there are a lot of metal ions imprinted polymers have been prepared, including Pb(II) [23], Ni(II) [24,25], Pd(II) [26], Dy(III) [27], UO<sub>2</sub>(II) [28], Cd(II) [1,29], Th(IV) [30], Ca(II) [31] and Mg(II) [32] imprinted polymers. However, few people developed procedure to research Fe(III). In this study, a new Fe(III)-imprinted amino-functionalized silica gel sorbent was synthesized by combining a surface molecular imprinting technique for selective extraction or preconcentration of Fe(III).

A new method using Fe(III)-imprinted sorbent for preconcentrating trace iron in real solution samples prior to its determination by ICP-AES was established. The proposed method presented high selectivity and adsorption capacity for Fe(III), and possessed simple, convenient and accurate characteristics.

## 2. Experimental

### 2.1. Instruments and apparatus

An IRIS advantage ER/S inductively coupled plasma spectrometer (TJA, USA) was used for the determinations of all metal ions. The operation conditions and the wavelengths were summarized in Table 1.

A pHS-10C digital pH meter (Xiaoshan Instrument Factory, China) was used for the pH adjustments. Infrared spectra were recorded on a Nicolet NEXUS 670 FT-IR apparatus (USA).

An YL-110 peristaltic pump (General Research Institute for Nonferrous Metals, Beijing, China) was used in the preconcentration process. A self-made glass microcolumn (45 mm × 2.5 mm i.d.) was used in this study.

### 2.2. Chemicals and reagents

Reagents of analytical and spectral purity were used for all experiments and doubly distilled deionized water was used throughout. Standard stock solutions of Fe(III) and Cr(III) (1 mg mL<sup>-1</sup>) were prepared by dissolving spectral pure-grade

Table 1  
Instrumental and operating conditions for ICP-AES measurements

Parameter	Type or amount
R.F. Power (kW)	1.15
Carrier gas (Ar) flow rate (L min <sup>-1</sup> )	0.6
Auxiliary gas (Ar) flow rate (L min <sup>-1</sup> )	1.0
Coolant gas (Ar) flow rate (L min <sup>-1</sup> )	14
Nebulizer flow (psi)	30
Pump rate (rpm)	100
Observation height (mm)	15
Integration time (s)	
On-axis	20
Off-axis	5
Wavelength (nm)	
Fe	259.940
Cr	267.716

FeCl<sub>3</sub>·6H<sub>2</sub>O (Tianjin Yaohua Chemical Factory, Tianjin, China) and CrCl<sub>3</sub>·6H<sub>2</sub>O (Shanghai First Reagent Factory, Shanghai, China). Silica gel (60–100 mesh, Mouping Kangbinuo Chemical Factory, Yantai, China) and 3-aminopropyltrimethoxysilane (APS, Qingdao Ocean University Chemical Company, Qingdao, China) were used to prepare the ion-imprinted and non-imprinted functionalized silica gel sorbent.

### 2.3. Sample preparation

The reference materials (GBW 08301, river sediment and GBW 08303, polluted farming soil) were obtained from the National Research Center for Certified Reference Materials (Beijing, China). Qinghai Lake water was collected from Qinghai Lake, Qinghai, China. Yellow River water was collected from Yellow River, Lanzhou, China. To oxidize organic matter such as humic acid, the sample was digested by oxidizing UV-photolysis in the presence of 1% H<sub>2</sub>O<sub>2</sub> using a low pressure Hg-lamp which was integrated in a closed quartz vessel [33]. The digested samples were immediately filtered through a Millipore cellulose nitrate membrane, pore size 0.45 μm, acidified to pH 3 with hydrochloric acid and stored in precleaned polyethylene bottles. Tap water samples taken from our research laboratory were analyzed without pretreatment. The pH value was adjusted to 3 with 0.1 mol L<sup>-1</sup> HCl or 0.1 mol L<sup>-1</sup> NH<sub>3</sub>·H<sub>2</sub>O prior to use.

Balsam pear leaves was obtained from Anning village, Lanzhou, China. The plant samples were dried in an oven at 80 °C to constant weight. A 1.000 g balsam pear leaves samples were weighted and transferred to a digestion tube before adding 5 mL of concentrated HNO<sub>3</sub>. Following the directions found in the literature [34], the tube was left at room temperature for one night. Then it was placed in a digester block and heated slowly until the temperature was up to 165 °C. This temperature was maintained until no more brown fumes evolved. After the tube had cooled down, 1.3 mL perchloric acid was added into it. Then the temperature was raised to 210 °C until white fumes begin to form. The volume was adjusted to 100 mL with doubly distilled deionized water after the tube had cooled off.

#### 2.4. Preparation of the Fe(III)-imprinted amino-functionalized silica gel sorbent

The silica gel surfaces were activated by refluxing 8 g of silica gel (60–100 mesh) with 60 mL of 6 mol L<sup>-1</sup> hydrochloric acid under stirring for 8 h, then the activated silica gel was filtered and washed with doubly distilled water to neutral and dried under vacuum at 70 °C for 8 h.

To prepare the Fe(III)-imprinted amino-functionalized silica gel sorbent, 2.271 g of FeCl<sub>3</sub>·6H<sub>2</sub>O was dissolved in 80 mL of methanol under stirring and heating, then 4 mL of APS was added into the mixture. The solution was stirred and refluxed for 1 h, to which 6 g of activated silica gel was added. After 20 h of stirring and refluxing the mixture, the product was recovered by filtration, washed with ethanol to remove the remnant APS, and stirred in 50 mL of 6 mol L<sup>-1</sup> hydrochloric acid for 2 h to remove metal ions from the polymer. The final product was filtered, washed with doubly distilled water to neutral and dried under vacuum at 80 °C for 12 h. The non-imprinted functionalized silica gel sorbent was also prepared using an identical procedure without adding FeCl<sub>3</sub>·6H<sub>2</sub>O.

#### 2.5. General procedure for preconcentration/separation of Fe(III)

##### 2.5.1. Static adsorption test

A portion of standard or sample solution containing Fe(III) was transferred into a 10 mL beaker, and the pH value was adjusted to the desired value with 0.1 mol L<sup>-1</sup> HNO<sub>3</sub> or 0.1 mol L<sup>-1</sup> NH<sub>3</sub>·H<sub>2</sub>O. Then the volume was adjusted to 10 mL with doubly distilled deionized water. And 50 mg of Fe(III)-imprinted amino-functionalized silica gel sorbent was added, and the mixture was shaken vigorously for 30 min to facilitate adsorption of the metal ions onto the ion-imprinted sorbent. After the solution was centrifuged, the concentrations of the metal ions in the solution were directly determined by ICP-AES.

##### 2.5.2. Dynamic adsorption test

Firstly, the glass column (45 mm in length and 2.5 mm in diameter) was packed with 50 mg of the imprinted functionalized silica gel sorbent. A small amount of glass wool was placed at both ends to prevent loss of the polymer particles during sample loading. Before use, pH 3 of HNO<sub>3</sub> solution and doubly distilled deionized water were successively passed through the microcolumn in order to equilibrate, clean and neutralize it. Each solution was passed through the column at a flow rate of 1.0 mL min<sup>-1</sup> (controlled by a peristaltic pump) after adjusting pH 3. The metal ions adsorbed on the column were eluted with 0.5 mol L<sup>-1</sup> HCl. The analytes in the elution were determined by ICP-AES.

##### 2.5.3. Constants

The adsorption capacity, the extraction percentage, the distribution ratio, the selectivity coefficient and the relative selectivity

coefficient were calculated as the following equations:

$$Q = \frac{(C_0 - C_e)V}{W}, \quad E = \frac{(C_0 - C_e)}{C_e}, \quad D = \frac{Q}{C_e},$$

$$\alpha_{\text{Fe/Cr}} = \frac{D_{\text{Fe}}}{D_{\text{Cr}}}, \quad \alpha_r = \frac{\alpha_i}{\alpha_n}$$

Where  $Q$  represents the adsorption capacity (mg g<sup>-1</sup>),  $C_0$  and  $C_e$  represent the initial and equilibrium concentration of Fe(III) (μg mL<sup>-1</sup>),  $W$  is the mass of Fe(III)-imprinted amino-functionalized silica gel polymer (g) and  $V$  is the volume of metal ion solution (L),  $E$  (%) is the extraction percentage,  $D$  is the distribution ratio (mL g<sup>-1</sup>),  $\alpha_{\text{Fe/Cr}}$  is the selectivity coefficient,  $\alpha_r$  is the relative selectivity coefficient,  $\alpha_i$  and  $\alpha_n$  represent the selectivity factor of imprinted sorbent and non-imprinted sorbent, respectively.

### 3. Results and discussion

#### 3.1. Preparation of the Fe(III)-imprinted amino-functionalized silica gel sorbent

Silica gel is an amorphous inorganic polymer having siloxane groups (Si–O–Si) in the bulk and silanol groups (Si–OH) on its surface. The latter are responsible for chemical modification that may occur on the silica surface. Because commercial silica gel contains a low concentration of surface silanol groups suitable for modification, the activation of silica gel surface is necessary. In this work hydrochloric acid was used for the activation of silica gel.

The complex was formed between Fe(III) and APS, then cohydrolyzed and co-condensed with the activated silica gel. Thus, the activated silica gel surface was grafted with the complex of Fe(III) and APS rather than just the free APS. After the remnant APS and Fe(III) were removed by ethanol and 6 mol L<sup>-1</sup> HCl, respectively, the imprinted functionalized silica gel sorbent which contained a tailor-made cavity for Fe(III) was formed.

#### 3.2. Characteristic of the FT-IR spectra

To ascertain the presence of APS in the functionalized silica gel sorbents, FT-IR spectra were obtained from activated silica gel, Fe(III)-imprinted and non-imprinted amino-functionalized silica gel sorbents. The observed features around 1101.5 and 964.6 cm<sup>-1</sup> indicated Si–O–Si and Si–O–H stretching vibrations, respectively. The presence of adsorption water was reflected by ν<sub>OH</sub> vibration at 3439.9 and 1635.1 cm<sup>-1</sup>. The bands around 802.6 and 468.4 cm<sup>-1</sup> resulted from Si–O vibrations. The ν<sub>NH<sub>2</sub></sub> band present in silica gel modified amine derivatives was absent in the IR spectra owing to the participation of the amino group in the Schiff base formation [35]. Imprinted and non-imprinted sorbent showed a very similar location and appearance of the major bands. It indicated that N–H was recovered after removal of Fe(III) in the imprinted sorbent.

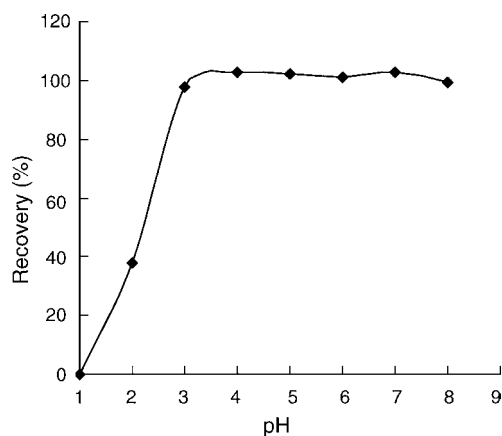


Fig. 1. Effect of pH on sorption of Fe(III) on Fe(III)-imprinted amino-functionalized silica gel sorbent. Other conditions: 50 mg of the sorbent; 1.0  $\mu\text{g mL}^{-1}$  of Fe(III); shaking time 30 min; temperature 25 °C.

### 3.3. Effect of pH

According to the recommended procedure (static method), the effect of pH on the adsorption of Fe(III) was tested by equilibrating 50 mg of Fe(III)-imprinted amino-functionalized silica gel sorbent with 10 mL of the buffer solutions containing 1.0  $\mu\text{g mL}^{-1}$  of Fe(III) under different pH conditions. It can be seen in Fig. 1, the sorption quantity of Fe(III) was very low when the pH was lower than pH 3 because of the protonation, but it increased dramatically with the pH. After pH 3, the sorption quantity remained relatively constant. In order to avoid hydrolyzing at higher pH values, pH 3 was selected as the enrichment acidity for subsequent experiments.

### 3.4. Effect of elution condition on recovery

Elution of Fe(III) from the column containing the Fe(III)-imprinted amino-functionalized silica gel sorbent was investigated by using 2 mL of various concentrations of HCl as eluent following the general procedure (dynamic method). When HCl is used as a desorption agent, the coordination spheres of chelated Fe(III) ions is disrupted and subsequently Fe(III) ions are released from the iron templates into the desorption medium. The quantitative recoveries (>95%) of Fe(III) can be obtained using 2 mL of 0.5 mol L<sup>-1</sup> HCl as eluent. Therefore, 2 mL of 0.5 mol L<sup>-1</sup> HCl was used as eluent in subsequent experiments.

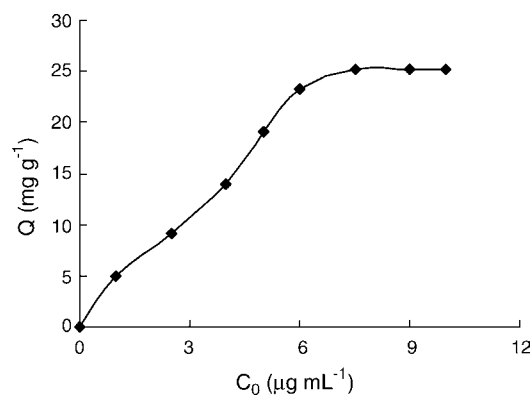


Fig. 2. The effect of Fe(III) initial concentration on the adsorption quantity of Fe(III)-imprinted amino-functionalized silica gel sorbent. Other conditions: 20 mg of ion-imprinted sorbent; pH 3; shaking time 30 min; temperature 25 °C.

### 3.5. Adsorption capacity of Fe(III)-imprinted sorbent for Fe(III)

The adsorption capacity is an important factor because it determines how much adsorbent is required to quantitatively concentrate the analytes from a given solution. The adsorption capacity was tested following the general procedure. To measure the static adsorption capacity, 20 mg of Fe(III)-imprinted or non-imprinted sorbent was equilibrated with 50 mL of various concentrations of Fe(III) solutions buffered with 0.1 mol L<sup>-1</sup> of HNO<sub>3</sub> or NH<sub>3</sub>·H<sub>2</sub>O at pH 3. As can be seen in Fig. 2, the amount of Fe(III) adsorbed per unit mass of IIPs increased with the initial concentrations of Fe(III). The initial Fe(III) concentrations were increased till the plateau values (adsorption capacity values) were obtained. The static adsorption capacity of the ion-imprinted and non-imprinted sorbent for Fe(III) was calculated as 25.21 and 5.10 mg g<sup>-1</sup>, respectively. The static adsorption capacity of the ion-imprinted was about five times of non-imprinted one. The results showed that the ion-imprinted polymers had a high adsorption capacity for Fe(III).

### 3.6. Selectivity of the imprinted sorbent

The Cr(III) ion was chosen as the competitive species with Fe(III) because these two ions have the same charge and similar ionic radius. As can be seen in Table 2, the *D* values of Fe(III)-imprinted amino-functionalized silica gel sorbent for Fe(III) were large, while *D* decreased significantly

Table 2  
Competitive loading of Fe(III) and Cr(III) by the Fe(III)-imprinted and non-imprinted silica gel sorbent

Sorbent	Initial solution ( $\mu\text{g mL}^{-1}$ )		Uptake (%)		Capacity ( $\text{mg g}^{-1}$ )		<i>D</i> ( $\text{mL g}^{-1}$ )		$\alpha$	$\alpha_r$
	Fe(III)	Cr(III)	Fe(III)	Cr(III)	Fe(III)	Cr(III)	Fe(III)	Cr(III)		
Fe(III)-imprinted	1	0	99.75		1.995		798112.0			
	1	1	99.66	39.4	1.994	0.788	586352.9	1300	451.0	49.9
	1	2	99.41	53.2	1.986	2.128	279684.5	2273.1	123.0	42.4
Non-imprinted	1	0	98.2		1.964		109106.7			
	1	1	97.3	86.38	1.946	1.727	114470.6	12683.1	9.03	
	1	2	97.2	84	1.944	1.680	15185.6	5250.4	2.9	

for Cr(III). The  $\alpha_r$  values were 49.9 and 42.4, which were greater than 1 for Fe(III)-imprinted amino-functionalized silica gel sorbent of Fe(III)/Cr(III). The results indicated that the Fe(III)-imprinted amino-functionalized silica gel sorbent had higher selectivity for Fe(III). And these results demonstrated that Fe(III) could be determined even in the presence of Cr(III) interference.

### 3.7. Effect of flow rate

The flow rate of the Fe(III) solution through the packed volume is a very important parameter because the retention of elements on adsorbent depends upon the flow rate of the sample solution. Its effect was examined under the optimum conditions (pH, eluent, etc.) by passing 50 mL of sample solution through the column with a peristaltic pump. Faster flow rates could not be investigated due to the back-pressure generated by the column. So the flow rates were adjusted in the range of 0.5–3.0 mL min<sup>-1</sup>. The adsorption in this system is a rapid kinetic process and at higher flow rates the contact time of iron ions with the column material is shorter. In the test, the quantitative recoveries of the metal ions will decrease with the further increasing of the flow rate that is over 1.5 mL min<sup>-1</sup>. Thus, a flow rate of 1.0 mL min<sup>-1</sup> was selected in this work.

### 3.8. Maximum sample volume and enrichment factor

The enrichment factor was studied by recommended column procedure by increasing volume of Fe(III) solution and keeping the total amount of loaded Fe(III) constant to 1.0  $\mu$ g. For this purpose, 10, 50, 100, 150, 200, 250 and 300 mL of sample

solutions containing 1.0  $\mu$ g of Fe(III) were passed through the column at the optimum flow rate. The maximum sample volume can be up to 150 mL with the recovery >95%. Therefore, 150 mL of sample solution was adopted for the preconcentration of analytes from sample solutions. And a high enrichment factor of 75 was obtained because 2 mL of 0.5 mol L<sup>-1</sup> HCl was used as eluent in these experiments.

### 3.9. Effect of coexisting ions

Different foreign ions were added to equal quantities of the diluted mixed standard solutions and enriched and determined according to the general procedure. The results showed that up to 4000  $\mu$ g mL<sup>-1</sup> of K(I), 4000  $\mu$ g mL<sup>-1</sup> of Na(I), 200  $\mu$ g mL<sup>-1</sup> of Ca(II), 200  $\mu$ g mL<sup>-1</sup> of Mg(II), 200  $\mu$ g mL<sup>-1</sup> of Ni(II), 200  $\mu$ g mL<sup>-1</sup> of Mn(II), 200  $\mu$ g mL<sup>-1</sup> of Zn(II), 100  $\mu$ g mL<sup>-1</sup> of Co(II), 50  $\mu$ g mL<sup>-1</sup> of Cd(II), 50  $\mu$ g mL<sup>-1</sup> of Cu(II), 50  $\mu$ g mL<sup>-1</sup> of Pb(II), 50  $\mu$ g mL<sup>-1</sup> of Hg(II) had no significant interferences with the determination of 1  $\mu$ g mL<sup>-1</sup> of Fe(III). There are three possible factors for this reason [29]. One is the amino-functionalized group inherent selectivity. The amino group is a soft base and it would not interact with alkali metal and alkali earth metal ions that are classified as hard acids. The second is the hole-size selectivity. The size of Fe(III) exactly fits the cavity of the Fe(III)-imprinted sorbent. The third is the coordination-geometry selectivity because the Fe(III)-imprinted silica gel sorbent can provide the ligand groups arranged in a suitable way required for coordination of Fe(III) ion. Although some ions have similar size with Fe(III) ion, and some ions have high affinity with the amino ligand, the Fe(III)-imprinted amino-functionalized silica gel sorbent still exhibits high selectivity for extraction of Fe(III) in the presence of other metal ions. These results suggest that the coordination-

Table 3  
Analytical results for the determination of trace ferric in standard reference materials, plant sample and natural water samples

Samples	Fe(III) added ( $\mu$ g mL <sup>-1</sup> )	Measured			Certified (mg g <sup>-1</sup> )	Founded with ICP-AES (mg g <sup>-1</sup> )	Recovery (%)
		Standard materials (mg g <sup>-1</sup> )	Plant sample (mg g <sup>-1</sup> )	Water samples ( $\mu$ g mL <sup>-1</sup> )			
GBW 08301		36 ± 1.4			39.4 ± 0.12		
GBW 08303		27 ± 2.2			29.7 ± 0.20		
Balsam pear leaves			3.48 ± 0.09			3.59 ± 0.12	
Qinghai Lake water	0.00			0.17 ± 0.02			–
	0.50			0.66 ± 0.03			98.0
	1.00			1.55 ± 0.05			98.0
	5.00			5.13 ± 0.02			99.2
Yellow River water	0.00			6.65 ± 0.03			–
	0.50			7.14 ± 0.02			98.0
	1.00			7.67 ± 0.06			102
	5.00			11.58 ± 0.07			98.6
Tap water	0.00			0.05 ± 0.02			–
	0.50			0.53 ± 0.03			96.0
	1.00			1.03 ± 0.05			98.0
	5.00			5.10 ± 0.08			101

The value following “±” is the standard deviation.



geometry selectivity may dominate in the selectivity enhancement.

### 3.10. Analytical precision and detection limits

Under the selected conditions, eight portions of standard solutions were enriched and analyzed simultaneously following the general procedure. The relative standard deviations (R.S.D.) of the method was lower than 2.0%, which indicated that the method had good precision for the analysis of trace Fe(III) in solution samples. In accordance with the definition of IUPAC [36,37], the detection limit of the method was calculated based on three times of the standard deviation of 11 runs of the blank solution. The detection limit ( $3\sigma$ ) of the proposed method was  $0.34 \mu\text{g L}^{-1}$ .

### 3.11. Application of the method

The proposed method was applied to the analysis of iron in two certified reference materials (GBW 08301, river sediment and GBW 08303, polluted farming soil), plants, tap water and river water samples. The results were listed in Table 3. The analytical results for the standard material were in good agreement with the certified values. The analytical results for plant sample were in agreement with the ICP-AES method. For the analytical of natural water samples, the standard addition method was used, the recoveries of iron were in the range of 96–105%. These results indicated the suitability of Fe(III)-imprinted amino-functionalized silica gel sorbent for selective solid-phase extraction and determination of trace Fe(III) in environmental samples.

## 4. Conclusions

In this paper, a selective and sensitive method for the determination of trace levels of iron was developed using Fe(III)-imprinted amino-functionalized silica gel (prepared by a surface imprinting technique) as a solid-phase extractant. The preparation of Fe(III)-imprinted amino-functionalized silica gel sorbent was relatively simple and rapid. The ion-imprinted sorbent had higher adsorption capacity and selectivity for Fe(III), and the method was successfully applied to the analysis of trace iron in plants and water sample solutions. The precision and accuracy of the method are satisfactory.

## References

- [1] Y. Liu, X. Chang, S. Wang, Anal. Chim. Acta 519 (2004) 173.
- [2] A. Junker-Buchheit, M. Witznabacher, J. Chromatogr. A 737 (1996) 67.
- [3] K. Pyrzynska, M. Trojanowicz, Crit. Rev. Anal. Chem. 29 (1999) 313.
- [4] J. Mary Gladis, T. Prasada Rao, Anal. Lett. 35 (2002) 501.
- [5] C.F. Poole, Trends Anal. Chem. 22 (2003) 362.
- [6] P.K. Jal, S. Patel, B.K. Mishra, Talanta 62 (2004) 1005.
- [7] D.C. Locke, J. Chromatogr. Sci. 11 (1973) 120.
- [8] N. Becker, K. Unger, Z. Fresenius, Anal. Chem. 304 (1980) 374.
- [9] T. Seshadri, G. Dietz, H. Haupt, Z. Fresenius, Anal. Chem. 319 (1984) 403.
- [10] D.E. Leyden, G.H. Luttrell, Anal. Chem. 47 (1975) 1612.
- [11] R. Kocjan, M. Garbacka, Talanta 41 (1994) 131.
- [12] M.E. Mahmoud, A.A. Soayed, O.F. Hafez, Microchim. Acta 143 (2003) 6.
- [13] K. Haupt, Analyst 126 (2001) 747.
- [14] K. Haupt, K. Mosbach, Chem. Rev. 100 (2000) 2495.
- [15] H. Nishide, J. Deguchi, Chem. Lett. (1976) 169.
- [16] K. Tsukagoshi, K.Y. Yu, M. Maeda, M. Takagi, Bull. Chem. Soc. Jpn. 66 (1993) 114.
- [17] R. Garcia, C. Pinel, C. Madic, M. Lemaire, Tetrahedron Lett. 39 (1998) 8651.
- [18] S.Y. Bae, G.L. Southard, G.M. Murray, Anal. Chim. Acta 397 (1999) 173.
- [19] S. Daniel, P.E.J. Babu, Prasada Rao S T.P., Talanta 65 (2005) 441.
- [20] H. Nishide, E. Tsuchida, Makromol. Chem. 177 (1976) 2295.
- [21] K.Y. Yu, K. Tsukagoshi, M. Maeda, M. Takagi, Anal. Sci. 8 (1992) 701.
- [22] I.A. Nicholls, J.P. Rosengren, Bioseparation 10 (2002) 301.
- [23] X. Zeng, G.M. Murray, Sep. Sci. Technol. 31 (1996) 24.
- [24] T. Panasyuk, V.C. Dallorto, G. Marraza, A. Elskaya, S. Piletsky, I. Rezzano, Anal. Lett. 31 (1998) 1809.
- [25] A. Ersöz, R. Say, A. Denizli, Anal. Chim. Acta 502 (2004) 91.
- [26] S. Daniel, J.M. Gladis, T. Prasada Rao, Anal. Chim. Acta 488 (2003) 173.
- [27] V.M. Biju, J. Mary Gladis, T. Prasada Rao, Anal. Chim. Acta 478 (2003) 43.
- [28] P. Metilda, J. Mary Gladis, T. Prasada Rao, Anal. Chim. Acta 512 (2004) 63.
- [29] G.-Z. Fang, J. Tan, X.-P. Yan, Anal. Chem. 77 (2005) 1734.
- [30] S. Büyüktiryaki, R. Say, A. Ersöz, E. Birlik, A. Denizli, Talanta 67 (2005) 640.
- [31] T. Rosatzin, L.I. Anderson, W. Simon, K. Mosbach, J. Chem. Soc. Perkin Trans. 28 (1991) 1261.
- [32] P.K. Dhal, F.H. Arnold, J. Am. Chem. Soc. 113 (1991) 7417.
- [33] C. Gueguen, C. Belin, B.A. Thomas, F. Monna, P.Y. Favarger, J. Dominik, Anal. Chim. Acta 386 (1999) 155.
- [34] E.S. Miranda Carlos, B.F. Reis, N. Baccan, A.P. Packer, M.F. Gine, Anal. Chim. Acta 453 (2002) 301.
- [35] M.E. Mahmoud, E.M. Soliman, Talanta 44 (1997) 15.
- [36] G.L. Long, J.D. Winefordner, Anal. Chem. 52 (1980) 2242.
- [37] G.L. Long, J.D. Winefordner, Anal. Chem. 55 (1983) 712A.

# On-line bi-directional electrostacking for As speciation/preconcentration using electrothermal atomic absorption spectrometry

Luciana M. Coelho<sup>a</sup>, Nívia M.M. Coelho<sup>b</sup>, Marco A.Z. Arruda<sup>a</sup>, Miguel de la Guardia<sup>c,\*</sup>

<sup>a</sup> Universidade Estadual de Campinas, Instituto de Química, Cidade Universitária Zeferino Vaz, CP 6154, CEP 13083-970, Campinas, São Paulo, Brazil

<sup>b</sup> Universidade Federal de Uberlândia, Instituto de Química, Av. João Naves de Ávila, 2180, CP 593, CEP 38.408.100, Uberlândia, Minas Gerais, Brazil

<sup>c</sup> Universitat de València, Dr. Moliner, 50, E-46100, Burjassot, València, Espanha

Received 9 January 2006; received in revised form 31 March 2006; accepted 6 April 2006

Available online 15 May 2006

## Abstract

A method using bi-directional electrostacking (BDES) in a flow system is presented for As preconcentration and speciation analysis. Some parameters such as electrostacking time and applied voltage, support buffers and their concentrations were investigated. Boric acid plus sodium hydroxide at 0.1 mol/l concentration was selected as support buffer to improve the pre-concentration factor (PF) for As(V). An analytical range from 2.0 to 50.0  $\mu\text{g l}^{-1}$ , and 0.35  $\mu\text{g l}^{-1}$  as limit of detection, when applied 750 V for 20 min, were achieved. Under these conditions, a pre-concentration factor of 4.8 was obtained. The proposed method was applied to determine As(V) in mineral water and natural water samples (river, fountain and gold mine) from Ouro Preto city. Recoveries from 93.5 to 106.4% were achieved at 10  $\mu\text{g l}^{-1}$  added As level (R.S.D.s between 3 and 7%). Potassium permanganate (10  $\text{mg l}^{-1}$ ) was used for oxidising As species in order to determine total As, being established the concentration of As(III) from the difference between total As and As(V).

© 2006 Elsevier B.V. All rights reserved.

**Keywords:** Arsenic; Speciation; Preconcentration; Water; On-line bi-directional electrostacking; Electrothermal atomic absorption spectrometry (ETAAS)

## 1. Introduction

The complexity of some matrices and the levels of the elements to be determined, sometimes involve the necessity of a separation and/or pre-concentration step [1]. Due to the importance of these steps in the analytical sequence, different strategies which vary from liquid-liquid extraction to solid phase preconcentration [2,3] have been applied in this context [4–6], also including original methods based on cloud point extraction [7].

Besides those already commented strategies commonly applied to separation/pre-concentration, a recent proposed alternative is the on-line electrostacking [8–12]. For this task, the samples are diluted either in pure water or in a low concentration buffer, which has the same components as the support buffer system. Due to the big difference on electric field strength, the migration of the ions is carried out from the sample region to

the support buffer. The migration speed is greatly reduced at the concentration boundary between sample and support buffer, resulting the separation and preconcentration of ionic species.

He et al. proposed the first on-line bi-directional electrostacking flow-injection system (BDES-FI) [9]. In that work, the speciation and pre-concentration of Cr(III) and Cr(VI) were carried out, and some parameters, such as ionic mobility, electric field strength, pH of the solutions, among others were investigated. The measurements were performed by flame atomic absorption spectrometry. The BDES voltage (1000 V) and time (600 s) were the optimised parameters, and a pre-concentration factor of 2.6 was obtained. The pH influence on both, support buffer and sample solutions were also investigated, and respectively chosen as 5.0 and 3.4.

Yang et al. [10] used the BDES for separation and preconcentration of Cr(VI) and Pb(II) in drinking water. The influence of sample tube (ST) and buffer tube (BT) lengths, sample medium concentration and the BDES time on the pre-concentration factor was studied. This factor was improved to 16 times when decreased the BT to 4 cm and increased the ST to 4.6 cm. A maximum pre-concentration factor for Pb(II) and Cr(VI) of 20

\* Corresponding author. Tel.: +34 96 3544838; fax: +34 96 3544838.  
E-mail address: [miguel.delaguardia@uv.es](mailto:miguel.delaguardia@uv.es) (M. de la Guardia).

Table 1  
Furnace program used for As determination

Step	Temperature (°C)	Ramp (s)	Hold (s)	Ar flow rate (ml min <sup>-1</sup> )
1	130	5	30	250
2	1300	10	20	250
3	2300	0	5	0
4	2450	1	3	250

and 27 times, respectively, was achieved when 32 min of BDES time was applied.

Due to the importance for determining As species, the extremely low concentration for total As (0.1–10 µg l<sup>-1</sup>) [13] as well as the novelty of BDES-FI for arsenic speciation and preconcentration, the aim of this work was to investigate the potentialities of an on-line BDES for preconcentration and speciation of As(III) and As(V) using ET AAS. Some parameters in the electrostacking system such as sample pH, applied and time voltage, system design, and sampled zone were investigated. For As speciation, the oxidation of As(III) to As(V) was carried out using potassium permanganate.

## 2. Experimental

### 2.1. Instruments and apparatus

A Perkin–Elmer AAnalyst 600 atomic absorption spectrometer (Norwalk, USA) equipped with a longitudinal Zeeman-effect background correction system, was employed as well as transversely heated graphite atomizer (THGA) tubes with integrated platforms.

All measurements were based on integrated absorbance and performed at 193.7 nm with a spectral bandwidth of 0.7 nm. The arsenic electrodeless discharge lamp from Perkin–Elmer was operated at 350 mA, and the recommended operating conditions for arsenic determination are given in Table 1.

An electrophoresis power supply EPS-1001, from GE (Upsala, Sweden) was employed and the conditions used for current and power were 4 mA and 4 W, respectively.

A model D20 Digimed (Santo Amaro, Brazil) potentiometer, a Micronal B331 (São Paulo, Brazil) conductivity meter and a Marconi MA 4025 hot plate (Piracicaba, Brazil) were also used.

### 2.2. Standards, reagents and samples

All solutions were prepared with analytical reagent-grade chemicals and deionised water (18.2 MΩ cm) obtained from a Milli-Q water purification system (Millipore, Bedford, USA) was used throughout. Polyethylene flasks were employed for storing the solutions.

Working standard solutions (2–50 µg l<sup>-1</sup>) of As(V) were prepared from AsHNa<sub>2</sub>O<sub>4</sub>·7H<sub>2</sub>O (Fluka, USA) by sequential dilutions from a stock solution of 250 mg l<sup>-1</sup>. A 500 mg l<sup>-1</sup> As(III) stock solution was prepared by dissolution of 0.660 g of As<sub>2</sub>O<sub>3</sub> (Vetec, Brazil) in 2.5% (w/v) NaOH. When necessary HNO<sub>3</sub> was used for attained the proper pH value. Working stan-

dard solutions of As(III) were prepared by appropriate dilutions from the stock one. The pH and conductivity of the As(V) and As(III) working standard solutions were 7.0 and 240 µS cm<sup>-1</sup>, respectively.

Potassium permanganate, 10 mg l<sup>-1</sup> concentration, was prepared by appropriate dilution from a 100 mg l<sup>-1</sup> stock solution.

Different buffer solutions were employed, such as glycine (J.T. Baker, USA) plus sodium hydroxide (Merck, Brazil), boric acid (Merck, Brazil) plus sodium hydroxide, and finally, tris(hydroxymethyl)aminomethane-Tris (Synth, Brazil) plus hydrochloric acid (Mallinckrodt, Mexico). Their concentrations, pH values and conductivity were always 0.1 mol l<sup>-1</sup>, 9.0 and 4.5 mS cm<sup>-1</sup>, respectively. Nitric acid was purchased from Mallinckrodt (Mexico). Agar-agar purchased from J.T. Baker (USA) was employed for preparing salt bridges (SB). The salt bridges should be immersed into a test tube containing the electrode solution, and kept in a refrigerator after their use. The parameters concerned to the salt bridge and electrode solutions were 0.5 mol l<sup>-1</sup>, pH 9.0 and 20 mS cm<sup>-1</sup>.

The mineral water was purchased at the local market. The initial conductivity and pH were 25–50 µS cm<sup>-1</sup> and 5.5–6.7, respectively. After the KCl (Merck, USA) addition, the conductivity was between 220 and 350 µS cm<sup>-1</sup>. The sample pH was adjusted at 7.0 ± 0.2.

Different water samples from river, fountain and an abandoned gold mine in the neighbourhoods of Ouro Preto city (Minas Gerais state, Brazil) were analyzed. The initial conductivity and pH varied from 19 to 107 µS cm<sup>-1</sup>, and from 5.2 to 7.6, respectively. The conductivity and pH were controlled and the As(III) and the As(V) were determined in each one of the samples. The KCl solution was employed to adjust the conductivity of buffers, standard solutions and samples.

### 2.3. On-line BDES-FI and operational conditions

Fig. 1 shows the diagram of the on-line BDES. This system comprises two Ismatec PC peristaltic pumps (Glattbrugg, Switzerland), which were employed to transport the support buffer solution (P1) and the standard or sample solutions (P2). Polytetrafluoroethylene (PTFE) tubes of 0.5 mm i.d. were used as transport lines. The BDES system also comprises four connectors (C) built in acrylic (0.5 and 1.5 mm i.d.), one sample tube with 4.1 cm length and 1.2 mm i.d., two support buffer tubes (BT) of PTFE with 6.1 cm length and 1 mm i.d. and two salt bridges tubes of PTFE with 12 cm length and 1 mm i.d. A three-piece injector commutator device (IC) built in acrylic was used for controlling the flow direction of the support buffer. The ST was manufactured by coupling two pieces of polypropylene syringes, both with 1 ml of capacity.

The salt bridges were prepared by dissolving 4% (w/v) agar-agar in 0.5 mol l<sup>-1</sup> buffer, heated at ca. 60 °C in a hot plate, and then injected into the PTFE tubes. The ends of the salt bridges were blocked up with cotton wool to prevent the gel sliding. Platinum filament (0.5 mm) was used as electrodes, and they were immersed together with the salt bridges into a 10 ml test tube containing 0.5 mol l<sup>-1</sup> buffer. The electrodes were fixed inside the test tubes by electric sockets.

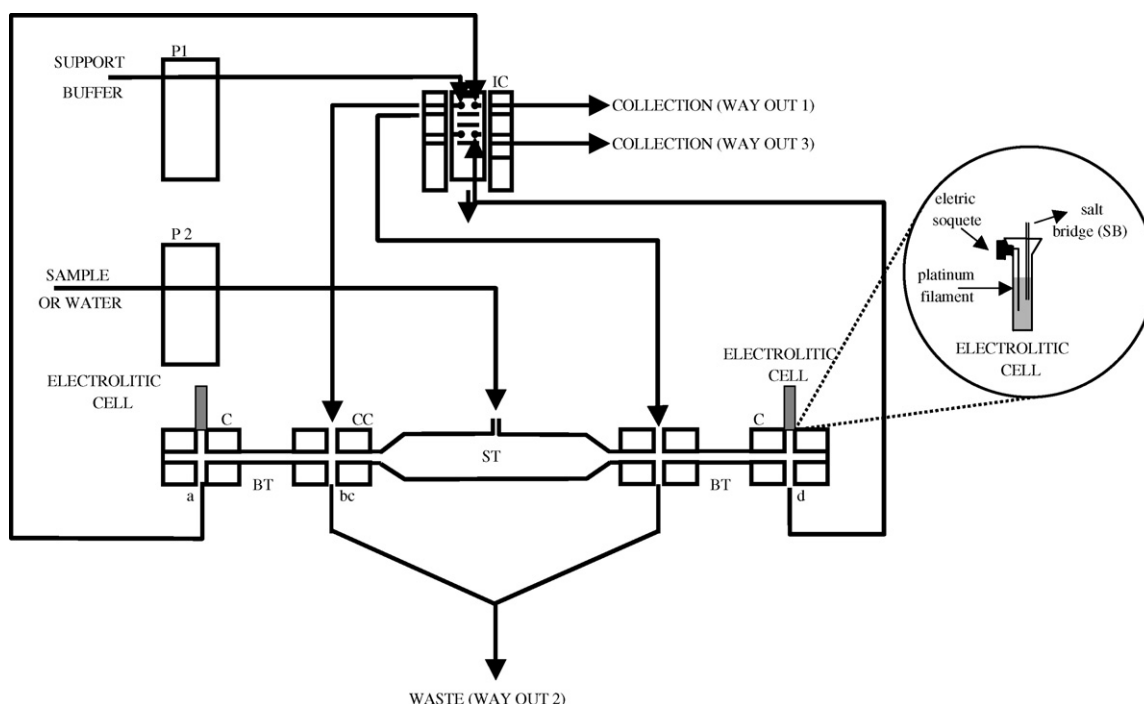


Fig. 1. Schematic diagram of BDES unit for on-line As determination. Points a, b, c and d indicate the flow directions, ST, sample tube, BT, buffer tube, P1 and P2, peristaltic pumps, IC, injector commutator, C, connectors and SB, salt bridge.

The set-up depicted in Fig. 1 was operated in accordance to the procedure summarized in Table 2. During the first step, P1 was stopped and the BDES unit was washed at a flow rate of  $6.5 \text{ ml min}^{-1}$  with deionised water driven by P2. The second step was employed to fill the sample tube with the sample solution. During this step, P1 keep still off and P2 pushed the sample solution into the sample tube. The flow direction was from the middle of sample tube to its end (Fig. 1b and c) until way out 2. In the third step, P2 was stopped and P1 carried the support buffer through left channel (from b to a) to way out 1 (IC). In the fourth step, with P2 still stopped, P1 carried the support buffer through the right channel (from c to d) to way out 3 (IC). In this sense, a concentration boundary was created, which was located at the frontier between the connector (C) and sample tube (ST). The fifth step comprised the preconcentration process, being both peristaltic pumps turned off. The voltage and time of BDES were investigated in a range from 500 to 1000 V and 5 to 20 min, respectively. In the sixth step, the pre-concentrated samples were pushed out by turning on the P1 pump. When the pre-concentrated sample was driven to the flow system, the way out 2 was closed. At this step, 12 aliquots of  $150 \mu\text{l}$  of the pre-

concentrated sample were collected. Six of them were sampled in each side of the BDES unit in order to increase the salt bridges and electrode solutions work lifetime, as long as 60 h. In this sense, the polarity of the power supply was changed after each performance [9]. As consequence, the pre-concentrated samples were sometimes collected in the left or right channel.

It must be noticed that, based on previous experiments it was confirmed that As(III) species does not migrates and thus As(V) could be determined selectively by electrothermal atomic absorption spectrometry (ETAAS) after BDES. On the other hand the speciation of As(III) and As(V) was based on the direct determination of As(V) and that of total As after oxidation by permanganate being established the As(III) concentration by the difference between total As and As(V) concentration.

### 3. Results and discussion

#### 3.1. Evaluation of the BDES-FI system parameters

An As(V) solution of  $9.0 \mu\text{g L}^{-1}$  was used to evaluate the parameters which affect the BDES. In the preliminary tests with

Table 2  
BDES operation procedure for As preconcentration

Step	Function	Pump P1 ( $\text{ml min}^{-1}$ )	Pump P2 ( $\text{ml min}^{-1}$ )	Way out 1	Way out 2	Way out 3
1	Water washing	0	6.5	Closed	Open	Closed
2	Fill with sample	0	6.5	Closed	Open	Closed
3	Fill with support buffer (left channel)	2.5	0	Open	Closed	Closed
4	Fill with support buffer (right channel)	2.5	0	Closed	Closed	Open
5	Electrostacking	0	0	Closed	Closed	Closed
6	Collection	2.5	0	Open <sup>a</sup>	Closed	Open <sup>a</sup>

<sup>a</sup> Way out 1 and 3 were sequentially open according to the polarity of the electrolytic cell.



the system depicted in the Fig. 1, the sampling tube was shortened from 12.4 cm (i.d. 0.6 cm) to 4.1 cm (i.d. 1.2 cm) length in order to avoid sample dispersion during the electrostacking process. With this simple system modification, the As results were increased by a 2.65 factor. This behaviour can be explained because of the dependence of the ion migration speed on the electric field intensity,  $E$ , and it is determined by the magnitude of the potential applied ( $V$ /volts) and by the distance between the electrodes ( $d$ /cm). In this way the relationship between  $E$ ,  $V$  and  $d$  is given by  $E = V/d$ . According to this equation there is an increase on the ion migration speed when the distance between the electrodes is shortened [14].

After the aforementioned modification, the variables involved in the BDES system, such as sampled zone, voltage and its application time, sample pH, as well as the nature and concentration of both support and electrode buffer solutions were investigated.

### 3.1.1. Sampling zone

It was evaluated the proper sampled zone where the As pre-concentration factor (PF) was as high as possible. In this way, six 150  $\mu$ l-aliquots were sequentially collected in the auto sampler tubes (1 ml) and the As determined in each one. The third and fourth sampled aliquots (from 300 to 600  $\mu$ l) produced the best results (PF of ca. 1.5 and R.S.D., as a repeatability index, lower than 4.0%). The conditions used in this test for applied voltage and time were 1000 V and 10 min, respectively, and they were based on previous work [9].

In order to check possible contamination problems, the same test was performed, but now using the buffer as the sample. In this way, only small As concentration ( $0.47 \pm 0.03 \mu\text{g l}^{-1}$ ) was achieved. It is interesting to point out that this value was lower than the LOQ (ca.  $1.2 \mu\text{g l}^{-1}$ ) of the method.

In all experiments, Tris–HCl was used as buffer solution and the sample pH was adjusted to 7.0.

### 3.1.2. Applied voltage and time

Applied voltage and time were varied in order to optimise the conditions for improving the PF value. In this way, applied voltage (500, 750 and 1000 V) and time (5, 10, 15 and 20 min) were tested. For all situations, both  $9.0 \mu\text{g l}^{-1}$  As(V) standard solution and the Tris buffer solution ( $0.1 \text{ mol l}^{-1}$ ) were used.

As can be see from Fig. 2, the highest As concentration was obtained using 1000 V as applied voltage and 20 min as electrostacking time. Although these parameters produced the best results, sometimes a great amount of bubbles was formed during the process, interrupting the electric circuit and making the BDES unstable.

It is interesting to note that although the advantageous effect of the increase on both voltage and time in order to improve the sensitivity, a temperature increase is also noted due to the Joule heating, making easier the bubble formation [10,15]. As a compromise between sensitivity and robustness of the system, 750 V and 20 min were chosen for following studies. At these conditions, an R.S.D. of 5% and PF value of 3.5 were obtained.

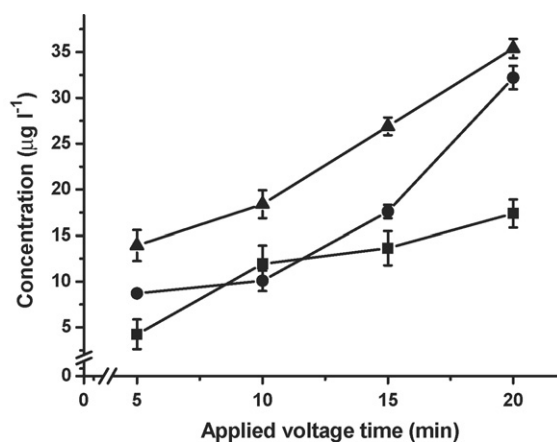


Fig. 2. Arsenic concentration obtained ( $\mu\text{g l}^{-1}$ ) after BDES by varying the applied voltage time. The symbols  $\blacksquare$ ,  $\bullet$  and  $\blacktriangle$  indicate the use of 500, 750 and 1000 V, respectively.

The condition of 0 V and 20 min was also applied in order to check the efficiency of the electrostacking. An interesting result was obtained because the arsenic species were not dispersed at the buffer solution. So, the result obtained ( $0.56 \pm 0.11 \mu\text{g l}^{-1}$ ) reflects the arsenic concentration present in the buffer solutions. This concentration was similar to that already reported (see Section 3.1.1).

In all experiments, Tris–HCl was used as buffer solution and the sample pH was adjusted at 7.0.

### 3.1.3. Sample pH

As the pH plays an important role in the electrostacking system, the pH values of 4, 7, 8 and 12 were evaluate to promote the preconcentration of As.

According to data reported in Fig. 3, one can see that the use of pH 7 provide precise results and the maximum preconcentration, being found a R.S.D. of 3% and a PF of 3.44, respectively. For pH values higher than seven the signal decreased. It can be explained due to the presence of  $\text{OH}^-$  ions which induce a low speed of migration of the  $\text{AsO}_4^{3-}$  species to the cathode. As a consequence, the electrophoretic mobility is decreased, also favouring a poorer As preconcentration [14].

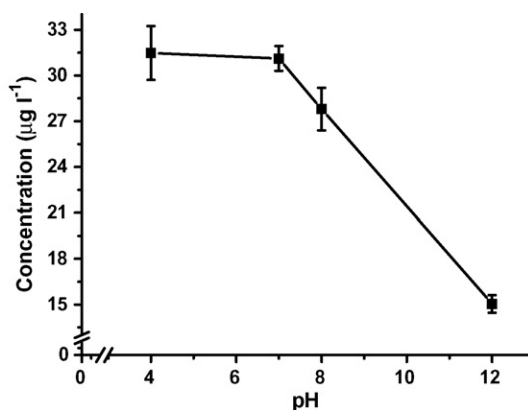


Fig. 3. Arsenic concentration obtained ( $\mu\text{g l}^{-1}$ ) after BDES as a function of sample pH using unbuffered solutions.



### 3.1.4. Study of the buffering conditions

Three buffer systems were tested: (i) Tris plus hydrochloric acid (BS1); (ii) boric acid plus sodium hydroxide (BS2) (iii), and glycine plus sodium hydroxide (BS3), which present  $pK$  of 8.06, 9.23 and 9.78, respectively. The concentration of the support buffer was  $0.1 \text{ mol l}^{-1}$  and that in the salt bridge was  $0.5 \text{ mol l}^{-1}$ . These values were established according to results obtained in a previous work [10]. For testing the buffer system, the same conditions already established were employed. In this way, the results obtained for As using BS1 to 3 were respectively,  $32.2 \pm 2.3 \mu\text{g l}^{-1}$  (PF=3.6),  $43.1 \pm 2.3$  (PF=4.8) and  $17.4 \pm 1.9$  (PF=1.9). According to these results boric acid plus sodium hydroxide was chosen for further experiments.

Poor PF results for glycine can be explained due to its mobility. Considering the  $pK$  of the carboxyl and amine groups as 2.35 and 9.78, respectively for glycine, the isoelectric point is achieved at pH 6.1. At this pH value the migration of the glycine molecules is worsted when the electric potential is applied, while for pH values higher than 6.1, the glycine molecules are deprotonated [14]. The migration of these molecules to the anode can probably create difficulties for the As ions migration to the cathode, decreasing the PF factor when glycine is compared to the others buffers tested here.

With the support buffer already defined, it was evaluated the effect of its concentration in the range between  $0.05$  and  $0.2 \text{ mol l}^{-1}$ . Similar results were achieved for As ( $43.4 \pm 2.0 \mu\text{g l}^{-1}$ ) when compared to those already obtained. It is interesting to note that only slight variations on the As results (ca. 2%) were achieved when the concentration of the buffer solution varied from  $0.5$  to  $1.0 \text{ mol l}^{-1}$ . In this way, the concentration of the buffer system was fixed at  $0.05 \text{ mol l}^{-1}$  and  $0.5 \text{ mol l}^{-1}$  for support buffer and electrode buffer solution, respectively. These values were also chosen in order to maintain a great difference in the concentration between the two buffer solutions, improving both, the electrostacking performance and the pre-concentration factor.

### 3.1.5. As speciation

For As speciation, the As(III) species were oxidized using  $1.5 \text{ ml}$  potassium permanganate solution ( $10 \text{ mg l}^{-1}$ ) in acidic medium ( $3.0 \text{ ml}$  of  $0.01 \text{ mol l}^{-1} \text{ H}_2\text{SO}_4$ ). Then, the excess of permanganate was removed with some drops of 3% (v/v)  $\text{H}_2\text{O}_2$  followed by heating the solution at  $40^\circ\text{C}$  until the vanishing the pink colour. The oxidation efficiency was verified through 5 days by preparing fresh  $10 \mu\text{g l}^{-1}$  As(III) solution in each day and carrying out its oxidation. Satisfactory results [ $50.96 \pm 2.18 \mu\text{g l}^{-1}$  for As(III) solutions previously oxidized] were obtained. Additionally, the oxidation efficiency ranged from 75 to 85%.

Blank solutions were also prepared in parallel, which indicated no contamination problem.

### 3.2. Analytical performance and analysis of water samples

The proposed BDES was remarkable stable. After 8 h working period, the slope of the calibration curve underwent only slight variations (lower than 8%). Linear range was obtained up to  $50 \mu\text{g l}^{-1}$  As(V) ( $r=0.9975$ ;  $n=4$ ) and the detection and

Table 3  
Arsenic determination in mineral water through BDES-ETAAS

Sample	As concentration added ( $\mu\text{g l}^{-1}$ )	As concentration found ( $\mu\text{g l}^{-1}$ )	Recovery %
Mineral water A	0	$2.5 \pm 0.3$	–
	10	$13.7 \pm 1.7$	112
Mineral water B	0	$0.7 \pm 0.1$	–
	10	$10 \pm 2$	95
Mineral water C	0	$1.6 \pm 0.2$	–
	10	$10.6 \pm 0.5$	90
Mineral water D	0	$<0.35$	–
	10	$9.6 \pm 0.6$	96
Mineral water E	0	$0.6 \pm 0.2$	–
	10	$11.6 \pm 0.2$	110
Mineral water F	0	$1.2 \pm 0.06$	–
	10	$11.7 \pm 0.4$	105
Mineral water G	0	$0.4 \pm 0.1$	–
	10	$10.6 \pm 0.3$	102
Mineral water H	0	$<0.35$	–
	10	$10.7 \pm 0.2$	107

Table 4  
Speciation of As in water samples from Ouro Preto area (Minas Gerais state, Brazil) through BDES and ETAAS

Natural water samples	Total As ( $\mu\text{g l}^{-1}$ )	As(III) ( $\mu\text{g l}^{-1}$ )	As(V) ( $\mu\text{g l}^{-1}$ )
Gold mine water 1	$9.88 \pm 0.16$	$5.77 \pm 0.21$	$4.11 \pm 0.21$
Gold mine water 2	$10.53 \pm 0.08$	$6.37 \pm 0.25$	$4.16 \pm 0.16$
Gold mine water 3	$9.38 \pm 0.13$	$5.30 \pm 0.10$	$4.08 \pm 0.15$
River	$8.47 \pm 0.22$	$<0.35$	$8.47 \pm 0.20$
Fountain	$7.52 \pm 0.15$	$4.65 \pm 0.22$	$2.87 \pm 0.10$

quantification limits were  $0.35$  and  $1.18 \mu\text{g l}^{-1}$ , respectively, according to IUPAC recommendations [16]. The precision was estimated as 7% R.S.D. for five independent measurements made on the same day and as 5% R.S.D. for five independent analyses.

The developed procedure was applied to the determination of As in eight mineral drinking water samples (see Table 3) and five natural water samples from Ouro Preto city (Table 4). Two mineral water samples (with gas) were sonicated during 30 min in order to eliminate the gas bubbles. The conductivity was controlled ( $<200 \mu\text{S cm}^{-1}$ ) and a current of  $2.3 \text{ mA}$  was obtained during the voltage application.

An amount of  $10 \mu\text{g l}^{-1}$  As was added to each mineral drinking water sample and the recovery obtained ranged from 91 to 110% with R.S.D.s between 3 and 7 % for three independent measurements of each sample (Table 3). An average pre-concentration factor of 3.5 was found for these samples.

Table 4 illustrates the results obtained for As speciation. As(III) was undetectable in sample 4. In other samples the As(III) concentration ranged from  $4.65$  to  $6.37 \mu\text{g l}^{-1}$ . According to Hall et al., the highest As(III) concentration than As(V) is due to the action of bacteria present in water samples, which make favourable the reduction of As species [17].

## 4. Conclusions

It has been evidenced that BDES offers an alternative for As preconcentration and speciation, in water samples. With

some modifications in the BDES-FI system, it was possible to determine As at  $\mu\text{g l}^{-1}$  concentration, expanding the BDES-FI application to those samples presenting low As concentration.

The proposed system was remarkable stable and can be applicable in the majority of the analytical laboratories because its components are easily available. In addition, the BDES-FI can open the possibility for on-line hyphenations by using different detectors.

### Acknowledgements

The authors are grateful to the Spanish Ministerio de Ciencia y Tecnología, Project AGL 2002-00729, the Brazilian Conselho Nacional de Desenvolvimento Científico e Tecnológico (CNPq) for fellowships of LCM and MAZA, and Fundação de Amparo a Pesquisa do Estado de São Paulo–FAPESP for financial support.

### References

- [1] A. Sanz-Medel, *Spectrochim. Acta* 53B (1998) 197–211.
- [2] S.L.C. Ferreira, H.C. dos Santos, A.C.S. Costa, M. de la Guardia, *Appl. Spectrosc. Rev.* 39 (2004) 457–474.
- [3] M.G. Pereira, E.R. Pereira-Filho, H. Berndt, M.A.Z. Arruda, *Spectrochim. Acta* 59B (2004) 515–521.
- [4] C.G. Yuan, G.B. Jiang, B. He, *J. Anal. At. Spectrom.* 20 (2005) 103–110.
- [5] D.Q. Hung, O. Nekrassova, R.G. Compton, *Talanta* 64 (2004) 269–277.
- [6] R.E. Paproski, X.C. Le, *Anal. Chim. Acta* 526 (2004) 69–76.
- [7] F. Shemirani, M. Baghdadi, M. Ramezani, *Talanta* 65 (2005) 882–887.
- [8] Y.Z. He, M.L. Cervera, A. Pastor, M. de la Guardia, *Anal. Chim. Acta* 447 (2001) 135–142.
- [9] Y.Z. He, M.L. Cervera, M.I. Garrido-Ecija, M. de la Guardia, *Anal. Chim. Acta* 421 (2000) 57–65.
- [10] L. Yang, Y.Z. He, W.E. Gan, M. Li, Q.S. Qu, X.Q. Lin, *Talanta* 55 (2001) 271–279.
- [11] L. Yang, Y.Z. He, W. Gan, N. Deng, M. Li, X.Q. Lin, Application of portable electrokinetic flow analysis system for determination of chromium(VI) and cadmium(II) in mineral water, *Chin. J. Anal. Chem.* 29 (2001) 555–557.
- [12] L. Yang, Y.Z. He, W. Gan, X.Q. Lin, H.C. Zhang, Determination of nitrate in pure water by electrodynamic flow analysis system, *Chin. J. Anal. Chem.* 28 (2000) 248–252.
- [13] A. Shraim, N.C. Sekaran, C.D. Anuradha, S. Hirano, Speciation of arsenic in tube-well water samples collected from West Bengal, India, by high-performance liquid chromatography-inductively coupled plasma mass spectrometry, *Appl. Organomet. Chem.* 16 (2002) 202–209.
- [14] G. Zweig, J.R. Whitaker (Eds.), *Paper Chromatography and Electrophoresis*, Academic Press Inc., London, 1967.
- [15] M. Melvin (Ed.), *Electrophoresis*, John Wiley & Sons, London, 1987.
- [16] Analytical Methods Committee, *Analyst* 112 (1987) 199–204.
- [17] G.E.M. Hall, J.C. Pelchat, G. Gauthier, Stability of inorganic arsenic (III) and arsenic (V) in water samples, *J. Anal. Atom. Spectrom.* 14 (1999) 205–213.

# Comparison of different sorbents for multiresidue solid-phase extraction of 16 pesticides from groundwater coupled with high-performance liquid chromatography

Angelo Antonio D'Archivio\*, Maria Fanelli, Pietro Mazzeo, Fabrizio Ruggieri

*Università degli Studi di L'Aquila, Dipartimento di Chimica, Ingegneria Chimica e Materiali, Via Vetoio, 67010 Coppito, L'Aquila, Italy*

Received 10 October 2005; received in revised form 16 February 2006; accepted 3 March 2006

Available online 18 April 2006

## Abstract

A procedure based on solid-phase extraction (SPE) followed by high-performance liquid chromatography (HPLC) with diode array detection has been developed for the simultaneous analysis of 16 widely used pesticides in groundwater samples. The compounds analysed were: aldicarb, atrazine, desethylatrazine, desisopropylatrazine, carbofuran, 2,4-D, dicloran, fenitrothion, iprodione, linuron, metalaxyl, metazachlor, phenmedipham, procymidone, simazine and vinclozolin. Five different SPE sorbents, C<sub>18</sub> bonded silica (Isolute SPE C18 (EC)), graphitised carbon black (Superclean Envi-Carb), highly cross-linked polystyrene–divinylbenzene (Lichrolut EN), divinylbenzene-*N*-vinylpyrrolidone (Oasis HLB) and surface modified styrene–divinylbenzene (Strata X), were compared. HPLC separation and quantification of the selected pesticides was carried out under isocratic conditions by means of a new reversed-phase column (Gemini from Phenomenex) based on C<sub>18</sub> bonded to organic–silica particles. Oasis HLB and Strata X provided the best results in the preconcentration of 1-l samples, yielding average recoveries higher than 70%, except for phenmedipham that rapidly degrades in groundwater. Detection limits of the target pesticides provided by the proposed SPE-HPLC procedure were between 0.003 and 0.04 μg l<sup>-1</sup>.

© 2006 Elsevier B.V. All rights reserved.

**Keywords:** Pesticides; Solid-phase extraction; Multiresidue analysis; HPLC; Groundwater

## 1. Introduction

Pesticide is a generic term that identifies a wide spectrum of synthetic compounds with biocide activity worldwide used to contrast weeds, fungi and insects with the scope of increasing productivity in agriculture. As the result of massive global consumption [1], pesticides and their degradation products can contaminate surface and groundwater with potential risks for wildlife and human health connected with proven or suspect toxicity of many of these compounds [2,3]. Groundwater, being the main source of drinking water in most of the European countries and in the USA, is subjected to restrictive legislation aimed at control of chemical pollutants [1]. As concerns pesticides, a European Community Directive fixes permitted levels in drinking water to 0.1 μg l<sup>-1</sup> for individual compounds and some of their degra-

dation products, and 0.5 μg l<sup>-1</sup> for the sum of all compounds [4].

Gas chromatography and high-performance liquid chromatography (HPLC) coupled with various detection systems [5–10] are the most powerful tools for the analysis of pesticides in water. However, in order to reach the low concentration levels permitted in potable water, a preliminary concentration step is required before chromatographic analysis [1,11,12]. Solid-phase extraction (SPE) is nowadays the most appropriate method for enrichment of pesticides in aqueous matrices. As compared with conventional liquid–liquid extraction, SPE exhibits lower cost, reduced processing time and solvent consumption [1,12]. C<sub>8</sub> or C<sub>18</sub> bonded silica, graphitised carbon, ionic exchange resins or polymeric materials [13], commercially available in cartridge and disk systems, are the most extensively used SPE sorbents for preconcentration and clean-up of water samples [1,10–12,14–19]. Extraction is a critical step of multiresidue analysis of water micropollutants. Ideally, this procedure should ensure large concentration factors for all target analytes. However, because of selective interaction mechanism of most of the

\* Corresponding author. Tel.: +39 0862433777; fax: +39 0862433753.  
E-mail address: [darchivi@univaq.it](mailto:darchivi@univaq.it) (A.A. D'Archivio).

available SPE sorbents, this is a difficult task in the circumstance that the analytes exhibit different physico-chemical properties (polarity, acidity, solubility).

In the present study, we developed a SPE-HPLC procedure for the simultaneous analysis of 16 widely used pesticides, namely: aldicarb, atrazine, desethylatrazine, desisopropylatrazine, carbofuran, 2,4-D, dicloran, fenitrothion, iprodione, linuron, metalaxyl, metazachlor, phenmedipham, procymidone, simazine and vinclozolin. Apart from interest related to large use of these compounds in modern agriculture, many deserve attention because of their toxicological potential, such as aldicarb and carbofuran, classified as extremely and highly hazardous, respectively [2], or linuron, atrazine and vinclozolin, suspected to be endocrine disruptors [3].

To achieve the most efficient preconcentration of the 16 pesticides we investigated the retention ability of five commercially available SPE cartridges based on different kinds of sorbents. Four sorbents, such as octadecyl-bonded silica (Isolute SPE C18 (EC)), graphitised carbon black (Envi-Carb), highly cross-linked polystyrene-divinylbenzene (LiChrolut EN) and divinylbenzene-*N*-vinylpyrrolidone copolymers (Oasis HLB), are quite popular. In addition to these, we tested a SPE cartridge based on surface modified styrene-divinylbenzene polymer (Strata X) suitable for the simultaneous extraction of analytes with different physico-chemical properties [20,21].

The identification and quantification of the investigated pesticides was carried out by means of HPLC coupled with diode array detection (DAD) at isocratic conditions. We used a new reversed-phase column (Gemini from Phenomenex) featured by C<sub>18</sub> chains bonded to silica particles covered by a layer of silica-organic material, which applications, as far as we know, have not been published yet.

## 2. Experimental

### 2.1. Chemicals and solvents

Pesticide standards were obtained from Labor Dr. Ehrenstorfer-Schäfers (Augsburg, Germany) and were used without further purification. Stock solutions (1.00 g l<sup>-1</sup>) were prepared by dissolving accurately weighed 10 mg of each pesticide in 10 ml of acetonitrile. Standard working solutions (100 mg l<sup>-1</sup>) of each compound were prepared by appropriate dilution of respective stock solutions with acetonitrile and were stored at 4 °C.

HPLC-grade acetonitrile, dichloromethane and methanol were purchased from Carlo Erba Reagenti (Milano, Italy). Distilled water obtained from a Milli-Q water filtration/purification system (Millipore, Bedford, MA, USA), acidified with H<sub>3</sub>PO<sub>4</sub> (Carlo Erba Reagenti), was used for the preparation of the mobile phase.

### 2.2. Materials for SPE

The following cartridges were used: LiChrolut EN, 3 ml, 200 mg (Merck, Darmstadt, Germany); Supelclean ENVI-Carb, 3 ml, 250 mg (Supelco, Bellefonte, PA, USA); Oasis HLB,

6 ml, 200 mg (Waters, Mildford, MA, USA); Strata X, 6 ml, 200 mg (Phenomenex, Torrance, CA, USA) and Isolute SPE C18 (EC), 3 ml, 200 mg (International Sorbent Technology Ltd., Mid Glamorgan, UK).

### 2.3. Sampling and sample preparation

Groundwater samples were taken from a well in the agricultural-industrial settlement of Fucino plain, (L'Aquila, Italy) and stored at 4 °C. In order to evaluate the recovery of extraction, 1 l of sample was spiked with the 16 pesticides, by addition of suitable aliquots of the respective working standard solutions, to finally give 0.1, 0.2 or 0.5 μg l<sup>-1</sup> of each compound. Prior to extraction, the spiked water samples were filtered by filter paper Whatman 5, diameter 5 cm, pore size 0.45 μm (Whatman International Ltd., Maidstone, England) to remove the particulate matter.

### 2.4. HPLC equipment

Separation was performed using an HPLC apparatus consisting of a 4.0 mm × 3.0 mm precolumn SecurityGuard C18 (Phenomenex), a 250 mm × 4.6 mm column Gemini C18 (Phenomenex) with 5 μm particle size, a 515 pump and a 996 Photodiode Array Detector (Waters). The system was controlled by a Millennium software (Waters).

### 2.5. Chromatographic analysis

The HPLC analyses were carried out at room temperature, constant flow-rate (1 ml min<sup>-1</sup>) and isocratic conditions using a mixture (50:50, v/v) of acetonitrile and water acidified with H<sub>3</sub>PO<sub>4</sub> (0.1%) as mobile phase. UV spectra of the analytes were recorded from 210 to 400 nm. The working wavelength for quantitative analysis of each analyte (Table 1) was selected to have the maximum absorbance and best peak resolution. Calibration curves of all analytes were obtained from triplicate experiments using five standard samples in the concentration range 0.1–1.0 mg l<sup>-1</sup> obtained by appropriate dilution of working standard solutions with acetonitrile. The relevant chromatographic parameters were obtained by averaging the results of two chromatographic runs.

### 2.6. SPE procedure

The SPE sorbents were conditioned by washing with 10 ml of dichloromethane, followed by 10 ml of acetonitrile and finally 10 ml of Milli-Q water. The solvents were forced through the cartridge by means of a positive pressure at a rate of 1 ml/min. The water sample (1 l), immediately after spiking, was passed through the cartridge approximately at a flow-rate of 10 ml min<sup>-1</sup> by applying a moderate vacuum. After that, the cartridges were washed with a water-methanol mixture (95:5, v/v) and successively dried for approximately 10 min by fluxing air. The retained analytes were eluted by 5 ml of acetonitrile and 5 ml of methanol. The elutes were collected as one and evaporated to dryness at room temperature in a Supelco dry-

Table 1  
Analytical data for the HPLC method

Pesticide	$t_R$ (min)	$\lambda$ (nm)	$r^2$	LOD ( $\text{mg l}^{-1}$ )	LOQ ( $\text{mg l}^{-1}$ )
Desysopropylatrazine	3.4	220	0.9999	0.005	0.015
Desethylatrazine	4.0	220	0.9999	0.005	0.015
Aldicarb	5.2	245	0.9998	0.05	0.2
Simazine	5.8	220	0.9999	0.005	0.015
Carbofuran	6.8	275	0.9986	0.035	0.13
Metalaxyl	7.3	220	0.9995	0.035	0.12
Atrazine	7.9	220	0.9989	0.005	0.015
2,4-D	8.6	220	0.9984	0.04	0.14
Metazachlor	9.7	220	0.9940	0.03	0.1
Dicloran	12.4	360	0.9997	0.015	0.05
Phenmedipham	12.8	238	0.9951	0.015	0.05
Linuron	14.1	248	0.9993	0.01	0.05
Iprodione	20.6	220	0.9994	0.02	0.075
Procymidone	22.6	220	0.9999	0.03	0.1
Fenitrothion	24.4	270	0.9954	0.075	0.25
Vinclozolin	29.4	220	0.9929	0.05	0.14

Approximate retention time ( $t_R$ ), wavelength for quantification ( $\lambda$ ), correlation coefficient ( $r^2$ ) of calibration curve, detection limit (LOD) and quantification limit (LOQ) of the target pesticides.

ing attachment working under vacuum in nitrogen atmosphere (procedure A). As an alternative, the elute was transferred into a 15 ml pear-shaped evaporating flask and evaporated by means of a rotavapor Büchi RE 111 at 40 °C under a moderate vacuum (procedure B). The dry residue was finally dissolved in 500  $\mu\text{l}$  of a water–acetonitrile mixture with the same composition of the HPLC mobile phase (50:50, v/v). Twenty microliters aliquots were injected into chromatograph for evaluation of the extraction recovery.

### 3. Results and discussion

#### 3.1. HPLC analysis

The chromatographic separation of the 16 pesticides was carried out by using a new reversed-phase column based on  $\text{C}_{18}$  chains covalently bonded to silica particles with the external surface covered by a silica–organic layer. The mobile phase composition was optimised to achieve the best separation under isocratic conditions. The isocratic method, that does not require column re-equilibration after each chromatographic run, was adopted to limit the overall analysis time in the circumstance that a great number of samples needs to be consecutively investigated. Optimisation of an extraction protocol as that presented in this paper is a typical case. Using water–acetonitrile (50:50, v/v) as eluent, a chromatogram consisting of separated and symmetric peaks was obtained in about 30 min. Fig. 1 shows the HPLC-DAD chromatograms of a 0.2  $\text{mg l}^{-1}$  standard solution of the 16 pesticides extracted at 220, 238 and 360 nm. Retention time and wavelength for quantification of the analytes are collected in Table 1. Identification of the pesticides was based on both retention time and their UV spectra. Quantification was carried out on the maximum absorbance (220 nm for many pesticides) unless peaks overlapped. In this circumstance the wavelength was selected on the basis of differences of UV spectra of the unresolved analytes. As an example, dicloran and phen-

medipham, that exhibit almost identical retention times, were quantified at 360 and 238 nm, respectively, i.e. in conditions of selective adsorption for each compound (see Fig. 1).

Good linearity of the response of the chromatographic method was found in the concentration range investigated (0.1–1  $\text{mg l}^{-1}$ ), with regression coefficients ranging between 0.9929 and 0.9999 (Table 1). The detection limits (LODs) and the quantification limits (LOQs) of the HPLC method, estimated on the basis of a signal-to-noise ratio of 3 and 10, respectively, are collected in Table 1. LOD and LOQ ranges from 50 to 5 and 200 to 15  $\mu\text{g l}^{-1}$ , respectively, except for fenitrothion that exhibits slightly larger LOD and LOQ values (75 and 250  $\mu\text{g l}^{-1}$ , respectively), as a consequence of its relatively weak absorbance.

#### 3.2. Recovery studies

A SPE procedure to be applied prior to the chromatographic analysis, allowing pesticide quantification at 0.1  $\mu\text{g l}^{-1}$  level, as demanded by the European legislation for potable

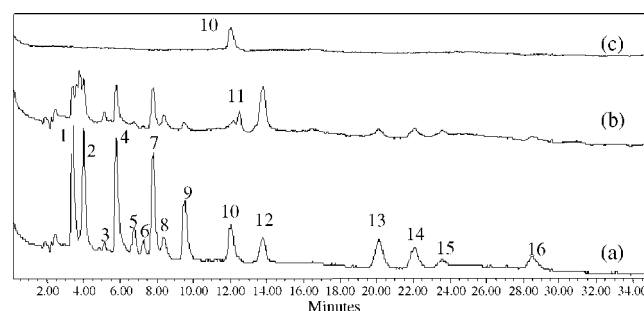


Fig. 1. Chromatograms of 0.2  $\text{mg l}^{-1}$  standard solution of pesticides extracted at 220 nm (a), 238 nm (b) and 360 nm (c). Peaks: (1) desysopropylatrazine, (2) desethylatrazine, (3) aldicarb, (4) simazine, (5) carbofuran, (6) metalaxyl, (7) atrazine, (8) 2,4-D, (9) metazachlor, (10) dicloran, (11) phenmedipham, (12) linuron, (13) iprodione, (14) procymidone, (15) fenitrothion, and (16) vinclozolin.



water, was here developed. In this context, we investigated the capacity to retain the pesticides of five commercially available SPE sorbents. In addition to quite popular sorbents, such as C<sub>18</sub> bonded silica (Isolute SPE C18 (EC)), graphitised carbon black (Superclean Envi-Carb), highly cross-linked polystyrene–divinylbenzene (Lichrolut EN) and divinylbenzene–*N*-vinylpyrrolidone copolymers (Oasis HLB), we evaluated the retention ability of Strata X, based on surface modified styrene–divinylbenzene polymer. One liter of groundwater spiked with the 16 pesticides at a concentration of 0.2 or 0.5  $\mu\text{g l}^{-1}$  was subjected to SPE to compare the extraction ability of the five cartridges. Oasis HLB and Strata X, that on the basis of recovery results at these concentrations (see below) exhibited the best efficiency, were also assayed at the concentration of 0.1  $\mu\text{g l}^{-1}$ . Acetonitrile and methanol were used to elute the analytes from the cartridges. The influence of the solvent volume on the recovery was carefully evaluated. Finally, 5 ml of each solvent was used, which ensured the complete desorption of the analytes from the sorbents in the investigated range of pesticide concentration.

The average extraction recoveries (*R*%) together with relative standard deviations (R.S.D.), obtained from experiments carried out in triplicate, are collected in Table 2. Apparently, the overall performance of the selected cartridges is not appreciably influenced by pesticide concentration, except when Oasis HLB is used. In this case, *R*% of many pesticides significantly decreases as concentration increases from 0.2 to 0.5  $\mu\text{g l}^{-1}$ , suggesting that breakthrough may take place for concentrations of all pesticides greater than 0.2  $\mu\text{g l}^{-1}$ . This condition, however, is unlikely to occur in real groundwater samples. The behaviour of phenmedipham needs to be discussed. We observed that this pesticide, although relatively stable in organic solvents and HPLC-grade water, degrades rapidly in groundwater, as also previously reported by other authors [22]. As a consequence, phenmedipham

cannot be completely recovered. Moreover, the observed *R*% of this analyte can be significantly influenced by the experimental conditions, particularly by the time taken for sample preconcentration. Thus, the experiments carried out in different days (for instance, the recovery studies at different spiked levels), in which the above variables are not exactly controlled, do not provide homogeneous results.

The cartridges Isolute SPE C18 and Superclean Envicarb are not able to retain some of the pesticides (aldicarb and 2,4-D in the former case, 2,4-D, dicloran and phenmedipham in the latter). On the other hand, Lichrolut EN, Oasis HLB and Strata X retain all pesticides with variable recoveries. Comparison of the behaviour of these three cartridges reveals that Oasis HLB and Strata X provide an overall comparable efficiency, significantly better than that of Lichrolut EN. This is demonstrated by a markedly better ability to retain carbofuran and 2,4-D and a moderately higher recovery of iprodione, whereas all other pesticides are recovered with similar yields by the three sorbents.

### 3.3. Optimisation of the SPE procedure

It must be noted that some pesticides are poorly or partially recovered regardless of the employed sorbent. These are dicloran, fenitrothion and viclozolin, which recoveries do not exceed 60–70%, and aldicarb, for which *R*% is lower than 47%. Previous studies [8] showed that aldicarb, as well as some other volatile pesticides, can be lost in the evaporation step. In order to evaluate the effect of possible evaporation of the analytes on the observed recoveries, we performed a test of volatility, as suggested in reference [8]. To this purpose, the desorption solution (5 ml of acetonitrile and 5 ml of methanol), after spiking with the 16 pesticides (0.2  $\mu\text{g l}^{-1}$ ), was subjected to evaporation under the same conditions used in the recovery studies (evaporation procedure A). Indeed, the following HPLC analysis of the

Table 2  
Comparison of retention ability of the five selected sorbents

Sorbent (spiked level ( $\mu\text{g l}^{-1}$ ))	Isolute SPE C18		Superclean Envi-Carb		Lichrolut EN		Oasis HLB			Strata X		
	0.2	0.5	0.2	0.5	0.2	0.5	0.1	0.2	0.5	0.1	0.2	0.5
Pesticide												
Desysopropylatrazine	12(6)	15(4)	77(5)	69(2)	82(4)	85(1)	99(2)	94(5)	68(6)	80(5)	89(4)	85(5)
Desethylatrazine	21(7)	29(6)	75(2)	73(3)	84(2)	92(2)	100(2)	97(5)	85(4)	100(1)	86(4)	95(6)
Aldicarb	0	0	34(10)	27(6)	20(24)	26(14)	40(6)	28(10)	31(6)	47(3)	43(11)	45(6)
Simazine	78(1)	85(4)	61(6)	62(2)	97(2)	87(3)	86(1)	79(6)	61(2)	75(5)	80(1)	81(5)
Carbofuran	62(2)	68(5)	79(2)	68(2)	21(3)	22(10)	84(3)	79(3)	71(1)	86(3)	90(4)	81(2)
Metalaxyl	71(3)	88(2)	98(2)	94(2)	103(3)	103(2)	98(2)	90(2)	85(5)	100(3)	91(3)	89(2)
Atrazine	85(1)	95(1)	81(2)	80(2)	98(2)	94(1)	89(4)	90(6)	72(3)	82(2)	83(3)	86(4)
2,4-D	0	0	0	0	29(6)	29(2)	100(1)	103(3)	99(1)	98(1)	105(5)	99(3)
Metazachlor	93(3)	95(2)	80(2)	72(3)	104(1)	87(1)	103(1)	87(4)	88(3)	95(4)	88(2)	91(1)
Dicloran	43(3)	47(8)	0	0	68(8)	62(1)	63(1)	65(3)	43(6)	48(1)	50(5)	60(3)
Phenmedipham	66(4)	47(4)	0	0	20(4)	20(6)	77(5)	71(5)	48(7)	40(8)	61(5)	35(1)
Linuron	90(3)	94(4)	21(3)	21(7)	94(2)	84(4)	89(5)	84(3)	65(3)	78(6)	87(2)	85(4)
Iprodione	85(2)	72(2)	6(3)	9(2)	53(6)	50(1)	78(3)	77(3)	60(4)	78(7)	74(2)	66(9)
Procymidone	76(3)	78(3)	65(4)	73(3)	83(1)	79(3)	84(3)	85(3)	63(3)	61(1)	77(1)	70(3)
Fenitrothion	35(5)	54(2)	33(7)	40(4)	61(5)	58(4)	62(4)	59(3)	54(7)	49(2)	50(2)	57(5)
Vinclozolin	26(1)	34(5)	36(3)	40(2)	56(2)	48(4)	43(7)	59(9)	51(6)	52(3)	42(9)	33(1)

Average recovery values and, in parentheses, relative standard deviations ( $n=3$ ) obtained preconcentrating 1 l of groundwater reinforced with different pesticide concentrations. Evaporation procedure A was followed.

Table 3  
Analytical data for the best SPE-HPLC procedure

Pesticide	R%		LOD ( $\mu\text{g l}^{-1}$ )	LOQ ( $\mu\text{g l}^{-1}$ )
	Oasis HLB	Strata X		
Desisopropylatrazine	90(5)	82(2)	0.003	0.009
Desethylatrazine	90(1)	92(3)	0.003	0.009
Aldicarb	74(6)	71(4)	0.035	0.14
Simazine	86(4)	85(5)	0.003	0.009
Carbofuran	99(1)	97(5)	0.02	0.06
Metalaxyl	111(8)	100(4)	0.02	0.06
Atrazine	95(7)	90(4)	0.003	0.009
2,4-D	101(5)	113(4)	0.02	0.07
Metazachlor	85(3)	90(4)	0.02	0.06
Dicloran	86(6)	84(5)	0.01	0.03
Phenmedipham	54(10)	66(2)	0.014	0.05
Linuron	86(5)	93(2)	0.01	0.05
Iprodione	72(5)	71(3)	0.014	0.05
Procymidone	79(1)	74(6)	0.02	0.07
Fenitrothion	86(5)	97(1)	0.04	0.15
Vinclozolin	71(7)	88(10)	0.035	0.1

Average recovery values and, in parentheses, relative standard deviations ( $n = 3$ ) obtained preconcentrating 1 l of groundwater spiked with  $0.2 \mu\text{g l}^{-1}$  of pesticides by means of Oasis HLB and Strata X cartridges, following procedure B for elute evaporation. LOD and LOQ values for the SPE-HPLC procedure (the two sorbents provide comparable values).

residue revealed incomplete recoveries for aldicarb ( $42 \pm 15\%$ ), dicloran ( $52 \pm 6\%$ ), fenitrothion ( $57 \pm 4\%$ ) and vinclozolin ( $45 \pm 4\%$ ). A moderate loss in the evaporation step was also found for carbofuran, linuron and procymidone (observed recoveries between 82 and 86%), whereas all other pesticides were almost completely recovered (90–107%). On the basis of this evidence, a different procedure for the evaporation of the desorption solution was adopted with the aim of minimising the loss of the analytes. Table 3 shows the recoveries obtained with Oasis HLB and Strata X, i.e. the sorbents providing the best results in the previous recovery study, for a spiked concentration of  $0.2 \mu\text{g l}^{-1}$ , when the evaporation was carried out by means of a rotavapor (procedure B, described in Section 2). Comparison of these data with those obtained when the evaporation protocol A was followed (given in Table 2) reveals that, while R% of non-volatile pesticides are substantially confirmed, recoveries do remarkably improve in the case of aldicarb, dicloran, fenitrothion and vinclozolin, i.e. the most volatile analytes. However, intra-day repeatability of recovery seems to be independent of the evaporation procedure: R.S.D. values typically fall within 2–7% for both applied procedures.

### 3.4. Analytical data for the best SPE-HPLC procedure

Inspection of Table 3 confirms the quite similar behaviour of Strata X and Oasis HLB. By applying the evaporation procedure B, all pesticides are recovered with remarkably good yields, R% being greater than 70%, except in the case of phenmedipham. Fig. 2 shows the HPLC chromatogram of a real groundwater sample reinforced with  $0.1 \mu\text{g l}^{-1}$  of each pesticide after extraction on Oasis HLB compared with the chromatogram of a not spiked sample. At the detection wavelength of 220 nm, used for the majority of the analytes, the matrix effects are mostly

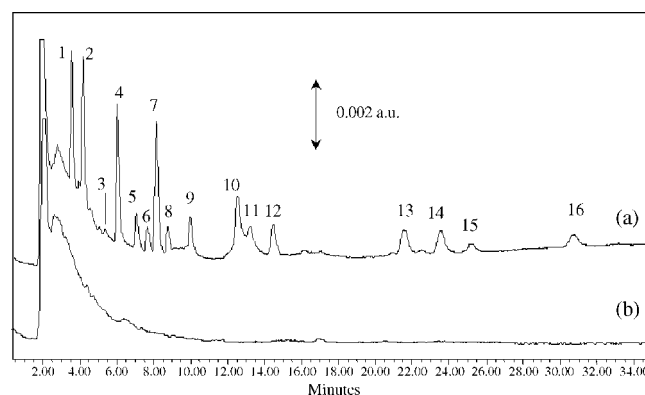


Fig. 2. HPLC chromatogram ( $\lambda = 220 \text{ nm}$ ) obtained by analysing 1-l sample of groundwater spiked with  $0.1 \mu\text{g l}^{-1}$  of each pesticide (a) and not spiked (b) after SPE on Oasis HLB and following evaporation procedure B. Peak numbers as in Fig. 1.

significant and result in a large peak at the beginning of the chromatogram. However, the analytes co-eluting with the unresolved matrix components still exhibit well distinct peaks. As to aldicarb, even if detectable (peak 3), as a consequence of low absorbance, it appears as a very low peak partially masked by the initial band. On the other side, the matrix interference seems to be negligible in the case of analytes with longer retention times, for which, however, sensitivity is reduced as a consequence of peak enlargement. LOD and LOQ of the SPE-HPLC procedure (the values are comparable when Oasis HLB and Strata X are used for extraction) are given in Table 3. For the majority of the investigated pesticides, LOD are between  $0.003$  and  $0.02 \mu\text{g l}^{-1}$  and LOQ between  $0.01$  and  $0.07 \mu\text{g l}^{-1}$ , i.e. significantly below the permitted concentration levels. As outlined above, some pesticides, owing to low absorption (aldicarb), significant peak broadening (vinclozolin), or both effects (fenitrothion), exhibit slightly larger values (LOD between  $0.035$  and  $0.04$  and LOQ between  $0.1$  and  $0.15 \mu\text{g l}^{-1}$ ). Thus, quantification of these analytes at a concentration level significantly lower than that demanded by European legislation requires a more sensitive and selective detection system, such as mass spectrometry, possibly combined with a gradient elution method able to avoid peak enlargement for the most retained pesticides.

The actual ability of the sorbents to retain phenmedipham could be evaluated taking into account its degradation kinetics. Phenmedipham concentration was observed to decrease in groundwater according to a first-order kinetics with half-life time of about 120 min. Maximum recovery can be identified with the ratio of the average residual concentration and the spiked concentration, the average being calculated over the time taken for the extraction (variable between approximately 90 and 150 min). Under these conditions, the maximum recovery is expected to fall between 67 and 78%, which compared with the observed recoveries, demonstrates a good ability of Strata X and Oasis HLB to retain also phenmedipham. It must be stressed, however, that, as a consequence of fast rate of degradation, it is unlikely to found detectable traces of phenmedipham in real groundwater samples. Degradation products should be rather identified and quantified.

#### 4. Conclusions

This work describes a simple method for the quantification of 16 pesticides in groundwater at low  $0.1 \mu\text{g l}^{-1}$  level. HPLC separation and quantification was carried out at isocratic conditions using a stationary phase based on  $\text{C}_{18}$  bonded to silica–organic particles. Five commercially available sorbents were assayed in order to optimise the simultaneous extraction of the selected analytes. The best recoveries were provided by two polymeric sorbents based on divinylbenzene-*N*-vinylpyrrolidone (Oasis HLB) and surface modified styrene-divinylbenzene (Strata X). By concentrating 1 l of groundwater, detection and quantification limits significantly below the permitted concentration levels were reached for most of the pesticides. Some pesticides (aldicarb, fenitrothion and vinclozolin) can be detected at concentration levels lower than  $0.1 \mu\text{g l}^{-1}$ , but their quantification limits approach the permitted concentration levels. Recovery studies showed that the evaporation of the elute is a critical step of the extraction procedure, because some volatile pesticides (aldicarb, dicloran, fenitrothion and vinclozolin) can be partially lost during evaporation. Phenmedipham cannot be detected in real groundwater samples as a consequence of fast degradation. It would be rather useful to quantify the degradation products of this pesticide.

#### References

- [1] H. Sabik, R. Jeannot, B. Rondean, *J. Chromatogr. A* 885 (2000) 217.
- [2] WHO, The WHO Recommended Classification on Pesticides by Hazard and Guidelines to Classification 2000–2002, World Health Organization Programme on Chemical Safety, Geneva, 2001.
- [3] European Commission, Communication from the Commission to the Council and European Parliament, Implementation of the Community Strategy for Endocrine Disruptors: a range of substances suspected of interfering with the hormone systems of humans and wildlife (COM (1999) 706), Brussels Belgium 14-06-2001, COM (2001) 262 final.
- [4] EEC, Drinking Water Guideline, 80/779/EEC, EEC No. L229/11-29, Brussels, 1980.
- [5] A. Di Corcia, A. Costantino, C. Crescenzi, R. Samperi, *J. Chromatogr. A* 852 (1999) 465.
- [6] A.C. Hogenboom, W.M.A. Niessen, U.A.Th. Brinkam, *J. Chromatogr. A* 794 (1998) 201.
- [7] K. Vandecasteele, I. Gaus, W. Debreuck, K. Walraevens, *Anal. Chem.* 72 (2000) 3093.
- [8] S. Guenu, M.C. Hennion, *J. Chromatogr. A* 737 (1996) 15.
- [9] C. Aguilar, I. Ferrer, F. Borrull, R.M. Marcé, D. Barceló, *J. Chromatogr. A* 794 (1998) 147.
- [10] H. Sabik, R. Jeannot, *J. Chromatogr. A* 818 (1998) 197.
- [11] D. Barceló, M.C. Hennion, *Analitica Chimica Acta* 338 (1997) 3.
- [12] V. Pacáková, K. Štulc, J. Jiskra, *J. Chromatogr. A* 754 (1996) 17.
- [13] N. Masqué, R.M. Marcé, F. Borrull, *Trends Anal. Chem.* 17 (1998) 384.
- [14] N. Masqué, R.M. Marcé, F. Borrull, *J. Chromatogr. A* 793 (1998) 257.
- [15] S. Guenu, M.C. Hennion, *J. Chromatogr. A* 737 (1996) 15.
- [16] R. Carabias-Martínez, E. Rodríguez-Gonzalo, E. Herrero-Hernández, F.J. Sánchez-San Roman, M.G. Prado Flores, *J. Chromatogr. A* 950 (2002) 157.
- [17] N. Masqué, M. Galià, R.M. Marcé, F. Borrull, *J. Chromatogr. A* 803 (1998) 147.
- [18] R.A. McLaughlin, B.S. Johnson, *J. Chromatogr. A* 790 (1997) 161.
- [19] N. Fontanals, P. Puig, M. Galià, R.M. Marcé, F. Borrull, *J. Chromatogr. A* 1035 (2004) 281.
- [20] M.H. Hilton, K.V. Thomas, *J. Chromatogr. A* 1015 (2003) 129.
- [21] M.D. Marazuela, M.C. Moreno-Bondi, *J. Chromatogr. A* 1034 (2004) 25.
- [22] C. Hidalgo, J.V. Sancho, F.J. López, F. Hernández, *J. Chromatogr. A* 823 (1998) 121.

# Determination of trace elements in natural waters by inductively coupled plasma time of flight mass spectrometry after flow injection preconcentration in a knotted reactor

Boryana Dimitrova-Koleva<sup>a</sup>, Karima Benkhedda<sup>b</sup>, Elisaveta Ivanova<sup>a,\*</sup>, Freddy Adams<sup>b</sup>

<sup>a</sup> Institute of General and Inorganic Chemistry, Bulgarian Academy of Sciences, Analytical Chemistry, Bl. 11, Acad. G. Bontchev Street, 1113 Sofia, Bulgaria

<sup>b</sup> Micro-Trace Analysis Centre, Department of Chemistry, University of Antwerp, Drie Eiken Campus, B-2610 Antwerp, Belgium

Received 31 October 2005; received in revised form 20 February 2006; accepted 3 March 2006

Available online 18 April 2006

## Abstract

A flow injection on-line sorption system was developed for the separation and preconcentration of traces of Ag, Cd, Co, Ni, Pb, U and Y from natural water samples with subsequent detection by ICP TOF MS. Simultaneous preconcentration of the analytes was achieved by complexation with the chelating reagent 1-phenyl-3-methyl-4-benzoylpyrazol-5-one immobilized on the inner walls of a (200 cm × 0.5 mm) PTFE knotted reactor. The analytes were eluted and transported to an axial ICP TOF MS system with 1% (v/v) HNO<sub>3</sub> containing 0.3 μg l<sup>-1</sup> of Rh as an internal standard using ultrasonic nebulization. The detection limits (3σ) varied from 0.3 ng l<sup>-1</sup> for Y to 15.2 ng l<sup>-1</sup> for Ni and the precision (R.S.D.) was better than 4%. Using a loading time of 90 s and a sample flow rate of 4.5 ml min<sup>-1</sup>, enhancement factors of 3–14 were obtained for the different analytes in comparison with their direct determination by ICP TOF MS with ultrasonic nebulization without preconcentration. The accuracy of the method was demonstrated by analysis of water based certified reference materials.

© 2006 Elsevier B.V. All rights reserved.

**Keywords:** Trace elements; Preconcentration; Waters; Inductively coupled plasma time of flight mass spectrometry

## 1. Introduction

The determination of trace elements in natural waters is of increasing importance for routine monitoring of environmental pollution and studies on the ecological and physiological role of the essential and toxic elements. However, direct trace analysis of environmental waters is frequently difficult because of very low analyte concentrations and high salt content.

Inductively coupled plasma mass spectrometry (ICP MS) is now a widely utilized instrumental technique, offering nearly complete elemental coverage over a broad concentration range, reaching very low detection limits with a high sample throughput and low sample consumption. However, the direct determination of trace elements in saline waters remains limited because of the sensibility of ICP MS to matrix interferences such as signal suppression by elements with low ionization potentials, polyatomic ion formation, space charge effects and salt deposition

on the sampler and skimmer cones, resulting in reduced sensitivity and compromising long-term stability. A pretreatment is usually necessary for trace element analysis of natural waters in order to remove the matrix while simultaneously preconcentrating the analytes. Off-line procedures such as coprecipitation [1], solvent extraction [2,3] and solid-phase extraction [4,5] are generally used but such procedures are time consuming, require significant manual efforts, need large sample volumes and suffer risks of contamination and analyte loss. These drawbacks are avoided by implementing the separation/preconcentration techniques in flow injection analysis [3,6–9].

Fang et al. [10] first used a knotted reactor (KR) made from Microline tubing as a filterless collector of organic precipitates in on-line coprecipitation–dissolution with subsequent flame atomic absorption spectrometric detection. Later, a KR made from PTFE tubing was shown to be capable of retaining metal complexes with a number of chelating reagents, e.g., ammonium pyrrolidinedithiocarbamate (APDC) [6,11–13], sodium diethyldithiocarbamate [14], 5-bromo-2-pyridylazo-5-diethylaminophenol [15], diethylthiourea [16], 1-phenyl-3-methyl-4-benzoylpyrazol-5-one (PMBP) [17,18] on its inner

\* Corresponding author. Tel.: +359 2 9792571; fax: +359 2 8702450.  
E-mail address: [eliva@svr.igic.bas.bg](mailto:eliva@svr.igic.bas.bg) (E. Ivanova).

walls through sorption under appropriate experimental conditions. The conventional preconcentration scheme involves on-line merging of sample and reagent solutions and sorption of the chelate complexes obtained onto the inner walls of the KR. In a former work [17], a preconcentration scheme based on the use of a KR pre-coated with the reagent was developed, which creates more favorable conditions for trace element preconcentration, expressed in higher sensitivity.

Since the introduction of commercially available ICP MS in the early 1980s, most instruments incorporate quadrupole mass filters, as these combine the necessary resolution with reasonable cost. Quadrupole ICP MS instruments are scanning-based spectrometers and suffer from performance limitations especially when they are used to detect transient signals. Myers and Hieftje [19] described in 1993 an ICP MS instrument based upon the time of flight (TOF) principle. In TOF MS all ions that comprise a single mass spectrum are simultaneously extracted from the plasma at a rate of typically more than 20,000 full spectra per second. As a result of this high spectral generation rate, the main drawbacks of scanning MS, such as the compromise between mass coverage and sensitivity/precision, do not apply to the TOF MS. ICP TOF MS has been already used for multi-element detection of transient signals derived from several hybrid techniques based on flow injection [12,16,20,21], gas chromatography [22,23], liquid chromatography [24] and laser ablation [25,26].

In this work, a selective, sensitive and fast method for the determination of trace levels of Ag, Cd, Co, Ni, Pb, U and Y in natural water samples is described. FI on-line sorption separation/preconcentration of the elements is performed in a KR pre-coated with the chelating reagent 1-phenyl-3-methyl-4-benzoylpyrazol-5-one with subsequent ICP TOF MS detection. The analytes are eluted and transported into the ICP TOF MS system with 1% (v/v) HNO<sub>3</sub>, containing 0.3 μg l<sup>-1</sup> Rh as an internal standard, using ultrasonic nebulization. The accuracy of the method is demonstrated by analysis of certified reference materials of natural waters.

## 2. Experimental

### 2.1. Instrumentation

An axial ICP TOF MS instrument (Renaissance, LECO, St. Joseph, MI, USA) was used for the determination of Ag, Cd, Co, Ni, Pb, U and Y. A CETAC (Omaha, NE, USA) ultrasonic nebulizer (USN), Model U-6000 AT<sup>+</sup> with membrane desolvator was used as an interface between the FI system and the ICP TOF MS spectrometer. The instrumental settings and operating conditions of the USN-ICP TOF MS system are summarized in Table 1. The selected isotopes, their relative abundance and the main polyatomic interferences caused by the common components of natural waters are given in Table 2. The net value of each monitored *m/z* was obtained by subtracting the signal of *m/z* = 220, at which no isotope is measured, and which reflects the fluctuations in the background signal level. Excel and Origin Professional software were used for processing the data. Peak area measurements of the transient signals were used for quantification.

Table 1  
USN-ICP TOF MS instrumental settings and operating conditions

ICP source settings	
Frequency (MHz)	40.68
Forward power (kW)	1.44
Plasma gas flow rate (l min <sup>-1</sup> )	14.5
Auxiliary gas flow rate (l min <sup>-1</sup> )	1.4
Carrier gas flow rate (l min <sup>-1</sup> )	0.75
Mass spectrometer, V	
Flight tube	-1490
Reflectron low	200
Reflectron high	1550
X steering	-1480
Y steering	-1650
Einzel lens 1	-910
Einzel lens 2	-1070
Ion lens 1	-772
Ion lens 2	-913
Detector	-2400
Data acquisition parameters	
Scanning mode	Peak transient
Integration time (ms)	500
Detecting mode	Counting, analog
Ultrasonic nebulizer parameters	
Heater temperature (°C)	140
Cooler temperature (°C)	3
Membrane desolvator parameters	
Heater temperature (°C)	160
Sweep gas flow rate (l min <sup>-1</sup> )	2.1

On-line separation and preconcentration was performed with a Perkin-Elmer Model FIAS-400 accessory equipped with a Perkin-Elmer 2 × 4 channel, 16-port double layer rotary injector valve and controlled by a separate computer using Perkin-Elmer AA Winlab software. The scheme of the FI manifold used through this work is presented in Fig. 1. A knotted reactor of 200 cm length made of PTFE tubing (0.5 mm i.d.) was used for the collection of the complexes formed with the analytes under investigation. Eluent loops of 100, 200, 250 and 300 μl were made of PTFE tubing of 0.5 mm i.d. The connections and conduits were made of PTFE tubing of 0.35 mm i.d. Ismaprene pump tubes (Ismatec, Wertheim, Germany) were employed to

Table 2  
Selected isotopes, their relative abundance and main potential interferences

Isotope	Relative abundance (%)	Interferent (relative abundance (%)) <sup>a</sup>
<sup>59</sup> Co	100	<sup>40</sup> Ar <sup>18</sup> O <sup>1</sup> H <sup>+</sup> (0.20), <sup>40</sup> Ca <sup>18</sup> O <sup>1</sup> H <sup>+</sup> (0.13)
<sup>58</sup> Ni	68.27	<sup>40</sup> Ar <sup>18</sup> O <sup>+</sup> (0.20), <sup>40</sup> Ca <sup>18</sup> O <sup>+</sup> (0.84), <sup>58</sup> Fe <sup>+</sup> (0.28), <sup>116</sup> Cd <sup>2+</sup> (7.58)
<sup>60</sup> Ni	26.10	<sup>44</sup> Ca <sup>16</sup> O <sup>+</sup> (2.08)
<sup>89</sup> Y	100	–
<sup>107</sup> Ag	51.84	<sup>67</sup> Zn <sup>40</sup> Ar <sup>+</sup> (4.10)
<sup>109</sup> Ag	48.16	–
<sup>114</sup> Cd	28.73	<sup>114</sup> Sn <sup>+</sup> (0.65), <sup>98</sup> Mo <sup>16</sup> O <sup>+</sup> (24.11)
<sup>111</sup> Cd	12.80	<sup>95</sup> Mo <sup>16</sup> O <sup>+</sup> (15.89)
<sup>208</sup> Pb	52.40	–
<sup>238</sup> U	99.27	–

<sup>a</sup> Data from Renaissance ICP TOF MS software.



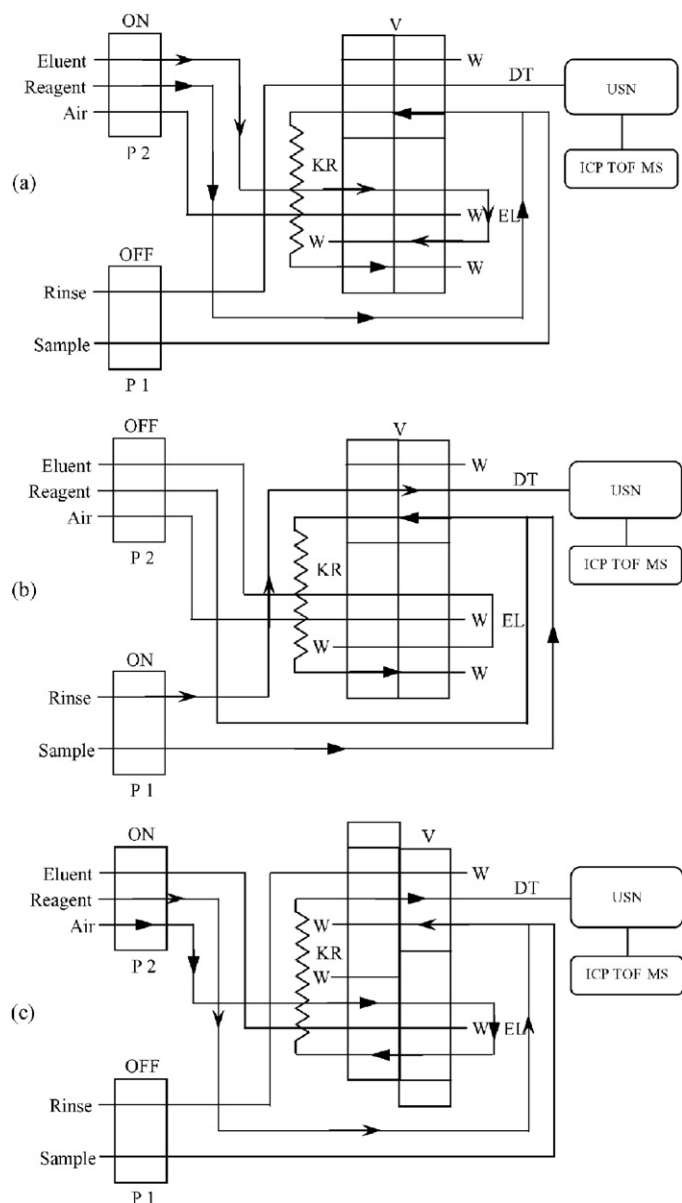


Fig. 1. FI on-line preconcentration manifold: P1 and P2, peristaltic pumps; V, valve; KR, knotted reactor; EL, eluent loop; W, waste; USN, ultrasonic nebulizer–membrane desolvator interface; DT, delivery tube: (a) KR coating/KR washing; (b) complexation; (c) elution.

propel the sample, reagent, eluent, air and rinse solution. A 40 cm PTFE delivery tube was used to connect the FI system with the USN interface.

## 2.2. Reagents

All reagents used were of the highest available purity. Doubly de-ionized water (18.2 M $\Omega$  cm) obtained from a Milli-Q water system (Millipore, Bedford, MA, USA) was used throughout. Nitric acid (65%), ammonia (25%) and acetic acid (96%) were all Suprapur from Merck (Darmstadt, Germany). The chelating reagent PMBP was purchased from Fluka (Buchs, Switzerland). A 0.05% (m/v) PMBP solution was daily prepared by dissolving a weighed portion of the reagent in a minimum amount of

aqueous ammonia, diluting with Milli-Q water and adjusting the pH of the solution to 9 with dilute nitric acid.

The mass calibration stock solution containing Li, Mg, Sc, Co, Y, In, Ce, Ba, Pb, Bi and U at 1000 mg l<sup>-1</sup> was obtained from Z-TEK (Amsterdam, The Netherlands). A diluted mass calibration solution (5  $\mu$ g l<sup>-1</sup> in 1% (v/v) HNO<sub>3</sub>) was used for the daily optimization of the ICP TOF MS parameters. A multi-element stock solution containing 10 mg l<sup>-1</sup> of Ag, Cd, Co, Ni, Pb, U and Y in 1% (v/v) HNO<sub>3</sub> was prepared from single stock solutions of the elements (Z-TEK). The working standard solutions were prepared daily by dilution of the multi-element stock solution with 0.01 mol l<sup>-1</sup> ammonium acetate buffer of pH 5.6. The eluent was 1% (v/v) HNO<sub>3</sub> containing 0.3  $\mu$ g l<sup>-1</sup> of Rh as an internal standard.

Two certified reference materials, synthetic fresh water (SRM 1643d) from the National Institute of Standards and Technology, USA (NIST) and river water (SLRS-4) from the National Research Council of Canada (NRCC), were analyzed. Sample pretreatment was restricted to dilution and pH adjustment by buffer addition. A blank sample based on doubly de-ionized water was prepared in the same way.

## 2.3. FI on-line separation and preconcentration procedure

The fully automated FI manifold is described in detail elsewhere [12]. The operation sequence of the FI on-line KR preconcentration procedure is given in Table 3. A pre-fill stage is only used when a new sample is introduced in order to flush the sample line. During the first step – KR coating (Fig. 1a) – the reagent is sorbed on the inner walls of the KR. In step 2 (Fig. 1b), the sample solution is directed to the KR where the analyte complexes with the immobilized reagent are formed; simultaneously, a 0.5% (v/v) NH<sub>4</sub>OH solution enters the ICP MS system to rinse the nebulizer and the sampling cone. The third step – KR washing – is shown in Fig. 1a. The washing solution is sucked through the KR to remove the residual matrix and then is discharged to the waste. During the same step, the eluent loop is filled with the eluent. In the last step (Fig. 1c), the analyte complexes are eluted with 250  $\mu$ l of 1% (v/v) HNO<sub>3</sub>, containing 0.3  $\mu$ g l<sup>-1</sup> of Rh and after nebulization and solvent elimination in the USN, are introduced into the ICP MS.

## 2.4. Optimization of the ICP TOF MS

The instrumental settings, summarized in Table 1, underwent slight everyday modifications. After the plasma ignition and prior to the optimization, it was important to ensure that argon and oxygen species are deflected to avoid detector overload. A 5  $\mu$ g l<sup>-1</sup> mass calibration solution was used for optimization of the instrumental settings by maximizing the signal intensity of <sup>115</sup>In. The optimization started with adjustment of the torch position by changing the X and Y positions and the carrier gas flow. The potentials on ion lenses 1 and 2, Einzel lenses 1 and 2 were also optimized. For optimal resolution, <sup>208</sup>Pb and <sup>209</sup>Bi should be observed as separate peaks. The reflectron settings were adjusted in a way to obtain symmetrical peaks with no tail-

Table 3

Operating sequence of the FI on-line KR separation and preconcentration system coupled with ICP TOF MS

Step	Function	Pumped medium	Pump active	Valve position	Flow rate (ml min <sup>-1</sup> )	Time (s)
1	KR coating	Reagent	2	Fill	4.5	30
2	Complexation, rinsing of USN and cones	Sample, rinse solution	1	Fill	4.5	90
3	KR washing, EL filling	Reagent, eluent	2	Fill	3.4	60
4	Elution	Air	2	Inject	1.0	70

ing or fronting. Mass calibration was following all optimization events prior to data collection.

### 3. Results and discussion

#### 3.1. Optimization of the FI on-line KR preconcentration/separation

With a view to eliminating most of the interferences shown in Table 2 and obtaining reliable analytical results for the trace element content in natural waters, a FI on-line KR separation and preconcentration system was coupled to the ICP TOF MS. The efficiency of the preconcentration/separation process is critically dependent on numerous variables which need to be carefully optimized. In the present work the chemical (pH, reagent concentration, nature of the eluent) and flow injection (flow rate and time) variables were separately optimized for all steps of the preconcentration process: KR coating, analyte complexation, KR washing and elution.

To find the optimum conditions for the simultaneous preconcentration of Ag, Cd, Co, Ni, Pb, U and Y, the effect of pH on the analytical signal of a 0.2 μg l<sup>-1</sup> multi-element standard solution was studied. A preliminary investigation was carried out in the pH range 1–9, followed by a more precise optimization in the pH range 4–7 (Fig. 2). As can be seen, the signals of Ag, Cd, Co and Ni gradually increase in the examined pH range, while those of Pb, Y and U decrease at pH values above 5.8. As the aim of this work was the simultaneous preconcentration of Ag, Cd, Co, Ni, Pb, U and Y, the complexation was performed at a compromise pH of 5.6, maintained by means of 0.01 mol l<sup>-1</sup> ammonium acetate buffer. Under these conditions, the alkali and alkaline earth metals do not form complexes with PMBP [18].

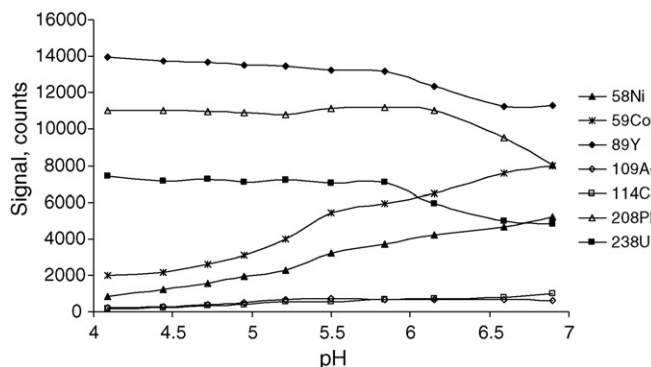


Fig. 2. Effect of pH of the sample solution on the signal intensity of a 0.2 μg l<sup>-1</sup> multi-element standard.

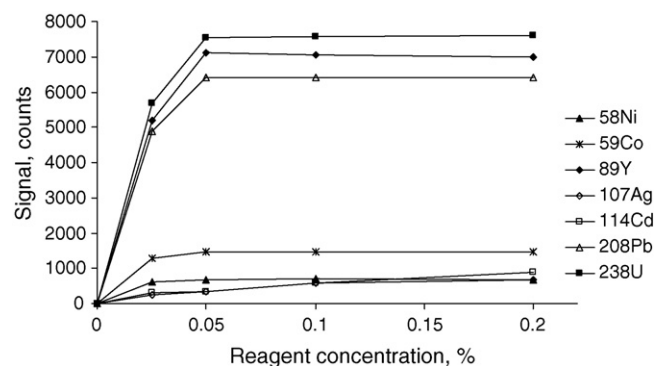


Fig. 3. Effect of reagent concentration on the signal intensity of a 0.2 μg l<sup>-1</sup> multi-element standard.

The effect of the acidity of the reagent solution used for KR coating on the signal of the analytes was studied over a wide pH range. For all analytes, the maximum intensities were registered with a reagent solution of pH 8.7–9.3. Consequently, the chelating reagent was kept at pH 9 for the rest of the work.

The effect of the reagent concentration was investigated between 0 and 0.2% (m/v). No elements were preconcentrated in the KR without PMBP pre-coating. As Fig. 3 shows, there is no significant increase in the analyte signals in the range 0.05–0.2% (m/v) PMBP. Owing to the relatively high blanks observed with the higher reagent concentrations, 0.05% PMBP was used in further work.

An almost linear increase in the analyte signals upon increasing the sample flow rate from 2.3 to 4.5 ml min<sup>-1</sup> was observed. A similar effect was registered upon increasing the flow rate of the reagent solution in the same range during KR coating. Consequently, 4.5 ml min<sup>-1</sup> flow rates of the sample and reagent solutions were adopted in further work.

The increase in the KR coating time from 30 to 90 s caused a slight increase only in the signals of U, Y and Pb while 30 s of coating were sufficient for the other analytes. A longer coating time has two drawbacks: (i) it increases the total duration of the FI procedure and (ii) it leads to higher blank signals. Therefore, 30 s of coating time were further used. Fig. 4 shows the effect of the sample loading time on the signal for 0.2 μg l<sup>-1</sup> of each analyte. There is a linear increase in the signals of Pb, U and Y as a function of the loading (complexation) time up to 90 s, but an insignificant change in the signals of Ag, Cd, Co and Ni for loading times longer than 30 s. The behavior of Ag, Cd, Co and Ni could be explained with the assumption that the chelate active sites of the immobilized PMBP are saturated after 30 s of loading time. The prolonged sorption of Pb, U and Y up to 90 s could be attributed to the possibility of their bonding to the

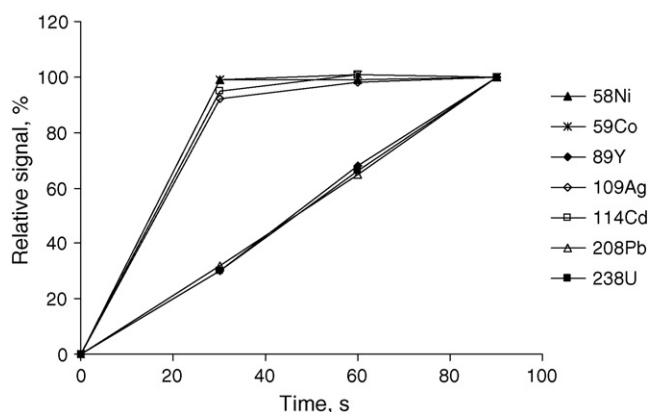


Fig. 4. Effect of loading time on the relative signal of a  $0.2 \mu\text{g l}^{-1}$  multi-element standard.

nitrogen atoms of the pyrazole ring of PMBP [27] which act as additional specific active sites. Ninety seconds were considered as the optimum loading time.

### 3.2. KR washing

The effect of KR washing on the efficiency of the overall pre-concentration process has been discussed in details elsewhere [28]. The removal of the non-complexed constituents of the matrix and any weakly bound concomitant elements aims at avoiding clogging of the interface and the sampling cone of ICP MS and minimizing matrix interferences. With the present FI scheme, it is only possible to use the reagent solution as a washing solution [12]. The flow rate and time of the washing step were optimized in the ranges  $1.7\text{--}3.4 \text{ ml min}^{-1}$  and  $0\text{--}90 \text{ s}$ , respectively. The washing flow rate did not affect the analyte signals; therefore, the washing step was performed with the maximum flow rate of  $3.4 \text{ ml min}^{-1}$ . As Fig. 5 shows, the signals of Pb, U and Y decrease with washing times above  $20\text{--}30 \text{ s}$ . This may be related to the fact that during the washing step, the slightly alkaline PMBP solution shifts the pH of the medium to a higher value, less favorable for the complexation of Pb, U and Y (cf. Fig. 2). Since washing for short time did not efficiently remove

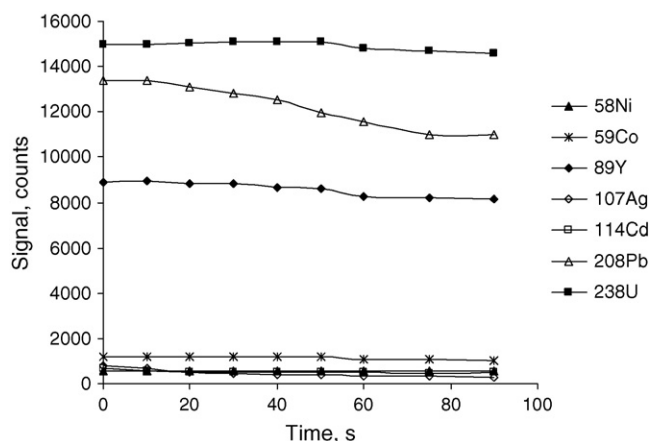


Fig. 5. Effect of the time of KR washing on the signal intensity of a  $0.2 \mu\text{g l}^{-1}$  multi-element standard.

the matrix components in the real samples,  $60 \text{ s}$  duration of the washing step was chosen.

### 3.3. Elution

For desorption of the analyte–PMBP complexes from the KR walls and their transportation to the detection system, several media were investigated— $\text{HNO}_3$ ,  $\text{NH}_4\text{OH}$ ,  $\text{MeOH}$  and acidified  $\text{MeOH}$ . The  $1\% \text{ HNO}_3$  showed the best elution characteristics. The eluent volume needed for the quantitative desorption of the complexes was determined by varying the eluent loop from  $100$  to  $300 \mu\text{l}$ . An eluent volume of  $250 \mu\text{l}$  was found to be sufficient for quantitative stripping of the analyte complexes from the  $200 \text{ cm}$  KR and their transportation to the plasma. The effect of elution flow rate was studied in the range  $0.8\text{--}2.2 \text{ ml min}^{-1}$ . Maximum sensitivity was registered at flow rates  $0.8\text{--}1.0 \text{ ml min}^{-1}$ . At higher elution flow rates lower peaks were observed. This could be attributed to both lower elution efficiency and reduced nebulization efficiency. Therefore, the elution flow rate was kept at  $1.0 \text{ ml min}^{-1}$ .

### 3.4. Analytical performance of the FI on-line KR pre-concentration/separation-ICP TOF MS system

The most important figures of merit of the FI on-line KR sorption/pre-concentration-ICP TOF MS determination of Ag, Cd, Co, Ni, Pb, U and Y are summarized in Table 4.

The calibration graphs were linear up to  $0.5 \mu\text{g l}^{-1}$  for Ag, Cd, Co and Ni and up to  $0.2 \mu\text{g l}^{-1}$  for Pb, U and Y. This is certainly not as large a dynamic range as expected when using ICP TOF MS. The limitation is imposed by the capacity of the KR, particularly when a large number of analytes are simultaneously pre-concentrated under FI conditions [18].

The enhancement factors were evaluated as the ratio between the analyte signal intensity after pre-concentration and that obtained by direct nebulization of  $250 \mu\text{l}$  of an aqueous multi-element standard solution. Enhancement factors from 3 to 14 were achieved at a loading time of  $90 \text{ s}$  and a sample loading rate of  $4.5 \text{ ml min}^{-1}$ . The low enhancement factors for Ag, Cd, Co and Ni may be attributed to the saturation of the chelate active sites of PMBP within  $30 \text{ s}$  of loading time, as discussed above (Fig. 4).

The detection limits (DLs) of the analytes were calculated on the basis of three times the standard deviation for nine replicate determinations of the blank. Irrespectively of the lower enhancement factors for Ag, Cd, Ni and Pb in comparison with those in a similar KR on-line pre-concentration-ICP TOF MS system using APDC [12], lower DLs of these analytes were obtained in the present work. As shown in Table 4, the precision of the method is better than  $4\% \text{ R.S.D.}$

The accuracy of the determination of Ag, Cd, Co, Ni, Pb, U and Y in natural waters after their FI on-line separation/pre-concentration in a KR was checked by analysis of two water certified reference materials prepared as described in Section 2 and analyzed under the conditions given in Tables 1 and 3. As Table 5 shows, the results obtained by the developed procedure agree well with the certified values or those reported in the

Table 4

Performance of the FI on-line KR separation and preconcentration-ICP TOF MS system for the determination of trace elements under the optimized conditions

Analyte	Enhancement factor (EF) <sup>a</sup>	Detection limit (DL) (ng l <sup>-1</sup> ) <sup>b</sup>	Precision (R.S.D.) (%) <sup>c</sup>	Correlation coefficient
Ag	3	0.6	2.1	0.9999
Cd	3	1.1	1.0	0.9999
Co	3	7.9	2.3	0.9997
Ni	3	15.2	2.9	0.9999
Pb	10	4.5	1.6	0.9996
U	10	0.4	3.7	0.9996
Y	14	0.3	2.5	0.9996

<sup>a</sup> Compared with the direct nebulization of 250 µl of an aqueous multi-element standard.<sup>b</sup> Based on 3σ of nine replicate determinations of the blank.<sup>c</sup> Calculated for nine replicate determinations of a 0.2 µg l<sup>-1</sup> (Ag, Cd, Co and Ni) and 0.04 µg l<sup>-1</sup> (Pb, U and Y) multi-element standard.

Table 5

Results (mean ± σ, n = 5) of the analysis of certified reference materials—NIST 1643d (synthetic fresh water) and SLRS-4 (river water)

Element	NIST 1643d		SLRS-4	
	Found (µg l <sup>-1</sup> )	Certified (µg l <sup>-1</sup> )	Found (µg l <sup>-1</sup> )	Certified (µg l <sup>-1</sup> )
Ag	1.28 ± 0.05	1.270 ± 0.057 1.23 ± 0.06 <sup>a</sup>	0.039 ± 0.007	0.035 ± 0.005 <sup>b</sup>
Cd	6.56 ± 0.36	6.47 ± 0.37 7.15 ± 0.41 <sup>a</sup>	0.011 ± 0.004	0.012 ± 0.002
Co	25.69 ± 1.26	25.00 ± 0.59 26.1 ± 1.3 <sup>a</sup>	0.035 ± 0.009	0.033 ± 0.006
Ni	56.81 ± 2.84	58.1 ± 2.7 56.3 ± 3.2 <sup>a</sup>	0.62 ± 0.12	0.67 ± 0.08
Pb	18.58 ± 0.58	18.15 ± 0.64 19.2 ± 1.1 <sup>a</sup>	0.093 ± 0.016	0.086 ± 0.007
U	0.03 ± 0.01	0.032 ± 0.017 <sup>c</sup>	0.049 ± 0.008	0.050 ± 0.003
Y	0.008 ± 0.002	0.0077 ± 0.002 <sup>c</sup>	0.151 ± 0.011	0.146 ± 0.008 <sup>b</sup>

<sup>a</sup> Data from Ref. [12].<sup>b</sup> Data from Ref. [30].<sup>c</sup> Data from Ref. [29].

literature, which points to the lack of matrix interferences on both the FI separation/preconcentration and the ICP TOF MS detection of the analyte elements. This is an evidence for the accuracy of the developed method for the determination of trace levels of Ag, Cd, Co, Ni, Pb, U and Y in natural water samples.

### Acknowledgement

B. Dimitrova-Koleva thanks the European Commission for a Marie Curie Training Site fellowship (EC-HPMT-CT-2001-00310).

### References

- [1] Q. Zhang, H. Minami, S. Inoue, I. Atsuya, *Anal. Chim. Acta* 508 (2004) 99.
- [2] G.J. Batterham, N.C. Munksgaard, D.L. Parry, *J. Anal. At. Spectrom.* 12 (1997) 1277.
- [3] K. Ndungu, R.P. Franks, K.W. Bruland, A.R. Flegal, *Anal. Chim. Acta* 481 (2003) 127.
- [4] M.L. Wells, K.W. Bruland, *Mar. Chem.* 63 (1998) 145.
- [5] A.R. Turker, S. Baytak, *Anal. Sci.* 20 (2004) 329.
- [6] S.C. Nielsen, E.H. Hansen, *Anal. Chim. Acta* 422 (2000) 47.
- [7] H.H. Chen, D. Beauchemin, *J. Anal. At. Spectrom.* 16 (2001) 1356.
- [8] M.S. Jimenez, R. Velarte, J.R. Castillo, *Spectrochim. Acta Part B* 57 (2002) 391.
- [9] H. Karami, M.F. Mousavi, Y. Yamini, M. Shamsipur, *Anal. Chim. Acta* 509 (2004) 89.
- [10] Z. Fang, M. Sperling, B. Welz, *J. Anal. At. Spectrom.* 6 (1991) 301.
- [11] E. Ivanova, K. Benkhedda, F. Adams, *J. Anal. At. Spectrom.* 13 (1998) 527.
- [12] K. Benkhedda, H.G. Infante, E. Ivanova, F.C. Adams, *J. Anal. At. Spectrom.* 15 (2000) 1349.
- [13] F.A.M. Silva, C.L. Porto da Silveira, N. Miekeley, I.L. Kuechler, *Anal. Sci.* 20 (2004) 1295.
- [14] J.A. Salonia, R.G. Wuilloud, J.A. Gasquez, R.A. Olsina, L.D. Martinez, *J. Anal. At. Spectrom.* 14 (1999) 1239.
- [15] S. Cerutti, J.A. Salonia, J.A. Gasquez, R.A. Olsina, L.D. Martinez, *J. Anal. At. Spectrom.* 18 (2003) 1198.
- [16] K. Benkhedda, B. Dimitrova, H.G. Infante, E. Ivanova, F.C. Adams, *J. Anal. At. Spectrom.* 18 (2003) 1019.
- [17] K. Benkhedda, E. Ivanova, F. Adams, *J. Anal. At. Spectrom.* 14 (1999) 957.
- [18] K. Benkhedda, H.G. Infante, E. Ivanova, F.C. Adams, *J. Anal. At. Spectrom.* 16 (2001) 995.
- [19] D.P. Myers, G.M. Hieftje, *Microchem. J.* 48 (1993) 259.
- [20] D.M. McClenathan, S.J. Ray, G.M. Hieftje, *J. Anal. At. Spectrom.* 16 (2001) 987.
- [21] S.N. Willie, R.E. Sturgeon, *Spectrochim. Acta Part B* 56 (2001) 1707.

- [22] P. Jitaru, H.G. Infante, F.C. Adams, *Anal. Chim. Acta* 489 (2003) 45.
- [23] A.M. Leach, M. Heisterkamp, F.C. Adams, G.M. Hieftje, *J. Anal. At. Spectrom.* 15 (2000) 151.
- [24] C.N. Ferrarello, M.M. Bayon, R.F. de la Campa, A. Sanz-Medel, *J. Anal. At. Spectrom.* 15 (2000) 1558.
- [25] A.M. Leach, G.M. Hieftje, *J. Anal. At. Spectrom.* 17 (2002) 852.
- [26] N.H. Bings, *J. Anal. At. Spectrom.* 17 (2002) 759.
- [27] E. Ivanova, O. Todorova, M. Stoimenova, *Fresenius J. Anal. Chem.* 344 (1992) 316.
- [28] E. Ivanova, F. Adams, *Fresenius J. Anal. Chem.* 361 (1998) 445.
- [29] D.B. Peart, R.C. Antweiler, H.E. Taylor, D.A. Roth, T.I. Brinton, *Analyst* 123 (1998) 455.
- [30] D. Yeghicheyan, J. Carignan, M. Valladon, M. Bouhnik Le Coz, F. Le Cornec, M. Castrec-Rouelle, M. Robert, L. Aquilina, E. Aubry, C. Churlaud, A. Dia. Deberdt, B. Dupre, R. Freydier, G. Gruau, O. Henin, A.-M. de Kersabiec, J. Mace, L. Marin, N. Morin, P. Petitjean, E. Serrat, *Geostand. Newslett.* 25 (2001) 465.



# Synthesis of a liposome incorporated 1-carboxyalkylxanthine-phospholipid conjugate and its recognition by an RNA aptamer

Katie A. Edwards, Antje J. Baeumner\*

*Department of Biological and Environmental Engineering, Cornell University, Ithaca, NY 14853, United States*

Received 31 January 2006; received in revised form 7 April 2006; accepted 7 April 2006

Available online 7 July 2006

## Abstract

RNA or DNA aptamers have received much attention in recent literature as therapeutic agents and chromatographic matrices, however, their use in analytical methodologies is relatively unexplored. We describe here investigations aiming to combine this promising technology with versatile liposomes in a competitive assay format. Thus, a phospholipid derivative of an unsymmetrical 1,3-disubstituted xanthine (1-carboxyethyl-3-methylxanthine-DPPE) was prepared for incorporation into the lipid bilayers of dye-encapsulating liposomes. Its synthesis and characterization using GC-MS, <sup>1</sup>H NMR, and HPLC are described. Equilibrium filtration experiments using enzyme linked immunosorbent assays (ELISAs) were completed to assess the affinity for theophylline of an unmodified RNA aptamer and one that had been modified on the 3' end with biotin. A dissociation constant ( $K_d$ ) for theophylline with the unmodified RNA aptamer of 0.9  $\mu$ M and biotinylated aptamer of 1.0  $\mu$ M was determined which showed that this modification did not affect the aptamer's affinity using this technique. The observed  $K_d$  values correlated with the previously reported value of 0.6  $\mu$ M. Experiments were also carried out in a competitive manner with the prepared 1-carboxypropyl-3-methylxanthine intermediate, and the final 1-carboxypropyl-3-methylxanthine-DPPE conjugate once it had been incorporated into the bilayers of liposomes. The  $K_d$  value for 1-carboxypropyl-3-methylxanthine was approximately 2.7  $\mu$ M. Finally, successful binding to theophylline-analog-tagged liposomes in a competitive assay format was shown versus liposomes prepared without the tag.

© 2006 Elsevier B.V. All rights reserved.

**Keywords:** Aptamer; Liposome; 1-Carboxypropyl-3-methylxanthine-DPPE

## 1. Introduction

Aptamers are single-stranded RNA or DNA oligonucleotides that can bind a variety of non-nucleic acid targets, ranging from ions such as  $Zn^{2+}$  [1], small molecules such as ATP [2,3], and proteins such as thrombin [4]. To date, they have been investigated for many purposes, including inhibitors for certain enzymes for therapeutic purposes, as biorecognition elements in biosensors, and as packing materials for affinity-chromatography type applications [5–7]. They are produced from random oligonucleotide pools by the in vitro selection process systematic evolution of ligands by exponential enrichment (SELEX), which has recently been reviewed elsewhere [8,9].

Briefly, the SELEX process is accomplished by passing a random pool of oligonucleotides through a column packed with a suitable material to which is conjugated the analyte of interest. Oligonucleotides which do not have affinity for the support are removed by washing, then the column is washed with a solution of the free analyte. Those sequences which elute with the free analyte are then reverse transcribed to form DNA, amplified exponentially using a reverse transcriptase polymerase chain reaction (RT-PCR), then transcribed back into RNA resulting in a large pool of potentially binding aptamers. This pool is applied to the column and the cycle is repeated. With successive cycles, the final pool of oligonucleotides rinsed from the column is less diverse and a higher proportion of binding aptamers is present than the previous run. Further specificity is conferred through washing column-bound oligonucleotides with structural analogs of the target molecule in a process known as 'counter-SELEX'.

A common detection format in bioanalytical chemistry is the competitive assay where analyte molecules compete with the analyte conjugated to a tag for a limited number

*Abbreviations:* BSTFA, bis(trimethylsilyl)trifluoroacetamide; DPPC, dipalmitoyl phosphatidylcholine; DPPG, dipalmitoyl phosphatidylglycerol; sodium salt; TMB, 3,3',5,5'-tetramethylbenzidine

\* Corresponding author. Tel.: +1 607 255 5433; fax: +1 607 255 4080.

E-mail address: [ajb23@cornell.edu](mailto:ajb23@cornell.edu) (A.J. Baeumner).

of biorecognition element binding sites. The biorecognition element which captures the unlabeled or native analyte is typically composed of antibodies. DNA oligonucleotides which relied on Watson–Crick pairing yielding hybridization to target molecules have also been successfully used in this manner [10]. Aptamers hold great promise as a biorecognition element in affinity-based biosensors substituting antibodies and receptors for the specific recognition of target analytes. Since aptamers have the potential of rational design and can be generated using a chemical process rather than a complex biological system such as cell culture or whole animals, their use in bioanalytical systems has been of interest in recent years [11,12]. They can confer exquisite target specificity, give improved resistance to denaturation and degradation versus antibodies, and provide recognition towards non-immunogenic or toxic compounds. These factors have contributed to their employment as biorecognition elements in a variety of assay formats found in recent literature [13–16]. However, few studies have utilized aptamers as biorecognition elements in competitive binding assays [17]. In such assays, after a separation step to remove unbound materials, the remaining tagged conjugate is used to generate a signal indirectly proportional to the concentration of analyte originally in the sample. While enzymes are most commonly used for this purpose [18–21], a variety of other tags have been used as well, including fluorophores [22,23], bioluminescent photoproteins [24], nanoparticles [25], and liposomes [26,27]. Some of these signaling means are considered in more detail in several recent review articles [28,29]. While enzymes can provide a low limit of detection, one advantage to non-enzymatic tags is the reduction in time required for signal generation. As an alternative, liposomes can encapsulate hundreds of thousands of small signaling molecules and also can provide instantaneous signal generation [30,31]. As such, they have been employed in a variety of assay formats, as summarized in several review articles [32–34].

We describe here investigations towards combining an RNA aptamer as a biorecognition element with small-molecule-tagged liposomes in a competitive assay format. A theophylline–RNA aptamer was chosen as a model biorecognition element since it had been previously reported and well characterized [35–37]. It was developed against the 1-carboxypropyl analog of theophylline and immobilized onto a solid support through an amide linkage [37]. By conjugation through the 1-position of theophylline, the structural features that distinguished theophylline from other common xanthine derivatives remained available for interaction with the aptamer. As a consequence of the analog chosen and SELEX process modifications, the resulting aptamer showed exceptional specificity towards theophylline over other xanthine derivatives [37]. Theophylline is of clinical importance as a bronchodilator, but has a narrow therapeutic index. Thus, methods to monitor its concentration are necessary to ensure a therapeutic effect and to avoid toxic side effects.

In this work, the synthesis of a 3-methylxanthine-lipid conjugate and its incorporation into the bilayer of dye-encapsulating liposomes is described (see Fig. 1). The affinity of both an unmodified and 3'-biotinylated RNA aptamer for theophylline

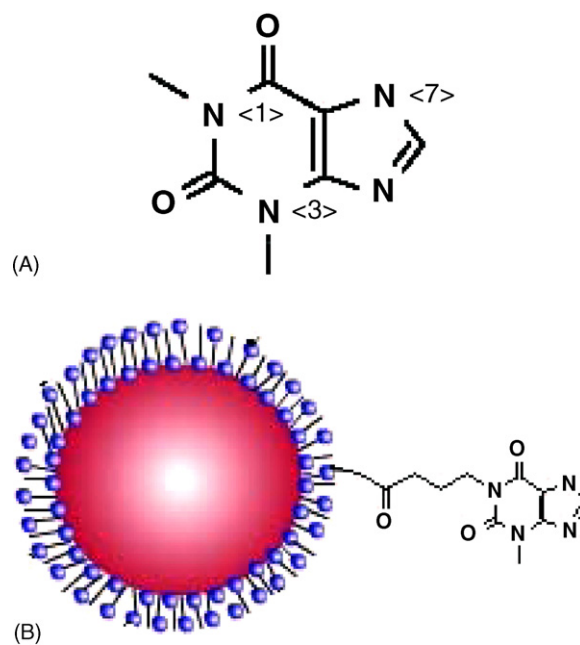


Fig. 1. (A) Theophylline. (B) Representation of 1-carboxypropyl-3-methylxanthine-tagged liposome (not to scale).

was assessed by the equilibrium filtration method. The affinity of the unmodified aptamer for the 1-carboxypropyl-3-methylxanthine intermediate was investigated in a competitive format. Lastly, the 1-carboxyethyl-3-methylxanthine lipid conjugate-tagged liposomes were then compared to untagged liposomes for their ability to compete for unmodified aptamer.

## 2. Materials and methods

Reagent grade chemicals were purchased from Sigma Chemical Company and were used as received. All reactions were carried out under nitrogen. The lipids, dipalmitoylphosphatidylethanolamine (DPPE), dipalmitoylphosphatidylcholine (DPPC) and dipalmitoylphosphatidylglycerol (DPPG) and the extrusion membranes were purchased from Avanti Polar Lipids (Alabaster, AL). Streptavidin and sulforhodamine B (SRB) were purchased from Molecular Probes Inc. (Eugene, OR). All other reagents used in these experiments were purchased from VWR (Bridgeport, NJ). The 42-mer RNA aptamer (5'-AAgUgCUACCAgCAUCgUCUUGAUgCCCUUggCAGCACUUCA-3') was purchased from Dharmacon Research (LaFayette, CO). A 3'-biotinylated RNA sequence was acquired from the same source. A DNA oligonucleotide of the same sequence was synthesized by the BioResource Center, Cornell University (Ithaca, NY). RNase free reagents for use with the aptamer were purchased from Ambion (Austin, TX). The aptamer was diluted with 100 mM HEPES, 50 mM NaCl, 5 mM MgCl<sub>2</sub> to a concentration of 100 pmol/μL. Theophylline ELISA kits were purchased from Neogen (Lexington, KY). HPLC analysis was run on an HP 1100 using a Phenomenex Aqua column, C18, 125 μm, 4.6 × 250 mm with UV detection at 220 nm. At a flow rate of 1 mL/min., the HPLC method used 100% water for the first 5 min, a gradient to 50% acetonitrile ending at 15 min,

isocratic 50% acetonitrile/water until 24 min, a second gradient to 10% water ending at 30 min, followed by isocratic elution at 10% water, 90% acetonitrile for the remaining 15 min. GC–MS analysis was performed on an Agilent 6890 GC equipped with an HP-5MS column, 30 m × 250 μm × 0.25 μm, and model 5973 mass selective detector. Samples were derivatized with either acetic anhydride or 10:1 (v/v) 10:1 bis(trimethylsilyl)trifluoro-acetamide:trimethylsilyl chloride (BSTFA:TMS-Cl) [38] for 15 min at 60 °C in anhydrous acetonitrile prior to GC–MS analysis. <sup>1</sup>H NMR data was obtained using a Varian Inova 400 MHz spectrometer. The liposome size distribution was determined by dynamic light scattering using a DynaPro LSR (Proterion Corporation, Piscataway, NJ).

## 2.1. Synthesis of the 1-carboxyalkyl-3-methylxanthine-lipid conjugate

The chemical structures of all synthesis intermediates are shown in Scheme 1 and their numbers indicated in parentheses here.

### 2.1.1. 3-Methyl-7-[(pivaloyloxy)methyl]xanthine (2)

3-Methylxanthine (1) (0.3 g, 18.1 mmol) was suspended in DMF and heated to 60 °C for 15 min. Sodium carbonate (0.2 g, 19.0 mmol) was then added and the solution was heated to 60 °C for 15 min. Chloromethyl pivalate (0.274 mL, 19.0 mmol) was then added gradually and the mixture was maintained at 60–65 °C for 17 h. The volume of solvent was then reduced under vacuum and the product in residual DMF was carried on to the next step generally without further purification. By HPLC, this reaction typically formed 76% of the desired 7-POM-3-methylxanthine (2, Ret. time = 18.03 min) and ~8% of the undesired 1,7-diPOM-3-methylxanthine (7, Ret. time = 30.79 min, TLC, RF<sub>100% EtOAc</sub> = 0.61) TLC (100% EtOAc) RF = 0.43, <sup>1</sup>H NMR (DMSO-*d*<sub>6</sub>) δ 1.07 ppm (s, 9H), 3.35 ppm (s, 3H), 6.09 ppm (s, 2H), 8.18 (s, 1H). GC–MS, *m/z* 280 [M<sup>+</sup>], 166 [M<sup>+</sup> – C<sub>6</sub>H<sub>11</sub>O<sub>2</sub>].

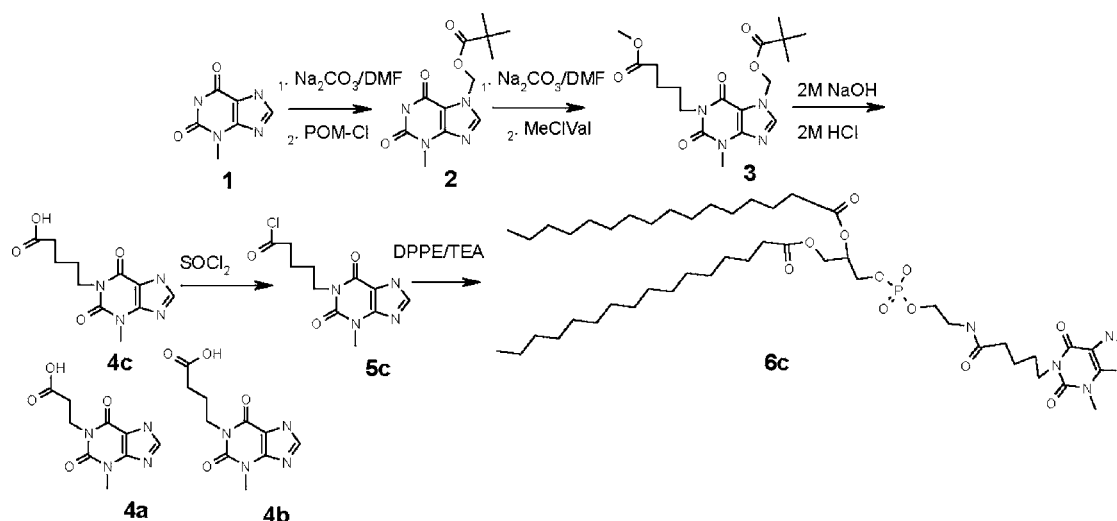
### 2.1.2. 3-Methyl-7-[(pivaloyloxy)methyl]-1-butylxanthine (3)

To the slurry of 2 in DMF was charged 0.4 g Na<sub>2</sub>CO<sub>3</sub>. This mixture was then heated to 60 °C for 15 min. Methyl 5-chlorovalerate (0.52 mL, 3.62 mmol) in DMF was then added dropwise and the reaction was maintained at 65 °C for 24 h. The resulting slurry was then filtered and ethyl acetate was used to wash the filter cake containing primarily inorganic solids. The solvent was removed and the crude oil was purified using silica gel and 100% ethyl acetate. This purification served to remove minor components such as 1,7-diPOM-3-methylxanthine 7, and 1,7-dialkyl-3-methylxanthine 8. The product was obtained as a clear colorless oil in ~70% yield (yield calculated based on input of 1). Other alkylating agents used for this synthesis included methyl-3-bromopropionate and methyl 4-chlorobutyrate yielding of shorter chain 1-substituted versions of 3 (a&b) which were also carried through the remaining steps of this synthesis. Subsequent NMR and GC–MS results refer to alkyl chain length of *n* = 4.

HPLC Ret. times: 3a = 22.00 min, 3b = 22.74 min, 3c = 24.70 min. TLC (100% EtOAc) 3a RF = 0.42, 3b RF = 0.5, 3c RF = 0.54, <sup>1</sup>H NMR (CDCl<sub>3</sub>) δ 1.02 ppm (s, 9H), 1.6 ppm (m, 4H), 2.22 ppm (t, 2H), 3.45 ppm (s, 3H), 3.55 ppm (s, 3H), 3.84 ppm (t, 2H), 6.08 ppm (s, 2H), 7.75 (s, 1H). GC–MS, *m/z* 394 [M<sup>+</sup>]. <sup>1</sup>H data are similar to published literature values for the 3-carboxypropyl-1-methyl-7-POM-xanthine derivative [43].

### 2.1.3. 1-Carboxylbutyl-3-methylxanthine (4)

The purified oil 3 (0.39 g) was mixed with 1.5 mL 2 M NaOH at 60 °C for 90 min. The initial mixture was immiscible, but the subsequent formation of a homogeneous solution generally signified reaction completion. The solution was then cooled to 0 °C and 2 M HCl was gradually added until the pH reached 2.0 while the temperature was maintained below 10 °C. White solids precipitated from solution during this addition, which were then filtered and washed with cold water followed by



Scheme 1. Synthetic scheme for the 1-carboxybutyl-3-methylxanthine-DPPE conjugate. Shorter alkyl chain derivatives were prepared using either 3-bromomethylpropionate or 4-chloromethylbutyrate in the conversion of 2 to 3. Representative structures are shown in 4a and 4b.

diethyl ether. The product was obtained in 53% yield. HPLC Ret. times: **4a** = 11.83 min, **4b** = 12.29 min, **4c** = 12.95 min. <sup>1</sup>H NMR (DMSO-*d*<sub>6</sub>) δ 1.45 ppm (m, 2H), 1.55 ppm (m, 2H), 2.25 ppm (t, 2H), 3.42 ppm (s, 3H), 3.85 ppm (t, 2H), 8.02 (s, 1H). GC–MS, *m/z* 483 [M + 3(Si(CH<sub>3</sub>)<sub>3</sub>)], 410 [M + 2(Si(CH<sub>3</sub>)<sub>3</sub>)], 337 [M + Si(CH<sub>3</sub>)<sub>3</sub>], and 265 [M – H<sup>+</sup>].

#### 2.1.4. 1-Carboxyalkyl-3-methylxanthine-DPPE conjugate (**6**)

Compound **4** (0.535 mmol) was diluted with toluene and was stringently maintained under N<sub>2</sub> throughout this reaction. Thionyl chloride (5.35 mmol) was added dropwise to this slurry and the reaction was heated to 80 °C for 1 h to form the acid chloride (**5**). Samples for HPLC, TLC, and GC–MS were quenched into anhydrous methanol to form the methyl ester prior to analysis. The solvent was evaporated and residue reconstituted with CHCl<sub>3</sub>. A yield for this material was not obtained and this solution was used without further purification in the next step.

Triethylamine (3.57 mmol) was added to a solution of DPPE (0.178 mmol) in chloroform at ambient temperature. The solution of **5** in CHCl<sub>3</sub> was transferred to this thin slurry gradually via cannula. Vigorous gas evolution was noted during this addition. Several TLC visualization methods were necessary for monitoring this reaction: UV (254 nm) was used to monitor the depletion of **5** and formation of **6**; ninhydrin was used to monitor the depletion of DPPE; molybdenum blue/H<sub>2</sub>SO<sub>4</sub> was used to visualize remaining DPPE as well as the formation of **6**. The reaction was complete within 30 min. The reaction was concentrated, then chromatographically purified using 100% EtOAc. TLC (100% EtOAc) **6a** RF = 0.35; **6b** RF = 0.43; **6c** RF = 0.5.

#### 2.2. Liposome preparation

DPPC, DPPG, cholesterol, and 1-carboxyethyl-3-methylxanthine-DPPE (40.3:21:51.7:0.452 μmol, respectively) were first dissolved in a solvent mixture containing 3 mL chloroform, 0.5 mL methanol, and 3 mL isopropyl ether and sonicated to ensure homogeneous mixing. A 45 °C solution of dye (2 mL sulforhodamine B, 150 mM, in 0.2 M potassium phosphate, pH 7.4) was added to the lipid mixture while sonicating for a total of 5 min. The mixture was then placed onto the rotary evaporator and the solvent was removed at 45 °C. The mixture was then transiently vortexed preceding and following an additional introduction of 2 mL 45 °C 150 mM SRB. The mixture was then returned to the rotary for 20 min, then was permitted to rotate without vacuum at 45 °C for 30 min before being extruded at 60 °C seven times through 2.0 μm membranes, followed by seven times through 0.4 μm membranes. The liposomes were then passed through a 19.7 × 1.7 cm column packed with Sephadex G-50 at ~4 mL/min. using 1xPBS-sucrose buffer (10 mM potassium phosphate, 150 mM sodium chloride, 0.01% sodium azide at pH 7.0), osmolality adjusted with sucrose (0.28 M) to 75 mmol/kg greater than the sulforhodamine B encapsulant, which was ~600 mmol/kg. The liposome fractions containing high liposome densities were then combined and dialyzed overnight against the sucrose-phosphate-saline buffer. One batch of liposomes was prepared without the

1-carboxyethyl-3-methylxanthine-DPPE tag for use as a control. Liposomes were also prepared with the synthesized longer chain carboxylalkyl (*n* = 3&4) derivatives, but these liposomes included a biotinylated lipid for further assay development and hence are not discussed further in this manuscript. The number of liposomes was estimated by dividing the concentration of SRB by the calculated internal volume based on the experimentally determined diameter. This calculation assumes unilamellarity, that the entrapped concentration of SRB equaled the input concentration, and a bilayer thickness of 4 nm [39,40].

#### 2.3. Equilibrium filtration experiments

##### 2.3.1. Affinity measurements

Aptamer-theophylline binding studies were carried out using modifications of the procedure of equilibrium filtration, as described by Jenison et al. [37]. The aptamer (either unmodified or biotinylated, 0.067–8.0 μM) and theophylline (12 μL, 100 ng/mL), were incubated at 65 °C for 5 min in 100 mM HEPES, 50 mM NaCl, and 5 mM MgCl<sub>2</sub> (total volume 150 μL). This mixture was transferred to the filtration unit of Microcon YM-10 devices following cooling to ambient temperature and centrifuged at 6200 rpm for 9 min. The theophylline concentration in the filtrates was assessed using ELISAs (see below). The data were then plotted against the aptamer concentration for estimating the dissociation constants of the non-biotinylated and the 3'-biotinylated aptamer. Similar experiments were carried out with the DNA aptamer using oligonucleotide concentrations ranging from 0.067 μM to 120 μM. Experiments were run in the absence of the aptamer to determine non-specific binding to the dialysis chamber and membrane and no detectable non-specific binding of theophylline was detected.

##### 2.3.2. Competitive binding: theophylline versus 1-carboxyethyl-3-methylxanthine-tagged liposomes

Twelve microliters of theophylline (100 ng/mL), 6 μL RNA aptamer (100 pmol/μL), 1-carboxyethyl-3-methylxanthine-tagged or control liposomes (0.1–6 μL, volume adjusted to compensate for concentration differences), and sufficient diluent (composed of 100 mM HEPES, 50 mM NaCl, and 5 mM MgCl<sub>2</sub>) to bring the volume to 150 μL were mixed in Eppendorf vials to yield final concentrations of 8 ng/mL theophylline and 4 μM aptamer. The mixtures were heated in a water bath at 65 °C for 5 min, then permitted to cool to room temperature over 5 min. The solutions were then transferred to Microcon YM-10 centrifugal filters and centrifuged for 9 min at 6200 rpm. The volumes of the filtrates were recorded and composition assayed by an ELISA.

##### 2.3.3. Competitive binding: theophylline versus and 1-carboxypropyl-3-methylxanthine

This competitive binding experiment was also run using 1-carboxypropyl-3-methylxanthine that was not coupled to liposomes. Twelve microliters of theophylline (100 ng/mL), 6 μL unmodified RNA aptamer (100 pmol/μL), 1-carboxypropyl-3-methylxanthine (10<sup>-8</sup> M to 10<sup>-2</sup> M), and sufficient diluent to bring the volume to 150 μL were mixed in Eppendorf vials to



yield final concentrations of 8 ng/mL theophylline and 4  $\mu$ M aptamer. The mixtures were heated in a water bath at 65 °C for 5 min, then permitted to cool to room temperature over 5 min. The solutions were then transferred to Microcon YM-10 centrifugal filters and centrifuged for 9 min at 6200 rpm. The volumes of the filtrates were recorded and composition assayed by an ELISA.

Eq. (1) was used to calculate the concentration of analyte that was bound to the recognition element.

$$\% \text{Bound} = 100\% \times \frac{\text{nmol}_{\text{initial}} - \text{nmol}_{\text{unbound}}}{\text{nmol}_{\text{initial}}} \quad (1)$$

#### 2.4. Enzyme linked immunosorbent assays (ELISAs)

The ELISA measurements were performed according to the manufacturer's directions. Twenty microliters of each sample was applied in duplicate to the 96-well ELISA plate. Theophylline standards were run in one of the first, middle, and last columns to ensure that the response to theophylline was equivalent across the plate. One hundred and eighty microliters of a 1:180 dilution of the theophylline-HRP conjugate in ELISA buffer was added to each well. The plate was covered with a polypropylene bag and gently agitated periodically to facilitate mixing during the 1 h incubation at room temperature. The contents of the plate were then discarded and each well was washed with  $3 \times 300 \mu\text{L}$  of a 1:10 ELISA wash buffer:water solution. The plate was gently tapped dry between washes.  $150 \mu\text{L}$  of TMB (3,3',5,5'-tetramethylbenzidine) substrate were then added to each well and the plate was covered then permitted to stand at room temperature for 30 min. Finally,  $50 \mu\text{L}$  of the Red Stop solution was added to each well. The plate was gently agitated to ensure mixing then was read at 650 nm in duplicate on a Spectra Rainbow plate reader using Tecan XREAD Plus software, version 4.11. The cross-reactivity of 1-carboxypropyl-3-methylxanthine in the ELISAs was determined.

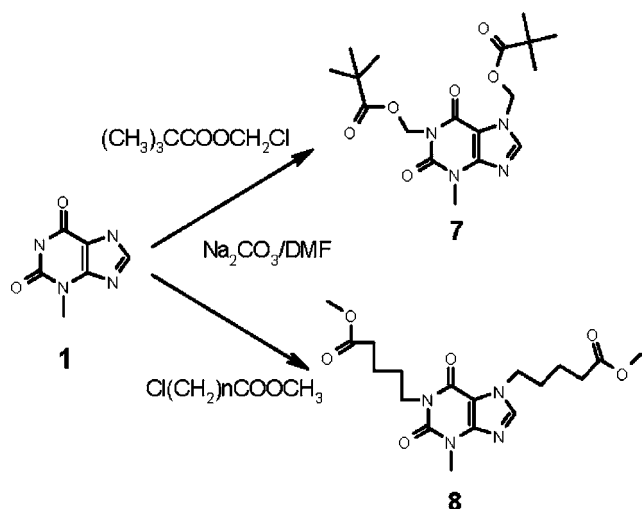
### 3. Results and discussion

In this work, a 42-nt RNA aptamer against theophylline was used as a model for preliminary investigations towards the development of a liposome-enhanced competitive biosensor. As a consequence of the immobilized analog chosen (1-carboxypropyl-3-methylxanthine) and counter-SELEX steps used during the initial discovery, this aptamer had shown exceptional specificity towards theophylline over other xanthine derivatives [37]. By conjugation through the 1-position of theophylline, the structural features that distinguished theophylline from other common xanthine derivatives (namely, the N-7 hydrogen and N-3 methyl group) remained available for interaction with the aptamer. In order to maintain the selectivity of the RNA aptamer to theophylline in this work, it was necessary to produce a liposome-linked conjugate of theophylline (1,3-dimethylxanthine) through its 1-position. 1-substituted theophylline analogs amenable to this conjugation were not commercially available, thus 3-methylxanthine (**1**, Scheme 1) served as a convenient starting material. The order

of proton acidity for xanthine compounds has previously been reported to be  $3 > 7 > 1$  [41], therefore it was expected that the 7-position of 3-methylxanthine would become alkylated prior to the alkylation of the desired 1-position [42]. Amine protection using hydroxylamine-*O*-sulfonic acid was previously reported [42], but the selectivity towards the 7-position and yield could not be reproduced in our hands. Using this approach, 1,7-diamino-3-methylxanthine, was formed in approximately equal amounts as the desired 7-amino-3-methylxanthine and residual 3-methylxanthine starting material. The introduction of additional hydroxylamine-*O*-sulfonic acid only resulted in the increased formation of the undesired 1,7-diamino-3-methylxanthine. Therefore, a method developed previously for the protection of the 7-position on 1-methylxanthine using chloromethyl pivalate [43] was adapted for this experiment.

Chloromethyl pivalate was a useful protecting agent for this synthesis due to its stability under the anhydrous basic conditions used in the alkylation and lability under the aqueous basic conditions used in the ester hydrolysis. Other amine-blocking agents were tried, including trityl chloride, acetyl chloride, and t-BOC, however, these agents either were poorly selective for the 7-position, or were inefficient overall as protecting agents under the conditions tried for this xanthine molecule. When Cl-POM was used in slight excess, the desired 7-protected product (**2**) formed predominantly (~75%) while ~12% starting material (**1**) remained and ~8% of the bis-protected xanthine (**7**, Scheme 1) was generated. The small amount of this byproduct that was generated was readily separable by column chromatography following the subsequent alkylation step and could be converted back to the starting material through hydrolysis with aqueous 2 M NaOH. Once the 7-position had been successfully blocked to yield **2**, the 1-position could then undergo alkylation (**3**) with either 3-bromomethylpropionate, 4-chloromethylbutyrate or 5-chloromethylvalerate, using a general alkylation procedure [44,45]. Alkylation of the 1-position using these agents could lead to the minor formation of the 1,7-disubstituted compound (**8**) if residual starting material remained, but like **7**, this impurity could easily be removed by chromatography. When 5-chloromethylvalerate was used as an alkylating agent, the identity of which structural isomer was present (**7** or **8**) could be revealed by the fragmentation pattern in their mass spectra. Purification at this stage was necessary as 1-carboxyalkyl-3-methylxanthine (**4**) would not crystallize out of solution when the input containing **3** was crude. Treatment with aqueous base simultaneously deprotected the 7-position while hydrolyzing the ester group of the 1-position to yield a carboxylic acid derivative (**4**) [43]. This derivative then underwent treatment with thionyl chloride to form the acid chloride (**5**), which was then reacted with the amine group of 1,2-dipalmitoyl-*sn*-glycero-3-phosphoethanolamine (DPPE) (Scheme 1). GC-MS, HPLC, NMR and TLC data, as well as successful binding of the theophylline-selective aptamer, support the conclusion that the desired phospholipid conjugate (**6**) of this theophylline analog was successfully prepared. The hydrophobic tails of the resulting conjugate were then incorporated into the lipid bilayer of liposomes using standard techniques [46] (Scheme 2).





Scheme 2. Impurities formed during the synthesis. The bis-protected compound (7) formed in low amounts ( $\sim 8\%$  by HPLC) during intended formation of the desired 7-protected compound (2). The bis-alkylated impurity (8) shown was formed from reaction of residual starting material (1) with 5-chloromethylvalerate.

During liposome preparation, the hydrophobic tails of this lipid become incorporated into the liposome bilayer and serve to immobilize the theophylline analog tag onto the liposome surface, thus approximately 50% of the tag lies on the exterior of the liposome and is available for binding. Conjugations of tags to preformed liposomes are possible, but less desirable since a change of liposome stability, size and entrapment efficiency can occur during coupling procedures. Thus, more reliable and less varying liposome populations can be prepared when using tagged lipids rather than tagging preformed liposomes. In order to show the success of the synthesis with respect to recognition by the theophylline aptamer and the incorporation of the product into the lipid bilayers of the liposomes, a number of experiments were carried out. Equilibrium filtration was done to determine dissociation constants of the unmodified and biotinylated aptamers, and when performed in competitive binding studies, these experiments provided information on the ability of the aptamers to recognize tags on the liposome surface. ELISAs were used to quantify the amount of unbound theophylline and were thus an indirect measure for the aptamer binding.

### 3.1. Determination of aptamer-theophylline dissociation constants

In order to determine the dissociation constants of the aptamers towards theophylline, and to rule out interference of the biotin tag on the aptamer with theophylline recognition, equilibrium filtration experiments were carried out (Fig. 2). In these experiments, the amount of theophylline which is aptamer bound is retained in the upper portion of centrifugal filtration devices, while unbound theophylline can freely pass through the semi-permeable membrane upon centrifugation [37].

The non-biotinylated RNA aptamer had a dissociation constant of approximately  $0.9 \mu\text{M}$  determined as the aptamer concentration at which 50% of the theophylline was bound. This

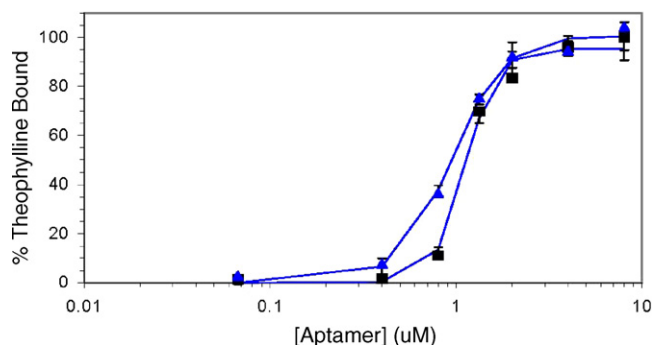


Fig. 2. The fraction of theophylline bound as a function of unmodified RNA aptamer ( $\blacktriangle$ ) and 3'-biotinylated RNA aptamer ( $\blacksquare$ ) concentrations is plotted. Measurements were taken at  $25^\circ\text{C}$  in 100 mM HEPES, 100 mM NaCl, 5 mM  $\text{MgCl}_2$  using the equilibrium filtration method.

correlated well with the dissociation constant reported by the original investigators of this aptamer ( $0.6 \mu\text{M}$ ). The biotinylated aptamer had a dissociation constant of  $1.0 \mu\text{M}$  suggesting that the addition of a 3'-biotin tag had little, if any, effect on the ability of the RNA aptamer to bind theophylline. Similar experiments were carried out with the DNA aptamer composed of the same sequence using oligonucleotide concentrations ranging from  $0.067 \mu\text{M}$  to  $120 \mu\text{M}$ , however no affinity of this oligonucleotide for theophylline was observed. Although the predicted secondary structure for the RNA and DNA oligonucleotide was the same using M-fold software, the predictions also suggested that the folded DNA structure was less stable [47,48]. The observation that the DNA aptamer had no apparent affinity for theophylline was not surprising since such post-SELEX substitutions have reportedly not proven to be successful for other aptamers [49]. However, biotinylated molecules are desirable entities in biosensor development due to their interaction with streptavidin yielding a high affinity ( $K_d \sim 10^{-15} \text{ M}$ ), non-covalent complex [50]. Previous authors have noted the use of biotinylated aptamers towards other target molecules in microarrays [51,52]. The similarity in affinity of the biotinylated aptamer to the unmodified variant is advantageous as it will facilitate immobilization in our proposed competitive biosensor.

### 3.2. Competitive binding between theophylline and 1-carboxypropyl-3-methylxanthine

Competitive binding between theophylline and 1-carboxypropyl-3-methylxanthine (4) for the unmodified RNA aptamer was studied using equilibrium filtration experiments. These experiments were carried out to determine whether the synthesized 1-carboxypropyl-3-methylxanthine (4) that was used as a tag for the liposomes could compete with theophylline for the available aptamer. When increasing the concentration of 1-carboxypropyl-3-methylxanthine, less theophylline binding to the aptamer was observed which indicated that this molecule successfully competed with theophylline for aptamer binding sites. The dissociation constant ( $K_d$ ) from this experiment, determined from its  $\text{IC}_{50}$ , for 1-carboxypropyl-3-methylxanthine was approximately  $2.7 \mu\text{M}$  which correlated well with the previously reported  $K_d$  for 1-carboxypropyl-3-methylxanthine at

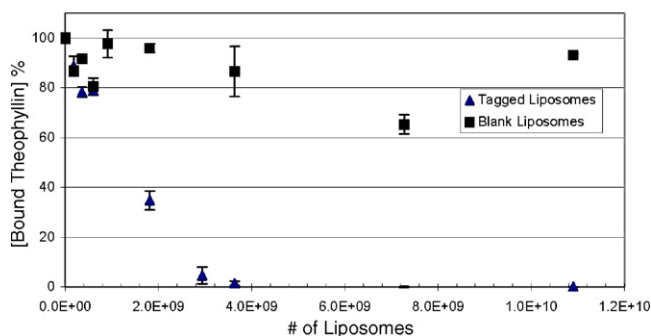


Fig. 3. Competitive binding between theophylline-analog-tagged (▲) or blank liposomes (■) and theophylline for binding sites at the unmodified RNA aptamer. Measurements were taken at 25 °C in 100 mM HEPES, 100 mM NaCl, 5 mM MgCl<sub>2</sub> using the equilibrium filtration method. The number of liposomes on the *x*-axis was calculated based on their diameter and entrapped dye content, as described in Section 2.

~0.7–1.1 μM [37]. Prior to running this experiment, the cross-reactivity of 1-carboxypropyl-3-methylxanthine with the antibody used in the commercial ELISA kit was investigated. Although the ELISA showed no cross-reactivity with the synthesized 1-carboxypropyl-3-methylxanthine for concentrations ranging from  $1 \times 10^{-10}$  M to  $1 \times 10^{-4}$  M, significant cross-reactivity was noted at concentrations greater than  $1 \times 10^{-3}$  M.

### 3.3. Competitive binding between theophylline and 1-carboxyethyl-3-methylxanthine-tagged liposomes

Competitive binding experiments between theophylline and liposomes tagged with 1-carboxyethyl-3-methylxanthine or blank liposomes to the non-biotinylated aptamer were carried out to determine if the tagged liposomes could compete with theophylline for binding to the RNA aptamer. Both liposome batches had an average diameter of  $300 \pm 65$  nm. The experiments with blank liposomes were carried out to determine whether this competition was specific to the theophylline-tag, or if non-specific binding to blank liposomes was responsible for the observed competition.

Increasing the concentration of 1-carboxyethyl-3-methylxanthine-tagged liposomes decreased the percentage of free theophylline that is bound to the aptamer (Fig. 3). By contrast, similar experiments performed with liposomes without any tag showed no competitive behavior. While  $\geq 69\%$  of theophylline was bound to the aptamer when blank liposomes were used, 0% of theophylline was bound when an equivalent volume of theophylline-analog-tagged liposomes were used. It can be concluded that the aptamer is thus capable of binding the free 1-carboxypropyl-3-methylxanthine, and also the liposome-bound form of this analyte. Therefore, the analyte-tagged liposomes could be used in a competitive assay format to quantify the presence of theophylline.

## 4. Conclusions

A conjugate of an unsymmetrical 1,3-disubstituted xanthine and phospholipid has been successfully prepared. After incorporation into liposomes, this phospholipid derivative was success-

fully recognized by an RNA aptamer to theophylline. This not only confirmed that the phospholipid-xanthine analog structure had formed, but also indicated that the two methylene groups between the xanthine structure and phospholipid provided sufficient separation from the liposome surface to permit recognition by the aptamer. We have not yet investigated longer spacer lengths and their affect on aptamer recognition. Since the RNA aptamer was successfully able to recognize a liposome-bound target in a competitive assay format, future work in this laboratory will be focused on adapting this aptamer for use in a biosensor for theophylline intended for clinical sample application. Dye-encapsulating liposomes have been utilized in a variety of formats, including sequential injection analysis (SIA), microfluidic devices, and lateral flow assays [53–55] where they have provided substantial signal enhancement over single-tagged fluorophores. The finding that the biotinylated version of this aptamer had similar affinity for theophylline will facilitate further development of a competitive biosensor using tagged liposomes, pending the identification of a suitable immobilization surface.

## Acknowledgements

The authors would like to thank Dr. Larsson-Kovach and IR-4 group for permitting use of their facilities, Anthony Condo at the Cornell University NMR facility for his assistance with acquiring the NMR data; and Allison Pelletier for editing the manuscript.

## References

- [1] J. Ciesiolka, J. Gorski, M. Yarus, *RNA* 1 (1995) 538–550.
- [2] D. Huizanga, J. Szostak, *Biochemistry* 34 (1995) 656–665.
- [3] M. Sassanfar, J. Szostak, *Nature* 364 (1993) 550–553.
- [4] J. Latham, R. Johnson, J. Toole, *Nucleic Acids Res.* 22 (1994) 2282–2817.
- [5] R. Kotia, L. Li, L. McGown, *Anal. Chem.* 72 (2000) 827–831.
- [6] T. Romig, C. Bell, D. Drolet, *J. Chromatogr.* 731 (1999) 275–284.
- [7] M. Minunni, S. Tombelli, A. Gulloto, E. Luzi, M. Mascini, *Biosens. Bioelectron.* 20 (2004) 1149–1156.
- [8] C. Tuerk, L. Gold, *Science* 249 (1990) 505–510.
- [9] S. Klug, M. Famulok, *Mol. Biol. Rep.* 20 (1994) 97–107.
- [10] M. Esch, A. Baeumner, R. Durst, *Anal. Chem.* 73 (2001) 3162–3167.
- [11] S. Tombelli, M. Minunni, M. Mascini, *Biosens. Bioelectron.* 20 (2005) 2424–2434.
- [12] C. O’Sullivan, *Anal. Bioanal. Chem.* 372 (2002) 44–48.
- [13] K. Stadtherr, H. Wolf, P. Lindner, *Anal. Chem.* 77 (2005) 3437–3443.
- [14] H.-M. So, K. Won, Y.H. Kim, B.-K. Kim, B.H. Ryu, P.S. Na, H. Kim, J.-O. Lee, *J. Am. Chem. Soc.* 127 (2005) 11906–11907.
- [15] S. Tombelli, M. Minunni, E. Luzi, M. Mascini, *Bioelectrochemistry* 67 (2005) 135–141.
- [16] F. Kleinjung, S. Klussman, V. Erdmann, F. Scheller, J. Furste, F. Bier, *Anal. Chem.* 70 (1998) 328–331.
- [17] M. Lee, D. Walt, *Anal. Biochem.* 282 (2000) 142–146.
- [18] M. Hennion, D. Barcelo, *Anal. Chim. Acta* 362 (1998) 3–34.
- [19] S. Wang, C. Zhang, Y. Zhang, *Anal. Chim. Acta* 535 (2005) 219–225.
- [20] M. Ducey Jr., A. Smith, X. Guo, M. Meyerhoff, *Anal. Chim. Acta* 357 (1997) 5–12.
- [21] Y. Jin, J.W. Jang, C.H. Han, M.H. Lee, *J. Agric. Food Chem.* 53 (2005) 7639–7643.

- [22] A. Brecht, A. Klotz, C. Barzen, G. Gauglitz, R.D. Harris, G.R. Quigley, J.S. Wilkinson, P. Sztajn bok, R. Abuknasha, J. Gascón, et al., *Anal. Chim. Acta* 362 (1998) 69–79.
- [23] K.E. Sapsford, P.T. Charles, C.H. Patterson Jr., F.S. Ligler, *Anal. Chem.* 74 (2002) 1061–1068.
- [24] I.A. Darwish, D.A. Blake, *Anal. Chem.* 73 (2001) 1889–1895.
- [25] M. Seydack, *Biosens. Bioelectron.* 20 (2005) 2454–2469.
- [26] J. Ho, R. Wauchope, *Anal. Chem.* 74 (2002) 1493–1496.
- [27] M. Roberts, R. Durst, *Anal. Chem.* 67 (1995) 482–491.
- [28] W.R.G. Baeyens, S.G. Schulman, A.C. Calokerinos, Y. Zhao, A.M. García Campaña, K. Nakashima, D. De Keukeleire, *J. Pharm. Biomed. Anal.* 17 (1998) 941–953.
- [29] L. Kricka, *Ann. Clin. Biochem.* 39 (2002) 114–129.
- [30] G. Rule, R. Montagna, R. Durst, *Anal. Biochem.* 244 (1997) 260–269.
- [31] A. Plant, M. Brizgys, L. Locascio-Brown, R. Durst, *Anal. Biochem.* 176 (1989) 420–426.
- [32] D. Monroe, *J. Liposome Res.* 1 (1989) 337–339.
- [33] H. Rongen, A. Bult, W. Bennekom, *J. Immunol. Methods* 204 (1997) 105–133.
- [34] K. Edwards, A. Baeumner, *Liposomes in Analyses*, *Talanta* 68 (2006) 1421–1431.
- [35] G. Zimmermann, T. Shields, R. Jenison, C. Wick, A. Pardi, *Biochemistry* 37 (1998) 9186–9192.
- [36] G. Zimmermann, R. Jenison, C. Wick, J. Simorre, A. Pardi, *Nat. Struct. Biol.* 4 (1997) 644–649.
- [37] R. Jenison, S. Gill, A. Pardi, B. Polisky, *Science* 263 (1994) 1425–1429.
- [38] T. Kuhara, C. Ohdoi, M. Ohse, *J. Chromatogr. B* 758 (2001) 1–14.
- [39] D. Small, *J. Lipid Res.* 8 (1967) 551–557.
- [40] J. Israelachvili, D. Mitchell, *Biochim. Biophys. Acta* 389 (1975) 13–19.
- [41] L. Cavalieri, J. Fox, A. Stone, N. Chang, *J. Am. Chem. Soc.* 76 (1954) 1119–1122.
- [42] V. Kuz'menko, A. Gulevskays, A. Pozharskii, *Z. Org. Khim.* 24 (1988) 1373–1377.
- [43] M. Hu, P. Singh, E. Ullman, *J. Org. Chem.* 45 (1980) 1711–1713.
- [44] H. Cottam, H. Shih, L. Tehrani, B. Wasson, D. Carson, *J. Med. Chem.* 39 (1996) 2–9.
- [45] R. Cavallaro, L. Filocamo, A. Galuppi, A. Galione, M. Brufant, A. Genazani, *J. Med. Chem.* 42 (1999) 2527–2534.
- [46] F. Szoka, D. Papahadjopoulos, *Proc. Natl. Acad. Sci. USA* 75 (9) (1978) 4194–4198.
- [47] D. Mathews, J. Sabina, M. Zuker, D. Turner, *J. Mol. Biol.* 288 (1999) 911–940.
- [48] M. Zuker, D. Mathews, D. Turner, Algorithms and thermodynamics for RNA secondary structure prediction: a practical guide, in: J. Barciszewski, B.F.C. Clark (Eds.), *RNA Biochemistry and Biotechnology*, NATO ASI Series, Kluwer Academic Publishers, 1999, pp. 11–43.
- [49] L. Gold, B. Polisky, M. Yarus, *Annu. Rev. Biochem.* 64 (1995) 763–797.
- [50] M. Wilchek, E. Bayer, *Immunol. Today* 5 (1984) 39–43.
- [51] J. Collett, E. Cho, A. Ellington, *Methods* 37 (2005) 4–15.
- [52] J. Collett, E. Cho, J. Lee, M. Levy, A. Hood, C. Wan, A. Ellington, *Anal. Biochem.* 338 (2005) 113–123.
- [53] M. Lee, R. Durst, R. Wong, *Anal. Chim. Acta* 354 (1997) 23–28.
- [54] S. Kwakye, A. Baeumner, *Anal. Bioanal. Chem.* 376 (2003) 1062–1068.
- [55] G. Rule, R. Montagna, R. Durst, *Clin. Chem.* 42 (1996) 1206–1209.

# Chemical enrichment and separation of uranyl ions in aqueous media using novel polyurethane foam chemically grafted with different basic dyestuff sorbents

M.F. El-Shahat<sup>a</sup>, E.A. Moawed<sup>b,\*</sup>, A.B. Farag<sup>c</sup>

<sup>a</sup> Chemistry Department, Faculty of Science, Ain Shams University, Cairo, Egypt

<sup>b</sup> Chemistry Department, Faculty of Science, Mansoura University, Damietta, Egypt

<sup>c</sup> Chemistry Department, Faculty of Science, Helwan University, Ain Helwan, Egypt

Received 24 November 2005; received in revised form 20 March 2006; accepted 23 March 2006

Available online 8 May 2006

## Abstract

The new type of the grafted polyurethane foam sorbents were prepared by coupling polyether polyol, toluene diisocyanate and basic dyestuff (Methylene blue, Rhodamine B and Brilliant green). The Me.B-PUF, Rh.B-PUF and Br.G-PUF were characterized using UV/vis, IR and TGA. The adsorption properties and chromatographic behaviour of these new adsorbents for preconcentration and separation of uranium(VI) ions at low concentrations from aqueous thiocyanate media were investigated by a batch process. The maximum sorption of U(VI) was in the pH ranges 1–4. The kinetics of sorption of the U(VI) by the Grafted-PUF were found to be fast with half life of sorption ( $t_{1/2}$ ) in 2.43 min. The average sorption capacity of different sorbents 0.124 meq g<sup>-1</sup> for uranyl ions, enrichment factors  $\approx 40$  and the recovery 98–100% were achieved (R.S.D.  $\approx 0.73\%$ ). The basic dyestuff Grafted-PUF could be used many times without decreasing their capacities significantly. The value of the Gibbs free energy ( $\Delta G$ ) for the sorbents is  $-7.3$  kJ mol<sup>-1</sup>, which reflects the spontaneous nature of sorption process. The sorption mechanism of the metal ion onto Grafted-PUF was also discussed.

© 2006 Elsevier B.V. All rights reserved.

**Keywords:** Uranium(VI); Enrichment; Separation; Polyurethane foam; Basic dyestuff

## 1. Introduction

The determination of low level of U(VI) in environmental samples and its removal from the water in inexpensive processing are very important. Several methods have been described for the separation and determination of uranyl ions precipitation, solvent extraction [1–3], silica gel [4,5], micellar ultrafiltration [6], organic and inorganic ion exchange [7–9]. Also, many types of organic adsorbents, e.g. organosilicon [10], octylsilane [11], polypropylene fiber [12], polyacrylonitrile [13], and polyurethane foam [14–17] have been developed and tested for recovery of uranium from aqueous media.

Polyurethane foam has been used as a sorbent to separate and preconcentrate a wide variety of inorganic and organic species from different media by conventional methods [18].

Polyurethane foam can be used without pretreatment and reagent immobilization [19–25]. Two main problems necessitate the need for preparation of PUF in which organic reagents are chemically bonded: lack of selectivity of unloaded foams and leaching of reagents from loaded ones. The Grafted-PUF was used as an excellent sorbent, which has good stability, high capacity for metal ions and good flexibility [26–29]. Also, the interesting property of Grafted-PUF is due to its relatively fast separation and preconcentration of metal ions compared to other solid sorbents [29].

In the present work we used a water soluble basic dyestuff (Brilliant green, Methylene blue and Rhodamine B) in grafting the PUF to obtain a new type of PUF having more functional groups capable of forming ion association complexes with the anionic complexes of metal ions through the quaternary ammonium group. The preparation of the grafted polyurethane foam (Br.G-PUF, Me.B-PUF and Rh.B-PUF) by coupling polyether polyol, basic dyestuff and toluene diisocyanate are the subject of the present paper. They are identified by using UV–vis,

\* Corresponding author. Tel.: +966 050 524 1921; fax: +966 003 827 8173.  
E-mail address: [eamoawed@yahoo.com](mailto:eamoawed@yahoo.com) (E.A. Moawed).

IR and TGA. The Grafted-PUF was found to be very suitable for the separation and preconcentration of uranium from aqueous thiocyanate media. The importance of this work is the development of the Grafted-PUF containing non-washable reagent, and stable chelate forming resin matrix, which has been recycled many times without decreasing their capacities significantly.

## 2. Material and methods

### 2.1. Reagents and materials

All reagents used were of analytical reagent grade. Standard uranium solution (0.1 mg/mL) was prepared by dissolving 0.1787 g of uranyl acetate in distilled water containing 1 mL of concentrated HNO<sub>3</sub> and the solution was completed to 1 L with distilled water. Ammonium thiocyanate solution (50%) was prepared by dissolving 50 g of NH<sub>4</sub>SCN in 100 mL of distilled water.

### 2.2. Synthesis of Br.G-PUF, Me.B-PUF and Rh.B-PUF

The Grafted-PUF was synthesized by mixing 20 g of the polyether polyol, 1 g distilled water, 0.04 g of dimethylene ethanol amine, 0.04 g of stannous octoate, 0.25 g of polyether polysiloxane and 0.2 g of basic dyestuff. The mixture was then stirred to complete homogeneity, 13 g of toluene diisocyanate was added gradually and the mixture was finally poured in a box. Grafted-PUF was washed with 0.1 M HCl followed by distilled water, then acetone and dried at 25 °C [26].

### 2.3. Apparatus

All spectrophotometric measurements are performed using UV–vis Perkin-Elmer 3 B spectrophotometer. Glass columns of about 15 cm × 1.5 cm i.d. were employed for the chromatographic separations.

### 2.4. General procedures

#### 2.4.1. Sorption investigations

Separation of U(VI) was carried out by a batch technique at 25 °C except otherwise specified. A 0.2 g portion of the Grafted-PUF was mixed with 25 mL aliquot of tested metal ion solution (1.6 µg/mL) in a shaker thermostated to the desired temperature and adjusted to a desired shaking speed. After fixed intervals, aliquots of solution were withdrawn and the concentration of U(VI) ions was determined spectrophotometrically. The following equations have been used to calculate the distribution coefficients ( $K_d = (C_0 - C)/C \times V/M$ ), where  $C_0$  and  $C$  are the initial and final concentrations, respectively, of metal ions in solution,  $V$  the volume of solution and  $M$  is the mass of the Grafted-PUF.

#### 2.4.2. Chromatographic separations

To study the preconcentration, the breakthrough capacities, the chromatographic behaviour, and the separation of the uranyl

ion, a compact column of 15 cm × 1.5 cm i.d. was packed with 1 g of the Grafted-PUF, by the procedure described previously [18]. Solutions were passed through the column at flow rate of 10 mL/min.

## 3. Results and discussion

Basic dyestuff has found considerable applications in the extraction of metals bound to ions such as thiocyanate or other ligands. The ion association complexes formed by the dyestuff and anionic complexes of metals are usually extracted into non-polar solvent. Methylene blue (azine dye), Rhodamine B (xanthene dye) and Brilliant green (triphenyl methane dye) are the basic dyestuff that has found to be used in the separation of anionic complexes. This paper describes the preparation and characterization of grafted polyurethane foam. This new chelating polymers are used for the preconcentration and separation of U(VI) from aqueous thiocyanate solution.

### 3.1. Characterization of Grafted-PUF

The densities of the White-PUF and Grafted-PUF were measured. The values obtained are 34.5 and 73.4 kg/m<sup>3</sup>, respectively. These results indicate that the Grafted-PUF is denser and has more crosslinkage than the White-PUF due to additional bonds between the basic dye and other group in the PUF.

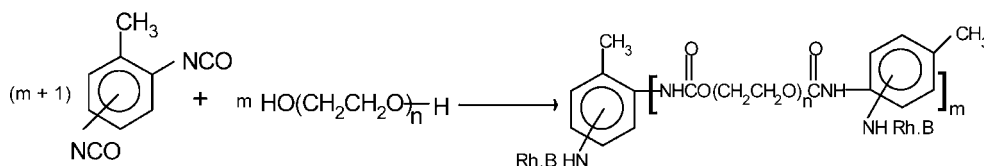
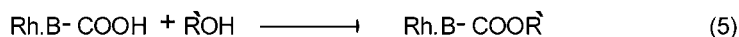
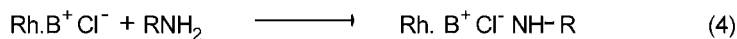
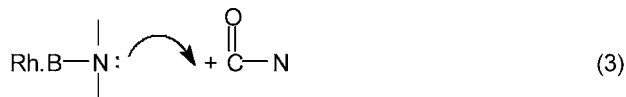
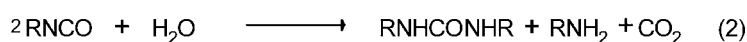
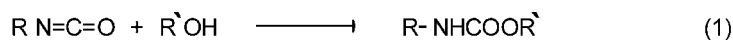
UV/vis spectrum of Grafted-PUF was compared with that of White-PUF. There are additional peaks at 660, 560 and 430 nm which appear in Me.B-PUF, Rh.B-PUF and Br.G-PUF, respectively due to reaction of PUF with dyes.

The infrared spectra of White-PUF and Grafted-PUF were tested using potassium bromide technique. The results obtained show that the absorption band at 2274.4 cm<sup>-1</sup> characteristic of isocyanate (–NCO) group disappears. Also, the broad band in 3600–3100 cm<sup>-1</sup> characteristic of the NH and OH groups of White-PUF is shifted. These results indicate that the coupling between group of the reagent and NCO group of PUF is due to the formation of ionic bond between the dyes molecule and amine product, and formation of ester in case of Rhodamine B dye.

Thermogravimetric analysis (TGA) of Grafted-PUF showed that the thermal decomposition beginning at 230 °C, the weight loss were 1.4, 35.1, 49.1 and 14.4% at 233, 337, 400 and >400 °C, respectively and two endothermic peak at 328 and 390 °C have appeared. TGA curves Grafted-PUF showed that the reagent was reacted with foam matrix. The adsorbed gases were loss at 233 °C and the endothermic peaks at 328 and 390 °C correspond to the thermal decomposition between 328 and 390 °C. Also, the Grafted-PUF has good thermal stability, compared with other chelating resins.

The leaching of reagent from Grafted-PUF with different solvents in batch mode was tested. According to the forgoing results, Grafted-PUF shows a good chemical stability in the presence of 1–10 M H<sub>2</sub>SO<sub>4</sub>, 1–6 M HCl, benzene, toluene, diethyl ether, isopropanol, chloroform, methyl propyl ketone and acetone. The expected scheme for the preparation of Grafted-PUF (Rh.B-PUF) is represented:





### 3.2. Optimum condition for preconcentration and separation of uranium(VI)

The effect of pH and acidity on the sorption of anionic complex,  $[UO_2(SCN)_4]^{-2}$  onto White-PUF and Grafted-PUF were examined. The distribution coefficients ( $K_d$ ) of U(VI) was plotted against the pH values. The results show that the maximum sorption of U(VI) onto White-PUF, Br.G-PUF and Me.B-PUF occurs in the pH ranges 2–4 while the maximum sorption occurs in pH 1–3 range for Rh.B-PUF (Fig. 1). The distribution coefficients sequence was in order Rh.B-PUF > Br.G-PUF > Me.B-PUF, which depends on the basic group of the dye molecule. The similarity of the curves of White-PUF and the Grafted-PUF could reasonably suggest that the sorption of metal ion complex onto White-PUF may proceed via both mechanism, weak anion exchange and ion association mechanism. While, the possible mechanisms that have been previously proposed for the sorption of metal ions onto White-PUF are surface sorption [31,32], etherlike solvent extraction [30,32], anion exchanger [33], cation chelation [34–36], and ion association [37].

The distribution ratio of uranyl ions ( $4.2 \times 10^{-5}$  mol/L) with White-PUF and Grafted-PUF were found to be strongly dependent on the thiocyanate concentration, thus the concentration of thiocyanate in the extraction medium was examined at con-

centration range from 0.1 to 5 mol/L  $NH_4SCN$ . The minimum concentration level necessary for the maximum uptake of U(VI) was 1.9 mol/L (Fig. 2). Also, the uptake of uranyl ions sorption onto Grafted-PUF is larger than those of White-PUF. This confirms that the Grafted-PUF is more efficient than the White-PUF due to the incorporation of quaternary ammonium group of basic dye which forms ion-pairs with metal thiocyanate complex.

The effect of shaking time on the sorption U(VI) onto White-PUF and Grafted-PUF was studied. From the results obtained, the time required for sorption equilibrium was found to be 20 and 10 min, respectively (Fig. 3). The sorption of uranyl ions on PUF may involve three steps: bulk transport of solute in solution, film transfer involving diffusion of solute through a hypothetical film boundary layer, and diffusion of the solute within the pore volumes of the adsorbent and along pore-wall surfaces to active adsorption sites. In order to study the particle diffusion mechanism of the sorption of U(VI) onto White-PUF and Grafted-PUF, the Morris–Weber ( $q_t = k_M \sqrt{t}$ ) equation was applied. Where  $q_t$  is the amount of metal ions sorbed at time  $t$  and  $k_M$  is the rate constant of interparticle transport. The obtained data show that the plots of  $q_t$  versus  $\sqrt{t}$  are linear and the values of  $k_M$  are 1.21 and 1.97  $\mu\text{mol g}^{-1} \text{min}^{-1/2}$  for the sorption of U(VI) with White-PUF and Grafted-PUF, respectively (Fig. 4). According

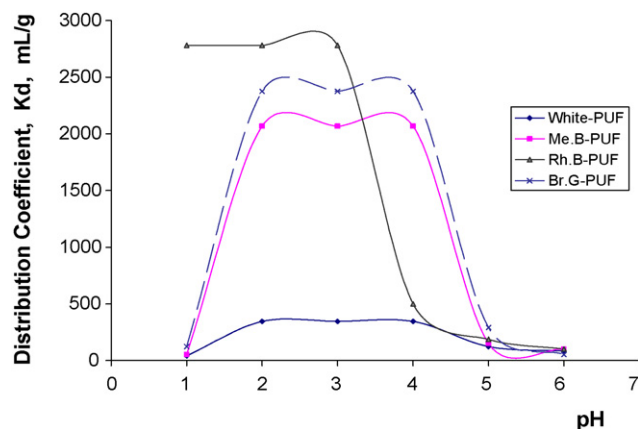


Fig. 1. Effect of pH on the sorption of uranyl ion onto Grafted-PUF.

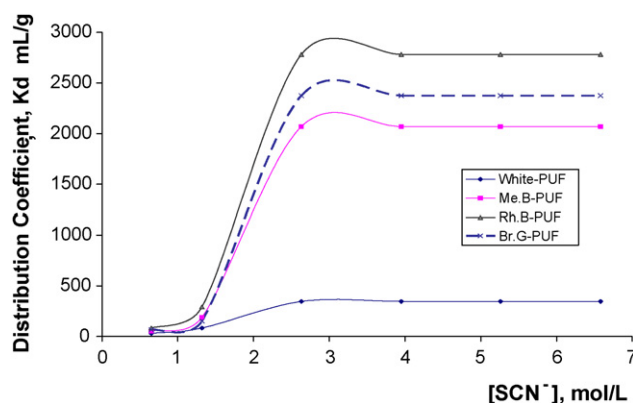


Fig. 2. Effect of thiocyanate concentration on the extraction of uranyl ion onto Grafted-PUF.

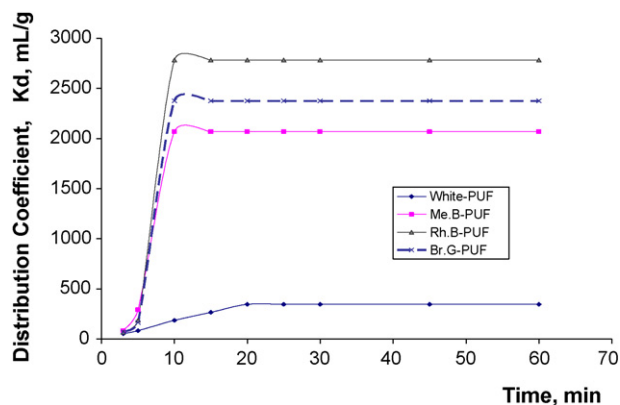
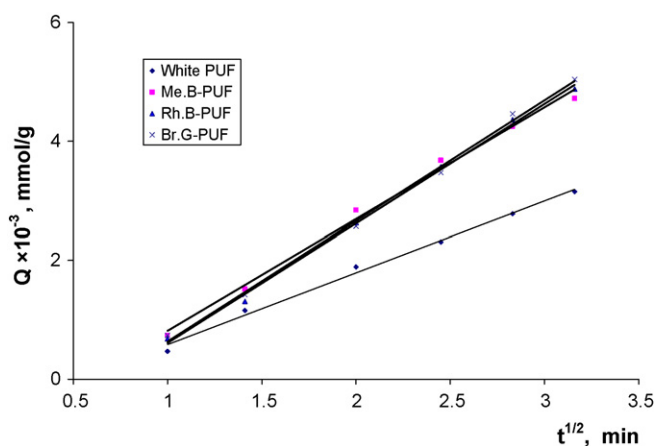


Fig. 3. Effect of shaking time on the extraction of uranyl ion onto Grafted-PUF.

Fig. 4. The plot of  $q_t \times 10^{-6}$  vs.  $t_{1/2}$  for the sorption of uranyl ion onto Grafted-PUF.

to the foregoing results, the diffusion rate is rapid. Also, the kinetic data was calculated according to first order reaction, Lagergren equation ( $\log(q_e - q_t) = \log q_e - k_1 t / 2.303$ ). Where  $q_e$  and  $q_t$  are the amount of metal ions sorbed at equilibrium and at time  $t$  and  $k_1$  is the rate constant of the sorption. A plot of  $\log(q_e - q_t)$  versus  $t$  shows a straight line, which indicates that the process is a first order reaction with respect to the adsorbed concentration of each metal ion. The half life of sorption uranyl ions ( $t_{1/2}$ ) onto White-PUF and Grafted-PUF calculated from the slope are 3.96 and 2.42 min, respectively (Table 1). These results show that the rate of sorption of the uranyl ions separation with Grafted-PUF is relatively fast and more efficient as compared to the White-PUF.

The uptake of the uranyl ions onto White-PUF and Grafted-PUF was determined as a function of metal ion concentration in the aqueous solution. The resultant isotherms show a good

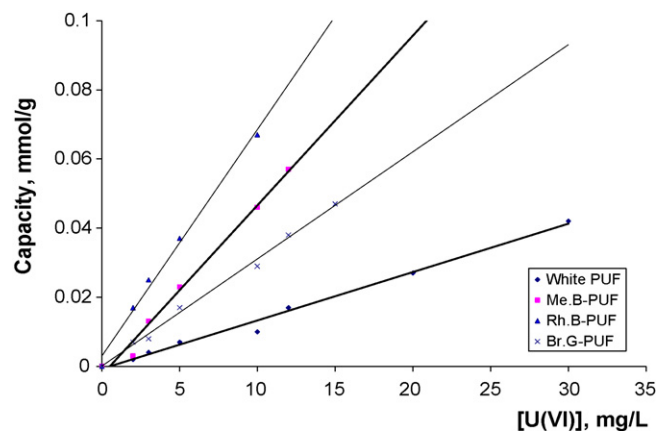


Fig. 5. Isotherm curve of the sorption of uranyl ion onto Grafted-PUF and White-PUF.

linear (correlation coefficient,  $r = 0.993$ ) relationship over relatively wide range of elements concentrations (Fig. 5). The isotherm capacity ( $Q_1$ ) of the White-PUF and Grafted-PUF for U(IV) using batch technique was calculated. The values obtained were 0.07 and 0.124 meq  $g^{-1}$ , respectively. The capacity sequence was in the order of Rh.B-PUF > Me.B  $\approx$  Br.G-PUF > White-PUF, which depends on the carboxylic group of the Rhodamine B. From these results the Grafted-PUF is more efficient than White-PUF [14–18,30] and other resins [12,13]. The dependence of sorption of uranyl ion on White-PUF and Grafted-PUF with temperature have been evaluated using the equations ( $\Delta G = -RT \ln K_c$ ), where  $\Delta G$  and  $T$  are Gibbs free energy and absolute temperature, respectively.  $R$  is the gas constant (8.314 J  $mol^{-1} K^{-1}$ ) and  $K_c$  is the equilibrium constant. The values of  $\Delta G$  at room temperatures for the sorption of U(VI) are given in Table 2. The average values of ( $\Delta G$ ) are  $-2.1$  and  $-6.57$  kJ  $mol^{-1}$  for White-PUF and Grafted-PUF, respectively. The negative values of  $\Delta G$  are attributed to the spontaneous chemisorptions nature of sorption process.

The uptake of sorption of U(VI) onto White-PUF and Grafted-PUF were determined at equilibrium condition as a function of salt concentration (0.1–1 M) of  $Li_2SO_4$ ,  $Na_2SO_4$ ,  $K_2SO_4$  and  $(NH_4)_2SO_4$ . The results obtained show that there was no effect of salt concentration on the separation of uranyl ion.

To determine the breakthrough capacity ( $Q_B$ ) of White-PUF and Grafted-PUF for uranyl ion, 0.25 g of PUF in the column is saturated with U(VI) under optimum conditions. A 250 mL aliquot of 10  $\mu g/mL$  of uranyl thiocyanate complex solution was percolated through the column with flow rate 10 mL/min. From the breakthrough curves presented in Fig. 6, the saturation of

Table 1

Kinetic parameters for the sorption and desorption of metal ions onto White-PUF and Grafted-PUF

Sorbent	Rate constant of interparticle transport, $k_M$ ( $\mu mol g^{-1} min^{-1/2}$ )	Rate constant of sorption, $k_1$ ( $min^{-1}$ )	Rate constant of desorption, $k_{-1}$ ( $min^{-1}$ )	Overall rate constant, $k'$ ( $min^{-1}$ )	Half life of sorption, $t_{1/2}$ (min)
White-PUF	1.21	0.175	0.075	0.250	3.96
Me.B-PUF	1.88	0.299	0.033	0.332	2.32
Rh.B-PUF	2.01	0.288	0.022	0.310	2.41
Br.G-PUF	2.03	0.272	0.011	0.283	2.55

Table 2  
Characteristics of the isotherm curves of the sorption of metal ions using White-PUF and Grafted-PUF sorbents

Resin	Least square equation		Correlation coefficient ( $r$ )	Free energy, $\Delta G$ (kJ mol <sup>-1</sup> )	Capacity, $Q$ (meq g <sup>-1</sup> )	Distribution coefficient, $K_d$ (mL/g)
	Intercept $\hat{i}$ ( $\times 10^{-3}$ )	Slope $\hat{s}$ ( $\times 10^{-3}$ )				
White-PUF	-0.78	1.38	0.986	-2.52	0.070	346.7
Me.B-PUF	-1.56	4.83	0.997	-6.94	0.121	2067.9
Rh.B-PUF	2.98	6.58	0.992	-7.67	0.131	2781.9
Br.G-PUF	0.39	3.05	0.996	-7.28	0.121	2375.0

each column is reached after passage of 80–160 mL of the uranyl ions. The capacities of White-PUF and Grafted-PUF columns are estimated to be 0.066 and 0.111 meq g<sup>-1</sup>, respectively. These capacities are quite reasonable in comparison with the previously reported results for different chelating resins [12].

The elution of tested metal ions from the White-PUF and Grafted-PUF columns was examined at different flow rates of eluting agent (5–20 mL/min). The uranyl ion was eluted from the PUF columns using 0.1 M NaOH. The chromatogram indicates that the U(VI) could be completely eluted in the first 150 mL. Generally the curves are symmetrical with relatively sharp peak. The values of HETP were obtained from the elution curves using Glueckauf ( $HETP = (L/16)(W^2/V_R^2)$ ) and Van Deemeter ( $HETP = A + (B/U) + CU$ ) equations, where  $N$  is the number of theoretical plates,  $V_R$  the volume of elutes at peak maximum,  $W$  the width of the peak, and  $L$  is the length of the foam bed. Good column efficiency as indicated by a low value of HETP was important if good separations were to be achieved. The HETP value was found equals to 0.5–1.4 mm at flow rate 5–10 mL/min.

### 3.3. Analytical application of Grafted-PUF for preconcentration and separation of uranyl ion

The performance of the Grafted-PUF columns in the preconcentration of U(VI) from different volume (25–1000 mL) of aqueous solution was studied. U(VI) was eluted in less or complete recover (98–100%) from the Grafted-PUF column at flow rate of 10 mL/min. These results show that the metal ions can be sensitively concentrated from large volumes of dilute aqueous solutions using Grafted-PUF packed columns. The preconcentration

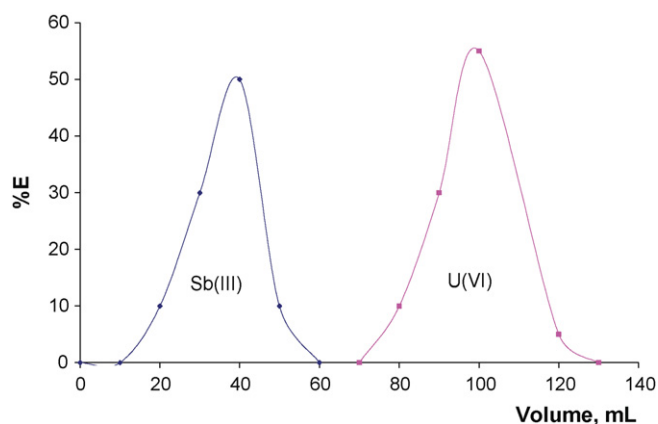


Fig. 7. Separation of U(VI), Fe(III) and Sb(III) from aqueous solution through Grafted-PUF column by using 0.1 M NaOH.

factor was estimated to be 40 with average R.S.D.  $\approx$  0.73. Finally, the Grafted-PUF could be used many times without decreasing their capacities significantly.

The separation of mixture of 50  $\mu$ g for U(VI), Sb(III) and Fe(III) using Br.G-PUF column was examined. Iron(III) is reduced using few drops of 2 M of ascorbic acid. Then 10 mL of 50% NH<sub>4</sub>SCN was passed through the Br.G-PUF column. Fe(III) was separated in the original solution and U(VI) and Sb(III) were retained in the column. U(VI) and Sb(III) were recovered with 0.1 M NaOH at flow rate of 10 mL/min (Fig. 7). This technique selectively allows the determination of each metal ion from the other ions in mixture.

## 4. Sorption mechanism

The average value of free energy ( $\Delta G$ ) is  $-7.3$  kJ mol<sup>-1</sup> for the sorption of uranyl ion onto Grafted-PUF which confirms the spontaneous chemisorptions type. The rate constant of interparticle transport and the values for the half life of adsorption ( $t_{1/2}$ ) of U(VI) were in the order Br.G-PUF > Rh.B-PUF > Me.B-PUF showing that the adsorption process depends on the reaction between the basic groups of dyes and the anionic uranyl complex and also depends on the molecular weight of the dyes. Finally, the Grafted-PUF is more efficient than the White-PUF due to the incorporation of quaternary ammonium group of basic dye which forms ion-pairs with uranyl thiocyanate complex (Figs. 1–3). The optimum pH ranges to extract uranyl ion onto Me.B-PUF and Br.G-PUF (pH 2–4) were similar to the sorption onto White-PUF (Fig. 1). Also, the values of the distribution coefficient decrease with the increase of the pH values

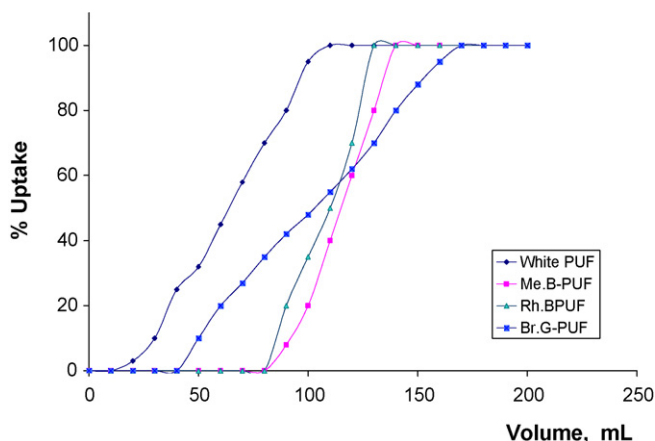


Fig. 6. Breakthrough curve for extraction of U(VI) from aqueous solution.

indicating that the protonated active sites of White-PUF could reasonably suggest that the sorption of uranyl ion complex onto White-PUF may proceed via ion association mechanism.

## 5. Conclusion

The present work deals with the preparation of new polymeric extractors, polyurethane foam, based on the reagent incorporated into the structure through covalent bond. This new extractors were used to separate of uranyl ion from aqueous solutions. Characterization of the Grafted-PUF and White-PUF indicates that the Grafted-PUF ( $0.124 \text{ meq g}^{-1}$ ) is more stable and capacity than the White-PUF ( $0.07 \text{ meq g}^{-1}$ ), which has been recycled many times after regeneration using 1 M HCl and NaOH without decreasing their capacities significantly. The negative values of  $\Delta G$  indicate that the spontaneous nature of the sorption of the uranyl ion. The uranyl ion was completely separated in the pH ranges 1–4 in 2 mol/L of  $\text{NH}_4\text{SCN}$ . Also, the half life of sorption uranyl ions ( $t_{1/2}$ ) was 2.42 min. Finally, the Grafted-PUF is more efficient for separation and determination of uranyl ion than White-PUF [14–18,30] and other resins [12,13].

## References

- [1] Z. Marczenko, Separation and Spectrophotometric Determination of Elements, Ellis Harwood, Chichester, 1986.
- [2] P.K. Mohapatra, V.K. Manchanda, Talanta 47 (1998) 1271.
- [3] Y.K. Agrawal, P. Shrivastav, S.K. Menon, Sep. Purif. Technol. 200 (2000) 177.
- [4] F. Barbette, F. Rascalou, H. Chollet, J.L. Babouhot, F. Denat, R. Guillard, Anal. Chim. Acta 502 (2004) 179.
- [5] P. Michard, E. Guibal, T. Vincent, P. Le Cloirec, Microporous Mater. 5 (1996) 309.
- [6] E. Pramauro, A.B. Prevot, V. Zelano, M. Gulmini, G. Viscardi, Analyst 121 (1996) 1401.
- [7] A.C.Q. Ladeira, C.A. Morais, Miner. Eng. 18 (2005) 1337.
- [8] A.C. Thomas, N. Dacheus, P. Le Coustumer, V. Brandel, M. Genet, J. Nucl. Mater. 295 (2001) 249.
- [9] F.F. Fondeur, D.T. Hobbs, S.D. Fink, M.J. Barnes, Sep. Sci. Technol. 40 (2005) 571.
- [10] A.F. Arruda, A.D. Campiglia, B.P.S. Chauhan, P. Boudjouk, Anal. Chim. Acta 396 (1999) 263.
- [11] Dj. Dojozan, M.H. Pournaghi-Azar, J. Toutouchi-Asr, Talanta 46 (1998) 123.
- [12] P.A. Kavakh, N. Seko, M. Tamada, O. Güven, Sep. Sci. Technol. 39 (2004) 1631.
- [13] N. Pekel, O. Güven, Colloids Surf. A 212 (2003) 155.
- [14] S. Katragadda, H.D. Gesser, A. Chow, Talanta 44 (1997) 1865.
- [15] M.S. El-Shahawi, A.M. Othman, H.M. Nassef, M.A. Abdel-Fadeel, Anal. Chim. Acta 536 (2005) 227.
- [16] M.S. El-Shahawi, A.M. Othman, M.A. Abdel-Fadeel, Anal. Chim. Acta 546 (2005) 221.
- [17] Y. Toker, M. Eral, Ü. Hiçsönmez, Analyst 123 (1998) 51.
- [18] T. Braun, J.D. Navartil, A.B. Farag, Polyurethane Foam Sorbents in Separation Science, CRC Press, Boca Raton, Florida, 1985.
- [19] M.M. Saeed, A. Rusheed, M. Ahmed, J. Tolgyessy, Sep. Sci. Technol. 29 (1994) 2143.
- [20] H. Matsunaga, W. Sun, A. Chow, Sep. Sci. Technol. 30 (1995) 3229.
- [21] D. Walidhagen, V. Krivan, Anal. Chim. Acta 274 (1993) 257.
- [22] S. Belyukova, G. Balamtsarashvili, Talanta 42 (1995) 1833.
- [23] A. Ramesh, K.R. Mohan, K. Seshiah, N.D. Jeyakumar, Anal. Lett. 34 (2001) 219.
- [24] V.A. Lemos, S.L.C. Ferreira, Anal. Chim. Acta 441 (2001) 281.
- [25] V.A. Lemos, R.E. Santelli, M.S. de Carvalho, S.L.C. Ferreira, Spectrochim. Acta 55 (2000) 1497.
- [26] M.F. El-Shahat, E.A. Moawed, M.A.A. Zaid, Talanta 59 (2003) 851.
- [27] E.A. Moawed, M.A.A. Zaid, M.F. El-Shahat, Anal. Lett. 36 (2003) 405.
- [28] E.A. Moawed, Ph.D. Thesis, Faculty of Science, Ain Shams University, Cairo, Egypt, 1994.
- [29] E.A. Moawed, Acta Chromatographica 14 (2004) 298.
- [30] T.C. Huang, D.H. Chen, M.C. Shieh, C.T. Huang, Sep. Sci. Technol. 27 (1992) 1619.
- [31] H.J.M. Bowen, J. Chem. Soc. A (1970) 1082.
- [32] M.S. El-Shahawi, H.A. Nassif, Anal. Chim. Acta 481 (2003) 29.
- [33] S.M. Hasany, M.M. Saeed, M. Ahmed, Sep. Sci. Technol. 35 (2000) 379.
- [34] S.M. Hasany, M.M. Saeed, M. Ahmed, Talanta 54 (2001) 89.
- [35] R.F. Hamon, A.S. Khan, A. Chow, Talanta 29 (1982) 313.
- [36] S.J. AL-Bazi, A. Chow, Talanta 30 (1983) 487.
- [37] P. Fong, A. Chow, Talanta 39 (1992) 825.

# Coffee varietal differentiation based on near infrared spectroscopy

I. Esteban-Díez, J.M. González-Sáiz, C. Sáenz-González, C. Pizarro\*

Department of Chemistry, University of La Rioja, C/Madre de Dios 51, 26006 Logroño (La Rioja), Spain

Received 21 November 2005; received in revised form 16 March 2006; accepted 23 March 2006

Available online 27 April 2006

## Abstract

Near infrared spectroscopy (NIRS) was used to discriminate between *arabica* and *robusta* pure coffee varieties and blends of varied varietal composition. Direct orthogonal signal correction (DOSC) pre-processing method was applied on a set of 191 roasted coffee NIR spectra from both pure varieties and blends varying the final *robusta* content from 0 to 60% (w/w) in order to remove information unrelated to the actual varietal composition of samples. The corrected NIR spectra, as well as raw NIR spectra, were used to develop separate classification models using the potential functions method as class-modelling technique, exploring several options more or less restrictive according to the final number of considered categories. All constructed classification models were compared to evaluate their respective qualities and to show the suitability of applying DOSC method as pre-processing step for developing improved classification models for coffee varietal identification purposes.

© 2006 Elsevier B.V. All rights reserved.

**Keywords:** Food authentication; NIR spectroscopy; Direct orthogonal signal correction; Potential functions; Coffee varieties

## 1. Introduction

Food authentication is one of the most crucial issues in food quality control and safety. Food industry, regulatory authorities and consumer groups are all interested in authenticate raw materials and food products in order to satisfy the food quality and food safety requirements, in such a way that food quality assurance has become an essential tool to meet consumer demands and expectations [1,2].

Coffee identification or classification has gained increasing attention as a means to control and avoid coffee adulteration, mainly considering the great variability of the final sale price depending on coffee varietal or geographic origin. Most commercially available coffees are produced from *arabica* and *robusta* roasted beans or blends of these two species. Both varieties differ not only in relation to their botanical, chemical and organoleptic characteristics, but also in terms of commercial value, with *arabica* coffees achieving market prices 20–25% higher than *robusta*. Therefore, suitable methods are required, for quality and economical reasons, in order to differentiate these varieties and to avoid the possible mixing with other cheaper coffees, thus ensuring coffee authenticity.

Varietal classification for coffee authenticity has been tackled using different types of compositional data including metal content [3], volatile compounds [4], chlorogenic acids and caffeine content [5], fatty acids profile [6], sterolic profile [7], diterpenic alcohols [8], amino acids enantiomers [9], tocopherols and triglycerides [10]. In spite of the relative success showed by many of these approaches in coffee varietal identification, it is important to consider that many analytical reference methods used to assess the chemical components to be later used as discriminant parameters between coffee varieties in the classification model development may be quite expensive, elaborate and/or time-consuming.

For this reason, industry is looking for faster methods, and a rapid, clean and low cost technique, such as an automated classification on the basis of NIR spectra directly acquired on untreated samples could be a very useful tool. In fact, near infrared spectroscopy (NIRS) has emerged in the last years as a very promising alternative method for constructing on the basis of spectral features, and in combination with pattern recognition methods, reliable classification models for assessing the quality of a given product in many food applications [11–17], including several approaches applying NIR to the problem of coffee varietal authentication [18–20].

In this context and in order to search for an optimal classification model, some of us have recently proposed a strategy for developing improved classification models for differenti-

\* Corresponding author. Tel.: +34 941299626; fax: +34 941299621.  
E-mail address: [consuelo.pizarro@dq.unirioja.es](mailto:consuelo.pizarro@dq.unirioja.es) (C. Pizarro).



ate between *arabica* and *robusta* pure coffee varieties based on their NIR spectra and using potential functions Method as class-modelling technique [21]. In this former paper and to minimise certain physical light effects, thus enhancing the relevant chemical information contained in the spectra, two orthogonal signal correction methods were applied on raw NIR spectra to remove information not related to the caffeine content of samples, which was selected as response variable precisely due to its high discriminating power between coffee varieties. Although it was shown that original NIR spectra of roasted coffee samples might be used directly to develop a classification model with a moderately high discrimination ability between pure varieties, the classification models constructed after applying the orthogonal signal correction methods yielded excellent classification results also with a notable reduction in model complexity.

Therefore, given that this strategy appeared to have great promise for coffee varietal authentication purposes, we decided to deeper explore its actual applicability options, and to evaluate in the present work if a similar strategy (combination of direct orthogonal signal correction (DOSC)) method [22] and potential function class-modelling method [23–25]) can be successfully applied not only to discriminate between pure coffee varieties, but also between pure varieties and different blends of the two species on the basis of NIR spectra.

Moreover, it should be noticed that in this modified application no additional chemical variable need to be determined for those samples forming the calibration set in order to perform on its basis the orthogonal correction of spectra, since the response variable to be used in DOSC application is directly the percentage of *robusta* coffee contained in each sample, so it is easy to be realized the notable simplification and cheapening that this fact implies.

One decisive design parameter that has to be set prior to any classification model development is the number of categories to be considered and the particular requirements that a sample has to fullfit in order to be assigned to a certain class. In this study, two different approaches were explored differing in the number and particular properties of classification categories to be taken into account. In an initial and more flexible approach three separate classes were defined a priori: (1) pure *arabica*; (2) *arabica-robusta* blends; (3) pure *robusta*. Next, a more constrained approach taking into account five different categories was evaluated, in such a way that the only class previously defined as '*arabica-robusta* blends' was split into three separate classes in order to try to differentiate between blends with a low *robusta* content (from  $\approx 5$  to 20%), blends with a medium *robusta* content (from  $\approx 25$  to 40%) and blends with a high *robusta* content (from  $\approx 45$  to 60%). In both cases, for evaluating the effect of the orthogonal correction applied on NIR spectra on the quality of the final classification model constructed, the results obtained before and after transforming the spectra were analysed and compared.

It should be clarified that the aim of this study was not to provide a definitive and immutable NIR classification model for discriminating between pure coffee varieties and blends, but to propose a novel strategy capable of accomplishing this task and proving its reliability and effectiveness to assess the genuineness

of coffee samples. Although the data set used in this work was designed to cover insofar as possible the great natural variability inherent to commercially available coffees by considering different roasting conditions and degrees, and varied geographical origins, it is quite clear that the dynamic nature of the coffee market and the particular needs and production lines of a given coffee company would demand a more exhaustive or specific collection of the calibration samples to develop the final class-model with the methodology here presented.

## 2. Experimental

### 2.1. Samples

The data set used in the present study comprised 83 roasted coffee samples from varied origins and varieties (36 *arabica* and 47 *robusta* coffees), which were processed under different roasting conditions. In addition, 108 blends of *arabica* and *robusta* coffee varieties were prepared in laboratory by combining the three coffee samples most representative of each variety which were previously selected. The application of PCA on mean centred NIR spectra provided an effective and easy-to-implement tool for selecting representative samples from *arabica* and *robusta* varieties. Fig. 1 shows a bidimensional representation of PC1 and PC2 scores accounting for 88.33% of the variance in the roasted coffee NIR spectral data, labelled according to their coffee variety: (1) *arabica* coffees; (2) *robusta* coffees. Two sample groups appeared slightly separated by the first bisectrix of the two component axes, suggesting the presence of two different clusters just associated with the two varieties considered. Thus, the centroid and two extreme samples within each class were selected in order to later generate on their basis suitable coffee blends with a *robusta* content in the final blends ranged from 0 to 60% (w/w). This specific range of blending (based on adding increasing *robusta* amounts to final blends) was precisely studied as an attempt to develop reliable classification models mainly focused on detecting *arabica* coffees

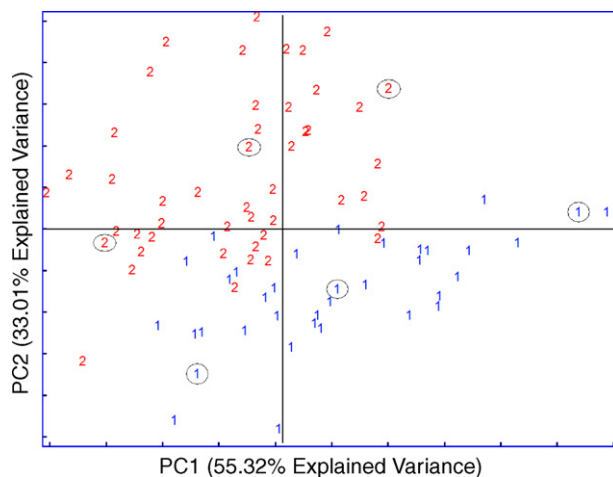


Fig. 1. Scores of the 83 roasted coffee samples from *arabica* (labelled as 1) and *robusta* (labelled as 2) pure varieties on the first two principal components explaining the variability in the NIR spectral data.

adulteration, since when a fraudulent practice is committed in the elaboration procedure of coffee blends from *arabica* and *robusta* pure coffee varieties the motivation behind is purely economical, i.e., to reduce costs due to the lower price of *robusta* coffee as compared to *arabica* coffee, increasing the actual *robusta* percentage in the final blends despite they will be sold as mostly based on *arabica* variety.

The resulting data set was split into two independent subsets: a calibration set with 100 samples and a test set with 91 samples. The main cautions taken in order to select a suitable composition of the external test set were to include samples of both pure varieties and different compositional blends, in such a way that the contained blends covered the whole range of *robusta* percentages studied.

## 2.2. Apparatus and software

NIR spectra were recorded on a near infrared spectrophotometer NIRSystems 5000 (Foss NIRSystems, Raamsdonksveer, The Netherlands) equipped with a reflectance detector and a sample transport module. The instrument was controlled by a compatible PC, and Vision 2.22 (Foss NIRSystems, Raamsdonksveer, The Netherlands) was used to acquire the data.

Data pre-processing treatments and potential functions class-modelling technique were applied by means of V-PARVUS 2004 (M. Forina et al., Dipartimento di Chimica e Tecnologie Farmaceutiche ed Alimentari, Università di Genova, Italy). The DOSC routine was implemented in MATLAB 6.5 (Mathworks, Natick, USA). Specifically, the DOSC method developed by Westerhuis et al. [21] was used for the DOSC calculations. Data for isopotential lines obtained from PARVUS were later mapped using Surfer 8 (Golden Software Inc.).

## 2.3. Recording of NIR spectra

Reflectance spectra were obtained directly from untreated samples. Due care was taken to ensure that the same amount of sample was always used to fill up the sample cell. Each spectrum was obtained from 32 scans performed at 2 nm intervals within the wavelength range 1100–2500 nm, with five replicates for each individual sample. The samples were decompacted between recordings. An average spectrum was subsequently computed from the collected replicates.

## 2.4. Validation of classification models

Usually, the potential functions class-modelling technique validates the predictive ability of the constructed classification models by cross-validation, since when working with potential functions is not recommended to waste objects to make up an external evaluation set. It is, however, well-known that orthogonal signal correction methods can produce a notable overfitting when applied on the spectra forming the calibration set. For this reason, although all potential functions classification models were constructed by cross-validation, we decided to also validate the actual predictive abilities of resulting models by

testing their performance on an external test set to guard against overfitting.

## 2.5. Data processing

The whole data matrix was composed of 191 objects, 700 spectral variables (NIR absorbance values within the wavelength range 1100–2500 nm), and a response variable (percentage of *robusta* content in samples) to be used in the orthogonal correction. The initial set of 191 roasted coffee samples was divided into two subsets: the calibration set (100 objects) used to develop the classification models and the external test set (91 objects) used to evaluate the actual predictive ability of the constructed models.

The models used to classify roasted coffee samples were constructed by using the potential functions method in its modified form as a class-modelling technique. The optimal value of the smoothing parameter was selected by means of a cross-validation procedure, in such a way that the amplitude of each individual potential, defined by this smoothing parameter, was the same for all the objects in the category (fixed potential functions). Model boundaries were computed from the estimate of the equivalent determinant. The class-models were constructed at a level of significance corresponding to 95%. The same a priori class probability was applied to both categories (equal to 1). When classification models were developed on the basis of NIR data, given the large number of spectroscopic variables, a prior step of dimensionality reduction computing a small number of principal components was required. One crucial step in modelling based on NIR spectra is the selection of the optimal number of PCs to be used in the model development. The optimal complexity of each model was assessed by cross-validation (all the classification models were built by cross-validation using five deletion groups). When the DOSC method was applied to find classification models with a high predictive ability and avoid over-fitted solutions, the suitable orthogonal correction degree to be applied was determined as follows: the number of orthogonal-PCs to be removed from raw spectra was varied from 1 to 5, in such a way that the optimal number of orthogonal components to be subtracted was chosen according to the results obtained in the cross-validation procedure. All models were constructed on centred data.

The quality of the results provided by the different class-models constructed was compared according to several evaluation parameters:

- total classification (prediction) rate (TR)

$$TR = \frac{\sum_c m_{cc}}{N} \quad (1)$$

- category *c* rate ( $R_c$ )

$$R_c = \frac{m_{cc}}{N_c} \quad (2)$$

These equations were applied in both classification and prediction, where  $m_{cc}$  is the number of correct classifications (predictions) for a certain category *c*,  $\sum_c m_{cc}$  is the total number of

Table 1  
Percentages of correctly classified samples

PCs	Classification (%)				External prediction (%)			
	RC1	RC2	RC3	TR	RC1	RC2	RC3	TR
Raw NIR spectra								
1	19.1 (17)	43.1 (33)	52.4 (10)	40.0 (60)	26.7 (11)	44.0 (28)	65.4 (9)	47.3 (48)
3	81.0 (4)	93.1 (4)	81.0 (4)	88.0 (12)	86.7 (2)	98.0 (1)	88.5 (3)	88.5 (6)
5	85.7 (3)	94.8 (3)	95.2 (1)	93.0 (7)	93.3 (1)	94.0 (3)	100	95.6 (4)
7	85.7 (3)	98.3 (1)	100	96.0 (4)	93.3 (1)	94.0 (3)	100	95.6 (4)
DOSC-corrected NIR spectra (three orthogonal-PCs removed)								
3	100	100	100	100	100	100	96.2 (1)	98.9 (1)

Total rate (TR) and category rates (RC1, RC2 and RC3) both in classification and external prediction, working on original and DOSC-corrected spectra. The number of samples incorrectly classified appears in brackets.

correct classifications (predictions),  $N_c$  is the number of classifications (predictions) for a certain category  $c$  and  $N$  is the number of total classifications (total predictions). It should be noticed that  $N_c$  does not always equal the number of objects belonging to class  $c$ , in the same way as  $N$  does not always represent the number of total objects, since, for instance, during cross-validation, an object can be classified several times.

Graphical tools, such as isopotential lines and Coomans plots, were also used to analyse the goodness of the models.

### 3. Results and discussion

#### 3.1. Three-class approach

In the first part of this study three separate categories ((1) pure *arabica* coffees; (2) *arabica-robusta* blends; (3) pure *robusta* coffees) were considered, accounting for 191 samples that were divided at random into calibration (21 *arabica* coffees; 58 blends; 21 *robusta* coffees) and test (15 *arabica* coffees; 50 blends; 26 *robusta* coffees) sets.

Table 1 summarised the classification and prediction rates corresponding to the class-models developed on the basis of mean-centred raw NIR spectra of roasted coffee samples using the potential functions method with model complexities from 1 to 7 PCs for the three-class problem analysed. The table shows the influence on the number of PCs used to construct the class-model, in such a way that 7 PCs were used to compute the model to achieve the maximum correct classification rates in

the cross-validation procedure, accounting for the 99.99% of the variance in the data. Table 2 shows the results corresponding to the same classification models developed from raw data expressed in terms of sensitivity and specificity for the three classes studied. Sensitivity is the proportion of samples belonging to a certain category correctly identified by the mathematical model corresponding to that class, i.e., it is a measure of the ability to correctly predict 'true' positives. Specificity is the proportion of samples not belonging to a certain class classified as foreign, i.e., it is a measure of the ability to discriminate against 'false' positives. In spite of the relatively good results obtained in both classification and prediction when considering the 7-PCs class-model developed from raw NIR spectra, the specificity of the model of category 1 for category 2 is 34.5%, whereas the specificity of the model of category 3 for category 2 is 10.4%, which indicates that many blends can be classified as 'false' pure varieties, leading to a high 'false' positives probability. Likewise, the observed specificity of the model of category 3 for category 1 is not neither too high (only 61.9%) which may suggest potential problems to discriminate even between pure varieties. These two parameters (sensitivity and specificity) are a very valuable diagnostic tool, since a class-model should not only accept samples belonging to the considered category but also it should reject foreign samples.

These numerical results can be also confirmed graphically. Fig. 2(a) shows the Coomans plot corresponding to the class-model computed with 7 PCs from raw NIR spectra. Bearing in mind the categories considered, the axes of the Coomans plot

Table 2  
Sensitivity and specificity values for the potential functions models constructed for categories 1 (pure *arabica*), 2 (*arabica-robusta* blends) and 3 (pure *robusta*)

PCs	Category 1		Category 2		Category 3				
	Sensitivity	Specificity for class		Sensitivity	Specificity for class				
		2	3		1	3	1	2	
Raw NIR spectra									
1	95.2	0.0	0.0	96.6	4.8	4.8	95.2	4.8	17.2
3	95.2	5.2	52.4	94.8	90.5	90.5	95.2	33.3	17.2
5	90.5	46.6	100	86.2	90.5	100	90.5	85.7	25.9
7	95.2	34.5	100	81.0	90.5	100	90.5	61.9	10.4
DOSC-corrected NIR spectra (three orthogonal-PCs removed)									
3	100	100	100	94.8	85.7	100	90.5	100	100

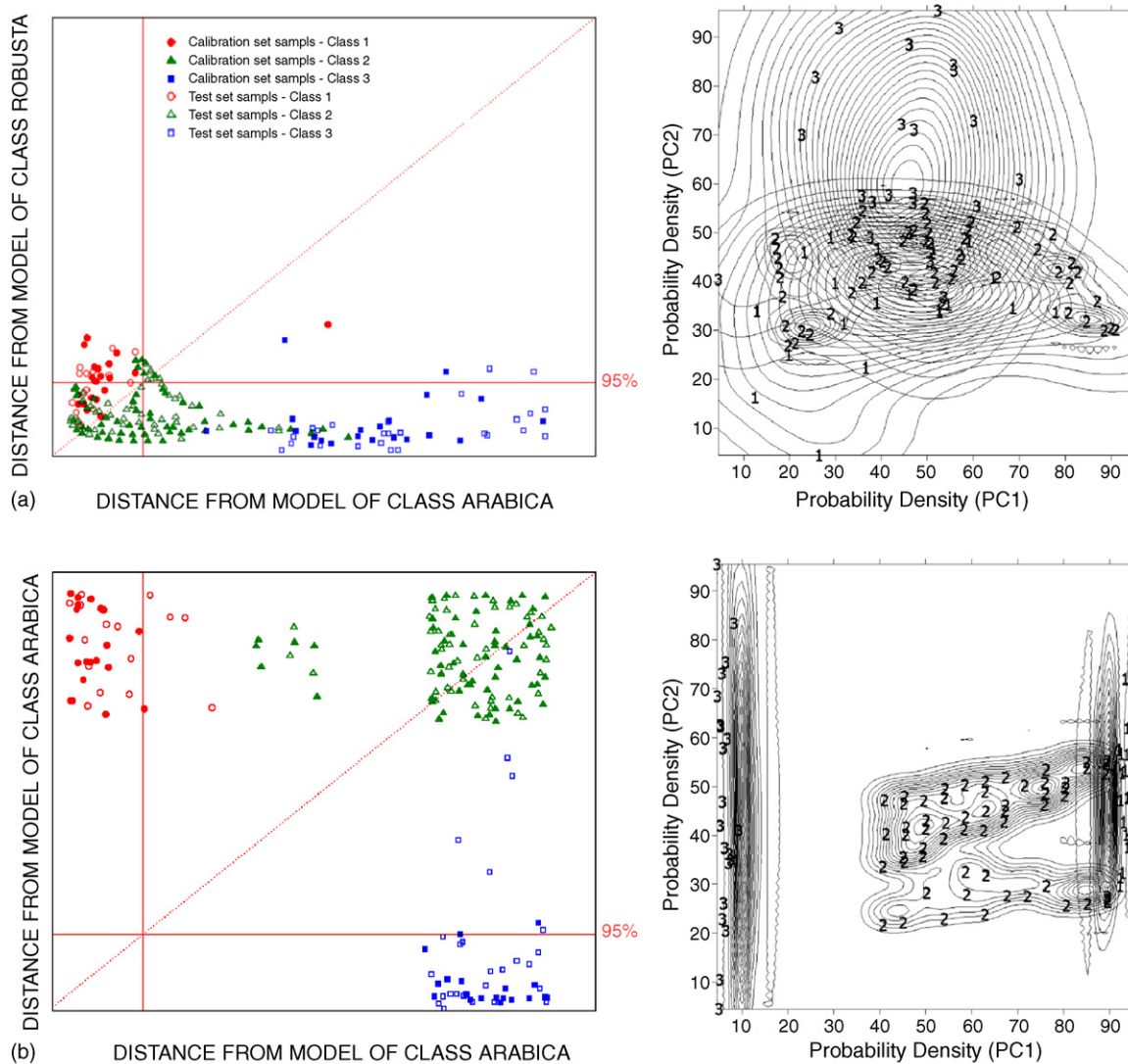


Fig. 2. Coomans and isopotential lines plots corresponding to a: (a) 7-PCs class-model developed from original NIR spectra, (b) 3-PCs class-model constructed from NIR spectra after removing three orthogonal PCs by DOSC; for the three-class problem analysed.

represent the class-models of *arabica* coffees (labelled as 1) in abscissas and *robusta* coffees (labelled as 3) in ordinates. Thus, the upper right quadrant will correspond to the samples rejected by the two models represented. In this case, the

samples expected to be located in this quadrant would be the *arabica-robusta* blends (labelled as 2). Samples contained in the test set are plotted as 0. The large number of samples plotted in the class-space common to the two models representing pure

Table 3  
Percentages of correctly classified samples

PCs	Classification (%)						External prediction (%)					
	RC1	RC2	RC3	RC4	RC5	TR	RC1	RC2	RC3	RC4	RC5	TR
Raw NIR spectra												
1	0.0 (21)	55.6 (8)	16.7 (15)	0.0 (22)	0.0 (21)	13.0 (87)	13.3 (13)	83.3 (3)	16.7 (15)	7.1 (13)	34.6 (17)	33.0 (61)
3	66.7 (7)	83.3 (3)	72.2 (5)	86.4 (3)	76.2 (5)	77.0 (23)	86.7 (2)	88.9 (2)	72.2 (5)	78.6 (3)	88.5 (3)	83.5 (15)
5	85.7 (3)	83.3 (3)	83.3 (3)	72.7 (6)	95.2 (1)	84.0 (16)	86.7 (2)	94.4 (1)	66.7 (6)	85.7 (2)	100	87.9 (11)
7	85.7 (3)	88.9 (2)	83.3 (3)	68.2 (7)	100	85.0 (15)	93.3 (1)	94.4 (1)	66.7 (6)	85.7 (2)	100	89.0 (10)
DOSC-corrected NIR spectra (three orthogonal-PCs removed)												
1	100	100	100	100	100	100	100	100	100	100	100	100

Total rate (TR) and category rates (RC1, RC2, RC3, RC4 and RC5) both in classification and external prediction, working on original and DOSC-corrected spectra. The number of samples incorrectly classified appears in brackets.



Table 4  
Sensitivity and specificity values for the potential functions models constructed for categories 1 (pure *arabica*), 2 (low *robusta* content blends), 3 (medium *robusta* content blends), 4 (high *robusta* content blends) and 5 (pure *robusta*)

PCs	Category 1					Category 2					Category 3					Category 4					Category 5									
	Sensitivity					Specificity for class					Sensitivity					Specificity for class					Sensitivity					Specificity for class				
	2	3	4	5	5	1	3	4	5	5	1	2	4	5	5	1	2	3	5	5	1	2	3	5	5	1	2	3	4	
Raw NIR spectra																														
1	95.2	0.0	0.0	0.0	0.0	100	33.3	33.3	18.2	28.5	94.4	4.8	5.6	0.00	4.8	90.9	4.8	27.8	16.7	4.8	95.2	4.8	33.3	22.2	0.0	4.8	33.3	22.2	0.0	
3	95.2	0.0	11.1	4.6	52.4	83.3	85.7	72.2	95.5	100	100	85.7	72.2	40.9	90.5	100	85.7	88.9	33.3	76.2	95.2	33.3	33.3	16.7	4.6	33.3	33.3	16.7	4.6	
5	90.5	0.0	33.3	95.5	100	83.3	90.5	77.8	100	100	94.4	100	72.2	63.6	100	86.4	100	100	55.6	100	90.5	85.7	44.4	33.3	4.5	85.7	44.4	33.3	4.5	
7	95.2	0.0	27.8	68.2	100	72.2	90.5	83.3	100	100	94.4	100	72.2	63.6	100	86.4	100	100	55.6	100	90.5	61.9	33.3	0.0	0.0	61.9	33.3	0.0	0.0	
DOSC-corrected NIR spectra (three orthogonal-PCs removed)																														
1	100	100	100	100	100	100	100	100	100	100	88.9	100	100	100	100	95.5	100	100	100	100	95.2	100	100	100	100	100	100	100	100	

varieties demonstrated a low degree of specificity of the model based on raw spectra. It deserves special attention the fact that most samples belonging to the blends category appear in this area. The potential functions method also enabled us to obtain potentials for contour plots (isopotential lines plots) considering all samples and categories to be used as an additional visualizing tool. Fig. 2(a) displays the isopotential lines plot relative to the potential functions model of the three considered categories. As can be seen, class-models did not appear clearly separated, showing a high degree of overlapping between all categories.

In sight of the numerical and graphical results derived from the analysed raw spectra based classification model, it could be stated that, despite its acceptable discrimination ability which might be considered satisfactory for differentiating between *arabica* coffees, blends and *robusta* coffees, the lack of specificity showed between classes could reveal potential problems for classification of future samples. This finding stresses the relevance of the aims pursued in the present study, i.e., trying to improve the quality of the final classification model constructed in terms of both sensitivity and specificity to enable a more accurate practical application.

In order to try to solve the already discussed specificity problems associated with models based on raw data, DOSC was applied on NIR spectra taking into account the percentage of *robusta* variety contained in each sample as response variable and varying the number of orthogonal-PCs to be removed from 1 to 5 to determine the suitable orthogonal correction degree to be applied. The corrected resulting spectra were then used to develop the respective potential functions class-models. Considering all the models based on spectra corrected by the DOSC method, it was observed that when the number of orthogonal-PCs to be removed from the raw data increased, the quality of the respective potential functions models improved significantly and their corresponding complexity decreased once each orthogonal component had been removed. Nevertheless, this gradual improvement in class-model performance was limited, and thus, the model developed after removing three orthogonal-PCs by DOSC was considered the most suitable one, since further corrections did not provide any substantial advantage. The results corresponding to the classification model finally selected expressed as correct classification and prediction rates are shown in Table 1. It can be observed that the optimal class-model constructed after the removal of three orthogonal-PCs not only reduced the model complexity to only three components (explaining almost the 100% of the variance in the data), but also exhibited excellent results in both classification and prediction. It must be particularly underlined the great improvement achieved in terms of sensitivity, and more remarkably concerning specificity between categories (Table 2). Coomans and isopotential lines plots showed in Fig. 2(b) also confirmed the high quality of the classification model developed from DOSC-corrected NIR spectra for discrimination between pure coffee varieties and blends. Both plots showed a high degree of interclass specificity and a patently clear separation between class-models, considerably improved with regard to that provided by the model constructed from raw spectra.



### 3.2. Five-class approach

At this point, and without underestimating the very good results obtained in the first part of the study when considering only three separate categories to deal with the problem of varietal classification for coffee authenticity, we decided to study the same problem in more depth considering a higher number of a priori defined categories by limiting the qualitative requirements to be met for belonging to a certain class. The increase in the number of considered categories was aimed at discriminating, at least roughly between several degrees of *robusta* contents in a blend.

In this way, five separate categories were defined: (1) pure *arabica* coffees; (2) blends with a low *robusta* content; (3) blends with a medium *robusta* content; (4) blends with a high *robusta* content; (5) pure *robusta* coffees. The 191 total roasted coffee samples were split randomly into calibration (21 *arabica* coffees; 18 low *robusta* content blends; 18 medium *robusta* content blends; 22 high *robusta* content blends; 21 *robusta* coffees)

and test (15 *arabica* coffees; 18 low *robusta* content blends; 18 medium *robusta* content blends; 14 high *robusta* content blends; 26 *robusta* coffees).

Table 3 shows the results in both classification and prediction (expressed as percentages of correctly classified samples) provided by the potential functions class-models developed from raw spectra, varying the number of PCs computed in the model development from 1 to 7 for the five-class problem studied. Table 4 summarised the results corresponding to the same class-models in terms of sensitivity and specificity percentages. Taking into account the numerical results collected in these tables, several conclusions can be drawn about the classification models developed from raw NIR spectra. Even though when a large number of PCs were used in the model construction (e.g. 7 PCs explaining for the 99.99% of the variance in the system), the fact of dividing the category of *arabica-robusta* blends (which initially has a 'global' nature) into three sub-categories according to the greater or lesser *robusta* content of samples gave rise to a notable worsening of the quality of the final classification

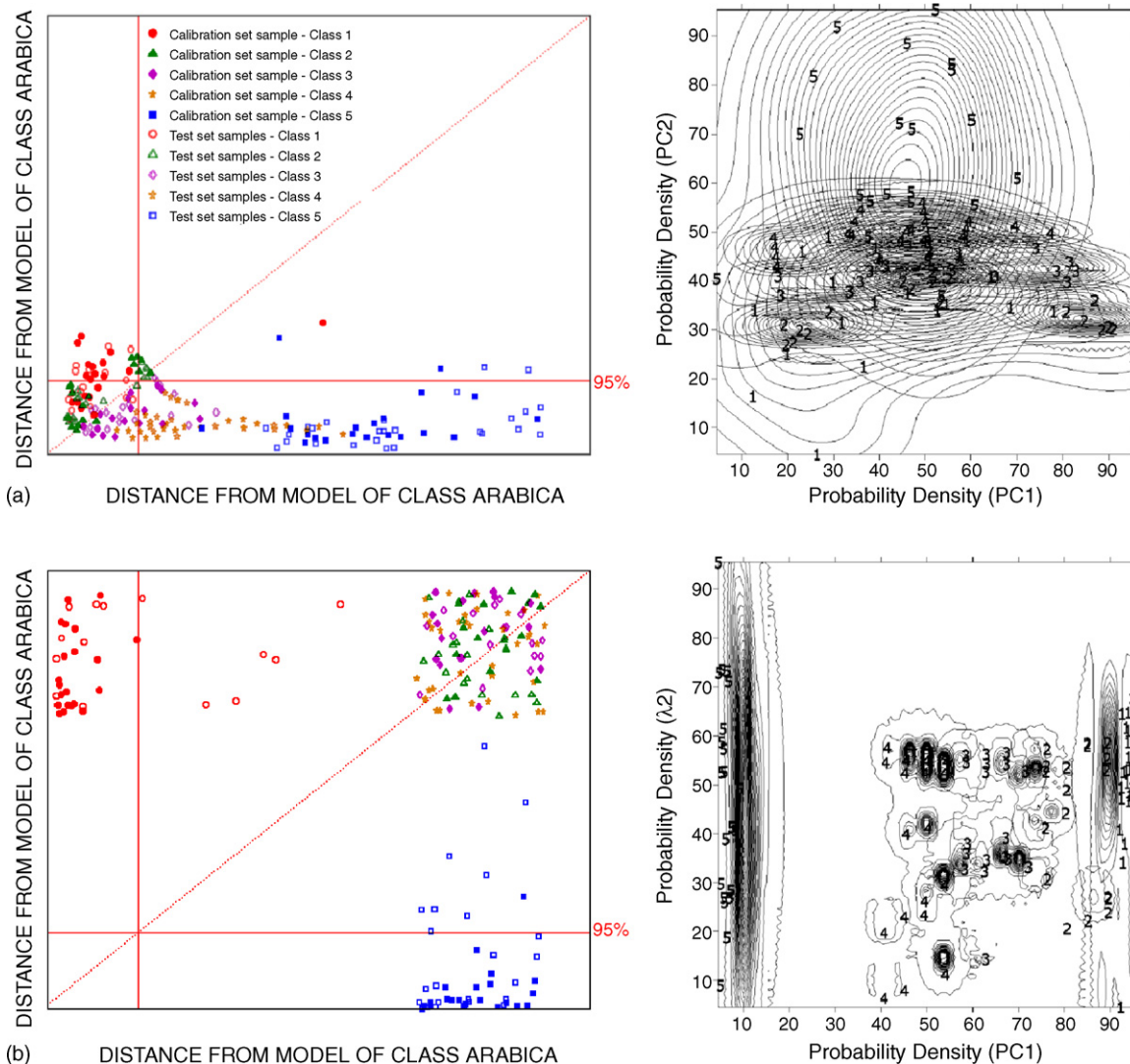


Fig. 3. Coomans and isopotential lines plots corresponding to: (a) 7-PCs class-model developed from raw NIR spectra, (b) 1-PC class-model constructed from NIR spectra after the removal of three orthogonal PCs by DOSC; for the five-class problem studied.

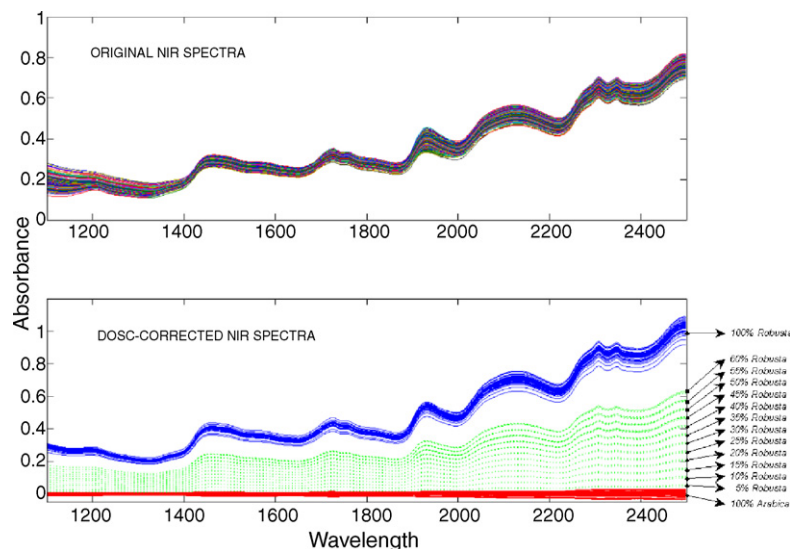


Fig. 4. Spectra of the 191 samples contained in the roasted coffee data set: (a) without pre-treatment and (b) after applying DOSC.

model. The category and total rates decreased appreciably in both calibration and prediction (particularly in the case of blends of medium and high *robusta* content), and the obtained specificity values between categories indicated an even higher risk of ‘false’ positives than in the case of only considering three classes. Fig. 3(a) show the Coomans plot and the isopotential lines plot corresponding to the 7-PCs potential functions model developed from raw data to discriminate between the five analysed categories. Again, in the Coomans plot, the class-model of *arabica* coffees (1) was represented in abscissas and the class-model of *robusta* coffees (5) was plotted in ordinates, so samples expected to be rejected by both displayed class-models (i.e., coffee blends belonging to categories 2, 3 and 4) should appear in the upper right quadrant. As in the previous case, external test samples are labelled as 0. From the samples distribution observed in the Coomans plot, it can be concluded that the model constructed on the basis of raw spectra was not able to neatly separate the five categories. The extremely strong overlapping between the five classes showed in the isopotential lines plot confirmed the serious lack of specificity of the model and its unsuitability to ensure an accurate classification.

Notably improved results were yielded by the potential functions model constructed after the application of DOSC pre-processing method on NIR spectra considering the *robusta* content in each sample as response variable to be used in the orthogonal correction (once selected the optimal number of orthogonal-PCs to be subtracted). As can be seen, the finally selected classification model developed after removing three orthogonal-PCs (we decided not to perform more exhaustive corrections because they did not provide any appreciable improvement in terms of model quality) and with the minimum complexity (only 1 PC explaining the 99.99% of the variance in the spectral data) not only provided 100% correct classifications in both calibration and prediction (Table 3), but also a great specificity between the five considered classes (Table 4), visually confirmed in Coomans and isopotential lines plot (Fig. 3(b)). Obviously, a slight longitudinal overlapping mainly between the

three categories dealing with *arabica-robusta* blends, which can be observed in the isopotential lines plot, was not only expected but logical, due to the narrow margin that existed between the quantitative limits defining each one of these qualitative categories of blends.

### 3.3. Spectral profiles

The main objective of the present study was focused on minimising certain physical light effects that occur inherently in diffuse reflectance near-infrared spectroscopy, to develop improved classification models for coffee varietal authentication purposes.

The results obtained and discussed in this study, in both approaches analysed, have already demonstrated the practical usefulness and efficiency of applying an orthogonal signal correction method prior to the development of a high quality classification model. Nevertheless, a visual comparison between NIR spectral profiles before and after applying the orthogonal correction on roasted coffee NIR spectra (Fig. 4) can contribute to additionally show up the goodness of the strategy used here. A clear distinction is observed between the DOSC pre-treated spectra, but not for the original spectra, in such a way that corrected spectral profiles appeared perfectly grouped according to the particular percentage of *robusta* coffee contained in samples. Since DOSC method was applied directly on raw spectra (no pre-treatment was previously performed on data), it works as a kind of background subtraction: for the *arabica* coffee (0% *robusta* content), the spectrum is filtered away.

## 4. Conclusions

The results reported in this study have demonstrated that the combination of near-infrared spectroscopy with an orthogonal signal correction method and with a powerful class-modelling technique, such as potential functions method can be used as an optimal strategy not only for discriminating between *arabica* and *robusta* pure coffee varieties, but also for differentiating

between pure varieties and blends of the two species, even when separate categories of blends were defined depending on the actual robusta content in samples. In both cases studied (varying the number of separate categories to be considered) a very substantial improvement in the global quality of the finally constructed class-model (particularly in terms of specificity between classes) was achieved in comparison with the respective model developed from original NIR spectra. The applied strategy did not imply any additional reference analysis, since the response variable to be considered in the orthogonal signal correction was precisely the percentage of *robusta* coffee in each sample (already known for calibration samples). Therefore, the applied classification strategy only relied on NIR measurements. This fact, together with the great results obtained, could make it very suitable for use in authenticity assessment of coffee. It should, however, be noticed that the work here presented is only a feasibility study, so further studies are required to properly evaluate its actual performance.

### Acknowledgements

The authors thank the Ministry of Science and Technology (Project No. 2FD1997-0491), the Autonomous Government of La Rioja – *Consejería de Educación, Cultura, Juventud y Deportes* (Project No. ACPI2000/08) and the University of La Rioja (Research grant FPI-2001) for their financial support, as well as Professor Michele Forina for providing us with the last version of Parvus package.

### References

- [1] M. Lees (Ed.), *Food Authenticity and Traceability*, Woodhead Publishing Ltd., Cambridge, UK, 2003.
- [2] C. Cordella, I. Moussa, A.C. Martel, N. Sbirrazzuoli, L. Lizzani-Couvelier, *J. Agric. Food Chem.* 50 (2002) 1751.
- [3] M.J. Martin, F. Pablos, A.G. Gonzalez, *Food Chem.* 66 (1999) 365.
- [4] C.P. Bicchì, M.P. Ombretta, G. Pellegrino, A.C. Vanni, *J. Agric. Food Chem.* 45 (1997) 4680.
- [5] M.J. Martin, F. Pablos, A.G. Gonzalez, *Talanta* 46 (1998) 1259.
- [6] M.J. Martin, F. Pablos, A.G. Gonzalez, M.S. Valdenebro, M. Leon-Camacho, *Talanta* 54 (2001) 291.
- [7] F. Carrera, M. Leon-Camacho, F. Pablos, A.G. Gonzalez, *Anal. Chim. Acta* 370 (1998) 131.
- [8] N. Frega, F. Bocci, G. Lercker, *Industrie Alimentari* 34 (1995) 705.
- [9] S. Casal, M.R. Alves, E. Mendes, M.B.P.P. Oliveira, M.A. Ferreira, *J. Agric. Food Chem.* 51 (2003) 6495.
- [10] A.G. Gonzalez, F. Pablos, M.J. Martin, M. Leon-Camacho, M.S. Valdenebro, *Food Chem.* 73 (2001) 93.
- [11] G. Downey, *J. Near Infrared Spectrosc.* 4 (1996) 47.
- [12] D.G. Evans, C.N.G. Scotter, L.Z. Day, M.N. Hall, *J. Near Infrared Spectrosc.* 1 (1993) 33.
- [13] B.G. Osborne, B. Mertens, M. Thompson, T. Fearn, *J. Near Infrared Spectrosc.* 1 (1993) 77.
- [14] P.J. Gemperline, L.D. Webber, F.O. Cox, *Anal. Chem.* 61 (1989) 138.
- [15] U.G. Indahl, N.S. Sahni, B. Kirkhus, T. Næs, *Chemom. Intell. Lab. Syst.* 49 (1999) 19.
- [16] K.I. Hildrum, T. Isaksson, T. Næs, A. Tandberg, *Near Infra-Red Spectroscopy. Bridging the Gap Between Data Analysis and NIR Applications*, Ellis Horwood, Chichester, 1992.
- [17] M.J. Sáiz-Abajo, J.M. González-Sáiz, C. Pizarro, *J. Agric. Food Chem.* 52 (2004) 7711.
- [18] G. Downey, J. Boussion, D. Beauchêne, *J. Near Infrared Spectrosc.* 2 (1994) 85.
- [19] G. Downey, J. Boussion, *J. Sci. Food Agric.* 71 (1996) 41.
- [20] G. Downey, R. Briandet, R.H. Wilson, E.K. Kemsley, *J. Agric. Food Chem.* 45 (1997) 4357.
- [21] I. Esteban-Díez, J.M. González-Sáiz, C. Pizarro, *Anal. Chim. Acta* 514 (2004) 57.
- [22] J.A. Westerhuis, S. de Jong, A.K. Smilde, *Chemom. Intell. Lab. Syst.* 56 (2001) 13.
- [23] D. Coomans, I. Broeckart, *Potential Pattern Recognition in Chemical and Medical Decision-Making*, Research Studies Press, Letchworth, 1986.
- [24] M. Forina, C. Armanino, R. Leardi, G. Drava, *J. Chemom.* 5 (1991) 435.
- [25] D.L. Massart, L. Kaufman, *The Interpretation of Analytical Chemical Data by the Use of Cluster Analysis*, Wiley, New York, 1983.

## Novel oxygen sensitive complexes for optical oxygen sensing

J.F. Fernández-Sánchez<sup>a,b,\*</sup>, T. Roth<sup>b</sup>, R. Cannas<sup>b</sup>, Md. K. Nazeeruddin<sup>c</sup>,  
S. Spichiger<sup>b</sup>, M. Graetzel<sup>c</sup>, U.E. Spichiger-Keller<sup>b</sup>

<sup>a</sup> Department of Analytical Chemistry, Faculty of Science, University of Granada, C/Fuentenueva s/n, E-18071 Granada, Spain

<sup>b</sup> Centre for Chemical Sensors, Swiss Federal Institute of Technology Zurich (ETHZ), Technoparkstrasse 1, CH-8005 Zürich, Switzerland

<sup>c</sup> Laboratory for Photonics and Interfaces, Institute of Chemical Sciences and Engineering, Ecole Polytechnique Fédérale de Lausanne, CH-1015 Lausanne, Switzerland

Received 7 December 2005; received in revised form 16 March 2006; accepted 23 March 2006

Available online 2 May 2006

### Abstract

Novel optical sensing films for oxygen based on highly luminescent iridium (III) and ruthenium (II) complexes have been developed. These demonstrate excellent long-term photostability (several months) when incorporated into polystyrene membranes. The influence of different plasticizers on the specific luminescence quantum yield, the Stern–Volmer constant, the reversibility and the response time were evaluated. Additionally the sensing films can be sterilized by chemical cleaning and gamma-ray irradiation.

© 2006 Elsevier B.V. All rights reserved.

**Keywords:** Optical sensor; Luminescence; Oxygen; Ruthenium complex; Iridium complex; Sterilization

### 1. Introduction

Molecular oxygen is one of the most important gases in our environment since it is found as either a reactant or a product in a vast number of chemical and biochemical reactions. Thus, the determination of oxygen is important in various fields of chemical and clinical analysis, packaging, process control, as well as in environmental monitoring [1–9].

Several oxygen detection systems have been reported based on redox titration [10], polarography [11] or measuring the chemiluminescence intensity [12]. To date, the Clark electrode and its modifications [11,13], which are based on the electrochemical-reduction of O<sub>2</sub> on a polarized cathode, have been among the most widely used O<sub>2</sub> detectors. Some limitations of Clark electrodes, such as the consumption of O<sub>2</sub> and their relatively long response times, are well known. Chemical instabilities were reported by Choi et al. [14] and Hartmann et al. [15]. In summary, the oxygen electrode is limited by the stability of the electrode surface and by instabilities in the oxygen diffusion barrier [16].

The Clark electrode is the most reliable oxygen-sensitive sensor and traditionally used in medicine as well as for process control in bioreactor processes. In the latter application, the electrode is sterilized along with the bioreactor itself. The Clark electrode is, however, not suitable as a disposable sensor. Therefore, a variety of optical devices and sensors have been developed to measure molecular oxygen [17]. The advantages of these optical sensors based on luminescence quenching are basically that they do not consume O<sub>2</sub> during the analytical process, they do not require reference electrodes and they are inert against sample flow rate or stirring speed [18]. Moreover, they are immune to exterior electromagnetic field interference and can be produced as disposable sensors. The latter two properties are especially attractive for the use of these sensors in biotechnology and disposable bioreactors [19,20].

These optical devices are based on the luminescence quenching of organometallic complexes by paramagnetic oxygen [17,21–23]. Table 1 shows an overview of luminescence probes used for analyzing oxygen. On the other hand, Nazeeruddin et al. [35] introduced two new iridium dyes, [Ir(ppy)<sub>2</sub>(NCS)<sub>2</sub>]<sup>+</sup> (N-833) and [Ir(ppy)<sub>2</sub>(CN)<sub>2</sub>]<sup>+</sup> (N-837) (ppy = 2-phenylpyridine) for developing organic light emitting diodes, which exhibit unprecedented luminescence quantum yields (97 ± 3%) with excited-state lifetimes of 1–3 μs in Argon-degassed dichloromethane solutions at 298 K, reduced to 70–90 ns in air-equilibrated

\* Corresponding author. Tel.: +34 958248593; fax: +34 958249510.  
E-mail address: [jffernan@ugr.es](mailto:jffernan@ugr.es) (J.F. Fernández-Sánchez).

Table 1  
Overview of luminescence probes used for analyzing oxygen

Probe	Support for immobilization	$\lambda_{\text{exc/em}}$ (nm)	$\Phi_{\text{L}}$	$I_0/I_{100}$	Reference
Pyrene-1-butylic acid	Poly(dimethylsiloxane)	365/396		1.5	[24]
Ru(dpp) <sub>3</sub> <sup>2+</sup>	Silicone	457/610	0.5	4.4	[17]
	Polystyrene	457/610	0.5	1.1	[17]
	PVC	457/610	0.5	3.5	[17]
	Poly(dimethylsiloxane)	457/610	0.5	4.5	[17]
Re(I)L(CO) <sub>3</sub> CN <sup>+</sup>	L = bpy	250/448	0.59	2.2	[25]
	L = phen	232/458	0.77	5.4	[25]
	L = Me4phen	274/462	0.68	41.0	[25]
Os(dpp) <sub>3</sub> <sup>2+</sup>	Poly(dimethylsiloxane)	502/729	–	4.5	[26]
Ir(ppy) <sub>3</sub>	Polystyrene	376/512	–	15.3	[27]
Platinum(II) octaethylporphyrin	Polystyrene	535/646	–	4.5	[28]
Platinum(II) tetrakis(pentafluorophenyl) porphyrin	Polystyrene	508/648	–	3.0	[29]
Platinum(II) octaethyl porphine ketone	PVC	592/758	0.01	2.0	[30]
	Polystyrene	586/758		20.0	[31]
Palladium(II) octaethylporphyrin	Polystyrene	546/663	0.12	11.5	[32]
Palladium(II) octaethyl porphine ketone	PVC	602/790	0.01	8.0	[30]
	Polystyrene	602/790		28.0	[31]
Aluminum tetraphenoxo PcOH	Polystyrene	606/705	–	1.0	[33]
(dppe)Pt{S <sub>2</sub> C <sub>2</sub> (CH <sub>2</sub> CH <sub>2</sub> N-2-pyridinium)	Cellulose acetate	470/710	0.01	2.5	[19]
Aluminum ferron	Sol gel (TMOS and MTMOS)	380/5/80	–	5.0	[34]
ETH <sup>T</sup> 3003	Polystyrene	460/620	0.19	3.5	This work
N-926	Polystyrene	400/526	0.80	2.4	This work
N-833	Polystyrene	402/529	0.60	1.3	This work
N-837	Polystyrene	398/528	0.38	1.8	This work

*Abbreviations:* dpp = 4,7-diphenyl-1,10-phenanthroline; bpy = 2,2'-bipyridine; phen = 1,10-phenanthroline; Me<sub>4</sub>phen = tetramethyl-1,10-phenanthroline; t-Bu = tetrabutyl; ppy = 2-phenylpyridine anion; PcOH = phthalocyanine hydroxide; dppe = 1,2-bis(diphenylphosphino)ethane; ferron = 8-hydroxy-7-iodo-5-quinolinesulfonic acid; TMOS = tetramethoxysilane; MTMOS = methyltrimethoxysilane.

dichloromethane solutions. The use of high luminescence quantum yield compounds as potential oxygen sensors may reduce the sensitivity for scattering interferences, thus permitting the use of less sensitive detectors in the development of optical oxygen sensors.

In this paper, we propose the lipophilization of [Ru(dpp)<sub>3</sub>]<sup>2+</sup> to achieve a higher lipophilicity of the compound and more options for homogenous incorporation into various polymers. The lipophilicity generally improves the retention of the organometallic complex (OMC) in very apolar polymer films, such as those used for chemical sensing. Thus, we describe the synthesis, characterization and analytical investigations of a more lipophilic ruthenium complex, called ETH<sup>T</sup> 3003 (tris(4,7-bis(4-octylphenyl)-1,10-phenanthroline) ruthenium (II) bis(perchlorate) monohydrate, Ru(8-dpp)(ClO<sub>4</sub>)<sub>2</sub>).

In addition, we also propose the two high-luminescence quantum-yield iridium complexes, which were described by Nazeeruddin et al. [35], tetrabutylammonium bis(isothiocyanato) bis(2-phenylpyridinyl)-iridium (III) (N-833), and tetrabutylammonium bis(cyanide) bis(2-phenylpyridinyl)-iridium (III) (N-837) and a novel more lipophilic iridium complex N-926 (bis(2-phenylpyridinyl)-*N,N,N,N*-tetramethyl-(4,4'-diamine-2,2'-bipyridinyl)-iridium (III) chloride) as oxygen-sensitive compounds (see Fig. 1).

The metal complexes are incorporated into polystyrene (PS), plasticized with and without the plasticizers *o*-nitrophenyl octyl

ether (*o*-NPOE) and *o*-cyanophenyl octyl ether (*o*-CPOE), which can be used as oxygen-sensitive compounds. PS was used to give mechanical strength to the films and to permit their sterilization by heating. Both, the use of PS and the more lipophilic complexes make the sensing layers more useful in the determination of oxygen: if the sensing films are applied to liquids, leaching of the dye is reduced and the metal center, which complexes the ligands, is shielded from attacks by such media as ligand exchange, and reducing and oxidizing compounds [36].

The crystal structure of the [Ru(dpp)<sub>3</sub>]<sup>2+</sup> was investigated by X-ray analysis. The XRD-structure of ETH<sup>T</sup> 3003 is shown in Fig. 2. Optical sensing films based on these compounds have high luminescence quantum yields, fast responses, high photostability and large Stokes' shifts. In view of the potential applications in bioreactors, the fact that the sensors can be sterilized by chemical cleaning and gamma irradiation makes them especially attractive. In the following section their use fullness for biotechnological applications is demonstrated.

## 2. Experimental

### 2.1. Chemicals and reagents

For the synthesis of ETH<sup>T</sup> 3003, the following chemicals were used: sodium *m*-nitrobenzenesulfonate (Fluka, pract.)



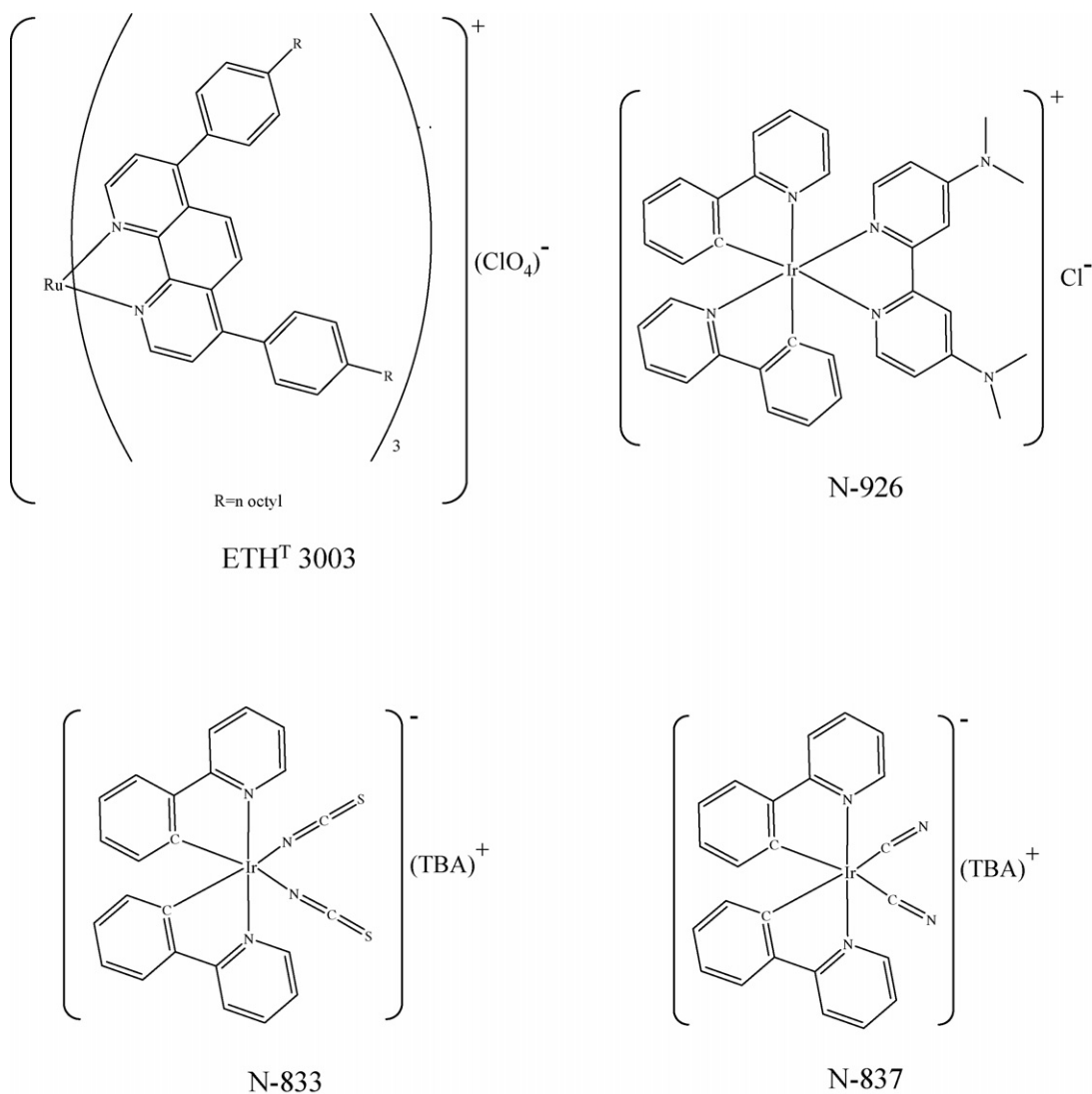


Fig. 1. Chemical structures of the metal complexes used in this study.

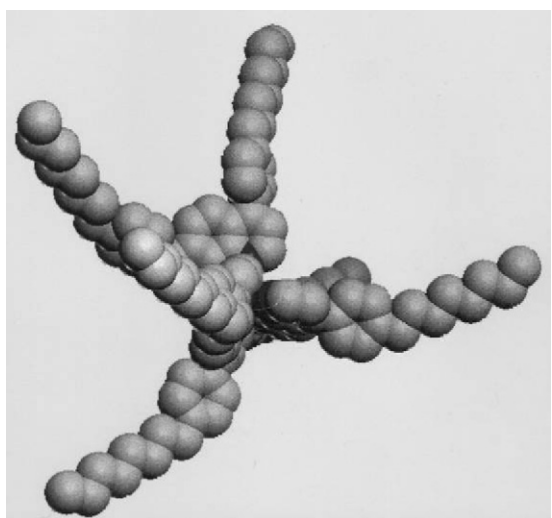


Fig. 2. Structure of ETH<sup>T</sup> 3003 calculated with the software package Sybyl based on the crystal structure of [Ru(dpp)<sub>3</sub>]<sup>2+</sup>; ETH<sup>T</sup> 3003 is the octyl-derivate of [Ru(dpp)<sub>3</sub>](ClO<sub>4</sub>)<sub>2</sub>. The two perchlorate ions have been omitted.

ruthenium trichloride monohydrate, 3-chloropropionylchloride (both from Fluka, purum), *n*-octylbenzene, aluminium trichloride, anhydrous zinc chloride, 1,2-phenylenediamine, carbon disulfide, ethanol, and hexamethylphosphoramide (all from Fluka, puriss.).

For the preparation of the membranes, synthesized dyes were used as well as chloroform (Fluka), Rhodamine 101 (Fluka), polystyrene (Scientific Polymers, USA), *o*-nitrophenyl octyl ether and *o*-cyanophenyl octyl ether (both from Fluka, puriss.). The gas flow-system was supplied by 50 L gas bottles at 200 bars with nitrogen 60 and oxygen 55 (both from Carbagas, Switzerland).

## 2.2. Synthesis of ETH<sup>T</sup> 3003

The synthesis of ETH<sup>T</sup> 3003 is a three-step synthesis (see Fig. 3). The first step is a *Friedel–Crafts* reaction [37]. The next step is, according to Skraup, similar to the method proposed by Hiti and Young [38], which is a standard procedure [39].

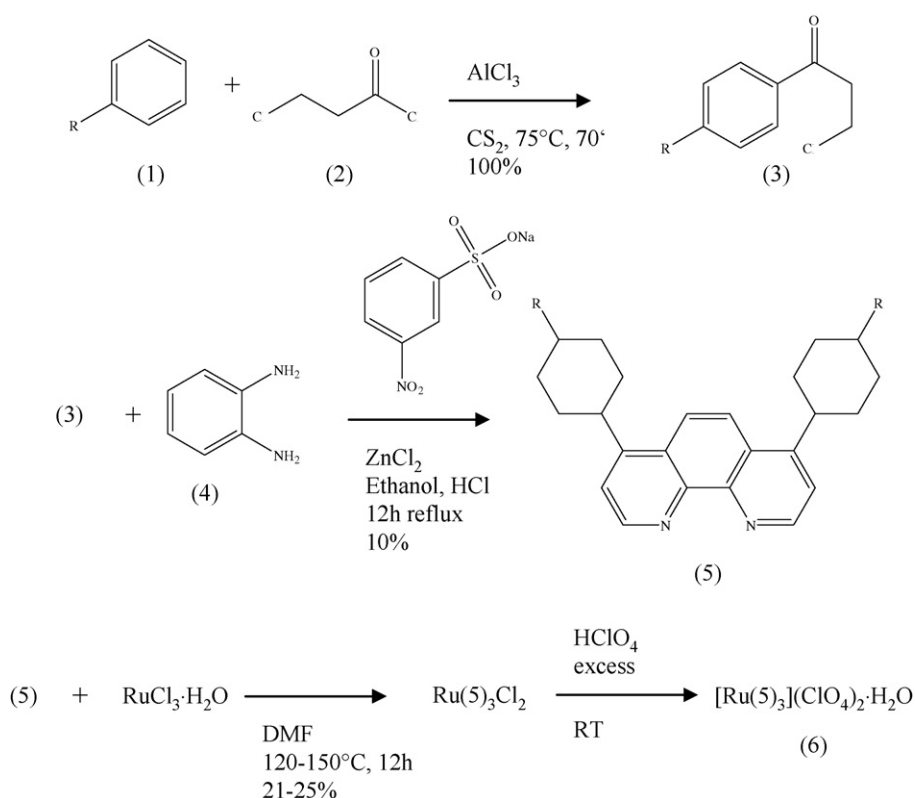


Fig. 3. Synthesis of the ETH<sup>T</sup> 3003 dye (R = *n*-octyl).

A solution of 29.8 g (156.6 mmol, 34.8 mL,  $M_r$  190.32) *n*-octylbenzene (**1**) in 90 g (71.3 mL) of carbon disulfide was first well stirred and then 21.9 g (164.1 mmol,  $M_r$  133.34) of aluminium trichloride were added. The resulting suspension was put under argon. A solution of 22.62 g (178.8 mmol,  $M_r$  126.97) 3-chloropropionyl chloride (**2**) in 5 mL carbon disulfide was added dropwise for 20 min. The resulting yellow solution was refluxed for 20 min at 75 °C. The mixture was cooled and poured onto 150 g ice in 150 mL concentrated hydrochloric acid. The organic phase for the subsequent extraction with ethylacetate were joined and washed twice with 200 mL 2 M NaOH each and once with saturated brine, dried over MgSO<sub>4</sub> and the solvent evaporated under vacuum. Upon standing, the residue quickly solidified, yielding 40.81 g (0.16 mol, 100%) of (2-chloroethyl)-(4-octylphenyl)ketone (**3**) as a plate yellow powder,  $R_f$  0.84 (hexane/ethylacetate, 6:4; developed with sulfuric acid/vanillin, yielding olive-green spots), m.p. 51–52 °C (Found: C, 72.65%; H, 8.91%. C<sub>17</sub>H<sub>25</sub>OCl with  $M_r$  280.83 requires C, 72.71%; H, 8.9%).

A nearly white suspension of 1.40 g (13.0 mmol,  $M_r$  108.14) 1,2-phenylenediamine (**4**), 7.42 g (33.0 mmol,  $M_r$  212.15) sodium *m*-nitrobenzenesulfonate and 492 mg (3.6 mmol,  $M_r$  136.28) anhydrous zinc chloride was made in 50 mL ethanol at 60 °C. Half a solution of 6.68 g (23.8 mmol,  $M_r$  280.83) (**3**) in 30 mL EtOH was added, to A, resulting in a yellow color. Through a second funnel 9.8 mL of concentrated hydrochloric acid were added to the reaction mixture, which then turned orange-red. After adding the other half of (**3**),

the solution was refluxed for 12 h. After 24 h of further stirring at room temperature, the solvent was removed in vacuo and the residue suspended in a mixture of 100 mL concentrated aqueous ammonia and 75 mL dichloromethane. The organic phase was separated and the remaining aqueous phase extracted a second time with dichloromethane. The pooled organic phases were washed with saturated brine and concentrated at reduced pressure. An orange-brown oil resulted, which was chromatographed on silica gel (gradient of hexane/pyrrolidine, 9:1 to hexane/ethylacetate/pyrrolidine, 6:3:1). After fraction collection and five-fold recrystallization from pure hexane 0.67 g (1.2 mmol, 5% with respect to (**3**)), 4,7-bis(4-octylphenyl)-1,10-phenanthroline (**5**) were produced as a beige, amorphous mass,  $R_f$  0.10 (hexane/pyrrolidine, 9:1 on UV<sub>254</sub>), m.p. 71–72 °C (Found: C, 86.26%; H, 8.63%; N, 5.10%. C<sub>40</sub>H<sub>48</sub>N<sub>2</sub> with  $M_r$  556.83 requires C, 86.28%; H, 8.69%; N, 5.03%).

<sup>1</sup>H NMR (CDCl<sub>3</sub>, 200 MHz): 9.22 (d,  $J$  = 5 Hz, 2H), 7.90 (s, 2H), 7.58 (d,  $J$  = 5 Hz, 2H), 7.45 (d,  $J$  = 8 Hz, 4H), 7.34 (d,  $J$  = 8 Hz, 4H), 2.72 (t,  $J$  = 7.7 Hz, 4H), 1.78–1.60 (m, 4H), 1.44–1.24 (m, 20H), 0.98 (t,  $J$  = 6.6 Hz, 6H).

<sup>13</sup>C NMR (CDCl<sub>3</sub>, 50 MHz): 149.9 (d), 148.6 (s), 147.1 (s), 143.6 (s), 135.3 (s), 129.7 (d), 128.8 (d), 126.6 (s), 124.1 (d), 123.6 (d), 35.7 (t), 31.9 (t), 31.4 (t), 29.4 (t), 29.3 (t), 29.2 (t), 22.6 (t), 14.1 (q).

A suspension of 429 mg (0.77 mmol,  $M_r$  556.83) (**5**) and 88 mg (0.39 mmol,  $M_r$  225.44) ruthenium trichloride monohydrate in 6 g (6.3 mL) dimethylformamide was stirred overnight

at 120–150 °C. This results in an intensely orange-colored solution. After the mixture was allowed to cool to ambient temperature, it was dissolved in 50 mL acetone and 7 mL of 70% perchloric acid were added. After standing for 12 h, the solvent was evaporated, leaving the crude products as a dark, viscous oil. Three subsequent chromatographic separations on aluminium oxide (neutral, activity III, with at least a 100-fold excess of aluminium oxide with respect to the raw product, eluant: ethylacetate/hexane/triethylamine 9:1:1, UV<sub>254</sub>) yielding 116 mg (0.18 mmol, 21–25% with respect to (5)) of ETH<sup>T</sup> 3003 (6) as an orange powder, *R<sub>f</sub>* 0.15–0.3 (hexane/ethylacetate/triethylamine, 2:9:1.7 at UV<sub>366</sub> smears, orange luminescence) (Found: C, 72.47%; H, 7.34%; N, 4.18%; O, 7.29%. C<sub>120</sub>H<sub>144</sub>N<sub>6</sub>O<sub>8</sub>RuCl<sub>2</sub> with *M<sub>r</sub>* 1970.47 requires C, 72.48%; H, 7.40%; N, 4.23%; O, 7.24%).

<sup>1</sup>H NMR (CDCl<sub>3</sub>, 300 MHz): 8.47 (d, *J* = 5.6 Hz, 6H), 8.24 (s, 6H); 7.82 (d, *J* = 5.6 Hz, 6H); 7.55 (d, *J* = 8.1 Hz, 12H); 7.35 (d, *J* = 8.1 Hz, 12H); 2.69 (t, *J* = 7.7 Hz, 12H); 1.67 (m, 12H); 1.42–1.20 (m, 60 H); 0.88 (t, *J* = 7 Hz, 18H).

<sup>13</sup>C NMR (CDCl<sub>3</sub>, 75 MHz): 153.2 (d); 149.1 (s); 148.5 (s); 146.0 (s); 133.1 (s); 130.2 (d); 129.3 (d); 128.8 (s); 127.2 (d); 126.1 (d); 35.8 (t); 31.9 (t); 31.4 (t); 29.5 (t); 29.4 (t); 29.3 (t); 22.7 (t); 14.1 (q).

The synthesis of Iridium dyes was carried out following the procedure described by Nazeeruddin et al. [35].

### 2.3. Membrane preparation and characterization

The cocktails were prepared in sealable 4 mL flasks. Compounds were weighed into the flask on an AT 261 balance (Mettler-Toledo, Greifensee, Switzerland) with ±0.01 mg precision. They were then filled up to 2 mL solution volume with chloroform. Table 2 shows the composition and the nomenclature of the different cocktails, which were shaken on an IKA-Vibramax-VXR (IKA-Labortechnik, Staufen, Germany) until all components were dissolved. The membranes were obtained using a spin-coating technique. An amount of 0.3 mL of the cocktail was injected onto a rotating glass plate of a spinning device [40]. The resulting layers showed a thickness between 2 and 7 μm, depending on the rotational speed and viscosity of the polymer mixture.

A standard protocol was used for characterizing the membranes. Then standard settings for all the experiments were:

Table 2  
Nomenclature and composition of the oxygen-sensitive membranes

Name	wt.% PS	Plasticizer		wt.% dye
		Kind	% Plasticizer	
PS0X	98.6	–	0	1.4
PS1XC	83.6	<i>o</i> -CPOE	15	1.4
PS2XC	68.6	<i>o</i> -CPOE	30	1.4
PS1XN	83.6	<i>o</i> -NPOE	15	1.4
PS2XN	68.6	<i>o</i> -NPOE	30	1.4

PS, polystyrene; *o*-CPOE, *o*-cyanophenyl octyl ether; *o*-NPOE, *o*-nitrophenyl octyl ether.

excitation slit 2.5 nm wide, emission slit 5.0 nm wide, excitation wavelengths of 400 nm for N-926, 402 nm for N-833, 398 nm for N-837 and 460 nm for the ruthenium complex, emission wavelengths of 526 nm for N-926, 529 nm for N-833, 528 nm for N-837 and 620 nm for ETH<sup>T</sup> 3003, with the 515 nm cut-off filter in place and a flow-rate of 200 mL min<sup>-1</sup>.

To obtain the Stern–Volmer Plot (SVP), the oxygen partial pressures were calculated from the measured oxygen/nitrogen flows, assuming a constant environmental pressure of 1000 mbar. Intensity measurements were made at 14 different oxygen partial pressures between 0 and 1 bar.

All the measurements were carried out in triplicate to evaluate the error. The experimental results were expressed as the average of three replicas ± error (*st*/√*n*), where *s* is the standard deviation, *t* the student *t* and *n* the number of replicas.

### 2.4. Instrumentation

All luminescence measurements were carried out on a Perkin-Elmer LS-50B luminescence spectrometer. This was fitted with a xenon flash lamp and a Hamamatsu R-928 red-sensitive photomultiplier, which has ±1 nm accuracy by the specified wavelength and ±0.5 nm reproducibility of wavelength, in the way usual for solid samples with a 30°/60° excitation/emission geometry. A self-built flow-through cell was used in all the experiments [36].

A gas-handling system was designed to control the gas composition, copper and stainless steel tubing were used up to the flow-through cell. For gas mixing, two mass flow controllers of Type 1179 from MKS Instruments (Andover, MA, USA) were used. After the mass flow controlled, stainless steel tubing was used up to the mixing T-union and to the two-fold solenoid valve from Cole-Parmer Instrument Company (Vernon Hills, IL, USA).

The system was controlled by a self-written LabVIEW 5.1 program connected to a National Instrument card with RS-232 interface, which fully controls the PE LS-50B via the serial interface and the MKS mass flow controllers via RS-485.

## 3. Results and discussion

### 3.1. Crystal structure of ETH<sup>T</sup> 3003

The crystal structure [Ru(dpp)<sub>3</sub>]<sup>2+</sup> was determined by Goldstein et al. [41]. They claim that [Ru(dpp)<sub>3</sub>]<sup>2+</sup> forms an orthorhombic system of the space group *Pbca* with the dimensions *a* = 13.085(2) Å, *b* = 24.173(1) Å and *c* = 22.773(4) Å, with *Z* = 4.

The structure of ETH<sup>T</sup> 3003 is shown in Fig. 2. The structure is based on investigations of the X-ray diffraction of [Ru(dpp)<sub>3</sub>]<sup>2+</sup> perchlorate by Volker Gramlich at ETHZ on a SYNTEX P21 diffractometer. Since it was not possible to crystallize the octyl-substituted complex and no ruthenium parameter set was available, the phenanthroline moieties were fixed in space based on the crystal structure of [Ru(dpp)<sub>3</sub>](ClO<sub>4</sub>)<sub>2</sub>. The structure of Ru(8-dpp)(ClO<sub>4</sub>)<sub>2</sub> was force-field optimized in

vacuo with the software package Sylbyl 6.3 (TRIPOS Inc., St. Louis, USA).

### 3.2. Absorption and emission data of complexes

The UV–vis absorption spectrum of the ETH<sup>T</sup> 3003 in ethanol shows peaks at 465 ( $\epsilon = 3.45 \times 10^4 \text{ M}^{-1} \text{ cm}^{-1}$ ), 440 ( $\epsilon = 3.48 \times 10^4 \text{ M}^{-1} \text{ cm}^{-1}$ ) and 280 nm ( $\epsilon = 15.09 \times 10^4 \text{ M}^{-1} \text{ cm}^{-1}$ ). The strong UV band at 280 nm is due to a charge transfer transition from the  $\pi-\pi^*$  orbital of the ligand and the visible bands at 440 and 465 nm to the metal  $t_{2g}$  orbital to the  $\pi^*$  orbital of the ligand [42].

The absorption spectra of the iridium complexes N-833, N-837 and N-926 display bands in the UV and the visible region due to intra ligand ( $\pi-\pi^*$ ) and metal-to-ligand charge transfer transitions (MLCT), respectively [43]. The low energy MLCT band in complex N-837 (463 nm), which is significantly blue shifted compared to the complexes N-833 (478 nm) and N-926 (480 nm), indicates the extent of  $\pi$ -acceptor strength of the CN–ligand compared to the NCS. The spectral shifts are consistent with the electrochemical data of these complexes. Hay, in a recent paper, analyzed the spectral properties of iridium (III) phenylpyridine complexes using density functional theory (DFT), in which the low-lying transitions are categorized as metal-to-ligand charge transfer transitions and the high-energy bands at above 280 nm are assigned to the intra ligand  $\pi-\pi^*$  transition of 2-phenylpyridine [44].

The ethanol solution of the Ru(8-dpp)(ClO<sub>4</sub>)<sub>2</sub> complex exhibits an intense bright orange luminescence maximum at 618 nm upon excitation at the metal-to-ligand charge transfer maxima at 465 nm, which is consistent with the literature [45].

As discussed in the Introduction, the luminescence quantum yield of ETH<sup>T</sup> 3003 in solution was  $0.56 \pm 0.05$  [36].

In contrast, iridium complexes exhibit luminescence maximum around 530 nm when they are excited within the  $\pi-\pi^*$  and MLCT absorption band.

Table 2 shows the composition and the terminology of the different sensing films studied, and Table 3 shows the photophysical properties of the organometallic complexes incorporated into polystyrene films. The luminescence quantum yields of thin films containing ruthenium and iridium complexes were measured and calculated using the following equation:

$$\phi_{L,X} K_{\text{opt}} = \phi_{L,r} \frac{(D/A_{\text{exc}})_X}{(D/A_{\text{exc}})_{r,\text{liquid membrane}}} \quad (1)$$

The subscript X denotes the substance whose luminescence quantum yield is determined and r the reference substance ( $2.25 \times 10^{-6} \text{ M}$  rhodamine 101 in ethanol) [46].  $K_{\text{opt}}$  is the optical factor, which refers to the considerably higher refractive index of the membrane ( $n_D(\text{PS}) = 1.5894$ ) compared to the solution ( $n_D(\text{ethanol}) = 1.3611$ ). It was calculated according to Roth [36] and amounted to 0.661 (for more information, see supporting information).  $D$  is the integrated area under the emission spectrum;  $A_{\text{exc}}$  is the absorbance at the excitation wavelength.  $\phi_{L,r}$  the luminescence quantum yield of rhodamine 101, is assumed to be 1.0 [46].

The iridium complexes display significantly higher luminescence quantum yields than the complexes of Ru(II) when incorporated into a polymer. Orthometallated iridium complexes are known to have the highest triplet luminescence quantum yields for several reasons: (a) iridium shows large d-orbital splitting compared to other metals in the series; (b) the strong ligand

Table 3

Luminescence excitation,  $\lambda_{\text{exc}}$ , and emission,  $\lambda_{\text{em}}$ , wavelengths, luminescence quantum yields and Stern–Volmer constants,  $K_{\text{SV}}$ , of the dyes incorporated into polystyrene membranes

Dye	Membrane	$\lambda_{\text{exc}}$ (nm)	$\lambda_{\text{em}}$ (nm)	Luminescence quantum yield <sup>a</sup>	$K_{\text{SV}}$ (bar <sup>-1</sup> ) <sup>a</sup>
ETH <sup>T</sup> 3003	PS0X	460	620	$0.19 \pm 0.05$	$1.63 \pm 0.02$
	PS1XC			$0.16 \pm 0.06$	$1.33 \pm 0.00$
	PS2XC			$0.13 \pm 0.06$	$1.17 \pm 0.01$
	PS1XN			$0.15 \pm 0.07$	$1.29 \pm 0.00$
	PS2XN			$0.15 \pm 0.09$	$1.17 \pm 0.01$
N-926	PS0X	400	526	$0.80 \pm 0.02$	$1.20 \pm 0.03$
	PS1XC			$0.66 \pm 0.13$	$0.76 \pm 0.02$
	PS2XC			$0.58 \pm 0.13$	$0.59 \pm 0.04$
	PS1XN			$0.32 \pm 0.10$	$0.32 \pm 0.00$
	PS2XN			$0.44 \pm 0.04$	$0.18 \pm 0.01$
N-833	PS0X	402	529	$0.60 \pm 0.06$	$0.34 \pm 0.00$
	PS1XC			$0.70 \pm 0.01$	$0.23 \pm 0.04$
	PS2XC			$0.55 \pm 0.08$	$0.25 \pm 0.01$
	PS1XN			$0.54 \pm 0.04$	$0.09 \pm 0.03$
	PS2XN			$0.35 \pm 0.09$	$0.03 \pm 0.00$
N-837	PS0X	398	528	$0.38 \pm 0.05$	$0.71 \pm 0.04$
	PS1XC			$0.41 \pm 0.02$	$0.66 \pm 0.09$
	PS2XC			$0.43 \pm 0.07$	$0.68 \pm 0.01$
	PS1XN			$0.16 \pm 0.01$	$0.09 \pm 0.04$
	PS2XN			$0.18 \pm 0.02$	$0.00 \pm 0.00$

<sup>a</sup> The experimental results are expressed as the average of three replicas  $\pm st/\sqrt{n}$  ( $n = 3$ ,  $t = 4.30$  ( $2P = 0.05$ )).

field strength of the phenyl anion ligand increases the energy between  $t_{2g}$  and  $e_g$  orbitals and leads to an enhanced gap between the  $e_g$  and LUMO of the ligand; (c) the close lying  $\pi-\pi^*$  and MLCT states together with the heavy atom effect enhance the spin-orbit coupling. The even more effective strategy to magnify the luminescence quantum yields of this class of complexes is to increase further the gap between the  $e_g$  and LUMO orbitals by introducing ligands such as 4,4'-dimethylamino-2,2'-bipyridine, which is known to have strong ligand field stabilization energy. In such type of complexes, the charge transfer excited states decay through radiative pathways.

Table 3 also shows the luminescence quantum yields for the dyes in PS with different percentages of plasticizers. The incorporation of the dyes into PS decreases the luminescence quantum yield referred to solution (the luminescence quantum yields of the dyes in deoxygenated solution were  $0.56 \pm 0.05$  for ETH<sup>T</sup> 3003 in Ethanol,  $0.99 \pm 0.05$  for N-833 in  $\text{CH}_2\text{Cl}_2$  and  $0.94 \pm 0.05$  for N-837 in  $\text{CH}_2\text{Cl}_2$ ) [36,35]. In addition, the luminescence quantum yields decrease with increasing concentrations of the plasticizer. Therefore, the membrane composition with the best luminescence quantum yield is based on dye N-926 incorporated into PS without using a permanent solvent (luminescence quantum yield of  $80 \pm 2\%$ ).

### 3.3. Oxygen sensing properties

The measurement of the oxygen partial pressure relies on the quenching of the intense emission from the metal-to-ligand charge transfer excited state to the ground state triplet oxygen by energy transfer. If luminescence quenching is entirely diffusional, then the luminescence intensities are related to the quencher concentration by the Stern–Volmer equation

$$\frac{I_0}{I} = 1 + K_{SV}[Q] \quad (2)$$

where  $I_0$  is the luminescence intensity in the absence of a quencher,  $I$  is the intensity at a given quencher concentration and  $K_{SV}$  is the Stern–Volmer constant.

For the organometallic complexes investigated here, an entirely diffusional quenching process is assumed because the experimental data can be fitted to the Stern–Volmer equation with a correlation coefficient ( $r$ ) > 0.999. Fig. 4 shows the Stern–Volmer Plot for the Ir(III) complex N-926. Assuming that the hypothesis of dynamic diffusional quenching holds true, the dynamic range of an oxygen optode is governed by the respective quenching function and Stern–Volmer constant (2). The variation in the luminescence intensity as a function of the relative oxygen concentration or partial pressure to nitrogen is given by the Stern–Volmer equation

$$\frac{I_0}{I} = 1 + K_{SV}p_{O_2} \quad (3)$$

where  $I_0$  is the luminescence intensity of the sensor in the absence of oxygen,  $I$  is the intensity at a given partial pressure of oxygen,  $p_{O_2}$ , and  $K_{SV}$  is the Stern–Volmer constant.  $K_{SV}$

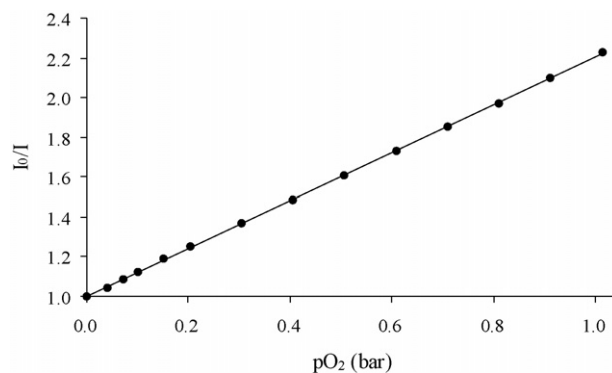


Fig. 4. Stern–Volmer plot  $I_0/I = f(p_{O_2})$  for N-926 incorporated into PS without plasticizer (PSOX membrane)  $\lambda_{exc/em} = 400/526$  nm, slits width $_{exc/em} = 2.5/5$  nm.

is equivalent to the slope of the response function/correlation function.

The experimental results are reported in Table 3. They show that the ruthenium complex is characterized by a more prominent Stern–Volmer constant than the iridium complexes, and therefore show a higher sensitivity to  $O_2$ . As a consequence, a higher luminescence quantum yield does not necessarily lead to a higher Stern–Volmer constant and a higher sensitivity to oxygen. However, the use of a dye with a high luminescence quantum yield and an adequate Stern–Volmer constant, e.g. N-926, may reduce scattering interferences and thus permit the use of less sensitive detectors.

On the other hand, the use of plasticizers decreases the  $K_{SV}$ . *o*-NPOE decreases  $K_{SV}$  more than *o*-CPOE. *o*-NPOE was observed to quench the luminescence emission of the metal complexes and thus reduce the amount of dye that can be quenched by oxygen. In addition, an increase in the concentration of the plasticizer goes along with a decrease in the Stern–Volmer constant. Therefore, the most  $O_2$ -sensitive membrane yielding the highest  $K_{SV}$  is still based on ETH<sup>T</sup> 3003 incorporated into polystyrene (PS) (Table 3).

The completely reversibility of the luminescence emission of the oxygen-sensitive films do possible the continuously monitor increasing and decreasing  $p_{O_2}$ . The physico-chemical quenching reaction is a reversible process. In addition, the oxygen-sensitive membranes show quick response times: the  $t_{95}$  response times of the sensors are <1 s when changing from pure  $N_2$  to 4 vol.%  $p_{O_2}$ , and <2 s when changing from 4 vol.%  $p_{O_2}$  to pure  $N_2$ .

### 3.4. Photostability and long-term stability

The photochemistry of ruthenium and iridium complexes in solution is dominated by ligand loss and photoanation of one or more ligands by solvent molecules or counter ions. The photoproducts are non-emissive at room temperature [15]. For this reason, it is very important to know the photostability and long-term stability of the iridium complexes incorporated into PS. The experimental results (see “supporting information” for details) show that the tested membranes present similar photostability in air and nitrogen, the presence of *o*-NPOE as a solvent increases



Table 4  
Stern–Volmer constants,  $K_{SV}$ , before and after two consecutive “cleaning in place (CIP)” sterilization processes (50 °C/30 min)

Dye	Cleaning agent	Membrane	Before	$K_{SV}$ (bar <sup>-1</sup> ) <sup>a</sup>	
				First sterilization (% decreasing)	Second sterilization (% decreasing)
ETH <sup>T</sup> 3003	NaOH 1M	PS0X	1.63 ± 0.02	1.45 ± 0.03 (11)	1.40 ± 0.03 (14)
		PS1XC	1.33 ± 0.00	1.25 ± 0.02 (6)	1.27 ± 0.01 (5)
		PS2XC	1.17 ± 0.01	1.00 ± 0.02 (15)	0.87 ± 0.04 (26)
	H <sub>3</sub> PO <sub>4</sub> 2.5%	PS0X	1.63 ± 0.02	1.34 ± 0.02 (18)	1.31 ± 0.02 (20)
		PS1XC	1.33 ± 0.00	1.30 ± 0.02 (2)	1.18 ± 0.02 (11)
		PS2XC	1.17 ± 0.01	0.91 ± 0.02 (22)	0.79 ± 0.02 (32)
N-926	NaOH 1M	PS0X	1.20 ± 0.03	1.07 ± 0.03 (11)	1.03 ± 0.05 (14)
		PS1XC	0.76 ± 0.02	0.71 ± 0.03 (7)	0.72 ± 0.03 (5)
		PS2XC	0.59 ± 0.04	0.18 ± 0.03 (69)	0.11 ± 0.05 (81)
	H <sub>3</sub> PO <sub>4</sub> 2.5%	PS0X	1.20 ± 0.03	0.99 ± 0.04 (18)	0.97 ± 0.04 (19)
		PS1XC	0.76 ± 0.02	0.74 ± 0.03 (3)	0.67 ± 0.03 (12)
		PS2XC	0.59 ± 0.04	0.13 ± 0.04 (78)	0.06 ± 0.05 (90)
N-833	NaOH 1M	PS0X	0.34 ± 0.00	0.29 ± 0.02 (15)	0.26 ± 0.03 (24)
		PS1XC	0.23 ± 0.04	0.23 ± 0.03 (0)	0.23 ± 0.05 (0)
		PS2XC	0.25 ± 0.01	0.18 ± 0.01 (28)	0.17 ± 0.02 (32)
	H <sub>3</sub> PO <sub>4</sub> 2.5%	PS0X	0.34 ± 0.00	0.31 ± 0.02 (9)	0.33 ± 0.01 (3)
		PS1XC	0.23 ± 0.04	0.21 ± 0.03 (9)	0.21 ± 0.04 (9)
		PS2XC	0.25 ± 0.01	0.23 ± 0.02 (8)	0.22 ± 0.02 (12)
N-837	NaOH 1M	PS0X	0.71 ± 0.04	0.82 ± 0.05 (-15)	0.84 ± 0.05 (-18)
		PS1XC	0.66 ± 0.09	0.63 ± 0.08 (5)	0.55 ± 0.05 (17)
		PS2XC	0.68 ± 0.01	0.63 ± 0.03 (7)	0.40 ± 0.03 (41)
	H <sub>3</sub> PO <sub>4</sub> 2.5%	PS0X	0.71 ± 0.04	0.76 ± 0.03 (-7)	0.80 ± 0.02 (-13)
		PS1XC	0.66 ± 0.09	0.56 ± 0.05 (15)	0.53 ± 0.05 (20)
		PS2XC	0.68 ± 0.01	0.51 ± 0.02 (25)	0.46 ± 0.02 (32)

<sup>a</sup> The experimental results are expressed as the average of three replicas  $\pm st/\sqrt{n}$  ( $n=3$ ,  $t=4.303$  ( $2P=0.05$ )).

the photobleaching of the dyes and the presence of *o*-CPOE minimizes the photodecomposition of the dyes. In the absence of a plasticizer, the photobleaching of the dyes is increased with respect to *o*-CPOE membranes. However, both PS and PS-CPOE membranes show sufficient light stability to be used as oxygen sensors. Since their analytical performance ( $K_{SV}$ ) did not change over 3 months storage under ambient conditions, the long-term stability of all the oxygen-sensitive membranes was considered to be sufficiently good for measurements in the gas phase.

### 3.5. Sterilizability

For many applications, especially for biotechnology, the sensors have to be sterilized. The oxygen-sensitive membranes based on the novel organometallic ruthenium and iridium complexes incorporated into PS with and without plasticizers were exposed to different sterilization processes. The sterilizability was established taking the change in their analytical performance (Stern–Volmer constant) into account.

Two sterilization protocols were tested: chemical cleaning (cleaning in place; CIP) [47] and gamma irradiation [47].

The CIP protocol consists of treating the membranes by NaOH (1 M) or H<sub>3</sub>PO<sub>4</sub> (2.5%) at 50 °C for 30 min, then purging with de-ionized water and, finally, drying under ambient conditions. The oxygen-sensitive membranes were subjected to this treatment twice consecutively.  $K_{SV}$  was evaluated before CIP, after the first sterilization run and again after the second run (see Table 4). The experimental results show that the oxygen-

sensitive membranes based on ETH<sup>T</sup> 3003, N-837, N-833 and N-926 incorporated into PS with or without plasticizers can be sterilized with both acid and basic CIP. In general, a low concentration of *o*-CPOE makes the membranes more stable to CIP. High concentrations of *o*-CPOE decrease the Stern–Volmer constant of the membrane after CIP, except for N-837, for which the presence of plasticizer decreases the sensitivity of the

Table 5  
Stern–Volmer constants,  $K_{SV}$ , before and after the gamma-ray sterilization process (14.5 kGy/30 min) (plasticizer-free membranes and polystyrene membranes dissolved in CPOE)

Dye	Membrane	$K_n$ (bar <sup>-1</sup> ) <sup>a</sup>	
		Before	After (% decrease)
ETH <sup>T</sup> 3003	PS0X	1.63 ± 0.02	1.32 ± 0.02 (19)
	PS1XC	1.33 ± 0.00	1.05 ± 0.02 (21)
	PS2XC	1.17 ± 0.01	1.00 ± 0.05 (15)
N-926	PS0X	1.20 ± 0.03	0.97 ± 0.02 (19)
	PS1XC	0.76 ± 0.02	0.60 ± 0.02 (21)
	PS2XC	0.59 ± 0.04	0.50 ± 0.15 (15)
N-833	PS0X	0.34 ± 0.00	0.22 ± 0.00 (35)
	PS1XC	0.23 ± 0.04	0.16 ± 0.00 (30)
	PS2XC	0.25 ± 0.01	0.14 ± 0.00 (44)
N-837	PS0X	0.71 ± 0.04	0.45 ± 0.07 (37)
	PS1XC	0.66 ± 0.09	0.50 ± 0.09 (24)
	PS2XC	0.68 ± 0.01	0.44 ± 0.03 (35)

<sup>a</sup> The experimental results are expressed as the average of three replicas  $\pm st/\sqrt{n}$  ( $n=3$ ,  $t=4.303$  ( $2P=0.05$ )).

membrane. Therefore, the Stern–Volmer constants were conserved better in plasticizer-free membranes.

The gamma-irradiation protocol involved exposing the membrane to 14.5 kGy for 30 min. Table 5 shows  $K_{SV}$  of the oxygen-sensitive membranes before and after the gamma irradiation. The experimental results show that the oxygen-sensitive membranes based on ETH<sup>T</sup> 3003, N-837, N-833 and N-926 incorporated into PS with or without plasticizers can be sterilized by gamma irradiation. Similar results to those with CIP were obtained and a low concentration of *o*-CPOE made the membranes more stable with gamma ray than membranes without plasticizer, but high concentrations of *o*-CPOE decrease the Stern–Volmer constant of the membrane with gamma-ray irradiation. The beneficial effect of the plasticizer during gamma-ray treatment has to do with an improved heat dissipation. The temperature within the goods to be sterilized may rise up to 60 °C.

#### 4. Conclusions

This report on highly luminescence metal complexes for analyzing oxygen in the gas phase and oxygen-sensitive membranes, describes how they show significant photostability and complete reversibility with short response times. It is also possible to sterilize them with gamma radiation. These novel oxygen-sensitive films can be used in current solid-state opto-electronics monitoring devices. They can be immobilized by incorporating them into nanostructured materials in which they are still photostable and in which they can still be sterilized.

#### Acknowledgements

The authors gratefully acknowledge financial support, in the form of a work contract, from the Junta de Andalucía (Ayuda para el Perfeccionamiento de Doctores en Universidades Fuera de Andalucía). They also thank their colleagues Dr. R. Steiger for revising the paper and Volker Gramlich of the Laboratorium für Kristallographie at ETH-Zürich for the X-ray experiment with the ruthenium complex. Some of our work received financial support from the Swiss National Science Foundation under NRP 47.

#### Appendix A. Supplementary data

Supplementary data associated with this article can be found, in the online version, at doi:10.1016/j.talanta.2006.03.043.

#### References

- [1] C. Preininger, I. Klimant, O.S. Wolfbeis, *Anal. Chem.* 66 (1994) 1841.
- [2] R.C. Martin, S.F. Malin, D.J. Bartnil, A.M. Schilling, S.C. Furlong, *Proc. SPIE* 2131 (1994) 426.
- [3] M.J. Atkinson, F.I.M. Thomas, N. Larson, E. Terril, K. Morita, C.C. Lium, *Deep-Sea Res.* I 42 (1995) 761.
- [4] H.S. Voraberger, H. Kreimaier, K. Biebnik, W. Kern, *Sens. Actuators B* 74 (2001) 179.
- [5] F.C. O'Mahony, T.C. O'Riordan, N. Papkovskaia, V.I. Ogurtsov, J.P. Kerry, D.B. Papkovsky, *Packag. Technol. Sci.* 14 (2004) 225.
- [6] W.L. Rumsey, J.M. Vanderkooi, D.F. Wilson, *Science* 241 (1988) 1649.
- [7] P. Babilas, G. Liebsch, V. Schacht, I. Klimant, O.S. Wolfbeis, R.M. Szeimies, C. Abels, *Microcirculation* 12 (2005) 477.
- [8] T.C. O'Riordan, D. Buckley, V. Ogurtsov, R. O'Connor, D.B. Papkovsky, *Anal. Biochem.* 278 (2000) 221.
- [9] T.C. O'Riordan, H. Voraberger, J.P. Kerry, D.B. Papkovsky, *Anal. Chim. Acta* 530 (2005) 135.
- [10] D.A. Skoog, D.M. West, F.J. Holler, *Fundamentals of Analytical Chemistry*, Saunders, Philadelphia, 1988, p. 344.
- [11] L.C. Clark, *US Patent* 2,913,386 (1959).
- [12] T.M. Freeman, W.R. Seitz, *Anal. Chem.* 53 (1981) 98.
- [13] M.C. Hitchman, *Measurement of Dissolved Oxygen*, Wiley, New York, 1978, p. 130.
- [14] M.M.F. Choi, D. Xiao, *Anal. Chim. Acta* 403 (2000) 57.
- [15] P. Hartmann, M.J.P. Leiner, P. Kohlbacher, *Sens. Actuator B* 51 (1998) 196.
- [16] Y. Fujiwara, Y. Amao, *Sens. Actuator B* 89 (2003) 187.
- [17] Y. Amao, *Microchip. Acta* 143 (2003) 1–12.
- [18] S. Arain, G.T. John, C. Krause, J. Gerlach, O.S. Wolfbeis, I. Klimant, *Sens. Actuators B* 113 (2006) 639–648.
- [19] Y. Kostov, G. Rao, *Sens. Actuators B* 90 (2003) 139.
- [20] S. Arain, G.T. John, C. Krause, J. Gerlach, O.S. Wolfbeis, I. Klimant, *Sens. Actuators B* 113 (2006) 639.
- [21] A. Gomez-Henz, M.P. Aguilar-Caballeros, *TRAC Trends Anal. Chem.* 23 (2004) 127.
- [22] G. Orellana, D. García-Fresnedillo, in: R. Narayanaswamy, O.S. Wolfbeis (Eds.), *Optical Sensors*, Springer, Berlin-Heidelberg, Germany, 2004, pp. 309–357.
- [23] J.M. Costa-Fernández, A. Sanz-Medel, in: A. Fernandez Gutierrez, S.G. Schulman (Eds.), *Analytical Molecular Fluorescence: A Practical Approach*, Editorial Universidad de Granada, Granada, Spain, 2001, pp. 355–395 (in Spanish language).
- [24] A. Sharma, O.S. Wolfbeis, *Appl. Spect.* 42 (1988) 1009.
- [25] L. Sacksteder, J.N. Demas, B.A. DeGraff, *Anal. Chem.* 65 (1993) 3480.
- [26] W.Y. Xu, K.A. Kneas, J.N. Demas, B.A. DeGraff, *Anal. Chem.* 68 (1996) 2605.
- [27] Y. Amao, Y. Ishikawa, I. Okura, *Anal. Chim. Acta* 445 (2001) 177.
- [28] S.-K. Lee, I. Okura, *Spectrochim. Acta A* 54 (1998) 91.
- [29] S.-K. Lee, I. Okura, *Anal. Commun.* 34 (1997) 185.
- [30] P. Hartmann, W. Trettnak, *Anal. Chem.* 68 (1996) 2615.
- [31] D.B. Papkovsky, G.V. Ponomarev, W. Trettnak, P. O'Leary, *Anal. Chem.* 67 (1995) 4112.
- [32] Y. Amao, T. Miyashita, I. Okura, J. Porphyrin. *Phthalocyanine* 5 (2001) 433.
- [33] Y. Amao, K. Asai, I. Okura, *Anal. Chim. Acta* 407 (2000) 41.
- [34] J.M. Costa-Fernandez, M.E. Díaz-García, A. Sanz-Medel, *Anal. Chim. Acta* 360 (1998) 17.
- [35] Md.K. Nazeeruddin, R. Humpry-Baker, D. Berner, S. Rivier, L. Zuppiroli, M. Graetzel, *J. Am. Chem. Soc.* 125 (2003) 8790.
- [36] T. Roth, *Ruthenium (II) diimine complexes for luminescence-based oxygen sensors*, Ph.D. Thesis, Diss. ETH No. 14001, Swiss Federal Institute of Technology, Zurich, 2000, p. 245.
- [37] S. Masuda, T. Nakajima, S. Suga, *Bull. Chem. Soc. Jpn.* 56 (1983) 1089.
- [38] J. Hiti, C.C. Young, *Patent US9/02057* (1992).
- [39] E.E. Seddon, K.R. Seddon, *The Chemistry of Ruthenium*, Elsevier Science Publishers B.V., Amsterdam, 1984.
- [40] K. Seiler, *Ion-selective optode membranes*, Fluka Chemie AG, CH-9470 Buchs, 1993.
- [41] B.M. Goldstein, J.K. Barton, H.M. Berman, *Inorg. Chem.* 25 (1986) 842.
- [42] R.J. Watts, G.A. Crosby, *J. Am. Chem. Soc.* 93 (1971) 3184.
- [43] Schmid, F.O. Garces, R.J. Watts, *Inorg. Chem.* 33 (1994) 9.
- [44] Hay, J. *Phys. Chem. A* 106 (2002) 1634.
- [45] R.J. Watts, G.A. Crosby, *J. Am. Chem. Soc.* 93 (1971) 3184.
- [46] T. Kartens, K. Kobs, *J. Phys. Chem.* 84 (1980) 1871.
- [47] S. Ahmed, G.P. Rigby, P. Crump, P.M. Vadgama, *Biosens. Bioelectron.* 15 (2000) 159.

# Application of a novel chemometric approach to the determination of aqueous photolysis rates of organic compounds in natural waters

Dimosthenis L. Giokas, Athanasios G. Vlessidis\*

*Laboratory of Analytical Chemistry, Department of Chemistry, University of Ioannina, 45110 Ioannina, Greece*

Received 28 March 2006; accepted 31 March 2006

Available online 11 May 2006

## Abstract

The utility of multivariate optimization methods in the determination of aqueous photolysis rates of organic compounds is examined in this study. A basic pursue was to designate the appropriate experimental design plan that extend the analytical utility of multivariate methods from qualitative data interpretation approaches, as applied thus far, to quantitative estimation methods. A three-level second-order central composite design with parameter concentrations (factor levels) beyond the environmental realistic concentrations was employed for that purpose enabling statistically significant effects to be determined. Method application is demonstrated in the first photodegradation study of two UV absorbing chemicals in natural waters. The results suggest that the proposed approach of enables a good approximation of the real behavior in terms of both qualitative and quantitative data interpretation with minimal loss of information.

© 2006 Elsevier B.V. All rights reserved.

*Keywords:* Chemometrics; Multivariate optimization; Natural waters; Photodegradation; Sunscreen agents

## 1. Introduction

Sunlight induced photochemical reactions are probably the most important abiotic processes determining the aquatic fate of organic compounds in natural waters. Two photoinduced alteration processes are commonly met in the surface layers of aquatic systems: direct and indirect photolysis. In direct photolysis, the organic compounds absorb UV light a procedure that either enables them to react with the constituents of water or induce self-decomposition. Indirect photolysis involves the photodegradation of organic compounds caused by photosensitizers like oxygen and hydroxyl or peroxy radicals produced by the photolysis of humic and inorganic substances [1].

Although both processes can occur simultaneously, indirect photolysis plays the most important role in the behavior and environmental half-life of organic contaminants. That is because natural waters contain a variety of substances (dissolved organic matter (DOM), bicarbonates, nitrates, chloride) that may either inhibit [2] or enhance [3] the photo-alteration of organic compounds, by scavenging or generating photo-oxidant agents com-

prised of both reactive oxygen species and other non-reactive oxygen species transient [4,5]. Thus, irrespectively of the effect of direct photolysis, indirect pathways are ubiquitous.

The ability and contribution of each reactive transient on the systematic removal of organic compounds is concentration depended, and is determined by the steady-state concentration of the reactants as a result of the mass balance between their production and consumption rates. This in turn is affected by the composition of natural waters thus the magnitude of each processes will vary depending on the synergistic or antagonistic action among the reactive transients. However, for simplicity reasons, the majority of research articles published hitherto have focused on the univariate investigation of each of the parameters that affect indirect photolysis [6,7]. As a result, the observed environmental photodegradation rates and quantum yield of the photochemical reactions, which are a superposition of many intricate reactions and depend on a variety of factors subject to diurnal variations, are simplified representations of the actual behavior and endanger loss of information.

In order to provide a more realistic description of real-life photoinduced transformations, multivariate methods have been set forth [8–11]. The advantage of these methods is that many factors can be investigated simultaneously thus obtain a better insight into naturally occurring processes. Photofate, a multivari-

\* Corresponding author. Tel.: +30 26510 98401; fax: +30 26510 44831.  
E-mail address: [avlessid@cc.uoi.gr](mailto:avlessid@cc.uoi.gr) (A.G. Vlessidis).

ate laboratory-based test system, was the first systematic attempt towards the combinational investigation of the contributions of various reactive transient species to the kinetics of indirect photolysis reactions in environmentally realistic mixtures [9]. The system has been shown to provide a more realistic provision of environmental photodegradation pathways for various organic contaminants compared to previous protocols [9,11]. Although innovative, the experimental design employed in Photofate has several shortcomings. In the first place, it is not based on a specific experimental design but on empirical observations depending on the number of constituents (factors) and the concentration levels. As a result, it does not allow for parameter interactions to be quantitatively described with a proper mathematical model in order to predict the photolysis rate constants as a function of matrix constituents. Furthermore, this approach is limited to a specific number of permutations that can be performed in a single photodegradation experiment, in other words it is limited by the space availability of the photosimulator. Thus, if the sequence of experiments has to be randomized (e.g. interrupted over-night), the method does not reflect systematic changes in the experimental conditions.

A more coherent approach has been proposed by Walse et al. [10] using a second-order central composite design to assess the influence of bicarbonate, nitrate and DOM interactions on the photodegradation of the insecticide Fipronil. On the basis of this design, they tried to describe linear and non-linear interactions and develop a multivariate kinetic model of Fipronil photodegradation. Although the latter effort was successful, no interactions were observed since only DOM was found to exert a statistically significant effect. Therefore, no mathematical equation able to estimate the photodegradation constants could be derived. One possible reason is that the factor levels were chosen to emulate concentrations that bracket those commonly found in natural waters, thus the differences between factorial ( $2^4$  kernel design) and star ( $2k$  star points) levels were too small to produce a statistically significant effect at the 95% probability level.

From the above discussion it is made clear that multivariate methods presented so far, although efficiently described parameter interactions in a qualitative manner, they had not been able to provide an adequate representation of aqueous photolysis on a quantitative basis. In this context, the primary aim of this study is to extend the scope and application of multivariate techniques by designating the conditions that enable the quantitative description of parameters affecting aqueous photolysis. To achieve this goal, factor levels were assigned values below and above the environmental realistic concentrations, in order to increase the absolute distance between factorial and star point levels, and fitted to a response surface second-order polynomial model. Data for verification were produced by investigating the photodegradation kinetics of two UV absorbing chemicals (also called sunscreen agents) in natural waters, a task which has seemingly never been reported before. The results suggest that the proposed approach provides a discrete response for each parameter and reduces the uncertainty between factor interactions thus enabling the quantitative interpretation of aqueous photolysis data.

## 2. Experimental

### 2.1. Reagents

3-(4-Methylbenzylidene)-camphor (Eusolex 6300 or E6300) and octyl methoxy cinnamate (Eusolex 2292 or E2292) were purchased from Merck (Darmstadt, Germany). Humic acid standard were purchased from Fluka. The solvents used ethyl acetate, dichloromethane, methanol, acetonitrile and water were of the highest available purity (HPLC grade) and were obtained by Labscan, Ltd., (Dublin, Ireland).  $C_{18}$  cartridges (500 mg) were obtained from Chromabond (Machereu Nagel Gmd H&Co.) and fitted to a 12-port SPE vacuum apparatus (Supelco Preppy) purchased from Supelco (Bellefonte, USA).

### 2.2. Chromatographic conditions

The decrease of E6300 and E2292 concentrations during photolysis was monitored using a chromatographic system comprised of a Shimadzu on-line degassing system DGU-14A coupled to a FCV-10AL controller unit and an LC-10AD high-pressure solvent delivery pump, with a 20  $\mu$ L sample loop injector. Analytes identification and quantitation was performed with an SPD-M6A UV/diode-array detector working under the Class M10A Software (version 1.20). The column material was an APEX  $C_{18}$  (Jones Chromatography, UK), with particle size of 5  $\mu$ m, (25 cm  $\times$  4.6 mm i.d.). Isocratic elution was used for the elution of the UV absorbing chemicals from the column with a mobile phase composed of acetonitrile/water (80/20%, v/v) [12]. Data collection was performed by obtaining one spectrum per second. The peaks representing the target species were recognized both by their retention time and their spectrum profile.

### 2.3. Irradiation experiments

The aqueous photolysis of Eusolex 6300 and Eusolex 2292 ( $0.2 \mu\text{g mL}^{-1}$ ) was performed separately with synthetic field water (60 mL) which composition varied according to the setup of the experimental design. The experiments were performed in temperature controlled (to maintain the temperature below 30 °C) continually stirred cylindrical Pyrex cells (to filter wavelengths below 290 nm). The initial solutions were allowed to equilibrate for 10 min with rapid mixing before a sample was withdrawn to determine the actual (initial) concentration of the examined sunscreen agents. The solutions were irradiated with a water refrigerated 150 W high-pressure mercury vapour lamp (Heraeus TQ 150, Hanau, Germany) ( $\lambda > 290$  nm) from 0 to 240 min. This light source was allowed to stabilize for 15 min prior to use.

Three sample points were sampled over the irradiation period for each compound. Linear regression of the logarithmic concentration values determined as a function of time was used to generate the pseudo-first-order reaction rate constants as the slope of the equation:  $C_t = C_0 e^{-kt}$  where  $C_t$  is the concentration at time  $t$ ,  $C_0$  the initial (actual) concentration and  $k$  is the rate constant (slope). The actual phototransformation constants were calculated by subtracting the exponents of the degradation



curves representing the apparent degradation and the degradation owned to hydrolysis and volatilization calculated from EPI suite v3.10 [13]. In that way the calculated constants and half-lives were more realistic minimizing the contribution of other factors that could overemphasize the importance of photolysis.

#### 2.4. Analytical methods

Aliquots of 3 mL were removed from the reactor with an aid of an automated 5 mL pipette. Due to the low concentrations of the analytes the samples were preconcentrated on C<sub>18</sub> cartridges. Before extraction, the cartridges were conditioned with 2.5 mL ethyl acetate/dichloromethane (1:1), followed by 5 mL of methanol and 3 mL of deionized water. Next, the sample was percolated through the cartridge under vacuum at a flow rate of 1 mL/min and the cartridge was dried for about 5 min. The analytes were extracted with 4 mL of ethyl acetate/dichloromethane (1:1). The extracts were evaporated to dryness under a gentle stream of nitrogen and re-dissolved in 50  $\mu$ L of methanol in scaled Ependorf vials. Extraction efficiencies, assessed by fortifying aqueous solutions with the maximum concentrations of the indirect photolysis factors used in this study (19 mg/L DOM, 19 mg/L NO<sub>3</sub><sup>-</sup> and 32 g/L NaCl), were 96.0  $\pm$  0.7% for Eusolex 6300 and 97.2  $\pm$  0.9% for Eusolex 2292.

### 3. Results and discussion

#### 3.1. Selection of the experimental design approach

When trying to investigate naturally occurring processes several factors must be considered. In this context, the selection of the appropriate experimental design method is an essential prerequisite for obtaining as realistic results as possible.

Two-level screening designs ( $2^k$  full factorial designs) enable the estimation of main effects and interactions between factors which by definition limits their application to case-specific studies where there is previous experience that the concentration of the investigated factors does not vary significantly [14] (e.g. seasonal changes). Their most important limitation though is that the number of experimental units increases rapidly as the number of factors increase, rendering the overall effort time-consuming and costly.

Fractional factorial designs ( $2^{k-p}$  designs) solve the problem of increasing experimental runs with the number of factors but they are still of limited use since they are based on the assumption of two-levels for each factor (high-low) while they assume that certain interactions between factors are negligible or even impossible, a situation which is rather unlikely for environmental studies and prone to information loss [14,15].

Three-level designs overcome the barriers imposed by the previous methods offering the most realistic solution. Central composite and Box–Behnken designs are the most powerful candidate options. Box–Behnken designs are more versatile but they are limited by the representation of the dependence of the responses in dependence of a single factor [16]. Central composite designs (CCD) consist of a full or fractional factorial design and an additional design, often a star design, where the centers of

both designs coincide. In CCD the number of experimental runs is calculated from:  $r = 2^{k-p} + 2k + n_0$ , where  $k$  is the number of factors,  $p$  the number of reduction of the full design and  $n_0$  is the number of experiments in the center of the design. The only limitation of this method is that the star points are outside the hypercube so that the number of levels that need to be adjusted for every factor is actually five instead of three [15,16]. However, this statistical attribute may be advantageous in environmental photolysis studies since it enables a clear provision of the effect of each factor on the final response.

Taking all the above into consideration, a three-level CCD with five levels for each factor and two orthogonal blocks was built. The factorial block 1 contains 8 factorial points and 2 center points, that is, 10 experiments. The axial block 2 has 6 axial points plus 1 center point, that is, 7 experiments. Thus, block orthogonality is ensured. The corresponding star arm is then calculated as:

$$a = \left\{ k \times \frac{1 + f_{s0}/f_s}{1 + f_{c0}/f_c} \right\}^{1/2} \approx 1.7$$

where  $a$  stands for the distance of the star points from the center of the design;  $k$  is the number of factors in the design;  $f_{s0}$  the number of center points in the star portion of the design;  $f_s$  the number of non-center star points in the design;  $f_{c0}$  the number of center points in the cube portion of the design and  $f_c$  is the number of non-center cube points in the design.

The selected factors and their levels are listed in Table 1. These levels were chosen on the basis of examining the effect of each variable in various conditions ranging from clear to polluted water in order to obtain a clear response on the effect of each variable. Initial sunscreen concentrations were not considered as a separate factor and maintained constant in order to reduce the experimental points. To quantify and interpret the relationships between responses and factor effects the response surface method (RSM) was employed. The response  $y$  (reaction rate constants) as a function of the variables (factors) and all possible interactions was estimated as:

$$y = b_0 + \sum_{i=1}^k b_i x_i + \sum_{1 \leq i < j}^k b_{ij} x_i x_j + \sum_{i=1}^k b_{ii} x_i^2$$

with  $k$  the number of variables (factors),  $b_0$  the intercept parameter and  $b_i$ ,  $b_{ij}$ ,  $b_{ii}$  regression parameters for linear, interaction and quadratic factor effects, respectively. The corresponding design matrix (Fig. 1) consisted of 17 experiments of which 14

Table 1  
Factor definitions, coded levels and design points of the three-factor CCD

Coded Levels	X <sub>1</sub> : nitrate (NO <sub>3</sub> )	X <sub>2</sub> : dissolved organic matter (DOM)	X <sub>3</sub> : sodium chloride (NaCl)
− $\alpha$	1	1	1
−1	5	5	6000
0	10	10	15000
+1	15	15	25000
+ $\alpha$	19	19	32000

All values are in mg/L.



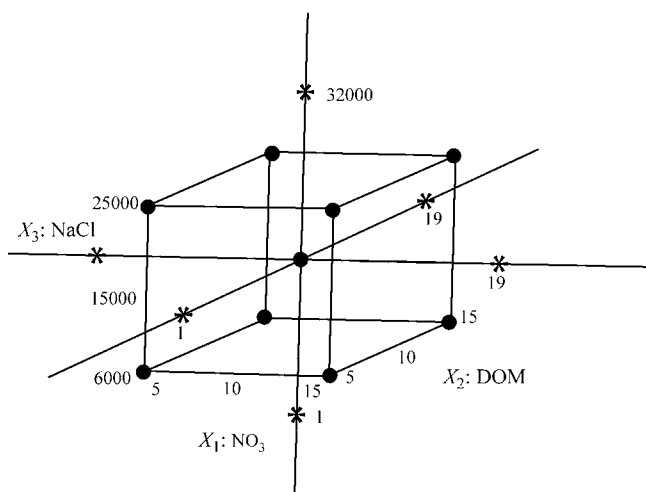


Fig. 1. Three-dimensional (3D) plane of the selected three-factor central composite design composed of six cube points, six axial points and three center points.

where experimental points and 3 center point (star) replications (Table 2).

### 3.2. Multivariate photolysis

#### 3.2.1. Evaluation of main effects

The main effects of each of the parameters on the photolysis rate constants of the target UV absorbing chemicals are given in Fig. 2. From these plots it can be inferred that maximum photodegradation of E6300 can be accomplished at the medium value of DOM (0 coded level), minimum value of NaCl ( $-\alpha$  coded level) and maximum value for  $\text{NO}_3^-$  ( $+\alpha$  coded level). Maximum depletion can also be achieved for E2292 at the lowest DOM concentration ( $-\alpha$  coded value), the medium NaCl concentration (0 coded level) and the highest  $\text{NO}_3^-$  level ( $+\alpha$  coded level). However, these plots only reveal the optimum

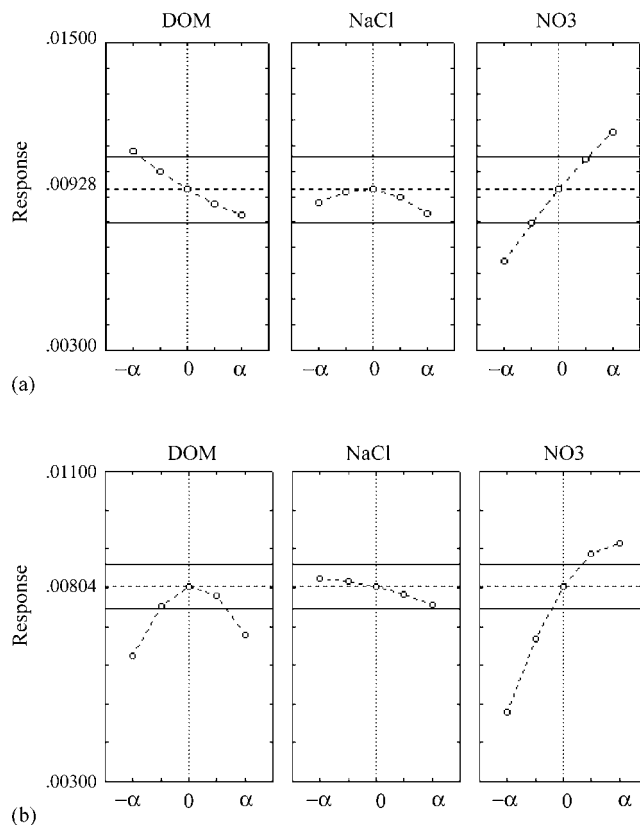


Fig. 2. Plot of main effects for (a) E2292 photolysis rate constants and (b) E6300 photolysis rate constants.

(maximum depletion) conditions but do not enable neither the investigation of the interactions among the factors nor the prediction of photodegradation rate constants at various combinations of factor levels. To accommodate factor interactions and the prediction of photodegradation rates, multivariate analysis was deployed.

Table 2  
Listing of experimental parameters, observed rate constants of E6300 and E2292 and experimental blocking

Run	Block	$\text{NO}_3$	DOM	NaCl	$k_{\text{photo}}$ (E2292)	$k_{\text{photo}}$ (E6300)	$r^2$ (E2292) <sup>a</sup>	$r^2$ (E6300) <sup>a</sup>
1	1	5	5	6000	0.00732	0.00552	0.95	0.94
2	1	5	15	6000	0.00708	0.00782	0.97	0.95
3	1	5	5	25000	0.0072	0.00449	0.97	0.96
4	1	5	15	25000	0.00696	0.00552	0.99	0.97
5	1	15	5	6000	0.01164	0.00736	0.96	0.94
6	1	15	15	6000	0.01008	0.00840	0.92	0.96
7	1	15	5	25000	0.01116	0.00966	0.95	0.97
8	1	15	15	25000	0.00984	0.00782	0.94	0.99
9 <sup>b</sup>	1	10	10	15000	0.0096	0.00817	0.99	0.98
10 <sup>b</sup>	1	10	10	15000	0.00972	0.00794	0.95	0.99
11	2	10	1	15000	0.01177	0.00713	0.98	0.99
12	2	10	19	15000	0.00781	0.00690	0.97	0.98
13	2	10	10	1	0.00902	0.00874	0.99	0.94
14	2	10	10	32000	0.00858	0.00805	0.97	0.97
15	2	1	10	15000	0.00737	0.00518	0.96	0.95
16	2	19	10	15000	0.01111	0.00978	0.95	0.98
17 <sup>b</sup>	2	10	10	15000	0.00858	0.00851	0.92	0.96

<sup>a</sup> Coefficient of determination for  $\ln[\text{concentration after time } t]/[\text{initial concentration at } t_0]$  vs. time.

<sup>b</sup> Indicates center point experiment.

### 3.2.2. Evaluation of multivariate interactions

To account for the photolysis rates as a function of factor interactions a reduced model was set forth which takes into account only the significant contributions. The outcome of the statistical treatment along with the analysis of variance (ANOVA) for the fit of the full second-order model to the data from the three-factor CCD is summarized in Table 3. The coefficients of multiple determinations,  $r^2$ , representing the fit of the models to the experimental data was 0.8993 for E2292 and 0.9758 for E6300 which means that 90 and 97% of the data about their mean was accounted for by the factor effects in the model. The statistically significant variables (noted in bold font in Table 3) at 95% level of confidence (i.e. student  $t < 0.05$ ) were the linear and quadratic effects of  $\text{NO}_3^-$ , the quadratic effect of DOM and

all cross-product terms in the case of E6300, while for E2292 only the linear effects of DOM and  $\text{NO}_3^-$  were found to affect the reaction rate constant. For the other factors, non-significant interactions were observed at the concentration zones studied. Interestingly, the block effect was also not significant indicating lack of systematic error in the experimental conditions.

After dropping the insignificant coefficients, the regression equations in the dimensional form are:

$$k_{\text{photo}}^{\text{E6300}} = 0.008286 + (0.001291X_1) + (-0.000518X_1X_2) \\ + (0.000633X_1X_3) + (-0.000518X_2X_3) \\ + (-0.000375X_1^2) + (-0.000538X_2^2),$$

$$k_{\text{photo}}^{\text{E2292}} = 0.009335 + (0.001497X_1) + (-0.000734X_2)$$

Table 3  
Multivariate results and analysis of variance of the central composite design (d.f. = degrees of freedom)

	Coefficient	Standard error	$t$ for null hypothesis	Sum of squares	d.f.	Mean squares	$p$ -Value
<b>E2292 parameters<sup>a</sup></b>							
$b_0$ : intercept	0.009335	0.000501	18.65111		1		<b>0.000002</b>
$b_1$ : $\text{NO}_3$	0.001497	0.000234	6.39360		1		<b>0.000689</b>
$b_2$ : DOM	-0.000734	0.000234	-3.13269		1		<b>0.020255</b>
$b_3$ : NaCl	-0.000124	0.000234	-0.53150		1		0.614167
$b_{11}$ : $\text{NO}_3 \cdot \text{NO}_3$	-0.000103	0.000258	-0.39903		1		0.703684
$b_{22}$ : DOM·DOM	0.000092	0.000258	0.35530		1		0.734522
$b_{33}$ : NaCl·NaCl	-0.000258	0.000258	-1.00250		1		0.354805
$b_{12}$ : $\text{NO}_3 \cdot \text{DOM}$	-0.000300	0.000306	-0.98038		1		0.364758
$b_{13}$ : $\text{NO}_3 \cdot \text{NaCl}$	-0.000060	0.000306	-0.19608		1		0.851022
$b_{23}$ : DOM·NaCl	0.000030	0.000306	0.09804		1		0.925095
Blocks				$5.86 \times 10^{-8}$	1	$5.86 \times 10^{-8}$	0.789
Regression model				$3.99 \times 10^{-5}$	9	$4.43 \times 10^{-6}$	
Linear				$3.82 \times 10^{-5}$	3	$1.27 \times 10^{-5}$	0.021
Square				$7.56 \times 10^{-7}$	3	$2.52 \times 10^{-7}$	
Interaction				$9.67 \times 10^{-7}$	3	$3.22 \times 10^{-7}$	
Residual error				$4.49 \times 10^{-6}$	6	$7.48 \times 10^{-7}$	
Lack of fit				$4.49 \times 10^{-6}$	5	$8.98 \times 10^{-7}$	0.068
Pure error				$7.20 \times 10^{-9}$	1	$7.20 \times 10^{-9}$	
Corrected total				$4.44 \times 10^{-5}$	16	$2.78 \times 10^{-6}$	
<b>E6300 parameters<sup>b</sup></b>							
$b_0$ : intercept	0.008286	0.000224	37.019		1		<b>0.000</b>
$b_1$ : $\text{NO}_3$	0.001291	0.000105	12.323		1		<b>0.000</b>
$b_2$ : DOM	0.000157	0.000105	1.498		1		0.185
$b_3$ : NaCl	-0.000203	0.000105	-1.937		1		0.101
$b_{11}$ : $\text{NO}_3 \cdot \text{NO}_3$	-0.000375	0.000115	-3.257		1		<b>0.017</b>
$b_{22}$ : DOM·DOM	-0.000538	0.000115	-4.668		1		<b>0.003</b>
$b_{33}$ : NaCl·NaCl	-0.000050	0.000115	-0.436		1		0.678
$b_{12}$ : $\text{NO}_3 \cdot \text{DOM}$	-0.000518	0.000137	-3.782		1		<b>0.009</b>
$b_{13}$ : $\text{NO}_3 \cdot \text{NaCl}$	0.000633	0.000137	4.622		1		<b>0.004</b>
$b_{23}$ : DOM·NaCl	-0.000518	0.000137	-3.782		1		<b>0.009</b>
Blocks				$1.01 \times 10^{-6}$	1	$1.01 \times 10^{-6}$	0.102
Regression model				$3.60 \times 10^{-5}$	9	$4.00 \times 10^{-6}$	
Linear				$2.36 \times 10^{-5}$	3	$2.36 \times 10^{-5}$	<0.001
Square				$4.88 \times 10^{-6}$	3	$4.88 \times 10^{-6}$	0.021
Interaction				$7.49 \times 10^{-6}$	3	$7.49 \times 10^{-6}$	0.022
Residual error				$8.99 \times 10^{-7}$	6	$1.50 \times 10^{-7}$	
Lack of fit				$8.72 \times 10^{-7}$	5	$1.74 \times 10^{-7}$	0.287
Pure error				$2.65 \times 10^{-8}$	1	$2.65 \times 10^{-8}$	
Corrected total				$3.70 \times 10^{-5}$	16	$2.31 \times 10^{-6}$	

<sup>a</sup>  $r = 0.9483$ ,  $r^2 = 0.8993$ , adjusted  $r^2 = 0.7315$ .

<sup>b</sup>  $r = 0.9878$ ,  $r^2 = 0.9758$ , adjusted  $r^2 = 0.9355$ .

Once the regression models have been formulated, their adequacy of fit and their residual variance (lack of fit) were calculated in order to ensure that the models are an adequate approximation of the data. The  $F$ -values for E6300 and E2292 were 0.027 and 0.17, respectively, which are both lower than the tabulated  $F$ -value (4.15) signifying that the models can adequately represent the data. The  $F$ -statistics for the lack of fit tests was 6.59 and 124.65 for E6300 and E2292, respectively. For a significant lack of fit, the  $F$ -values would have to be as large as 230.2 (tabulated  $F_{0.05(5,1)}$  value) indicating that all differences between the means obtained in the different experimental conditions can be sufficiently explained by the produced models and there are no additional significant effects that need to be accounted for.

The visualisation of E6300 and E2292 photodegradation rate constants as a function of two of the studied variables was

attained keeping constant the rest of the variables at the medium level ('0' in coded units) of the experimental domain. The three-dimensional response surfaces of this polynomial fit and for all possible parameter combinations are depicted in Fig. 3.

Based on these graphs and the parameter coefficients of Table 3 we attempted to interpret the behavior of the sunscreen compounds as a function of matrix constituents. The negative value of DOM coefficient ( $b_2$ ) indicates retardation of E2292 photodegradation in the presence of organic matter. This can be explained by a competition process between DOM and E2292 for the available photons, thus slowing down the direct photochemical reaction (optical filter effect) [17]. Another reason may be the partial binding between DOM and E2292 by hydrophobic partitioning or weak van der Waals forces, a fraction that is not available to photolysis action. Furthermore, DOM has been recognized as the most important scavenger of  $\bullet\text{OH}$  radicals in

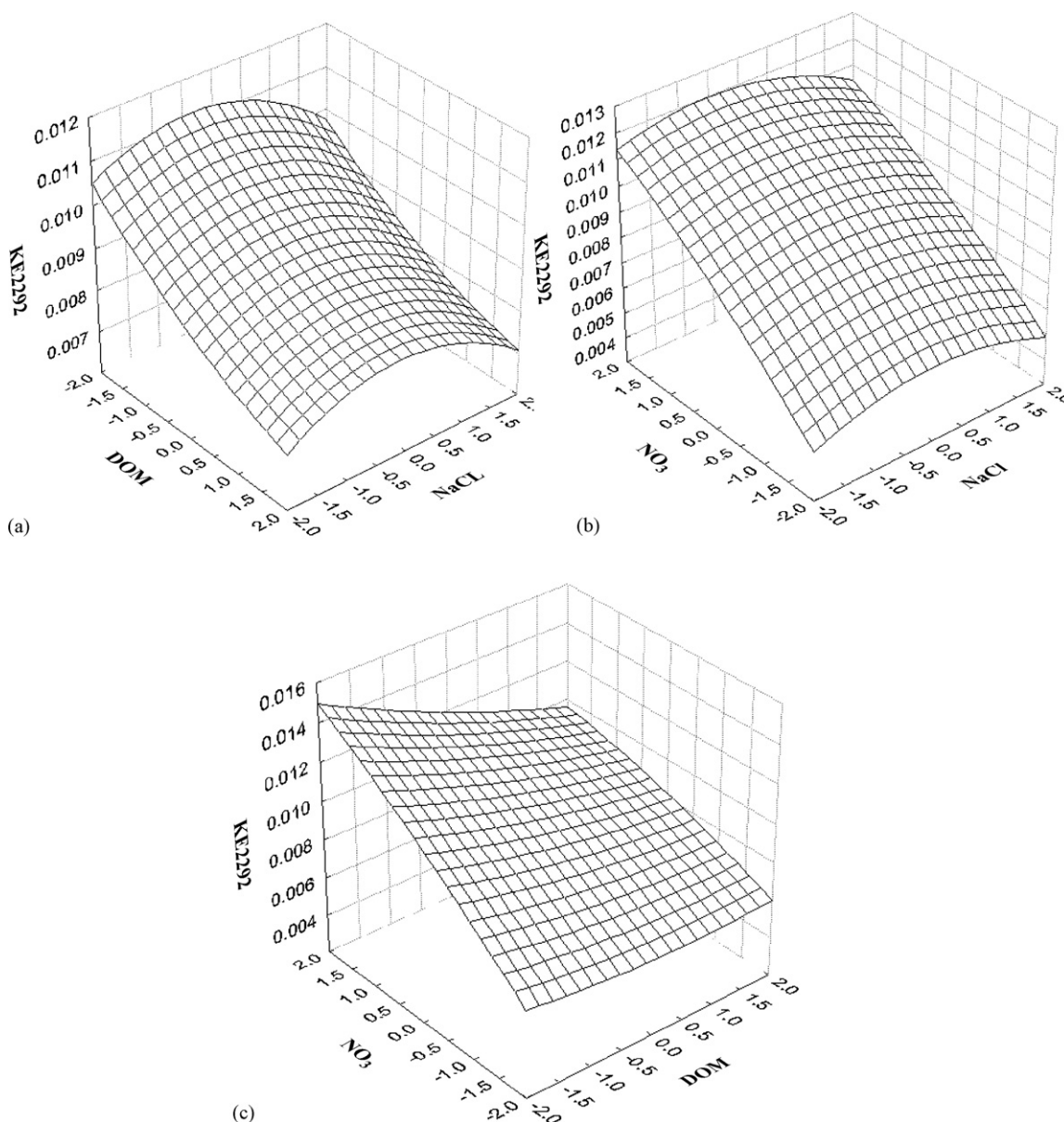


Fig. 3. Three-dimensional (3D) response surfaces of the multivariate optimization for E2292 (a–c) and E6300 (d–f). Factor levels in coded units.

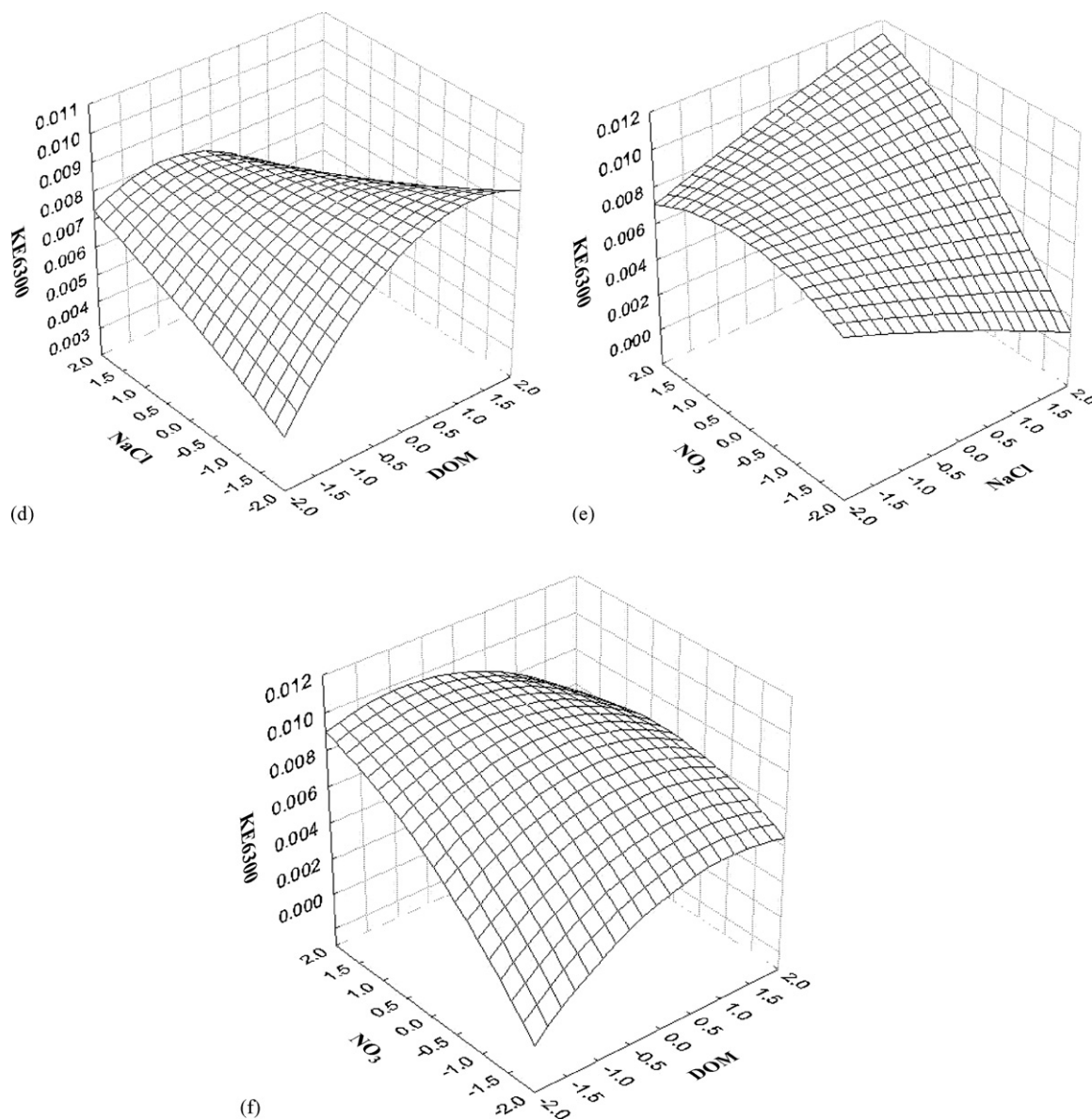


Fig. 3. (Continued).

low-alkalinity waters therefore the reduction of oxidizing radicals may be another reason for this pattern [18]. With regards to nitrate, the positive sign of  $NO_3^-$  linear effect ( $b_1X_1$ ) indicate acceleration of photolysis rate with increasing concentrations. This can be ascribed to the photochemical production of hydroxyl radicals which have been shown to act as photosensitizers to the light mediated transformation of organic compounds in natural waters [19]. For the other parameters no statistically significant interactions were observed therefore their influence plays a secondary role. The most interesting finding is that chloride retarded the photodegradation rate at concentrations equivalent to estuarine or seawaters a situation which is consistent with  $\bullet OH$  scavenging by chloride ions [20].

For E6300, the linear effects of  $NO_3^-$  and DOM ( $b_1X_1$  and  $b_2X_2$ ) gathered in Table 3 suggest that the influence of these matrix constituents increase of its photodegradation rate. This means that DOM act as photosensitizer a case which has been

verified in both laboratory and field experiments [8,9], especially at low nitrate levels. The negative sign of the interaction term between  $NO_3^-$ –DOM ( $b_{12}X_{12}$ ) may be due to the scavenging of aqueous electrons from nitrate produced upon the photolysis of DOM [21]. This is further supported by the theory that DOM is both an important photosensitizer and a scavenger of reactive intermediates and photons [8,22] and its behavior is a function of sample matrix composition [8,9]. Supportive to this observation are the negative coefficients of the quadratic terms indicating deceleration of the photolysis rates. In the case of DOM, beyond scavenging of  $\bullet OH$  radicals, this can also be attributed to the competitive light absorption of DOM over E6300 (optical filter effect). In the case of  $NO_3^-$ , it has been reported that at elevated  $NO_3^-$  levels increasing DOM concentrations reduce the photodegradation rate constants [9]. Since the quadratic effects of the investigated parameters have been examined by keeping the rest constant at the medium level (0 coded units) this observation



is not strange. With regards to NaCl, almost all coefficients were holding a negative sign implying that chloride ions scavenge hydroxyl radicals thus reduce the photolysis rates especially at the maximum NaCl and DOM concentrations (Fig. 3d). This may be attributed to increased E6300 binding to DOM as water salinity increases, a case which has also been observed for other organic contaminants [23].

An interesting observation from the second-order polynomial models is that they can detect (environmental) parameter interactions irrespectively of the effect of the linear terms on the photolysis rate constants, a case which is not possible with univariate methods. In the case of E6300 both  $\text{NO}_3^-$  and DOM have the largest positive coefficients but their quadratic and interaction products have negative signs. Similar observations can be made with E2292. This indicates that the produced coefficients can quantitatively reflect qualitative changes in the photolysis rates induced by parameter interactions. However, the coefficients values will be produced on the grounds of obtaining the best polynomial equation that efficiently estimates photolysis rates. In the compromise of these two aspects (data interpretation and simulation) some coefficients may not always have a physical meaning or the mechanisms responsible for the observed behavior may be too intricate to be accounted for by the present approach. In that case, more complex designs or specifically oriented experiments should be considered as supplementary. In our study, the interaction term of  $\text{NO}_3^-$  with NaCl for E6300 holds a negative sign which is rather unexpected. A possible explanation could be given by inspecting the graphs of Fig. 3 where the maximum NaCl and  $\text{NO}_3^-$  concentrations increase the photolysis rate while reduction of either NaCl or  $\text{NO}_3^-$  have the opposite effect. Intuitively, we inferred that this trend reflects the relative importance of DOM (as previously discussed) on the influence of  $\text{NO}_3^-$  and NaCl but the design could not lead to secure conclusions.

#### 4. Conclusions

In this study, the analytical utility of multivariate chemometric techniques in the investigation of aqueous photolysis of organic compounds has been demonstrated. The novelty of the method lies not only with the investigation of photolysis behavior of sunscreen agents in natural waters but also with the formulation of the experimental design. In contrast to pre-

vious methods where environmentally realistic sample matrixes were used, this study demonstrates that in order to delineate complex factor interactions their effect should be investigated over a large concentration range. In that manner, the absolute and relative contribution of each parameter can accurately be defined on both a qualitative and a quantitative basis. As with most mathematical models, some loss of physical information may be observed. However, the results suggest that the proposed method is subject to minor interferences of this kind.

#### References

- [1] S.O. Pehkonen, Q. Zhang, *Crit. Rev. Environ. Sci. Technol.* 32 (2002) 17.
- [2] J. Bachman, H. Patterson, *Environ. Sci. Technol.* 33 (1999) 874.
- [3] S. Canonica, U. Jans, K. Stemmler, J. Hoigne, *Environ. Sci. Technol.* 29 (1995) 1822.
- [4] X. Zhou, K. Mopper, *Mar. Chem.* 30 (1990) 71.
- [5] O.C. Zafriou, J. Jousset-Dubien, R.G. Zepp, R.G. Zika, *Environ. Sci. Technol.* 18 (1984) 358A.
- [6] M. Mansour, E.A. Feicht, A. Behechti, I. Scheunert, *Chemosphere* 35 (1997) 39.
- [7] Y.P. Chin, P.L. Miller, L. Zeng, K. Cawley, L.K. Weavers, *Environ. Sci. Technol.* 35 (2004) 5888.
- [8] P.L. Miller, Y.P. Chin, *J. Agric. Food Chem.* 50 (2002) 6758.
- [9] M.W. Lam, K. Tantuco, S.A. Mabury, *Environ. Sci. Technol.* 37 (2003) 899.
- [10] P. Walse, S.L. Morgan, L. Kong, J.L. Ferry, *Environ. Sci. Technol.* 38 (2004) 3908.
- [11] M.W. Lam, C.J. Young, S.A. Mabury, *Environ. Sci. Technol.* 39 (2005) 513.
- [12] N.A. Parisi, D.L. Giokas, A.G. Vlessidis, N.P. Evmiridis, *J. Chromatogr. A* 1097 (2005) 17.
- [13] SRC, EPI Suite, version 3.10, Syracuse Research Corporation, Syracuse, NY, on behalf of the US Environmental Protection Agency, 2000.
- [14] M. Otto, *Chemometrics*, Wiley, Weinheim, 1999.
- [15] S.J. Haswell, *Practical Guide to Chemometrics*, Marcel Dekker, Inc., New York, 1992.
- [16] V. Kavarov, *Cybernetic Methods in Chemistry and Chemical Engineering*, MIR Publishers, Moscow, 1976.
- [17] R.A. Larson, E.J. Weber, *Reactions Mechanisms in Environmental Organic Chemistry*, CRC Press, Boca Raton, 1994.
- [18] P.L. Brezonik, J. Fulkeron-Brekken, *Environ. Sci. Technol.* 32 (1998) 3004.
- [19] P.P. Vaughan, N.V. Blough, *Environ. Sci. Technol.* 32 (1998) 2947.
- [20] C. Liao, S. Kang, F. Wu, *Chemosphere* 44 (2001) 1193.
- [21] R.G. Zepp, A.M. Braun, J. Hoigne, J.A. Leenheer, *Environ. Sci. Technol.* 21 (1987) 485.
- [22] P. Westerhoff, G. Aiken, G. Amy, J. Debroux, *Water Res.* 33 (1999) 2265.
- [23] S. Chiron, J. Abian, M. Ferrer, F. Sanchez-Baeza, A. Messegue, D. Barcelo, *Environ. Toxicol. Chem.* 14 (1995) 1287.



# Determination of poisonous metals in wastewater collected from paint manufacturing plant using laser-induced breakdown spectroscopy

M.A. Gondal<sup>a,\*</sup>, T. Hussain<sup>b</sup>

<sup>a</sup> *Laser Research Laboratory, Physics Department, King Fahd University of Petroleum & Minerals Box 5047, Dhahran 31261, Saudi Arabia*

<sup>b</sup> *Institute of Environmental Science & Engineering, National University of Sciences and Technology (NUST), Tamiz Ud din Road, Rawalpindi, Pakistan*

Received 31 January 2006; received in revised form 7 March 2006; accepted 7 March 2006

Available online 18 April 2006

## Abstract

Laser-induced breakdown spectroscopy (LIBS) system was developed for determination of toxic metals in wastewater collected from local paint manufacturing plant. The plasma was generated by focusing a pulsed Nd:YAG laser at 1064 nm on the solid residue from wastewater collected from paint industry. The concentration of different elements of environmental significance like, lead, copper, chromium, calcium, sulphur, magnesium, zinc, titanium, strontium, nickel, silicone, iron, aluminum, barium, sodium, potassium and zirconium, in paint wastewater were 6, 3, 4, 301, 72, 200, 20, 42, 4, 1, 35, 120, 133, 119, 173, 28 and 12 mg kg<sup>-1</sup>, respectively. The evaluation of potential and capabilities of LIBS as a rapid tool for paint industry effluent characterization is discussed in detail. Optimal experimental conditions were evaluated for improving the sensitivity of our LIBS system through parametric dependence study. The laser-induced breakdown spectroscopy (LIBS) results were compared with the results obtained using standard analytical technique such as inductively coupled plasma emission spectroscopy (ICP). The relative accuracy of our LIBS system for various elements as compared with ICP method is in the range of 0.03–0.6 at 2.5% error confidence. Limits of detection (LOD) of our LIBS system were also estimated for the above mentioned elements.

© 2006 Elsevier B.V. All rights reserved.

**Keywords:** Laser-induced breakdown spectroscopy (LIBS); Multi-elemental analysis; Lead poisoning and detection; Laser diagnostics; Paint industry effluent; Atomic emission plasma spectroscopy; Environmental challenges related with paint industry waste; Environmental impacts of trace metals; Trace metals detection; LIBS applications

## 1. Introduction

An unfortunate consequence of industrialization and industrial production is the generation and release of toxic waste products which are polluting our environment. The paint industry is one of the major contributors for polluting the soil and water resources with poisonous substances such as Pb, Cr and Cd. The paint industry uses about 300 different types of raw materials for production of different kinds and qualities of paints. About 15% raw materials of this industry is petroleum-based [1]. The major raw material of paint industry is pigments, zinc oxide, titanium oxide, lithopone, mineral, turpentine, resins, vegetable resins and gums. Metal and metal oxides are added to paint for pigmentation, film strength, spreading quality and to enhance weather resistance [2]. The paint is categorized in two board

classes: water-based paint and other solvent based paint. The paint industry in Saudi Arabia produces a wide range of finished and intermediate products which are pigments, distempers, plastic emulsion, enamel, undercoat, primers, rubber paint, air craft paint, marine paint, anticorrosive paint, antifouling paint, etc. [3]. The main source of wastewater in any paint industry is the manufacturing plant water-based paint. The estimated quantity of process wastewater is 3–7 m<sup>3</sup>/day for a normal operating day for a typical paint industry [4]. Usually high volume of wastewater is generated during washing activities at paint industrial units in the water-based paint manufacturing area and water-based resin manufacturing area and lead-chromate pigment manufacturing process zone. The environmental challenges for the paint industry are associated with wastewater generation, air emission and solid waste contaminated with toxic metals such as lead, chromium and cadmium [5,6].

Many studies have warned us about the health risks due to toxic metal-containing paint at our homes, work place and other industrial units using paint. For example lead (Pb) poisoning

\* Corresponding author. Tel.: +966 38602351; fax: +966 38604281.

E-mail address: [magondal@kfupm.edu.sa](mailto:magondal@kfupm.edu.sa) (M.A. Gondal).

may be one of the most prevalent diseases of environmental and occupational origin due to the use of lead in paints in buildings. Its toxic effects, which include anemia, neurological problems (which may be largely irreversible), colic, renal and reproductive problems, are various and can be severe. Children and developing fetuses are especially at risk for Pb poisoning [7]. Just a few  $\mu\text{g}/\text{dl}$  can cause developmental problems in children, while  $>100 \mu\text{g}/\text{dl}$  can cause death in children.

Wastewater from paint industry can be highly toxic to the environment as well. It harms fish, wildlife, and contaminates the food chain if poured down a storm drain. It can also pollute groundwater if dumped onto the ground. Excessive paint pouring down the drain disrupts microbes and causes sewage treatment to be less effective. Paint has also adverse effects on human health occupants [8]. If used in closed area, its chemical components can irritate eyes, skin and lungs and causes headaches and nausea. It can also contribute to respiratory problems, muscle weakness, liver and kidney damage. The other metals along with lead which are present in paint such as chromium and cadmium also pose many health risks [9]. To understand and minimize the hazardous effects of paint on environment and human health, there is a great need for the development of an analytical tool which could determine the heavy metals content in paint and wastewater from paint industry accurately and rapidly.

Laser-induced breakdown spectroscopy (LIBS) is an emerging technique for the rapid and accurate analysis of solid waste. Till date, most of the work on quantitative and qualitative analysis using LIBS has been focused to solid samples and much less work has been carried out on liquid samples [10,11]. The main reason for application of LIBS for solid samples could be that analysis of liquid samples by existing analytical techniques is well established and does not require preparatory steps as often required for the analysis of solid samples using conventional analytical techniques (i.e. atomic absorption spectrometer, ICP, etc.). In addition, the LIBS applications for analysis of liquid samples is not straight forward matter and could embrace many problems with laser-plasma generation mechanism from liquids, as compared with laser produced plasmas from solid samples. This could be due to the low density of liquids as compared with solids and also shock waves associated with vaporization of liquid samples to create aerosol above the liquid surface. These aerosols may disturb the incident laser radiations and the plasma emitted light returning to the spectrometer [12]. In addition, these aerosols could damage the optical components employed for guiding the laser beam onto liquid surface and for the collection laser produced plasma emission. It is also probable that laser pulse could induce bubbles inside liquids that are not transparent to laser-induced plasma and could affect the reproducibility of the results.

In order to overcome the above mentioned problems for analysis of paint samples in liquid by using LIBS, residue of wastewater from paint industry was collected on a filter paper and laser produced plasma from paint residue on filter paper was then analyzed using our LIBS spectrometer. This approach was adopted in this study to test the effluent of paint industry wastewater samples collected from local paint manufacturing plant. The foundation for LIBS setup is a solid-state, short-pulsed Nd:YAG

laser that is focused on a sample to generate a high-temperature plasma. Upon cooling, the excited atomic, ionic, and molecular fragments produced within the plasma emit radiation that is characteristic of the elemental composition of the material in the volatilized sample. The LIBS technique has proven capable of detecting many metals of environmental concern in both natural and anthropogenic materials. Because off-site analysis is unnecessary, the measurement complexity is greatly reduced and there is no chance for sample loss or cross-contamination during transport or complicated preparations for laboratory analysis. Additional LIBS advantages include the ability to conduct standoff distance measurements (perhaps up to 100 m) which allows access to difficult (i.e. contaminated) locations, a small sample size ( $<1 \mu\text{g}$ ) which allows for discreet elemental analysis of individual particles, and the analysis of certain elements outside the capability of other current field portable techniques (such as X-ray fluorescence, XRF). Due to this reason, a system based on LIBS principle is being developed for future missions of NASA for remote analysis of geological rocks present on Mars surface [13]. Laser-induced breakdown spectroscopy (LIBS) has a lot of applications as a fast and simple method to analyze and to determine the elemental composition of various solid samples such as alloys, glass, paint and soil [14–19].

The important parameter [20,21] which can influence the sensitivity of LIBS system include the laser pulse characteristics (pulse width, energy), the sample homogeneity and the sampling geometry (distance from the focusing lens to the sample, focal length of the collecting lens, fiber optics, etc.). All these parameters were optimized to achieve the best limit of detection using our system prior to its applications for the analysis of wastewater samples collected from local paint manufacturing plant. The aim of this work is to analyze the wastewater of paint manufacturing plant using LIBS spectrometer for environmental concerns. The data obtained concerning concentration of the contaminants with our LIBS spectrometer was crosschecked with the standard method such as inductively coupled plasma (ICP) spectrometer. The results obtained with our LIBS setup were in excellent agreement with ICP results. The development of the LIBS system for environmental and other analytical applications such as monitoring of toxic metals in paint industrial wastewater is a continuity of our group activities for development of laser based pollution monitoring systems like photo-acoustic and LIDAR system [22–29].

## 2. Experimental setup details

A schematic diagram of the experimental setup applied for the analysis of wastewater of paint manufacturing plant is shown in Fig. 1. LIBS system used in this study consists of Ocean Optics LIBS 2000+ spectrometer, a sample chamber, OOILIBS software, Nd:YAG laser (Spectra Physics, Model GCR100). It can deliver maximum pulse energy of 1 J with a laser pulse width of 8 ns and operate at a 10 Hz pulse repetition rate, operating in Q-switched mode. Here 1064 nm radiations emitted at fundamental frequency from Nd:YAG laser were applied for production of plasma spark at target surface. A pulse from this Q-switched Nd:YAG laser at fundamental wavelength 1064 was

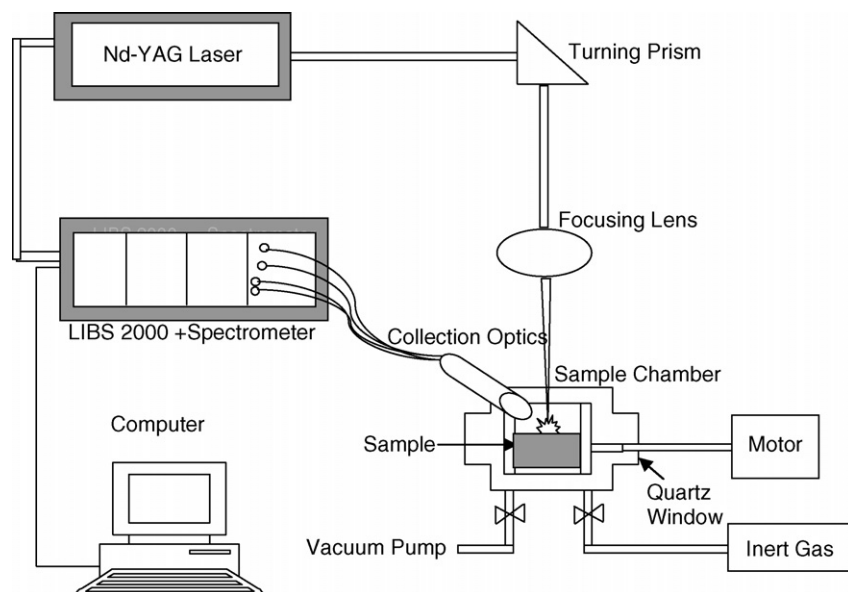


Fig. 1. Schematic diagram of the experimental setup applied for the analysis of industrial paint wastewater samples.

focused by a convex lens of focal length 30 mm onto the residue sample of paint industry collected on a filter paper to create a plasma spark or breakdown in the sample. The laser energy was measured with a calibrated energy meter (Ophir Model 300) for the study of dependence of LIBS signal on incident laser energy.

The pulse energy utilized in this experiment was in the range of 50–120 mJ. The light from the plasma spark is collected by a collimating lens using UV graded fused silica 1 m, multi-mode sampling fiber with SMA connector and is transferred to LIB2000+ spectrometer (Ocean Optics). Our LIBS 2000+ has four spectrometer modules to provide high resolution (FWHM 0.1 nm) in the 200–620 nm wavelength region. The detector has a gated CCD camera having 14,336 pixels. This makes it possible to measure a LIBS spectrum over broad spectral range (200–620 nm) simultaneously with high spectral resolution (0.1 nm). The emission is observed at a 45° angle to the laser pulse. Software built in the spectrometer read the data from the chip and reconstructed the spectrum. For each LIBS analysis, a sample of paint residue on filter paper was pasted on a stain less steel platform disc shaped (20 mm diameter × 10 mm long) mounted on a rotary table. The table was positioned such that the focal volume of the laser pulse was centered in the disk holding the sample. Twenty laser pulses were directed into the cup to complete one measurement. The table was rotated using a step motor having 12 revolutions per minutes. The concentrations of different trace metals present in the wastewater samples were also measured with a calibrated ICP spectrometer to verify the results achieved with our calibrated LIBS method.

The gating of the ICCD camera is important for the improvement of LIBS sensitivity. The first trigger from the delay generator fired the flash lamp of the laser, while the second one was sent to the Q-switched of the laser build in LIBS spectrometer with delay of 145 μs relative to the first trigger. Here trigger is sent to the ICCD which gate the input to the ICCD camera.

### 2.1. Sample preparation and reagent used for LIBS and ICP analysis

The wastewater generated by pigment manufacturing process at paint manufacturing plant located in Industrial City Riyadh, Saudi Arabia contains heavy metals especially lead and chromium. Usually the wastewater is discharged without any treatment. Only few units have installed sedimentation tanks for physical treatment of wastewater before discharging into sewerage line. Depending on the size of the unit about 90–300 l of used solvent is generated per day, from a solvent-based-paint plant. But during cleaning of different containers discharge level increases five times higher than the normal level. We took the samples of wastewater during normal peak working hours of plant in plastic bottles according to the standard procedure. The plastic bottles were thoroughly washed to avoid any contamination before taking samples.

Analytical-reagent grade chemicals without further purification were used for the calibration and analysis of paint samples by ICP and LIBS method. For calibration purposes, the metals used are lead, copper, chromium, calcium, sulphur, magnesium, zinc, titanium, strontium, nickel, silicone, iron, aluminum, barium, sodium, potassium and zirconium. All these metals in powder forms were of high purity (99.99%) and procured from Fisher Scientific, USA. For the construction of the calibration curves, different stoichiometric samples comprising these metals were prepared. Pure metals in powder form were mixed with the matrix material KBr in a ball milling apparatus in order to ensure good mixing and homogeneity. It was thoroughly mixed and grinded to make a homogeneous mixture. Here the KBr used as binding material (matrix) was of high purity (99.99%) procured from Fluka, Germany.

For the analysis of paint samples using ICP technique, the wastewater sample collected from paint manufacturing plant was digested with nitric acid (99.99%, Fisher Scientific, USA) and left over night. The resulting residue was then ashed at

500 °C. The ashed sample was further diluted with nitric acid (99.99%, Fisher Scientific, USA) and the resulting solution was analyzed for poisonous metals using inductively coupled plasma spectrometer calibrated using reference standards of three level accuracy. For laser-induced breakdown spectroscopy, wastewater collected from a paint manufacturing plant was filtered on a filter paper and the residue was thoroughly mixed and were dried at 105 °C in an oven. The dried paint waste residue was then shifted to LIBS ablation chamber. In order to test the homogeneity of our samples, several LIBS measurements were performed at different locations of the surface of residue paint sample.

### 3. Results and discussion

The important experimental parameters, which can affect the limit of detection (LOD) in LIBS, are laser energy, gate delay time, focusing lens for incident laser radiation, collecting lens for laser produced emission and target rotation speed. The main parameters which were studied in this experiment for improvement of LOD and are mentioned in this work are laser energy, gate delay time while other were optimized for best signal to noise ratio of LIBS signal.

#### 3.1. Dependence of LIBS signal intensity on incident laser energy

In LIBS, one requires high-pulse energy of laser beam to generate plasma and to excite the sample species into ionic and neutral atomic transitions. The laser energy can affect the property of the induced plasma and eventually the figure of merit of LIBS measurement. The signal of the analyte lines is proportional to the laser energy [30] while the laser produced plasma is in the optical thin region. This has been confirmed from constant ratios of the multiplet lines of the test elements over the range of the data.

We recorded the emission spectra at different laser energies to study the effect of the laser energy on the line emission intensity. Plasma emission spectra were recorded for most of the elements under investigation at different laser energies. A time delay of 4.0  $\mu\text{s}$  was used throughout this study. To study the effect of laser energy on the intensity for 280.2 nm emission line of lead (signature of Pb), laser produced plasma emission spectra from paint samples were recorded in the 200–620 nm region at laser energies of 50, 60, 70, 80, 90, 100, 110 and 120 mJ. A time delay of 4.0  $\mu\text{s}$  was used where maximum signal intensity of LIBS signal for lead was achieved. Fig. 2 shows a typical trend of dependence of laser produced plasma on incident laser energy for lead element present in a test sample. Here the line intensity variation versus incident laser energy is plotted. It is clear from Fig. 2 that the line intensity increases with rise in incident laser energy from 50 to 120 mJ. The line intensity dependence (for lead) shows linear dependence on the incident laser energy which is clear from the least square fit,  $R^2 = 0.9999$ . It is worth mentioning that an incident laser pulse energy = 120 mJ was enough for detection of toxic metals present in paint samples under investigation.

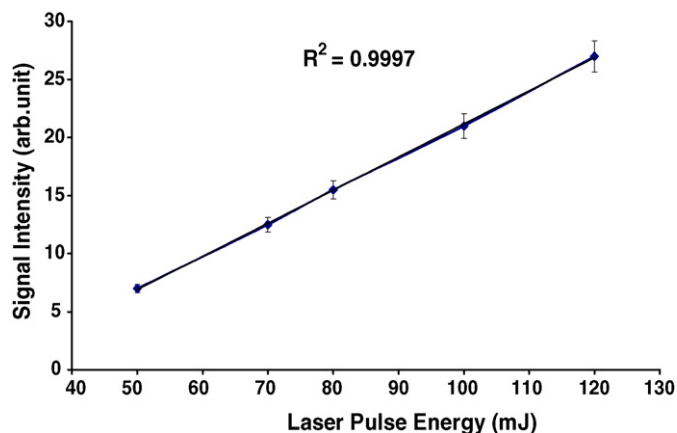


Fig. 2. The dependence of the intensity of the Pb 280.2 nm emission line on laser energy recorded with our LIBS system wastewater sample collected from local paint manufacturing plant.

#### 3.2. LIBS signal intensity dependence on time delay

The importance of the time delay between laser pulse initiating plasma spark and detector (gated ICCD camera) has been stressed in several papers during the past few years [30,31] and as a matter of fact, the LIBS spectra shows a dramatic time evolution. Delay times were controlled by a Q switch trigger pulse to the laser and the trigger pulse to gate the ICCD camera. A series of measurements were made to find the optimum time delay between the laser pulse and the beginning of the LIBS spectra acquisition. The delay times were chosen according to the detection of maximum LIBS signal intensity for each element. These delay times were controlled by a Q switch trigger pulse to the laser and the trigger pulse to gate the ICCD camera. This option is provided in the LIBS 2000+ spectrometer and our YAG laser applied in this study.

Elements under investigation show the maximum spectral line intensity between 3.0 and 4.0  $\mu\text{s}$  delay time. Clean shots were applied to clean the sample surface before the actual measurements were made.

#### 3.3. Calibration curves for elements under investigation

The total intensity of a spectral line ' $I$ ' from an excited atom or ion in homogenous and optically thin plasma for a transition from state  $j \rightarrow i$  is given by [32]:

$$I = h\nu_{ji}A_{ji}N_j \quad (1)$$

where  $\nu_{ji}$  is the frequency of the transition from state  $j \rightarrow i$ ,  $A_{ji}$  the Einstein coefficient for spontaneous emission,  $N_j$  the population of the upper level  $j$  and  $h$  is the Planck constant.

If the energy levels concerned are in local thermodynamic equilibrium (LTE), then population density of upper level  $N_j$  is related to ground level number density ( $N$ ) by Boltzman equation [33,34]:

$$N_j = Ng_j Q^{-1} \exp\left(-\frac{E_j}{kT}\right) \quad (2)$$

Here  $g_j$  and  $E_j$  are the statistical weight and energy of upper level  $j$ , respectively and  $Q$  is the partition function of relevant species,  $K$  is the Boltzman's constant and  $T$  is the electron temperature of the plasma. So from above two equations, we get:

$$I = hv_{ji}A_{ji}Ng_jQ^{-1} \exp\left(-\frac{E_j}{kT}\right) \quad (3)$$

According to Eq. (3), one can determine the population density of the relevant species (atoms or ions) for an element in plasma from a measurement of the absolute intensity of corresponding transition and knowledge of the excitation temperature and atomic constants. However it is not possible to derive a theoretical expression relating  $N$  and concentration of that element in solid sample under investigation. Hence, in practice, an empirical relationship is sought between the observed line intensity ( $I_j$ ) and corresponding concentration ( $C$ ), i.e.:

$$I_j = F(C) \quad (4)$$

Here  $F(C)$  is called analyte calibration function and the graph between the LIBS intensity of a line of specific element and the concentration is called the calibration curve. Such curve can be drawn by measurements of reference samples of known concentrations termed as standard samples and can be used to determine the elemental concentration in unknown sample like our paint sample.

A plot of intensity  $I_{ji}$  as a function of elemental concentration  $n_j$  yields the calibration curve. If the dependence of LIBS signal intensity on the elemental concentration is linear then one can determine the unknown concentration of particular element at any LIBS signal intensity  $I_{ji}$  provided that the same experimental parameters (time delay, incident laser energy, collecting

fiber optics and incident focusing optics distance, target rotation speed, atmospheric pressure) are selected.

In this experimental work, four samples of known concentration of 10, 1, 0.1 and 0.01 weight percent (wt.%) of elements under investigation were prepared in the matrix of KBr. The LIBS spectra were recorded for these four (10, 1, 0.1 and 0.01 wt.%) concentrations of each element. All these spectra were recorded with an average of 20 laser shots, at three different locations on the sample surface. The calibration curve for each element under investigation was established by plotting the LIBS signal intensity of specific transition of each element as a function of the wt.%. The LIBS signal intensity showed linear dependence on the concentration of lead and copper in the standard sample as predicted by Eq. (1).

The line interference is the most sever problem for emission identification, thus we choose those lines for analysis which are free from interference or those which have minimal effect are selected to get better results.

### 3.4. Limit of detection

The determination of the detection limit is very important for samples under investigation. Detection limit here means the lowest concentration that can be detected with LIBS. The detection limit (LOD) can be estimated using the equation [35–37]:

$$\text{LOD} = \frac{2\sigma_B}{S} \quad (5)$$

where  $\sigma_B$  the standard deviation of the back ground and  $S$  is the sensitivity which is given by the ratio of the intensity to the concentration. The detection limit for LIBS analysis of paint samples under investigation was calculated by using the above mentioned equation. The relative standard deviation (R.S.D.) is

Table 1  
Elements detected in wastewater collected from paint industry and comparison of LIBS with ICP

Elements detected in wastewater	Wave length (nm) <sup>a</sup>	Comparison of LIBS and ICP and relative accuracy (RA)			Standard deviation (S.D.) LIBS	Limit of detection LOD of LIBS (mg kg <sup>-1</sup> )	Maximum permissible safe limits (mg kg <sup>-1</sup> ) <sup>b</sup>
		LIBS (mg kg <sup>-1</sup> )	ICP (mg kg <sup>-1</sup> )	RA			
Al	394.4	133.2	129.0	0.03	1.09	12	30
Ba	553.54	119.2	114.0	0.04	1.12	14	2.0
Ca	393.37	301.7	293.0	0.03	1.16	12	–
Cr	428.9	3.70	2.46	0.56	0.99	2	1.0
Fe	567.9	119.7	115.0	0.04	0.71	10	25
Cu	324	3.20	2.65	0.26	0.95	2	1.2
Mg	518.29	199.6	192.0	0.04	0.75	3	–
K	404.72	28.0	25.3	0.11	1.33	4	–
Na	588.9	172.6	166.0	0.04	0.92	5	1000
Ni	352.4	1.20	0.51	0.60	1.16	0.2	2.5
P	255.3	237.9	230.0	0.03	1.23	4	50
Pb	280.2	6.19	5.90	0.07	0.99	3	.5
S	547.9	71.6	67.6	0.06	1.12	7	800 for sulphate
Si	250.69	35.2	32.6	0.08	1.43	10	–
Sr	460.73	4.1	3.2	0.32	1.60	2	–
Ti	445.7	42.05	39.30	0.07	1.43	10	–
Zn	334.5	20.1	18.3	0.11	1.12	5	10
Zr	487.2	12.30	9.25	0.34	1.73	4	–

<sup>a</sup> Reference for wavelengths: [38] and NIST database.

<sup>b</sup> Environmental Regulation Standards for Saudi Industries set by Royal Commission Jubail, Saudi Arabia.



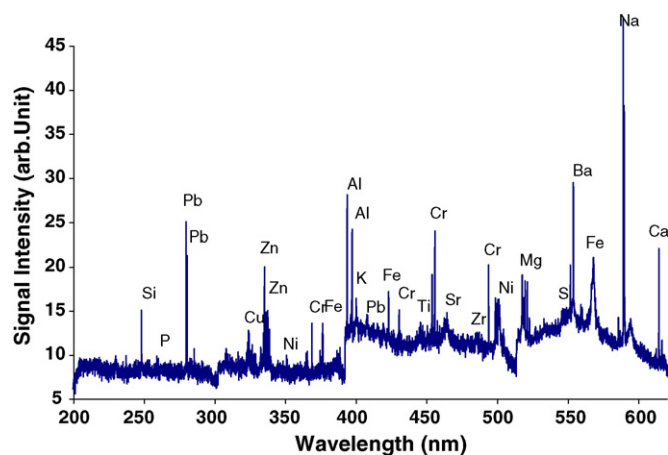


Fig. 3. Typical LIBS spectra of wastewater sample collected from local paint manufacturing plant in the region of 200–620 nm recorded at delay time of 4.0  $\mu$ s and laser pulse energy = 120 mJ.

given by the equation:

$$\text{R.S.D. (\%)} = \frac{\text{standard deviation}}{\text{mean}} \times 100 \quad (6)$$

The relative standard deviation decreased with the number of shots but no improvement in R.S.D. after 20 shots. The R.S.D. value in our case was 3.4%. The paint samples results were comparable to the results obtained by inductively coupled plasma emission spectroscopy (ICP). The limit of detection for some elements under investigation is given in Table 1.

### 3.5. LIBS analysis of samples

A typical LIBS spectra due to wastewater of paint manufacturing plant sample recorded in the 200–620 nm spectral region with our setup is depicted in Fig. 3. Here the delay time between laser trigger and the opening of shutter of ICCD camera was set at 4  $\mu$ s and the laser pulse energy was 120 mJ. The distance between the optical fiber and the plasma was 10 mm. Average spectra due to 20 laser shots were recorded for each data point. The averaging of the 20 laser shots spectra reduces the background noise to a great extent when compared to the single shot spectrum of the sample. The trace metals present in the wastewater of industrial paint sample were identified and are marked in Fig. 3. The major elements detected in the sample are lead, copper, chromium, calcium, sulphur, magnesium, zinc, titanium, strontium, nickel, silicone, iron, aluminum, barium, sodium, potassium and zirconium.

The 518.36 nm emission line of Mg (signature of Mg), the 521.82 nm emission line of Cu (signature of Cu), the 280.2 nm emission line of Pb (signature of Pb), the 393.38 nm emission line of Ca (signature of Ca), 394.37 nm emission line of Al (signature of Al), 428.97 nm emission line of Cr (signature of Cr), 334.5 nm emission line of Zn (signature of Zn) and 588.9 nm emission line of Na (signature of Na) have been selected for quantitative analysis. These emission lines have minimal interference from other emission lines, do not involve the ground state so that self-absorption is almost absent, and are intense enough. Due to these reasons, these lines are useful for quantitative

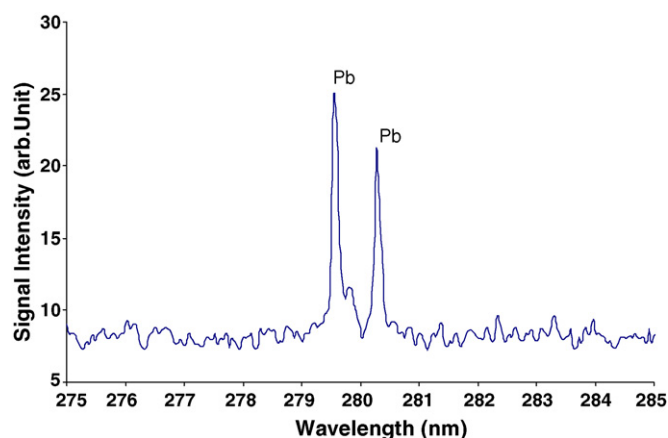


Fig. 4. Fine structure component of Pb present in wastewater sample collected from local paint manufacturing plant. This spectrum was recorded in the 275–285 nm region at delay time of 4.0  $\mu$ s and laser pulse energy of 120 mJ.

analysis. The fine structure component of these trace metals are also well resolved with our LIBS spectrometer. A typical fine structure spectrum of Pb is also presented in Fig. 4. All the spectral lines for above mentioned elements recorded with our LIBS setup were identified using the NIST atomic spectral database and also using the reference [38].

Similarly the wavelengths for Ba, Fe, P, Sr, Ti, Cu, Si, K, Zr, etc. are listed in Table 1. The above mentioned selected lines were employed to study the effect of the different experimental parameters and to compare the signal intensities with the calibration curves of the elements under investigation. In this work, the experimental parameters, which can affect LIBS data precision and limit of detection, are delay time, laser pulse energy, number of shots accumulated, the distance between the plasma and collecting optical fiber.

The concentration determined with our LIBS set up for each element, is also listed in Table 1 and has been confirmed by the analysis using conventional analytical technique such as ICP. The values obtained with our LIBS setup are in well agreement with the ICP results. The concentration of lead measured with our system is 6.19 mg kg<sup>-1</sup> which is quite high as compared with the standard permissible safe limit of 0.5 mg kg<sup>-1</sup> set by EPA and other regulatory authorities.

Lead is basically found in the effluent due to the use of lead chromate in the paint production process. The main reason that the paint industries in developing countries could not be able to meet the environmental standards for effluent is due to the loss of pigment during supernatant decanting and discharging the pigments slurry filtrate into the sewer without treatment. Lead can be found in the effluent in the following forms such as: Pb<sup>2+</sup>, PbCr<sub>2</sub>O<sub>7</sub> (the solubility of lead dichromate is very high), PbCrO<sub>4</sub> (pigment, the solubility of lead chromate is low, about 7  $\times$  10<sup>-6</sup> g/100 g water) and Pb(Ac)<sub>2</sub> (the solubility of lead acetate is very high and is about 55 g/100 g water). However LIBS system cannot distinguish between these different forms of lead and could detect only the elemental compositions of trace metals present in the wastewater.

Similarly for chromium, the maximum permissible limit is 1 mg kg<sup>-1</sup> and the detected value in the wastewater of industrial

paint was  $3.7 \text{ mg kg}^{-1}$ . This high concentration of chromium in the effluent is found due to the manufacturing of lead chromate which is used in the pigment manufacturing process. Although limited amount of chromium is an essential nutrient that helps the body to use sugar, protein, and fat. However, breathing high levels of chromium can cause irritation to the nose, such as runny nose, nosebleeds, and ulcers and holes in the nasal septum. Ingesting large amounts of chromium can cause stomach upsets and ulcers, convulsions, kidney and liver damage, and even death. Skin contact with certain chromium compounds can cause skin ulcers. Some people are extremely sensitive to chromium. Allergic reactions consisting of severe redness and swelling of the skin have been noted.

### 3.6. Comparison of the data from two detection systems and LIBS accuracy

The accuracy and precision for the paint sample under investigation obtained from these two detection systems (LIBS and ICP) are compared in table [1]. The relative accuracy (RA) is calculated as follows [39]:

$$RA = \frac{|d| + S.D. \times t_{0.975}/\sqrt{n}}{M} \quad (7)$$

where  $d$  is the difference between the LIBS measurement and the ICP (standard method). S.D. is the standard deviation of LIBS measurement,  $M$  is the measurement from standard method,  $n$  is the number of measurements and  $t_{0.975}$  is the  $t$  value at 2.5% error confidence. As clear from Table 1, the relative accuracy is in the range of 0.03–0.6 which is quite acceptable for any good instrument.

In order to achieve the better accuracy and precision with our method, following precautions were undertaken. Few laser shots were applied to clean the sample surface prior to actual measurements were carried out on the sample. The trace elements were identified using the NIST Atomic Data Base for neutral and ionized elements and reference data book [38]. Fluctuation of laser pulse was also considered during the performance of the experiment for betterment of precision and accuracy. In order to overcome this problem, sufficient warm up time was permitted for the laser to be stabilized prior to start of the measurements. In addition to stabilization of laser energy over longer periods of time, the LIBS spectra were averaged for 20 laser pulses. The variation in LIBS signal intensity was stabilized by averaging for different laser shots while the relative standard deviation (R.S.D.) decreased with the increasing of number of laser shots.

## 4. Conclusions

The concentration of various elements present in the wastewater collected from local paint manufacturing plant located in industrial city of Riyadh, Saudi Arabia was measured accurately using our LIBS system. The accuracy of our system in terms of qualitative as well as quantitative analysis is obvious from the comparison of LIBS results and the results obtained with a standard method such as inductively coupled plasma spectrometer (ICP). The concentrations of contaminants detected with our

setup for most of the toxic elements like Pb, Cr, Al, Ba, Cu, Fe, P and Zn were higher than the safe permissible limits set by the Saudi Royal commission responsible for environmental standards for water (see Table 1) in the Kingdom of Saudi Arabia. In addition, the sensitive lines for above mentioned elements were identified for the elemental analysis and the calibration curves were effective in quantifying the trace metal concentration in paint water samples. The experience gained through this work can be useful for the development of a portable system for on line analysis of wastewater at paint industrial plants.

## Acknowledgements

The support by the Physics Departments and King Fahd University of Petroleum and Minerals is gratefully acknowledged. One of the author (TH) is thankful to National University of Science and Technology and Government of Pakistan for financial support for his PhD work. He is also thankful to KFUPM for its hospitality and permission to work at its research facilities.

## References

- [1] E.W. Flick, Handbook of Paint Raw Materials, 2nd ed., Noyes Data Corp., Park Ridge, NJ, 1989.
- [2] G.P.A. Turner, Introduction to Paint Chemistry and Principles of Paint Technology, 3rd ed., Chapman & Hall, New York, 1988.
- [3] Royal Commission, Jubail Industrial City, Saudi-Arabian Environmental Regulation Standards, September 1999 and American Public Health Association, Standard Methods for the examination of water and wastewater, 18th ed., American Public Health Association, Washington, DC, 1992.
- [4] M.A. Briggs, Paint Research Association Technical Report TR14177, Paint Research Association, Teddington, UK, 1977.
- [5] G.E. Weismantel, Paint Hand Book, McGraw-Hill, New York, 1981.
- [6] C.H. Martens, Emulsion and Water-soluble Paints and Coatings, Reinhold Publishing Company, New York, 1964.
- [7] B.E. Davies, Water, Air, Soil Pollut. 94 (1997) 85.
- [8] E.A. Mackey, P.R. Becker, R. Demiralaph, P.R. Greenberg, B.J. Koster, S.A. Wise, Arch. Environ. Contam. Toxicol. 30 (1996) 503.
- [9] P.N. Lee, D.M. Corning (Eds.), Experimental Toxicology, Cambridge, 1993.
- [10] A.A. Adeniyi, Environ. Int. 22 (1996) 62.
- [11] J.B. Stiger, H.P.M. De Haan, R. Guichert, C.P.A. Deckers, M.L. Daane, Environ. Pollut. 107 (2000) 451.
- [12] P. Ficht, P. Mauchien, J.F. Wangner, C. Moulin, Anal. Chim. Acta 429 (2001) 269.
- [13] O. Samek, D.C.S. Beddows, J. Kaiser, S.V. Kukhlevsky, M. Liska, H.H. Telle, J. Young, Opt. Eng. 39 (2000) 2248.
- [14] T. Bundschuh, W. Hauser, J.I. Kim, R. Knopp, F.J. Scherbaum, J. Colloids Surf. 180 (2001) 285.
- [15] A.K. Knight, N.L. Scherbarth, D.A. Cremers, M.J. Ferris, Appl. Spectrosc. 4 (2000) 331.
- [16] F. Colao, R. Fantoni, V. Lazic, A. Paolini, G. Ori, L. Marinangeli, Planet. Space Sci. 52 (2004) 117.
- [17] H. Morita, K. Semba, Z. Bastl, J. Pola, J. Photochem. Photobiol. 116 (1998) 91.
- [18] B.J. Marquard, S.R. Goode, S.M. Angel, Anal. Chem. 68 (1996) 977.
- [19] H. Kurniawan, S. Nakajima, J.E. Batubara, M. Marpaung, M. Okamoto, K. Kagawa, Appl. Spectrosc. 49 (1995) 1067.
- [20] B.T. Fisher, H.A. Johnson, S.G. Buckley, W. Hahn, Appl. Spectrosc. 55 (2001) 1312.
- [21] J. Winefordner, I. Gornushkin, D. Pappas, O. Matveev, B. Smith, J. Anal. At. Spectrom. 15 (2000) 1161.
- [22] M.A. Gondal, Appl. Opt. 36 (1997) 3195.

- [23] M.A. Gondal, J. Mastromarino, *Appl. Opt.* 40 (2001) 2010.
- [24] M.A. Gondal, M.A. Baig, M.H. Shwehdi, *IEEE Trans. Dielect. Electr. Insul.* 9 (2002) 421.
- [25] M.A. Gondal, M.H. Shwehdi, A. Dastgeer, *Talanta* 62 (2004) 131.
- [26] M.A. Gondal, J. Mastromarino, *Talanta* 53 (2000) 147.
- [27] M.A. Gondal, J. Mastromarino, U.K.A. Klein, *Opt. Lasers Eng.* 38 (2002) 589.
- [28] B. Lal, H. Zheng, F. Yueh, J.P. Singh, *Appl. Opt.* 43 (2004) 2792.
- [29] B. Lal, F. Yueh, J.P. Singh, *Appl. Opt.* 44 (2005) 3668.
- [30] B. Castle, K. Talabardon, B.W. Smith, J.D. Winefordner, *Appl. Spectrosc.* 52 (1998) 649.
- [31] B. Sallé, D.A. Cremers, S.M. Roger, C. Wiens, *Spectrochim. Acta B* 60 (2005) 479.
- [32] G.A. Latif, H. Imam, *Spectrochim. Acta B* 57 (2002) 1155.
- [33] E.H. Piepmeier, *Analytical Applications of Lasers*, Krieger Pub. Co., New York, 1986.
- [34] K. Song, Y.I. Lee, J. Sneddon, *Appl. Spectrosc. Rev.* 32 (1997) 183.
- [35] J. Sneddon, T.L. Thiem, Y.I. Lee (Eds.), *Lasers in Analytical Atomic Spectroscopy*, John Wiley & Sons, New York, 1997.
- [36] L.J. Radziemski, R.W. Solaz, J.A. Paisner, *Laser Spectroscopy and Applications*, Marcel Dekker, Inc., New York, 1989.
- [37] L.J. Radziemski, D.A. Cremers (Eds.), *Laser-induced Plasma and Application*, Marcel Dekker, New York, 1989.
- [38] A. Striganove, N. Sventitski, *Table of Spectral Lines of Neutral and Ionized Atoms*, Plenum Press, New York, 1968.
- [39] M.G. Natrella, *Experimental Statistics*, NBS Handbook, vol. 91, National Institute of Standards and Technology, Gaithersburg, MD, 1963.

## Discarded free PEG-based assay for obtaining the modification extent of pegylated proteins

Xing Wen Gong, Dong Zhi Wei\*, Ming Lei He, Yu Chun Xiong

State Key Laboratory of Bioreactor Engineering, Institute of New World Biotechnology, East China University of Science and Technology, Shanghai 200237, China

Received 30 August 2005; received in revised form 26 March 2006; accepted 10 April 2006  
Available online 16 May 2006

### Abstract

Free polyethylene glycol (PEG) is a byproduct produced during the process of pegylation and should be removed for the purification of pegylated proteins. In this paper, it was used to develop a new method for obtaining the modification extent of pegylated proteins. This method included two steps of operation. Firstly, the free PEG was separated from crude reaction mixture of pegylated proteins by CM-Sepharose FF. Then PEG was determined based on the formation of a complex with barium chloride and iodine solution. The effective detective range of PEG was 0–7.5  $\mu\text{g/ml}$ . The modification extent was calculated according to a formula. This method is simple, sensitive, and applicable to all of the PEG derivatives. The most distinctive aspect is that it does not consume proteins.

© 2006 Elsevier B.V. All rights reserved.

*Keywords:* Polyethylene glycol; Pegylated protein; Free PEG; Modification extent

### 1. Introduction

Polyethylene glycol (PEG) modification, i.e. pegylation, is a procedure of growing interest for enhancing the therapeutic and biotechnological potential of proteins [1]. More than 100 kinds of proteins have been modified with PEG [2], and five of them, namely ADAGEN<sup>®</sup> (pegylated adenosine deaminase), ONCASPAR<sup>®</sup> (pegylated asparaginase), PEG-Intron<sup>®</sup> (pegylated interferon- $\alpha$ -2b), Pegasys<sup>®</sup> (pegylated interferon- $\alpha$ -2a), Pegfilgrastim<sup>®</sup> or NEULASTA<sup>®</sup> (pegylated granulocyte colony stimulating factor), have been approved for human use by FDA [3]. Meanwhile, a variety of activated PEG derivatives have been developed for the pegylation, whose targets include amino groups, sulfhydryl groups, carboxyl groups, etc. Some detailed reviews regarding the chemistry of pegylation are available [1–5].

The determination of polymer content in pegylated proteins, i.e. modification extent, is essential in order to control the half-life, maintain manufacturing uniformity, and satisfy regulatory concerns. Due to its speed and simplicity, TNBS method [6] is

the most commonly used procedure for obtaining the modification extent. But this method usually gives overestimated results [7–9]. Meanwhile, TNBS method is only applicable to PEG derivatives which target to amino groups of proteins. This is also one of the problems of fluorimetric method [10,11], which is another simple method for the determination of modification extent. Moreover, fluorimetric method is deeply affected by the environment of the fluorophore [8]. A variety of techniques that could be used to all of the PEG derivatives have also been utilized for this purpose. These methods include NMR [12], amino acid analysis [8,12], capillary zone electrophoresis (CE) [9], matrix assisted laser desorption/ionization–mass spectrometry (MALDI–MS) [9], Fourier-transform infrared spectroscopy (FTIR)[9], Raman spectroscopy [9], and online size-exclusion high-performance liquid chromatography light scattering differential refractometry methods [13]. These methods are more accurate than TNBS and fluorimetric method, but are hard to be popularized because of the needs of tedious operations, sophisticated equipments, and skilled operators. Therefore, it is necessary to develop a simple method which is applicable to all of the PEG derivatives. Furthermore, the above-mentioned methods are all based on the direct analysis of pegylated proteins. Consequently, these methods would inevitably consume pegylated proteins. Since the proteins used for and via pegylation

\* Corresponding author. Tel.: +86 21 64252981; fax: +86 21 64250068.  
E-mail address: [dzhwei@ecust.edu.cn](mailto:dzhwei@ecust.edu.cn) (D.Z. Wei).

are generally costly, it would be more meaningful to develop a method which does not consume proteins.

It is known that, for the purification of pegylated proteins, free PEG in the crude reaction mixture should be removed. Meanwhile, some methods for the determination of PEG are available [14–20]. Therefore, it is possible to obtain the modification extent indirectly by the determination of free PEG in the crude reaction mixture. As to above-mentioned methods, some of them are based on the determination of partitioning of dye [14] or chromophore [15,16] in two-phase systems, while the others are based on the determination of a complex formed between PEG and barium iodide [17–20]. In this paper, one of the latter [17] was used to develop a new method for the determination of modification extent of pegylated proteins, while one of the former [16] as a comparison.

## 2. Experimental

### 2.1. Materials and reagents

Recombinant interleukin-2 (rIL-2) and interferon $\alpha$ -2b (IFN $\alpha$ -2b) were obtained from Shanghai Huaxin Biotech. Co. Ltd. (Shanghai, China). CM-Sepharose FF was product of Pharmacia Fine Chemicals (Uppsala, Sweden). Crystalline bovine serum album (BSA), *N*-hydroxysuccinimide (NHS) and Coomassie Brilliant Blue G-250 were from Sigma Chemical Co. (St. Louis, MO, USA). Monomethoxy polyethylene glycol with nominal molecular weight of 5000 (PEG5000) and 12000 (PEG12000) were purchased from Sunbio Corporation (Anyang, South Korea). Other reagents and chemicals were of analytical grade and made in China.

### 2.2. Synthesis of SC-PEG

Succinimidyl carbonate of PEG (SC-PEG) was synthesized according to the procedure of Zalipsky et al. [21]. Monomethoxy polyethylene glycol (12 mmol), dried by azeotropic removal of toluene, was dissolved in toluene/dichloromethane (3/1, 200 ml) and treated with a toluene solution of phosgene (30 ml, 57 mmol) overnight. The solution was evaporated to dryness and the remainder of phosgene was removed under vacuum. The residue was redissolved in toluene/dichloromethane (2/1, 150 ml) and treated with solid *N*-hydroxysuccinimide (2.1 g, 18 mmol) followed by triethylamine (1.7 ml, 12 mmol). After 3 h the solution was filtered and evaporated to dryness. The residue was dissolved in warm (50 °C) ethyl acetate (600 ml), filtered from trace of insolubles, and cooled to facilitate precipitation of the polymer. The product was collected by filtration and then recrystallized once more from ethyl acetate. Both PEG5000 and PEG12000 were used to synthesize the SC-PEG, and the relevant products were labeled as SC-PEG5000 and SC-PEG12000, respectively.

### 2.3. Sample preparation

The protein used for pegylation was adjusted to concentration of 1 mg/ml with 0.2 M phosphate buffer (pH 7.0), and

then 50-fold molar excess of SC-PEG was added. The mixture was kept standing for 30 min at room temperature, and then excessive acetic acid was added to terminate the modification. The crude reaction mixtures of SC-PEG5000 modified Recombinant interleukin-2 (rIL-2), interferon $\alpha$ -2b (IFN $\alpha$ -2b) and bovine serum album (BSA) were named as PEG5000-rIL-2, PEG5000-IFN $\alpha$ -2b, and PEG5000-BSA, respectively, while those of SC-PEG12000 modified ones labeled as PEG12000-rIL-2, PEG12000-IFN $\alpha$ -2b, and PEG12000-BSA, respectively.

CM-Sepharose FF (10  $\times$  1.0 cm) was pre-equilibrated five times (column volume) with 20 mM sodium phosphate, pH5.5 (buffer A). Then the crude reaction mixture was loaded onto it. The column was washed three times (column volume) with buffer A to remove unbonded substances such as free PEG, *N*-hydroxysuccinimide (NHS) and so on. The eluates were collected, mixed and diluted to 100 ml precisely with distilled water. It was labeled as fraction A and used for the determination of modification extent with the new method. The column was washed with 20 mM sodium phosphate, pH 7.5, containing 0.25 M NaCl (buffer B), to elute the protein. The flow rate was 1.0 ml/min and the absorbance was measured at 280 nm. The eluate was labeled as fraction B and used to determine the modification extent with the method of Li et al. [16].

### 2.4. Preparation of reagents

There were two kinds of reagents used for the determination of PEG, namely barium chloride solution and iodine solution. The barium chloride solution was prepared by dissolving the solute in 1 M hydrochloric acid to form a 5% (w/v) solution, while the iodine solution was prepared by dissolving 1.27 g iodine in 100 ml of 2% (w/v) potassium iodide.

### 2.5. Determination of modification extent

The free PEG in fraction A (see Section 2.3) was determined according to the procedure of Sims and Snape [17] with some modifications. Briefly, samples were diluted with distilled water to final concentrations of PEG within the range of 0–7.5  $\mu$ g/ml. To a 800  $\mu$ l sample, 200  $\mu$ l barium chloride solution and 100  $\mu$ l iodine solution were added in turn. The reagent blank was prepared as above with distilled water instead of sample. Solutions were agitated to ensure adequate mixing. Color was allowed to develop for 15 min at room temperature, and then absorbance was read at 535 nm. Unactivated PEG, which has the same molecular weight with the free PEG, was used to prepare a standard curve. The concentration of free PEG was estimated from the standard curve. Modification extent was calculated according to Eq. (1):

$$ME = \frac{ma - mc}{mb \times Nb} \times 100\% \quad (1)$$

where ME is the modification extent, ma the molar amount of PEG used for modification, mb the molar amount of protein mc the molar amount of free PEG and Nb is the amount of target group in one protein molecule.



## 2.6. The procedure of Li et al.

The procedure of Li et al. [16], which is based on the partitioning of a chromophore in a two-phase system, was used for a comparison. Firstly, fraction B (see Section 2.3) was concentrated to protein concentration about 10 mg/ml. To 100  $\mu$ l concentrated sample, 2  $\mu$ l sodium hydroxide (5 M) were added. The alkaline hydrolysis was performed at room temperature for 25 min, and then 2  $\mu$ l hydrochloric acid (5 M) were added for neutralization. This solution (100  $\mu$ l) was added to a two-phase system comprising of 1 ml chloroform and 1 ml aqueous ammonium ferrioxalate (0.1 M). After vigorous vortexing for 30 min and centrifugation at  $3500 \times g$  for 3 min, lower chloroform layer was collected. Absorbance was recorded at 510 nm. The concentration of unactivated PEG was plotted against the corresponding absorbance resulting in a standard curve. The amount of released PEG was obtained from the standard curve. Modification extent was calculated according to Eq. (2):

$$ME = \frac{md}{mb \times Nb} \times 100\% \quad (2)$$

where ME represents the modification extent, mb the molar concentration of protein md the molar concentration of released PEG, and Nb is the amount of target group in one protein molecule.

## 2.7. Protein determination

Protein concentrations were determined spectrophotometrically using Coomassie Brilliant Blue G-250, according to Bradford method [22]. Crystalline bovine serum albumin (BSA) was used to prepare standard curve. Absorbance was read at 595 nm.

## 3. Results and discussion

### 3.1. Comparison with the procedure of Li et al.

The procedure of Li et al. [16] is a promising method for the determination of PEG because it could determine free and conjugated PEG simultaneously. Therefore, it was used for a comparison in this paper. The results were shown in Table 1. For both SC-PEG5000 and SC-PEG12000 modified proteins, the results from the two methods were basically consistent. How-

Table 1  
Modification extents obtained by the procedure of Li et al and the new procedure presented in this paper

Sample	Modification extent (%) <sup>a</sup>	
	Procedure of Li et al.	New procedure
PEG5000-BSA	9.14 $\pm$ 0.63	8.89 $\pm$ 0.59
PEG5000-rIL-2	12.92 $\pm$ 0.91	12.46 $\pm$ 1.0
PEG5000-IFN $\alpha$ -2b	13.94 $\pm$ 1.04	13.16 $\pm$ 1.05
PEG12000-BSA	9.35 $\pm$ 0.62	8.70 $\pm$ 0.37
PEG12000-rIL-2	12.09 $\pm$ 0.95	11.35 $\pm$ 0.84
PEG12000-IFN $\alpha$ -2b	15.16 $\pm$ 1.13	14.26 $\pm$ 0.43

<sup>a</sup> The data shown were the mean and the standard deviation (S.D.) of three replicate measurements.

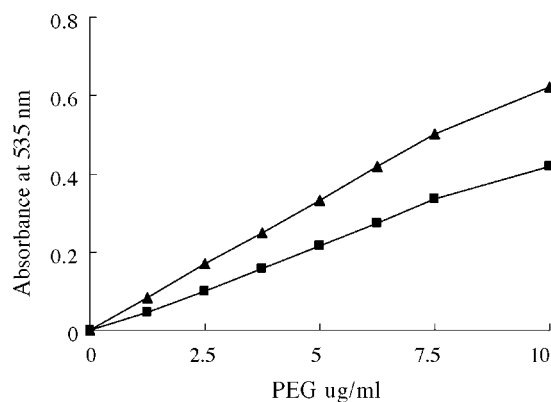


Fig. 1. Effect of varying concentration of PEG on the absorbance in the new method ( $\blacktriangle$ , PEG5000;  $\blacksquare$ , PEG12000).

ever, in comparison with the method we proposed, there exist some flaws in the procedure of Li et al. [16]. Firstly, the procedure is tedious (including 7 steps of operation), thus needs more time to be accomplished. Secondly, the procedure, with the lowest detection limit about 100  $\mu$ g/ml, was not as sensitive as the method we proposed, which gave a linear response to PEG concentration from 0 to 7.5  $\mu$ g/ml (Fig. 1). Thirdly, the procedure needs high initial protein concentration (about 10 mg/ml) that result in higher final PEG concentration. Therefore, after alkaline hydrolysis, PEG is released at high concentration. It was known that PEG was frequently used for precipitation of proteins although conjugated PEG could increase the solubility [23]. Perhaps it was the reason why precipitation occurred in our experiment and even in the paper of Li et al. [16]. The precipitated proteins would interfere with the absorbance of lower chloroform layer, which is used for the determination of PEG, and impair the accuracy of the method of Li et al. [16].

### 3.2. Comparison with the procedure of Sims and Snape

The procedure of Sims and Snape [17] is a simple and sensitive method for the determination of PEG and has been used to visualize the PEG in gels of SDS-PAGE [18–20]. It gives a linear response to PEG concentration from 0 to 7.5  $\mu$ g/ml. Furthermore, the presence of proteins affects the accuracy of this method. In this paper, we confirmed the two points. Meanwhile, we found that the trichloroacetic acid (TCA), which was used to precipitate proteins by Sims and Snape [17], could not completely precipitate pegylated proteins. The reason of which might be the increased solubility caused by pegylation [24]. In this paper, cation exchange chromatography, which has been used for the purification of some pegylated proteins [7,25–27], was employed to separate free PEG. The results indicated that there were no proteins being eluted with free PEG simultaneously.

Furthermore, we found that the ratio of reagents could be improved. In the procedure of Sims and Snape [17], to a 4 ml sample, 1 ml barium chloride solution and 1 ml iodine solution were added. But in this paper, the proportion of them was 8:2:1, which could lighten the color of reagent blank and decrease the standard deviation (S.D.) of the mean (Table 2). The stan-

Table 2

Absorbance obtained from the procedure of Sims and Snape and the new procedure presented in this paper

PEG ( $\mu\text{g/ml}$ )	Absorbance (mean $\pm$ S.D.) <sup>a</sup>	
	Procedure of Sims and Snape	New procedure
1.25	0.084 $\pm$ 0.002	0.084 $\pm$ 0.001
2.50	0.170 $\pm$ 0.002	0.170 $\pm$ 0.002
3.75	0.249 $\pm$ 0.003	0.250 $\pm$ 0.003
5.0	0.330 $\pm$ 0.003	0.330 $\pm$ 0.002
6.25	0.421 $\pm$ 0.003	0.420 $\pm$ 0.002
7.50	0.50 $\pm$ 0.003	0.50 $\pm$ 0.001

<sup>a</sup> The data shown were the mean and the standard deviation (S.D.) of three replicate measurements.

standard curve showed that such a proportion was sufficient for the determination of PEG with concentrations within the range of 0–7.5  $\mu\text{g/ml}$  (Fig. 1).

### 3.3. Interfering substances

The procedure of Sims and Snape [17] has shown a good recovery of PEG. Therefore, in the new method, the potential interfering substances are those related to pegylation of proteins. Because proteins used for pegylation are generally purified and devoid of impurities, it is needless to worry about their interference. As to the PEG derivatives used for modification, the hydrolyzed or ammonolyzed *N*-hydroxysuccinimide (NHS) is the most commonly seen impurity, but it does not interfere with this method. Furthermore, buffer solution is a potential source of the interfering substance. Therefore, the phosphate buffer was used in this paper and it did not interfere with this method. On the other hand, it should be noted that, to dilute free PEG to concentrations within the range of 0–7.5  $\mu\text{g/ml}$ , at least 100-fold dilution with distilled water is needed. Therefore, even if the interfering substances exist, their interference on this method would be very limited.

### 3.4. Key points

In this method, there are several key points that should be noted. Firstly, when separating free PEG from crude reaction mixture, the pH of eluant should be low enough to avoid pegylated proteins being eluted. Secondly, to impair the influence of potential interfering substances, the dilution of free PEG should be made in distilled water. Thirdly, to prevent from the potential interfering substances, we suggest using phosphate buffer for pegylation of proteins and separation of free PEG. Finally, unactivated PEG, which was used for the preparation of standard curve, should have the same molecular weight with the determined free PEG.

## 4. Conclusions

It is known that the removing of free PEG is indispensable for the purification of pegylated proteins and the free PEG is usu-

ally discarded. In this paper, based on the determination of free PEG, we developed a new method for obtaining the modification extent of pegylated proteins. This method is simple, sensitive, economical and applicable to all of the PEG derivatives. These advantages make it a promising method for the analysis of pegylated proteins.

## Acknowledgements

This work was supported by grants from National 863 Project (No. 2002AA2Z3451) and the Key Disciplinary Foundation of Shanghai, China.

## References

- [1] F.M. Veronese, *Biomaterials* 22 (2001) 405–417.
- [2] Y. Kodera, A. Matsushima, M. Hiroto, H. Nishimura, A. Ishii, T. Ueno, Y. Inada, *Prog. Polym. Sci.* 23 (1998) 1233–1271.
- [3] R.B. Greenwald, Y.H. Choe, J. McGuire, C.D. Conover, *Adv. Drug Deliv. Rev.* 55 (2003) 217–250.
- [4] S. Zalipsky, *Adv. Drug Deliv. Rev.* 16 (1995) 157–182.
- [5] M.J. Roberts, M.D. Bentley, J.M. Harris, *Adv. Drug Deliv. Rev.* 54 (2002) 459–476.
- [6] S.L. Snyder, P.Z. Sobocinski, *Anal. Biochem.* 64 (1975) 284–288.
- [7] P. McGoff, A.C. Baziotis, R. Maskiewicz, *Chem. Pharm. Bull.* 36 (1988) 3079–3091.
- [8] L. Sartore, P. Caliceti, O. Schiavon, C. Monfardini, F.M. Veronese, *Appl. Biochem. Biotechnol.* 31 (1991) 213–222.
- [9] J. Bullock, S. Chowdhury, A. Severdia, J. Sweeney, D. Johnston, L. Pachla, *Anal. Biochem.* 254 (1997) 254–262.
- [10] S. Udenfriend, S. Stein, P. Bohlen, W. Dairman, W. Leimgruber, M. Weigle, *Science* 178 (1972) 871–872.
- [11] S.J. Stocks, A.J. Jones, C.W. Ramey, D.E. Brooks, *Anal. Biochem.* 154 (1986) 232–234.
- [12] C.-J.C. Jackson, J.L. Charlton, K. Kuzminski, G.M. Lang, A.H. Sehon, *Anal. Biochem.* 165 (1987) 114–127.
- [13] B.S. Kendrick, B.A. Kerwin, B.S. Chang, J.S. Philo, *Anal. Biochem.* 299 (2001) 136–146.
- [14] C. Guermant, J. Brygier, D. Baeyens-Volant, M. Nijs, J. Vincentelli, C. Paul, Y. Looze, *Anal. Biochem.* 230 (1995) 254–258.
- [15] A. Nag, G. Mitra, P.C. Ghosh, *Anal. Biochem.* 237 (1996) 224–231.
- [16] S.K. Li, Z.J. Yang, X.H. Sun, Y.Y. Tan, S. Yagi, R.M. Hoffman, *Anal. Biochem.* 313 (2003) 335–337.
- [17] G.E.C. Sims, T.J. Snape, *Anal. Biochem.* 107 (1980) 60–63.
- [18] M.M. Kurfürst, *Anal. Biochem.* 200 (1992) 244–248.
- [19] S.B. Zimmerman, L.D. Murphy, *Anal. Biochem.* 234 (1996) 190–193.
- [20] O.W. Odom, W. Kudlicki, G. Kramer, B. Hardesty, *Anal. Biochem.* 245 (1997) 249–252.
- [21] S. Zalipsky, R. Seltzer, S.M. Rudolph, *Biotechnol. Appl. Biochem.* 15 (1992) 100–114.
- [22] M.M. Bradford, *Anal. Biochem.* 72 (1976) 248–254.
- [23] S.C.B. Yan, D.A. Tuason, V.B. Tuason, W.H. Frey II, *Anal. Biochem.* 138 (1984) 137–140.
- [24] L. Doretto, D. Ferrara, P. Gattolin, S. Lora, F. Schiavon, F.M. Veronese, *Talanta* 45 (1998) 891–898.
- [25] O.B. Kinstler, D.N. Brems, S.L. Lauren, A.G. Paige, J.B. Hamburger, M.J. Treuheit, *Pharm. Res.* 13 (1996) 996–1002.
- [26] T. Uchio, M. Baudyš, F. Liu, S.C. Song, S.W. Kim, *Adv. Drug Deliv. Rev.* 35 (1999) 289–306.
- [27] Y.S. Wang, S. Youngster, M. Grace, J. Bausch, R. Bordens, D.F. Wyss, *Adv. Drug Deliv. Rev.* 54 (2002) 547–570.

# Classification of reversed-phase columns based on their selectivity towards vancomycin compounds

Erik Haghedooren<sup>a</sup>, José Diana<sup>a</sup>, Béla Noszál<sup>b</sup>, Jos Hoogmartens<sup>a</sup>, Erwin Adams<sup>a,\*</sup>

<sup>a</sup> *Katholieke Universiteit Leuven, Laboratorium voor Farmaceutische Chemie en Analyse van Geneesmiddelen, O & N 2, PB 923, Herestraat 49, B-3000 Leuven, Belgium*

<sup>b</sup> *Semmelweis University, Department of Pharmaceutical Chemistry, Hőgyes E.u. 9, H-1092 Budapest, Hungary*

Received 18 October 2005; received in revised form 24 February 2006; accepted 3 March 2006

Available online 18 April 2006

## Abstract

The selection of a reversed-phase liquid chromatographic (RP-LC) column with suitable selectivity for a particular separation is difficult if the brand name of the column is not known. The monographs of the *European Pharmacopoeia* and other official compendia for drug analysis only give a general description of the stationary phase to be used in the operating procedure of a liquid chromatographic method. A project to develop a chromatographic test procedure to characterise RP-LC C<sub>18</sub> columns was started earlier and resulted in a fast, simple, repeatable and reproducible test procedure. Four column parameters, determined on 69 RP-LC C<sub>18</sub> columns, allowed the characterisation and ranking of these columns. In this paper, an overview of this column classification system is given with an application on the separation of vancomycin and some of its impurities. It is shown that the column ranking system is a helpful tool in the selection of a suitable column.

© 2006 Elsevier B.V. All rights reserved.

**Keywords:** Reversed-phase liquid chromatography; Column characterisation; Chromatographic tests; Column classification; Vancomycin

## 1. Introduction

Official compendia, like the *European Pharmacopoeia* (Ph. Eur.) [1] and the *United States Pharmacopoeia* (USP) [2] prescribe many different liquid chromatographic (LC) analyses. In most cases, the use of RP-LC is prescribed with C<sub>18</sub> stationary phases. Nowadays, an extended number of different C<sub>18</sub> reversed-phase (RP) columns is available on the market. Since monographs of the Ph. Eur. and other official compendia for drug analysis only give a general description of the stationary phase to be used in the operating procedure of an LC method, the selection of a suitable column can be problematic. The problem also rises when a column, prescribed in literature or by compendia, is not available in the laboratory. Proper column selection is also needed during method development when an analyst wants to try columns giving different selectivity.

The issue of RP-LC column selection was discussed earlier by Steffek et al. [3] and Engelhardt and Grüner [4].

Dolan and Snyder characterised more than 300 columns based on an empirical equation including conditions-dependent properties of the solute and conditions-independent properties of the column. Five determined parameters ( $H$ ,  $S^*$ ,  $A$ ,  $B$  and  $C$ ) can be combined to an  $F_s$  value, to evaluate the (dis)similarity of two selected columns [5–10].

Euerby et al. studied 170 columns based on 6 chromatographic parameters, defining surface coverage, hydrophobic selectivity, shape selectivity, hydrogen bonding capacity and ion-exchange capacity at pH 2.7 and 7.6. Principal component analysis led to the study of a subset of the database including only C<sub>18</sub> phases with non-acidic silica material [11,12].

Vander Heyden et al. tested 8 chromatographic parameters on 28 columns, using chemometric techniques like Pareto-optimality concept, principal component analysis and Derriinger's desirable function. Column selection based on the Pareto-optimality concept led to a subset of columns, but was found less flexible when new columns were added to the original dataset [13].

Many other papers, describing methods to characterise columns, were published to solve this issue, but only recently published articles are cited here [14–19].

\* Corresponding author. Tel.: +32 16 3234 44; fax: +32 16 3234 48.  
E-mail address: [erwin.adams@pharm.kuleuven.be](mailto:erwin.adams@pharm.kuleuven.be) (E. Adams).

In our laboratory, a general test method was developed by selection of the most appropriate test methods from the literature. This column characterisation and classification system allows the selection of columns with selectivity similar to or different from a chosen reference column [20–26]. The column classification system would also allow to follow up column ageing so that analysts can check whether the characteristics of their columns have changed over time.

In this work, a short overview is given of the development of our column classification system and an application is shown, using the separation of vancomycin (VM) from some of its impurities. Vancomycin was already used by Forlay-Frick et al., combining 28 different chromatographic conditions, i.e. 7 stationary phases with 4 different mobile phases to study the replacement of columns. This was evaluated based on the theoretical plate number and symmetry factor of three test compounds; benzoic acid, *N,N*-dimethylaniline and vancomycin [27]. Three columns out of seven had the same stationary phase as used in this article: LiChrospher, Purospher and Symmetry, but the columns had different dimensions, making comparison between the two systems troublesome.

VM is a glycopeptide antibiotic used in the prophylaxis and treatment of infections caused by Gram-positive bacteria,

including methicillin-resistant and oxacillin-resistant staphylococci [28,29]. It is a branched tricyclic glycosylated non-ribosomal peptide produced by the fermentation of the Actinobacteria species *Amycolatopsis orientalis*, formerly *Nocardia orientalis*, appearing as a mixture of similarly structured compounds of which many components have not yet been identified [30–33]. See Fig. 1 for the structure of known components. VM B is the main compound. Monodechlorovancomycin 2 (MDCV 2) is a side-product isolated from fermentation broth. Selective dehalogenation of VM results in monodechlorovancomycin 1 (MDCV 1) [34]. VM degrades into a crystalline degradation product (CDP-I) by hydrolytic loss of ammonia [35,36]. CDP-I exists in two isomeric forms, the major form (CDPM) and the minor form (CDPm) [36–38]. Aglucovancomycin (AGLUV) and desvancosaminylvancomycin (DESV) are other degradation products resulting from the loss of the disaccharide moiety and the vancosamine sugar, respectively [39]. The LC method that is used to analyse vancomycin on the different columns has been discussed previously [40]. The peaks that are considered in the discussion of the classification correspond to vancomycin B (VM B), monodechlorovancomycin 1, monodechlorovancomycin 2 and two isomeric forms of a crystalline degradation product, the major form and the minor form.

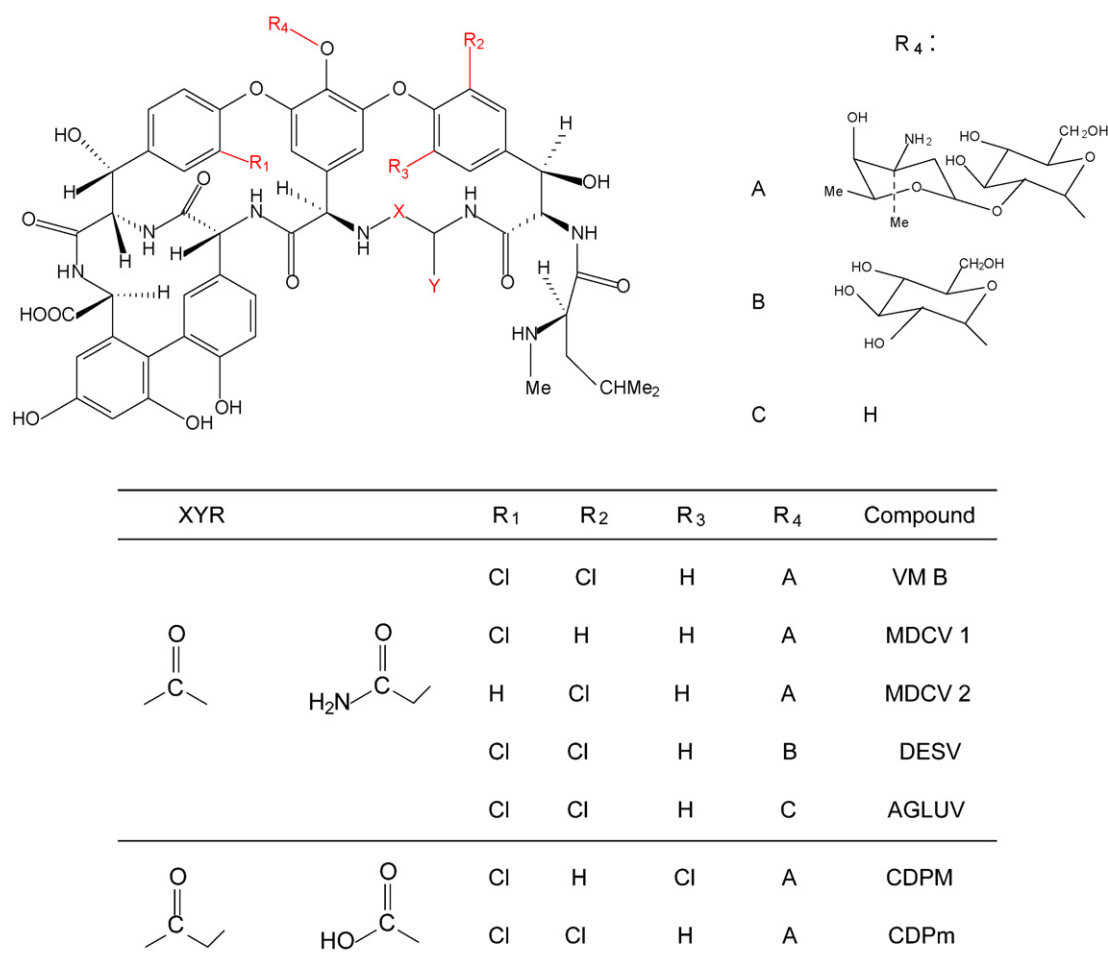


Fig. 1. Structure of vancomycin B and related substances.

## 2. Experimental

### 2.1. Reagents and samples

Acetonitrile HPLC grade was purchased from Biosolve LTD (Valkenswaard, The Netherlands). Dioxane HPLC grade and formic acid were purchased from Acros Organics (Geel, Belgium). Concentrated ammonia and tetrahydrofuran were from Riedel-de Haën (Seelze, Germany). Water was purified in the laboratory by distillation of demineralised water. Reference substances of VM B, MDCV 1, MDCV 2, DDCV, CDPM and CDPm were obtained from Abbott Laboratories (Abbott Park, IL, USA). Vancomycin samples were prepared at a concentration of 2 mg/ml. Solutions of reference substances were prepared at a final concentration of 0.05–0.1 mg/ml. Both samples and reference substances were dissolved in mobile phase. Sample solutions slightly degraded within one day when they were kept at room temperature, but they could be used for several days when they were stored at 4 °C.

### 2.2. Instrumentation and liquid chromatographic conditions

The LC apparatus consisted of a L-6200 Intelligent Pump (Merck Hitachi, Darmstadt, Germany), an autosampler Model 655A-40 (Merck Hitachi) equipped with a 20 µl loop, a Linear UVIS 200 UV detector (Thermo Separation Products, San Jose, CA, USA) set at 280 nm and Chromperfect 4.4.23 software (Justice Laboratory Software, Fife, UK) for data acquisition. A set of 37 RP-LC C<sub>18</sub> columns (Table 1) was investigated. The columns were kept at 35 °C in a water bath heated by a Julabo EC thermostat (Julabo, Seelbach, Germany).

A mobile phase consisting of dioxane–0.3 M ammonium formate, pH 1.7–water (6:5:89, v/v/v) was used for all columns at a flow rate of 1.0 ml/min. The mobile phases were degassed by sparging helium. To prepare the 0.3 M ammonium formate solution, the appropriate amount of concentrated ammonia was diluted in water and adjusted to the required pH using 10% (v/v) formic acid, before bringing to volume.

Table 1  
Specifications for the examined columns

Column number	Name of the column	Length (mm)	Particle size (µm)	Manufacturer/supplier
1	µBondapak	250	10	Waters
2	ACE 5	250	5	Advanced Chrom. Tech./Achrom
3	Alltima	250	5	Alltech
4	Apex Basic	250	5	Jones Chromatography/Sopachem
5	Apex ODS II	250	5	Jones Chromatography/Sopachem
6	Brava BDS	250	5	Alltech
7	Discovery	250	5	Supelco
8	Hypersil BDS	250	5	ThermoQuest
9	Hypersil ODS	250	5	ThermoQuest
10	Kromasil (EKA)	250	5	Akzo Nobel/SerCoLab
11	Kromasil (MN)	250	5	Macherey-Nagel/Filter Service
12	LiChrospher	250	5	Merck
13	Luna	150	5	Phenomenex/Bester
14	Nucleosil	250	5	Macherey-Nagel/Filter Service
15	Nucleosil HD	250	5	Macherey-Nagel/Filter Service
16	Nucleosil Nautilus	250	5	Macherey-Nagel/Filter Service
17	OmniSpher	250	5	Varian
18	Platinum	250	5	Alltech
19	Platinum EPS	250	5	Alltech
20	Purospher	250	5	Merck
21	Purospher endcapped	250	5	Merck
22	Purospher STAR	250	5	Merck
23	Spheri-5	250	5	PerkinElmer
24	Spherisorb ODS2	250	5	Waters
25	Supelcosil LC-18	250	5	Supelco
26	Supelcosil LC-18 DB	250	5	Supelco
27	Superspher	250	5	Merck
28	Symmetry	250	5	Waters
29	TracerExcel ODS A	250	5	Teknokroma/SerCoLab
30	Uptisphere HDO	250	5	Interchrom/Achrom
31	Uptisphere ODB	250	5	Interchrom/Achrom
32	Validated	250	5	PerkinElmer
33	Wakosil HG	250	5	SGE/Achrom
34	YMC-Pack Pro	150	3	YMC Sep. Techn./ThermoQuest
35	Zorbax Eclipse XDB	250	5	Agilent Technologies
36	Zorbax Extend	250	5	Agilent Technologies
37	Zorbax SB	250	5	Agilent Technologies



### 3. Results and discussion

#### 3.1. Development of the column classification system

The column characterisation and classification project consisted of three major parts. First, a procedure, allowing the measurement of a number of parameters, reflecting chromatographic characteristics was developed. In order to make the procedure as user friendly as possible, the number of test parameters was kept minimal. The second part intended to classify RP-LC columns with closely related characteristics. The third part consisted in performing pharmaceutical separations to check the usefulness of the developed ranking system of the columns in practice.

In the first part, test methods from the literature for characterisation of RP-LC columns were critically evaluated. Properties of RP-LC stationary phases can be checked by both non-chromatographic and chromatographic methods. Carbon content, amount of metal impurities, particle size, surface area, pore size, packing density and acidity can be determined by non-chromatographic methods. However, these techniques are not readily performed and cannot be carried out on the packed column without destruction. Therefore the choice of chromatographic methods was obvious. Visky et al. made a selection of 36 test parameters from literature, testing as many as possible different properties of RP-LC columns, like column efficiency, hydrophobicity and silanol activity. Eight chromatographic methods were developed, allowing to determinate the 36 test parameters [20]. Since a general procedure needs to use repeatable and reproducible test parameters, the eight methods were examined in three different laboratories. Of the initial 36 parameters, 24 proved to be repeatable and reproducible, based on the calculation of the relative standard deviation [21]. Iványi et al. applied chemometrics to diminish the number of parameters, while maintaining the classification. Principal component analysis (PCA) was found to offer the possibility to evaluate column clustering or differentiation [22]. Similar to this approach, the 24 parameters of our study were reduced to 4 parameters: the retention factor of amylbenzene,  $k'_{\text{amylbenzene}}$  ( $k'_{\text{amb}}$ ), the relative retention factor benzylamine/phenol at pH 2.7,  $\text{rk}'_{\text{benzylamine/phenol}}$  ( $\text{rk}'_{\text{ba/ph pH 2.7}}$ ), the relative retention factor triphenylene/*o*-terphenyl,  $\text{rk}'_{\text{triphenylene/o-terphenyl}}$  ( $\text{rk}'_{\text{tri/o-ter}}$ ) and the retention factor of 2,2'-dipyridyl,  $k'_{2,2'\text{-dip}}$  ( $k'_{2,2'\text{-dip}}$ ).

In the second part of the project, PCA of the four parameters was at first used to distinguish groups of columns (groups Ia, Ib, IIa, IIb, IIc and III) [23]. These groups were constructed based on the different reversed phases described in the Ph. Eur. and on information provided by the column manufacturers. A more practical approach to rank RP-LC columns was introduced by using  $F$ -values:

$$F = (k'_{\text{amb,ref}} - k'_{\text{amb},i})^2 + (\text{rk}'_{\text{ba/ph pH 2.7,ref}} - \text{rk}'_{\text{ba/ph pH 2.7},i})^2 + (k'_{2,2'\text{-dip,ref}} - k'_{2,2'\text{-dip},i})^2 + (\text{rk}'_{\text{tri/o-ter,ref}} - \text{rk}'_{\text{tri/o-ter},i})^2 \quad (1)$$

The  $F$ -value of a column  $i$  equals the sum of squares of the differences between each parameter value of a chosen reference column and of the column  $i$ . The smaller the  $F$ -value, the more similar is column  $i$  to the reference column. In order to have the same weighing of each parameter in this equation, the parameters are autoscaled using formula (2) before being introduced in Eq. (1):

$$\frac{x_{ij} - \bar{x}_j}{s_j} \quad (2)$$

where  $x_{ij}$  is the value of parameter  $j$  on column  $i$ ,  $\bar{x}_j$  the mean of parameter  $j$  on all tested columns and  $s_j$  is the standard deviation on the mean parameter value. With this  $F$ -value, a ranking of all columns is obtained, indicating how close columns are to the selected reference column. Low  $F$ -values correspond to high ranking [24].

The third part of the project consisted in performing pharmaceutical analyses to check the performance of the column classification system in real separations. Dehouck et al. carried out the separation of acetylsalicylic acid (aspirin) according to the Ph. Eur. monograph. The system suitability test (SST) prescribed by the Ph. Eur. to distinguish between suitable and non-suitable columns was also evaluated. It was concluded that this SST could not always predict the suitability of the column to separate all the aspirin components. Alternatively, the suitability was investigated by calculation of the chromatographic response function (CRF). The CRF value is equal to 1 if all the peaks are baseline separated, and equal to 0 if two peaks are coeluted. Partial separations lead to intermediate values. The column ranking approach starts with the choice of a reference column or of reference parameters. For each column, the  $F$ -value versus this reference column was calculated and the columns were ranked according to their  $F$ -value, starting with the smallest one. It was concluded that the chance of selecting a suitable column clearly increased with a smaller  $F$ -value. All columns with an  $F < 2$  gave baseline separation for all peaks (CRF = 1) while this number decreased to 43% for columns with  $2 < F < 6$  and to 18% for columns with  $F > 6$ . The column ranking system is freely accessible on our website: <http://www.pharm.kuleuven.be/pharmchem/columnclassification>.

This database contains already more than 50 types of RP-LC C<sub>18</sub> columns and new types are being characterised in our laboratory at this moment. Analysts can either classify all columns from the database with regard to a freely chosen reference column from the list or they can fill in four parameter values, determined on their own column [24,25].

In order to further investigate the possibilities of this column classification system, its performance towards the separation of vancomycin compounds is examined here.

#### 3.2. Column classification system based on vancomycin analyses

Each of the 37 columns in Table 1 was used for the separation of vancomycin and its impurities. The suitability of the stationary phases for this separation was examined by calculating the CRF, which is a measure for the overall selectivity and which is

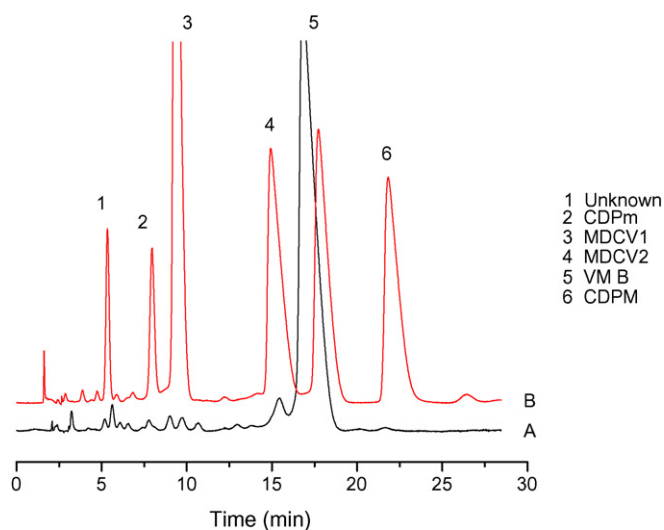


Fig. 2. Typical chromatogram of: (A) VM commercial sample (2 mg/ml) and (B) a mixture of VM and some of its potential impurities (1 mg/ml) analysed during columns investigation. Column: Symmetry, maintained at 30 °C with dioxane–0.3 M ammonium formate, pH 1.7–water (6:5:89, v/v/v) as mobile phase. Detection: UV at 280 nm; flow rate: 1.0 ml/min; injection volume: 20  $\mu$ l.

calculated as follows:

$$\text{CRF} = \prod_{i=1}^{n-1} \frac{f_i}{g_i} \quad (3)$$

where  $n$  is the total number of peaks,  $g$  the interpolated peak height between two peaks, i.e. the distance between the baseline and the line connecting the two peak tops, at the location of the valley, and  $f$  is the depth of the valley, measured from the line connecting the two peak tops [41,42]. This means that a baseline-separated peak pair has an  $f/g$  ratio of 1, a coeluting pair has a value of 0, while a partly separated peak pair has an intermediate value. The CRF was calculated based on the following peaks: unknown, CDPm, MDCV 1, MDCV 2, VM B and CDPM (Fig. 2).

From the separations, it was observed that complete baseline separation for all peaks ( $\text{CRF} = 1$ ) could only be obtained on two columns, Nucleosil HD (column 15) and Spheri-5 (column 23). Some columns did not separate all peaks and therefore had a CRF of 0. However, many columns showed a CRF above 0.91. This is mainly due to partially coelution of CDPm (peak 2 in Fig. 2) and MDCV 1 (peak 3 in Fig. 2). Fig. 3 shows an example of a separation with  $\text{CRF} = 0.50$ , 0.91 and 1, respectively. As can be observed, a CRF of 0.91 still gives a very acceptable separation. Therefore, the criterion of a good separation was set at a CRF of more than 0.90. For each test parameter, the average of all columns, matching the criterion of  $\text{CRF} > 0.90$ , was calculated to obtain a ‘virtual suitable column’. With these four values as reference, a ranking was obtained based on the  $F$ -values (Table 2), calculated from the measured parameter values, as discussed above. It was observed that all columns with  $F < 2$  are suitable for the analysis of vancomycin and its impurities ( $\text{CRF} > 0.90$ ). For columns with  $F > 2$  the probability of separation of impurities clearly decreases. When  $F$  is between 2 and 6, 6 out of 10 (60.0%) columns gave a CRF

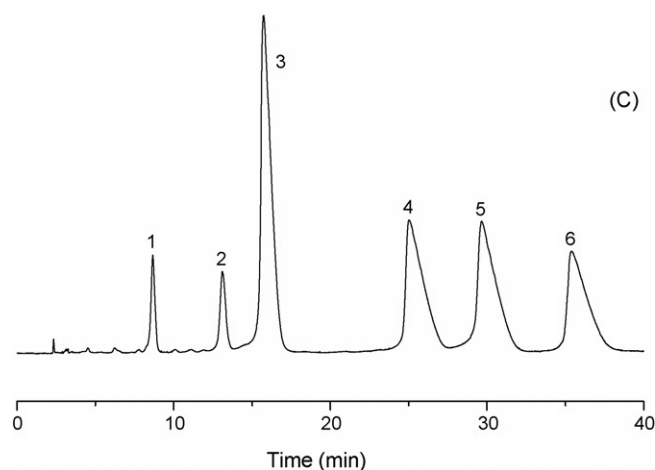
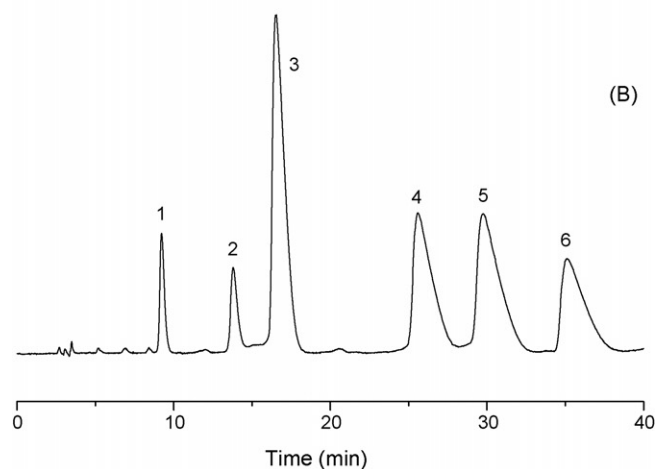
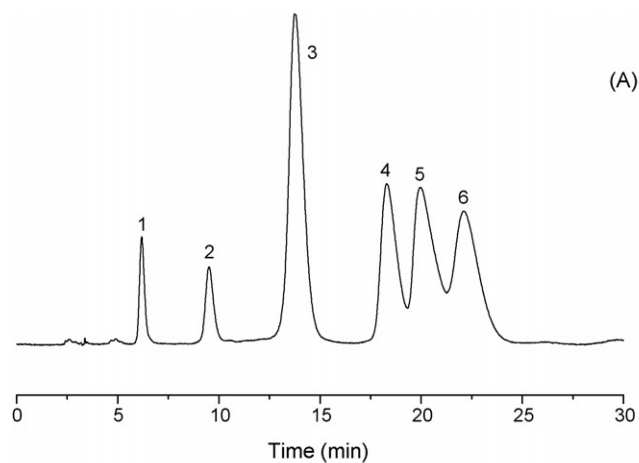


Fig. 3. Chromatogram of the test mixture on: (A) Nucleosil Nautilus with  $\text{CRF} = 0.50$ , (B) Brava BDS with  $\text{CRF} = 0.91$  and (C) Nucleosil HD with  $\text{CRF} = 1$ . The chromatographic conditions were as in Fig. 2. The peak numbering of Fig. 2 was maintained.

value above 0.90, while for  $F$ -values above 6, only 1 out of 8 (12.5%) showed an appropriate selectivity. Although suitable columns can be found among the low-ranked columns as well, the probability has clearly decreased. So, the column classification system is a helpful tool in finding a suitable stationary phase, since any column having an  $F$ -value lower than 2.0 appeared to

Table 2

Column ranking according to the  $F$ -values, calculated vs. a 'virtual ideal column' with  $k'_{amb} = 5.78$ ,  $rk'_{ba/ph\ pH\ 2.7} = 0.09$ ,  $k'_{2,2'-dip} = 9.76$ ,  $rk'_{ti/o-ter} = 1.46$

	$k'_{amb}$	$rk'_{ba/ph\ pH\ 2.7}$	$k'_{2,2'-dip}$	$rk'_{ti/o-ter}$	$F$ -value	CRF
Reference column						
Virtual suitable column	5.78	0.09	9.76	1.46		
Column						
Validated C <sub>18</sub>	0.34	-0.424	-0.10	-0.44	0.075	0.93
Nucleosil HD	0.54	-0.349	-0.48	-0.27	0.150	1
Tracerexcel 5	0.52	-0.429	-0.36	-0.61	0.253	0.97
Uptispher ODB5	0.70	-0.418	-0.28	-0.61	0.295	0.94
Zorbax Extend C18	0.62	-0.434	-0.62	-0.14	0.318	0.92
Wakosil HG 5_25	0.14	-0.413	-0.65	-0.44	0.401	0.94
Superspher	0.75	-0.231	-0.27	0.33	0.440	0.94
Symmetry	0.81	-0.563	-0.34	0.20	0.459	0.96
Kromasil NM	0.64	-0.445	-0.23	0.50	0.594	0.93
YMC-Pack-Pro C18-3	0.36	-0.526	-0.57	-0.82	0.626	0.94
Zorbax Eclipse XDB	0.54	-0.413	-0.58	-0.91	0.732	0.93
Purospher Star	1.05	-0.461	0.51	0.12	0.977	0.97
Uptispher HDO5	0.39	-0.354	-0.86	-0.91	1.024	0.97
Alltima 5	1.26	-0.402	0.41	-0.23	1.055	0.96
Kromasil EKA	1.37	-0.386	-0.22	0.20	1.130	0.94
ACE C18-5	-0.31	-0.343	-0.99	-0.01	1.283	0.97
Zorbax SB-C18	-0.02	-0.434	-0.27	-1.25	1.296	0.95
OmniSpher	1.42	-0.365	-0.18	0.67	1.840	0.94
Luna 5	0.36	-0.617	-0.41	-1.55	1.984	0.93
Supelcosil LC-18 DB 5	-0.64	0.097	-0.95	-0.61	2.055	0.92
Nucleosil NM	-0.40	-0.188	0.80	0.63	2.207	0.96
Hypersil BDS	-0.88	-0.080	-0.93	0.20	2.484	0
Brava BDS 5	-1.20	-0.172	-1.07	-0.06	3.464	0.91
Purospher endcapped	1.53	-0.472	0.96	0.84	3.620	0.88
Discovery	-1.19	-0.338	-1.49	-0.06	4.366	0.95
Purospher	-0.34	-0.778	0.26	1.65	4.386	0
Bondapak	-1.50	-0.316	-0.72	-1.25	5.014	0.19
Spherisorb ODS2	0.25	0.569	1.94	0.16	5.179	0.93
Spheri	1.16	0.451	1.94	-0.40	5.456	1
Platinum 5	-1.79	0.236	-0.33	-1.21	6.066	0
LiChrospher	0.78	0.059	1.94	1.10	6.258	0.96
Nucleosil HD Nautilus	-1.08	-0.708	-0.98	1.86	7.371	0.5
Platinum EPS 5	-2.38	1.368	-0.07	1.57	13.595	0.39
Hypersil ODS	-0.88	2.473	1.94	-0.87	13.989	0
Supelcosil LC18	-0.54	3.294	1.94	-0.35	18.019	0.67
Apex Basic	-1.70	-0.778	-0.66	3.44	18.229	0
Apex ODS	-0.69	3.294	1.94	-0.48	18.388	0

be suitable for the separation of vancomycin and some of its impurities.

It should be noted that the column ranking does not distinguish between "good" and "bad" columns. A column with a higher  $F$ -value only indicates that it has properties different from that of the reference column. For another application, using other reference values, such a column may be ranked high. Even a column that ranks low for many applications may be of great value for some other, specific applications.

#### 4. Conclusions

This paper discusses the performance of 37 RP-LC C<sub>18</sub> columns for the separation of vancomycin and some of its impurities. The columns were characterised by a set of four chromatographic test parameters. To determine whether a sep-

aration was good or poor, the overall selectivity was evaluated using the Chromatographic Response Function. Average values of the four test parameters were calculated for columns showing a CRF > 0.90. Using these values as a reference for a "suitable" column, the  $F$ -values were calculated and a ranking was obtained. All columns with an  $F$ -value below 2 were found suitable. An  $F$ -value between 2 and 6 still offered a 60% possibility to find a good column. Above 6, the chances to find a suitable column were very low. These findings are in accordance with the conclusions drawn from a previous experiment with aspirin. In the future, more complex case studies (also using gradient elution) will have to be performed to examine the correlation between the column test parameters and their separation characteristics. The final aim of the project is to provide a simple column test procedure with accompanying limits, which can help to predict the suitability of a column for real separations.

## Acknowledgments

The authors thank the manufacturers and the suppliers for the gift of columns. E. Haghedooren enjoys a grant of the Institute for the Promotion of Innovation through Science and Technology in Flanders (IWT-Vlaanderen). E. Adams is a post-doctoral fellow of the Fund for Scientific Research (FWO)-Flanders, Belgium. Financial support to this project is given by a Research Grant of the Fund for Scientific Research-Flanders (Belgium).

## References

- [1] European Pharmacopoeia, fifth ed., Council of Europe, Strasbourg, France, 2005, p. 2671.
- [2] United States Pharmacopoeia, vol. 28, The United States Pharmacopoeial Convention, Rockville, MD, USA, 2005, p. 2013.
- [3] R.J. Steffek, S.L. Woo, R.J. Weigand, J.M. Anderson, LC–GC 13 (1995) 720.
- [4] H. Engelhardt, R. Grüner, *Inter. Lab.* (1999) 34.
- [5] L.R. Snyder, A. Maule, A. Heebsh, R. Cuellar, S. Paulson, J. Carrano, L. Wrisley, C.C. Chan, N. Pearson, J.W. Dolan, J.J. Gilroy, *J. Chromatogr. A* 1057 (2004) 49.
- [6] J.W. Dolan, A. Maule, D. Bingley, L. Wrisley, C.C. Chan, M. Angod, C. Lunte, R. Krisko, J.M. Winston, B.A. Homeier, D.V. McCalley, L.R. Snyder, *J. Chromatogr. A* 1057 (2004) 59.
- [7] L.R. Snyder, J.W. Dolan, P.W. Carr, *J. Chromatogr. A* 1060 (2004) 77.
- [8] D.H. Marchand, K. Croes, J.W. Dolan, L.R. Snyder, *J. Chromatogr. A* 1062 (2005) 57.
- [9] D.H. Marchand, K. Croes, J.W. Dolan, L.R. Snyder, R.A. Henry, K.M.R. Kallury, S. Waite, P.W. Carr, *J. Chromatogr. A* 1062 (2005) 65.
- [10] J. Pellett, P. Lukulay, Y. Mao, W. Bowen, R. Reed, M. Ma, R.C. Munger, J.W. Dolan, L. Wrisley, K. Medwid, *J. Chromatogr. A* 1101 (2006) 122.
- [11] M.R. Euerby, P. Petersson, *J. Chromatogr. A* 994 (2003) 13.
- [12] M.R. Euerby, P. Petersson, *J. Chromatogr. A* 1088 (2005) 1.
- [13] E. Van Gysegem, M. Jimidar, R. Sneyers, D. Redlich, E. Verhoeven, D.L. Massart, Y. Vander Heyden, *J. Chromatogr. A* 1042 (2004) 69.
- [14] M. Kele, G. Guiochon, *J. Chromatogr. A* 830 (1999) 41.
- [15] W. Verstraeten, J. de Zeeuw, J. Crombeen, N. Vonk, *Int. Lab. (March)* (2000) 20.
- [16] U.D. Neue, K. Van Tran, P.C. Iraneta, B.A. Alden, *J. Sep. Sci.* 26 (2003) 174.
- [17] K. Le Mapihan, J. Vial, A. Jardy, *J. Chromatogr. A* 1061 (2004) 149.
- [18] R. Kaliszan, M.A. van Straten, M. Markuszewski, C.A. Cramers, H.A. Claessens, *J. Chromatogr. A* 855 (1999) 455.
- [19] T. Baczek, R. Kaliszan, K. Novotna, P. Jandera, *J. Chromatogr. A* 1075 (2005) 109.
- [20] D. Visky, Y. Vander Heyden, T. Iványi, P. Baten, J. De Beer, B. Noszál, E. Roets, D.L. Massart, J. Hoogmartens, *Pharmeuropa* 14 (2002) 288.
- [21] D. Visky, Y. Vander Heyden, T. Iványi, P. Baten, J. De Beer, Zs. Kovács, B. Noszál, E. Roets, D.L. Massart, J. Hoogmartens, *J. Chromatogr. A* 977 (2002) 39.
- [22] T. Iványi, Y. Vander Heyden, D. Visky, P. Baten, J. De Beer, I. Lázár, D.L. Massart, E. Roets, J. Hoogmartens, *J. Chromatogr. A* 954 (2002) 99.
- [23] D. Visky, Y. Vander Heyden, T. Iványi, P. Baten, J. De Beer, Z. Kovács, B. Noszál, P. Dehouck, E. Roets, D.L. Massart, J. Hoogmartens, *J. Chromatogr. A* 1012 (2003) 11.
- [24] P. Dehouck, D. Visky, G. Van den Bergh, E. Haghedooren, E. Adams, A. Kerner, Y. Vander Heyden, D.L. Massart, Zs. Kovács, B. Noszál, J. Hoogmartens, LC–GC Eur. 17 (2004) 592.
- [25] P. Dehouck, D. Visky, Y. Vander Heyden, E. Adams, Z. Kovács, B. Noszál, D.L. Massart, J. Hoogmartens, *J. Chromatogr. A* 1025 (2004) 189–200.
- [26] D. Visky, E. Haghedooren, P. Dehouck, Zs. Kovács, K. Kóczyán, B. Noszál, J. Hoogmartens, E. Adams, *J. Chromatogr. A* 1101 (2006) 103–114.
- [27] P. Forlay-Frick, J. Fekete, K. Héberger, *Anal. Chim. Acta* 536 (2005) 71.
- [28] P.F. Smith, W.P. Petros, M.P. Soucie, K.R. Copeland, *Ther. Drug Monit.* 20 (1998) 231.
- [29] M. Adamczyk, E.M. Brate, E.G. Chiappetta, S. Ginsburg, E. Hoffman, C. Klein, M.M. Perkowski, S.D. Rege, P.P. Chou, A.G. Costantino, *Ther. Drug Monit.* 20 (1998) 191.
- [30] G.K. Best, N.H. Best, N.N. Durham, *Antimicrob. Agents Chemother.* 4 (1968) 115.
- [31] R.L. Kirchmeier, R.P. Upton, *Anal. Chem.* 50 (1978) 349.
- [32] J.R. Uhl, J.P. Anhalt, *Ther. Drug Monit.* 1 (1979) 75.
- [33] E.L. Inman, *J. Chromatogr.* 410 (1987) 363.
- [34] C.M. Harris, R. Kannan, H. Kopecka, T.M. Harris, *J. Am. Chem. Soc.* 107 (1985) 6652.
- [35] F.J. Marshall, *J. Med. Chem.* 8 (1965) 18.
- [36] C.M. Harris, H. Kopecka, T.M. Harris, *J. Am. Chem. Soc.* 105 (1983) 6915.
- [37] M.P. Williamson, D.H. Williams, *J. Am. Chem. Soc.* 103 (1981) 6580.
- [38] D.W. Armstrong, Y. Tang, S. Chen, Y. Ahou, C. Bagwill, J.R. Chen, *Anal. Chem.* 66 (1994) 1473.
- [39] R. Nagarajan, A.A. Schabel, *J. Chem. Soc. Chem. Commun.* (1988) 1306.
- [40] J. Diana, D. Visky, E. Roets, J. Hoogmartens, *J. Chromatogr. A* 996 (2003) 115.
- [41] S.L. Morgan, S.N. Deming, *J. Chromatogr.* 112 (1975) 267.
- [42] W. Naidong, S. Hua, E. Roets, J. Hoogmartens, *J. Planar Chromatogr.* 5 (1992) 92.

## Development of a long-life capillary enzyme bioreactor for the determination of blood glucose

Ja-an Annie Ho<sup>a,b,\*</sup>, Li-chen Wu<sup>b</sup>, Nien-Chu Fan<sup>a</sup>, Ming-Shih Lee<sup>c,d</sup>,  
Hung-Yi Kuo<sup>b</sup>, Chung-Shi Yang<sup>b</sup>

<sup>a</sup> Department of Chemistry, National Tsing Hua University, Hsinchu 300, Taiwan

<sup>b</sup> Department of Applied Chemistry, National Chi-Nan University, Puli, Nantou 545, Taiwan

<sup>c</sup> Department of Medical Laboratory, Taichung Veterans General Hospital, Taichung 407, Taiwan

<sup>d</sup> Department of Medical Technology, Chung Shan Medical University, Taichung 402, Taiwan

Received 11 January 2006; received in revised form 11 April 2006; accepted 11 April 2006

Available online 5 June 2006

### Abstract

A long-life capillary enzyme bioreactor was developed that determines glucose concentrations with high sensitivity and better stability than previous systems. The bioreactor was constructed by immobilizing glucose oxidase (GOx) onto the inner surface of a 0.53 mm i.d. fused-silica capillary that was part of a continuous-flow system. In the presence of oxygen, GOx converts glucose to gluconic acid and hydrogen peroxide (H<sub>2</sub>O<sub>2</sub>). Hydrogen peroxide detection was accomplished using an amperometric electrochemical detector. The integration of this capillary reactor into a flow-injection (FIA) system offered a larger surface-to-volume ratio, reduced band-broadening effects, and reduced reagent consumption compared to packed column in FIA or other settings. To obtain operational (at ambient temp) and storage (at 4 °C) stability for 20 weeks, the glucose biosensing system was prepared using an optimal GOx concentration (200 mg/mL). This exhibited an FIA peak response of 7 min and a detection limit of 10 μM (S/N = 3) with excellent reproducibility (coefficient of variation, CV < 0.75%). It also had a linear working range from 10<sup>1</sup> to 10<sup>4</sup> μM. The enzyme activity in this proposed capillary enzyme reactor was well maintained for 20 weeks. Furthermore, 20 serum samples were analyzed using this system, and these correlated favorably (correlation coefficient,  $r^2 = 0.935$ ) with results for the same samples obtained using a routine clinical method. The resulting biosensing system exhibited characteristics that make it suitable for *in vivo* application.

© 2006 Elsevier B.V. All rights reserved.

**Keywords:** Continuous-flow system; Flow-injection analysis; FIA; Glucose; Blood glucose; Glucose oxidase

### 1. Introduction

Human body needs to maintain blood glucose within a very narrow range of 70–110 mg/dL. People who have diabetes or increased fasting levels of glucose have elevated blood glucose levels because of an inability to use insulin properly. This is often referred to as insulin resistance. Statistics show that diabetes has reached epidemic levels in the U.S. because of increased incidence among older Americans, as well as more obesity in the population. About 2200 people are diagnosed with diabetes each day, but about one-third of the individuals who have diabetes are not aware of it until one of its life-threatening complications has developed. Diabetes results in long-term health consequences,

including cardiovascular disease, nephropathy, neuropathy, diabetic retinopathy and blindness. Recent research has indicated that hyperglycemia is common in critically ill patients, even in those without diabetes mellitus. It has been reported that aggressive glycemic control may reduce mortality in this population [1]. However, the relationship among mortality, the control of hyperglycemia, and the administration of exogenous insulin is still unclear. Therefore, it is very important to have a simpler, more-stable, and more-sensitive method that allows the monitoring of blood glucose in clinics and laboratories.

The glucose sensor reported by Clark and Lyons in 1962 [2] has generally been recognized as the first biosensor. Since then, many types of sensors have been developed for medical diagnosis applications. The use of glucose oxidase (GOx)-based electrodes is a well-established method of detection for *in vivo* levels of circulating glucose [3–5]. In this approach, glucose is converted to gluconic acid and easily detectable hydrogen perox-

\* Corresponding author. Tel.: +886 3571 5131x31286; fax: +886 3 571 1082.  
E-mail address: [jaho@mx.nthu.edu.tw](mailto:jaho@mx.nthu.edu.tw) (J.-a.A. Ho).



ide ( $\text{H}_2\text{O}_2$ ) by the enzyme glucose oxidase. The process requires oxygen as a cosubstrate. The produced  $\text{H}_2\text{O}_2$  is then measured using a charged platinum electrode surface. Hydrogen peroxide has become by far the most widely used method of signal transduction in enzyme biosensors, and a majority of all biosensors (65%) use hydrogen peroxide detection [6]. According to Wilson and Thevenot [7], the construction of a hydrogen peroxide sensor usually involves a platinum anode and a silver/silver chloride cathode. When the anode is poised at +0.6–0.7 V [8], the plateau of oxidation of peroxide is reached at the anode. The enzyme employed in the construction of hydrogen peroxide-producing biosensors frequently involves the immobilization of oxido-reductases to the surface of the sensor by glutaraldehyde cross-linking [8]. Other methods have been reported for the immobilization of enzyme, such as physical deposition onto solid supports, covalent binding [9], and entrapment within a polymer matrix [10]. In recent years, sol–gel technology has been widely used to entrap enzyme for different uses [11–14], because it retains better enzyme activity compared to the free enzyme. Matrixes are usually prepared under ambient conditions and exhibit tunable porosity, high thermal stability, and chemical inertness [12]. However, the silica sol–gel matrixes have some drawbacks, including fragility, complicated preparation procedures, and a tendency to be hydrolyzed at high acidity, which often results in the loss of enzyme stability and also limits their application and feasibility in the development of electrochemical sensors [15,16].

Many methods have been developed in an effort to find a noninvasive detection system for circulating glucose at *in vivo* levels, including ultrasound-assisted transdermal monitoring, electromagnetic-based sensor, and fluorescence-affinity hollow-fiber sensors [17–27]. Other methods of glucose determination that have been reported include those based on a genetically engineered protein [28], on concanavalin A [29], and on a microcantilever [30].

In this work we develop a longer-life capillary enzyme bioreactor for the determination of glucose. The greatly improved activity and stability of this new enzyme bioreactor is facilitated by the direct attachment of GOx to the wall of a 530  $\mu\text{m}$  i.d. fused-silica capillary. To the best of our knowledge this is the first demonstration of the capillary glucose oxidase bioreactor with improved enzyme stability and longer shelf life, which provides a higher surface-to-volume ratio, maximizing the interaction between glucose and GOx compared to bead-packed column. The results from blood sample analysis promised well for the use of this biosensing system in online blood glucose monitoring of critically ill patients before and after surgical operations. Reduced mortality can therefore be achieved by intensive glycemic control.

## 2. Materials and methods

### 2.1. Reagents and materials

D-(+)-Glucose, glucose oxidase (glucose: oxygen oxidoreductase E.C. 1.1.3.4, from *Aspergillus niger*, 181.6 U/mg), 3-glycidoxy propyltrimethoxysilane, potassium carbonate,

sodium metaperiodate, sodium cyanoborohydride and triethanolamine, glycine, and Trizma<sup>®</sup> Base tris[hydroxymethyl]aminomethane (Tris) were obtained from Sigma Chemicals Co. (St. Louis, MO). The fused-silica capillary (0.53 mm i.d.) was obtained from Alltech (Deerfield, IL). All other inorganic chemicals and organic solvents were of reagent grade or better and were purchased from Aldrich Chemical Co. (St. Louis, MO). The pre-analyzed blood plasma samples from patients were obtained fresh from the Veteran General Hospital—Taichung (VGHTC). The use of these samples in no way contradicts the Helsinki Declaration. De-ionized distilled water was obtained from a Milli-Q system (Milford, MA).

### 2.2. Methods

#### 2.2.1. Capillary modification

For a sensitive flow-injection analysis (FIA) enzyme reactor, we required a high-enzyme loading comparable to the dead volume of the bed. For such an enzyme assay, the immobilization support must be rigid and have a mild, very stable, covalent immobilization chemistry. Our group has previously demonstrated the successful immobilization of biomolecules such as antibody without loss of activity and decreased stability on the inner surface of capillary column precoated with a glycerylpropyl layer to minimize the adsorption of the analyte. In the current study the microcapillary enzyme reactor was modified based on previously described procedures [31–36]. Detailed modification procedures were as follows:

Step 1: The 85 cm fused-silica capillary (0.53 mm i.d.) was treated with 1 M NaOH overnight.

Step 2: 1 M HCl and distilled water were used to rinse the capillary, which was subsequently filled with 3-glycidoxypropyltrimethoxysilane (GPTMS) and heated at 90 °C for 2 h.

Step 3: The capillary was rinsed and treated with 10 mM sulfuric acid at 90 °C for 10 min to convert the residual epoxy groups to diols.

Step 4: After washing with distilled water, diols were cleaved and oxidized to aldehydes with sodium metaperiodate containing potassium carbonate at room temperature for 2 h.

Step 5: 190  $\mu\text{L}$  of GOx (200 mg/mL) and sodium cyanoborohydride (5 mg/mL) in 0.1 M phosphate buffer (pH 7.3) were passed slowly into the capillary and incubated overnight to reduce the Schiff base.

Step 6: The capillary was rinsed with 0.2 M triethanolamine buffer (pH 8.2), 1 M NaCl, 0.1 M glycine/HCl buffer (pH 2.5), and Tris buffered saline (TBS), pH 7.0, sequentially. Finally, the capillary enzyme reactor, filled with TBS (pH 7.0), was then stored at 4 °C until use. In this way glucose oxidase was covalently attached on the inner wall of capillary column.

### 2.3. Flow-injection analysis system

The flow-injection analysis system (schematic diagram shown at Fig. 1) consists of a Hewlett Packard 1050 HPLC pump (Agilent, Foster City, CA) at the inlet of the capillary glu-

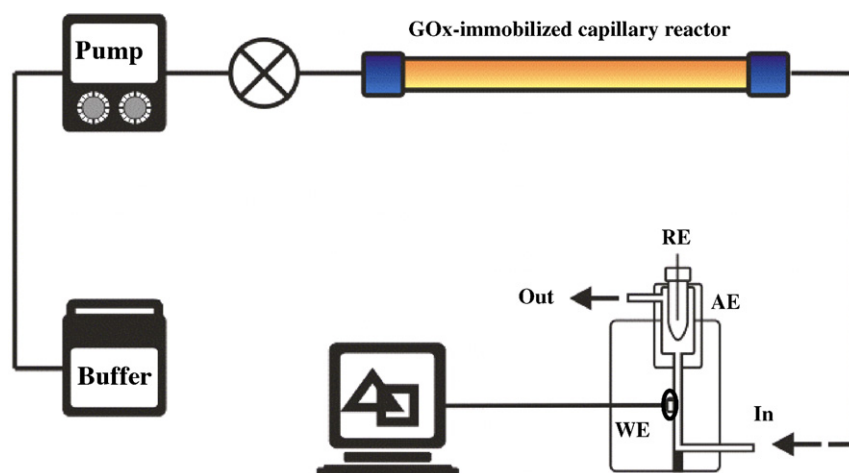


Fig. 1. A schematic diagram of enzymatic flow injection analytical system for blood glucose. WE: working electrode; RE: reference electrode; AE: counter electrode.

cose biosensing system that maintains a flow rate of 0.3 mL/min and a Rheodyne (Model 7725) injector with a 20  $\mu\text{L}$  sample loop (Rainin, Emeryville, CA) for injection of the samples. Commercially available polyetheretherketone (PEEK) tubing (0.020 in. i.d.) and standard fingertight fittings were purchased from Upchurch Scientific Inc. (Oak Harbor, WA). The carrier used was 0.1 M potassium phosphate buffer (pH 7.2) containing 0.1 M NaCl that was vacuum-filtered before use. A HW-2000 Chromatography workstation, used for data collection, was purchased from Great Tide Instrument Co. (Taipei, Taiwan).

Final signal integration was performed using the HW-2000 Chromatography workstation system running on an Intel Celeron 2.20 GHz computer. All electrochemical measurements were performed on an electrochemical analyzer (model CL-4C amperometric detector) obtained from BAS (West Lafayette, IN). A BAS model CC-5E electrochemical flow cell was employed in these measurements. The conventional three-electrode system was made up of a dual platinum electrode for thin-layer cross-flow cell (model MF-1012, BAS) as working electrode (3 mm in diameter), Ag|AgCl as reference (model MW-2078, BAS), and steel wire as counter electrode.

#### 2.4. Experimental procedures

For the determination of glucose, 20  $\mu\text{L}$  of glucose standards were injected into the carrier stream and subjected to flow-injection analysis using the constructed microcapillary glucose oxidase enzyme reactor as described above, where the catalytic reaction involves glucose oxidation to produce hydrogen peroxide. The amperometric signal produced by hydrogen peroxide was measured by the amperometric detector in the system, which applied a potential to the electrochemical cell and monitored the resulting electrochemical reaction. The dual platinum working electrode was initially prepared by polishing for 3 min with 0.05  $\mu\text{m}$  diamond polish on a polishing disk. After polishing, the dual electrode surface was rinsed with distilled water and maintained at 0.350 V versus Ag|AgCl for hydrogen peroxide measurements. The electrochemical oxidation of hydrogen peroxide at the dual 3 mm platinum electrode was measured with an

amperometric detector, and the current output was also stored on HW-2000. The height of a given FIA peak reflects the number of moles injected onto the capillary enzyme reactor. At a given analyte concentration, the peak height varies with sample volume, which is determined by the volume of the injection loop. The calibration curves for each assay were expressed in terms of the injected molar content in order to determine the linear dynamic range of the capillary FIA system for glucose.

#### 2.5. Real-sample analysis

Fresh human serum (20  $\mu\text{L}$ ) was diluted with 180  $\mu\text{L}$  of 0.1 M potassium phosphate buffer (pH 7.2) containing 0.1 M NaCl and subsequently injected via the valve. The results obtained using this capillary-based method were compared to those obtained with a clinically used glucose analyzer (Hitachi 7170 automated analyzer).

### 3. Results and discussion

#### 3.1. Optimization of parameters and characterization of the biosensing system

A series of experiments was performed to establish the conditions for maximum peak height. The applied voltage (0.300–0.500 V), sample injection volume (5–20  $\mu\text{L}$ ), enzyme concentration (100–200 mg/mL), and flow rate (0.1–0.5 mL/min) were investigated.

To evaluate the effect of the voltage on the sensitivity of the biosensing system, different voltages were applied to the system. The voltages varied from 0.300 to 0.500 V. The maximum sensitivity was achieved at an applied voltage of 0.500 V versus Ag|AgCl using model glucose standards. However, this high voltage suffered from a low signal-to-noise ratio problem, and there was severe interference from the medium during serum sample analysis (Fig. 2). Oxidation of hydrogen peroxide at higher voltage (at a platinum electrode) is prone to interference from many other electroactive substances, such as ascorbic acid and uric acid; however, oxidation signals obtained

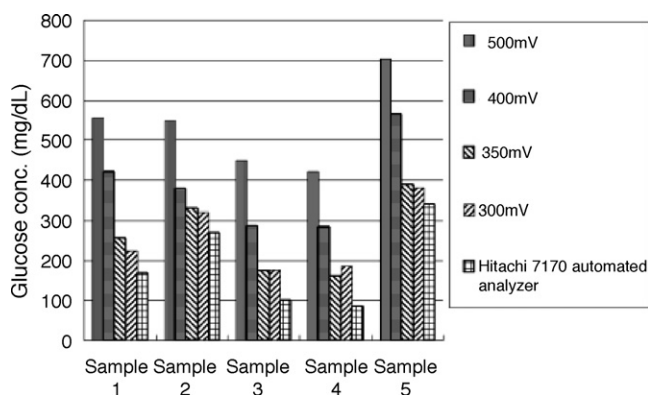
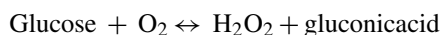


Fig. 2. The effect of applied voltage on real-sample analysis.

at lower potential minimize these interference effects. Therefore, a voltage of 0.350 V was selected, and the system became more tolerant of interference. Although results obtained from Hitachi 7170 autoanalyzer and proposed FIA system correlated well, differences were still observed between these two sets of data. The accuracy of the proposed system should be satisfactory for screening purpose. The injected-sample volume was varied by changing sample loop size relative to the injection valve. The peak height increased with increasing injected-sample size. A sample volume of 20  $\mu\text{L}$  was selected as a suitable volume. The enzyme concentration for the immobilization on the inner wall of capillary was varied from 100 to 200 mg/mL. The maximum peak height was obtained with GOx at 200 mg/mL. Due to the relatively high cost of glucose oxidase, enzyme concentration higher than 200 mg/mL was not considered in this study. The length of bioreactor (25–100 cm) was also an investigated parameters. The longer the bioreactor, the higher signal output could be obtained. However, broaden peaks were often found when length of bioreactor was longer than 85 cm. The flow rate was a very important parameter of the proposed system because the slower flow allowed sample glucose to react with immobilized enzyme more completely, and therefore higher signal output could be collected; however, the slow flow rate often resulted in peak broadening and limited sample throughput. After considering all of these factors, a flow rate of 0.3 mL/min was chosen for acceptable peak height and sample throughput.

### 3.2. Assay performance

The present enzyme-based capillary glucose biosensing system was based on glucose oxidase.



In the reaction sequence shown above, glucose oxidase catalyses the oxidation of  $\beta$ -D-glucose to gluconic acid, using oxygen as the electron acceptor. Since the gluconic acid level cannot be measured by the change in pH [8], the oxidation of hydrogen peroxide was measured by means of a charged platinum-based working electrode surface [3]. Based on earlier research [37–40], potassium phosphate buffered saline (pH 7.2) with a similar nature to physiological fluids was selected as the medium solu-

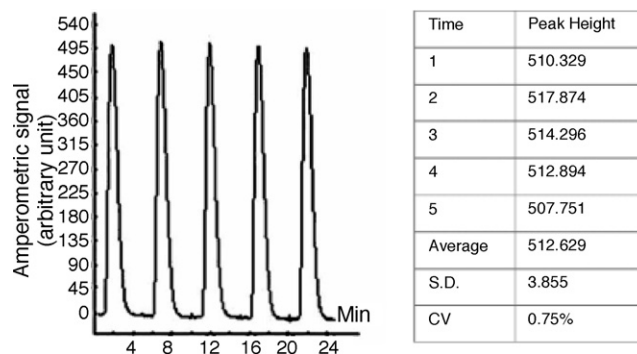
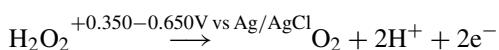


Fig. 3. Reproducibility of the signals generated by five replicates of a glucose standard (concentration = 10 mM).

tion for the glucose standards.



The amperometric signal was obtained upon the injection of variable glucose concentrations into the electrode cell under flow conditions, no signal was found in the absence of glucose. The linear response was observed between  $10^{-2}$  mM (10  $\mu\text{M}$ ) and 10 mM of glucose standard solution with the regression equation of amperometric signal = 49.879 mM + 2.21 ( $R^2 = 1.000$ ). The sensing system was used for an average of 8 h a day, and the capillary enzyme reactor remained stable for at least 120 days at 25  $^\circ\text{C}$  in operation condition and for the remainder of the time at 4  $^\circ\text{C}$  in storage conditions. The repeatability and reproducibility of the proposed system was examined by injecting a 10 mM glucose standard. The uniformity of the FIA-amperometric peaks generated by five replicate injections is shown in Fig. 3. The largest value for the coefficient of variation (CV) for five replicate measurements was 0.75%, indicating that the reproducibility of this enzyme-based capillary glucose sensing system is acceptable. The proposed method was also validated for its accuracy by employing interday studies for 5 days where a glucose standard was measured, also at a concentration of 10 mM. As shown in Fig. 4, the coefficient of variation based on the peak height was found to be 3.05%. Additionally, though Pt electrode is prone to fouling by protein components in physiological fluids, no serious interference was found when our model serum solution (BSA spiked in glucose standard solution at final concentration of 7 mg/mL) was tested.

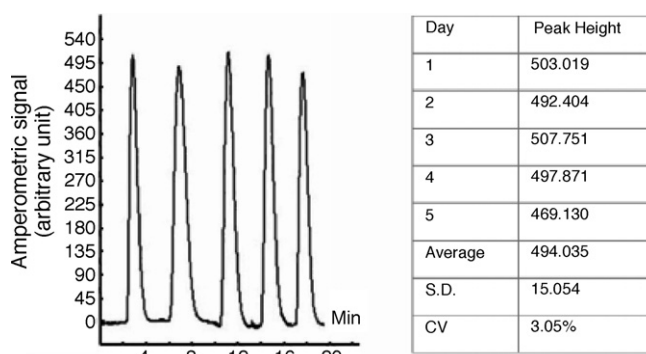


Fig. 4. Interday deviation for the enzyme-based capillary biosensing system. Glucose standard concentration: 10 mM.

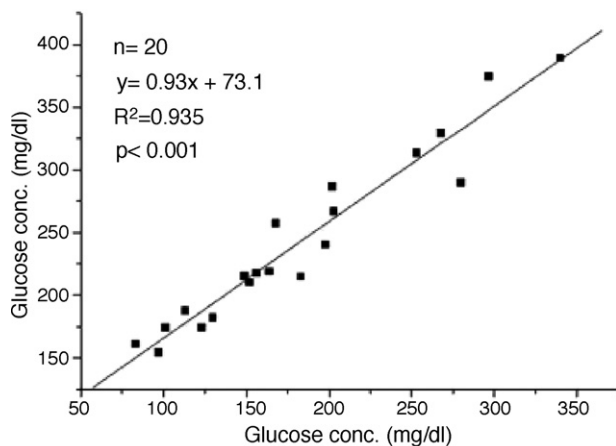


Fig. 5. Linear regression of the correlation between glucose results measured by the proposed capillary glucose biosensing system and reference clinical measurements of blood samples obtained from 20 patients. X-axis: results of clinical measurements; Y-axis: results from the capillary glucose biosensing system. Each point represents the mean of three measurements.

### 3.3. Application

The comparison study in measuring blood glucose of patients with proposed system and clinically used glucose analyzer (Hitachi 7170) is very important in validating a new analytical methodology towards its clinical applications. In this study, glucose was determined in human serum from adults by using the proposed system. Prior to analysis the sample serum was diluted with 0.1 M potassium phosphate buffer containing 0.1 M NaCl (pH 7.2) and centrifuged at  $2000 \times g$  at room temp for 5 min. Twenty microliters was taken directly from the supernatant and injected into the system. Linear regression of the correlation between blood glucose results measured by the enzyme-based capillary glucose biosensing system and a clinically used glucose analyzer (Hitachi 7170) is shown in Fig. 5. The largest value of the CV for five replicate injections was 6.05%. The best-fit regression line of the average of enzyme-based capillary glucose sensing system versus that determined using the clinical Hitachi 7170 automated analyzer indicated a strong correlation between the two data sets ( $r^2 = 0.935$ ). This shows that the proposed system is comparable to the Hitachi 7170 automated analyzer presently used in the Medical Laboratory Department at Taichung Veterans General Hospital.

### 4. Conclusions

In summary, we have demonstrated the successful attachment of glucose oxidase to the inner wall of a fused-silica capillary while retaining enzymatic activity for more than 120 days. Our study has shown that an enzyme-based capillary glucose biosensing system was developed based on flow-injection analysis with amperometric detection. Operational and storage stability for greater than 4 months permitted the measurement of more than 300 samples. The glucose biosensing system prepared using the optimal GOx concentration (200 mg/mL) exhibited a FIA-amperometric current response at 7 min. The sample throughput was about 9/h, and the reagent consumption was reduced. This

flow-injection type of sensing system holds promise for the determination of glucose content in clinical samples as well as in fruit juice.

The proposed glucose sensing system was found to be responsive to glucose over a wide range of concentrations and has the following characteristics: a detection limit of  $10 \mu\text{M}$  (based on the signal-to-noise characteristics,  $S/N = 3$ ), linearity up to  $10^4 \mu\text{M}$ , and reproducibility of under 0.75% coefficient of variation. These results clearly show the usefulness of this platform for direct detection of glucose and clinical diagnosis without complicated sample preparation and labeling. This proposed biosensing system has demonstrated its feasibility as a means of determining blood glucose in serum. The integration of this capillary system into a flow-injection system offers the advantages of a large surface-to-volume ratio, laminar flow, and reduced band-broadening effects compared to previous packed-column systems. These all help to increase the sensitivity and reproducibility of this capillary glucose measurement system. The current focus of our group is to use an enzyme-immobilization technique on microfluidic enzyme chips to improve the sample throughput. Future efforts will include attempts to incorporate an insulin biosensor into the present sensing system that will allow the parallel measurement of glucose and insulin. This will simplify studies on whether blood glucose level or the amount of insulin administered is associated with reduced mortality in critically ill patients.

### Acknowledgements

This work was supported by the National Science Council in Taiwan, ROC, under grant NSC 91-2113-M-260-011 and the Taichung Veterans General Hospital-National Chi-Nan University Joint Research Program under grant VGHCN 92-72-02.

### References

- [1] S.J. Finney, C. Zekveld, A. Elia, T.W. Evans, *JAMA* 290 (2003) 2041.
- [2] L.C. Clark Jr., C. Lyons, *Ann. N Y Acad. Sci.* 102 (1962) 29.
- [3] G.G. Guilbault, G.J. Lubrano, *Anal. Chim. Acta* 64 (1973) 439.
- [4] Y. Zhang, G.S. Wilson, *Anal. Chim. Acta* 281 (1993) 513.
- [5] Y. Hu, G.S. Wilson, *J. Neurochem.* 68 (1997) 1745.
- [6] J. Davis, D.H. Vaughan, M.F. Cardosi, *Enzyme Microbiol. Technol.* 17 (1995) 1030.
- [7] G.S. Wilson, D.R. Thevenot, in: A.E.G. Cass (Ed.), *Biosensor, A Practical Approach*, IRL Press, Oxford, UK, 1990, pp. 1–17.
- [8] J. Woodward, in: A. Mulchandani, K.R. Rogers (Eds.), *Enzyme and Microbial Biosensor, Techniques and Protocols*, Humana Press, New Jersey, USA, 1998, pp. 67–79.
- [9] K.T. Lee, C.C. Akoh, *Food Rev. Int.* 14 (1998) 17.
- [10] D. Parra-Diaz, D.P. Brower, M.B. Medina, G.J. Piazza, *Biotechnol. Appl. Biochem.* 18 (1993) 359.
- [11] A. Hsu, T.A. Foglia, S. Shen, *Biotechnol. Appl. Biochem.* 31 (2000) 179.
- [12] J. Yu, H. Ju, *Anal. Chem.* 74 (2002) 3579.
- [13] Th. Noguier, D. Szydłowska, J.-L. Marty, M. Trojanowicz, *Polish J. Chem.* 78 (2004) 1679.
- [14] Y. Tang, E.C. Tehan, Z. Tao, F.V. Bright, *Anal. Chem.* 75 (2003) 2407.
- [15] Q. Chen, G.L. Kenasis, A. Heller, *J. Am. Chem. Soc.* 120 (1998) 4582.
- [16] O. Lev, M. Narvaez, E. Dominguez, I. Katakai, *J. Electroanal. Chem.* 425 (1997) 1.

- [17] M. Gourzi, A. Rouane, R. Guelaz, M. Nadi, F. Jaspard, *J. Med. Eng. Technol.* 27 (2003) 276.
- [18] J. Kost, S. Mitragotri, R. Gabbay, M. Pishko, R. Langer, *Nature* 6 (2000) 347.
- [19] R. Ballerstadt, J.S. Schultz, *Anal. Chem.* 72 (2000) 4185.
- [20] M. Gerritsen, J.A. Jansen, A. Kros, R.J.M. Nolte, J.A. Lutterman, *Invest. Surg.* 11 (1998) 163.
- [21] R. Ballerstadt, J.S. Schultz, *Anal. Chim. Acta* 345 (1997) 203.
- [22] E. Wilkins, P. Atanasov, B.A. Muggenburg, *Biosens. Bioelectron.* 10 (1995) 485.
- [23] D.L. Meadows, J.S. Schultz, *Anal. Chim. Acta* 280 (1993) 21.
- [24] S. Mansouri, J.S. Schultz, *Biotechnology* 2 (1984) 885.
- [25] P. Abel, A. Muller, U. Fischer, *Biomed. Biochim. Acta* 3 (1984) 577.
- [26] J.C. Pickup, D.R. Thevenot, European achievements in sensor research dedicated to in vivo monitoring, in *Advances in biosensors*, supplement 1, JAI Press, London, UK, 1993, pp. 273–288.
- [27] S. Jung, J.R. Trimarchi, R.H. Sanger, P.J.S. Smith, *Anal. Chem.* 73 (2001) 3759.
- [28] L. Tolosa, I. Gryczynski, L.R. Eichhorn, J.D. Dattelbaum, F.N. Castellano, G. Rao, J.R. Lakowicz, *Anal. Biochem.* 267 (1999) 114.
- [29] R.J. Russell, M.V. Pishko, *Anal. Chem.* 71 (1999) 3126.
- [30] J. Pei, F. Tian, T.B. Thundat, *Anal. Chem.* 76 (2004) 292.
- [31] P. Larsson, *Methods Enzymol.* 104 (1984) 212.
- [32] M. de Frutos, S.K. Paliwal, F.E. Regnier, *Anal. Chem.* 65 (1993) 2159.
- [33] M.Y. Lee, R.A. Durst, *J. Agric. Food Chem.* 44 (1996) 4032.
- [34] J.A. Ho, R.A. Durst, *Anal. Chim. Acta* 414 (2000) 61.
- [35] F.E. Regnier, R. Noel, *J. Chromatogr. Sci.* 14 (1976) 316.
- [36] L.C. Wu, C.M. Cheng, *Anal. Biochem.* 346 (2005) 234.
- [37] J. Wang, M. Chatrathl, A. Ibañez, *Analyst* 126 (2001) 1203.
- [38] M.G. Booutelle, L.K. Fellows, C. Cook, *Anal. Chem.* 64 (1992) 1790.
- [39] T. Hoshi, J. Anzai, T. Osa, *Anal. Chem.* 67 (1995) 770.
- [40] S. Hrapovic, J.H.T. Luong, *Anal. Chem.* 75 (2003) 3308.



# Estimating the chemical rank of three-way data arrays by a simple linear transform incorporating Monte Carlo simulation

Le-Qian Hu, Hai-Long Wu<sup>\*</sup>, Jian-Hui Jiang, Qing-Juan Han, A-Lin Xia, Ru-Qin Yu

*State Key Laboratory of Chemo/Biosensing and Chemometrics, College of Chemistry and Chemical Engineering, Hunan University, Changsha 410082, China*

Received 13 January 2006; received in revised form 8 April 2006; accepted 9 April 2006  
Available online 24 May 2006

## Abstract

Estimating an appropriate chemical rank of a three-way data array is very important to second-order calibration. In this paper, a simple linear transform incorporating Monte Carlo simulation approach (LTMC) to estimate the chemical rank of a three-way data array was suggested. The new method determines the chemical rank through performing a simple linear transform procedure on the original cube matrix to produce two subspaces by singular value decomposition. One of two subspaces is derived from the original three-way data array itself and the other is derived from a new three-way data array produced by the linear transformation of the original one. Projection technique incorporating the Monte Carlo approach acts as distinguishing criterion to choose the appropriate component number of the system. Simulated three-way trilinear data arrays with different noise types (homoscedastic and heteroscedastic), various noise level as well as high collinearity are used to illustrate the feasibility of the new method. The results have shown that the new method could yield accurate results with different conditions appended. The feasibility of the new method is also confirmed by two real arrays, HPLC-DAD data and excitation–emission fluorescent data. All the results are compared with the other three factor-determining methods: factor indicator function (IND), core consistency diagnostic (CORCONDIA) and two-mode subspace comparison (TMSC) approach. It shows that the newly proposed algorithm can objectively and quickly determine the chemical rank to fit the trilinear model.

© 2006 Elsevier B.V. All rights reserved.

*Keywords:* Rank estimation; Chemical rank of three-way data arrays; Linear transform; Monte Carlo simulation; Projection technique

## 1. Introduction

Tensor calibration is increasingly being used for establishing regression models and predicting the concentration from experimental data. It can be classified into zero- to first- to second-order calibration and beyond in terms of the order of the analytical instruments [1]. The first- and second-order calibrations are the most commonly used ones in the analytical chemistry field. The first-order calibration methods comprise several important regression models, such as multivariate linear regression (MLR), principal components regression (PCR), partial least squares regression (PLS) [2]. The insufficiency of the first-order calibration (two-way data analysis) is that it requires every spectrally active species in a future unknown sample must be included in the calibration sample [1] i.e., the components

contained in the calibration sample and predicted sample should coincide. Otherwise, the predicted result will be inaccurate when a sample with one or more species (interferences) is not represented in the calibration model.

In practical situations dealing with complex chemical and physical systems, such as process analysis, environmental analysis, food and pharmaceutical analysis, the interferences are often encountered in the mixture investigated [3]. On such occasions only the second-order calibration (three-way data analysis) can obtain more satisfactory result. Thus three-way data (derived from the hyphenated analytical techniques such as HPLC-DAD or excitation/emission matrix spectrofluorometer) analysis has become one of the most active areas in analytical chemometrics and other areas [4–9]. Unlike two-way analysis techniques, three-way data analysis enables one to quantify the components of analytical interest even in the presence of unknown interferences not included in the calibration sample i.e., the second-order advantage [1]. The other advantage of it is that the solution produced by the trilinear data analysis is rotation

<sup>\*</sup> Corresponding author. Tel.: +86 731 8821818; fax: +86 731 8821818.  
E-mail address: [hlwu@hnu.cn](mailto:hlwu@hnu.cn) (H.-L. Wu).

dependent [3,6]. Primarily, in terms of their sensitivity for the chemical rank (the number of principal factors responsible for the trilinear model), there are two main types of methodologies for the three-way data resolution in chemometrics. Methods of the first type are sensitive to the rank of three-way data arrays, i.e., the underlying factors, such as Tucker3 [10], PARAFAC [11], bilinear least squares (BLLS) [5], generalized rank annihilation (GRAM) [12] and trilinear decomposition (TLD) method [13]. However, methods of the second type are insensitive to the underlying factors of the system. These are developed mainly by our laboratory, including alternating trilinear decomposition (ATLD) [14], alternating slice-wise diagonalization (ASD) [15], self-weighted alternating trilinear decomposition (SWATLD) [16], and pseudo-alternating least squares (PALS) [17], etc. The first type requires a correct determination of the underlying factors of the complex system. Otherwise it would produce an inaccurate result. The second type only requires the factors selected are not less than the accurate underlying factors. The result would be inaccurate when the chemical rank was underdetermined for any methods. Thus, it is requisite to determine the underlying factors for fitting the trilinear model beforehand. The analytes are often unknown in practical analysis process. Therefore, determining the underlying species in the mixture is always the key step to further qualitative and quantitative analysis in all forms of spectral data treatment whichever type is employed.

In chemometrics, choosing the chemical rank of a data matrix focuses mainly on first-order data arrays [18]. Here, the chemical rank of a data matrix denotes the number of principal factors responsible for the model. Sometime it can also be called pseudo-rank or underlying factor or number of significant component of the mixture system. Some authors have given some good reviews about these methods in their literatures [12,19]. Contrarily, deciding the appropriate rank of three-way data array is very difficult and different from two-way data arrays. Kruskal has pointed out six distinctions from the first-order data [20]. Only several methods have been used for the determination of significant factors of three-way data arrays. Primarily, they can be divided into two groups. The first group applies trilinear model to estimate the chemical rank of three-way data array, such as core-consistency-diagnostic [21] and add-up-one [22] approach. Core-consistency-diagnostic compares the results from the core matrix of the Tucker3 and PARAFAC models with different factors attempted, and the add-up-one algorithm unfolds the three-way data along with the two orders into two cube matrices, then runs PARAFAC algorithm [11] twice to compare the residuals of different factors. Some literatures have used the core-consistency-diagnostic in their papers [3,8]. However, these methods used to be time-consuming for their requiring PARAFAC to run once or twice times. At the same time, two-factor degeneracy [23,24] may make these two methods suffer from heavy computation burden and produce erroneous result. The second group is the non-model method. They include split-half analysis [25], multi-way cross-validation [26], two-mode subspace comparison (TMSC) [27] and principal norm vector (PNV) [28] approaches, etc. Wu et al. [14] also suggested general formula for deducing the chemical rank

of three-way data arrays. In practical application, it is difficult to select the appropriate splitting scheme for split-half analysis. The performance of the multi-way cross-validation is more inconvenient to the general user. At the same time, TMSC and PNV only adopt a group of subspace to determine the chemical rank, which may lead to losing some useful information. On the other hand, any of these methods cannot ensure to obtain the accurate result for a practical mixture system. Two or more methods are often used to estimate the appropriate component number of the mixture to confirm the result [3]. Thus, developing the method of choosing the significant components for fitting the trilinear model should be encouraged [9]. In this paper, a simple linear transform method incorporating Monte Carlo simulation (LTMC) to estimate the chemical rank of three-way data arrays was proposed. Its feasibility was validated through the simulated and real three-way data sets. The new method offered an alternative to estimating the chemical rank of three-way data array from a complex system.

## 2. Theory

### 2.1. Trilinear model for second-order calibration

Trilinear instrumental response, say the two-way matrices obtained using HPLC-DAD, for  $K$  mixture samples can be expressed as

$$\mathbf{X}_{..k} = \sum_{n=1}^N \mathbf{a}_n \mathbf{b}_n^T c_{kn} + \mathbf{E}_{..k}, \quad k = 1, 2, \dots, K \quad (1)$$

where  $\mathbf{X}_{..k}$  is the response matrix for the  $k$ th sample ( $I$  wavelengths by  $J$  retention times).  $\mathbf{a}_n$  and  $\mathbf{b}_n$  are the spectral and the chromatographic profiles, respectively, for the  $n$ th component and  $c_{kn}$  is the concentration of the  $n$ th component in the  $k$ th sample. It is important to note that it is implied by Eq. (1) that  $\mathbf{a}_n \mathbf{b}_n^T$  is the two-way response of the pure  $n$ th component of unit concentration.  $\mathbf{E}_{..k}$  is the measurement error matrix for the  $k$ th sample.  $N$  denotes the underlying factors, which should be considered as the total number of detectable species, containing physically meaningful component(s) of interest and background as well as uncalibrated interferences (interferent(s) that are not present in the calibration samples). The superscript  $T$  denotes the transpose of a matrix or a vector. Note that, throughout this paper, scalars are shown in italics, vectors are bold lowercase letters, two-way matrices are bold uppercase letters.

### 2.2. Algorithm

The mathematical formulation of HPLC-DAD or emission-excitation fluorescent approach for  $N$  components sample can also be expressed as the following:

$$\mathbf{X}_{..k} = \mathbf{A} \text{diag}(\mathbf{c}(k)) \mathbf{B}^T + \mathbf{E}_{..k}, \quad k = 1, 2, \dots, K \quad (2)$$

where  $\mathbf{X}_{..k}$  is still the response matrix for the  $k$ th sample.  $\mathbf{E}_{..k}$  is the measurement error matrix.  $\mathbf{A}$  and  $\mathbf{B}$  are the matrices which collect spectral and chromatographic profiles for all  $N$  components, respectively. They can be expressed as  $\mathbf{A} = (\mathbf{a}_1, \mathbf{a}_2, \dots, \mathbf{a}_N)$

and  $\mathbf{B} = (\mathbf{b}_1, \mathbf{b}_2, \dots, \mathbf{b}_n)$ .  $\mathbf{c}_{(k)}$  is the  $k$ th row of  $\mathbf{C}$  (the concentration matrix with size  $K \times N$ ).  $\text{diag}(\mathbf{c}_{(k)})$  denotes the diagonal matrix whose diagonal elements are the corresponding ones of  $\mathbf{c}_{(k)}$ . Now we suppose the only two mixture samples that both included  $N$  components were measured by hyphenated instrument and then two response data matrices were obtained, respectively. They are only different with variable concentration. If one decomposes the two sample matrices by singular value decomposition (SVD), the first  $N$  columns of two left and right eigenvector matrices will be uniform to each other in the absence of noise. In the presence of noise, the first  $N$  columns of left and right eigenvector matrices will span the same subspace but the  $(N + 1)$ th column is nearly orthogonal. Refs. [29,30] have adopted this idea to determine the chemical rank of the excitation–emission matrix by applying repeated experiments and bootstrap resampling scheme. For three-way data analysis, one can obtain  $K$  (here  $K$  is often greater than two sample matrices synchronously, including calibration samples and prediction samples. Generally, each sample matrix does not always comprise of the same component especially for the prediction samples. The prediction samples often contain the uncalibrated interferences that are not included in the calibration sample. Thus the above idea does not fit to estimate the chemical rank of three-way data set obtained from multi-samples. In this paper, we apply a simple linear transform approach to choosing the appropriate component in the trilinear data arrays. First we will add together the  $K$  sample matrices:

$$\mathbf{R1} = \sum_{k=1}^K \mathbf{X}_{..k} \quad k = 1, 2, \dots, K \quad (3)$$

Then we multiply a stochastic number  $w_k$  ( $0 < w_k < 1$ ,  $k = 1, 2, \dots, K$ ) to each sample matrix as the following:

$$\mathbf{X}_{..k}^* = w_k \mathbf{X}_{..k} = \mathbf{A} \text{diag}(w_k \mathbf{c}_{(k)}) \mathbf{B}^T + \mathbf{E}_{..k}^* \quad k = 1, 2, \dots, K \quad (4)$$

This can be considered to be a linear transform of concentration term to produce  $K$  new sample matrices. In succession we also add together the new  $K$  sample matrices as former:

$$\mathbf{R2} = \sum_{k=1}^K \mathbf{X}_{..k}^* \quad k = 1, 2, \dots, K \quad (5)$$

Matrices  $\mathbf{R1}$  and  $\mathbf{R2}$  represent the compressed sample matrices. One can decomposes the matrix  $\mathbf{R1}$  and the reproduced matrix  $\mathbf{R2}$  by singular value decomposition (SVD):

$$[\mathbf{U}, \mathbf{S}, \mathbf{V}] = \text{svd}(\mathbf{R1}), \quad [\mathbf{U}^*, \mathbf{S}^*, \mathbf{V}^*] = \text{svd}(\mathbf{R2})$$

It supposes that there are  $N$  component(s) in the complex systems. One can find the two subspaces spanned by the first  $N$  columns of two eigenvector matrices  $\mathbf{U}$  and  $\mathbf{U}^*$  are nearly coincident while they are nearly orthogonal for the two subspaces spanned by the later  $(N + 1)$ th,  $(N + 2)$ th, ..., columns of eigenvector matrices  $\mathbf{U}$  and  $\mathbf{U}^*$ , because the later  $(N + 1)$ th,  $(N + 2)$ th, ..., columns represent the noise space that is independent. It is identical to the other two eigenvector matrices  $\mathbf{V}$  and

$\mathbf{V}^*$ . The idea can lead us to estimate the rank of three-way data arrays.

Several algorithms can be used to distinguish the difference between two subspaces produced, such as projection approach, subspace difference approach. Subspace included angle approach [31] and canonical correlation analysis [29,30], etc. In this paper, only projection method was used to determine the chemical rank of three-way data arrays.

Projection technique is a conventional method in chemometrics. In this paper it is used to determine the coherency between the subspace  $\mathbf{U}$  and  $\mathbf{U}^*$ . The factors from one to  $F$  ( $F \gg N$ ,  $N$  is the appropriate component number to fit the trilinear model) were selected. Just as discussed above, the first  $N$  columns of matrices  $\mathbf{U}$  and  $\mathbf{U}^*$  are high correlation but low correlation for the later  $N + 1$  column. Therefore, the projection residuals for the first  $N$  factors will keep very small values or decrease gradually to the minimum value when the factors selected increase from one to  $N$ . Thereafter the projection residuals of the  $N + 1$  factor selected will enhance remarkably and keep relatively large value for the subsequent factors. The performance result of eigenvector matrices  $\mathbf{V}$  and  $\mathbf{V}^*$  will be coincide with the above conclusion. Here we incorporate them together as following:

$$F(f) = \left( \left\| (\mathbf{I}_U - \mathbf{U}_f \mathbf{U}_f^+) \mathbf{U}_f^* \right\| + \left\| (\mathbf{I}_V - \mathbf{V}_f \mathbf{V}_f^+) \mathbf{V}_f^* \right\| \right) / f \quad (6)$$

here  $\mathbf{I}_U$  and  $\mathbf{I}_V$  denote the identity matrices with same dimension to the  $\mathbf{U}_f \mathbf{U}_f^+$  and  $\mathbf{V}_f \mathbf{V}_f^+$ , respectively.  $f$  denotes the factor attempted to decide the chemical rank of the mixture.  $\mathbf{U}_f$  and  $\mathbf{U}_f^*$  denotes subspaces which collect the first  $f$  columns of  $\mathbf{U}$  and  $\mathbf{U}_f^*$ .  $\mathbf{V}_f$  and  $\mathbf{V}_f^*$  denotes subspaces which collect the first  $f$  columns of  $\mathbf{V}$  and  $\mathbf{V}^*$ .  $\| \cdot \|$  denotes matrix norm. It should be noticed, if one or several matrices were multiplied by a very small stochastic value  $w_k$  (close to zero), it may lead to losing some useful information contained in those samples and the final result may be inaccurate. To overcome the deficiency, Monte Carlo (MC) simulation [32] is used to produce at least 50 groups of stochastic number (each group contains  $k$  stochastic numbers  $w_k$ , respectively) to repeat above computation procedure 50 times. The projection residuals of each time will be added up and a mean value can be obtained. Therefore, comparing with TMSC and PNV, which only adopt a group of subspace, the newly proposed method will be more robust than them from statistics' point of view for it applies MC approach to producing multiple groups of subspace. At the same time, the newly proposed method runs faster than add-up-one and core consistency diagnostic approach for it does not require running PARAFAC. Thus the first  $N$  factor(s) corresponding to the small projection residuals will be considered to be the chemical rank of the mixture system. The subsequent factors corresponding to the large projection residuals will not be deemed to be the significant components to fit the trilinear model. It is also worth noting that the newly proposed method chooses the chemical rank of the mixture system based on the trilinear model. Therefore, it does not fit the non-trilinearity data arrays produced by some factors, such as retention time shift in the chromatographic analysis and Rayleigh scattering in the spectrofluorimetric analysis, etc.

The newly proposed method of estimating the underlying factors in the three-way data arrays can be described as the following:

- (1) The original cube  $\mathbf{X}$  is unfolded into  $K$  matrices  $\mathbf{X}_{I \times J}$ , and then each matrix  $\mathbf{X}_{I \times J}$  is multiplied by the scalar  $w_{..k}$  to produce  $K$  new matrices  $\mathbf{X}_{I \times J}^*$ , here  $w_{..k}$  is produced by Monte Carlo simulation.
- (2) Then add the  $K$  matrices  $\mathbf{X}_{I \times J}$  and  $K$  new matrices  $\mathbf{X}_{I \times J}^*$  together, respectively, to produce two compressed matrices  $\mathbf{R1}$  and  $\mathbf{R2}$ .
- (3) Two compressed matrices  $\mathbf{R1}$  and  $\mathbf{R2}$  were decompose by SVD, respectively.
- (4) The eigenvector matrices  $\mathbf{U}$  and  $\mathbf{U}^*$  as well as eigenvectors matrices  $\mathbf{V}$  and  $\mathbf{V}^*$  are performed by the projection method together.
- (5) Monte Carlo (MC) simulation is used to produce at least 50 groups of stochastic numbers to repeat steps (1)–(4) at least 50 times (more times can make the result more obvious). All 50 groups of projection residuals are added up and a mean value can be obtained. Here  $f$  values ranging from 1 to  $F$  are attempted to determine the chemical rank of the mixture system. The process will stop when the projection residuals increase remarkably from a very small value to a large value. The factors corresponding to those small residuals can be considered to be the chemical rank of the three-way data arrays. In this paper, 10 factors ( $F = 10$ ) are attempted in each data array to interpret the feasibility of the newly suggested method. In practices, the maximum factor attempted must not be predefined. The procedure can stop automatically when the projection residuals increase from a small value to a large value.

The newly proposed method was compared with the following three methods: factor indication function (IND) [12], core consistency diagnostic (CORCONDIA) and two-mode subspace compare (TMSC) approach. The first compared method was often used to estimate the chemical rank of two-way data arrays. The last two methods used to decide the underlying factor of three-way data arrays. The chemical rank is the factor corresponding to the minimum factor indication function value in the IND approach. For the two-mode subspace compare approach, the chemical rank denotes the factor which corresponds to the minimum projection residuals. The core consistency diagnostic utilizes core consistency to choose the chemical rank. The total factor numbers which have the maximal percentage of explained variation are considered to be the underlying factor for fitting the trilinear model. None of the selected methods requires human involvement. In this paper, three sets of simulated three-way data and two real three-way data arrays have been used to valuate the performance of the proposed method.

All computer programs were written in the MATLAB (MathWorks) programming environment, and all calculations were carried out on a personal computer (Pentium IV processor).

### 3. Experimental

#### 3.1. Simulated HPLC-DAD data arrays with homoscedastic and heteroscedastic noises

In order to investigate the feasibility of the newly proposed method to resolve the three-way trilinear data arrays, a simulated data set measured using a HPLC system with diode array detection on 10 samples containing three species was simulated. Here the first six samples only contained the two components of analytical interest. The remaining four samples contained two analytical species and one interference, i.e., three components. Two types of noise, homoscedastic noise and heteroscedastic noise were constructed to join into the simulated three-way to produce two trilinear data arrays, respectively. Homoscedastic and heteroscedastic noises are produced basing on the following schemes:

$$\text{homo\_noise} = a_{\text{homo}} \times \text{RANDN} \times \max(\mathbf{X}_{..k}),$$

$$\text{heter\_noise} = a_{\text{heter}} \times \text{RANDN} \circ \mathbf{X}_{..k}$$

Where  $a_{\text{homo}}$  and  $a_{\text{heter}}$  are two parameters controlling the homoscedastic and heteroscedastic noise levels [20]. The symbol ‘ $\circ$ ’ represents Hadamard product. In this paper,  $a_{\text{homo}}$  changes from 0.4% to 4.0% and  $a_{\text{heter}}$  changes from 0.8% to 20%, respectively.

#### 3.2. Simulated emission–excitation fluorescent collinearity data array

Resolving collinearity data is a difficult task while estimating the chemical rank of a three-way data array. In this paper, a simulated excitation–emission fluorescent data set of 10 samples with four components was constructed. The simulated data set is also divided into calibration sample and predicted sample as the above. The fourth component is only contained in the last four predicted samples. The methods from the literature [20] were used to produce collinearity data arrays, i.e., the spectrum of the fourth component with spectral profile reproduced by the equation:  $\mathbf{sp} = \text{norm}(\mathbf{sp}_4 + a_{\text{collinearity}} \times \mathbf{sp}_3)$ , here,  $\text{norm}$  is a function normalizing vectors to unit length,  $\mathbf{sp}_3$  and  $\mathbf{sp}_4$  symbolize the spectra of components 3 and 4, respectively,  $a_{\text{collinearity}}$  is a parameter regulating the degree of collinearity. In this paper,  $a_{\text{collinearity}}$  equals to 0.9, 1.2 and 1.4, respectively. Homoscedastic noise level is fixed to be 0.6% in these data arrays.

#### 3.3. Real HPLC-DAD data array

Twelve samples containing different amounts of 1-chloro-2,4-dinitrobenzene, 3,5-dinitrobenzoic acid and 2,4-dinitrobenzoic acid were analyzed using HPLC-DAD. Twelve samples are divided into two sets, i.e., the first eight samples are the calibrated sets and the remaining four are the predicted sets. 2,4-Dinitrobenzoic acid is considered as interference in predicted samples. The response data used for second-order calibration were taken over an elution time range of 1.313–1.860 min (1/150 min intervals) and a wavelength range of 220.0–310.0 nm



(2 nm intervals). All chemical substance was of analytical grade. A three-way data array of size  $83 \times 46 \times 12$  was collected. Detailed can be found in Ref. [33].

### 3.4. Real excitation–emission fluorescent data array

Determination of the reserpine in human plasma was investigated by model F-4500 fluorescence spectrophotometer (HITACHI). Reserpine with different concentrations was done in 10 samples. The first six samples only contain reserpine and the last four predicted samples were spiked to human plasma as background or interferences. The excitation wavelength was set from 310.0 to 420.0 nm at an interval of 5.0 nm, and the emission wavelength varied from 430.0 to 505.0 nm with an interval of 5.0 nm. Thus, a  $22 \times 15 \times 10$  data array can be assembled. Rayleigh scattering in all response matrices was roughly corrected just by subtracting the average response matrix of the three blank solutions. Data arrays were assembled by the Rayleigh scattering corrected response matrices.

## 4. Results and discussions

### 4.1. Simulated HPLC-DAD data arrays with homoscedastic and heteroscedastic noises

In the simulated HPLC-DAD data set, various homoscedastic noise levels (0.4–4.0%) were first considered to inspect the feasibility of the newly proposed method. It was found that the new method performed well when the error level changed. The projection residuals of the 10 factors with different magnitude homoscedastic errors were listed in Fig. 1. From the results one can find that the projection residuals decrease gradually from one to three and increase suddenly to a large value for the later factors. It clearly shows that the chemical rank of the simulated HPLC-DAD data array is three, i.e., the simulated sample set requests three underlying factors to fit the trilinear model accu-

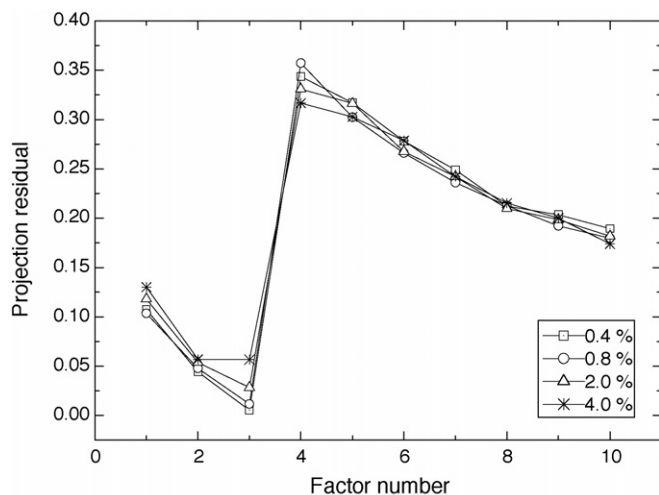


Fig. 1. The projection residuals of 10 factors for simulated three-component HPLC-DAD data set with different magnitude homoscedastic noise (0.4–4.0%).

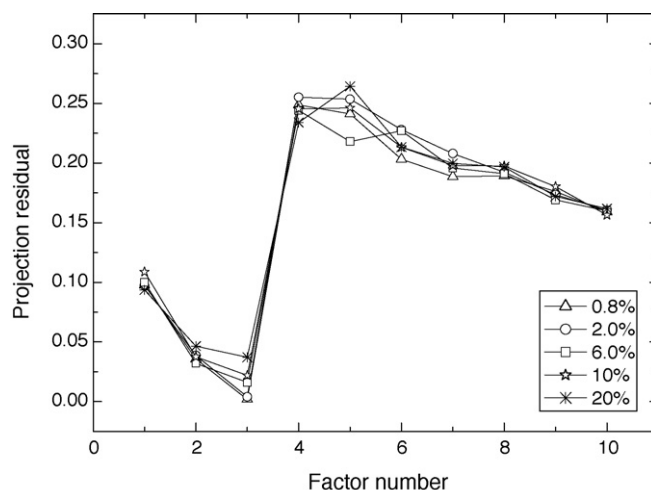


Fig. 2. The projection residuals of 10 factors for simulated three-component HPLC-DAD data set with different magnitude heteroscedastic noise (0.8–20%).

rately. It is coincident with the practical. It shows the newly suggested method could be used to estimate the chemical rank of the three-way data arrays.

Fig. 2 displays the projection residuals of 10 factors with different magnitude heteroscedastic noise (0.8–20%). It can also be clearly found that the third factor selected corresponds to the smallest projection residuals among 10 factors attempted. The projection residuals corresponding to the fourth factor enhance remarkably to a large value. Therefore, there were three appropriate components in the simulated HPLC-DAD data set. Running the PARAFAC algorithm is completely correct. It shows that the new method can give a correct estimate of the underlying factors in the three-way data arrays with heteroscedastic noise.

The simulated HPLC-DAD data sets were also performed by the other three factor-determining methods, respectively. Tables 1 and 2 list the results calculated by the four factor-determining methods. The TMSC and CORCONDIA give excellent result for the simulated data set with different conditions appended. Contrarily, the IND method failed to give the true result when the noise level is high enough. It validates three components when noise is small enough but underestimates one component for 4% homoscedastic and 20% heteroscedastic noise level. This shows that the IND may be deficient for its utilizing the eigenvalue to decide the rank of the compound. It will fail when the noise is relatively high.

Table 1

The performances of four factor-determining methods for simulated three-component HPLC-DAD data array with different magnitude homoscedastic noise

	LTMC	TMSC	CORCONDIA	IND
0.4%	3	3	3	3
0.8%	3	3	3	3
2.0%	3	3	3	3
4.0%	3	3	3	2



Table 2

The performances of four factor-determining methods for simulated three-component HPLC-DAD data array with different magnitude heteroscedastic noise

	LTMC	TMSC	CORCONDIA	IND
0.8%	3	3	3	3
2.0%	3	3	3	3
6.0%	3	3	3	3
10%	3	3	3	3
20%	3	3	3	2

#### 4.2. Simulated emission–excitation fluorescent collinearity data array

The feasibility of resolving high collinearity three-way data array discussed by the new method. Different  $a_{\text{collinearity}}$  (0.9, 1.2, 1.4) is changed to control the collinearity, respectively. The result of the newly proposed method is listed in Fig. 3. It can be found the projection residuals of the first four factors keep very small value and increase rapidly to a large value for latter factors. It indicates that there are four underlying factors in the simulated emission–excitation fluorescent data set. The result

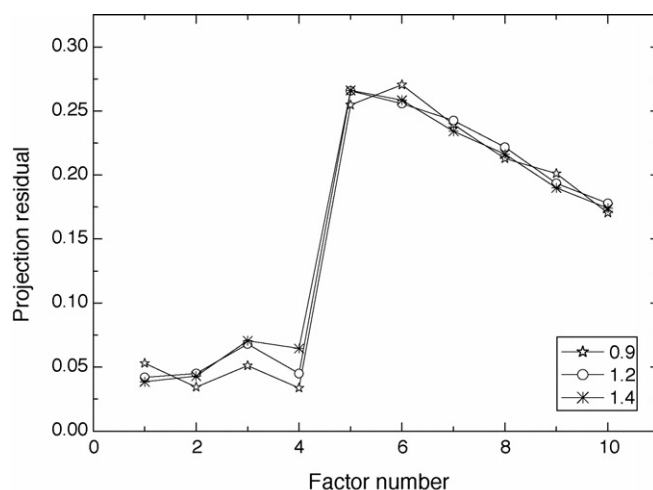


Fig. 3. The projection residuals of 10 factors for simulated four-component emission–excitation fluorescent data with different collinearity (homoscedastic noise level is fixed to be 0.6%).

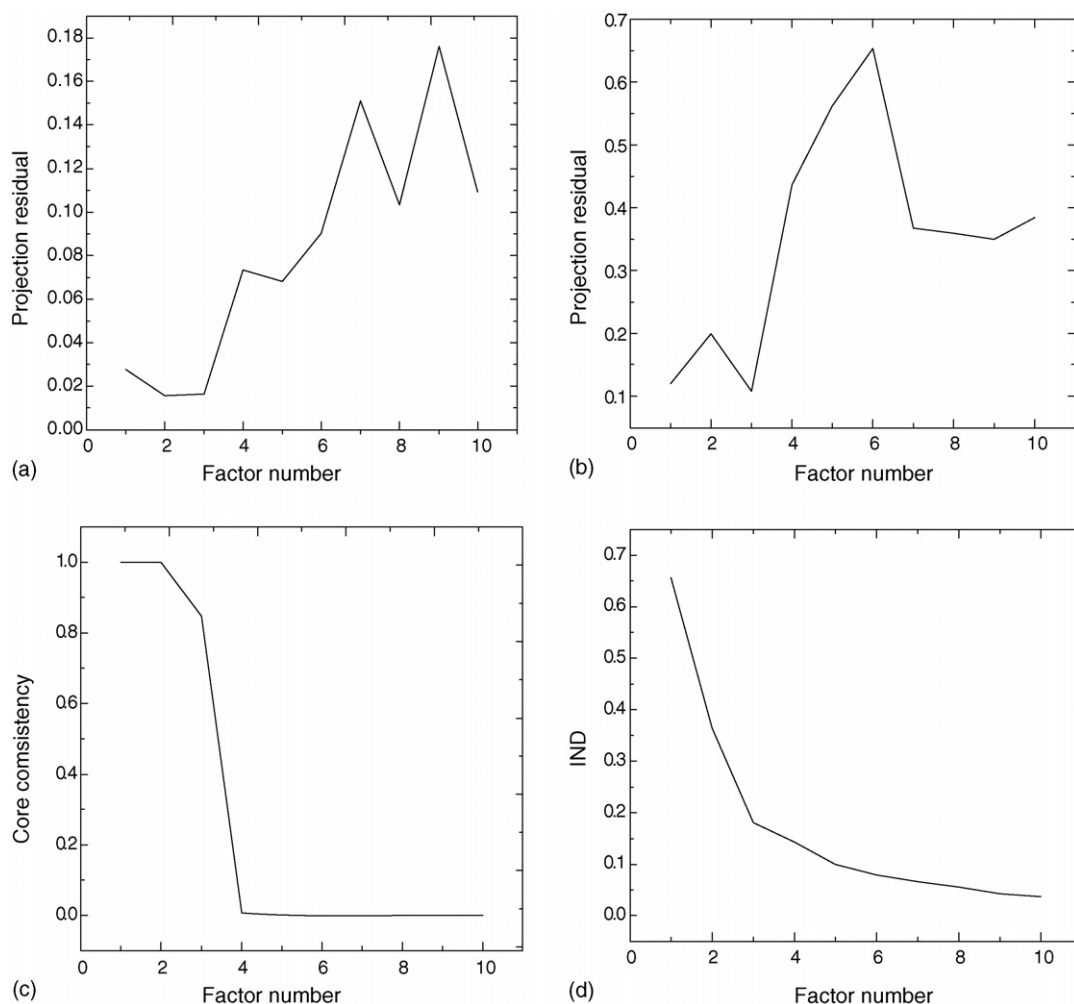


Fig. 4. Rank-deducing results of LTMC (a), TMSC (b), CORCONDIA (c) and IND (d) methods for the real HPLC-DAD data array.

Table 3

The performances of four factor-determining methods for simulated four-component data array with different collinearity

	LTMC	TMSC	CORCONDIA	IND
$a=0.9$	4	4	4	4
$a=1.2$	4	4	4	4
$a=1.4$	4	4	4	4

Homoscedastic noise level is fixed to be 0.6%.

can be substantiated by successful application of PARAFAC algorithm. It shows that the LTMC approach can overcome the impact of high collinearity in the complex system. The other factor-determining methods give accurate chemical rank in the simulated emission–excitation fluorescent collinearity data. The result can be found in Table 3.

#### 4.3. Real HPLC-DAD data array

In the real HPLC-DAD data arrays, the factors attempted from 1 to 10 are calculated using LTMC. The result is listed in Fig. 4. One can find that the projection residuals of the first three factors maintain a relatively small value and suddenly enhance

to a very large value for the later factors. It shows that there are three underlying factors in the complex system. The result can be substantiated by the successful application of PARAFAC algorithm and comparing to the true value. The results of the other three methods are also plotted in Fig. 4, respectively. The TMSC and CORCONDIA also give excellent result for the real three-way data arrays. Contrarily, the IND method failed to give the true result. This shows that the newly proposed method can be used to determine the rank of the practical three-way data arrays.

#### 4.4. Real excitation–emission fluorescent data array

In the real emission–excitation fluorescent data array, the human plasma was added to the system except the calibration set. Fig. 5 displays the result obtained by the newly proposed method. The projection residuals of the first two factors corresponded to the small value and increased remarkably to a large value for the subsequent factors. It shows that the system has two underlying factors. The result of the CORCONDIA and IND method are listed in Fig. 5. It gives the same result as the LTMC. In Fig. 5, one can find the TMSC method cannot give a clear conclusion. It shows that the factor-determining method may be successful at some circumstances but fail to the other

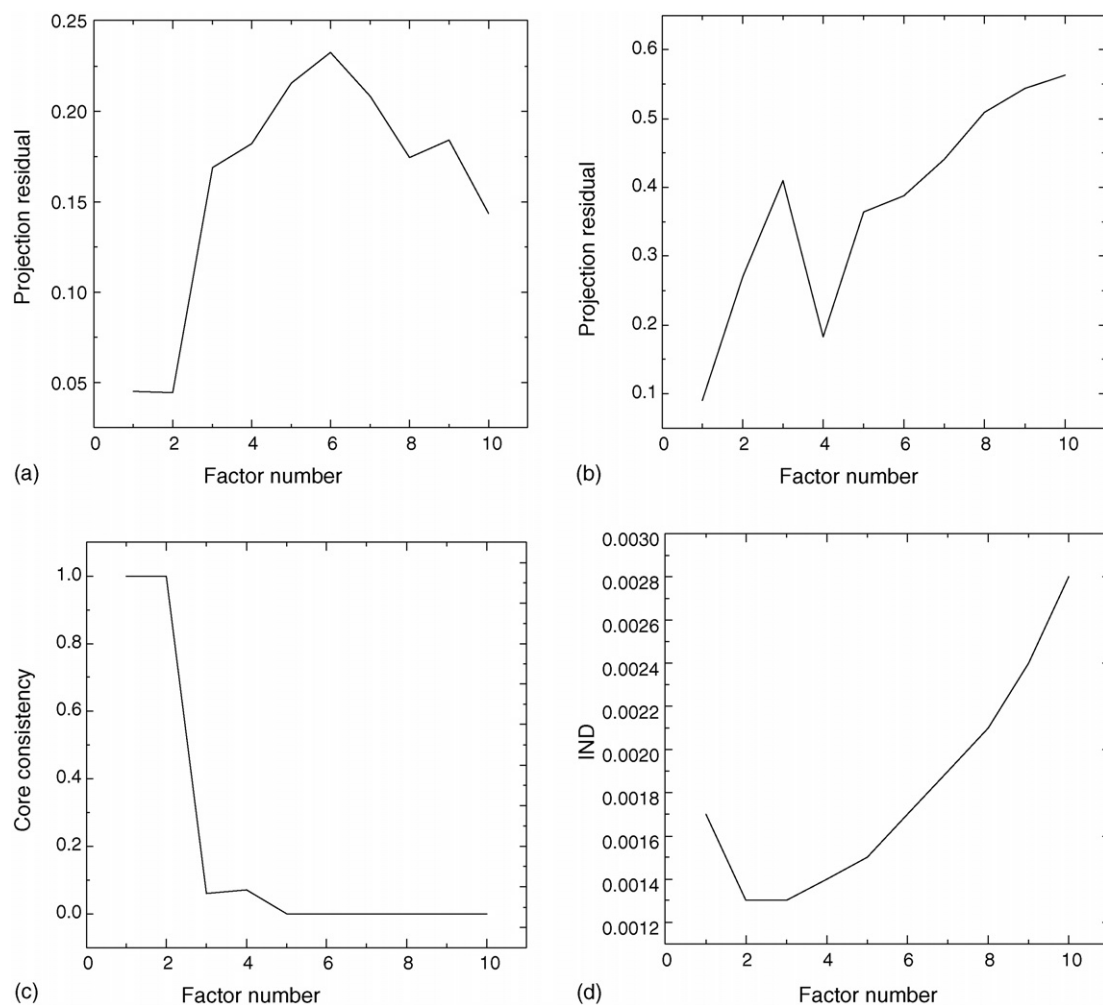


Fig. 5. Rank-deducing results of LTMC (a), TMSC (b), CORCONDIA (c) and IND (d) methods for the real emission–excitation fluorescent data array.

instances. Thus, it is often recommended to adopt two or more methods to estimate the appropriate component number of the mixture. Here one and two factors were considered to run the PARAFAC algorithm, respectively. The result is proved to be correct in contrast with the true value when component number equates to two. It shows that the plasma introduced interference to the mixture. The underlying factors should be equal to the summation of the species investigated and interferences. The results show that the newly proposed method can be used to estimate the chemical rank of three-way data array obtained from the practical system and give the correct conclusion.

## 5. Conclusion

A simple linear transform procedure incorporating Monte Carlo simulation (LTMC) approach to estimate the chemical rank of three-way data arrays (LTMC) was proposed in this paper. Applications of the simulated three-way data arrays and real experiment have showed the LTMC algorithm is feasible to determine the chemical rank of the complex system studied. Comparing with the other factor-determining methods, the outstanding feature of the LTMC method can be extremely easy to calculate and quickly determine the appropriate component to fit the trilinear model. Simultaneously it must not produce a standard to determine when the progress of factor-determining stopped. The figure of projection residuals will yield a clear conclusion to correctly estimating the chemical rank of the three-way data arrays.

## Acknowledgement

The research was financially supported by the National Natural Science Foundation of China (Grant Nos. 20475014 and 20375012) and by K.C. Wong Education Foundation, Hong Kong.

## References

- [1] K.S. Booksh, B.R. Kowalski, *Anal. Chem.* 66 (1994) 782A–791A.
- [2] B.G.M. Vandeginste, D.L. Massart, L.C.M. Buydens, S. de Jong, P.J. Lewi, J. Smeyers-Verbeke, *Handbook of Chemometrics and Qualimetrics: Part B*, Elsevier, Amsterdam, 2003, pp. 349–379.
- [3] C.M. Andersen, R. Bro, *J. Chemom.* 17 (2003) 200–215.
- [4] A.K. Smilde, *Chemom. Intell. Lab. Syst.* 15 (1992) 143–157.
- [5] P.C. Damiani, A.J. Nepote, M. Bearzotti, A.C. Olivieri, *Anal. Chem.* 76 (2004) 2798–2806.
- [6] L.A. Hergert, G.M. Escandar, *Talanta* 60 (2003) 235–246.
- [7] Z.G. Wang, J.H. Jiang, Y.J. Ding, H.L. Wu, R.Q. Yu, *Talanta* 68 (2006) 1371–1377.
- [8] V. Pravdova, C. Boucon, S. de Jong, B. Walczak, D.L. Massart, *Anal. Chim. Acta* 462 (2002) 133–148.
- [9] R. Bro, *Chemom. Intell. Lab. Syst.* 38 (1997) 149–171.
- [10] L.R. Tucker, *Psychometrika* 31 (1966) 279–311.
- [11] R.A. Harshman, *UCLA Working Pap. Phonetics* 16 (1970) 1–84.
- [12] E.R. Malinowski, *Factor Analysis in Chemistry*, 3rd ed., Wiley, New York, 2002, pp. 73–130.
- [13] E. Sanchez, B.R. Kowalski, *J. Chemom.* 4 (1990) 29–45.
- [14] H.L. Wu, M. Shibukawa, K. Oguma, *J. Chemom.* 12 (1998) 1–26.
- [15] J.H. Jiang, H.L. Wu, Z.P. Chen, R.Q. Yu, *J. Chemom.* 14 (2000) 15–36.
- [16] Z.P. Chen, H.L. Wu, J.H. Jiang, R.Q. Yu, *J. Chemom.* 15 (2001) 439–453.
- [17] Z.P. Chen, H.L. Wu, J.H. Jiang, R.Q. Yu, *J. Chemom.* 15 (2001) 149–167.
- [18] M. Meloun, J. Capek, P. Miksik, R.G. Brereton, *Anal. Chim. Acta* 423 (2000) 51–68.
- [19] M. Wasim, R.G. Brereton, *Chemom. Intell. Lab. Syst.* 72 (2004) 133–151.
- [20] J.B. Kruskal, Rank, decomposition, and uniqueness for 3-way and N-way arrays, in: R. Coppi, Bolasco (Eds.), *Multiway Data Analysis*, Elsevier, Amsterdam, 1989, pp. 8–18.
- [21] R. Bro, H.A.L. Kiers, *J. Chemom.* 17 (2003) 274–286.
- [22] Z.P. Chen, Z. Liu, Y.Z. Cao, R.Q. Yu, *Anal. Chim. Acta* 444 (2001) 295–307.
- [23] B.C. Mitchell, D.S. Burdick, *J. Chemom.* 8 (1994) 155–168.
- [24] W.S. Rayens, B.C. Mitchell, *Chemom. Intell. Lab. Syst.* 38 (1997) 173–181.
- [25] R.A. Harshman, M.E. Lundy, The PARAFAC model for three-way factor analysis and multidimensional scaling, in: H.G. Law, C.W. Snyder, J.A. Hattie, R.P. McDonald (Eds.), *Research Methods for Multimode Data Analysis*, Praeger, New York, 1984, pp. 122–215.
- [26] D.J. Louwse, A.K. Smilde, H.A.L. Kiers, *J. Chemom.* 13 (1999) 491–510.
- [27] H.P. Xie, J.H. Jiang, N. Long, G.L. Shen, H.L. Wu, R.Q. Yu, *Chemom. Intell. Lab. Syst.* 65 (2003) 101–115.
- [28] H.P. Xie, J.H. Jiang, G.L. Shen, R.Q. Yu, *Comput. Chem.* 26 (2002) 183–190.
- [29] X.M. Tu, *Anal. Chem.* 61 (1989) 2219–2224.
- [30] X.M. Tu, *J. Chemom.* 5 (1991) 333–343.
- [31] H.L. Shen, Y.Z. Liang, O.M. Kvalheim, R. Manne, *Chemom. Intell. Lab. Syst.* 51 (2000) 49–59.
- [32] C. Jacoboni, A new approach to Monte Carlo simulation, in: *International Electron Devices Meeting*, IEEE Electron Devices Society, Washington, DC, 1989, pp. 469–472.
- [33] Y.J. Ding, H.L. Wu, D.M. Fang, H. Cui, X.Y. Sun, A.L. Xia, L.Q. Hu, R.Q. Yu, *Chem. J. Chin. Univ.* 26 (2005) 1255–1257.

# Development of prototype heterogeneous chitosan membrane using different plasticizer for glutamate sensing

I.M. Isa, S. Ab Ghani\*

*Pusat Pengajian Sains Kimia, Universiti Sains Malaysia, 11800 USM, Pulau Pinang, Malaysia*

Received 23 January 2006; received in revised form 14 April 2006; accepted 15 April 2006

Available online 12 June 2006

## Abstract

This paper describes the preparation of and experimentation undertaken by heterogeneous chitosan membrane as ion selective electrode for glutamate ion. The linearity response was obtained in the range of  $1.0 \times 10^{-5}$  to  $1.0 \times 10^{-1}$  M with a detection limit of  $1.0 \times 10^{-6}$  M. The performance of the electrode was found in the pH range of 4.0–8.0 at temperature  $25 \pm 3$  °C. The response time was at 5–35 s and was useful for a period of more than 4 months. The selectivity values towards some anions indicates good selectivity over a number of interfering anions. No significant improvement of membrane performance over additional of plasticizers such as 2-NPOE, BEHA and DOPP. The electrodes gave sufficient Nernstian responses with the exception of membrane with 2-NPOE.

© 2006 Elsevier B.V. All rights reserved.

**Keywords:** Chitosan; Plasticizer; Glutamate; Heterogeneous; Membrane electrode

## 1. Introduction

Mono sodium glutamate, better known as MSG, is essentially a drug which may act as an excitatory neurotransmitter. It is, however, highly toxic to neuron [1] if available in large amounts. Basically, what the MSG does is to initiate the nerve cells to discharge electrical impulses—this is the basis of its use as a flavor enhancer. Common fast foods are well known to contain this material. Besides, MSG is also used as additive in processed, canned and packed foods. At one time, most cooked Chinese dishes contained MSG and the so-called ‘Chinese Restaurant Syndrome’ [2] is the after effect that is synonymous with large intake of MSG. The extra consumption of MSG will also produce symptoms such as chest pain, numbness, headache and sweat. Nevertheless, due to demands of MSG in food industries, its annual production is reported to reach 900,000 tons per year and is increasing [3]. The presence of glutamate in a sample is usually determined by either chromatographic techniques [4–8] or electrochemical techniques [9–15]. For the later, the electrodes used are mainly of enzyme electrode, thence, amperometric technique is applied.

Chitosan, a poly-[1-4]- $\beta$ -D-glucosamine, is a derivative of chitin, a naturally occurring polysaccharide found in insects, arthropods and crustaceans. A quantitative amount of chitosan is obtained by deacetylation of chitin’s acetoamide groups in a strong alkaline solution. Chitosan is well known for complexing transition metal ions, through chelation at its amino group [16,17]. Chitosan is also widely believed capable of removing fat, hence is used for slimming purposes for ladies. However, there is no reporting on the uptake of fat, i.e. carboxylic acid as yet. On the other hand, chitosan is reported capable of reacting with amino acids or proteins, humic acid and *o*-phthalic acid [18–20]. However, there are some analytical application of chitosan membrane such as adsorption of lysozyme [21], urea [22] and separation of aqueous alcoholic solutions [23,24].

The objective of this work is to prepare a heterogeneous membrane of chitosan and then its application for the determination of glutamate.

## 2. Experimental

### 2.1. Reagents

High-molecular weight poly(vinyl chloride) (PVC), 2-nitrophenyloctylether (2-NPOE), *bis*(2-ethylhexyl)adipate (BEHA) and dioctyl phenylphosphonate (DOPP) were obtained from

\* Corresponding author.

E-mail address: [sag@usm.my](mailto:sag@usm.my) (S. Ab Ghani).

Fluka Chemika (Switzerland). Analytical grade potassium and sodium salts of all anions and tetrahydrofuran (THF) were obtained from MERCK (Germany). All solutions were prepared using pure water from MiliQ Plus, Millipore Corp. (USA). The pH adjustments were made with dilute hydrochloric acid and sodium hydroxide solution as required. A stock solution of glutamate was freshly prepared by dissolving appropriate amount of analytical grade sodium salt of L-glutamate acid from BDH chemicals (England) in pure water. Chitosan PM 100 (granular, 100 mesh) was obtained from Chito Chem(M) Sdn. Bhd. (Malaysia) and was used without purification.

## 2.2. Preparation of membrane electrode

The membrane electrode was prepared by mixing thoroughly 50 mg chitosan, 50 mg PVC and 10 drops of plasticizer (2-NPOE/BEHA/DOPP) in a beaker prior to dissolving in about 2 ml THF. The mixture had to be vigorously stirred immediately after the addition of THF for an easy dissolution of PVC. The heterogeneous mixture so obtained was poured in a glass ring (3.5 cm i.d.), that sat on a surface of glass plate. A filter paper was placed on top of the glass ring to prevent dust and air streams from spoiling the mixture. The mixture was left to cure overnight at room temperature. The obtained, heterogeneous membrane was later peeled off from the glass. A membrane disc of 6 mm diameter was then cut and glued to one end of Pyrex® glass tube with Araldite®. The glass tube was then filled with an internal solution of saturated sodium salt of L-glutamic acid. Electrical contact was done by immersing a platinum wire in the solution. The final assembly was first conditioned by soaking the membrane in  $1.0 \times 10^{-5}$  M sodium salt of L-glutamic acid for a period of 24 h prior to use.

## 2.3. Measurements

Potential measurements were carried out with Orion 720A, Mass. (USA) pH meter. A saturated calomel electrode of Russell, Fife, Scotland (UK) with a fiber junction was used as a reference electrode. Whilst, pH value was determined by using Orion, 915600, Mass. (USA) glass-pH electrode. All measurements were carried out at  $25 \pm 3$  °C with the following schematic cell:

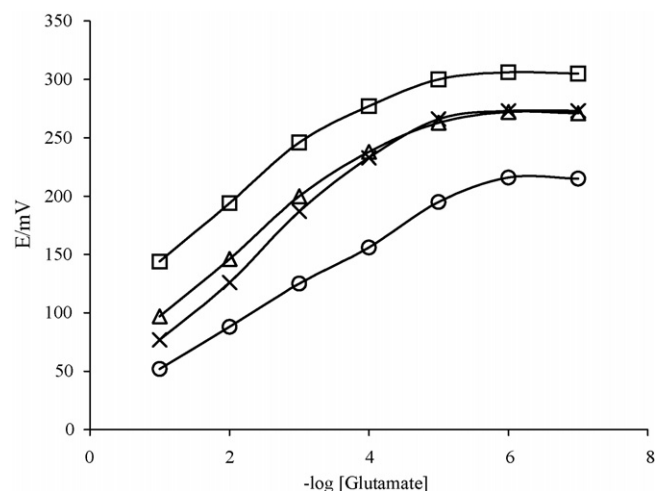
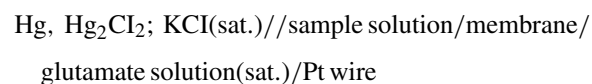


Fig. 1. Potentiometric response of the glutamate-ISE using optimized membrane electrode with various plasticizer. (x: control/without plasticizer, □: DOPP, △: BEHA, ○: 2-NPOE).

Before every measurement, the electrode was preconditioned in stirred water until the reading was stable. A series of 25.0 mL standard glutamate solutions in the concentration range from  $1.0 \times 10^{-7}$  to  $1.0 \times 10^{-1}$  M were prepared. The solutions were continuously stirred during measurement and a steady potential reading was then taken.

## 3. Results and discussion

It is well known that the sensitivity and selectivity obtained for a given heterogeneous membrane depend significantly on its composition. A plasticizer is useful in increasing both the elasticity and the working range of the membrane [25]. It also critical of the amount and type of plasticizer being used. Usually, in preparation of PVC membrane electrodes, a PVC/plasticizer ratio (w/w) of nearly 2 has resulted in very suitable electrode performance [26]. However, in this study, the ratio (w/w) of PVC to plasticizer equal to 1, literally, gave the good response for glutamate. The response of the prepared membrane using various plasticizer is shown in Fig. 1.

In all experiments, the potential response was done at optimum pH, i.e. pH 5. It was found that the membrane without plasticizer (control) gave a slightly better response to glutamate as the Nernstian slope of  $53 \pm 1.0$  mV decade<sup>-1</sup> ( $n = 1$ ) (see Table 1). Generally, the electrodes gave full Nernstian responses

Table 1  
Characteristics of optimized glutamate membrane electrode

Plasticizer	Control	2-NPOE	BEHA	DOPP
Linear range (M)	$1.0 \times 10^{-5}$ to $1.0 \times 10^{-1}$	$1.0 \times 10^{-5}$ to $1.0 \times 10^{-1}$	$1.0 \times 10^{-5}$ to $1.0 \times 10^{-1}$	$3.0 \times 10^{-5}$ to $1.0 \times 10^{-1}$
Slope (mV per decade)	$53 \pm 1.0$	$35 \pm 1.0$	$50 \pm 1.0$	$52 \pm 1.0$
pH range	4.0–8.0	4.0–7.0	5.0–8.0	4.0–8.0
Detection limit (M)	$1.0 \times 10^{-6}$	$1.0 \times 10^{-6}$	$1.0 \times 10^{-6}$	$1.0 \times 10^{-6}$
Response time (s)	20–35	20–35	20–35	5–15
Life time (month)	>4	>4	>4	>4



Table 2  
Comparison between heterogeneous chitosan membrane electrode and other electrochemical amperometric technique

	Technique	Working range (M)
Isa et al.	Chitosan membrane electrode	$1.0 \times 10^{-5}$ to $1.0 \times 10^{-1}$
Ling et al. [27]	Enzyme amperometric	$5.0 \times 10^{-5}$ to $5.0 \times 10^{-2}$
Hanko et al. [28]	LC with integrated pulsed amperometric	Down to $10^{-4}$
Stalikas et al. [29]	Enzyme amperometric	$5.0 \times 10^{-4}$ to $1.0 \times 10^{-2}$

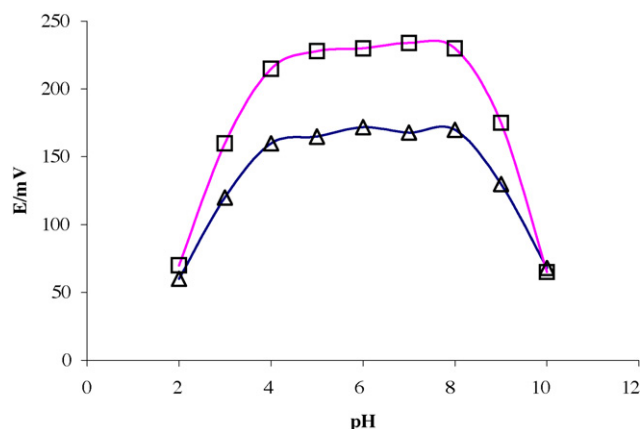


Fig. 2. Effect of pH on electrode potential at ( $\Delta$ )  $1.0 \times 10^{-3}$  M and ( $\square$ )  $1.0 \times 10^{-4}$  M glutamate without plasticizer (control).

with the exception of membrane with 2-NPOE. Even though the improved response time of the plasticizer added membrane is not that significant as and when cost factor is taken into consideration. The sub Nernstian slope value for 2-NPOE added membrane could be due to restriction of mobility of exchange ion within the membrane that effect Donnan exclusion.

It is, however, the results so obtained compared favorably if not better than many other reported glutamate detector (Table 2).

The influence of pH on the response of the membrane was done in glutamate solutions  $1.0 \times 10^{-3}$  and  $1.0 \times 10^{-4}$  M. Typical response for the chitosan membrane without plasticizer (control) is shown in Fig. 2. The potential of the membrane electrode remains constant at pH 4.0–8.0. A sharp decrease in pH value below 4.0 could be due to protonation of glutamate to glutamic acid, which results in a loss of membrane ability to interact with glutamate ions in solution. At a higher pH value than 8.0, the potential drop may be because of interference of hydroxyl ion which competed for the cation site in the membrane. Therefore,

Table 3  
Selectivity coefficients of membranes towards various interfering ions

Interfering ion	$K^{\text{pot}}$			
	Control	DOPP	BEHA	2-NPOE
$\text{Cl}^-$	$3.55 \times 10^{-3}$	$1.00 \times 10^{-3}$	$7.08 \times 10^{-4}$	$5.01 \times 10^{-4}$
$\text{Br}^-$	$2.51 \times 10^{-3}$	$4.00 \times 10^{-3}$	$5.00 \times 10^{-3}$	$3.55 \times 10^{-4}$
$\text{NO}_3^-$	$2.24 \times 10^{-3}$	$3.55 \times 10^{-3}$	$5.01 \times 10^{-3}$	$2.24 \times 10^{-4}$
$\text{CH}_3\text{COO}^-$	$2.51 \times 10^{-3}$	$3.16 \times 10^{-3}$	$5.01 \times 10^{-4}$	$5.60 \times 10^{-3}$
$\text{SO}_4^{2-}$	$2.51 \times 10^{-3}$	$2.82 \times 10^{-3}$	$1.58 \times 10^{-3}$	$1.03 \times 10^{-3}$
$\text{C}_2\text{O}_4^{2-}$	$5.62 \times 10^{-3}$	$7.94 \times 10^{-3}$	$3.16 \times 10^{-3}$	$6.31 \times 10^{-3}$
$\text{PO}_4^{3-}$	$2.51 \times 10^{-3}$	$3.55 \times 10^{-4}$	$6.31 \times 10^{-4}$	$5.60 \times 10^{-4}$
Ascorbate	$5.62 \times 10^{-3}$	$5.62 \times 10^{-3}$	$3.16 \times 10^{-3}$	$2.00 \times 10^{-5}$

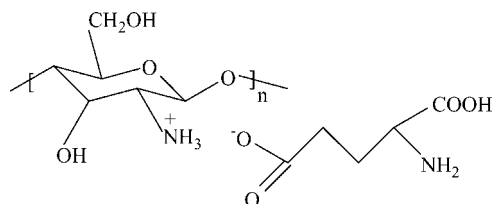
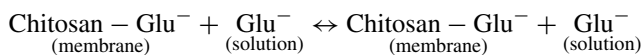


Fig. 3. Expected structural formula of chitosan-glutamate.

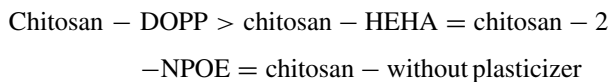
from Table 1 shows, the best performance for glutamate electrode based on chitosan-2-NPOE membrane should be achieved in the pH range of 4.0–7.0, chitosan-BEHA in the pH range of 5.0–8.0 while chitosan-DOPP and chitosan without plasticizer in the pH range of 4.0–8.0.

The ISE response is solely attributed to the ion exchange mechanism at the membrane-solution interface because of its univalent charge of glutamate. Chitosan behaves as a charge carrier for glutamate. The possible mechanism that are responsible for the potentiometric response is:



The expected structural formula of chitosan-glutamate is shown in Fig. 3. This is an analogy to the formation of an ammonium salt, e.g.  $\text{NH}_4\text{Cl}$ .

It is interesting to note that a reasonably fast response time was obtained, which was within 20 s. Table 1 shows the relative response time of the membranes as:



The potentials generated across the membrane were stable within a period of 4 months without any appreciable drift in potential.

The selectivity of the electrode against other ions was done by mixed-solution method. The potential response was measured by mixing various concentration of interfering ion solution with  $1.0 \times 10^{-4}$  M glutamate. List the potentiometric selectivity coefficient data of the sensor for several anions with relative to glutamate is shown in Table 3.

Generally, the  $K^{\text{Pot}}$  value are less than 1 indicating that the electrode is more selective to the analyte than to the interfering ion. In conclusion, the interference ions studied do not interfere in the determination of glutamate.

#### 4. Conclusion

A simple and accurate method has been developed to determine monosodium glutamate. It can be carried out in any laboratory equipped with pH-ionmeter. The method is selective and sensitive down to the microgram levels. This technique is also comparable to enzyme immobilized amperometric methods. Our next paper will be dealt with FIA using coated wire electrode version of this electrode.

#### Acknowledgements

The authors are indebted to the Univ. Sains Malaysia for grant: 131/0250/0580. One of us, I.M. Isa is thankful to the Universiti Pendidikan Sultan Idris for SLAB sponsorship.

#### References

- [1] H.P. Rang, M.M. Dale, J.M. Ritter, P.K. Moore, *Pharmacology*, 5th edn., Churchill Livingstone, Scotland, 2003, p. 491.
- [2] <http://health.allrefer.com/health/chinese-restaurant-syndrome-info.html>.
- [3] S. Delauney, P. Gourden, P. Lapujade, E. Maily, E. Oriol, J.M. Engasser, N.D. Lindley, J.L. Goergen, *Enzyme Microb. Technol.* 25 (1999) 762.
- [4] M.J. Lu, T.C. Chiu, P.L. Chang, H.T. Ho, H.T. Chang, *Anal. Chim. Acta* 538 (2005) 143.
- [5] J. Qu, W. Chen, G. Luo, Y. Wang, S. Xiao, Z. Ling, G. Chen, *Analyst* 127 (2002) 66.
- [6] V.P. Hanko, J.S. Rohrer, *Anal. Biochem.* 324 (2004) 29.
- [7] G. Halmos, B. Lendvai, A. Gaborjan, M. Baranyi, L.Z. Szabo, C. Vitez, *Neurochem. Int.* 40 (2002) 243.
- [8] Y.V. Tcherkas, A.D. Denisenko, *J. Chromatogr. A* 913 (2001) 309.
- [9] D. Ling, G. Wu, C. Wang, F. Wang, G. Song, *Enzyme. Microb. Tech.* 27 (2000) 515.
- [10] W.K. Xin, X.X. Gao, *Analyst* 121 (1996) 687.
- [11] C.D. Stalikas, M.I. Karayannis, S.M.T. Karayanni, *Analyst* 118 (1993) 723.
- [12] M.R. Ryan, J.P. Lowry, R.D. O'Neill, *Analyst* 122 (1997) 1419.
- [13] R. Shi, K. Stein, *Analyst* 121 (1996) 1306.
- [14] M. Montagne, H. Durliat, M. Comtat, *Anal. Chim. Acta* 278 (1993) 25.
- [15] O. Niwa, T. Horiuchi, R. Kurita, H. Tabei, K. Torimitsu, *Anal. Sci.* 14 (1998) 947.
- [16] W.S. Wan Ngah, I.M. Isa, *J. Appl. Polym., Sci.* 67 (1998) 1067.
- [17] W.S. Wan Ngah, S. Ab Ghani, A. Kamari, *Bioresource Technol.* 96 (2005) 443.
- [18] S.P. Meyers, *Diss. Abstr. (Int.)* (1987) 1459, AAI8811429.
- [19] C. Senstad, K.A. Almas, in: T. Muzzarelli, C.G. Jeuniaux, W. Graham (Eds.), *Chitin Nat. Technol. (Proc. Int. Conf. Chitin Chitosan)* Pub. 1986, Plenum, New York, USA, 3rd 1985, pp. 568–570.
- [20] K. Inoue, Y. Baba, K. Yashizuka, H. Noguchi, M. Yoshizaki, *Chem. Lett.* 200 (1988) 1281.
- [21] X. Chen, J. Liu, Z. Feng, Z. Shao, *J. Appl. Polym., Sci.* 96 (2005) 1267.
- [22] X. Chen, J. Liu, Z. Shao, P. Zhou, *J. Appl. Polym., Sci.* 90 (2003) 1108.
- [23] T. Uragami, H. Kinoshita, H. Okuno, *Angew. Makromol.* 209 (1) (1993) 41.
- [24] J.-J. Shieh, R.Y.M. Huang, *J. Memb. Sci.* 148 (1998) 243.
- [25] L.P. Singh, J.M. Bhatnagar, S. Tanaka, H. Tsue, M. Mori, *Anal. Chim. Acta* 546 (2005) 199.
- [26] C. Hongbo, E.H. Hansen, J. Ruzicka, *Anal. Chim. Acta* 169 (1985) 209.
- [27] D. Ling, G. Wu, C. Wang, F. Wang, G. Song, *Enzyme Microb. Technol.* 27 (2000) 515.
- [28] V.P. Hanko, J.S. Rohrer, *Anal. Biochem.* 324 (2004) 29.
- [29] C.D. Stalikas, M.I. Karayannis, S.M.T. Karayanni, *Analyst* 118 (1993) 723.

# Determination of trace elements in coal and coal fly ash by joint-use of ICP-AES and atomic absorption spectrometry

Akira Iwashita<sup>a</sup>, Tsunenori Nakajima<sup>a</sup>, Hirokazu Takanashi<sup>a</sup>, Akira Ohki<sup>a,\*</sup>,  
Yoshio Fujita<sup>b</sup>, Toru Yamashita<sup>b</sup>

<sup>a</sup> Department of Bioengineering, Faculty of Engineering, Kagoshima University, 1-21-40 Korimoto, Kagoshima 890-0065, Japan

<sup>b</sup> Coal Research Laboratory, Idemitsu Kosan Co. Ltd., 3-1 Nakasode, Sodegaura, Chiba 299-0267, Japan

Received 16 January 2006; received in revised form 24 March 2006; accepted 24 March 2006

Available online 3 May 2006

## Abstract

Microwave-acid digestion (MW-AD) followed by inductively coupled plasma-atomic emission spectrometry (ICP-AES), graphite furnace atomic absorption spectrometry (GFAAS), and hydride generation atomic absorption spectrometry (HGAAS) were examined for the determination of various elements in coal and coal fly ash (CFA). Eight certified reference materials (four coal samples and four CFA samples) were tested. The 10 elements (As, Be, Cd, Co, Cr, Mn, Ni, Pb, Sb, and Se), which are described in the Clean Air Act Amendments (CAAA), were especially considered. For coal, the HF-free MW-AD followed by ICP-AES was successful in the determination of various elements except for As, Be, Cd, Sb, and Se. These elements (except for Sb) were well-determined by use of GFAAS (Be and Cd) and HGAAS (As and Se). For CFA, the addition of HF in the digestion acid mixture was needed for the determination of elements, except for As, Sb, and Se, for which the HF-free MW-AD was applicable. The use of GFAAS (Be and Cd) or HGAAS (Sb and Se) resulted in the successful determination of the elements for which ICP-AES did not work well. The protocol for the determination of the 10 elements in coal and CFA by MW-AD followed by the joint-use of ICP-AES, GFAAS, and HGAAS was established.

© 2006 Elsevier B.V. All rights reserved.

**Keywords:** Coal; Coal fly ash; Trace elements; Graphite furnace atomic absorption spectrometry; Hydride-generation atomic absorption spectrometry

## 1. Introduction

Recently, there has been a growing interest in the presence of trace elements in coal and coal fly ash (CFA). In the United States, 11 elements (As, Be, Cd, Co, Cr, Hg, Mn, Ni, Pb, Sb, and Se) in coal have been identified as being of particular concern, and limitations are placed on their emission levels by the passage of the Clean Air Act Amendments (CAAA) in 1990. After combustion, majority of the trace elements in coal is distributed in solid combustion residues, such as CFA, although some of the elements are released into air [1–3].

When solid samples, such as coal and CFA, are analyzed by atomic spectrometries, the analytes need to be transferred from solid phase into solution in order to confirm the sample introduction systems of the spectrometers. Recently, acid digestion

assisted by microwave processing is popularly utilized for such a pretreatment of the solid samples.

There have been many studies on the determination of trace elements in coal and CFA by use of the microwave-acid digestion (MW-AD) [4–20]. Rodushkin et al. studied the optimization of MW-AD as well as the use of laser ablation, and discussed the difference between coal and CFA for the determination of trace elements [9]. Also, the optimization of MW-AD has been done by several researchers [16,19]. So far, it has been thought that the addition of HF is needed in the acid mixture of MW-AD, because coal contains an appreciable amount of inorganic matters, which mainly consists of aluminosilicate matrix. In our previous paper, we have proved that the addition of HF is not necessary for MW-AD of coal for trace elements [14]. Also, Wang et al. has reported that the HF-free digestion can be applied to the determination of many elements in coal [12,13]. However, for CFA, we have pointed that the addition of HF is necessary to attain the determination of trace elements [20]. Although there have been some studies about the difference between coal and

\* Corresponding author. Tel.: +81 99 285 8335; fax: +81 99 285 8339.  
E-mail address: [ohki@be.kagoshima-u.ac.jp](mailto:ohki@be.kagoshima-u.ac.jp) (A. Ohki).

CFA for the determination of trace elements by use of MW-AD [7,9], still systematic studies have not yet been fully done. Such an information should be important in the determination of trace elements in various residues obtained during coal utilization processes, because such residues will be available in the form of something in between coal and ash.

In our previous papers about the optimization of MW-AD conditions, we have focused on the elements which can be measured by inductively coupled plasma-atomic emission spectrometry (ICP-AES) [14,20]. Compared to inductively coupled plasma-mass spectrometry (ICP-MS), ICP-AES is more widely used, because it has several advantages, such as low initial cost and easy maintenance, although the detection limits of ICP-AES are usually inferior to those of ICP-MS. Further, ICP-MS inherently involves a problem of isobaric interference, so that the determination of some hazardous elements of very concern, such as As and Se, is sometimes faced with difficulties [13].

A combination of hydride generation and atomic absorption spectrometry (HGAAS) provides an excellent determination of some specific elements, such as As, Sb, and Se. Also, the detection limits of graphite furnace atomic absorption spectrometry (GFAAS) are comparable to those of ICP-MS for some elements, although GFAAS is generally single element measurement. It must be important to establish a proper protocol for each of coal and CFA in terms of the determination of trace elements by a joint-use of ICP-AES and atomic absorption spectrometry, which are rather wide spread analytical instruments.

In this study, we investigated the determination of trace elements in coal and CFA by use of MW-AD followed by ICP-AES and atomic absorption spectrometry; especially we noted the 10 elements (except for Hg) described in CAAA. Thus, the elements, which cannot be favorably determined by ICP-AES, are analyzed by HGAAS or GFAAS. The determination of Hg in coal has been already established by use of a mercury analyser, which is usually based on cold-vapor atomic absorption spectrometry, and thus the element was omitted in this study. For each measurement method, the effect of acid composition in the MW-AD conditions upon the recovery of elements was examined. Also, the difference between coal and CFA in terms of the determination of trace elements is discussed.

## 2. Experimental

### 2.1. Coal and CFA samples

Four certified reference coals and four certified reference CFAs from National Institute of Standards and Technology, USA (NIST; 1632c (coal) and 1633b, 2689, and 2690 (CFAs)), Community Bureau of Reference, EC (BCR-180 (coal)), SA Bureau of Standards, Republic of South Africa (SARM; 19 and 20 (coals)), and State Bureau of Metrology, China (GBW-08401 (CFA)), were used. These coals and CFAs were provided with certified or reference values for various elements, which include major and trace elements.

### 2.2. Reagents and instrumentation

Nitric acid ( $\text{HNO}_3$ , 61%), hydrogen peroxide solution ( $\text{H}_2\text{O}_2$ , 30%), hydrofluoric acid (HF, 46%) were analytical grade reagents from Wako Pure Chemical Ind. Ltd. Distilled water was further purified by a Milli-Q system and used throughout the experiments. For the ICP-AES measurement, a multielement standard solution (Merck) was used for the elements shown in Table 2 except for Ti and V, for which single element standard solutions (Wako) were added. When HGAAS (As, Sb, and Se) and GFAAS (Be and Cd) were carried out, a single element standard solution of each element was used. The microwave digestion was carried out by using a Milestone ETHOS1600, which was equipped with an evaporation module (SSM60). ICP-AES measurement was performed using a Perkin-Elmer Optima 3100RL equipped with pneumatic cross-flow type nebulizer, quartz torch, and alumina injector, which enabled us to apply samples containing HF in a small amount. HGAAS (Nippon Jarrel Ash, model 890 +HYD-10) and GFAAS (Thermo Elemental SOLAAR MQZ) instruments were also used. These instrumental parameters are listed in Table 1.

The limit of quantitation (LOQ) for each element of the ICP-AES, HGAAS, and GFAAS instruments was calculated as the concentration equal to 10 times the standard deviation of the background signal (the signal of the blank solution), which was multiplied by the dilution factor. The results are shown in Table 2.

### 2.3. Digestion procedures and measurement

A 0.25 g portion of coal or 0.1 g portion of CFA sample was weighed and transferred into a pressure-resistant PTFE vessel (volume 100 ml), and the mixture of acids was added. Procedures of MW-AD in this study (Methods A and B) are seen in Fig. 1. The vessel was then sealed and mounted in a sleeve (outer vessel). According to the manufacturer's protocol and our previous paper [14], the conditions of microwave processing were determined. Total of six samples were evenly spaced in the microwave oven carousel and the digestion program was set as listed in Table 3 (Stage 1); the program was automatically processed. The vessels were removed and carefully vented in a fume hood after cooling to room temperature in a water-bath. Further a mixture of  $\text{HNO}_3 + \text{H}_2\text{O}_2$  (2 + 1 ml) was quickly added to each sample. The vessels were returned to the microwave oven and the second processing was applied to the samples under the conditions as described in Table 3 (Stage 2). When HF was not used (Method A), the reaction mixture was filtered, and the filtrate was diluted to a fixed volume (25 ml) with ultrapure water.

When HF was used in the digestion acid mixture (Method B), the removal of HF was needed for the following analytical procedure. The reaction mixture was subjected to an evaporation procedure by use of the evaporation module in order to remove the acids after the final digestion. Then the residue was dissolved in 1.3 M  $\text{HNO}_3$  solution and filtrated, and the filtrate was diluted to a fixed volume (25 ml) with ultrapure water. The ICP-AES, HGAAS, and GFAAS measurements were performed for the

Table 1  
Instrumental operating conditions for ICP-AES, GFAAS, and HGAAS

ICP-AES			
RF power (W)	1300		
Plasma flow (L/min)	15		
Auxiliary flow (L/min)	0.5		
Carrier gas flow (L/min)	0.8		
Pump rate (ml/min)	1.5		
GFAAS			
	Be	Cd	
Wavelength (nm)	234.9	228.8	
Lamp current (mA)	10	10	
Ashing temperature (°C)	1100	600	
Atomization temperature (°C)	2600	1000	
Matrix modifier	Mg(NO <sub>3</sub> ) <sub>2</sub>	Mg(NO <sub>3</sub> ) <sub>2</sub> + Pd(NO <sub>3</sub> ) <sub>2</sub>	
HGAAS			
	As	Sb	Se
Wavelength (nm)	193.7	217.6	196.0
Lamp current (mA)	12	14	12
Pre-reduction solution	30% KI	30% KI	Boiling with HCl (6 M)
NaBH <sub>4</sub> solution concentration (%)	2.5	1.0	1.0
HCl solution concentration (mol/l)	5.8	2.0	5.8

Table 2  
Limits of quantitation (LOQ) in the determination of elements in coal and CFA by ICP-AES, GFAAS, and HGAAS (μg/g)

Elements	Coal <sup>a</sup>			CFA <sup>b</sup>		
	ICP-AES	GFAAS	HGAAS	ICP-AES	GFAAS	HGAAS
Al	0.50			1.3		
As	5.0	0.10	0.05	13	0.25	0.125
Be	0.01	0.05		0.025	0.125	
Ca	0.18			0.45		
Cd	0.50	0.02		1.3	0.05	
Co	0.10			0.25		
Cr	0.40			1.0		
Cu	0.60			1.5		
Fe	0.50			1.3		
Mg	0.32			0.80		
Mn	0.10			0.25		
Ni	1.0			2.5		
Pb	1.0			2.5		
Sb	1.0	0.30	0.10	2.5	0.75	0.20
Se	10	0.30	0.05	25	0.75	0.125
Ti	0.05			0.13		
V	0.10			0.25		
Zn	0.10			0.25		

<sup>a</sup> Dilution factor (DF) = 100.

<sup>b</sup> Dilution factor (DF) = 250.

Table 3  
Microwave digestion program

Step	Stage 1			Stage 2		
	Time (min)	Power (W)	Temp. <sup>a</sup> (°C)	Time (min)	Power (W)	Temp. <sup>a</sup> (°C)
1	2	250	110	5	250	130
2	1	0	110	5	400	130
3	5	250	110	5	500	130
4	5	400	110	5	600	130
5	5	500	110	15	400	130
6	20	400	110			

<sup>a</sup> Temperature at the sleeve (outer vessel).



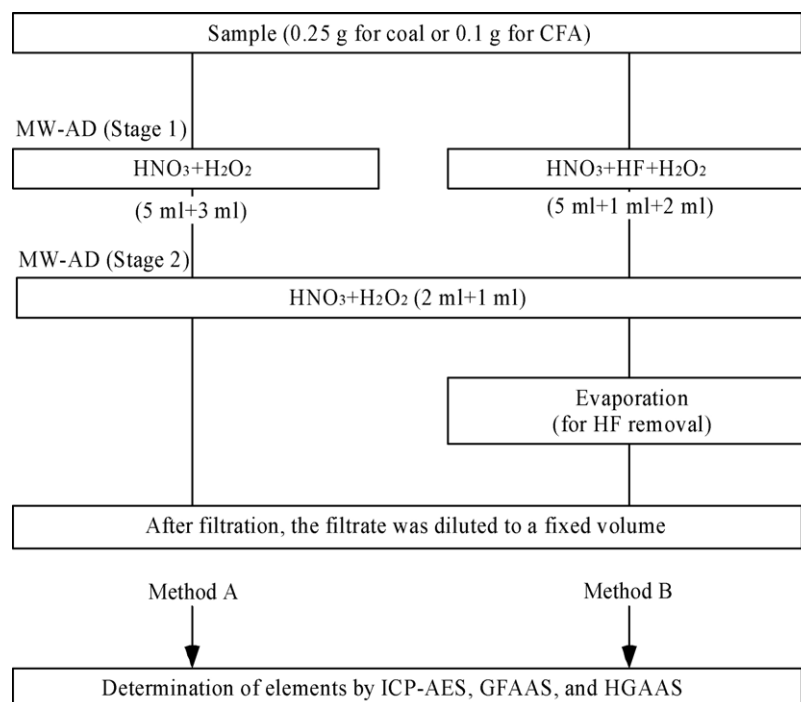


Fig. 1. Procedures of MW-AD used in this study.

diluted solutions. The concentration of each element in each diluted solution was measured.

For each run, samples were prepared at least triplicates, and the analysis of each digested samples was carried out twice. From these more than six measurements, mean value and standard deviation for the metal concentration were obtained.

### 3. Results and discussion

#### 3.1. Determination of elements in coal by ICP-AES

A certified reference material of coal, NIST-1632c, was digested by MW-AD (Method A, see Fig. 1) followed by the ICP-AES measurement. The results are presented in Table 4 together with the certified or reference values. In our previous paper, it was reported that the HF-free MW-AD could be applied to the determination of various elements in coal; the elements include major elements (Al, Ca, Fe, and Mg) as well as trace elements (Co, Cr, Cu, Mn, Ni, Pb, and Zn) [14]. For Method A, in which HF was not added in the digestion acids, the determination of elements (Al, Ca, Co, Cr, Cu, Fe, Mg, Mn, Ni, Pb, Ti, V, and Zn) gave satisfactory recoveries (Table 4). In this paper, “satisfactory” or “good” recoveries mean 90–110% recoveries, which have been adopted by many researchers [7,12–14,17,19,20].

Consequently, it is proved that the HF-free MW-AD (Method A) followed by ICP-AES favorably works for the five elements (Co, Cr, Mn, Ni, and Pb) among the elements described in CAAA. However, for several CAAA elements, As, Be, Cd, Sb, and Se, the determination was not successful, mainly due to low LOQ values of these elements for ICP-AES as seen in Table 2.

#### 3.2. Determination of elements in coal by GFAAS and HGAAS

We applied GFAAS to the determination of Be and Cd in coal, while HGAAS to that of As, Sb, and Se. A coal NIST-1632c was digested by MW-AD (Method A) followed by the GFAAS and HGAAS measurements, and the results are recorded in Table 5. The HF-free MW-AD (Method A) provided good recoveries

Table 4  
Determination of elements in a coal (NIST-1632c) by MW-AD (Method A) with ICP-AES

Elements	Certified <sup>a</sup>	Measured	Recovery <sup>b</sup> (%)
Al (mg/g)	(9.15 ± 0.14)	8.36 ± 0.31	91
Ca (mg/g)	(1.45 ± 0.30)	1.43 ± 0.09	99
Fe (mg/g)	(7.35 ± 0.11)	7.14 ± 0.33	97
Mg (mg/g)	(0.38 ± 0.03)	0.35 ± 0.02	92
As (μg/g)	(6.18 ± 0.27)	<sup>c</sup>	–
Be (μg/g)	(1.0)	0.20 ± 0.01	20
Cd (μg/g)	0.072 ± 0.007	<sup>c</sup>	–
Co (μg/g)	3.48 ± 0.20	3.7 ± 0.1	106
Cr (μg/g)	(13.73 ± 0.20)	13.8 ± 0.5	101
Cu (μg/g)	(6.01 ± 0.25)	5.5 ± 0.2	97
Mn (μg/g)	13.04 ± 0.53	12.7 ± 0.7	97
Ni (μg/g)	(9.32 ± 0.51)	9.4 ± 0.5	101
Pb (μg/g)	(3.79 ± 0.07)	3.9 ± 0.1	103
Sb (μg/g)	0.461 ± 0.029	<sup>c</sup>	–
Se (μg/g)	1.326 ± 0.071	<sup>c</sup>	–
Ti (μg/g)	517 ± 32	501 ± 19	97
V (μg/g)	(23.72 ± 0.51)	22.4 ± 0.7	94
Zn (μg/g)	12.1 ± 1.3	11.7 ± 0.5	97

<sup>a</sup> Values in parentheses are not certified (reference value).

<sup>b</sup> Recovery (%) = [(mean measured value)/(certified or reference value)] × 100.

<sup>c</sup> Not detected.

Table 5  
Determination of elements in a coal (NIST-1632c) by MW-AD (Method A) with GFAAS and HGAAS

Elements	Certified <sup>a</sup> ( $\mu\text{g/g}$ )	Measured ( $\mu\text{g/g}$ )	Recovery <sup>b</sup> (%)	Analytical method
As	(6.18 ± 0.27)	6.11 ± 0.31	99	HGAAS
Be	(1.0)	0.94 ± 0.04	94	GFAAS
Cd	0.072 ± 0.007	0.074 ± 0.002	103	GFAAS
Sb	0.461 ± 0.029	0.29 ± 0.21	63	HGAAS
Se	1.326 ± 0.071	1.25 ± 0.06	94	HGAAS

<sup>a</sup> Values in parentheses are not certified (reference value).

<sup>b</sup> Recovery (%) = [(mean measured value)/(certified or reference value)] × 100.

for As, Be, Cd, and Se. The recovery of Sb was not good. The decrease in dilution factor as well as the use of standard addition method was tried in order to improve the recovery of Sb. However, these attempts were not successful. Although the reason for the low recovery of Sb is not clear, it is presumed that some

loss of the element occurs during the MW-AD process due to vaporization etc.

Other three certified reference materials of coal, BCR-180, SARM-19, and SARM-20, were tested by use of MW-AD (Method A) with GFAAS for the determination of Be and Cd as well as with HGAAS for that of As, Sb, and Se. As shown in Table 6, satisfactory recoveries were obtained for As, Be, Cd, and Se, whereas Sb was not favorably determined. Consequently, the HF-free MW-AD (Method A) followed by GFAAS and HGAAS efficiently works for the determination of As, Be, Cd, and Se in coal, although the determination of Sb is impossible by the method.

### 3.3. Determination of elements in CFA by ICP-AES

In our previous paper, we reported that the addition of HF in the digestion acids was needed when CFA was digested by MW-AD [20]. For a certified reference material of CFA, NIST-

Table 6  
Determination of As, Be, Cd, Sb, and Se in three certified reference coals by MW-AD (Method A) with HGAAS and GFAAS

Elements	BCR-180			SARM-19			SARM-20			Analytical method
	Certified <sup>a</sup> ( $\mu\text{g/g}$ )	Measured ( $\mu\text{g/g}$ )	Recovery <sup>b</sup> (%)	Certified <sup>a</sup> ( $\mu\text{g/g}$ )	Measured ( $\mu\text{g/g}$ )	Recovery <sup>b</sup> (%)	Certified <sup>a</sup> ( $\mu\text{g/g}$ )	Measured ( $\mu\text{g/g}$ )	Recovery <sup>b</sup> (%)	
As	4.23 ± 0.19	4.05 ± 0.10	96	7 ± 1	6.40 ± 0.22	91	4.7 ± 1.2	4.35 ± 0.10	93	HGAAS
Be	0.81 <sup>c</sup>	0.83 ± 0.01	–	2.8 ± 1	2.94 ± 0.09	105	2.5 ± 1.2	2.36 ± 0.11	94	GFAAS
Cd	0.212 ± 0.011	0.229 ± 0.016	108	0.17 <sup>d</sup>	0.160 ± 0.010	–	NA	0.12 ± 0.01	–	GFAAS
Sb	NA	<sup>e</sup>	–	(0.3)	0.03 ± 0.02	10	(0.4)	<sup>e</sup>	–	HGAAS
Se	1.32 ± 0.06	1.21 ± 0.03	92	(1)	0.97 ± 0.05	97	0.8 ± 0.2	0.73 ± 0.03	91	HGAAS

<sup>a</sup> NA: not available; values in parentheses are not certified (reference value).

<sup>b</sup> Recovery (%) = [(mean measured value)/(certified or reference value)] × 100.

<sup>c</sup> From Wang et al. [12].

<sup>d</sup> From Wang et al. [13].

<sup>e</sup> Not detected.

Table 7  
Determination of elements in a CFA (NIST-1633b) by MW-AD with ICP-AES

Elements	Certified <sup>a</sup>	Method A		Method B	
		Measured	Recovery <sup>b</sup> (%)	Measured	Recovery <sup>b</sup> (%)
Al (mg/g)	150.5 ± 2.7	60.1 ± 2.1	40	13.5 ± 0.6	9
Ca (mg/g)	15.1 ± 0.6	8.41 ± 1.1	56	1.41 ± 0.21	9
Fe (mg/g)	77.8 ± 2.3	59.6 ± 3.1	77	74.3 ± 0.9	96
Mg (mg/g)	4.8 ± 0.1	1.60 ± 0.09	33	0.24 ± 0.09	5
Ti (mg/g)	7.91 ± 0.14	1.91 ± 0.10	24	7.30 ± 0.07	92
As ( $\mu\text{g/g}$ )	136.2 ± 2.6	129.7 ± 2.4	95	132.5 ± 5.8	97
Be ( $\mu\text{g/g}$ )	13.4 <sup>c</sup>	6.00 ± 0.12	–	9.68 ± 0.39	–
Cd ( $\mu\text{g/g}$ )	0.784 ± 0.006	<sup>d</sup>	–	<sup>d</sup>	–
Co ( $\mu\text{g/g}$ )	(50)	26.9 ± 0.5	54	54.3 ± 0.6	109
Cr ( $\mu\text{g/g}$ )	198.2 ± 4.7	153.5 ± 2.1	77	180.5 ± 1.9	91
Cu ( $\mu\text{g/g}$ )	112.8 ± 2.6	52.8 ± 1.8	47	120.7 ± 7.1	107
Mn ( $\mu\text{g/g}$ )	131.8 ± 1.7	60.1 ± 0.7	46	119.3 ± 5.7	91
Ni ( $\mu\text{g/g}$ )	120.6 ± 1.8	59.3 ± 0.5	49	114.9 ± 0.3	95
Pb ( $\mu\text{g/g}$ )	68.2 ± 1.1	30.9 ± 5.2	45	62.7 ± 2.0	92
Sb ( $\mu\text{g/g}$ )	(6)	<sup>d</sup>	–	<sup>d</sup>	–
Se ( $\mu\text{g/g}$ )	10.26 ± 0.17	<sup>d</sup>	–	<sup>d</sup>	–
V ( $\mu\text{g/g}$ )	295.7 ± 3.6	135.3 ± 9.1	46	275.2 ± 5.3	93
Zn ( $\mu\text{g/g}$ )	(210)	93.2 ± 0.5	44	191.0 ± 5.1	91

<sup>a</sup> Values in parentheses are not certified (reference value).

<sup>b</sup> Recovery (%) = [(mean measured value)/(certified or reference value)] × 100.

<sup>c</sup> From Rodushkin et al. [9].

<sup>d</sup> Not detected.

Table 8  
Determination of elements in a CFA (NIST-1633b) by MW-AD with GFAAS and HGAAS

Elements	Certified <sup>a</sup> (μg/g)	Method A		Method B		Analytical method
		Measured (μg/g)	Recovery <sup>b</sup> (%)	Measured (μg/g)	Recovery <sup>b</sup> (%)	
As	136.2 ± 2.6	140 ± 3	103	135 ± 1	99	HGAAS
Be	13.4 <sup>c</sup>	10.6 ± 0.8	–	13.8 ± 0.8	–	GFAAS
Cd	0.784 ± 0.006	0.337 ± 0.015	43	0.724 ± 0.039	92	GFAAS
Sb	(6)	6.18 ± 0.19	103	5.74 ± 0.33	96	HGAAS
Se	10.26 ± 0.17	9.92 ± 0.07	97	9.55 ± 0.18	93	HGAAS

<sup>a</sup> Values in parentheses is not certified (reference value).

<sup>b</sup> Recovery (%) = [(mean measured value)/(certified or reference value)] × 100.

<sup>c</sup> From Rodushkin et al. [9].

1633b, MW-AD (Methods A and B) followed by the ICP-AES measurement was performed for the determination of various elements in CFA. The results are shown in Table 7, together with the certified or reference values. When the HF-added MW-AD (Method B, see Fig. 1) was performed, many elements (As, Co, Cr, Cu, Fe, Mn, Ni, Pb, Ti, V, and Zn) provided satisfactory recoveries, although Al, Ca, and Mg gave quite poor recoveries due to the formation of insoluble fluoride salts [20]. For almost all elements, the HF-free MW-AD (Method A) was not favorably carried out. When coal is burned in a boiler, the matrix melts according to its heat history. The elements in coal should be trapped in the matrix and/or transformed into more insoluble oxide forms. Thus, the HF-free MW-AD is inadequate for the complete decomposition of CFA matrix. For Cd, Sb, and Se, the determination was not successful, probably because the LOQ values of these elements are quite low. On the other hand, it appears that the low recovery of Be is ascribed to an interference caused by some coexisting ions [21]. Consequently, as for the 10 elements described in CAAA, it is found that the HF-added MW-AD (Method B) followed by ICP-AES can be useful for the determination of 6 elements (As, Co, Cr, Mn, Ni, and Pb), whereas 4 elements (Be, Cd, Sb, and Se) cannot be well-determined.

### 3.4. Determination of elements in CFA by GFAAS and HGAAS

The determination of Be and Cd in CFA was carried out by GFAAS, while that of As, Sb, and Se was done by HGAAS. A CFA NIST-1633b was digested by MW-AD (Methods A and

B) followed by the GFAAS and HGAAS measurements, and the results are recorded in Table 8. For both Methods A and B, As, Sb, and Se provided satisfactory recoveries. Jones described that those elements in CFA are likely to leach out because the oxides of these elements are quite hydrophilic [22]. Therefore, the complete decomposition of matrix is not needed for the determination of these elements, so that even the HF-free MW-AD (Method A) favorably works. The concentration of Sb in CFA is much higher than that in coal, leading to the successful determination.

For Be and Cd, Method A provided low recoveries, while Method B gave good recoveries. This result for Be and Cd was similar to that for other elements, such as Co, Cr, Cu, Fe, Mn, Ni, Pb, Ti, V, Zn shown in Table 7. It appears that these elements including Be and Cd form remarkably insoluble oxide species [23]. In conclusion, the HF-free MW-AD (Method A) is useful when As, Sb, and Se in CFA are determined, whereas for other elements the addition of HF in the digestion acids (Method B) is needed. The effect of the amount of added HF on the recoveries of Be and Cd was examined, when GBW-08401 was subjected to MW-AD followed by GFAAS. As shown in Fig. 2, the recoveries of these elements increased with an increase in the HF amount, and the satisfactory recoveries were achieved above the HF amount of 1.0 ml. This result is similar to that for several heavy metals described in our previous paper [20].

Other three certified reference materials of CFA, GBW-08401, NIST-2689, and NIST-2690, were tested for the determination of elements, and the results are shown in Table 9. The HF-free MW-AD (Method A) followed by HGAAS provided good recoveries for As, Sb, and Se, while the determination of

Table 9  
Determination of elements in three certified reference CFAs by MW-AD with GFAAS and HGAAS

Elements	GBW-08401			NIST-2689			NIST-2690			MW-AD method	Analytical method
	Certified <sup>a</sup> (μg/g)	Measured (μg/g)	Recovery <sup>b</sup> (%)	Certified <sup>a</sup> (μg/g)	Measured (μg/g)	Recovery <sup>b</sup> (%)	Certified <sup>a</sup> (μg/g)	Measured (μg/g)	Recovery <sup>b</sup> (%)		
As	11.4 ± 0.6	11.5 ± 0.2	101	(200)	188 ± 5	94	(26)	24.9 ± 0.5	96	Method A	HGAAS
Be	10.7 ± 0.9	10.3 ± 0.4	96	(21)	20.2 ± 0.8	96	(8)	8.28 ± 0.39	104	Method B	GFAAS
Cd	0.16 ± 0.04	0.159 ± 0.010	99	(3)	2.70 ± 0.15	90	(0.7)	0.654 ± 0.042	93	Method B	GFAAS
Sb	NA	2.02 ± 0.10	–	(9)	8.86 ± 0.25	98	(6)	5.74 ± 0.33	96	Method A	HGAAS
Se	1.13 ± 0.16	1.18 ± 0.02	104	(7)	6.34 ± 0.05	91	(0.8)	0.75 ± 0.02	94	Method A	HGAAS

<sup>a</sup> NA: not available; values in parentheses are not certified (reference value).

<sup>b</sup> Recovery (%) = [(mean measured value)/(certified or reference value)] × 100.

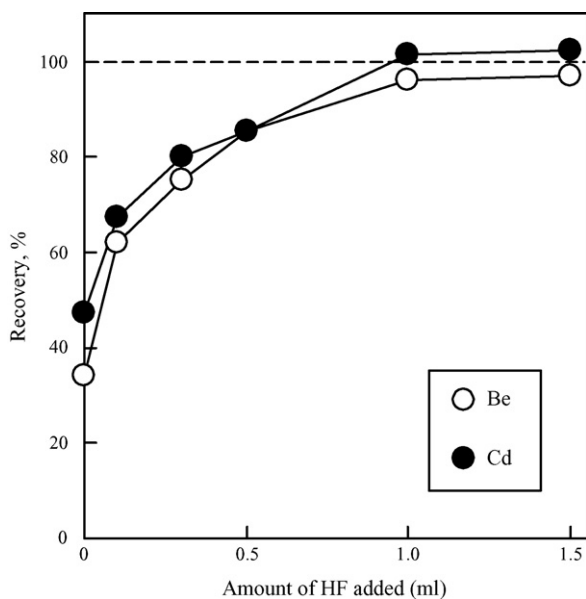


Fig. 2. Effect of the amount of added HF on the recoveries of Be and Cd (GBW-08401; Method B; GFAAS).

Be and Cd was successful by the HF-added MW-AD (Method B) followed by GFAAS. These results are similar to those for NIST-1633b, and it is proved that such a combination of MW-AD and HGAAS or GFAAS can give satisfactory recoveries for certain elements in CFA.

#### 4. Conclusion

For the determination of various elements in coal and CFA, MW-AD followed by ICP-AES, GFAAS, and HGAAS was carried out. The elements include 10 hazardous elements (As, Be, Cd, Co, Cr, Mn, Ni, Pb, Sb, and Se) described in CAAA. When coal was analyzed, the HF-free MW-AD (Method A) with ICP-AES was favorably applied to many elements including the five elements (Co, Cr, Mn, Ni, and Pb), whereas this did not work well for As, Be, Cd, Sb, and Se. By use of GFAAS (Be and Cd) and HGAAS (As and Se), these elements except for Sb were successfully determined. For CFA, many elements including the six elements (As, Co, Cr, Mn, Ni, and Pb) were efficiently determined by the HF-added MW-AD (Method B) followed by ICP-AES. The determination of several elements (Be, Cd, Sb, and Se) by ICP-AES was not successful, whereas those elements

were favorably determined by GFAAS (Be and Cd) and HGAAS (Sb and Se). For the determination of As, Sb, and Se in CFA, the HF-free MW-AD (Method A) could be applied.

#### References

- [1] L.B. Clarke, L.L. Sloss, Trace Elements-Emissions from Coal Combustion and Gasification, IEA Coal Research, London, 1992, IEACR/49.
- [2] R.M. Davidson, L.B. Clarke, Trace Elements in Coal, IEA Coal Research, London, 1996, IEAPER/21.
- [3] L.L. Sloss, I.M. Smith, Trace Element Emissions, IEA Coal Research, London, 2000, CCC/34.
- [4] E. Hatanpaa, K. Kajander, T. Laitinen, S. Piepponen, H. Revitzer, Fuel Process Technol. 51 (1997) 205.
- [5] E. Ikavalko, T. Laitinen, H. Revitzer, Fresenius J. Anal. Chem. 363 (1999) 314.
- [6] K.L. Laban, B.P. Atkin, Int. J. Coal Geol. 41 (1999) 351.
- [7] H. Lachas, R. Richaud, E. Jarivis, A.A. Herod, D.R. Dugwell, R. Kandiyoti, Analyst 124 (1999) 177.
- [8] R. Richaud, H. Lachas, A.E. Healey, G.P. Reed, J. Haines, K.E. Jarvis, A.A. Herod, D.R. Dugwell, R. Kandiyoti, Fuel 79 (2000) 1077.
- [9] I. Rodushkin, M.D. Axelsson, E. Burman, Talanta 51 (2000) 743.
- [10] M.L.D.P. Godoy, J.M. Godoy, L.A. Roldao, At. Spectrosc. 22 (2001) 235.
- [11] G.C. Turk, L.L. Yu, M.L. Salit, W.F. Guthrie, Fresenius J. Anal. Chem. 370 (2001) 259.
- [12] J. Wang, T. Nakazato, K. Sakanishi, O. Yamada, H. Tao, I. Saito, Anal. Chim. Acta 514 (2004) 115.
- [13] J. Wang, T. Nakazato, K. Sakanishi, O. Yamada, H. Tao, I. Saito, Talanta 68 (2006) 1584.
- [14] Y.-H. Xu, A. Iwashita, T. Nakajima, H. Yamashita, H. Takanashi, A. Ohki, Talanta 66 (2005) 58.
- [15] R.A. Nadkarni, Anal. Chem. 56 (1984) 2233.
- [16] T. Laitinen, H. Revitzer, M. Tolvanen, Fresenius J. Anal. Chem. 354 (1996) 436.
- [17] M. Bettinelli, S. Spezia, U. Baroni, G. Bizzarri, Microchem. J. 59 (1998) 203.
- [18] Z. Mester, M. Angelone, C. Brunori, C. Creminini, H. Muntau, R. Morabito, Anal. Chim. Acta 395 (1999) 157.
- [19] K. Swami, C.D. Judd, J. Orsini, K.X. Yang, L. Husain, Fresenius J. Anal. Chem. 369 (2001) 63.
- [20] A. Iwashita, T. Nakajima, H. Takanashi, A. Ohki, Y. Fujita, T. Yamashita, Fuel 85 (2006) 257.
- [21] G.S. Chowdary, K. Satyanarayana, N. Mathur, At. Spectrosc. 13 (1992) 213.
- [22] D.R. Jones, in: D.J. Swaine, F. Goodarzi (Eds.), Environmental Aspects of Trace Elements in Coal, Kluwer Academic Publishers, Dordrecht, 1995 (Chapter 12).
- [23] D.R. Lide (Ed.), CRC Handbook of Chemistry and Physics, CRC press, Boca Raton, 1995.

# Hexacyanoferrate(III) as a mediator in the determination of total iron in potable waters as iron(II)-1,10-phenanthroline at a single-use screen-printed carbon sensor device

Jan Jezek<sup>1</sup>, John W. Dilleen<sup>2</sup>, Barry G.D. Hagggett, Arnold G. Fogg, Brian J. Birch<sup>\*</sup>

*Luton Institute of Research in the Applied Natural Sciences University of Luton, The Spires, 2 Adelaide Street, Luton LU1 5DU, United Kingdom*

Received 7 September 2005; received in revised form 14 March 2006; accepted 23 March 2006

Available online 12 May 2006

## Abstract

Hexacyanoferrate(III) was used as a mediator in the determination of total iron, as iron(II)-1,10-phenanthroline, at a screen-printed carbon sensor device. Pre-reduction of iron(III) at  $-0.2$  V versus Ag/AgCl (1 M KCl) in the presence of hexacyanoferrate(II) and 1,10-phenanthroline (pH 3.5–4.5), to iron(II)-1,10-phenanthroline, was complete at the unmodified carbon electrode surface. Total iron was then determined voltammetrically by oxidation of the iron(II)-1,10-phenanthroline at  $+0.82$  V, with a detection limit of  $10 \mu\text{g l}^{-1}$ .

In potable waters, iron is present in hydrolysed form, and it was found necessary to change the pH to 2.5–2.7 in order to reduce the iron(III) within 30 s. A voltammetric response was not found at lower pH values owing to the non-formation of the iron(II)-1,10-phenanthroline complex below pH 2.5.

Attempts to incorporate all the relevant reagents (1,10-phenanthroline, potassium hexacyanoferrate(III), potassium hydrogen sulphate, sodium acetate, and potassium chloride) into a modifying coated PVA film were partially successful. The coated electrode behaved very satisfactorily with freshly-prepared iron(II) and iron(III) solutions but with hydrolysed iron, the iron(III) signal was only 85% that of iron(II).

© 2006 Elsevier B.V. All rights reserved.

**Keywords:** Iron; Potable water; Single-use; Sensor

## 1. Introduction

Iron is an essential element in human metabolism. Most is found in haemoglobin with smaller quantities in myoglobin and in iron–sulphur enzymes [1]. About 15% of the body's iron is in storage and is mobilised if the dietary intake becomes insufficient. The body normally maintains its physiological iron status by controlling the amount of iron absorbed from food [2]. Excessive intake of iron can be harmful due to its slow excretion from the body, which results in over accumulation in body tissues and organs [3]. Monitoring of iron in potable waters is therefore important.

Iron(II), which is generally the more soluble form, is readily oxidised to iron(III). Therefore, iron(III) predominates in oxygenated water and is present as highly insoluble oxyhydroxides [4]. The solubility of iron(III) increases with the acidity of the solution. Current legislation on the quality of drinking water within the European Union derives from a directive [5], which sets the limit for iron at  $200 \mu\text{g l}^{-1}$ . The International Standards Organisation (ISO) method [6] for determination of total dissolved iron in drinking water is spectroscopic, based on the formation of a coloured complex between iron(II) and 1,10-phenanthroline. Measurement of total iron requires sample pretreatment in strong acid followed by chemical reduction of iron(III) to iron(II) prior to complex formation. The method is applicable to concentrations in the range  $0.01$ – $5 \text{ mg l}^{-1}$ .

There is a large literature on the determination of iron in a wide range of matrices. Much recent methodology has been directed at the determination of iron in seawater: A recent review [4] also covers recommendations for sampling and storage of samples. These techniques assume that the iron in seawater is

\* Corresponding author. Tel.: +44 1582 743724; fax: +44 1582 74301.

E-mail address: [Brian.Birch@luton.ac.uk](mailto:Brian.Birch@luton.ac.uk) (B.J. Birch).

<sup>1</sup> Present address: Insense Ltd, Colworth Science Park, Sharnbrook, Bedford MK44 1LQ, UK.

<sup>2</sup> Present address: Stirling Medical Innovations, Unit 10, Scion House, Stirling University Innovation Park, Stirling FK9 4NF, United Kingdom.



totally as iron (III) since no chemical oxidation of iron (II) is carried out.

Many colorimetric techniques have been described, which allow direct measurement of a particular oxidation state of iron. Determination of total iron is achieved after chemical oxidation or reduction. Whilst a detection limit of approximately  $100 \mu\text{g l}^{-1}$  can be achieved using bathophenanthroline [7] or tiron [8,9] as chelating agents for iron(II), the use of norfloxacin to complex iron(III) allows measurement of iron down to  $10 \mu\text{g l}^{-1}$  [10]. In general, the sensitivity of measurements can be improved to sub- $\mu\text{g l}^{-1}$  by pre-concentration of iron on a chromatographic column loaded with chelating agent. A ferrozine based C-18 column [11], and a 3-(2-pyridyl)-5,6-diphenyl-1,2,4-triazine based C-18 column [12] have been used, as has a charge-sensitive film preloaded with 2-2'-bipyridine [13]. Chemiluminescence techniques have been described [14,15] based on the reaction between iron(II), brilliant sulphoflavin and hydrogen peroxide: whilst pre-concentration on a cationic exchange column gave a detection limit of about  $0.1 \mu\text{g l}^{-1}$ . The detection of sub- $\mu\text{g l}^{-1}$  concentrations of iron has also been reported using the fluorescence quenching of pyoverdin by iron(III) [16]. Atomic absorption spectrometric techniques [17] allowed determination of iron down to  $20 \mu\text{g l}^{-1}$ .

Various electrochemical techniques for determining iron have also been reported. The most sensitive methods are based on cathodic stripping voltammetry at a hanging mercury drop electrode. Various chelating agents including 2,3-dihydroxynaphthalene [18], 1-nitroso-2-naphthol [19], and 2-(2-thiazolylazo)-*p*-cresol [20] have been used to accumulate iron complexes on the electrode surface. Further sensitivity was achieved by using catalytic cathodic stripping voltammetry in which the iron(II) is reoxidised chemically as it is formed. It is then available for repeated electrochemical reduction. Concentrations of  $10 \text{ ng l}^{-1}$  can be determined using this technique. The use of solid glassy carbon electrodes has been reported [21] to give a detection limit of  $10 \mu\text{g l}^{-1}$  based on the use of chitosan. Gao et al. [22] used a carbon paste working electrode containing 1,10-phenanthroline and Nafion to determine iron(II) with a detection limit of approximately  $1 \mu\text{g l}^{-1}$ .

The work reported in here is concerned with the development of a disposable screen-printed carbon sensor device for the determination of total iron in potable water. The 1,10-phenanthroline based voltammetric method of Gao et al. [22] was adapted for this purpose. Various chemical and electrochemical methods of reducing iron(III) to iron(II) prior to the determination were studied; electrochemical reduction being favoured. The investigations included studies of the dissolution of sparingly soluble iron(III) species. Finally attempts were made to incorporate all the reagents onto the surface of the sensors in order to avoid the need to pre-treat the sample solution prior to iron measurement.

## 2. Experimental details

### 2.1. Chemicals

Iron(II) sulphate heptahydrate, iron(III) nitrate, 1,10-phenanthroline (abbreviated to 'phe'), 1,10-phenanthroline

iron(II) sulphate complex ('ferroin'), potassium hexacyanoferrate(III) and potassium hexacyanoferrate(II) were purchased from Sigma-Aldrich. Unless stated otherwise, solutions were prepared in  $18 \text{ M}\Omega$  deionised water (Elgastat, Elga Ltd.). Two 'types' of iron solution were used in this work. These are referred to as 'pre-dissolved iron solution' and 'natural iron solution'. Pre-dissolved iron stock solution was prepared by dissolving iron(II) sulphate or iron(III) nitrate in 10 mM hydrochloric acid and diluting to the required concentration with deionised water shortly before use. Natural iron solutions were prepared from iron(II) sulphate or iron(III) nitrate added directly to deionised water. Solutions were kept in polyethylene bottles to avoid adsorption of the insoluble iron species onto the walls of the vessel [4]. A stock solution of 1,10-phenanthroline ( $100 \text{ mg l}^{-1}$ ) was prepared in deionised water, the mixture being stirred in a water bath ( $50^\circ\text{C}$ ) for 10 min to achieve dissolution.

### 2.2. Single-use electrochemical sensor devices

Sensor devices ( $1 \text{ cm} \times 4.5 \text{ cm}$ ) were prepared in-house by screen-printing onto an alumina substrate. Carbon ink (ED5000, Electra Ltd.) was used to print working and counter electrodes, conducting tracks and connector pads. Silver–silver chloride paste (Gwent Electronic Materials Ltd., GEM) was used to print reference electrodes and dielectric (D1, GEM) was used to insulate the conductive tracks [23]. Unless indicated otherwise, potentials are quoted with respect to the screen-printed silver–silver chloride reference electrode bathed in potassium chloride (0.1 M), i.e. Ag–AgCl (0.1 M KCl).

The sample was confined between the electrodes and a top-cap positioned over the alumina substrate with a gap of about  $150 \mu\text{m}$ . Electrochemistry was carried out using an electrochemical workstation (AutoLab, EcoChimie BV) with GPES software in differential pulse mode. Peak height (automatic search; linear baseline) was used as the chief characteristic of the voltammetric peaks.

### 2.3. Preparation of sensors with reagent layers

The reagent layer for the measurement of total iron consisted of polyvinyl alcohol (PVA;  $M_r$  85,000–146,000; >99% hydrolysed) as the support structure to contain the reagents. PVA ( $0.05\text{--}1 \text{ g l}^{-1}$  depending on the experiment) was dissolved in deionised water by stirring for 15 min in a bath of almost boiling water. The following reagents were added to the PVA solution to achieve the indicated concentrations: potassium chloride (100 mM), potassium hexacyanoferrate(III) (1 mM), potassium hydrogen sulphate (29.5 mM), sodium acetate (20.5 mM) and pre-dissolved 1,10-phenanthroline ( $100 \text{ mg l}^{-1}$ ).

Sensor devices were washed in deionised water and dried. PVA/reagent solution ( $15 \mu\text{l}$ ) was pipetted onto the sensor (in the region of the working, reference and counter electrodes) and spread using the side of the pipette tip so that the electrodes were evenly covered with the reagent cocktail. The sensor devices were dried at room temperature and stored in a dessicator over self-indicating silica gel.

## 2.4. Spectrophotometry

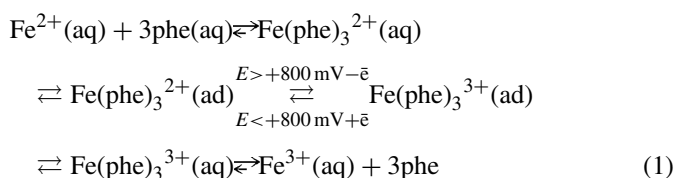
A diode-array spectrophotometer (Hewlett-Packard 8452A) with HPUV software was used for measurements of UV–vis spectra. Cuvettes with a path length of 1 cm were used and an integration time of 5 s was selected.

## 3. Results and discussion

### 3.1. Determination of total predissolved (i.e. unhydrolysed) iron

#### 3.1.1. Chemical reduction of iron(III)

Iron(II) solutions, in the presence of 1,10-phenanthroline, exhibited an oxidation peak (see Fig. 1) when scanned (differential pulse mode) from +0.4 to +1.2 V, and a corresponding reduction peak when the scan was reversed (not shown). The height of the reduction peak was independent of the time that the working electrode was held at +1.2 V before commencing the scan. No peak was observed when iron(III) was used in place of iron(II). The following reaction scheme was tentatively assigned:



This indicates that formation of the 1,10-phenanthroline complex with iron(III) was not favoured and required to be driven by an appropriately oxidising electrode potential. The height of the reduction peak ( $I_{p,c}$ ) correlated linearly with the iron(II) concentration,

$$\begin{aligned} \frac{I_{p,c}}{nA} &= (0.111 \pm 0.002)[\text{iron(II)}]/\mu\text{g l}^{-1} + (5.3 \pm 1.7) \\ R^2 &= 0.998, \end{aligned} \quad (2)$$

across a broad concentration range (0–5000  $\mu\text{g l}^{-1}$ ) with a detection limit calculated to be 10  $\mu\text{g l}^{-1}$ . The peak height and peak

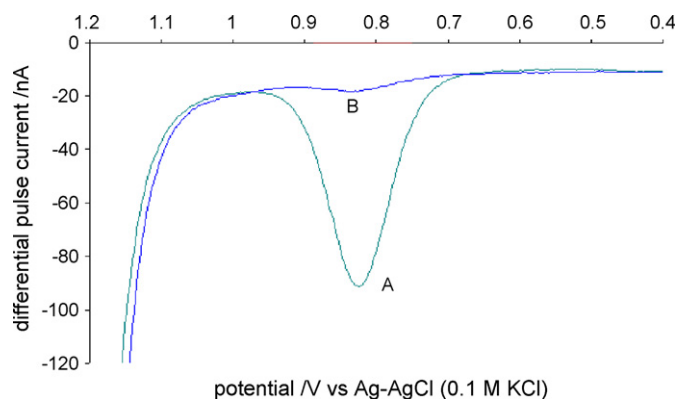


Fig. 1. Differential pulse voltammetry of 1,10-phenanthroline complex with iron(II). Iron(II)/ $\mu\text{g l}^{-1}$ : (A) 640; (B) 0. [1,10-phenanthroline] = 100  $\text{mg l}^{-1}$ ; acetate/ $\text{HSO}_4^-$  buffer, pH 4.5. Modulation amplitude, 50 mV; modulation time, 0.05 s; interval time, 0.2 s; step size, 2 mV; and initial potential, +1.2 V.

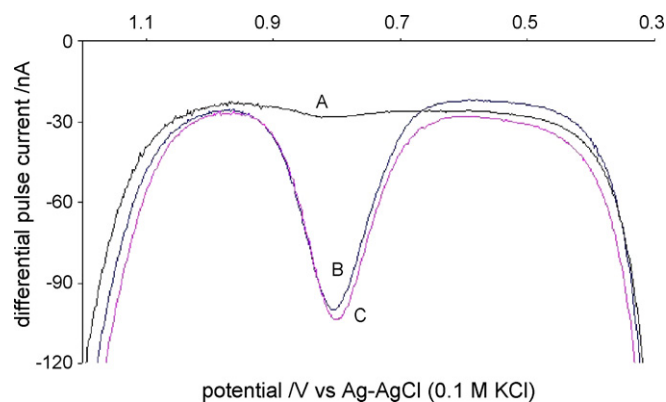


Fig. 2. Differential pulse voltammetry of iron-1,10-phenanthroline complex with potassium hexacyanoferrate(II) (2 mM). [iron(II)] and [iron(III)]/ $\mu\text{g l}^{-1}$ : (A) 0 and 0; (B) 640 and 0; (C) 0 and 640; [1,10-phenanthroline] = 100  $\text{mg l}^{-1}$ ; acetate/ $\text{HSO}_4^-$  buffer, pH 4.5.

potential were independent of pH in the range 2.1–7 in accord with the reported formation of a stable complex between pH 2 and 9 [24]. No experiments were carried out at pH higher than 7 in this work but the magnitude of the voltammetric peak diminished rapidly as the pH was decreased below 2.1.

Hydroxylamine was used to reduce iron(III) to iron(II) to enable complex formation with 1,10-phenanthroline. However, the electroactivity of hydroxylamine resulted in a rising background current and consequently a less sensitive detection limit (40  $\mu\text{g l}^{-1}$ ) compared with the measurement of iron(II) in the absence of the reducing agent (10  $\mu\text{g l}^{-1}$ ). Hexacyanoferrate(II) was identified as a more suitable reducing agent. Although hexacyanoferrate(II) could not be used to reduce iron(III) directly, the reaction was facilitated by 1,10-phenanthroline. The formation of  $\text{Fe}(\text{phe})_3^{2+}$  in mixtures of iron(III), hexacyanoferrate(II) and 1,10-phenanthroline was demonstrated both electrochemically (differential pulse peak at +820 mV, see Fig. 2) and optically (absorption band, max 510 nm; see Fig. 3). Visible spectrophotometry also demonstrated (see Fig. 3) that formation of the

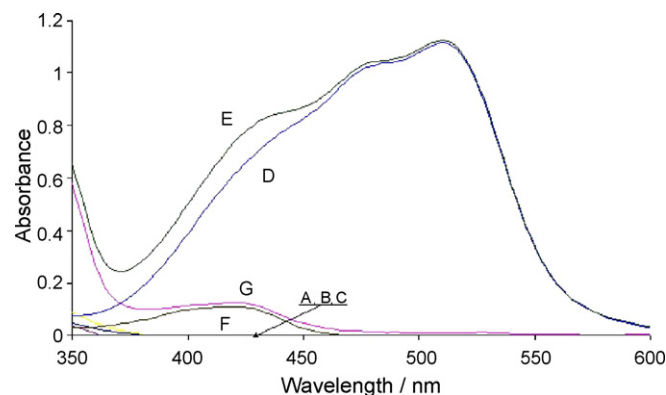
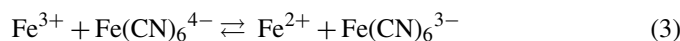


Fig. 3. Absorbance spectra of various mixtures of iron(III), hexacyanoferrate(II) and 1,10-phenanthroline in acetate/ $\text{HSO}_4^-$  buffer (pH 3.5): (A)  $\text{Fe}^{3+}$  (0.1 mM) from  $\text{Fe}(\text{NO}_3)_3$ ; (B) potassium hexacyanoferrate(II) (0.5 mM); (C) 1,10-phenanthroline (0.5  $\text{g l}^{-1}$ ); (D)  $\text{Fe}(\text{phe})_3^{2+}$  complex (0.1 mM); (E) mixture of  $\text{Fe}^{3+}$  (0.1 mM), hexacyanoferrate(II) (0.5 mM) and 1,10-phenanthroline (0.5  $\text{g l}^{-1}$ ); (F) potassium hexacyanoferrate(III) (0.1 mM); and (G) spectrum E–spectrum D.

complex was accompanied by the formation of hexacyanoferrate(III) (absorption band at 420 nm). The mechanism of the reaction was not investigated but it is assumed that the reaction was driven by formation of the 1,10-phenanthroline complex:

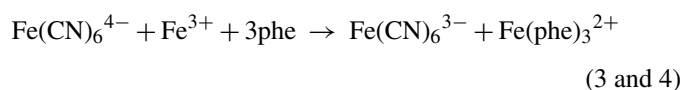


On the time scale of the measurement, the reaction process was effectively instantaneous at pH >2.3 and importantly, iron(III) added to an excess of 1,10-phenanthroline and hexacyanoferrate(II) was converted quantitatively to  $\text{Fe}(\text{phe})_3^{2+}$  (Fig. 3).

The presence of hexacyanoferrate(II) had almost no effect on the magnitude of the voltammetric signal for the  $\text{Fe}(\text{phe})_3^{2+}$  complex but the peak position was shifted about 20 mV towards more negative potentials in the presence of hexacyanoferrate(II) (1 mM). A large current reflected the reduction of hexacyanoferrate(III) at potentials more negative than +400 mV but it was clearly distinguishable from the iron peak. The peak positions for separate measurements of both iron(II) and iron(III) were the same, and the magnitude of the signals for iron(II) and iron(III) solutions of the same concentration were comparable (see Fig. 2). The background current of the differential pulse scan was slightly higher in the presence of hexacyanoferrate(II) but, in marked contrast to the use of hydroxylamine, the baseline was almost horizontal, the peaks were almost symmetrical and the detection limit for pre-dissolved iron was  $10 \mu\text{g l}^{-1}$ . Clearly, hexacyanoferrate (II) is ideal for reducing iron(III) in this application.

### 3.1.2. Mediated electroreduction of iron(III)

**3.1.2.1. Determination at uncoated sensor devices.** Chemical reduction of iron(III) could be replaced by reduction at the surface of a suitably poised working electrode, thus avoiding the use of unstable chemical reducing agents. Direct reduction of iron(III) at the working electrode (−350 mV) was inefficient; pre-treatment for >5 min was required to obtain a signal >95% of that for iron(II) of the same concentration. Considerably more rapid conversion of iron(III) to iron(II) was achieved using electroreduction mediated by hexacyanoferrate(III):



It was established in the previous section that reactions (2) and (3) were effectively instantaneous at pH >2.3. Therefore, with hexacyanoferrate(II) present in the mixture, reduction at the electrode produced hexacyanoferrate(II), which, in turn, reduced iron(III) in the vicinity of the electrode resulting in its quantitative conversion to the  $\text{Fe}(\text{phe})_3^{2+}$  complex. Hexacyanoferrate(III)-mediated electroreduction of iron(III) was considerably faster than unmediated reduction at the electrode. Measurement of total iron could be effected in  $\geq 20$  s using mediated reduction. Calibration graphs were obtained using

the method (not shown). Linear correlation between the signal and the concentration of total iron was found between 10 and  $5000 \mu\text{g l}^{-1}$ :

$$\frac{I_{\text{p.c}}}{nA} = (0.121 \pm 0.001)[\text{Fe}^{2+}/\mu\text{g l}^{-1}] + (13 \pm 2) \\ R^2 = 0.999 \quad (6)$$

$$\frac{I_{\text{p.c}}}{nA} = (0.117 \pm 0.001)[\text{Fe}^{3+}/\mu\text{g l}^{-1}] + (11 \pm 2) \\ R^2 = 0.998 \quad (7)$$

Providing that the pre-dissolved form of iron was used, the analysis could be carried out at a pH between 2.3 and 4.5.

1,10-Phenanthroline is known [24] to form complexes with a range of metal ions, including  $\text{Zn}^{\text{II}}$ ,  $\text{Cu}^{\text{II}}$ ,  $\text{Mn}^{\text{II}}$ , and  $\text{Co}^{\text{II}}$ . Therefore, possible interference by other metals was studied, using both direct electrode reduction of iron(III) (i.e. in the absence of hexacyanoferrate(III)) and using hexacyanoferrate(III) as the electrochemical mediator. Of the metals tested ( $\text{Mn}^{\text{II}}$ ,  $\text{Cu}^{\text{II}}$ ,  $\text{Al}^{\text{III}}$ ,  $\text{Zn}^{\text{II}}$ ,  $\text{Ag}^{\text{I}}$ ,  $\text{Pb}^{\text{II}}$ ,  $\text{Co}^{\text{II}}$ ,  $\text{Cr}^{\text{III}}$ , at  $500 \mu\text{g l}^{-1}$ ) only zinc showed interference in the absence of hexacyanoferrate(III), the reduction peak potential ( $E_{\text{p.c}}$ ) being indistinguishable from that of iron. The magnitude of the signal for zinc was approximately 25% of that for iron(II) for the same concentrations.  $\text{Mn}^{2+}$  and  $\text{Ag}^+$  showed some interfering electroactivity. In these cases, however,  $E_{\text{p.c}}$  was either more positive ( $\text{Ag}^+$ ) or more negative ( $\text{Mn}^{2+}$ ) than that for iron(II). Importantly, the interferences of Zn, Mn and Ag were negligible in the presence of hexacyanoferrate(III). This is most probably due to precipitation of the interfering metal species by hexacyanoferrate(III) or hexacyanoferrate(II).

**3.1.2.2. Determination at coated sensor devices.** It was found to be possible to immobilise all the necessary reagents (1,10-phenanthroline, potassium hexacyanoferrate(III), potassium hydrogen sulphate, sodium acetate and potassium chloride) on the sensor surface in a PVA matrix, then to measure total dissolved iron without the need for sample pre-treatment.

The layer of PVA was positioned to cover the working, reference and counter electrodes. Adherence of the layer to the sensor devices was satisfactory and the PVA also assisted wetting of the electrodes. The measurement consisted of applying the sample solution onto the sensor device, pre-treatment at −0.2 V for 30 s to convert iron(III) to iron(II), followed immediately by a voltammetric scan from +1.2 to +0.4 V to measure the reduction of the iron(II)1,10-phenanthroline complex. When pre-dissolved iron(II) and iron(III) sample solutions were used, the magnitude of the signal was comparable for both iron(II) and iron(III) (compare Figs. 2 and 4). The magnitude of the signal was very similar to those obtained using the reagents in solution.

### 3.2. Determination of total iron in natural iron solutions using coated sensor devices

Measurement of total iron directly in natural samples (e.g. potable water), where most of the iron is present in the form of insoluble iron(III) species (particularly oxyhydroxides),

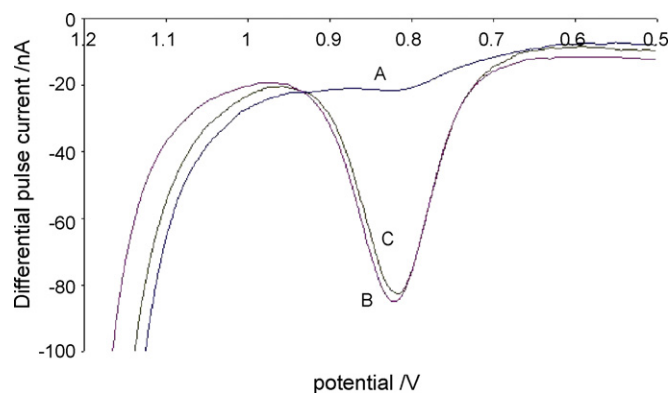
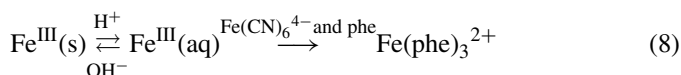


Fig. 4. Differential pulse voltammetry of iron using sensor devices with immobilised reagents and hexacyanoferrate(III) mediated electroreduction of iron(III). Stock solutions of iron ( $100 \text{ mg l}^{-1}$ ) were prepared in  $10 \text{ mM}$  hydrochloric acid and diluted to the required concentration with deionised water.  $[\text{Iron(II)}]$  and  $[\text{Iron(III)}]/\mu\text{g l}^{-1}$ : (A) 0 and 0; (B) 640 and 0; (C) 0 and 640. Electroreduction was performed for 30 s at  $-0.2 \text{ V}$  prior to the voltammetric scan.

requires the dissolution of the insoluble iron species present as part of the measurement process.

Initial experiments showed that dissolution of colloidal iron species was a lengthy process, even at pH values as low as 2.1—the minimum pH at which it was feasible to carry out the 1,10-phenanthroline-based voltammetric measurement. Below pH 2.1, formation of the  $\text{Fe}(\text{phe})_3^{2+}$  complex was slow and incomplete. Dissolution of iron(III) oxyhydroxides was considerably faster when the dissolved iron(III) was rapidly and irreversibly converted to the strong  $\text{Fe}(\text{phe})_3^{2+}$  complex by reaction with hexacyanoferrate(II) and 1,10-phenanthroline:



The rate of  $\text{Fe}(\text{phe})_3^{2+}$  formation from iron(III) in the presence of hexacyanoferrate(II) and 1,10-phenanthroline is shown as a function of pH in Fig. 5. The most rapid dissolution was achieved at pH 2.3–2.5. Slow dissolution at pH 2.1 may be explained by a slow rate of complex formation between iron(II) and 1,10-phenanthroline, whilst at pH values higher than 2.3 the initial dissolution of sparingly soluble iron(III) was the rate limiting factor. The electrochemical determinations in natural iron solutions were achieved by electroreduction of hexacyanoferrate(III) for 5 min to produce excess hexacyanoferrate(II) which, in combination with the low pH (2.5), led to dissolution of the insoluble species and the subsequent formation of the  $\text{Fe}(\text{phe})_3^{2+}$  complex. The approach was tested using sensor devices with immobilised reagents. In this case, however, the magnitude of the signal for iron(III) species tended to be smaller than that for iron(II) species at the same concentration. Employing longer pre-treatment times (up to 10 min) did not improve the results. However, it was found that the following factors had an effect on the magnitude of the signal for iron(III):

- the degree of hydrolysis of PVA—the signal for iron(III) tended to be larger using PVA with a high degree of hydrolysis;

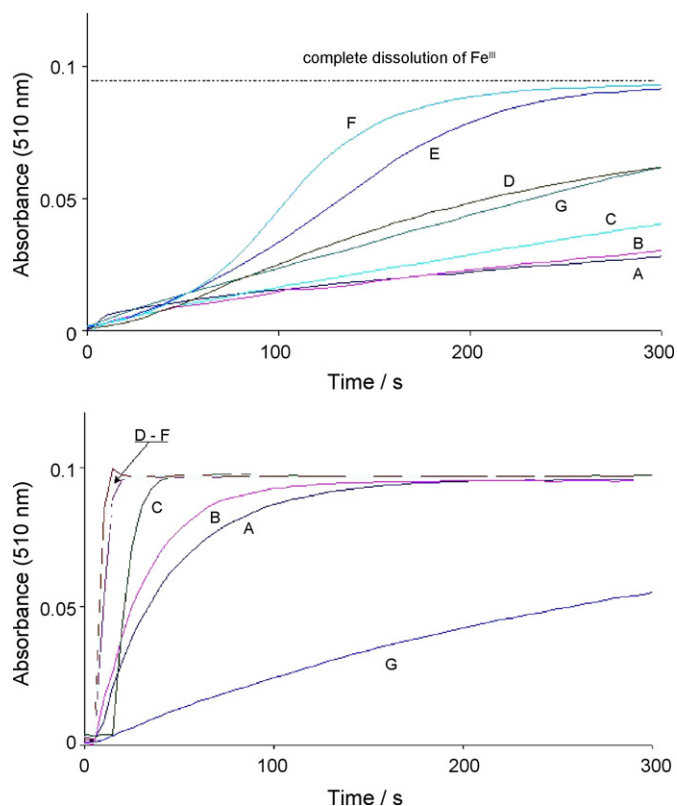


Fig. 5. Effect of pH on the rate of formation of  $\text{Fe}(\text{phe})_3^{2+}$  complex in mixtures of iron, hexacyanoferrate(II) and 1,10-phenanthroline. The reaction was started at time 0 by adding (top) iron(III) (from nitrate;  $1 \text{ mg l}^{-1}$ ) or (bottom) iron(II) (from sulphate;  $1 \text{ mg l}^{-1}$ ) to an equal volume of the mixture of ferrocyanide ( $2 \text{ mM}$ ) and 1,10-phenanthroline ( $0.2 \text{ g l}^{-1}$ ) in acetate/ $\text{HSO}_4^-$  buffer. The pH of the buffer was (A) 4.5; (B) 4.0; (C) 3.3; (D) 2.7; (E) 2.5; (F) 2.3; and (G) 2.1.

- the concentration of PVA in the reagent layer—the signal for iron(III) tended to be larger using smaller concentrations of PVA.

These effects were not investigated exhaustively but the best results were obtained using a layer of 0.05% PVA (>99% hydrolysed;  $M_r = 85,000$ – $146,000$ ) and >4 min electrode-reduction at  $-0.2 \text{ V}$ . These conditions gave signals for iron(III) species in natural solutions that were about 85% of those for equivalent concentrations of iron(II) species. Smaller concentrations of PVA reduced the effectiveness of PVA as a spreading layer.

#### 4. Conclusions

A novel method for the quantitative determination of total iron was developed in this work. Although the possibility of measuring iron voltammetrically based on complexation with 1,10-phenanthroline had been reported previously, this work added some novel practical features to the technique. Firstly, the method was adapted to the use of screen-printed disposable sensor devices. This provides the possibility to determine the concentration of the total dissolved iron simply and quickly. Screen-printed single-use sensor devices lend themselves to routine in-field use using simple procedures and relatively inexpen-

sive equipment. Secondly, an effective way of reducing iron(III) to iron(II) prior to the voltammetric measurement was identified. Iron(III) was reduced at the surface of a suitably poised working electrode using hexacyanoferrate(III) as a mediator, thus avoiding the need to use unstable chemical reagents. The method allowed complete reduction of iron(III) in the vicinity of the electrode within 30 s. A subsequent voltammetric scan permitted the determination of total iron with a detection limit of  $10 \mu\text{g l}^{-1}$ . Thirdly, the simplicity of the measurement was improved further by immobilisation of all the necessary reagents on the sensor devices, which allowed measurement of total dissolved iron without any sample pre-treatment.

Techniques for total iron are typically preceded by dissolution of iron(III) species in a strong acid. The possibility of measuring total iron in natural samples without a separate pre-dissolution step was investigated and was found to be feasible. Insoluble iron(III) was dissolved at pH 2.3–2.5 on the sensor during the measurement. The rate of dissolution, which is rather slow at this pH, was enhanced by the presence of hexacyanoferrate(II) generated at the working electrode. The total iron measurement, including the dissolution of iron(III) species using this technique, took approximately 5 min, without any sample pretreatment being required.

However, this method of dissolving iron(III) appeared to be less effective when tested with reagents immobilised in the PVA layer. In this case the signal was typically smaller for iron(III) than for iron(II) at the same concentration. The composition of the layer was optimised to improve the signal for iron(III) and this resulted in a signal which was about 85% of that for iron(II).

The detection limit of  $10 \mu\text{g l}^{-1}$  of this method was not as good as that described previously using catalytic cathodic stripping voltammetry on a mercury electrode. Nevertheless, it was comparable with a range of other methods including the official ISO spectrometric method for determination of total iron in drinking water.

## Acknowledgement

This work was carried out with funding from the European Union under the FW5 Competitive and Sustainable Growth Programme project GRD1-1999-10868.

## References

- [1] L. Stryer, Biochemistry, in: W.H. Freeman (Ed.), second ed., San Francisco, 1981.
- [2] T.H. Bothwell, R.W. Charlton, J.D. Cook, C.A. Finch, Iron Metabolism in Man, Blackwell Scientific, Oxford, 1979.
- [3] J.V. Corbett, Am. Matern. Child. Nurs. 20 (1995) 234.
- [4] E.P. Achtenberg, T.W. Holland, A.R. Bowie, R.F.C. Mantoura, P.J. Worsfold, Anal. Chim. Acta 442 (2001) 1.
- [5] European Council Directive 98/83/EC, 3 Nov 1998.
- [6] ISO 6332:1988.
- [7] A. Quinteros, R. Farre, M.J. Lagarda, Food Chem. 75 (2001) 365.
- [8] M. Kassand, A. Ivaska, Talanta 58 (2002) 1131.
- [9] L.V. Mulaudzi, J.F. van Staden, R.I. Stefan, Anal. Chim. Acta 467 (2002) 35.
- [10] T. Pojanagaroon, S. Watanesk, V. Rattanaphani, S. Liawrungrath, Talanta 58 (2002) 1293.
- [11] S. Blain, P. Treguer, Anal. Chim. Acta 308 (1995) 425.
- [12] P.L. Croot, K.A. Hunter, Anal. Chim. Acta 406 (2000) 289.
- [13] J.N. Richardson, A.L. Dyer, M.L. Stegemiller, I. Zudans, C.J. Seliskar, W.R. Heineman, Anal. Chem. 74 (2002) 3330.
- [14] V.A. Elrod, K.S. Johnson, K.H. Coale, Anal. Chem. 63 (1991) 893.
- [15] S. Hirata, H. Yoshihara, M. Aihara, Talanta 49 (1999) 1059.
- [16] P. Pulido-Tolfino, J.M. Barrero-Moreno, M.C. Perez-Conde, Talanta 51 (2000) 537.
- [17] E.K. Paleologos, D.L. Giokas, S.M. Tzouwara-Karayanni, M.I. Karayannis, Anal. Chim. Acta 458 (2002) 241.
- [18] H. Obata, C.M.G. van den Berg, Anal. Chem. 73 (2001) 2522.
- [19] A.P. Aldrich, C.M.G. van den Berg, Electroanalysis 10 (1998) 369.
- [20] P.L. Croot, M. Johansson, Electroanalysis 12 (2000) 565.
- [21] G. Lu, X. Yao, X. Wu, T. Zhan, Microchem. J. 69 (2001) 81.
- [22] Z. Gao, P. Li, G. Wang, Z. Zhao, Anal. Chim. Acta 241 (1990) 137.
- [23] J.W. Dilleen, S.D. Sprules, B.J. Birch, B.G.D. Hagggett, Analyst 123 (1998) 2905.
- [24] Official Methods of Analysis, in: S. Williams (Ed.), 14th ed., AOAC Inc., 1984.



# Determination of bismuth and copper using adsorptive stripping voltammetry couple with continuous wavelet transform

Shokooh S. Khaloo, Ali A. Ensafi\*, T. Khayamian

*Department of Chemistry, Isfahan University of Technology, Isfahan 84156, Iran*

Received 22 November 2005; received in revised form 27 March 2006; accepted 6 April 2006

Available online 30 May 2006

## Abstract

A new method is proposed for the determination of bismuth and copper in the presence of each other based on adsorptive stripping voltammetry of complexes of Bi(III)-chromazorul-S and Cu(II)-chromazorul-S at a hanging mercury drop electrode (HMDE). Copper is an interfering element for the determination of Bi(III) because, the voltammograms of Bi(III) and Cu(II) overlapped with each other. Continuous wavelet transform (CWT) was applied to separate the voltammograms. In this regards, wavelet filter, resolution of the peaks and the *fitness* were optimized to obtain minimum detection limit for the elements. Through continuous wavelet transform Symlet4 (Sym4) wavelet filter at dilation 6, quantitative and qualitative analysis the mixture solutions of bismuth and copper was performed. It was also realized that copper imposes a matrix effect on the determination of Bi(III) and the standard addition method was able to cope with this effect. Bismuth does not have matrix effect on copper determination, therefore, the calibration curve using wavelet coefficients of CWT was used for determination of Cu(II) in the presence of Bi(III). The detection limits were 0.10 and 0.05 ng ml<sup>-1</sup> for bismuth and copper, respectively. The linear dynamic range of 0.1–30.0 and 0.1–32.0 ng ml<sup>-1</sup> were obtained for determination of bismuth in the presence of 24.0 ng ml<sup>-1</sup> of copper and copper in the presence of 24.0 ng ml<sup>-1</sup> of bismuth, respectively. The method was used for determination of these two cations in water and human hair samples. The results indicate the ability of method for the determination of these two elements in real samples.

© 2006 Elsevier B.V. All rights reserved.

**Keywords:** Continuous wavelet transform; Resolving the overlapped voltammogram; Bismuth; Copper

## 1. Introduction

Bismuth compounds have application in semiconductors, cosmetic preparations, metallurgy and alloy industry, iron castings, electronics, lubricating oils and greases, pigments, medicines for treatment of helicobacter pyloric- induced gastritis, contact lens cleaning solution, nuclear reactor cooling fluids and reagent for purification of sugar [1–3]. Copper is an essential constituent of enzymes, therefore is biologically essential trace elements [4] and play an important role in water as pollutant or essential element [5] dependent on its concentration. Therefore, it is not surprising that many techniques have been developed for determination of bismuth and copper. Among the different methods, electrochemical stripping analysis is favor because of ease and speed of operation and sensitivity [6–10].

There are a variety of electrochemical stripping methods including anodic stripping voltammetry (ASV) and adsorptive cathodic stripping voltammetry (AdCSV) for the determination of bismuth and copper [6–14]. Although, these techniques offer the desired sensitivity but, they suffer from some practical difficulties. The advantage of the highly sensitive stripping techniques is often overshadowed by the interference of Cu(II), which its peak overlaps with Bi(III) peak [9]. Therefore, accurate determination of these two elements in the presences of each other is not possible by common electroanalytical methods. Several efforts have been made to resolve the interference of copper. Accumulation of bismuth onto the surface of a chemically modified electrode containing 1-(2-pyridylazo)-2-naphthol [14] is a selective voltammetric method for the determination of bismuth in presence of copper. In this method the interference of copper was overcome by using an excess amount of iodide to the deposition medium. However, it is not possible to determine copper by this method. Zen et al have developed poly (4-vinyl pyridine)/mercury film electrode to overcome the interference of copper [9]. Limson has mentioned that simultaneous detection

\* Corresponding author. Tel.: +98 311 3912351; fax: +98 311 3912350.  
E-mail address: [ensafi@cc.iut.ac.ir](mailto:ensafi@cc.iut.ac.ir) (A.A. Ensafi).

of Cu(II), Pb(II), Bi(III) and Cd(II) can be performed by using appropriate concentration of each cation. Since there is strong interference between bismuth and copper, determination of one cation is possible only in the presence of very low concentration of another one [10]. However, it is not possible to control the concentration of these cations in real samples.

Resolving and quantifying the overlapped peaks has long been an interesting subject in analytical chemistry. Many efforts have been made to resolve overlapped signals by chemical, instrumental and mathematical methods. In chemometrics, different methods such as linear or non-linear regression analysis, curve fitting [15,16], the Fourier self deconvolution (FSD) [17], artificial neural networks (ANN) [14,18], and factor analysis [19] were employed to overcome this problem. The Fourier self deconvolution is an effective means of resolving overlapped band, but this method requires a mathematical model to yield deconvolution and it is quite sensitive to noise in unresolved bands [20]. In the past decade, wavelet transform (WT) has also been employed to find the individual peak position in overlapped signals [21–23]. Wu and co-workers [24] performed CWT in a single dilation to find positions of overlapped peak of square wave voltammogram (SWV) that could be described by the  $\text{sech}^2$ -function. Xiaoquan et al. have developed a method to estimate the number of peaks and individual peak position in an overlapped signal. They have used CWT not on a single dilation but on an appropriate dilation range [25].

In this work, chromazorul-S has been used as a chelating agent in cathodic adsorptive stripping voltammetry of bismuth and copper on a hanging mercury drop electrode (HMDE). In the presence of chromazorul-S as a new complexing agent for determination of Bi(III), interference of Cu(II) was observed by overlapping of cathodic peak of Cu(II)-chromazorul-S. Despite of optimization of chemical and instrumental parameter there is still severe overlapping between the voltammograms of these two elements. Therefore, using mathematical method for resolving of these voltammograms is unavoidable. CWT is a very powerful preprocessing method to estimate the number of peaks, their positions and to obtain the individual peak in an overlapped signal and was proposed to resolve and quantify the overlapped voltammogram of these two cations. Maximums of wavelet coefficients were used to find the number of peaks and their positions. By using the proposed method Bi(III) was determined in the presence of Cu(II) in concentration as high as 200 times more than bismuth concentration. The determination of copper was performed in mixture solution without the matrix effect of Bi(III) on Cu(II) voltammogram.

## 2. Theory of the wavelet transforms

A detailed description of the wavelet and wavelet transform can be found in some references [26,27] and book [28]. A brief overview of this theory is presented.

Wavelet is defined as a series of function  $\psi_{a,b}(t)$  derived from a mother function  $\psi(t)$  by dilation and translation

$$\psi_{a,b}(t) = |a|^{-1/2} \psi\left(\frac{t-b}{a}\right) \quad a, b \in R \text{ and } a \neq 0 \quad (1)$$

where  $a$  is the scale parameter that controls dilation and  $b$  is the shift parameter that controls the translation of wavelet. For a signal  $f(t)$  in time domain, its CWT could be described as Eq. (2)

$$W_f(a, b) = |a|^{-1/2} \int_{-\infty}^{+\infty} f(t) \psi\left(\frac{t-b}{a}\right) dt \quad (2)$$

$a$  or  $b$  is a certain constant and the CWT under a certain dilation  $W_{f(a)}(b)$  or under certain translation  $W_{f(b)}(a)$  can be obtained [28].

Because WT is a linear transformation, the peak position of the data set would not change before and after WT. In the other hand, the information of the signal will remain in the transformed coefficients for further regression analysis. Therefore, after preprocessing with CWT, the obtained coefficients of the spectra can be used for calibration or regression with partial least squares (PLS) and artificial neural network or other methods [24]. This means, quantitative and qualitative analysis can be performed by using wavelet coefficients. If one signal  $f(t)$  increases  $K$  times the CWT coefficients increase  $K'$  time (quantitative analysis) and the position of the maximum of  $W_{f(a)}(b)$  is the same as the peak position of original signal (qualitative analysis).

Selection of a wavelet filter that is matched to the data is very important. CWT based on incorrect wavelet function could not detect the exact peak number and position [25]. Theoretically, there are many wavelet functions could be used to run CWT, but the Harr, daubelets, coiflets and symlets are widely used for signal processing [29]. Among these 22 orthonormal wavelet functions (Haar, nine daubelets, five coiflets and seven symlets), selection of an appropriate wavelet filter may be guided by empirical rules applied to data size and signal continuity. The typical way is to visually inspect the data first, and select an appropriate wavelet filter [29]. The other way is to consider the peak position, peak number and degree of separation ( $R$ ) as criteria. Resolution of two peaks defines as,

$$R = \frac{x_2 - x_1}{0.5(y_2 - y_1)} \quad (3)$$

where  $x_1$  and  $x_2$  are the peak positions,  $y_1$  and  $y_2$  the bottom widths of peaks and  $R$  is degree of separation [25].

In addition to wavelet function, dilation has also an important role to get maximum resolution and sensitivity. A proper dilation was selected using the introduced criterion by Xiaoquan et al. [25]

$$\text{fitness}(a) = \sum_{b=1}^{\text{length } f(x)} [|W_{f(a)}(b)| - |f(b)|]^2 \quad (4)$$

$\text{fitness}(a)$  represents the cumulated difference between the wavelet coefficients  $W_{f(a)}(b)$  and the original data at each transition. The dilation which makes the  $\text{fitness}(a)$  have the minimum value would be chosen as the best dilation.

### 3. Experimental

#### 3.1. Experimental data

##### 3.1.1. Reagents

All chemicals were reagent grade and doubly distilled water was used in preparation of all solutions.

Stock solutions ( $1000 \mu\text{g ml}^{-1}$ ) of Bi(III) and Cu(II) were prepared by dissolving 0.2400 g of  $\text{Bi}(\text{NO}_3)_3 \cdot 6\text{H}_2\text{O}$  and 0.3920 g of  $\text{Cu}(\text{NO}_3)_2$  in 2 ml nitric acid and water, respectively. The result solutions were diluted with double distilled water to 100 ml in 100 ml volumetric flasks.

Chromazurol S solution,  $1.00 \times 10^{-3} \text{ M}$ , was prepared by dissolving 0.0600 g of the reagent in water in a 100 ml volumetric flask, diluted to the mark and stored in fridge.

##### 3.1.2. Apparatus

All electrochemical experiments were performed with potentiostat and galvanostat (Auto lab AUT 72036 electrochemical system) in conjunction with a 663 VA Stand Metrohm electrochemical cell. A conventional three-electrode system, comprising a medium-sized hanging mercury drop electrode as a working electrode, a platinum wire counter electrode and an Ag/AgCl reference electrode (saturated KCl) was used in all experiment.

##### 3.1.3. Procedure

Ten milliliter of buffer solution (acetate, pH 3.7) and  $4.0 \mu\text{M}$  of chromazurol-S were added in the electrochemical cell as a blank and the solution was purged with the nitrogen gas for at least 4 min. The adsorption preconcentration was carried out from the stirred solution for a period of 60 s at a  $-0.20 \text{ V}$  versus Ag/AgCl, at a fresh mercury drop. Afterward, a differential pulse voltammogram was recorded from  $+0.16$  to  $-0.08 \text{ V}$ , with a potential scan rate of  $20 \text{ mV s}^{-1}$ . The voltammogram for the blank solution ( $E_b$ ) was measured. Then, Bi(III) or Cu(II) standard solutions were added to the cell while maintaining a nitrogen atmosphere over the solution and a differential pulse voltammogram was recorded. The sample voltammogram ( $E_s$ ) was measured at the same conditions. Measurements were obtained in room temperature ( $25^\circ\text{C}$ ).

All computations were carried out on a Pentium4, 1.5 GHz PC. The CWT algorithm was written in Matlab 6.1 software by the authors.

#### 3.2. Simulated data

In order to find out the optimized variables, the method was applied to simulated overlapped peaks. The details of procedure that were used in this work can be summarized as the following steps: (1) create a simulated overlapped signal by using the Gaussian equation

$$y = \frac{1}{\sigma\sqrt{2\pi}} e^{-(x-\mu)^2/2\sigma^2} \quad (5)$$

(2) select a wavelet function and set an initial value as the scale parameter, (3) perform CWT of the signal on a selected dilation

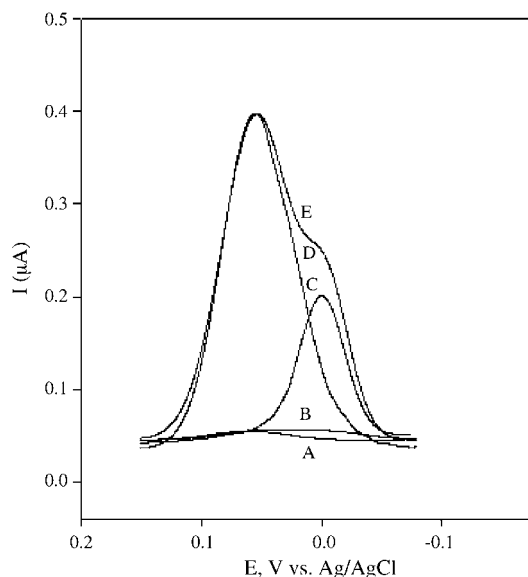


Fig. 1. The original DPSV for: (A) the blank solution contain  $4.0 \mu\text{M}$  chromazurol-S in acetate buffer pH 3.7; (B) the solution contains  $18.0 \text{ ng ml}^{-1}$  Bi(III) and  $9.0 \text{ ng ml}^{-1}$  Cu(II) in acetate buffer, pH 3.7; (C) (A) plus  $5.0 \text{ ng ml}^{-1}$  Bi(III); (D) (A) plus  $6.0 \text{ ng ml}^{-1}$  Cu(II); (E) (A) plus  $5.0 \text{ ng ml}^{-1}$  Bi(III) and  $6.0 \text{ ng ml}^{-1}$  Cu(II).

by convolution the wavelet function on all the signal and obtain data  $Wf_{(a)}(b)$  and (4) detect the peak numbers, peak positions and degree of separation according to the wavelet coefficients,  $Wf_{(a)}(b)$ , and compare with those of the original signal, to find the best wavelet filter. After optimization of wavelet filter according to the criteria, dilation was studied. Values of  $fitness(a)$  were calculated according to Eq. (4) and minimum of  $fitness$  was selected as optimized value for the scale. Then optimized dilation and filter function were obtained by using the simulated overlapped signals were used to perform CWT on real voltammograms. Maximum of wavelet coefficients,  $Wf_{(a)}(b)$ , were used to plot the calibration curves and calculation of concentration of cations.

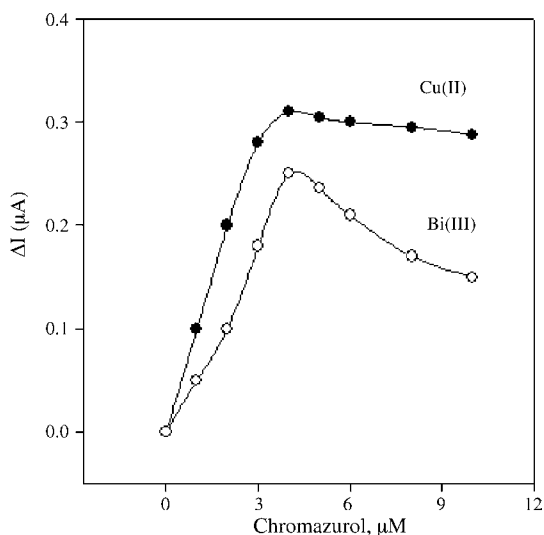


Fig. 2. Effect of chromazurol S concentration on the peak current of a solution contains  $10.0 \text{ ng ml}^{-1}$  Bi(III) or Cu(II) in acetate buffer, pH 3.7. Conditions:  $E_{ac} = -0.15$ ;  $t_{ac} = 60 \text{ s}$  and scan rate =  $15 \text{ mV s}^{-1}$ .

Table 1  
Optimized parameter for determination of Bi(III) and Cu(II)

Parameter	Range	Optimized value for Cu	Optimized value for Bi	Selected optimized value for mixture
pH	2–6	4	3.7	3.7
Chromazurol-S ( $\mu\text{M}$ )	0–10	4.0	4.0	4.0
$E_{ac}$ (V)	0.18 to $-0.5$	$-0.14$	$-0.2$	$-0.2$
$t_{ac}$ (s)	0–140	50	60	60
Scan rate ( $\text{mV s}^{-1}$ )	5–40	20	20	20
Pulse height (V)	0.02–0.12	0.1	0.1	0.1

## 4. Result and discussion

### 4.1. Adsorptive and voltammetric characteristic of the Bi(III) and Cu(II)-chromazurol-S complexes

Fig. 1 shows the differential pulse stripping voltammograms for solutions contain  $4.0 \mu\text{M}$  of chromazurol-S in acetate buffer pH 3.7 in presence of Bi(III) and Cu(II) under different conditions. In the absence of chromazurol-S as a complexing agent, there is not any reduction peak current for  $18.0 \text{ ng ml}^{-1}$  Bi(III) or  $9.0 \text{ ng ml}^{-1}$  Cu(II). Chromazurol-S does not have any electrochemical activity in this potential range (Fig. 1B). However, in the presence of Bi(III) and Cu(II) alone or in mixture solutions and chromazurol-S, corresponding peaks are observed (Fig. 1C–E). The voltammograms of Bi(III), Cu(II) and chromazurol-S system recorded without accumulation and in different accumulation times. The results show that the peak currents increase with increasing accumulation time prior to the potential scan, indicate that the Bi(III) and Cu(II) chromazurol-S complexes is readily adsorbed onto the HMDE. In addition, depression of the peak current upon addition of  $10.0 \mu\text{g ml}^{-1}$  Triton X-100 into the solution shows the adsorptive characteristic of the complex onto the HMDE.

The effect of chemical parameters such as pH and chromazurol-S concentration and instrumental parameters such as accumulation potential, accumulation time, pulse amplitude

and scan rate were investigated to obtain maximum resolution and sensitivity. Fig. 2 is a typical graph shows the influence of chromazurol-S concentration on the peak current of solutions of  $10.0 \text{ ng ml}^{-1}$  Bi(III) and Cu(II). The sensitivity of determination of both copper and bismuth increased with increasing chromazurol-S concentration up to  $4.0 \mu\text{M}$ . At higher concentrations, peak currents decrease with increasing chromazurol-S concentration. This effect is due to competition adsorption of free ligand and complexes on the surface of mercury electrode. Therefore,  $4.0 \mu\text{M}$  chromazurol-S concentration was selected as optimized value for both elements.

All of the other parameters were optimized in a similar way. The results are summarized in Table 1. Despite of optimization of chemical and instrumental parameters there is still severe overlapping between the voltammograms of these two cations.

### 4.2. Selection of an appropriate wavelet filter and dilation

#### 4.2.1. Simulated overlapped signal

In this paper three criteria (peak position, peak number and resolution) were used to find the best wavelet filter. In this regard, overlapped simulated signal according to the Gaussian function (Eq. (5)) was used. Fig. 3 exhibits two simulated peaks (A and B), which their peak positions are  $P_1 = 0.020$  and  $P_2 = -0.044$ . CWT was performed using 22 orthonormal wavelet functions

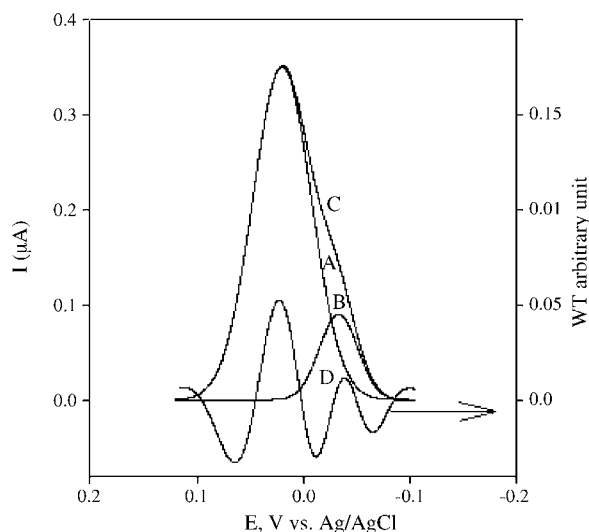


Fig. 3. Simulated signals (A–C) and corresponding wavelet transform (D) using sym4 at dilation 7.

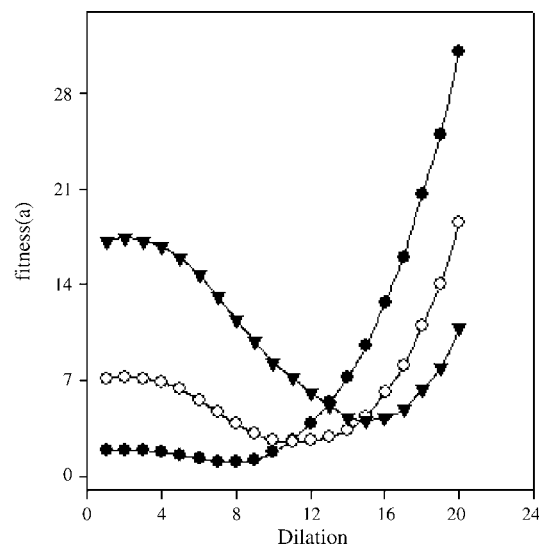


Fig. 4. fitness(a) for simulated overlapped signals when the peak heights of  $P_1$  are constant and peak height of  $P_2$  changed from (▼)  $P_2:P_1$  1:3; (○)  $P_2:P_1$  1:5 and (●)  $P_2:P_1$  1:7.

Table 2  
Regression equation<sup>a</sup> and limit of determination (LOD) of Cu(II) and Bi(III) in different dilution

Dilution	Bi(III)		Cu(II)	
	Regression (P.h.)	LOD (ng ml <sup>-1</sup> )	Regression	LOD (ng ml <sup>-1</sup> )
4	0.038 × C + 0.02	0.20	0.015 × C + 0.01	0.10
6	0.042 × C + 0.02	0.10	0.017 × C + 0.01	0.08
8	0.040 × C + 0.02	0.15	0.014 × C + 0.01	0.13
10	0.036 × C + 0.01	0.25	0.013 × C + 0.01	0.17

<sup>a</sup> P.h.: peak height in arbitrary unit, C: concentration in ng ml<sup>-1</sup>.

in the same dilution. According to the above criteria, Sym4 was selected as the best filter for resolving overlapped signal. Fig. 3D shows deconvolution of signal by using Sym4 wavelet filter with dilution 7. The relative errors of peak positions after wavelet transform were 1.9 and 2.9% for  $P_1$  and  $P_2$ , respectively. The degree of separation  $R$  is 0.74.

To obtain maximum resolution and sensitivity an optimized dilution is also necessary to perform CWT. The minimum value of fitness( $a$ ) was selected as a criterion to optimize dilution. Since the individual peaks overlap with a different overlap degrees in different peak heights therefore, optimum value of the dilution is dependent to concentration of analytes. Fig. 4 shows the values of the fitness( $a$ ) for simulated overlapped signal when the peak heights of  $P_1$  is constant and the other one,  $P_2$ , is changed. Results show whenever the optimization of dilution is performed when peak height of  $P_2$  is low (e.g. less than 20% of peak height of  $P_1$ ) limit of detection for  $P_2$  is improved. Xiaoquan and et al. used an appropriate dilution range to perform CWT instead of single dilution [25]. Since main goal of this work is the determination of low concentration of bismuth in the presence of high concentration of copper therefore, a dilution that shows a minimum detection limit was selected.

#### 4.2.2. Experimental data

In order to confirm the optimized variables based on the mentioned criteria, the same procedure, which was used for the simulated data, was repeated for the experimental data to find out the optimized variable performing CWT. The same optimized wavelet filter and dilution were obtained for the experimental data.

Table 2 shows the equation of regressions and limit of determinations of Bi(III) in different dilutions. The best limit of determination was obtained at dilution 6.

#### 4.3. Quantitative analysis

The linear property of CWT is one of the main characteristic of WT that can be used in quantitative analysis then, the  $Wf_{(a)}(b)$ , can be employed as a response to construct the calibration plot. Fig. 5a and b shows the DPSV and their corresponding  $Wf_{(a)}(b)$  to quantify Bi(III) in presence of 8.0 ng ml<sup>-1</sup> of Cu(II). Calibration graphs were obtained by using the maximum of wavelet coefficients of decomposed signals (Fig. 5b) at peak potential corresponding bismuth (around -0.02 V) versus concentration of Bi(III). On the other hand, a baseline correction for  $Wf_{(a)}(b)$

can be performed by linking the minimum points of bismuth peak and shift the peak in positive direction.

The calibration graphs for both methods have been shown in the corresponding inset figures. The regression coefficients in both methods are acceptable but, whenever baseline correction is done, the slope of calibration graph is greater than the other one, i.e. by baseline correction sensitivity and limit of detection improves. A similar investigation was performed when concentration of copper increases in presence of 10.0 ng ml<sup>-1</sup> bismuth. The results have been shown in Fig. 6a and b.

In comparing Figs. 5a and 6a, the results show that presence of copper can interfere for bismuth determination but, presence of bismuth does not have any interference for copper determination. To confirm this claim, the Cu(II) calibration plot was investigated in different conditions, e.g. (1) in the absence of bismuth and (2) in the presence of different concentration of bismuth. Table 3 shows the results of this investigation. Calibration plot of Bi in the presence of different concentration of copper was also investigated. The results have been summarized in last four rows of Table 3. Calibration graphs have been constructed after CWT without baseline correction. The results show the peak current of bismuth in presence of copper is still linear, however the slopes of the Bi(III) calibration curve in absence of copper is significantly different from those when copper is present. The statistical results of  $t$ -test show copper has a matrix effect on determination of bismuth and confirm the above claim. Therefore, standard addition method couple with CWT was proposed for quantitative analysis of bismuth in presence of copper. Statistical results show there is not any matrix effect of bismuth on copper determination therefore, calibration curve after CWT can be used for determination of copper in presence of bismuth.

To investigate the accuracy and applicability of the proposed method for quantitative determination of Bi(III) and Cu(II) in mixed solutions, the method was employed for determination of bismuth or copper in several synthetic samples with different concentrations of other element. The results are given in Table 4. The good recoveries show the method is capable to determine Bi(III) in the presence of high concentration of copper and vice versa.

#### 4.4. Interference study

The influence of various metal ions on the determination of copper and bismuth were examined. The obtained results for



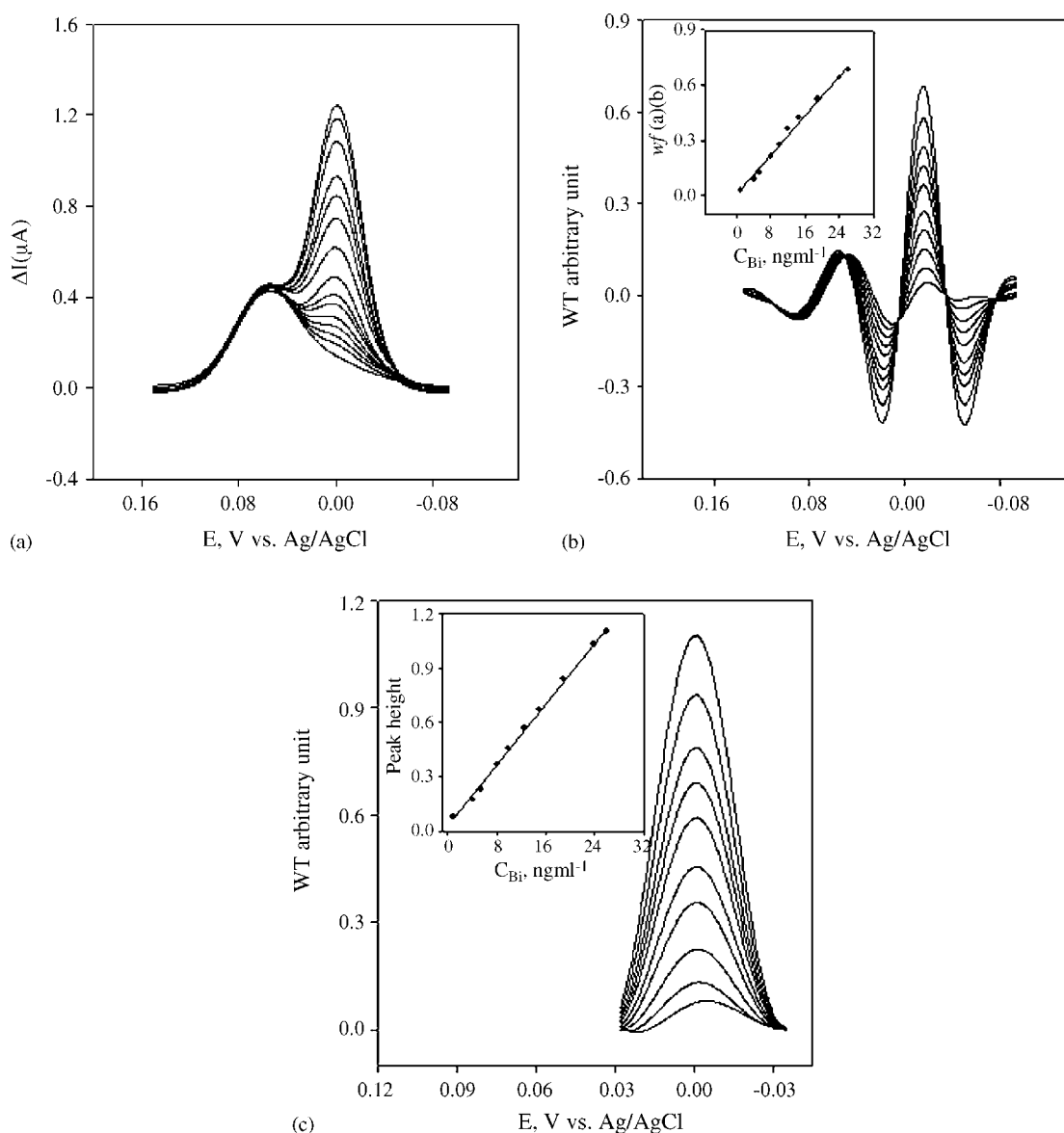


Fig. 5. (a–c) Show the DPSV, corresponding wavelet transform without baseline correction and baseline correction, respectively, using standard addition method to quantify Bi(III) in solution containing  $8.0 \text{ ng ml}^{-1}$  Cu(II). The insets figures show the corresponding peak heights vs. Bi(III) concentration.

$10.0 \text{ ng ml}^{-1}$  of each cation with 60 s preconcentration time are summarized in Table 5. The tolerance limit was defined as the concentration, which gave an error of  $<3.0\%$  in the determination of copper and bismuth. From the results, it is concluded that the method is free from many interferences of foreign ions.

#### 4.5. Analysis of real samples

In order to study applicability of the proposed method in a practical analytical situation, the method was used for the determination of copper and bismuth in tap water, river water and

Table 3  
Statistical results for comparison slope of the calibration curve of Cu(II) (1–3) and Bi(III) (4–7) in presence of different concentration of the other cation

Sample	Bi(III) ( $\text{ng ml}^{-1}$ )	Cu(II) ( $\text{ng ml}^{-1}$ )	Slope ( $\times 10^{-3}$ )	$F_{\text{exp}}$	$F_{\text{tab}}(0.05,9,9)$	$S_{\text{pooled}} (\times 10^{-3})$	$t_{\text{exp}}$	$t_{\text{tab}}(0.05,18)$
1	0.0	–	$12.3 \pm 0.6$	–	–	–	–	–
2	10.0	–	$11.5 \pm 0.3$	2.9	3.18	5.5	1.9	2.10
3	20.0	–	$12.1 \pm 0.3$	3.1	3.18	5.6	2.0	2.10
4	–	0.0	$35.3 \pm 0.8$	–	–	–	–	–
5	–	8.0	$27.2 \pm 0.3$	1.9	3.18	4.1	2.5	2.10
6	–	15.0	$11.1 \pm 0.3$	3.	3.18	3.9	2.8	2.10
7	–	24.0	$8.1 \pm 0.4$	1.9	3.18	4.0	2.6	2.10

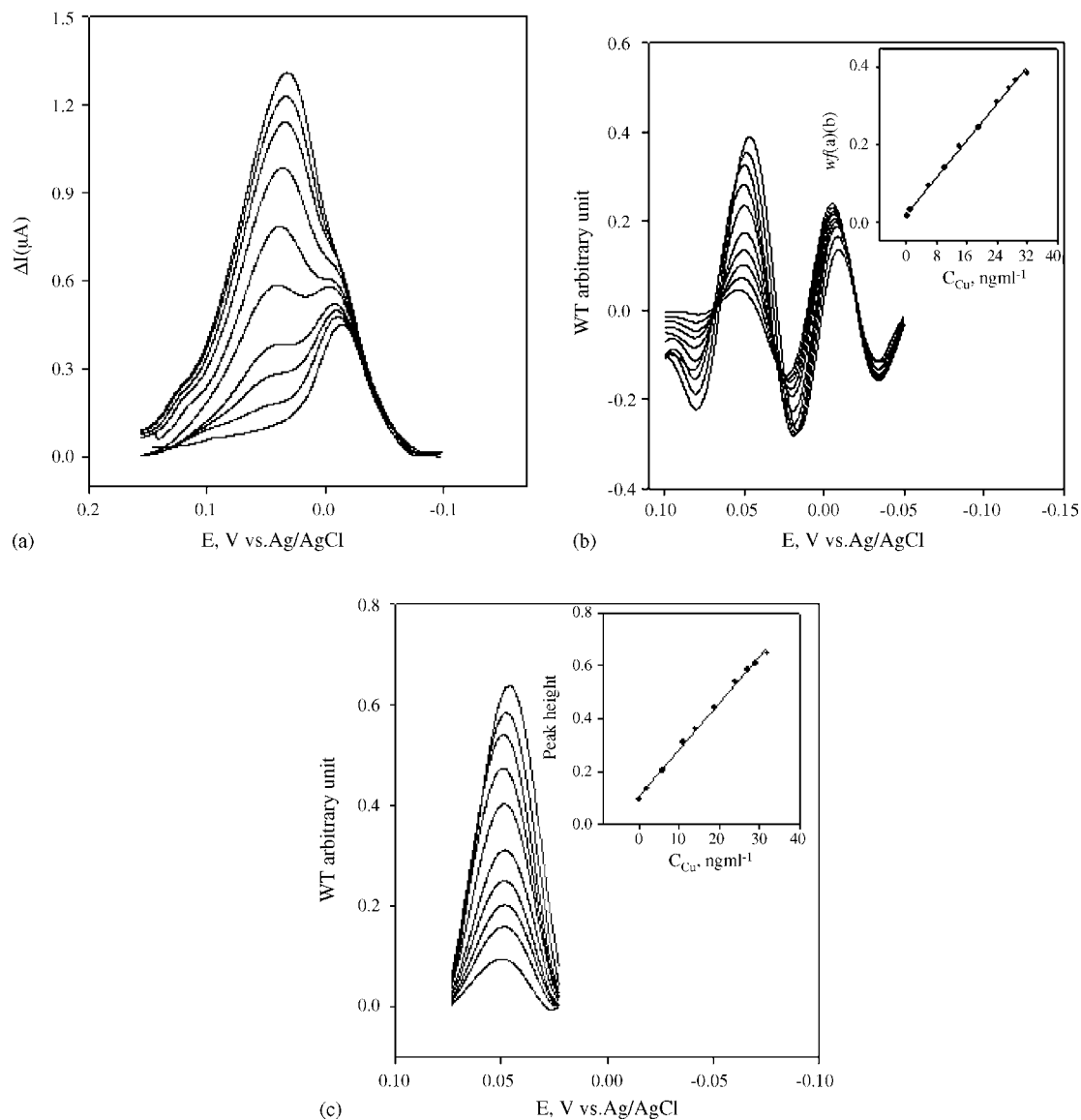


Fig. 6. (a–c) Individually show the DPSV, corresponding wavelet transform without baseline correction and baseline correction, respectively, to quantify Cu(II) in a solution containing  $8.0 \text{ ng ml}^{-1}$  Bi(III). The inset figures show the corresponding peak heights vs. Cu(II) concentration.

Table 4  
Recovery percentage of Bi(III)<sup>a</sup> and Cu(II)<sup>b</sup> in synthetic samples

Sample	Actual ( $\text{ng ml}^{-1}$ )		Found ( $\text{ng ml}^{-1}$ )		Recovery (%)
	Cu(II)	Bi(III)	Cu(II)	Bi(III)	
1	8.0	6.0	–	$5.89 \pm (0.24)$	98.2
	8.0	20.0	–	$19.20 \pm (0.62)$	96.0
2	24.0	9.0	–	$8.71 \pm (0.34)$	96.7
	24.0	20.0	–	$19.22 \pm (0.57)$	96.1
3	3.0	10.0	$2.94 \pm (0.08)$	–	98.0
	20.0	10.0	$20.28 \pm (0.71)$	–	101.4
4	3.0	20.0	$2.91 \pm (0.07)$	–	97.0
	20.0	20.0	$19.84 \pm (0.59)$	–	99.2

<sup>a</sup> Standard addition method.

<sup>b</sup> Calibration curve.

Table 5  
Interference study for determination of Cu(II) and Bi(III) under optimized condition

Species	Tolerance limit
Zn(II), Ni(II), Co(II), Ba(II), Mg(II), Na <sup>+</sup> , K <sup>+</sup> , Ag <sup>+</sup> , Ca(II), Mn(III), NO <sub>3</sub> <sup>-</sup> , SO <sub>4</sub> <sup>2-</sup> , Br <sup>-</sup> , Cl <sup>-</sup> , CN <sup>-</sup> , SCN <sup>-</sup> , Fe(II), Fe(III), Mo(VI), W(VI)	500
In(III), ClO <sub>4</sub> <sup>-</sup> , Hg(II), V(III), Cr(III)	300
Al(III), Cd(II), Pb(II)	200

Table 6  
Determination of copper and bismuth in real samples

Sample	Found (ng ml <sup>-1</sup> )		Added (ng ml <sup>-1</sup> )		Found (ng ml <sup>-1</sup> )		Recovery (%)	
	Cu(II)	Bi(III)	Cu(II)	Bi(III)	Cu(II)	Bi(III)	Cu(II)	Bi(III)
Tap water	3.1	–	3.0	2.0	6.0	2.1	98.4	105.0
River water	7.1	0.3	3.0	2.0	9.8	2.3	97.0	99.0
Human hair1 <sup>a</sup>	8.3	0.6	3.0	2.0	11.0	2.5	97.3	96.1
Human hair2 <sup>a</sup>	5.7	0.8	3.0	2.0	8.0	2.7	96.3	96.4

<sup>a</sup> μg g<sup>-1</sup>.

human hair samples. The Cu(II) and Bi(III) contents in water samples were determined after filtering without more preparation. Hair samples were digested as follow and then analyzed by the proposed method. About 5.0 g of hair samples were washed with water, immersed in ethanol for 1 h and then rinsed with double distilled water several times, dried at 110 °C and then weighed. The samples were placed in crucible and heated gradually in a furnace at 250 °C for 1 h and at 600 °C for 1.5 h and then cooled. They were dissolved in 2.0 ml of hot HCl (1:1), then transferred to a 50 ml volumetric flask, and diluted to marker. A suitable volume of samples was transferred into a cell for determination of copper and bismuth by the proposed method.

No bismuth was detected in water samples so they were spiked with appropriate amounts of Bi(III). The results are collected in Table 6. As results show, the recoveries of spiked samples are very good and indicate that the proposed method is feasible for the determination of Bi(III) and Cu(II) in various matrixes.

## 5. Conclusion

In this paper we have shown that chromazurol-S is a useful ligand for the highly sensitive determination of Bi(III) and Cu(II) by adsorptive stripping voltammetry on HMDE. However, copper is an interfering element because, its voltammogram overlap with the bismuth voltammogram and this element has a matrix effect on bismuth determination. Cu(II) generally considers as a major interference on the determination of Bi(III) by voltammetric methods, since Bi(III) peak may be easily overlapped or even shielded by the peak of copper. Therefore, it is very important to be able to measure Bi(III) concentration in presence of Cu(II). Thomsen and co-workers [14] used an excess amount of iodide in deposition medium to overcome the interference of copper on a chemically modified electrode. However, it is not possible to determine copper by this method. Hajian and Shams used different concentration of ligand and accumulation potential for sequential determination of copper and bismuth [13]. Here, we

used CWT to extract the individual peaks from the severe overlapped DPSV of Bi(III) and Cu(II) without change the medium, adding any chemical or any pretreatment of sample. The proposed method, was used for determination of copper and bismuth in the presence of each other. The best variable (wavelet filter and dilation) was selected to obtain the best separation of voltammogram and minimum detection limit. Although, a dilation range can be selected to perform CWT but, in this study single dilation was used to improve limit of detection for bismuth determination and to simplify the software have been written for deconvolution of voltammograms and plotting calibration curves. The proposed baseline correction is another way to improve sensitivity and detection limit. The obtained results for real samples analysis show that standard addition method couple with CWT is a very good tool for determination of Bi(III) and Cu(II) in presence of each other.

## Acknowledgements

The authors gratefully acknowledge the support of this work by the Isfahan University of Technology, Sensor excellency. The authors also thanks for Dr. Sadrei and Mr. Saidei for their helpful guides.

## References

- [1] P.J. Sadler, J. Inorg. Biochem. 67 (1997) 4.
- [2] L.B. Yang, J. Eshraghi, R. Fassihi, J. Control. Release 57 (1999) 215.
- [3] D.W. Thomas, in: E. Merin (Ed.), Metals and Their Compounds in the Environment, VCH, Weinheim, 1991, p. 789.
- [4] E.I. Stiefel, Science 272 (1996) 1599.
- [5] B. Venngopal, T.D. Luckey, Metal Toxicology in Mammals, vol. 2, Plenum Press, New York, 1978.
- [6] K. Giao, W. Jin, H. Metzger, Anal. Chim. Acta 260 (1992) 35.
- [7] Y.C. Sun, J. Mierzwa, C.R. Lan, Talanta 52 (2000) 417.
- [8] J.M. Zen, M.J. Chung, Anal. Chim. Acta 320 (1996) 43.
- [9] J. Limson, T. Nyokong, Anal. Chim. Acta 344 (1997) 87.
- [10] M.H. Pournaghi-Azar, D. Djozan, H. Abdolmohammadzadeh, Anal. Chim. Acta 437 (2001) 217.

- [11] H.Y. Yang, W.Y. Chen, I.W. Sun, *Talanta* 50 (1999) 977.
- [12] H. Guo, Y. Li, P. Xiao, N. He, *Anal. Chim. Acta* 534 (2005) 143.
- [13] R. Hajian, E. Shams, *Anal. Chim. Acta* 491 (2003) 63.
- [14] K.L. Dong, L. Kryger, J.K. Christensen, K.N. Thomsen, *Talanta* 38 (1991) 101.
- [15] D. Ozdenir, R.R. Williams, *Appl. Spectrosc.* 51 (1997) 749.
- [16] M.L. Phillips, R.L. White, *J. Chromatogr. Sci.* 35 (1997) 175.
- [17] R.S. Jackson, P.R. Griffiths, *Anal. Chem.* 63 (1991) 2557.
- [18] S.R. Gallant, S.P. Fraleigh, S.M. Cramer, *Chemom. Intell. Lab. Syst.* 18 (1993) 41.
- [19] F.C. Sanchez, S.C. Ruran, M.D.G. Garcia, D.L. Massart, *Chemom. Intell. Lab. Syst.* 36 (1997) 153.
- [20] J.B. Zheng, H.Q. Zhang, H. Cao, *Sci. China (B)* 43 (2000) 1–9.
- [21] T.R. Griffiths, K. King, H. Hubbard, M.J. Schwingwiell, J. Meullestre, *Anal. Chim. Acta* 143 (1982) 163.
- [22] R.S. Jackson, P.R. Griffiths, *Anal. Chem.* 63 (1991) 2557.
- [23] X.Q. Zhaeng, H. Gao, *Anal. Chim. Acta* 443 (2001) 117.
- [24] L. Nie, S.G. Wu, J.W. Wang, L.Z. Zheng, X. Lin, L. Rui, *Anal. Chim. Acta* 450 (2001) 185.
- [25] L. Xiaoquan, L. Hongde, X. Zhonghua, Z. Qiang, *J. Chem. Inf. Comput. Sci.* 44 (2004) 1228.
- [26] B.K. Alsberg, A.M. Woodward, D.B. Kell, *Chemom. Intell. Lab. Syst.* 37 (1997) 215.
- [27] A.K. Melung, F.T. Chau, J.B. Gao, *Chemom. Intell. Lab. Syst.* 43 (1998) 165.
- [28] B. Walczak (Ed.), *Wavelet in Chemistry*, Elsevier Science Publishers B.V., 2000.
- [29] C. Cai, P.D.B. Harrington, *J. Chem. Inf. Comput. Sci.* 38 (1998) 1161–1170.

## Potentiometric measurements in sequential injection analysis lab-on-valve (SIA-LOV) flow-system

Timo Kikas<sup>b</sup>, Ari Ivaska<sup>a,\*</sup>

<sup>a</sup> *Process Chemistry Centre, c/o Laboratory of Analytical Chemistry, Åbo Akademi University, FIN-20500 Turku-Åbo, Finland*

<sup>b</sup> *Institute of Physical Chemistry, Tartu University, Tartu, Estonia*

Received 4 November 2005; received in revised form 23 February 2006; accepted 20 March 2006

Available online 9 May 2006

### Abstract

Advantages of using sequential injection analysis lab-on-valve (SIA-LOV) in potentiometric measurements are studied with Ca<sup>2+</sup> sensitive solid-contact ion-selective electrodes (SC-ISE) and pH electrode based on polyaniline (PANI). Experiments show that Ca<sup>2+</sup>-SC-ISE requires a stopped flow mode to be used in order to get longer equilibration time. On the other hand, PANI based pH electrode gives better results under flow conditions. SIA-LOV was found to be a flexible solution handling system for potentiometric measurements. The technique gives a possibility to fine-tune the calibration range or even recondition the electrode before every measurement without losing in linear range of calibration.

© 2006 Elsevier B.V. All rights reserved.

*Keywords:* Sequential injection; Lab-on-valve; Ion-selective electrodes

### 1. Introduction

Ion-selective electrodes (ISEs) are widely used in variety of analytical applications [1–3]. Applications range from clinical to industrial and environmental analysis and include both organic and inorganic ions as targets [4–6]. Conventional ISEs are based on an ion-selective membrane containing ionophores that have affinity to specific ions. The membrane has to contain also some other components in order to allow a potential to be developed at the membrane/sample solution interface [2]. However, this is not the only construction of ISE that is possible. There are ISEs based on conducting polymers [7] and even some conducting polymers themselves have selectivity to certain kind of ions, e.g. polyaniline (PANI) is sensitive to pH [8,9]. PANI has three different oxidation states and the emeraldine salt (ES) form is in pH equilibrium with the emeraldine base form (EB) giving the sensitivity to H<sup>+</sup> ions. ES is the electrically conducting form of PANI. The protonation process is rather reversible and therefore PANI can be used as pH sensitive material in solid-state pH-ISE [9].

One of the complications in conventional potentiometric measurements is solution handling. The experiments are normally done manually and are therefore rather time consuming. One practical way to solve the problem with solution handling is to use a flow injection analysis (FIA) instrument. FIA is a powerful tool for many kind of solution handling problems. Modern versions of FIA instruments like sequential injection analysis (SIA) and lab-on-valve (LOV) are based on small volumes and confined spaces [10]. Therefore, they require miniaturization of the sensing system and often also the ability to use it in a non-vertical position. Conventional ISEs with internal solution are difficult to miniaturize and to use them in a non-vertical position create additional practical problems. However, in the concept of solid-contact ion-selective electrode (SC-ISE) the internal reference electrode and solution have been replaced by a layer of conducting polymer which functions as the ion-to-electron transducer [11,12]. By using the SC-ISE concept the electrode can be both miniaturized and used in any position imaginable. Therefore, using SC-ISE with SIA-LOV makes an ideal combination of the methods and uses the best characteristics of both of them.

The objective of this work is to demonstrate the use of miniaturized all-solid-state electrodes in potentiometric measurements with the SIA-LOV system.

\* Corresponding author. Tel.: +358 2 215 4420; fax: +358 2 215 4479.  
E-mail address: [ari.ivaska@abo.fi](mailto:ari.ivaska@abo.fi) (A. Ivaska).



## 2. Experimental

### 2.1. Chemicals

The monomer 3,4-ethylenedioxythiophene (EDOT, trade name: Baytron M) was obtained from Bayer AG (D-51368, Leverkusen, Germany). Poly(sodium-4-styrenesulfonate) (NaPSS) (MW ~70,000) was obtained from Aldrich. Aniline was obtained from Baker and distilled before use. ETH 1001, ETH 500, *o*-nitrophenyloctylether (*o*-NPOE), poly(vinylchloride), potassium tetrakis(4-chlorophenyl)borate, and KCl were obtained from Fluka. All reagents were analytical-reagent grade. HPLC grade tetrahydrofuran (THF) was obtained from lab-scan analytical sciences. All aqueous solutions were prepared from distilled deionized water with resistance  $\geq 18.2 \text{ M}\Omega$ .

### 2.2. Solid-contact $\text{Ca}^{2+}$ ionselective electrodes (ISE)

Solid-contact  $\text{Ca}^{2+}$ -ion-selective electrodes were prepared on glassy carbon (GC) electrode (diameter 1 mm) by first depositing a poly(3,4-ethylenedioxythiophene) (PEDOT) film as a solid contact material on the GC substrate. The PEDOT film was electrochemically polymerized by cyclic voltammetry in deaerated 0.01 M 3,4-ethylenedioxythiophene (EDOT) solution using 0.1 M poly(sodium-4-styrenesulfonate) (NaPSS) (MW ~70,000) as the supporting electrolyte. Electropolymerization was performed in 20 cycles at 50 mV/s in the potential range from  $-0.2$  to  $0.84 \text{ V}$  against the Ag/AgCl/3 M KCl reference electrode. A GC rod was used as the auxiliary electrode. Electrochemical polymerization was done by using an Autolab General Purpose Electrochemical System (AUT20.FRA2-Autolab, Eco Chemie B.V., The Netherlands) and a conventional one-compartment three-electrode electrochemical cell. Prior to the electropolymerization process, the GC working electrode was polished with  $0.3 \mu\text{m}$  alumina, rinsed thoroughly with deionized water and ultrasonicated for at least 15 min. Resulting GC/PEDOT(PSS) electrodes were conditioned in a 0.1 M  $\text{CaCl}_2$  solution for at least 24 h before further use. This process was found to be useful to incorporate  $\text{Ca}^{2+}$  in the PEDOT(PSS) film.

The GC/PEDOT(PSS) electrodes were then coated with ion-selective membrane. The solutions used for casting the ion-selective membranes were 15–18% dry fraction (DF) solutions in tetrahydrofuran (THF), where DF contained 65.5% polar plasticizer (*o*-nitrophenyloctylether), 32.5% polymer (poly(vinylchloride) (PVC)), 0.94% ionophore (ETH1001), 0.33% ion-exchanger (potassium tetrakis(4-chlorophenyl)borate) (KTPCIPB), 0.75 % background electrolyte (ETH 500) [6]. The casting solution was applied on the upside turned working electrodes and the solvent was evaporated and a dry film was formed on top of the working electrode. The resulting  $\text{Ca}^{2+}$  solid-contact ISE was conditioned in 0.1 M  $\text{CaCl}_2$  solution for at least 24 h prior to use.

The SIA-LOV experiments were carried out by injecting  $\text{Ca}^{2+}$  solutions with different concentrations into carrier stream of the background electrolyte solution (0.1 M KCl). Volume of the injected sample was  $300 \mu\text{L}$ . All  $\text{Ca}^{2+}$  standard solutions were also made in the same background electrolyte solution to avoid

any differences in ionic strength of the sample and the carrier solutions. Samples were delivered into the measurement cell by propelling the carrier solution through the SIA-LOV system. In the stopped flow experiments sample plugs were stopped in the measurement cell for longer equilibration times. At the end of each experiment the sample plug was discarded into waste.

### 2.3. Solid-state pH electrodes based on polyaniline

Potentiometric solid-state pH electrodes were prepared on a platinum rod (diameter  $300 \mu\text{m}$ ) by depositing a film of PANI on the Pt surface. The films were deposited by cyclic voltammetry in deaerated 0.05 M aniline solution using 1.0 M HCl as the supporting electrolyte. The PANI film was deposited during 200 cycles at 50 mV/s in the potential range from  $-0.2$  to  $0.84 \text{ V}$  against the Ag/AgCl/3 M KCl reference electrode. A GC rod was used as the auxiliary electrode. Instrumentation was the same as in the PEDOT polymerization experiment. Prior to coating, the Pt working electrode was polished with  $0.3 \mu\text{m}$  alumina, rinsed thoroughly with deionized water and ultrasonicated for at least 15 min. Resulting Pt/PANI electrodes were conditioned in 1.0 M HCl solution for at least 24 h before further use.

In the pH experiments the standard solutions were made of universal buffer (25 mM solution of each of the following components: citric acid,  $\text{KH}_2\text{PO}_4$ , sodium tetraborate, Tris and KCl). HCl or NaOH was added to adjust the pH value of the buffer solution. Standard solutions ranged from pH 2–10. Volume of injected sample was  $300 \mu\text{L}$ . In SIA-LOV experiments the carrier was usually universal buffer solution with neutral pH. In the experiments where carrier effect was considered, the carrier solution was changed to 1.0 M HCl, universal buffer solution with pH = 2, or universal buffer solution with pH = 10.

### 2.4. SIA-LOV set-up

The sequential injection analysis lab-on-valve (SIA-LOV) set-up was configured as shown on Fig. 1. FIALab 3000 system (from FIALab instruments) was used as a basic solution handling unit and the measurements were done in the lab-on-valve unit (from FIALab instruments). Both the indicator and reference electrodes are tailor made to fit in the canals of the LOV. The working electrode is placed in the canal adjacent to the sample inlet in order to have the best contact with the sample. The reference electrode is placed next to the outlet from LOV and should always be placed upstream from the working electrode to avoid disturbances from the leaking electrolyte. The inlet and outlet of the measurement cell were electrically grounded to avoid the streaming potential buildup. Potentials were measured with a conventional potentiometer.

## 3. Results and discussion

### 3.1. $\text{Ca}^{2+}$ solid-contact ISE

Preliminary experiments with  $\text{Ca}^{2+}$  ISEs in SIA-LOV showed the importance of using grounding of the measurement cell (see Fig. 1) due to buildup of streaming potential. It was also

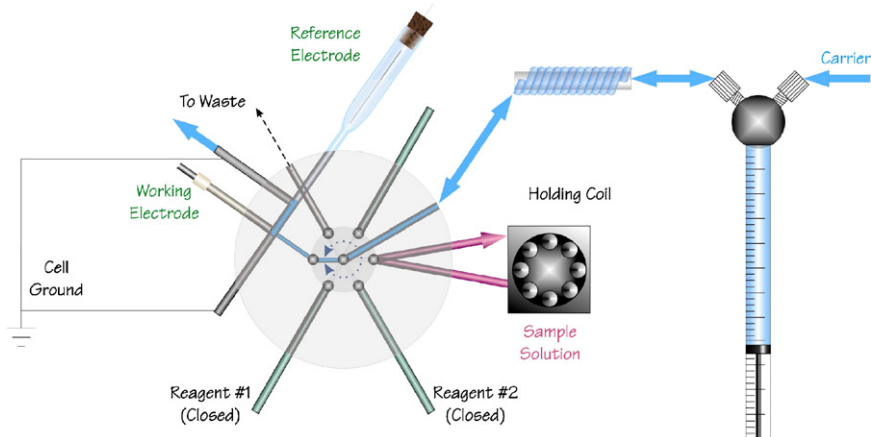


Fig. 1. Experimental set-up of the SIA-LOV instrument for potentiometric experiments with a solid state ISE.

found that although the primary response (3 s to reach 90% signal) to  $\text{Ca}^{2+}$  was fast, it still required longer time to reach the equilibrium potential. Continuous flow did not allow proper equilibration and moreover, the baseline of continuous flow measurements was not stable either. Stopped-flow technique, however, showed good reproducibility and reasonable linear range (see Fig. 2) as this technique gives ion selective mem-

brane enough time for reaching equilibrium with the sample solution.

In the sequence of stopped flow experiments the measurement cell was washed with the carrier electrolyte in the beginning of each measurement cycle. The syringe was filled with carrier solution, syringe valve position was changed toward the LOV and the sample was aspirated into the holding coil through the sample port. Next, the LOV port was changed to the measurement cell position and the sample was pushed from holding coil into the cell. Flow was stopped at the moment when the maximum signal (concentration) was reached (this had earlier been determined with a trace curve) and was then kept stationary for 4 min. Finally the sample was pushed into waste to empty the cell for next cycle. The resulting response of Ca-ISE was slightly subnernstian (with the slope of 25.0 mV/decade). The linear calibration range extended from  $10^{-1}$  to  $10^{-4}$  M, which does not deviate much from the range achieved in batch measurements with conventional Ca-ISEs. The sampling rate in this study was 10 samples/hour but the maximum rate would be 20 samples/h.

### 3.2. Solid-state pH electrode

The PANI based solid-state pH electrode measurements in the stopped flow system did not show the same stable response as the measurements with Ca-ISEs. Although the PANI-pH electrode showed fast response on the sample solution entering into the cell, the signal, however, started to decrease when the flow was stopped. This is obviously due to formation of a depletion layer near the PANI membrane as  $\text{H}^+$  ions are consumed in the reaction between the PANI membrane and the sample solution. Unlike Ca-ISE though, it showed a well-developed response under the continuous flow conditions (Fig. 3). This can be attributed to the different potential formation mechanisms in the two electrodes studied. In both cases the potential is formed due charge separation at the solution/membrane interface. In the PANI-pH electrode the change in pH at the surface of the membrane results in a fast change in the pH controlled emeraldine salt (ES)–emeraldine base (EB) equilibrium in the surface region of the PANI membrane whereas the response in the Ca-ISE is due

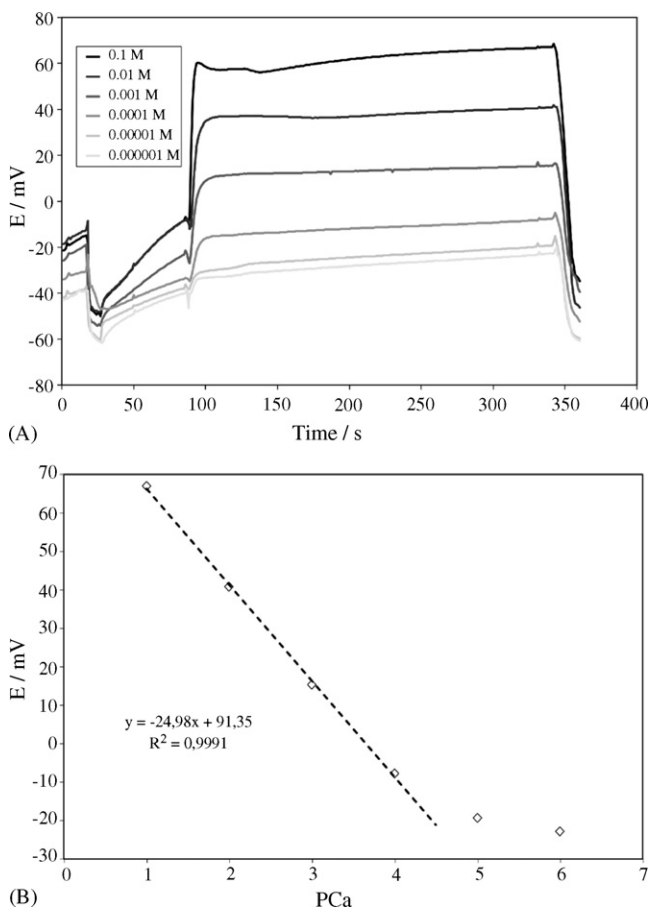


Fig. 2. Calibration curve of the  $\text{Ca}^{2+}$  sensitive SC-ISE in the SIA-LOV system. (A) Shows the time series of experiments with different concentrations and (B) resulting in linear calibration graph. Sample size was  $300 \mu\text{L}$ , carrier solution was 0.1 M KCl and stopped flow regime was used.

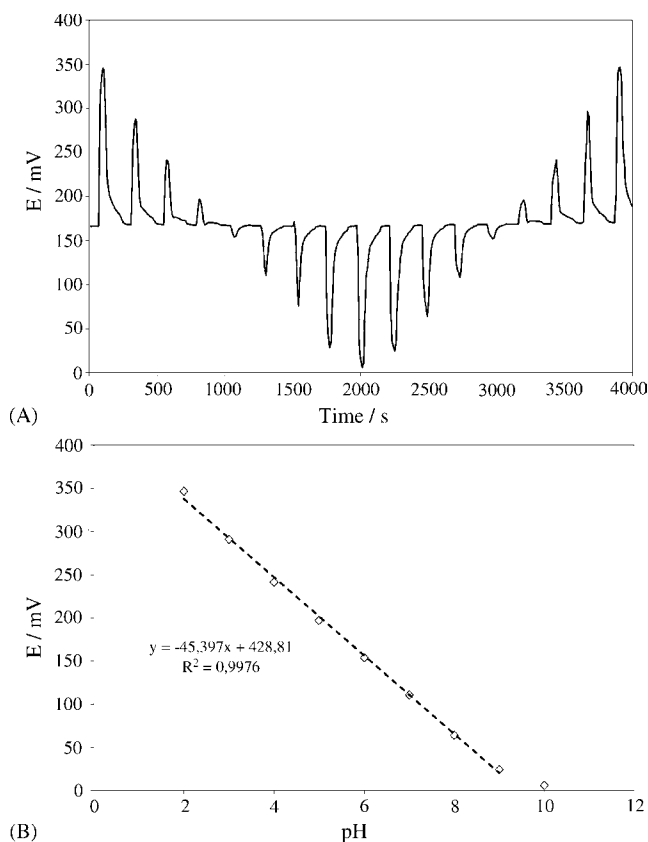


Fig. 3. Calibration of pH sensitive SC-ISE in SIA-LOV system. (A) Shows the timeseries of the experiment and (B) resulting linear calibration graph. Sample size was  $300 \mu\text{L}$ , carrier solution was neutral ( $pH=6$ ) universal buffer and continuous flow regime was used.

to the equilibrium between  $\text{Ca}^{2+}$  in the ionophore complex in the membrane and in the solution phase.

### 3.3. Effect of the carrier

In the continuous flow measurements with the PANI-pH electrode it was noticed that the linear part of the calibration curve and its upper and lower limits varied depending on the  $pH$  of the carrier solution. In the cases when the buffer solution with low  $pH$  ( $pH=2$ ) was used as the carrier the linear range shifted to lower  $pH$  values as well. In the cases when the buffer solution with midrange  $pH$  ( $pH=6$ ) was used the linear range was longest and in the middle of the  $pH$  scale. Cases when alkaline buffer was used as the carrier solution ( $pH=10$ ) rendered two linear ranges—one with subnernstian ( $40.6 \text{ mV/pH}$ ) and other with supernernstian ( $69.8 \text{ mV/pH}$ ) slope value (Fig. 4). Furthermore, when acidic carrier solution (buffer with  $pH=2$  or  $1.0 \text{ M HCl}$ ) was used it was noticed that the peaks did not have a normal plateau type shape that is expected when large sample volumes were used, i.e. quasi steady state response was reached. In fact, the larger was the difference in  $pH$  between the sample the carrier solution the more a peak shape response was observed. It was also noticed that the response peaks at higher sample  $pH$  values did not reach a plateau at all but rather the signal kept rising till the end of the sample plug. Volume of the injected sample was

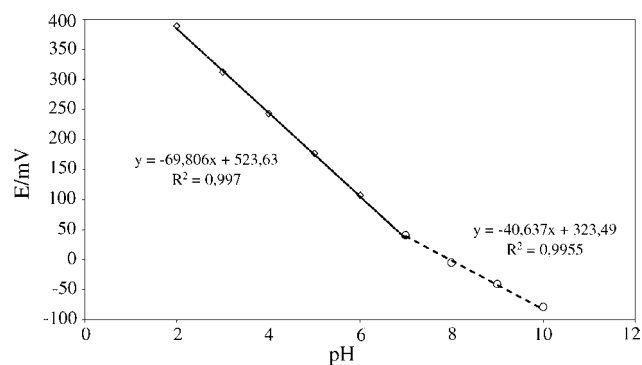


Fig. 4. Calibration of PANI pH electrode in SIA-LOV system with basic ( $pH=10$ ) buffer as a carrier solution. The squares show concentrations that fall into linear region with supernernstian slope and the circles concentrations that fall into linear region with subnernstian slope. Sample size was  $300 \mu\text{L}$ , carrier solution was basic ( $pH=10$ ) universal buffer and continuous flow regime was used.

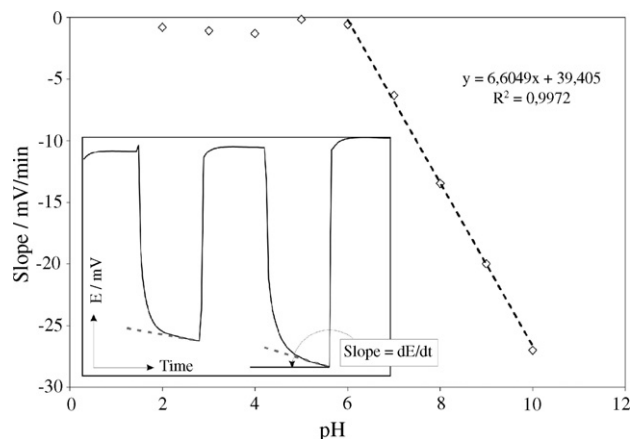


Fig. 5. Calibration of PANI pH electrode in SIA-LOV system with acidic carrier solution ( $1.0 \text{ M HCl}$ ) using the slope of the peak as a parameter. Sample size was  $300 \mu\text{L}$ , carrier solution was  $1.0 \text{ M HCl}$  and continuous flow regime was used. The inset shows slope determination from the peak.

$300 \mu\text{L}$ . Therefore, each peak had different final rising slope (see Fig. 5. insert), specifically in the higher  $pH$  region. The exact mechanism of signal formation is not clear yet. The response time of the PANI electrode is rather fast, about  $1 \text{ s}$  to reach  $90\%$  of the steady state signal, and therefore we can assume that the shape of the peak is entirely due to dispersion of the sample plug. The final slopes of the increase in the response, change in potential in time, were calculated. When the final slopes of the peaks were plotted against the corresponding  $pH$  values the calibration curve given in Fig. 5 was observed. This shows that it is possible to use the kinetics of the response as a parameter in order to prolong the linear range of the measurements. This is made possible by the high reproducibility of the solution handling in the SIA systems. The sampling rate in this study was  $16 \text{ samples/h}$  but the maximum rate would be  $30 \text{ samples/h}$ .

## 4. Conclusions

It was shown that SIA-LOV as the solution-handling and automation system gives additional possibilities in

potentiometric measurements compared with the conventional batch method. Ca-SC-ISE used in the system showed similar linear range as that of the conventional method but with minimized work and higher sample throughput. Although the stopped flow method had to be used in order to obtain better results the measurement time is still in the same time span as in the case of conventional method where at least couple of minutes are needed to reach a stable potential reading. Furthermore, in the case of SIA-LOV the sample intake and cell washing stages of the experiment can also be used to recondition the Ca-SC-ISE. Thus every following sample is measured by a freshly reconditioned electrode that further equalizes the starting-point for each sample and minimizes the possibility for hysteresis in the measurements.

In the case of PANI based pH electrode the advantages are even more obvious with measurements in the continuous flow system. Similarly to Ca-SC-ISE, sample intake and cell washing stages of the experiment can be used to recondition the electrode in the original conditioning solution or condition it in the carrier solution for some specific pH range. By choosing 1.0 M HCl as the carrier solution the PANI sensor can be reconditioned between each measurement to its original electronic state. Furthermore, the carrier solution can be chosen with the specific pH value that falls in the middle of the pH range of interest thus maximizing the performance in that range.

Further, experiments showed that reconditioning the PANI pH electrode between each sample with the original conditioning solution (1.0 M HCl) rendered peaks with a different final slope. When that slope was plotted against pH it showed a linear relationship. Therefore, it may also be used as a parameter to extend the linear region of the PANI pH electrode.

Reproducibility of the measurements was 2–5% with both Ca<sup>2+</sup> electrodes and pH(PANI) electrodes when done with physically different electrodes but prepared with the same procedure. Repeatability of the electrode signal between different injections

was about 1%. These results show that potentiometric measurements can well be used with the SIA-LOV technique.

As demonstrated in this work all-solid-state electrodes can conveniently be used in the SIA-LOV system. Use of conventional ISEs would be more difficult and very unpractical. In general it can be stated that one of the main advantages of using the SIA-LOV in potentiometric measurements is the increase in the sample throughput compared with the conventional batch measurement system.

### Acknowledgement

This work is part of the activities at the Åbo Akademi Process Chemistry Centre within the Finnish Centre of Excellence Program (2000–2005) by the Academy of Finland.

### References

- [1] Y. Umezawa, *CRC Handbook of Ion-Selective Electrodes: Selectivity coefficients*, CRC Press, Boca Raton, 1990.
- [2] E. Bakker, P. Buehlmann, E. Pretsch, *Chem. Rev.* 97 (1997) 3083.
- [3] P. Buehlmann, E. Pretsch, E. Bakker, *Chem. Rev.* 98 (1998) 1593.
- [4] E. Bakker, D. Diamond, A. Lewenstam, E. Pretsch, *Anal. Chim. Acta* 393 (1999) 11.
- [5] J. Bobacka, T. Alaviuhkola, V. Hietapelto, H. Koskinen, A. Lewenstam, M. Lämsä, J. Pursiainen, A. Ivaska, *Talanta* 58 (2002) 341.
- [6] M. Vazquez, K. Mikhelson, S. Piepponen, J. Rämö, M. Sillanpää, A. Ivaska, A. Lewenstam, J. Bobacka, *Electroanalysis* 13 (2001) 1119.
- [7] J. Bobacka, A. Ivaska, A. Lewenstam, *Electroanalysis* 15 (2003) 366.
- [8] A.A. Karyakin, M. Vuki, L.V. Lukachova, E.E. Karyakina, A.V. Orlov, G.P. Karpachova, J. Wang, *Anal. Chem.* 65 (1999) 2534.
- [9] T. Lindfors, A. Ivaska, *J. Electroanal. Chem.* 531 (2002) 43.
- [10] J. Ruzicka, *Analyst* 125 (2000) 1053.
- [11] A. Cadogan, Z. Gao, A. Lewenstam, A. Ivaska, D. Diamond, *Anal. Chem.* 64 (1992) 2496.
- [12] J. Bobacka, T. Lindfors, A. Lewenstam, A. Ivaska, *Am. Lab.* 36 (2004) 13.

# Improvement of an enzyme electrode by poly(vinyl alcohol) coating for amperometric measurement of phenol

Gha-Young Kim, Nguyen Manh Cuong, Seung-Hee Cho,  
Joonmok Shim, Jung-Je Woo, Seung-Hyeon Moon\*

*Department of Environmental Science and Engineering, Gwangju Institute of Science & Technology (GIST),  
1 Oryong-dong, Buk-gu, Gwangju 500-712, South Korea*

Received 12 January 2006; received in revised form 16 March 2006; accepted 16 March 2006  
Available online 12 May 2006

## Abstract

A poly(vinyl alcohol) film cross-linked with glutaraldehyde (PVA–GA) was introduced to the surface of a tyrosinase-based carbon paste electrode. The coated PVA–GA film was beneficial in terms of increasing the stability and reproducibility of the enzyme electrode. The electrode showed a sensitive current response to the reduction of the *o*-quinone, which was the oxidation product of phenol, by the tyrosinase, in the presence of oxygen. The effects of the PVA and PVA–GA coating, the pH, and the GA:PVA ratio on the current response were investigated. The sensitivity of the PVA–GA–Tyr electrode was 130.56  $\mu\text{A}/\text{mM}$  (1.8  $\mu\text{A}/\mu\text{M cm}^2$ ) and the linear range of phenol was 0.5–100  $\mu\text{M}$ . At a higher concentration of phenol (>100  $\mu\text{M}$ ), the current response showed the Michaelis–Menten behavior. Using the PVA–GA–Tyr electrode, a two-electrode system was tested as a prototype sensor for portable applications.

© 2006 Elsevier B.V. All rights reserved.

**Keywords:** Tyrosinase; Poly(vinyl alcohol); Glutaraldehyde; Carbon paste electrode; Phenol

## 1. Introduction

Phenol and substituted phenols are widely generated and used in many industries. Due to their toxicity, analytical methods, such as liquid chromatography, gas chromatography, and capillary electrophoresis, were developed to measure them [1–3]. These methods are sensitive and specific but expensive and time-consuming. Using an electrochemical biosensor, however, it is possible to detect them selectively and rapidly, since it is working at a relatively low potential compared to the direct amperometric detection [4] and at a low cost of preparation and storage with the potential for miniaturization and automation. Many types of tyrosinase (Tyr) electrodes have been studied for a long time to prepare a phenol-detecting sensor in a wide variety of matrices, including carbon paste [3,5–10,17,18], nafion membrane [11], PVI-Os redox hydrogel [12], graphite [13], conducting polymers [14,15], and biopolymers [16].

One of them, the carbon paste electrode, has many advantages, such as fast-charge transport and reasonable sensitivity, specificity, easy-to-handle, and durable detection and measurement of phenol and several *p*-substituted phenols [6,7]. Moreover, renewal and modification of the surface are easy, and the adhesion of the coating can be completed without difficulty [8].

There have been previous reports on the construction and operation of carbon paste electrodes for the enhancement of electrode performance. Marko-Varga et al. investigated the effect of the use of various oils, such as mineral, paraffin, and silicon [5]; Lutz et al. studied the addition of polymeric and small-molecular-weight compounds [9]; Lindgren et al. researched on the use of redox mediators [10]; and Wang et al. investigated the effects of short-chain hydrocarbon-binding liquids on the electrodes [6]. Moreover, Rogers et al. modified the electrodes with respect to the effect of the relative polarity or viscosity of the carbon paste electrode binders [3].

The main disadvantage of carbon paste electrodes, however, is their lack of stability, especially when they are exposed for a longer period or in the presence of organic solvents in the solution. To overcome this problem, the composite materials were modified with various polymeric materials, such as epoxy

\* Corresponding author. Tel.: +82 62 970 2435; fax: +82 62 970 2434.  
E-mail address: [shmoon@gist.ac.kr](mailto:shmoon@gist.ac.kr) (S.-H. Moon).



resins [17], silicone [18], Teflon [19], and polypyrrole [20], but they are complicated to prepare and handle and have a possibility to deactivate the enzyme activity and less wide detecting range than bare carbon paste electrode. Moreover, there are problems of the storage stability of the carbon paste electrodes as well as their working stability [5].

Poly(vinyl alcohol), a hydrophilic polymer, is frequently used in biomedical applications and protein immobilization. Besides its hydrophilicity, it forms hydrogels that are biocompatible and non-toxic. Due to its low price, easy availability, and chemical properties, it is applied in large areas [21]. It has a high swelling index, however, and it dissolves readily in water when not cross-linked [22]. This problem was solved with the use of  $\gamma$ -rays [22] and glutaraldehyde (GA) [23]. In this study, PVA was cross-linked with GA, after which the cross-linked PVA–GA film was introduced to the Tyr-based carbon paste electrode (PVA–GA–Tyr electrode) to modify and protect the electrode surface and to improve its storage and working stability. The PVA–GA–Tyr electrode was compared with a bare Tyr electrode and a PVA–Tyr electrode, and cyclic voltammetry (CV) and amperometry were measured to investigate the electrode performance and the enhanced stability.

## 2. Experimental methodology

### 2.1. Materials

Tyrosinase (Tyr, from mushrooms, EC 1.14.18.1, 50,000 units/mg), graphite powder, ferrocenemonocarboxylic acid, and mineral oil were used to prepare the carbon paste. Poly(vinyl alcohol) (PVA), glutaraldehyde (25 wt%), and 0.1 M  $\text{H}_2\text{SO}_4$  were used to make a PVA–GA film. A phosphate buffer solution (PBS, 0.1 M, pH 7) was prepared with  $\text{Na}_2\text{HPO}_4$  and  $\text{NaH}_2\text{PO}_4$  as the electrolytes. All the chemicals used in this study were analytical reagent grade and were supplied by Sigma–Aldrich (USA). All the solutions were prepared with Milli-Q water (18 M $\Omega$ ). The test solutions were saturated with oxygen by aeration.

### 2.2. Electrode preparation

The electrode materials were prepared by mixing tyrosinase, graphite powder, ferrocene–ormosil (organically modified silicate) powder [24], and mineral oil at a predetermined weight ratio. The ferrocene–ormosil powder was made following; first, methanol, 0.01 M HCl, methyltrimethoxysilane (MTMOS), 3-aminopropyltrimethoxysilane (APTOS), and ferrocene was mixed and then kept at room temperature for 24 h. After solidifying, the ferrocene–ormosil was grounded. In this procedure, the ferrocene was coated by ormosil layer and increased stability due to lower solubility while preserving the function as an electron transfer mediator. The mixed electrode material was immersed in the hole of the electrode body (BAS MF2010, diameter = 3 mm, USA), and the electrode surface was polished with a weighing paper. Then the electrode was stored overnight at 4 °C. PVA (0.5 g) was dissolved in 5 mL of distilled water by heating while it was stirred. When its color became transparent,

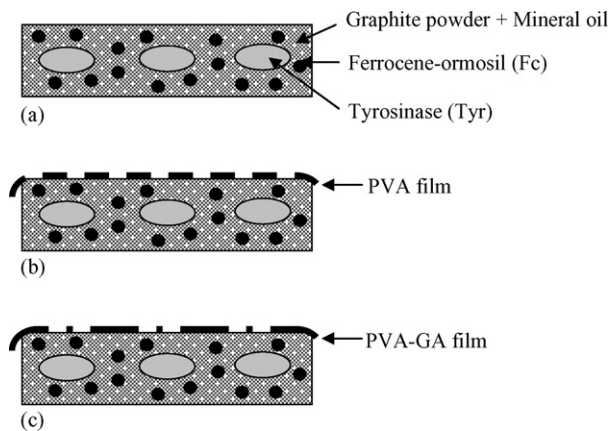


Fig. 1. Configuration of the Tyr-based carbon paste electrodes and electrode materials: (a) the bare Tyr electrode, (b) the PVA–Tyr electrode, and (c) the PVA–GA–Tyr electrode.

the heating was stopped and 1 mL of 0.1 M  $\text{H}_2\text{SO}_4$  and 1.5 mL of GA (25 wt%) were added to the PVA solution, then the solution was mixed well and cooled to room temperature. Afterwards, the electrode surface was coated with 10–30  $\mu\text{L}$  of the PVA–GA solution and solidified for one day at 4 °C. The configuration of the prepared Tyr electrodes and the structure of the cross-linked PVA [14] are shown in Figs. 1 and 2, respectively.

### 2.3. Electrochemical measurements

Electrochemical experiments were performed with a PGSTAT30/GPES system (Autolab, The Netherlands) and picoammeter (M 6487, Kiethley, USA). A three-electrode cell equipped with a platinum wire counter electrode, a silver/silver chloride (Ag/AgCl, model RE-1, BAS) reference electrode, and the prepared Tyr electrode as the working electrode was used for all the electrochemical experiments. A two-electrode system was operated with the prepared Tyr and reference electrode. The effective area of the working electrode was 0.07 cm<sup>2</sup>. All the experiments were performed at room temperature in 0.1 M PBS (pH 7) as the background electrolyte. The amperometric experiments were performed at an applied potential, which was investigated from the cyclic voltammetry measurement under well-mixed conditions. Before each measurement, the solution was saturated with oxygen by aeration.

## 3. Results and discussion

### 3.1. Current response of the bare Tyr electrode

Using the bare Tyr electrode, a cyclic voltammetry measurement was conducted with 1 mM of the phenol solution. As shown in Fig. 3, an anodic peak and a cathodic peak of phenol were observed at 0.9 and 0.2 V versus NHE, respectively. When phenol was added to the air-saturated PBS (0.1 M, pH 7), it was diffused to the electrode and oxidized not only by electrochemical reaction but also by enzymatic reaction. The electrochemical oxidation of phenol occurred at 0.9 V versus NHE ( $E_{\text{pa}}$ ), and the anodic peak current ( $I_{\text{pa}}$ ) was linearly correlated with the (scan

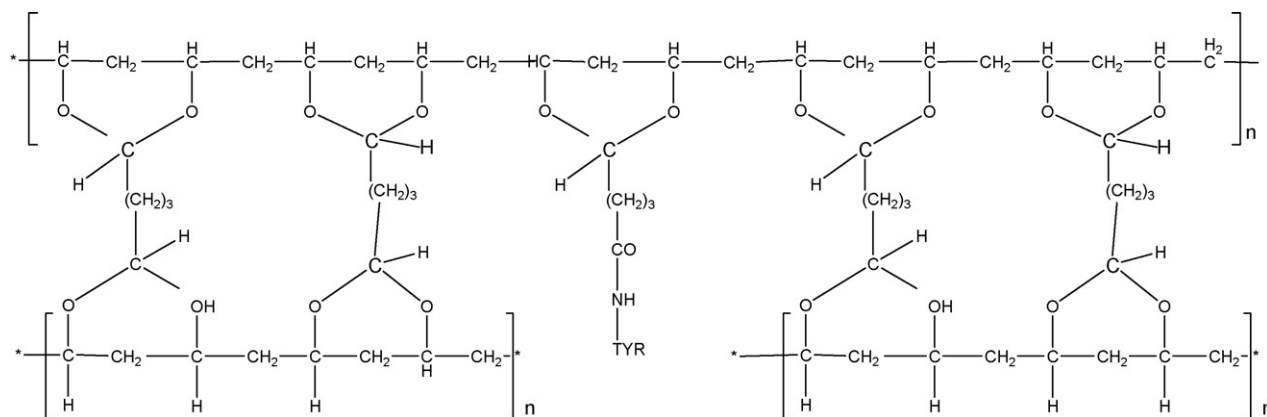


Fig. 2. Structure of the GA-cross-linked PVA and Tyr.

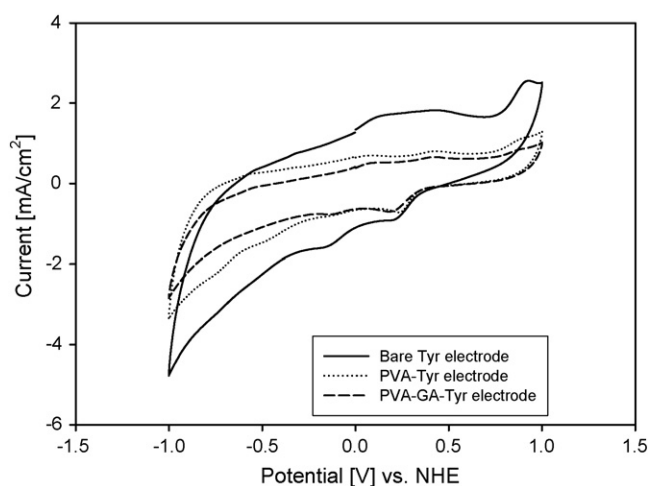


Fig. 3. Cyclic voltammograms of the bare Tyr, PVA-Tyr, and PVA-GA-Tyr electrodes with 1 mM phenol to air-saturated PBS (0.1 M, pH 7) at 25 mV/s.

rate)<sup>1/2</sup>, which indicates the diffusion limitation phenomenon (data not shown). The enzymatic oxidation was identified with the appearance of the cathodic peak, which was due to the reduction of oxidized product through enzymatic reaction, at 0.2 V versus NHE ( $E_{pc}$ ). The reaction mechanism is shown in Fig. 4.

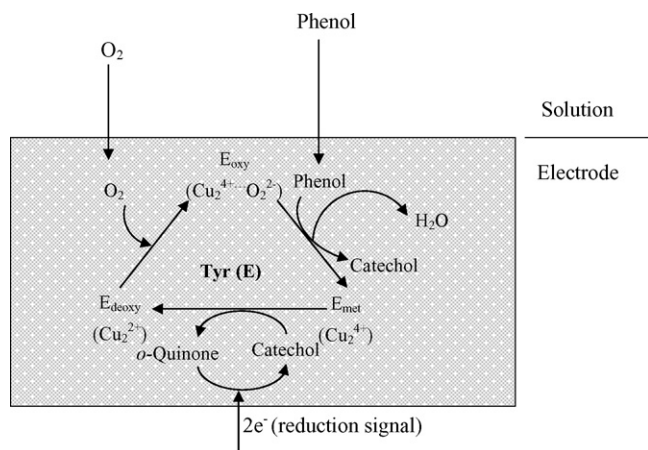


Fig. 4. Reaction mechanism for the enzymatic oxidation of phenol and catechol by tyrosinase and its coupling to an electrode.

In the first step, tyrosinase oxidizes phenol, which is diffused and reaches the electrode surface in the presence of molecular oxygen, which forms catechol. Then the catechol is in turn further oxidized to *o*-quinone by tyrosinase. It is known that the *o*-quinone is electrochemically active and can be efficiently reduced at a low potential (close to or below 0.24 V versus NHE) [25,26]. Moreover, this paves the way for the recycling of catechol and gives rise to the amplification of the signal. The liberated *o*-quinone is reduced to catechol, which is oxidized again by Tyr, and a cathodic peak current ( $I_{pc}$ ) is generated at  $E_{pc}$ . Therefore, using this cathodic current, the phenolic substance can be detected. In addition, a cathodic peak appeared at  $-0.2$  V versus NHE and it was found for the bare carbon paste electrode also (data was not shown), implying that the peak was irrelevant to the enzyme reaction.

Based on the reaction mechanism, the current response of the bare Tyr electrode to the addition of phenol was measured while stirring and applying a cathodic peak potential (0.2 V versus NHE). The calibration curve in the phenol concentration is shown in Fig. 5(a). After 1 week, a much higher current value was measured and unstable behavior was observed. It was thought that the large surface area was exposed to the solution with the loss of the binder (mineral oil) due to its continuous use, and that consequently the loose carbon material (graphite powder) allowed to pass more current due to the lower impedance.

### 3.2. Current responses of the PVA-Tyr electrode

In the case of the bare Tyr electrode, there was less stability and reproducibility with the absence of a protected layer on the electrode surface to prevent the exposure of the excess electrode surface. To protect the electrode surface and to increase its stability, the poly(vinyl alcohol) (PVA) film was introduced. Fig. 3 shows the cyclic voltammograms of the PVA-Tyr electrode with 1 mM of the phenol solution. Similarly, the redox peak of phenol was observed at the same potential as that of the bare Tyr electrode but with a lower peak current. This was due to the presence of the PVA layer. After the PVA coating, there was a limitation in the mass transfer of phenol, and less phenol reached the electrode surface. Thus, a lower peak current value was obtained. To investigate the effect of the PVA coating and its

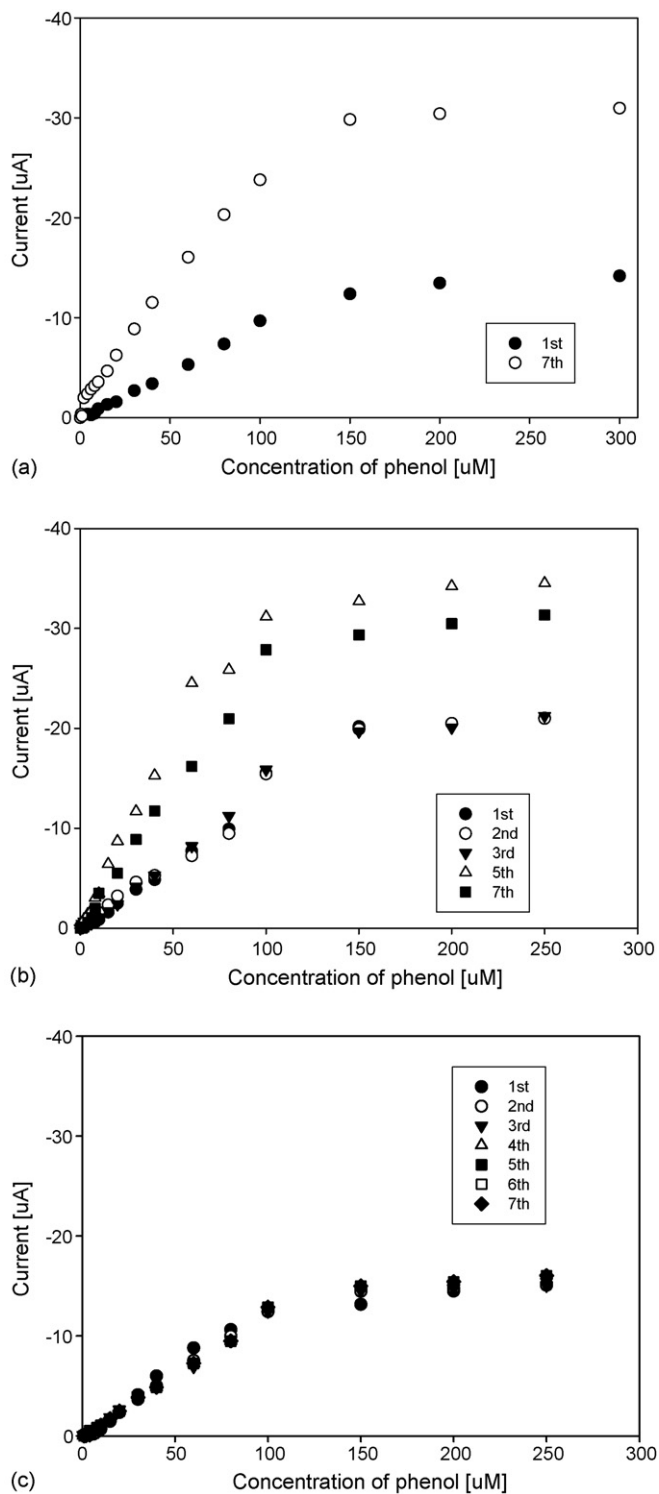


Fig. 5. Calibration curves of the: (a) bare Tyr electrode, (b) PVA-Tyr electrode, and (c) PVA-GA-Tyr electrode upon successive additions of phenol to air-saturated PBS (0.1 M, pH 7) at 0.2 V vs. NHE (the numbering means 1 day, the calibration curves were measured at least three times a day).

response to the addition of phenol, its current response was measured using amperometry, with successive additions of phenol. Fig. 5(b) shows the calibration curve that was obtained from the amperometric experiments. As shown in the figure, there was a stable current response for three days. Afterwards a higher cur-

rent value was obtained for the same concentration of phenol. It was assumed that the coated PVA film was damaged and the surface of the carbon paste electrode was exposed. The result is coincident with the cyclic voltammograms in Fig. 3, showing the current differences in  $I_{pc}$  for the three types of electrodes, bare, PVA coated, and PVA-GA coated Tyr electrode at the 1 mM of phenol.

### 3.3. Current responses of the PVA-GA-Tyr electrode

Due to the high swelling index of PVA, it has weak mechanical strength and is dissolved readily in water when not cross-linked [21]. Thus, PVA was cross-linked with the use of glutaraldehyde, after which the enzyme electrode was coated with the cross-linked PVA solution. Using the PVA-GA-Tyr electrode, a cyclic voltammogram was obtained with the phenol solution, and the redox peaks were obtained at the same potential values as those of the bare and PVA-coated Tyr electrodes (Fig. 3). Compared with the bare Tyr electrode, a much lower current flow and little discrepancies were obtained with the PVA-Tyr electrode. This implies that the mass transfer resistance of PVA layer existed, but there was no significant difference between PVA and cross-linked PVA layers. Also the Tyr activity did not decrease, although GA (the cross-linking reagent) is known to be toxic for some enzymes. There were fewer discrepancies in the cathodic peak currents than the anodic peak currents for the three types of Tyr electrodes. As discussed previously, the anodic peak current was due to the direct electrochemical oxidation of phenol and depended on the mass transfer, while the cathodic peak current was due to the reduction of the oxidized product of phenol by tyrosinase, and that the mainly controlling parameter was the enzyme activity. Therefore, at  $E_{pc}$ , the limiting parameter was the enzyme reaction and the difference in  $I_{pc}$  was relatively smaller than  $I_{pa}$  although the PVA film was coated.

To examine the performance of the PVA-GA-Tyr electrode, its current response was measured with the addition of phenol at a constant potential ( $E_{pc} = 0.2$  V versus NHE), which was determined from the CV tests. The calibration curve of the PVA-GA-Tyr electrode in the phenol concentration range of 0.5–100  $\mu$ M is shown in Fig. 5(c). The linear range of the PVA-GA-Tyr electrode was almost the same as those of the bare and PVA-Tyr electrodes. The current response was stable, however, and the linear range did not change within 1 week of continuous use. Therefore, the results revealed that the stability of the Tyr electrode was significantly improved after it was coated with the PVA-GA film.

### 3.4. Effects of the GA:PVA ratio on the current response of the TYR electrode

When PVA was cross-linked with GA, it no longer easily dissolved in water, improving the stability of the PVA-coated Tyr electrode. Although GA would improve the enzyme stability, GA could inhibit the enzyme activity due to its toxicity. To investigate the effect of cross-linking and to determine its optimal content, PVA films with three different GA con-

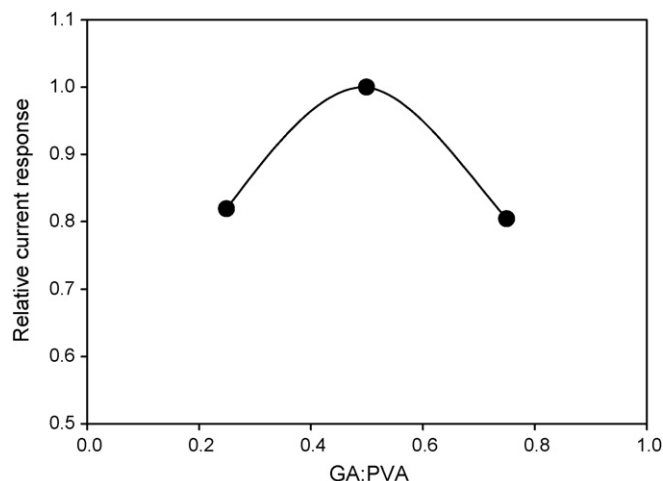


Fig. 6. Relative current response of the PVA–GA–Tyr electrode to 1 mM phenol in 0.1 M PBS of various GA:PVA ratios.

tent were prepared and used to coat the Tyr electrode. The effect of the ratio of GA:PVA on the current response of the PVA–GA–Tyr electrode is shown in Fig. 6. The optimal current response was observed at the ratio of GA:PVA 0.5. Under the condition, the inhibition of GA on the enzyme electrode was minimized.

### 3.5. Sensitivity and linear range of the PVA–GA–Tyr electrode

Based on the GA:PVA ratio and the voltammetric and amperometric experiments, the PVA–GA–Tyr electrode was prepared and the current responses were obtained. Table 1 shows a comparison of the performance of the Tyr-based carbon paste electrodes for phenol detection in this and previous studies. The

sensitivity of  $130.56 \mu\text{A}/\text{mM}$  ( $1.8 \mu\text{A}/\mu\text{M cm}^2$ ) is greater than the values reported earlier, as shown in Table 1, except a previous study [20], while the electrode used in this study has the wider linear range. It was thought that the increase in sensitivity resulted from the presence of ferrocene–ormosil as an electron transfer mediator, and the wider in linear range resulted from covering the cross-linked PVA layer and/or increasing stability of enzyme. When the concentration of phenol was higher than  $100 \mu\text{M}$ , the amperometric responses of both the bare Tyr and PVA–GA–Tyr electrodes exhibited characteristics of the Michaelis–Menten kinetic mechanism. The apparent Michaelis–Menten constants ( $K_M^{\text{app}}$ ) of the bare Tyr and PVA(–GA)–Tyr electrodes were about  $70$  and  $50 \mu\text{M}$ , using phenol as the substrate (Fig. 5). The  $K_M^{\text{app}}$  values are lower than that for the free enzyme in the solution ( $=700 \mu\text{M}$ ). This behavior may be due to an electroenzymatic recycling phenomenon that gives rise to the decrease in the apparent Michaelis constant of the entrapped enzyme [27,32]. The  $K_M^{\text{app}}$  value is also lower than the  $133$ ,  $168$ , and  $245 \mu\text{M}$  values found for the tyrosinase-based carbon paste electrode with different binders [6,27]. This was due to the interaction of some factors, such as the diffusional constraints of the substrate and the oxygen, the enzyme activity in the carbon paste, and ferrocene–ormosil [27].

### 3.6. Stability of enzyme electrodes

After 20 days, it retained 90% of the initial current response. The current response was almost the same even after 1 week, indicating that the PVA–GA–Tyr electrode can be operated for a longer period than suggested in previous studies. It was assumed that not only the protecting PVA–GA layer but also the ferrocene–ormosil and/or the cross-linked Tyr contribute

Table 1  
Tyrosinase-based modified carbon paste electrodes

Composition of paste	Sensitivity		Detection limit	Linear range	Stability	Reference
	$\mu\text{A}/\text{mM}$	$\mu\text{A}/\mu\text{M cm}^2$				
Graphite powder, mineral oil, Fc-ormosil	130.56	1.8		0.5–100 $\mu\text{M}$ (0.5–10 ppm)	7 day (continuous use) 90% after 20 days	This study
Graphite powder, nujol oil, polypyrrole		3.13		$\sim 20 \mu\text{M}$	80% after 1 month	[20]
Graphite powder, light mineral oil, poly(40vinylpyridine)				14 ppb to 2.5 ppm		[28]
Ruthenium on carbon, mineral oil, octadecylamine				0.8–80 $\mu\text{M}$		[29]
Graphite powder, mineral oil	77			$\sim 100 \mu\text{M}$		Flow cell system, [3]
Graphite powder, epoxy resin		0.01	0.96 $\mu\text{M}$	$\sim 300 \mu\text{M}$	70–75% after 15 days	Flow injection analysis, [10]
Graphite powder, paraffin oil, colloidal gold		12.3	6.1 nM (at $3\sigma$ )	4–48 $\mu\text{M}$	90% after 20 days	[27]
Graphite powder, paraffin oil, magnetic $\text{MgFe}_2\text{O}_4$ nanoparticles	54.2		0.6 $\mu\text{M}$	1–250 $\mu\text{M}$	92, 85, and 70% after 10, 20, and 30 days, respectively	[30]
Carbon paste/sol–gel	$1.28 \times 10^3$			0.4–20 $\mu\text{M}$	50% after 15 days	[31]



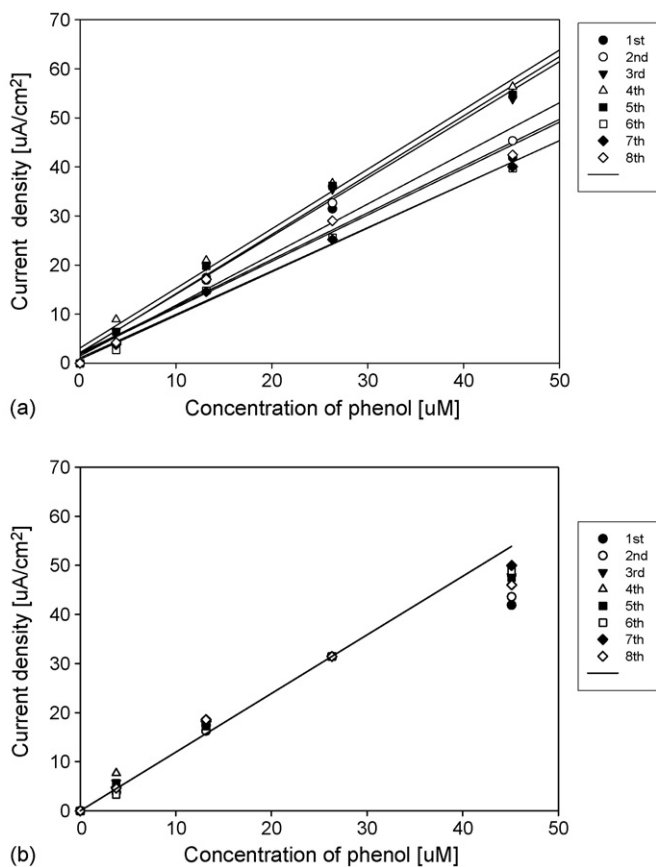


Fig. 7. (a) Current responses of the PVA-GA-Tyr electrode in a two-electrode system and (b) one-point recalibration curve.

the increased stability. The ferrocene-ormosil is the coated ferrocene with ormosil, which was formed by sol-gel reaction of silanes, and has less solubility. So it acts as an electron transfer mediator for a longer period. Also in the course of coating of PVA-GA layer, the Tyr might be cross-linked, and the stability was enhanced.

### 3.7. Two-electrode system

Using a two-electrode system equipped with the PVA-GA-Tyr and reference electrode, the current response was measured with the addition of phenol, which is more portable and appropriate to field application. Similarly with a three-electrode experiment, a current was measured with the different concentrations of phenol under the constant potential in the presence of flow. The current responses and one-point recalibration curves based on 27  $\mu\text{M}$  for 8 days were presented in Fig. 7(a and b), respectively. From the results, it was found that the prepared Tyr electrode works reasonably under 30  $\mu\text{M}$  and that the application of the prepared Tyr electrode to a two-electrode system as a portable sensor is feasible.

## 4. Conclusions

It was demonstrated that the coated PVA film, which was cross-linked with GA, improved the stability of the enzyme elec-

trode in the preparation of the tyrosinase-based carbon paste electrode. The PVA-GA-Tyr electrode showed a sensitive current response to the reduction of the oxidation product of phenol by the immobilized tyrosinase in the presence of dissolved  $\text{O}_2$ . The optimal pH and GA:PVA ratio was identified through the measurement of the current response. Although the coated PVA film act as a protecting layer, the influence of the layer on the performance was negligible due to its hydrophilicity. Also it was tested in a two-electrode system for more portable and practical applications.

## Acknowledgment

This work was supported by the ECO project of the Korea Institute of Environmental Science and Technology (Project No. 071-051-080).

## References

- [1] K.R. Rogers, J.Y. Becker, J. Wang, F. Lu, *Field Anal. Chem. Technol.* 3 (1999) 161.
- [2] J.C. Schmidt, *Field Anal. Chem. Technol.* 2 (1998) 351.
- [3] K.R. Rogers, J.Y. Becker, J. Cembrano, *Electrochim. Acta* 45 (2000) 4373.
- [4] W.P. King, K.T. Joseph, P.T. Kissinger, *J. Assoc. Off. Anal. Chem.* 63 (1) (1980) 137.
- [5] G. Marko-Varga, J. Emnéus, L. Gorton, T. Ruzgas, *Trends Anal. Chem.* 14 (1995) 319.
- [6] J. Wang, F. Lu, S.A. Kane, Y.-K. Choi, M.R. Smyth, K. Rogers, *Electroanalysis* 9 (1997) 1102.
- [7] M.E. Rice, Z. Galus, R.N. Adams, *J. Electroanal. Chem.* 2 (1983) 143.
- [8] D. Diamond (ed.), *Principles of Chemical and Biological Sensors*, John Wiley & Sons, Inc., 1998.
- [9] M. Lutz, E. Buresdt, J. Emnéus, H. Lidén, S. Gobhadi, L. Gorton, G. Marko-Varga, *Anal. Chim. Acta* 305 (1995) 8.
- [10] A. Lindgren, T. Ruzgas, J. Emnéus, E. Csoregi, L. Gorton, G. Marko-Varga, *Anal. Lett.* 29 (1996) 1055.
- [11] J. Furbee, C. Thomas, R. Kelly, M. Malachowski, *Anal. Chem.* 65 (1993) 1654.
- [12] F. Daigle, D. Leech, *Anal. Chem.* 69 (1997) 4108.
- [13] C. Nistor, J. Emnéus, L. Gorton, A. Ciucu, *Anal. Chim. Acta* 387 (1999) 309.
- [14] A. Arslan, S. Kiralp, L. Toppare, Y. Yagci, *Intl. J. Biol. Macromol.* 35 (2005) 163.
- [15] V. Christophe, F. Silvia, T. Canh, *Talanta* 59 (2003) 535.
- [16] L. Aihua, H. Itaru, Z. Haoshen, *Electrochem. Commun.* 7 (2005) 233.
- [17] P. Önerfjord, J. Emnéus, G. Marko-Varga, E. Domínguez, L. Gorton, *Biosens. Bioelectron.* 10 (1995) 601.
- [18] M.P. Connor, J. Sanchez, J. Wang, M.R. Smith, S. Mannino, *Analyst* 114 (1989) 1427.
- [19] B. Serra, A.J. Riveiro, C. Parrado, J.M. Pingarron, *Biosens. Bioelectron.* 14 (1999) 503.
- [20] P. Mailley, E.A. Cummings, S.C. Mailley, B.R. Eggins, E. McAdams, S. Cosnier, *Anal. Chem.* 75 (2003) 5422.
- [21] M. Constantin, G. Fundueanu, F. Bortolotti, R. Cortesi, P. Ascenzi, E. Menegatti, *Int. J. Pharm.* 285 (2004) 87.
- [22] S.K. Jha, S.F. D'Souza, *J. Biochem. Bioph. Methods* 62 (2005) 215.
- [23] L.B. Carvalho Jr., A.M. Araujo, A.M.P. Almeida, W.M. Azevedo, *Sens. Actuators B* 35 (1996) 427.
- [24] P.C. Pandey, S. Upadhaya, S. Sharma, *J. Electrochem. Soc.* 150 (2003) H85.



- [25] Z. Liu, B. Liu, J. Kong, J. Deng, *Anal. Chem.* 72 (2000) 4707.
- [26] L. Gorton, *Electroanalysis* 7 (1995) 23.
- [27] S. Liu, J. Yu, H. Ju, *J. Electroanal. Chem.* 540 (2003) 61.
- [28] M. Bonakdar, J.L. Vilchez, H.A. Mottola, *J. Electroanal. Chem.* 266 (1989) 47.
- [29] J. Wang, F. Lu, D. Lopez, *Biosens. Bioelectron.* 9 (1994) 9.
- [30] Z. Liu, Y. Liu, H. Yang, Y. Yang, G. Shen, R. Yu, *Anal. Chim. Acta* 533 (2005) 3.
- [31] J. Li, L.S. Chia, N.K. Goh, S.N. Tan, *Anal. Chim. Acta* 362 (1998) 203.
- [32] J.L. Bescombes, C. Cosnier, P. Labbe, G. Reverdy, *Anal. Chim. Acta* 317 (1995) 275.

## On-line enrichment system for manganese determination in water samples using FAAS

Marta Knap, Krzysztof Kilian, Krystyna Pyrzynska\*

*Department of Chemistry, Warsaw University, Pasteura 1, 02-093 Warsaw, Poland*

Received 20 December 2005; received in revised form 6 April 2006; accepted 13 April 2006

Available online 26 May 2006

### Abstract

An on-line preconcentration procedure for the determination of manganese using flow-injection approach with flame atomic absorption spectrometry as a detection method is described. The proposed method is based on the complexation between Mn(II) and 5,10,15,20-tetrakis(4-carboxyphenyl)porphyrin (TCPP). Two approaches were investigated for enrichment of manganese; the formation of Mn–TCPP complex in a solution followed by its retention on a sorbent and the sorption of manganese ions onto the TCPP-modified resin. The best results was obtained for the first approach when  $10^{-5}$  M reagent was on-line mixed with an aqueous sample solution and passed through the microcolumn packed with anion-exchange resin Amberlite IRA-904 for 5 min. The sorbed complexes were then eluted with 0.5 ml of 2 M  $\text{HNO}_3$ . A good precision (2.2–3.1% R.S.D. for  $50 \mu\text{g l}^{-1}$  manganese) and the enrichment factor of 30 were obtained with the detection limit of  $12 \mu\text{g l}^{-1}$  for 5 min loading time. The interference of anions and cations has been studied to optimize the conditions and the method was applied for determination of manganese in natural water samples. The results obtained by FI–FAAS and ETAAS (as a reference method) were not statistically different for a significance level of 0.05.

© 2006 Elsevier B.V. All rights reserved.

**Keywords:** Manganese; On-line preconcentration; FI–FAAS; TCPP

### 1. Introduction

The determination of manganese in natural water samples is of great importance in environmental chemistry. It helps to elucidate the biochemical cycles in which this element is involved such as bioaccumulation in living organisms, burial into sediments as well as adsorption–desorption equilibria with colloidal and suspended particles [1]. Manganese is very sensitive to redox conditions and is relatively mobile. In aerated conditions, the thermodynamically stable form is Mn(IV) as colloidal oxo-hydroxide. However, in the estuaries permanent oxygenated conditions are not presented and by consequence Mn(II) could be also occur as the long-lived metastable form. The iron–manganese–aluminum colloids can act either as efficient trap for metal ions from the solution phase, or as a source of soluble manganese. It was found that about 80% of manganese in pond and groundwater samples was in dissolved fraction that

was passing through a membrane filter of  $0.05 \mu\text{m}$  pore size [2,3]. According to the elaborated “in field” procedure, the dissolved manganese part in river water was in the range of 5–14% [4]. The requirements for manganese speciation and the analytical methods applied to such studies have been recently presented by Pearson and Greenway [5]. Although manganese has relatively low toxicity, in chronic overdose or moderate exposure over an extended period, Mn compounds are neurotoxic substances that target the central nervous system [6].

Although the sensitivity of analytical methods has increased in recent years, the routine determination of trace manganese in complex media is still difficult. The preliminary step is generally required for enrichment and elimination of interfering ions [7,8]. Several authors have chosen solid phase extraction due to its specificity and high preconcentration factors. Iminodiacetic resin [9], Chrome-Azurol-S-loaded resin [10], 8-hydroxyquinoline immobilized on controlled-pore glass [11] as well as microorganism *Agrobacterium tumefaciens* immobilized on Amberlite XAD-2 [12] have been used as a solid phase. The alternative procedures, based on the solid phase extraction of manganese complexes with Eriochrome Black T

\* Corresponding author. Tel.: +48 22 8220211; fax: +48 22 8223532.  
E-mail address: [kryspyrz@chem.uw.edu.pl](mailto:kryspyrz@chem.uw.edu.pl) (K. Pyrzynska).

[13], 2-(5-bromo-2-pyridylazo)-5-diethylaminophenol [14] and 5,7-dichlorooxime [15] have been also investigated. Abollino et al. [16] proposed a procedure for speciation of manganese based on the retention of metal species onto a cation or anion exchange resin. Recently, on-line electrochemical preconcentration of manganese for its determination in urine samples has been proposed [17].

In this paper, an on-line preconcentration procedure for the determination of manganese using flow-injection (FI) approach with flame atomic absorption spectrometry (FAAS) as a detection method is described. The system combining FI with on-line preconcentration is very effective in enhancing the sensitivity and selectivity of trace metals determination in samples with complex matrices. On-line procedures have also the advantage of working in closed systems, thereby reducing contamination of the samples due to the laboratory environment. Only a few papers describe the coupling of flow-injection system to FAAS method for preconcentration and determination of Mn(II) [11,15,17]. The proposed method is based on the complexation between Mn(II) and 5,10,15,20-tetrakis(4-carboxyphenyl)porphyrin (TCPP). Different approaches were investigated for enrichment of manganese; the formation of Mn–TCPP complex in a solution followed by its retention on a sorbent and the sorption of manganese ions onto the TCPP-modified resin.

## 2. Experimental

### 2.1. Reagents and materials

Analytical reagent-grade chemicals were used as well as deionised water from a Milli-Q-system. Standard solutions of manganese were prepared by the appropriate dilution of 1000 mg l<sup>-1</sup> of a stock solution from Merck. 5,10,15,20-tetrakis(4-carboxyphenyl)porphyrin (TCPP) from Fluka was used without further purification.

The macroporous anion-exchange resin Amberlite IRA-904 (50–100 mesh) from Bio Rad Laboratories was applied to prepare the microcolumns.

Buffer components were of analytical grade and used without further purification. The phosphate buffer (0.05 M) was used for pH 6–8 and borate buffer (0.05 M) for pH 8–10.

### 2.2. Apparatus

A Perkin-Elmer 3110 atomic-absorption spectrometer equipped with a deuterium background corrector utilised the Mn 279.5 nm line. An air–acetylene flame was adjusted according to the manufacturer's recommendation. Time-resolved absorbance signals of the elution peaks were displayed on the monitor and printed together with the peak height values (evaluation of the spectrometer was operated with a time contact of 1 s).

### 2.3. Procedures

The FI systems used, shown schematically in Fig. 1, consisted of an Ismatec MS/4 Reglo peristaltic pump, two Rheodyne RH

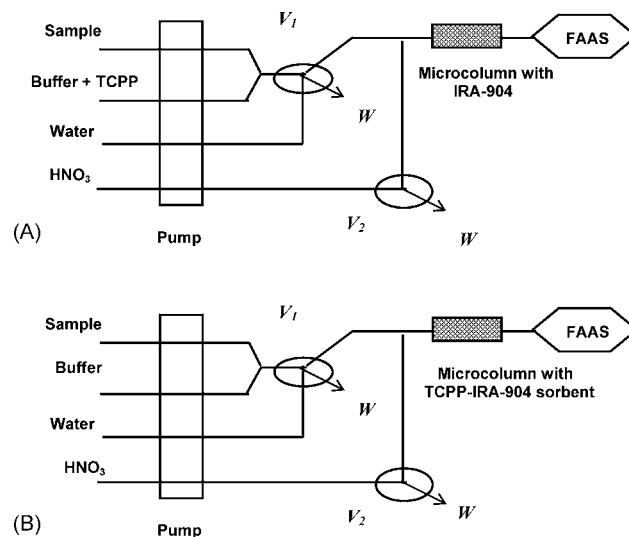


Fig. 1. FI manifolds used for on-line preconcentration of Mn(II).

5020 low-pressure injection valves and a microcolumn manufactured from a pipette tip (the ends of which were fitted with cotton to retain the sorbent in the tube). The microcolumn (packed with 200 mg of sorbent) was integrated into the system between the eluent injection valve and the nebulizer of the instrument. It was initially washed with 2 M HNO<sub>3</sub> and deionised water before use. PTFE tubes (0.8 mm i.d.) were employed for the coils. The flow system was operated in the time-based mode and deionised water served as the carrier stream.

Two different approaches were applied for the preconcentration step. In the first one (Fig. 1A) a sample was mixing with TCPP and buffer in the manifold followed by retention of the formed Mn–TCPP complex for selected interval time. In the second approach a sample was pumped through the microcolumn packed with Amberlite IRA-904 loaded with TCPP (Fig. 1B). In all cases after preconcentration step, the first injection valve was switched to its other position and 0.5 ml of 2 M HNO<sub>3</sub> solution was injected by means of a second valve in order to release manganese directly into the nebulizer of the spectrometer. Finally, the blank carrier (deionised water) was passed through the microcolumn for 30 s (at 6.8 ml min<sup>-1</sup>) in order to prepare it for the following sample loading.

## 3. Results and discussion

Porphyrin nucleus are macrocyclic ligands and metal complexation takes place through the nitrogen atoms [18]. Our studies on complexation reaction between TCPP and some metal ions [19] showed that this ligand forms with Mn(II) the negatively charged complex with 1:1 molar ratio. The presence of the carboxylic groups, located apart from the coordination site, allows the retention of the Mn–TCPP complex as well as a ligand alone on a microcolumn packed with anion-exchange resin. Additionally, the  $\pi$ – $\pi$  interactions between aromatic structure of the resins matrix and chelating agent molecule has to be taken into consideration.

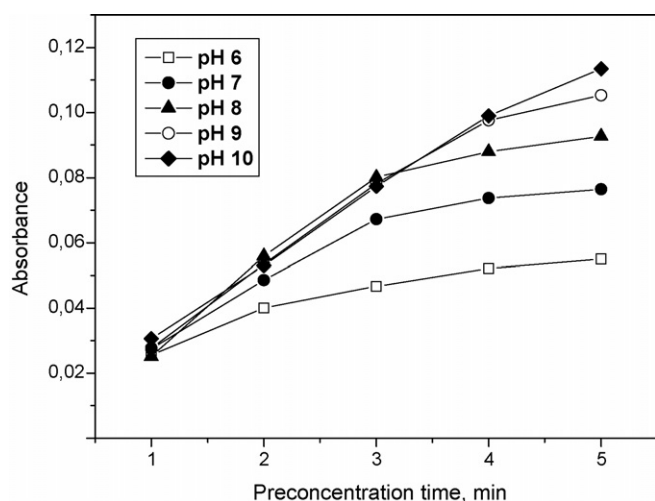


Fig. 2. Effect of pH on analyte response for different loading times ( $0.6 \mu\text{g l}^{-1}$  Mn solution).

### 3.1. Chemical and flow optimization

The pH value of the medium is one of the most important factors controlling the limit of metal ions sorption, because hydrogen ions compete with metal ions in the complex formation reaction. In order to determine the optimum conditions of manganese sorption, the pH conditions were examined using manifold shown in Fig. 1A. A time-based system was applied for used FI configuration because it is more flexible as time can be changed in order to load desired amount of analyte onto the microcolumn. The sample solutions containing  $0.6 \text{ mg l}^{-1}$  of Mn(II) and TCPP ( $1 \times 10^{-5} \text{ M}$ ) were adjusted to the appropriate pH with phosphate or borate buffers and were passed through the microcolumns packed with Amberlite IRA-904 resins (200 mg) for selected interval time. Fig. 2 shows the effect of pH on manganese absorbance signal for different loading times. The best linearity of response ( $r^2 = 0.9964$ ) was observed up to 5 min of loading time for sample pH of 10. The observed relationship means that retention of manganese complex is constant. The adjustment of the sample pH to the optimum value can be achieved by using TCPP solution with 0.05 M borate buffer.

The effect of porphyrin concentration (in 0.05 M borate buffer) was investigated. The results showed that the absorption signal for  $1.2 \mu\text{g}$  of manganese increased when the concentration of TCPP was increasing up to  $10^{-5} \text{ M}$ , since the equilibrium was shifted toward complex formation. The variation in the absorbance signal along with a further increase in the ligand concentration was negligible.

The changes in a flow rate during preconcentration step between  $0.6$  and  $3 \text{ ml min}^{-1}$  ( $15 \text{ ml}$  of a Mn standard of  $100 \mu\text{g l}^{-1}$ ) resulted in very small variations in measured signal (Fig. 3). At higher flow rates, the analytical signal decreased owing to short residence time of the sample, which resulted in an incomplete retention of manganese. In further study for sample and TCPP solutions flow rates of  $3 \text{ ml min}^{-1}$  were applied.

Elution of preconcentrated manganese ions could be done by breaking the metal-chelate bond using mineral acids.  $500 \mu\text{l}$  of 2 M nitric acid was more sufficient than similar volume of HCl

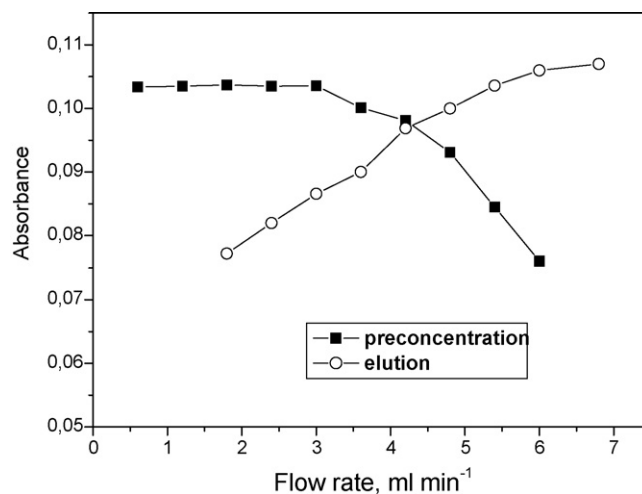


Fig. 3. Effect of flow rates during preconcentration (■) and elution (○) on the absorbance ( $15 \text{ ml}$  of a Mn standard of  $100 \mu\text{g l}^{-1}$ ).

solution. Moreover, leaching of ligand by  $\text{HNO}_3$  is much lower in comparison with hydrochloric acid [20]. Two subsequent elutions with  $\text{HNO}_3$  on the same loaded column confirmed that no manganese was present in the second aliquot. The elution rate is also important for good precision and better sensitivity. The eluent flow rate was varied from  $1.8$  to  $6.9 \text{ ml min}^{-1}$  (Fig. 3). The absorbance increased in a regular manner along with an increase of in the flow rate up to the natural aspiration rate of the nebulizer ( $6.8 \text{ ml min}^{-1}$ ) owing to the increasing nebulizer efficiency, at higher flow overpressure was observed. After the elution step, the sorbent needs to be prepared for the next loading step. Pumping deionised water for 30 s at the natural aspiration rate of the nebulizer ( $6.8 \text{ ml min}^{-1}$ ) was found to optimum to prevent analyte to be eluted prematurely.

The capacity of the resin towards Mn–TCPP complex was estimated with the manual column preconcentration technique and it was found to be  $0.17 \mu\text{mol g}^{-1}$ . A microcolumn such as the one used in this study is able to retain  $1.8 \mu\text{g}$  of Mn; this value is well above the content of this metal in  $100 \text{ ml}$  of river or seawater sample [9,13]. In the case when concentration of the analyte exceeding the capacity of the microcolumn, a larger amount of sorbent can be used.

### 3.2. Analytical performance

Using a manifold presented in Fig. 1A (ligand in solution) a linear correlation between the absorbance and the manganese concentration was obtained up to  $150 \mu\text{g l}^{-1}$  of Mn(II). When Amberlite IRA-904 resin modified with TCPP was used (Fig. 1B) good linearity was observed in the range of  $20$ – $120 \mu\text{g l}^{-1}$  ( $r^2 = 0.9995$ ). The lower linear calibration range may be due to the fact that many exchange sites on TCPP-loaded resin is inaccessible to the metal ions. The detection limit based on three-times standard deviation of the peak absorbance was  $12$  and  $16 \mu\text{g l}^{-1}$ , respectively, using a preconcentration time of 5 min. The precision obtained at the  $50 \mu\text{g l}^{-1}$  level of Mn(II), expressed as R.S.D., was  $2.2$ – $3.1\%$  ( $n = 10$ ).

The experimental enrichment factor (EF), defined as the ratio of the slopes of the calibration graphs obtained with and without preconcentration was 30 (for 15 ml sample solution). The efficiency of preconcentration essentially depends on the sample volume and the time taken for the sample solution to pass through a microcolumn. The application of longer loading time improves the enrichment, but simultaneously leads to a decrease in a sample rate [14,21]. For example, metal ions, including manganese, were preconcentrated on Amberlite XAD-16 functionalized with 1,3-diethyl-3-aminopropan-1-ol reaching the enrichment factor as high as 300. However, 3000 ml volume of sample was used and the time required for one cycle of preconcentration and determination of manganese took above 2 h to get one results [21]. Hence, it seems to be very appropriate to use the concentration efficiency (CE) and the consumptive index (CI) for comparing of various systems. CE is the product of the EF and the sampling frequency in number of samples analysed per hour, while CI is defined as the volume of sample in millilitres consumed to achieve a unit EF [22]. Using our method, CE and CI were  $5 \text{ min}^{-1}$  and 2 ml, respectively.

Upon comparing these results with previously published concerning manganese preconcentration coupled to flame AAS detection, lower detection limit was reported for 2-(5-bromo-2-pyridylazo)-5-diethylaminophenol complexes sorbed on thermal modified Kaolinite [14] and Mn-PAR complexes enriched on activated carbon [8]. However, these procedures were conducted in off-line mode and their limitation is rather long time of analysis. In the works of Doi et al. [9] and Sarzanini et al. [13] much more sensitive detection methods, such as chemiluminescence and ETAAS, were applied. The method proposed by Tony et al. [15] with FAAS detection using  $\text{C}_{18}$  bonded silica gel seems to show better analytical performance.

Interferences from co-existing ions were evaluated for both complexation approaches, e.g. complexation in solution and onto the sorbent phase. TCPP does not form strong complexes with alkali and alkaline earth metals [20], commonly encountered matrix components in natural waters. However, in order to identify their potential interference on the on-line sorption of the Mn-TCPP complex, high concentration of them were tested. Different amounts of metal ions were added individually to a  $100 \mu\text{g l}^{-1}$  Mn solution and passed for 5 min through the columns containing 200 mg of Amberlite IRA-904 alone or modified with TCPP. The obtained results show that the presence of NaCl (up to  $100 \text{ mg l}^{-1}$ ) and  $\text{Na}_2\text{SO}_4$  (up to  $140 \text{ mg l}^{-1}$ ) did not significantly affect the determination of magnesium, when the analyte was complexed before sorption on the microcolumn. More serious interferences were observed when TCPP-modified sorbent was used;  $\text{Na}_2\text{SO}_4$  concentrations greater than  $60 \text{ mg l}^{-1}$  decrease the absorbance signal by about 20%. The presence of  $\text{MgCl}_2$  and  $\text{MgSO}_4$  up to  $20 \text{ mg l}^{-1}$  could be tolerated for both complexation approaches. Heavy metal ions may cause interferences owing to their competition for the chelating agent and their TCPP complexes for active sites on the sorbent. Metals such as Ni(II), Cu(II), Co(II) and Pb(II) could be tolerated up to  $0.6 \text{ mg l}^{-1}$ . Fe(III) could be tolerated up to  $0.1 \text{ mg l}^{-1}$ , but strongly lowering the absorbance signal at its higher content. Increasing the amount of the sorbent up to 500 mg at the expense

of lowering the enrichment factor was not successful. Thus, the proposed method could be sufficient for application to water samples, except for those which are heavily polluted with iron.

### 3.3. Application to natural samples

To study the accuracy of the method and the possible effects from the real matrix, the recovery tests were applied to natural pond water. The aliquots of pond water (pH 6.9) were spiked with Mn(II) solution and passed through the microcolumns containing 200 mg of anion-exchange resin Amberlite IRA-904 and TCPP-modified Amberlite, respectively, for 5 min using manifolds presented in Fig. 1. Manganese was then eluted by  $500 \mu\text{l}$  of 2 M  $\text{HNO}_3$  and determined by FAAS. The recoveries for spiked addition ( $50 \mu\text{g l}^{-1}$  of Mn(II)) gave a mean result of  $(98.1 \pm 3.9)\%$  for five replicate experiments when the sample was mixed with TCPP solution before sorption process. Lower recovery was obtained for TCPP-modified sorbent ( $86.2 \pm 4.6\%$ ). Thus, these results proved that the earlier approach is not affected by matrix interferences and can be satisfactory applied for on-line manganese preconcentration from water samples.

The practical feasibility of the proposed method for the determination of manganese with on-line preconcentration was tested on several natural water samples collected from different sources. After filtration using  $0.45 \mu\text{m}$  filter, four replicates were performed for each sample combining complexation of Mn(II) with TCPP in the flow system with FAAS detection. The manganese content in these samples together with the results obtained by ETAAS method is presented in Table 1. To compare the obtained results, the Student's *t*-test [25] was applied. The experimental values of *t* from our results were in the range of 1.66–2.28. As for 8 degree of freedom, the critical value of  $t_8$  is 2.31 ( $P=0.05$ ), the differences between the results obtained by FI-FAAS and ETAAS methods are not significant at the 5% level. Our methodology was shown to be an effective approach for improving the sensitivity of flame AAS manganese determination in natural water samples.

The permissible limits of Mn in the drinking water in Poland as well as in other European Union countries [23] is  $50 \mu\text{g l}^{-1}$ , however, World Health Organization guidelines [24] increases this level up to  $100 \mu\text{g l}^{-1}$ . Doi et al. [9] found that in the unfiltered samples of seawater, the concentration of manganese

Table 1  
Analysis of manganese in natural water samples<sup>a</sup>

Sample	Determined value ( $\mu\text{g l}^{-1}$ )	
	FI-FAAS	ETAAS
Drinking water (Smyczkowa) <sup>b</sup>	$12.7 \pm 0.6$	$13.7 \pm 0.8$
Drinking water (Powsin) <sup>b</sup>	$15.8 \pm 0.8$	$15.0 \pm 0.7$
Pond water (Pasteura) <sup>b</sup>	$18.5 \pm 1.6$	$19.6 \pm 1.0$
Well water (Ursynów)	$44.5 \pm 1.0$	$43.3 \pm 0.9$
Well water (Powsin) <sup>b</sup>	$22.3 \pm 1.2$	$23.6 \pm 0.7$
Well water (Smyczkowa)	$95 \pm 4$	–

<sup>a</sup> Mean of five determination  $\pm$  standard deviation ( $P=0.95$ ).

<sup>b</sup> 15 min sample loading time.



was slightly higher than in the filtered samples (0.2  $\mu\text{m}$ ). They applied preconcentration step (iminodiacetate-immobilized on silica gel) prior to detection, which implies that not only dissociated manganese but also particulate Mn was adsorbed partially onto the microcolumn. These differences could show the possibility of evaluating the labile fraction of particulate manganese and its reactivity.

#### 4. Conclusion

The on-line enrichment procedure developed allows manganese determination at trace levels by FAAS. The main advantages achieved with the proposed method are reduction of sample contamination as well as analyte losses because less manipulation of the sample is required compared with off-line methods. The sensitivity of the method could still be improved by increasing preconcentration time and/or by using a larger microcolumn packing.

#### References

- [1] M. Miyazawa, M.A. Pavan, P.L. Machado, E.L. de Oliveira, M. Yamashita, *Soil Sci.* 162 (1997) 641.
- [2] S.A. Sanudo-Wilhelmy, F.K. Rossi, H. Bokuniewicz, R.J. Paulsen, *Environ. Sci. Technol.* 36 (2002) 1435.
- [3] A. Itoh, T. Nagasawa, Y. Zhu, K.H. Lee, E. Fujimori, H. Haraguchi, *Anal. Sci.* 20 (2004) 29.
- [4] K. Zih-Perényi, A. Lászyity, *Spectrochim. Acta Part B* 60 (2005) 385.
- [5] G.F. Pearson, G.M. Greenway, *Trends Anal. Chem.* 9 (2005) 803.
- [6] D.G. Ellingsen, S. Hetland, Y. Thomassen, *J. Environ. Monit.* 5 (2003) 84.
- [7] M. Grotti, R. Leardi, C. Gnecco, R. Frache, *Spectrochim. Acta Part B* 54 (1999) 845.
- [8] A.C. Ferreira, M.G.A. Korn, S.L.C. Ferreira, *Microchim. Acta* 146 (2004) 271.
- [9] T. Doi, H. Obata, M. Maruo, *Anal. Bioanal. Chem.* 378 (2004) 1288.
- [10] Z. Moldovan, L. Vlădescu, *Talanta* 43 (1996) 1573.
- [11] C.G. Bruhn, E.E. Pino, V.H. Campos, J.A. Nóbrega, *Anal. Bioanal. Chem.* 374 (2002) 131.
- [12] A. Baytak, A.R. Türker, *Talanta* 65 (2005) 938.
- [13] C. Sarzanini, O. Abollino, E. Mentasti, *Anal. Chim. Acta* 435 (2001) 343.
- [14] D. Afzali, M.A. Taher, A. Mostafavi, S.Z.M. Moharakeh, *Talanta* 65 (2005) 476.
- [15] K.A. Tony, S. Kartikeyan, B. Vijayalakshmy, T.P. Rao, Ch.S. Iyer, *Analyst* 124 (1999) 191.
- [16] O. Abollino, M. Aceto, E. Bruzzoniti, E. Mentasti, C. Sarzanini, *Anal. Chim. Acta* 375 (1998) 299.
- [17] M. Burguera, J.L. Burguera, D. Rivas, C. Rondón, P. Carrero, O.M. Alarcón, Y.P. de Peña, M.R. Brunetto, M. Galignani, O.P. Márquez, J. Márquez, *Talanta* 68 (2005) 219.
- [18] M. Biesaga, K. Pyrzynska, M. Trojanowicz, *Talanta* 51 (2000) 209.
- [19] K. Pyrzynska, K. Kilian, *J. Sep. Sci.* 2 (2006) 282.
- [20] K. Kilian, K. Pyrzynska, *Chem. Anal. (Warsaw)* 47 (2002) 439.
- [21] D. Prabhakaran, M.S. Subramanian, *Talanta* 59 (2003) 1227.
- [22] Z.I. Fang, *Flow Injection Atomic Absorption Spectrometry*, Wiley, Chichester, 1995.
- [23] Council Directive of 3 November 1998 on the quality of water intended for human consumption. *Official Journal of European Communities*. L.330/32, 5.12/98.
- [24] WHO, *Guidelines for Drinking Water Quality*. Vol. 1. Recommendations, 2nd ed., WHO, Geneva, 1993.
- [25] J.N. Miller, J.C. Miller, *Statistics and Chemometrics for Analytical Chemistry*, 5th ed., Pearson Education Ltd, 2005.

# A liquid chromatography/positive ion tandem mass spectrometry method for the determination of cilazapril and cilazaprilat in human plasma

Heon-Woo Lee, Wan-Su Park, Sung-Hee Cho, Min-Hwan Kim, Ji-Hyung Seo,  
Yong-Won Kim, Sung-Su Kim, Yong-Sup Lee, Kyung-Tae Lee\*

College of Pharmacy, Kyung Hee University, Hoegi-Dong, Dongdaemun-Ku, Seoul 130-701, Republic of Korea

Received 22 January 2006; received in revised form 6 March 2006; accepted 6 March 2006

Available online 31 March 2006

## Abstract

A simple, rapid, and sensitive high-performance liquid chromatography (HPLC)–electrospray ionization (ESI) tandem mass spectrometric method (LC–MS/MS) has been developed for simultaneous determination of cilazapril levels and its active metabolite, cilazaprilat, in human plasma using enalapril as internal standard. The acquisition was performed in the multiple reaction monitoring mode; monitoring the transitions:  $m/z$  418.4 > 211.1 for cilazapril and  $m/z$  390.3 > 211.1 for cilazaprilat. The method involves a simple single-step liquid–liquid extraction with ethyl acetate. The analyte was chromatographed on an YMC C<sub>8</sub> reversed-phase chromatographic column by isocratic elution with 10 mM ammonium formate buffer-methanol (10:90, v/v; pH 3.2 with formic acid). Numerous compounds did not interfere with specific multiple reaction monitoring in tandem mass spectrometric detection following C<sub>8</sub> reversed-phase chromatographic separation under conditions that eluted cilazapril, cilazaprilat, and enalapril within 2 min. This method was validated over 0.1–500 ng ml<sup>-1</sup> of cilazapril and 0.5–50 ng ml<sup>-1</sup> of cilazaprilat. Cilazapril and cilazaprilat were stable in standard solution and in plasma samples under typical storage and processing conditions. The assay was successfully applied to a pharmacokinetic study of cilazapril given as a single oral dose (5 mg) to healthy volunteers.

© 2006 Elsevier B.V. All rights reserved.

**Keywords:** Cilazapril; Cilazaprilat; Determination; LC–MS/MS; Pharmacokinetic study

## 1. Introduction

Cilazapril, [1S-[1 $\alpha$ ,9 $\alpha$ (R\*)]]-9-[[1-ethoxycarbonyl]-3-phenylpropyl]amino]octa-hydro-10-*oxo*-6H-pyridazino[1,2a][1,2] diazepine-1-carboxylic acid monohydrate is a potent and specific angiotensin-converting enzyme (ACE) inhibitor, which lowers peripheral vascular resistance without affecting heart rate. It is used in the treatment of hypertension and congestive heart failure [1], was rationally designed based on binding to the active site of ACE [2,3]. ACE inhibition prevents the conversion of angiotensin I to angiotensin II, a potent vasoconstrictor, to cause vasodilatation and lower blood pressure [3,4]. It also prevents the reabsorption of sodium and water from renal tubules and decreases the heart flow rate [5].

Following oral administration, cilazapril undergoes de-esterification in the liver to its active di-acid form, cilazaprilat. This active metabolite is more polar than cilazapril, making it more difficult for the intestine to absorb, but cilazapril, although not active, is well absorbed orally. Doses of cilazapril range from 0.5 to 5 mg per day [6]. Bioavailability of cilazaprilat is 57% and it is excreted almost exclusively by the kidney and no further metabolism occurs. The elimination kinetic of cilazaprilat is biphasic, with a distribution half-life of 1.5–2 h and a terminal elimination half-life of 30–50 h [5,7,8].

Various methods for determining levels of cilazapril and cilazaprilat in urine and other matrices have been developed. The activity of these compounds is usually assayed indirectly by measuring ACE inhibition, angiotensin II, or renin levels [1,3,6,9]. Enzyme immunoassay has been used for the direct determination in plasma and serum [10], and HPLC with amperometric detection for its analysis in urine [11]. Methods applied to the analysis of cilazapril in tablets include UV spectrophotometry [12], as well as HPLC with photometric [13] and amperometric detection [11]. Other structurally similar ACE inhibitors

\* Corresponding author at: Department of Pharmaceutical Biochemistry, College of Pharmacy, Kyung Hee University, Dongdaemun-Ku, Hoegi-Dong, 130-701 Seoul, Republic of Korea. Tel.: +82 2 9610860; fax: +82 2 9663885.

E-mail address: [ktee@khu.ac.kr](mailto:ktee@khu.ac.kr) (K.-T. Lee).

have been analysed in biological fluids by GC–MS, but this involves two derivatization steps for the amine group and the carboxylic acid that are very slow and can significantly affect the results [14–18]. To our knowledge, no reports of simultaneous determination of cilazapril and its active metabolite cilazaprilat using LC–MS/MS has been published until now.

The aim of this work was to develop and validate a simple and accurate LC–MS/MS method for simultaneous quantification of cilazapril and cilazaprilat using liquid/liquid extraction. Additionally, this method was applied to a pharmacokinetic study of cilazapril (5 mg) tablets in 24 healthy Korean volunteers.

## 2. Experimental

### 2.1. Chemicals

Cilazapril and enalapril maleate (Fig. 1) were obtained from Myungmoon Pharm. Co., Ltd. (Kyunggi-Do, South Korea) and Sigma–Aldrich (Steinheim, Germany), respectively. Cilazaprilat was prepared from cilazapril by alkaline hydrolysis as described previously [11]. All these compounds were checked by HPLC and were found to be >99% pure. Methanol, ethyl acetate, dimethyl sulfoxide (DMSO) and formic acid (all HPLC-grade) were purchased from Fisher Scientific (Fair Lawn, NJ, USA). A Milli-Q® (Millipore Co., Milford, MA, USA) water purification system was used to obtain the purified water used for the HPLC analysis. All other chemicals and solvent were of the highest analytical grade available.

### 2.2. Sample preparation

Stock solutions containing 1 mg ml<sup>-1</sup> of cilazapril, cilazaprilat, and enalapril were prepared in DMSO. Separate solutions were prepared for the calibration curve and quality control samples. Further solutions were obtained by serial dilution of stock solutions with 100% methanol. Calibration curves for cilazapril were prepared by spiking blank plasma at 0.1, 0.2, 1, 10, 100, and 500 ng ml<sup>-1</sup>. The quality control solutions of cilazapril (0.5, 50, and 500 ng ml<sup>-1</sup>) were similarly prepared. For cilazaprilat, the calibration standard solutions were 0.5, 1, 2, 5, 10, 20, and 50 ng ml<sup>-1</sup>, and the quality control solutions were 1, 10, and 50 ng ml<sup>-1</sup>. The internal standard solution was prepared by dilution of the stock solution with methanol to a final concentration of 20 µg ml<sup>-1</sup>. Calibration curves for cilazapril and cilazaprilat were constructed from a blank sample (a plasma sample processed without the I.S.), a zero sample (a plasma sample processed with the I.S.), and nonzero samples covering

the range of 0.1–500 and 0.5–50 ng ml<sup>-1</sup>, respectively. All stock solution and plasma samples were stored at –70 °C.

A 250 µl volume of human plasma was introduced into a glass tube followed by 20 µl I.S. solution (20 µg ml<sup>-1</sup> of enalapril), and acidified with 20 µl 10% phosphoric acid. After the samples were vortexed for 1 min, ethyl acetate was added (6 ml) to the tubes and extraction was performed by vortexing for 10 min. The tubes were centrifuged for 10 min at 3000 rpm. The organic phase was transferred to another set of clean glass tubes and evaporated to dryness under N<sub>2</sub> at 40 °C. Residues were dissolved in 0.1 ml of reconstitution solution (90% methanol in 10 mM ammonium formate), and 10 µl of reconstituted samples were injected into the LC–MS/MS system. Between the sample injections, the injection needle was washed with 50% methanol.

### 2.3. Liquid chromatography and mass spectrometry

A Waters 2795 separation module HPLC system and a Waters Micromass Quattro Premire triple quadrupole mass spectrometer (Milford, MA, USA) were used. The analytical column was a Hydrosphere C<sub>8</sub> (50 mm × 2 mm i.d. S-3 µm, 12 nm; YMC, Kyoto, Japan). The mobile phase, consisting of 90% methanol and 10% Milli-Q water containing 10 mM ammonium formate (pH 3.2 with formic acid), was filtered and degassed. The flow rate of 0.2 ml min<sup>-1</sup> was adequate for sample analysis and the temperature of the autosampler was 4 °C.

Micromass Masslynx 4.0 and Quanlynx were used for data management. Electrospray ionization was performed using nitrogen as a desolvation gas at 600 × 1 h<sup>-1</sup> flow rate, at 50 × 1 h<sup>-1</sup> cone gas flow rate and 350 °C desolvation temperature. Collision cell gas pressure was 2.8 × 10<sup>-3</sup> mbar. Other ion source parameters were: capillary voltage, 3.5 kV; extractor, 2.0 V; RF lens, 0.2 V; source temperature, 120 °C. MS analyzer parameters were: resolution 1, 14 (LM) and 14 (HM); ion energy 1, 1.0 V; collision cell entrance potential, 2.0 V; collision cell exit potential, 2.0 V; resolution 2, 14 (LM) and 14 (HM); ion energy 2, 1.0 V; multiplier, 650 V; dwell time, 0.5 s; cone voltage, 24 V (cilazapril), 20 V (cilazaprilat) and 30 V (enalapril) and collision energy, 20 V (cilazapril), 18 V (cilazaprilat) and 23 V (enalapril), respectively. Three channels of positive ion multiple reaction monitoring (MRM) mode were used to detect *m/z* 418.4 > 211.1 (cilazapril), *m/z* 390.3 > 211.1 (cilazaprilat) and *m/z* 377.4 > 234.2 (enalapril).

### 2.4. Recovery and stability

Recovery was evaluated by comparing the mean detector response of different QC samples post-extracted with those prepared by adding compound to extracted drug free plasma at the corresponding concentrations. To test the stability of extracted cilazapril and cilazaprilat, three QC samples, containing 0.5, 50 and 500 ng ml<sup>-1</sup> (cilazapril), and 1, 10 and 50 ng ml<sup>-1</sup> (cilazaprilat) concentrations, were determined after three freeze and thaw cycles, by thawing at room temperature for 2–3 h and freezing for 12–24 h. The short-term stabilities of the samples in plasma during storage for 24 h at 4 °C, room temperature

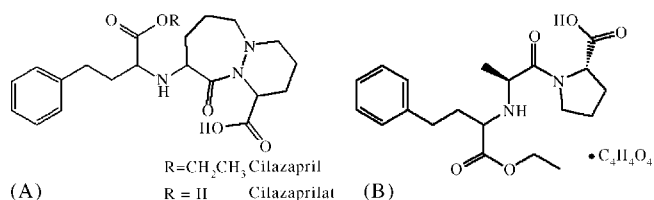


Fig. 1. Chemical structures of (A) cilazapril and cilazaprilat, and (B) enalapril maleate.

and  $-20^{\circ}\text{C}$ , and extracted samples during storage for 12 h at  $4^{\circ}\text{C}$  were also determined. The long-term storage stability of the samples in plasma during storage at  $-70^{\circ}\text{C}$  was determined after 30 days.

### 2.5. Method validation and clinical test

Quantitative analysis was performed using an internal standard. Standard calibration curves were obtained by the chromatographic area ratios of cilazapril and cilazaprilat against enalapril. Concentrations of cilazapril and cilazaprilat were calculated from their area ratio and the calibration curve.

The intra- and inter-day accuracy and precision were studied by performing five separate analyses per day for 5 days with cilazapril (0.1, 0.5, 50 and  $100\text{ ng ml}^{-1}$ ) and cilazaprilat (0.5, 1, 10 and  $50\text{ ng ml}^{-1}$ ). The limit of detection (LOD) was measured by signal to noise ratio ( $S/N$ ) = 3 and a lower limit of quantitation (LLOQ) measured by means of  $S/N$  = 10. The precision and accuracy of LLOQ was required to be within 20% by FDA guidelines [19].

For the clinical test, 24 healthy male volunteers were given a single oral dose of cilazapril (5 mg). Plasma samples were obtained by centrifuging blood samples collected before dosing and at 0.25, 0.5, 0.75, 1, 1.5, 2, 2.5, 3, 4, 6, 8, and 12 h after intake. Plasma samples were frozen at  $-70^{\circ}\text{C}$  until analysis.

## 3. Results and discussion

### 3.1. LC-MS/MS method

Multiple reaction monitoring (MRM) afforded by tandem mass spectrometry has great advantage in reducing interference and enhancing sensitivity over the selected ion monitoring (SIM). MRM was set for the detection of cilazapril, cilazaprilat and enalapril in this study. To optimize the LC-MS/MS method capillary voltage, cone voltage and collision energy were varied. Using MS scan mode at optimal voltages, protonated molecular ions ( $\text{MH}^+$ ) of cilazapril, cilazaprilat, and enalapril gave sharp signals at  $m/z$  418.4, 390.3, and 377.4, respectively. Tandem mass spectra for all the analytes are shown in Fig. 2. The most abundant product ions at the selected voltages were  $m/z$  211.1 from the parent  $m/z$  418.4 ion, 211.1 from 390.3, and 234.2 from 377.4. Therefore, MRM mode was used at  $m/z$  418.4 > 211.1 for cilazapril,  $m/z$  390.3 > 211.1 for cilazaprilat and  $m/z$  377.4 > 234.2 for enalapril. Optimum tandem MS parameters including resolution, ion energy, entrance and exit potential and collision energy were set to maximize the product ions and the optimum values mentioned in the experimental section were obtained.

### 3.2. Recovery and stability

The recoveries were calculated from the average peak areas of extracted fortified plasma samples read against that of reference solutions in diluent (analytical standards) of the same

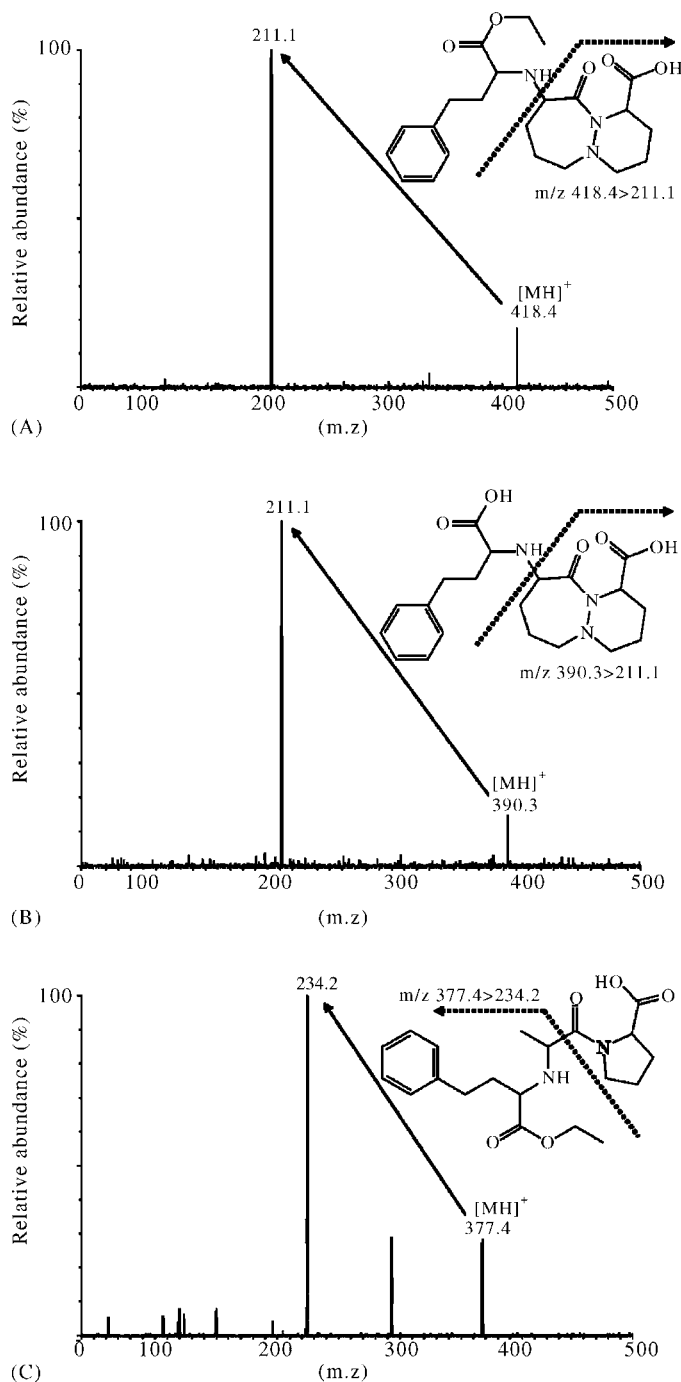


Fig. 2. MS/MS product ion spectra of (A) cilazapril, (B) cilazaprilat and (C) enalapril.

concentration, as there was no appreciable matrix suppression. To decrease LLOQ and analysis time, liquid-liquid extraction was performed using four different extraction solvents (ethyl acetate, hexane, dichloromethane and methyl-*t*-butyl ether). Ethyl acetate was chosen to allow for good recovery of analytes (data not shown). Under acidic conditions, cilazapril and cilazaprilat had higher recovery (Table 1). Cilazaprilat shows the highest recovery at pH 3.2, so plasma pH was adjusted to 3.2 by adding  $20\ \mu\text{l}$  phosphoric acid (10%, v/v). The average absolute recoveries for cilazapril and cilazaprilat in pH 3.2 were

Table 1

Recovery of cilazapril and cilazaprilat using different plasma pH for extraction in the LC–MS/MS method

pH	Cilazapril (%)	Cilazaprilat (%)
7.1	35.0 ± 7.3	4.9 ± 6.8
4.5	95.4 ± 12.2	40.2 ± 9.4
3.2	69.5 ± 5.8	71.2 ± 6.1
2.4	43.2 ± 6.5	43.5 ± 9.6
2.1	35.2 ± 8.1	32.8 ± 4.9
1.9	12.5 ± 12.5	32.4 ± 13.0
1.8	3.9 ± 10.4	29.8 ± 18.2

69.5 ± 5.8 and 71.2 ± 6.1%, respectively. The recovery of I.S. was 76.8 ± 4.4. The extents of recovery of cilazapril, cilazaprilat and enalapril were consistent, precise, and reproducible, which was satisfactory.

To evaluate analytes stability in human plasma, drug-free plasma samples were spiked at 0.5, 50 and 500 ng ml<sup>-1</sup> (cilazapril), and 1, 10 and 50 ng ml<sup>-1</sup> (cilazaprilat). After extraction, samples were arranged in the autosampler and were analyzed. No significant deterioration was observed under any of these conditions (Table 2).

### 3.3. Specificity, linearity, limit of detection, precision and accuracy

The YMC column, with a mobile phase of methanol with 10 mM ammonium formate (pH 3.2 with formic acid) at a ratio of 90:10 (v/v), produced a short chromatographic run time (2.0 min) with satisfactory separation of cilazapril, cilazaprilat, and enalapril. Fig. 3 shows typical chromatograms of the sample analysis. No interference with constituents from drug-free human plasma was observed. Cilazapril, cilazaprilat and the internal standard separated from the biological background at 1.21, 1.12, and 1.19 min, respectively. The total analysis time for each run was 2 min.

Assay linearity was evaluated with calibration curves ranging from 0.1 to 500 ng ml<sup>-1</sup> of cilazapril and 0.5 to 50 ng ml<sup>-1</sup> of cilazaprilat. A good linear relationship between peak area ratios and concentrations was established: for cilazapril,  $y = 0.002203x + 0.000143$ ;  $r^2 = 0.99995$ , where  $y$  is the peak area ratio (cilazapril/enalapril) and  $x$  is the concentration (ng ml<sup>-1</sup>) of cilazapril, and  $y = 0.000147x + 0.000395$ ;  $r^2 = 0.99980$  for cilazaprilat. An LOD of 0.01 ng ml<sup>-1</sup> for cilazapril and 0.1 ng ml<sup>-1</sup> for cilazaprilat were determined at a signal to noise ratio of 3, which was more sensitive than reported methods [11–13]. An LLOQ of 0.1 ng ml<sup>-1</sup> for cilazapril and 0.5 ng ml<sup>-1</sup> for cilazaprilat were determined at S/N = 10, with precision and accuracy within 20% for LC–MS/MS. With dual extensive washes (five washes per injection) of the syringe, the carryover was not observed, allowing us to reach an LLOQ.

Within-assay and between-assay precision and accuracy in human plasma for four levels of concentration of cilazapril and cilazaprilat are summarized in Table 3. All results were within appropriate ranges for precision (%) and accuracy (%), and were acceptable for bio-analytical applications.

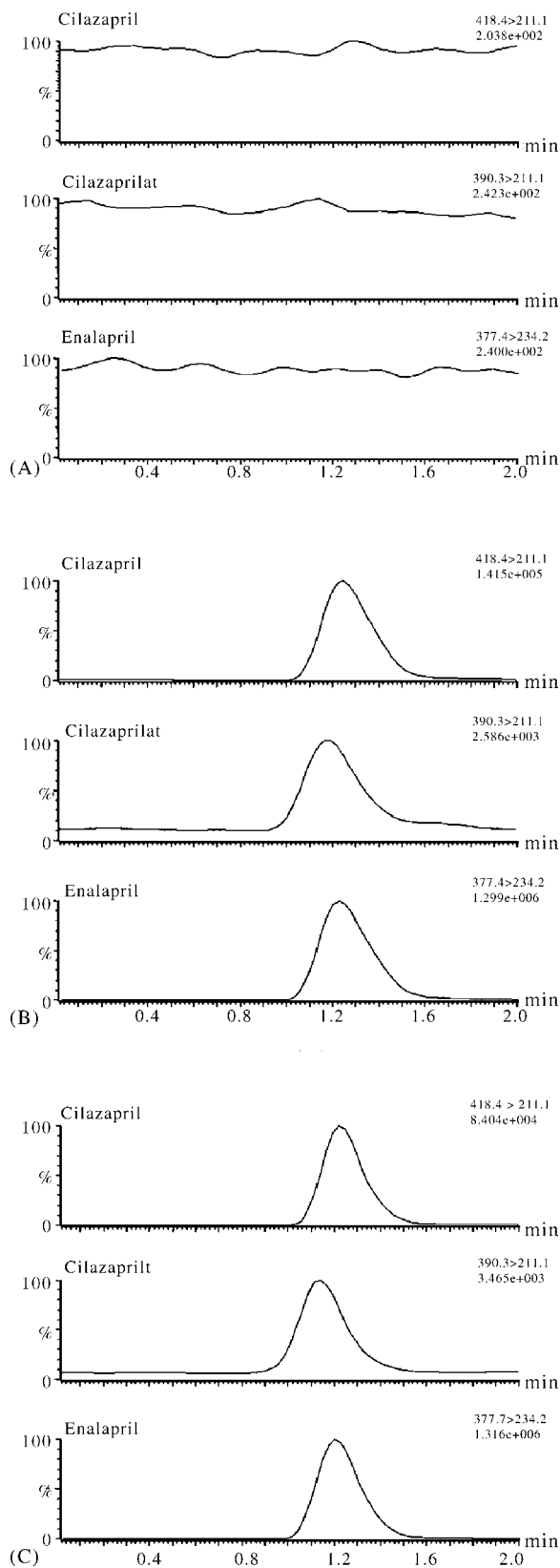


Fig. 3. Chromatogram of (A) blank human plasma, (B) plasma spiked with 50 ng ml<sup>-1</sup> cilazapril and 10 ng ml<sup>-1</sup> cilazaprilat, and (C) sample plasma (measured cilazapril concentration: 27.2 ng ml<sup>-1</sup> and cilazaprilat: 15.8 ng ml<sup>-1</sup>).



Table 2  
Stability data for cilazapril and cilazaprilat (mean  $\pm$  S.D.,  $n = 3$ )

Theoretical concentration (ng ml <sup>-1</sup> )	Cilazapril			Cilazaprilat		
	0.5	50	500	1	10	50
<b>Short term</b>						
24 h, 4 °C (%)	96.4 $\pm$ 8.1	95.4 $\pm$ 4.7	98.6 $\pm$ 6.8	104.8 $\pm$ 9.4	92.7 $\pm$ 9.0	98.9 $\pm$ 11.4
24 h, room temperature (%)	98.6 $\pm$ 5.7	105.3 $\pm$ 8.4	96.1 $\pm$ 9.1	98.6 $\pm$ 10.2	93.2 $\pm$ 4.2	106.8 $\pm$ 10.5
24 h, -20 °C (%)	103.8 $\pm$ 7.6	95.6 $\pm$ 9.9	92.0 $\pm$ 12.6	103.9 $\pm$ 9.0	108.2 $\pm$ 12.2	98.8 $\pm$ 12.8
12 h, 4 °C, extracted (%)	105.8 $\pm$ 4.9	107.2 $\pm$ 6.1	99.4 $\pm$ 5.6	97.5 $\pm$ 5.9	101.7 $\pm$ 9.6	105.4 $\pm$ 8.8
<b>Long term</b>						
30 days, -70 °C (%)	96.4 $\pm$ 5.9	97.9 $\pm$ 13.1	99.1 $\pm$ 10.3	91.2 $\pm$ 12.4	105.8 $\pm$ 10.8	109.5 $\pm$ 7.5
Freeze-thaw stability (%)	94.3 $\pm$ 12.5	98.2 $\pm$ 9.7	109.4 $\pm$ 7.6	89.7 $\pm$ 13.2	92.0 $\pm$ 8.4	87.1 $\pm$ 14.1

### 3.4. Application to the clinical test

The proposed method was applied to the determination of cilazapril and cilazaprilat in human plasma after a single oral administration of cilazapril (5 mg tablet) to 24 healthy male volunteers. Plasma concentrations of cilazapril and cilazaprilat were in the standard range and remained above 0.1 ng ml<sup>-1</sup> (cilazapril) and 0.5 ng ml<sup>-1</sup> (cilazaprilat) for the entire sampling period. All 312 clinical samples were divided into two batches, with each batch consisting of a calibration curve, 156 samples from 12 subjects, and 6 quality controls. It took about half an hour for sample preparation and 7 h for sample analysis. All samples were analyzed in 2 days. A typical plasma concentration versus time profiles of cilazapril and cilazaprilat were shown in Fig. 4. The area under the plasma concentration versus time curve from time 0 to 12 h sampling time (AUC<sub>12h</sub>) were 240.8  $\pm$  163.7 (cilazapril) and 73.6  $\pm$  30.6 (cilazaprilat) ng ml<sup>-1</sup> h, respectively. And, the area under the plasma concentration versus time curve from time 0 to infin-

Table 3  
Precision and accuracy data for the analysis of cilazapril and cilazaprilat in human plasma ( $n = 5$ )

Analyte	Nominal concentration (ng ml <sup>-1</sup> )	Measured concentration (ng ml <sup>-1</sup> )	Precision (%)	Accuracy (%)
<b>Within-assay</b>				
Cilazapril	0.1	0.11 $\pm$ 0.01	8.33	105.00
	0.5	0.50 $\pm$ 0.01	1.95	99.72
	50	49.58 $\pm$ 0.26	0.52	99.16
	500	493.29 $\pm$ 2.10	0.43	98.66
Cilazaprilat	0.5	0.49 $\pm$ 0.05	10.52	97.20
	1	1.01 $\pm$ 0.06	6.33	101.00
	10	10.77 $\pm$ 0.62	5.76	107.69
	50	46.15 $\pm$ 1.18	2.56	92.31
<b>Between-assay</b>				
Cilazapril	0.1	0.11 $\pm$ 0.01	7.82	107.00
	0.5	0.52 $\pm$ 0.05	9.46	103.02
	50	48.41 $\pm$ 0.82	1.70	96.83
	500	485.87 $\pm$ 5.14	1.06	97.17
Cilazaprilat	0.5	0.50 $\pm$ 0.02	3.20	100.45
	1	1.03 $\pm$ 0.03	3.26	103.38
	10	10.52 $\pm$ 0.71	6.77	105.22
	50	46.64 $\pm$ 2.45	5.26	93.28

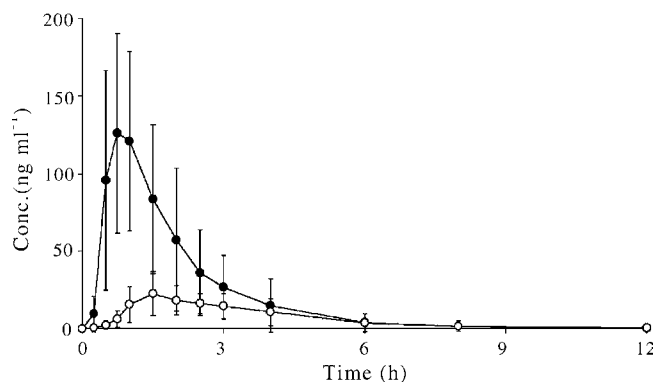


Fig. 4. Mean concentration-time pharmacokinetic profile of cilazapril (●) and cilazaprilat (○) in human plasma from 24 healthy male volunteers after single oral administration of cilazapril tablet (5 mg).

ity (AUC<sub>inf</sub>) were 241.8  $\pm$  166.1 (cilazapril) and 77.5  $\pm$  31.6 (cilazaprilat) ng ml<sup>-1</sup> h, respectively. The observed maximum plasma concentration ( $C_{max}$ ) of cilazapril and cilazaprilat were 139.9  $\pm$  60.5 and 25.7  $\pm$  14.1 ng ml<sup>-1</sup>, respectively. The average  $T_{max}$  of cilazapril was 0.8  $\pm$  0.2 h and that for cilazaprilat was 1.8  $\pm$  0.7 h. Half-life of drug elimination during the terminal phase ( $t_{1/2}$ ) were 1.4  $\pm$  0.3 (cilazapril) and 2.3  $\pm$  1.1 (cilazaprilat), respectively. This method is well suited for routine high-throughput analyses, such as in a pharmacokinetic study.

### 4. Conclusion

We developed a simple, rapid, and sensitive LC-MS/MS method for the simultaneous determination of cilazapril and cilazaprilat in human plasma and fully validated it according to FDA guidelines. The present method affords the sensitivity, accuracy, and precision necessary for quantitative measurements in pharmacokinetic studies and therapeutic monitoring of cilazapril and cilazaprilat.

### Acknowledgement

This work was supported by a grant no. R13-2002-020-01002-0 from the Korea Science & Engineering Foundation.

**References**

- [1] I.L. Natoff, J.S. Nixon, R.J. Francis, L.R. Klevans, M. Brewster, J. Budd, A.T. Patel, J. Wenger, E. Worth, J. Cardiovasc. Pharm. 7 (1985) 569.
- [2] J.R. Rosenthal, U. Osowski, Cardiology 87 (1996) 54.
- [3] I.L. Natoff, S. Redshaw, Drug. Future 12 (1987) 475.
- [4] M. Litter, Farmacología Experimental y Clínica, 7th ed., El Ateneo, Buenos Aires, 1986.
- [5] F. Deget, R.N. Brogden, Drugs 41 (1991) 799.
- [6] T. Szucs, Drugs 41 (1991) 18.
- [7] U. Tamer, O.N. Pekmez, O. Atay, A. Yildiz, J. Pharm. Biomed. Anal. 29 (2002) 43.
- [8] J. Essig, G.G. Belz, A. Wellstein, Br. J. Clin. Pharmacol. 27 (1989) 217S.
- [9] A.A. Ajayi, H.L. Elliott, J.L. Reid, Br. J. Clin. Pharmacol. 22 (1986) 167.
- [10] H. Tanaka, Y. Yoneyama, M. Sugawara, I. Umeda, Y. Ohta, J. Pharm. Sci. 76 (1987) 224.
- [11] J.A. Prieto, R.M. Jiménez, R.M. Alonso, J. Chromatogr. B 714 (1998) 285.
- [12] N. Erk, F. Onur, Anal. Lett. 29 (1996) 1963.
- [13] A. Gumieniczek, L. Przyborowski, J. Liq. Chromatogr. R. T. 20 (1997) 2135.
- [14] A. Sioufi, F. Pommier, J. Chromatogr. 434 (1988) 239.
- [15] H.J. Leis, M. Leis, W. Welz, J. Chromatogr. 529 (1990) 299.
- [16] N. Goto, T. Kamata, K. Ikegami, J. Chromatogr. 578 (1992) 195.
- [17] H. Shioya, M. Shimojo, Y. Kawahara, Biomed. Chromatogr. 6 (1992) 59.
- [18] H.H. Maurer, T. Kraemer, J.W. Arlt, Ther. Drug. Monit. 20 (1998) 706.
- [19] FDA Guidance for Industry, Statistical Approaches to Establishing Bioequivalence, US Department of Health and Human Services, Food and Drug Administration, Center for Drug Evaluation and Research (CDER), 2001. Website: <http://www.fda.gov/cder/guidance/index.htm>.

# A new room temperature ionic liquid 1-butyl-3-trimethylsilylimidazolium hexafluorophosphate as a solvent for extraction and preconcentration of mercury with determination by cold vapor atomic absorption spectrometry

Zaijun Li<sup>a,\*</sup>, Qin Wei<sup>b</sup>, Rui Yuan<sup>a</sup>, Xia Zhou<sup>a</sup>, Huizhen Liu<sup>a</sup>, Haixia Shan<sup>a</sup>, Qijun Song<sup>a</sup>

<sup>a</sup> College of Chemical and Materials Engineering, Southern Yangtze University, 170 Huihe Road, Wuxi 214036, PR China

<sup>b</sup> College of Chemistry and Chemical Engineering, Jinan University, Jinan 250022, PR China

Received 8 November 2005; received in revised form 5 February 2006; accepted 7 March 2006

Available online 17 April 2006

## Abstract

A new room temperature ionic liquid 1-butyl-3-trimethylsilylimidazolium hexafluorophosphate abbreviated as [C<sub>4</sub>tmsim][PF<sub>6</sub>] was synthesized and developed as a novel medium for liquid/liquid extraction of inorganic mercury in this work. Under optimal condition, *o*-carboxyphenyldiazoamino-*p*-azobenzene abbreviated as CDAA reacted with inorganic mercury to form a neutral Hg–CDAA complex, the complex was rapidly extracted into ionic liquid phase. After back-extracting into aqueous phase with sulfide sodium solution, the mercury concentration was detected by cold vapor atomic absorption spectrometry. The extraction and back-extraction efficiencies were 99.9 and 100.1% for 5.0 μg L<sup>-1</sup> standard mercury in 1000 mL of water solution, respectively. The detection limit, calculated using three times the standard error of estimate of the calibration graph, is 0.01 ng of mercury per milliliter water sample. The proposed method has been used to the determination of trace inorganic mercury in natural water with satisfactory results. Moreover, Zeta potential and surface tension of [C<sub>4</sub>tmsim][PF<sub>6</sub>] solution were measured and applied to explain the extraction mechanism of [C<sub>4</sub>tmsim][PF<sub>6</sub>] system.

© 2006 Elsevier B.V. All rights reserved.

**Keywords:** Room temperature ionic liquid; 1-Butyl-3-trimethylsilylimidazolium hexafluorophosphate; Solvent extraction; Inorganic mercury; Water; Cold vapor atomic absorption spectrometry

## 1. Introduction

Mercury is a global pollutant and is identified as a highly toxic element because of its accumulative and persistent character in the environment and living organisms. Therefore, routine monitor and control of mercury is becoming increasingly important, especially in water system. In literatures, many modern technologies such as atomic absorption/emission spectrometry [1,2], inductively coupled plasma mass spectrometry [3,4], atomic fluorescence spectrometry [5] and voltammetric determination [6] have been reported to the determination of trace mercury, but these methods are difficult to directly apply to the determination of trace mercury in natural water due to their limited sensitiv-

ity. Recent years, professor Wang and Hansen developed many sample separation and preconcentration procedures based on the solvent extraction. The solvent extraction can effectively decrease the detection limit and eliminate matrix interference, these coupling above methods have been applied to determination of ultra-trace level heavy metals [7–9]. However, the use of classical extraction method requires large amounts of high purity solvents for the extraction, this may also result environmental and safety problems due to volatilization of the solvents

Room temperature ionic liquid has aroused increasing interest for their promising role as alternative medium in synthesis [10], separation [11,12] and electrochemistry [13] as a result of their unique chemical and physical properties [14]. As ionic liquids have no detectable vapor pressure and are relatively thermal stable, hence many environmental and safety problems associated with organic solvents are avoided. Recently, the applications of ionic liquid in analytical chemistry have also

\* Corresponding author. Tel.: +86 5105811863; fax: +86 5105811863.  
E-mail address: [zaijunli@263.net](mailto:zaijunli@263.net) (Z. Li).

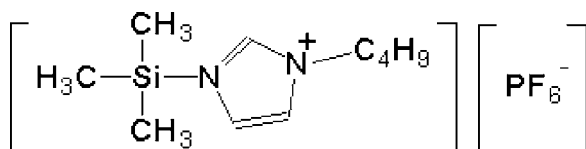


Fig. 1. The molecule structure of [C<sub>4</sub>tmsim][PF<sub>6</sub>].

started to receive attention [15–19], in which a typical room temperature ionic liquid 1-butyl-3-methylimidazolium hexafluorophosphate abbreviated as [C<sub>4</sub>mim][PF<sub>6</sub>] was often studied as extraction medium [20]. Because the volume of the sample is usually smaller than 5 mL in the most of previous works, the enrichment effect usually was not very ideal. In this study, we attempt to use [C<sub>4</sub>mim][PF<sub>6</sub>] as solvent for the extraction of inorganic mercury in a relatively large water sample (1000 mL of water). It was found that the extraction efficiency of the inorganic mercury is very low due to its relatively high water solubility when the volume of [C<sub>4</sub>mim][PF<sub>6</sub>] was smaller than 25 mL. In order to resolve the problem, a new room temperature ionic liquid, 1-butyl-3-trimethylsilylimidazolium hexafluorophosphate abbreviated as [C<sub>4</sub>tmsim][PF<sub>6</sub>], was designed and synthesized in the laboratory (shown in Fig. 1). Experiment indicated that [C<sub>4</sub>tmsim][PF<sub>6</sub>] has much lower water solubility (0.5 g L<sup>-1</sup>) than [C<sub>4</sub>mim][PF<sub>6</sub>] (18 g L<sup>-1</sup>), but also can extract the mercury complex more effectively. So, [C<sub>4</sub>tmsim][PF<sub>6</sub>] can be used as an excellent solvent for liquid/liquid extraction of trace mercury in a relatively large volume samples.

*o*-Carboxyphenyl diazoamino *p*-azobenzene abbreviated as CDAA is a sensitive and selective chromogenic reagent for spectrophotometric determination of mercury [21]. Unlike dithizone, CDAA reacts with inorganic mercury to form a stable complex, which do not react with organic mercury in the same conditions, the reaction condition is simple and easy to control. Therefore in this work CDAA was employed as chelator to form a neutral mercury complex to evaluate the [C<sub>4</sub>tmsim][PF<sub>6</sub>] extraction system. After the preconcentration, cold vapor atomic absorption spectrometry was used to as a detection method for the determination of trace mercury in natural water. Proposed method offers the advantages of rapidity, simplicity and high sensitivity without the need for potentially toxic organic solvent.

## 2. Experimental

### 2.1. Reagents

All reagents were of analytical reagent grade and ultra pure water (18.2 MΩ cm) was used throughout the experiment. A stock solution of 1.0 mg mL<sup>-1</sup> mercury(II) was prepared by dissolving appropriate amounts of analytical reagent grade Hg(NO<sub>3</sub>)<sub>2</sub> in 2% nitric acid solution. Working solutions were prepared immediately before use. All glassware used was soaked with 10% nitric acid for 1 day and rinsed with ultra pure water before use. The chelating agent, CDAA was purchased from Shanghai Zhongke Chemical Limit Company (Shanghai, China). A 1.0 × 10<sup>-3</sup> mol L<sup>-1</sup> CDAA solution was prepared by dissolving appropriate amounts of CDAA in 95% ethanol. 1-

Trimethylsilylimidazole was provided by Linhai Kaile Chemical Company (Linhai city, China), and other all reagents employed were purchased from Shanghai Chemical Company (Shanghai, China).

### 2.2. Apparatus

The mercury measurements were performed with a Perkin-Elmer 2380 atomic absorption spectrometer, equipped with a deuterium background corrector, a hollow cathode mercury lamp, a PE3030 mercury vapor generator with MHS-20 hydride atomizer. A UV-240 spectrophotometer (Shimadzu, Tokyo) was used for recording the UV spectra. A DRX-500 nuclear magnetic resonance (NMR) spectrometer was used for <sup>1</sup>H NMR and <sup>13</sup>C NMR analyses (Bruker, Russ, Germany).

### 2.3. Preparation of ionic liquid

Transfer equal amounts (0.5 mol) of 1-bromobutane and 1-trimethylsilylimidazole (distilled freshly) to 500 mL round bottom flask which is fitted with reflux condenser and nitrogen protecting facilities. Add 50 mL of toluene to the flask as solvent. After the mixture was stirred at 70 °C for 18 h, a transparent viscous product, 1-butyl-3-trimethylsilylimidazolium bromide was formed. The liquid was cooled and transferred to a 2000 mL beaker. And then 500 mL of potassium hexafluorophosphate (0.5 mol) was added to the well stirred mixture. After the addition of the reagent, the mixture was continuously stirred for 4 h. And then the water phase was discarded and the formed ionic liquid [C<sub>4</sub>tmsim][PF<sub>6</sub>] was washed with water until bromide ion was wiped off completely using a silver nitrate test. The collected ionic liquid was heated to 110 °C under vacuum to remove water, the solvent and unreacted reagents, total yield was about 80%. The NMR data of the product were listed in the following: <sup>1</sup>H NMR (500 MHz, CD<sub>3</sub>OCD<sub>3</sub>), 0.454 (s, 9H), 0.886 (t, 3H), 1.316 (m, 2H), 1.862 (m, 2H), 4.24 (m, 2H), 7.495 (d, 1H), 7.661 (d, 1H), 8.64 (d, 1H); <sup>13</sup>C NMR (500 MHz, CD<sub>3</sub>OCD<sub>3</sub>), 136.74, 123.78, 122.93, 50.72, 32.96, 20.46, 14.14, 14.11.

### 2.4. Measurement extraction efficiencies of the complex and CDAA

A 1000 mL of the synthesized water sample containing 5 μg of standard mercury and 1.0 × 10<sup>-6</sup> mol L<sup>-1</sup> CDAA was used to investigate extraction efficiencies of the complex. After addition of 5 mL [C<sub>4</sub>tmsim][PF<sub>6</sub>] to above solution, the biphasic system was shaken to ensure it was fully mixed. Wait until the phase separation complete, the upper aqueous phase was taken out and the concentration of mercury that was left in the aqueous phase was measured by cold vapor atomic absorption spectrometry. The extraction efficiencies of the complex abbreviated as *E<sub>c</sub>* were calculated by *E<sub>c</sub>* (%) = (C<sub>0</sub> - C<sub>1</sub>)/C<sub>0</sub> × 100, where C<sub>0</sub> and C<sub>1</sub> are the concentration of mercury in aqueous phase before and after extraction, respectively. The extraction efficiency of CDAA was determined using a similar preparation procedure, but without the addition of standard mercury. Absorption spectrum of the aqueous phase was measured on the spectrophotometer against

water. Its extraction efficiency abbreviated as  $E_R$  were calculated by  $E_R (\%) = (A_0 - A_1)/A_0 \times 100$ , where  $A_0$  and  $A_1$  are the absorbance in aqueous phase at corresponding maximum absorption before and after extraction, respectively.

### 2.5. Surface tension and Zeta potential measurements

Surface tension measurements were made by using the Wilhelmy plate technique. The Wilhelmy plate (sand-blasted platinum, ca. 5-cm perimeter) was hung from the arm of a Bethlehem dial-type torsion balance with solutions immersed in a constant temperature bath at the desired temperature,  $20 \pm 1$  °C. The instrument was calibrated against the quartz-condensed water each day. Sets of measurements were taken at 30 min intervals until no significant change occurred; Zeta potential of the ionic liquid solution was performed with Zetasizer model 2000 (Malvern Instruments Ltd., UK).

### 2.6. Procedure for preconcentration of trace mercury

An aliquot of 1000 mL of the natural water or synthesized water sample was transferred to a 2000 mL segregator. 1.0 mL of concentration ammonia and 1.0 mL of  $1.0 \times 10^{-3}$  mol L<sup>-1</sup> CDAA solution were added subsequently. After the solution was shaken up, the extraction of Hg–CDAA complex was performed by mixing 5 mL ionic liquid with the complexes and shaking for about 1.0 min and deposited for 5.0 min to separate the two phases. After the separation of the aqueous phase, to the ionic liquid phase 5.0 mL of  $1.28 \times 10^{-4}$  mol L<sup>-1</sup> sulfide sodium solution was added to strip the mercury ion. For different concentration of mercury, an appropriate amount of upper aqueous solution was introduced into the reduction vessel for determination of mercury.

## 3. Results and discussion

### 3.1. The formation of Hg–CDAA complex

CDAA was good organic reagent for spectrophotometric determination of mercury, the analytical characteristic in selectivity and sensitivity are remarkably superior over most of the reagents for the determination of mercury in literatures, and the reaction condition is simple and easy to control [21]. For the reason, CDAA was employed as a chelator to form a neutral Hg–CDAA complex to test the liquid/liquid extraction of mercury with [C<sub>4</sub>tmsim][PF<sub>6</sub>]. In order to adapt to the extraction of very low level of inorganic mercury in a relatively large volume water sample, the reaction condition for the formation of Hg–CDAA complex was investigated. Although an addition of non-ionic surfactant Triton X-100 can increase the absorbance of the complex remarkably, the addition of Triton X-100 will result that the remove of ionic liquid from aqueous phases required a longer time and have to use of centrifuge to expedite the separation. In order to overcome the problem, the reaction of mercury ion with CDAA in the absence of surfactant was studied. The results showed that CDAA can react with inorganic mercury ion to form stable complex, thus a simple procedure, i.e., without

addition of surfactant was adopted in the work. The reaction of CDAA with mercury ions can carry out in a wide pH value range from 9.0 to 13. For a large volume water samples such as 1000 mL of water, a small volume of concentrated ammonia can provide the required acidity for the reaction. Therefore in this work a final concentration of ammonia used was 0.015 mol L<sup>-1</sup> and it was also found that  $5.0 \times 10^{-6}$  mol L<sup>-1</sup> CDAA is enough to extract up to 20 µg of mercury in 1000 mL of water.

### 3.2. Effect of the amounts of ionic liquid on the extraction

Once the solution of Hg–CDAA complexes was mixed with [C<sub>4</sub>tmsim][PF<sub>6</sub>], Hg–CDAA was removed from aqueous phase and the characteristic absorption peak of Hg–CDAA complex in aqueous phase disappeared. It was found that amounts of ionic liquid remarkably affect on the extraction efficiency. With the increase of the volume of ionic liquid, the extraction efficiency increased rapidly at first and then leveled off after the volume of ionic liquid was greater than 4.0 mL. Thus, an addition of 5.0 mL ionic liquid is recommended. In order to compare with old ionic liquid, the effect of another typical room temperature ionic liquid [C<sub>4</sub>mim][PF<sub>6</sub>] amounts was also investigated using a similar procedure, in which a 5 min of centrifuging separation at 3000 r/min was used to accelerate the separation of ionic liquid from aqueous phase. It was found the extraction efficiency is very poor when the volume of [C<sub>4</sub>mim][PF<sub>6</sub>] is smaller than 20 mL. The results indicated that [C<sub>4</sub>tmsim][PF<sub>6</sub>] has better performance in the liquid/liquid extraction than [C<sub>4</sub>mim][PF<sub>6</sub>]. The reason is that [C<sub>4</sub>mim][PF<sub>6</sub>] is difficult to form an immiscible extraction phase when its volume is less than 12 mL due to relatively high water solubility.

### 3.3. Select of method for back-extraction of mercury ions from ionic liquid

Since the Hg–CDAA complex was formed at an alkaline medium, the complex may be decomposed to mercury ion and enter aqueous phase by using strong acid solution. Basing on the consideration, various mineral acids were used to back-extraction of mercury from ionic liquid including nitric acid, sulfuric acid, hydrochloric acid and phosphoric acid. The experiments indicated although all strong acid can decompose the Hg–CDAA complex, a high acid concentration and long heating time were required to obtain good back-extraction efficiency due to the complex good stability in ionic liquid. However, EDTA and sulfide sodium are better reagents for decomposing organometallic compounds. The experiments indicated sodium sulfide can decompose Hg–CDAA complex rapidly with an ideal the recovery. When  $1.28 \times 10^{-4}$  mol L<sup>-1</sup> sodium sulfide excess 4.0 mL, almost all mercury ions were back-extracted to aqueous phase from ionic liquid. Thus, an addition of 5 mL of  $1.28 \times 10^{-4}$  mol L<sup>-1</sup> sulfide sodium solution was selected in the following experiments.

### 3.4. Characteristics of the complex

Under optimal conditions, Hg–CDAA complex could immediately formed and could stabilize for 4 h at room temperature.



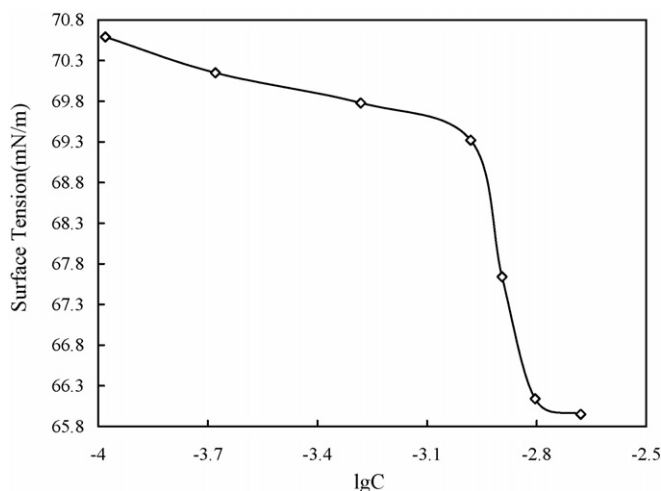


Fig. 2. Surface tension and critical micelle concentration of  $[C_4tmsim][PF_6]$ , measurement temperature:  $25 \pm 0.1^\circ C$ .

The composition ratio of Hg–CDAA complex obtained using Job's method of continuous variation and the slope-ratio method was 1:2 (Hg:CDAA). Because absorption spectra of the complexes in aqueous and ionic liquid phase have a very similar shape, this attest the extraction do not influence on the complex's composition. In addition, it was also observed the stability of the complex in ionic liquid is better than that in the aqueous solution, the absorbance can remain stable for at least 24 h under room temperature.

### 3.5. Extraction mechanism study

To study extraction mechanism of  $[C_4tmsim][PF_6]$  system, the surface tension and Zeta potential of the ionic liquid solution were investigated in detail. It was found the surface tension of the solution decreased with increase of the concentration of  $[C_4tmsim][PF_6]$  solution, its critical micelle concentration and surface tension of saturated  $[C_4tmsim][PF_6]$  solution are  $1.59 \times 10^{-3} \text{ mol L}^{-1}$  and  $65.95 \text{ Nm/m}$  (see Fig. 2), respectively. Above data showed ionic liquid has high surface activity, this property allow the ionic liquid to fully interact with the complex or CDAA in aqueous phase and easy to extract the complex into the ionic liquid phase due to micelle extraction function, which is unique property of surfactant. On the other hand, the Zeta potential value of saturated  $[C_4tmsim][PF_6]$  solution was found to be  $+2.1 \text{ mV}$ . The result showed the double electron layer at the  $[C_4tmsim][PF_6]$ –water interface existed the positive charge. The positive charge will produce strong interaction between Hg–CDAA complex or CDAA species and ionic liquid surface. Above two factors allow ionic liquid has a higher the extraction efficiency than ordinary organic solvent. It should be stated that Zeta potential may be positive or negative value for different ionic liquid, that decide various ionic liquid has different extraction performance. In order to test suggested extraction mechanism, the extraction efficiencies of CDAA in different acidity was researched by using a procedure in Section 2.4. The result is very interesting that the order of the extraction efficiency of CDAA is in base > neutral > acid medium. Because CDAA is a

weak organic acid, its dissociation product three reagent species in water, these are  $RH_2$ ,  $RH^-$  and  $R^{2-}$ , respectively, in which CDAA was replaced by  $RH_2$  in order to simple. In strong base solution, reagent specie is  $R^{2-}$  mainly, it is easy to extract into ionic liquid due to its strong negative electric charge, the order accord with suggested extraction mechanism.

### 3.6. Analytical parameters

The linearity of the response in the range from 10 to 120 ng of mercury in the reduction vessel was checked. Inorganic mercury  $y = 0.00975x + 0.00102$ ,  $r = 0.9998$ , in which  $y$  is absorbance,  $x$  is amounts of mercury in reduction vessel. The detection limits, defined as the mercury concentration corresponding to three times the standard deviation of 11 reagent blanks, in which reagent and calibration graph were prepared using a previous preconcentration procedure described in Section 2.6, is  $0.01 \text{ ng}$  of mercury per milliliter of water sample.

The precision of the procedure was estimated from the values obtained in the independent analysis of 10 synthesized water samples ( $5 \mu\text{g}$  of standard mercury was added in  $1000 \text{ mL}$  of ultra pure water). Samples were extracted and back-extraction, then  $50 \mu\text{L}$  aliquot of  $5 \text{ mL}$  of this solution was introduced into the digestion vessel. Mean mercury value is  $4.98 \mu\text{g}$ , the relative standard deviation was  $1.2\%$ . These values can be considered acceptable for a trace element measurement. Accuracy of proposed method was also determined through the analysis of spiked tap natural water sample using standard addition calibration method. The sample was analyzed after the sample was preconcentration using a procedure in Section 2.6, the recovery was between  $98.3$  and  $101.4\%$ . The data indicated proposed method has an excellent precision and accuracy.

### 3.7. Interference in the extraction of inorganic mercury with ionic liquid

Except for cadmium(II) and silver(I), all foreign ions studied do not react with CDAA to form stable the complex in an ammonia medium and interfere with the extraction of inorganic mercury with ionic liquid. The effect of cadmium and silver ions on the extraction efficiency of inorganic mercury was researched in detail. Results indicated the complex of cadmium and silver with CDAA can be extracted into ionic liquid phase effectively, but 20-fold of cadmium and silver do not reduce the extraction efficiency of inorganic mercury obviously when the concentration of CDAA is bigger than the two times stoichiometric concentration of the metal ions. Although methylmercury always coexist in the natural water due to biotic processes and may effect on the determination of inorganic mercury, it is difficult to extract into ionic liquid phase effectively because methylmercury cannot react with CDAA to form a stable complex in the same condition, the results showed that equal methylmercury do not interfere with the determination of inorganic mercury. Moreover, the anions are assumed to compete with CDAA for complex formation and may lead to interference. The results indicated that the interference of anions on the extraction of

Table 1  
Analysis of inorganic mercury in natural waters

Sample	Inorganic mercury added (ng L <sup>-1</sup> )	Mercury found (ng L <sup>-1</sup> ) <sup>a</sup>	Recovery (%)
Lake water	0.0	22.16 ± 1.2	101.2
	30.0	52.53 ± 1.8	
Tap water	0.0	32.56 ± 2.2	98.3
	50.0	81.7 ± 1.2	
Sea water	0.0	23.54 ± 2.0	101.4
	25.0	48.88 ± 3.3	

<sup>a</sup> Mean ± standard deviation (*n* = 5).

inorganic mercury is negligible. This is due to large formation constant of Hg–CDAA complex.

### 3.8. Sample analysis

In order to validate the methodology, the method proposed for mercury determination was applied to natural waters analysis. Lake water and river water containing mercury were collected from Wuxi station in Taihu Lake, where effluents from various industries mix with lake water and river water. Sea water samples were collected from Yellow Sea around Shandong area. The water samples were filtered through 0.45 μm pore size milipore membrane filters. Trace mercury in samples was preconcentrated by using a procedure described in Section 2.6. Upper aqueous solution was used for the determination of mercury by cold vapor atomic absorption spectrophotometry (*l* = 253.7 nm, lamp intensity 8 mA, slit width 0.7 nm). A silicone drop was added to 2 mL of the solution which was transferred to the reduction vessel, 1.0 mL of 1% (w/v) SnCl<sub>2</sub> solution was added, and then air was vigorously bubbled into the mixture. The measured peak height corresponded to the mercury. Once the signal had gone to the base line, 0.5 mL of the oxidizing solution followed by 1.0 mL of 1% (w/v) NaBH<sub>4</sub> were added. The signal corresponded to the mercury present in the vessel. The results were listed in Table 1. Accuracy of proposed method was also determined through the analysis of spiked tap water sample using standard addition calibration method. Real water samples spiked with standard inorganic mercury solution. The sample was analyzed by using above procedure, the results were listed in Table 1.

### 3.9. Recycling ionic liquid

The feasibility of recycling [C<sub>4</sub>tmsim][PF<sub>6</sub>] in liquid/liquid extraction of 1.0 μg of mercury at 0.015 mol L<sup>-1</sup> ammonia medium with CDAA was examined. After the extraction, the ionic liquid phase was mixed with 1.28 × 10<sup>-4</sup> mol L<sup>-1</sup> sulfide

sodium solution to remove mercury ion from the ionic liquid. Then, the ionic liquid was recycled for reuse. This extraction and stripping process was repeated six cycles. Cold vapor atomic absorption spectrometry was used to measure the concentration of mercury ion in acidic aqueous phase after each stripping process. Average extraction efficiency of 99.4% was obtained. The results indicate that ionic liquid can be recycled for reuse in liquid/liquid extraction of mercury.

### 3.10. Conclusions

Low water solubility of [C<sub>4</sub>tmsim][PF<sub>6</sub>] and good extraction efficiency for neutral molecule and organic negative ion allow its use in solvent extraction of hydrophobic compounds, especially to extraction of trace amounts of metal ions in large volume water samples. Since [C<sub>4</sub>tmsim][PF<sub>6</sub>] can be reused, proposed procedure is very economical, thus, it can be used as novel medium to replace traditional volatile organic solvents in various routine analysis.

### References

- [1] J.L. Capelo, G.M. Rivas, L.G. Oliveira, C. Vilhena, A.C. Santos, T. Valada, M. Galesio, P. Oliveira, M.D.R. Gomes da Silva, E.M. Gaspair, S. Alves, C. Fernandez, C. Vaz, *Talanta* 68 (2006) 813–818.
- [2] A.N. Anthemidis, G.A. Zachariadis, J.A. Stratis, *Talanta* 64 (2004) 1053–1057.
- [3] J. Qvarnstrom, W. Frech, *J. Anal. Atom. Spectrom.* 17 (2002) 1486–1491.
- [4] P. Jitaru, H.G. Infante, F.C. Adams, *Anal. Chim. Acta* 489 (2003) 45–47.
- [5] T. Stoichev, R.C. Rodriguez Martin-Doimeadios, E. Tessier, D. Amouroux, O.F.X. Donard, *Talanta* 62 (2004) 433–438.
- [6] N.L.D. Filho, D.R. do Carmo, *Talanta* 68 (2006) 919–927.
- [7] J.H. Wang, E.H. Hansen, *Anal. Chim. Acta* 456 (2002) 283–292.
- [8] J.H. Wang, E.H. Hansen, *J. Anal. Atom. Spectrom.* 17 (2002) 1284–1289.
- [9] E.H. Hansen, J.H. Wang, *Anal. Chim. Acta* 467 (2002) 3–12.
- [10] F. Favre, H. Olivier-Bourbigou, D. Commereuc, L. Saussine, *Chem. Commun.* (2001) 1360–1361.
- [11] A.E. Visser, R.D. Rogers, *J. Solid State Chem.* 171 (2003) 109–113.
- [12] J.G. Huddleston, H.D. Willauer, R.P. Swatoski, A.E. Visser, R.D. Rogers, *Chem. Commun.* (1998) 1765–1766.
- [13] I.W. Sun, C.L. Hussey, *Inorg. Chem.* 28 (1989) 2731–2737.
- [14] J.L. Anthony, E.J. Maginn, J.F. Brennecke, *J. Phys. Chem. B* 105 (2001) 10942–10949.
- [15] J.F. Liua, J.F. Peng, Y.G. Chi, G.B. Jiang, *Talanta* 65 (2005) 705–709.
- [16] H. Luo, S. Dai, P.V. Bonnesen, *Anal. Chem.* 76 (2004) 2773–2779.
- [17] C.D. Zhang, S.V. Malhotra, *Talanta* 67 (2005) 560–563.
- [18] J. Sirieix-Plénet, L. Gaillon, P. Letellier, *Talanta* 63 (2004) 979–986.
- [19] D. Giovanelli, M.C. Buzzeo, N.S. Lawrence, C. Hardacre, K.R. Seddon, R.G. Compton, *Talanta* 62 (2004) 904–911.
- [20] N. Hirayama, M. Deguchi, H. Kawasumi, T. Honjo, *Talanta* 65 (2005) 255–260.
- [21] S. Chatterjee, A. Pillai, V.K. Gupta, *Talanta* 57 (2002) 461–465.

# A novel method of the determination of boron in the presence of a little methanol by discoloring spectrophotometry in pharmaceutical and biological samples

Quanmin Li\*, Tiantian Zhang

*College of Chemistry and Environmental Science, Henan Normal University; Henan Key Laboratory for Environmental Pollution Control, Xixiang, Henan 453007, PR China*

Received 12 January 2006; received in revised form 21 March 2006; accepted 4 April 2006  
Available online 15 May 2006

## Abstract

It is the first time that boron is determined in the presence of a little methanol by discoloring spectrophotometry in this paper. A russet product can be formed by the reaction between glycine (Gly) and sodium 1,2-naphthoquinone-4-sulfonate (NQS) in alkaline solution. When boron is added to the solution, the system will be discolored, and the addition of a little methanol will improve the discoloration. Beer's law is obeyed in the range of boron concentrations of 0.86–43.24  $\mu\text{g ml}^{-1}$  at the maximal discoloring wavelength of 382 nm. The equation of linear regression is  $A = -0.07581 - 86.79186C$  ( $\text{mol l}^{-1}$ ), with a linearly correlation coefficient of 0.9979. The detection limit is 0.80  $\mu\text{g ml}^{-1}$  and R.S.D. is 4.2%. The method is successfully applied to the determination of boron in pharmaceutical and biological samples. The average recoveries are in the range of 98.2–104.1%. Analytical results obtained with this novel method are satisfactory.

© 2006 Elsevier B.V. All rights reserved.

**Keywords:** Boron; Glycine; Sodium 1,2-naphthoquinone-4-sulfonate; Methanol; Discoloring spectrophotometry

## 1. Introduction

In recent years, boron has been considered as an essential trace element for plant, animal and human [1]. The World Health Organization's Expert Committee on Trace Elements in Human Nutrition concluded that boron is probably essential in human ultra-trace nutrition (WHO, 1996) [2]. Boron exists widely in vegetables and fruits, especially in plums and apricots [3]. It can keep bones and joints functioning normally, which was demonstrated by Newnham [4] with a large amount of experimental, nutritional and epidemiological evidence. Boron helps to prevent osteoporosis and osteoarthritis, and stimulates immune system and hormonal responses together with other minerals, such as calcium, magnesium and vitamin D [5]. Excess boron, however, is harmful for the health of human, a minimum of daily dose has not been determined, but 3 mg per day of boron is recommended as a nutrient supplement [1,6]. The amounts greater than 500 mg per day may cause nausea, vomiting and diarrhea [5].

Obviously, it is significant to build up an intelligent, accurate and simple method to determine the concentration of boron, so as to access the beneficial therapy with this element in different kinds of human ailments.

The analytical techniques used for the determination of boron range from simple electrochemical methods to complex nuclear methods [7]. The most common methods for the determination of boron are spectrophotometric and plasma-source spectrometric methods [8]. Among the plasma-source spectrometric methods, application of inductively coupled plasma optical emission spectrometry (ICP-AES) [3,9] and electrothermal atomic absorption spectrometry (ETAAS) [10] has remained limited because these methods have poor sensitivity and they suffer from serious memory effects and interferences [8,10]. Though ICP-mass spectrometry (ICP-MS) [11,12] provides a high sensitivity and a low detection limit, the treatment of samples of this method is uncharitably required, or the capillary tube to the nebulizer may be clogged. Moreover, expensive apparatus are needed in all atomic spectroscopic methods mentioned above, and the high cost of the instruments and their operation do not permit their use in most laboratories.

\* Corresponding author. Tel.: +86 373 3326335; fax: +86 373 3326445.  
E-mail address: [mercury6068@hotmail.com](mailto:mercury6068@hotmail.com) (Q. Li).

Most spectrophotometric methods and fluorimetric methods are based on the reaction between boron and reagents, such as Azomethine-H [13–18], curcumin [19], carmimic acid [20], crystal violet [21], Alizarin red [22], methyl orange (MO) [23,24], and so on. Furthermore, several new derivatives of these organic dyes were synthesized and studied for spectrophotometric determination of boron [12,25,26]. It, however, is very troublesome and time consuming to synthesize new reagents.

This paper presents a novel method for the determination of boron with the system of glycine (Gly) and sodium 1,2-naphthoquinone-4-sulfonate (NQS) in the presence of a little methanol by discoloring spectrophotometry in pharmaceutical and biological samples. It has been reported that procaine hydrochloride [27], isoniazid [28] and some other drugs were determined using NQS to react with amino group of a primary amine in a nucleophilic substitution reaction. The study shows that a russet complex can be formed by the reaction between Gly and NQS in alkali medium, and the system is discolored after the boron is added ( $\lambda_{\max} = 382 \text{ nm}$ ). The addition of a little methanol will enhance the discoloration of the system. Consequently, boron can be determined using this discoloring system. The linear range is  $0.86\text{--}43.24 \mu\text{g ml}^{-1}$ , and the limit of detection is  $0.80 \mu\text{g ml}^{-1}$ . Compared with the methods mentioned above, this proposed method is fast, simple and sensitive. It has a wide line scope and does not need expensive apparatus, and all reagents used are easy obtained. At the same time, in order to demonstrate the performance of the described method, the determination of boron was carried out in pharmaceutical samples and biological samples, respectively. Analytical results obtained with this novel method are satisfactory.

## 2. Experimental

### 2.1. Reagents and solutions

Unless specially stated, all reagents used were of analytical grade and all solutions were prepared with distilled water. The main solutions were prepared as follows. A standard boron stock solution ( $0.1000 \text{ mol l}^{-1}$ ) was prepared by dissolving 3.1013 g of boric acid (BA) (Beijing Xinguang Chemical Reagent Plant, Beijing, China) and 3.7280 g of KCl (Taishan Chemical Reagent Plant, Guangdong, China) in distilled water heated for a few minutes. This solution was stored in a 500 ml standard flask [29] and used to prepare working boron standards by suitable dilutions. A stock of standard solution of  $1.25 \times 10^{-3} \text{ mol l}^{-1}$  of glycine was prepared by dissolving 0.0188 g Gly (Beijing Abxing Biological Technology Co. Ltd.) in 200 ml distilled water (the solution was preserved at  $4^\circ\text{C}$  without light). A stock of standard solution of  $5.0 \times 10^{-3} \text{ mol l}^{-1}$  sodium 1,2-naphthoquinone-4-sulfonate (from ACROS ORGANICS) was obtained by dissolving 0.6505 g in 500 ml standard flask with distilled water (The solution was preserved at  $4^\circ\text{C}$  without light). Buffer solution of pH 12.00 was obtained by mixing 12.00 ml solution of  $0.20 \text{ mol l}^{-1}$  NaOH and 50 ml solution of  $0.20 \text{ mol l}^{-1}$  KCl in

200 ml standard flask [30], and adjusted by a pH 3C digital pH meter (Shanghai Lei Ci Device Works, Shanghai, China). A 0.1% solution of alkylphenol polyoxyethylene (OP-10) was prepared by dissolving 0.50 g in 500 ml distilled water. A 0.1% solution of sodium dodecanesulphonate (SLS) (Sinopharm Medicine Holding Beijing Co. Ltd., Beijing, China) was prepared by dissolving 0.50 g in 500 ml distilled water. A 0.1% solution of cetyl trimethyl ammonium bromide (CTMAB) (Beijing Chemical Reagent Plant, Beijing, China) was prepared in the same way.

### 2.2. Sample preparation

Prior to analysis, 0.5000 g of the certified reference material (CRM) of Bingpeng Hanpian (The Pharmacy Group Co. Ltd. of Xi'an Jiaotong University) (There are Borax, Borneol, Cinnabar and refined mirabilite in the material) was accurately weighed using a BS 110s electro-analytical balance (Beijing Sartorius balance Ltd., Beijing, China), and then dissolved in distilled water with 2.00 ml of  $0.2 \text{ mol l}^{-1}$  HCl. The solution was filtrated, and the filtrate was taken into a 100 ml standard flask. Subsequently, the solution was diluted to the mark, mixed well and preserved without light at  $4^\circ\text{C}$ .

Two tablets of Bingpeng Hanpian ( $0.5 \text{ g} \times 2$ ) were ground well. 0.5000 g of the sample powder was also accurately weighed, and then prepared in the same way as the solution of CRM and preserved without light at  $4^\circ\text{C}$ .

### 2.3. Apparatus

A model 7230 spectrophotometer (Xiamen Analytical Instrument Plant, Xiamen, China) was employed for photometric measurements. A TU-1810 UV-vis spectrophotometer (Pgeneral Instrument plant, Beijing, China) was used for scanning the absorption spectrum. All pH measurements were performed with a pH 3C digital pH meter (Shanghai Lei Ci Device Works, Shanghai, China). A model CS-501 super constant temperature instrument (Chongqing Experiment Equipment Plant, Chongqing, China) was used for temperature measurements.

### 2.4. Procedure

2.50 ml of  $1.25 \times 10^{-3} \text{ mol l}^{-1}$  Gly was taken to a 25.0 ml color comparison tube. Sequentially, 2.00 ml NaOH-KCl buffer solution of pH 12.00 and 2.00 ml of  $5.0 \times 10^{-3} \text{ mol l}^{-1}$  NQS were added, and then some amount of  $0.1000 \text{ mol l}^{-1}$  BA was added and diluting the solution to 12.5 ml with distilled water. The mixture was shaken well and the pH of solution was measured with a pH 3C digital pH meter. This solution stood for 35 min at room temperature, and the absorbance of the solution was measured at 382 nm (382 nm proved to be the maximal discoloring wavelength of the system by determining its absorbance at different wavelengths) against a reagent blank prepared in the same way, but no BA ( $\text{H}_3\text{BO}_3$ ).



### 3. Results and discussion

#### 3.1. Absorption spectrum

The absorption spectrum of the discoloring system is shown in Fig. 1. It can be seen that the discoloring system has a minimal absorption at 382 nm. In order to obtain the highest sensitivity, all the following measurements were carried out at 382 nm.

#### 3.2. Effect of pH

The effect of pH on the coloring system of Gly–NQS and the discoloring system of BA and Gly–NQS (compared with the coloring system) were examined by varying pH from 1.00 to 13.00, respectively (see Fig. 2).

As shown in Fig. 2, at pH 1.00–7.00, the absorbance of Product I (formed from Gly and NQS) is close to 0, indicating that under high acidity, it is difficult for Gly to react with NQS. The possible reason may be that amino group ( $-\text{NH}_2$ ) of Gly is protonized and it turns into protonated amine salt ( $-\text{NH}_3^+$ ) in acidic

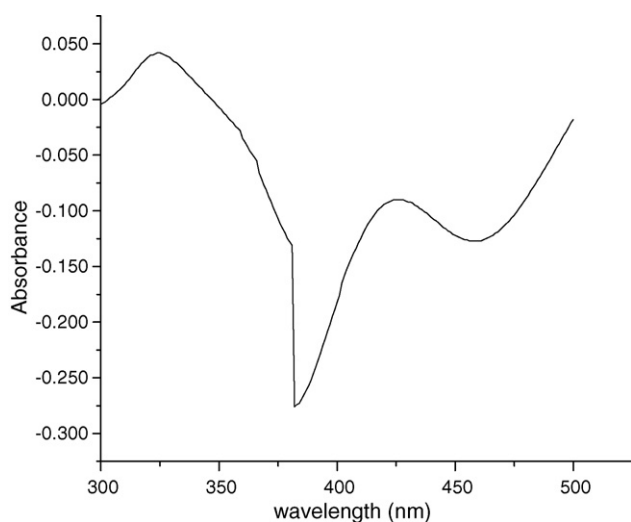


Fig. 1. The absorption spectrum of the discoloring system.

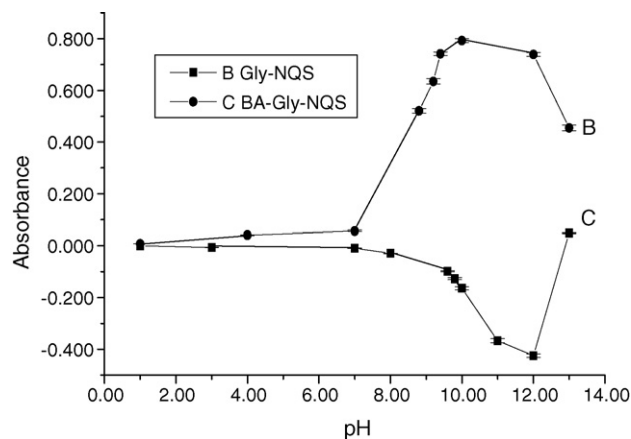


Fig. 2. Effect of pH on absorbance of the coloring system and the discoloring system BA ( $0.1000 \text{ mol l}^{-1}$ ): 1.00 ml; Gly ( $1.25 \times 10^{-3} \text{ mol l}^{-1}$ ): 2.50 ml; NQS ( $5.0 \times 10^{-3} \text{ mol l}^{-1}$ ): 2.00 ml; reaction time: 35 min.

medium. So it loses nucleophilic capacity for 4-sodium sulfonate of NQS, and the nucleophilic substitution reaction cannot take place easily. Correspondingly, the discoloration of the system is weak (see Fig. 2). If  $\text{pH} > 7.00$ , the absorbance of Product I increases rapidly corresponding to the growth of pH. Probably, the protonated amine salt ( $-\text{NH}_3^+$ ) of Gly turns back into amino group ( $-\text{NH}_2$ ) when the acidity of solution becomes low. The higher pH is, the more effectively the protonated amino group removes the proton, and more easily the nucleophilic substitution reaction happens. At the same time the discoloration of the system is enhanced, too (see Fig. 2). According to the literature [31], boron can chelated with N and O in Azomethine-H, and then amino group ( $-\text{NH}_2$ ) of Gly is possible to chelated with boron, hence the degree of the reaction between Gly and NQS declines, and the system is discolored, which leads to the descent of the absorbance. Fig. 2 shows that the absorbance of Gly–NQS reaches its maximal at pH 10.00, in other words, the degree of the nucleophilic substitution reaction is also maximal. While as also can be seen from Fig. 2, the system is discolored to the greatest extent by boron at pH 12.00, presumably as a result of the greatest degree of the reaction between boron and Gly. When pH continues to increase, absorbance of the system of Gly–NQS decreases, while that of the system of BA–Gly–NQS increases. Probably it may be the increase of the amount of hydroxide ion that holds back the nucleophilic substitution reaction between Gly and chromogenic reagent NQS, which results in the reduction of the absorbance of Product I. While in the discoloring system, high concentration of  $\text{OH}^-$  can chelated with BA to form  $[\text{B}(\text{OH})_4]^-$  [32], interfering with the chelate of BA and Gly. In order to keep the high sensibility for determination of boron, the experiment was carried out at pH 12.00.

#### 3.3. Effect of amount of Gly, NQS and buffer solution

##### 3.3.1. Effect of amount of Gly

The absorbance was determined when the amounts of BA and NQS were kept unchanged and the amount of Gly increased gradually (see Fig. 3). The absorbance descends with the

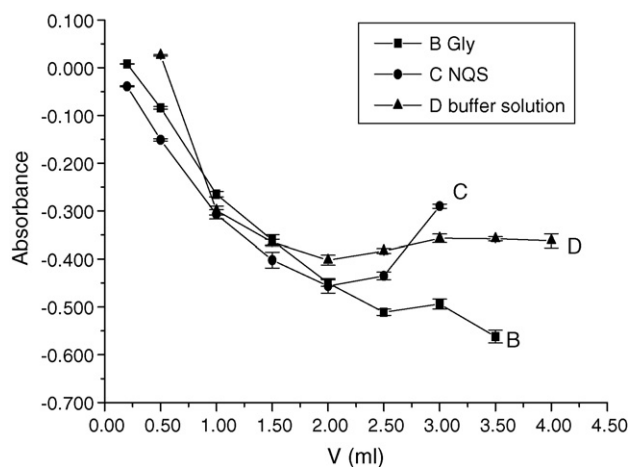


Fig. 3. Effect of amount of Gly, NQS and buffer solution BA ( $0.1000 \text{ mol l}^{-1}$ ): 1.00 ml; Gly ( $1.25 \times 10^{-3} \text{ mol l}^{-1}$ ); NQS ( $5.0 \times 10^{-3} \text{ mol l}^{-1}$ ); NaOH–KCl buffer solution (pH 12.00); reaction time: 35 min.



increase of the amount of Gly. When 2.50 ml of Gly is added, the absorbance is  $-0.511$ ; 3.00 ml,  $-0.494$ ; 3.50 ml,  $-0.562$ . Absorbance has been plotted as function of the concentration of BA using Gly 2.50 and 3.50 ml, respectively. Two calibration curves were obtained, and the linearly dependent coefficient of the former is higher than that of the latter. Therefore, 2.50 ml of Gly was selected as the optimum.

### 3.3.2. Effect of amount of NQS

In order to study the effect of amount of NQS on the determination of boron, the amount of NQS ranging from 0.20 to 5.00 ml was submitted to the proposed procedure. Fig. 3 shows that the absorbance decreases rapidly with the rise of amount of NQS when the amount is below 2.00 ml. It is likely that the coloration of the system of Gly–NQS is enhanced with the increase of the amount of NQS, and the discoloration of the system of BA and Gly–NQS is also enhanced correspondingly. The degree of the discoloration becomes greatest when the amount of NQS is 2.00 ml. When the amount, however, is above 2.00 ml, the absorbance rises from  $-0.456$  (2.00 ml) to  $-0.290$  (3.00 ml). It is probable that the ability of boron to compete with NQS to react with Gly weakens when there are more than 2.00 ml of NQS, and consequently the degree of the discoloration of the system declines. Hence, 2.00 ml of NQS was chosen as the condition of determination.

### 3.3.3. Effect of amount of buffer solution

The effect of amount of buffer solution on the absorbance of discoloring system was studied according to the procedure, keeping pH at 12.00. Fig. 3 shows that absorbance gets to the minimum when the amount of buffer solution is 2.00 ml. When the amount is above 2.00 ml, there is a small increase in absorbance, from  $-0.402$  (2.00 ml) to  $-0.362$  (4.00 ml). The possible reason is that when more than 2.00 ml of buffer solution was added to the 25.0 ml comparison tube and diluted to 12.5 ml, pH value has not changed approximately, but then the multiple of dilution has descended 50% corresponding to the amount of buffer solution rising from 2.00 to 4.00 ml. Thereby the concentration of  $\text{OH}^-$  in the solution has a little increase, then the ability of  $\text{OH}^-$  to chelated with BA to form  $[\text{B}(\text{OH})_4]^-$  enhances, which results in that the chelate of boron and Gly is interfered to a little extent. In order to keep the high sensitivity of the determination, 2.00 ml of buffer solution was chosen.

### 3.4. Effect of temperature and standing time

The absorbance of the system was measured at room temperature every 5 min. The absorbance decreases from 0.027 to  $-0.415$  after standing for 35 min, then increases to  $-0.375$  after standing for 60 min. It is found that the absorbance gets to its minimum after 35 min at room temperature.

The absorbance of discoloring system was determined at different temperature with 8 min reaction time. It is shown that the absorbance of the discoloring system is greatly affected by temperature and becomes minimal when the temperature is  $50^\circ\text{C}$ .

The absorbance of the discoloring system at  $50^\circ\text{C}$  reacting for 8 min is  $-0.403$ , while it is  $-0.415$  at room temperature after

standing for 35 min. The latter is 3.0% bigger than the former. In another word, it is more sensitive when the reaction takes place at room temperature after standing for 35 min. In addition, NQS, which as a chemical derivative chromogenic reagent is required to be preserved at  $4^\circ\text{C}$  without light, maybe unstable at high temperature. In order to make the determination more sensitive, stable and simpler, the condition of 35 min standing time at room temperature was chosen as the optimum.

### 3.5. Effect of organic solvent

Keeping other conditions constant, the effects of various organic solvents on the determination of boron were studied. When 1.00 ml of ethanol is added to the solution, the absorbance of the system decreases from  $-0.391$  to  $-0.417$ , and it indicates that there is little effect of ethanol on the determination of boron. With the amount of dioxane increasing, the absorbance of the discoloring system, however, increases, and gets to  $-0.293$  when the amount is 1.00 ml. Presumably boron can chelated with O [33–35] in dioxane, which interferes with the chelation of boron and amino group ( $-\text{NH}_2$ ) of Gly. But then the addition of methanol reduces the absorbance of the system to a greater extent, in another word, methanol promotes the discoloration of the system. Probably at pH 12.00 methanol turns into methoxide and competes against Gly to react with NQS, resulting in the descending of absorbance. In addition, a good linear relationship is obtained when the amount of methanol is from 0.00 to 0.80 ml, but when 1.00 ml of methanol was added, the absorbance increases to  $-0.551$ . The absorbance gets to its minimum ( $-0.596$ ) when the amount is 0.80 ml. Therefore 0.80 ml of methanol was chosen as the optimum when the calibration curve was plotted.

### 3.6. Potential interference

A systematic study of the influence of common ions was carried out on the determination of boron. The tolerance levels are defined with an error less than  $\pm 5\%$  in the analysis. A conclusion is drawn as follows:  $560\text{ mg l}^{-1}$  ( $\text{K}^+$ ,  $\text{Na}^+$ ,  $\text{NO}_3^-$ ,  $\text{Cl}^-$ ,  $\text{SO}_4^{2-}$ ),  $240\text{ mg l}^{-1}$  ( $\text{CO}_3^{2-}$ ),  $208\text{ mg l}^{-1}$  ( $\text{Mg}^{2+}$ ),  $160\text{ mg l}^{-1}$  ( $\text{Ca}^{2+}$ ),  $6.40\text{ mg l}^{-1}$  ( $\text{Co}^{2+}$ ),  $3.20\text{ mg l}^{-1}$  ( $\text{Fe}^{3+}$ ),  $0.80\text{ mg l}^{-1}$  ( $\text{Zn}^{2+}$ ,  $\text{Cu}^{2+}$ ,  $\text{Mn}^{2+}$ ,  $\text{Ni}^{2+}$ ) do not affect the determination of boron. As can be seen from the above, the concentrations of  $\text{Co}^{2+}$ ,  $\text{Fe}^{3+}$ ,  $\text{Zn}^{2+}$ ,  $\text{Cu}^{2+}$ ,  $\text{Mn}^{2+}$  and  $\text{Ni}^{2+}$  are relatively lower. The possible reason may be that these metal ions can chelated with Gly [36], which keeps back the nucleophilic substitution reaction between Gly and NQS.

### 3.7. Calibration curve

According to the procedure, the absorbance of the discoloring system was measured, and has been plotted as function of the concentration of BA. The linear range of boron in this calibration curve is  $13.84\text{--}172.96\text{ }\mu\text{g ml}^{-1}$ . It has been shown in Section 3.7 that boron can discolor the system of Gly–NQS to a greater degree in the presence of methanol, in other words, methanol can enhance the sensitivity of the proposed discoloring

oring system. Therefore,  $0.8 \times 10^{-4}$ ,  $2.0 \times 10^{-4}$ ,  $4.0 \times 10^{-4}$ ,  $8.0 \times 10^{-4}$ ,  $12 \times 10^{-4}$ ,  $20 \times 10^{-4}$  and  $40 \times 10^{-4} \text{ mol l}^{-1}$  of BA solution were prepared, respectively, and then the absorbance of the discoloring system in the presence of 0.80 ml of methanol was determined under the optimum conditions. Absorbance has been plotted as function of the concentration of BA. A linear regression equation is attained as  $A = -0.07581 - 86.79186C$  ( $\text{mol l}^{-1}$ ) with a linearly dependent coefficient of 0.9979. The linear range of boron is  $0.86\text{--}43.24 \mu\text{g ml}^{-1}$ . The minimal concentration of detection has descended about 16 times, which is beneficial to the determination of low level of boron.

### 3.8. Determination of reproducibility and detection limit

According to the procedure, the solution of BA was determined 11 times ( $n = 11$ ) with a R.S.D. of 4.2%. Then a reagent blank solution was measured 11 times ( $n = 11$ ), too. The standard deviation of the reagent blank ( $\sigma$ ) is 0.002136. Therefore, the limit of detection of this proposed method evaluated by calibration curve ( $3\sigma/k$ ) is  $0.80 \mu\text{g ml}^{-1}$ .

## 4. The study of kinetic property and reaction mechanism

### 4.1. Kinetic curve of reaction

In accordance with the procedure, keeping the temperature at  $25^\circ\text{C}$ , the absorbance of the discoloring system was determined at different reaction time in initial rate method. Then a good linear relationship was obtained. Obviously, the reaction order between boron and Product I is one. Since the quantity of NQS is much more than that of boron in solution, and the concentration variation is relatively small, hence this reaction can be regarded as pseudo first order reaction.

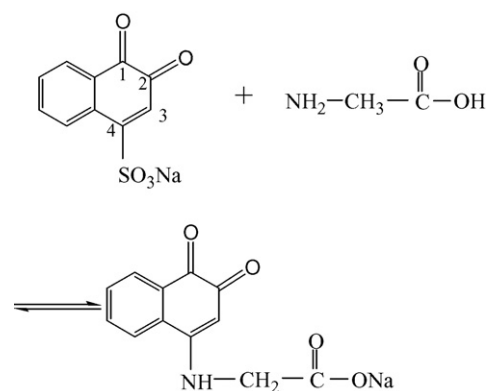
### 4.2. Apparent rate constant and activation energy

By dealing with  $A\text{--}T$  data obtained above, the apparent rate constants at  $20^\circ\text{C}$  and  $30^\circ\text{C}$  can be obtained, respectively. Then in light of Arrhenius Formula of  $E_a = RT_2T_1/(T_2 - T_1) \ln k'_2/k'_1$  and different pairs of  $K\text{--}T$  data, the activation energy of nucleophilic substitution reaction was calculated.  $k'(20^\circ\text{C})$ ,  $k'(30^\circ\text{C})$  and  $E_a$  is  $1.9 \times 10^{-3}(\text{s}^{-1})$ ,  $3.2 \times 10^{-3}(\text{s}^{-1})$  and  $35.94(\text{KJ mol}^{-1})$ , respectively.

As activation energy of the reaction is smaller than  $40 \text{ KJ mol}^{-1}$ , it indicates that the nucleophilic substitution reaction can easily take place. Hence, the described discoloring system can be used to determine boron.

### 4.3. Discussion of reaction mechanism

It has been reported that NQS can react with amino group of primary amine derivative [27]. Amino group of Gly takes on nucleophilicity due to the fact that its lone pairs of electron of nitrogen can attack the electron deficiency center. 3,4-C=C of NQS can bond conjugate with 2-C=O, as a result 4-C becomes electron lacking center. So Gly can react with NQS in a nucleophilic substitution reaction. It seems reasonable that the reaction equation is as follows:



As boron lacks electron,  $\sigma$ -bond tends to be formed from electron pair donor ( $-\text{NH}_2$ ) and boron as electron pair ceptor. When BA was added to this system, boron can break the dative bond of  $-\text{NH}_2$  and NQS, chelated with Gly, and discolor the system of Gly-NQS.

## 5. Sample analysis

### 5.1. Analysis boron in pharmaceutical sample

Five solutions of certified reference materials were measured, and the results are consistent with the certified values (see Table 1).

Then different concentrations of pharmaceutical sample solutions were measured, and the results agree well with those obtained using Azomethine-H as the chromogenic agent (see Table 2). In addition, the results are satisfactory with low R.S.D.

Table 1  
Determination of boron in certified reference materials (CRM) ( $n = 5$ ,  $t_{0.054} = 2.78$ )

Certified reference material	The certified ( $\mu\text{g ml}^{-1}$ )	Present method ( $\mu\text{g ml}^{-1}$ )	CRM content ( $\mu\text{g ml}^{-1}$ )	Added ( $\mu\text{g ml}^{-1}$ )	Found ( $\mu\text{g ml}^{-1}$ )	R.S.D. (%)	Recovery (%)
060201	129.57	$128.12 \pm 1.04$	31.08	34.59	$34.28 \pm 0.35$	0.81	99.1
060202	129.81	$127.86 \pm 0.96$	31.15	51.89	$51.01 \pm 0.39$	0.61	101.3
060318	141.22	$142.34 \pm 1.51$	33.89	34.59	$34.73 \pm 0.29$	0.67	100.4
060319	139.79	$136.91 \pm 1.34$	22.37	17.30	$17.08 \pm 0.22$	1.04	98.7
060320	139.72	$137.54 \pm 0.83$	44.71	34.59	$34.24 \pm 0.52$	1.21	99.0

Table 2  
Determination of boron in pharmaceutical samples ( $n = 5$ ,  $t_{0.054} = 2.78$ )

Sample	The labelled (mg/tablet)	Present method (mg/tablet)	Azomethine-H method (mg/tablet)	Sample content ( $\mu\text{g ml}^{-1}$ )	Added ( $\mu\text{g ml}^{-1}$ )	Found ( $\mu\text{g ml}^{-1}$ )	R.S.D. (%)	Recovery (%)
1	12.88	12.54 $\pm$ 0.08	12.68	30.91	34.59	35.63 $\pm$ 0.13	0.30	103.0
2	12.88	12.45 $\pm$ 0.10	12.56	30.91	51.89	54.01 $\pm$ 0.29	0.44	104.1
3	12.88	13.40 $\pm$ 0.07	12.72	30.91	34.59	35.56 $\pm$ 0.25	0.58	102.8
4	12.88	12.82 $\pm$ 0.05	13.00	20.61	17.30	17.16 $\pm$ 0.11	0.53	99.2
5	12.88	13.16 $\pm$ 0.05	12.94	41.22	34.59	33.97 $\pm$ 0.12	0.29	98.2

Table 3  
Determination of boron in urine of patient ( $n = 5$ ,  $t_{0.054} = 2.78$ )

Sample urine (time)	Sample content ( $\mu\text{g ml}^{-1}$ )	Azomethine-H method ( $\mu\text{g ml}^{-1}$ )	Added ( $\mu\text{g ml}^{-1}$ )	Found ( $\mu\text{g ml}^{-1}$ )	R.S.D. (%)	Recovery (%)
2 h	69.07 $\pm$ 0.05	68.92	25.94	26.09 $\pm$ 0.07	0.23	100.6
4 h	23.42 $\pm$ 0.08	23.25	25.94	25.77 $\pm$ 0.09	0.27	99.3
6 h	11.39 $\pm$ 0.06	11.47	25.94	25.65 $\pm$ 0.13	0.41	98.9

and high recovery. As the sample in the experiment is the compound prescription, it also shows that other components in the pharmaceutical sample do not affect the determination of boron with the discoloring system and the results are satisfactory.

### 5.2. Analysis of boron in urine of patient

Three urine samples of the same patient who has taken the medicine after different time were measured with the proposed method, and the results are shown in Table 3. These results are in agreement with those obtained using Azomethine-H as the chromogenic agent, and have high accuracy and good recovery, which indicates that the proposed method can be successfully applied to the determination of boron in biological samples.

## 6. Conclusion

It is the first time that determination of boron was carried out with the system of BA and Gly–NQS in the presence of a little methanol by discoloring spectrophotometry.

The experiment was carried out in the pH 12.00 solution at room temperature standing for 35 min, and the amounts of Gly, NQS and NaOH–KCl buffer solution are 2.50, 2.00 and 2.00 ml, respectively. In the presence of 0.80 ml of methanol the linear range of boron is 0.86–43.24  $\mu\text{g ml}^{-1}$ . A simple, sensitive, rapid and reliable method is developed. The proposed method can be successfully applied to the determination of boron in pharmaceutical and biological samples with satisfactory results. If other reagents with amino group of primary amine derivative (R–NH<sub>2</sub>) can react with NQS to form a coloring system, then boron may be determined by the discoloring of the system of NQS–R–NH<sub>2</sub>. Compared with other methods mentioned in this paper, the proposed method needs neither the complicated apparatus, nor new reagents to be synthesized. Therefore the determination of boron by discoloring spectrophotometry has got an important value and practical foreground.

## References

- [1] F.H. Nielsen, Essential and Toxic Trace Elements in Human Health and Disease: an update, Wiley-Liss, New York, 1993, p. 355.
- [2] K. Usuda, K. Kono, T. Dote, K. Miyata, H. Nishiura, M. Shimahara, K. Sugimoto, Sci. Total Environ. 220 (1998) 45.
- [3] A. Krejcová, T. Cernohorsky, Food Chem. 82 (2003) 303.
- [4] Rex E. Newnham, Environ. Health Perspect. 102 (1994) 83.
- [5] A. Economou, D.G. Themelis, H. Bikou, P.D. Tzanavaras, P.G. Rigas, Anal. Chim. Acta 510 (2004) 219.
- [6] E. Mindell, Prague: Euromedia Group, Knizniklub, 2000.
- [7] R.N. Sah, P.H. Brown, Plant Soil 193 (1997) 15.
- [8] R.N. Sah, P.H. Brown, Microchem. J. 56 (1997) 285.
- [9] A.S. Szabo, D.W. Golightly, J. Food Compos. Anal. 8 (1995) 220.
- [10] M. Burguera, J.L. Burguera, C. Rondon, P. Carrero, Spectrochim. Acta B 56 (2001) 1845.
- [11] D.H. Sun, R.L. Ma, C.W. McLeod, X.R. Wang, A.G. Cox, J. Anal. At. Spectrom. 15 (2000) 257.
- [12] A. Sabarudin, K. Oshita, M. Oshima, S. Motomizu, Talanta 66 (2005) 136.
- [13] P. Carrero, A. Malave, E. Rojas, C. Rondon, Y.P. de Pena, J.L. Burguera, M. Burguera, Talanta 68 (2005) 374.
- [14] J.F.V. Staden, T.A.V. der Merwe, Analyst 125 (11) (2000) 2094.
- [15] F.J. Krug, J. Mortal, L.C.R. Pessenda, E.A.G. Zagatto, H. Bergamin, Anal. Chim. Acta 125 (1981) 29.
- [16] P. Carrero, J.L. Burguera, M. Burguera, C. Rivas, Talanta 40 (1993) 1967.
- [17] M.A.Z. Arruda, E.A.G. Zagatto, Anal. Chim. Acta 199 (1987) 137.
- [18] S. Sato, S. Uchikawa, Anal. Chim. Acta 143 (1982) 283.
- [19] S. Thangavel, S.M. Dhavile, K. Dash, S.C. Chaurasia, Anal. Chim. Acta 502 (2004) 265.
- [20] H. Pan, X. Zheng, Chin. J. Adm. Technol. Environ. Monit. 12 (5) (2000) 30.
- [21] N. Chimpalee, D. Chimpalee, B. Boonyanitchayakul, D.T. Burns, Anal. Chim. Acta 282 (1993) 643.
- [22] I. Sekerka, J.F. Lechner, Anal. Chim. Acta 234 (1990) 199.
- [23] K. Nose, M. Zenki, Analyst 116 (1991) 712.
- [24] J.F. van Staden, M. Tsanwani, Talanta 58 (2002) 1103.
- [25] Z.J. Li, Z.W. Cui, J. Tang, Food Chem. 94 (2006) 310.
- [26] Z.J. Li, Q.J. Song, Z.W. Cui, Q. Wei, J. Zheng, Talanta 66 (2005) 136.
- [27] M.O. Ozgur, S. Sungur, Rev. Anal. Chem. 22 (1) (2003) 1.
- [28] P. Nagaraja, K.C. Srinivasa Murthy, H.S. Yathirajan, Talanta 43 (1996) 1075.

- [29] W.B. Chang, K.A. Li, *A concise Analytical Chemistry Handbook*, first ed., Peking University Press, Beijing, China, 1981, p. 263.
- [30] Analytical Chemistry Studio of Zhongnan Mineral College, *Handbook of Chemical Analysis*, Science Press, Beijing, China, 1984, p. 383.
- [31] H. Hagen, S. Reinoso, M. Albrecht, J. Boersma, A.L. Spek, G.V. Koten, *J. Organomet. Chem.* 608 (2000) 27.
- [32] Inorganic Chemistry Studio of Beijing Normal University, Huazhong Normal University and Nanjing Normal University, *Inorganic Chemistry*, third ed., Higher Education Press, Beijing, China, 1992, p.602.
- [33] P. Denis, O.N. Ventura, *J. Mol. Struct. (Theochem)* 537 (2001) 173.
- [34] K.Y. Law, *J. Photochem. Photobiol. A* 107 (1997) 115.
- [35] D.A. Oxspring, S. McClean, E. O'Kane, W.F. Smyth, *Anal. Chem. Acta* 317 (1995) 295.
- [36] G.G. Mohamed, N.E.A. El-Gamel, *Spectrochim. Acta A* 60 (2004) 3141.

# Determination of clarithromycin in rat plasma by HPLC–UV method with pre-column derivatization

Wei Li, Huijuan Jia, Kang Zhao\*

*The College of Pharmaceuticals and Biotechnology, Tianjin University, Tianjin, PR China*

Received 24 January 2006; received in revised form 29 March 2006; accepted 10 April 2006

Available online 24 May 2006

## Abstract

A novel high-performance liquid chromatographic (HPLC) method using pre-column derivatization and UV detection at 275 nm for the determination of clarithromycin in rat plasma has been validated. Clarithromycin was extracted from plasma sample spiked with internal standard (erythromycin) under alkaline condition with ethyl ether and derivatized with trimethylbromosilane. The analyses were run on a C<sub>18</sub> column, maintained at 40 °C during elution, using a mobile phase comprised of potassium dihydrogen phosphate (50 mM, pH 6.8, contained 0.7% triethylamine), acetonitrile, and methanol (30:45:25, v/v/v). The standard calibration curve for clarithromycin was linear ( $r^2 = 0.9998$ ) over the concentration range of 0.1–10  $\mu\text{g ml}^{-1}$  in rat plasma. The limit of detection (LOD) and limit of quantitation (LOQ) was 30  $\text{ng ml}^{-1}$  and 0.1  $\mu\text{g ml}^{-1}$  respectively. The intra- and inter-day assay variability range was 2.6–7.4% and 3.3–8.5%, respectively. This method has been successfully applied to a pharmacokinetic study of clarithromycin in rats.

© 2006 Elsevier B.V. All rights reserved.

**Keywords:** Derivatization; Clarithromycin; Trimethylbromosilane; Rat plasma; High-performance liquid chromatography

## 1. Introduction

Clarithromycin (Fig. 1A) is a semi-synthetic macrolide antibiotic with good antimicrobial activity against a wide range of gram-positive and gram-negative organisms. Its structure is identical to that of erythromycin (Fig. 1B), except that the *O*-methyl group has been substituted for a hydroxyl group at position six of the lactone [1]. Clarithromycin has a good stability in gastric acid, a better bioavailability and a more favorable pharmacokinetic profile than erythromycin [2].

The analytical methods reported previously for the quantification of clarithromycin in biological fluids include microbiological bioassay [3] and high-performance liquid chromatography (HPLC); detection methods include electrochemical detection [4–12], mass-spectrometry [13], fluorescence detection after pre-column derivatization [14], and UV detection [15–17].

As lacking a suitable chromophore, clarithromycin has only a weak UV absorbance in the low wavelength range (<220 nm) which makes it difficult to develop a specific, selective and sen-

sitive UV method according to the occurrence of substantial UV absorption, particularly when using complex matrices such as biological fluids. But the UV detector is more widely distributed than all of the other detectors and also more inexpensive compared to HPLC–MS, the development of a HPLC–UV method for clarithromycin continue to be needed for trials aimed at pharmacokinetic and efficacy. A sensitive HPLC–UV method was reported by Amini and Ahmadiani recently [15]. But the large volume of plasma (1 ml) required to achieve the high sensitivity limits its application when only small volume of plasma is available.

Chemical derivatization can increase detection sensitivity and improve selectivity by means of pre-column or post-column HPLC [18], so we developed and validated a novel HPLC–UV method for the determination of clarithromycin in rat plasma which can be used in pharmacokinetic study of clarithromycin. This method involved pre-column derivatization with trimethylbromosilane (TMBS, Fig. 1C) as the derivatization reagent and erythromycin as the internal standard (IS). The possible construction of the derivatization product is also showed in Fig. 1D. This method offered a selective and sensitive determination of clarithromycin with a limit of detection (LOD) of 30  $\text{ng ml}^{-1}$  and a limit of quantitation (LOQ) of 0.1  $\mu\text{g ml}^{-1}$  through employing

\* Corresponding author. Tel.: +86 22 27404031; fax: +86 22 27405190.  
E-mail address: [combinology@yahoo.com](mailto:combinology@yahoo.com) (K. Zhao).



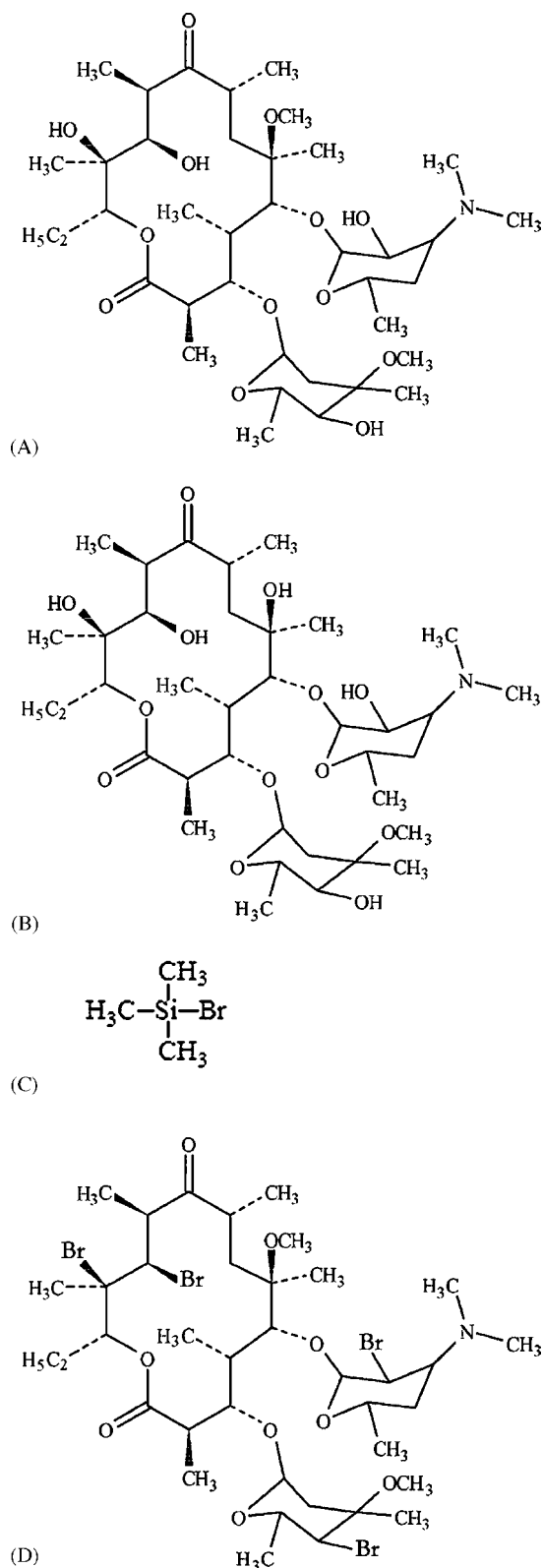


Fig. 1. The chemical structure of clarithromycin (A), internal standard erythromycin (B), the derivatization reagent trimethyl-bromosilane (C), and the possible structure of derivatization product (D).

a micro volume of plasma (150  $\mu\text{l}$ ) which ensures the applicability of the method when only small volume of plasma is available.

## 2. Experimental

### 2.1. Materials and reagents

Clarithromycin was supplied by Zhejiang Huayi Pharmaceutical Co., Ltd (949.7  $\mu\text{g mg}^{-1}$ , China). Certified reference materials (CRMs) of clarithromycin (972  $\mu\text{g mg}^{-1}$ ) and erythromycin (888  $\mu\text{g mg}^{-1}$ ) were applied by National Institute for the Control of Pharmaceutical and Biological Products (Beijing, China). HPLC grade acetonitrile (ACN) and methanol (MeOH) were obtained from Fisherchemicals (New Jersey, USA). Trimethylbromosilane was supplied by Rich Trading Ltd. (Beijing, China). Analytical grade triethylamine (TEA), potassium dihydrogen phosphate, ethyl ether, sodium hydroxide (NaOH), concentrated phosphate acid and dichloromethane ( $\text{CH}_2\text{Cl}_2$ ) were obtained from Kewei Reagents Company (Tianjin, China). Heparin sodium salt was obtained from Aoboxing Biotechnical Company (Beijing, China). Healthy male Wistar rats were obtained from the laboratory animal center of Academy of Military Medical Sciences (Beijing, China).

### 2.2. Instrumentation and chromatography

The apparatus used for HPLC analysis was an Agilent 1100 quaternary pump, with a variable wavelength detector, thermostatted autosampler and column thermostat. A Hyper-sil ODS<sub>2</sub> C<sub>18</sub> column (250 mm  $\times$  4.6 mm ID, 5  $\mu\text{m}$ , Thermo, UK) was fitted with a Phenomenex guard column packed with octadecyl C<sub>18</sub> (Phenomenex, USA). UV spectrophotometric measurements were made using a UV-visible spectrophotometer (UV-2450, Shimadzu, Japan). The pH value was measured using a pHS-3C precision pH meter (Leici Devices Factory of Shanghai, China).

The mobile phase comprised of 50 mM potassium dihydrogen phosphate (contained 0.7% TEA, v/v, adjust with concentrated phosphate acid to pH 6.8)—acetonitrile—methanol (30:45:25, v/v/v). Analyses were run at a flow rate of 1.0  $\text{ml min}^{-1}$  at 40  $^\circ\text{C}$ .

### 2.3. Standard solutions

The stock solutions of clarithromycin and erythromycin were prepared through dissolving 50 mg of corresponding CRMs in 50 ml of methanol. Separate standard solutions of clarithromycin were prepared by serial dilutions of stock solutions with water for the calibration standards. These solutions were added to drug free plasma in volumes not exceeding 8% of the plasma volume. The internal standard solution was diluted in water to produce a final concentration of 150  $\mu\text{g ml}^{-1}$ .

### 2.4. Sample preparation

To 150  $\mu\text{l}$  of plasma sample in an Eppendorf tube (1.5 ml capacity), 10  $\mu\text{l}$  of the internal standard erythromycin solution

(150  $\mu\text{g ml}^{-1}$ ) and 20  $\mu\text{l}$  of 0.25 M NaOH were added. The solution was vortexed briefly then 1.0 ml of ethyl ether was added and vortexed for 5 min and centrifuged for another 5 min at 4000 rpm. The organic layer was transferred into another clean Eppendorf tube and dried under a stream of  $\text{N}_2$  at room temperature. The residue was resolved with 600  $\mu\text{l}$  of frappe  $\text{CH}_2\text{Cl}_2$ , and then 50  $\mu\text{l}$  of trimethylbromosilane was added and kept at 0 °C for 10 min. Then 200  $\mu\text{l}$  of water was added and vortexed 1 min to terminate the reaction. The solution was centrifuged for 5 min and the water layer was discarded, the organic layer was dried under a stream of  $\text{N}_2$  at room temperature. The residue was reconstituted with 150  $\mu\text{l}$  mobile phase. A 100  $\mu\text{l}$  of the reconstituted solution was injected onto the HPLC column.

### 2.5. Calibration curve and assay validation

Standard calibration curve was constructed by spiking drug free plasma with a known amount of clarithromycin in the concentration range of 0.1–10  $\mu\text{g ml}^{-1}$ . The plasma standards were also used to determine the intra-day and inter-day precision and accuracy of the method.

The concentration of clarithromycin was calculated through the ratio between the peak areas of clarithromycin and internal standard. Calibration curve was obtained by plotting the peak area ratios on the abscissa and the respective drug concentrations on the ordinate.

Absolute recoveries at seven different concentration levels of clarithromycin (0.1–10  $\mu\text{g ml}^{-1}$ ) in rat plasma were determined by assaying the samples as the procedure described above and comparing the peak areas of clarithromycin with those obtained from clarithromycin solutions in  $\text{CH}_2\text{Cl}_2$  of corresponding concentrations assayed as the same procedure except the extraction.

### 2.6. Pharmacokinetic protocol

Five male Wistar rats (250–300 g) were used in this experiment. The rats were fasted overnight before use and received an oral gavage of 150  $\text{mg kg}^{-1}$  clarithromycin in a 0.5% carboxymethylcellulose (CMC) suspension (4  $\text{ml kg}^{-1}$ ). Blood samples (0.4 ml) were collected using heparin sodium salt as anti-coagulant from the plexus venosus at fundus oculi through a glass capillary inserted along the angulus oculi medialis. The sampling time-points were 15, 30, 60, 120, 180, 240, 300, 360, 420 and 480 min postdose. Plasma samples were harvested after centrifugation and stored frozen at –20 °C until analysis.

### 2.7. Pharmacokinetic data analysis

The pharmacokinetic analysis was conducted through using Practical Pharmacokinetic Program-Version 97 (3P97, published by Chinese Pharmacological Association, Beijing, China).

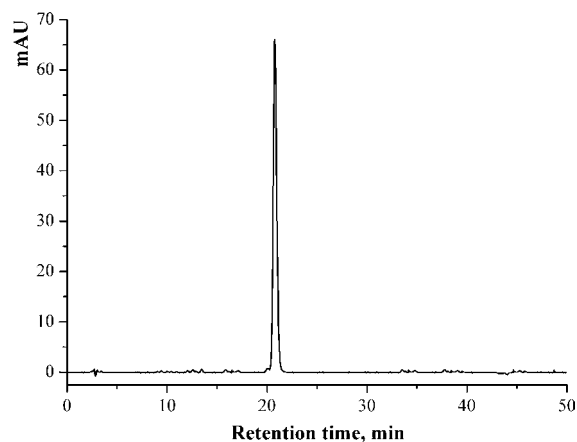


Fig. 2. The chromatography of the products of the derivatization.

## 3. Results and discussion

### 3.1. Derivatization

Derivatization of clarithromycin with the TMBS was employed for the detection and quantification of clarithromycin. The reagent TMBS was found to react readily with clarithromycin in  $\text{CH}_2\text{Cl}_2$  solution. According to the known reaction between TMBS and hydroxy group, the hydroxy groups of clarithromycin are believed to react with TMBS to yield brominated derivate. The reaction was monitored by HPLC and the chromatography showed that there was only one major product when the reaction was terminated (Fig. 2).

Absorption spectra in the range (200–400 nm) were obtained for the clarithromycin and derivatized clarithromycin (Fig. 3). The derivate exhibited two absorption maxima (at 206 and 275 nm). The 275 nm was chosen as detection wavelength which can improve the sensitivity and selectivity of method greatly because of the high molar absorptive coefficient of the derivate and the elimination of the substantial UV absorption at 275 nm.

Compared with 9-fluorenylmethyloxycarbonylchloride (FMOC-Cl), a derivatization reagent also has been applied for the detection and quantification of clarithromycin [14], the TMBS consumed much shorter time to complete the

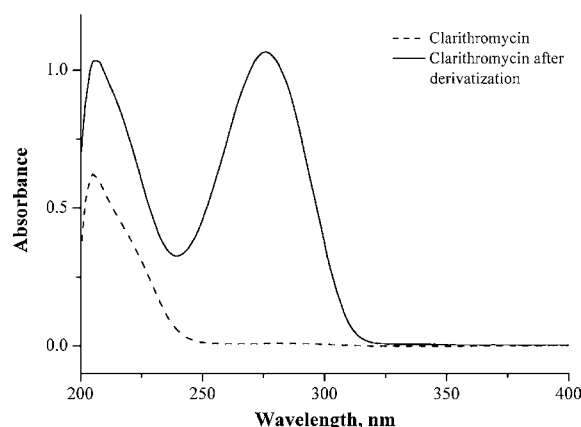


Fig. 3. The absorption spectra of clarithromycin (200  $\mu\text{g ml}^{-1}$ ) before and after derivatization.

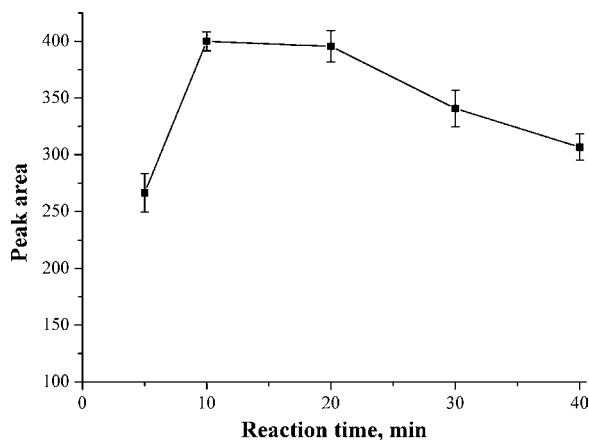


Fig. 4. The optimization of reaction time (mean  $\pm$  S.D.,  $n=4$ ). Test solution contained  $5 \mu\text{g ml}^{-1}$  clarithromycin was used.

derivatization reaction. The optimal reaction time of TMBS is 10 min according to the result of the optimization test (Fig. 4) while the corresponding parameter of FMOC-Cl is 40 min [14]. So the cycle of sample pretreatment will be shortened and the efficiency can be improved greatly.

### 3.2. Chromatography

The aim of this work, a novel HPLC–UV method to determine clarithromycin in rat plasma has been developed. A satisfactory separation of clarithromycin from endogenous components in rat plasma was obtained.

Representative chromatograms of blank rat plasma, drug free rat plasma spiked with clarithromycin and internal standard, and rat plasma after administration of the clarithromycin are shown in Fig. 5.

The mobile phase comprised of 50 mM potassium dihydrogen phosphate (contained 0.7% TEA, v/v, pH 6.8)—acetonitrile–methanol (30:45:25, v/v/v) was used. The influences of different organic modifiers in the mobile phases and the different pH values of the phosphate buffer on the performance of the method were investigated and summarized in Tables 1 and 2. According to the results, the retention time and peak symmetry of clarithromycin decreased when the content of MeOH or the pH value of the phosphate buffer in mobile phase decreased. The appropriate content of MeOH and neutral pH value were necessary to achieve satisfactory peak symmetry and enduring retention time simultaneously. Eventually, the pH 6.8 and the ratio of The final composition of the mobile phase was

Table 1  
Influences of different organic modifiers on the performance of method<sup>a</sup>

Organic modifier	Retention time (min)	Peak symmetry
MeOH	40.3	0.98
MeOH:ACN = 9:5 (v/v)	29.1	0.91
MeOH:ACN = 5:9 (v/v)	20.9	0.85
MeOH:ACN = 1:6 (v/v)	13.7	0.60
ACN	11.6	0.42

<sup>a</sup> The content of organic modifier in mobile phase is 70% and the pH value of phosphate buffer is 6.8.

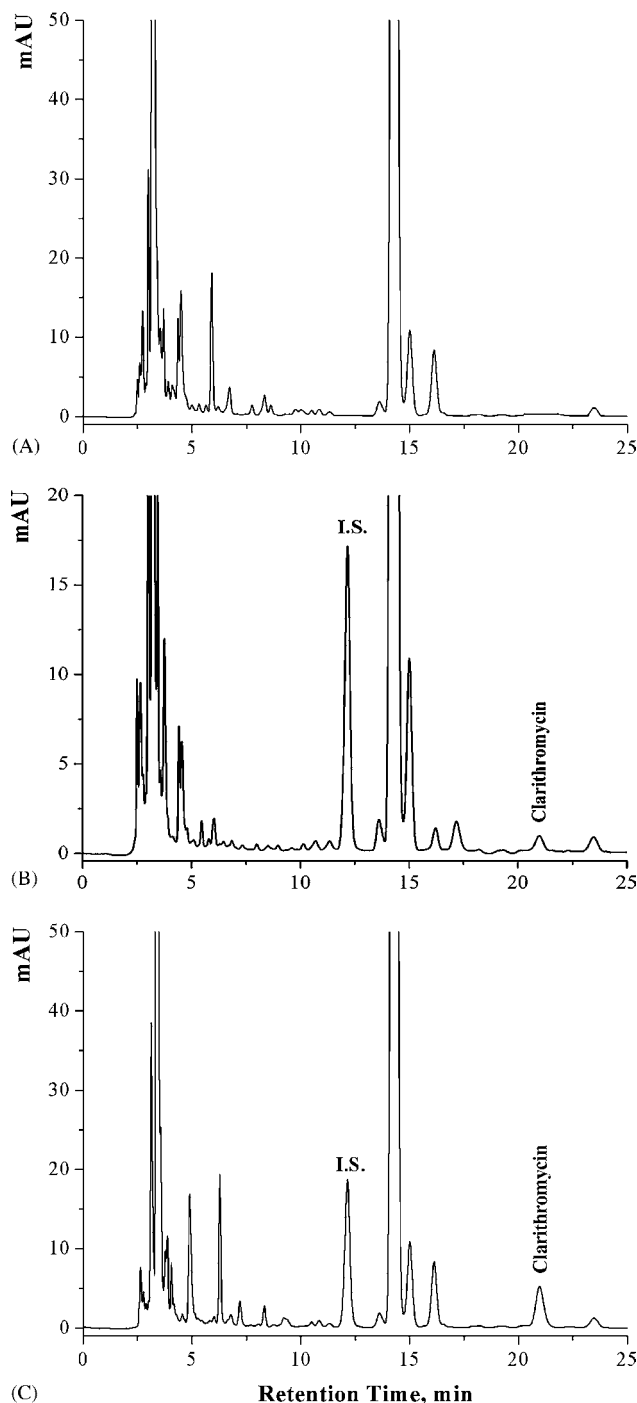


Fig. 5. (A) HPLC chromatogram of drug free rat plasma. (B) HPLC chromatogram of rat plasma containing erythromycin (I.S.,  $10 \mu\text{g ml}^{-1}$ ) and clarithromycin ( $0.2 \mu\text{g ml}^{-1}$ ). (C) A collected rat plasma sample after 1 h of the start clarithromycin administration ( $150 \text{ mg kg}^{-1}$ ).

chosen to achieve the best peak resolution, appropriate retention time, acceptable peak shape and satisfactory separation of clarithromycin from endogenous components in rat plasma.

### 3.3. Calibration curve and assay validation

A good linear relationship was found, as described by the following linear regression equation:  $y = 6.0783x + 0.0009$

Table 2

Influences of different pH values of phosphate buffer on the performance of method<sup>a</sup>

pH values of phosphate buffer	Retention time (min)	Peak symmetry
7.6	22.7	0.87
7.2	21.3	0.85
6.8	20.9	0.85
6.4	17.6	0.72
6.0	14.4	0.69

<sup>a</sup> The mobile phase is comprised of acetonitrile–methanol–phosphate buffer (45:25:30, v/v/v).

( $r^2 = 0.9998$ ), where  $y$  is the concentration ( $\mu\text{g ml}^{-1}$ ) and  $x$  is the ratio of the peak area of clarithromycin and internal standard. The coefficient of determination is satisfactory.

The limit of detection (LOD) was determined as the concentration of component giving a signal to noise ratio = 3:1. The limit of detection for clarithromycin in rat plasma was found to be  $30 \text{ ng ml}^{-1}$ . The limit of quantitation (LOQ) of clarithromycin in rat plasma was chosen as the concentration used for the lowest concentration level on the calibration curve ( $0.1 \mu\text{g ml}^{-1}$ ) which offer a signal to noise ratio = 10:1. The method LOQ is equal to that of some electrochemical methods [8–10] with an LOQ of  $0.1 \mu\text{g ml}^{-1}$ , but much more sensitive than the fluorescence method [14] with an LOQ of  $0.2 \mu\text{g ml}^{-1}$ .

The percentage recoveries ( $n = 6$ ) of clarithromycin ranged from 82.2 to 90.8% over the entire concentration range (Table 3).

The intra- and inter-days variations and accuracy of the clarithromycin determinations in rat plasma are summarized in Table 4. All results are within the ranges acceptable for bio-analytical purposes.

### 3.4. Application

The developed method has been successfully applied to an analysis of plasma samples collected from rats administered with clarithromycin. The concentration–time curve (mean  $\pm$  S.D.) of clarithromycin after oral administration of clarithromycin ( $150 \text{ mg kg}^{-1}$ ) is shown in Fig. 6.

A two-compartment model was fitted to the concentration–time profiles of the administered animals by the 3P97 program. The pharmacokinetic parameters estimated as parts of the model were summarized in Table 5.

Table 3

Absolute recovery and corresponding relative standard deviation (R.S.D) of clarithromycin ( $n = 6$ )

Concentration ( $\mu\text{g ml}^{-1}$ )	Recovery (mean%)	R.S.D. (%)
0.1	88.5	6.4
0.2	90.8	4.9
0.5	82.6	4.1
1.0	82.7	5.5
2.0	82.2	4.1
5.0	88.3	4.7
10.0	85.9	5.2

Table 4

The intra- and inter-day variations and accuracy of clarithromycin ( $n = 6$ )

Concentration ( $\mu\text{g ml}^{-1}$ )	Precision (R.S.D. %)	Accuracy (%)
Intra-day		
0.1	7.0	106.8
0.2	6.4	103.7
0.5	7.4	100.5
1.0	4.3	97.1
2.0	4.6	97.3
5.0	3.5	102.5
10.0	2.6	99.8
Inter-day		
0.1	7.7	113.9
0.2	8.2	110.4
0.5	6.6	104.1
1.0	8.5	97.9
2.0	5.9	97.7
5.0	5.0	100.8
10.0	3.3	100.2

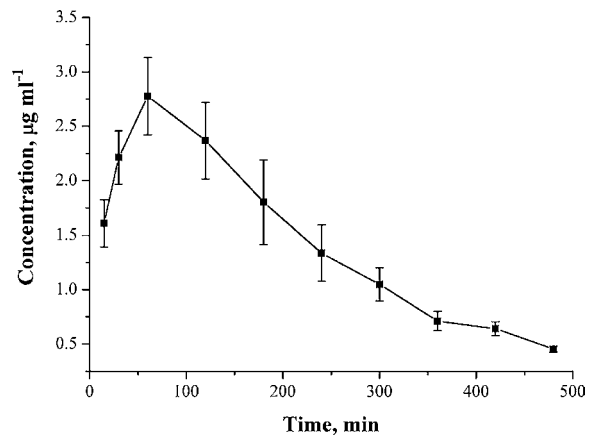


Fig. 6. The concentration–time profile (mean  $\pm$  S.D.) of clarithromycin after administered to rats ( $n = 5$ ).

Table 5

Pharmacokinetic parameters of clarithromycin in rat ( $n = 5$ )

Parameter <sup>a</sup>	Value (mean $\pm$ S.D.)
$A$ ( $\mu\text{g/ml}$ )	$3.42 \pm 1.72$
$\alpha$ (1/min)	$0.013 \pm 0.0038$
$B$ ( $\mu\text{g/ml}$ )	$4.25 \pm 1.38$
$\beta$ (1/min)	$0.0047 \pm 0.0020$
$k_a$ (1/min)	$0.033 \pm 0.012$
$t_{1/2\alpha}$ (min)	$55.86 \pm 13.96$
$t_{1/2\beta}$ (min)	$164.15 \pm 57.58$
$t_{1/2k\alpha}$ (min)	$28.86 \pm 9.70$
$k_{10}$ (1/min)	$0.011 \pm 0.0034$
$k_{12}$ (1/min)	$0.0056 \pm 0.0015$
$k_{21}$ (1/min)	$0.00087 \pm 0.00038$
AUC (min $\mu\text{g/ml}$ )	$686.75 \pm 117.72$
$CL_{(s)}$ (mg/kg/min/( $\mu\text{g/ml}$ ))	$0.20 \pm 0.060$
$T_{max}$ (min)	$71.75 \pm 23.0$
$C_{max}$ ( $\mu\text{g/ml}$ )	$2.66 \pm 0.72$

<sup>a</sup>  $A$ : distribution phase;  $B$ : elimination phase;  $\alpha$ : distribution rate constant;  $\beta$ : elimination rate constant;  $k_a$ : absorption rate constant;  $t_{1/2\alpha}$ : distribution half-life time;  $t_{1/2\beta}$ : elimination half-life time;  $t_{1/2k\alpha}$ : absorption half-life time;  $k_{12}$  and  $k_{21}$ : transportation constants;  $k_{10}$ : elimination constant; AUC: area under curve;  $CL_{(s)}$ : clearance;  $C_{max}$ : maximum concentration;  $T_{max}$ : time of  $C_{max}$ .

#### 4. Conclusion

A novel sensitive, specific HPLC–UV method was developed and validated. We significantly improved the UV detection of clarithromycin through using the trimethylbrosilicon as the derivatization reagent. According to our knowledge, this is the first time that the trimethylbromosilane is used as the derivatization reagent for the determination of clarithromycin and this reagent offers a more efficient derivatization procedure than the method has been published [14].

Most of the published methods use 0.3–1 ml of human plasma for analysis, and are not verified for preclinical animal study with rat or mice where less than 0.3 ml is usually available for each plasma sample. The present work requires only 150  $\mu$ l of plasma for the analysis which is almost seven times less than the HPLC–UV method reported by Amini and Ahmadiani [15]. The LOQ of this method is 0.1  $\mu$ g ml<sup>-1</sup>, which is sufficient to study the plasma pharmacokinetics of clarithromycin in rats after a single oral dose of 150 mg kg<sup>-1</sup> body weight.

#### Acknowledgements

K.Z. acknowledges the Tianjin Municipal Science and Technology Commission (#043186011), the Outstanding Young Scholarship from NSFC (#30125043), the Basic Research Project (#2002CCA01500) of the MOST, and the Cheung Kong Scholars Programme for financial support.

#### References

- [1] I.I. Salem, in: H.G. Brittain (Ed.), *Analytic Profiles of Drug Substances and Excipients*, vol. 24, Academic Press, San Diego, 1996, p. 45.
- [2] D.H. Peters, S.P. Clissold, *Drugs* 44 (1992) 117–164.
- [3] A.L. Barry, R.R. Packer, *Eur. J. Clin. Microbiol.* 5 (1986) 536–540.
- [4] F. Kees, S. Spangler, M. Wellenhofer, *J. Chromatogr. A* 812 (1998) 287–293.
- [5] S.-Y. Chu, L.T. Sennello, S.T. Bunnell, L.L. Varga, D.S. Wilson, R.C. Sonders, *J. Chromatogr.* 571 (1991) 199–208.
- [6] M. Janecek, M.A. Quilliam, M.R. Bailey, *J. Chromatogr.* 619 (1993) 63–69.
- [7] M. Hedenmo, B.-M. Eriksson, *J. Chromatogr. A* 692 (1995) 161–166.
- [8] I. Niopas, A.C. Daftsios, *Biomed. Chromatogr.* 15 (2001) 507–508.
- [9] S.J. Choi, S.B. Kim, H.-Y. Lee, D.H. Na, Y.S. Yoon, S.S. Lee, J.H. Kim, K.C. Lee, H.S. Lee, *Talanta* 54 (2001) 377–382.
- [10] J.I.D. Wibawa, P.N. Shaw, D.A. Barrett, *J. Chromatogr. B* 783 (2003) 359–366.
- [11] T. Chieko, O. Hisakazu, H. Erika, K. Hajime, S. Hitoshi, I. Tatsuji, *J. Chromatogr. B: Biomed. Sci. Appl.* 738 (2000) 405–411.
- [12] A. Pappa-Louisi, A. Papageorgiou, A. Zitroua, S. Sotiropoulos, E. Georgarakis, F. Zougrou, *J. Chromatogr. B: Biomed. Sci. Appl.* 755 (2001) 57–64.
- [13] G.F. van Rooyen, M.J. Smit, A.D. de Jager, H.K.L. Hundt, K.J. Swart, A.F. Hundt, *J. Chromatogr. B* 768 (2002) 223–229.
- [14] J. Sastre Torano, H.J. Guchelaar, *J. Chromatogr. B: Biomed. Sci. Appl.* 720 (1998) 89–97.
- [15] H. Amini, A. Ahmadiani, *J. Chromatogr. B* 817 (2005) 193–197.
- [16] P.O. Erah, D.A. Barret, P.N. Shaw, *J. Chromatogr. B* 682 (1996) 73–78.
- [17] P.O. Erah, A.F. Goddard, D.A. Barrett, P.N. Shaw, R.C. Spiller, *J. Antimicrob. Chemother.* 39 (1997) 5–12.
- [18] J. You, Y. Ming, Y. Shi, X. Zhao, Y. Suo, H. Wang, Y. Li, J. Sun, *Talanta* 68 (2005) 448–458.



## Determination of proteins by flow injection analysis coupled with the Rayleigh light scattering technique

Ying Li<sup>a</sup>, Lijun Dong<sup>a</sup>, Yaheng Zhang<sup>a</sup>, Zhide Hu<sup>a,b,\*</sup>, Xingguo Chen<sup>a</sup>

<sup>a</sup> Department of Chemistry, Lanzhou University, Lanzhou, GanSu Province 730000, China

<sup>b</sup> Institute of DunHuang Studies of Lanzhou University, Lanzhou University, Lanzhou, GanSu Province 730000, China

Received 29 December 2005; received in revised form 6 March 2006; accepted 14 March 2006

Available online 5 May 2006

### Abstract

A novel flow injection analysis (FIA) method with Rayleigh light scattering (RLS) detection was developed for the determination of protein concentrations. This method is based on the weak intensity of RLS of *p*-nitrohenzene-azo-3,6 disulfo-1-amino-8-naphthol-7-azo-benzene disodium salt (Amide Black-10B) which can be enhanced by addition of protein in weakly acidic solution. It has proved that the application of this method to quantify the proteins by using human serum albumin was available in real samples. In addition, this method is very sensitive (the determination limits are 0.11 µg/mL for human serum albumen (HSA) and 0.85 µg/mL for bovine serum albumen, BSA), simple, rapid and tolerance of most interfering substances. The FIA–RLS method was more stable than the general RLS method and the average R.S.D. value of FIA–RLS less than general RLS. The effects of different interfering substances will be also examined. The amount of proteins in human serum sample was determined and the maximum relative error was no more than 3.00% as well as the recovery was between 94.9 and 105.9%.

© 2006 Elsevier B.V. All rights reserved.

**Keywords:** Rayleigh light scattering; Flow injection analysis; Amide Black-10B; Protein

### 1. Introduction

It is deemed that quantitative analysis of proteins is a basic requisite in biochemistry because it is often used as a reference for the measurements of other components in biological samples. Up to now, most methods widely accepted of protein determination are spectrophotometric, such as the Lowry et al. [1], Coomassie brilliant blue (CBB) [2,3], bromophenol blue [4], and bromocresol green [5] methods. However, undoubtedly, there are some limitations on them in terms of sensitivity, selectivity, stability and simplicity. Therefore, a great number of assays have been developed.

Recent years sensitive methods for protein and nucleic acids have been developed based on enhanced Rayleigh light scattering (RLS). RLS measurements usually are performed at wavelengths away from absorption bands of the species. The technique has been extensively studied and applied to a variety of problems for many years [6,7]. Pasternack et al. studied por-

phyrin associates with DNA and the aggregation of chlorophyll by resonance light scattering, and pointed out that light scattering is very sensitive for probing the aggregation of macromolecules [6]. Huang et al. firstly applied this technique to analytical assays because enhanced intensity of RLS was obtained with  $\alpha,\beta,\gamma,\delta$ -tetrakis[4-(trimethylammonium)phenyl]porphyrin [8]. Later, Ma et al. also used this technique for protein assay [9]. Currently, RLS spectroscopy has gradually become a useful technique which be used in analytical chemistry, including the determination of inorganic ions [10], nucleic acids [11] and proteins [12–17]. However, relatively less satisfactory is know about the reproducibility of a general RLS method for unstable dye-staining systems. Despite greatly improved selectivity and sensitivity, newly developed RLS techniques which include RLS imaging [18] and the total internally reflected RLS [19] still have not overcome the fluctuation of signals. Also, it is not easy to perform automated analysis for these improved RLS techniques. Thus, it is necessary to develop new methods for coupled automated injection systems to overcome these shortcomings [20–23].

Flow injection technique becomes an affective instrumental tool which can increases the sampling rate, reduces the use of

\* Corresponding author. Tel.: +86 931 8912540; fax: +86 931 8912582.  
E-mail address: [huzd@lzu.edu.cn](mailto:huzd@lzu.edu.cn) (Z. Hu).

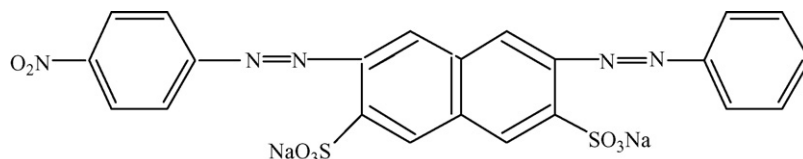


Fig. 1. Structure of Amide Black-10B.

reagents and contributes to development of automation of analysis. These features of FIA make it very suitable for analysis in clinical analytical control [24,25].

*p*-Nitrohenzene-azo-3,6-disulfo-1-amino-8-naphthol-7-azobenzene disodium salt (Amide Black-10B) (structure in Fig. 1) is a good chromogenic reagent, it has not been paid much attention in the determination of proteins. The aim of this study is to use Amide Black-10B (AB-10B) as a binding reagent for protein determination because a high sensitivity to RLS intensity was observed. By considering the advantages on automation of laboratory processes, an FIA system with RLS detection was developed and optimized in order to automate the determination of total protein in serum samples, with high sample throughput.

## 2. Experimental

### 2.1. Instrument and apparatus

The spectrum and the intensity of RLS were obtained with a RF-5301PC spectrofluorophotometer (Shimadzu) with a 150 W xenon lamp. The excitation and emission bands widths were 3 nm. The pH measurements were made with a model PHS-10A pH meter (Xiaoshan, China).

A schematic diagram of the flow system for the determination of proteins was shown in Fig. 2. Two peristaltic pumps and eight-way injection valve (Wenzhou, China) were used to assemble the system. A flow cell with a 90  $\mu$ L inner volume was employed to measure the FIA–RLS signals. PTFE tubing (i.d. 0.5 mm) was used to connect all components in flow system.

### 2.2. Reagents

Amide Black-10B was obtained from Shanghai Experimental Reagent Limited and was directly dissolved in water to prepare stock solution of  $1.0 \times 10^{-3}$  mol/L. Human serum albumin

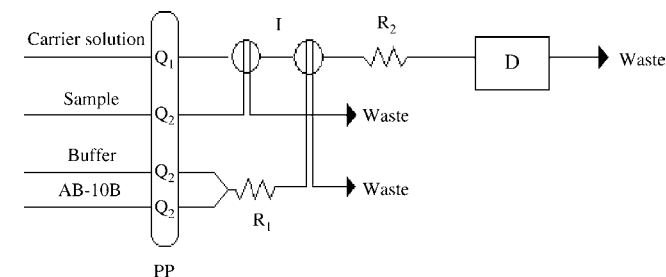


Fig. 2. FIA system for the determination of proteins. PP: peristaltic pump; Q<sub>1</sub>: 2.80 mL/min; Q<sub>2</sub>: 1.95 mL/min; I: injector (eight-way valve); R<sub>1</sub>, R<sub>2</sub>: reactor; D: detector.

and Bovine serum albumin were purchased from Sino-American Biotechnology Company (China), were applied without further purification. All protein solutions were prepared in doubly distilled water to prepare stock solutions of 2.0 mg/mL and the protein stock solutions were kept in the dark at 277 K.

Britton–Robinson buffer was utilized to control the pH values of carrier flow. All other chemicals were of analytical grade or the best grade are commercially available. Human serum samples were obtained from the Hospital of Lanzhou University. The serum samples were diluted 250-fold with doubly distilled water to prepare stock solutions and stored at 277 K.

### 2.3. Procedure

Fig. 2 shows a schematic diagram of the FIA system for the quantification of protein. The carrier solution (Britton–Robinson buffer, pH 4.1) was propelled by a peristaltic pump in the reservoir. The sample flow system consisted of another peristaltic pump connected to a sample injection valve (eight-way injection valve) equipped with sample loops. The reagent stream merged with a buffer solution inside the reactor (R<sub>1</sub>) to obtain suitable pH. Then the sample and reagent are transported to another reactor (R<sub>2</sub>) while being mixed. Lastly, the mixed solution was transported to a spectrofluorometer with a flow-through cell connected to a recorder and finally to a waste tank. The Rayleigh light scattering intensity was measured at  $\lambda_{\text{ex}} = \lambda_{\text{em}} = 265$  nm with a spectrofluorometer. The flow system was operated at room temperature.

The RLS spectra were obtained with the excitation and emission monochromators of fluorometer scanned synchronously through the wavelength range of 220–500 nm.

### 2.4. Theory for the determination by the RLS

In general, the intensity of light scattering is related to the volume of the species, the wavelength of incident light, and the real and imaginary parts of the scatterer's polarizability. When the medium is transparent and the wavelength is determined, the intensity of scattering is only related to the concentration of samples, which is the quantitative basis of Rayleigh light scattering [12].

The intensity of RLS was calculated by Anglister and Steinberg [26] to be

$$R(90^\circ) = \left( \frac{4000\pi^2 n^2 C}{\lambda^4 N_A} \right) \left[ \left( \frac{dn}{dC} \right)^2 + \left( \frac{dk}{dC} \right)^2 \right] \quad (1)$$

where  $R(90^\circ)$  is the Rayleigh ratio for the incident beam and total scattered light at  $90^\circ$ ,  $n$  the refractive index of the medium,

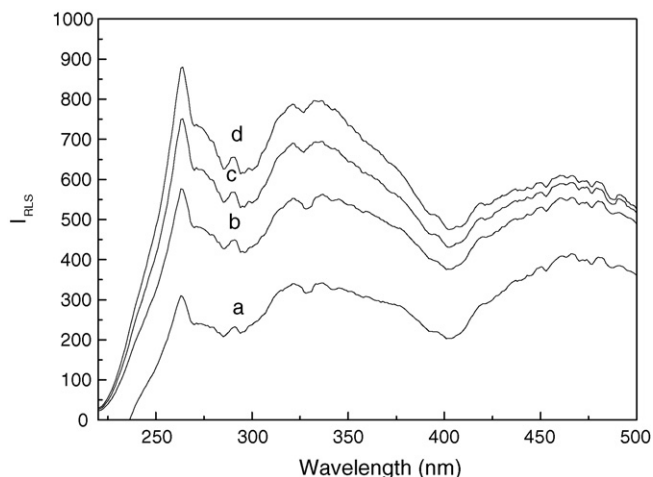


Fig. 3. The RLS spectra of (AB-10B)–HSA system. (a)  $1.0 \times 10^{-4}$  mol/L AB-10B; (b–d)  $1.0 \times 10^{-4}$  mol/L AB-10B in the presence of 8.0, 16.0, 24.0  $\mu\text{g/mL}$  HSA; pH 4.1;  $\lambda_{\text{ex}} = \lambda_{\text{em}} = 265$  nm.

$\lambda$  the wavelength of incident light,  $N_A$  the Avogadro constant,  $C$  the molarity of the scattering particle, while  $dn/dC$  and  $dk/dC$  are the increments of the real and imaginary components and of the refractive index of the solution due to the scattering particles, respectively.

### 3. Results and discussion

#### 3.1. Spectra features of (AB-10B)–proteins interaction

The light scattering intensity was measured at 265 nm with 3 nm slit width for both excitation and emission radiation. The light scattering spectrum was obtained by scanning simultaneously with the same excitation and emission wavelengths. Fig. 3 indicates the RLS spectra AB-10B and (AB-10B)+HSA obtained under the optimum experimental conditions ( $1.0 \times 10^{-4}$  mol/L AB-10B; pH 4.1). A low light scattering intensity of AB-10B was found between 220 and 500 nm. However, when the HSA was present, an important enhanced light scattering was obtained. We consequently conclude that AB-10B reacted with HSA and produced a complex, its RLS intensity was much higher than that of AB-10B under the same optimal condition. From Fig. 3, it can be seen that there are two RLS peaks for (AB-10B)–HSA system at 265 and 320 nm. As the enhanced signal at 265 nm is greater than that at 320 nm, 265 nm was chosen as the excitation and emission wavelengths.

#### 3.2. Optimization of the flow system

In order to obtain the best experimental result, FIA variables (flow rate, reactor lengths, sample volume, and reaction time) were optimized.

The effect of the flow rate was investigated by injecting a sample solution of the analyte (20.0  $\mu\text{g/mL}$ ) at different flow rates. Increasing flow rate resulted in decrease of peak heights

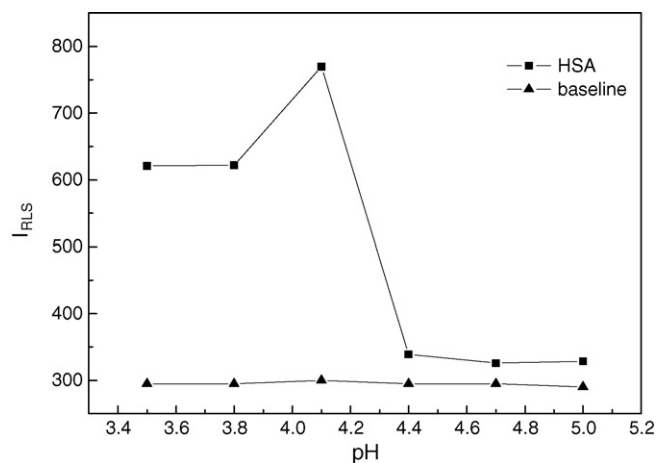


Fig. 4. Effect of pH on the interaction between AB-10B and HSA. Concentrations:  $1.0 \times 10^{-4}$  mol/L AB-10B; 20.0  $\mu\text{g/mL}$  HSA.

and over-pressure was caused in the system, however, it was not impossible to obtain a higher sampling frequency. The flow rate was studied in the range 3.33–1.20 mL/min. A flow rate of 2.80 mL/min working with  $Q_1$  peristaltic pumps, simultaneously, was adopted as a compromise between sensitivity and throughput. The flow rate of  $Q_2$  could be decreased to 1.95 mL/min. The reactor length was investigated in the range 50–250 mm. It can be seen that the sensitivity increases with increasing rate of carrier stream flow, and that the sensitivity was independent of length of reaction coil. The interaction between AB-10B and proteins was incomplete when the reaction coils length too short, whereas the RLS signals could decrease when it is too long. So, the reactor proper length of  $R_1R_2$  was 150 mm.

The effect of the sample volume was also studied. Using sample volumes between 50 and 250  $\mu\text{L}$  of 20.0  $\mu\text{g/mL}$  HSA standard solution, the increase of RLS was linear in the range 50–200  $\mu\text{L}$  (higher volumes did not increase significantly the signal). In this work, the sample volume was 200  $\mu\text{L}$ . Reaction time was one of important variables. The RLS intensity was independent of reaction time. So, the intensity of RLS did not increase with long reaction time. Reaction time between AB-10B and proteins was 10 s.

#### 3.3. Effect of pH

The effect of pH on RLS was investigated at pH 3.5–5.0. The scattering intensity of the assay system is greatly affected by the pH whereas the RLS of the reagent blank is not affected.

Fig. 4 shows that the scattering intensity of the (AB-10B)–HSA complex was affected greatly by pH. The highest intensity was obtained at pH 4.1, so this pH was chosen for the assay. The effect of pH can be explained as follows: the greater negative charge on AB-10B would enhance the interaction with the pH increased between dye and positively charged HSA. On the other hand, an increase in pH also causes an increase in the negative charge on the protein, which would weaken the binding of dye to HSA. These two opposing effects of pH resulted in the

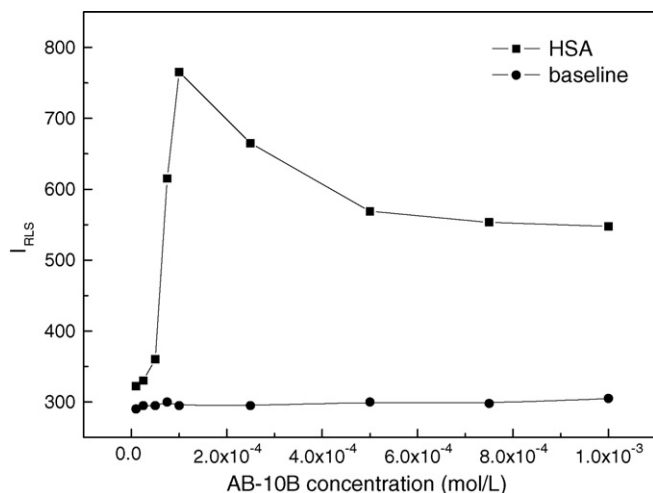


Fig. 5. Effect of AB-10B concentration on the interaction between AB-10B and HSA. Concentrations: 20.0  $\mu\text{g/mL}$  HSA; pH 4.1.

strongest binding and hence the maximum RLS intensity at pH 4.1.

### 3.4. Effect of AB-10B concentrations

The effect of AB-10B concentration on the response of the reaction is tested in the range of  $1.0 \times 10^{-5}$  to  $1.0 \times 10^{-3}$  mol/L. It can also be seen from Fig. 5 that the highest sensitivity and intensity was reached at an AB-10B concentration of  $1.0 \times 10^{-4}$  mol/L, above which the sensitivity decreased with the increase of the dye concentration. At this concentration, all available AB-10B was bound so that further protein addition cannot lead to further (AB-10B)–protein interaction. This phenomenon is owing to the higher concentration of the free dye at which resulted in a higher absorbance and thus less enhancement of the scattering. Thus  $1.0 \times 10^{-4}$  mol/L AB-10B was used in this assay to get a higher sensitivity.

Table 1  
Effect of interfering substances on the RLS<sup>a</sup> method for HSA determination

Interfering substance <sup>b</sup>	Change of RLS (%)	Interfering substance <sup>b</sup>	Change of RLS (%)
D-Leu-OH	−0.83	L-Try	−6.47
D-Glu-OH	−6.54	L-Iso	0
D-Asp-OH	−5.40	Glucose	−0.72
L-Pro	−4.68	Urea	−1.81
L-H-Ser-OH	1.44	$\beta$ -CD	2.16
L-Hyp-OH	0.72	$\text{Cl}^-$	−1.08
L-Leu-OH	0.72	$\text{NO}_3^-$	3.96
L-H-Val-OH	−1.15	$\text{CO}_3^{2-}$	14.08
L-Gly	−3.60	$\text{SO}_4^{2-}$	−1.08
L-Glu	−4.67	$\text{K}^+$	−0.20
L-Lys	−3.33	$\text{Na}^+$	−3.24
L-His	−0.35	$\text{Ca}^{2+}$	−2.68
L-Arg	0.01	$\text{Mg}^{2+}$	0
L-Leu	−4.31	$\text{Mn}^{2+}$	−2.52
L-Phe	−1.08	$\text{Zn}^{2+}$	−3.24
DL-Met	−3.60	$\text{Pb}^{2+}$	−13.67

<sup>a</sup> Concentration of AB-10B  $1.0 \times 10^{-4}$  mol/L; HSA 20.0  $\mu\text{g/mL}$ ; pH 4.1; average of five measurements.

<sup>b</sup> Concentration of interfering substance was 40.0  $\mu\text{g/mL}$ .

### 3.5. Effect of interfering substances

Considering that the matrix compositions are usually quite complex in biological samples, i.e., various components in biological sample might cause interferences for the assay of protein. The potential interfering effects of some of those species frequently encountered in biological samples were investigated in the present system. The influences of coexisting substances were tested, and the results are shown in Table 1. The experimental results indicated that for the assay of 20.0  $\mu\text{g/mL}$  HSA, no interfering effects were observed arising from amino acids and metal ions at the concentration levels. So no special preparation was needed to take before serum sample analysis.

### 3.6. Comparison of the stability of the FIA–RLS method to the general RLS method

Fig. 6 shows FIA gram of (AB-10B)–HSA with increasing HSA. It can be seen that the addition of HSA induced very RLS signals.

Fig. 6 shows that the reproducibility is satisfactory. The reproducibility of the two methods (the FIA–RLS method and the general RLS method) was assessed by using relative standard deviations (R.S.D.). The R.S.D. was calculated by running assays ( $n=5$ ) on different days. The average R.S.D. value of general RLS was 5.38% for 20.0  $\mu\text{g/mL}$  (AB-10B)–HSA (20.0  $\mu\text{g/mL}$  HSA), while the average R.S.D. value of FIA–RLS was 1.47% for 20.0  $\mu\text{g/mL}$  (AB-10B)–HSA (20.0  $\mu\text{g/mL}$  HSA). We consequently concluded that the FIA–RLS method was more reproducible than the general RLS method and the average R.S.D. value of FIA–RLS less than general RLS.

### 3.7. Calibration graphs and sensitivity

Using the optimized flow injection scheme, a calibration graph was obtained for protein. The analytical parameters for

Table 2  
Standard regression equations of various protein

Protein	Standard regression equation ( $C$ , mg/mL)	Linear range ( $\mu\text{g/mL}$ )	Regression coefficient	Determination limits ( $\mu\text{g/mL}$ )
HSA	$Y = 8.65 + 23.80C$	0.50–32.00	0.9991	0.11
BSA	$Y = 48.41 + 16.30C$	2.00–36.00	0.9969	0.85

<sup>a</sup>Concentration of AB-10B  $1.0 \times 10^{-4}$  mol/L; HSA 20.0  $\mu\text{g/mL}$ ; pH 4.1; average of five measurements.

Table 3  
Determination results for protein in human serum

Sample number	The Biuret method $C_p$ (mg/mL) <sup>a</sup>	The proposed method $C_p$ (mg/mL) <sup>b</sup>	R.S.D. (%)	Relative error (%)
1	74.00	75.70	0.32	2.30
2	74.00	74.75	1.32	1.01
3	72.00	71.83	2.58	−0.24
4	84.00	83.38	1.21	−0.74
5	80.00	80.12	1.30	0.15
6	61.00	60.28	0.71	−1.18

<sup>a</sup> The data obtained from the Hospital of Lanzhou University.

<sup>b</sup> Average of five measurements.

the determination are shown in Table 2. It can be seen from Table 2, the linear ranges for HSA and BSA are 0.50–32.00 and 2.00–36.00  $\mu\text{g/mL}$ . The possible reason is that different proteins have different isoelectric points. At the same time, the weight, size and shape of the molecules are also different, so the RLS signals for various proteins are different. The limit of detection is calculated using following formula:

$$C_L = \frac{kS_{b1}}{S} \quad (2)$$

where  $C_L$  is the limit of detection,  $k$  the constant related to the confidence level, according to the suggestion of the IUPAC,  $k = 3$ ,  $S_{b1}$  the standard deviation of five blank-solution measurements and  $S$  is the slope of the calibration graph.

Detection limit estimated were 0.11  $\mu\text{g/mL}$  (HSA) and 0.85  $\mu\text{g/mL}$  (BSA), sample throughput was  $90 \text{ h}^{-1}$ .

### 3.8. Application to sample analysis

The determination of protein is very important in clinical analysis and biochemistry. By using the present method, proteins in human serum samples were measured (shown in Table 3). For each sample, five parallel experiments were conducted, and the maximum relative standard deviation was 2.58%. The results were compared with those assayed by the Biuret method (the data obtained from the Hospital of Lanzhou University), the maximum relative error was 2.30%. The recovery of the samples also was determined. Fixed amounts of HSA standard were added to six samples of known HSA content and the mixtures were analyzed with the proposed procedure. The results were listed in Table 4 and the recovery was between 94.9 and 105.9%. Compared to the standard method, the results are very satisfactory.

Table 4  
The recovery for the determination of HSA sample

Sample number	Diluted sample ( $\mu\text{g/ml}$ ) <sup>a</sup>	Found value ( $\mu\text{g/ml}$ )	R.S.D. <sup>b</sup> (%)	Standard added ( $\mu\text{g/ml}$ )	Total recovery ( $\mu\text{g/ml}$ )	Recovery (%)
1	7.40	7.62	0.40	10.00	17.38	98.9
				20.00	27.92	100.6
2	7.40	7.51	1.52	10.00	17.36	99.3
				20.00	27.09	99.8
3	7.20	7.17	3.17	10.00	16.80	94.9
				20.00	26.87	96.9
4	8.40	8.68	1.33	10.00	18.95	99.2
				20.00	28.54	102.9
5	8.00	8.23	1.27	10.00	18.51	105.9
				20.00	28.35	101.3
6	6.10	6.13	0.85	10.00	16.30	100.5
				20.00	26.76	101.3

<sup>a</sup> The sample obtained from the Hospital of Lanzhou University.

<sup>b</sup> Average of five measurements.



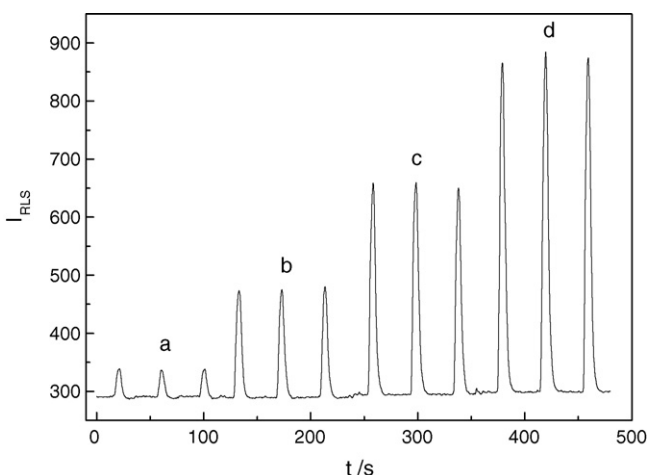


Fig. 6. FIA gram of (AB-10B)–HSA interaction in flow injection analysis. Carrier: BR buffer; (a–d)  $1.0 \times 10^{-4}$  mol/L AB-10B in the presence of 2.0, 8.0, 16.0, 24.0  $\mu\text{g}/\text{mL}$  HSA; pH 4.1. Flow injection analysis variables: sample volume, 200  $\mu\text{L}$ ; carrier flow rate, 2.80 ml/min; time for reaction, 10 s.

#### 4. Conclusion

The presented method offers a simple, rapid and reproducible way for the determination of protein. Automatic Rayleigh light scattering detection techniques were established with flow injection, which avoid the poor reproducibility of unstable system, simplify the detection procedure and facilitate on-line detection of proteins. Moreover, there is no sample matrix interference, which is crucial to determine the protein in real samples.

#### References

- [1] O.H. Lowry, N.J. Rosebrough, A.L. Farr, R.J. Randall, *J. Biol. Chem.* 193 (1951) 265.
- [2] M.M. Bradford, *Anal. Biochem.* 72 (1976) 248.
- [3] T. Zor, Z. Selinger, *Anal. Biochem.* 236 (1996) 302.
- [4] R. Flores, *Anal. Biochem.* 88 (1978) 605.
- [5] R.L. Rodkey, *Clin. Chem.* 11 (1965) 478.
- [6] R.F. Pasternack, C. Bustamante, P.J. Collings, A. Giannetto, E.J. Gibbs, *J. Am. Chem. Soc.* 115 (1993) 5393.
- [7] R.F. Pasternack, K.F. Schaefer, P. Hambright, *Inorg. Chem.* 33 (1994) 2062.
- [8] C.Z. Huang, K.A. Li, S.Y. Tong, *Anal. Chem.* 68 (1996) 2259.
- [9] C.Q. Ma, K.A. Li, S.Y. Tong, *Anal. Chim. Acta* 338 (1997) 255.
- [10] M. Oshima, N. Goto, J.P. Susanto, S. Motorizo, *Analyst* 121 (1996) 1085.
- [11] C.Z. Huang, K.A. Li, S.Y. Tong, *Anal. Chem.* 69 (1997) 514.
- [12] Y. Liu, C.Q. Ma, K.A. Li, F.C. Xie, S.Y. Tong, *Anal. Biochem.* 268 (1999) 187.
- [13] G. Yao, K.A. Li, S.Y. Tong, *Talanta* 50 (1999) 585.
- [14] H. Zhong, N. Li, F.L. Zhao, K.A. Li, *Talanta* 62 (2004) 37.
- [15] R.P. Jia, L.J. Dong, Q.F. Li, X.G. Chen, Z.D. Hu, Y.K. Nagaosa, *Anal. Chim. Acta* 442 (2001) 249.
- [16] H. Zhong, K. Wang, H.Y. Chen, *Anal. Biochem.* 330 (2004) 37.
- [17] H. Zhong, J.J. Xu, H.Y. Chen, *Talanta* 67 (2005) 749.
- [18] C.Z. Huang, Y. Liu, Y.H. Wang, H.P. Guo, *Anal. Biochem.* 321 (2003) 236.
- [19] P. Feng, W.Q. Shu, C.Z. Huang, Y.F. Li, *Anal. Chem.* 73 (2001) 4307.
- [20] X.W. Chen, W.X. Wang, J.H. Wang, *Analyst* 130 (2005) 1240.
- [21] K.J. Tian, Y.F. Li, C.Z. Huang, *Luminescence* 20 (2005) 176.
- [22] E. Vidal, M.E. Palomeque, A.G. Lista, B.S. Fernández Band, *Anal. Bioanal. Chem.* 376 (2003) 38.
- [23] X.W. Chen, J.H. Wang, Z.L. Fang, *Talanta* 67 (2005) 227.
- [24] J. Ruzicka, G.D. Marshall, *Anal. Chim. Acta* 237 (1990) 329.
- [25] T. Bo, Z. Li, G. Yue, *Talanta* 65 (2005) 769.
- [26] J. Anglister, I.Z. Steinberg, *Chem. Phys. Lett.* 65 (1979) 50.

## Electrochemical studies of the interaction of Basic Brown G with DNA and determination of DNA

You Qin Li<sup>a,b</sup>, Yu Jing Guo<sup>a,\*</sup>, Xiu Fang Li<sup>a</sup>, Jing Hao Pan<sup>a</sup>

<sup>a</sup> School of Chemistry and Chemical Engineering, Shanxi University, Taiyuan 030006, PR China

<sup>b</sup> Department of Chemistry, Datong University, Datong 037009, PR China

Received 18 October 2005; received in revised form 19 February 2006; accepted 15 March 2006

Available online 18 April 2006

### Abstract

A new method of electrochemical probe has been proposed for the determination of Herring Sperm DNA (DNA) based on its interaction with Basic Brown G (BBG). The electrochemical behavior of interaction of BBG with DNA was investigated on Hg electrode. In 0.1 mol L<sup>-1</sup> NH<sub>3</sub>–NH<sub>4</sub>Cl buffer solution (pH 8.0), BBG can be reduced on Hg electrode with a well-defined voltammetric peak at –0.67 V (versus SCE). In the presence of DNA, the reduction peak current of BBG decreases and the peak potential shifts to a more positive potential without the appearance of new peak. The study shows that a new BBG–DNA complex is formed by linear sweep voltammetry (LSV) and spectrophotometry. The decrease of the second order derivative of reductive peak current ( $\Delta i_p''$ ) of BBG is proportional to the concentration of DNA in the range of 0.10–36  $\mu\text{g mL}^{-1}$ . Limit of detection of DNA is 0.04  $\mu\text{g mL}^{-1}$ . DNA of Hepatitis B Virus in serum samples was determined satisfactorily. Additionally, the binding mechanism was preliminarily discussed. The mode of interaction between BBG and DNA was found to be intercalation binding.

© 2006 Elsevier B.V. All rights reserved.

**Keywords:** Herring Sperm DNA (DNA); Basic Brown G (BBG); Electrochemical probe; Interaction; Determination

### 1. Introduction

The study on the interaction of small molecules such as metal, drugs, organic dyes with DNA is one of interest because it is important in the design of new and more efficient drugs targeted to DNA [1,2]. A variety of small molecules are bound by electrostatic with the exterior sugar-phosphate backbone or by hydrophobic interaction along the minor groove of DNA or by intercalative interaction between the stacked bases pairs of native DNA from the major groove [2,3]. Among the three modes, the most effective mode of the drugs targeted to DNA is intercalation binding [4]. Thus the research of interaction of intercalation agent with DNA is vital. The studies for the binding interaction with DNA so far have been performed using various methods [5–9]. Based on these interactions, analytical methods for DNA can be established. However, most of these methods suffer from low sensitivity, high costs and procedural complications.

In recent years, electrochemical methods are increasingly used in bioanalytical chemistry [10–15]. They provide a use-

ful complement compared to other analytical methods, on one hand, because they are low-cost, fast response, simple and easily implemented, on the other hand, the interpretation of electrochemical data can contribute to elucidation of the mechanism by which DNA interacts with drugs in an approach to the real action that occurs in the living cells in vivo [16]. In addition, electrochemical methods have special advantages when the substance which can interact with DNA show UV absorbance near 260 nm, which will disturb the absorbance value of bases of DNA. Bard and co-workers pioneered the field of electrochemical study of the interaction of metal complex with DNA [17,18]. However, it is difficult to avoid background current in DNA detection and the large amount of DNA used [3]. Li and co-workers [19–21] studied the interaction of DNA with some electrochemically active compounds such as 9,10-anthraquinone or porphyrin. Zhang et al. [10] reported the interaction of lomefloxacin–Mg(II) complex with DNA and its analytical of DNA determination. Long et al. [22] investigated the electrochemical behavior of CuII–Triazolylazo supramolecular interaction with DNA and developed the method of detection of DNA. However, only a narrow range of relatively high DNA concentration is used for assay and construction of the calibration graph in the above methods.

\* Corresponding author. Tel.: +86 351 7011333; fax: +86 351 7011688.  
E-mail address: [guoyj@sxu.edu.cn](mailto:guoyj@sxu.edu.cn) (Y.J. Guo).

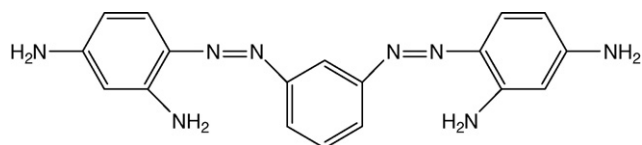


Fig. 1. Molecular structure of Basic Brown G.

Among the most commonly used of all kinds of DNA binders, organic dye has received a great deal of attention, because it serves as effective probes of the structures and functions of biological macromolecules and as study models of some biophysical processes [23]. It is today a generally accepted concept that the planar dyes molecules, such as acridine dyes, phenazine dyes, bind to DNA by intercalation. Wang et al. determined the concentration of DNA in human urine by fluorescence probe of Acridine Orange [24]. Huang et al. detected concentration of nucleic acids with Safranin T by a resonance light-scattering technique [25]. It is well known that electrochemical signals of nucleic acids are so weak that the direct determination is difficult. However, many of the organic dyes have proven to be more effective conductors, thus they can be employed as an electrochemical probe in the detection of DNA.

But to our knowledge, organic dye as an electrochemical probe has seldom been reported for determination of DNA. The major focus of this paper is to develop an electrochemical method as a sensitive and convenient technique for the determination of DNA based on its interaction with organic dye.

Basic Brown G (C.I. Basic Brown 1) is an easily available basic azo dye and can be applied for dyeing materials such as silk, fleece, leather, and paper [26]. Its structure is shown in Fig. 1. In this paper, it is used as the electrochemical probe for the determination of DNA. The electrochemical behavior of the interaction of DNA with BBG was studied on Hg electrode. The binding interaction of BBG with DNA produced a new complex in  $0.1 \text{ mol L}^{-1} \text{ NH}_3\text{-NH}_4\text{Cl}$  buffer solution (pH 8.0), which results in the decrease of the reductive peak currents of BBG. The decrease of the second order derivative of reductive peak current ( $\Delta i_p''$ ) of BBG is proportional to the concentration of DNA within a certain range, thus the concentration of DNA can be determined. The binding ratio and binding constant of DNA with BBG have been detected. Furthermore, the binding mechanism between BBG and DNA is also discussed. It is concluded that the mode of interaction between BBG and DNA is intercalative binding.

## 2. Experimental

### 2.1. Reagents

The following chemicals were used: Herring Sperm DNA (Beijing Xiasi Biotechnology Co. Ltd., China) was commercially purchased and accepted for use without further purification. The stock solutions were prepared by dissolving the solid DNA in  $0.1 \text{ mol L}^{-1} \text{ NaCl}$  solution and stored in the refrigerator at  $0\text{--}4^\circ\text{C}$  for no more than a week. The concentration of DNA was determined according to the absorbance at 260 nm

after establishing that the absorbance ratio  $A_{260}/A_{280}$  was in the range of 1.80–1.90 for DNA indicating that the DNA was free of protein. The molar extinction coefficient  $\epsilon_{260}$  was taken as  $6600 \text{ L mol}^{-1} \text{ cm}^{-1}$ .

The Basic Brown G was purchased from Hebei Jinzhou Chemical Plant, China. Stock solution of  $1.0 \times 10^{-3} \text{ mol L}^{-1}$  BBG was prepared by dissolving BBG directly in doubly distilled water.  $0.1 \text{ mol L}^{-1} \text{ NH}_3\text{-NH}_4\text{Cl}$  was used as buffer solution. The operating solutions of BBG and DNA were obtained by diluting their stock solutions with water just before use. All other reagents were of analytical reagent grade and were used without purification. Doubly distilled water was used throughout.

### 2.2. Apparatus

Linear sweep voltammetric experiments were carried out by using a model JP-303 polarographic analyzer (ChengDu Instrumental Factory, China) with a three-electrode system, namely mercury working electrode, a saturated calomel reference electrode and a platinum-wire counter electrode. Cyclic voltammetry was performed on a BAS-100A electrochemical analyzer (USA) with a PAR-303 electrode system serving as the working electrode used. A saturated calomel electrode was used as the reference electrode and a platinum-wire as counter electrode. A DMP-40 Digital Plotter (USA) was also used. The absorption spectra measurement was performed on a TU-1901 double-beam spectrophotometer (Beijing Puxi Instrument Limited Co., China). All the pH values were measured with a SA-720pH acidity meter (Shenzhen Shanlong Technology Limited Co., China).

### 2.3. General procedure

#### 2.3.1. Electrochemical measurement

To a 10 mL colorimetric tube, solutions were added in the following order: 1.0 mL of  $0.1 \text{ mol L}^{-1} \text{ NH}_3\text{-NH}_4\text{Cl}$  buffer solution (pH 8.0), 0.70 mL of  $1.0 \times 10^{-3} \text{ mol L}^{-1}$  BBG and an appropriate amount of standard DNA. The mixture was diluted to 10 mL with water. After that it was shaken thoroughly and allowed to equilibrate at room temperature for 10 min. The linear sweep second order derivative voltammetric peak currents ( $i_p''$ ) were recorded in the potential range from  $-0.40$  to  $-1.00 \text{ V}$  (versus SCE). Under the same conditions, the voltammetric peak current ( $i_{po}''$ ) of the BBG solution without DNA was obtained and then the difference of peak currents ( $\Delta i_p'' = i_{po}'' - i_p''$ ) was used to determine the concentration of DNA.

#### 2.3.2. Spectroscopic measurement

The absorption spectra were performed by keeping the concentration of BBG constants while varying the concentration of DNA.

## 3. Results and discussion

### 3.1. Study on the interaction of DNA with BBG by spectrophotometry

Absorption spectra behavior of the interaction of DNA with BBG was investigated in the  $0.1 \text{ mol L}^{-1} \text{ NH}_3\text{-NH}_4\text{Cl}$  buffer

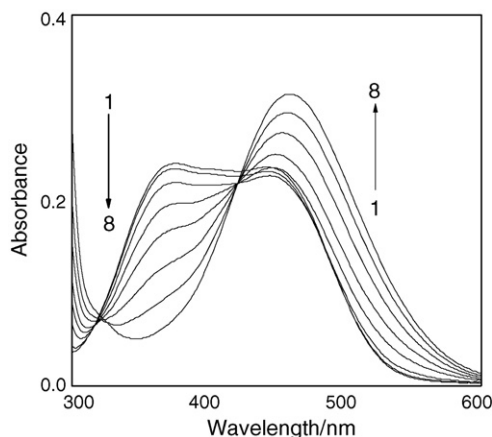


Fig. 2. Absorption spectra of  $7.0 \times 10^{-5} \text{ mol L}^{-1}$  BBG in different concentrations of DNA at pH 8.0. The concentrations of DNA ( $\mu\text{g mL}^{-1}$ ): (1) 0; (2) 50; (3) 100; (4) 150; (5) 200; (6) 250; (7) 300; (8) 350.

solution (pH 8.0), obtained by keeping the BBG concentration constants but changing the DNA concentration. The experimental results are shown in Fig. 2. It can be seen that the BBG molecule has a maximal absorption wavelength at 370 nm. In the presence of DNA, with increasing the concentration of DNA, the absorption at 370 nm linearly decreased whereas the absorption at 425 nm gradually increased. With further addition of DNA, however, large wavelength bathochromic shift and hyperchromic effect were obtained; moreover, an isobestic point at 418 nm was also observed. The change of absorption spectra implied that there are intensive binding interactions between DNA and BBG and a new DNA–BBG complex is formed. The obvious isobestic point at 418 nm also provided the evidence of the formation of new complex.

Hypochromism was suggested to be due to the strong interaction between the electronic state of the intercalating chromophore and that of the DNA bases. Since the strength of this electronic interaction is expected to decrease as the cube of the distance of separation between the chromophore and the DNA bases. The observed large hypochromism strongly suggests a close proximity of BBG molecule to the DNA bases. For example, intercalation of the BBG molecule into the double helix and strong overlap of the  $\Pi-\Pi^*$  states it with the electronic states of the DNA bases are consistent with the observed spectral changes. In addition to the increase intensity, big red shift and isobestic point were also observed in the spectra. Based on the above analysis, we suggest that the interactive mode between BBG and DNA is intercalative binding, which is in agreement with the proposal in literature [27].

### 3.2. Study on the interaction of DNA with BBG by LSV

The nucleic acids, the only electroactive groups are the nitrogenous bases adenine (A), guanine (G), and cytosine (C) [28]. But there is no measurable voltammetric peak at the potential range from  $-0.40$  to  $-1.00$  V (versus SCE). A typical voltammogram of  $7.0 \times 10^{-5} \text{ mol L}^{-1}$  BBG in the absence and presence DNA is shown in Fig. 3. Curve 1 is the voltammogram of  $7.0 \times 10^{-5} \text{ mol L}^{-1}$  BBG without DNA in  $\text{NH}_3\text{-NH}_4\text{Cl}$

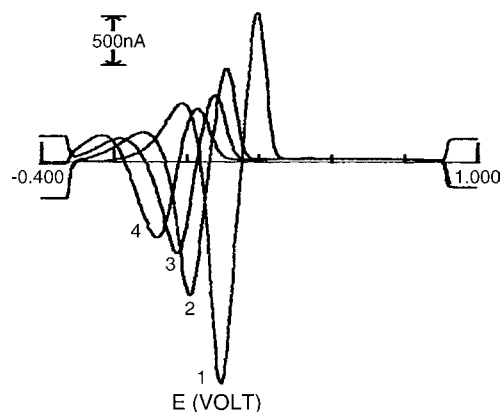


Fig. 3. Second order derivative linear sweep voltammogram of  $7.0 \times 10^{-5} \text{ mol L}^{-1}$  BBG in the  $\text{NH}_3\text{-NH}_4\text{Cl}$  (pH 8.0) buffer solution in the absence (1) and presence (2–4) of  $3 \mu\text{g mL}^{-1}$  (2);  $6 \mu\text{g mL}^{-1}$  (3);  $9 \mu\text{g mL}^{-1}$  (4) DNA.

buffer solution (pH 8.0). It has a well-defined voltammetric peak at  $-0.67$  V (versus SCE), which is related to the electrode reduction of the  $-\text{N}=\text{N}-$  group of the BBG molecule [29]. Curves 2–4 are the voltammograms of the mixture of DNA with BBG. On the addition of DNA, a decrease in the peak current and positive shift in the peak potential were observed for BBG. The remarkable changes mean the complex of BBG–DNA is formed. The decrease in the peak current is attributed to the formation of BBG–DNA complex, which results in the decrease of equilibrium concentration of BBG in solution.

According to above experiment phenomena and references [16,17], it can be inferred that the binding mode of BBG to DNA should be intercalative binding under our experiment conditions, which is in agreement with the results from spectrophotometry. The  $\Delta i_p''$  of BBG is proportional to the added DNA concentration in some ranges, which might be used to determine the concentration of DNA. The plots of  $i_p''$  versus  $v^{1/2}$  are linear both in the absence and presence of DNA, indicating that the electron transfer process involves diffusing species [30].

In addition, a repetitive cyclic voltammogram of BBG–DNA in  $\text{NH}_3\text{-NH}_4\text{Cl}$  buffer solution (pH 8.0) on Hg electrode was examined. The results reveal the cathodic peak potential is about  $-0.67$  V (versus SCE) and no anodic peak indicating that the reduction of BBG is an irreversible process. The repetitive cyclic voltammogram also shows that the cathodic peak current decreases in second cycle, which means that the peak current had adsorption behavior both without and with DNA. The first derivative curve shows that the height of down branch is greater than that of up branch, which also means that the peak current has adsorption behavior [30] in the absence and presence DNA on Hg electrode. All of the above given matter suggested that the peak currents of BBG and its complex with DNA not only are controlled by diffusion but also have adsorption behavior in the experiment.

### 3.3. Determination of binding constant and binding ratio

According to references [31,32], if it is assumed that BBG and DNA only produce a single complex, where M,  $n$ , and  $\text{M}-n\text{DNA}$  represent the dye, binding ratio, and DNA–dye

complex, respectively, a reaction equation is as follows:



The binding constant  $\beta$  can be obtained:

$$\beta = \frac{[M-n\text{DNA}]}{[M][\text{DNA}]^n} \quad (2)$$

If  $M-n\text{DNA}$  is not electrochemically active, it is assumed that the decreasing value of the peak current  $I$  is proportional to the concentration of  $M-n\text{DNA}$  complex:

$$\Delta I = k[M-n\text{DNA}] \quad (3)$$

The following equation can be deduced:

$$C_m = [M] + [M-n\text{DNA}] \quad (4)$$

$$\Delta I_{\max} = kC_m \quad (5)$$

$$\Delta I_{\max} - \Delta I = k(C_m - [M-n\text{DNA}]) = k[M] \quad (6)$$

The Eqs. (3) and (6) are deduced to Eq. (2) and then:

$$\beta = \frac{\Delta I}{(\Delta I_{\max} - \Delta I)[\text{DNA}]^n}$$

$$\text{or } \frac{1}{\Delta I} = \frac{1}{\Delta I_{\max}} + \frac{1}{\beta \Delta I_{\max}} \frac{1}{[\text{DNA}]^n} \quad (7)$$

where  $\beta$  is in  $(\text{L mol}^{-1})^n$ ,  $k$  in  $\text{nA L mol}^{-1}$ ,  $\Delta I$  and  $\Delta I_{\max}$  in  $\text{nA}$ ,  $[M-n\text{DNA}]$ ,  $[M]$ ,  $[\text{DNA}]$  and  $C_m$  all in  $\text{mol L}^{-1}$ . At last let  $\Delta I''$  replace  $\Delta I$  and that is to say, when  $n$  is 1, 2, 3, ..., respectively, the plots of  $1/\Delta I''$  versus  $1/[\text{DNA}]^n$  give some curves. The value of  $n$  is the binding ratio when the curve becomes a straight line and the value of  $\beta$  is  $1/\Delta I_{\max}$  versus  $1/\beta \Delta I_{\max}$ . Based on our experimental data, A linear regression equation  $y=0.0004x+4.8338$  (correlation coefficient,  $r=0.9950$ ) was obtained when  $n=1$  and  $\beta=1.2 \times 10^4 \text{ L mol}^{-1}$ , which proves the binding ratio of DNA–BBG complex is 1:1. DNA interacting with BBG forms a complex of one molar BBG per molar base pair.

### 3.4. The optimum conditions of DNA determination

#### 3.4.1. Effect of additional reagents sequence and pH

The different addition orders of buffer solution, DNA and BBG were investigated and different  $\Delta i_p''$  were observed. The buffer solution and BBG were first mixed, then DNA solution added, a maximum  $\Delta i_p''$  was obtained for this sequence. Spectrophotometry was utilized to further probe this system and the result was good in accordance with LSV. Therefore, this above additional sequence was selected as an experimental condition. The results of experiment indicate that different buffers also have an effect on the system. Among the tested buffers, such as  $\text{HAc-NaAc}$ ,  $\text{Na}_2\text{HPO}_4\text{-KH}_2\text{PO}_4$ ,  $\text{NaCl}$ ,  $\text{Tris-HCl}$ , and  $\text{NH}_3\text{-NH}_4\text{Cl}$ .  $\text{NH}_3\text{-NH}_4\text{Cl}$  buffer is suitable for studying the system of BBG–DNA. The pH of buffer greatly affects the formation of complex BBG–DNA, the  $\text{NH}_3\text{-NH}_4\text{Cl}$  buffer of different pH values were selected as supporting electrolyte to

Table 1  
Analytical parameters for the determination of DNA

Concentration range of DNA ( $\mu\text{g mL}^{-1}$ )	Linear equation	Correlation coefficient ( $r$ )
0.10–2.0	$\Delta i_p'' = 968.6m - 283.0$	0.9969 ( $n=8$ )
2.0–18	$\Delta i_p'' = 85.46m + 4.558$	0.9922 ( $n=8$ )
18–36	$\Delta i_p'' = 5.155m + 1282$	0.9934 ( $n=8$ )

determine the formation of the complex. BBG and DNA concentrations were fixed at  $1.0 \times 10^{-5} \text{ mol L}^{-1}$  and  $5.0 \mu\text{g mL}^{-1}$ , respectively.  $\Delta i_p''$  primarily increased and then decreased with the increasing of pH value and it reached its maximum at pH 8.0. An optimal pH of 8.0 was therefore chosen. In the final 10 mL solution, 0.5–2.0 mL of  $\text{NH}_3\text{-NH}_4\text{Cl}$  buffer solutions were suitable. But the amount of buffer was 1.0 mL, which  $\Delta i_p''$  produced the maximum. Therefore, 1.0 mL  $\text{NH}_3\text{-NH}_4\text{Cl}$  was selected for subsequent characterizations.

#### 3.4.2. Effect of BBG concentration

The effect of BBG concentration on the system was studied with  $10.0 \mu\text{g mL}^{-1}$  DNA. The result showed that  $\Delta i_p''$  increased firstly and then decreased with increasing the concentration of BBG. The concentration of  $7.0 \times 10^{-5} \text{ mol L}^{-1}$  BBG gave the maximum  $\Delta i_p''$ , therefore  $7.0 \times 10^{-5} \text{ mol L}^{-1}$  BBG was employed for further assay.

Table 2  
Effect of the foreign substances on the system

Foreign substance	Concentration ( $\mu\text{mol L}^{-1}$ )	Change $\Delta i_p$ (%)
Zn(II), $\text{SO}_4^{2-}$	8.50	–2.6
K(I), $\text{Cl}^-$	8.50	4.6
Mn(II), $\text{Cl}^-$	4.24	–4.4
Co(II), $\text{SO}_4^{2-}$	4.24	–0.9
Na(I), $\text{Br}^-$	4.24	–3.5
Cr(III), $\text{Cl}^-$	4.24	–4.7
Mg(II) $\text{Cl}^-$	4.24	0.5
Cu(II), $\text{SO}_4^{2-}$	0.50	–6.4
Fe(III), $\text{Cl}^-$	0.50	7.1
Ca(II), $\text{Cl}^-$	0.50	–6.1
$\text{Na}^+$ , $\text{PO}_4^{3-}$	85.0	–2.3
DL-Serine	85.0	–1.7
DL-Histidine	4.24	4.6
Threonine	0.85	0.5
L-Glutamine	0.85	–2.9
DL-Valine	0.50	4.6
$\beta$ -CD	10.0	–0.6
Gelation	0.01 <sup>a</sup>	–2.4
Sodium lauryl sulfate	0.01 <sup>a</sup>	–2.8
Cetyl-pyridine bromide	0.01 <sup>a</sup>	5.2
Protein, BSA	10.0	3.4
Glucose	10.0	–3.7
Maltose	10.0	–3.8
Lactose	10.0	–3.8
Sucrose	10.0	–1.8
Cytosine	10.0	–1.4
Guanine	10.0	–2.7
6-Azouracil	10.0	–1.8

<sup>a</sup> Values in percent.



Table 3  
Result of determination of DNA samples

Sample	DNA ( $\mu\text{g mL}^{-1}$ )	DNA added ( $\mu\text{g mL}^{-1}$ )	DNA found ( $\mu\text{g mL}^{-1}$ )	Recovery (%)
1	5.0	2.0	7.10	105
2	5.0	4.0	8.99	99.7
3	5.0	5.0	10.05	101
4	5.0	6.0	11.24	104
5	5.0	7.0	11.71	95.8

Table 4  
Comparison of determination result for serum samples by fluorescence PCR and electrochemical method

Method	1	2	3	4	5
Fluorescence PCR (copies $\text{mL}^{-1}$ )	$5.52 \times 10^3$	$1.26 \times 10^3$	$<1.0 \times 10^3$	$<1.0 \times 10^3$	$<1.0 \times 10^3$
Electrochemical method	$5.40 \times 10^3$	$1.35 \times 10^3$	$3.06 \times 10^2$	$2.75 \times 10^2$	$2.60 \times 10^2$

### 3.4.3. Effect of ionic strength

The effect of ionic strength on BBG–DNA system was investigated by the addition of a strong electrolyte. The result shows that when NaCl solution was added to the BBG solution in the presence of DNA, the peak current is sensitive to change of ionic strength. The effect of ionic strength comes from the increasing stability of the double helix of nucleic acids with increasing ionic strength. As a controller of ionic strength of the solution,  $\text{Na}^+$  act as counter ions to decrease the unwinding tendency due to electrostatic repulsion between the negatively charged phosphate groups on adjacent nucleotides. So the ionic strength controller also leads to change of the state of nucleic acids. Therefore, appropriate salt medium should be maintained [33].

### 3.4.4. Reaction time, stability, and optimization of instrument conditions

The reaction between BBG and DNA occurs rapidly at the ambient temperature within 10 min and keeps constant for at least 35 min. So the system was equilibrated for 10 min to measure the samples. The scan rate and the dropping mercury static period of the instrument for the assay were studied. The peak current of the complex increases with increasing scan rate. The scan rate ranged from 50 to 1000  $\text{mV s}^{-1}$  every other 100 mV and  $\Delta i_p''$  increased continually and  $\Delta i_p''$  reached a maximum at 600  $\text{mV s}^{-1}$ . Also the peak current increased with increasing of the static period and  $\Delta i_p''$  decreased after the static period was more than 9 s. The static period for the assay was selected at 9 s and the scan rate was fixed at 600  $\text{mV s}^{-1}$ .

## 3.5. The determination of DNA

### 3.5.1. Calibration curve and limits of detection

In this paper, the linear sweep voltammetric technique was applied to determine the concentration of DNA. Under optimal conditions, a linear relationship was obtained between  $\Delta i_p''$  and the concentration of DNA in  $7.0 \times 10^{-5} \text{ mol L}^{-1}$  BBG solution. The calibration regression equations for different concentration range were presented in Table 1. The  $\Delta i_p''$  of BBG is proportional to the concentration of DNA in the range of 0.10–36  $\mu\text{g mL}^{-1}$ . The limit of detection of DNA is 0.04  $\mu\text{g mL}^{-1}$ .

### 3.5.2. Tolerance of the foreign substances

Under the optimum conditions, the influences of the foreign substances such as metal ions, bases, surfactant, carbohydrate, amino acids and protein were tested when the concentration of DNA was 1.0  $\mu\text{g mL}^{-1}$  according to the standard procedure. The interference levels are summarized in Table 2. The experiment results indicated that small amounts of the foreign substances did not disturb the determination of DNA.

### 3.5.3. Analysis of sample and recovery test

The standard addition method was further evaluated for the determination of synthetic and practical samples of DNA. Synthetic samples were prepared based on the interferences of foreign substances and DNA of Hepatitis B Virus in serum sample was obtained from the People's Hospital of Shanxi province. The analytical result is listed in Tables 3 and 4. Synthetic sample recovery was 95.8–105% with the assay. The relative standard deviation was 3.5% for 5.0  $\mu\text{g mL}^{-1}$  DNA ( $n = 10$ ). The determination results of practical sample in Table 4 obtained by electrochemical method were consistent with those obtained by fluorescence polymerase chain reaction (PCR) method. It can be seen that DNA in samples can be determined with satisfactory and reliable results. This also means the proposed electrochemical method is acceptable for the determination of DNA.

## 4. Conclusion

Based on the interaction between BBG and DNA, a new method for the detection of DNA was established. The method is simple, rapid, reliable and cost-effective and can be used to determine DNA in serum sample. The intercalative binding between BBG and DNA was suggested by electrochemical method and spectrophotometry.

## Acknowledgements

All authors herein gratefully acknowledge the support by the National Natural Science Foundation of China (No. 20172035) and the Natural Science Foundation of Shanxi province (No. 20041015).

## References

- [1] M.J. Waring, in: G.C.K. Roberts (Ed.), *Drug Action at the Molecule Level*, Macmillan, London, 1977, p. 167.
- [2] G.M. Zhang, S.M. Shuang, C. Dong, D.S. Liu, M.M.F. Choi, *J. Photochem. Photobiol. B* 74 (2004) 127.
- [3] C. Li, S.L. Liu, L.H. Guo, D.P. Chen, *Electrochem. Commun.* 7 (2005) 23.
- [4] R.Y. Zhang, D.W. Pang, R.X. Cai, *Chem. J. Chin. Univ.* 20 (1999) 1210.
- [5] Y.L. Zhou, Y.Z. Li, *Colloids Surf. A: Physicochem. Eng. Aspects* 233 (2004) 129.
- [6] H.M. Zhang, X.Q. Guo, Y.B. Zhao, D.Y. Wang, J.G. Xu, *Anal. Chim. Acta* 361 (1998) 9.
- [7] S. Mahadevan, M. Palaniandavar, *Inorg. Chim. Acta* 254 (1997) 291.
- [8] J.K. Barton, S.R. Paranawithana, *Biochemistry* 25 (1986) 2205.
- [9] Y.C. Cao, R. Jin, C.S. Thaxton, C.A. Mirkin, *Talanta* 67 (2005) 449.
- [10] N. Zhang, X.L. Zhang, Y.F. Zhao, *Microchem. J.* 75 (2003) 249.
- [11] W. Sun, K. Jiao, *Talanta* 56 (2002) 1073.
- [12] C.Q. Ma, K.A. Li, F.L. Zhao, S.Y. Tong, *Acta Chim. Sinica* 57 (1999) 385.
- [13] J.Q. Liu, J.N. Tian, Z.D. Hu, X.G. Chen, *Biopolymers* 73 (2004) 443.
- [14] H. Zhong, J.J. Xu, H.Y. Chen, *Talanta* 67 (2005) 749.
- [15] C. Tlili, H. Korri-Youssoufi, L. Ponsonnet, C. Martelet, N.J. Jaffrezic-Renault, *Talanta* 68 (2005) 131.
- [16] X.M. Wang, H.Y. Chen, S.Y. Li, J.D. Wang, *Anal. Chim. Acta* 290 (1994) 349.
- [17] M.T. Carter, M. Rodriguez, A.J. Bard, *J. Am. Chem. Soc.* 111 (1989) 8901.
- [18] M.T. Carter, A.J. Bard, *J. Am. Chem. Soc.* 109 (1987) 7528.
- [19] Q. Feng, N.Q. Li, Y.Y. Jiang, *Talanta* 45 (1998) 787.
- [20] Z. Zhu, N.Q. Li, *Microchem. J.* 59 (1998) 294.
- [21] Z. Zhu, N.Q. Li, *Microchem. J.* 59 (1998) 307.
- [22] D.W. Long, C.Y. Liu, H.Y. Zhao, G.H. Lu, *Chin. J. Anal. Chem.* 30 (2002) 1250.
- [23] Y.J. Wei, S.Y. Tong, K.A. Li, *Acta Chim. Sinica* 53 (1995) 83.
- [24] J.W. Wang, X.P. Zhu, W. Sun, J.G. Xue, Z.X. Wang, M.G. Fu, *Spectrosc. Spectral Anal.* 23 (2003) 899.
- [25] C.Z. Huang, Y.F. Li, X.D. Liu, *Anal. Chim. Acta* 375 (1998) 89.
- [26] H.L. He, *Handbook of Industry of Fine Chemical*, Chemistry Industry Press, Beijing, 2004, p. 188.
- [27] E.C. Long, J.K. Barton, *Acc. Chem. Res.* 23 (1990) 271.
- [28] E.L. Palecek, in: G. Milazo (Ed.), *Topic in Bioelectrochemistry and Bioenergetics*, Wiley, London, 1983.
- [29] Q.L. Li, *Electroanalytical Chemistry*, first ed., Beijing Normal University Publishing House, Beijing, 1995, p. 173.
- [30] X.R. Yao, L.Q. Zhang, *Polarographic Catalytic Wave Atlas*, Geology Publishing House, Beijing, 1988, p. 5.
- [31] N.Q. Li, X.X. Gao, *Chin. J. Anal. Chem.* 1 (1971) 40; N.Q. Li, X.X. Gao, *Chin. J. Anal. Chem.* 2 (1974) 459.
- [32] X.X. Gao, X.R. Yao, *Polarographic Catalytic Wave of the Element of Group*, Pt. Science Press, Beijing, China, 1977, p. 122.
- [33] T. Shen, J.Y. Wang, *Biochemistry*, second ed., Higher Education Press, Beijing, 1993, p. 350.

# Chromatographic fingerprints of industrial toluic acids established for their quality control

Hongzhen Lian\*, Yuna Wei

Key Laboratory of Analytical Chemistry for Life Science (Education Ministry of China), School of Chemistry and Chemical Engineering & Center of Materials Analysis, Nanjing University, 22 Hankou Road, Nanjing 210093, PR China

Received 31 December 2005; received in revised form 20 March 2006; accepted 26 March 2006

Available online 2 May 2006

## Abstract

The chromatographic fingerprints of industrial *o*-toluic acid, *m*-toluic acid and *p*-toluic acid have been established by HPLC-UV detection according to their impurity groups. HPLC separation of all relative substances involved in the groups was developed on a Kromasil C<sub>18</sub> column by using methanol–water–NH<sub>4</sub>Ac–HAc buffer (100 mM, pH 4.70) 15/65/20 (v/v/v) as the mobile phase at a flow rate of 1.5 mL/min, and detection was operated by UV adsorption at a wavelength of 254 nm. The ultraviolet spectra corresponding to each chromatographic peak were also recorded for further identification of all components. Whether the limits of relative impurities residues in a toluic acid product are qualified or not can be intuitively estimated by analyzing its chromatogram with comparison to the fingerprint. This protocol has successfully provided some Chinese manufacturers with a simple and feasible method for quality control of toluic acids for industrial use.

© 2006 Elsevier B.V. All rights reserved.

**Keywords:** Chromatographic fingerprint; Fine chemical intermediate; *o*-Toluic acid; *m*-Toluic acid; *p*-Toluic acid; HPLC; Ultraviolet spectrum

## 1. Introduction

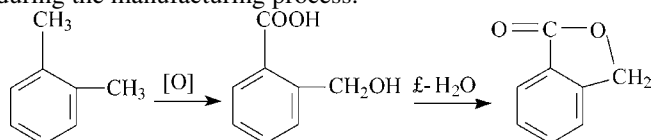
Chromatographic fingerprint analysis is a rational approach for quality assessment of natural products such as herbal medicine, etc., and the industrial products of natural origins such as wine, edible oil and petroleum, etc., each of which contains many compounds that may be relevant to the medical, nutrient or other putative activity [1–4]. A chromatographic fingerprint is, in practice, a chromatographic pattern of extract of some common chemical components. This chromatographic profile is featured by the fundamental attributions of “integrity” and “fuzziness” or “sameness” and “difference” so as to chemically represent the samples investigated. This strategy has been playing more and more important role in traditional Chinese medicine (TCM) quality control [1]. In the last two to three decades, China has been becoming a main exporter of fine chemical intermediate (FCI) in the world. FCI products require strict quality control to enter the international market [5,6]. Analytical methods are needed not only to verify the product purity but also to iden-

tify the nature of related substances existed, and are of primary importance in fine chemical industry [7,8]. Based on the current situation of analysis and testing of fine chemicals including intermediates in China, we put forward the conception of FCI chromatographic fingerprint and suggested that the fingerprint should be established by using the experience of TCM [6]. The significance of the chromatographic fingerprint for research, development, manufacture and trade of FCIs was presented. The feasibility of establishment of FCI chromatographic fingerprints was discussed, and moreover, the general procedures and the essential techniques for the strategy were introduced in detail [6]. Without doubt, HPLC is one of the dominating techniques for this purpose. As exemplified with chromatographic fingerprints of *o*-toluic acid (OTA), *m*-toluic acid (MTA) and *p*-toluic acid (PTA) for industrial use, which have been built by HPLC combined with spectrophotometric detection, these fingerprints have been successfully applicable for the routine quality control in some chemical plants manufacturing the three products.

OTA, MTA and PTA are all fundamental organic synthetic and fine chemical intermediates, and extensively used in pesticides, medicines, dyestuff, and other fine chemicals. Although there are many ways to obtain these three chemicals, the preparation is mainly based on the partial oxidation of *o*-, *m*- and

\* Corresponding author. Tel.: +86 25 83686075; fax: +86 25 83325180.  
E-mail address: [hzlian@nju.edu.cn](mailto:hzlian@nju.edu.cn) (H. Lian).

*p*-xylene, respectively, using different oxidants and catalysts, etc. under certain conditions. So *o*-phthalic acid (OPA), *m*-phthalic acid (MPA) and *p*-phthalic acid (PPA) would easily be the byproducts of industrial OTA, MTA and PTA, respectively, originating from the excessive oxidation of *o*-, *m*- and *p*-xylene. For OTA product, the formation of an additional impurity phthalide (PA) may occur owing to the under-mentioned reaction. Because most of xylenes as the input materials of toluic acids contain more or less amount of toluene and ethylbenzene, benzoic acid (BA) is inevitably present in all final products. In addition, the tiny isomers coexisting in a certain kind of xylene produce corresponding impurities in the reaction. For example, as an isomer of *o*-xylene, *p*-xylene may be turned into PTA and then PPA as impurities in OTA product, such-and-such. To sum up, in the final individual product of toluic acids, BA, OPA, MPA, PPA, even OTA, MTA and PTA, and sometimes PA are all the possible impurities [9–11]. Therefore, the contents of the relative substances in each toluic acid product have to be controlled during the manufacturing process.



Very few reports about the HPLC analysis with regard to industrial toluic acids have been published up to date [12–15]. The analytical methods used only aimed at the purity assay of a single product such as MTA [12], or determination of impurities in a single product such as OTA [13] or PTA [14,15], OPA, MTA, PTA and their related impurities being just regarded as waifs and strays. In fact, all of these compounds are interdependent and interknit. Accordingly, the term “impurity group” was introduced to describe the integrated product profile that is composed of all relative substances existed reasonably and allowably in a FCI product. For instance, BA, OPA, MPA, PPA, MTA, PTA and PA constitute the impurity group of industrial OTA, also, BA, OPA, MPA, PPA, OTA and PTA constitute that of industrial MTA, and BA, OPA, MPA, PPA, OTA and MTA constitute that of industrial PTA, respectively. Therefore, fingerprints of OTA, MTA and PTA products can be drawn based on their impurity groups. In this paper, an HPLC-UV method for the simultaneous determination of eight chemicals specified has been developed. The optimization of the experimental conditions was comprehensively investigated. On the basis of good separation and reliable determination, furthermore, we established the chromatographic fingerprints of OTA, MTA and PTA products, by which quality assessment could be facilitated of industrial toluic acids.

## 2. Experimental

### 2.1. Apparatus

Instrumentation for HPLC analysis included a Varian 5060 liquid chromatograph (Varian, Walnut Creek, USA), a Rheodyne 7725i injector valve equipped with a 10- $\mu$ L loop (Rheodyne, Cotati, USA), a Waters 486 tunable UV absorbance detec-

tor (Waters, Milford, USA). Data acquisition and processing was performed on a JS-3050 chromatographic working station (Dalian Johnson Separation Science and Technology Corporation, Dalian, PRC). The UV spectra of eight chemicals were obtained by Waters Alliance 2695 Separations Module equipped with a vacuum degasser, a quaternary pump, an autosampler and a 996 UV-vis photodiode-array detector (PDA), and Millennium<sup>32</sup> chromatography manager system (Waters). The latter HPLC system also was used to assess the comparability of chromatographic fingerprints in different apparatus.

### 2.2. Reagents and chemicals

Reference substances (RS) of OTA, MTA, PTA, OPA, MPA, PPA and PA (99.0% purity) were purchased from Shanghai First Reagent Factory (Shanghai, PRC), Tianjin Second Reagent Factory (Tianjin, PRC), Nanjing Chemical Reagent Factory (Nanjing, PRC) or Taixing Seventh Chemical Factory (Taizhou, PRC). RS of BA (99.5%, purity) was from Shanghai First Reagent Factory. Industrial products of toluic acids were kindly provided by various manufacturers of China. Methanol was HPLC grade (Hanbang Sci & Tech Co. Ltd., Jiangsu, Huai'an, PRC). Water was Wahaha purified water (Wahaha Group Ltd., Hangzhou, PRC).

### 2.3. HPLC conditions

The column was a Kromasil C<sub>18</sub>, 150 mm  $\times$  4.6 mm i.d., packed with 5  $\mu$ m particle (Hanbang). The mobile phase was methanol–water–buffer (15/65/20, v/v/v). The buffer was NH<sub>4</sub>Ac-HAc (100 mM, pH 4.70). The separation was carried out by isocratic elution with a flow rate of 1.5 mL/min and the column temperature was constantly maintained at 30 °C. The optimum UV wavelength was 254 nm and 10  $\mu$ L each was applied into HPLC system.

## 3. Results and discussion

### 3.1. Development of analytical method

#### 3.1.1. Linear range and detection limit

Individual OTA, MTA, PTA, OPA, MPA, PPA, PA and BA standard stock solutions (1.0 mg/mL) used for calibration purpose were prepared by separately weighting about 25.00 mg of RS into eight 25-mL volumetric flasks and adding methanol to make up to the mark. Then transfer each stock solution 2.50 mL into a 25-mL volumetric flask, mix and add methanol to the volume. The final concentration of each component in this mixed standard solution was 100  $\mu$ g/mL. Its chromatogram is shown in Fig. 1. Mixed standard solutions at concentration of 0.2–80  $\mu$ g/mL each component were prepared by serial dilution of the above mixed standard solution with methanol. Linear relationship between peak areas versus concentrations of standards were obtained within the range 0.2–100  $\mu$ g/mL for PPA, 0.4–100  $\mu$ g/mL for OPA, and 0.6–100  $\mu$ g/mL for MPA, BA, PA, OTA, MTA and PTA, respectively. The regression equations with correlation coefficients (*r*) were

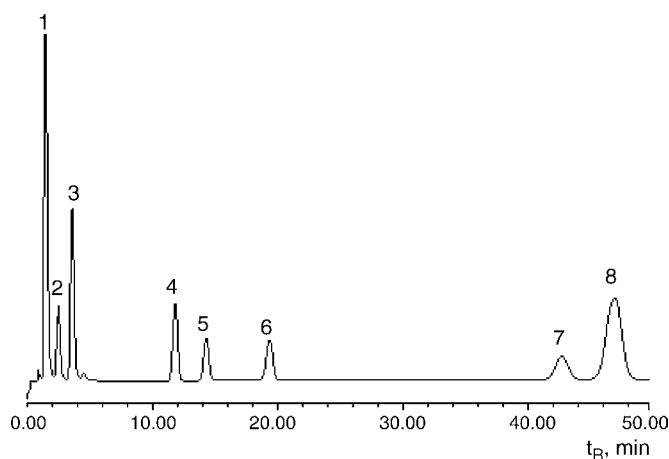


Fig. 1. Chromatogram of standard solution of mixture, 0.1 mg/mL each. Peaks: (1) PPA; (2) MPA; (3) OPA; (4) BA; (5) PA; (6) OTA; (7) MTA; (8) PTA.

$A_{PPA} = 1.493 \times 10^5 C_{PPA} + 33.262$  (0.9995),  $A_{MPA} = 1.011 \times 10^4 C_{MPA} + 2.488$  (0.9994),  $A_{OPA} = 2.847 \times 10^4 C_{OPA} - 5.912$  (0.9997),  $A_{BA} = 2.015 \times 10^4 C_{BA} - 3.182$  (0.9998),  $A_{PA} = 1.270 \times 10^4 C_{PA} - 5.757$  (0.9996),  $A_{OTA} = 1.587 \times 10^4 C_{OTA} - 10.715$  (0.9998),  $A_{MTA} = 1.936 \times 10^4 C_{MTA} - 21.343$  (0.9995) and  $A_{PTA} = 7.688 \times 10^4 C_{PTA} - 26.153$  (0.9999). The limits of detection ( $S/N=3$ ) were 0.05  $\mu\text{g/mL}$  for PPA, 0.1  $\mu\text{g/mL}$  for OPA, 0.2  $\mu\text{g/mL}$  for MPA, BA, PA, OTA and PTA, and 0.4  $\mu\text{g/mL}$  for MTA, respectively.

### 3.1.2. Precision of method

The sample solution for the impurity analysis was prepared by weighting accurately about 30 mg of toluic acid industrial product into a 10-mL volumetric flask and adding methanol to make up to the mark. The peak area relative standard deviations (R.S.D.s) of five injections were 4.5, 1.8, 1.6, 1.7% for OPA, BA, PA and MTA in an OTA sample solution, 1.0 and 5.2% for BA and OTA in a MTA sample solution, and 1.2% for PPA in a PTA sample solution, respectively. The analytical results of impurities in three representative OTA, MTA and PTA industrial products, with the intra-day and inter-day precision, are summarized in Table 1.

### 3.1.3. Choice of experimental conditions

**3.1.3.1. Effect of mobile phase pH.** An important factor for the separation of these eight compounds is pH of mobile phase. The composition of the mobile phase was fixed at methanol–water– $\text{NH}_4\text{Ac}$  buffer (100 mM) (15/65/20, v/v/v). The buffer pH value was adjusted from 3.75 to 6.08 by acetic acid or ammonia (Fig. 2). Except for PA, the retention times of the other seven organic acids are reduced when the mobile phase pH increases. This is because PA is a lactone other than an acid, which retention time does not alter with pH. It is interesting that the retention time change of OPA is not evident. This may be explained by the following reason. A hydrogen bond takes place between the adjacent carboxylic groups in OPA, reducing the amount of free carboxylic acid that is prone to dissociate in aqueous mobile phase. As a result, eight compounds could be completely separated when pH is about 4.70, which

Table 1  
The determination of impurities in three typical industrial toluic acids (%)<sup>a</sup>

Sample	Intra-day ( $n=5$ )								Inter-day ( $n=3$ )							
	PPA	MPA	OPA	BA	PA	OTA	MTA	PTA	PPA	MPA	OPA	BA	PA	OTA	MTA	PTA
OTA product	nd	nd	0.04 (2.8)	0.15 (2.3)	0.20 (1.7)	n/a	0.40 (3.4)	nd	nd	0.04 (1.0)	0.14 (2.8)	0.19 (0.4)	n/a	0.41 (3.6)	nd	
MTA product	nd	nd	nd	0.67 (3.1)	nd	0.13 (4.1)	n/a	nd	nd	nd	0.66 (3.7)	nd	0.12 (3.6)	n/a	nd	
PTA product	0.05 (4.1)	nd	nd	nd	nd	nd	nd	0.04 (0.7)	nd	nd	nd	nd	nd	nd	n/a	

<sup>a</sup> The data in parentheses are R.S.D. (%).



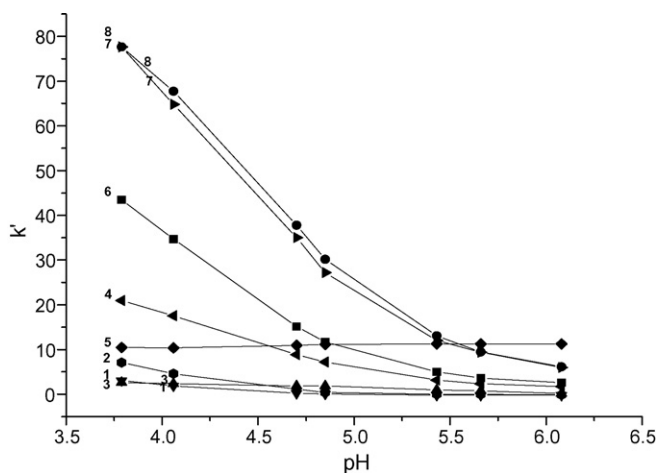


Fig. 2. Effect of mobile phase pH. Lines: (1) PPA; (2) MPA; (3) OPA; (4) BA; (5) PA; (6) OTA; (7) MTA; (8) PTA.

was selected as the pH of the mobile phase in the following experiments.

**3.1.3.2. Effect of ionic strength in mobile phase.** When methanol content was fixed at 15% we also observed the effect of the buffer concentration in mobile phase on separation by adding different proportion of  $\text{NH}_4\text{Ac-HAc}$  solution (100 mM, pH 4.70). It was found that the buffer concentration in the range of 10–80% has little influence on the retention times of all eight compounds involved, but their retention times slightly increased when the proportion was below 10%. Accordingly, we chose 20% as the buffer proportion, that is, the concentration of buffer in the holistic mobile phase was 20 mM.

**3.1.3.3. Effect of the methanol content in mobile phase.** In this experiment, we fixed the proportion of  $\text{NH}_4\text{Ac-HAc}$  buffer (100 mM, pH 4.70) and adjusted the content of methanol ranging from 10 to 60% in mobile phase. By comparing with separation phenomenon under various methanol contents, it indicated that eight compounds could be separated perfectly on baseline when methanol proportion was 15%.

## 3.2. Chromatographic fingerprints of toluic acids for industrial use

### 3.2.1. Identification and verification of impurities in toluic acids

PDA detection following HPLC separation can provide on-line ultraviolet spectrum for each individual peak in chromatograms of toluic acids. In addition to retention time, UV–vis information makes the qualitative analyses of related impurities much easier and more reliable. Thus, ultraviolet spectra of eight compounds of the impurity groups were recorded by PDA (not shown) and employed for peak purity checking and peak identification in order to ensure the accuracy of chromatographic fingerprints for toluic acids. For a certain toluic acid industrial product, the existence of impurities with spectra out of those included in its impurity group suggests that this product should be a questionable one. Consequently, the proposed fingerprints contain both chromatographic and spectral information.

### 3.2.2. Establishment of fingerprints and similarity of toluic acids

We are able to use the chromatographic technique to obtain a relatively complete profile of a FCI product, which is in common called chromatographic fingerprint to represent the so-called equivalence. Obtaining a good fingerprint depends on many factors. The most important one is that a lot of samples of different sources must be analyzed to ensure representativeness, reliability and repeatability. The integrated feature of the chromatographic fingerprint of OTA industrial product can be clearly shown in Fig. 3a. Despite tiny differences, the chromatograms are fairly constant from one batch to the next, and equivalence in these profiles is obvious. The construction of a chromatographic fingerprint aims at evaluating the quality of an intermediate. As discussed above, the fundamental reason of quality control was based on the concept of equivalence, then used this conception to identify the real one and the false one, and further completed precise determination. Thus, the intuitive screen method is to compare the shape similarity of the chromatographic fingerprints. The most commonly used standards for evaluation of similarity of the multivariate systems was Euclidean dis-

Table 2  
Similarity of 10 industrial OTA samples

No.	OPA		BA		PA		Similarity
	Content (%)	R.S.D. (% , n = 3)	Content (%)	R.S.D. (% , n = 3)	Content (%)	R.S.D. (% , n = 3)	
1	0.04	3.7	0.14	1.2	0.20	1.4	0.9515
2	0.04	3.9	0.14	1.5	0.20	1.7	0.9420
3	0.02	3.5	0.14	3.2	0.25	3.3	0.8717
4	0.03	3.3	0.17	2.9	0.28	2.8	0.7983
5	0.04	3.7	0.14	1.9	0.20	2.1	0.9349
6	0.04	2.9	0.15	1.7	0.20	2.0	0.9424
7	0.04	3.9	0.15	2.1	0.20	1.9	0.9365
8	0.04	3.8	0.15	2.3	0.20	1.5	0.9688
9	0.04	3.9	0.15	2.1	0.20	0.9	0.9442
10	0.04	3.9	0.15	2.1	0.20	1.9	0.9442
Average	0.04	–	0.15	–	0.21	–	1

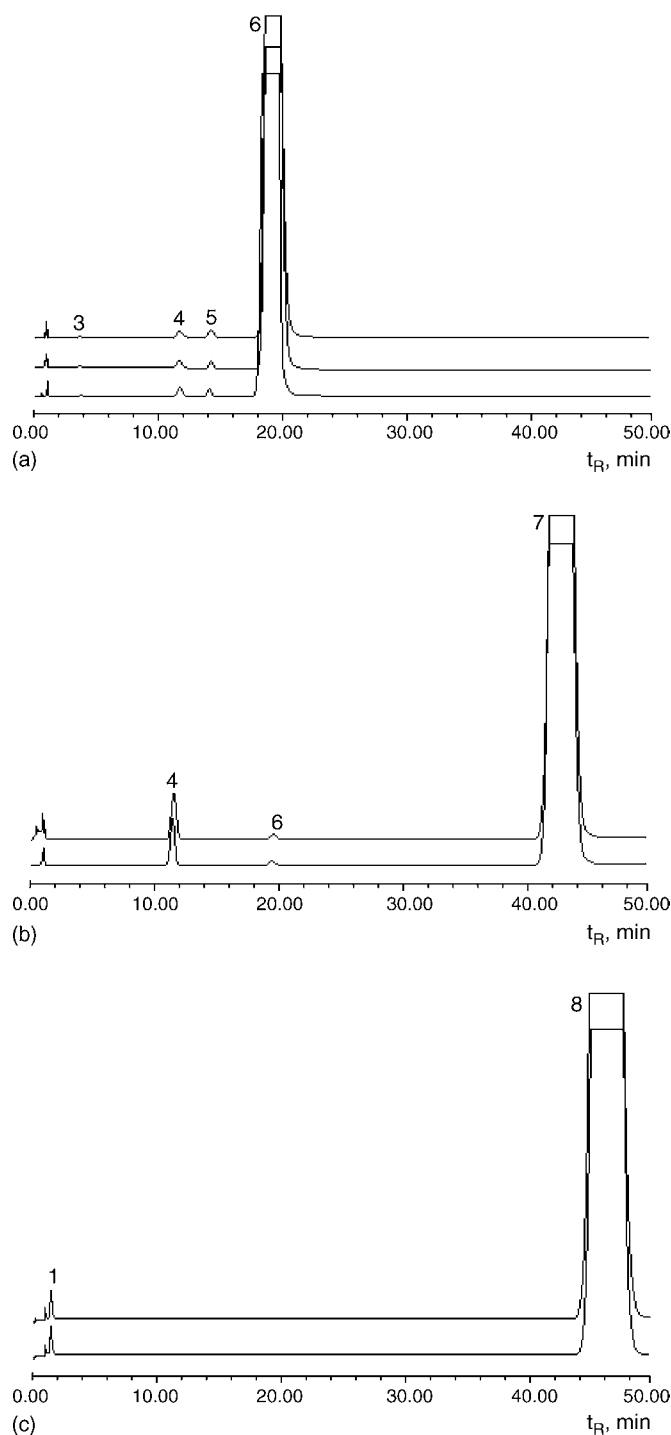


Fig. 3. Chromatographic fingerprint of industrial toluic acids: (a) OTA; (b) MTA; (c) PTA. Peaks: same as in Fig. 1.

tances similarity [1,16]. The similarity of 10 OTA industrial products is shown in Table 2. By the same way, we obtained the chromatographic fingerprints of MTA and PTA industrial products (Fig. 3b and c). The results of similarity are shown in Tables 3 and 4. As can be seen, relative substances constructing a toluic acid fingerprint must fall on the respective impurity group, but the number of these substances is not exactly equal to that in the group. Sometimes, the components of a FCI impu-

Table 3  
Similarity of 10 industrial MTA samples

No.	BA		OTA		Similarity
	Content (%)	R.S.D. (% , n = 3)	Content (%)	R.S.D. (% , n = 3)	
1	0.69	2.4	0.12	3.5	0.9381
2	0.70	2.7	0.13	2.9	0.9376
3	0.64	2.6	0.13	3.3	0.9409
4	0.66	3.1	0.13	1.9	0.9646
5	0.67	1.9	0.13	2.0	0.9579
6	0.68	2.6	0.28	3.4	0.8490
7	0.66	2.7	0.17	2.2	0.9875
8	0.64	2.4	0.16	3.5	0.9645
9	0.64	1.8	0.17	2.9	0.9642
10	0.63	2.5	0.16	3.3	0.9531
Average	0.66	–	0.16	–	1

urity group should depend upon the synthesis approach, raw and processed materials used, subsequent application and the specification requirements in international markets.

### 3.2.3. Application of chromatographic fingerprints

Once a correct and reliable chromatographic fingerprint is established, we can know if a product is up to sample or not. If the chromatogram of some toluic acid product is similar with its fingerprint, we can rapidly estimate that it is primarily eligible. Otherwise, it is unqualified. In other words, abnormal chromatograms imply failed products. For these failed products, it is not necessary to carry through further analysis and testing. A whole set of multi-items and multi-step analytical procedure for a FCI quality inspection normally is laborious, time-consuming and costly. On the other hand, it is impractical for chemical factories to elucidate any unknown impurities structurally, which generally needs combining HPLC-mass spectrometry (MS) and/or HPLC-nuclear magnetic resonance spectroscopy (NMR) [7,8]. So prescreening defective products by FCI fingerprint is an economical method for quality control. It is of great significance for many manufacturers in developing countries especially in China.

Table 4  
Similarity of 10 industrial PTA samples

No.	PPA		Similarity
	Content (%)	R.S.D. (% , n = 3)	
1	0.05	0.8	0.9881
2	0.05	0.9	0.9797
3	0.04	1.4	0.9726
4	0.05	0.7	0.9961
5	0.04	1.2	0.9589
6	0.05	1.1	0.9956
7	0.05	0.9	0.9343
8	0.05	2.0	0.9904
9	0.05	1.5	0.9904
10	0.04	0.8	0.9718
Average	0.05	–	1

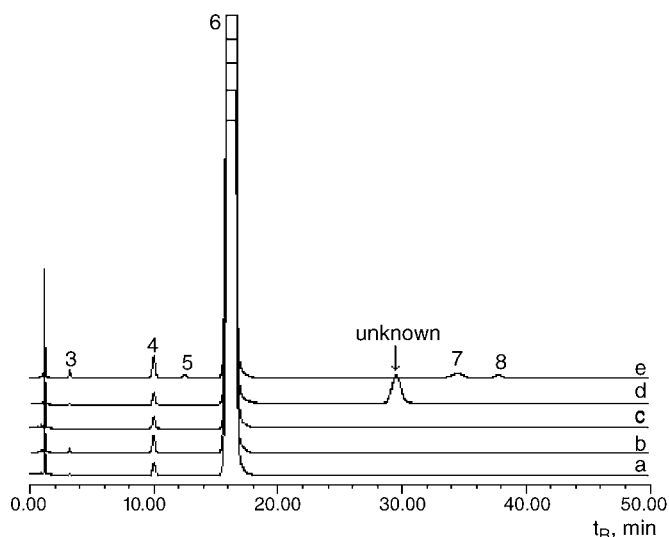


Fig. 4. Chromatographic fingerprint of OTA in other HPLC apparatus. Peaks: same as in Fig. 1.

### 3.2.4. Comparison of chromatographic fingerprints in different apparatus

Using different HPLC apparatus, we would have similar chromatograms of toluic acid product under the same experimental condition. For example, Fig. 4 is a chromatographic fingerprint of industrial OTA, which was obtained under chromatographic conditions identical to Fig. 3a, but using another HPLC instrument, Waters Alliance 2695-996 PDA. Comparing Fig. 4 with Fig. 3a, we can clearly find that the chromatographic profiles of product (a), (b) and (c) look like those in Fig. 3a, although the retention time of every component is a little shift. In addition, product (d) and (e) contained an unknown impurity, MTA and

PTA, respectively, we can judge that they are unqualified. It is shown that this is a comparable and propulsive protocol in different laboratories, and even in different countries. Consequently, chromatographic fingerprint would become a key technique for FCI quality control and a powerful support for the progress of fine chemicals.

### Acknowledgments

This project is supported by the National Natural Science Foundation of China (No. 20575027), and the Analysis & Test Fund of Nanjing University.

### References

- [1] Y.Z. Lian, P.S. Xie, K. Chan, J. Chromatogr. B 812 (2004) 53.
- [2] P. Karásek, J. Planeta, E. Varad'ová Ostrá, M. Mikešová, J. Goliáš, M. Roth, J. Vejrosta, J. Chromatogr. A 1002 (2003) 13.
- [3] M. Hajimahmoodi, Y. Vander Heyden, N. Sadeghi, B. Jannat, M.R. Oveisi, S. Shahbazian, Talanta 66 (2005) 1108.
- [4] L.S.M. Wiedemann, L.A. d'Avila, D. de A. Azevedo, J. Braz. Chem. Soc. 16 (2005) 139.
- [5] H.Z. Lian, Fine Spec. Chem. 13 (2005) 6.
- [6] H.Z. Lian, Fine Chem. Intermed. 34 (2004) 1.
- [7] P. Novak, P. Tepeš, M. Cindrić, M. Ilijaš, S. Dragojević, K. Mihaljević, J. Chromatogr. A 1033 (2004) 299.
- [8] P. Novak, M. Cindrić, P. Tepeš, S. Dragojević, M. Ilijaš, K. Mihaljević, J. Sep. Sci. 28 (2005) 1442.
- [9] M.G. White, A.V. Iretski, US Patent 6,281,382 (2001).
- [10] M.M. Schwartz, L.E. Stark, US Patent 4,675,438 (1987).
- [11] G.H. Du, X.L. Luo, Petrochem. Technol. 27 (1998) 82.
- [12] Y.C. Zhang, Z.Y. Pan, C.M. Lin, J. Zhejiang Univ. Technol. 26 (1998) 78.
- [13] H.J. Yang, M.Y. Ding, J. Liq. Chromatogr. Relat. Technol. 25 (2002) 2709.
- [14] Y.R. Sun, Petrochem. Technol. 30 (2003) 805.
- [15] X. Du, Y. Shi, X.H. Liu, Chem. Res. Appl. 16 (2004) 107.
- [16] M.J. Chen, Y.Y. Cheng, R.C. Lin, Chin. Tradit. Pat. Med. 24 (2002) 905.

# Prediction of gas-phase reduced ion mobility constants ( $K_0$ ) based on the multiple linear regression and projection pursuit regression

Huanxiang Liu<sup>a</sup>, Xiaojun Yao<sup>a,\*</sup>, Mancang Liu<sup>a</sup>, Zhide Hu<sup>a</sup>, Botao Fan<sup>b</sup>

<sup>a</sup> Department of Chemistry, Lanzhou University, Lanzhou 730000, China

<sup>b</sup> Université Paris 7-Denis Diderot, ITODYS 1, Rue Guy de la Brosse, 75005 Paris, France

Received 31 December 2005; received in revised form 25 March 2006; accepted 26 March 2006

Available online 11 May 2006

## Abstract

Multiple linear regression and projection pursuit regression were used to develop the linear and nonlinear models for predicting the gas-phase reduced ion mobility constant ( $K_0$ ) of 159 diverse compounds. The six descriptors selected by heuristic method were used as the inputs of the linear and nonlinear models. The linear and nonlinear models gave very satisfactory results; the square of correlation coefficient was 0.9082 and 0.9379, the squared standard error was 0.0043 and 0.0030, respectively for the whole data set. The proposed models can identify and provide some insight into what structural features are related to the  $K_0$  of compounds. They can also help to understand the separation mechanism in ion mobility spectrometry. Additionally, this paper provided two simple, practical and effective methods for analytical chemists to predict the  $K_0$  of compounds in ion mobility spectrometry.

© 2006 Elsevier B.V. All rights reserved.

**Keywords:** Ion mobility spectrometry; QSPR; Heuristic method; Projection pursuit regression

## 1. Introduction

As a tool for the separation of mixtures of components, the use of ion mobility spectrometry (IMS) has attracted great interest in the past few years. The features of IMS, including high speed, excellent detection limits, amenability to miniaturization, and ruggedness for field operation, make it an ideal analyzer in applications that require portability. Due to these advantages, IMS has been widely used for the rapid detection of explosives, chemical agents, and toxic industrial chemicals [1–3]. In addition, it also can be used for high-throughput drug screening [4] and proteomics studies [5–7] by coupling ion mobility spectrometry (IMS) with time-of-flight mass spectrometry.

The basic concept of IMS is that an ion will drift at a constant velocity when exposed to an electric field at ambient pressure. The ion accelerates in the electric field before colliding with a neutral molecule and stopping [8]. The continuous series of accelerations and collisions leads to the apparent constant velocity. The ratio of the drift velocity of a given ion to the electric

field gives rise to the ion mobility value, typically denoted as  $K$ . In most IMS instruments, the value of  $K$  can be derived from the following equation [9]:

$$K = \frac{L^2}{Vt} \quad (1)$$

where  $L$  is the length of the drift tube region of the spectrometer,  $V$  is the applied voltage, and  $t$  is the drift time of the ion. For purposes of standardization, the reduced mobility constant,  $K_0$ , is typically reported for any particular analyte ion.  $K_0$  values are calculated using the following equation [9]:

$$K_0 = K \left( \frac{273}{T} \right) \left( \frac{P}{760} \right) \quad (2)$$

where  $T$  is the operating temperature of the instrument and  $P$  is the current ambient pressure. The standardized ion mobility is particular for a particular ion and not dependent on the experimental condition, which provides the possibility to predict the reduced mobility constant from molecular structure alone [8,10].

In addition, the prediction of  $K_0$  values is very important for several reasons. First, the basic mechanism in IMS technique discussed above is the differences in the analytes' ion mobility, so ion mobility is the most important parameter governing the

\* Corresponding author. Tel.: +86 931 891 2578; fax: +86 931 891 2582.  
E-mail address: [xjyao@lzu.edu.cn](mailto:xjyao@lzu.edu.cn) (X. Yao).

separation of solutes in IMS. At the same time, the determination by experiments is often costly and time-consuming. Thus any attempt to provide a computational method to calculate the ion mobility is very useful. Second, there are limited experimental  $K_0$  values that have been published. Third, predicted  $K_0$  values may provide an initial value for algorithms used to calibrate instrument-specific measurements. Finally, a prediction equation could provide valuable insights into the principle dynamics that have the greatest effects on ion mobility.

There have been some studies on the prediction of  $K_0$ . A method for calculating  $K_0$  directly from structure has been reported [11]. Prior to that report, there was no known way to accurately predict  $K_0$  values for diverse sets of organic compounds. Several efforts to correlate  $K_0$  with ion mass have been reported. The correlation between the mass and the inverse of mobility has been applied to homogeneous sets of compounds with some success. However, the obtained results were not satisfactory when applied to a diverse set of compounds [12–15]. Jurs and co-workers developed a neural network model, which was able to predict  $K_0$  values with over 99% accuracy for a defined set of relatively simple compounds [11] and a somewhat lower (i.e., 91.1%) accuracy for an expanded set containing more diverse compounds [9]. The weights and node links of neural nets are constructed to optimize predictions by specific criteria, however, without providing the user a method of relating inputs to predictions. Although this model has good predictive ability, it is difficult to interpret the relationship between the inputs and response. Tolley et al. built several models using multiple linear regression method for different groups [16]. An  $R^2$  value of 80.1% between the calculated  $K_0$  values and measured  $K_0$  values was obtained for 162 compounds. When two outliers were removed, the predictability increased to an  $R^2$  value of 87.4%. This model is difficult to generalize because it has different regression equations for different series of compounds. In addition, the model was not tested by the external test set.

In the present investigation, the calculated descriptors based on the software CODESSA from structure alone were used to predict the reduced ion mobility constants of a more diverse set of 159 compounds by using the heuristic method (HM) and projection pursuit regression (PPR). The aim was to explore the mobility behavior of these compounds in ion mobility spectrometry, to establish a new quantitative structure–mobility relationship (QSMR) model to seek for the structural factors affecting the mobility behavior of these compounds in ion mobility spectrometry and the essential difference of the different compounds. The predicted results were very satisfactory for both training set and test set compounds. Moreover, the HM and PPR methods used in this investigation are very simple, effective and practical regression methods for chemists.

## 2. Methods

### 2.1. Data set

The gas-phase reduced ion mobility constants ( $K_0$ ) of 162 compounds with diverse structures were collected from [16]. This reference indicated that two compounds, chloroacetophe-

none and 3-xylyl bromide (3-methylbenzyl bromide) had very large residuals and should be taken out from the data set. In addition, the compound dichloro-(2-chlorovinyl) arsine contains an arsenic atom (arsenic element has many special features). In order to build a general model, the rest 159 compounds were studied. The data set was randomly separated into a training set of 120 compounds and a test set of 39 compounds. The training set was used to build the model, and the test set was used to evaluate its prediction ability.

### 2.2. Calculation and selection of the descriptors

To obtain a QSPR model, compounds are often represented by the molecular descriptors. The calculation process of the molecular descriptors is described as below: All molecules were drawn into Hyperchem and pre-optimized using MM+ molecular mechanics force field [17]. A more precise optimization was done with semi-empirical AM1 method in MOPAC6.0 [18]. All calculations were carried out at restricted Hartree Fock level with no configuration interaction. The molecular structures were optimized using the Polak-Ribiere algorithm until the root mean square gradient was 0.01. With the final geometry structures obtained by MOPAC as inputs, CODESSA (Version 2.63, Semicem, Inc.) software was used to calculate five classes of descriptors: constitutional (number of various types of atoms and bonds, number of rings, molecular weight, etc.); topological (Wiener index, Randic index, Kier-Hall shape index, etc.); geometrical (moments of inertia, molecular volume, molecular surface area, etc.); electrostatic (minimum and maximum partial charges, polarity parameter, charged partial surface area descriptors, etc.); and quantum chemical (reactivity index, dipole moment, HOMO and LUMO energies, etc.) [19].

After the calculation of descriptors, the heuristic method in CODESSA was used to accomplish the pre-selection of the descriptors and build the linear model. Its advantages are the high speed and no software restrictions on the size of the data set. The heuristic method can either quickly give a good estimation about what quality of correlation to expect from the data, or derive several best regression models. Besides, it will demonstrate which descriptors have bad or missing values, which descriptors are insignificant, and which descriptors are highly intercorrelated. This information will be helpful to reduce the number of descriptors in QSAR/QSPR studies.

First of all, all descriptors are checked to ensure: (a) that values of each descriptor are available for each structure and (b) that there is a variation in these values. Descriptors for which values are not available for every structure in the data are discarded. Descriptors having a constant value for all structures in the data set are also discarded. Thereafter, all possible one-parameter regression models are tested and insignificant descriptors removed. As a next step, the program calculates the pair correlation matrix of descriptors and further reduces the descriptor pool by eliminating highly correlated descriptors. All two-parameter regression models with remaining descriptors are subsequently developed and ranked by the regression correlation coefficient  $R^2$ . A stepwise addition of further descriptor scales is performed to find the best multi-parameter regression models



with the optimum values of statistical criteria (highest values of  $R^2$ , the cross-validated  $R_{cv}^2$ , and the  $F$ -value).

The heuristic method usually produces correlations 2–5 times faster than other methods with comparable quality [20]. The rapidity of calculations from the heuristic method renders it the first choice in practical research. Thus, in the present investigation, we used this method to select descriptors and build the linear model.

### 2.3. Projection pursuit regression

Projection pursuit (PP) is a powerful tool for seeking interesting projections of high dimensional data in one, two or three dimensions. It can overcome the curse of dimensionality. At present, projection pursuit has been applied in density estimation, classification and regression problems [21–23]. In this investigation, we mainly apply this technique to solve a regression problem. So, we only introduce the principle of projection pursuit regression (PPR).

For many practical problems, the data is usually high dimensional. It has been a common practice to use lower dimensional linear projections of the data for visual inspection. The lower dimension is usually 1 or 2 (or maybe 3). More precisely,  $X_1, \dots, X_n$   $X \in IR^p$  are  $p$ -dimensional data, then a  $k$ -dimensional ( $k < p$ ) linear projections is  $Z_1, \dots, Z_n$ ,  $Z \in IR^k$  where  $Z_i = \alpha^T X_i$  for some  $p \times k$  matrix  $\alpha$  such that  $\alpha^T \alpha = I_k$ , the  $k$ -dimensional identity matrix. Such a matrix  $\alpha$  is often called *orthonormal*. Since there are infinitely many projections from a higher dimension to a lower dimension, it is important to have a technique to pursue a finite sequence of projections that can reveal the most interesting structures of the data. Friedman and Turkey successfully implemented the idea combining both projection and pursuit, which is called projection pursuit (PP) [21].

The two basic elements of projection pursuit are: a PP index and a PP algorithm. A PP index,  $I(\alpha)$ , is a measure of how interesting a projection by  $\alpha$  is, where  $I(\alpha) = I(\alpha|X)$  implicitly depends on the data  $X = (X_1, \dots, X_n)$ . The larger the index value, the more interesting the projection is. A PP algorithm is a numerical optimization algorithm which maximizes the index over all possible  $\alpha$ . In the implementation of PP by Friedman and Turkey [21], the first several maxima found by a PP algorithm provide the most interesting projections.

In a typical regression problem,  $(X, Y)$  is an observable pair of random variables from a distribution  $F$ , where  $X \in IR^p$  is a  $p$ -dimensional variable (called predictor) and  $Y \in IR$  is a response; and the goal is to estimate the regression function.

$$f(x) = E(Y|X = x),$$

i.e. the conditional expectation of  $Y$  given  $X = x$ , using a random sample  $(X_1, Y_1), \dots, (X_n, Y_n)$  from  $F$ . PPR approximates the regression function  $f(x)$  by a finite sum of ridge functions

$$g^{(m)}(x) = \sum_{i=1}^m g_i(\alpha_i^T x)$$

where  $\alpha_i$  are  $p \times k$  orthonormal matrices,  $m$  is the number of ridge functions. PPR model can be used to approximate a large class of function by suitable choices of  $\alpha_i$  and  $g_i$ .

In this investigation, the PPR algorithm proposed by Friedman was used to construct a PPR model. In this algorithm,  $g_i$  are found by smoothing operation that entails a backfitting. Specially, given  $g^{(0)} = 0$ , for  $i \geq 1$ , it iteratively estimates  $\alpha_i$  by maximum of an index and  $g_i$  by a low dimensional nonparametric regression estimate based on the projected data  $(z_j, r_j)$ , where  $r_j = Y_j - g^{(i-1)}(X_j)$  are the residuals at the  $i$ th step and  $z_i = \alpha_i^T X_j$ ,  $j = 1, \dots, n$ . The procedure is repeated forward (and perhaps a backward fitting is allowed to adjust for the previous fitted pair) until the residual sum of squares  $\sum r_j^2$  is less than a predetermined values.

A different smoother for  $g_i$ , or index, or fitting order may be used and hence yields a different PPR algorithm. In the present work, we used Friedman's super smoother as a smoother. Friedman's super smoother is a running lines smoother which chooses between three spans for the lines. If 'span' is specified, a single smoother with span 'span \*  $n$ ' is used, where ' $n$ ' is the number of data points. PPR algorithm was performed using R script.

## 3. Results and discussion

### 3.1. The HM and MLR models

A total of 646 descriptors were calculated by the CODESSA program for each compound. After the heuristic reduction, the pool of descriptors was reduced to 192. To select the set of descriptors that are most relevant to the mobility of compounds, the linear models with the number of variables from 1 to 9 were built. When adding another descriptor did not improve significantly the statistics of a model, it was determined that the optimum subset size was achieved. The influences of the number of the descriptors on the correlation coefficient ( $R^2$ ) and the standard deviation ( $s$ ) were shown in Fig. 1. From Fig. 1, it can be seen that six descriptors appear to be sufficient for a success-

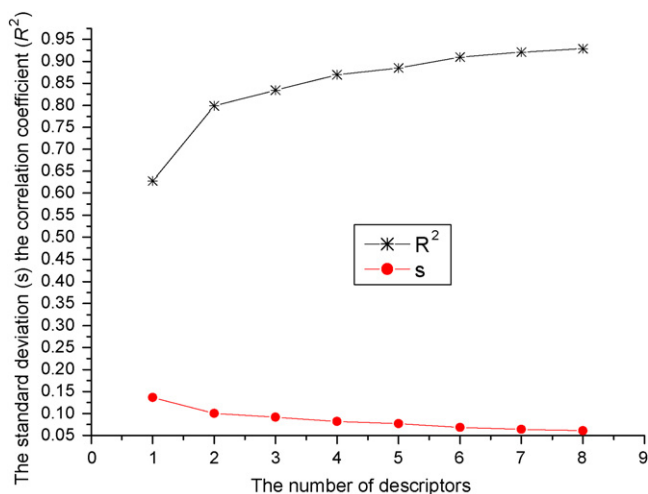


Fig. 1. Influence of the number of descriptors on the correlation coefficient ( $R^2$ ) and the standard deviation ( $s$ ) of the regression models.

Table 1  
Descriptors, coefficients, standard error, and *t*-values for the best linear model

Descriptor	Coefficient	Error	<i>t</i> -test value
Intercept	2.57E + 00	2.11E – 01	12.173
WPSA3 weighted PPSA (PPSA3*TMSA/1000) [Zefirov's PC]	–9.75E – 02	1.14E – 02	–8.5779
Max bonding contribution of a MO	–5.40E – 01	8.87E – 02	–6.0938
Min atomic orbital electronic population	9.60E – 01	8.30E – 02	11.5654
Average Complementary Information content (order 0)	–1.17E – 01	1.69E – 02	–6.9094
RPCS Relative positive charged SA (SAMPOS*RPCG) [Zefirov's PC]	–1.93E – 02	2.19E – 03	–8.794
RNCG Relative negative charge (QMNEG/QTMINUS) [Quantum Chemical PC]	6.82E – 01	1.05E – 01	6.4832

$$R^2 = 0.9096, F = 255.04, s^2 = 0.0047, n = 159.$$

ful regression model. Thus, the 6-parameter model was chosen as the best linear model, which was given in Table 1.

By interpreting the descriptors in the regression model, it is possible to gain some insight into factors that are likely to govern the mobility of the compounds and understand which interactions play an important role during the separation of these compounds.

In this model, there are one topological descriptor, two electrostatic descriptors and three quantum chemical descriptors. According to the *t*-test, the most important descriptor is topological descriptor average complementary information content (order 0) (ACIC0) [24]. The average complementary information contents are defined on the basis of the Shannon information theory. They can be calculated for different orders of neighborhoods,  $r$  ( $r = 0, 1, 2, \dots, \rho$ ), where  $\rho$  is the radius of the molecular graph  $G$ . At the 0th-order level, the atom set is partitioned solely on the basis of its chemical nature. This descriptor can express the size of the molecule. The high correlation between this descriptor and the  $K_0$  indicates that the size of a compound is the most important factor during the IMS separation process.

Both electrostatic descriptors, weighted PPSA (PPSA3\*TMSA/1000) [Zefirov's PC] and RPCS Relative positive charged SA (SAMPOS\*RPCG) [Zefirov's PC], belong to CPSA (Charged Partial Surface Area) descriptor. The electrostatic descriptor WPSA3 weighted PPSA (PPSA3\*TMSA/1000) [Zefirov's PC], which equals to PPSA3 (Atom Charged Weighted Partial Positive Surface Area) multiplied by total molecular surface area. RPCS [24,25] is the product of the solvent accessible surface area of the most positive atom by the relative positive charge (RPCG). The chemical charges in the molecule are calculated using the approach proposed by Zefirov, based on the Sanderson's electronegativity scale [19]. The two descriptors can roundly reflect how charge is distributed in the molecule and loosely show molecular size as well.

Three quantum chemical descriptors involved in the model include RNCG relative negative charge (QMNEG/QTMINUS) [Quantum Chemical PC], max bonding contribution of a MO and Minimum atomic orbital electronic population, respectively. The relative negative charge (RNCG) [19], a quantum-chemical descriptor, represents or depends directly on the quantum-chemically calculated charge distribution in the molecules. The quantum chemical descriptor max bonding contribution of a MO is related to the strength of intramolecular bonding interactions and characterizes the stability of the molecules [19]. Minimum

atomic orbital electronic population for a given atomic species in the molecule is a simplified index to describe the electrophilic ability of the molecule. The first step of the IMS experiments is to produce primary ions in a carrier gas from a neutral gas molecule. Thus, the  $K_0$  value is correlated with the stability and the electrophilic ability of the molecules.

From the above discussion, we can conclude that the factors influencing the  $K_0$  of compounds in IMS process mainly included the molecular size, the electrostatic features and stability of molecules. The best 6-parameter model gave a root mean square (RMS) error of 0.0047 and the corresponding correlation coefficients ( $R^2$ ) were 0.9096, confirming the good fitness capability of the model.

In QSPR study, generally, the quality of a model is expressed by its fitting ability and prediction ability, and the prediction ability is more important. To test the built model, the dataset were divided into a training set of 120 compounds and a test set of 39 compounds. The training set was used to build model and test set was used to test the built model. Table 2 gave the obtained linear model for the training set based on the selected parameters by using multiplier linear regression (MLR) method. With the test set, the prediction results were obtained, confirming the predictive capability of the model. The statistical parameters for the test set were  $R^2 = 0.9067$ ;  $F = 359.55$ ;  $n = 39$ ;  $s = 0.0047$ . Fig. 2 showed a plot of the calculated versus experimental  $K_0$  for the training set and the test set.

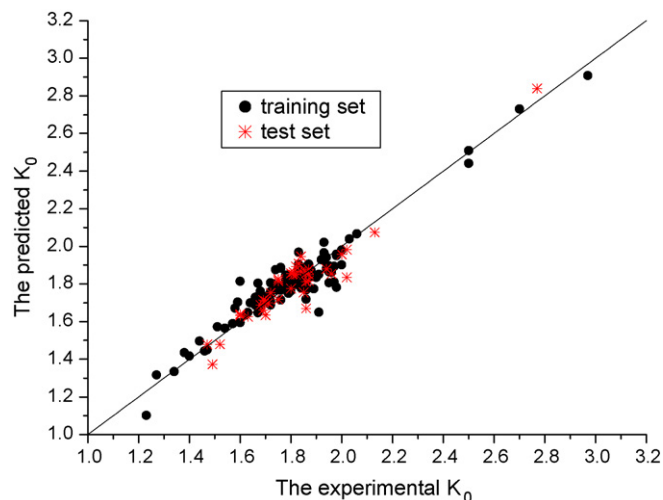


Fig. 2. Predicted  $K_0$  values vs. experimental values by MLR method.

Table 2  
The linear model of training set compounds based on the selected six parameters

Descriptor	Coefficient	Error	<i>t</i> -test value
Intercept	2.60E + 00	2.40E – 01	10.8264
WPSA3 weighted PPSA (PPSA3*TMSA/1000) [Zefirov's PC]	–1.05E – 01	2.13E – 02	–4.9314
Max bonding contribution of a MO	–1.94E – 02	2.53E – 03	–7.6754
Min atomic orbital electronic population	–1.10E – 01	1.56E – 02	–7.0165
Average Complementary Information content (order 0)	–5.44E – 01	9.90E – 02	–5.494
RPCS Relative positive charged SA (SAMPOS*RPCG) [Zefirov's PC]	8.93E – 01	1.12E – 01	7.9651
RNCG Relative negative charge (QMNEG/QTMINUS) [Quantum Chemical PC]	7.36E – 01	1.18E – 01	6.2515

$R^2 = 0.9116$ ,  $F = 194.22$ ,  $s^2 = 0.0048$ ,  $n = 120$ .

### 3.2. The projection pursuit regression model

After building the linear MLR model, projection pursuit regression was applied to build the nonlinear model. In this investigation, all calculation programs implementing projection pursuit regression were written in R-file based on R script. For projection pursuit regression, there are several parameters “*n*terms”, “*optlevel*” and “*span*” need to be determined. The parameter “*n*terms” controls the number of terms to be included in the final model. The levels of optimization (argument ‘*optlevel*’) differ in how thoroughly the models are refitted during this process. At level 0 the existing ridge terms are not refitted. At level 1 the projection directions are not refitted, but the ridge functions and the regression coefficients are. Levels 2 and 3 refit all the terms and are equivalent for one response; level 3 is more careful to re-balance the contributions from each regressor at each step and so is a little less likely to converge to a saddle point of the sum of squares criterion. *Span* defined the fraction of the observations in the span of the running lines smoother. In this investigation, the three parameters “*n*terms”, “*optlevel*” and “*span*” were determined as 6, 2 and 0.75, respectively. The predicted results of the optimal PPR model were shown in Fig. 3. The model gave an standard error of 0.0032 for the training set, 0.0022 for the prediction set and the corresponding correlation coefficients ( $R^2$ ) were 0.9337, 0.9569,

Table 3  
Comparison of Different QSPR Models for the prediction of the  $K_0$

Models	$s^2$	$R^2$	<i>F</i> -test	<i>t</i> -test	Sig
Ref [16]	0.0092	0.7640	508.155	22.542	0.000
MLR	0.0043	0.9082	1565.98	39.572	0.000
PPR	0.0030	0.9379	2345.35	48.429	0.000

respectively. From Fig. 3, it can be seen that the predicted values are in agreement with the experimental values for most of compounds.

### 3.3. Comparison of the results obtained by different approaches

To test the suitability of PPR model, we have compared the obtained predicted results for all 159 compounds by PPR and MLR with those obtained in [16]. Table 3 showed the statistical parameters of the results obtained from the three studies for the same set of compounds. Thus, from the Table 3, it can be seen that this PPR model give the best results.

## 4. Conclusion

Multiple linear regression and pursuit projection regression were used to develop the linear and nonlinear models for predicting the  $K_0$  of 159 diverse compounds based on calculated descriptors. Very satisfactory results were obtained with the proposed methods. By analyzing the obtained results, it can be concluded that: (1) The proposed models could identify and provide some insight into what structural features are related to the  $K_0$  of compounds and help to improve the understanding for the separation mechanism of compounds in IMS. (2) Non-linear models using PPR produced better models with good predictive ability than heuristic method. Non-linear relationship can describe accurately the relationship between the structural parameter and the  $K_0$  of the studied compounds. Additionally, this paper provided two simple, practical and effective methods for analytical chemists to predict the  $K_0$  of compounds in IMS.

## References

- [1] W.E. Steiner, B.H. Clowers, L.M. Matz, W.F. Siems, H.H. Hill Jr, Anal. Chem. 74 (2002) 4343.

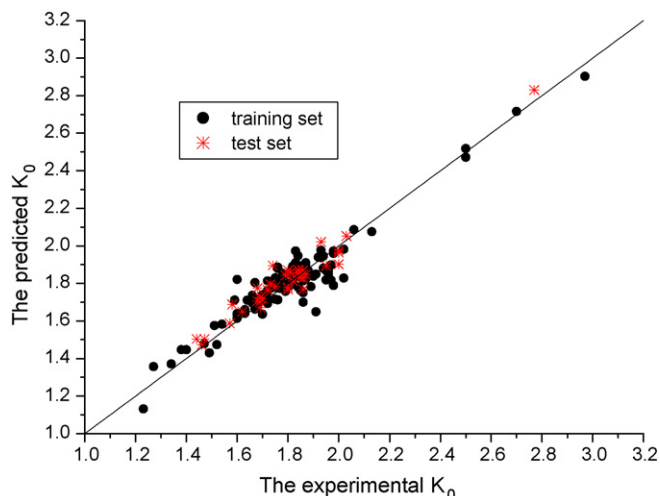


Fig. 3. Predicted  $K_0$  values vs. experimental values by PPR method.

- [2] J. St. Taylor, L.J. Piper, J.A. Connor, J. Fitzgerald, J.H. Adams, S. Ch. Harden, D.B. Schoff, D.M. Davis, R.G. Ewing, *IJIMS* 1 (1998) 58.
- [3] G.M. Bota, P.B. Harrington, *Talanta* 68 (2006) 629.
- [4] D.C. Collins, M.L. Lee, *Fresenius J. Anal. Chem.* 369 (2001) 225.
- [5] S. Myung, Y.J. Lee, M.H. Moon, J. Taraszka, R. Sowell, S. Koeniger, A.E. Hilderbrand, S.J. Valentine, L. Cherbas, P. Cherbas, T.C. Kaufmann, D.F. Miller, Y. Mechref, M.V. Novotny, M.A. Ewing, C.R. Sporleder, D.E. Clemmer, *Anal. Chem.* 75 (2003) 5137.
- [6] J.A. McLean, D.H. Russell, *J. Proteome Res.* 2 (2003) 427.
- [7] R.W. Purves, D.A. Barnett, B. Ells, R. Guevremont, *J. Am. Soc. Mass Spectrom.* 12 (2001) 894.
- [8] H.H. Hill Jr, W.F. Siems, R.H. St. Louis, D.G. McMinn, *Anal. Chem.* 62 (1990) 1201A.
- [9] M.D. Wessel, J.M. Sutter, P.C. Jurs, *Anal. Chem.* 68 (1996) 4237.
- [10] H.E. Revercomb, E.A. Mason, *Anal. Chem.* 47 (1975) 970.
- [11] M.D. Wessel, P.C. Jurs, *Anal. Chem.* 66 (1994) 2480.
- [12] G.W. Griffin, I. Dzidic, D.I. Carroll, R.N. Stillwell, E.C. Horning, *Anal. Chem.* 45 (1973) 1204.
- [13] S.N. Lin, G.W. Griffin, E.C. Horning, W.E. Wentworth, *J. Chem. Phys.* 60 (1974) 4994.
- [14] S.A. Benezra, *J. Chromatogr. Sci.* 14 (1976) 122.
- [15] F.W. Karasek, S.H. Kim, S. Rokushika, *Anal. Chem.* 50 (1978) 2013.
- [16] N. Agbonkonkon, H.D. Tolley, M.C. Asplund, E.D. Lee, M.L. Lee, *Anal. Chem.* 76 (2004) 5223.
- [17] HyperChem. 4.0, Hypercube (1994).
- [18] J.P.P. Stewart, MOPAC 6.0, Quantum Chemistry Program Exchange; QCPE, No. 455, Indiana University, Bloomington, IN, 1989.
- [19] A.R. Katritzky, V.S. Lobanov, M. Karelson, *Comprehensive Descriptors for Structural and Statistical Analysis, Reference Manual, Version 2.0*; 1994.
- [20] A.R. Katritzky, R. Petrukhin, R. Jain, M. Karelson, *J. Chem. Inf. Comput. Sci.* 41 (2001) 1521.
- [21] J.H. Friedman, W. Stuetzle, *J. Am. Stat. Assoc.* 76 (1981) 817.
- [22] Y. Du, Y. Liang, D. Yun, *J. Chem. Inf. Comput. Sci.* 42 (2002) 1283.
- [23] Q.N. Hu, Y.Z. Liang, X.L. Peng, H. Yin, K.T. Fang, *J. Chem. Inf. Comput. Sci.* 44 (2004) 437.
- [24] D.T. Stanton, P.C. Jurs, *Anal. Chem.* 62 (1990) 2323.
- [25] D.T. Stanton, L.M. Egolf, P.C. Jurs, *J. Chem. Inf. Comput. Sci.* 32 (1992) 306.

# Separation and determination of alpinetin and cardamonin in *Alpinia katsumadai* Hayata by flow injection–micellar electrokinetic chromatography

Lihong Liu, Xingguo Chen\*, Zhide Hu

Department of Chemistry, Lanzhou University, Lanzhou 730000, China

Received 18 December 2005; received in revised form 16 March 2006; accepted 18 March 2006

Available online 5 May 2006

## Abstract

A simple, rapid, and accurate method for the separation and determination of alpinetin and cardamonin in *Alpinia katsumadai* Hayata was developed by combination of flow injection (FI)–micellar electrokinetic chromatography (MEKC) for the first time. The analysis was carried out using an unmodified fused-silica capillary (50  $\mu\text{m}$  i.d.; total length 13.6 cm; effective length 10.3 cm) and direct ultraviolet (UV) detection at 214 nm. The sample throughput was 11–24 samples per hour using the background electrolyte (BGE) containing 4 mM sodium borate–8 mM  $\text{NaH}_2\text{PO}_4$  (pH 8.1)–8 mM sodium dodecyl sulfate (SDS)–19% (v/v) ethanol. The repeatabilities ( $n = 4$ ) reached relative standard deviation values (R.S.D.) of 3.0% and 2.5% for the peak areas and 2.5% and 3.1% for peak heights of alpinetin and cardamonin, respectively. Regression equations revealed linear relationships ( $r^2$ : 0.9993–0.9994) between the peak area of each analyte and the concentration. Recoveries were in the range 90–92% and 99–105% for alpinetin and cardamonin, respectively.

© 2006 Elsevier B.V. All rights reserved.

**Keywords:** Flow injection–micellar electrokinetic chromatography; Alpinetin; Cardamonin; *Alpinia katsumadai* Hayata

## 1. Introduction

Alpinetin and cardamonin are the two major similar components of the seeds of *Alpinia katsumadai* Hayata. They have long been known to show many pharmacological activities including antiemetic, depriving dampness, and expelling cold. The analytes are important due to its decoction of lower than 1% concentration stimulates, while that higher than 1% inhibits the intestines of guinea-pigs in vitro [1]. So it is necessary to establish a suitable analytical method to evaluate or control the quality of the herbal medicine. However, under acid or alkaline conditions, alpinetin (7-hydroxy-5-methoxyflavanone) and cardamonin (2, 4-dihydroxy-6-methoxychalcone) can transfer each other (see Fig. 1). Hitherto, only high performance liquid chromatography [2] has been reported for the separation and determination of alpinetin and cardamonin. No application of CE has been reported.

MEKC, which was first introduced by Terabe et al. [3], has been widely used to separate nonionic compounds using the

electrokinetic phenomena, and it is also applied to improve the separation selectivity of charged analytes [4,5]. However, the discontinuous sample introduction mode confined the sample throughput and precision. Compared to conventional sample introduction for CE, the combined FI–CE system provides a continuous, reproducible, and readily automated sample introduction means with enhanced sample throughput and improved repeatability [6–13]. Previous studies have indicated that MEKC is the method of choice for separation of mixtures of small molecules, such as pharmaceutical agents [14–16]. In this paper, an FI–MEKC method was firstly developed for the separation and detection of alpinetin and cardamonin. The method was simple, rapid, and continuous automated sampling technique, and it was also applied to the analysis of alpinetin and cardamonin in *A. katsumadai* Hayata with good results.

## 2. Experimental

### 2.1. Chemicals and materials

Alpinetin and cardamonin were obtained from the National Institute for the Control of Pharmaceutical and Biological

\* Corresponding author. Tel.: +86 931 8912763; fax: +86 931 8912582.  
E-mail address: [chenxg@lzu.edu.cn](mailto:chenxg@lzu.edu.cn) (X. Chen).



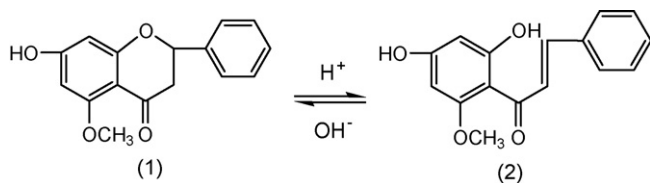


Fig. 1. Structures of (1) alpinetin and (2) cardamonin.

Products, China. The purity of standard analytes was checked by determined alpinetin and cardamonin by FI–CE, respectively. In this study, we obtained single peak for alpinetin and cardamonin, respectively. The crude drug of *A. katsumadai* Hayata was purchased from local drug store. Ethanol was purchased from Tianjin Chemical Corporation (Tianjin, China). SDS was purchased from Tianjin Guangfu Fine Chemical Institute (Tianjin, China). All chemicals were of analytical reagent grade and were used as received. All solution and buffer were made in distilled water. Distilled water was used in all the experiments.

## 2.2. Solutions preparation

Stock standard solutions of alpinetin and cardamonin were prepared in ethanol (500  $\mu\text{g}/\text{mL}$ ), degassed in an ultrasonic bath and filtered through a 0.45  $\mu\text{m}$  membrane filter. Standard solutions, ranging 10–500  $\mu\text{g}/\text{mL}$  of alpinetin and cardamonin, were prepared from stock standard solutions with ethanol. The carrier solution (functioning also as BGE) was freshly prepared. The BGE for the studies was 4 mM sodium tetraborate–8 mM  $\text{NaH}_2\text{PO}_4$  (pH 8.1) containing 8 mM SDS–19% (v/v) ethanol. The BGE was prepared daily from stock solution of 0.1 M sodium tetraborate, 0.1 M  $\text{NaH}_2\text{PO}_4$ , 0.2 M SDS and ethanol. The buffer pH was determined before addition of the organic modifier.

## 2.3. Sample preparation

The powdered (2 g) of *A. katsumadai* Hayata was accurately weighed and extracted with 35 mL ethanol in an ultrasonic bath for 1 h, and filtered through 0.45  $\mu\text{m}$  syringe filters. The extracted solution was directly injected into the CE equipment by the FI system. All solutions were filtered through 0.45  $\mu\text{m}$  syringe filters before use.

## 2.4. Apparatus

All electrophoresis experiments were performed with an HPE-100 CE system with 12 kV maximum voltage (Bio-Rad, Hercules, CA) equipped with a UV absorbance detector. Detection was done by absorption at 214 nm. Uncoated fused-silica capillaries of 50  $\mu\text{m}$  i.d., 375  $\mu\text{m}$  o.d., and 13.6 cm total length (10.3 cm effective length) were purchased from Yongnian Optical Fiber Factory (Handan, Hebei, China). Chroma chromatography collection system (Bio-Rad) was used for data acquisition and manipulation.

A K-1000 flow injection analyzer (Hitachi, Japan) was equipped with a peristaltic pump, a 16-way injection valve and a

plunger pump. 0.5 mm i.d. polytetrafluoroethylene (PTFE) tubing was used for connecting all components of the FI system, including 33 cm length transport line from the valve to an H-channel microchip, which was used to combine the FI system and the CE instrument. The detailed description of the H-channel has been given elsewhere [9]. A sample loop and two reagent loops were made from PTFE. The time period for the injecting sample was defined through man/access mode.

## 2.5. Operation procedure

An unmodified fused-silica capillary was used for all analysis. At the beginning of each working day, the capillary was flushed sequentially with distilled water (5 min), 0.1 M NaOH (5 min), and distilled water (5 min), followed by running buffer (5 min) from the capillary outlet reservoir using a water-circulating vacuum pump. Simultaneously the CE instrument was warmed up until a stable baseline was achieved. The capillary was left filled with distilled water overnight.

For the FI operations, the carrier stream was driven by the plunger pump, and in turn was passed through a pressure damper, a pressure gauge, and the 16-way valve. A sample solution and two carrier solutions (In this study, there was not reaction, and carrier solution was injected into reagent loop.) were delivered to a sample loop and two reagent loops (volume: 20  $\mu\text{L}$ , respectively) in the 16-way injection valve by the peristaltic pump, respectively. Injection of the sample and the carrier solutions into the carrier stream was carried out by actuating automatically the 16-way valve. The sample solution was sandwiched by the carrier solutions and transported through the connecting conduit into the anodic reservoir, where the flow was split and a fraction of the sample zone injected by FI system was introduced into the separation capillary by electrokinetic means. A series of samples was injected continuously without interrupting the high voltage (3.4 kV).

## 3. Results and discussion

### 3.1. Selection of electrolyte solution

Since the separation mechanism in MEKC involves partitioning between the mobile phase, any manipulation of the buffer system will have some effect on the distribution coefficient and therefore on the migration of solutes [17]. The mixed buffer of sodium borate and phosphate has been reported [18]. In addition to stable pH, the borate ions can form complexes with phenols, which enhance the selectivity for phenols separation [19]. In this study, the analytes wholly overlapped without sodium borate in buffer. The effect of the concentrations of borate–phosphate on the separation was studied in the range from 11 mM to 17 mM. The buffer containing 4 mM sodium borate and 8 mM  $\text{NaH}_2\text{PO}_4$  at pH 8.1 was found to produce the highest resolution.

#### 3.1.1. Effect of ethanol

When organic solvent was added in the running buffer, the hydrophobicity and ionic strength of buffer were changed, consequently resulting in the change of the EOF and the resolution.

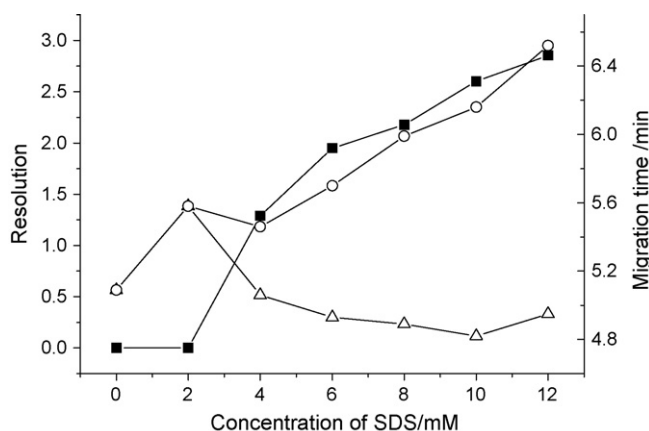


Fig. 2. Influence of SDS concentrations on the migration time and resolution of the peaks (■, resolution of alpinetin and cardamomin) and migration time (△, alpinetin, ○, cardamomin). Conditions: 50  $\mu\text{m}$  i.d.  $\times$  375  $\mu\text{m}$  o.d.  $\times$  13.6 cm length (10.3 cm effective length), uncoated; buffer, 4 mM sodium borate–8 mM  $\text{NaH}_2\text{PO}_4$  (pH 8.1)–19% (v/v) ethanol, voltage, 3.0 kV; detection wavelength, 214 nm; sample volume, 20  $\mu\text{L}$ ; carrier flow rate, 1.32 mL/min; sample: 100  $\mu\text{g}/\text{mL}$  alpinetin and cardamomin.

In this study, peak splitting was observed when the concentration of ethanol was below 13% (v/v). So we investigated the effect of ethanol contents changed from 15% to 23% (v/v) on the separation behavior of alpinetin and cardamomin. When the amount of ethanol was increased from 15% to 23% (v/v), there was an increase in the migration time, and the resolution between the analytes was reduced. It may be because the fact that the use of ethanol at low concentrations increases the migration time for two reasons: (1) an increase in viscosity of the running buffer and (2) addition of ethanol changes in hydrophobicity of mobile phase resulting in different distribution of analytes between the pseudostationary phase and mobile phase, and changes in charge and solvation of analytes in the mobile phase. However, peak shape (height/width) of cardamomin was greatly improved with increasing ethanol. On considering the resolution, migration time and peak shape of the analytes, the optimized concentration of ethanol was selected at 19% (v/v).

### 3.1.2. Effect of SDS

In MEKC mode, micelles added to the buffer solution form with the neutral compound a charged complex with an effective electrophoretic mobility [20]. The differential partition of the neutral species in the retentive phase obtained gives rise to the separation due to their differential migration rates [5]. A significant variable for MEKC separation optimization is surfactant concentration. Influence of the SDS on the resolution and migration time of alpinetin and cardamomin was studied in a range from 0 mM to 12 mM using 4 mM sodium borate–8 mM  $\text{NaH}_2\text{PO}_4$  (pH 8.1)–19% (v/v) ethanol, 1.32 mL/min rate, 20  $\mu\text{L}$  sample loop volume and 3.0 kV applied voltage. Based on the structure and hydrophobicity of the compounds, the separation was affected by the SDS concentration differently (Fig. 2). When the concentration of SDS was increased from 2 mM to 12 mM, there was an increase in the migration time from 5.09 min to 6.52 min for cardamomin, however, the migration time of alpinetin was decreased. It can be seen in Fig. 2 that the resolution increased

with increasing SDS concentration. Although 6 mM SDS can achieve baseline separation, it was unfavorable to the analytes' separation in real samples. Accordingly, the SDS concentration was fixed at 8 mM for the following experiments.

### 3.1.3. Effect of flow rate

With fixed sample injection volumes, the carrier flow rate determined the residence time of the sample zone within the flow-through reservoir and therefore the time available for electrokinetic split-sampling into the capillary [21]. We investigated the effect of flow rate changed from 0.76 mL/min to 1.5 mL/min on the separation behavior of the analytes using 4 mM sodium borate–8 mM  $\text{NaH}_2\text{PO}_4$  (pH 8.1)–8 mM SDS–19% (v/v) ethanol. With increasing flow rate, the migration time was shortened, however, the peak area of the analytes was decreased, and a higher flow rate consumed more buffer solution. On considering the resolution of these analytes, peak area, and consumption of buffer solution, 1.36 mL/min was finally chosen as the flow rate of buffer solution.

### 3.1.4. Effect of separation voltage

Attempts were made to optimize the separation condition by using different applied voltages ranging from 2.6 kV to 3.8 kV. As may be expected, increasing the voltage gave shorter migration times, but this also caused the decrease of resolution and peak area. It was probably owing to an increase in the EOF. The lower voltage would result in longer broadening peaks due to diffusion effects. In this study, when separation voltage was higher than 3.4 kV, the migration times of the analytes were shortened, however, the analytes in real samples could not be completely separated with unknown peak. With concurrent considerations in peak area, peak shape, migration time, and resolution, the separation voltage finally chosen was 3.4 kV.

### 3.1.5. Final optimization

Final conditions were 4 mM sodium borate–8 mM  $\text{NaH}_2\text{PO}_4$  (pH 8.1)–8 mM SDS–19% (v/v) ethanol, 3.4 kV voltage, 20  $\mu\text{L}$  sample volume, 214 nm UV detection, 1.36 mL/min flow rate of buffer solution.

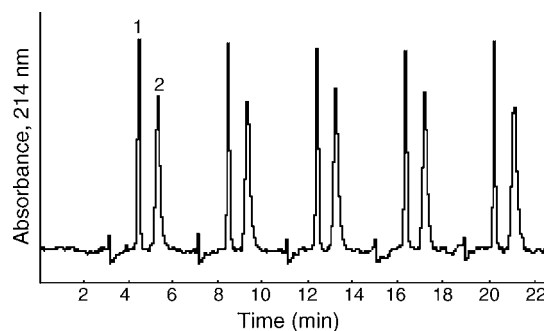


Fig. 3. Recordings of five consecutive injections of a standard mixture of alpinetin and cardamomin. Peaks: 1 = alpinetin, 2 = cardamomin. Sample: 500  $\mu\text{g}/\text{mL}$  alpinetin and cardamomin. Separation condition: 4 mM sodium borate–8 mM  $\text{NaH}_2\text{PO}_4$  (pH 8.1)–8 mM SDS–19% (v/v) ethanol, voltage, 3.4 kV; detection wavelength, 214 nm; sample volume, 20  $\mu\text{L}$ ; carrier flow rate, 1.36 mL/min.

Table 1  
Analytical performance of the FI–CE and HPLC methods in pharmaceutical preparation testing system ( $n = 7$ )

	Alpinetin		Cardamonin	
	FI–MEKC	HPLC <sup>a</sup>	FI–MEKC	HPLC
Peak area R.S.D. (%)	3.0	–	2.5	–
Peak height R.S.D. (%)	2.5	0.75	3.1	1.2
Regression equation	$y_1 = 106.44x_1 + 111.91^b$	$y_2 = 0.00023x_2 + 0.00175^c$	$y_1 = 139.28x_1 - 866.15$	$y_2 = 0.000203x_2 - 0.000674$
$r^2$	0.9993	0.9992	0.9994	0.9996
LOD ( $S/N = 3$ )	3.6 $\mu\text{g/mL}$	445 $\text{mm}/\mu\text{g}$	4.9 $\mu\text{g/mL}$	582 $\text{mm}/\mu\text{g}$
Linear range	10–500 $\mu\text{g/mL}$	0.05–0.26 $\mu\text{g}$	10–500 $\mu\text{g/mL}$	0.05–0.26 $\mu\text{g}$
Migration time R.S.D. (%)	0.68	–	0.50	–
Analysis time of real sample (min)	6	14	6	14
Sample throughput ( $\text{h}^{-1}$ )	11–24	–	11–24	–

<sup>a</sup> The data from reference [2].

<sup>b</sup>  $y_1$ , peak area;  $x_1$ , standard concentration ( $\mu\text{g/mL}$ ).

<sup>c</sup>  $y_2$ , peak height;  $x_2$ , injected amount ( $\mu\text{g/mL}$ ).

Table 2  
Results for the determination of the two components in *Alpinia katsumadai* Hayata ( $n = 4$ )

Ingredient	Content (mg/g)	Concentration spiked ( $\mu\text{g/mL}$ )	Concentration found ( $\mu\text{g/mL}$ )	Recovery (%)
Alpinetin	$5.8 \pm 0.2$	100	$90 \pm 4.8$	$91 \pm 1.0$
		150	$136 \pm 7.3$	
		250	$229 \pm 5.6$	
Cardamonin	$5.2 \pm 0.1$	100	$105 \pm 5.1$	$103 \pm 3.2$
		150	$149 \pm 8.6$	
		250	$261 \pm 13.8$	

Each value represents the mean  $\pm$  S.D. ( $n = 4$ ).

### 3.1.6. Performance of the combined FI–CE

The regression equation, linear range, detection limits, and repeatability were studied for the present FI–MEKC method. Calibration graphs were obtained by injecting standard solutions at seven different concentrations. Each point on the calibration graph corresponded to the mean value obtained from three independent peak area measurements. The equation of the calibration curve was then used to calculate the concentrations of the analytes in sample. The repeatability of the method was determined with a standard mixture solution containing 500  $\mu\text{g/mL}$  of alpinetin and cardamonin. The analytes were repeatedly injected into the CE system every 4 min. Five consecutive injections were performed. The electropherograms obtained are shown in Fig. 3. The peak areas were employed for quantification. The performance of this method is summarized in Table 1. The sampling frequency achievable per hour could be estimated according to

Fang's equation [21]. The limit of detection (LOD) was calculated as the peak height at a signal-to-noise ratio of 3 ( $S/N = 3$ ).

### 3.1.7. Application

To test the applicability of the developed method based on FI–MEKC system, quantitative analysis was performed under the optimum conditions obtained from the experiments described above. The method was applied to the analysis of alpinetin and cardamonin in *A. katsumadai* Hayata. The contents of the analytes are given in Table 2. The typical electropherograms of *A. katsumadai* Hayata is shown in Fig. 4. The peaks were identified by the standard addition methods. The accuracy of the methods and the potential matrix effects were established by analyzing spiked samples. The results are presented in Table 2.

## 4. Conclusions

In this paper, we adopted MEKC mode with ethanol as organic modifiers to improve resolution and avoid peak splitting. The coupling of FI system with CE equipment has been successfully used to analyze alpinetin and cardamonin in *A. katsumadai* Hayata for the first time. The result indicates the FI provides repeatable and reliable sample introduction for CE. The repeatability was 3.0% and 2.5% with peak area evaluation and 0.68% and 0.50% with migration time evaluation for alpinetin and cardamonin, respectively. Furthermore, the capillary used in above methods was relatively short (effective length 10.3 cm) which made the analysis time relatively short. The separation

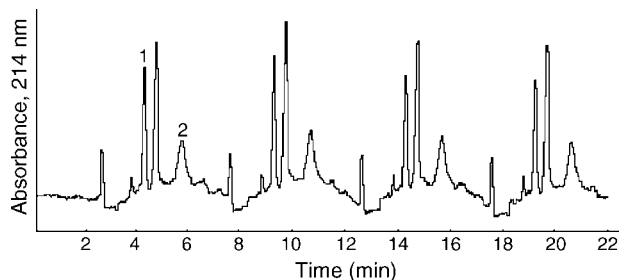


Fig. 4. Electrochromatogram of *Alpinia katsumadai* Hayata. Other conditions as in Fig. 3.

could be achieved within 6 min (14 min in reference [2]). This technique does not need expensive chromatogram column, the consumption of organic reagent is lower and the replacing of capillary is very convenient. This sample introduction scheme has several compelling advantages over provided method in the reference [2], including ease of operation and automation, enhanced sampling frequencies (standard solution: 24 h<sup>-1</sup>, real samples: 11 h<sup>-1</sup>).

### Acknowledgement

We kindly acknowledge the National Science Foundation of China (No. 20275014) for supporting this work.

### References

- [1] M. Ou, Chinese–English Manual of Common-Used in Traditional Chinese Medicine, Publisher of Guangdong Science and Technology, Guangzhou, 1992, p. 449.
- [2] W.W. Rao, Y.D. Lin, Chin. Pharm. J. 33 (1998) 743.
- [3] S. Terabe, K. Otsuka, K. Ichikawa, T. Ando, Anal. Chem. 56 (1984) 111.
- [4] A.K. Su, Y.S. Chang, C.H. Lin, Talanta 64 (2004) 970.
- [5] D.A. El-Hadya, N.A. El-Maalaa, R. Gottib, V. Andrisanob, Talanta 66 (2005) 253.
- [6] P. Kuban, A. Engstrom, J.C. Olsson, G. Thorsen, R. Tryzell, B. Karlberg, Anal. Chim. Acta 337 (1997) 117.
- [7] H.W. Chen, Z.L. Fang, Anal. Chim. Acta 355 (1997) 135.
- [8] P. Kuban, B. Karlberg, Anal. Chem. 69 (1997) 1169.
- [9] L.Y. Fan, H.L. Chen, X.G. Chen, Z.D. Hu, J. Sep. Sci. 26 (2003) 1376.
- [10] P. Kuban, B. Karlberg, Talanta 45 (1998) 477.
- [11] B.M. Simonet, A. Rios, F. Grases, M. Valcarcel, Electrophoresis 24 (2003) 2092.
- [12] P. Kuban, P. Kuban, V. Kuban, Electrophoresis 24 (2003) 1935.
- [13] L.H. Liu, L.Y. Fan, H.L. Chen, X.G. Chen, Z.D. Hu, Electrophoresis 26 (2005) 2999.
- [14] A. Laskaridou-Monnerville, J. Chromatogr. A 838 (1999) 293.
- [15] W.J. Zheng, S.F. Wang, X.G. Chen, Z.D. Hu, Biomed. Chromatogr. 18 (2003) 167.
- [16] S.F. Wang, Y.Q. Wu, Y. Ju, X.G. Chen, J. Chromatogr. A 1017 (2003) 27.
- [17] J. Cheng, K.R. Mitchelson, J. Chromatogr. A 761 (1997) 297.
- [18] H. Long, A.J. Huang, Y.L. Sun, Chin. Chem. Lett. 9 (1988) 87.
- [19] Y. Li, H. Long, H.W. Liu, J. Chin. Pharm. Sci. 9 (2000) 80.
- [20] S.M. Lunte, D.M. Radzik, Pharmaceutical and Biomedical Applications of Capillary Electrophoresis, Elsevier Science B.V., Guildford, 1996.
- [21] Z.L. Fang, Z.S. Liu, Q. Shen, Anal. Chim. Acta 346 (1997) 135.

# Number of species in complexation equilibria of *o*-, *m*- and *p*-CAPAZOXS with Cd<sup>2+</sup>, Co<sup>2+</sup>, Ni<sup>2+</sup>, Pb<sup>2+</sup> and Zn<sup>2+</sup> ions by PCA of UV–vis spectra

Milan Meloun\*, Tomáš Syrový

Department of Analytical Chemistry, Faculty of Chemical Technology, University of Pardubice, CZ-532 10 Pardubice, Czech Republic

Received 1 March 2005; received in revised form 23 February 2006; accepted 15 March 2006

Available online 9 May 2006

## Abstract

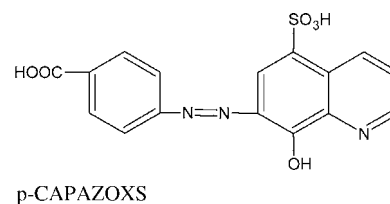
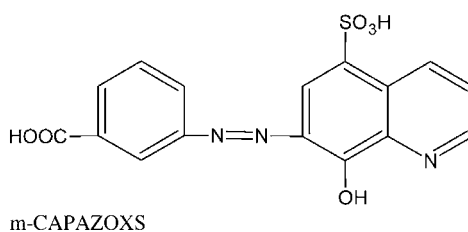
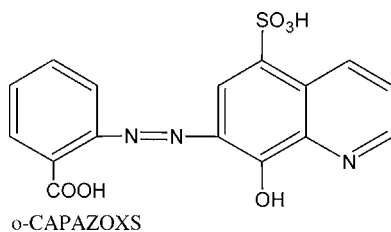
A critical comparison of the selected derivative principal component analysis (PCA) methods on the absorbance matrix data concerning the complexation equilibria between *o*-CAPAZOXS and Cd<sup>2+</sup>, Pb<sup>2+</sup> and Zn<sup>2+</sup> or *m*-CAPAZOXS and Cd<sup>2+</sup>, Co<sup>2+</sup>, Ni<sup>2+</sup> and Zn<sup>2+</sup> or *p*-CAPAZOXS and Cd<sup>2+</sup> and Zn<sup>2+</sup> at 25 °C is provided. As the number of complex species in a complex-forming equilibria mixture is an important step in spectral data treatment, the nine selected index functions for the prediction of the number of light-absorbing species that contribute to a set of spectra is critically tested by the PCA. An improved identification with the second SD(AE) or third derivative TD(AE) and derivative ratio function ROD(AE) for the average error criterion AE is preferred. After the number of various complexes formed the stability constants of species ML, ML<sub>2</sub> (and ML<sub>3</sub>, respectively) type  $\log \beta_{11}$ ,  $\log \beta_{12}$  (and  $\log \beta_{13}$ , respectively) for the system of *o*-CAPAZOXS (ligand L) with the metals (the standard deviation  $s(\log \beta_{pq})$  of the last valid digits is given in brackets) Cd<sup>2+</sup> (6.39(5) and 11.51(9)), Pb<sup>2+</sup> (4.24(2) and 9.01(2)) and Zn<sup>2+</sup> (5.18(7) and 9.06(10)) and for the system of *m*-CAPAZOXS with Cd<sup>2+</sup> (6.59(20) and 11.51(32)), Co<sup>2+</sup> (7.19(6) and 12.19(8)), Ni<sup>2+</sup> (7.64(7) and 13.39(12)) and Zn<sup>2+</sup> (4.83(3) and 9.57(3)) and for the system of *p*-CAPAZOXS with Cd<sup>2+</sup> (6.44(5), 10.99(10) and 14.57(25)) and Zn<sup>2+</sup> (6.84(16), 13.05(29) and 18.74(43)) at 25 °C are estimated using SQUAD(84) nonlinear regression of the mole-ratio spectrophotometric data. The computational strategy is presented with goodness-of-fit tests and various regression diagnostics capable of proving the reliability of the chemical model proposed.

© 2006 Elsevier B.V. All rights reserved.

**Keywords:** Principal component analysis (PCA); Factor analysis (FA); Rank of matrix; Number of species; Number of components; Spectrophotometer error

## 1. Introduction

The protonation and complex-forming equilibria of some sulphoazoxine oligomers have been studied systematically in the authors laboratory [1]. The protonation constants and the number of oligomer species for five 7-arylazo derivatives of 8-hydroxyquinoline-5-sulphonic acid, sometimes differing only in the steric arrangement of their molecules, viz. SNAZOXS and naphthylazoxine 6S [1] or *o*-, *m*-, *p*-CAPAZOXS, were studied.



The five substances are frequently applied as metalochromic indicators in analytical practice, as they form complex compo-

unds, usually yellow in color, with a series of metals. Analysis of solution equilibria is, in general, performed in several steps: in the first step the number of components is determined, and then concentrations of all of the complex species involved

\* Corresponding author. Tel.: +420 466037026; fax: +420 466037068.  
E-mail address: milan.meloun@upce.cz (M. Meloun).



Table 1  
Estimated number of light-absorbing species  $n_c = k$  and the experimental error,  $s_{\text{inst}}(A) = s_k(A)$  by the derivative technique of PCA methods (INDICES program) for the *o*-CAPAZOXS (three metals), *m*-CAPAZOXS (four metals) and *p*-CAPAZOXS (two metals) complex-forming systems with different metals

System	$s_k(A)$	R.S.D.	RMS	AE	$\chi^2$	RPV	$\psi$	IE	IND
<i>o</i> -CAPAZOXS									
Cd <sup>2+</sup>	3, 0.63	3, 0.56	3, 0.50	3, 0.50	5	3	1	8	8
Pb <sup>2+</sup>	3, 0.56	3, 0.49	3, 0.40	3, 0.40	3	3	1	6	6
Zn <sup>2+</sup>	3, 0.50	3, 0.46	3, 0.40	3, 0.40	3	3	1	5	5
<i>m</i> -CAPAZOXS									
Cd <sup>2+</sup>	3, 0.63	3, 0.20	3, 0.20	0.18	3	3	1	5	5
Co <sup>2+</sup>	3, 0.50	3, 0.20	3, 0.20	0.16	3	3	1	5	5
Ni <sup>2+</sup>	3, 0.71	3, 0.32	3, 0.28	0.25	3	3	1	6	6
Zn <sup>2+</sup>	3, 0.63	3, 0.20	3, 0.18	0.16	3	3	1	8	5
<i>p</i> -CAPAZOXS									
Cd <sup>2+</sup>	4, 0.32	4, 0.18	4, 0.16	4, 0.11	4	4	1	6	6
Zn <sup>2+</sup>	4, 0.25	4, 0.18	4, 0.16	4, 0.13	4	4	1	6	6

Predicted  $k$  and corresponding  $s_k(A)$  [mAU] for precise methods and  $k$  for approximate methods. The  $n \times m$  absorbance matrix is for  $n$  solutions with total concentrations of  $c_M$ ,  $c_L$  and  $c_H$ , with molar ratio  $q_M = c_M/c_L$  and measured at  $m$  wavelengths. Index algorithms used:  $s_k(A)$ , Kankare's residual standard deviation; R.S.D., residual standard deviation; RMS, root mean square error; AE, average error criterion;  $\chi^2$ , Bartlett  $\chi^2$  criterion; RPV, Scree test;  $\psi$ , Exner  $\psi$  function; IE, imbedded error function; IND, factor indicator function.

are calculated. Several instrumental methods have been devised for the second step, and depend on the chemical model of all equilibria and the experimental design. Predicting the number of components is pertinent to all methods of chemical model determination.

Determining the number of complex species in a mixture with the use of spectroscopic data is the first step towards further qualitative and quantitative analysis. Procedures for determining the chemical rank of a matrix comprising a variety of empirical and statistical methods based on principal component analysis (PCA), have been reported and critically compared [1–9]. In the study of complex-forming equilibria, for instance,

a reliable determination of the number of components involved will help to obtain a reasonable interpretation of the various complexes.

The aim of this study is to make a critical comparison of the various PCA methods on the absorbance matrix data concerning the complex-forming equilibria of three sulphoneazoxines with selected metal cations.

## 2. Theoretical

The application of various modifications of principal component analysis for determining the number of components that

Table 2  
The most probable chemical model in complex-forming equilibria of the *m*-CAPAZOXS + Me<sup>2+</sup> system by regression spectra analysis using SQUAD(84) with the standard deviations of the estimated stability constant,  $\log \beta_{pqr}(s(\beta_{pqr}))$  of the last valid digits in brackets

	<i>m</i> -CAPAZOXS + Cd <sup>2+</sup>	<i>m</i> -CAPAZOXS + Co <sup>2+</sup>	<i>m</i> -CAPAZOXS + Ni <sup>2+</sup>	<i>m</i> -CAPAZOXS + Zn <sup>2+</sup>
$c_L$ [mol/L]	0.000221	0.00022	0.000187	0.000218
Range $q_M$	0.05–0.88	0.05–2.63	0.05–5.00	0.05–1.35
Range pH	4.759–4.777	4.723–4.777	4.690–4.778	4.749–4.777
$n$	13	18	14	14
$m$	28	28	28	28
$n_c$	3	3	3	3
$s_k(A)$ [mAU]	0.44	0.42	0.64	0.65
Estimated stability constant, $\log \beta_{pqr}(s(\beta_{pqr}))$				
ML	6.59(21)	7.19(6)	7.64(7)	4.83(3)
ML <sub>2</sub>	11.51(32)	12.19(8)	13.39(12)	9.57(3)
The degree-of-fit test by the statistical analysis of residuals				
$\bar{e}$ [mAU]	0	0	0	0
$ \bar{e} $ [mAU]	1.22	0.83	1.04	1.08
$s(e)$ [mAU]	1.88	1.37	1.57	1.53
$g_1(e)$ ( $\approx 0$ )	–0.25	0.93	–0.24	–0.2
$g_2(e)$ ( $\approx 3$ )	2.59	7.54	3.78	2.27
$R$ [%] (<0.5)	0.44	0.34	0.38	0.37

The parameter reliability is proven with degree-of-fit statistics such as the mean of residuals  $\bar{e}$  [mAU], the mean residual  $|\bar{e}|$  [mAU], the standard deviation of the residual  $s(e)$  [mAU] which is equal to the standard deviation of absorbance after termination of the regression process,  $s(A)$  [mAU], the residual skewness  $g_1(e)$  and residual kurtosis  $g_2(e)$  and the Hamilton  $R$ -factor [%]. *Experimental conditions*:  $c_L$  (*m*-CAPAZOXS),  $I = 0.1$  (NaClO<sub>4</sub> + Na<sub>3</sub>PO<sub>4</sub> + HClO<sub>4</sub>), 25 °C, path length 1.000 cm,  $s_{\text{inst}}(A) = 0.45$  mAU (Specord M40, Zeiss, Jena Germany).

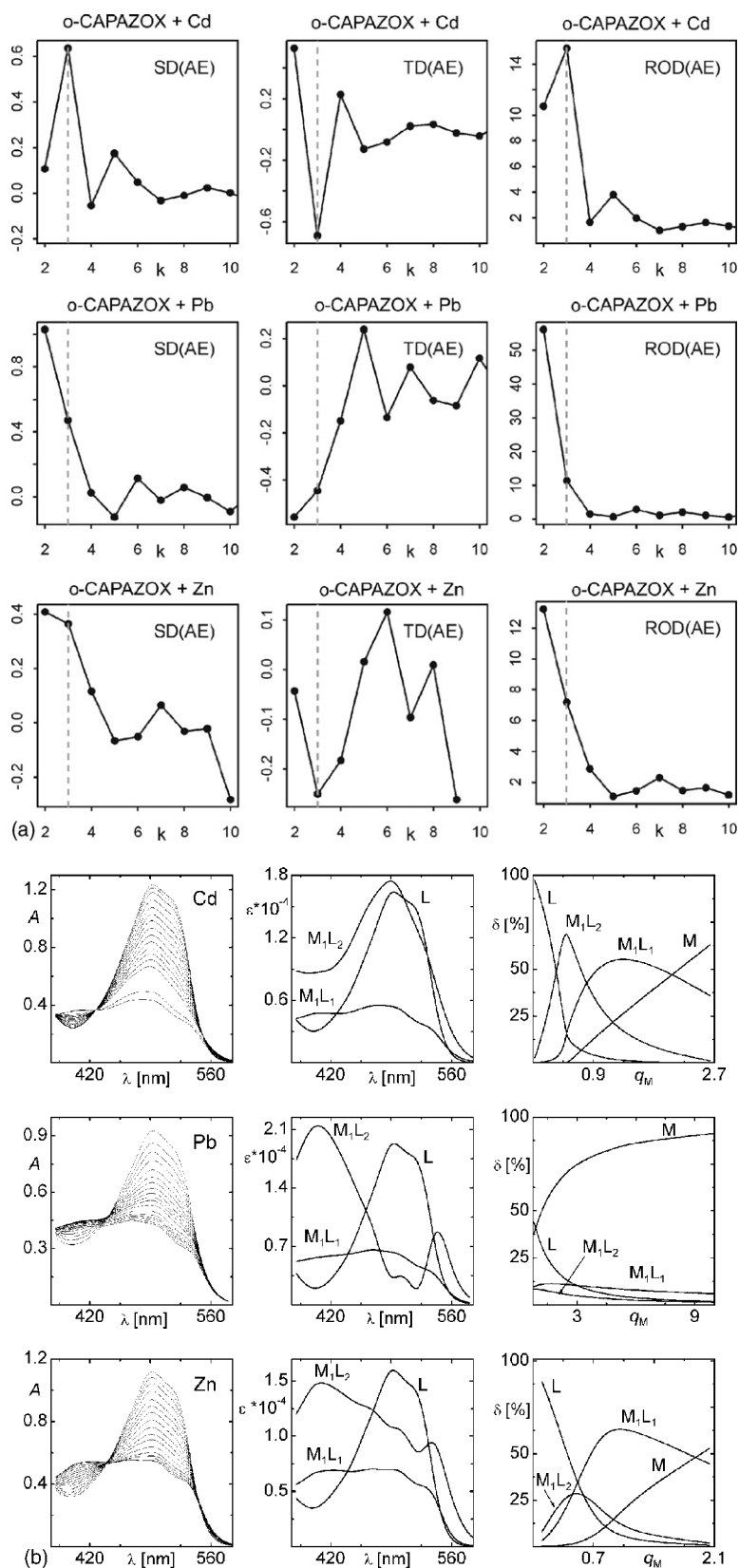


Fig. 1. (a) The derivatives detection criteria SD(AE), TD(AE) and ROD(AE) applied to the absorbance data set of complex-forming equilibria from the system of *o*-CAPAZOXs and Cd<sup>2+</sup> in the first row, *o*-CAPAZOXs and Pb<sup>2+</sup> in the second row and *o*-CAPAZOXs and Zn<sup>2+</sup> in the third row. (b) Complex-forming equilibria of the *o*-CAPAZOXs systems with three metal ions presented on the absorption spectra at 25 °C (left), the spectra of molar absorptivities vs. wavelengths for all of the complex species (middle) and the distribution diagram of the relative concentrations of all of the complex species in equilibrium: (first row) *o*-CAPAZOXs + Cd<sup>2+</sup>, (second row) *o*-CAPAZOXs + Pb<sup>2+</sup> and (third row) *o*-CAPAZOXs + Zn<sup>2+</sup>.

contribute to the absorption spectra of multicomponent systems has been described in a previous paper for this journal [1]. All notation and computations relating to the determination of stability constants were performed by regression analysis of the spectra and have been described previously [1].

### 3. Experimental

The actual concentration of sulphoazoxine was determined by emf titration with NaOH and evaluated by regression program analysis with the ESAB [18] and MAGEC [19] programs. The purity of *o*-, *m*- and *p*-CAPAZOXS has previously been described in this way [8]. The impurities were mostly inorganic salts. Other solutions, the apparatus and the procedure of spectrophotometric titration were described in earlier papers [1,20].

## 4. Results and discussion

### 4.1. The number of complex species

Determination of the number of light-absorbing components in an equilibrium mixture is an important point prior to the formulation of the hypothesis of a chemical model. When the absorbance matrix monitoring the complex-forming equilibria of CAPAZOXS with various metal cations was subjected to PCA indices analysis using covariance about the origin, nine characteristics  $s_{\text{inst}}(A)$ , R.S.D., RMS, AE,  $\chi^2$ ,  $\psi$ , RPV, IE and IND resulted. The break on the curve  $PC(k)=f(k)$  may be used as a guide to selecting the primary eigenvalues. Deducing the exact size of the true component space is usually a difficult problem because of experimental error. The various techniques applied to solve this problem may be divided into precise

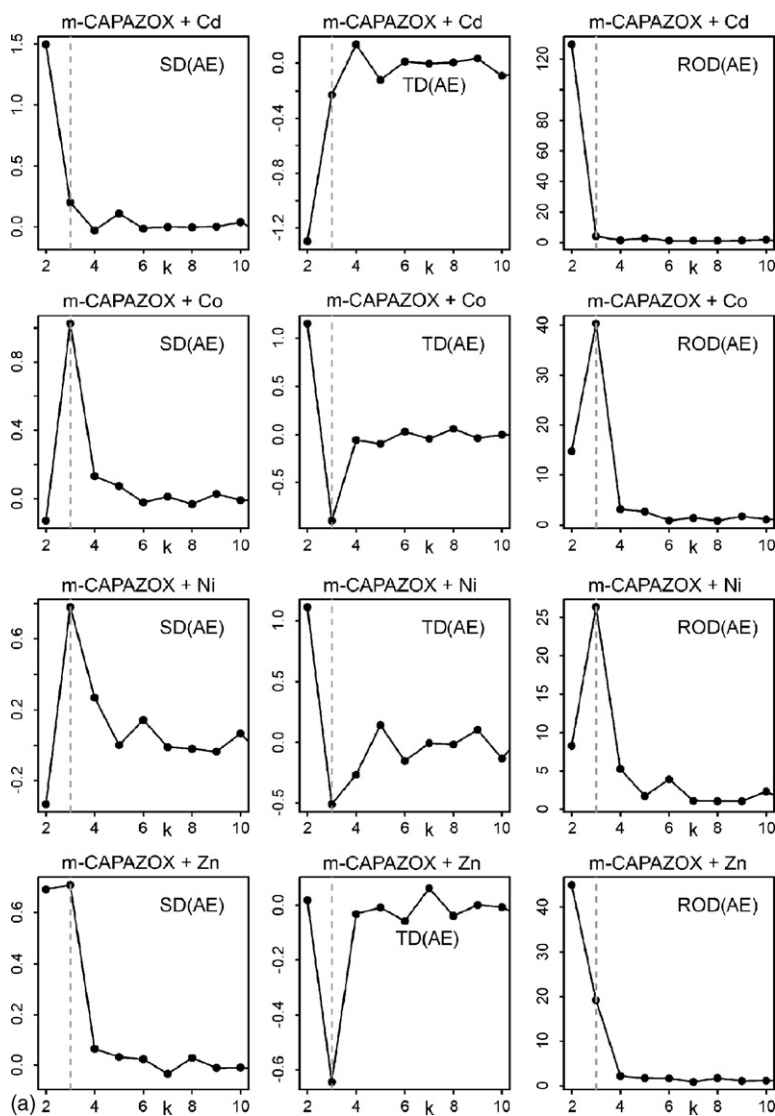


Fig. 2. (a) The derivatives detection criteria SD(AE), TD(AE) and ROD(AE) applied to the absorbance data set of complex-forming equilibria from the system of *m*-CAPAZOXS and Cd<sup>2+</sup> in the first row, *m*-CAPAZOXS and Co<sup>2+</sup> in the second row, *m*-CAPAZOXS and Ni<sup>2+</sup> in the third row and *m*-CAPAZOXS and Zn<sup>2+</sup> in the fourth row. (b) Complex-forming equilibria of the *m*-CAPAZOXS systems with four metal ions presented on the absorption spectra at 25 °C (left), the spectra of molar absorptivities vs. wavelengths for all of the complex species (middle) and the distribution diagram of the relative concentrations of all of the complex species in equilibrium: (first row) *m*-CAPAZOXS + Cd<sup>2+</sup>, (second row) *m*-CAPAZOXS + Co<sup>2+</sup>, (third row) *m*-CAPAZOXS + Ni<sup>2+</sup> and (fourth row) *m*-CAPAZOXS + Zn<sup>2+</sup>.

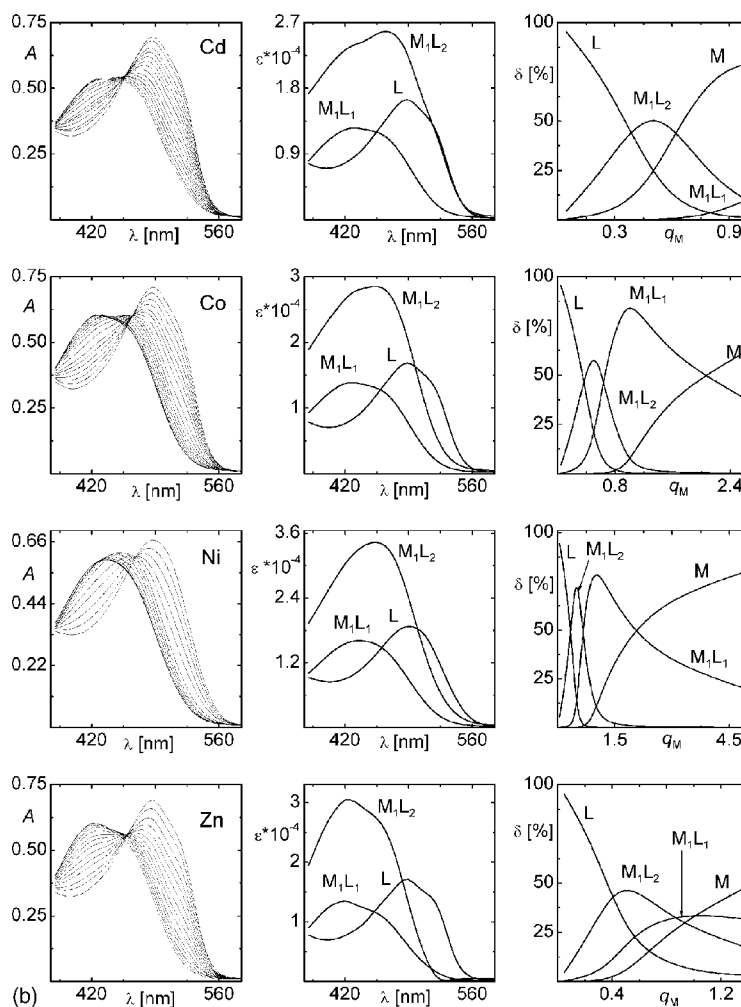


Fig. 2. (Continued).

methods –  $s_{\text{inst}}(A)$ , R.S.D., RMS and AE based on a knowledge of the experimental error of absorbance of spectrophotometer used  $s_{\text{inst}}(A)$  – and approximate methods ( $\chi^2$ ,  $\psi$ , RPV, IE and IND) requiring no knowledge of this experimental error [2–17]. Obviously, methods in the first category are preferred when the error is known [6–10]. The number of light-absorbing components  $n_c$  can be estimated from indices by comparing them with the experimental error, using the noise level  $s_{\text{inst}}(A)$ , R.S.D.<sub>inst</sub>, RMS<sub>inst</sub> and AE<sub>inst</sub> as a threshold. This is the common criterion to determine  $n_c$  for precise methods. The point where  $k = n_c$  from dependence of the indices on the number of principal components  $k$  to calculate them is then proposed for use. The average error criterion AE seems to be one of the best and most reliable indices and the index value AE( $k$ ) was used for elucidation. Comparing an index value, AE( $k$ ) calculated for the variable index  $k$  to the estimated experimental error: if the AE( $k$ ) is greater than the estimated error AE<sub>inst</sub>, then the number of factors  $k$  is insufficient. If the AE( $k$ ) is approximately equal to the estimated error AE<sub>inst</sub>, then the proper number of factors  $k$  is appropriate. Generally, the dependence PC( $k$ ) =  $f(k)$  decreases steeply with an increasing index  $k$ , as long as the  $k$ 's are significant, i.e. one finds the point where the slope of the indicator

function PC( $k$ ) =  $f(k)$  changes (Table 1). The number of complex species in the mixture was evaluated more reliably with the use of the second derivatives SD(AE), the third derivatives TD(AE) and the derivatives ratio ROD(AE), using the following rules (Figs. 1–3): (a) the curve of the second derivative of the index function SD(AE( $k$ )) =  $f(k)$  exhibits a maximum for the true index  $k = n_c$ . (b) The curve of the third derivative of the index function TD(AE( $k$ )) =  $f(k)$  crosses 0 and reaches a negative minimum which can be used as a criterion for the best estimate of index  $k$  being equal to  $n_c$ ,  $k = n_c$ . (c) The curve of the ratio of derivatives ROD(AE( $k$ )) =  $f(k)$  should reach a first maximum at the point where  $k = n_c$ . Tables 1–3 show the predicted number of complex species of the three CAPAZOXS complex-forming systems with selected metal cations, using the methods in Figs. 1–3.

#### 4.2. Complexation equilibria of *o*-, *m*- and *p*-CAPAZOXS

Multicomponent spectral analysis SQUAD(84) and  $\beta_{pqr}$  and  $\epsilon_{pqr}$  adjustment for a given spectra by fitting the predicted absorbance-response surface to given spectral data, with one dimension representing the dependent variable (absorbance), and the other two dimensions representing the independent

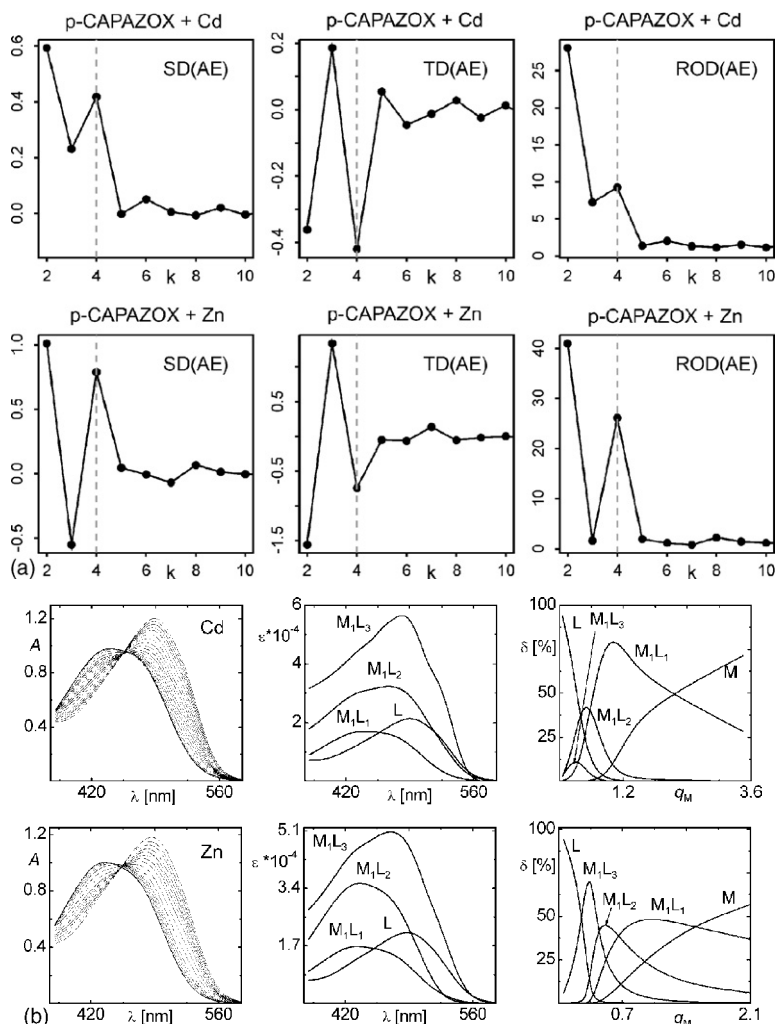


Fig. 3. (a) The derivatives detection criteria SD(AE), TD(AE) and ROD(AE) applied to the absorbance data set of complex-forming equilibria from the system of *p*-CAPAZOXs and Cd<sup>2+</sup> in the first row and *p*-CAPAZOXs and Zn<sup>2+</sup> in the second row. (b) Complex-forming equilibria of the *p*-CAPAZOXs systems with two metal ions presented on the absorption spectra at 25 °C (left), the spectra of molar absorptivities vs. wavelengths for all of the complex species (middle) and the distribution diagram of the relative concentrations of all of the complex species in equilibrium: (first row) *p*-CAPAZOXs + Cd<sup>2+</sup> and (second row) *p*-CAPAZOXs + Zn<sup>2+</sup>.

variables (the total component concentrations  $n_s$  solutions at  $n_w$  wavelengths). The parameters to be determined are [13,17]: (i) the number of species  $n_c$  and their stoichiometric indices  $(p, q, r)_j, j = 1, \dots, n_c$ , (ii) their stability constants  $\beta_{pqr}$  and molar absorptivities  $\varepsilon_{pqr}$  and (iii) the free concentrations  $[M_pL_qH_r]_j, j = 1, \dots, n_c$ , of all the species in the chemical model proposed. The general equations for complexes are  $pM + qL + rH = M_pL_qH_r$  with  $\beta_{pqr} = [M_pL_qH_r]/([M]^p [L]^q [H]^r)$ , where charges are omitted for simplicity. For the  $i$ th solution and  $k$ th wavelength, the absorbance  $A_{ik}$  is given by relation  $A_{ik} = \sum_{j=1}^{n_c} (\varepsilon_{pqr,k} \beta_{pqr} [M]^p [L]^q [H]^r)_j$  where  $\varepsilon_{pqr,k}$  is the molar absorptivity of species  $[M_pL_qH_r]$  at the  $k$ th wavelength. When the estimated  $\beta_{pqr}$  and  $\varepsilon_{pqr}$  values have been refined, the agreement between the experimental and predicted data can be examined. The residuals are analysed to discover whether the refined parameters adequately represent the data. To analyse the residuals a degree-of-fit test is performed by the statistical analysis of residuals (Tables 2 and 3): the residual mean  $\bar{e}$  should be nearly 0, the mean residual  $|\bar{e}|$  and the standard deviation of

residuals  $s(e)$  should be at the same level as the instrumental noise  $s_{\text{inst}}(A)$ , the residual skewness  $g_1(e)$  should be 0 so proving a symmetric distribution and  $g_2(e)$  should be 3, so proving the Gaussian distribution of residuals, and finally the Hamilton  $R$ -factor for relative fit  $R$  [%] should be less than 0.5% for an excellent fitness achieved (Tables 2 and 3).

Applying the procedure of efficient experimentation and computational strategy on the mole-ratio spectra, the ratio  $q_M = c_M/c_L$  is varied by keeping  $c_L$  constant and varying  $c_M$ . The metalochromic indicator CAPAZOXs mostly forms yellow complexes with cadmium(II), cobalt(II), copper(II), lead(II), nickel(II) and zinc(II) at pH 5. In solutions with an excess of the ligand,  $q_M < 0.5$ , the complex  $ML_3$  can also exist, while in equimolar solutions only  $ML_2$  and  $ML$  complexes are present. Table 2 presents the results of the chemical model determination for the *m*-CAPAZOXs system and Table 3 for the *o*- and *p*-CAPAZOXs system. The chemical model concerns a guess as to the number of light-absorbing species  $n_c$  coexisting in the equilibrium mixture, their stoichiometry, their stability constants



Table 3

The most probable chemical model in complex-forming equilibria of the *o*- and *p*-CAPAZOXS + Me<sup>z+</sup> system by regression spectra analysis using SQUAD(84) with the standard deviations of the estimated stability constant, log  $\beta_{pqr}(s(\beta_{pqr}))$  of the last valid digits in brackets

	<i>o</i> -CAPAZOXS + Cd <sup>2+</sup>	<i>o</i> -CAPAZOXS + Pb <sup>2+</sup>	<i>o</i> -CAPAZOXS + Zn <sup>2+</sup>	<i>p</i> -CAPAZOXS + Cd <sup>2+</sup>	<i>p</i> -CAPAZOXS + Ni <sup>2+</sup>	<i>p</i> -CAPAZOXS + Zn <sup>2+</sup>
$c_L$ [mol/L]	0.000391	0.0000234	0.000397	0.000293	0.000278	0.000297
Range $q_M$	0.03–2.63	0.8–33.33	0.10–2.04	0.06–3.45	0.04–6.25	0.05–2.5
Range pH	4.685–4.777	2.981–2.966	4.703–4.774	4.685–4.777	4.627–4.778	4.709–4.777
$n$	16	18	17	20	15	18
$m$	28	21	28	28	28	28
$n_c$	3	3	3	4	4	4
$s_k(A)$ [mAU]	0.54	0.3	1.03	0.24	0.76	0.18
Estimated stability constant, log $\beta_{pqr}(s(\beta_{pqr}))$						
ML	6.39(5)	4.24(2)	5.18(7)	6.44(5)	7.72(18)	6.84(16)
ML <sub>2</sub>	11.51(9)	9.01(2)	9.06(10)	10.99(10)	13.86(34)	13.05(29)
ML <sub>3</sub>	–	–	–	14.57(25)	17.88(63)	18.74(43)
The degree-of-fit test by the statistical analysis of residuals						
$\bar{e}$ [mAU]	0	0.000002	0	0	0	0
$ \bar{e} $ [mAU]	1.03	0.99	1.67	0.69	1.03	1
$s(e)$ [mAU]	1.83	1.49	2.68	1.2	1.73	1.76
$g_1(e)$ ( $\approx 0$ )	0.59	–0.39	0.41	1.04	0.4	0.23
$g_2(e)$ ( $\approx 3$ )	6.02	3.67	4.11	6.84	3.83	3.8
$R$ [%] (<0.5)	0.34	0.3	0.5	0.17	0.24	0.25

The parameter reliability is proven with degree-of-fit statistics such as the mean of residuals  $\bar{e}$  [mAU], the mean residual  $|\bar{e}|$  [mAU], the standard deviation of residual  $s(e)$  [mAU] which is equal to the standard deviation of absorbance after termination of the regression process,  $s(A)$  [mAU], the residual skewness  $g_1(e)$  and residual kurtosis  $g_2(e)$  and the Hamilton  $R$ -factor [%]. *Experimental conditions*:  $c_L$  (*o*-, *p*-CAPAZOXS),  $I = 0.1$  (NaClO<sub>4</sub> + Na<sub>3</sub>PO<sub>4</sub> + HClO<sub>4</sub>), 25 °C, path length 1.000 cm,  $s_{inst}(A) = 0.45$  mAU (Specord M40, Zeiss, Jena Germany).

estimated by regression analysis and at the same time the curves of molar absorption coefficients dependent on wavelength. For a set of current values of  $\beta_{pqr}$  the free concentrations of metal [M] and ligand [L], followed by the concentrations of all the complexes in the equilibrium mixture  $[M_pL_qH_r]_j$ ,  $j = 1, \dots, n_c$ , for  $n$  solutions the matrix **C**, and are presented in the form of a distribution diagram of relative concentrations in Figs. 1b, 2b and 3b.

In addition to the fit achieved, it is also necessary to examine the physico-chemical sense of the model parameter estimates, such as positive values in the concentration matrix, positive values of molar absorptivities and the concentration fraction of the complex species in the mixture. If a complex species is present in a fraction lower than 5–10%, the evaluation of such an equilibrium can fail: from the spectral point of view it acts merely as “noise”, insufficient for an evaluation of its own equilibrium and complicating the evaluation of other equilibria. This problem can be solved by augmenting the set of spectra with a single spectrum of the molar absorptivities of the unknown species. In searching for a chemical model the hypothesis of three species L, ML and ML<sub>2</sub> was tested in the first step. In accordance with results of the PCA indices analysis the hypothesis of four species was also tested and better fitness through spectra points was not obtained for *o*- and *m*-CAPAZOXS. Therefore, the final chemical model contained three light-absorbing components ML, ML<sub>2</sub> and L in most systems for *o*- and *m*-derivates. However, *p*-CAPAZOXS exhibits four species in equilibrium ML, ML<sub>2</sub>, ML<sub>3</sub> and L.

Cherkesov [21] has explained the formation of a covalent bond of the central metal ion to the azo group nitrogen. In this

case the six-membered chelate ring is completed by the bond of the central ion to the azo group nitrogen more remote from the quinoline ring. As the pH of solutions increases the bond of the central ion to the azo group nitrogen is disrupted, and a bond of the ion to the heterocycle nitrogen of the quinoline system is formed.

## 5. Conclusion

1. Generally, the most reliable index methods seem to be those based on a knowledge of the experimental error of absorbance. The average error criterion seems to be the most reliable method for the determination of the instrumental standard deviation of the spectrophotometer used.
2. Index methods are all based on finding the point at which the slope of the index function changes, and therefore the application of derivatives is very useful. For more than three components in the mixture, the modification of Elbergali et al. with the second or third derivative and derivative ratio function seem to be an useful resolution tool, enabling the correct prediction of the number of components in spectra for all index functions.
3. Precise methods based on a knowledge of the instrumental error  $s_{inst}(A)$  are preferred as the more reliable procedure, as they always predict the correct number of components and even the presence of minor species in the mixture.
4. A chemical model (i.e. the number of complexes, their stoichiometry, their stability constants and their curves of molar absorption coefficients with a distribution diagram of relative concentrations of all species) of the following systems

was found at  $I \approx 0.1$  and  $25^\circ\text{C}$ . The standard deviations of the estimated stability constant,  $\log \beta_{pqr}(s(\beta_{pqr}))$  of the last valid digits in brackets are in brackets:

*o*-CAPAZOXS +  $\text{Cd}^{2+}$ : For  $q_M$  0–2.6 leading to three light-absorbing species L, ML and  $\text{ML}_2$  with estimates of stability constants  $\log \beta_{110} = 6.39(5)$  and  $\log \beta_{120} = 11.51(9)$ .

*o*-CAPAZOXS +  $\text{Pb}^{2+}$ : For  $q_M$  1–33 leading to three light-absorbing species L, ML and  $\text{ML}_2$  with  $\log \beta_{110} = 4.24(2)$  and  $\log \beta_{120} = 9.01(2)$ .

*o*-CAPAZOXS +  $\text{Zn}^{2+}$ : For  $q_M$  0–53 leading to three light-absorbing species L, ML and  $\text{ML}_2$  with  $\log \beta_{110} = 5.18(7)$  and  $\log \beta_{120} = 9.06(10)$ .

*m*-CAPAZOXS +  $\text{Cd}^{2+}$ : For  $q_M$  0–1 leading to three light-absorbing species L, ML and  $\text{ML}_2$  with  $\log \beta_{110} = 6.59(20)$  and  $\log \beta_{120} = 11.51(32)$ .

*m*-CAPAZOXS +  $\text{Co}^{2+}$ : For  $q_M$  0–2.6 leading it lead to three light-absorbing species L, ML and  $\text{ML}_2$  with  $\log \beta_{110} = 7.19(6)$  and  $\log \beta_{120} = 12.19(8)$ .

*m*-CAPAZOXS +  $\text{Ni}^{2+}$ : For  $q_M$  0–5 it leading three light-absorbing species L, ML and  $\text{ML}_2$  with  $\log \beta_{110} = 7.64(7)$  and  $\log \beta_{120} = 13.39(12)$ .

*m*-CAPAZOXS +  $\text{Zn}^{2+}$ : For  $q_M$  0–1.4 leading to three light-absorbing species L, ML and  $\text{ML}_2$  with  $\log \beta_{110} = 4.83(3)$  and  $\log \beta_{120} = 9.57(3)$ .

*p*-CAPAZOXS +  $\text{Cd}^{2+}$ : For  $q_M$  0–3.5 leading to three light-absorbing species L, ML,  $\text{ML}_2$  and  $\text{ML}_3$  with  $\log \beta_{110} = 6.44(5)$ ,  $\log \beta_{120} = 10.99(10)$  and  $\log \beta_{130} = 14.57(25)$ .

*p*-CAPAZOXS +  $\text{Zn}^{2+}$ : For  $q_M$  0–2.5 leading to four light-absorbing species L, ML,  $\text{ML}_2$  and  $\text{ML}_3$  with  $\log \beta_{110} = 6.84(16)$ ,  $\log \beta_{120} = 13.05(29)$  and  $\log \beta_{130} = 18.74(43)$ .

## Acknowledgements

The financial support of the Internal Grant Agency of the Czech Ministry of Health (grant no. NR 9055-4/2006) and of the Czech Ministry of Education (grant no. MSMT 0021627502) is gratefully acknowledged.

## References

- [1] M. Meloun, T. Čapek, T. Syrový, Talanta 66 (2005) 547.
- [2] E.R. Malinowski, Factor Analysis in Chemistry, second ed., Wiley, New York, 1991.
- [3] M. Meloun, J. Havel, E. Högfeltdt, Computation of Solution Equilibria, Horwood, Chichester, 1988.
- [4] E.R. Malinowski, J. Chemom. 13 (1999) 69.
- [5] E.R. Malinowski, Anal. Chem. 49 (1977) 612.
- [6] A.K. Elbergali, J. Nygren, M. Kubista, Anal. Chim. Acta 379 (1999) 143.
- [7] J.M. Dean, in: R.G. Brereton (Ed.), Multivariate Pattern Recognition in Chemometrics Illustrated by Case Studies, Elsevier, Amsterdam, 1992.
- [8] M. Meloun, J. Čapek, P. Mikšík, R.G. Brereton, Anal. Chim. Acta 423 (2000) 51.
- [9] M. Meloun, K. Kupka, J. Čapek, T. Syrový, INDICES Algorithm, <http://meloun.upce.cz> and the block Algorithms.
- [10] J.J. Kankare, Anal. Chem. 42 (1970) 1322.
- [11] M.S. Bartlett, Br. J. Psych. Stat. Sec. 2 (1950) 77.
- [12] R.D. Catell, Multivar. Behav. Res. 1 (1966) 245.
- [13] (a) D.J. Leggett (Ed.), Computational Methods for the Determination of Formation Constants, Plenum Press, New York, 1985, pp. 99–157; (b) D.J. Leggett (Ed.), Computational Methods for the Determination of Formation Constants, Plenum Press, New York, 1985, pp. 291–353; (c) J. Havel, M. Meloun, Computational Methods for the Determination of Formation Constants, Plenum Press, New York, 1985, p. 19; (d) J. Havel, M. Meloun, Computational Methods for the Determination of Formation Constants, Plenum Press, New York, 1985, p. 221.
- [14] D.J. Leggett, W.A.E. McBryde, Anal. Chem. 47 (1975) 1065.
- [15] M. Meloun, M. Javůrek, J. Havel, Talanta 33 (1986) 513, available online at <http://meloun.upce.cz>.
- [16] M. Meloun, J. Havel, E. Högfeltdt, Computation of Solution Equilibria, Ellis Horwood, Chichester, 1988.
- [17] (a) M. Meloun, J. Militký, M. Forina, PC-Aided Regression and Related Methods, vol. 2, Ellis Horwood, Chichester, 1994; (b) M. Meloun, J. Militký, M. Forina, PC-Aided Statistical Data Analysis, vol. 1, Ellis Horwood, Chichester, 1992.
- [18] (a) C. Rigano, M. Grasso, S. Sammartano, Ann. Chim. Rome 74 (1984) 537; (b) C. De Stefano, P. Princi, C. Rigano, S. Sammartano, Ann. Chim. Rome 77 (1987) 643.
- [19] P.M. May, D.R. Williams, P.W. Linder, R.G. Torrington, Talanta 29 (1982) 249.
- [20] M. Meloun, V. Říha, J. Žáček, Chem. Listy 82 (1988) 765, available online at <http://meloun.upce.cz>.
- [21] A.I. Cherkosov, Zh. Anal. Khim. 17 (1962) 16.

# Optimization of a GFAAS method for determination of total inorganic arsenic in drinking water

Jérôme Michon, Véronique Deluchat\*, Raad Al Shukry, Christophe Dagot, Jean-Claude Bollinger

*Laboratoire des Sciences de l'Eau et de l'Environnement, Faculté des Sciences et Techniques, 123 avenue Albert Thomas, 87 060 Limoges, France*

Received 8 December 2005; received in revised form 31 May 2006; accepted 7 June 2006

Available online 13 December 2006

## Abstract

The new  $10 \mu\text{g l}^{-1}$  arsenic standard in drinking water has been a spur to the search for reliable routine analytical methods with a limit of detection at the  $\mu\text{g l}^{-1}$  level. These methods also need to be easy to handle due to the routine analyses that are required in drinking water monitoring. Graphite furnace atomic absorption spectrometry (GFAAS) meets these requirements, but the limit of detection is generally too high except for methods using a pre-concentration or separation step. The use of a high-intensity boosted discharge hollow-cathode lamp decreases the baseline noise level and therefore allows a lower limit of detection. The temperature program, chemical matrix modifier and thermal stabilizer additives were optimized for total inorganic arsenic determination with GFAAS, without preliminary treatment. The optimal furnace program was validated with a proprietary software. The limit of detection was  $0.26 \mu\text{g As l}^{-1}$  for a sample volume of  $16 \mu\text{l}$  corresponding to  $4.2 \text{pg As}$ . This attractive technique is rapid as 20 samples can be analysed per hour. This method was validated with arsenic reference solutions. Its applicability was verified with artificial and natural groundwaters. Recoveries from 91 to 105% with relative standard deviation <5% can be easily achieved. The effect of interfering anions and cations commonly found in groundwater was studied. Only phosphates and silicates (respectively at 4 and  $20 \text{mg l}^{-1}$ ) lead to significant interferences in the determination of total inorganic arsenic at  $4 \mu\text{g l}^{-1}$ .

© 2006 Elsevier B.V. All rights reserved.

**Keywords:** Graphite furnace atomic absorption spectrometry (GFAAS); UltraAA-Lamp®; Trace inorganic arsenic determination; Drinking water; Data processing software

## 1. Introduction

Arsenic is a ubiquitous element with metalloid properties. Its chemistry is complex and, in nature, it is widely distributed in many minerals and organic arsenic compounds [1], as the result of biological activity. In water, arsenic is predominantly present in inorganic form, as As(III) and As(V); a minor amount of methyl and dimethyl arsenic compounds being detected. In many parts of the world, groundwater is polluted with arsenic. This pollution is due to natural occurrence in soils (especially as arsenopyrite or as metal arsenates) or to anthropogenic activities (mining, agriculture, forestry, feed additives, glass and ceramic industries, ...) [1,2]. Arsenic is recognized as carcinogenic (class A), it causes cancers of the skin, lungs and bladder [2–4]. These effects are primarily due to consumption of

arsenic-contaminated drinking waters [5]. Due to arsenic's health and toxicological effects, many regulatory agencies, such as the WHO and the U.S. EPA, have revised the maximum contaminant level to  $10 \mu\text{g l}^{-1}$  [6,7]. Further to the European Directive of 1998 [8], all drinking water supply systems within the European Union should comply with this limit; it is also the case in some countries such as Jordan, and Japan [9], among others. Efficient and easy to handle analytical methods to measure total arsenic at such a low concentration have therefore to be developed.

The most important commercially available multielement instruments for trace element determination are inductively coupled plasma (ICP)-based, especially the ICP-MS [10]. ICP-MS enables reliable arsenic determination with a very low limit of detection (LOD below  $1 \mu\text{g l}^{-1}$ ) [11,12]. However, a drawback of this method is the difficulty in analysing samples with a high salt concentration [12,13], which may be due to natural occurrence or addition of HCl for sample preservation [14]. Moreover, the MS detector is rather complex and expensive,

\* Corresponding author. Tel.: +33 555 457 468; fax: +33 555 457 203.  
E-mail address: [veronique.deluchat@unilim.fr](mailto:veronique.deluchat@unilim.fr) (V. Deluchat).

which limits the widespread use of ICP-MS for routine and quality control, especially in small drinking water plants and labs [13,15].

Hydride generation atomic absorption spectrometry (HG-AAS) is often used for the determination of arsenic trace levels in water [10–12]. This analytical method is the most widely accepted procedure for the analysis of arsenic at  $\mu\text{g l}^{-1}$  level. However, the atomisation signal is nevertheless dependent on the oxidation state and the hydride system used [16,17].

Currently, graphite furnace atomic absorption spectrometry (GFAAS) is one of the most reliable and powerful analytical techniques for the determination of trace and ultra-trace elements in water, soil, clinical and biological samples [13,15,18,19]. It offers good sensitivity with a short analysis time, low cost (in comparison with ICP-MS [13]) and requires a low sample volume (2–100  $\mu\text{l}$ ) [15]. However, most of the reported methods for arsenic determination based on GFAAS need a pre-concentration/separation step, in order to determine arsenic at such low concentration range ( $\mu\text{g l}^{-1}$ ) and to reach LOD lower than  $1 \mu\text{g l}^{-1}$  [11,12,20,21]. These combined techniques are expensive and time-consuming [15].

GFAAS alone is suitable only for the determination of the total inorganic arsenic concentration in the sample solution. Thus, the determination conditions must be optimized so that all the inorganic arsenic species are atomized equally at the same temperature. To this aim, the use of a chemical matrix modifier is necessary [22,23]. It decreases interferences and stabilizes the analyte to higher temperatures. It also allows separation between background and analyte atomic absorption signals [22]. An ideal chemical modifier is thus a reagent which not only diminishes the background signal and interference effects, but also enhances the analyte sensitivity. Furthermore, the use of a specific hollow-cathode lamp (UltrAA-Lamp<sup>®</sup>) allows reduction of both the baseline noise level and the background signal. Background correction is however often necessary. It is therefore necessary to select operating parameters in order to (i) remove the maximum amount of matrix material during the ashing stage, (ii) provide adequate analytical sensitivity and (iii) separate the analyte peak from non-atomic absorption peaks.

The aim of the present study was thus to develop a simple and rapid method (without preliminary treatment of the sample) for the determination of total inorganic arsenic in aqueous solutions with an arsenic concentration lower than  $10 \mu\text{g l}^{-1}$ . This method should be applicable to routine analyses and monitoring studies. A high-intensity hollow-cathode lamp (UltrAA-Lamp<sup>®</sup>) was used in order to decrease the LOD and increase the sensitivity of the method [24]. The analytical conditions were optimized by a new proprietary data-processing software, ATOM<sup>®</sup>. Different temperature programs, chemical matrix modifiers (Ni, Pd and a Pd–Mg mixture) and thermal stabilizer solutions were tested.

## 2. Materials and methods

### 2.1. Standards and reagents

All solutions were prepared with high-purity de-ionised water (resistivity  $18.2 \text{ M}\Omega \text{ cm}$ ) obtained with a Milli-Q water

purification system (Millipore Milli-Q Gradient A10 and Purelab Prima). All glassware and polyethylene bottles were cleaned by soaking in 10%  $\text{HNO}_3$  (Prolabo, Normapur) and rinsed three times with de-ionised water. Synthetic standard stock solutions ( $1000 \text{ mg l}^{-1}$  As) of arsenate and arsenite were prepared by dissolving respectively disodium arsenate heptahydrate  $\text{Na}_2\text{HAsO}_4 \cdot 7\text{H}_2\text{O}$  (Fluka, purity >98.5%) and sodium (meta)arsenite  $\text{NaAsO}_2$  (Fluka, purity >99%) in de-ionised water. Calibration standard solutions were prepared daily from  $10 \text{ mg l}^{-1}$  solutions in de-ionised water.

A secondary reference material solution (Fluka [As(III)] =  $998 \pm 2 \text{ mg l}^{-1}$ , purity >99.95%, certificate number KI-0102, product No. 11078), certified by EMPA (St. Gallen, Switzerland), was diluted in 0.1%  $\text{HNO}_3$  (v/v, pH lower than 3) in order to obtain an As(III) concentration of  $5.0 \pm 0.1 \mu\text{g l}^{-1}$ .

The chemical matrix modifiers, for the arsenic determination with the GFAAS analytical technique, were Ni, Pd and a Pd–Mg mixture: i.e. the most commonly mentioned in the literature [15,23]. The Ni modifier was a  $1000 \text{ mg l}^{-1}$   $\text{Ni}(\text{NO}_3)_2$  (Fluka, purity >99%) solution. The palladium modifier was a  $2000 \text{ mg l}^{-1}$   $\text{Pd}(\text{NO}_3)_2$  (Fluka, As <0.000001%) solution. Finally, the Pd–Mg solution was prepared by mixing 900  $\mu\text{L}$  of  $2000 \text{ mg l}^{-1}$   $\text{Pd}(\text{NO}_3)_2$  (Fluka, As <0.000001%) and 100  $\mu\text{L}$  of  $10000 \text{ mg l}^{-1}$   $\text{Mg}(\text{NO}_3)_2$  (Fluka, purity >99%). These chemical modifiers were prepared in de-ionised water. The reagents used as thermal stabilizer additives were KI (Merck, purity >99%, As <0.000001%), NaOH (Merck, purity >99%, As <0.0001%) and  $\text{HNO}_3$  (Merck, Suprapur, As <0.0000001%).

### 2.2. Samples

Artificial water, based on an original compilation of 23 groundwater compositions from granitic areas, was prepared according to Lenoble et al. [25]. This artificial water, spiked with As(III) and/or As(V), was used to test arsenic determination with a constant composition medium. Moreover, three real life contaminated groundwater samples were collected in polyethylene bottles, near Limoges, France. These samples were immediately acidified with 0.1% of concentrated HCl (Merck, Suprapur, As <0.0000001%), which provided a pH lower than 2 [14]. The samples were then filtered in the laboratory using a  $0.45 \mu\text{m}$  pore size membrane filter (Macherey-Nagel, PTFE) to remove suspended solids. The water compositions are given in Table 1.

### 2.3. Instrumentation

#### 2.3.1. Apparatus

Measurements were carried out with a Varian SpectrAA 880Z atomic absorption spectrometer equipped with a GTA 100Z graphite furnace, with Zeeman background correction. An arsenic high-intensity boosted discharge hollow-cathode lamp (Varian, serial number: OOH0 770), called “UltrAA-Lamp<sup>®</sup>”, was used. It uses the existing lamp current but applies a second discharge within the lamp to increase the emission intensity. A conventional hollow-cathode lamp (Varian, serial number: OYH 6072) was used to compare the sensitivity of both system

Table 1  
Arsenic and associated mineral matrix in artificial water and in three groundwater samples from near Limoges, France

Water samples	As ( $\mu\text{g l}^{-1}$ )	pH	$\text{HCO}_3^-$ ( $\text{mg l}^{-1}$ )	$\text{Na}^+$ ( $\text{mg l}^{-1}$ )	$\text{K}^+$ ( $\text{mg l}^{-1}$ )	$\text{Mg}^{2+}$ ( $\text{mg l}^{-1}$ )	$\text{Ca}^{2+}$ ( $\text{mg l}^{-1}$ )	$\text{Cl}^-$ ( $\text{mg l}^{-1}$ )	$\text{NO}_3^-$ ( $\text{mg l}^{-1}$ )	$\text{SO}_4^{2-}$ ( $\text{mg l}^{-1}$ )	$\text{PO}_4^{3-}$ ( $\text{mg l}^{-1}$ )	$\text{SiO}_2$ ( $\text{mg l}^{-1}$ )
Artificial	N.D.	6.0	1.2	6.9	0.8	1.3	3.2	8.1	9.9	3.4	–	9.0
Sample 1	$4.69 \pm 0.11$	5.5	6.9	5.5	1.0	0.8	3.6	5.7	2.0	1.4	N.D.	10.9
Sample 2	$2.36 \pm 0.12$	6.0	–	10.9	10.7	3.0	9.2	24.7	57.3	7.9	N.D.	N.D.
Sample 3	$0.65 \pm 0.06$	6.5	–	12.9	4.1	6.4	20.1	13.6	51.5	61.1	N.D.	N.D.

N.D.: not detectable. Standard deviation for cations and anions:  $\pm 5\%$ .

accessories. A wavelength of 193.7 nm and a 0.5 nm slit-width were selected from previous optimizations. Pyrolytic graphite coated tubes (Varian 63-100012-00) with forked pyrolytic platforms (Varian 63-100024-00) were used. The volume injected was 21  $\mu\text{l}$  including 5  $\mu\text{l}$  of chemical matrix modifier. All measurements were carried out with at least three replicates and based on integrated absorbance. Argon was used as protective gas throughout.

### 2.3.2. Advanced temperature optimization methodology (ATOM<sup>®</sup>) software

In order to optimize the temperature program, the ATOM<sup>®</sup> software was used. It has been developed by Varian France (Version 1.0.0, reference: SRM20020624) specially for GFAAS. Based on experimental design procedures, the studied system is characterized by a complete polynomial of the second order. The analytical response is a function of two parameters: the pyrolysis and atomization temperatures. The combination of these two temperatures should give an optimal answer. Mathematical and statistical calculations then determine two shapes (the 3D shape and the Contour Graph shape). The interpretation of these two shapes allows the optimum pyrolysis and atomization temperatures and the best chemical matrix modifier in agreement with the method used.

## 3. Results and discussion

### 3.1. Optimization of spectroscopic conditions

Arsenic determination experiments were carried out with and without the arsenic UltrAA-Lamp<sup>®</sup>. Typical atomization

response signals for analysis of water spiked with arsenic are shown in Fig. 1. The use of the UltrAA-Lamp<sup>®</sup> enabled an increase in sensitivity of up to 40%: the maximum absorbance for a sample containing 5  $\mu\text{g l}^{-1}$  As(V) was 0.084 U with a normal hollow-cathode lamp and 0.111 U with an UltrAA-Lamp<sup>®</sup>. This result was better than those obtained by Bezur [24]: the slope of the calibration curve increased in 30% with his high-intensity boosted cathode lamp, compared to the results obtained with a usual hollow cathode lamp. The baseline noise was also reduced with the use of the UltrAA-Lamp<sup>®</sup>: the ratio peak area/noise increased up to 2.5 times when compared with a conventional lamp. The LOD obtained was thus improved. The best LOD was obtained for a lamp current of 10 mA and a wavelength of 193.7 nm with a slit-width of 0.5 nm. For a slit-width of 0.2 nm (value usually used in literature [15,23]), the absorbance of the signal observed was not sufficient to obtain a satisfactory measurement, particularly for arsenic concentrations below 2  $\mu\text{g l}^{-1}$ .

### 3.2. Optimization of the graphite furnace temperature program and analytical conditions

The GFAAS conditions were optimized so that As(III) and As(V) species were atomized equally at the same atomization temperature and so that the same furnace program and a common calibration graph, could be used for measuring either of these two inorganic arsenic species. The optimization of the furnace program was therefore focused on two different points: first, the time and temperature of the pyrolysis and atomization steps, secondly, the selection and the amount of the chemical matrix modifier and the thermal stabilizer. The first one

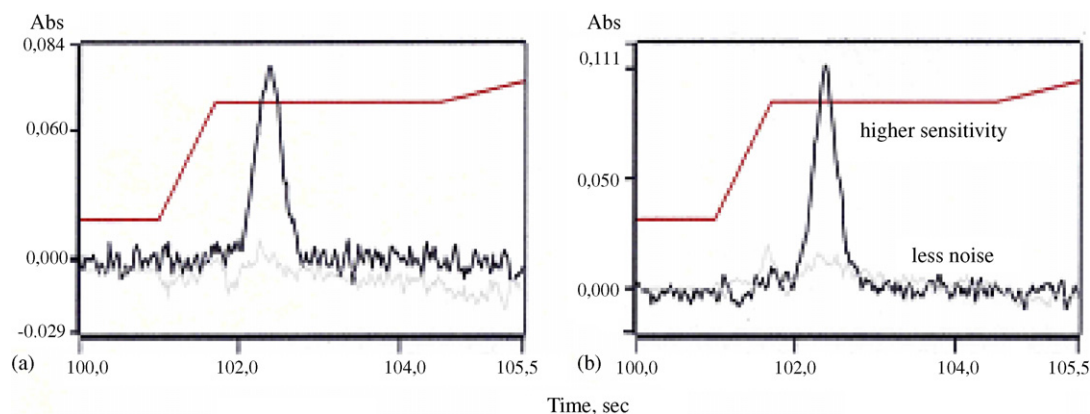


Fig. 1. Atomization profiles of water spiked with 5  $\mu\text{g As(V) l}^{-1}$  for a GFAAS using an (ordinary) arsenic hollow-cathode lamp (a), and an arsenic UltrAA-Lamp<sup>®</sup> (b).



Table 2  
Results obtained with the ATOM<sup>®</sup> software

Matrix modifier	Pyrolysis guideline (step: 300 °C)	Atomisation guideline (step: 250 °C)	3D-shape	Contour shape	Selected pyrolysis value (°C)	Selected atomization value (°C)
Ni	1000	2000	–	–	None	None
		2400	+	–	1130	2330
Pd	1200	2000	–	–	None	None
		2400	+	–	1250	2330
	1600	2000	+	–	1430	2200
		2400	+	–	1480	2250
Pd–Mg	1200	2000	+	–	1135	2230
		2400	+	+	1178	2395
	1600	2000	–	–	None	None
		2400	–	–	None	None

+: an optimal 3D or contour shape was selected by the ATOM software. –: no convenient 3D or contour shape was selected by the ATOM<sup>®</sup> software.

Table 3  
Optimized furnace program for the analysis of As in liquid solution

Step	Temperature (°C)	Ramp (s)	Hold (s)	Ar flow rate (l min <sup>-1</sup> )
Drying 1	140	5	30.0	3.0
Drying 2	180	5	35.0	3.0
Pyrolysis 1	1200	10	20.0	3.0
Pyrolysis 2	1200	1.0	0.0	0.0
Atomization	2400	0.8	2.7	0.0
Cleaning	2600	1.0	1.0	3.0

reduced the interference effects and enhanced the analyte sensitivity, whereas the second one stabilized the signal during the atomization step.

These optimizations were validated by the ATOM<sup>®</sup> software. Sample and chemical matrix modifier (Ni, Pd or Pd–Mg mixture) were both injected in a pre-heated tube at 100 °C. The injection flow rate was 7  $\mu\text{l s}^{-1}$  and the injected volume was 21  $\mu\text{l}$ : 16  $\mu\text{l}$  of a 10  $\mu\text{g l}^{-1}$  As(V) solution and 5  $\mu\text{l}$  of the chemical matrix modifier. The different conditions tested with the ATOM<sup>®</sup> software were chosen from literature data [15,22,26] and are presented in Table 2.

The best results were obtained with a Pd–Mg mixture as the chemical matrix modifier and selected temperatures of 1178 °C (pyrolysis) and 2395 °C (atomization) (Table 2). Therefore, for routine analyse, the pyrolysis and atomization temperatures chosen were 1200 and 2400 °C, respectively (Table 3). The ratio of the Pd–Mg chemical matrix modifier was then studied. The best accuracy was obtained for a Pd–Mg mixture ratio of 1/5 (w/w), with Pd and Mg concentrations of 2 and 10  $\text{g l}^{-1}$ , respectively.

Table 4  
Analytical characteristics of the As(III) and As(V) calibrant solutions for the proposed method

Species	As(III)	As(V)
Calibration	$A = 0.00553(\pm 0.00007)[\text{As}] + 0.00043(\pm 0.00009)$	$A = 0.00593(\pm 0.00012)[\text{As}] - 0.00001(\pm 0.00007)$
Linear analytical range ( $\mu\text{g l}^{-1}$ )	0.26–10.0	0.26–10.0
Coefficient of determination	$R^2 = 0.996$	$R^2 = 0.993$
R.S.D. ( $[\text{As}] = 5 \mu\text{g l}^{-1}$ ; $N = 5$ )	2.9%	3.5%

A: absorbance; [As] expressed in  $\mu\text{g l}^{-1}$ ; N: number of measurements.

The ramp and hold times of each step were also studied. Moreover, in the optimized furnace program, two drying steps at 140 and 180 °C were applied, in order to achieve a correct dryness for liquid calibrants without splatter. After atomization, a final cleaning step was applied at a slightly higher temperature (2600 °C) to prevent memory effects.

Three thermal stabilizer solutions, KI, NaOH and HNO<sub>3</sub>, were tested over a range of concentrations from 0.1 to 3% (v/v). With NaOH, the background signal obtained did not change whereas with KI and HNO<sub>3</sub>, it decreased. However, with the use of the KI solution, a yellow coloration of the capillary, due to potassium iodide decomposition, was observed. The thermal stabilizer chosen was therefore HNO<sub>3</sub>. For the concentration range tested, the best result obtained was for an arsenic solution containing 1% (v/v) of HNO<sub>3</sub>.

Finally, in the optimized furnace program (Table 3), the standard solution mixed with 1% (v/v) of HNO<sub>3</sub>, was introduced at 100 °C. Two drying steps were applied and then pyrolysis and atomization, at 1200 and 2400 °C, respectively. The chemical matrix modifier used was a Pd/Mg mixture (ratio Pd–Mg equal to 1/5, w/w).

### 3.3. Calibration graph and LOD

In order to compare the behaviour of inorganic arsenic species during the analysis program, As(III) and As(V) solutions were studied separately. Two linear calibrations of five measurements were obtained for As(III) and As(V) in the concentration range of 1–10  $\mu\text{g l}^{-1}$  (Table 4). The peak shapes and area obtained

Table 5  
Recoveries of the arsenic species

As concentration ( $\mu\text{g l}^{-1}$ )	As species	Calibrant solution used	Recovery (%)	R.S.D. (%)
1.65	As(III)	As(III)	97	3.7
	As(III)	As(V)	105	4.1
	As(V)	As(V)	95	3.5
	As(V)	As(III)	96	4.2
	As(III) + As(V) <sup>a</sup>	As(V)	102	4.3
	As(III) + As(V) <sup>a</sup>	As(III)	104	4.6
4.70	As(III)	As(III)	102	1.9
	As(III)	As(V)	105	2.9
	As(V)	As(V)	95	2.0
	As(V)	As(III)	101	2.1
	As(III) + As(V) <sup>a</sup>	As(V)	97	1.7
	As(III) + As(V) <sup>a</sup>	As(III)	98	1.9
7.5	As(III)	As(III)	103	0.3
	As(III)	As(V)	98	0.8
	As(V)	As(V)	101	0.4
	As(V)	As(III)	102	0.6
	As(III) + As(V) <sup>a</sup>	As(V)	97	0.4
	As(III) + As(V) <sup>a</sup>	As(III)	101	0.3

<sup>a</sup> Ratio As(III)/As(V): 1/1 (w/w).

looked the same for As(III) and As(V) solutions. In order to confirm that As(III) and As(V) were atomized equally at the same temperature and that a common calibration graph could be used for these two inorganic arsenic species, arsenic determinations in As(III) and As(V) solutions, were carried out with the two calibration curves. Standard solutions of As(III), As(V) and As(III) + As(V) were prepared simply by diluting As(III) and As(V) standard stock solutions with de-ionised water. Table 5 shows that recovery percentages from 95 to 105% were obtained whatever the calibration curves used. The R.S.D. value of three replicate samples was below 5%. Thus, the procedure was well suited to the determination of total inorganic As in drinking water for a range of 0.26–10  $\mu\text{g l}^{-1}$ . Subsequently the As(V) solution was used as calibrant solution: absorbance = 0.00593 ( $\pm 0.00012$ ) [As] – 0.00001 ( $\pm 0.00007$ ).

The LOD was calculated according to IUPAC recommendations [27]: 3.29 times the standard deviation of the blank solutions. For this calculation, 20 measurements were carried out. These values were then related to the slope value of the calibration equation of As(V) (Table 4). The LOD obtained was 0.26  $\mu\text{g l}^{-1}$  As for a sample volume of 16  $\mu\text{l}$  corresponding to 4.2 pg As. This LOD was lower than that obtained with GFAAS studies carried out without pre-concentration step [19,21,22]. Moreover, this LOD was comparable with that obtained by more elaborated analytical techniques (flow injection hydride generation atomic absorption spectrometry (FI-HG-AAS) and liquid chromatography-inductively plasma mass spectrometry (LC-ICP-MS)) [17,28].

The quantification limit, which marked the ability of the apparatus to adequately “quantify” an analyte, calculated as the concentration corresponding to 10 times the standard deviation of the blank [27], was 0.79  $\mu\text{g l}^{-1}$  As.

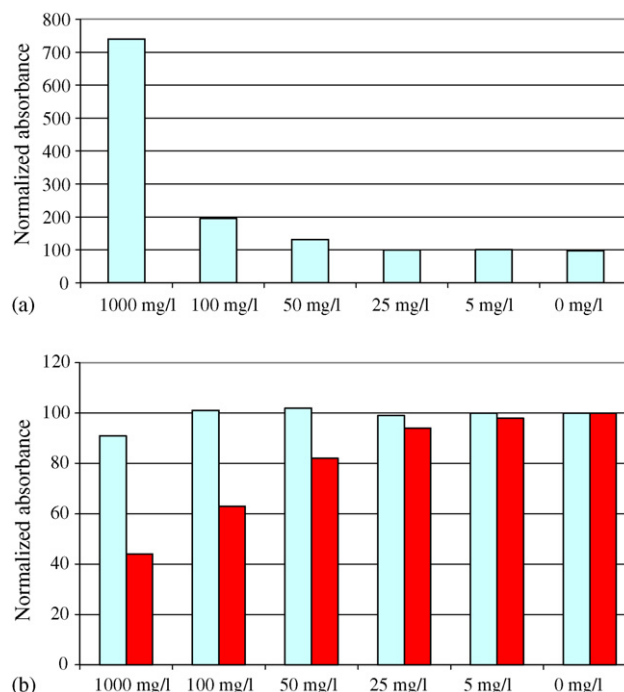


Fig. 2. Interference effect of the  $\text{SO}_4^{2-}$ ,  $\text{SiO}_4^{4-}$  and  $\text{PO}_4^{3-}$  anions on the determination of total inorganic arsenic: (a)  $\text{SiO}_4^{4-}$  (b)  $\square$   $\text{SO}_4^{2-}$  and  $\blacksquare$   $\text{PO}_4^{3-}$  ([As] = 4  $\mu\text{g l}^{-1}$ ). Normalized absorbance of 100 corresponding to the response obtained without interfering anions.

### 3.4. Precision and accuracy

The R.S.D. value of three replicate samples was below 4%, for the calibration range studied. Moreover, the short-term reproducibility values for the same sample (R.S.D. day to day) was lower than 5%, and the long-term reproducibility (month to month) was below 8%. The accuracy of the method was evaluated with analyses of the inorganic secondary reference material solution certified by EMPA (see Section 2.1). Our result was [As] = 5.1  $\pm 0.2 \mu\text{g l}^{-1}$ , in good agreement with the value of the diluted solution [As] = 5.0  $\pm 0.1 \mu\text{g l}^{-1}$ .

Table 6

Experimental recovery on arsenic determination by GFAAS in artificial and natural water samples spiked with As(V)

	As concentration ( $\mu\text{g l}^{-1}$ )	Recovery (%)
Artificial water + 2 $\mu\text{g l}^{-1}$	1.93 $\pm$ 0.11	93.3
Artificial water + 5 $\mu\text{g l}^{-1}$	5.08 $\pm$ 0.09	100.2
Artificial water + 8 $\mu\text{g l}^{-1}$	7.94 $\pm$ 0.07	98.4
Sample 1	4.69 $\pm$ 0.11	–
Sample 1 + 2 $\mu\text{g l}^{-1}$	6.56 $\pm$ 0.07	98.1
Sample 1 + 5 $\mu\text{g l}^{-1}$	9.85 $\pm$ 0.03	101.7
Sample 2	2.36 $\pm$ 0.12	–
Sample 2 + 2 $\mu\text{g l}^{-1}$	4.45 $\pm$ 0.11	102.1
Sample 2 + 5 $\mu\text{g l}^{-1}$	7.35 $\pm$ 0.05	99.9
Sample 3	0.65 $\pm$ 0.06	–
Sample 3 + 2 $\mu\text{g l}^{-1}$	2.43 $\pm$ 0.07	91.7
Sample 3 + 5 $\mu\text{g l}^{-1}$	5.54 $\pm$ 0.04	98.1

Table 7  
Comparison of the performance and characteristics between the GFAAS method optimized and two others methods used for arsenic determination without preliminary treatment

Analytical parameters	GFAAS (present study)	FI-HG-AAS [17]	LC-ICP-MS [28]
Arsenic species	Total inorganic arsenic	As(III) and As(V)	As(III), As(V), DMA, MMA
Linearity range	0.26–10 $\mu\text{g l}^{-1}$	10–100 $\mu\text{g l}^{-1}$	2–100 $\mu\text{g l}^{-1}$
Limit of detection (As(III), As(V))	0.26 $\mu\text{g l}^{-1}$	0.3 $\mu\text{g l}^{-1}$ (As(III)) 0.5 $\mu\text{g l}^{-1}$ (As(V))	0.2 $\mu\text{g l}^{-1}$ 0.1 $\mu\text{g l}^{-1}$ (DMA, MMA)
Precision	R.S.D. < 5%	R.S.D. < 3%	R.S.D. < 5%
Experimental recovery	91–105%	96–108%	80–110%
Interference	$\text{SO}_4^{2-}$ , $\text{SiO}_4^{4-}$ , $\text{PO}_4^{3-}$	$\text{Fe}^{3+}$ , $\text{Cu}^{2+}$ , $\text{Ni}^{2+}$ , $\text{Sb}^{2+}$ , $\text{Sn}^{4+}$ , $\text{Se}^{4+}$	$\text{Cl}^-$
Sample preparation preparation	No sample preparation except filtration and acidification (HCl)	No sample preparation except acidification (HCl)	No sample except filtration
Drinking water labs Instrument availability	Easily available	Easily available	Rare
Running cost	Low	Low	High
Time consuming	Rapid (20 samples per hour)	Very rapid (120 samples per hour)	Slow (6 samples per hour)

FI-HG-AAS: flow injection hydride generation atomic absorption spectrometry; LC-ICP-MS: liquid chromatography–inductively plasma mass spectrometry.

### 3.5. Interference studies

The effects of some cationic ( $\text{Na}^+$ ,  $\text{K}^+$ ,  $\text{Ca}^{2+}$ ,  $\text{Mg}^{2+}$ ,  $\text{Fe}^{2+}$  and  $\text{NH}_4^+$ ) species were studied by spiking at three different concentrations representing an excess of 250, 25,000, and 250,000 times the arsenic concentration ( $4 \mu\text{g l}^{-1}$ ): no interference was observed. Anionic species ( $\text{Cl}^-$ ,  $\text{SO}_4^{2-}$ ,  $\text{SiO}_4^{4-}$  and  $\text{PO}_4^{3-}$ ) were also tested.  $\text{Cl}^-$  did not induce interferences even with concentrations representing an excess of 250,000 times the arsenic concentration. Fig. 2b shows that if  $\text{SO}_4^{2-}$  slightly interfered in the total inorganic arsenic determination, serious interferences were due to  $\text{SiO}_4^{4-}$  (Fig. 2a) and  $\text{PO}_4^{3-}$  (Fig. 2b). Therefore, for an arsenic concentration of  $4 \mu\text{g l}^{-1}$ ,  $\text{SO}_4^{2-}$ ,  $\text{SiO}_4^{4-}$  and  $\text{PO}_4^{3-}$  can be tolerated without interference up to a 25,000-, 6000-, and 1000-fold excess, respectively.  $\text{PO}_4^{3-}$  caused the strongest interference effect, as expected due to the similar chemical properties of arsenate and phosphate [4]. The optimized method therefore allowed arsenic determination in drinking waters containing  $\text{SO}_4^{2-}$ ,  $\text{SiO}_4^{4-}$  and  $\text{PO}_4^{3-}$  of concentrations respectively lower than 100, 24 and  $4 \mu\text{g l}^{-1}$ .

### 3.6. Application of the method

This GFAAS arsenic determination method was used for analyses of various artificial and real groundwater samples, spiked with As(V). The recoveries of total inorganic arsenic concentration were calculated by comparing the average arsenic concentration of the replicate samples with the real value (measured initial value + spiked concentration) (Table 6). While the recovery percentages obtained were always higher than 91%, they were also higher than 98% for samples containing more than  $4.45 \mu\text{g l}^{-1}$  As. These results indicated that the procedure is suitable for arsenic analysis in waters.

## 4. Conclusion

A graphite furnace atomic absorption spectrometer with an UltrAA-Lamp<sup>®</sup> was optimized to determine total inorganic arsenic concentration at the  $\mu\text{g l}^{-1}$  level in water. This method needed no pre-concentration or separation step. The furnace pro-

gram was optimized by a proprietary data-processing software, ATOM<sup>®</sup>, and was applied with success to real life groundwaters. The use of an UltrAA-Lamp<sup>®</sup>, such as a hollow-cathode lamp, a Pd–Mg chemical matrix modifier and  $\text{HNO}_3$  as a thermal stabilizer lead to performances and characteristics comparable with two other common current analytical techniques used for arsenic determination but without sample preparation (Table 7). With a sample dispenser (Varian, mod. 31–972), 20 samples per hour can be analysed. The absence of pre-concentration/separation steps means that this is an economical, simple and sensitive technique for routine determination of trace amounts of total inorganic arsenic in water samples, below  $10 \mu\text{g l}^{-1}$ , the limit value currently recommended by regulatory agencies.

## Acknowledgements

This work was financially supported by the Project RITEAU of the French Government. JM receives a PhD stipend from the French Ministry of Universities. Arsenic studies at LSEE were made possible by grants from the Contrat de Plan Etat-Région Limousin and the Conseil Régional du Limousin. The authors thank Dr B. Serpaud for scientific discussions and comments.

## References

- [1] P.L. Smedley, D.G. Kinniburgh, Appl. Geochem. 17 (2002) 517.
- [2] B.K. Mandal, K.T. Suzuki, Talanta 58 (2002) 201.
- [3] T. Yoshida, H. Yamauchi, G.F. Sun, Toxicol. Appl. Pharmacol. 198 (2004) 243.
- [4] M.F. Hughes, Toxicol. Lett. 133 (2002) 1.
- [5] A.H. Smith, M.M.H. Smith, Toxicology 198 (2004) 39.
- [6] WHO, Arsenic Compounds Environmental Health Criteria 224, second ed., World Health Organisation, Geneva, 1996.
- [7] U.S. EPA, National Primary Drinking Water Regulation, Federal Register, vol. 66, 2001, p. 6976.
- [8] European Council Directive 98/83/EC, Off. J., 330 (1998) 32.
- [9] WHO Draft, Drinking Water Guidelines and Standards, World Health Organisation, Geneva, 2003 (Chapter 5).
- [10] K.A. Francesconi, D. Kuehnelt, Analyst 129 (2004) 373.
- [11] M. Burguera, J.L. Burguera, Talanta 44 (1997) 1581.
- [12] D.Q. Hung, O. Nebrassova, R.G. Compton, Talanta 64 (2004) 269.
- [13] M.C. Hsiang, Y.H. Sung, S.D. Huang, Talanta 62 (2004) 791.

- [14] R.B. McCleskey, D.K. Nordstrom, A.S. Maest, *Appl. Geochem.* 19 (2004) 995.
- [15] S. Latva, M. Hurta, S. Peräniemi, M. Ahlgrén, *Anal. Chim. Acta* 418 (2000) 11.
- [16] J. Aggett, A.C. Aspell, *Analyst* 101 (1976) 341.
- [17] N.M.M. Coelho, A. Cosmen da Silva, C. Moraes da Silva, *Anal. Chim. Acta* 460 (2002) 227.
- [18] K. Anazaki, I. Nakatsuka, K. Ohzenki, *Anal. Sci.* 15 (1999) 829.
- [19] V.R.A. Filho, K.G. Fernandes, M. De Moraes, J.A. Gomes Neto, *At. Spectrosc.* 23 (2002) 7.
- [20] D. Pozebon, V.L. Dressler, J.A. Gomes Neto, A.J. Curtius, *Talanta* 45 (1998) 1167.
- [21] F. Shemirani, M. Baghdadi, M. Ramezani, *Talanta* 65 (2005) 882.
- [22] E.C. Lima, J.L. Brasil, J.C.P. Vaghetti, *Talanta* 60 (2003) 103.
- [23] B. Welz, M. Sperling, *Atomic Absorption Spectrometry*, third ed., Wiley-VCH, Weinheim, 1999, pp. 485–486.
- [24] L. Bezur, *Microchem. J.* 59 (1998) 107.
- [25] V. Lenoble, C. Chabroulet, R. Al Shukry, B. Serpaud, V. Deluchat, J.C. Bollinger, *J. Colloid Interface Sci.* 280 (2004) 62.
- [26] D.E. Shrader, L.M. Voth, L.A. Covick, *Varian Instruments At Work, Application Notes AA-31*, Varian, Palo Alto, CA, 1983.
- [27] L.A. Currie, *Anal. Chim. Acta* 391 (1999) 105.
- [28] K.F. Akter, Z. Chen, L. Smith, D. Davey, R. Naidu, *Talanta* 68 (2005) 406.

## Peroxidase-like catalytic activity of Mn<sup>3+</sup>-octabromo-tetrakis(4-sulfophenyl)porphine on linoleate hydroperoxide and its analytical application

Masaki Mifune<sup>a,\*</sup>, Hidenori Kamiguchi<sup>b</sup>, Taka-aki Tai<sup>b</sup>, Seigo Kuremoto<sup>b</sup>, Makiko Yamamoto<sup>b</sup>, Ikuko Tsukamoto<sup>c</sup>, Madoka Saito<sup>b,c</sup>, Youji Kitamura<sup>a</sup>, Yutaka Saito<sup>a</sup>

<sup>a</sup> Department of Pharmaceutical Sciences, Graduate School of Medicine and Dentistry and Pharmaceutical Sciences, Okayama University, Tsushima-Naka, Okayama 700-8530, Japan

<sup>b</sup> Department of Pharmaceutical Chemistry, Graduate School of Natural Science and Technology, Okayama University, Tsushima-Naka, Okayama 700-8530, Japan

<sup>c</sup> Faculty of Medicine, Kagawa University, Ikenobe, Miki-Cho, Kagawa 761-0793, Japan

Received 16 March 2006; received in revised form 19 April 2006; accepted 19 April 2006

Available online 19 May 2006

### Abstract

To reveal an enzyme-like catalytic activity of metal-octabromo-tetrakis(sulfophenyl)porphines (M-OBPSs), their peroxidase-like catalytic activity on linoleate hydroperoxide (LOOH) were evaluated on the basis of dye-formation in the coloring reaction between *N,N*-diethylaniline and 4-aminoantipyrine that yields a quinoid-type dye. Among M-OBPSs tested, Mn<sup>3+</sup>-OBPS allowed to produce the largest amount of dye. The optimal conditions of the coloring reaction catalyzed by Mn<sup>3+</sup>-OBPS for the determination of LOOH were determined. A good linear calibration curve was obtained in the concentration range of 0.025–0.4 μmole LOOH with good reproducibility (coefficient of variance = 1.23%), suggesting that Mn<sup>3+</sup>-OBPS is a good artificial mimesis of the peroxidase for LOOH. In addition, Mn<sup>3+</sup>-OBPS was highly specific for LOOH even in the presence of cumene hydroperoxide or hydrogen peroxide. It was revealed that the peroxidase-like activity of Mn<sup>3+</sup>-OBPS is attributable to the redox cycle of Mn<sup>3+</sup> ↔ Mn<sup>4+</sup>.

© 2006 Elsevier B.V. All rights reserved.

**Keywords:** Linoleate hydroperoxide; Determination; Peroxidase; Metal-porphyrin

### 1. Introduction

Metal-porphyrin plays a central role for the activity of oxygen carriers such as hemoglobin and enzymes including catalase and peroxidase. Investigations into various metal porphyrins have been carried out for evaluating the enzyme-like catalytic activities, especially oxidative catalytic activities, such as superoxide dismutase (SOD) [1–3], cytochrome P450 [4,5] and peroxidase [6,7]. Other investigations were directed to the reaction between a metal porphyrin and peroxide, such as lipid hydroperoxide or the inhibitory effect of a metal porphyrin on peroxidation of a lipid [8]. Although an ordinary metal porphyrin exerts peroxidase- or catalase-like catalytic activities

in the presence of peroxides such as hydrogen peroxide, a catalytic reaction with such a metal porphyrin generally results in a suicide reaction [9]. For this reason, a metal porphyrin was not used as an enzyme-like catalyst in a liquid state and had to be immobilize on ion-exchanging resins or the like [10–12].

Recently, metal-octabromo-porphyrin derivatives having non-planar structure were synthesized, and SOD activity of Mn<sup>2+</sup>-octabromo-porphyrin, electric characteristics of metal-octabromo-tetrakis(sulfophenyl)porphine (M-OBPSs), or the like has been investigated [4,13–15]. The present study is focused on the application of a remarkable characteristic of M-OBPSs, i.e., high resistance to oxidation as compared to ordinary (not octabrominated) metal-porphyrins. It was expected that a M-OBPSs could exert a peroxidase-like catalytic activity in a liquid state, if it possesses the above-mentioned characteristic in the presence of a peroxide.

\* Corresponding author. Tel.: +81 86 251 7952; fax: +81 86 251 7953.  
E-mail address: [mifune@pharm.okayama-u.ac.jp](mailto:mifune@pharm.okayama-u.ac.jp) (M. Mifune).



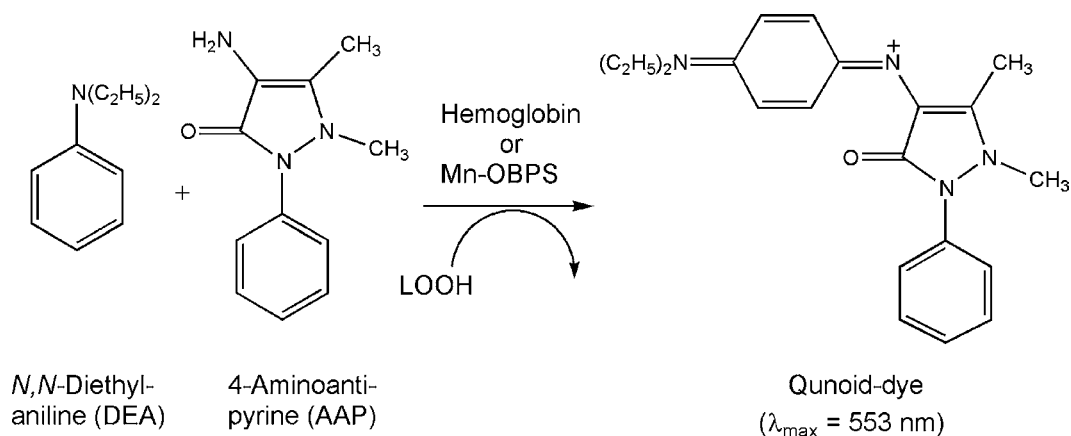


Fig. 1. Principle of determination of LOOH.

In this study, to reveal an enzyme-like catalytic activity of M-OBPSs, they were examined for the peroxidase-like activity on linoleate hydroperoxide (LOOH), one of organic peroxides, on the basis of dye-formation in the coloring reaction between *N,N*-diethylaniline (DEA) and 4-aminoantipyrine (AAP) as shown in Fig. 1, which reaction is catalyzed by hemoglobin [16]. It was revealed that one metal-octabromo-porphyrin,  $\text{Mn}^{3+}$ -octabromo-tetrakis(4-sulfophenyl)-porphine (Mn-OBPS), has the peroxidase-like activity and is possibly useful as a catalyst in the determination of LOOH.

## 2. Experimental

### 2.1. Reagents

Cu-tetraphenylporphine (Cu-TPP) and tetrakis(4-sulfoxyphenyl)porphine ( $\text{H}_2$ -TSPP) were purchased from Sigma–Aldrich Co. (St. Louis, MO, USA) and used as they were. Linoleic acid (super high grade) was purchased from Nacalai Tesque (Kyoto, Japan) and lipoxidase from Sigma–Aldrich Co.

Cumene hydroperoxide (COOH) and hydrogen peroxide were purchased from Nacalai Tesque and Wako Pure Chem. Co. (Osaka, Japan), respectively. The other reagents were of super high grade.

### 2.2. Synthesis of metal-octabromotetrakis(sulfophenyl)-porphine (M-OBPS, Fig. 2)

#### 2.2.1. Synthesis of $\text{H}_2$ -octabromotetrakisphenylporphine ( $\text{H}_2$ -OBPP)

Cu-OBPS was synthesized using Cu-TPP and bromine according to the method of Bhyrappa and Krishnan [17]. The resulting crude Cu-OBPP was dissolved in *n*-hexane and reprecipitated with acetone. After repeating these procedures, the resulting Cu-OBPP was dried in vacuo at 130 °C for 3 h and used in the experiments. The purity of the obtained Cu-OBPP was confirmed by elementary analysis.

$\text{H}_2$ -OBPP was prepared by demetalizing Cu-OBPP with 70% perchloric acid according to the method described in the literature [17]. The crude products were purified by re-precipitation from benzene/*n*-hexane.

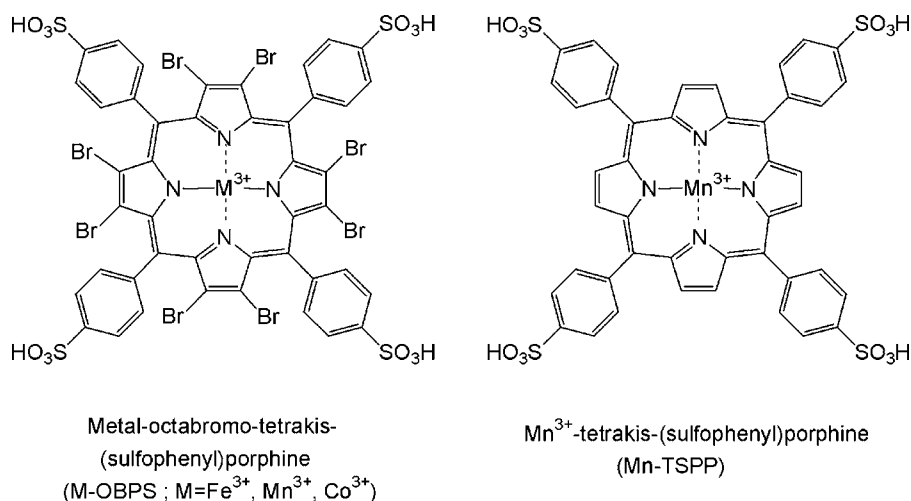


Fig. 2. Structures of metal-porphyrins.

### 2.2.2. Synthesis of M-OBPS

H<sub>2</sub>-OBPP was sulfonated by 97% sulfonic acid according to a method described in a literature [18]. The resulting crude H<sub>2</sub>-OBPS was purified by several times of re-precipitation. The re-precipitation involved repetitions of a process where crude products are dissolved in water and 36% hydrochloric acid is added. The precipitated crystals were washed with diluted hydrochloric acid, and dried over solid sodium hydroxide in vacuo to remove water and hydrogen chloride completely. The resultant H<sub>2</sub>-OBPS and corresponding metal chloride were used to synthesize Mn-, Co- and Fe-OBPSs according to a similar method that used for the synthesis of metal-TPPS [19].

### 2.3. Apparatus

Absorption spectra and absorbances were measured on a Shimadzu UV 160 or 180 spectrophotometer (Kyoto, Japan) with 10 mm fused-silica cells.

### 2.4. Preparation of sample solutions

A sample solution containing LOOH was prepared on demand in the following manners. First, a mixture of linoleic acid in ethanol (18 mg/ml, 10.0 ml), 0.05 mole/l boric acid–0.2 mole/l potassium hydroxide buffer (5.0 ml) and purified water (25.0 ml) was prepared. As need arises, lipoxidase solution (12560 U/ml, 5.0 ml) and purified water (70.0 ml) were added to the mixture (30.0 ml) and shaken at 20 °C for 1.0 h. The LOOH concentration was determined on the basis of molar absorption coefficient of conjugated diene ( $\epsilon = 2.7 \times 10^4$  l/cm/mole), and the solution was diluted with purified water appropriately to obtain LOOH sample solutions ( $2.5\text{--}40 \times 10^{-2}$   $\mu\text{mole/ml}$ ).

A COOH sample solution was prepared by diluting COOH with ethanol to a concentration of 0.50  $\mu\text{mole/ml}$ . A hydrogen peroxide sample solution was prepared by diluting hydrogen peroxide with purified water to a concentration of 0.60  $\mu\text{mole/ml}$ .

### 2.5. Recommend procedure for determination of LOOH

To an LOOH sample solution ( $2.5\text{--}40 \times 10^{-2}$   $\mu\text{mole/ml}$ , 1.0 ml) are added a chromogen solution (8.0 ml, 1:1:6 mixture of 1.0 mg/ml DEA, 1.0 mg/ml AAP and 0.1 mole/l pH 8.0 borate buffer solutions) and an aqueous  $1.0 \times 10^{-5}$  mole/l Mn-OBPS solution (1.0 ml), and the mixture is shaken briefly. The solution is allowed to stand at about 25 °C for 30 min. The LOOH concentration can be then determined from a calibration curve prepared using absorbance of quinoid-dye at 553 nm.

## 3. Results and discussion

In general, a catalytic activity such as peroxidase-like activity on LOOH is evaluated on the basis of initial rate of the reaction. However, from the viewpoint of developing analytical application, the catalytic activity was evaluated on the basis of the amount of the reaction product quinoid-dye, i.e., the absorbance of the reaction solution, in the present study.

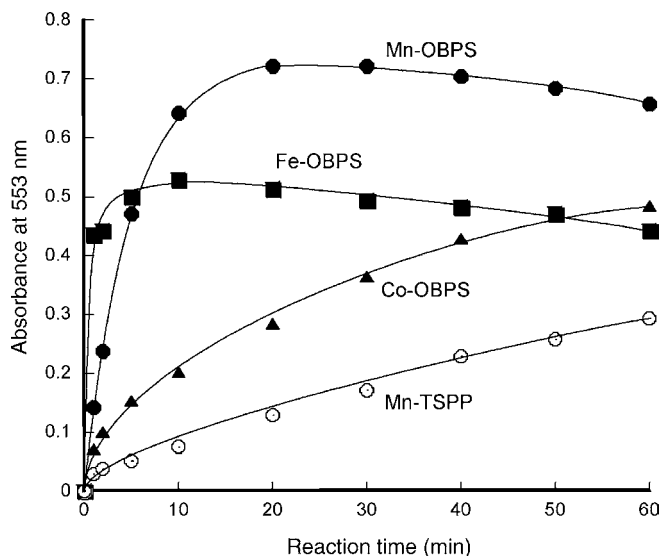


Fig. 3. Peroxidase-like activities of metal-porphyrins on LOOH. LOOH: 0.41  $\mu\text{mole/ml}$ , pH 8.0, 25 °C.

### 3.1. Effect of central-metal

Considering the results of previous studies on metal-porphyrins immobilized on carriers [10], Mn<sup>3+</sup>, Co<sup>3+</sup> and Fe<sup>3+</sup> were selected as a potentially active central metal. The effect of the central metal on the absorbance was examined with time. The results are shown in Fig. 3 together with that obtained using the non-brominated counterpart Mn-TSPP. It is clear from Fig. 3 that Mn-OBPS gives the largest amount of the dye and the highest absorbance. Mn-OBPS seems to have the most superior activity when evaluated on the basis of the amount of the dye. On the other hand, Fe-OBPS seems to have the most superior POD-like activity among the metal-OBPSs tested when evaluated on the basis of reaction rate. However, the amount of the dye produced with Fe-OBPS is only about 70% compared to that produced with Mn-OBPS. From these results, it was considered that Fe-OBPS acts as a scavenger of lipid peroxide as well a POD-like catalyst, or, alternatively, reacts with LOOH. Non-brominated Mn-TSPP showed lower reaction rate and produced less amount of the dye than Mn-OBPS, indicating that the bromination of porphyrin ring changes the activity greatly. Thus, the activity of M-OBPS depends on not only the central metal but also the porphyrin ring.

In the present study, the optimal conditions for determining LOOH were examined using mainly Mn-OBPS which gave the highest absorbance.

### 3.2. Determination of optimal condition

For the determination of optimal conditions, 1.0 ml of a 0.40  $\mu\text{mole/ml}$  LOOH sample solution was used.

#### 3.2.1. Effect of pH and reaction time

The effect of pH on absorbance was examined using Mn-OBPSs over the pH range of 4.0–11.0. The results are shown in Fig. 4. As can be seen from Fig. 4, the reaction solution contain-

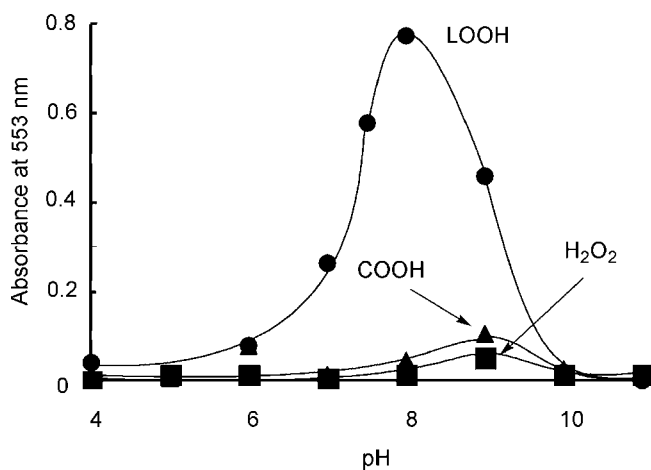


Fig. 4. Effect of pH. LOOH: 0.43  $\mu\text{mole/ml}$ ; COOH: 0.50  $\mu\text{mole/ml}$ ; hydrogen peroxide: 0.60  $\mu\text{mole/ml}$ , 25  $^{\circ}\text{C}$ .

ing Mn-OBPS showed the highest absorbance at pH 8.0. Thus, pH 8.0 was selected as the optimal pH for the determination of LOOH.

The reaction time at pH 8.0 was examined up to 60 min as shown in Fig. 3. The absorbance is almost highest when the reaction time is around 30 min. Accordingly, the reaction time was set to 30 min in the present study.

### 3.2.2. Effect of concentration of Mn-OBPS and chromogens

The effect of amount of Mn-OBPS to be used on the dye-formation was examined over the concentration range of  $1.0 \times 10^{-6}$  to  $1.0 \times 10^{-5}$  mole/l. It was revealed that both the reaction rate and the amount of the dye produced at the time of 30 min were increased as the concentration of Mn-OBPS became higher. In the present study,  $1.0 \times 10^{-5}$  mole/l of Mn-OBPS was selected. Although the reaction rate is improved when  $4 \times 10^{-5}$  mole/l or higher concentration of Mn-OBPS exists, such a higher concentration affects adversely to the determination of LOOH, since Mn-OBPS and resulting dye have the absorption band in the same region.

The amount of chromogens, DEA and AAP, to be used is then examined. The results are shown in Fig. 5. The both chromogens

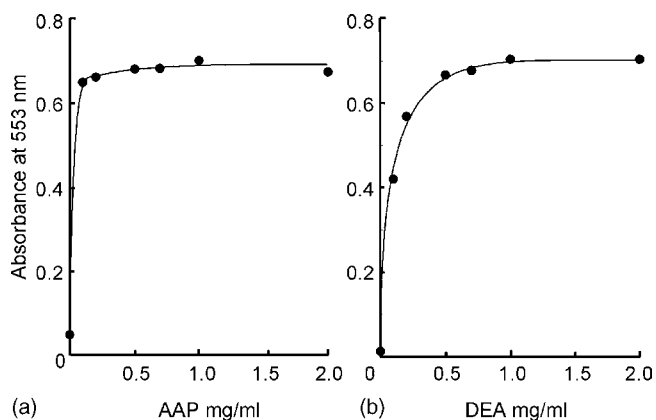


Fig. 5. Effect of concentration of chromogens on absorbance. LOOH: 0.40  $\mu\text{mole/ml}$ , pH 8.0, 30 min, 25  $^{\circ}\text{C}$  (a) in the presence of 1.0 mg/ml DEA and (b) in the presence of 1.0 mg/ml AAP.

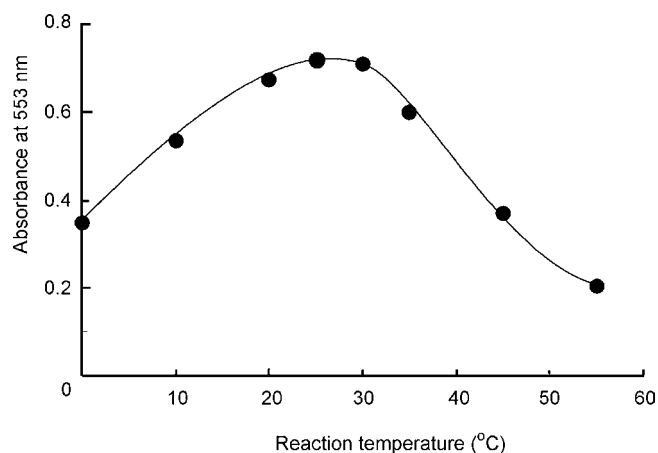


Fig. 6. Effect of reaction temperature. LOOH: 0.40  $\mu\text{mole/ml}$ , pH 8.0, 30 min.

can yield a sufficient amount of the dye when used as a 1.0 mg/ml solution. In the present study, 1.0 mg/ml of chromogen solutions were used.

### 3.2.3. Effect of temperature

The reaction temperature was examined over the temperature range of 0–55  $^{\circ}\text{C}$ . The results are shown in Fig. 6. It can be seen that the absorbance is highest at 25  $^{\circ}\text{C}$ . Accordingly, 25  $^{\circ}\text{C}$  was set as the optimal temperature.

### 3.3. Calibration curve and sensitivity

A calibration curve was prepared according to the recommended procedures above. This procedure was more convenient than those required when ion-exchange resins modified with metal-porphine was used [10], because filtration of the modified resins was unnecessary. A good linear curve passing the origin was obtained over the examined LOOH concentration range from 0.025 to 0.40  $\mu\text{mole/10 ml}$  ( $y = 1.6786x - 0.0022$ ,  $R^2 = 0.9999$ ). The apparent molar absorbance coefficient of LOOH was  $1.7 \times 10^4$  l/cm/mole. This value is twice as large and about threefold compared with that obtained using the modified resins and hemoglobin, respectively [10]. The variation coefficient is 1.23% at 0.40  $\mu\text{mole}$  LOOH indicating a good reproducibility. The lower and upper limits were around 0.02 and 0.6  $\mu\text{mole/10 ml}$ , respectively.

### 3.4. Specificity

The substrate specificity of Mn-OBPS was evaluated by examining the peroxidase-like activity on LOOH (0.40  $\mu\text{mole}$ ), COOH (0.50  $\mu\text{mole}$ ), an organic peroxide, and hydrogen peroxide (60  $\mu\text{mole}$ ) according to the recommended procedures described in Section 2.4. The results obtained between pH 4.0 and pH 11.0 are shown in Fig. 3. It is clear that, as for COOH and hydrogen peroxide, a slight amount of the dye was produced around pH 9.0, and the maximum absorbance was only 12 and 6% of that of LOOH in the cases of COOH and hydrogen peroxide, respectively. At pH 8.0, the maximum absorbance for these two substances was 4% or less of that for LOOH. These results indi-

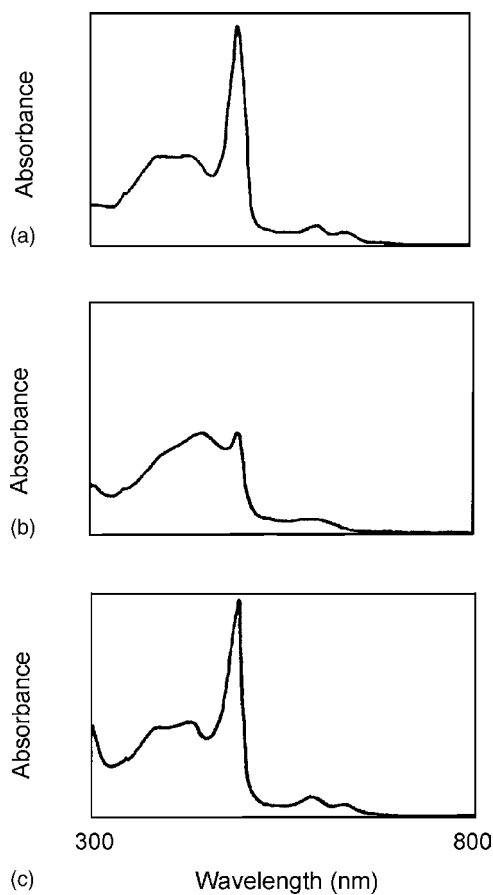


Fig. 7. UV/V absorption spectra of Mn-OBTS. (a) A mixture of  $5.0 \times 10^{-5}$  mole/l Mn-OBPS (1 ml) and pH 8.0 buffer (10 ml) solutions, (b) after adding a LOOH solution to the solution (a) and (c) after adding DEA solution to the solution (b).

cate that the method of determination developed in the present study is highly specific for LOOH even in the presence of other peroxides. In the case of the resins modified with Mn-TSPP, hydrogen peroxide gave larger absorbance than LOOH by 1.12 times [10]. Thus, it is of interest that octa-bromination of porphine-ring affects the specificity of the peroxidase-like catalytic activity.

### 3.5. Estimation of catalytic mechanism by UV/V spectra

According to the determination method used in the present study,  $1.0 \times 10^{-8}$  mole Mn-OBPS can promote the reaction of  $4.0 \times 10^{-7}$  mole LOOH, which means that Mn-OBPS catalyzes the reaction of 40 times or higher concentration of LOOH. To elucidate the mechanism of peroxidase-like catalytic action of Mn-OBPS, the UV/V spectra of Mn-OBPS in the presence of LOOH or a chromogen were investigated by using  $5.0 \times 10^{-5}$  mole/l Mn-OBPS solution, five fold more concentration. The results are shown in Fig. 7. The UV/V spectrum of the Mn-OBPS solution (Fig. 7a) was hardly changed by adding a solution of DEA, 4-AAP or a mixture of DEA and 4-AAP, indicating that Mn-OBPS does not interact through a coordination with neither DEA nor 4-AAP, or the coordination, if

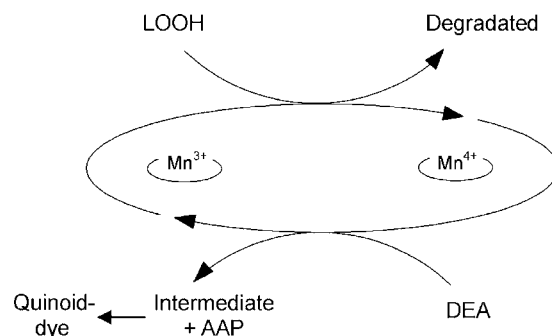


Fig. 8. Proposed reaction mechanism.

any, is not strong enough to affect the UV/V spectrum. On the other hand, when a solution of LOOH is added, the spectrum changed and the absorption band corresponding to  $\text{Mn}^{4+}$ -OBPS [8] became apparent as can be seen from Fig. 7b, indicating that manganese in Mn-OBPS was oxidized from  $\text{Mn}^{3+}$  to  $\text{Mn}^{4+}$  by LOOH. Further, adding DEA to the LOOH solution, spectrum (Fig. 7b) changed to spectrum (Fig. 7c) that is the same as Fig. 7a. Adding 4-AAP to the solution (Fig. 7b), however, did not change the spectrum. These results indicate that Mn-OBPS exerts the catalytic activity through the repeated redox cycles of  $\text{Mn}^{3+} \leftrightarrow \text{Mn}^{4+}$  which is caused by LOOH and DEA as illustrated in Fig. 8. Further, DEA, an electron donor [20,21], seems to serve as an intermediate and reacts with 4-AAP to form the quinoid-dye.

## 4. Conclusion

As we have expected, Mn-OBPS exhibits a potent peroxidase-like activity on LOOH around neutral pH region and is useful for the specific determination of LOOH. Further, this activity was revealed to be attributable to the redox cycle of  $\text{Mn}^{3+} \leftrightarrow \text{Mn}^{4+}$ . Hopefully, the method of determining LOOH developed in the present study will be widely applied to the analysis of LOOH and contribute to analytical chemistry involving LOOH.

## References

- [1] N. Nagami, H. Umakoshi, T. Shimanouchi, R. Kuboi, *Biochem. Eng. J.* 21 (2004) 221–227.
- [2] I. Batinić-Haberle, S.I. Liochev, I. Spasojević, I. Fridovich, *Arc. Biochem. Biophys.* 342 (1997) 225–233.
- [3] F. Tani, M. Matsu-ura, S. Nakayama, Y. Naruta, *Coord. Chem. Rev.* 226 (2002) 219–226.
- [4] E. do Nascimento, G. de, F. Silva, F.A. Caetano, M.A.M. Fernandes, D.C. da Silva, M.E. de Carvalho, J.M. Pernaut, J.S. Rebouças, Y.M. Idemori, *J. Inorg. Biochem.* 99 (2005) 1193–1204.
- [5] V. Cantonetti, D. Monti, M. Venanzi, C. Bombelli, F. Ceccacci, G. Mancini, *Tetrahedron Asym.* 15 (2004) 1969–1977.
- [6] A. Sánchez-Sandval, D. Ramírez-Rosales, R. Zamorano-Ulloa, C. Álvarez-Toledano, M. Moya-Cabrera, Y. Reyes-Ortega, *Biophys. Chem.* 106 (2003) 253–265.
- [7] S. Ozaki, T. Matsui, M.P. Roach, Y. Watanabe, *Coord. Chem. Rev.* 198 (2000) 39–59.
- [8] A. Bloodsworth, V.B. O'Donnell, I. Batinić-Haberle, P.H. Chumley, J.B. Hurt, B.J. Day, J.P. Crow, B.A. Freeman, *Free Radic. Biol. Med.* 28 (2000) 1017–1029.

- [9] B. Valderrama, M. Ayala, R. Vazquez-Duhalt, *Chem. Biol.* 9 (2002) 555–565.
- [10] M. Mifune, T. Tai, A. Iwado, H. Akizawa, J. Oda, N. Motohashi, Y. Saito, *Talanta* 54 (2001) 319–327.
- [11] M. Mifune, D. Hino, H. Sugita, A. Iwado, Y. Kitamura, N. Motohashi, I. Tsukamoto, Y. Saito, *Chem. Pharm. Bull.* 53 (2005) 1006–1010.
- [12] H. Türk, H. Berber, *Int. J. Chem. Kinetics* 32 (2000) 271–278.
- [13] P. Hoffmann, G. Labat, A. Robert, B. Meunier, *Tetrahedron Lett.* 31 (1990) 1991–1994.
- [14] Q. Chen, D. Li, Q. Ahu, H. Yang, H. Zheng, J. Xu, *Anal. Chim. Acta* 406 (2000) 209–215.
- [15] F. D'Souza, Y. Hsieh, G.R. Deviprosad, *J. Porphy. Pthal.* 2 (1998) 429–437.
- [16] S. Ozaki, T. Matsui, M.P. Roach, Y. Watanabe, *Coord. Chem. Rev.* 198 (2000) 39–59.
- [17] P. Bhyrappa, V. Krishnan, *Inorg. Chem.* 30 (1991) 239–245.
- [18] E.B. Fleischer, J.M. Palmer, T.S. Srivastave, A. Chatterjee, *J. Am. Chem. Soc.* 93 (1971) 3162–3167.
- [19] A. Iwado, M. Mifune, J. Kato, J. Oda, M. Chikuma, N. Motohashi, Y. Saito, *Chem. Pharm. Bull.* 48 (2000) 1831–1832.
- [20] R. Liantonio, S. Luzzati, P. Metrangolo, T. Pilati, G. Resnati, *Tetrahedron* 58 (2002) 4023–4029.
- [21] A. Chakraborty, D. Seth, D. Chakraborty, P. Harza, N. Sarkar, *Chem. Phys. Lett.* 405 (2005) 18–25.



# Determination of trace metals by ICP-OES in plant materials after preconcentration of 1,10-phenanthroline complexes on activated carbon

Barbara Mikuła\*, Bożena Puzio

*Institute of Chemistry, Silesian University, 40-006 Katowice, Poland*

Received 11 February 2004; received in revised form 14 February 2006; accepted 17 March 2006

Available online 8 May 2006

## Abstract

In this work, 1,10-phenanthroline was used as a complexing agent for the separation and preconcentration of Cd(II), Co(II), Ni(II), Cu(II) and Pb(II) on activated carbon. The metals were adsorbed on activated carbon by two methods: static (1) and dynamic (2). The optimal condition for separation and quantitative preconcentration of metal ions with activated carbon for the proposed methods was for (1) in the static methods in the pH range 7–9. The desorption was found quantitative with 8 mol dm<sup>-3</sup> HNO<sub>3</sub> for Cd(II) (92.6%), Co(II) (95.6%), Pb(II) (91.0%), and with 3 mol dm<sup>-3</sup> HNO<sub>3</sub> for Cd(II) (95.4%), Pb(II) (100.2%). The preconcentration factor was 100 with R.S.D. values between 1.0 and 2.9%. For (2), the dynamic method (SPE), the pH range for the quantitative sorption was 7–9. The desorption was found quantitative with 8 mol dm<sup>-3</sup> HNO<sub>3</sub> for Cd(II) (100.6%), Pb(II) (94.4%), and reasonably high recovery for Co(II) (83%), Cu(II) (88%). The optimum flow rate of metal ions solution for quantitative sorption of metals with 1,10-phenanthroline was 1–2 cm<sup>3</sup> min<sup>-1</sup> whereas for desorption it was 1 cm<sup>3</sup> min<sup>-1</sup>. The preconcentration factor was 50 for all the ions of the metals with R.S.D. values between 2.9 and 9.8%.

The samples of the activated carbon with the adsorbed trace metals can be determined by ICP-OES after mineralization by means of a high-pressure microwave mineralizer. The proposed method provides recovery for Cd (100.8%), Co (97.2%), Cu (94.6%), Ni (99.6%) and Pb (100.0%) with R.S.D. values between 1.2 and 3.2%.

The preconcentration procedure showed a linear calibration curve within the concentration range 0.1–1.5 μg cm<sup>-3</sup>. The limits of detection values (defined as “blank + 3s” where *s* is standard deviation of the blank determination) are 5.8, 70.8, 6.7, 24.6, and 10.8 μg dm<sup>-3</sup> for Cd(II), Pb(II), Co(II), Ni(II) and Cu(II), respectively, and corresponding limit of quantification (blank + 10s) values were 13.5, 151.3, 20.0, 58.9 and 33.2 μg dm<sup>-3</sup>, respectively.

As a result, these simple methods were applied for the determination of the above-mentioned metals in reference materials and in samples of plant material.

© 2006 Elsevier B.V. All rights reserved.

**Keywords:** ICP-OES; 1,10-Phenanthroline; Activate carbon

## 1. Introduction

The determination of elements is usually preceded by their separation from the major components (matrix) of the sample, and it involves simultaneous preconcentration of the trace components.

Activated carbon is widely use a trace collector for multi-element preconcentration in analysis of water, high-purity substances, vegetable sample, etc. There are two general approaches to metal preconcentration using activated carbon, namely from

aqueous solution by simply adjusting the pH to an adequate value and by using a chelating agent.

A literature survey revealed that enrichment of heavy metals on actived carbon is usually carried out after chelation with 8-hydroxyquinoline [1–6], cupferron [7,8], dithiocarbamates [9–12], dithizone [13,14], potassium ethylxanthate [15,16], chrome azurol S [17] or the ammonium salt of dithiophosphoric acid *O,O*-diethyl ester [18]. Following desorption in a small volume of nitric acid, the metal concentration are measured by AAS or ICP-OES.

Zhang et al. [19] presents a method where by trace elements are adsorbed in NH<sub>4</sub>Cl–NH<sub>3</sub> medium on activated carbon and then determined by microwave plasma torch atomic emission spectrometry.

\* Corresponding author. Fax: +48 32 599978.

E-mail address: [bmikula@us.edu.pl](mailto:bmikula@us.edu.pl) (B. Mikuła).

1,10-Phenanthroline has been used as a complexing reagent for preconcentration trace metals [20–24].

Problems in using activated carbons for analytical work are related to the large variations in the physical and chemical properties of the different sources of carbon and difficulty in obtaining full desorption of organic and inorganic analytes.

The aim of the present work was to investigate activated carbon for the preconcentration and separation of cadmium, copper, nickel, cobalt and lead traces. 1,10-Phenanthroline was used as a complexing agent. The model system was used for the determination of heavy metals in plant materials.

## 2. Experimental

### 2.1. Apparatus and conditions

Mineralizer M-9 (WSL, Bytom); Mineralizer microwaves UniClever (Plasmatronika); Spectroflame, ICP Model M (Spectro Analytical Instruments).

The sequential spectrometer was used with following parameters: frequency, 27.12 MHz; power, 1.1 kW; demountable quartz torch, Ar/Ar/Ar; coolant gas Ar, 14.0 l min<sup>-1</sup>; auxiliary gas Ar, 0.5 l min<sup>-1</sup>; nebulizer gas Ar, 1.0 l min<sup>-1</sup>; nebulizer pressure, 2.4 bar; glass spray chamber according to Scott, sample flow rate, 1.0 ml min<sup>-1</sup>; observation height 11 mm; holographic grating, 2400 grooves mm<sup>-1</sup>; dispersion of grating in the first reciprocal order, 0.55 nm mm<sup>-1</sup>; wavelength range of monochromator 165–460 nm; integration time, 3 s. The wavelengths for Cd, 226.50 nm; Pb, 220.35 nm; Ni, 352.45 nm; Co, 228.62 nm; Cu, 324.75 nm.

### 2.2. Reagents

Standard solutions Cd(II), Cu(II), Pb(II), Ni(II) and Co(II) of concentration 1 mg dm<sup>-3</sup> (Merck). Activated carbon (AC), powder (J.T. Baker); 1,10-phenanthroline (POCH); conc. HNO<sub>3</sub> (POCH); H<sub>2</sub>O<sub>2</sub> 30% (POCH). All reagents used were of analytical or ultrapure grade. The water used for synthetic solutions was doubly distilled in a quartz apparatus. The 1,10-phenanthroline was prepared by dissolving 0.496(5) g of the reagent in 0.25 dm<sup>3</sup> of doubly distilled water.

### 2.3. Preconcentration procedure

The procedure of the concentration of cadmium, copper, nickel, cobalt and lead by adsorption on activated carbon with the use of 1,10-phenanthroline was as follows.

Activated carbon powder (J.T. Baker) was kept in nitric acid (1:1) solution for 24 h so as to remove the metal ions and other impurities sorbed on it. Then it was filtered and rinsed with doubly distilled water until it was free from acid. It was dried in a drying furnace at 110 °C. The complexing reagent and the activated carbon were added to a beaker with the 50 cm<sup>3</sup> model solution containing 5 µg each Pb(II), Co(II), Cu(II), Ni(II) and Cd(II). The pH of the solution was adjusted to desired value (pH ≈ 7). The required pH of the solution was adjusted by adding 0.1 mol dm<sup>-3</sup> hydrochloric acid or 0.1 mol dm<sup>-3</sup> sodium hydroxide.

The activated carbon, after the metals sorption, was rinsed with water and dissolved in 10 cm<sup>3</sup> of 3 and 8 mol dm<sup>-3</sup>. The metals concentration was determined with ICP-OES.

#### 2.3.1. Preconcentration of activated carbon by static method

A 10 cm<sup>3</sup> of the complexing reagent (0.01 mol dm<sup>-3</sup> 1,10-phenanthroline solution) and 0.1 g activated carbon were added to the sample and diluted to 50 cm<sup>3</sup>. The mixture was stirred with a magnetic bar for 25 min. Then the sample was prepared in two ways.

In the first method, the sample was filtered through a filter paper, rinsed with water and dissolved in 10 cm<sup>3</sup> of 3 and 8 mol dm<sup>-3</sup> HNO<sub>3</sub>.

In the second method, the mixture was filtered through a small filter paper (Millipore). Then a filter paper covered with activated carbon was mineralized by adding 3 cm<sup>3</sup> of nitric acid in a microwave mineralizer. The obtained solution was diluted to the volume of 10 cm<sup>3</sup>.

#### 2.3.2. Column method

The 500 mg of activated carbon was packed in a column SPE-PP (polypropylene-size 3 cm<sup>3</sup>).

The sample solution containing 5 µg Cd(II), Cu(II), Pb(II), Ni(II) and Co(II) and 2 cm<sup>3</sup> of 1,10-phenanthroline solution (pH ≈ 7.0) was passed through the columns filled with activated carbon after adjusting its pH to an optimum value at a flow rate of 1 cm<sup>3</sup> min<sup>-1</sup> used by BAKERBOND SPE system. The metals were then desorbed from the column with 10 cm<sup>3</sup> of 8.0 mol dm<sup>-3</sup> nitric acid.

#### 2.3.3. Mineralization of plant materials

The 1 g sample of potatoes of 1 mm grain size, dried previously to the constant air-dry mass was mineralized by adding 10 cm<sup>3</sup> of HNO<sub>3</sub> and H<sub>2</sub>O<sub>2</sub> (*t* ≈ 190 °C) in a mineralizer M-9. Then the obtained solution was diluted to the volume of about 50 cm<sup>3</sup>. The prepared samples were neutralized to pH 7–8 with the sodium hydroxide solution.

## 3. Results and discussion

The application of activated carbon for enrichment of trace elements in different materials is often presented in the analytical procedures. However, better results are to be expected when the metals are complexed with organic chelating agents before adsorption on AC. For these reasons 1,10-phenanthroline was chosen in this work as a complexing agent for enrichment on AC.

It was proved experimentally that nitric acid slightly influenced the simultaneous determination of Pb(II), Co(II), Cu(II), Ni(II) and Cd(II) by the ICP-OES method. Model standard curves (for the solutions containing the matrix reagents) were linear in the concentration range 0.1–1.5 µg cm<sup>-3</sup> for Cd, Cu, Ni, Co and 0.2–1.5 µg cm<sup>-3</sup> for Pb.

In the literature there are two methods proposed. One of them requires the complex compound to be added to the sample first and then adsorbed on the activated carbon. In the second, the

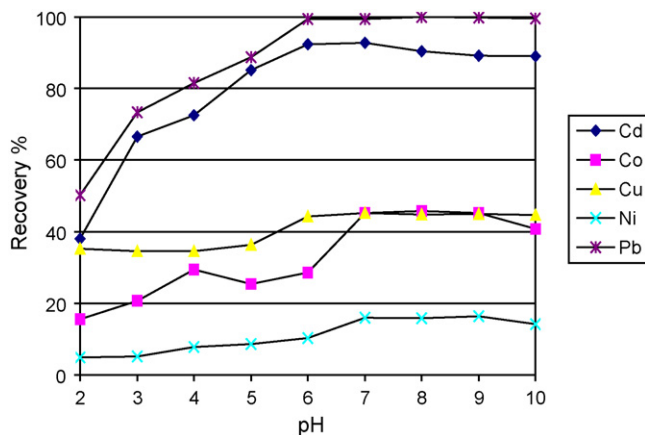


Fig. 1. The effect of pH on the recovery of metals with 1,10-phenanthroline by static method.

activated carbon is modified with a complexing reagent before contact with the ions of the metal. In this work the first method was applied.

In order to obtain quantitative recoveries of the metal ions on the activated carbon, the preconcentration procedure was optimized for the various analytical parameters such as sample preparation, pH, amount of activated carbon, complexing reagent, factor preconcentration and the stirring time were studied.

The effect of pH on the separation of metal ions was studied in the range 2–10, keeping the other parameters constant. As shown in Fig. 1, the optimum pH range for quantitative recoveries of Cu, Ni, Pb, Cd and Co was above 7. The effect of amount of activated carbon and 1,10-phenanthroline was examined in the range 50–300 mg and 5–20 cm<sup>3</sup> of 0.01 mol dm<sup>-3</sup> solution, respectively. In the proposed procedure, 100 mg AC and 10 cm<sup>3</sup> of 0.01 mol dm<sup>-3</sup> 1,10-phenanthroline were recommended for quantitative sorption of metal ions. For the 300 mg AC and above, the preconcentration was not quantitative. The stirring time of the solution was tested in the range 10–40 min. The result of the stirring time effect demonstrated that the sorption of the complex was quantitative after 25 min.

For the group desorption Pb(II), Co(II), Cu(II), Ni(II) and Cd(II), 8 mol dm<sup>-3</sup> of eluent (nitric acid) proved to be efficient. However, for the desorption of Cd(II) and Pb(II), it was sufficient to apply 3 mol dm<sup>-3</sup> HNO<sub>3</sub> as an eluent, obtaining almost 100% recovery of metals (Table 1). The results showed that des-

Table 1

Effect on the concentration of elution solutions on results of determination of heavy metals after preconcentration on AC with 1,10-phenanthroline by the static method

C <sub>HNO<sub>3</sub></sub> (mol dm <sup>-3</sup> )	Recovery (%)				
	Cd	Co	Cu	Ni	Pb
3	95.4	81.4	45.2	21.4	100.2
4	95.2	94.2	50.8	21.8	99.4
5	94.0	86.3	69.8	22.0	98.6
6	93.6	90.0	70.4	35.4	96.0
7	93.2	93.2	67.6	36.0	93.0
8	92.6	95.6	78.4	42.6	92.6
9	86.8	93.8	74.1	41.2	90.0
10	84.4	93.6	70.5	46.6	85.6

pH 7–8; 10 cm<sup>3</sup> eluent volume; ligand: 0.01 mol dm<sup>-3</sup> 1,10-phenanthroline.

orption was not quantitative for nickel and copper. Therefore, the activated carbon with adsorbed metals was mineralized with 3 cm<sup>3</sup> of nitric acid. The results presented in Table 2 confirm the efficiency of preconcentration of metals on activated carbon using 1,10-phenanthroline. Difficulties with the elution of adsorbed metals are probably due to formation of metal complexes strongly adsorbed on activated carbon.

This procedure was also applied to the preconcentration of the investigated elements by the column method. The influence of the flow rate in the range 1.0–3.0 cm<sup>3</sup> min<sup>-1</sup> on the sorption of metals into SPE and elution was studied. The preconcentration and elution flow rate was quantitative for this range and hence 1.0 cm<sup>3</sup> min<sup>-1</sup> was chosen for preconcentration and elution in the later studies. Table 2 shows the results of the preconcentration of the complexes of metal ions with 1,10-phenanthroline by the static and column method. The results of the preconcentration in column method gave good R.S.D. but recoveries of the elements were lower than in the static method. Quantitative preconcentration and elution of metals was obtained by increasing the dilution of 5 µg metal ions in the range 25–500 cm<sup>3</sup> (final volume: 10 cm<sup>3</sup>). The enrichment factor was found to be approximately 50. The limit of detection values (defined as “blank + 3s” where *s* is the standard deviation of the blank determination) were 5.8, 70.8, 6.7, 24.6, and 10.8 µg dm<sup>-3</sup> for Cd(II), Pb(II), Co(II), Ni(II) and Cu(II), respectively. The corresponding limit of quantification (blank + 10s) values were 13.5, 151.3, 20.0, 58.9 and 33.2 µg dm<sup>-3</sup>, respectively.

Table 2

Results of analysis of metal ions by ICP-OES after preconcentration on AC

M	Column method, elution		Static method			
	Recovery (%)	R.S.D. (%)	Elution		Mineralized AC	
			Recovery (%)	R.S.D. (%)	Recovery (%)	R.S.D. (%)
Cd	100.6	2.9	92.6	2.9	100.8	3.1
Co	83.0	9.0	95.4	2.6	97.2	3.2
Cu	87.6	9.4	78.6	1.0	94.6	2.4
Ni	24.6	9.0	39.4	3.0	99.6	1.2
Pb	94.4	9.8	91.0	2.7	100.0	2.3

pH 7–8; eluent: 10 cm<sup>3</sup> of 8 mol dm<sup>-3</sup> HNO<sub>3</sub>; ligand: 0.01 mol dm<sup>-3</sup> 1,10-phenanthroline.

Table 3

Results of determining of Cd, Pb, Co, Ni and Cu in references material (oriental tobacco leaves, CTA-OTL-1) by ICP-OES methods after preconcentration of metals with 1,10-phenanthroline on activated carbon

Metal	Certified value ( $\mu\text{g g}^{-1}$ )	Determined ( $\mu\text{g g}^{-1}$ )		
		Column method, elution	Static method	
			Elution	Mineralize AC
Cd	1.12 ± 0.12	1.07 ± 0.13	1.05 ± 0.06	1.15 ± 0.07
Pb	4.91 ± 0.80	5.25 ± 0.1	5.31 ± 0.08	5.02 ± 0.01
Co	0.879 ± 0.039	0.70 ± 0.09	0.84 ± 0.06	0.89 ± 0.01
Ni	6.32 ± 0.65	1.28 ± 0.07	1.55 ± 0.08	6.25 ± 0.09
Cu	14.1 ± 0.5	14.1 ± 0.1	6.0 ± 0.1	13.9 ± 0.1

pH 7–8; eluent:  $10\text{ cm}^3$  of  $8\text{ mol dm}^{-3}$   $\text{HNO}_3$ ; ligand:  $0.01\text{ mol dm}^{-3}$  1,10-phenanthroline.

Different amounts of the metals were preconcentrated by the proposed methods in the range 1.0–15  $\mu\text{g}$  in  $500\text{ cm}^3$  solution. The R.S.D. and the average recovery preconcentration were comparable (Table 2).

In order to establish the validity of the proposed procedure, the method has been applied to the determination of the content of the studied elements in standard reference material-oriental tobacco leaves (CTA-OTL-1). The results of the metal analyses after preconcentration on activated carbon using two different methods (the static and column methods) are reported in Table 3. The use of both methods gave good recovery for cadmium, lead and cobalt. Only the recovery obtained for copper and nickel in the references material was significantly lower, but recovery of metals was comparable with the values obtained for the model solutions, and can also be applied to determine the approximate contents of these metals.

The AC mineralization method allowed to obtain about 100% recovery.

These results proved also that the procedure can be applied satisfactorily for the determination of metals in contaminated samples of plant materials. The preconcentration procedures were applied to the determination of Co(II), Pb(II), Ni(II), Cd(II) and Cu(II) in potatoes by ICP-OES (Table 4). The R.S.D. values were less than 10%. In the investigated samples of plant material, in spite of the application of separation and preconcentration methods, traces of cobalt were found, but the amount was below the detection limit.

Table 4

Results of Cd, Co, Cu, Ni and Pb in potatoes by ICP-OES method

Metal	Determined ( $\mu\text{g g}^{-1}$ )		
	Column method, elution	Static method	
		Elution	Mineralized AC
Cd	0.41 ± 0.04	0.41 ± 0.02	0.38 ± 0.02
Co	<0.1	<0.1	<0.1
Cu	4.1 ± 0.1	5.2 ± 0.3	4.82 ± 0.06
Ni	0.22 ± 0.01	0.26 ± 0.03	0.50 ± 0.09
Pb	0.91 ± 0.06	1.3 ± 0.1	0.91 ± 0.07

pH 7–8; eluent:  $10\text{ cm}^3$  of  $8\text{ mol dm}^{-3}$   $\text{HNO}_3$ ; ligand:  $0.01\text{ mol dm}^{-3}$  1,10-phenanthroline.

Preconcentrating of heavy metals on activated carbon by the static and column methods, using elution with proper acid, recovery of some metals was not quantitative. That is why mineralization of activated carbon with adsorbed metals was preferred.

#### 4. Conclusion

The proposed static and column methods of the preconcentration of Co(II), Pb(II), Ni(II), Cd(II) and Cu(II) as complexes with 1,10-phenanthroline with the use of activated carbon were found simple and accurate. The static method may be used for preconcentration and determination of Cd, Co and Pb. For preconcentration of Cd and Pb, the static and column methods may be applied. However, for the group determination of the metals, mineralization of activated carbon with adsorbed metals was proposed. It was found that there was no significant difference between achieved results by proposed methods and certified results. The methods of preconcentration of heavy metals can be used for their determination in plant materials by the ICP-OES.

#### References

- [1] B.M. Vanderborcht, R.E. Van Grieken, *Anal. Chem.* 49 (1977) 311.
- [2] J. Shiowatana, K. Benyatiab, A. Siripinyanond, *At. Spectrosc.* 21 (2000) 179.
- [3] L.F. Kozin, N.V. Mashkova, F.D. Manilevich, *Russ. J. Appl. Chem.* 73 (2000) 1162.
- [4] Y. Sakai, T. Tomura, K. Ohshita, S. Koshimizu, *J. Radioanal. Nucl. Chem.* 230 (1998) 261.
- [5] S. Cerutti, M.F. Silva, J.A. Gaseguez, R.A. Olsina, L.D. Martinez, *Spectrochim. Acta B* 58 (2003) 43.
- [6] Y. Okamoto, A. Murata, T. Kumamura, *Anal. Sci.* 7 (1991) 879.
- [7] M. Yaman, S. Gucer, *Ann. Chim.* 88 (1998) 555.
- [8] M. Yaman, *J. Anal. At. Spectrom.* 14 (1999) 27.
- [9] M. Soyak, L. Elci, M. Dogan, *Fresenius Environ. Bull.* 5 (1996) 148.
- [10] R. Tezcan, H. Tezcan, *Fresenius Environ. Bull.* 5 (1996) 156.
- [11] L. Monser, N. Adhoum, *Sep. Purif. Technol.* 26 (2002) 137.
- [12] M. Kimura, K. Kawanami, *Talanta* 26 (1979) 901.
- [13] E. Jackwerth, J. Lohmar, G. Wittler, *Fresenius Z. Anal. Chem.* 266 (1973) 1.
- [14] E. Beinrohr, J. Rojcek, J. Garaj, *Analyst* 113 (1988) 1831.
- [15] M. Kimura, *Talanta* 24 (1997) 194.

- [16] P.R. Devi, G.R.K. Naidu, *Analyst* 115 (1990) 1469.
- [17] A.J. Ambrose, A.L. Ebdon, P. Jones, *Anal. Proc.* 26 (1989) 337.
- [18] V.L.A. Monte, A.J. Curtius, *J. Anal. At. Spectrom.* 5 (1990) 21.
- [19] H. Zhang, X. Yuan, X. Zhao, O. Jin, *Talanta* 44 (1997) 1615.
- [20] M. Ali Taher, B.K. Puri, *Indian J. Chem. A* 42 (2003) 2963.
- [21] M. Ali Taher, *Indian J. Chem. Technol.* 10 (2003) 661.
- [22] M. Ali Taher, *Bull. Korean Chem. Soc.* 24 (2003) 1177.
- [23] M. Ali Taher, *Chem. Anal. (Warsaw)* 47 (2002) 147.
- [24] A. Ali, X. Yin, H. Shen, Y. Ye, X. Gu, *Anal. Chim. Acta* 392 (1999) 283.



# A novel method for flow injection analysis of total antioxidant capacity using enzymatically produced ABTS<sup>•+</sup> and biamperometric detector containing interdigitated electrode

Stjepan Milardovic<sup>a,\*</sup>, Irena Kereković<sup>a</sup>, Romano Derrico<sup>a</sup>, Vlatko Rumenjak<sup>b</sup>

<sup>a</sup> Department of General and Inorganic Chemistry, Faculty of Chemical Engineering and Technology, University of Zagreb, Marulićev trg 19, HR-10000 Zagreb, Croatia

<sup>b</sup> Sveti duh General Hospital, Sveti duh 64, Hr-10000 Zagreb, Croatia

Received 15 November 2005; received in revised form 20 March 2006; accepted 23 March 2006

Available online 2 May 2006

## Abstract

Application of interdigitated array microelectrodes as electrochemical sensors for determination of antioxidant capacity is reported. Electrochemical measurements with interdigitated electrodes (IDE) were studied in both stationary solutions and the flow system. The method is based on biamperometric measurements using ABTS<sup>•+</sup>|ABTS redox couple in phosphate buffer solution, pH 7.40. During analysis, the ABTS radical cation was enzymatically produced by peroxidase in a tubular flow-through reactor. The performance of bioreactor was tested at different concentrations of immobilized enzyme, ABTS and hydrogen peroxide. The influence of flow rate on proper operation of the bioreactor was also studied. The results of antioxidant activity were determined using Trolox as a standard. The applied IDE detector accomplished good sensitivity of 0.3 nA/μM of Trolox and offered linear range between 20 to 500 μM of Trolox.

The comparison of results ( $R^2 = 0.9915$ ) for antioxidant activity between spectroscopic and FIA biamperometric measurements by interdigitated electrodes confirmed the applicability of the proposed method for determination of antioxidant capacity.

© 2006 Elsevier B.V. All rights reserved.

**Keywords:** Interdigitated electrodes; Antioxidant; ABTS<sup>•+</sup>|ABTS redox couple; Biamperometry; Trolox

## 1. Introduction

Interdigitated electrodes (IDE) have various advantages concerning their ability to enhance the current response, and offer higher sensitivity than the macro-electrode. Therefore interdigitated electrode has been used in a variety of electrochemical applications including development of sensors, electrochemical measurements in highly resistant media, detection of intermediate species, and trace determination of easily oxidizable organic and inorganic species.

Sanderson and Anderson described the electrochemical behavior of IDE almost 20 years ago [1]. Morita and coauthors studied electrochemical measurements with carbon-based interdigitated array electrodes in batch mode and in flow system [2], while Kudera et al. presented application of multi microelectrode

array of eight different sizes in biological electrochemistry [3]. Application of interdigitated array electrodes for determination of enzyme activity was also described [4]. Xie et al. used a chip with four separated parallel arrays of iridium-made ultramicroelectrodes and miniaturized flow device for trace heavy metal measurements in water [5]. The measuring system consisting of four pairs of thin gold interdigitated electrodes and two auxiliary electrodes fixed on micro fluidic platform was described as a chip-based detector for rapid detection and quantification of nucleic acids [6]. Interdigitated ultramicroelectrode arrays (IDUAs) as possible transducers in a portable microfluidic-based biosensor were designed with the aim to maximize signal-to-noise ratio [7], while palladium nanoscaled interdigitated array electrode was made with deep UV lithography and applied for the detection of binding affinity of biomolecular structures by impedimetric measurements [8].

Biamperometric measurements involve electrochemical detection by two identical working electrodes, polarized with a small voltage difference, and applied in the solution contain-

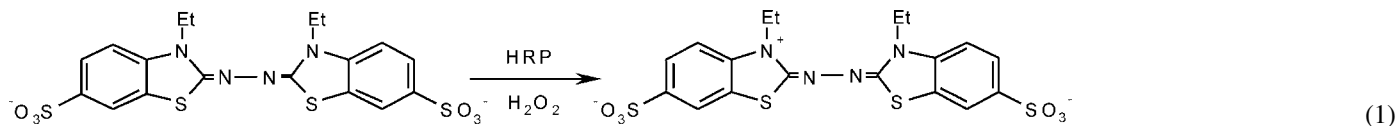
\* Corresponding author. Tel.: +385 1 4597 289; fax: +385 1 4597 260.  
E-mail address: [stjepan.milardovic@fkit.hr](mailto:stjepan.milardovic@fkit.hr) (S. Milardovic).

ing indicating reversible redox couple. Indirect biamperometric method of measurements is based on homogeneous reaction between an analyte and an indicating reversible redox couple. The most considered indicating systems for biamperometric determination include  $\text{Fe}^{3+}|\text{Fe}^{2+}$ ,  $\text{I}_2|\text{I}^-$ ,  $\text{Br}_2|\text{Br}^-$ ,  $\text{VO}_3^-|\text{VO}^{2+}$ ,  $\text{Ce}(\text{IV})|\text{Ce}(\text{III})$  and  $\text{Fe}(\text{CN})_6^{3-}|\text{Fe}(\text{CN})_6^{4-}$ .

Tougas and coauthors explained the basis for flow injection analysis by biamperometric technique [9]. Determination of various analytes as components of complex biological samples (urine, blood) was possible due to high selectivity of biamperometric method [10,11].

In recent years, a considerable interest has been focused on analytical methods for evaluation of antioxidant activity of food [12,13] and beverage samples [14,15]. One of the most widely used method for antioxidant activity evaluation is based on decolorization assay based on the scavenging of stable ABTS radical cation (2,2'-azino-bis(3-ethylbenzo thiazoline-6-sulfonic-acid)) [16,17]. Iveković et al. explained electrochemical generation of ABTS radical cation and its application for flow injection analysis of antioxidant activity by spectrophotometric detection [18]. Determination of antioxidant activity by amperometric and biamperometric method using DPPH|DPPH• redox couple and classic glassy carbon disc electrode in the batch mode of measurements has recently been presented [19,20]. Kadnikova and Kostić described biocatalytical oxidation of ABTS by hydrogen peroxide using horseradish peroxidase encapsulated in the sol-gel glass [21]. Campanella and coworkers have recently presented an electrochemical method for determination of antioxidant capacity using a biosensor [22].

The aim of this study was the development of an electrochemical method for the flow injection analysis of antioxidant capacity, based on continuous enzymatic production of  $\text{ABTS}^{\bullet+}$  and biamperometric detection by interdigitated electrode (IDE). In this study  $\text{ABTS}^{\bullet+}|\text{ABTS}$  redox couple was used as indicating redox pair.  $\text{ABTS}^{\bullet+}$  radical cation represents an oxidized form while ABTS is a reduced form of the redox pair. During the analysis, continuous one electron oxidation of 2,2'-azino-bis(3-ethylbenzothiazoline-6-sulfonic-acid) into corresponding radical cation  $\text{ABTS}^{\bullet+}$  (Eq. (1)) was achieved by peroxidase-catalyzed reaction in the flow-through tubular reactor.



Enzymatically produced  $\text{ABTS}^{\bullet+}$  react in the mixing coil with different compounds of antioxidant AH (analyte) producing ABTS according to reaction (2).



After reaction,  $\text{ABTS}^{\bullet+}$  concentration was reduced. In the proposed biamperometric measurement by IDE, current intensity is proportional to the residual reduced concentration of  $\text{ABTS}^{\bullet+}$  after reaction with an antioxidant. When analyzed solution contains a suitable ratio of reduced/oxidized forms of indicating redox pair, the interferences from the analytically undesirable oxidative or reductive species presented in the

solution are minimized. Consequently, in the case of the studied method, possible interferences caused by oxidative form of antioxidants designated as  $\text{A}^{\bullet}$  in Eq. (2) would be avoided.

The applied interdigitated electrodes contributed to biamperometric measurements of antioxidant capacity with many advantages including high selectivity, short response time, high rate of steady state current, high sensitivity, and also enabled application of the flow injection analysis.

## 2. Experimental

### 2.1. Reagents and solutions

Commercially available chemicals of the highest purity were used. L-Ascorbic acid, and uric acid, L-glutathione (reduced form), 6-hydroxy-2, 5,7,8-tetramethylchroman-2-carboxylic acid (Trolox, 97%), ABTS (2,2-azino-bis(3-ethylbenzo-thiazoline-6-sulfonic acid) diammonium salt, 98%), N, N'-methylenebisacrylamide (99%), 2,2-dimethoxy-2-phenylacetophenone (99%), and peroxidase (147 units/mg) from horseradish (type 1) were obtained from Sigma-Aldrich (St. Louis, USA). Acrylamide was purchased from Fluka (Buchs, Switzerland). Sodium dihydrogen phosphate, sodium hydrogen phosphate, potassium chloride, hydrogen peroxide (30%) were from Kemika (Zagreb, Croatia). Potassium peroxodisulfate ( $\text{K}_2\text{S}_2\text{O}_8$ ) was from Merck (Germany). Ten milliliter of 10 mM solutions of antioxidants were prepared daily. The solutions of water-soluble antioxidants (L-ascorbic acid, L-glutathione, Trolox, uric acid (5 mM), gallic acid and N-acetyl-L-cysteine) were prepared using double deionized water from Millipore-MilliQ system (USA). The  $\text{ABTS}^{\bullet+}$  solution (50 ml) was prepared 24 h before the spectrophotometric analysis by mixing 0.2 ml 65 mM  $\text{K}_2\text{S}_2\text{O}_8$  and 10 ml 5 mM ABTS using phosphate buffer, pH 7.4.

### 2.2. Apparatus and instrumentation

Electrochemical measurements were carried out on Potentiostat 273 A (Princeton Applied Research, USA) connected to

a computer for data collection and analysis. Cyclic voltammetry was performed in a standard three-electrode electrochemical cell for preconditioning of IDE. Interdigitated electrodes (IDE) IME 1525.3 FD Au P (ABTCH, Richmond, USA) were employed as working electrodes while a disc glassy carbon electrode was used as an auxiliary electrodes and  $\text{Hg}_2\text{Cl}_2|3\text{M KCl}$  was used as a reference electrode. Interdigitated array electrodes was microolithographically fabricated sensor chip, formed from magnetron sputtered gold on borosilicate glass substrate and consist two separated working electrode arrays on chip (6.4 mm × 5.5 mm, digit length  $W_a = 2.985$  mm, digit width ( $W_g$ ) = 15 μm, interdigit space ( $W$ ) = 15 μm and the number of digit pairs = 25),

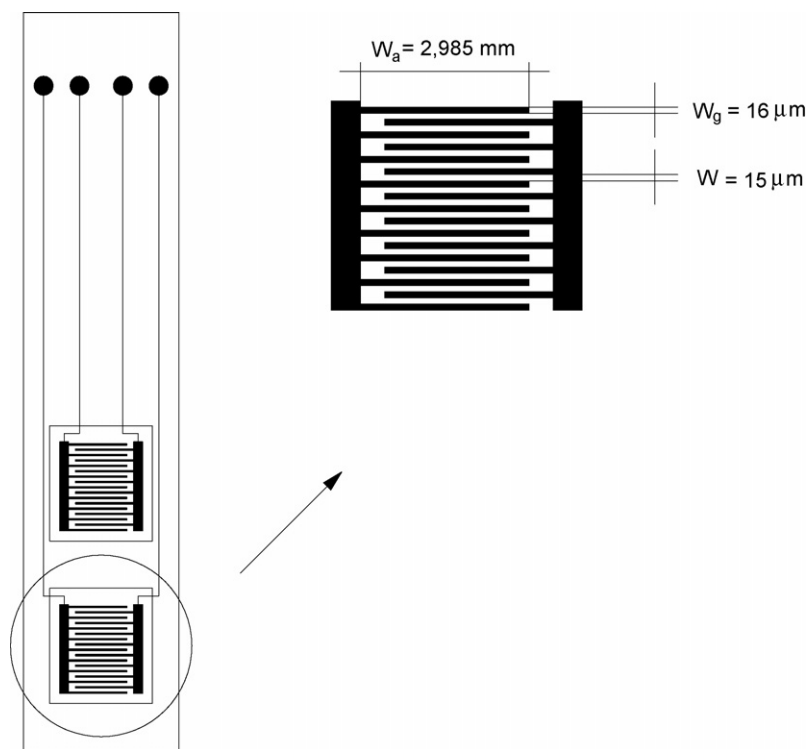


Fig. 1. Graphical presentation of IDE.

Fig. 1. The applied potential scan rate in cyclic voltammetry was 50 mV/s. Current-time measurements utilized the pair of interdigitated electrodes fixed in flow-through measuring cell. Transportation of the carrier solution in FIA mode (Fig. 2) was made by double tubing peristaltic pump. Sample injection into carrier stream was done by a syringe using injector valve Rheodyne Model 7125 and the sample loop of 10  $\mu$ l. Knitted coil reactor was made using a Teflon tube (1 mm in diameter, 60 cm long).

The absorbance of ABTS<sup>•+</sup> was measured at 730 nm on a double-beam DMS 80 (USA) spectrophotometer connected to a computer for data acquisition.

### 2.3. Interdigitated electrode (IDE) conditioning

Prior to measurement, interdigitated electrodes were cleaned and preconditioned according to manufacturer's recommendations. The conditioning was made in 0.8 M sulfuric acid by three-fold cycling potentials in the range between  $-600$  to  $1000$  mV using 50 mV/s scan rate. The preconditioning was repeated for each part of IDE pairs using Hg<sub>2</sub>Cl<sub>2</sub>/3 M KCl as a reference electrode and the disc glassy carbon electrode as an auxiliary electrode.

### 2.4. Spectroscopic determination

One milliliter ABTS<sup>•+</sup> in the phosphate buffer solution (pH 7.40, initial absorbance of 0.7) was placed in a plastic spectroscopic 1.5 ml cell (12.5 mm  $\times$  12.5 mm  $\times$  45 mm, Brand, Germany). After reaching steady state of absorbance at 730 nm, 5  $\mu$ l of the measuring sample (Trolox standard, pure antioxidant

samples or actual sample) were added to the cuvette and mixed for 10 s. The changes in absorbance were read after 20 s as this period was needed for mixing the sample and ABTS<sup>•+</sup> in the coil reactor applied for FIA biamperometric analysis.

### 2.5. Flow-through bioreactor: production of ABTS<sup>•+</sup>

Immobilization of peroxidase was made in polyacrylamide gel. Acrylamide solution was prepared by 0.43 g acrylamide, 66 mg *N,N*-methylenebisacrylamide and 2.4 mg 2,2-dimethoxy-2-phenylacetophenone dissolved in 1 ml deionized water and 1.5 ml of glycerol. In 600  $\mu$ l of acrylamide solution, 3.9 mg of peroxidase (147 units/mg) were added and mixed well for 30 min. The solution was placed on a glass plate and photopolymerized by illumination from a mercury lamp (Osram, ultravitalux, 300 W, Germany) during 2 min at the distance of 15 cm. The formed gel was cut by spatula to 3 mm  $\times$  3 mm pieces and filled into a tubular reactor (4 mm in diameter, 4 cm long). To obtain adequate porosity and continuous flow across the well-filled reactor, the silica-gel grains (2 mm in diameter) were packed together by polyacrylamide. Reactions in the bioreactor between immobilized peroxidase and ABTS and hydrogen peroxide were described by Eq. (1).

### 2.6. Actual antioxidant samples

Tea solutions were prepared by weighing 0.3 g of commercially available tea in 30 ml of deionized water heated to 60 °C. After 20 min of extracting, the samples were filtered and immediately used for analysis. Camomile and sage tea were used without further dilution while rosehip tea and tropic fruit tea

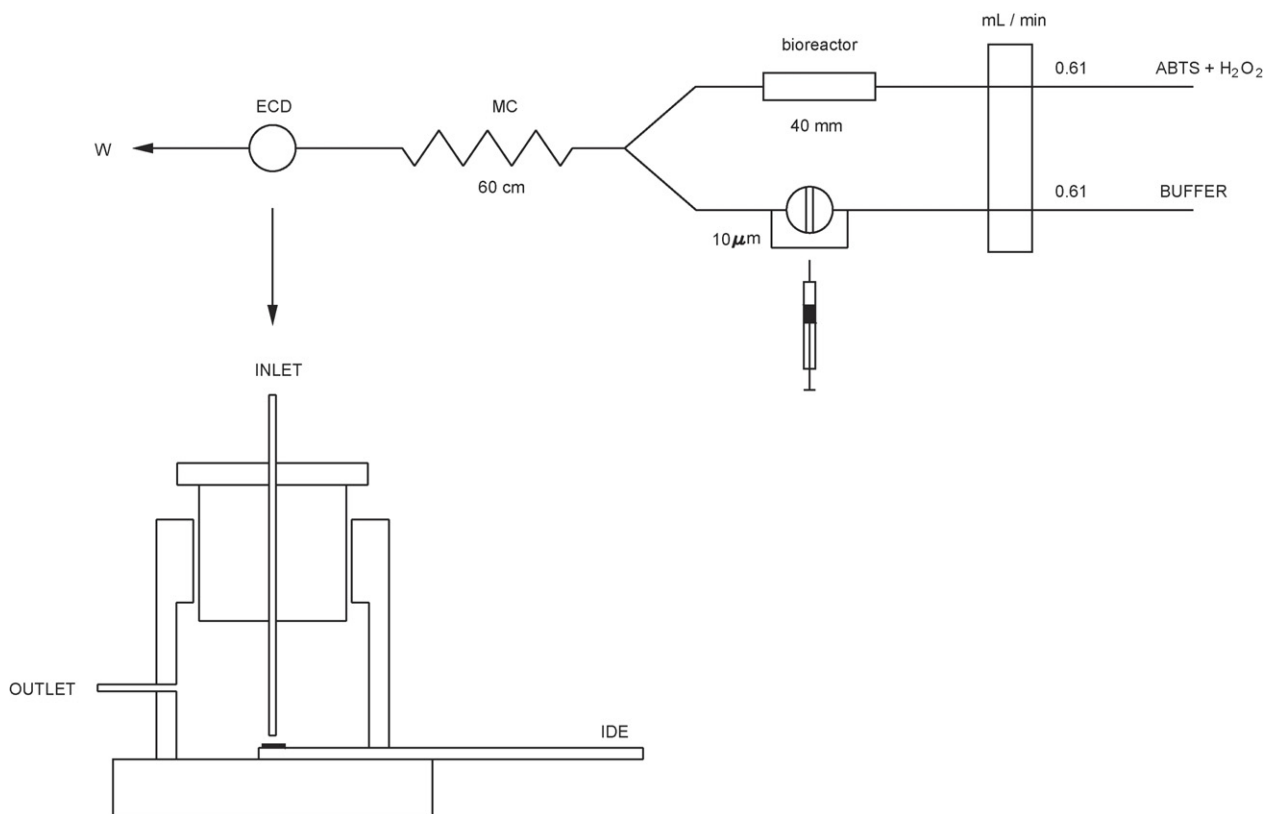


Fig. 2. Graphical presentation of FIA device and construction of a flow-through biamperometric IDE detector. MC: mixing coil, ECD: electrochemical detector, W: waste.

were diluted three-fold prior to analyses. The green tea was diluted six-fold by buffer solution before biamperometric or spectrophotometric measurements. The samples of black wine were ten-fold diluted while blueberry juice samples needed four-fold dilution. Orange juice, white wine and apple juice were analyzed by both techniques without dilution.

### 3. Results and discussion

#### 3.1. Electrochemical response of IDE

Fig. 3a shows the cyclic voltammograms of IDE in the phosphate buffer solution (0.05 M, 150 mM KCl, pH 7.4) containing 1 mM of ABTS after successive addition of  $\text{ABTS}^{\bullet+}$ . A potential scan rate of 5 mV/s was used. Curves 1–6 indicate IDE responses to concentrations of 12.6, 18.6, 24.4, 30, 35.4 and 40.52  $\mu\text{M}$  of  $\text{ABTS}^{\bullet+}$ , respectively. Increase in the concentration of  $\text{ABTS}^{\bullet+}$  resulted in increased current responses in both cathodic and anodic part of voltammograms. This phenomenon is indicated in Fig. 3b which shows linearity between current response of IDE, determined at potential of 100 mV, in the above mentioned concentration range of  $\text{ABTS}^{\bullet+}$ . Initially, measurements with applied buffer solution containing only 1 mM ABTS (designated as “o” in Fig. 1) resulted in low residual current. As evident in Fig. 3b, the current responses are a linear function of the bulk concentration of the radical form of ABTS, i.e. the current response is linear for those constituents of redox couple which were present in the measured sample in lower concentra-

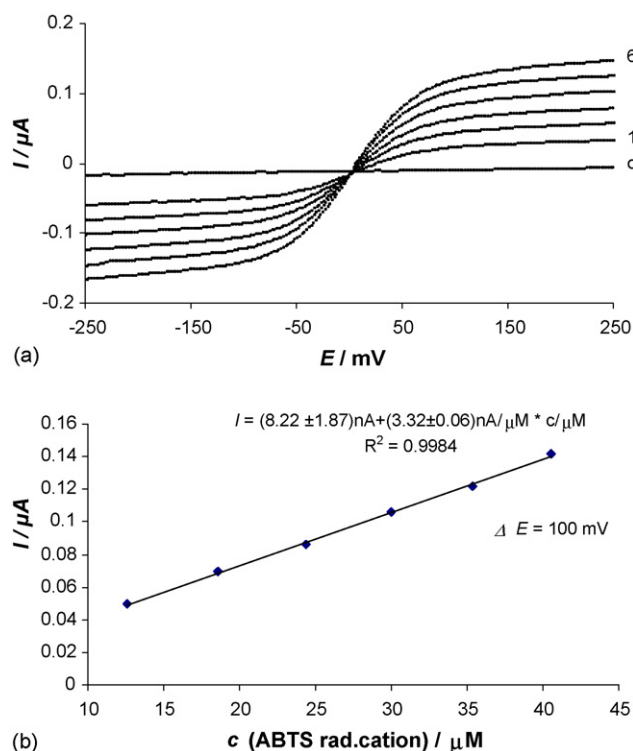


Fig. 3. (a and b) Cyclic voltammograms of IDE in the phosphate buffer solution, pH 7.4, containing 1 mM ABTS (curve “o”) and 12.6, 18.6, 24.4, 30.0, 35.4 and 40.5  $\mu\text{M}$   $\text{ABTS}^{\bullet+}$  (curves 1–6, respectively). Scan rate 5 mV/s.

tion. Also, the current response should be negligible in the case when only one constituent of the redox pair existed in the bulk solution.

### 3.2. Production of $ABTS^{\bullet+}$ by HRP immobilized and packed in the flow-through reactor

The effect of  $H_2O_2$  concentration on oxidation of ABTS catalyzed by HRP immobilized in flow-through tubular reactor can be seen in Fig. 4a. Applied tubular reactor was 4 mm in diameter and 2 cm long, while the mass of immobilized and packed HRP was 1.4 mg. Initial concentrations of ABTS were 1, 2 and 4 mM. Each point in the plots indicates hydrogen peroxide concentrations of 30, 60, 125, 250, 500 and 1000  $\mu M$ , respectively. The steady-state current was measured by IDE with imposed voltage difference of 100 mV, and the applied volume flow rate was 1.22 ml/min. According to Fig. 4a, production of ABTS in the tubular flow-through reactor increased upon increasing the concentration of hydrogen peroxide and the maximum value was reached at the concentration of 250  $\mu M$ . It was also observed that the double increase in ABTS concentration caused only 20% higher current response. The absorbance of produced ABTS radical

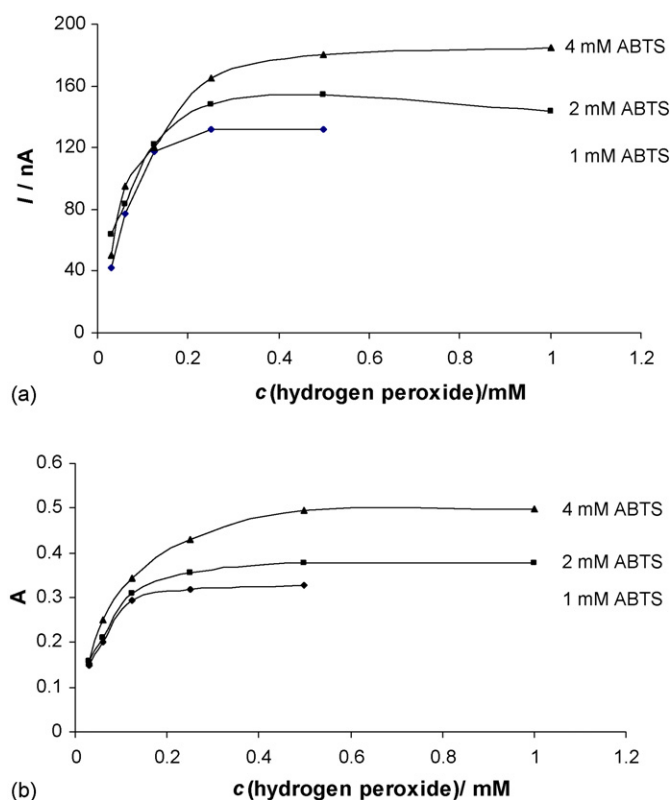


Fig. 4. (a) Effect of  $H_2O_2$  concentration on oxidation of ABTS catalyzed by HRP immobilized in flow-through tubular reactor. Initial concentrations of ABTS were 1, 2 and 4 mM. Each point in the plots designates hydrogen peroxide concentration of 30, 60, 125, 250, 500 and 1000  $\mu M$ , respectively. IDE was polarized by voltage difference of 100 mV and the applied volume flow rate was 1.22 ml/min. (b) Experimental conditions were the same as those in (a). Each point in the plot indicates absorbance of  $ABTS^{\bullet+}$  produced in a flow-through tubular enzymatic reactor after reaction between 1, 2 and 4 mM ABTS and 30, 60, 125, 250, 500 and 1000  $\mu M$  hydrogen peroxide, respectively.

ical cation shows the same dependence on the concentration of hydrogen peroxide and ABTS, as shown in Fig. 4b.

Determined absorbances at 250  $\mu M$  of hydrogen peroxide were 0.318 (1 mM ABTS), 0.357 (2 mM ABTS) and 0.43 (4 mM ABTS) while the concentrations of ABTS in the radical form, calculated using  $\epsilon = 1.5 \times 10^4 \text{ l mol}^{-1} \text{ cm}^{-1}$  [23], were 21.2, 23.8 and 28.7  $\mu M$ , respectively. The  $ABTS^{\bullet+}$  yields determined at 250  $\mu M$   $H_2O_2$  were in the range between 8.4 and 11.5%, between 16.4 and 18.4% for 120  $\mu M$   $H_2O_2$ , and approximately 34% for 30  $\mu M$   $H_2O_2$ . As the concentration of  $H_2O_2$  rose, the  $ABTS^{\bullet+}$  yields slightly decreased; therefore, to improve the yield of  $ABTS^{\bullet+}$  without the possibility to produce other oxidation forms of ABTS [23], the rest of experiments were conducted in the 4 cm long tubular reactor with 3.9 mg of immobilized HRP, using 2 mM ABTS because any further increase in  $H_2O_2$  concentration could not ensure significantly higher yield of  $ABTS^{\bullet+}$ .

Flow rate dependence of steady-state current and the absorbance obtained in the buffer solution of 2 mM ABTS and 120  $\mu M$   $H_2O_2$  catalyzed by HRP ( $m = 3.9$  mg) immobilized and packed in the flow-through tubular reactor are shown in Fig. 5a and b. The current response was measured by IDE polarized at voltage difference of 100 mV. Each point in Fig. 5a designates the current response for flow rates of 2.68, 1.71, 1.36, 1.16, 1.06 and 0.68 ml/min, respectively. Corresponding  $ABTS^{\bullet+}$  yields were in the range between 32.2% (77.3  $\mu M$  of  $ABTS^{\bullet+}$ ) and

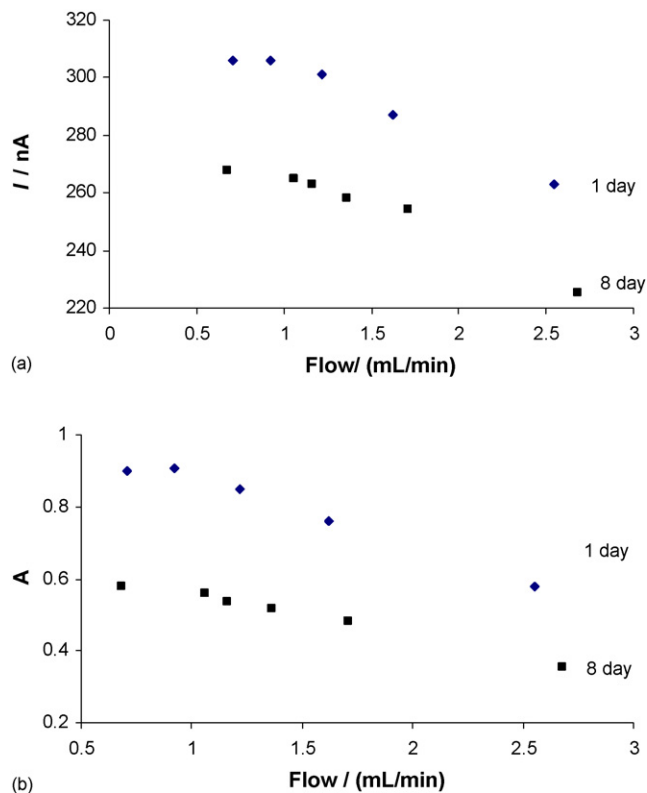


Fig. 5. (a) Flow rate dependence of steady-state current obtained in the buffer solution of 2 mM ABTS and 120  $\mu M$   $H_2O_2$  catalyzed by HRP ( $m = 3.9$  mg) immobilized and packed in the flow-through tubular reactor (reactor length = 4 cm). Current response was measured by IDE polarized at voltage difference of 100 mV. Each point indicates current response for flow rates of 2.68, 1.71, 1.36, 1.16, 1.06 and 0.68 ml/min, respectively.



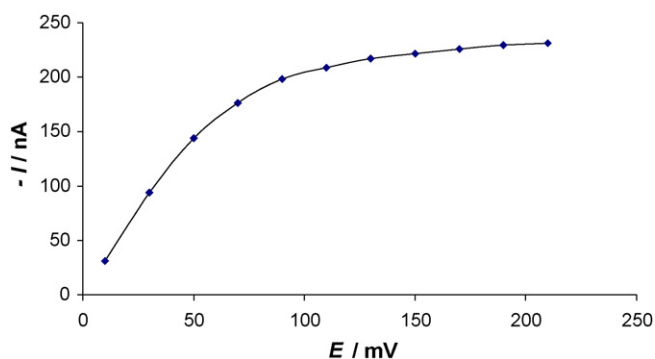


Fig. 6. Influence of the potential difference applied between IDE to current sensitivity. Experimental conditions were as follows:  $c(\text{ABTS}) = 2 \text{ mM}$ ,  $c(\text{H}_2\text{O}_2) = 120 \mu\text{M}$ , volume flow rate = 1.22 ml/min.

50% ( $120 \mu\text{M}$  of  $\text{ABTS}^{\bullet+}$ ) obtained in the reactor a day after preparation, and between 19.8 and 32.5%, 8 days after the bioreactor had been packed. The flow rate of 1.22 ml/min was used in all further experiments because the current response of IDE as the result of produced  $\text{ABTS}^{\bullet+}$  slightly changes in the range between 1.22 ml/min and 0.68 ml/min.

### 3.3. Effect of potential difference on the current sensitivity

Influence of the potential difference applied between IDE to the current sensitivity is shown in Fig. 6. Experimental conditions were as follows:  $c(\text{ABTS}) = 2 \text{ mM}$ ,  $c(\text{H}_2\text{O}_2) = 120 \mu\text{M}$ , volume flow rate = 1.22 ml/min,  $\Delta E$  was shifting in the range between 10 and 210 mV in the steps of 20 mV. The steady state current obtained rose as the imposed voltage difference increased. However, at a potential higher than 100 mV, the potential effect on current responses was minimized. Also, the possible interference of undesirable species presenting in the measured sample at the lower potential should be suppressed. All of these factors were considered and the potential of 100 mV was favored in all further experiments. The same behavior of IDE toward potential change was observed before in the batch mode of measurement, as seen in Fig. 3a.

### 3.4. Flow injection measurements

Fig. 7 shows the diagram obtained for Trolox in the concentration range between 20 and  $600 \mu\text{M}$ . The measurements were conducted in the 50 mM phosphate buffer solution, pH 7.4, containing ABTS ( $c = 2 \text{ mM}$ ) and  $\text{H}_2\text{O}_2$  ( $c = 120 \mu\text{M}$ ) at the potential imposed to IDE of 100 mV. The  $\text{ABTS}/\text{ABTS}^{\bullet+}$  molar ratio was 15.6:1. The applied flow rate was 1.22 ml/min. Biamperometric response of IDE was linearly related to Trolox concentration up to  $500 \mu\text{M}$  ( $I = (8.41 \pm 1.62) \text{ nA} + ((0.312 \pm 0.006) \text{ nA}/\mu\text{M}) c/\mu\text{M}$ ,  $R^2 = 0.9956$ ). The sensitivity of the method was  $0.312 \text{ nA}/\mu\text{M}$  of Trolox while the limit of detection accomplished by the used measuring device was  $6.5 \mu\text{M}$ . The absolute limit of detection was calculated as a triple value of the standard deviation of background current divided by sensitivity. According to diagram, the time needed for peak forming was approximately 65 s; 20 s was needed for

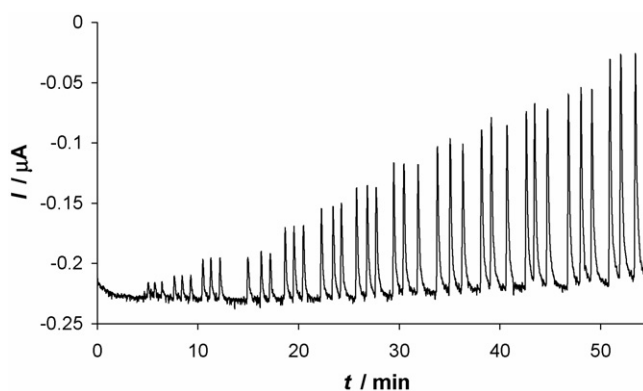


Fig. 7. The diagram obtained for Trolox. The measurements were conducted in the 50 mM phosphate buffer solution pH 7.4 containing ABTS ( $c = 2 \text{ mM}$ ) and  $\text{H}_2\text{O}_2$  ( $c = 120 \mu\text{M}$ ). Working potential was 100 mV, applied flow rate was 1.22 ml/min, sample loop volume was  $10 \mu\text{M}$ .

sample transporting from an injection valve through a mixing coil to the detector, so that the time of analysis was 85 s.

Flow injection analysis of water-soluble antioxidant is shown in Fig. 8. Experimental conditions were the same as in Fig. 7. The concentration of injected antioxidants was  $250 \mu\text{M}$  for Trolox, ascorbic acid and uric acid, and  $220 \mu\text{M}$  for reduced glutathione. Trolox equivalents, calculated by dividing current response of tested antioxidant by the current response of Trolox, were 0.995 for uric acid, 0.994 for ascorbic acid, and 0.817 for reduced glutathione, and are in good correlation to theoretical value 1 for uric and ascorbic acid, and 0.9 for reduced glutathione [24].

Antioxidant activity for sixteen pure compounds of antioxidants and actual samples of tea, wine and juices determined spectroscopically and biamperometrically is summarized in Table 1. Experimental conditions were the same as those for calibration diagram of Trolox. To suppress possible reaction between unreacted hydrogen peroxide and antioxidant that presented in the real sample, the inlet hydrogen peroxide concentration to flow-through reactor was reduced to  $30 \mu\text{M}$ . Correlation of the antioxidant activity determined by biamperometric FIA method and spectrophotometric determination is shown in Fig. 9. The injection of each sample of antioxidant or an actual sample of juices, wine or tea were repeated three-fold and the results of antioxidant capacity were determined by two points calibration graph of

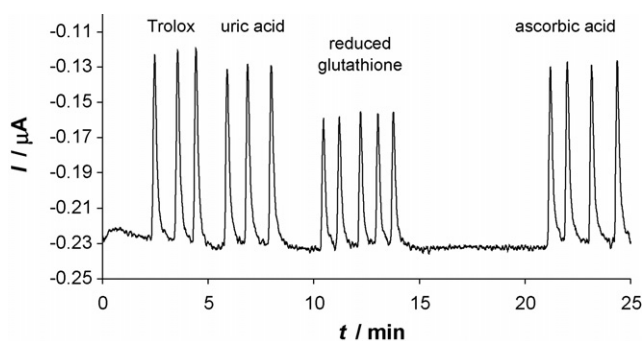


Fig. 8. Flow injection analysis of water-soluble antioxidant. Experimental conditions were the same as in Fig. 7. The concentration of injected antioxidants was  $250 \mu\text{M}$  for Trolox, ascorbic acid and uric acid, and  $220 \mu\text{M}$  for reduced glutathione.

Table 1  
Comparison of results for antioxidant capacity obtained by spectrophotometric (batch mode) and biamprometric measurements (FIA mode)

	Antioxidant capacity determined by IDE	Antioxidant capacity determined spectrophotometrically
Trolox	1.00	1.00
Water-soluble antioxidants		
L-Ascorbic acid	0.99	0.96
Uric acid	0.95	0.94
Gallic acid	2.33	2.99
N-Acetyl-L-cystein	1.25	1.48
L-Glutathione	0.82	0.92
Real samples		
Tea		
Rosehip tea	4.46	4.58
Tropic fruit tea	2.01	1.71
Green tea	7.50	7.38
Chamomile tea	0.48	0.42
Sage tea	0.94	0.87
Juices		
Orange juice	0.89	0.97
Blueberry juice	4.59	3.80
Apple juice	0.34	0.34
Wine		
Red wine	14.10	15.00
White wine	0.88	0.99

Trolox. The linearity was tested before and after measurements of real samples by two different Trolox concentrations, and the real samples were diluted every time when current response reached 0 value. The results of antioxidant capacity were calculated from the calibrating graph of Trolox and were expressed as the corresponding Trolox concentrations. The regression analysis (antioxidant capacity determined spectrophotometrically/mM =  $(-0.06 \pm 0.12) + (1.040 \pm 0.027)$  antioxidant capacity determined by IDE,  $R^2 = 0.9915$ ) for intercept close to 0 and the slope close to 1 confirmed good agreement between classic

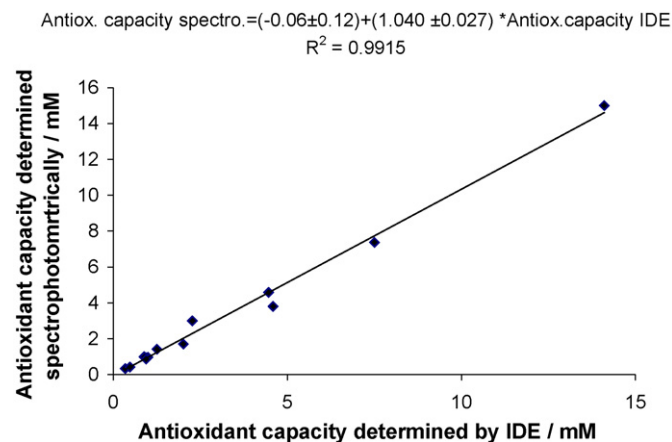


Fig. 9. Correlation between antioxidant capacity obtained by biamprometric FIA method and spectrophotometric determination. Experimental conditions:  $c(\text{ABTS}) = 2 \text{ mM}$ ,  $c(\text{hydrogen peroxide}) = 30 \text{ }\mu\text{M}$ , flow rate =  $1.22 \text{ ml/min}$ ,  $\Delta E = 100 \text{ mV}$ ,  $V(\text{sample loop}) = 10 \text{ }\mu\text{M}$ .

spectrophotometric (batch mode), and flow injection analysis based on biamprometric detection by IDE.

#### 4. Conclusion

The novel flow injection analysis of antioxidant capacity based on continuous enzymatic production of ABTS radical cation and biamprometric detection by interdigitated electrode was proposed. The production of  $\text{ABTS}^{\bullet+}$  enzymatically by the peroxidase immobilized and packed into a tubular flow-through reactor offered continuous analysis immediately after the time when reagents reached the enzymatic reactor, while the classic spectroscopic analysis utilized  $\text{ABTS}^{\bullet+}$  prepared 24 h prior to analysis. Immobilized peroxidase offered sufficiently high yields of  $\text{ABTS}^{\bullet+}$ , which is essential for practical work, and therefore achieved sufficiently wide linear range of biamprometric detector by the applied interdigitated electrode. IDE consisted of a pair of identical electrodes specifically suitable for biamprometric detection. Good linearity obtained for Trolox in the range between 20 and  $500 \text{ }\mu\text{M}$  and good agreement between the results of Trolox equivalents obtained by IDE detector and those presented in the literature confirmed the usefulness of biamprometric method for the determination of antioxidant capacity. Additionally, good correlation between spectrophotometric measurements and flow injection analysis by IDE biamprometric detector, established for a wide variety of samples, confirmed the applicability of the proposed method for antioxidant capacity analysis.

#### Acknowledgement

We are grateful to the Croatian Ministry of Science Education and Sports, project No. 0125-054, for the financial support of the presented study.

#### References

- [1] D.G. Sanderson, L.B. Anderson, *Anal. Chem.* 57 (1985) 2388.
- [2] M. Morita, O. Niwa, T. Horiuchi, *Electrochim. Acta* 42 (1997) 3177.
- [3] M. Kudera, H. Allen, O. Hill, P.J. Dobson, P.A. Leigh, W.S. McIntire, *Sensors* 1 (2001) 18.
- [4] U. Wollenberg, M. Paeschke, R. Hintsche, *Analyst* 119 (1994) 1245.
- [5] X. Xie, D. Stüben, Z. Berner, J. Albers, R. Hintsche, E. Jantzen, *Sens. Actuators* 97 (2004) 168.
- [6] M. Gabig-Ciminska, A. Holmgren, H. Andersen, K. Bundvig Barken, M. Wümpelmann, J. Albers, R. Hintsche, A. Breitenstein, P. Neubauer, M. Los, A. Czyz, G. Wegrzyn, G. Silfversparre, B. Jürgen, T. Scweder, S.-O. Enfors, *Biosens. Bioelectron.* 19 (2004) 537.
- [7] J.H. Min, A.J. Baumner, *Electroanalysis* 16 (9) (2004) 724.
- [8] P. Vangerwen, W. Laureyn, W. Laureys, G. Huyberechts, M.O. Debeek, K. Baert, J. Suls, W. Sansen, P. Jacobs, L. Hermans, R. Mertens, *Sens. Actuators B: Chem.* 49 (1/2) (1998) 73.
- [9] T.P. Tougas, J.M. Jannetti, W.G. Collier, *Anal. Chem.* 57 (1985) 1377.
- [10] J. Michałowski, M. Trojanowicz, *Anal. Chim. Acta* 281 (1993) 299.
- [11] C. Zhao, J. Zhang, J. Song, *Anal. Biochem.* 297 (2001) 170.
- [12] C. Sanchez-Moreno, *Food Sci. Tech. Int.* 8 (3) (2002) 121.
- [13] B. Tang, L. Zhang, Y. Geng, *Talanta* 65 (3) (2004) 665.
- [14] D. Villaño, M.S. Fernández-Pachón, A.M. Troncoso, M.C. García-Parrilla, *Talanta* 64 (2) (2004) 501.
- [15] M.H. Zhang, J. Luypaert, J.A. Fernández Pierna, Q.S. Xu, D.L. Massart, *Talanta* 62 (1) (2003) 25.

- [16] I.F.F. Benzie, J.J. Strain, *Meth. Enzymol.* 299 (1999) 15.
- [17] C. Rice-Evans, N.J. Miller, *Meth. Enzymol.* 234 (1994) 279.
- [18] D. Iveković, S. Milardović, M. Roboz, B.S. Grabarić, *Analyst* 130 (2005) 708.
- [19] S. Milardovic, D. Iveković, B.S. Grabarić, *Bioelectrochemistry* 68 (2005) 180.
- [20] S. Milardovic, D. Iveković, V. Rumenjak, B.S. Grabarić, *Electroanalysis* 17 (2005) 1847.
- [21] E.N. Kadnikova, N.M. Kostić, *J. Mol. Catal. B: Enzym.* 18 (2002) 39.
- [22] L. Campanella, E. Martini, M. Tomassetti, *Talanta* 66 (4) (2005) 902.
- [23] J.L. Scott, W.J. Chen, A. Bakac, J.H. Espenson, *J. Phys. Chem.* 97 (1993) 6710.
- [24] D. Armstrong, *Free Radical and Antioxidant Protocols*, Humana Press, Totowa, 1998, p. 294.

Short communication

# Simultaneous purification and spectrophotometric determination of nickel present in as-prepared single-walled carbon nanotubes (SWCNT)

S. Mohanapriya, V. Lakshminarayanan\*

*Raman Research Institute, C.V. Raman Avenue, Bangalore 560080, India*

Received 3 March 2006; received in revised form 1 April 2006; accepted 1 April 2006

Available online 9 May 2006

## Abstract

The quality of single-walled nanotubes (SWCNT) is usually assessed by means of electron microscopic techniques or Raman spectroscopy. However, these sophisticated techniques are not widely available and do not reliably estimate the impurities in highly heterogeneous samples containing metal particles, fullerenes and other carbonaceous materials. We have developed a simple, inexpensive and convenient spectrophotometric method to assess the purity of arc-discharge grown as-prepared SWCNT. Purification process consists of initial gas phase oxidation and refluxing with nitric acid at the optimal conditions including short time period during acid refluxing. We have shown that this method could remove the metal particles effectively with a good yield of high quality SWCNTs, as shown by the spectrophotometric and scanning tunneling microscope studies described here. The extent of removal of the nickel present in as-prepared carbon nanotube sample is followed by spectrophotometric analysis of the dissolved nickel analyte. The composition of nickel in the SWCNT sample is found to be 17.56%. The method is based on the chelating of  $\text{Ni}^{2+}$  with dimethylglyoxime in ammoniacal citrate medium to form nickel dimethylglyoxime complex. A second stage purification of SWCNT eliminates the residual metal particles. The purified SWCNT has been studied using scanning tunneling microscopy which shows clearly resolved individual carbon nanotubes.

© 2006 Elsevier B.V. All rights reserved.

**Keywords:** Single-walled nanotubes purification; Nickel nanoparticles; Spectrophotometric determination; STM of single-walled nanotubes

## 1. Introduction

The potential applications of single-walled carbon nanotube (SWCNT) both in basic science and technology originate from its exceptional physical and chemical properties [1,2]. The advanced technological application envisaged for SWCNTs mainly rely on the purity of the material. Most of the presently known techniques for production of SWCNT quote the purity of the sample to be about 10–90%. The as-produced SWCNT (AP-SWCNT) generally contains carbon encapsulated metal particles along with the non-tubular carbon forms (amorphous carbon particle, fullerenes, polyaromatic shells). A measurement of the metal content in as-produced SWCNT samples is important in realizing many of its potential applications. For example, the hydrogen uptake capacity of SWCNT shows a strong dependence on the amount of residual nickel present

in nanotube sample [3]. The unusual magnetic properties of SWCNT form the basis of nanoscale electronic devices. Obviously ferromagnetic nickel particles can have a significant influence on the magnetic behavior of CNT. In order to realize the potential applications of the magnetic properties of SWCNTs, the sample under investigation should be either free of nickel particles or should possess a known quantity of the metal. In other words, the efficiency of a purification process on the extent of the removal of nickel has to be monitored carefully.

The arc-discharge method of synthesizing SWCNT is a principal technique used for large-scale economic production of high quality SWCNT. Electric arc-derived AP-SWCNT contains significant amount of metallic impurities, predominantly nickel, which is used as a catalyst in its preparation. Although SEM and TEM methods are regularly used to evaluate the sample purity, these methods become highly unreliable when bulk samples are under investigation. For example, within one SEM frame, the amount of the material that can be seen and analyzed is of the order of a few micrograms and consequently only the materials with high homogeneity can be studied by SEM analysis. A crit-

\* Corresponding author. Tel.: +91 80 23610122; fax: +91 80 23610492.  
E-mail address: [narayan@ri.res.in](mailto:narayan@ri.res.in) (V. Lakshminarayanan).

ical step involved in TEM studies is the preparation of nanotube dispersion while in Raman and IR spectroscopic measurements, interpretation of the spectral data is rather complex and quantitative estimate of the metal content cannot be obtained [4]. Though thermo gravimetric analysis (TGA) is one of the widely used analytical tools for the determination of the metal content in SWCNT, the complications involved in TGA studies are, exothermic oxidation during the measurements and the dependence of the data on the temperature ramp rate.

In this communication, we report a simple and sensitive spectrophotometric method for the quantitative analysis of catalytic nickel present in as-prepared single-walled carbon nanotubes. The proposed method is a macro scale technique, which may readily be applied to purify several gram quantities of raw product. The purification procedure employed here involves initial gas phase oxidation of SWCNT sample at 350 °C followed by refluxing in HNO<sub>3</sub>. There are several methods based on different oxidising temperatures and sequences for gas phase oxidation and acid refluxing that are available in literature [5,6]. In our procedure, the air oxidized SWCNT is subjected to acid refluxing in 6N nitric acid to dissolve metal particles. A long time acid refluxing procedure usually employed attacks the defective sites of nanotube surface, which results in shortening or eventual destruction of SWCNT. We have employed a significantly short time period of 30 min for acid refluxing treatment in 6N nitric acid and we observe that this could effectively dissolve the metal nanoparticles without causing significant structural deformations to SWCNT. Owing to their nanometre size, the metal particles dissolve fast and the development of intense green color after 10 min of heating is indicative of the formation of nickel nitrate.

We have used gas phase purification, acid refluxing and vacuum filtration for separating the SWCNT from the metal impurities. A second stage purification of once purified SWCNT ensures the effectiveness of our purification process and spectrophotometric studies confirm the purity of CNT to be above 99% with respect to metal content. Finally, we have characterized the purified SWCNT by scanning tunneling microscopy.

## 2. Experimental

### 2.1. Reagents

All the chemicals used in this study are of analytical grade. The Millipore water with the resistivity of 18 MΩ cm was used throughout the experiments for the preparation of the aqueous solutions. A standard stock solution of nickel (1.7 mM) was prepared by warming the 0.01 g of nickel strip in 6N nitric acid at 60 °C for 25 min. The dissolved solution is evaporated to expel any oxides of nitrogen, transferred quantitatively to a 100 ml standard flask after cooling. The dimethylglyoxime reagent is prepared by dissolving 0.5 g of dimethylglyoxime in 250 ml of ammonia solution and diluting to 500 ml with water. A freshly prepared solution of DMG is used in all the experiments as the oxime group tends to get oxidized in air to form furoxane compound. The dilute ammonia solution was prepared by mixing the aqueous ammonia with water in the volume ratio of 1:1.

The SWCNT purchased from Carbolex Inc. (USA) consists of single-walled close-ended carbon nanotubes, prepared by arc-discharge synthesis using nickel and yttrium as catalysts. Though the arc-discharge method of producing SWCNT promises to be a convenient and relatively less expensive one, the pristine nanotube sample is generally associated with the metallic impurities. It is well known that arc-derived CNT is difficult to purify from the metal catalytic particles. There are some procedures described in the literature for the purification of SWCNTs grown by arc-discharge method [7,8].

### 2.2. Instrumentation

A spectrophotometer model SD 2000 (Ocean Optics, USA) fitted with a tungsten lamp source and a cell having a path length of 1 cm was employed to measure the absorbance spectra and analysis. The pH was measured with a digital hand held pH meter (Hanna Instruments), which is calibrated with a standard buffer solution before each measurement.

A home built scanning tunneling microscope (STM) in high-resolution mode described elsewhere [9] was used to probe the SWCNT dispersed on a highly oriented pyrolytic graphite (HOPG) surface. The STM images were obtained at room temperature in air and the instrument was operated in constant current mode of 1 nA at a sample bias voltage of +100 mV. Higher resolution images were acquired at constant height mode of operation. Prior to these experiments, the instrument was calibrated with highly oriented pyrolytic graphite (HOPG) (ZYA grade, Advanced Ceramic). A mechanically cut tungsten tip was used as the probe. The images shown here were plane corrected and in some cases Fourier filtered using scanning probe image processor (SPIP) software (Image Metrology, Denmark). To ensure that the images shown were representative of the CNT, multiple images were taken at different locations and scan ranges.

The STM studies of both the purified and as-prepared SWCNT samples were carried out. The SWCNT is dispersed in ethanol at a typical concentration of 0.1 mg/ml and a drop of the solution is spread on to a freshly cleaved HOPG substrate and used as a specimen for imaging.

### 2.3. Procedures

#### 2.3.1. Purification

The 200 mg of raw soot of SWCNT was subjected to air oxidation by heating the sample in air at 350 °C for 4 h to oxidize the non-tubular forms of the carbon. The SWCNT sample was then treated with 6N nitric acid under reflux at 60 °C for 30 min in order to dissolve the metal particles. After cooling, the sample was filtered using a cellulose nitrate filter paper with 0.2 μm pore size by applying vacuum suction. A clear green colored supernatant acidic solution was collected at the bottom of filtering unit; successive washing with Millipore water removes the substantial amount of trapped acid from the sediment. The SWCNT collected in the filter paper was dried in an oven at 50 °C for 30 min. The filtrate obtained was transferred to a 100 ml standard flask and made up to the mark using Millipore water and this solution is used for further spectrophotometric studies.



### 2.3.2. Spectrophotometric analysis

**2.3.2.1. Test for iron.** The presence of the iron in the CNT sample is analyzed by transferring 1 ml of test solution to a 25 ml graduated flask and the pH was adjusted to 3.5 by the addition of 0.2 M sodium acetate. To reduce the Fe (III) species into Fe (II), 10% aqueous solution of hydroquinone was added followed by 2 ml of 0.25% of 1,10-phenanthroline. The solution is made up to the mark and allowed to stand for 1 h in order to complete the reaction. No color formation is observed in this case. The absorbance of the sample was measured by a spectrophotometer after running a reagent blank. The absence of characteristic absorption peak in the spectra confirms that the carbon nanotube is free from iron.

**2.3.2.2. Test for cobalt.** A test for cobalt is carried out by the addition of dimethylglyoxime reagent under appropriate conditions. There is no formation of brown colored Co–DMG complex indicating that cobalt metal is not present in the pristine SWCNT material.

**2.3.2.3. Procedure for determination of the nickel content.** One millilitre of the test solution was transferred to a 100 ml standard flask containing water and shaken well so that the concentration of  $\text{Ni}^{2+}$  is uniform. On diluting the solution, the homogeneously distributed nickel ions become more readily available for binding with the ligand. Since the molecular mass of dimethylglyoxime reagent is very high compared to nickel, it reacts with nickel in the stoichiometric ratio of 1:2, and therefore a very small quantity of nickel could form a voluminous precipitate. The dilution process also helps in a facile extraction of the complex. Addition of 5 g of citric acid to avoid the interference of any trace iron has brought down the pH of the solution from 4.5 to 2.1. The optimum pH of 7.5 for complexing nickel with DMG has been adjusted by the addition of diluted  $\text{NH}_3$ . After cooling, it is transferred to a separatory funnel fitted with a Teflon stopcock, followed by the addition of 40 ml DMG solution. After allowing it to stand for 3 min, 6 ml of chloroform was added and shaken well to dissolve the  $\text{Ni}(\text{dmg})_2$  complex. The phases are allowed to settle out and the pale yellow colored nickel complex was extracted. Three more extracts in 4 ml portions of chloroform were collected and all the extractions were combined. Care has been taken to avoid any viscous film or foam formed between two phases to get into the extractions. The extract is quantitatively transferred into a 25 ml standard flask made up to the volume by chloroform. Since we find that the absorbance values increase slowly with time, each absorbance value had been recorded after 10 min of mixing. The absorbance of this yellow colored complex was measured in a 1 cm cell at a wavelength of 360 nm exactly after 10 min of mixing, with reference to reagent blank.

The aforementioned procedure is employed for a series of standard nickel solutions of nickel concentration in a range of 1–20  $\mu\text{g}/\text{ml}$ . From the absorbance data recorded by a spectrophotometer, a calibration graph of absorbance of the nickel dimethylglyoxime complex against the concentration of nickel was constructed.

## 3. Results and discussions

The spectrophotometric procedure developed here is used to determine the amount of nickel in inhomogeneous bulk soot without modifying the structure of the nanotubes. The proposed method does not consume any specific quantity of the sample because it is an integral part of purification steps. This is due to the fact that the filtrate with metal nitrates obtained during the purification process is used for the analysis. The stability of this test solution, which is used for spectrophotometric analysis, is indicated by its constant pH value (1.41) up to 100 days. When dimethyl glyoxime is used as a sequestering agent, one of the acidic hydrogen in DMG is replaced by one equivalent of  $\text{Ni}^{2+}$  ion and two molecules of DMG reacts with  $\text{Ni}^{2+}$  to give red voluminous precipitate. Ammonical citrate medium is employed to prevent the co-precipitation of other ions, which would generally form their hydroxides. Being a bidentate ligand, DMG forms a strong coordinate covalent bond through oxygen and nitrogen atoms. The color intensity of the Ni–DMG complex strongly depends on  $\text{OH}^-$  ion concentration. The stability of the complex is widely studied in various solvents and optimum pH for chelating is reported to be 7.5. This optimum pH is brought about by the addition of diluted  $\text{NH}_3$  solution. The use of diluted  $\text{NH}_3$  prevents the formation of crystalline  $\text{Ni}(\text{OH})_2$ . Under the experimental conditions employed, the absorption spectrum of Ni–DMG complex obtained is as shown in Fig. 1. The absorption maximum at 360 nm characterizes a typical metal to ligand charge transfer (MLCT) spectra which arises from the transition of an electron from one of the orbital of nickel into a  $\pi^*$  orbital of DMG generally represented as  $\text{M-L} \rightarrow \text{M}^+-\text{L}^-$ .

### 3.1. Analytical characteristics

Since the analytical application of spectrophotometry rely on the proportionality between absorbance and concentration, a calibration curve was constructed with the data obtained from spectrophotometric measurements. Fig. 2 shows the calibration

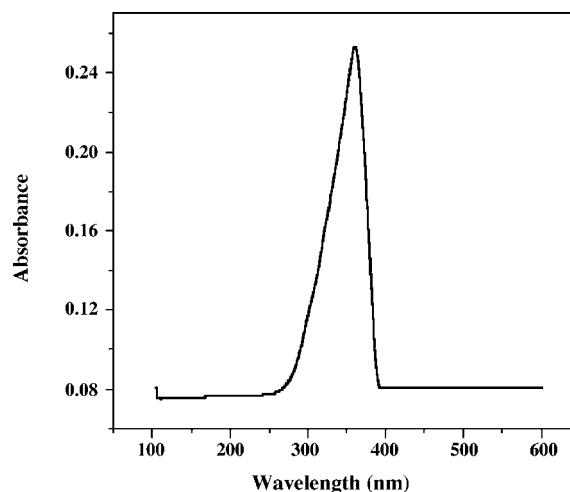


Fig. 1. The absorption spectra of dimethylglyoxime complex of nickel prepared from the filtrate obtained during the purification of SWCNT.

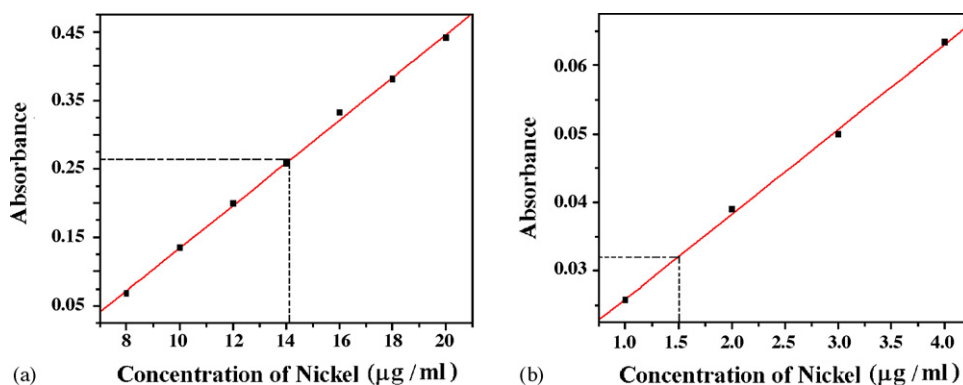


Fig. 2. The calibration graph of concentration of nickel vs. absorbance of nickel–dimethylglyoxime complex, illustrating the validity Lambert–Beer’s Law. (a) After first stage purification. The dotted lines correspond to the measured nickel concentration of 14.1  $\mu\text{g/ml}$  in the test solution. (b) After second stage purification. The dotted lines correspond to the measured nickel concentration of 1.5  $\mu\text{g/ml}$ .

graph illustrating the validity of Beer’s law up to a concentration of 20  $\mu\text{g/ml}$  for Ni–DMG complex at 360 nm.

A linear regression analysis of the data yields a correlation coefficient of 0.999. The obtained apparent molar absorbance coefficient was  $\epsilon = 5.206 \times 10^3 \text{ dm}^3 \text{ mol}^{-1} \text{ cm}^{-1}$ . From the calibration graph the concentration of nickel in the test solution is found to be 14.1  $\mu\text{g/ml}$  that corresponds to the nickel content of 17.5% in a given CNT sample. Three replicate analysis of the test solution containing the nickel by

the aforementioned procedure gave a variation coefficient of  $\pm 1\%$ .

The above-described procedure was repeated for the second stage purification of already once purified CNT sample. Due to the efficiency of our purification process there is an almost complete removal of metallic impurities. This has been confirmed by the analysis of the filtrate obtained during the second stage purification. From the calibration graph of Fig. 2, it can be observed that the test solution containing residual nickel shows

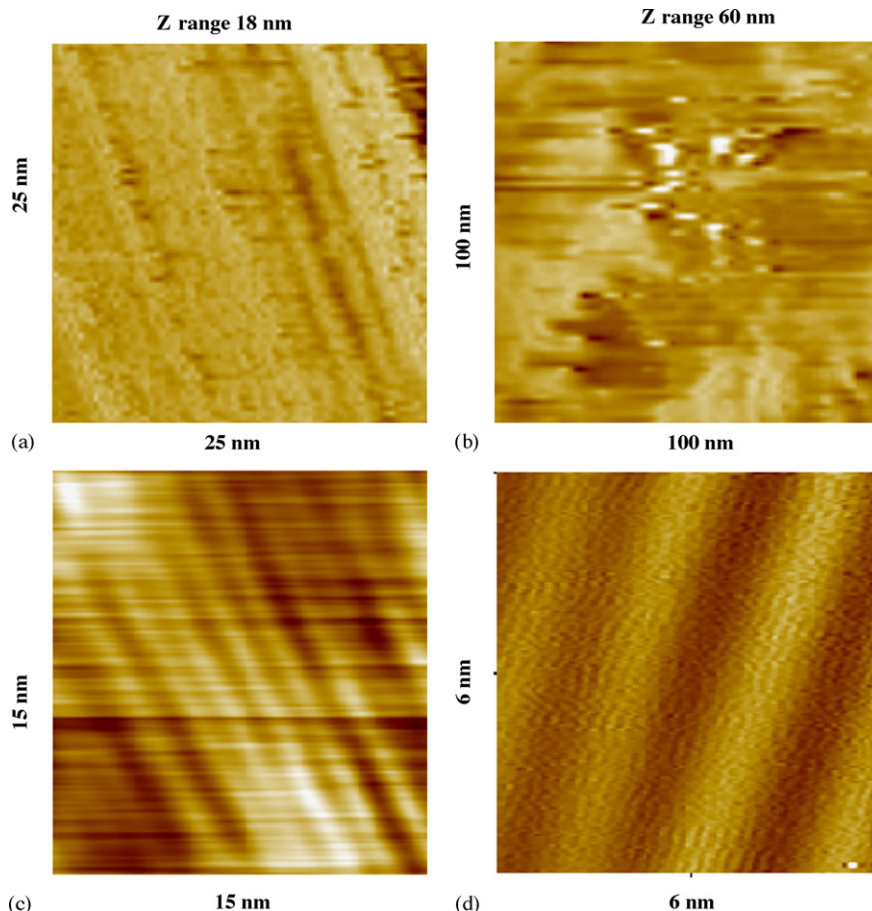


Fig. 3. Scanning tunneling microscope images of SWCNT on HOPG. (a and b) Constant current mode images before purification. (c and d) Constant height mode images after purification. The scanning parameters are tunneling current, 1 nA and bias voltage, +100 mV (substrate positive).

an absorbance value corresponding to 1.5  $\mu\text{g/ml}$ , which constitutes a nickel content of 0.234% in purified SWCNT sample.

The scanning tunneling microscope images of the SWCNT on HOPG surface both before and after purification treatment are shown in Fig. 3. The constant current STM image of the sample before purification can be seen to contain tight bundles of SWCNT where the individual nanotubes could be barely resolved as shown in Fig. 3(a). It can also be seen from Fig. 3(b), some clusters of nanoparticles probably encapsulated with carbon is imaged at a different location of the unpurified sample. The sizes of the nanoparticle clusters are about 10–12 nm. Presumably, these clusters contain several individual nanoparticles. Fig. 3(c) and (d) show the STM images of the purified samples at two different scan ranges of (c) 15 nm  $\times$  15 nm and (d) 6 nm  $\times$  6 nm from which individual CNTs can be clearly resolved. The scanning was carried out at a tunneling current of 1 nA and a bias voltage of +100 mV (substrate positive) in the constant height mode of imaging. The 15 nm  $\times$  15 nm image of Fig. 3(c) shows a bundle of SWCNT in which the individually resolved nanotubes can be clearly seen. The separation of the nanotubes are effected by the acid treatment which also functionalises the nanotubes with carboxylic groups. The diameter of the individual CNT is about 1.4 nm as can be seen from higher resolution image of Fig. 3(d). No Ni nanoparticle could be seen on different regions of the scanned surface showing the effectiveness of purification procedure adopted in this work.

#### 4. Conclusions

We have obtained highly pure SWCNT with minimum structural deformation by following a purification procedure combining air oxidation at 350° C for 4 h as an initial step and nitric acid refluxing. The optimum conditions to obtain pure and defect-free SWCNT involve acid refluxing for 30 min at 60° C. This reproducible procedure also permits the quantitative spectrophotometric analysis of nickel content. The procedure followed for

determining the nickel content in a CNT sample is based on simple spectrophotometry, which involves the sequestration of trace amount of nickel in ammoniacal citrate medium. The method employed here is simple and rapid and does not need sophisticated instrumentation facilities. The amount of nickel measured is in good agreement with the amount of the catalytic nickel used during the synthesis of CNT as reported in the literature. The second stage purification of SWCNT and the subsequent determination of nickel, validate the efficiency of our purification procedure, besides optimizing the conditions employed. Quantitative determination of nickel content in SWCNT sample opens a way for the systematic study of nickel-influenced properties of SWCNT. We have demonstrated the application of this method for the determination of nickel content of up to 0.24% with good reproducibility. We have also shown clearly resolved individual carbon nanotubes on the HOPG surface by the scanning tunneling microscopic studies.

#### References

- [1] H. Dai, J.H. Hafner, A.G. Rinzler, D.T. Colbert, R.E. Smalley, *Nature* 384 (1996) 147.
- [2] A.C. Dillon, K.M. Jones, T.A. Bekkedhal, C.H. Kiang, D.S. Bethune, M.J. Heben, *Nature* 386 (1997) 377.
- [3] P.M.J. Costa, K.S. Coleman, M.L.H. Green, *Nanotechnology* 16 (2005) 512.
- [4] M.E. Itkis, D.E. Perea, R. Jung, S. Noyogi, R.C. Haddon, *J. Am. Chem. Soc.* 127 (2005) 3439.
- [5] I.W. Chiang, B.E. Brinson, A.Y. Huang, P.A. Willis, M.J. Bronikowski, J.L. Margrave, R.E. Smalley, R.H. Hauge, *J. Phys. Chem. B* 105 (2001) 8297.
- [6] E. Dujardin, T.W. Ebbesen, A. Krishnan, M.M. Treacy, *Adv. Mater.* 10 (1998) 611.
- [7] K. Tohji, T. Goto, H. Takahashi, Y. Shinoda, N. Shimizu, B. Jeyadevan, I. Matsuoka, Y. Saito, A. Kasuya, T. Ohsuna, K. Hiraga, Y. Nishina, *Nature* 383 (1996) 679.
- [8] K. Tohji, T. Goto, H. Takahashi, Y. Shinoda, N. Shimizu, B. Jeyadevan, I. Matsuoka, Y. Saito, A. Kasuya, S. Oto, Y. Nishina, *J. Phys. Chem. B* 101 (1997) 1974.
- [9] M. Jayadevaiah, V. Lakshminarayanan, *Meas. Sci. Technol.* 15 (2004) N35.

# Use of fractional factorial design for optimization of digestion procedures followed by multi-element determination of essential and non-essential elements in nuts using ICP-OES technique

Awad A. Momen, George A. Zachariadis\*, Aristidis N. Anthemidis, John A. Stratis

*Laboratory of Analytical Chemistry, Department of Chemistry, Aristotle University, Thessaloniki GR-54124, Greece*

Received 7 February 2006; received in revised form 10 April 2006; accepted 14 April 2006

Available online 24 May 2006

## Abstract

Two digestion procedures have been tested on nut samples for application in the determination of essential (Cr, Cu, Fe, Mg, Mn, Zn) and non-essential (Al, Ba, Cd, Pb) elements by inductively coupled plasma-optical emission spectrometry (ICP-OES). These included wet digestions with HNO<sub>3</sub>/H<sub>2</sub>SO<sub>4</sub> and HNO<sub>3</sub>/H<sub>2</sub>SO<sub>4</sub>/H<sub>2</sub>O<sub>2</sub>. The later one is recommended for better analytes recoveries (relative error < 11%). Two calibrations (aqueous standard and standard addition) procedures were studied and proved that standard addition was preferable for all analytes. Experimental designs for seven factors (HNO<sub>3</sub>, H<sub>2</sub>SO<sub>4</sub> and H<sub>2</sub>O<sub>2</sub> volumes, digestion time, pre-digestion time, temperature of the hot plate and sample weight) were used for optimization of sample digestion procedures. For this purpose Plackett–Burman fractional factorial design, which involve eight experiments was adopted. The factors HNO<sub>3</sub> and H<sub>2</sub>O<sub>2</sub> volume, and the digestion time were found to be the most important parameters. The instrumental conditions were also optimized (using peanut matrix rather than aqueous standard solutions) considering radio-frequency (rf) incident power, nebulizer argon gas flow rate and sample uptake flow rate. The analytical performance, such as limits of detection (LOD < 0.74 μg g<sup>-1</sup>), precision of the overall procedures (relative standard deviation between 2.0 and 8.2%) and accuracy (relative errors between 0.4 and 11%) were assessed statistically to evaluate the developed analytical procedures. The good agreement between measured and certified values for all analytes (relative error < 11%) with respect to IAEA-331 (spinach leaves) and IAEA-359 (cabbage) indicates that the developed analytical method is well suited for further studies on the fate of major elements in nuts and possibly similar matrices.

© 2006 Elsevier B.V. All rights reserved.

**Keywords:** Experimental design; Essential and non-essential elements; Nuts; Sample digestion; ICP-OES

## 1. Introduction

The interest in elemental composition of plant materials is growing as a result of ongoing developments in agriculture, in nutrition and environmental studies, and in biological surveying and mineral prospecting. All these developments have led to increased demands for analysis of complicated biological matrices. Inductively coupled plasma-optical emission spectrometry (ICP-OES) has proved to be convenient technique for this task [1–4] and qualities such as capacity for simultaneous, rapid and precise determination with wide dynamic range and low limits of detection allow it to compete successfully with more traditional techniques like atomic absorption spectrometry, flame atomic

emission spectrometry, instrumental neutron activation analysis and X-ray fluorescence.

A wide range of digestion methods for plants have been published such as dry ashing, wet ashing with different mixtures of reagents or conventionally heating procedures, microwave dissolution and acid bomb digestion, etc. [1,2,5,6]. Although these methods are generally showed both good accuracy and precision, some of them are rather time-consuming. Depending on analysis task, several factors should be considered for sample digestion. These may include level of contamination, sample homogeneity, completeness of digestion, reproducibility, suitability of the analytical technique employed, time needed for sample preparation, economic aspects including labour and reagent consumption, equipment cost, etc. [1,2]. Common practice for digestion of plant matrices is the addition of H<sub>2</sub>O<sub>2</sub> to HNO<sub>3</sub>. Addition of H<sub>2</sub>O<sub>2</sub> to the digestion mixture increases the oxidation power of HNO<sub>3</sub> during digestion and enhances the

\* Corresponding author.

E-mail address: [zacharia@chem.auth.gr](mailto:zacharia@chem.auth.gr) (G.A. Zachariadis).



attack on organic material present in the sample. However, mixtures of  $\text{HNO}_3/\text{H}_2\text{O}_2$  alone cannot dissolve all the material that present in the sample, thus leading to poor recoveries for many elements [3]. Correspondingly, the use of oxidizing acids such as  $\text{HNO}_3$  and/or  $\text{H}_2\text{SO}_4$  is important especially for wet digestion of food samples high in carbohydrates and/or fats, to reduce carbonization and to ensure completeness of the digestion. Also, acid mixtures of  $\text{HNO}_3/\text{HClO}_4$  or  $\text{HNO}_3/\text{HCl}$  or combination of more than two acids are usually employed in wet digestions, while the use of  $\text{H}_2\text{O}_2$  may be needed when the sample material is difficult to decompose [2,7–9].

Nuts are considered to be one of the most economically and nutritionally available food in the world. They contain abundant amounts of antioxidants, vitamins, mineral silicates, carbohydrates and other beneficial nutrients. Also, they are fat, mineral and energy-dense (rich) foods; it has been valued for their oils (oil content ranges between 36 and 61%) [6]. The mineral composition of any food item is more or less variable factor and influenced by a number of factors such as, climate, soil characteristics (content of organic matter, pH and clay mineralogy), variety, transport, storage, and preparation. These factors vary from a region to another and even within the same country [10].

Magnesium, chromium, iron, manganese, copper and zinc are essential elements for human health, and they are playing an important role in human metabolism [11]. Environmental pollution is the main cause of heavy metal contamination in the food chain, and cadmium and lead are potentially harmful metals that have aroused considerable concern [12,13]. Moreover, aluminum and barium are non-essential elements, with unknown biological function for living organisms.

The aim of this study was to develop multi-element ICP-OES analytical method for nut samples after an appropriate wet digestion procedure using an open vessels technique. Taking into the accounts the contamination factors as minimum as possible. Optimization of the factors affecting the digestion process (adequate volume of acid combination, digestion time, temperature, etc.) using a complete factorial design requires a great many experiments [14]. The Plackett–Burman fractional factorial design [15] allows the main effects of a greater number of factors to be known with relatively few experiments without a substantial loss of information. Moreover, this design is adequate tool to optimize the variables affecting sample digestions. Also, it can make the analyst's task easier and quicker and provide a more reliable answer to the analytical question posed especially when a large numbers of variables are needed to be evaluated. But the main drawback of this design is that it did not allow the evaluation of interactions between variables. Due to this fact, in a large scale design the effects of the significant variables and their interaction should be re-evaluated, using another type of design like a central composite design. After preliminary study (carefully investigation and accurately evaluation) using IAEA-331 and IAEA-359 certified reference materials (CRMs), the most effective procedure was selected to optimize the ICP-OES parameters. The analytical performances of the whole procedure, such as limit of detection, precision and accuracy were assessed statistically to evaluate the developed procedure. The elemental contents of various

Table 1  
Operating conditions and description of ICP-OES instrument

rf Incident power <sup>a</sup>	1300 W
rf Generator	40 MHz (free running)
Nebulizer argon gas flow rate <sup>a</sup>	0.8 l min <sup>-1</sup>
Sample uptake flow rate <sup>a</sup>	1.0 ml min <sup>-1</sup>
Argon gas flow rates	0.5 l min <sup>-1</sup> (auxiliary); 0.8 l min <sup>-1</sup> (plasma)
Signal measurement mode	Peak area (three points per peak)
Torch alumina injector, id	2.0 mm
Spray chamber	Scott double-pass
Nebulizer type	Gem tips cross-flow
Pump	Peristaltic, three channel
Polychromator	Echelle grating
Resolution	0.006 nm at 200 nm
Detector	Segmented-array charge-coupled (SCD), 235 sub-arrays

<sup>a</sup> Optimized value.

commonly consumed commercial nut samples were also estimated.

## 2. Experimental

### 2.1. Instrumentation and apparatus

A Perkin-Elmer Optima 3100XL axial viewing ICP-optical emission spectrometer was used throughout. The quantitation was performed at two different spectral atomic (I) and ionic (II) lines for each analyte: Al 308.215 I; Al 237.313 I; Ba 233.527 II; Ba 230.424 II; Cd 214.440 II; Cd 226.502 II; Cr 283.563 II; Cr 284.325 II; Cu 324.752 I; Cu 224.700 II; Fe 238.204 II; Fe 239.562 II; Mg 279.077 II; Mg 280.271 II; Mn 257.610 II; Mn 259.372 II; Pb 220.353 II; Pb 217.000 I; Zn 213.857 I; Zn 202.548 II. The operation conditions employed are described in Table 1.

A peristaltic pump was used to introduce the sample solutions into the ICP and to discard the wastes. To avoid contamination factors as much as possible, all sample preparation apparatus, glassware, polytetrafluoroethylene (PTFE) digestion vessels and storage bottles were soaked in freshly prepared 10% (v/v)  $\text{HNO}_3$  for at least 48 h, and finally washed three times with double deionized water (DDW) before use. Crucibles were immersed in 20% (v/v)  $\text{HCl}$  for about two days, and rinsed with DDW several times to be used for the next experiment.

### 2.2. Standard reference materials and reagents

The accuracy of the analytical technique was checked by analyzing IAEA-331 (spinach leaves) and IAEA-359 (cabbage) supplied by IAEA, International Atomic Energy Agency, Monaco.

The following analytical reagents (Merck, Darmstadt, Germany) were used in this study:  $\text{HNO}_3$  (65%), Pro-analyti,  $\text{H}_2\text{SO}_4$  (97%), Pro analyti,  $\text{HCl}$  (37%), Pro-analyti,  $\text{H}_2\text{O}_2$  (30%), Pro-analyti. Also, 1000 mg l<sup>-1</sup> stock standard multi-element solution (Merck, Darmstadt, Germany) was used. All solutions were prepared with high purity DDW, prepared by suc-



cessfully passing tap water through two ion exchange columns. Also, DDW has been used for washing and rinsing of all apparatus and glassware.

### 2.3. Nut samples

Four nut species were analyzed: peanut, almond, hazelnut, and walnut. The edible part was analyzed for essential and non-essential elements. Since grinding of samples accelerates the digestion process, samples were first shelled, when necessary, grounded in a glass mortar, pestle and sieved into fine powders. Ten sub-samples from each type were dried to constant mass, cooled and weighed as soon as they reached room temperature for further sample digestion. IAEA-331 and IAEA-359 were used as bottled, without further grinding and sieving, but before digestion, they were dried as recommended by the supplier.

For ICP-OES analyses, all blank solutions, nut samples and CRMs were digested with the following composition of reagents: (1) HNO<sub>3</sub>/H<sub>2</sub>SO<sub>4</sub> and (2) HNO<sub>3</sub>/H<sub>2</sub>O<sub>2</sub>/H<sub>2</sub>SO<sub>4</sub>.

### 2.4. Digestion procedures

After the optimization of the digestion conditions, the selected factors (the optimum conditions) for each procedure were applied to an oven-dried nut samples (50 °C, 24 h). About 0.5 g of each sample was accurately weighed into dry, clean PTFE digestion vessels. 1 ml of DDW was added first and then, the appropriate volume of acid/oxidant combination at the selected level for each procedure as described in Table 3. When the initial reaction has subsided, vessels contents were gently mixed and the mixtures were left for the selected pre-digestion time. Then the contents were heated at the selected temperature until heavy evolution of fumes ceases. The final residues were dissolved in 2.5 ml of HCl and diluted to 50 ml with DDW. Both blanks and CRMs (IAEA-331, IAEA-359) were treated in the same way. Matrix effect studies were carried out by spiking some of the original un-digested samples (accurately weighed different amounts) with variable amounts of standard solution

of the metals. The spiked samples were then mineralized using the same digestion procedures as were applied to the non-spiked samples. All digestions were performed in triplicate.

### 2.5. Experimental design

The Plackett–Burman experimental matrix was used to optimize the working conditions for nut samples digestion. Differences between mean values were evaluated by Student's paired *t*-test because the measured values were distributed normally. Linear regression and correlation analysis were performed for calculation of slope (*b*), intercept (*a*) and correlation coefficient (*r*) of the regression lines. A sample mass of 0.5 g was used for all the experiments.

## 3. Results and discussion

### 3.1. Selection of emission lines

The employed ICP-OES instrument allows different spectral lines to be selected for analytes quantification. Therefore, all analytes were measured in two different emission lines. This will help to select wavelengths of no spectral interferences. The results of regression analysis of aqueous standard and standard addition solutions for the selected spectral lines (spectral lines with high sensitivity) are presented in Table 2, including the slope-values (a measure of sensitivity), the 95% confidence intervals of slopes and correlation coefficients (the correlation between data). The dynamic range of all analytes is extended at least up to 1 mg l<sup>-1</sup>, and is considered as sufficient for the accurate quantification of all analytes in various nuts samples, which commonly contain lower concentrations of the examined analytes.

### 3.2. Optimization of digestion factors

The Plackett–Burman fractional factorial design makes it possible to know the influence of up to seven factors (A–G) with

Table 2

Regression data and ICP limits of detection (calculated as μg l<sup>-1</sup> and expressed as μg g<sup>-1</sup>), for the selected wavelengths using aqueous standards and standard addition solutions of peanut digested by HNO<sub>3</sub>/H<sub>2</sub>SO<sub>4</sub>/H<sub>2</sub>O<sub>2</sub>

Element, wavelength (nm)	Aqueous standards			Standard addition solutions			<i>b</i> ratio <sup>a</sup> (%)	Limits of detection	
	<i>b</i> (cps μg <sup>-1</sup> l)	95% confidence interval of <i>b</i>	<i>r</i>	<i>b</i> (cps μg <sup>-1</sup> l)	95% confidence interval of <i>b</i>	<i>r</i>		μg l <sup>-1</sup> <sup>b</sup>	μg g <sup>-1</sup> <sup>c</sup>
Al I, 237.313	3.41	±0.61	0.998	2.58	±0.18	0.999	+24.34	2.0	0.2
Ba II, 233.527	20.01	±1.15	0.999	13.9	±2.6	0.998	+30.53	0.37	0.04
Cd II, 226.502	6.22	±0.95	0.999	7.0	±0.2	0.999	-11.14	1.21	0.12
Cr II, 284.325	46.5	±4.8	0.954	45.2	±1.3	0.999	+2.8	2.0	0.2
Cu I, 324.752	148	±15	0.997	152	±3	0.999	-2.7	0.84	0.08
Fe II, 238.204	37.2	±2.1	0.999	36.2	±3.4	0.998	+2.6	2.50	0.25
Mg II, 279.077	5.33	±0.75	0.977	5.24	±0.12	0.979	+1.68	2.73	0.27
Mn II, 259.372	128	±5	0.999	132	±2	0.999	-3	0.15	0.02
Pb I, 217.000	0.69	±0.16	0.982	0.41	±0.09	0.987	+40.57	7.34	0.73
Zn I, 213.857	27.6	±2.0	0.999	23.3	±0.3	0.999	+15.6	2.80	0.28

<sup>a</sup> Positive (+) ratio indicate *b* of aqueous standards is >*b* of standard addition techniques and vice versa.

<sup>b</sup> Concentration corresponding to three standard deviations of the signals of the blank solutions.

<sup>c</sup> Concentration corresponding to three standard deviations of the signals of the blank related to a sample mass of 0.5 g finally diluted to 50 ml.

Table 3  
Experimental definition for the digestion methods studied

Factors	Digestion with HNO <sub>3</sub> /H <sub>2</sub> SO <sub>4</sub>			Digestion with HNO <sub>3</sub> /H <sub>2</sub> SO <sub>4</sub> /H <sub>2</sub> O <sub>2</sub>		
	High level (+)	Low level (–)	Optimum conditions	High level (+)	Low level (–)	Optimum conditions
(A) Volume of HNO <sub>3</sub> (ml)	4	2	4	4	2	4
(B) Digestion time (h)	2	1	2	2	1	2
(C) Temperature (°C)	120	90	120	120	90	120
(D) Volume of H <sub>2</sub> SO <sub>4</sub> (ml)	2	1	2	2	1	1
(E) Pre-digestion time (min)	60	30	30	60	30	30
(F) Volume of H <sub>2</sub> O <sub>2</sub> (ml)	0	0	0	2	1	1
(G) Sample weight (g) <sup>a</sup>	0.5	0.5	0.5	0.5	0.5	0.5

<sup>a</sup> Non-optimized factor.

only eight experiments. The optimized method permits estimation of the main effects of the factors and disregards interactions between them. The studied factors as well as the values for each one (+ represent the maximum and – represents the minimum) are shown in Table 3. The eight experiments were summarized in the matrix (the table of signs) and are listed in Table 4. When the numbers of factors is less than seven and more than three, as in this study, the matrix must be restricted to columns corresponding to non-optimized factors (F and G in HNO<sub>3</sub>/H<sub>2</sub>SO<sub>4</sub> procedure and G in HNO<sub>3</sub>/H<sub>2</sub>SO<sub>4</sub>/H<sub>2</sub>O<sub>2</sub> procedure).

The influence of each factor was evaluated by comparing its effects with twice the overall average standard deviation ( $2s_{\text{overall}}$ ) assimilated to experimental error. The main effect of a factor (e.g., factor A) is calculated as the difference between the average value of results corresponding to both positive ( $A^+$ ) and negative ( $A^-$ ) levels as indicated in the following equation:

$$\text{Main effect of factor A} = A^+ - A^- = \frac{R_1 + R_2 + R_3 + R_5}{4} - \frac{R_4 + R_6 + R_7 + R_8}{4}$$

When the difference between the two averages is larger than  $2s_{\text{overall}}$ , the factor has a significant effect on the digestion. The negative level of the factor will be chosen if the result is negative and vice versa.

An acid-oxidant HNO<sub>3</sub>/H<sub>2</sub>SO<sub>4</sub> and HNO<sub>3</sub>/H<sub>2</sub>SO<sub>4</sub>/H<sub>2</sub>O<sub>2</sub> solutions were chosen in order to reach highest recoveries of elements from nut samples. It is possible that a certain acid

Table 4  
Plackett–Burman experimental matrix (table of signs)

Experiment	Factors							Result
	A	B	C	D	E	F	G	
1	+	+	+	–	+	–	–	R <sub>1</sub>
2	+	+	–	+	–	–	+	R <sub>2</sub>
3	+	–	+	–	–	+	+	R <sub>3</sub>
4	–	+	–	–	+	+	+	R <sub>4</sub>
5	+	–	–	+	+	+	–	R <sub>5</sub>
6	–	–	+	+	+	–	+	R <sub>6</sub>
7	–	+	+	+	–	+	–	R <sub>7</sub>
8	–	–	–	–	–	–	–	R <sub>8</sub>

Signs represent experimental levels (see Table 3).

could digest some constituents in nuts, so a second acid and/or oxidant are needed in order to digest all constituents. The acid-oxidant solution volume can be an important parameter, because a low acid solution volume can be more rapidly saturated by the metal than a high acid solution volume. A 3–10 ml range was chosen. The temperature can increase the digestion power of the acid solution. An elevated temperature can increase the oxidative power of the digestion acid. Two values of a temperature (90 and 120 °C) were studied. Moreover, the standing and the pre-digestion time is an important factor. The digestion processes occurs to a great extent when long pre-digestion times are used. A satisfactory yield can be obtained using a relatively short pre-digestion time. We selected a 30 and 60 min for our study.

The results in Table 5, indicated that for almost all analytes the digestion procedures (using the Plackett–Burman design) which applied for CRMs are nearly quantitative. High recoveries were reached in some runs. Also, it is indicated that three of the studied factors (the volume of HNO<sub>3</sub>, the volume of H<sub>2</sub>O<sub>2</sub>, and the digestion time), were found to be the most effective parameters when compared to other factors. Therefore, more attentions were taken for these three factors during sample preparation steps to provide a maximum analyte recovery (see Section 3.5). The optimum values for each factor, obtained as a maximum response (highest analyte recovery), were selected and applied for the tested digestion procedures (Table 3).

### 3.3. Effect of the factors

The analytical results obtained for CRMs in each of the digestion methods studied are shown in Table 5 and the effects of the factors, calculated by applying the equation which indicated in Section 3.2, are shown in Table 6. Digestion with HNO<sub>3</sub>/H<sub>2</sub>SO<sub>4</sub>, the HNO<sub>3</sub> volume shows positive effect on the determination of Cu and Zn, while the H<sub>2</sub>SO<sub>4</sub> volume and the digestion time have the same effects on the determination of Al. The temperature show negative effect on the determination Cu. In the digestion with HNO<sub>3</sub>/H<sub>2</sub>SO<sub>4</sub>/H<sub>2</sub>O<sub>2</sub>, the HNO<sub>3</sub> volume and the digestion time show positive effects on the determination of Zn. However, the H<sub>2</sub>O<sub>2</sub> volume has negative effect on the determination of Cd, Cu and Mn.

Taking the above into account, it may be concluded that Cu and Zn are the analytes that requiring more rigorous investigation before methods validation and selection of digestion conditions

Table 5

Analytical results obtained for analytes in IAEA-331 using HNO<sub>3</sub>/H<sub>2</sub>SO<sub>4</sub> and HNO<sub>3</sub>/H<sub>2</sub>SO<sub>4</sub>/H<sub>2</sub>O<sub>2</sub>

Exp. no.	Al	Ba	Cd	Cr	Cu	Fe	Mg	Mn	Pb	Zn
Analyte concentration <sup>a</sup> (μg g <sup>-1</sup> ) using HNO <sub>3</sub> /H <sub>2</sub> SO <sub>4</sub>										
1	299.1 ± 5.2	6.4 ± 0.4	2.0 ± 0.2	2.4 ± 0.1	12.8 ± 0.4	255.7 ± 5.3	8899 ± 188	77.2 ± 1.9	<LOD <sup>b</sup>	75.6 ± 3.0
2	298.5 ± 6.3	5.8 ± 0.5	1.8 ± 0.2	2.3 ± 0.2	13.5 ± 0.5	248.5 ± 6.1	8886 ± 171	75.1 ± 2.3	<LOD	73.2 ± 2.9
3	264.9 ± 5.7	5.5 ± 0.4	1.6 ± 0.1	2.1 ± 0.1	11.3 ± 0.4	235.6 ± 6.2	8890 ± 184	73.8 ± 1.7	<LOD	72.1 ± 3.2
4	271.0 ± 5.8	5.8 ± 0.3	1.7 ± 0.2	2.3 ± 0.1	11.1 ± 0.6	241.0 ± 6.5	8885 ± 154	71.9 ± 2.0	<LOD	68.8 ± 3.3
5	287.6 ± 6.7	5.6 ± 0.3	1.6 ± 0.1	1.9 ± 0.2	12.9 ± 0.5	247.3 ± 5.9	8890 ± 193	73.0 ± 1.8	<LOD	74.5 ± 3.8
6	282.2 ± 7.1	6.0 ± 0.4	1.9 ± 0.1	1.8 ± 0.2	10.5 ± 0.6	239.8 ± 5.6	8911 ± 185	78.4 ± 2.5	<LOD	67.0 ± 4.1
7	297.0 ± 5.2	5.9 ± 0.4	1.8 ± 0.2	2.0 ± 0.2	10.2 ± 0.5	245.7 ± 6.0	8903 ± 168	77.5 ± 2.4	<LOD	66.7 ± 3.5
8	279.8 ± 6.6	5.7 ± 0.3	1.7 ± 0.2	2.1 ± 0.1	12.5 ± 0.7	236.0 ± 5.8	8896 ± 173	73.6 ± 2.1	<LOD	64.3 ± 3.6
s <sub>overall</sub>	6.0	0.4	0.2	0.2	0.5	5.8	176	2.1	–	3.3
Analyte concentration <sup>a</sup> (μg g <sup>-1</sup> ) using HNO <sub>3</sub> /H <sub>2</sub> SO <sub>4</sub> /H <sub>2</sub> O <sub>2</sub>										
1	301.1 ± 9.1	6.7 ± 0.6	2.4 ± 0.2	2.6 ± 0.2	12.2 ± 0.5	265.9 ± 7.4	8910 ± 157	79.2 ± 2.3	<LOD	85.4 ± 3.6
2	296.8 ± 10.3	5.9 ± 0.4	2.1 ± 0.2	2.4 ± 0.2	12.7 ± 0.6	250.4 ± 6.9	8906 ± 171	74.4 ± 2.0	<LOD	82.6 ± 2.7
3	284.3 ± 8.1	5.8 ± 0.3	1.7 ± 0.1	2.2 ± 0.1	11.5 ± 0.4	245.6 ± 5.8	8898 ± 182	75.1 ± 1.9	<LOD	79.9 ± 3.4
4	291.6 ± 9.0	6.4 ± 0.4	1.8 ± 0.1	2.0 ± 0.1	11.4 ± 0.7	255.1 ± 6.4	8895 ± 174	73.0 ± 2.1	<LOD	78.2 ± 3.1
5	277.4 ± 6.7	6.2 ± 0.4	1.6 ± 0.1	2.5 ± 0.2	11.3 ± 0.6	247.5 ± 6.2	8890 ± 170	70.5 ± 1.9	<LOD	71.6 ± 2.2
6	280.8 ± 9.3	6.0 ± 0.4	2.3 ± 0.2	2.2 ± 0.1	12.7 ± 0.7	249.3 ± 6.1	8900 ± 175	78.7 ± 2.5	<LOD	70.8 ± 2.3
7	277.0 ± 6.2	5.8 ± 0.5	2.0 ± 0.2	2.3 ± 0.2	10.8 ± 0.5	235.0 ± 4.7	8902 ± 169	72.4 ± 2.3	<LOD	73.1 ± 2.5
8	289.7 ± 7.6	5.9 ± 0.4	2.2 ± 0.2	2.4 ± 0.1	12.4 ± 0.8	251.8 ± 6.6	8897 ± 183	77.9 ± 2.4	<LOD	69.0 ± 2.0
s <sub>overall</sub>	8.2	0.4	0.2	0.2	0.6	6.3	172	2.2	–	2.6

<sup>a</sup>  $\bar{x} \pm s$  = average of three determination ± standard deviation.<sup>b</sup> <LOD show that the results were lower than the limit of detection of ICP-OES; s<sub>overall</sub> = the overall average standard deviation.

(i.e., important consideration for the digestion conditions). On the other hand, Al, Cd and Mn are the analytes that requires careful control for the digestion conditions. Ba, Cr, Fe and Mg are the analytes presenting the least difficulty, providing that no significant effects of the factors studied were observed at any of the selected levels. Finally, the best factors were selected for each studied digestion method (Table 3).

### 3.4. Optimization of ICP-OES parameters

Once the digestion conditions are optimized, the next step was to optimize the instrumental conditions. It is important to optimize ICP-OES parameters in presence of the sample matrix because the intensity and shapes of the element signals are clearly depend on the matrix. In this study, the instru-

mental parameters namely radio-frequency (rf) incident power, sample uptake flow rate, nebulizer argon gas flow rate, auxiliary argon gas flow rate and plasma argon gas flow rate were optimized using digested peanut matrix rather than aqueous standard solution. The first three parameters have the most significant effect on emission intensities and depending on the type of emission line, they are subjected to change. The last two parameters have relatively small effects on sensitivity and are usually adjusted to accommodate a particular sample type, such as organic materials and high dissolved solids, rather than to improve the best limits of detection.

The sample uptake flow rate was investigated at three levels: 1.0, 2.0 and 3.0 ml min<sup>-1</sup>. It was found that the emission intensities for Ba, Mn, Cd, Fe and Pb were higher at 1 ml min<sup>-1</sup>,

Table 6

Main effect of the selected factors, calculated according to the equation described in Section 3.2

	Al	Ba	Cd	Cr	Cu	Fe	Mg	Mn	Pb	Zn
Digestion with HNO <sub>3</sub> /H <sub>2</sub> SO <sub>4</sub>										
A	5.0	0.1	-0.1	0.1	1.6 <sup>a</sup>	6.1	-8.0	-0.8	NQ <sup>b</sup>	7.1 <sup>a</sup>
B	12.8 <sup>a</sup>	0.2	0.1	0.3	0.1	8.1	-3.5	0.9	NQ	1.6
C	1.6	0.2	0.1	-0.1	-1.3 <sup>a</sup>	1.0	12.0	3.1	NQ	0.1
D	12.6 <sup>a</sup>	0.1	0.1	-0.2	-0.2	3.3	5.0	2.1	NQ	0.1
E	-0.1	0.3	0.1	-0.1	-0.1	4.5	2.5	0.3	NQ	2.4
Digestion with HNO <sub>3</sub> /H <sub>2</sub> SO <sub>4</sub> /H <sub>2</sub> O <sub>2</sub>										
A	5.2	0.1	-0.1	0.2	0.1	4.5	2.5	-0.7	NQ <sup>b</sup>	7.1 <sup>a</sup>
B	8.5	0.2	0.2	0.1	-0.2	3.1	7.0	-0.8	NQ	7.0 <sup>a</sup>
C	-3.1	-0.1	0.2	0.1	-0.2	-2.3	6.0	2.3	NQ	2.0
D	-8.6	-0.2	0.1	0.1	0.1	-9.1	-0.5	-2.3	NQ	-3.6
E	0.8	0.5	0.1	0.1	0.1	8.8	-2.0	0.5	NQ	0.3
F	-9.5	-0.1	-0.5 <sup>a</sup>	-0.2	-1.3 <sup>a</sup>	-8.5	-7.0	-4.7 <sup>a</sup>	NQ	-1.3

<sup>a</sup> Values higher than the experimental error (i.e., larger than twice the overall average standard deviation, >2s<sub>overall</sub>).<sup>b</sup> NQ: not quantitated due to <LOD.

Table 7  
Percent recoveries of analytes in IAEA-331 and IAEA-359<sup>a</sup> using two digestion methods

Element	HNO <sub>3</sub> /H <sub>2</sub> SO <sub>4</sub> digestion; recovery (%) <sup>b</sup>		HNO <sub>3</sub> /H <sub>2</sub> SO <sub>4</sub> /H <sub>2</sub> O <sub>2</sub> digestion; recovery (%) <sup>b</sup>	
	IAEA-331	IAEA-359	IAEA-331	IAEA-359
Al	86 ± 2	–	89 ± 3	–
Ba	–	94 ± 2	–	95 ± 3
Cd	95 ± 5	<LOD <sup>c</sup>	103 ± 5	<LOD
Cr	–	100 ± 5	–	104 ± 6
Cu	99 ± 5	99 ± 4	98 ± 5	100 ± 4
Fe	–	86 ± 4	–	101 ± 3
Mg	99 ± 3	88 ± 2	103 ± 3	96 ± 3
Mn	101 ± 5	90 ± 5	101 ± 4	98 ± 5
Pb	<LOD	<LOD	<LOD	<LOD
Zn	93 ± 5	104 ± 6	95 ± 5	100 ± 5

<sup>a</sup> IAEA certified values (mean ± standard deviation).

<sup>b</sup> Mean ± standard deviation ( $n=3$ ).

<sup>c</sup> <LOD show that the results were lower than the limits of detection of ICP-OES.

while for Zn, Al, Cu and Mg the flow rates were higher at 2 ml min<sup>-1</sup>, and only for Cr the intensity was slightly higher at 3 ml min<sup>-1</sup>. Therefore, in the present study, the sample uptake flow rate of 1 ml min<sup>-1</sup> which provide sufficient sensitivity and low sample consumptions, was chosen as optimal and applied for quantification throughout this study. Moreover, the rf incident power was optimized as it affects seriously the plasma temperature and improves atom excitation performance. It was studied in the range between 1100 and 1500 W. The results indicated that the sensitivity and the linearity are better at 1300 W for almost all analytes with some exceptional cases, and the stability of plasma was also improved. The effect of nebulizer argon gas flow rate was studied from 0.6 to 1.41 min<sup>-1</sup> appearing a maximum intensity at 0.81 min<sup>-1</sup> for almost all analytes. Thus, a 0.81 min<sup>-1</sup> nebulizer argon gas flow rate was adopted throughout this study, which provides high sensitivity and good precision. The optimum values for instrumental parameters are shown in Table 1.

### 3.5. Validation and comparison of the digestion methods

To verify the accuracy of the proposed methods, two CRMs (spinach leaves and cabbage) have been digested by the developed procedures and analyzed by ICP-OES using the operation conditions and the selected digestion conditions that are listed in Tables 1 and 3, respectively. These reference materials were chosen as they were the closest available to resemble the nut matrices. Also, they are certified for most of the analytes of interest to be determined. The results indicated that there are good agreement between measured and certified values within relative errors of less than 15% for wet digestion with HNO<sub>3</sub>/H<sub>2</sub>SO<sub>4</sub> and <11% for wet digestion with HNO<sub>3</sub>/H<sub>2</sub>SO<sub>4</sub>/H<sub>2</sub>O<sub>2</sub> (Table 7). Moreover, Student's *t*-test at 95% confidence level showed that there were insignificant differences between the means of the certified and obtained values for almost all analytes under investigation.

The two digestion methods were found to allow digestion of similar sample mass at same digestion time. According to recovery calculations (the accuracy of the proposed methods)

with respect to CRMs, rather than the effects of digestion factors, the wet digestion with HNO<sub>3</sub>/H<sub>2</sub>SO<sub>4</sub>/H<sub>2</sub>O<sub>2</sub> gave the best results for almost all of analytes (Table 7). The recovery result of Cr with HNO<sub>3</sub>/H<sub>2</sub>SO<sub>4</sub> digestion method was better. It is clear that the recoveries of Al and Fe obtained from HNO<sub>3</sub>/H<sub>2</sub>SO<sub>4</sub> digestion method were not so good. For the rest of the analytes wet digestion with HNO<sub>3</sub>/H<sub>2</sub>SO<sub>4</sub>/H<sub>2</sub>O<sub>2</sub> gave comparable or better recoveries than with HNO<sub>3</sub>/H<sub>2</sub>SO<sub>4</sub> digestion method, i.e., the digestion mixture HNO<sub>3</sub>/H<sub>2</sub>SO<sub>4</sub>/H<sub>2</sub>O<sub>2</sub> was capable to quantitatively extract almost all analytes in the CRMs. This indicates that, the presence of H<sub>2</sub>O<sub>2</sub> is very important for digesting food samples high in carbohydrates and/or fats, and was applied for samples digestion and analytes quantification throughout this study.

### 3.6. Limits of detection and precision

The solution LOD for the ICP-OES procedure were calculated as the concentration equal to three times the standard deviation (S.D.) of 10 blank measurements divided by the slope (*b*) of calibration line of aqueous standard or standard addition for each analyte (i.e., 3 × S.D./*b*). For the calculation of the LOD, ten separate blank solutions, which prepared independently, were analyzed. The obtained LOD (Table 2) are generally providing sufficient detection capability to determine elements of nutritional interest easily, at the concentrations present in nuts. Further improvement of LOD values for the solid material may be achieved by using larger sample weights and/or lower final dilutions. On the other hand, for the selected spectral lines (Table 2) for almost all analytes the *b*-values (slopes) that obtained for aqueous solutions were 2–16% higher than those obtained for standard addition solutions, with some exceptional cases for Al, Ba, Cd, Cu, Mn and Pb. These differences obviously result from chemical and/or matrix interferences (i.e., the chemicals, the analytes and as well as the sample matrices). This primary observation indicates that the sensitivities of the two techniques were quite different. Thus, aqueous standard can be used for Cd, Cr, Cu, Fe, Mg and Mn, while, standard addition technique was important for Al, Ba, Pb and Zn in order to elim-

Table 8

Method comparison test (using a linear regression line) for comparison of *b* and *r* of the regression lines for nut samples

Element	Peanut			Almond			Walnut			Hazelnut		
	<i>r</i>	<i>b</i> (cps $\mu\text{g}^{-1}$ l) <sup>a</sup>	Result <sup>b</sup>	<i>r</i>	<i>b</i> (cps $\mu\text{g}^{-1}$ l)	Result	<i>r</i>	<i>b</i> (cps $\mu\text{g}^{-1}$ l)	Result	<i>r</i>	<i>b</i> (cps $\mu\text{g}^{-1}$ l)	Result
Al	0.997	0.82 ± 0.15	S	0.999	0.81 ± 0.04	S	0.993	0.83 ± 0.23	NS	0.999	0.82 ± 0.08	S
Ba	0.999	0.91 ± 0.28	NS	0.999	1.02 ± 0.29	NS	0.991	1.10 ± 0.30	NS	0.993	1.34 ± 0.45	NS
Cd	0.999	0.39 ± 0.04	S	0.999	0.39 ± 0.02	S	0.999	0.44 ± 0.10	S	0.995	0.43 ± 0.30	S
Cr	0.995	1.03 ± 0.24	NS	0.998	0.94 ± 0.12	NS	0.992	0.95 ± 0.27	NS	0.999	0.93 ± 0.09	NS
Cu	0.997	0.79 ± 0.14	S	0.999	0.77 ± 0.08	S	0.985	0.76 ± 0.32	NS	0.997	0.78 ± 0.14	S
Fe	0.995	0.86 ± 0.20	NS	0.973	1.13 ± 0.62	NS	0.954	1.32 ± 0.95	NS	0.841	1.14 ± 0.21	NS
Mg	0.994	0.04 ± 0.03	S	0.994	1.16 ± 0.33	NS	0.999	0.06 ± 0.07	S	0.830	0.57 ± 0.26	S
Mn	0.995	0.87 ± 0.21	NS	0.999	0.81 ± 0.04	S	0.980	0.73 ± 0.34	NS	0.998	0.78 ± 0.12	S
Pb	0.990	1.30 ± 0.42	NS	0.985	1.16 ± 0.46	NS	0.987	1.50 ± 0.57	NS	0.988	1.39 ± 0.50	NS
Zn	0.997	0.55 ± 0.10	S	0.999	0.52 ± 0.05	S	0.977	0.49 ± 0.25	S	0.997	0.54 ± 0.10	S

<sup>a</sup> Mean ± standard deviation (*n* = 3).<sup>b</sup> Significant difference (S) or non significant difference (NS) at 99% probability level.

inate the interferences. Therefore, standard addition technique was used (to all analytes) for the rest of the study.

The precision of the method was determined by replicate determination of aqueous standard solution containing

250  $\mu\text{g l}^{-1}$  of each analyte. The calculated R.S.D. for all analytes was found in the range between 2.0 and 8.2%. The results indicate that the developed procedure offers good precision for all analytes.

Table 9

Al, Ba, Cd, Cr, Cu, Fe, Mg, Mn, Pb and Zn levels ( $\mu\text{g g}^{-1}$ ) reported in the literature for nuts

Sample	Al	Ba	Cd	Cr	Cu	Fe	Mg	Mn	Pb	Zn	Reference
<b>Almond</b>											
Spain	8.3	–	0.008	0.4	11.1	45.0	–	–	0.3	38.8	[17]
Spain	–	–	–	–	11.1	44.0	–	–	–	15.0	[20]
Italy	–	–	–	–	20 ± 0	140 ± 10	2400 ± 40	–	–	60 ± 3	[6]
UK	–	–	–	–	3.7	11.0	–	–	–	12.0	[18]
USA	–	–	–	–	11.1	43.0	–	–	–	33.6	[19]
Chile	–	–	–	–	10.4 ± 2.8	20.2 ± 8.0	–	–	–	24.4 ± 4.7	[24]
Greece	9.6 ± 1.0	0.11 ± 0.02	<LOD <sup>a</sup>	0.81 ± 0.06	9.9 ± 0.8	39.5 ± 2.3	1789 ± 52	11.6 ± 0.9	<LOD	33.9 ± 3.4	Present study
<b>Hazelnut</b>											
Spain	9.4	–	0.006	0.37	16.6	17.3	–	–	0.31	42.5	[17]
Spain	–	–	–	–	15.3	17	–	–	–	20	[20]
Italy	–	–	–	–	20 ± 0	80 ± 20	1700 ± 2	–	–	30 ± 10	[6]
UK	–	–	–	–	12.3	32.0	–	–	–	21	[18]
Greece	5.7 ± 0.8	0.07 ± 0.01	<LOD	0.68 ± 0.05	19.2 ± 2.3	76.0 ± 4.9	1273 ± 34	16.3 ± 1.7	<LOD	41.1 ± 4.0	Present study
<b>Peanut</b>											
Spain	1.9	–	0.009	0.38	6.9	22.8	–	–	0.29	31.9	[17]
Spain	–	–	–	–	0.1–10.5	6.6–39.4	–	–	–	–	[21]
Italy	–	–	–	–	10 ± 1	60 ± 1	1600 ± 500	–	–	40 ± 2	[6]
Bulgaria	–	–	0.45–1.04	–	–	–	–	–	5.2–9.7	47–80	[23]
USA	–	–	–	–	11.44	45.8	–	–	–	32.7	[19]
Chile	–	–	–	–	8.5 ± 1.8	12.4 ± 1.4	–	–	–	28.9 ± 3.2	[24]
China	–	–	0.36–0.55	–	12.7–19.8	–	–	–	0.13–0.78	57.9–65.3	[22]
Greece	3.4 ± 0.7	0.06 ± 0.01	<LOD	0.40 ± 0.04	18.8 ± 1.7	69.9 ± 4.1	966 ± 27	17.8 ± 1.7	<LOD	26.5 ± 2.7	Present study
<b>Walnut</b>											
Spain	4.7	–	0.006	0.35	22.0	22.5	–	–	0.24	28.50	[17]
Italy	–	–	–	–	20 ± 2	70 ± 3	1600 ± 300	–	–	40 ± 2	[6]
UK	–	–	–	–	14.6	29.0	–	–	–	27.0	[18]
USA	–	–	–	–	15.9	29.1	–	–	–	30.9	[19]
Chile	–	–	–	–	17.7 ± 5.8	26.1 ± 4.3	–	–	–	29.8 ± 7.9	[24]
France	–	–	–	–	12–15	18–24	1290–1910	24–43	–	18–19	[25]
California	–	–	–	–	13.0	24.0	1130	21.0	–	29.0	[26]
Greece	2.9 ± 0.5	<LOD	<LOD	0.53 ± 0.03	17.0 ± 1.2	45.0 ± 3.1	1330 ± 41	26.5 ± 2.3	<LOD	22.6 ± 3.0	Present study

<sup>a</sup> <LOD show that the results were lower than the limits of detection of ICP-OES.



### 3.7. Matrix effect and calibration techniques

In this study aqueous standards and standard addition solutions which prepared for the investigated samples using  $\text{HNO}_3/\text{H}_2\text{SO}_4/\text{H}_2\text{O}_2$  were utilized to select the calibration technique. To determine if the sample matrix could interfere with the analytes, linear regression statistical test at 99% probability level was applied. Slope ( $b$ ) and intercept ( $a$ ) are calculated by plotting the emission intensities of aqueous standards versus the emission intensities of standard addition solutions that prepared for nut samples. The calculated  $b$ -values were in the range of 0.8–1.2 cps  $\mu\text{g}^{-1}$  l (counts per second  $\mu\text{g}^{-1}$  l) (Table 8) for almost all analytes with some exceptional cases. The theoretical model assumes that, the value of  $b$  is equal to unity (absence of systematic errors) [16]. Practically, if the observed  $b$ -value did not differ significantly from unity then the sensitivities between the two techniques were similar, otherwise the two techniques were significantly different. It was found that the analytes were shown significant (S) or non-significant (NS) differences (at 99% probability level) depending on type of sample matrix. These differences obviously attribute to both the digestion mixture and sample matrices, which causes chemical interferences. Moreover, the theoretical model assumes that, the value of  $r$  is equal to unity (maximum accordance) [16]. It was found that the calculated  $r$ -values varied in the range of 0.850 and 0.999 (Table 8) for all analytes and  $r$ -values greater than 0.800 were assumed to be acceptable lower limit (i.e., the correlations were statistically NS at 99% probability level). The minor differences obviously attribute to the same reasons that are mentioned above. Consequently, calibrations using the standard addition technique are recommended for determination of these elements in nut samples, to overcome or to eliminate most of the errors due to non-linearity and/or matrix interferences that causes low sensitivity. On the overall, the results proved that, the developed procedures are in good accordance for analyzing nut samples for the selected analytes with acceptable accuracy.

### 3.8. Applications in mineral analysis of common nuts

The developed analytical method using  $\text{HNO}_3/\text{H}_2\text{SO}_4/\text{H}_2\text{O}_2$  as digestion mixture was applied for the determination of Al, Ba, Cd, Cr, Cu, Fe, Mg, Mn, Pb and Zn in four types of the most commonly consumed commercial nut samples (Table 9). In the whole, mineral composition of the analyzed samples showed high levels of Fe and Mg, and at the opposite very low level of Ba. Cd and Pb levels in all nut samples were lower than the LOD of ICP-OES.

Our data are in agreement with those of earlier reports shown in Table 9 except for Cd and Pb (i.e., Cd and Pb are <LOD of ICP-OES) [6,17–26]. With regard to minerals, the nutritional interest of nuts is mainly due to trace elements and Mg content. For that reason the higher content of Mg in almond is of particular interest as is the higher level of Zn in hazelnut.

## 4. Conclusions

The analytical ICP-OES technique which has been developed and validated for nut samples proved to be simple (0.5 g sample +  $\text{HNO}_3/\text{H}_2\text{SO}_4$  or  $\text{HNO}_3/\text{H}_2\text{SO}_4/\text{H}_2\text{O}_2$ ), rapid (<1 h), accurate ( $e < 11\%$ ) and precise (R.S.D. < 9%) for simultaneous determination of essential and non-essential elements (at least nine elements) in nut samples. Also, it can be considered as useful technique for routine analysis of trace elements in foods and possibly similar matrices and in quality control. The use of an experimental design may contribute to a good relation of cost and benefit and also permit the analyst to estimate the optimal conditions to guarantee quality assurance, including precision and accuracy. The Plackett–Burman design was proved to be a powerful tool to optimize the variables affecting samples digestion. Also, this design can make the analyst's task quicker (offers optimization of all variables with a minimum number of experiments) and provides more reliable answer to the question posed. For almost all analytes, calibration after standard addition was preferable to that, using aqueous standards. In some exceptional cases like Cd, Cu and Mn, for which the slopes of standard addition were 2–12% higher than those obtained for aqueous standards, the later can also, be used. The dynamic range of the method covers the range of the concentrations usually found in nut samples. The multi-element analysis capability provided by ICP-OES combined with its wide dynamic range will, however, make it a likely choice for any large-scale food composition studies.

## Acknowledgment

The financial support of this research by Greek State Scholarship Foundation (IKY) is gratefully acknowledged.

## References

- [1] I. Rodushkin, T. Ruth, A. Huhtasaari, *Anal. Chim. Acta* 378 (1999) 191.
- [2] S. Tuncel, S. Yenisoy-Karakas, A. Dogangun, *Talanta* 63 (2004) 273.
- [3] A. Sapkota, M. Krachler, C. Scholz, N. Cheburkin, W. Shotyk, *Anal. Chim. Acta* 540 (2005) 247.
- [4] F. Monaci, F. Moni, E. Lanciotti, D. Grechi, R. Bargagli, *Environ. Pollut.* 107 (2000) 321.
- [5] L. Hansson, J. Pettersson, A. Olin, *Talanta* 34 (1987) 829.
- [6] M. Plessi, D. Bertelli, A. Monzani, M. Simonetti, A. Neri, P. Damiani, *J. Food Comp. Anal.* 12 (1999) 91.
- [7] U. Tinggi, C. Reilly, C. Patterson, *Food Chem.* 60 (1997) 123.
- [8] AOAC Official Methods of Analysis, 15th ed., Association of Official Analytical Chemists, Arlington, Virginia, 1990, p. 778.
- [9] S. D'Illo, M. Alessandrelli, R. Cresti, G. Forte, S. Caroli, *Microchem. J.* 73 (2002) 195.
- [10] E. Santos, D. Lauria, P. Da Silveira, *Sci. Total Environ.* 327 (2004) 69.
- [11] E. Pelus, J. Arnaud, H. Faure, A. Favier, A.M. Roussel, *Int. J. Food Sci. Nutr.* 45 (1994) 63.
- [12] G. Seiler, A. Sigel, H. Sigel, *Handbook on Metals in Clinical and Analytical Chemistry*, Marcel Dekker, New York, 1994.
- [13] International Programme on Chemical Safety, *Environmental Health Criteria No. 134*, World Health Organization, Geneva, 1992.
- [14] A. Mohd, J. Dean, W. Tomlinson, *Analyst* 117 (1992) 1743.

- [15] M. Blanco, R. Ribo, X. Tomas, J. Obiols, *Anal. Proc. Including Anal. Commun.* 31 (1994) 353.
- [16] J. Miller, J. Miller, *Statistics for Analytical Chemistry*, 4th ed., Prentice Hall, New York, 2000.
- [17] C. Cabrera, F. Lioris, R. Gimenez, M. Olalla, C. Lopez, *Sci. Total Environ.* 308 (2003) 1.
- [18] B. Holland, I. Unwin, D. Buss, *First Supplement to McCance and Widdowson's. The Composition of Foods*, 5th ed., Royal Society of Chemistry, Cambridge, 1992.
- [19] USDA, *Food Composition and Nutrition Links*, 2001 (<http://www.nal.usda.gov>).
- [20] A. Jimenez, P. Cervera, M. Bacardi, *Tabla de Composicion de Alimentos*, Novartis Nutrition, Barcelona, 1998.
- [21] J. Anzano, P. Gonzalez, *Microchem. J.* 64 (2000) 141.
- [22] H. Liu, A. Probst, B. Liao, *Sci. Total Environ.* 239 (2005) 153.
- [23] K. Stefanov, K. Seizova, N. Yanishlieva, E. Marinova, S. Popov, *Food Chem.* 54 (1995) 311.
- [24] M. Olivares, F. Pizarro, S. de Pablo, M. Araya, R. Uauy, *J. Nutr.* 20 (2004) 205.
- [25] F. Laedrine, A. Ravel, A. Villet, V. Ducros, J. Alary, *Food Chem.* 68 (2000) 347.
- [26] M. Ravai, *Cereal Food Worlds* 37 (1992) 362.

## A new sensor for thermometric titrations

Fadhil M. Najib\*, Sardir Zewar, Ahmad M. Abdulla

*Chemistry Department, Collage of Science, Sulaimani University, Kurdistan Region, Iraq*

Received 24 May 2005; received in revised form 19 February 2006; accepted 17 March 2006

Available online 15 May 2006

### Abstract

A new thermometric sensor, which is a transistor (OC71), has been introduced to follow thermometric titrations successfully to clear end points. The sensor was suitable in both normal and differential modes of titration. It is possible to titrate down to 1.32  $\mu\text{mol}$  of HCl and 26.4  $\mu\text{mol}$  of  $\text{H}_3\text{BO}_3$  in a final 20 ml solution with accuracy and precision of 1%, 2.2% and 1.4%, 2.2%, respectively. The sensor, in association with a pH glass electrode, was used for the determination of  $\text{p}K$  values of some well established weak acids such as, acetic acid (4.77), phosphoric acid ( $\text{p}K_1 = 2.18$ ,  $\text{p}K_2 = 7.20$  and  $\text{p}K_3 = 12.32$ ) as well as for a very weak acid of uncertain  $\text{p}K$  values  $\text{H}_3\text{BO}_3$  ( $\text{p}K_1 = 9.20$ ,  $\text{p}K_2 = 12.7$  and  $\text{p}K_3 = 13.80$ ). The sensor was also examined for kinetic catalytic determination of iron(III) in water, milk and pharmaceuticals.

© 2006 Elsevier B.V. All rights reserved.

**Keywords:** Thermometric sensor; Transistor OC71; Thermometric titration;  $\text{p}K_a$  of boric acid; Silicon diode; Iron(III); Water; Milk; Pharmaceuticals

### 1. Introduction

The first thermometric titration reported was that of citric acid against aqueous ammonia using Beckmann thermometer [1] followed by more applications [2–9]. In 1941, Muller [10] replaced Beckmann thermometer with a multi junction thermopile, using a differential thermometric method.

The major breakthrough in the technique was that reported by Linde et al. [11] in 1953 using thermistors which were devices constructed from sintered metallic oxides of iron, copper, manganese, nickel . . . , etc. In contrast to the metals used in making thermocouples, which have positive temperature coefficient, for thermistors this coefficient is negative. Good reviews on the subject appeared in the literature [12,13]. Even recent workers have used a thermistor as a thermometric sensor [14–17], although recently diodes have been used as thermometers [18,19]. To best of our knowledge, no thermometric sensor, other than those mentioned above, has been found in the literature particularly transistors and diodes. The present work reports, for the first time, the use of a transistor type OC71 as a new sensor for thermometric titrations in analytical chemistry. The success of this

new sensor in thermometric titrations was tested by its application to locate the end points clearly in order to enable the determination of  $\text{p}K_a$  values of very weak acids such as  $\text{H}_3\text{BO}_3$ . The sensor was also applied for the determination of iron(III) at nanogram level in samples of water, milk and pharmaceuticals.

### 2. Experimental

#### 2.1. Chemicals and reagents

All chemicals were of A.R grade. Borax, phosphoric acid, 60% (w/v) ferric chloride solution, sodium periodate, 1,10-phenanthroline and  $\text{KNO}_3$  from (BDH), acetic acid (Tetnal Photowerk&Co.), boric acid (Lubico-Belgium), NaOH and 37% fuming HCl (Fluka).

Different concentrations of the acids and bases were prepared in the usual way. A standard stock solution of iron(III) (1000 ppm.) was prepared from the ferric chloride solution. Acetate buffer (pH 4.75) was prepared from crystalline sodium acetate (from Sheminab), and concentrated acetic acid. Standard sulphanilic acid solutions of different concentrations were prepared from solid substance (Merck) in acetate buffer (pH 4.75). This was done by dissolving the weighed quantities of 20.51 g crystalline sodium acetate and 0.9525 g of solid sulphanilic acid in a sufficient amount of 1 M acetic acid solution. The pH of this solution was then adjusted to 4.75 by slow addition of 1 M

\* Corresponding author.

E-mail addresses: [fadhilmn@yahoo.com](mailto:fadhilmn@yahoo.com) (F.M. Najib), [sardirzewar@yahoo.com](mailto:sardirzewar@yahoo.com) (S. Zewar), [meerahmaad56@yahoo.com](mailto:meerahmaad56@yahoo.com) (A.M. Abdulla).

acetic acid and controlling by a pH meter. Finally, the volume was completed to 250 ml in a volumetric flask. The concentration of sulphanilic acid in the final solution was  $2.2 \times 10^{-2}$  M and 1 M for each of acetate buffer components (sodium acetate and acetic acid).

### 3. Apparatus

A new thermometric sensor OC71 (Ge-P, pnp germanium type NF-V/Tr, 32 V, 10 mA, 0.125 W,  $B > 20$ ). An electronic circuit, which was a two stage differential amplifier, connected with the sensor, (details of construction can be obtained from one of the authors Mr. Zewar, an ISA member No. 20209146, who is the designer), a vertical stirrer, a pump (type: original-perfusor, spritze, 50 ml B. Braun) used for delivering the titrant through a large syringe of 60 ml capacity, a chart recorder, Universal Polarograph (type OH-105 from Radelkis Budapest), a digital avometer (perron MT 4063) used for the calibration of the recorder and watching its output, a digital thermometer, (testo 905-T2-Germany), a voltage stabilizer (stavol Matsunaga manufacturing Ltd. Japan), a 12 V storage battery used as a DC source, a digital pH meter (Orion701) equipped with a combined pH glass electrode (Orion Combined pH 910600), a vernier for measuring the distances on the enthalpograms.

### 4. Construction of the sensors

Two new sensors were tested, namely: a transistor type OC71 and a silicon diode (IN4148, SI.DI, 100 V, 0.2 A, 4 ns). The transistor sensor was fixed to one end of a glass tube (6 mm  $\phi$  and 100 mm long) by an adhesive glue (ATLAS a two components type from Tehran NOUH Co. Ltd) as shown in (Fig. 1(a)). The two wire leads of the sensor were shielded with aluminum foil, the other end of the tube was sealed with PVC tape.

The diode was fixed with the adhesive material to two thin glass tubes (3 mm diameter and 100 mm long) as shown in (Fig. 1(b)). The two wire leads were connected to the electronic circuit.

The above two sensors were arranged in the cell in such a way that, they can directly sense any change in heat inside the solution titrated.

A calibration resistance of 1000 k $\Omega$  was connected, fixed and the sensor together in their proper positions in the circuit. The position of the calibration resistance was replaced by another sensor identical to the first one, when differential thermometric titration procedure was applied. The circuit was fixed properly in an aluminum box (9 cm  $\times$  15 cm  $\times$  17.5 cm) having three dial

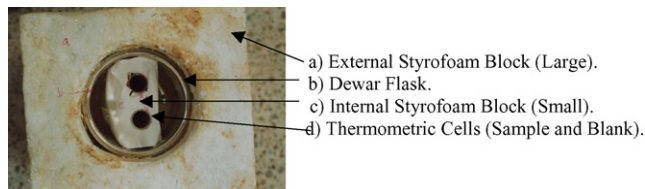


Fig. 2. Insulation of the thermometric titration vessels (a) external styrofoam block (large). (b) Dewar flask. (c) Internal styrofoam block (small). (d) Thermometric cells (sample and blank).

knobs outside, for initial adjustments. These adjustments were necessary as part of a successful measurement and they were:

- (1) Equilibrium adjustment of the two stages in the circuit. This was necessary when the calibration resistance or a new sensor was connected in addition to the periodic testing of the performance of the system or before the execution of a series of titrations or injections.
- (2) Zero adjustment.

### 5. The titration cell assembly

The titration cell was a polyethylene tube of 25 ml capacity for normal titration or two identical tubes in the differential mode. They were well isolated by fixing them in a thick block of styrofoam situated in a Dewar flask (of 1 l capacity) which itself was already insulated in a 6 cm wall thickness styrofoam as shown in Fig. 2. The whole cell was covered with the same thickness of styrofoam with small holes for fixing the sensor, passing the vertical stirrer and the titrant delivery tube. A sufficient length of this tube (50 cm long) was coiled inside, so that the titrant can maintain the same temperature for several titrations and finally performing the experiment in a constant-temperature room or a constant-temperature air box. All these insulations were performed after extensive tests of the whole system to minimize fluctuations due to temperature of the environment. Even stirring was studied and found effective in stabilizing the system. The titrant was delivered via this tube by a large syringe (60 ml capacity) fixed on a peristaltic pump.

### 6. The procedures

#### 6.1. Determination of the ionization constants

A portion of 20 ml sample (adjusted to 0.5 M ionic strength with solid  $\text{KNO}_3$ ) was placed in the cell, for differential mode

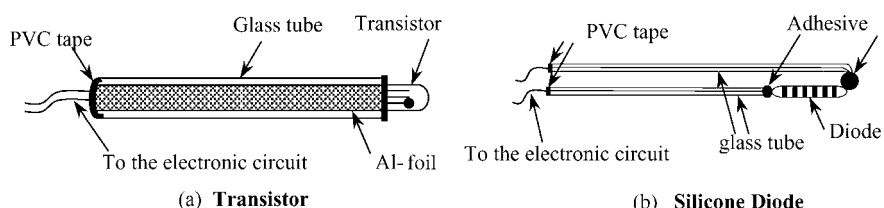


Fig. 1. Construction of the thermometric sensors. (a) Transistor; (b) silicone.

20 ml blank was also placed in the second cell. The lid, which was carrying the sensors, the delivery tube and a hole for a vertical stirrer, was pressed gently on the mouth of the Dewar flask and covering the whole block of titration. The titration was started by switching on both the pump and the chart recorder, at the same time. The complete enthalpogram was obtained from the chart recorder, in addition to exact value of  $\Delta mV$  read from a digital avometer. The titration was stopped when the last break of the end point was observed. Both the pump and the recorder's chart speeds were carefully optimized and manipulated in such a way to read the volume of the titrant directly from the chart paper with reasonable accuracy and precision.

Because of the small size of the cell in this work, the experiment was performed in two steps:

1. The differential thermometric titration of 0.01 M or higher concentration of the weak acid with 1.022 M NaOH solution was performed as described above.
2. The same titration above was repeated exactly in the same manner but a combined pH glass electrode was placed in the cell instead of the thermometric sensor. The pH was recorded manually during the course of titration each (5 s) for the same period of time used before. The pH scale was superimposed on the time scale of the enthalpogram. The final result was a thermogram with distinct breaks of the end points, in addition to pH values at any point required. This modification was needed to calculate the pK values of the weak acids. For this purpose also, the pH-glass electrode was calibrated using three standard buffers (pH 4.01, 7.04 and 10.12). In addition to that and at pH values higher than 10, the pH of the test solution was compared to the calculated pH of a standard NaOH solution having exactly the same pH value. This step was performed to account for the alkaline error of pH-glass electrode usually occur at such high pH values, but less effective at low temperature [20] as is in our case.

## 6.2. Determination of Iron(III)

A 5 ml portion of a mixture of sulphanic acid ( $2.2 \times 10^{-2}$  M), 1,10-phenanthroline ( $7.5 \times 10^{-4}$  M) in the acetate buffer solution (pH 4.75), was placed in the thermometric cell, and the desired volume of standard FeIII or sample solution was added and diluted to 19.5 ml. The cell was placed in its position and covered by the press-on lid. The solution was stirred while waiting for 2–3 min to attain thermal equilibrium. The output signals of both stages of the electronic circuit, were adjusted to zero until a smooth base line was obtained. Then a 0.5 ml portion of  $7.5 \times 10^{-3}$  M sodium periodate solution was injected rapidly, and the titration curve was recorded automatically on a strip chart recorder.

## 7. Results and discussion

It was not the authors' intention to discuss the theory of p-n semi conductors, which has been extensively studied in the literature [19] but rather have discovered their important capa-

bilities as sensors in different types of thermometric titrations in analytical chemistry.

## 8. Examination of the sensors

### 8.1. Selecting the sensor

In a rough titration of 0.01 M HCl with 1 M standard NaOH, one transistor of OC71 type and a silicon diode among several transistors and diodes were chosen for further investigations because they gave highest signals.

### 8.2. Resistance temperature behavior

The sensor was placed in a digital water bath and the changes in resistance were measured by a digital avometer and recorded manually for each 0.1 °C or more starting from 0 °C to 40 °C and the results are shown in Fig. 3(a and b). In spite of nonlinearity observed in these plots, which is quite usual with semiconductors [18,19], the figures show the existence of three linear regions of different mechanisms of response (Table 1).

The table shows clearly that even at highest value of the diode slope which is in region (I), it is about 6-folds of lower sensitivity than the minimum value of the transistor slope at region (III). In

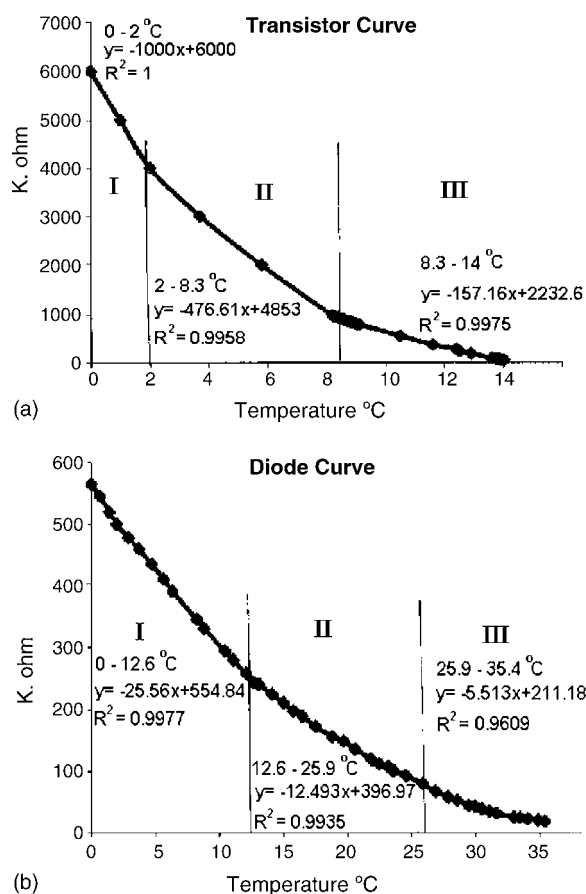


Fig. 3. (a) Resistance–temperature curve for transistor sensor. (b) Resistance–temperature curve for silicone diode.



Table 1

A comparison between the behavior of the transistor and the silicon diode, in the three linear regions shown in Fig. 3(a and b)

Region	Sensors type	Temperature-range degree (°C)	Slope ( $\Delta R/\Delta T$ ) K $\Omega$ /°C sensitivity
I	Transistor	0–2	–1000
	Diode	0–12.3	–25.06
II	Transistor	2–8.3	–477
	Diode	12.3–25.9	–12.49
III	Transistor	8–14	–157
	Diode	25.5–35	–5.5

another comparison between these two sensors and thermistors used in the literature, it was found that the transistor gave a maximum sensitivity of 200 mV/°C compared with 12.3 mV/°C and 67 mV/°C for both silicon diode and thermistors, respectively. Therefore, it was decided to complete the rest of the work with the transistor OC71.

Region III, which was chosen in the present work, was the least sensitive compared to regions (I and II), but it was most convenient for performing the experiments in the constant-temperature room used here. Furthermore, this region gave a good linearity between 8 °C and 14 °C as shown in Fig. 4. The other two regions could be used for higher sensitivities if proper conditions could be set carefully. If it is desired to work at the normal room temperature, the authors believe that this would be possible if a temperature-controlled air-bath, very well insulated, is used instead of working in a constant-temperature room.

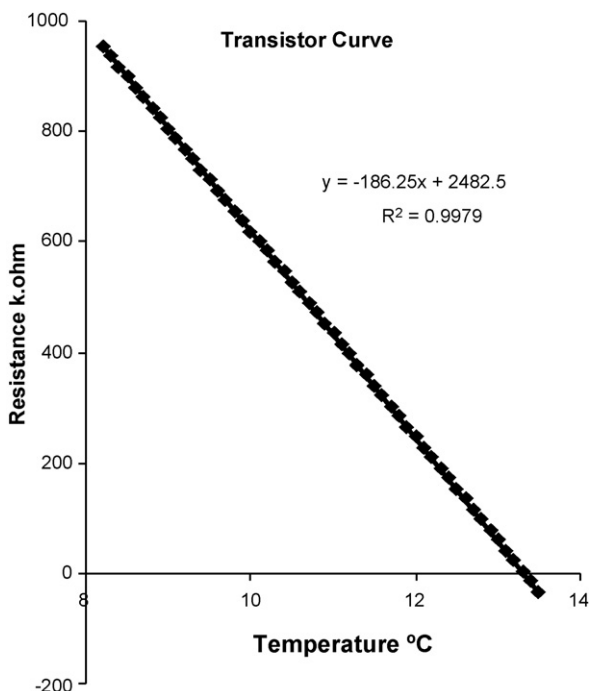


Fig. 4. Resistance–temperature curve for the transistor OC71 in the range 8–14 °C.

## 9. Testing the electronic circuit and the calibration resistance

In order to balance and calibrate the sensor before starting any experiment a reference resistance was needed in the circuit. The selection of this calibration resistance was found to depend on the sensor type used, as well as the working temperature. Although many resistances ranging between 800 k $\Omega$  and 1000 k $\Omega$  could satisfy balancing the sensor, but not all of these were suitable. The high sensitivity of the sensor to the temperature changes was causing the unbalancing of the system at some ranges of heat. At the working temperature of around 8–14 °C, the resistance value of 1000 k $\Omega$  was found satisfactory. An additional home-made electronic filter was also included into the circuit to smooth the outputs thermograms.

After these arrangements, the home-made electronic circuit was tested and compared with the usual Wheatstone bridge, commonly applied in thermometric titrations, and the results of the two outputs are shown in Fig. 5. A sensitivity of about 5-folds higher was obtained when the home-made electronic circuit was used (Fig. 5(a)).

The previous optimizations were performed on usual and differential titrations. In the differential mode, two identical sensors were used in two identical cells side by side in the same environment, one for the sample and the other for the reference. The second transistor was placed in the proper position instead of the calibration resistance. In this manner it was thought that most of the factors causing errors, especially variation in the environmental temperature will be eliminated or minimized, by difference. To evaluate all these primary tests, a series of simple titrations of standard HCl with 1.044 M NaOH, were performed.

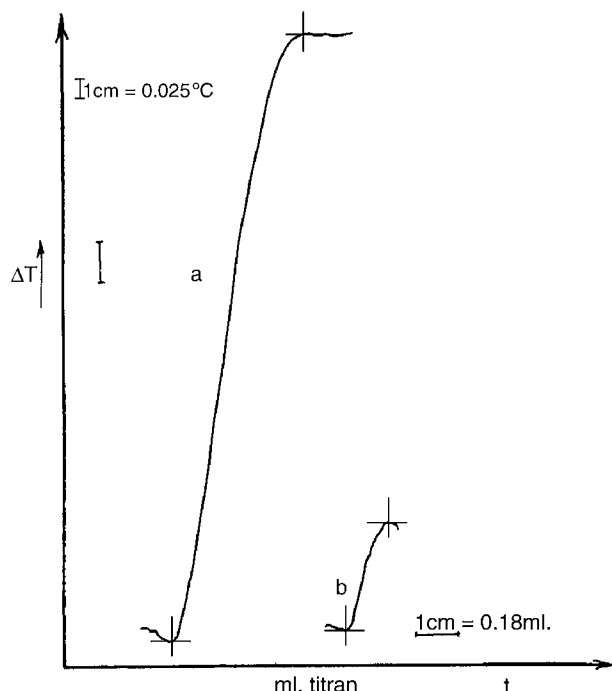


Fig. 5. Comparison between the output of (a) the home-made electronic circuit and (b) Wheatstone bridge in connection with the transistor sensor.

Table 2

Thermometric titrations of different concentrations of (20 ml) HCl or H<sub>3</sub>BO<sub>3</sub> in the cell with 1.044 M and 0.01455 M NaOH, as a titrant, respectively

Node	Acid type	Conc. (M)	μmoles present	Recovery R%	Error E%	R.S.D.%
Usual	HCl	$2.5 \times 10^{-2}$	500	101.80	+1.8	0.54
		$1.2 \times 10^{-2}$	240	104.73	+4.7	1.0
		$2.5 \times 10^{-3}$	50	121.94	+21.9	7.7
		$1.2 \times 10^{-3}$	24	126.53	+26.5	5.3
		$5.16 \times 10^{-4}$	10.32	131.77	+31.8	9.8
Differential	HCl	$1.2 \times 10^{-2}$	240	100.4	+0.4	1.2
		$1.6 \times 10^{-5}$	1.32	101.03	+1.03	2.2
	H <sub>3</sub> BO <sub>3</sub>	$1.32 \times 10^{-3}$	26.4	101.43	+1.43	2.2

Some of these titrations were repeated with HCl and also with H<sub>3</sub>BO<sub>3</sub> using the differential mode (Table 2).

The table shows that usual titration is only suitable at high concentration, not less than 240 μmol of HCl. On the other hand, the differential mode seems to have minimized the systematic error existed due to the environmental temperature variations. In this way, even a concentration down to 1.33 μmol of HCl and a very weak acid such as boric acid ( $K_a = 5.8 \times 10^{-10}$ ) down to (26.4 μmol) could be determined successfully with reasonable accuracy and precision, as shown in the table.

Furthermore, *t*-test was applied for the results of the differential mode and was found that there is no significant difference between  $\bar{X}$  and  $\mu$  since  $((\bar{X} - \mu) < t.s./\sqrt{n})$  at 95% C.L (DOF=9). This has emphasized that no systematic error was detected and the error present might just be a random error. It is important to point out that even visual titration with this acid was not successful unless some additives, such as mannitol or glucose, were added to enhance the acid property [21].

## 10. Determination of ionization constants of weak acids

Literature showed that the thermometric titration has not yet been used for the determination of ionization constants of weak acids and bases. The present method was applied to assist potentiometric titrations of very weak acids, or bases, to exactly locate the end points, followed, then, by the calculation of *pK* values in the usual way. In this sense, it will be extremely useful since a potentiometric titration of such systems is neither able to give sharp breaks at the end points, nor it can distinguish between the end points of a multibasic acids especially when they are too close to each other. In the latter case, such as H<sub>3</sub>BO<sub>3</sub>, which was examined in the present work, potentiometric titration was not successful because of unfavorable  $\Delta G$ . But, similar concentrations of this acid and the strong acid HCl, when titrated with NaOH gave almost identical end point sharpness, since both give close values of heat of neutralization 10.2 kcal/mol and 13.5 kcal/mol, respectively [12,22]. It is well known that in the titration of H<sub>3</sub>BO<sub>3</sub> with NaOH using thermistor as a sensor, although a sharp end point was obtained, the acid behaved as a monobasic acid [12]. As a matter of fact the reason was not due to the behavior of the acid but rather because the thermistor sensor was not sensitive enough to give

the three end point breaks, as it will be shown in the present work. But first to achieve reliability, the method was used for those acids having well established *pK<sub>a</sub>* values, such as the monobasic acetic and tribasic phosphoric acids. The procedure was then applied for the determination of the three (*pK<sub>a</sub>*) values of boric acid. Fig. 6(a and b) show the thermometric titrations of both H<sub>3</sub>PO<sub>4</sub> (Fig. 6(a)) and H<sub>3</sub>BO<sub>3</sub> (Fig. 6(b)) with standard NaOH solution. It can be seen that the present method is presenting sharp end points to the potentiometric method to complete the procedure. This was performed here by taking advantage of easy combination between the clear end points obtained by the present method and the possibility of quick change over of the thermometric sensor to a combined pH glass electrode for pH measurements of the same system by repeating the entire titration procedure followed by the location of the *pK<sub>a</sub>* positions.

Some handbooks and textbooks have given three *pK<sub>a</sub>* values for H<sub>3</sub>BO<sub>3</sub> [26,27] but they have neither given a reference nor did they give a procedure how these values were found.

To calculate *pK<sub>a</sub>*, the pH values were determined accurately at the half ways from the end points, where *pK<sub>a</sub>* = pH and the results are shown in Table 3. Apart from the results given in the present work, none of the methods listed in Table 3 has involved in thermometric titrations for the determination of *pK<sub>a</sub>* values.

A quick examination of the data obtained from the literature for both acetic and phosphoric acids, reveal that the results of the present work can be placed between, or very close to them. The literature values of *pK<sub>a</sub>* of acetic acid, for instance, ranged between 4.73 and 4.76 compared to 4.77 in the present work, which is only 0.4% higher.

If the values found in the literature were regarded as true values ( $\mu$ ), *t*-test has showed no significant difference between these results and those obtained in the present work at 95% C.L (DOF=5). All these confirm the reliability of the values in the present work, especially when such clear breaks are seen even at the third end point of H<sub>3</sub>PO<sub>4</sub> (Fig. 6(a)) which was not easily observed in potentiometric titrations, particularly in case of H<sub>3</sub>BO<sub>3</sub>. Thus, the values obtained in case of H<sub>3</sub>BO<sub>3</sub> were as well reliable.

Tyrrell [28] found, that sharp end points in thermometric titrations can be obtained when  $KC_A > 10^3$ , where *K* is the equilibrium constant of the reaction in which the total molar

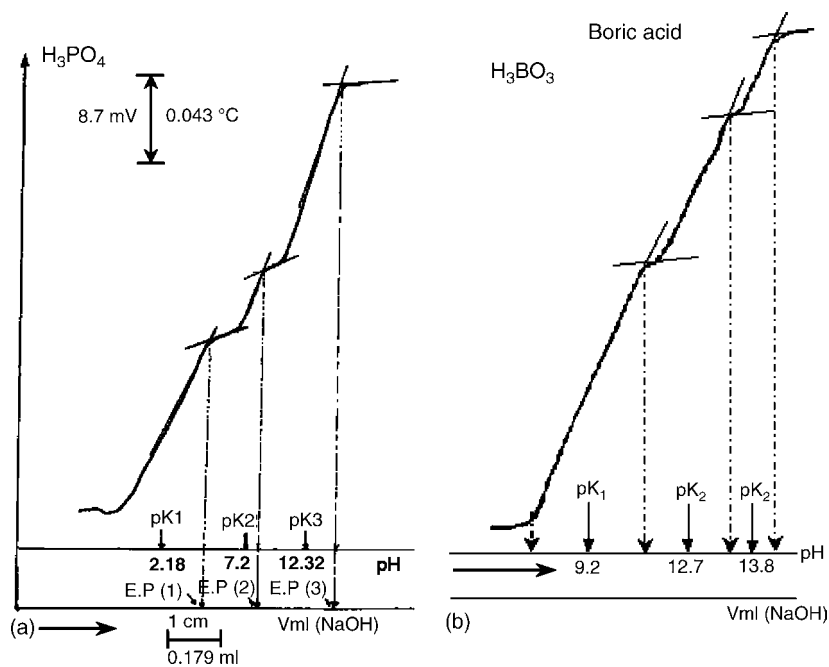


Fig. 6. Thermometric titration of 0.01 M of (a)  $\text{H}_3\text{PO}_4$  and (b)  $\text{H}_3\text{BO}_3$  with 1.022 M NaOH and the determination of their  $\text{pK}_a$  values.

concentration of the titrand is  $C_A$  providing that large enough heat of reaction is produced. He gave  $\text{H}_3\text{BO}_3$  as an example without referring to the neutralization steps. According to this theoretical finding, even the third end point in the titration between 0.01 M  $\text{H}_3\text{PO}_4$  and 1 M. NaOH cannot give a sharp end point since  $KC_A = 0.5$ .

In case of  $\text{H}_3\text{BO}_3$ , again according to Tyrrell the situation must even be worse, since none of the three end points can satisfy this theory. The results of the present work in Fig. 6(a and b) show reasonable, good and sharp end points for both  $\text{H}_3\text{PO}_4$  and  $\text{H}_3\text{BO}_3$ , this would suggest that more factors are missing and Tyrrell's theory has to be reconsidered. It is obvious that one of these factors must be the type of the sensor while the second may be the system of signal generation.

In the present work, these two factors which are the transistor sensor instead of thermistor, as shown before, and the home-made electronic circuit instead of Wheatstone bridge, as shown in Fig. 5, gave together more than 20-folds higher sensitivity than

a thermistor. Moreover, the heat of the reaction of the individual steps, which were not available to the authors, could also be other favourable factors.

## 11. Determination of iron(III)

Few Fe(III)-catalysed reactions have been reported [29–31] by thermometric techniques, although they have advantages over spectrophotometry for colored and turbid samples. The catalytic function of iron(III) on the oxidation of sulphanilic acid by potassium periodate has been applied successfully for the determination of iron(III) in tap water using the catalytic thermometric titration method (CTT) [29]. This method was exploited to examine the new sensor discovered in the present work for the determination of iron(III) in tap water, milk and some pharmaceutical drugs. Experiments were performed for optimization of conditions, including interferent studies, for iron(III) determination and the final results are presented in Table 4. The table

Table 3  
A Comparison between the ( $\text{pK}_a$ ) values of acids obtained by the present method with the values given in the literature

Acid	The present method	Ref. [21]	Ref. [23]	Ref. [24]	Ref. [25]	Ref. [26]	Ref. [27]
Acetic acid ( $\text{pK}_a$ )	4.77	4.73	4.76	4.76	4.76	4.75	4.757
Phosphoric acid ( $\text{pK}_{a1}$ )	2.18	2.12	2.23	2.12	2.00	2.12	2.148
( $\text{pK}_{a2}$ )	7.20	7.21	7.21	7.21	7.20	7.21	7.199
( $\text{pK}_{a3}$ )	12.32	12.67	12.32	12.30	12.37	12.67	12.15
Boric acid ( $\text{pK}_{a1}$ )	9.20	9.24	9.24	9.24	9.23	9.14	9.236
( $\text{pK}_{a2}$ )	12.70	–	–	–	–	12.74	12.74
( $\text{pK}_{a3}$ )	13.80	–	–	–	–	13.80	13.80

Table 4  
The optimum analytical conditions for the determination of iron(III) between (40 and 450) ppb, including interferences

Reagent	Concentration
pH	4.75 adjusted with acetate buffer
Sulphanilic acid	$2.2 \times 10^{-2}$ M
Sodium periodate	$7.5 \times 10^{-3}$ M
1,10-Phenanthroline	$7.5 \times 10^{-4}$ M
Interfering ions	Tolerance, limiting ratio [Ion]/[FeIII] folds giving no more than 5% error
Ce(IV), Mn(II)	<1
Co(II)	10
Ag(I)	20
Ni(II), Hg(II)	50
Cd(II), Cu(II), Pb(II), Ba(II)	100
Ca(II), Mg(II), Cr(III), Cr(VI), Zn(II)	250*
CO <sub>3</sub> <sup>2-</sup> , Cl <sup>-</sup> , NO <sub>3</sub> <sup>-</sup> , SO <sub>4</sub> <sup>2-</sup>	1000*

\* Maximum amount tested.

indicated sufficient selectivity in such a way that removing interferences was not required.

## 12. Preparation of the calibration curve

The calibration curve was obtained by two steps:

### (a) Slope measurement:

From the (temperature–time) curve obtained for each individual injection, a tangent was drawn for the initial part of the curve. The slope was measured as (mV s<sup>-1</sup>) or (°C s<sup>-1</sup>) by calibrating the Y-axis both in (mV) and (°C), as follows:

- (1) The calibration with (mV) was achieved using a digital avometer connected parallel with the recorder. The millivolts were converted to temperature readings (°C) according to the sensitivity of the transistor sensor, which was given before, in Table 1.
- (2) Time readings on (X-axis), were obtained from the chart speed of the recorder (cm/min), which was also examined periodically, without observation of any significant changes. The slope of the tangent was, then, calculated in the usual way after measuring the vertical and the

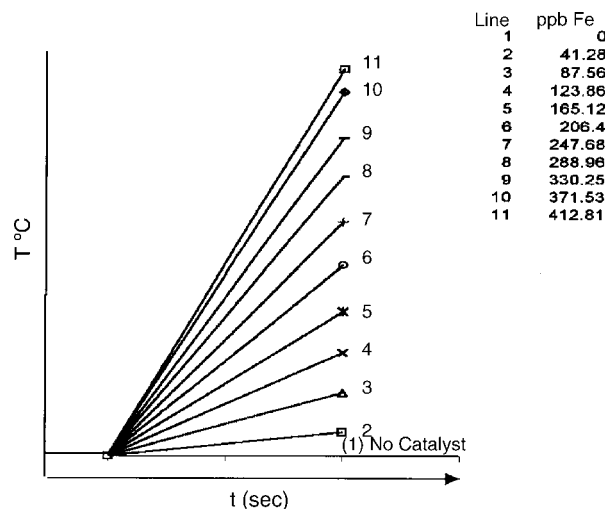


Fig. 7. Temperature–time plot in the presence of various concentrations of iron.

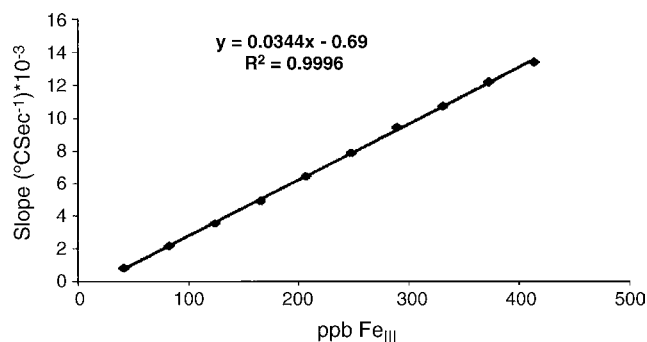


Fig. 8. Calibration curve between slope (°C s<sup>-1</sup>) with (ppb) Fe<sub>III</sub>.

horizontal distances with a vernier, the final results are shown in Fig. 7.

### (b) Final calibration:

The calibration curve was obtained by plotting the slopes obtained in step (a) as a function of standard iron(III) concentrations in (ppb), as shown in Fig. 8. The equation of the plot was ( $dT/dt = 0.0344 [\text{Fe}] - 0.69$ ) with the value of ( $R^2 = 0.9996$ ).

Iron(III) in the solid samples was determined after dry ashing and its amount in each sample was measured from the

Table 5  
Comparison between the results of iron(III) determination in different samples, by kinetic-thermometric titration of the present work and atomic absorption methods

No.	Samples	Iron(III) content	Present thermometric method			Atomic absorption method		
			Mean $\bar{X}$	E%	R.S.D.%	Mean $\bar{X}$	E%	R.S.D.%
1	Guigoze(I)	60 $\mu\text{g/g}^a$	62.13 $\mu\text{g/g}$	3.55	5.56	62.90 $\mu\text{g/g}$	4.83	2.64
2	Guigoze(I)	83 $\mu\text{g/g}^a$	86.25 $\mu\text{g/g}$	3.91	4.15	86.50 $\mu\text{g/g}$	4.21	1.53
3	Ferrosam tablets <sup>b</sup>	325 $\text{mg/g}^a$	315.3 $\text{mg/g}$	2.98	4.35	317.1 $\text{mg/g}$	2.43	1.47
4	Lentil	–	185.06 $\mu\text{g/g}$	–3.2 <sup>c</sup>	4.65	191.20 $\mu\text{g/g}$	–	0.49
5	Tap water I	–	210.98 $\text{ng/g}$	–3.6	3.66	203.60 $\text{ng/g}$	–	2.20
6	Tap water II	–	231.74 $\text{ng/g}$	–3.8	4.06	223.30 $\text{ng/g}$	–	2.62

<sup>a</sup> These values were obtained from the factory certificates.

<sup>b</sup> The solution was diluted (1000 times) before the measurement.

<sup>c</sup> If the results of A.A. were taken as nearest to the true values.

value of the slope ( $^{\circ}\text{C s}^{-1}$ ), which was obtained from the temperature–time curve. The results were compared with those obtained by flame atomic absorption (Table 5).

The comparison has been evaluated statistically using the paired comparison *t*-test. The results indicated that the difference between the two methods was not significant at 95% confidence limit (DOF = 5), and the present method was at least as good as the A.A. method. In some cases it was superior, for instance, turbid samples are preferably not analyzed by A.A., but made no problem in the present method.

Further statistical evaluations of the results shown in Table 5 were undertaken to examine the existence of a systematic error. The difference between the true value ( $\mu$ ) and the mean ( $\bar{X}$ ) was compared by using (*t*-test). For samples (1–3) the true values were obtained from the factories certificates, while the results of A.A. were given this credit for samples 4–6.

Statistical evaluation indicated no significant difference existed between the means and the true value at (95%) confidence limit (DOF = 5), thus no systematic errors were detected. The accuracy (2.98–3.91%) and precision (4.15–5.56) were acceptable for such low levels (ppb) of determinations.

### 13. Conclusions

In the present work, the transistor type OC71 was discovered to be a suitable sensor for use instead of thermistors in thermometric methods of analysis. The resistance–temp response showed three linear regions between (0–2)  $^{\circ}\text{C}$ , (2–8)  $^{\circ}\text{C}$  and (8–14)  $^{\circ}\text{C}$ . The sensitivity was about 200 mV/ $^{\circ}\text{C}$  in the region of (8–14  $^{\circ}\text{C}$ ) compared to 66.6 mV/ $^{\circ}\text{C}$  and 12.25 mV/ $^{\circ}\text{C}$  in case of thermistors (100 k $\Omega$ ) and silicon diode, respectively. This region was of lowest sensitivity but was most convenient to perform the experiments in a constant-temperature room. If conditions could be arranged, even higher sensitivity would be obtained using the other two regions. The sensor was tested and exploited in differential thermometric titrations for the determination of  $\text{pK}_a$  values of very weak acids, such as boric acid, which are usually difficult by other techniques. The method was also applied for the kinetic determination of iron (III) at nanogram level in water, milk and pharmaceuticals with reasonable accuracy and precision. This was based on its catalytic oxidation of sulphanilic acid by periodate ion in the presence of 1,10-phenanthroline

as an activator. Further applications are underway in future works.

### References

- [1] J.M. Bell, C.F. Cowell, J. Am. Soc. 35 (1913) 49.
- [2] P. Dutiot, E. Grobet, J. Chim. Phys. 19 (1921) 324.
- [3] B.C. Halder, J. Indian Chem. Soc. 23 (1947) 147; B.C. Halder, J. Indian Chem. Soc. 25 (1948) 439, 445.
- [4] A.K. Bahattachara, H.C. Gaur, Ibid (Cited from Ref. 12, p40) 25 (1948) 185.
- [5] S.K. Siddhanta, Ibid (Cited from Ref. 12, p40) 25 (1948) 579.
- [6] T. Somiya, J. Soc. Chem. Ind. (Japan) 30 (1927) 106.
- [7] T. Somiya, Chem. News 14 (1928) 137.
- [8] R. Paris, J. Robert, Compt. Rendus (Cited from Ref. 12, p40) 223 (1946) 1135.
- [9] T. Jordan, T.G. Alleman, Anal. Chem. 29 (1957) 9.
- [10] R.H. Muller, Ind. Eng. Chem. Anal. Edn. 13 (1941) 671.
- [11] H.W. Linde, L.B. Rogers, D.N. Hume, Anal. Chem. 25 (1953) 404.
- [12] L.S. Bark, S.M. Bark, Thermometric Titrimetry, Pergamon Press, 1969, p. 42.
- [13] L.S. Bark, P. Bate, J.K. Grime, Annu. Rev. Anal. Sci. 2 (1972) 121.
- [14] C.B.F. Jullio, M.A. Luiz, D.N. Graciliano, E.S.G. Oswald, Analyst 121 (1996) 559.
- [15] F.A. Biljana, D.T. Sanja, K.A. Borislav, F.G. Ferec, Analyst 121 (1996) 425.
- [16] Multititrator Ply Ltd., 1999, from Internet.
- [17] J.D.C. Mario, A.F.J. Mario, E.S.G. Oswald Jr., Braz. Chem. Soc. 13 (5) (2002) 692.
- [18] P.R.N. Childs, J.R. Greenwood, C.A. Long, Rev. Sci. Instrum. 71 (2000) 2659.
- [19] J.W. Precker, M.A. da Silva, Am. J. Phys. 70 (11) (2002) 1150.
- [20] N. Linnet, pH measurements in theory and practice, Radiometer (Copenhagen), 1970, pp. 80–83.
- [21] V. Alexeyev, Quantitative Analysis, second ed., Mir Publishers, Moscow, 1969.
- [22] J. Jordan, J. Chem. Educ. 40 (1963) A5.
- [23] I.M. Kolthoff, E. Sandell, E.J. Mehan, S. Backenstein, Quantitative Chemical Analysis, fourth ed., 1969.
- [24] Vogel's Textbook of Quantitative Analysis, fifth ed., Longman, 1989, p. 833.
- [25] D.A. Skoog, D.M. West, F.J. Holler, Fundamentals of Analytical Chemistry, seventh ed., Sanders College Publ., 1996.
- [26] R.C. Weast, (Ed.), Handbook of Chemistry and Physics, 58th ed., CRC Press, 1977–1978, p. D-151.
- [27] D.C. Harris, Exploring Chemical Analysis, second ed., Freeman & Co, 2001.
- [28] H.J.V. Tyrrell, Talanta 14 (1967) 843.
- [29] F. Borrul, P. Ramirez, H.N. Torres, V. Cerda, Thermochim. Acta 127 (1988) 209.
- [30] F. Borrul, V. Cerda, Thermochim. Acta 137 (1989) 263.
- [31] R. Forteza, I.M. Estela, V. Cerda, Analyst 115 (1990) 749.



# Chemiluminometric determination of the pesticide 3-indolyl acetic acid by a flow injection analysis assembly

A.I. Pimentel Neves, J.R. Albert-García, J. Martínez Calatayud\*

*Department of Analytical Chemistry, University of Valencia, Valencia, Spain*

Received 18 November 2005; received in revised form 23 March 2006; accepted 6 April 2006

Available online 24 May 2006

## Abstract

A new method is proposed for the chemiluminescent determination of the pesticide 3-indolyl acetic acid by means of an flow injection analysis system. The chemiluminescence emission is obtained by oxidation of the analyte with Ce (IV) in nitric acid and presence of  $\beta$ -cyclodextrine.

The continuous-flow method allows the determination of 159 samples  $\text{h}^{-1}$  of 3-indolyl acetic acid in an interval of concentrations over the range 0.5–15.0  $\text{mg l}^{-1}$ . The limit of detection was 0.1  $\mu\text{g l}^{-1}$  and the R.S.D. ( $n$ , 17) at 2.0  $\text{mg l}^{-1}$  of the pesticide level was 2.7%. The method was applied to water samples.

© 2006 Elsevier B.V. All rights reserved.

**Keywords:** Pesticides; Herbicides; Chemiluminescence; F.I.; Ce(IV)

## 1. Introduction

The massive use of pesticides, the persistence on the environment and the strong toxicity on animals and humans, imposes easy, quick and automated analytical methods for the control analysis of samples of environmental interest; samples like soil, water or parts of plants. Legal rules (more strict every day) in most of the countries also impose this search of quick and effective analytical procedures for the control analysis.

Analytical literature depicts a relatively small variety of analytical procedures for the determination of low amounts of pesticides or its residues on food or environmental samples: namely, HPLC, GC, immunoassays and by using few analytical detectors, mainly UV–vis absorption and fluorimetry or some electroanalytical.

The number of published procedures in the analytical literature which are dealing on F.I. and chemiluminescence for the determination of pesticides is relatively low. One of them and as a way of example [1] is based on the oxidation of bis(2,4,6-trichloro-phenyl) oxalate by hydrogen peroxide and the excited energy is transferred to a sensitizer. The system

was used for the determination of several organotin–quinoline complexes like dibutyldichlorostannane (II), dichlorodiphenylstannane (III), tributylchlorostannane (IV) and chlorotriphenylstannane (V). The procedure was based on the sample injection into a carrier solution containing the quinoline and then this stream merged with a buffered solution containing a mixture of hydrogen peroxide and (2,4,6-trichlorophenyl) oxalate. A procedure devoted to determination of paraoxon and aldicarb [2] is based on the inhibitory effect on acetyl cholinesterase; the generated choline enzyme was oxidized by the liberated hydrogen peroxide which diminution in turn is determined by the decreasing chemiluminescence of luminol. A F.I.-chemiluminescence procedure with the aid of an on-line photo-reactor was applied to the determination of carbofuran and promecarb [3]. The UV-irradiation as a preliminary treatment has been also used with the aid of the multicommutation continuous-flow methodology [4] for the chemiluminometric determination of the pesticides chlorsulfuron [5], aldicarb [6] and asulam [7].

The 3-indolyl acetic acid (IAA) also known as 3-indoleacetic acid according to IUPAC presents a molecular formulae  $\text{C}_{10}\text{H}_9\text{NO}_2$ ; a molecular weight 175.2 and a molecular structure as illustrated in Fig. 1. It melts over the range 166–168 °C and it is commercially available as a white powder. It is soluble in water (1500  $\text{mg l}^{-1}$ ) at room temperature; this solubility and the stability of the aqueous solutions (neutral or alkaline media)

\* Corresponding author at: University of Valencia, Department of Analytical Chemistry, Moliner 50, 46 100 Burjassot (Valencia), Spain.  
Tel.: +34 96 354 40 62; fax: +34 96 354 40 62.

E-mail address: [jose.martinez@uv.es](mailto:jose.martinez@uv.es) (J.M. Calatayud).

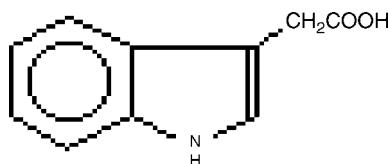


Fig. 1. Molecular structure of the 3-indolyl acetic acid.

make this pesticide a dangerous pollutant element to water environmental samples [8]. It is also soluble in some organic solvents as ethanol, acetone, diethyl ether and chloroform. It is a member of the auxin family, a group of hormones acting as promoters of the plant growth. About its toxic effects on humans, it affects the skin, eyes and internal skin of the respiratory system.

The analytical literature dealing with the determination of 3-indolyl acetic acid is mostly based on chromatographic separations. With HPLC and spectrophotometric detection extracts from plants have been analyzed [9,10] or animals [11]; and biological fluids by means of fluorimetry [12,13] and an electrochemical detector [14]. Other detectors have been connected to the chromatographic equipment and proposed for the determination of 3-indolyl acetic acid, like mass spectrometry-HPLC for biological fluids [15]; mass spectrometry-gas chromatography for bactericidal material [16]; for plant extracts have been proposed gas chromatography with the electron capture detector [17] and the amperometric detection in a liquid chromatograph [18]. There are published some determination methods by capillary electrophoresis on vegetal samples with spectrophotometric detection [19] and amperometric detector on plant extracts [20]; the couple amperometry-immunoassay has been proposed on crop samples [21]. Enzymatic immunoassays [22,23]; and voltamperometry determinations have also been proposed on plant extracts [24]. As far as authors know there are no published results dealing on the chemiluminescent behaviour of 3-indolyl acetic acid neither on the determination by means of a continuous-flow procedure.

This paper is a part of our research work on control analysis for pesticides in environmental samples in which we try to propose methods as simple, quick and cost-effective as possible. This objective is performed on different continuous-flow methods to be applied as a complete method or as a way to enhance the sensitivity of a separation procedure (like a post-column process). To reach this objective required a large screening on fluorescent and chemiluminescent properties of pesticides [25,26].

## 2. Experimental

### 2.1. Reagents and apparatus

All reagents used were analytically pure unless stated otherwise and prepared in purified water; reverse osmosis and deionized (18 M $\Omega$  cm) with a Sybron/Barnstead Nanopure II water purification system provided with a fibber filter of 0.2  $\mu$ m pore-size.

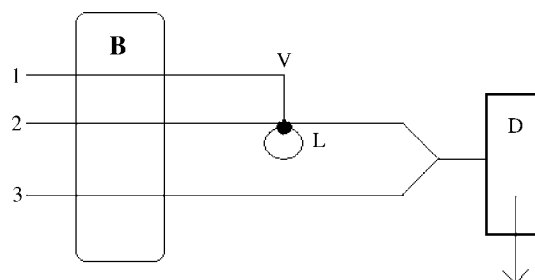


Fig. 2. Flow assembly proposed for the chemiluminescent determination of the 3-indolyl acetic acid. B, peristaltic pump; (flow-rate 700 a.u.); V, injection valve; L, sample loop (57 cm); D, detector; 1, sample channel; 2, carrier channel; 3, oxidative system channel.

### 2.1.1. Analyte solutions and stability

The 3-indolyl acetic acid was from Dr. Ehrenstorfer GmbH (99.0%, Germany) and the stability of the aqueous stock solutions of the pesticide was tested by preparing a solution containing 20 mg l<sup>-1</sup> of 3-indolyl acetic acid which was kept into a plastic bottle, protected from room light and into a refrigerator at 4 °C. The absorption spectrum was recorded everyday, up to 53 days. No changes were observed in these spectra.

Other used reagents were mineral acids, alkalis and salts, KMnO<sub>4</sub>, H<sub>2</sub>O<sub>2</sub>, formic acid, acetonitrile, 2-propanol (all from Panreac, Spain), Fe (NO<sub>3</sub>)<sub>3</sub>·7H<sub>2</sub>O, Ce (NH<sub>4</sub>)<sub>2</sub> (NO<sub>3</sub>)<sub>6</sub> (Probus, Spain), sodium dodecyl sulphate, hexadecyl pyridinium chloride,  $\beta$ -cyclodextrine (Fluka, Switzerland), benzalkonium chloride (Guinama, Valencia, Spain), *N*-cetyl-*N,N,N*-trimethyl ammonium bromide (Merck, Darmstadt, Germany), quinine sulphate (Sigma-Aldrich Química S.A, Spain), Triton-X 100, *N,N*-dimethylformamide (Scharlau, Spain), ethanol (Prolabo, Spain).

### 2.1.2. Flow assembly

The flow injection assembly is depicted in Fig. 2 and it consisted of a PTFE coil of 0.8 mm id; a Gilson (Worthington, OH, USA) Minipuls 2 peristaltic pump provided with pump tubing from Elkay Elreann (Galway, CO, USA); and the sample solution was inserted through a six port injection valve Rheodyne type 5041. The photo-reactor used for preliminary studies, consisted of PTFE tubing helically coiled around a low-pressure mercury lamp Zalux. The flow cell was a flat-spiral quartz tube of 1 mm id and 3 cm total diameter backed by a Al-foil mirror for maximum light collection. The photo detector package was a P30CWAD5F-29 Type 9125 photomultiplier tube (PMT) supplied by Electron Tubes operating at 1280 V; it was located in a laboratory-made light-tight box. The output was fed to a computer equipped with a counter-timer, also supplied by Electron Tubes.

## 3. Results and discussion

### 3.1. Preliminary tests

Preliminary assays were performed on Brompyrazon, Buminafos, Metobromuron and 3-indolyl acetic acid (auxin family) to check the photo-induced chemiluminescence emission; UV-irradiation was performed in different media and the

further oxidation with several oxidative systems. The photoreactor was provided with a low-pressure Hg lamp and each test was performed lamp ON and OFF.

The 3-indolyl acetic acid presented native chemiluminescent emission; which resulted in higher outputs with lamp OFF than ON. Then, the direct oxidation of the analyte (no photo-degradation) was selected for further work.

### 3.2. Selection of the oxidative system

The analyte solution contained  $20 \text{ mg l}^{-1}$  and was inserted into a pure water carrier stream (channel 2) which merged with the mixture oxidant and medium solutions. Tested oxidative systems were:  $10^{-3} \text{ mol l}^{-1} \text{ KMnO}_4$  in  $0.5 \text{ mol l}^{-1} \text{ H}_2\text{SO}_4$ ;  $10^{-3} \text{ mol l}^{-1} \text{ Ce (IV)}$  in  $0.5 \text{ mol l}^{-1} \text{ HClO}_4$ ;  $10^{-3} \text{ mol l}^{-1} \text{ Fe (CN)}_6^{3-}$  in  $0.5 \text{ mol l}^{-1} \text{ NaOH}$ ;  $10^{-3} \text{ mol l}^{-1} \text{ H}_2\text{O}_2$  in  $\text{H}_2\text{O}$ ; and,  $10^{-3} \text{ mol l}^{-1} \text{ Cr}_2\text{O}_7^{2-}$  in  $0.5 \text{ mol l}^{-1} \text{ HCl}$ . Outputs were compared with the corresponding blank experiment. No emission was observed with oxidants like hydrogen peroxide or dichromate; and, low outputs were presented by the oxidation with hexacyanoferrate (III). High emission was observed with Ce (IV) and potassium permanganate; with important differences among them; 54282.6 (in arbitrary units, a.u.) versus 2870.3 (a.u.) for Ce (IV) and  $\text{MnO}_4^-$ , respectively.

In order to confirm the oxidant providing the best analytical signal, new tests were performed to check the influence of different concentrations of oxidant on several concentrations of the analyte (pre-calibration graph assays); permanganate concentrations were assayed from  $10^{-3}$  to  $10^{-5} \text{ mol l}^{-1}$  in  $0.5 \text{ mol l}^{-1}$  sulphuric medium; and, the oxidation with Ce(IV) was tested over the concentrations range  $10^{-3}$ – $10^{-5} \text{ mol l}^{-1}$ , all in  $0.5 \text{ mol l}^{-1} \text{ HClO}_4$ . The prepared pesticide concentrations were 5, 10, 15 and  $20 \text{ mg l}^{-1}$ . Highest emission outputs were observed with  $10^{-3} \text{ mol l}^{-1} \text{ Ce (IV)}$  in  $0.5 \text{ mol l}^{-1} \text{ HClO}_4$  which was finally selected for further work.

Next step was to study the influence of the oxidation acidic medium ( $0.5 \text{ mol l}^{-1} \text{ H}_2\text{SO}_4$ ,  $\text{HClO}_4$ ,  $\text{HCl}$  and  $\text{HNO}_3$ ) on the emission intensity with  $10 \text{ mg l}^{-1}$  pesticide and  $10^{-3} \text{ mol l}^{-1} \text{ Ce(IV)}$ . The carrier stream was pure water. Emission outputs were higher for  $\text{HClO}_4$  and  $\text{HNO}_3$ ; however, as both acids resulted in similar outputs a new series of experiments was performed by varying the acid concentration from 0.1 to  $1.0 \text{ mol l}^{-1}$ ; each acid concentration was assayed with different concentrations of the herbicide, from 2.0 to  $15.0 \text{ mg l}^{-1}$ . Best results for each tested acid were observed with acid concentrations close to  $1.0 \text{ mol l}^{-1}$ . A new test was performed with the acid concentration range from 0.7 to  $1.2 \text{ mol l}^{-1}$  (analyte from 0.5 to  $10.0 \text{ mg l}^{-1}$ ) two facts were observed, the nitric acid presented higher outputs; and, the increase in the acid concentration also resulted in higher linear slope. Nitric acid was selected for further work.

The next empirical step was to check the influence of the nitric acid concentration on the chemiluminescent output; tested range was from 0.5 to  $1.5 \text{ mol l}^{-1}$  with solutions containing  $2.0 \text{ mg l}^{-1}$  of pesticide and  $1.0 \times 10^{-3} \text{ mol l}^{-1} \text{ Ce (IV)}$ ; the acidic medium was tested simultaneously on the sample, oxidant and carrier solutions. This first step revealed best outputs as minor was

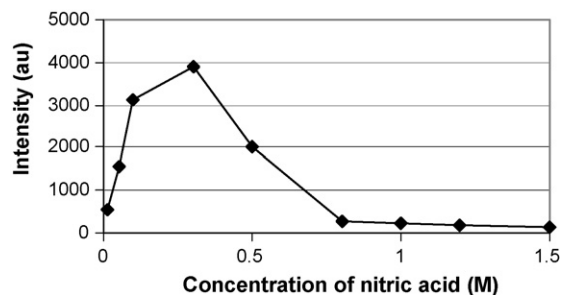


Fig. 3. Influence of the concentration of the nitric acid.

the acid concentration; a new series from 0.010; 0.050; 0.100; 0.300; 0.500 and  $0.800 \text{ mol l}^{-1}$ , resulted in higher outputs about  $0.300 \text{ mol l}^{-1}$ , as depicted in Fig. 3.

The influence of the concentration of the oxidant was performed with solutions containing  $2.0 \text{ mg l}^{-1}$  of pesticide and  $0.300 \text{ mol l}^{-1}$  of acid and the Ce (IV) concentration was varied from 0.0001 to  $0.1000 \text{ mg l}^{-1}$ . Depicted results in Fig. 4 shown the  $0.005 \text{ mol l}^{-1}$  as the suitable concentration to be selected for further work.

Temperature has a relatively complex effect on chemiluminescent systems [4,5]; redox reactions can be affected by temperature in both thermodynamic and kinetic terms. If the temperature increase affects the reaction kinetics—by accelerating the chemiluminescent process—, then, the optimum flow rate will also be affected by the temperature change. However, a temperature rise can decrease the emission intensity through an increased probability of deactivation via external conversions.

The influence of the temperature was tested by immersing three flasks into a water bath. (TECTRON 200 from J. P. Selecta); the immersed solutions were the carrier, the sample containing  $2.0 \text{ mol l}^{-1}$  of the pesticide; and, the oxidative system which was formed by a mixture containing  $0.0050 \text{ mol l}^{-1}$  of Ce (IV) and  $0.3000 \text{ mol l}^{-1}$  of  $\text{HNO}_3$ . The studied temperatures ranged from room temperature to  $80^\circ\text{C}$ . The results demonstrated a continuous decreasing of the analytical signal at higher temperatures; the decrease was specially relevant up to  $60^\circ$ .

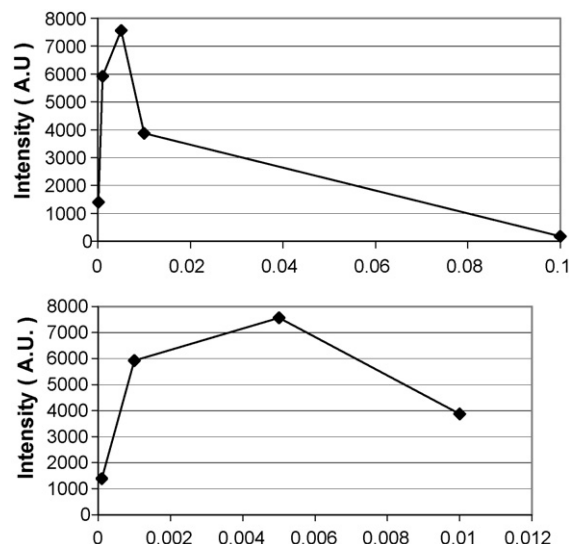


Fig. 4. Influence of the concentration of the oxidant Ce (IV).

### 3.3. Influence of organized media and sensitizers

The influence of organized media and/or sensitizers, can affect strongly to the chemiluminescence behaviour. The following substances were separately assayed by merging with the sample solution at the indicated concentration; between branches the chemiluminescent output minus blank (solution containing no pesticide). As reference was used the output 7560.6 (arbitrary units) from the solution containing  $2 \text{ mg l}^{-1}$  of 3-indolyl acetic acid). Observed outputs were:  $\beta$ -cyclodextrine 1.2% (14819.4); benzalkonium chloride 0.6% (1443.8); *N*-cethyl-*N,N,N*-trimethyl ammonium bromide 0.2% (4662.3); hexadecylpyridinium chloride 0.2% (3075.7); sodium dodecylsulphate 1.2% (1801.8); Triton X-100 0.06%, (1460.7). See Fig. 5a). The depicted results revealed the  $\beta$ -cyclodextrine as the most favourable; then was tested the influence of its concentration by testing 0.10; 0.25; 0.50; 0.75; 1.00; 1.20 and 1.50%; the concentration 1.20% was selected as presenting the best result, see Fig. 5b).

The procedure to test the influence of sensitizers was the same as described for organized media. Studied substances and con-

centrations were: dimethylformamide, 5.0%; ethanol, 20.0%; 2-propanol 20.0%; acetonitrile, 20.0%; quinine,  $10^{-4}$  M; and, formic acid, 0.5%. Higher outputs were observed (see Fig. 5c) with 5% dimethylformamide and 20% acetonitrile; with variations versus reference of 56% and 35%, respectively. The repeatability of both signals was (as % R.S.D., 15 replicates) 2.2% and 4.7%.

Then the combined influence of  $\beta$ -cyclodextrine and dimethylformamide was tested with two different carrier streams. Three different solutions in  $0.30 \text{ mol l}^{-1}$  of nitric acid were tested: (a) blank containing 1.2%  $\beta$ -cyclodextrine and 5.0% dimethylformamide; (b) reference solution containing  $2.0 \text{ mg l}^{-1}$  of pesticide; and (c) test solution containing 1.2% of  $\beta$ -cyclodextrine, 5.0% *N,N*-dimethylformamide and  $2.0 \text{ mg l}^{-1}$  of pesticide. The oxidant was  $0.0050 \text{ ml l}^{-1}$  Ce(IV) in  $0.30 \text{ mol l}^{-1}$  nitric acid. Chemiluminescent outputs were obtained by using two different carriers, pure water and  $0.30 \text{ mol l}^{-1}$  of nitric acid.

Obtained results, variation versus reference, were 39% and 119% with water or nitric acid (as carrier), respectively. Nitric acid was selected as carrier for next experiments.

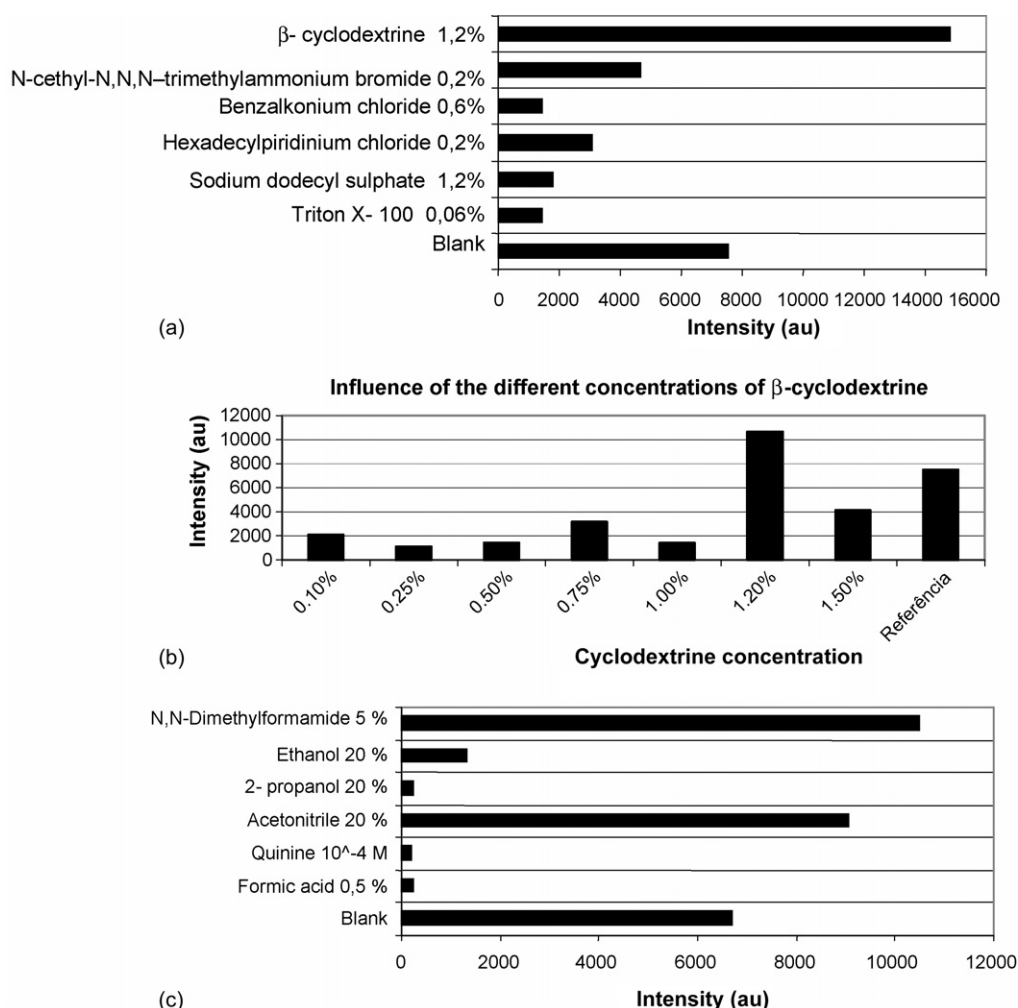


Fig. 5. Influence of organized media and sensitizers. (a) influence of organized media. (b) Influence of the concentration of  $\beta$ -cyclodextrine. (c) influence of sensitizers.



Table 1  
Analysis of water samples

Type of water sample	Collected in	Recovery (in %; <i>n</i> 3)
Magro river (San Juan Valencia, Spain)	1°10'12.686"W, 39°31'27.99"N	92.6 ± 2.3
Residual water (Chirivella, Valencia, Spain)	0°26'19.057"W, 39°27'10.642"N	93.7 ± 4.9
Underground water (San Antonio, Valencia, Spain)	1°9'9.993"W, 39°31'22.096"N	96.6 ± 2.7
Mineral bottled water (Bejis, Castellón, Spain)	Agua de Bejis (trade mark, commercially available)	98.0 ± 0.9

### 3.4. Optimization of hydrodynamic parameters and re-optimization (robustness of the method) of chemical parameters

The multiparametric strategy known as the modified simplex method (MSM) [27–29] was selected for the optimization of the hydrodynamic parameters insertion sample volume and the flow-rate of carrier and oxidant. Three series of experiments were consecutively performed to re-optimize former results; the last of them consisted in selecting the best vertices and to obtain the best compromise peak height (sensitivity of the measurement) – reproducibility (R.S.D) – sample throughput (wide of the base-peak). Best results were obtained by using 379  $\mu\text{l}$  of sample and flow-rate (in  $\text{ml min}^{-1}$ ) of 0.87 and 3.67 for carrier and oxidant solution, respectively.

With the selected flow conditions, each chemical parameter was confirmed (univariant method) by testing other values around the previously selected as optimum. This is also known as the robustness of the method. Tested parameters were the concentration of oxidant, nitric acid and  $\beta$ -cyclodextrine; flow-rates of carrier and oxidant and sample volume. The tested variations for each parameter were  $\pm 2$ ,  $\pm 5$ ,  $\pm 6$  and  $\pm 10\%$  around the formerly figure selected as optimum. Obtained results were compared with the obtained with the optimized conditions. Differences of concentration of the organized media resulted in relevant differences in outputs (even over 50%). However, the smallest observed variations were with the sample volume and the oxidant concentration.

## 4. Analytical figures of merit

With the optimized manifold, the calibration graph was studied up to  $30.0 \text{ mg l}^{-1}$ ; the parabolic profile fitted the equation  $I = 191.99 x^2 + 13000 x - 5860$ , the correlation coefficient was 0.9991 and presented a linear dynamic range comprised between 0.5 and  $15.0 \text{ mg l}^{-1}$ . This linear range fitted the equation  $I = 10131 x + 401$  with a correlation coefficient of 0.9989 (*n* 5). *x* means in both equations the analyte concentration in  $\text{mg l}^{-1}$ .

The inter-day reproducibility was checked by performing five different calibrations into the linear dynamic range (0.1 and  $1 \text{ mg l}^{-1}$ ) in five consecutive days with freshly prepared solutions; the calculated R.S.D. of the linear slope was 4.9%.

The limit of detection ( $0.1 \mu\text{g l}^{-1}$ ) was experimentally confirmed as the concentration yielding a signal higher than the corresponding to the blank plus three times the standard deviation of the blank (*n* 30).

The repetitive insertion of 17 samples containing  $2.0 \text{ mg l}^{-1}$  of pesticide resulted in a repeatability of RSD 1.8%; similar experiment dealing with  $0.1 \text{ mg l}^{-1}$  resulted in an RSD 2.7%. The average insertion rate was calculated from the average of the base-width (22.59 s) and was  $159 \text{ h}^{-1}$ .

Interferences were sought among some of the usual inorganic ions in water samples, namely:  $\text{Ca}^{2+}$ ,  $\text{Fe}^{3+}$ ,  $\text{Fe}^{2+}$ ,  $\text{Mg}^{2+}$ ,  $\text{Cu}^{2+}$ ,  $\text{Hg}^{2+}$ ,  $\text{Mn}^{2+}$ ,  $\text{Cd}^{2+}$ ,  $\text{Ni}^{2+}$ ,  $\text{Co}^{2+}$ ,  $\text{NH}_4^+$ ,  $\text{Na}^+$ ,  $\text{K}^+$ ,  $\text{SO}_4^{2-}$ ,  $\text{HPO}_4^{2-}$ ,  $\text{NO}_3^-$ ,  $\text{NO}_2^-$ ,  $\text{CH}_3\text{COO}^-$ ,  $\text{ClO}_4^-$  and  $\text{Cl}^-$ . Prepared solutions contained  $0.1 \text{ mg l}^{-1}$  of the pesticide and different concentrations of the tested potential interferent (maximum assayed concentration 500 and minimum  $0.1 \text{ mg l}^{-1}$ ). Results were compared with the solution containing only the pesticide; and, the chemical was considered as interferent when the difference versus reference was over  $\pm 5\%$ . Most of the tested ions resulted in high interference. Next step was to study the separation of interferents from the analyte by two different procedures: (a) elimination of interferences with sample passage through a mini-column containing strong ionic exchange resins to retain interferents; and (b) a column filled with adsorbents to retain the analyte and then eluting it. UV–vis spectra were recorded before and after sample passage through the column. Ion-exchange resins do not result in removing interferences completely; however, good results were obtained with the use of cartridges  $\text{C}_{18}$  (Bond Elut  $\text{C}_{18}$ , Varian), the analyte was completely retained and then, it was eluted with the aid of *N,N*-dimethylformamide. The experiments were performed with solutions containing  $0.1 \text{ mg l}^{-1}$  of the pesticide and  $200 \text{ mg l}^{-1}$  of all the proposed interferents; eluting solution was prepared with 1.33 ml of 5% *N,N*-dimethylformamide levelled to 25 ml with 1.2% of  $\beta$ -cyclodextrine solvent in  $0.3 \text{ mol l}^{-1}$  nitric acid. Results were  $-0.7\%$  (relative error) compared with the reference solution containing only pesticide and no interferents. The mini-columns can be integrated easily in a flow assembly.

Several water samples were collected from different places and types (see Table 1) and were spiked with a known amount of the pesticide ( $0.1 \text{ mg l}^{-1}$ ). As above reported, the resulting pesticide solutions were forced through the  $\text{C}_{18}$  cartridge and then elution was performed with the mixture *N,N*-dimethylformamide and  $\beta$ -cyclodextrine in  $\text{HNO}_3$  medium. Recoveries are depicted in the Table 1.

## 5. Conclusions

A new F.I.-chemiluminometric procedure is presented for the determination of the herbicide 3-indolyl acetic acid. The method is based on the direct chemiluminescence of the pesticide by means of the oxidation with Ce (IV) in acid nitric solution. The



analytical outputs were clearly increased with the presence of  $\beta$ -cyclodextrine and dimethylformamide 5.0%.

The procedure is performed by a simple F.I. assembly and at room temperature in which the aliquot of the sample solution was inserted into a nitric solution as carrier. It presents a competitive sample throughput ( $159 \text{ h}^{-1}$ ) and a detection limit of  $0.1 \mu\text{g ml}^{-1}$ . The selectivity in the determination of the herbicide in water samples was implemented by using (it can be added easily to the flow-manifold) a  $\text{C}_{18}$  solid-phase extraction cartridge.

## References

- [1] T. Fujimaki, T. Tani, S. Watanabe, *Anal. Chim. Acta* 282 (1993) 175.
- [2] A. Roda, P. Rauch, E. Ferri, S.A. Girotti, S. Ghini, O. Carrea, R. Bovara, *Anal. Chim. Acta* 294 (1994) 35.
- [3] T. Pérez-Ruiz, C. Martínez-Lozano, C. Tomás, J. Martín, *Analyst* 127 (2002) 1526.
- [4] J.V. García Mateo, Multicommutation in flow analysis. <http://www.uv.es/~martinej/Flow-Analysis/>.
- [5] K. Mervartová, M. Catalá Icardo, J. Martínez Calatayud, *Anal. Lett.* 38 (2005) 179.
- [6] M. Palomeque, J.A. García Bautista, M. Catalá Icardo, J.V. García Mateo, J. Martínez Calatayud, *Anal. Chim. Acta* 512 (2004) 149.
- [7] A. Chivulescu, M. Catalá Icardo, J.V. García Mateo, J. Martínez Calatayud, *Anal. Chim. Acta* 519 (2004) 113.
- [8] [http://www.scorecard.org/chemical-profiles/summary.tcl?edf\\_substance\\_id=87-51-4](http://www.scorecard.org/chemical-profiles/summary.tcl?edf_substance_id=87-51-4).
- [9] P. Hu, D.H. Liu, F. Hu, H. Yang, Fenxi- Shiyanshi. 20 (2001) 8.
- [10] Z. Zhang, Q. Zhang, Z.H. Wang, R.F. Lin, Y.R. Tao, *Sepu* 12 (1994) 140.
- [11] R.Z. Wang, L.T. Xiao, W.H. Lin, Y. Cao, X.Y. Bo, *Sepu* 20 (2002) 148.
- [12] J. Hansen - Moeller, *J. Chromatogr.* 624 (1992) 479.
- [13] K. Hoenicke, T.J. Simat, H. Steinhart, H.J. Koehler, A. Schwab, *J. Agric. Food Chem.* 49 (2001) 5494.
- [14] Y.G. Du, S.G. Li, H.L. Guo, *Sepu* 21 (2003) 507.
- [15] J.P. Danaceau, G.M. Anderson, W.M. McMahon, D.J. Crouch, *J. Anal. Toxicol.* 27 (2003) 440.
- [16] Z.X. Lu, W. Song, *Sepu* 18 (2000) 328.
- [17] D. Xiang, J. Ding, D. Xu, J. Pu, *Zhongguo-Yaoke-Daxue-Xuebao.* 19 (1988) 171.
- [18] J. Ramon-Guerrero, P. Garcia-Ruiz, J. Sanchez-Bravo, M. Acosta, M.B. Arnao, *J. Liq. Chromatogr. Relat. Technol.* 24 (2001) 3095.
- [19] A. Segura-Carretero, C. Cruces-Blanco, M. Soriano-Pena, S. Cortacero-Ramirez, A. Fernandez-Gutierrez, *J. Agric. Food Chem.* 52 (2004) 1419.
- [20] K.B. Wu, Y.Y. Sun, S.S. Hu, *Sens. Actuators B.* 96 (2003) 658.
- [21] J. Li, L.T. Xiao, G.M. Zeng, G.H. Huang, G.L. Sheng, R.Q. Yu, *Anal. Chim. Acta* 494 (2003) 177.
- [22] K. Manning, *J. Immunol. Methods* 136 (1991) 61.
- [23] H.Y. Gao, T.B. Jiang, W.R. Heineman, H.B. Halsall, J.L. Caruso, *Fresenius J. Anal. Chem.* 364 (1999) 170.
- [24] L. Hernandez, P. Hernandez, F. Paton, *Anal. Chim. Acta* 327 (1996) 117.
- [25] L. Lahuerta Zamora, Y. Fuster Mestre, M.J. Duart, G.M. Antón Fos, R. García Domenech, J. Gálvez Alvarez, J. Martínez Calatayud, *Anal. Chem.* 73 (2001) 4301.
- [26] M. Catalá Icardo, L. Lahuerta Zamora, G.M. Antón-Fos, J. Martínez Calatayud, M.J. Duart, *TrAC, Trends Anal. Chem.* 24 (2005) 782.
- [27] L.A. Yabro, S.N. Deming, *Anal. Chim. Acta* 73 (1974) 1043.
- [28] S.L. Morgan, S.N. Deming, *Anal. Chem.* 46 (1974) 1170.
- [29] J.A. Nelder, R. Mead, *Comput.* 7 (1965) 308.

# Application of manganese(IV) dioxide microcolumn for determination and speciation of nitrite and nitrate using a flow injection analysis–flame atomic absorption spectrometry system

Meissam Noroozifar<sup>a,\*</sup>, Mozhgan Khorasani-Motlagh<sup>b</sup>,  
Aboozar Taheri<sup>a</sup>, Marjan Homayoonfard<sup>a</sup>

<sup>a</sup> Analytical Research Laboratory, Department of Chemistry, University of Sistan & Baluchestan, Zahedan, P.O. Box 98165-181, Iran

<sup>b</sup> Inorganic Research Laboratory, Department of Chemistry, University of Sistan & Baluchestan, Zahedan, P.O. Box 98165-181, Iran

Received 7 February 2006; received in revised form 6 April 2006; accepted 6 April 2006

Available online 19 May 2006

## Abstract

A flow injection (FI) method with flame atomic absorption spectrometry (FAAS) detection was developed for the determination and speciation of nitrite and nitrate in foodstuffs and wastewaters. The method is based on the oxidation of nitrite to nitrate using a manganese(IV) dioxide oxidant microcolumn where the flow of the sample through the microcolumn reduces the MnO<sub>2</sub> solid phase reagent to Mn(II), which is measured by FAAS. The absorbance of Mn(II) is proportional to the concentration of nitrite in the samples. The injected sample volume was 400 μL with a sampling rate of analyses was 90 h<sup>-1</sup> with a relative standard deviation better than 1.0% in a repeatability study. Nitrate is reduced to nitrite in proposed FI–FAAS system using a copperized cadmium microcolumn and analyzed as nitrite. The calibration curves were linear up to 20 mg L<sup>-1</sup> and 30 mg L<sup>-1</sup> with a detection limit of 0.07 mg L<sup>-1</sup> and 0.14 mg L<sup>-1</sup> for nitrite and nitrate, respectively. The results exhibit no interference from the presence of large amounts of ions. The method was successfully applied to the speciation of nitrite and nitrate in spiked natural water, wastewater and foodstuff samples. The precision and accuracy of the proposed method were comparable to those of the reference spectrophotometric method. © 2006 Elsevier B.V. All rights reserved.

**Keywords:** Nitrite; Nitrate; Manganese(IV) dioxide; Flow injection analysis; Flame atomic absorption spectrometry; Mini-column

## 1. Introduction

Nitrite and nitrate ions take part in several important environmental transformations involving nitrogen. Nitrate is sources of nitrogen for the synthesis of proteins by microorganisms. However, large amounts of this species may be toxic and cause eutrophication [1,2]. Nitrite ions are toxic even in low concentrations and may cause death by asphyxia [1]. The toxicity of nitrite is primarily due to the fact that it can react with secondary or tertiary amines present in human body to form nitrosamines, which are known to be carcinogens, teratogenic and mutagenic [3–7]. Recent evidence suggests that plasma nitrite anion represents a latent substance that can be reacts with iron(III) of haemoglobin, forming methemoglobin which has no oxygen carrying ability and this disease is called methemoglobinemia [8–10]. There-

fore, the determinations of nitrite and nitrate in foodstuffs and wastewaters have attracted much attention and a simple, sensitive and specific determination of nitrite is highly desirable.

Several methods have been reported for the quantitative determination of nitrate and nitrite, including kinetic methods [11,12], chromatography [13,14], potentiometry [15,16], amperometry [17], polarography [18], capillary electrophoresis [19], spectrophotometry [20,21] and flow injection analysis (FIA) systems [22–25]. However, these methods have the disadvantage of the employment of large volumes of toxic reagents, low sample frequency, application of complicated flow injection systems, poor reproducibility, expensive and time-consuming procedures.

Solid-phase reagents (SPR) have been used for determination of inorganic and organic compounds in our laboratory, previously [26–30]. Today, it is known that the use of solid-phase reactors incorporated into FIA manifolds may offer certain advantages over homogeneous systems such as decreasing of reagent consumption, utility for the in situ preparation of

\* Corresponding author. Tel.: +98 541 244 6565; fax: +98 541 244 6888.  
E-mail address: [mnoroozifar@chem.usb.ac.ir](mailto:mnoroozifar@chem.usb.ac.ir) (M. Noroozifar).

unstable reagents and simplification of the system with fewer junctions for mixing of reagents, sample and carrier streams. So, it is important to find these kinds of reagents for application in every laboratory.

The presents study reports a new approach for speciation of inorganic nitrogen in which an on-line heterogeneous chemical/FIA–FAAS system were employed. Our basic study has been shown that in an acidic media, nitrite solutions readily dissolve  $\text{MnO}_2$ , and the manganese released as  $\text{Mn}^{2+}$  is determined by FAAS. Nitrate is reduced to nitrite in proposed FI–FAAS system using a copperized cadmium microcolumn and determined as nitrite.

## 2. Experimental

### 2.1. Reagents and solutions

All reagents were prepared from analytical reagent grade chemicals unless specified otherwise. All aqueous solutions were prepared with re-distilled water. Nitrite stock solution  $100 \text{ mg L}^{-1}$  was prepared freshly before each measurement by dissolving  $0.1500 \text{ g}$  sodium nitrite (Merck) in  $1000 \text{ ml}$  water. A  $100 \text{ mg L}^{-1}$  standard solution of nitrate was prepared by dissolving  $0.1371 \text{ g}$  of sodium nitrate (Merck) in  $1000 \text{ ml}$  water. Working standard solutions of nitrite were prepared daily by dilution of the standard stock solutions. The solution for the carrier stream was prepared by dilution of  $\text{H}_2\text{SO}_4$  (Merck) with re-distilled water to a final concentration of  $0.1 \text{ M}$ . The silica gel beads (mesh 230–400,  $0.04\text{--}0.063 \text{ mm}$ ; Merck) were treated for three hours at  $950^\circ\text{C}$  for irreversible dehydration [31] before mixing with manganese(IV) dioxide (Merck). Our standard spectrophotometric method for nitrite has been reported previously by Rincón and Martínez [32]. Reagents were prepared as follow:  $0.5 \text{ g}$  sulphanilamide ( $\text{NH}_2\text{C}_6\text{H}_4\text{SO}_2\text{NH}_2$ ) dissolved in  $30 \text{ ml}$  glacial acetic acid and added  $120 \text{ ml}$  of warm water, and filtered. Coupling reagent solution:  $0.25 \text{ g}$  *N*-(1-naphthyl)-ethylene diamine dihydrochloride ( $\text{C}_{12}\text{H}_{16}\text{C}_{12}\text{N}$ ) dissolved in water. Diluted to  $250 \text{ ml}$  with water. Stored in a well-stoppered brown bottle and kept in a refrigerator. Nitrate is reduced to nitrite using a copperized cadmium column and analyzed as nitrite [33].

### 2.2. Instrumentation

A schematic diagram of the single-line flow injection system is given in Fig. 1. A variable flow-rate peristaltic pump, (IKA.Schlauchpumpe, Janke & Kunkel GMBH, IKA. Labortechnik, PA.B1) was used to pump carrier-streams and the sample through the manifold at a flow rate of  $3.5 \text{ ml min}^{-1}$ . Manifold lines consisted of  $0.8 \text{ mm}$  i.d. polyethylene tubing. The six-way injection valve (Rheodyne, Model 7125) allowed the sample to be directly loaded into a  $400 \mu\text{L}$  loop, and subsequently injected into the carrier stream. The injection valve was kept in the load position for the first  $10 \text{ s}$  of every run to load the sample loop, after which it was switched to the inject position to place the sample plug into the carrier stream. The valve was kept in the inject position for a further  $30 \text{ s}$  to ensure that the entire

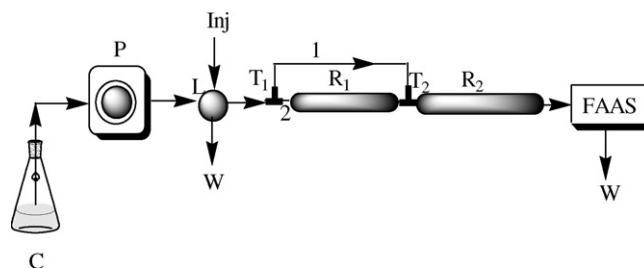


Fig. 1. Schematic representation of the FIA manifold employed for the determination and speciation of nitrite and nitrate. C, Carrier stream; P, Pump; Inj, Injector valve; L, Loop;  $T_1$  &  $T_2$ , Three way valve;  $R_1$ , Copperized cadmium mini-reactor and  $R_2$ ,  $\text{MnO}_2$  mini-reactor; FAAS, Flame atomic absorption spectrometer detector; W, Waste.

sample was flushed out of the sample loop. This was followed by switching the valve to the load position to fill the sample loop for the next run. Two three-way valves were employed for adjusted carrier and samples lines passing in reactor 2 ( $25\% \text{ (w/w)}$   $\text{MnO}_2$ ) or reactor1 (copperized cadmium)-reactor 2. After being placed in the carrier stream, the sample zones were pumped through the solid-phase reactors 2 (for determination of nitrite) or 1 and 2 (for determination of nitrate and nitrite). The products were channeled to a Philips flame atomic absorption spectrometer (Model PU 9110X) with an air-acetylene flame and  $5 \text{ cm}$  optical path-length (burner). The light source was a Mn hollow cathode lamp. The wavelength was set to  $279.5 \text{ nm}$  with a spectral slit-width of  $0.5 \text{ nm}$  and a lamp current of  $9.0 \text{ mA}$ .

### 2.3. The reducing copperized cadmium and $\text{MnO}_2$ solid-phase reactors

Metallic cadmium ( $R_1$ ) fillings between 40 meshes and 60 meshes were taken, stirred for  $2 \text{ min}$  with distilled water, stirred for  $2 \text{ min}$  with  $100 \text{ ml}$  of  $2\%$  copper sulphate solution, and then the supernatant liquid was removed. Metallic cadmium was washed with distilled water till the washings were free from precipitated copper. A Teflon tube ( $0.7 \text{ mm}$  i.d.) was carefully filled with prepared material up to  $7 \text{ cm}$  height on a glass wool support without any air bubbles [34]. The column was regenerated by pumping a carrier stream containing  $\text{EDTA}/\text{NH}_4\text{Cl}$  (prepared by dissolving  $0.4 \text{ g}$   $\text{EDTA}\cdot 2\text{H}_2\text{O}$  and  $70 \text{ g}$  ammonium chloride in  $1 \text{ dm}^3$  of water and pH was adjusted between 9 and 9.5 with ammonium solution) [35]. The solid-phase reactor ( $R_2$ ) was constructed from stainless tubing with i.d. of  $0.7 \text{ mm}$  and length of  $12.0 \text{ cm}$ . The tubing was packed by silica gel beads embedded in solid  $\text{MnO}_2$ . The reactor was prepared by mixing  $0.5 \text{ g}$  powdered solid manganese(IV) dioxide (Merck) and  $1.5 \text{ g}$  of silica gel beads. This mixture was homogenated using an IR vibration mill (Shimaadzu, Japan). Each packed reactor had to be conditioned for at least  $30 \text{ min}$  before use. Conditioning involved pumping re-distilled water through the reactor for  $15 \text{ min}$  followed by pumping the carrier stream,  $0.1 \text{ M}$   $\text{H}_2\text{SO}_4$ , for another  $15 \text{ min}$  at flow rate of  $3.5 \text{ ml min}^{-1}$ . The lifetime of each reactor was established by comparing absorbance for the same standards from day to day. When the absorbance started to decrease systematically and drastically, the reactor had to be

replaced. The total number of samples that could be processed with one column varied between 400 and 450 depending on the nitrite concentration. Nitrate is previously reduced to nitrite in a copperized cadmium column and analyzed as nitrite.

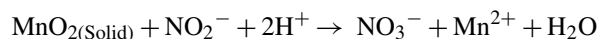
#### 2.4. Real samples

Our meat products preparation method for determination of nitrite and nitrate in meat products has been reported previously by Öztekin et al. [19]. Ten grams from meat products were weighed in a beaker. Deionized water (150 ml) was added and blended for 2 min in a laboratory blender. The suspension was incubated for 15 min in a warm water bath at 50 °C. After cooling, the volume was diluted to 250 ml and filtered through a Whatman filter paper no. 1. An aliquot of this solution was then filtered from a 0.45- $\mu\text{m}$  cellulose acetate filter disc. The resulting solution, after adequate dilution, was injected to proposed system. The proposed method was tested with different wastewaters; the samples were filtered with Whatman filter paper no. 1 and determined by the proposed method. The original nitrite concentration of these samples was also determined before spiking.

### 3. Results and discussion

#### 3.1. Analysis with $\text{MnO}_2$ and copperized cadmium reactors

It is the aim of the present work to investigate the possibility of using a solid-phase manganese(IV) dioxide reactor for on-line oxidation of  $\text{NO}_2^-$  in a FI system at room temperature and without any sample concentration. In this reactor, nitrite reduces  $\text{MnO}_2$  to Mn(II) and nitrate is formed. The equation for this reaction is:



Consumes manganese(IV) dioxide is proportional to the concentrations of nitrite in the samples. Hence, we used manganese(IV) dioxide solid reagent for the determination of nitrite in a FI system. Nitrite, when added in increasing amounts, consumes manganese(IV) dioxide and increases the Mn absorbance. Nitrate is reduced to nitrite in FI system using a copperized cadmium column (R1) and analyzed as nitrite. The absorbance is found to increase linearly with increasing concentration of nitrate, which forms the basis for speciation of nitrite and nitrate.

#### 3.2. Optimization of variables

The performance of the proposed flow-injection system depends on the efficiency of the reaction at the interface between the solid and liquid phases of the reactors. The acid  $\text{H}_2\text{SO}_4$  concentration in carrier stream, the  $\text{MnO}_2$  concentration in reagent section, the loop volume and the temperature also had major effects and had to be optimized.

The contact time between the sample zone containing  $\text{NO}_2^-$  and the reactor is very important for the reaction to proceed sufficiently. Because this depends on the flow rate of the sample zone through the reactor, a study of the flow rate of the carrier

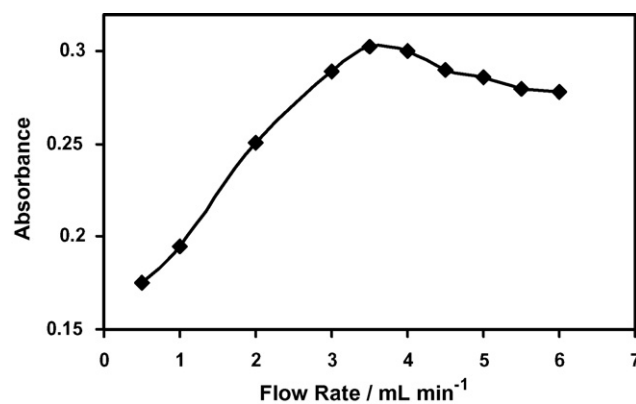


Fig. 2. Influence of the carrier flow rate on the analytical signal,  $[\text{NO}_2^-] = 8.0 \text{ mg L}^{-1}$ ,  $T = 25^\circ\text{C}$ ,  $[\text{MnO}_2] = 25\%$  (w/w), Loop volume =  $400 \mu\text{L}$ , carrier stream =  $0.1 \text{ mol L}^{-1} \text{ H}_2\text{SO}_4$ .

stream was conducted. Flow rates between  $0.5 \text{ ml min}^{-1}$  and  $6 \text{ ml min}^{-1}$  were evaluated. The optimization is shown in Fig. 2. The highest analytical signal (absorbance) was found for a rate of  $3.5 \text{ ml min}^{-1}$ . At the lower flow rates down to  $3.5 \text{ ml min}^{-1}$ , the resulting absorbance is low, because of increased longitudinal diffusion. Decreasing absorbance was found for flow rates above  $3.5 \text{ ml min}^{-1}$ , because the reaction between  $\text{NO}_2^-$  with  $\text{MnO}_2$  had not gone to completion. A carrier flow rate of  $3.5 \text{ ml min}^{-1}$  was selected in order to obtain maximum sensitivity and minimum residence times. Under these conditions, at least 90 injections per hour can be performed.

Based on the above reaction, an acidic carrier is required for the completion of the reaction between  $\text{NO}_2^-$  and  $\text{MnO}_2$ . Care should be taken that the concentration of the acid in the carrier stream will give optimum performance, but without any destruction to the response reactor. The response of oxidation reactor was studied by using  $\text{HCl}$ ,  $\text{H}_3\text{PO}_4$  and  $\text{H}_2\text{SO}_4$  acids in the carrier stream. The optimum acidity of the solution with  $\text{HCl}$  and  $\text{H}_3\text{PO}_4$  and  $\text{H}_2\text{SO}_4$  lies within the concentration range  $0.0001\text{--}0.5 \text{ mol L}^{-1}$ . The following media have been tried in the proposed experiments: hydrochloric acid, phosphoric acid and sulfuric acid solutions. Analytical parameters of these acids have been studied and reported in Table 1. It was found that the sensitivity of reaction is very low in  $\text{HCl}$  and  $\text{H}_3\text{PO}_4$  solutions. But the sensitivity is higher and the reproducibility is better only in sulfuric acid. Therefore, sulfuric acid was selected as the best reaction medium. Also, the effect of acid concentration (preparation from sulfuric acid) was evaluated (see Fig. 3). The

Table 1  
Analytical parameters of the proposed method for different mineral acids

Acid <sup>a</sup>	Intercept ( $a$ ) <sup>b</sup>	Slope ( $b$ ) <sup>b</sup>	$r^c$	DL <sup>d</sup> ( $\text{mg L}^{-1}$ )
$\text{H}_3\text{PO}_4$	0.006	0.0214	0.9973	0.22
$\text{HCl}$	0.005	0.0327	0.9948	0.28
$\text{H}_2\text{SO}_4$	0.002	0.0454	0.9979	0.07

<sup>a</sup> Acids concentration was  $0.1 \text{ mol L}^{-1}$ .

<sup>b</sup> The slope is obtained from equation;  $A = a + b \times [\text{NO}_2^-]$ , where  $A$  is the absorbance for concentration of nitrite,  $a$  is intercept and  $b$  is slope.

<sup>c</sup> Correlation coefficient.

<sup>d</sup> Detection limit.

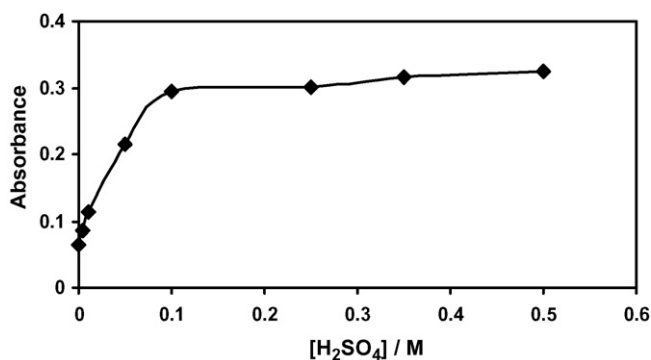


Fig. 3. Influence of the carrier stream H<sub>2</sub>SO<sub>4</sub> concentration on the analytical signal, [NO<sub>2</sub><sup>-</sup>] = 8 mg L<sup>-1</sup>, T = 25 °C, [MnO<sub>2</sub>] = 25% (w/w), Loop volume = 400 μL and flow rate = 3.5 ml min<sup>-1</sup>.

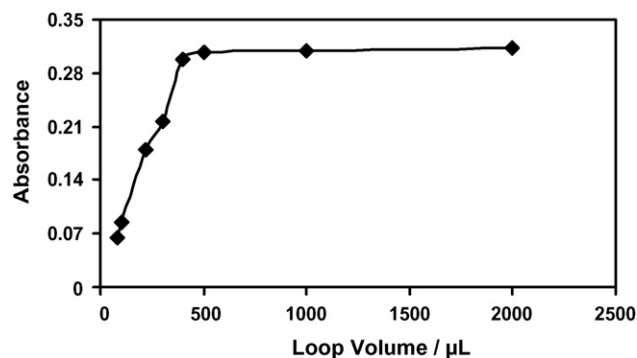


Fig. 5. Influence of the injection volume on analytical signal, [NO<sub>2</sub><sup>-</sup>] = 8 mg L<sup>-1</sup>, carrier stream = 0.1 mol L<sup>-1</sup> H<sub>2</sub>SO<sub>4</sub>, [MnO<sub>2</sub>] = 25% (w/w), T = 25 °C and flow rate = 3.5 ml min<sup>-1</sup>.

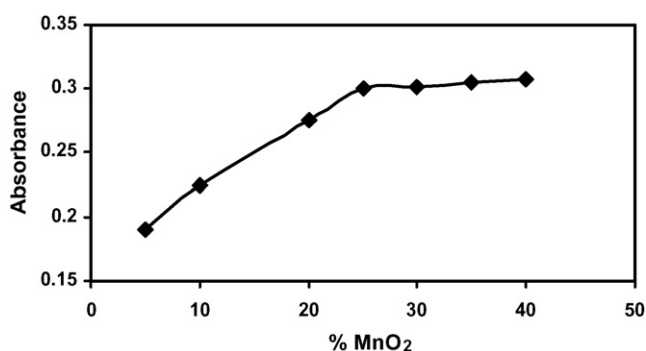


Fig. 4. Influence of the solid MnO<sub>2</sub>% (w/w) suspended on silica gel beads on analytical signal, [NO<sub>2</sub><sup>-</sup>] = 8 mg L<sup>-1</sup>, carrier stream = 0.1 mol L<sup>-1</sup> H<sub>2</sub>SO<sub>4</sub>, T = 25 °C, Loop volume = 400 μL and flow rate = 3.5 ml min<sup>-1</sup>.

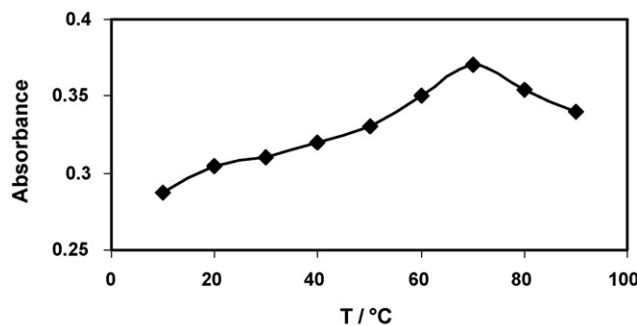


Fig. 6. Influence of the reactor temperature on analytical signal, [NO<sub>2</sub><sup>-</sup>] = 9 mg L<sup>-1</sup>, carrier stream = 0.1 mol L<sup>-1</sup> H<sub>2</sub>SO<sub>4</sub>, [MnO<sub>2</sub>] = 25% (w/w), Loop volume = 400 μL and flow rate = 3.5 ml min<sup>-1</sup>.

analytical signals increased with an increase in acid concentration from 0.0001 to 0.1 and then were constant, so 0.1 mol L<sup>-1</sup> H<sub>2</sub>SO<sub>4</sub> was chosen as the optimum concentration.

The effect of the oxidant (manganese(IV) dioxide) concentration on the performance of the method was evaluated between 5% and 40% (w/w) for MnO<sub>2</sub>:silica ratio. Fig. 4 shows the results of increasing the MnO<sub>2</sub>:silica ratio on the amount of absorbance. A 25% (w/w) MnO<sub>2</sub> mixture was chosen to ensure longer reactor lifetime and better sensitivity.

The loop volume has a significant effect on absorbance, range of linearity and sensitivity, as one would expect. The absorbance was found to increase with the injected sample volume (see Fig. 5). The height absorbance was obtained for loop volume upper of 400 μL. The loop volume of 400 μL was chosen as optimum.

Finally, the effect of the reactor temperature between 10 °C and 90 °C was evaluated. The optimization is shown in Fig. 6. The analytical signals increased slowly with increasing temperature between 10 °C to 70 °C and then decreased with an increase in temperature up to 90 °C. We chose 25 °C (r.t.) as the optimum temperature for a simple system.

### 3.3. Sample matrix interference

The investigation of interferences was carried out for the NO<sub>2</sub><sup>-</sup>-MnO<sub>2</sub> reaction, by adding the interfering element to a NO<sub>2</sub><sup>-</sup> standard solution. Tolerance is defined as the maximum weight ratio of foreign compounds to NO<sub>2</sub><sup>-</sup> producing an error of ±5% in the determination of 10 mg L<sup>-1</sup> NO<sub>2</sub><sup>-</sup>. According to this work, no interference is observed from anions such as ClO<sub>4</sub><sup>-</sup> with weight ratio up to 1500, NO<sub>3</sub><sup>-</sup> with weight ratio up to 1000, CO<sub>3</sub><sup>2-</sup>, Ca<sup>2+</sup>, Mg<sup>2+</sup>, Cl<sup>-</sup> with weight ratio up to 800,

Table 2  
Speciation of nitrite and nitrate in synthetic mixtures

Present (mg L <sup>-1</sup> )		[NO <sub>2</sub> <sup>-</sup> ]			[NO <sub>3</sub> <sup>-</sup> ]		
[NO <sub>2</sub> <sup>-</sup> ]	[NO <sub>3</sub> <sup>-</sup> ]	found (mg L <sup>-1</sup> )	R.S.D. (%) (n = 7)	Relative error (%)	found (mg L <sup>-1</sup> )	R.S.D. (%) (n = 7)	Relative error (%)
2.00	2.00	1.96	1.0	-2.00	1.95	0.56	-2.50
8.00	7.00	8.10	0.93	1.25	7.14	1.8	2.00
12.00	14.00	12.23	0.65	1.92	14.27	1.4	1.93
18.00	22.00	17.89	0.97	-0.61	22.60	0.60	2.73



Table 3  
Speciation of nitrite and nitrate in real samples and recovery test

Sample	Added		[NO <sub>2</sub> <sup>-</sup> ] found with		R.S.D. (%)		[NO <sub>3</sub> <sup>-</sup> ] found with		R.S.D. (%)		Recovery (%)	
	[NO <sub>2</sub> <sup>-</sup> ] (mg L <sup>-1</sup> )	[NO <sub>3</sub> <sup>-</sup> ] (mg L <sup>-1</sup> )	Proposed method (mg L <sup>-1</sup> )	Standard method (mg L <sup>-1</sup> )	Proposed method (n = 7)	Standard method (n = 7)	Proposed method (mg L <sup>-1</sup> )	Standard method (mg L <sup>-1</sup> )	Proposed method (n = 7)	Standard method (n = 7)	[NO <sub>2</sub> <sup>-</sup> ]	[NO <sub>3</sub> <sup>-</sup> ]
Waste water 1 <sup>a</sup>	0.00	0.00	1.54	1.49	0.91	1.35	64.23	63.12	0.52	1.53	–	–
	10.00	10.00	11.47	11.40	0.89	1.15	73.88	73.60	0.61	1.21	99.3	96.5
Waste water 2 <sup>a</sup>	0.00	0.00	1.31	1.29	0.83	0.97	56.08	57.10	0.70	1.47	–	–
	10.00	10.00	11.23	11.20	0.85	1.40	66.10	66.6	0.65	1.33	99.2	100.2
Zahedan city water	0.00	0.00	0.00	0.00	–	–	18.86	19.33	0.46	0.99	–	–
	1.000	10.00	9.95	9.86	1.0	1.72	29.05	28.87	0.64	1.01	99.5	101.9
Iranshahr <sup>b</sup> city water	0.00	0.00	0.00	0.00	–	–	14.12	14.23	0.79	1.25	–	–
	10.00	10.00	9.83	9.91	1.1	1.64	24.38	23.99	0.50	1.07	98.3	102.6
Meat product <sup>c</sup>	0.00	0.00	11.10	10.91	0.76	1.12	63.80	64.10	0.40	1.53	–	–
	10.00	10.00	21.28	22.00	0.64	1.73	73.69	74.78	0.83	1.44	101.8	98.9
Meat product <sup>d</sup>	0.00	0.00	31.10	30.85	1.1	1.03	54.21	53.46	0.58	1.69	–	–
	10.00	10.00	40.86	41.00	0.79	0.99	64.63	63.77	0.77	1.71	97.6	104.2
Well water 1	0.00	0.00	0.00	0.00	–	–	47.31	46.80	0.80	1.64	–	–
	10.00	10.00	9.87	9.80	0.80	1.33	56.96	56.78	0.86	1.55	98.7	96.5
Well water 2	0.00	0.00	0.00	0.00	–	–	120.10	120.96	0.79	1.47	–	–
	10.0	10.00	9.90	10.05	1.0	1.21	130.25	130.57	0.91	1.74	99.0	101.2

<sup>a</sup> University of Sistan and Baluchestan wastewaters.

<sup>b</sup> Iranian Sistan and Baluchestan province.

<sup>c</sup> Amol Juoneka Sausage.

<sup>d</sup> Amol Juoneka Calbus.

S<sub>2</sub>O<sub>8</sub><sup>2-</sup> with weight ratio up to 500, F<sup>-</sup>, H<sub>2</sub>PO<sub>4</sub><sup>-</sup> with weight ratio up to 300, CH<sub>3</sub>COO<sup>-</sup>, Fe<sup>3+</sup> with weight ratio up to 50 and B<sub>4</sub>O<sub>7</sub><sup>2-</sup>, S<sub>2</sub>O<sub>5</sub><sup>2-</sup> with weight ratio up to 50, Mo<sub>7</sub>O<sub>24</sub><sup>6-</sup> with weight ratio up to 10 IO<sub>3</sub><sup>-</sup>, BrO<sub>3</sub><sup>-</sup>, S<sub>2</sub>O<sub>4</sub><sup>2-</sup>, with weight ratio up to 1.

### 3.4. Evaluation of the method

Using the experimental conditions described above, the calibration graphs are linear from 0.1 mg L<sup>-1</sup> to 20 mg L<sup>-1</sup> and 0.5 mg L<sup>-1</sup> to 30 mg L<sup>-1</sup> and are described by the equation:  $A_1 = 0.0454 [\text{NO}_2^-] + 0.002$  with  $r = 0.9979$  and  $A_2 = 0.0232 [\text{NO}_3^-] + 0.003$  with  $r = 0.9992$  for  $n = 10$  for nitrite and nitrate respectively, where  $A$  is the absorbance,  $r$  the correlation coefficient and  $n$  represents the number of determinations.

The detection limit (DL) were calculated using the equation  $\text{DL} = 3S_{\text{bk}}/m$ , where  $S_{\text{bk}}$  is the standard deviation of blank signals for 10 determinations and  $m$  is the slope of the calibration graph. The calculated DL was found to be 0.07 mg L<sup>-1</sup> and 0.14 mg L<sup>-1</sup> for nitrite and nitrate, respectively.

### 3.5. Determination of nitrite and nitrate in a mixture

The present method was applied to determine nitrite and nitrate in synthetic mixtures at different mass ratios under the optimum conditions. The absorbance intensity of a nitrite and nitrate mixture was measured without reduction of nitrate. This gives the measure of nitrite originally present as nitrite in the mixture. Subtracting this from the total gives the concentration of nitrate present in the mixture after reduction of nitrate by copperized cadmium solid-phase reactor. Also, the repeatability of the proposed method was determined for nitrite and

nitrate mixtures (by seven repetitive analyses). The results are shown in Table 2. These results indicate that the relative standard deviation (R.S.D.%) and relative error (R.E.%) could be better than 1.0% and  $\pm 2.00$  for nitrite and 1.8% and  $\pm 2.73$  for nitrate, respectively.

### 3.6. Application to real samples and recovery tests

Recovery tests for nitrite and nitrate using the proposed method were performed using four different samples, and the test for each sample was carried out in triplicate. As shown in Table 3, the recoveries of nitrite and nitrate added to meat products and water samples were all between 97.6% to 101.8% and 96.5% to 104.2% for nitrite and nitrate, respectively. The results of the recovery tests are very good.

## 4. Conclusions

The results of this work demonstrate application of manganese(IV) oxide solid-phase reactor for the speciation of nitrite and nitrate using a FIA–FAAS system. The sample is forced through the reactor and the liberated manganese ions are then monitored by a flame atomic absorption spectrometer. The procedure resulted in a selectivity which fits well with that of water, wastewater and foodstuff samples. The MnO<sub>2</sub> reagent used is cheap, stable and readily available in every laboratory.

## Acknowledgement

The authors gratefully thank University of Sistan & Baluchestan (USB) for providing the financial support.

## References

- [1] S.E. Manahan, *Environmental Chemistry*, fourth ed., Brooks/Cole, Monterey, CA, 1984.
- [2] J.W. Moore, E.A. Moore, *Environmental Chemistry*, Academic Press, New York, 1976.
- [3] Ministry of Agriculture, Fisheries and Food, Great Britain (MAFF), 1992, Paper 32.
- [4] J.K. Hurst, S.V. Lumar, *Chem. Res. Toxicol.* 10 (1997) 804.
- [5] J.G. Henery, G.W. Heinke, *Environmental Science and Engineering*, second ed., Prentice Hall, New Jersey, 1996.
- [6] R.D. Cox, C.W. Frank, *J. Anal. Toxicol.* 6 (1982) 148.
- [7] M. Masuda, H.F. Mower, B. Pignatelli, I. Celan, M.D. Friesen, H. Nishino, H. Ohshima, *Chem. Res. Toxicol.* 13 (2000) 301.
- [8] C.J. Wang, H.P. Huang, T.H. Tseng, Y.L. Lin, S.J. Shiow, *Arch. Toxicol.* 70 (1995) 5.
- [9] R. Burakham, M. Oshima, K. Grudpan, Sh. Motomizu, *Talanta* 64 (2004) 1259.
- [10] Daniel B. Kim-Shapiro, Mark T. Gladwin, Rakesh P. Patel, Hogg. Neil, J. Inorg. Biochem. 99 (2005) 237.
- [11] M.A. Koupparis, K.M. Walczak, H.V. Malmstadt, *Analyst* 107 (1982) 1309.
- [12] B. Liang, M. Iwatsuki, T. Fukasawa, *Analyst* 119 (1994) 2113.
- [13] S.B. Butt, M. Riaz, M.Z. Iqbal, *Talanta* 55 (2001) 789.
- [14] D.C. Siu, A. Henshall, *J. Chromatogr. A* 604 (1998) 157.
- [15] J.Z. Li, X.C. Wu, R. Yuan, H.G. Lin, R.Q. Yu, *Analyst* 119 (1994) 1363.
- [16] U. Schaller, E. Bakker, U.E. Spichiger, E. Pretsch, *Talanta* 41 (1994) 1001.
- [17] M. Bertotti, D. Pletcher, *Anal. Chim. Acta* 337 (1997) 49.
- [18] M.I.N. Ximenes, S. Rath, F.G.R. Reyes, *Talanta* 51 (2000) 49.
- [19] N. Öztekin, M.S. Nutku, F.B. Erim, *Food Chem.* 76 (2002) 103.
- [20] AOAC Official methods of analysis (16th ed.). Gaithersburg: Association of Official Analytical Chemists, 1997.
- [21] T. Kawakami, S. Igrashi, *Anal. Chim. Acta* 333 (1996) 175.
- [22] M.F. Gine', F.H. Bergamin, E.A.G. Zagatto, B.F. Reis, *Anal. Chim. Acta* 114 (1980) 191.
- [23] R. Andradea, C.O. Viana, S.G. Guadagnin, F.G.R. Reyesb, S. Rath, *Food Chem.* 80 (2003) 597.
- [24] Y.-Q. Zhao, Y.-Z.H. He, W.-E. Gan, L. Yang, *Talanta* 56 (2002) 619.
- [25] L. Monser, S. Sadok, G.M. Greenway, I. Shah, R.F. Uglow, *Talanta* 57 (2002) 511.
- [26] K. Kargosha, M. Noroozifar, *Anal. Chim. Acta* 413 (2000) 57.
- [27] M. Noroozifar, M. Khorasani-Motlagh, S.-N. Hosseini, *Anal. Chim. Acta* 528 (2005) 269.
- [28] M. Noroozifar, M. Khorasani-Motlagh, *Asian J. Spec.* 6 (2002) 97.
- [29] M. Noroozifar, M. Khorasani-Motlagh, *Talanta* 61 (2003) 173.
- [30] M. Noroozifar, M. Khorasani-Motlagh, *Chem. Anal. (Warsaw)* 49 (2004) 929.
- [31] B. Ravindranath, *Principles and Practice of Chromatography*, John Wiley & Sons, New York, 1989, p. 248.
- [32] F. Rincón, B. Martínez, J.M. Delgado, *Meat Sci.* 65 (2003) 1421.
- [33] W. John Williams, *Handbook of Anion Determination*, Butterworths, USA, 1979, p. 127.
- [34] N. Gayathri, N. Balasubramanian, *Analisis* 27 (1999) 174.
- [35] R.A.S. Lapa, J.L.F. Clima, I.V.O.S. Pinto, *Anal. Sci.* 16 (2000) 1157.

## Determination of phenolic acids using *Trametes versicolor* laccase

Dilek Odaci<sup>a</sup>, Suna Timur<sup>a</sup>, Nurdan Pazarlioglu<sup>a</sup>, Maria Rita Montereali<sup>b</sup>,  
Walter Vastarella<sup>b</sup>, Roberto Pilloton<sup>b,\*</sup>, Azmi Telefoncu<sup>a</sup>

<sup>a</sup> Ege University, Faculty of Science, Biochemistry Department, 35100 Bornova-Izmir, Turkey

<sup>b</sup> ENEA, Via Anguillarese 301, SP061, Santa Maria di Galeria, 00060 Rome, Italy

Received 4 November 2005; received in revised form 6 March 2006; accepted 6 April 2006

Available online 12 June 2006

### Abstract

Two biosensors based on *Trametes versicolor* laccase (TvL) were developed for the determination of phenolic compounds. Commercial oxygen electrode and ferrocene-modified screen-printed graphite electrodes were used for preparation of laccase biosensors. The systems were calibrated for three phenolic acids. Linearity was obtained in the concentration range 0.1–1.0  $\mu\text{M}$  caffeic acid, 0.05–0.2  $\mu\text{M}$  ferulic acid, 2.0–14.0  $\mu\text{M}$  syringic acid for laccase immobilised on a commercial oxygen electrode and 2.0–30.0  $\mu\text{M}$  caffeic acid, 2.0–10.0  $\mu\text{M}$  ferulic acid, 4.0–30.0  $\mu\text{M}$  syringic acid for laccase immobilised on ferrocene-modified screen-printed electrodes. Furthermore, optimal pH, temperature and thermal stability studies were performed with the commercial oxygen electrode. Both electrodes were used for determination of a class of phenolic acids, achieving a cheap and fast tool and an easy to be used procedure for screening real samples of human plasma.

© 2006 Elsevier B.V. All rights reserved.

**Keywords:** Phenolic acid; Laccase biosensor; Ferrocene; Screen-printed electrode

### 1. Introduction

Phenolic acids and their derivatives are widely in plant kingdom (legumes, cereals, and fruits), their by-products (tea, cider, oil, wine, beverages) and medicinal plants [1,2]. Caffeic acid (3,4-dihydroxycinnamic acid), ferulic acid (3-methoxy-4-hydroxycinnamic acid), syringic acid (3,5-dimethoxy-4-hydroxybenzoic acid) have some important antioxidant characteristics for metabolism. Caffeic acid is a kind of phenolic acid, which has been found to be pharmacologically active as an antioxidant, antimutagenic, anticarcinogenic agent, lipoxygenase inhibitor and it also has antibacterial, antiinflammatory and stypic activities [3,4]. Ferulic acid arises from the metabolism of phenylalanine and tyrosine. It is the most abundant hydroxycinnamic acid in the plant world and occurs primarily in seeds and leaves both in its free form and covalently linked to lignin and other biopolymers. The dehydromers of ferulic acid are important structural components in the plant cell wall and serve to enhance its rigidity and strength [5,6]. Due to its phenolic

nucleus and an extended side chain conjugation, it readily forms a resonance stabilized phenoxy radical, which accounts for its potent antioxidant potential. UV absorption by ferulic acid catalyzes stable phenoxy radical formation and thereby potentiates its ability to terminate free radical chain reactions. By virtue of effectively scavenging deleterious radicals and suppressing radiation-induced oxidative reactions, ferulic acid may serve an important antioxidant function in preserving physiological integrity of cells exposed to both air and impinging UV radiation. Similar photoprotection is afforded to skin by ferulic acid dissolved in cosmetic lotions. Its addition to foods inhibits lipid peroxidation and subsequent oxidative spoilage. By the same mechanism, ferulic acid may protect against various inflammatory diseases. A number of other industrial applications are based on the antioxidant potential of ferulic acid [5]. Recently, phenolic acids have been determined in blood, wine, tea, fruit juice, oil and plant extracts by using HPLC with mass spectrometry, UV or electrochemical detection [7–11], capillary electrophoresis with UV or electrochemical detection [12,13], liquid chromatography [14], gas chromatography–mass spectrometry [15–18], fluorescence [19], electrochemical [20,21] detection and biosensor [22]. Compared with other methods, biosensors have the potential to overcome most of the disadvantages of conventional

\* Corresponding author.

E-mail address: [pilloton@casaccia.enea.it](mailto:pilloton@casaccia.enea.it) (R. Pilloton).

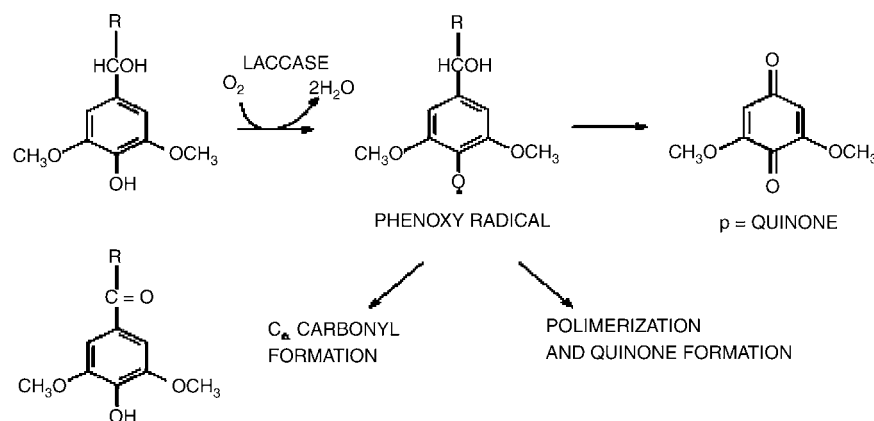


Fig. 1. Typical laccase-catalysed reactions [43].

methods [23]. Amperometric biosensors have been prepared as mediated and unmediated systems. Many electrodes combined with laccase have been developed for detection of phenolics [24–33].

Laccases (*p*-diphenol: dioxygen oxidoreductase, E.C. 1.10.3.2) are multi-copper oxidase having Type 1, Type 2, and Type 3 copper sites [34]. Although a few laccases have been isolated from plant sources (e.g., lacquer, sycamore, and tobacco) most of known laccases have fungal origins (e.g., white rot fungi) and are extracellular enzymes [35,36]. Very recently, it has been reported that laccases are widespread in bacteria [37]. As shown in Fig. 1, laccases reduce oxygen directly to water in a four-electron transfer step without intermediate formation of soluble hydrogen peroxide in expense of one-electron oxidation of a variety of substrates, e.g., phenolic compounds [26].

Instead of oxygen, mediator can be used as an electroactive compound. Ferrocene and its derivatives have been used in biosensors as redox mediators for the electron shuttling between enzyme active site and electrode [38,39]. Phenolic acids are oxidised by laccase. When ferrocene is present in the reaction medium, it acts as an electron donor during oxidation of phenolic acids. Mediator is oxidised by the working electrode. As a result, current is decreased and detected using the electrode system (Fig. 2).

In this study, alternative systems were developed for faster and cheaper determination of phenolic acids in real samples of human plasma by bioanalytical methods including *Trametes versicolor* laccase (TvL) and two different transducers: a commercial Clark electrode and a ferrocene-modified screen-printed graphite electrode.

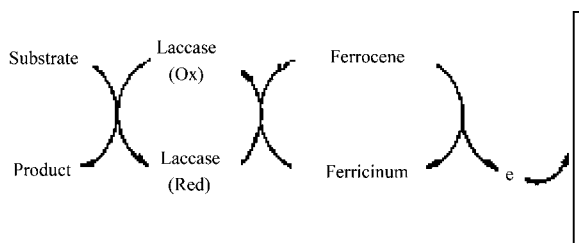


Fig. 2. Principle of ferrocene-mediated laccase biosensor.

## 2. Materials and methods

### 2.1. Reagents

All chemicals were commercially available and of reagent grade. Three-hundred bloom calf skin gelatin, glutaraldehyde (GA), ferulic acid, caffeic acid, syringic acid and 2,2-azinobis-(3-ethylbenzothiazoline-6-sulphonic acid) (ABTS) were obtained from Sigma Chem. Co. (St. Louis, MO, USA).

Plasma samples were obtained from a local hospital and denaturated by adding 70% HClO<sub>4</sub>. The obtained plasma sample was diluted 100-fold and spiked with known amount of standard solutions.

### 2.2. Apparatus

WTW InoLab Oxi Level 2 model dissolved oxygenmeter based on amperometric mode and WTW Cellox 325 Dissolved Oxygen Probe (Germany) were used for the experiments. Chronoamperometric measurements were carried out with the Radiometer (Voltalab PGP 201) electrochemical measurement system (France). Ag/AgCl and Pt were used as reference and counter electrodes, respectively.

### 2.3. Electrode preparation

Ferrocene-modified screen-printed electrodes were home made prepared on PVC substrates by using a HT10 Machine (Fleishle, Germany). Pastes for printing, working electrodes were prepared by using a commercially available graphite paste (GWENT Electronics Materials Inc.<sup>®</sup>). Printed electrodes were fabricated by depositing several layers of pastes on a PVC substrate. 5.6% Ferrocene (w/w) was added to graphite paste, the graphite working electrode, auxiliary electrode, conducting paths and pads were deposited directly on the PVC sheets using graphite pastes (GWENT Electronics Materials Inc.<sup>®</sup>). Then, an insulator paste (GWENT Electronics Materials Inc.<sup>®</sup>) was deposited. Finally, an Ag/AgCl paste (GWENT Electronics Materials Inc.<sup>®</sup>) was placed over the conducting paths (Fig. 3).

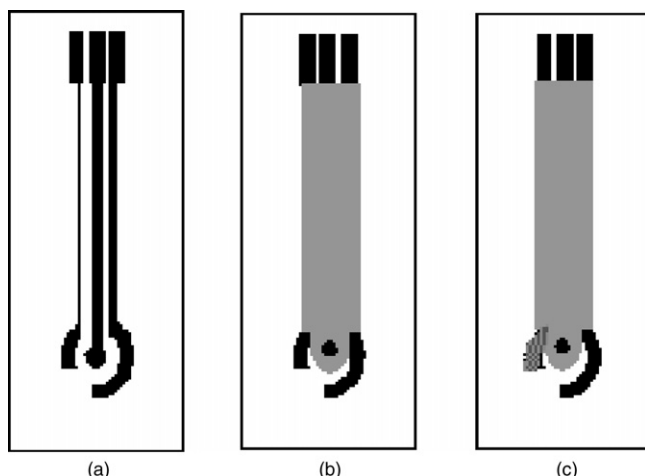


Fig. 3. SPG electrodes: from left to right the concentric lay-out of sequentially printed layers: (a) ferrocene/graphite auxiliary and working electrodes, conductive paths and pads; (b) insulator; (c) Ag/AgCl reference electrode.

#### 2.4. Culture medium of microorganism and laccase production

TvL was isolated from the culture filtrates of the white rot fungus *T. versicolor* (ATCC 11 235). *T. versicolor* was maintained at 4 °C on 2% malt agar and grown in 100 ml malt extract broth (2%) for 3 days. The laccase-production medium was a nitrogen-limited medium consisting of 10 g glucose, 1 g  $\text{NH}_4\text{H}_2\text{PO}_4$ , 0.05 g  $\text{MgSO}_4 \cdot 7\text{H}_2\text{O}$ , 0.01 g  $\text{CaCl}_2$  and 0.025 g yeast extract, per litre. The cultures of *T. versicolor* were incubated at 26 °C on a rotary shaker at 175 rpm. After 72 h cultivation, growing medium was used as a source of enzyme. Laccase production was assessed by measurement of enzyme oxidation of 2,2-azinobis-(3-ethylbenzothiazoline-6-sulphonic acid) at 427 nm ( $\epsilon = 3.6 \times 10^4 \text{ cm}^{-1} \text{ M}^{-1}$ ) [40]. The reaction mixture contained 300  $\mu\text{L}$  of extracellular fluid, 300  $\mu\text{L}$  of 1 mM ABTS and 0.1 M Na-acetate buffer (pH 4.5). 1.0 Unit of enzyme activity is defined as the amount of enzyme that oxidises 1  $\mu\text{mol}$  ABTS in 1 min. Final activity for TvL was 350  $\text{U ml}^{-1}$ .

#### 2.5. Preparation of biosensors

Both commercial oxygen electrode and ferrocene-modified screen-printed electrode were used for preparation of biosensors. Gelatin (10 mg) and 4 U of laccase in 250  $\mu\text{l}$  of phosphate buffer (pH 7.5, 50 mM) were mixed at 38 °C for few minutes. Then, the solution spread over probe surface and allowed to dry at 4 °C for 45 min. Moreover, for screen-printed electrodes the procedure was the same as reported above, with the exception of the deposition of 2.5  $\mu\text{l}$  of mixed solution on the surface of ferrocene-modified graphite working electrode. Four units laccase was used for both biosensors. Finally, they were immersed in 2.5% glutaraldehyde in 50 mM phosphate buffer (pH 7.5) for 5 min [41]. Thus, Type I biosensor including dissolved oxygen probe and Type II biosensor including ferrocene-modified screen-printed electrodes were prepared for detection of phenolic acids.

#### 2.6. Measurements

Oxygen consumption occurred in the enzymatic reaction was detected with Type I biosensor to determine the concentration of phenolic acids. All the measurements were done at 35 °C under continuous and constant stirring and varying substrate concentrations in steady-state conditions by using a thermostatic reaction cell. A baseline was obtained with the working buffer in 10 min, then the substrate solution was added individually to the reaction cell. Enzymatic reaction was completed in 10 min. The concentration of dissolved oxygen was measured. After completion of the measurement, the electrode was rinsed with distilled water and allowed to equilibrate before the following measurement. Fifty millimolars of acetate buffer, pH 4.5, was used as working buffer for laccase biosensor.

Under same working conditions, phenolic acid detection was obtained with Type II biosensors. The buffer solution was deaerated with  $\text{N}_2$  for 10 min before use. After phenolic acid addition, its oxidation took place in the bioactive layer and was sensed as a change in the current intensity with a potentiostat at 0.28 V versus Ag/AgCl pseudo-reference electrode.

### 3. Results and discussion

#### 3.1. Optimisation of assay conditions

Optimisation studies have been performed only with the commercial oxygen electrode, while all the remaining experiments have been done with both biosensors.

##### 3.1.1. Effect of pH

Fig. 4(a) and (b) show the results obtained from pH optimisation studies of the biosensors. The optimal pH value of 4.5 of both systems was obtained for caffeic acid, ferulic acid and syringic acid. A decrease was observed for lower and higher pH values. Our data on TvL perfectly agree with previous work [26], where the variation of laccase activity from different enzyme sources with pH was tested by using phenol as a substrate.

##### 3.1.2. Effect of temperature

Electrode response was measured at different temperatures ranging from 25 °C to 40 °C with Type I biosensor. As shown in Fig. 5, the maximum response was obtained at 35 °C, which is also known as optimum temperature value for laccase enzymes and well agrees with previous works, as cited above. Hence, this temperature was used for all measurements.

##### 3.1.3. Thermal stability

The thermal stability experiments were performed at working conditions (acetate buffer, pH 4.5, 50 mM and 35 °C) for Type I biosensor. Our data showed no decrease in biosensor response after 7 h. After that, only 7% decrease of the beginning activity of the biosensor was observed up to 8 h. In this period, approximately 28 measurements have been made. It could be also possible to make more measurements during the mentioned time.



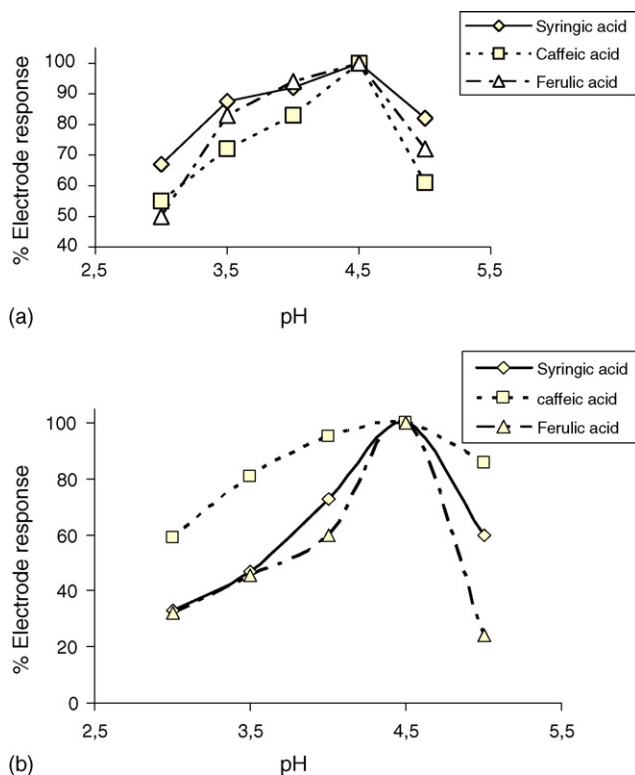


Fig. 4. Effect of pH on Type I (a) and Type II; (b) biosensor responses (pH 3.0–5.5, 50 mM acetate buffer, 35 °C).

### 3.2. Effect of applied potential

Hydrodynamic voltammograms of Type II biosensors based on graphite-ferrocene inks (Fig. 6) were previously performed in our laboratories with several immobilisation procedures and enzymes (peroxidase, tyrosinase, laccase), which have phenols as substrates. Tyrosinase [42] and peroxidase were immobilised on the SPE surface in a cross-linked glutaraldehyde BSA matrix, whereas TvL was immobilised as described above. Similar behaviour of the three biosensors (peroxidase voltammogram not shown in Fig. 6) were observed at different optimal potential as a consequence of experimental conditions and immobilisation procedures used. The optimal potential for Type II biosensor (+280 mV versus Ag/AgCl pseudo-reference electrode) was chosen according to Fig. 6.

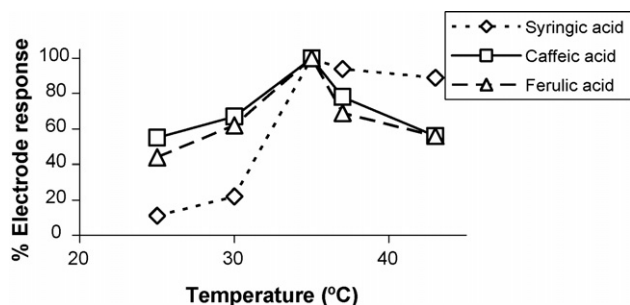


Fig. 5. Effect of temperature on the biosensor response (in acetate buffer, 50 mM, pH 4.5).

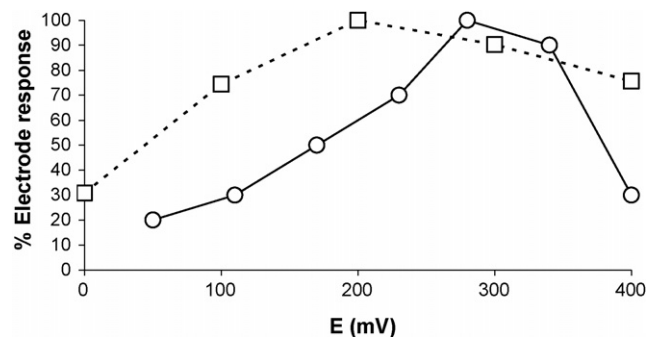


Fig. 6. Hydrodynamic voltammograms obtained with ferrocene-graphite electrodes coupled with cross-linked tyrosinase or TvL. Response to 1 mM phenol with (□) tyrosinase in a GA-BSA matrix (PB 0.1 M, pH 6.5, room temperature); (○) TvL in a gelatin matrix (acetate buffer; 50 mM, pH 4.5, 35 °C).

### 3.3. Analytical characteristics

Linearity was obtained in a concentration range 0.1–1.0  $\mu\text{M}$  caffeic acid, 0.05–0.2  $\mu\text{M}$  ferulic acid, 2.0–14.0  $\mu\text{M}$  syringic acid for laccase immobilised on commercial oxygen electrode and 2.0–30.0  $\mu\text{M}$  caffeic acid, 2.0–10.0  $\mu\text{M}$  ferulic acid, 4.0–30.0  $\mu\text{M}$  syringic acid for laccase immobilised on ferrocene-modified screen-printed electrodes (Table 1). At higher concentrations, calibration curves showed a deviation from linearity. The precision of biosensors was tested and results are shown in Table 1 as coefficient of variation (CV).

On the other hand, ascorbic acid, uric acid and paracetamol which could be catalytically oxidised by ferricinium ion were tested at different concentrations. No signal was detected with Type II biosensor at +280 mV at concentrations lower than 50  $\mu\text{M}$  ascorbic acid, 100  $\mu\text{M}$  uric acid and 25  $\mu\text{M}$  paracetamol. These concentrations are relatively higher than detection ranges for phenolic acids tested in this paper. At higher concentration signals have been recorded as 0.5, 1.15 and 0.95  $\mu\text{A cm}^{-2}$  for ascorbic acid (50  $\mu\text{M}$ ), uric acid (100  $\mu\text{M}$ ) and paracetamol (25  $\mu\text{M}$ ).

### 3.4. Phenolic acid determination of human plasma

Proposed biosensors were analytically evaluated with real samples of human plasma. TvL is specific for a class of compounds, not for a single compound and this characteristic has been exploited to obtain an analytical device for a wide spectrum of phenolic compounds. In addition, TvL shows different specificity for its substrates. Accuracy is then affected by the different specificity of the enzyme for all substrates. For this reason, recovery experiments on blind spiked samples were preferred with respect to the comparison with a reference method. For this purpose, denaturated plasma sample was prepared as described in material and method and used as stock solution. Plasma samples were added to reaction cell after equilibration and changes in the responses were recorded for both types of biosensors. Then, plasma samples with spiked amount of several phenols were added and signals were recorded. Finally, data were calculated from the calibration curves. All results including recovery coefficients (Table 2) are analytically acceptable.

Table 1  
Analytical features of the proposed laccase biosensors

	Biosensor					
	Type I biosensor			Type II biosensor		
	Caffeic acid <sup>a</sup>	Ferulic acid <sup>a</sup>	Syringic acid <sup>a</sup>	Caffeic acid <sup>a</sup>	Ferulic acid <sup>a</sup>	Syringic acid <sup>a</sup>
Slope of the calibration line <sup>b</sup>	0.239	1.040	0.130	0.110	0.130	0.013
Correlation coefficient ( $R^2$ )	0.991	0.997	0.996	0.993	0.996	0.998
Linearity range ( $\mu\text{M}$ )	0.10–1.00	0.05–0.20	2.0–14.0	2.0–30.0	2.0–10.0	4.0–30.0
LOD ( $\mu\text{M}$ ) <sup>c</sup>	0.06	0.01	0.5	1.6	1.8	1.5
LOQ ( $\mu\text{M}$ ) <sup>c</sup>	0.12	0.02	1.1	3.0	2.3	2.4
$\sigma$ ( $n=5$ ) <sup>d</sup>	$\pm 0.03$	$\pm 0.01$	$\pm 0.5$	$\pm 0.2$	$\pm 0.2$	$\pm 0.6$
CV <sup>e</sup> (%)	3.3	5.0	4.5	4.6	1.4	4.9

<sup>a</sup> Phenolic acid.

<sup>b</sup> Slope is given in  $\text{mg L}^{-1} \mu\text{M}^{-1}$  for Type I biosensor and in  $\mu\text{A cm}^{-2} \mu\text{M}^{-1}$  for Type II biosensor.

<sup>c</sup> LOD (limit of detection) and LOQ (limit of quantitation) have been calculated with the graphical method reported by Meier and Zund [44].

<sup>d</sup> Repeability measurements and standard deviation ( $\sigma$ ) calculation were performed with  $n=5$  replicates of 0.75  $\mu\text{M}$  caffeic acid, 0.1  $\mu\text{M}$  ferulic acid, 10.0  $\mu\text{M}$  syringic acid with Type I biosensor and 4.0  $\mu\text{M}$  caffeic acid, 6.0  $\mu\text{M}$  ferulic acid, 10.0  $\mu\text{M}$  syringic acid with Type II biosensor.

<sup>e</sup> Coefficient of variation.

Table 2  
Application of biosensors to human plasma

	Amount of phenolic acid in plasma ( $\mu\text{M}$ ) <sup>a</sup> ( $C_0$ )	Added phenolic acid ( $\mu\text{M}$ ) ( $C_{\text{add}}$ )	Detected total phenolic acid ( $\mu\text{M}$ ) ( $C_{\text{tot}}$ )	% Recovery ( $(C_{\text{tot}} - C_0)/C_{\text{add}}$ )
Type I biosensor				
Caffeic acid	<0.06	0.60	$0.58 \pm 0.03$	97
	0.09	0.70	$0.78 \pm 0.04$	99
Ferulic acid	0.05	0.10	$0.13 \pm 0.01$	80
	0.06	0.10	$0.18 \pm 0.01$	120
Syringic acid	<0.50	1.80	$2.1 \pm 0.6$	117
	3.20	7.00	$10.1 \pm 0.3$	99
Type II biosensor				
Caffeic acid	<1.60	2.70	$2.2 \pm 0.5$	81
	0.10	4.50	$4.8 \pm 0.8$	105
Ferulic acid	<1.80	2.10	$2.2 \pm 0.4$	105
	0.50	4.40	$5.0 \pm 0.3$	102
Syringic acid	0.70	5.30	$6.1 \pm 0.5$	102
	1.50	9.90	$11.6 \pm 0.3$	102

All results are given as value  $\pm$  S.D.,  $n=5$ .

<sup>a</sup> Added phenolic acid concentration were calculated after addition to the blank plasma sample using the standard curves obtained for each substrate.

The nature of sample does not affect the measurements. Moreover, interferences of some compounds were already mentioned in Section 3.3. Apart from these compounds, electrochemical response of each phenolic acid on naked screen-printed electrode (with or without ferrocene) was also tested and no response was obtained in each case. All data showed that in the detection ranges both types of biosensor could be used as an analytical system selective for the class of phenolic compound.

#### 4. Conclusion

In this study, TvL based biosensors were developed for determination of phenolic acids. Optimal working conditions were found at pH 4.5, 50 mM acetate buffer and 35 °C by using laccase modified oxygen electrode. Under these conditions, calibration analytical parameters, reproducibility studies, including sample application, were done for both laccase modified electrodes.

Laccase based biosensors are simple, rapid to prepare, reliable fast and of low cost. Furthermore, they offer a good method for screening phenolic acids in complex matrices like human plasma.

#### Acknowledgement

Authors thank Y.D. Unal for technical assistance during the enzyme production.

#### References

- [1] G. Maiani, M. Serafini, M. Salucci, E. Azzini, A. Ferro-Luzzi, J. Chromatogr. A 692 (1997) 311–317.
- [2] Y. Amakura, M. Okada, S. Tsuji, Y. Tonogai, J. Chromatogr. A 891 (2000) 183–188.
- [3] Y. Peng, F. Liu, J. Ye, Electroanalysis 17 (4) (2005) 356–362.

- [4] T.H. Tsai, Y.F. Chen, I.F. Chen, C.F. Chen, *J. Chromatogr. B* 729 (1999) 119–125.
- [5] E. Graf, *Free Radical Biol. Med.* 13 (4) (1992) 435–448.
- [6] S. Mathew, T.E. Abraham, *Crit. Rev. Biotechnol.* 24 (2–3) (2004) 59–83.
- [7] Y.S. Uang, F.L. Kang, K.Y. Hsu, *J. Chromatogr. B: Biomed. Sci. Appl.* 673 (1) (1995) 43–49.
- [8] A. Schieber, P. Keller, R. Carle, *J. Chromatogr. A* 910 (2001) 265–273.
- [9] A. Bolarinwa, J. Linseisen, *J. Chromatogr. B* 823 (2005) 143–151.
- [10] F. Buiarelli, G. Cartoni, F. Coccioli, Z. Levetsovitou, *J. Chromatogr. A* 695 (2) (1995) 229–235.
- [11] G. Shui, L.P. Leong, *J. Chromatogr. A* 977 (2002) 89–96.
- [12] A.C. Pancorbo, A.S. Carretero, A.F. Gutierrez, *J. Sep. Sci.* 28 (2005) 925–934.
- [13] J. Hernandez-Borges, G. Gonzalez-Hernandez, T. Borges-Miquel, M.A. Rodriguez-Delgado, *Food Chem.* 91 (2005) 105–111.
- [14] A. Cappiello, G. Famigliani, F. Mangani, M. Careri, P. Lombardi, C. Mucchino, *J. Chromatogr. A* 855 (1999) 515–527.
- [15] Y.C. Fiamegos, C.G. Nanos, J. Vervoort, C.D. Stalikas, *J. Chromatogr. A* 1041 (2004) 11–18.
- [16] T.Y. Chu, C.H. Chang, Y.C. Liao, Y.C. Chen, *Talanta* 54 (2001) 1163–1171.
- [17] K. Zhang, Y. Zuo, *J. Agric. Food Chem.* 52 (2) (2004) 222–227.
- [18] H. Wu, T. Haig, J. Pratley, D. Lemerle, M. An, *J. Chromatogr. A* 864 (1999) 315–321.
- [19] M. Muchuweti, A.R. Ndhkala, A. Kasiamhuru, *Food Chem.* 94 (2006) 415–419.
- [20] W.R. Sousa, C. Rocha, C.L. Cardoso, D. Helena, S. Silva, M. Valnice, B. Zanoni, *J. Food Compos. Anal.* 17 (2004) 619–633.
- [21] Y.H. Pyoa, T.C. Lee, L. Logendra, R.T. Rosen, *Food Chem.* 85 (2004) 19–26.
- [22] J. Li, L.S. Chia, N.K. Goh, S.N. Tan, *Anal. Chim. Acta* 362 (1998) 203–211.
- [23] B.D. Malhotra, R. Singhal, A. Chaubey, S.K. Sharma, A. Kumar, *Curr. Appl. Phys.* 5 (2005) 92–97.
- [24] A.J. Wilkołazka, T. Ruzgas, L. Gorton, *Talanta* 66 (2005) 1219–1224.
- [25] B. Haghghi, L. Gorton, T. Ruzgas, L.J. Jönsson, *Anal. Chim. Acta* 487 (2003) 3–14.
- [26] S. Timur, N. Pazarlioglu, R. Pilloton, A. Telefoncu, *Sens. Actuators B* 97 (2004) 132–136.
- [27] O.D. Leite, O. Fatibello-Filho, A.M. Barbosa, J. Braz. Chem. Soc. 14 (2) (2003) 297–303.
- [28] S.A.S.S. Gomes, J.M.F. Nogueiraa, M.J.F. Rebelo, *Biosens. Bioelectron.* 20 (2004) 1211–1216.
- [29] A.J. Wilkołazka, T. Ruzgas, L. Gorton, *Enzyme Microb. Technol.* 35 (2004) 238–241.
- [30] F. Vianello, A. Cambria, S. Ragusa, M.T. Cambria, L. Zennaro, A. Rigo, *Biosens. Bioelectron.* 20 (2004) 315–321.
- [31] D. Quan, Y. Kim, W. Shin, *J. Electroanal. Chem.* 561 (2004) 181–189.
- [32] J. Kulyš, R. Vidziunaite, *Biosens. Bioelectron.* 18 (2003) 319–325.
- [33] R.S. Freire, N. Duran, L.T. Kubota, *Talanta* 54 (2001) 681–686.
- [34] Y. Kim, N.S. Cho, T.J. Eom, W. Shin, *Bull. Korean Chem. Soc.* 23 (7) (2002) 985–989.
- [35] P. Schneider, M.B. Caspersen, K. Mondorf, T. Halkier, L.K. Skov, P.R. Ostergaard, K.M. Brown, S.H. Brown, F. Xu, *Enzyme Microb. Technol.* 25 (1999) 502–508.
- [36] M. Antorini, I.H. Gimbert, T. Choinowski, J.C. Sigoillot, M. Asther, K. Winterhalter, K. Piontek, *Biochim. Biophys. Acta* 1594 (2002) 109–114.
- [37] N. Duran, M.A. Rosa, A. D’Annibale, L. Gianfreda, *Enzyme Microb. Technol.* 31 (2002) 907–931.
- [38] A. Chaubey, B.D. Malhotra, *Biosens. Bioelectron.* 17 (2002) 441–456.
- [39] J. Razumiene, V. Gureviciene, A. Vilkanauskite, L. Marcinkeviciene, I. Bachmatova, V. Laurinavicius, *Sens. Actuators B* 95 (2003) 378–383.
- [40] R. Bourbannais, M.G. Paice, *Biochem. J.* 255 (1988) 445–450.
- [41] N. Ertaş, S. Timur, E. Akyilmaz, E. Dinçkaya, *Turk. J. Chem.* 24 (2000) 95–99.
- [42] M.R. Montereali, W. Vastarella, L. Della Seta, R. Pilloton, *Intern. J. Environ. Anal. Chem.* 85 (9–11) (2005) 795–806.
- [43] R.C. Minussi, G.M. Pastoreand, N. Duran, *Trends Food Sci. Technol.* 13 (2002) 205–216.
- [44] P.C. Meier, R.E. Zund, in: J.D. Winefordner (Ed.), *Statistical Methods in Analytical Chemistry*, vol. 123, J. Wiley & Sons Inc., New York, 1993, p. 87.

Review

# Determination of rhodium: Since the origins until today ICP-OES and ICP-MS

C. Bosch Ojeda, F. Sánchez Rojas\*

*Department of Analytical Chemistry, Faculty of Sciences, University of Málaga, Campus Teatinos, 29071 Málaga, Spain*

Received 21 November 2005; received in revised form 29 March 2006; accepted 6 April 2006

Available online 30 May 2006

## Abstract

Rh is contained in catalyst in much smaller quantities than Pt. For this reason, the database for this metal with respect to emissions from catalytic converters is much smaller than that for platinum, thus precluding a quantitative risk assessment.

Accurate determinations of the rhodium have always been difficult tasks. The metal is often present at trace levels in sample types of complex composition. This situation has improved recently due to developments of instrumental methods and their applications to analyses of rhodium in a variety of matrices. The purpose of this review is to describe the analytical sensitive methods by inductively coupled plasma spectrometry.

© 2006 Elsevier B.V. All rights reserved.

**Keywords:** Rhodium determination; Inductively coupled plasma atomic emission spectrometry; Inductively coupled plasma mass spectrometry; Sample preparation; Review

## Contents

1. Introduction	1
2. Inductively coupled plasma atomic emission spectrometry	2
3. Inductively coupled plasma mass spectrometry	4
3.1. Geological and industrial materials	4
3.2. Environmental materials	6
4. Conclusions	11
References	11

## 1. Introduction

Rhodium together with platinum and palladium play a decisive role in the performance of exhaust systems, worldwide applied in vehicles to reduce the emission of gaseous pollutants. However, the hot exhaust gases flowing through the converter cause abrasion of these units, leading to the emission of the metals to the environment. Thus, these novel anthropogenic metals

have an increasing impact on nature due to the increasing number of cars equipped with catalytic converters.

The monitoring of rhodium originating from the emission of the automotive catalytic converter attrition into environmental samples has paramount importance with respect to estimation of the future risk of the human health and the ecosystem. The concentration of this element is still relatively low in environmental compartments, thus their analysis requires analytical methods of high sensitivity, selectivity and the control of interference effects.

In two previous reviews, we have summarised the determination of rhodium by spectrophotometric methods [1] and atomic

\* Corresponding author. Tel.: +34 952137393; fax: +34 952132000.  
E-mail address: [fsanchezr@uma.es](mailto:fsanchezr@uma.es) (F.S. Rojas).

absorption spectrometry [2]. The aim of the present review is to evaluate the utility of atomic emission spectrometry (ICP-OES) and ICP-MS.

Atmospheric-pressure inductively coupled plasmas are flame-like electrical discharges that have revolutionized the practice of elemental and isotopic ratio analysis. In particular, the novel attributes of argon ICPs have made these plasmas a remarkable vaporization–atomisation–excitation–ionisation source for atomic emission and mass spectrometry. Since its introduction over three decades ago, the ICP has exhibited a large number of special attributes. ICP-OES and ICP-MS are the similar analytical methods from the viewpoint of the use of plasma as excellent excitation and ionisation sources.

Optical emission spectroscopy, with argon plasma as the excitation source, has gained worldwide acceptance as a versatile analytical technique. The technique is characterized by high temperature leading to few chemical interferences and wide linear response range (five to six orders of magnitude). ICP-OES has been used for many years, while applications of ICP-MS are of more recent origin.

The ICP-MS is characterized by low background, is one of the most sensitive analytical techniques presently available. It is being developed continuously, to increase the sensitivity, selectivity and capability to process fast transient signals.

Both techniques have provided accurate results rapidly when employed for simultaneous multi-element measurements.

## 2. Inductively coupled plasma atomic emission spectrometry

Plasma source developed from flames and are now very important tools for multi-element determinations in liquid sam-

ples and in solids following sample dissolution. In order to overcome the disadvantages related to the low temperatures of chemical flames but to develop sources with a similarly good temporal stability and versatility with respect to the sample introduction, efforts were directed towards electrically generated discharges called plasma sources. Plasma may be defined as “luminous volume of partially ionised gas”. The plasma is generated from radiofrequency (RF) magnetic fields induced by a copper coil wound around the top of a glass torch.

Sample is generally introduced as a solution and is nebulised to form a fine aerosol, that is transported into the centre of the plasma where it rapidly undergoes dissolution, vaporization to molecular level and dissociation into atoms; some of the atoms are ionised. Both atoms and ions become excited in the plasma and, as they revert to their ground state in the tail flame, they emit light; in ICP-OES their characteristic emission is measured using an optical spectrometer. The emission lines, detection limits and possible interferences applicable to ICP-OES in rhodium analysis are given in Table 1 [3].

As all elements present in the radiation source emit their spectrum at the same time, from the principles of OES it is clear that it is a multi-element method and is very suitable for the determination of many elements under the same working conditions. Apart from simultaneous determinations, so-called sequential analyses can also be carried out, provided the analytical signals are constant. Sequential and simultaneous multi-element spectrometers both have their own possibilities and limitations. For this reason, the majority of papers reported the determination of rhodium and other elements, principally noble metals. The determination of rhodium alone in catalysts is described by Watanabe et al. [4] using potassium xanthates to form complex which is extractable into xylene, the detection limit was

Table 1  
Emission lines, detection limits and possible interferences for the determination of rhodium and other precious metals by ICP-OES [3]

Element	Emission line	Wavelength (nm)	Detection limit (ng ml <sup>-1</sup> )	Interference and spectral line (nm)
Rh	I	343.489	60	V II 343.54
Pt	II	214.423	30	Al I 214.54 Fe II 214.44
Pd	I	340.458	44	Fe I 340.44 V II 340.44 Ti II 340.50 W I 340.53
Ru	II	240.272	30	Fe II 240.26
Ir	I	349.894	111	
	II	224.268	27	Cu II 224.26 Fe II 224.18 Ni I 224.29
Os	II	225.585	0.36	Fe II 225.58 Fe I 225.59 Ni I 225.59 Cr II 225.60
Au	I	242.795	17	Fe II 242.83
				Mn II 242.78
				Mn I 242.80
				V I 242.83
				V II 242.73
				W II 242.75
				Al I 197.84
				Al I 197.819
			38	



19 ng ml<sup>-1</sup> and the relative standard deviation for the determination of 25, 50 and 100 µg of Rh for 10 runs, ranged from 1.52 to 1.97%.

Many studies in ICP-OES were concentrated on the determination of impurities in fine precious metals and their alloys. Attention was also paid on the determination of these metals in ores and materials of industrial importance. For example, a method of decomposing placer platinum samples was proposed and this made it possible to determine Rh and Pt, Pd, Ir, Os, Ru, Au and some base metals simultaneously [5]. The decomposition procedure consists in treating the samples with potassium tetrafluorobromate and converting the complex fluorides into soluble complex chlorides.

In the analysis of geological materials, the most important method used for the preconcentration of platinum group metals (PGE) and Au and their separation from base metals and silicates is the fire assay. In the ICP-OES determination of PGE and Au in geological samples following the NiS fire assay and Te coprecipitation, the recovery of these elements was improved by employing screw-capped Teflon bombs for dissolving the NiS beads or the Te precipitates [6]. The precipitation of Crystal Violet–precious metals–tin(II) chloride has been applied to the enrichment of Rh and Pt, Pd, Ir and Au for ICP-AES determination [7]. Also, Rh and 12 impurities were analysed in Pt–Rh

and Pd–Rh alloys [8] and Rh, Au, Pd, Pt in technical solutions [9].

However the limited use of ICP-OES in precious metal analysis, as evinced by the fewer publications, is mainly due to the large sample to volume ratio required. The technique has been utilized for the determination of Rh and Pd in high-purity alloys [10]. Emission lines, detection limits and possible interferences in precious metal analysis are given in Table 1.

On the other hand, the ultra-trace levels of PGE in environmental samples require preconcentration of the analytes and/or separation of the matrix for their determination by ICP-OES. In this way, Lee et al. [11] applied on-line preconcentration of Rh, Pt and Pd as bis(carboxymethyl)-dithiocarbamate (CMDTC) complexes on an XAD-4 filled microcolumn after the off-line addition of solid CMDTC to the sample solution containing SnCl<sub>2</sub> and HCl. The sample solution was segmented in the preconcentration unit by air in order to prevent dispersion. The eluate was collected on-line in a PTFE loop and was forced either into the graphite furnace or into the ICP by the use of a carrier solution. The pH of sample solutions, the concentration of the complexing and reducing agents, and the flow rate in the column were also studied and optimised.

Table 2 describes the details of selected studies of rhodium and other metal ions.

Table 2  
Determination of rhodium and other elements by ICP-OES

Elements	Sample matrix	Methods	Ref.
Pt	Catalysts	Coprecipitation with Te in HCl 2 M by heating at 90° for 5 h	[12]
Pt, Pd	Catalysts	By acid pressure decomposition; with Y as an internal standard	[13]
Pt, Pd	Automotive catalytic converters	An ion-exchange method with a column of Amberlite IRA-93 anion exchange resin	[14]
Pt, Pd	Used automobile catalysts	Microwave digestion of sample with HNO <sub>3</sub> + HCl + H <sub>2</sub> O <sub>2</sub> . Filtration and analysis. NIST 2557 as standard	[15]
Pt, Pd	Catalytic converter	With multichannel array detector technology; using Carius tube dissolution	[16]
Pt, Pd, Au	Rocks, ores, concentrates and sulphide float	After reductive coprecipitation using Se as collector	[17]
Pt, Pd, Au	Minerals	Immobilized by the carbon powder containing diphenylthiourea	[18]
Pt, Pd, Au	Geological samples	After preconcentration with diphenylthiourea immobilized on aluminium oxide	[19,20]
Pt, Pd, Ir	–	Using AP chelating resin (α-aminopyridyl)	[21]
Pd, Ru, Au	Non-ferrous matrix	With a macroporous poly(vinyl-aminoacetone) chelating resin for preconcentration and separation	[22]
Pd, Ce, Y	Pt–Pd–Rh, Pt–Pd–Rh–Ce, Pt–Pd–Rh–Y alloys	The determination ranges of Ce (Y), Rh and Pd being 0.1–1, 0.6–6, and 2–20%, respectively	[23]
Pt, Pd, Ir, Ru	Catalysts	Y as an internal standard	[24]
Pt, Pd, Au, Ag	Geological samples	After poly(dithiocarbamate) resin pre-treatment; sample fusion with a lithium borate flux	[25]
PGE	Airborne particulate	Sample collected on glass filters, leached with HNO <sub>3</sub> /H <sub>2</sub> O <sub>2</sub> diluted with water. Solutions were mixed with Septonex cationic surfactant and HCl and separated using modified silica gel. Also determination by ICP-MS	[26]
PGE	Environmental samples	Preconcentrations as ionic associations of their halo complexes with cation-active tensides on modified silica-type sorbents and by sorption of their halo complexes on strongly basic anion exchangers	[27]
PGE, Au	Geological samples	Separation and preconcentration with a chelating resin (YPA4); the resin is treated by high temperature furnace, vaporized by continuous laser and introduced into ICP	[28]
PGE, Ag, Ta, Th, U	Geological materials	With a poly(dithiocarbamate) resin separation	[29]
Pd and 11 impurities	Platinum gauze for HNO <sub>3</sub> industry	With subtraction of equivalent concentrations	[30]

### 3. Inductively coupled plasma mass spectrometry

ICP-MS has been accepted as a rapid, accurate technique for multi-element analysis. Detection limits of ICP-MS for many elements are comparable or better to electrothermal atomic absorption spectrometry (ET-AAS), although ET-AAS is usually limited to the determination of one element at a time. In addition to excellent sensitivity and multi-element capability, ICP-MS can be used for isotope ratio measurements.

The ICP-MS technique combines advantages of the high temperature plasma source with the highly sensitive detection capabilities of the mass spectrometer. In this technique, the sample aerosol emerging from the plasma tail flame contains a mixture of atoms, ions, undissociated molecular fragments and unvolatilised particles. These are extracted into the mass spectrometer through a sampler cone followed by a skimmer cone. An electrostatic lens system is placed behind the skimmer in the region of high vacuum (at  $10^{-5}$  to  $10^{-6}$  Torr). These function as a focussing medium and the quadrupole system acts as a mass filter. A stable ion path exists along the axis of the four quadrupole rods for passage of ions of only one mass at a time. In addition to the RF voltage applied to opposite pair of rods a dc voltage is applied; the analyzer is scanned by ramping the RF and dc voltages applied to the rods, ions of selected masses are allowed through the detection system in a sequential mode; best results are achieved if the ratio of the voltages remains constant. This operation is usually carried out very rapidly. Ion detection is usually accomplished using electron multiplier detectors. The ability to count individual ions, coupled with very low background signals, results in excellent detection limits for nearly all elements.

The total dissolved content is generally kept below 0.2% to minimize solid deposition on the sampler and skimmer. The major spectroscopic interferences in ICP-MS fall into four categories: polyatomic ions, doubly charged ions, refractory oxides and isobaric ions. Non-spectroscopic interferences are frequently observed when sample matrix is complicated.

With wide linear dynamic range, essentially simultaneous multi-element analytical capability due to rapid scanning facility and a fair degree of tolerance to interference free measurement of analytical signal the ICP-MS today is a widely used analytical tool for trace metal analysis. In principle spectral interferences are not as common as in ICP-OES, but sometimes they can be very severe. However, non-spectral or matrix-induced interferences are more problematic. A major limiting factor is the low tolerance to high dissolved salts in the analyte solutions. Sometimes collision cell interface is used to remove interferences. If the neutral gas introduced to the collision cell is of low molecular weight relative to the ions to be analysed, the ions tend to lose kinetic energy and migrate toward the axis as a result of collision and it acts as a collisional focusing device. If the collision gas molecular weight is too large, the collisions lead to ion scattering out of the cell. Gas phase collisions with Xe and CH<sub>4</sub> have been used for reducing polyatomic ion interferences in ICP-MS.

ICP-MS has provided a powerful alternative method for the determination of the PGEs.

#### 3.1. Geological and industrial materials

Date et al. [31] describe a preliminary work on the application of fire assay and ICP-MS to the determination of PGEs in geological materials. A combination of the neoclassical nickel sulphide fire assay collection procedure with final determination by ICP-MS is considered in relation to the simplified procedure required for dissolution of the Ni sulphide button and the wealth of information inherent in ICP-MS spectra.

Jackson et al. [32] determined PGEs and Au in geological materials by NiS-FA and ICP-MS. The precious metals in the NiS residue were dissolved and then co-precipitated with Te. The precipitate was re-dissolved and analysed in the presence of two internal standards. Detailed studies for evaluating the optimum nickel sulphide button size in the estimation of PGEs by ICP-MS were carried out [33]. PGEs losses in various stages of the process have been studied. The results indicate that among the three button sizes investigated, i.e., 2.5, 5 and 8 g, the 2.5 g button was found to be adequate for the full recovery of the PGEs. Losses of PGE in the fusion slag and in the pulp at the second filtration stage have been found to be negligible. Tellurium coprecipitation was found to minimize the losses during the dissolution of the nickel sulphide button. The nickel sulphide fire assay followed by inductively coupled plasma mass spectrometry was used to determine the platinum group elements and gold in the certified reference material SARM-7 of feldspathic pyroxenite and in the two new reference materials CHR-Pt+ and CHR-Bkg of chromitite [34]. These results and results of reagent blank studies are reported. The nickel sulphide fire assay was also compared with the other commonly used pre-treatment methods, i.e., lead fire assay and aqua regia leach. The comparison was made using the above reference materials and 12 samples from different ore types of the Keivitsa mafic layered intrusion in northern Finland. Various rock types, quartz carbonate rock, hornblende and peridotite, were selected to study dependence of the results on the type of sample. The highest recoveries, considering all elements, were obtained by nickel sulphide fire assay. The results obtained by aqua regia leach support its use for preliminary ore analysis preceding fire assay for gold, platinum and palladium and for some rock types for rhodium and ruthenium.

Digestion in acids is sometimes used as a means of extraction of PGE and Au from geological samples as an alternative to fire assay procedures. However, results have not always been quantitative, and have depended upon the type of sample as well as the experimental conditions. The ratio of sample weight to the volume of acids is very important. PGE and Au were extracted from SRMs and samples by aqua regia, and the solutions were analysed by ICP-MS [35]. In this work, 10 g of sample were treated with 20 ml of acid; Pd and Au were recovered efficiently from a few standards; 20–40% of Pt, Rh, Ru, and Os were recovered, while 1–10% recovery was reported for Ir.

Dry chlorination was developed for the determination of very low concentrations of PGE and Au in rocks [36]. PGE and Au present in geological samples in the forms of native metals, natu-

ral alloys and as PGE- (or Au-) bearing sulphide group minerals were converted to the respective sodium salts in the presence of chlorine gas and sodium chloride at 580 °C. The salts were dissolved in weak HCl and were then separated from chlorination resistant materials by filtration. Precious metals in the filtrates were analysed using the method of standard additions. Samples as large as 25 g were analysed. Analysis of reference materials yielded results which were comparable to or better than results obtained by fire assay techniques. An important advantage of the dry chlorination method was the extremely low reagent blanks. The dry chlorination technique was subsequently extended to the analysis of larger (250 g) samples [37]. The capability of analysing large samples is important because small concentrations of precious metals are not uniformly distributed in rocks. Even samples of 20–30 g of non-ores may not be representative. The reaction vessel was a large, ribbed chlorination tube which was rotated slowly to provide good contact between the chlorine flow and the sample. Results of analyses of a number of standards were in good agreement with accepted values. Blanks were less than 0.1 ng g<sup>-1</sup> for most of the elements.

Dry chlorination for the determination of PGE and Au in the metallic fraction of a rock sample, i.e., the fraction of the sample that contains precious metals as native metals, natural alloys and sulphide group minerals, results in a chlorination resistant non-metallic fraction of the sample, which may contain precious metals also. PGE and Au in chlorination residues (or non-metallic fractions) were determined by microwave digestions of these residues and analyses of the solutions by ICP-MS [38]. The research provided a means of investigating PGE depletion in layered mafic intrusions which host PGE deposits. In this investigation, a much smaller quantity of NaCl (a five times reduction) was distributed efficiently throughout the sample. The lower total dissolved solids contents of the solution for analysis reduced the adverse effects of large salt concentrations in the ICP-MS determination. A more extensive study was undertaken of PGE and Au depletion in layered mafic intrusions. These are the results of penetrations of geological formations by basic igneous rocks while molten. The study involved analyses of drill core samples of the Fox River Sill (Canada) [39].

Sample introduction in the form of slurry has the advantages of fewer sample preparation steps and the need of only a minimum number of reagents. Slurry preparation and introduction was studied for analyses of four SRMs and an in-house standard [40]. Samples were prepared in the presence of a dispersing agent by grinding them to a particle size of <5 µm with zirconium beads in plastic bottles. The dispersing agent, a solution containing Na<sub>4</sub>P<sub>2</sub>O<sub>7</sub> and aqua regia, partially digested the samples during the grinding operation. A disadvantage of this method of sample preparation is the small sample size (0.2 g). Because there is no preconcentration step, low concentrations of precious metals in samples may be beyond the quantitation limits (0.04–0.2 µg g<sup>-1</sup>).

In other investigation, 0.5–1 g of SARM-7 and Merensky Reef PGE-ore samples were fused with Na<sub>2</sub>O<sub>2</sub>, in zirconium crucibles [41]. The acidic solution of the fusion bead was diluted sufficiently to obtain dissolved solids content of 0.25%, and the

solution was introduced to the instrument by FI. Results for Pt and Au agreed with the recommended values for SARM-7. Dilution of the solution for analysis is a disadvantage of this method. In addition, the attack of the flux on the crucible introduced elements whose polyatomic ions interfered in the determinations of the precious metals.

Two methods are described for the preparation of geological samples using microwave digestion prior to determination of the PGEs and Au by ICP-MS [42]. In one method, 0.5-g samples are dissolved in sealed all-PFA microwave digestion vessels using HNO<sub>3</sub>–HCl–HF–HClO<sub>4</sub> acids. Samples are transferred to open PTFE beakers and evaporated to incipient dryness, final solutions being taken up in 1 M HCl prior to analysis. The method has been evaluated using a suite of well-characterized international reference materials (RMs). In some cases, the method resulted in a complete digestion and quantitative data were obtained for Rh, Pd, Ir, Pt and Au, although insufficiently low limits of determination precluded the determination of all five elements in all materials. In other cases, an insoluble residue remained and recoveries of the PGEs and Au were dependent on the element concerned and the mineralogy of each sample. A second method employs 1 g samples and microwave digestion with aqua regia–HF, in higher-pressure Ultem-jacketed Teflon PFA sealed-vessels. Samples are subsequently evaporated to near dryness, digested in 0.5 M HCl, filtered, and the insoluble residues are fused with small quantities of 1:1 Na<sub>2</sub>O<sub>2</sub> + Na<sub>2</sub>CO<sub>3</sub> or Na<sub>2</sub>O<sub>2</sub>, before being dissolved in 0.5 M HCl. The combined solutions are analysed by ICP-MS. Data obtained for a wide range of RMs showed good agreement with reference values. Both methods provide viable means of quantifying Ru, Rh, Pd, Ir, Pt and Au in mineralised samples, but both are limited by modest lower limits of determination in samples of 0.2–1 µg g<sup>-1</sup>. Only the combined microwave digestion–minifusion technique yields fully quantitative data for samples containing refractory minerals. Other method for determination of Rh, Ru, Pd, Ir and Pt in geological samples, using microwave-assisted acid digestion and alkali fusion, separation of the PGEs by cation-exchange chromatography, and analysis by ICP-MS is described [43]. Experiments using synthetic multi-element solutions have been used to establish: conditions for cleaning and conditioning AG 50W-X8 cation-exchange resin; solution requirements for loading samples onto the resin; optimum column size and elution parameters. Recovery studies show no significant retention of Ru, Rh, Pd, Ir and Pt on the resin, at levels ranging from 0.1 to 500 µg. The optimised cation-exchange procedure has been evaluated using 1 g sub-samples of eight reference materials (DZE-1; DZE-2; MA-2a; PTA-1; PTC-1; PTM-1; SARM7; SU-1a), digested using microwave heating in sealed-vessels with aqua regia–HF, followed by alkali fusion of insoluble residues, evaporation of solutions to near dryness, and dissolution in 0.5 M HCl. Matrix elements were removed from sample solutions by cation-exchange chromatography on AG 50W-X8, prior to analysis by ICP-MS. Lower limits of quantitative analysis for 1 g sub-samples range from 1.3 ng g<sup>-1</sup> for Rh to 11 ng g<sup>-1</sup> for Pd, two orders of magnitude better than those achieved for unseparated samples. Good agreement with reference values has been obtained for Ru, Rh, Pd and Ir in most RMs. Preliminary work

indicates that, with minor modification, the method may be applied successfully to larger (5 g) sample sizes, and offers an alternative to fire assay for the determination of Ru, Rh, Pd and Ir.

Laser ablation (LA) is another means of sample introduction that does not require the extensive use of chemicals for sample preparation. Traditional methods for separating the PGEs and gold from ores and rocks have been adapted for use with laser ablation-inductively coupled plasma mass spectrometry (LA-ICP-MS) [44]. Samples were prepared using NiS fire assay techniques resulting in the production of a collector button weighing only  $\sim 1$  g. The button was ground to produce a flat surface and directly ablated using a Nd:YAG laser operating at fundamental wavelength. Quantitative data were obtained by external calibration against both natural geological reference materials (SARM-7, MINTEK 2/77 and CHR-Pt+) and synthetic NiS standard buttons produced by doping high-purity quartz sand with multi-element stock solutions. Analysis times are rapid, 30 s per analysis, and the sampling protocols developed offer the possibility of full automation. Precision of the measurements varied according to concentration and the elements concerned, but were typically 10–15% relative standard deviation or better. Accuracy of the data was assessed by comparison of measured and reference values. Accuracy was partly dependent on element. Data for Ru, Rh and Pd in 2/77 and Ru in CHR-Pt+ were in excellent agreement with reference values, while recoveries for Rh in CHR-Pt+ were a little high. Data for Os and Au could only be evaluated in SARM-7 where agreement with reference values was good. Platinum consistently showed poor recovery with values which were typically 30% low. Experimentally determined detection limits were similar for all elements, from 10 to  $90 \text{ ng g}^{-1}$ . The method provides for the rapid, simultaneous and sensitive determination of the PGEs and Au in rocks and ores.

Inductively coupled plasma mass-spectrometric procedures have been developed for the high-accuracy determination of three platinum group elements (Pt, Pd, and Rh) and Pb in two used automobile catalysts [45]. Isotope dilution quantification was applied for the certification of Pb, Pt, and Pd. The mononucleidic Rh was quantified using an internal standard after careful assessment of potential systematic errors from incomplete dissolution and instrumental interferences.

Alternative methods of sample introduction have also been used for the ICP-MS analysis of the PGEs, these include slurry sampling [40] and laser ablation [44]. There are few reports of the use of electrothermal vaporization (ETV) as a method of sample introduction for Rh. Recently, automobile exhaust gas has been analysed for some PGEs (Rh, Pt, Pd, Ir) by collecting particulate exhaust matter on graphite discs from which the sample was then electrothermally vaporized [46]. The mechanisms by which the PGEs are vaporized in the graphite furnace have been investigated using ETV-ICP-MS [47]. The results suggest that five of these elements (Ru, Rh, Pd, Ir and Pt) are reduced to their metallic state in the graphite furnace and then vaporized by direct sublimation of the metal. The addition of  $\text{TeCl}_2$  chemical modifier was found to have minimal effect on the vaporization mechanism and sensitivity for determination for five of the PGEs. Optimum conditions for the determination of the PGEs

by ETV-ICP-MS are reported, along with their absolute limits of detection; these range from 0.015 pg for Ir to 0.25 pg for Os.

A spark-based, solid-sampling cell is described for ICP-MS [48]. The cell is devised for the direct sampling of gold and silver beads produced by the classical lead fire assay procedure. The sampler produces a solid aerosol composed of submicron-sized vapor condensates and small ( $< 2 \mu\text{m}$ ) spherules. In contrast to solution nebulisation, the mass spectrum for spark-ICP-MS is relatively free of interfering metal oxide, polyatomic, and multiply charged ions. The measurement precision is 3% R.S.D. for Pt, Pd, and Rh preconcentrated into fire assay beads.

Determination of Pd, Rh and Pt in the catalysts by ID-ICP-MS is possible only after extensive treatment with highly corrosive acids in sealed quartz tubes at high temperatures. By contrast, glow discharge mass spectrometry (GD-MS) [49] permits the direct determination of noble metals in the catalysts without prior dissolution. Although the auto-catalyst powders are non-conducting, they may be combined with a metallic binder and analysed. Aluminium powders was chosen as the binder material for its superior gettering abilities, and because the Al mass spectrum in the vicinity of the Pd, Rh and Pt peaks was clear of interferences. Results from the GD-MS analysis of noble metals in NIST Standard Reference Material 2557 used auto-catalyst (monolith) are precise and accurate to  $< 10\%$  R.S.D. for Pd, Rh and Pt.

A simple and highly selective analytical procedure is presented for the concentration determination of Rh, Ru, Pd, Re, Os, Ir and Pt by isotope dilution, which is suitable for the investigation of geological and environmental materials [50]. Sample preparation consists of a sample digestion step in a high pressure asher (HPA-S) with concentrated  $\text{HNO}_3$  and HCl and drying down of the sample solution after the Os concentration was determined by sparging  $\text{OsO}_4$  into an ICP-MS. After drying and redissolution of the remaining solution the other PGEs are separated on-line from their matrix in a simple cation-exchange column that is coupled to a quadruple ICP-MS. Through this technique it is possible to monitor in every sample the isotopes of the analytes as well as of those elements that cause isobaric interferences or that potentially causes interferences through molecular species. Concentrations of the two or more isotopic elements can be calculated through isotope ratios, whereas Rh is calculated by the peak area.

### 3.2. Environmental materials

PGEs, especially Pt, Pd and Rh, have been used as components of automotive exhaust catalysts in order to reduce the concentrations of carbon monoxide, unburned hydrocarbons and nitrogen oxides in exhaust gases. As noted earlier, the catalysts are sources of airborne particulate matter.

During the past decade, the traffic-related emission of Pt, Rh, and Pd has strongly increased resulting in growing concentrations in specific environmental areas. To distinguish different aspects of time-dependent development, PGEs concentrations and element ratios in urban dust, road dusts, soil, and sewage sludge samples collected over the past decade were determined [51]. The short-term variation of PGE concentrations and ele-



ment ratios in road dust is due to wind and rain, whereas the long-term trend reflects the changing proportions of PGE used for converter production. In soil, the total input of PGE has been accumulated since the introduction of converter technology. Because of very low background values, this contamination results in rapidly increasing PGE concentrations, showing multiplied values over a period of 2 years at a typical highway site. The integration of these data permits an estimate of the total accumulation of PGE and means emission rates that are significantly higher than experimental results from stationary motor experiments. Runoff contributes to the composition of sewage but seems to be less important, compared to other sources, in total PGE input into urban sewage sludge. For the analyses of the PGE content in the road dust, soil, and sewage sludge ashes, the separation of the PGE from the sample matrices was done by NiS fire assay, followed by a wet-chemical attack. As the samples of airborne particulate matter were far too small for this high volume sample treatment, an alternative wet-chemical digestion was used where the separation of the PGE is achieved by tellurium coprecipitation. The final analysis was done by quadruple ICP-MS and special attention was given to possible mass interferences. Mass interferences were controlled by measuring the concentrations of the possibly interfering elements (Cu, Zn, Rb, Sr, Y, Mo, Hf, Pb). Because of the matrix separation, the residual concentrations of those elements were in the same range or even lower than those of the PGE. Hence, possible interferences were negligible and no mathematical correction was necessary.

The performance of a double-focusing inductively coupled plasma mass spectrometer equipped with a micro-concentric nebuliser was investigated for the direct simultaneous determination of Rh, Pd, and Pt in less than 1 ml of melted snow and ice samples originating from remote sites [52,53]. Ultra-clean procedures were adopted in the laboratories and during the pre-treatment steps, to avoid possible contamination problems. Spectroscopic and non-spectroscopic interferences affecting the determination of Rh, Pd, and Pt were carefully considered. Detection limits of 0.02, 0.08, and 0.008  $\mu\text{g g}^{-1}$  for Rh, Pd, and Pt, respectively, were obtained using the following isotopes:  $^{103}\text{Rh}$ ,  $^{106}\text{Pd}$ , and  $^{195}\text{Pt}$ . Repeatability of measurements, as R.S.D., was 27, 28, and 29%, for Rh, Pd, and Pt, respectively. The new method was applied to the analysis of samples coming from Greenland, Antarctica, and the Alps in order to assess the past natural background concentrations and to determine the present level of these polluting substances. The extremely low detection limits allowed the direct analysis of all samples except for two Greenland ice core sections dating from 7260 and 7760 years ago for which a preconcentration step was necessary. Concentration ranges for all snow samples were ( $\mu\text{g g}^{-1}$ ) as follows: Rh (0.0005–0.39), Pd (0.01–16.9), and Pt (0.008–2.7). The lowest concentrations were measured in the enriched Greenland ancient ice samples.

Quantification of three platinum group elements most relevant to environmental monitoring, i.e., Pt, Rh and Pd, was performed in road dust, exploiting the high mass resolution capabilities of ICP-SFMS [54]. Sample preparation involved complete microwave-assisted acid digestion of the silicate matrix with  $\text{HNO}_3$ – $\text{HCl}$ – $\text{HF}$  mixtures. An ultrasonic nebuliser,

incorporating a membrane desolvation unit was used as the introduction system. For Pt the Hf oxide interference could be eliminated effectively by membrane desolvation alone. For Rh and Pd, interferences, which could not be eliminated by mass resolution, were evaluated carefully by standard addition of the concomitant ions. It could be shown that no mathematical correction of the result was necessary for Rh, provided that membrane desolvation was employed. Pd in turn could not be measured interference free with this instrumental set-up. This work was focused on the methodology of the direct ICP-SFMS determination of the three PGE most relevant to environmental monitoring, i.e., Pt, Pd and Rh, in road dust. In contrast to previously published studies, high mass resolution capability and ultrasonic nebulisation combined with membrane desolvation were evaluated as instrumental strategies in order to mitigate spectral interferences. Road dust taken from the ceiling of a tunnel is suggested to be the ideal example for an environmental silica containing matrix, as it provides the PGE in the chemical form and matrix in which they were emitted from the car catalyts.

Laser ablation-inductively coupled plasma mass spectrometry (LA-ICP-MS) is a direct trace element measurement technique and can be used for the rapid characterization of metals in solid environmental matrices. The capability of LA-ICP-MS for the direct quantitative determination of PGEs in road sediments was assessed [55]. Two Nd:YAG laser systems operating at 266 and 1064 nm, respectively, were coupled to an ICP-MS. Uncontaminated road sediments were spiked with PGEs, both as solution and as solid certified reference material, and used to assess the analytical performance of the technique and to calibrate the instrument. Interferences due to the formation of molecular ions and double charged ions were investigated. The LA-ICP-MS was then used to determine the concentration of PGEs in recent urban road sediment and the results were compared with high resolution ICP-MS measurements after microwave sample digestion with aqua regia. The LA-ICP-MS allows the quantitative analysis of Pd, Pt, and Rh in road sediments at sub-microgram per gram levels with a relative standard deviation of 10% and with estimated detection limits in the lower nanogram per gram range. Good agreement between LA-ICP-MS and HR-ICP-MS analysis could be obtained for Pt and Rh whereas the determination of Pd remains subject to interferences.

In other study, a new on-line method developed for the determination of Pt, Rh, and Pd by ICP-QMS include separation of elements which might lead to spectral interference in the quadruple instrument [56]. The fused-silica capillaries generally used for transport of the sample to  $\mu$ -flow nebulisers have been chemically modified with ion-exchanger compounds to remove interfering elements such as Cu, Pb, or Hf. Characterization of the modification procedures by atomic-force microscopy showed that the quality of the quartz material and the kind of modification had a decisive influence on the yield of surface modification, and thus the exchange capacity of the capillaries.

Rauch et al. [57] show that scanning laser ablation-inductively coupled plasma mass spectrometry can identify and track individual particles released from automobile catalyts present in environmental particulates and sediments. Particles with high PGE concentrations were found in the exhaust of gaso-



line and diesel vehicles equipped with catalytic converters. The PGE–Ce association in individual particles provides a definitive fingerprinting for tracking catalyst particles in environmental compartments, while relative PGE signal intensity is an indication of the catalyst type. Scanning laser ablation-ICP-MS of road and aquatic sediments revealed a few PGE containing catalyst particles and it was possible to identify catalyst types for the origin of these particles.

Determinations of rhodium and other PGE and Au in seawater and saline liquids are difficult because of their low concentrations and the presence of large concentrations of salts. Concentrations of Au, Pt, Pd and Rh in Salton Sea geothermal brines were measured as part of a study of the solubilities and transport of these elements [58]. Samples were evaporated and the precious metals in the salts were concentrated by Pb–FA. Au concentrations ranged from 0.02 to 0.6 ng g<sup>-1</sup>. The largest Pd value was 0.02 ng g<sup>-1</sup>, while concentrations of Pt and Rh were 0.5 ng g<sup>-1</sup> or less.

Studies performed on platinum group elements in several environmental matrices have already highlighted their diffusion at a planetary level and their potential risk for human health. In order to evaluate their distribution in the environment and to understand their geochemical behaviour, it is important to study these elements also in non-conservative matrices, such as seawater. PGEs are present in seawater at very low levels (usually less than 1 pg g<sup>-1</sup>); only very sensitive instrumentation like ICP-SFMS, permits the determination of these elements in diluted seawater without any other manipulation of samples, reducing the risk of contamination associated with preconcentration techniques [59].

Rh, Pd and Pt concentrations in aerosol samples were monitored for 1 year in a high trafficked sampling site in Mestre (Venice) [60]. Samples were taken with a collector onto a mixed cellulose ester filter and analysed by ICP-SFMS. A desolvating system was used for sample introduction and the contribution of interfering species was determined.

Using ICP-MS and ICP-OES platinum group elements (Pt, Pd, Rh, Ru and Ir) and Ce, La, Nd, Pb and Zr have been determined in street dust, *Taraxacum officinale* (dandelion), *Plantago lanceolata* (plantain), *Lolium multiflorum* (annual ryegrass), *Rhytidiadelphus squarrosus* (moss) and *Vascellum pratense* (mushrooms) collected along highways and streets in Germany during 1999 [61]. Among the plants *Taraxacum officinale* (dandelion) reflects most adequately the pollution with the investigated elements matching the results from street dust. A strong positive correlation between all elements determined in the plants is established.

The interferences from Cd, Cu, Hf, Pb, Sr, Zn, Zr and Y on the inductively coupled plasma quadrupole mass spectrometry determination of Pt, Pd, Rh, Ru and Ir in geological and environmental samples (sediment, dust and plant sample) are evaluated using model solutions, real samples and comparison to ICP-OES results [62]. Pt, Rh, Ru and Ir can be determined usually after introduction of corrections for the interference in all investigated materials though in sediments the direct determination of Pt might be a problem depending on the actual Hf concentrations.

The results of the determination of physiological levels of precious metals in blood with a new type of magnetic sector field high resolution (HR)-ICP-MS instrument are presented [63]. HR-ICP-MS operating in the low resolution mode is advantageous for such ultra-trace analyses as it is about 100 times more sensitive than in the HR mode or conventional quadrupole (Q)-ICP-MS. It is also shown that the determination of Rh and Pd in the ng l<sup>-1</sup> range is impaired by spectral interferences originating from Cd<sup>+</sup>, Pb<sup>2+</sup>, SrO<sup>+</sup>, RbO<sup>+</sup>, CuAr<sup>+</sup> and ZnAr<sup>+</sup>. Using standard instrumental operating conditions on a Q-ICP-MS instrument, Pb<sup>2+</sup>:Pb<sup>+</sup> and SrO<sup>+</sup>:Sr<sup>+</sup> ratios were found to be about 0.1%, which results in a severe impairment of the determination of physiological Rh and Pd concentrations in body fluids. The resolution of the HR instrument used (m/Am = 7500) was not sufficient to separate Rh and Pd from all spectral overlaps. These remaining spectral interferences can only be overcome by an appropriate sample preparation step.

A method is described which is based on the use of a magnetic sector field ICP-MS for the determination of Pd, Pt and Rh at ng l<sup>-1</sup> levels in urine preliminarily digested by UV irradiation [64]. Several sample pre-treatment approaches were tested. The adverse effect of potentially interfering species on the mass-spectrometric determination of these metals was also taken into account. In particular, the role of other concomitants, such as Cd, Cu, Mo, Pb, Rb, Sr and Zn, was investigated in detail. A pilot investigation was performed to assess the exposure to these metals of 310 schoolchildren aged between 6 and 10 years from the urban and suburban area of Rome [65]. All determinations were performed by high-resolution magnetic sector inductively coupled plasma mass spectrometry after UV irradiation of the samples.

ICP-time of flight (TOF)-MS with ultrasonic nebulisation (USN) was combined on-line with a flow injection (FI) system for the determination of Pt, Rh and Pd in biological fluids (urine and blood serum) and road dust [66]. Simultaneous and selective preconcentration of the analytes was performed by sorption of their complexes formed on-line with diethylthiourea (DET) on the inner walls of a PTFE knotted reactor (KR), in a wide range of sample acidity (0.1–0.5 M HNO<sub>3</sub> for Pd and Rh and 0.05–0.2 M HNO<sub>3</sub> for Pt). A quantitative elution was achieved using 500 ml methanol acidified with 1% HNO<sub>3</sub>. Using a preconcentration time of 120 s and a sample flow rate of 5 ml min<sup>-1</sup>, enrichment factors of 55, 5 and 2 for Pd, Pt and Rh, respectively, were obtained in comparison with direct determination by ICP-MS without preconcentration. Special attention was paid to the study of the adverse effects of potentially interfering species present in the matrix (Cd, Cu, Pb, Sr, Fe, Y, Zn, Ni, Rb, Mn and Mo) on the preconcentration and the mass-spectrometric determination of the analytes. The accuracy of the method was demonstrated by the analysis of urine, blood serum and road dust certified reference materials. The method was applied to urine and serum samples of healthy subjects. The concentrations of Pt, Rh and Pd determined in these samples were comparable to reported values.

Specimens of samples from raptors are useful for the investigation of the impact of PGEs because these birds are found in both urban and rural environments and are invariably at the top

Table 3  
Determination of rhodium and other elements by ICP-MS

Elements	Sample matrix	Methods	Ref.
Pt, Ru, Os, Ir	Slurry made out of standard solutions, automobile catalyst	NiS fire assay; varying flux constituents; phase distribution study by electron microprobe	[72]
PGE, Au	Ore grade sample (SARM-7), komatiite (BF-4)	Effect of collector (NiS) mass and concentration of Ni, S, Cu and Zn in the sample on the recovery of precious metals	[73]
PGE, Au	Komatiite (WITS-1), SARM-7, sulphide concentrate (PTC-1)	NiS fire assay; low grade standard preparation using different techniques	[74]
PGE	Many CRMs comprising ultra basic rock, chromitite, Cu–Ni ore, etc.	NiS button dissolved in HCl/Te-coppt	[75,76]
Pt, Pd, Ru, Ir, Au	SARM-7, sulphide (SU-1a), NBM-6b	Aqua regia-microwave digestion	[77]
Pt, Pd, Ru, Ir, Au	Synthetic multi-element solutions, SARM-7, PTM-1, PTC-1	Different acid mixtures comprising HF, HNO <sub>3</sub> , HCl, HClO <sub>4</sub> followed by Dowex 1-X8 based anion exchange separation	[78]
Pt, Pd, Ir, Au	Geological and related materials	High pressure microwave digestion with HF and aqua regia; insoluble fused with Na <sub>2</sub> O <sub>2</sub> ; ion exchange separation of combined solutions	[79]
Pt, Pd, Ru, Ir, Au	Canadian certified reference materials	Peroxide fusion in zirconium crucibles and Se/Te as carriers	[80]
PGE, Au	Geological reference materials	UV laser ablation of the NiS button. Calibration using buttons prepared using doped quartz	[81]
Pt, V	Automotive catalytic converters	Spark ablation; milled sample mixed with graphite powder in pellet form is ablated at 30 A peak current with pre-burn time of 1 min, NIST SRM 2556 recycled pellet used as standard. DL was 1 µg g <sup>-1</sup> for Rh	[82]
Pt, Pd, Ti	Automotive catalytic converters	0.05–0.25 g of sample suspended in 1 ml of water treated with 4 ml of HNO <sub>3</sub> and 5 ml of HCl/HF (7:3); microwave digestion, followed by boric acid digestion	[83]
Pt, Pd, Ru, Ir, Au	Two Russian candidate reference materials	NiS fire assay preconcentration	[84]
PGE, Au	Geological reference materials	UV laser system coupled to high-resolution ICP-MS in NiS buttons prepared by the fire assay technique; Nd:YAG laser at 266 nm	[85]
Ir	Photographic emulsions	Samples where therefore first dissolved in concentrated ammonia solution and Rh was then directly measured by ICP-MS after dilution of the solution using an internal In standard for calibration; this procedure has the advantage of a simple sample preparation technique but introduces high amounts of Ag into the mass spectrometer and dilution of the sample restricts the DL; because of the similar chemical and physical behaviour of Ru and Rh, Ru was used as an internal standard during matrix separation and subsequent ICP-MS measurements of rhodium	[86]
Pt, Pd	Catalyst and car exhaust fumes	A new sampling procedure was developed in which whole raw exhaust fumes were taken for analysis and it was possible to distinguish between soluble and particulate PGE. Interference control and analytical methodology for ICP-MS determination were also studied	[87]
PGE, Au	Geological samples	Sample was decomposed with Na <sub>2</sub> O <sub>2</sub> in corundum crucible; after dissolving the fused disk with aqua regia and evaporating the solution to dryness for removing the SiO <sub>2</sub> , PGE were concentrated by Te coprecipitation	[88,89]
PGE, Au	Geological reference materials	NAA and UV laser ablation ICP-MS in NiS fire assay buttons: a comparison	[90]
Pt, Au	Iron-age pottery	By fire assay	[91]
Pt, Pd, Ru, Ir, Au	Geological samples	Double-focusing high resolution ICP-MS; sample fused by Na <sub>2</sub> O <sub>2</sub> ; enrichment by coprecipitation with Te	[92]
PGE, Au	Geochemical exploration	By NiS fire assay combined with isotope dilution of Os	[93]
PGE, Au	Geological materials	NiS fire assay and Te coprecipitation; the NiS dissolution step revisited	[94]
Pt, Pd	Airborne particulate matter; road dust	ICP-MS combined with ultrasonic nebulisation	[95]
Pt, Pd	Airborne particulate matter	By quadruple inductively coupled plasma mass spectrometry after mathematical correction of interferences	[96]
Pt, Pd	Road; urban river sediments	Ultrasonic nebulisation and high resolution ICP-MS; potential interferences were studied in low and high resolution modes	[97]
Pt	Airborne particulate matter; road dust	Study of distribution	[98]
Pt, Pd	Greenland snow	Inductively coupled plasma sector field mass spectrometry technique	[99]
Pt, Pd	Airborne; road dust	Te-coprecipitation after digestion with aqua regia–HF in a microwave oven	[100]
Pt, Pd	Size-classified urban aerosol	ICP-SFMS; microwave-assisted acid digestion	[101]
Pt, Pd, Au	Environmentally relevant samples	Measurement uncertainties resulting from sample preparation by either aqua regia leaching or NiS dokimasy	[102]
Pt, Pd	Auto-catalysts	Using a multi-collector ICP-MS; microwave digestion; comparison with conventional quadruple instrument	[103]
Pt, Pd	Geological samples	Comparison of silver and gold inquarting in the fire assay	[104]
Pt	Dust and plant samples	Microwave-assisted sample digestion; spectral interferences corrected using mathematical correction equations based on signal ratio measurement	[105]
Pt, Pd	Dust samples	Comparison of microwave-assisted digestion methods; selection of internal standards	[106]

Table 4  
Rhodium and other PGEs (platinum and palladium) in the environment: emission by automobile catalysts

Sample matrix	Remarks	Ref.
Soil	Varying parameters, such as pH, Cl <sup>-</sup> or S <sup>=</sup> concentration, the solubility was measured; comparison with different environmental materials; analytical techniques were GFAAS, XRF, ICP-MS, AV, XPS and SIMS	[107]
Soil	Typical distribution in roadside soil is compared to the distribution of Pb and Zn; effect of a barrier on airborne transport of aerosols is demonstrated as well as the influence of prevailing wind direction	[108]
Soil from the area Hanau (Germany)	The results confirm the existence of two different sources for anthropogenic PGE: automotive catalysts and PGE-processing plants	[109]
Two major U.K. roads	Temporal and spatial studies	[110]
Soils from Mexico city	Traffic-related PGE: concentrations in soils exposed to high traffic densities exceed the natural background values	[111]
Roadside soils from Sao Paulo, Brazil	Sampling made at four sites with varying traffic volumes and driving styles	[112]
Road dusts, roadside soils, Perth, Western Australia	Temporal variability of levels on a seasonal basis over a 12-month period	[113]
Infiltration basin and wetland sediments receiving urban runoff	Occurrence and spatial distribution	[114]
Airborne dust in the Frankfurt am Main area	Collected at three sites with different traffic densities	[115]
Road dust, tunnel dust, common grass, pine needles in Bialystok area, Poland	High resolution and quadruple ICP-MS: a pilot study	[116]
Whole raw exhaust fumes	A comparison of PGE emission between gasoline and diesel engine catalytic converters	[117]
Airborne particles and road dust sediments and bioaccumulation studies in aquatic organisms, plants and urine	The work is planned to ascertain the health and ecosystem risks of PGEs emitted through a series of interrelated objectives that address the pathway of these elements from the catalyst to the different environmental compartments	[118]
Soils and different types of plants	The transfer coefficient decreases from Pd > Pt greater than or equal to Rh	[119]
From urban particulates and sediments by the freshwater isopod <i>Asellus aquaticus</i>	In natural ecosystems and under laboratory conditions	[120]
Birds in Sweden	ICP-MS and laser ablation ICP-MS	[121]
Zebra mussel	Uptake and bioaccumulation	[122]

of the food chain [67,68]. Pt, Pd and Rh concentrations were determined by quadruple ICP-MS in eggs of the sparrow hawk (*Accipiter nisus*) and the peregrine falcon (*Falco peregrinus*), and in blood, liver and kidney of the peregrine falcon.

The applicability of size-exclusion chromatography (SEC) coupled on-line with a high resolution ICP-MS (HR-ICP-MS) to investigate the speciation of the platinum group elements, Rh, Pd and Pt, was evaluated [69]. Experiments were carried out to determine the efficiency of different hydrophilic and hydrophobic size-exclusion gel materials to select the optimal eluent in respect of resolution, recovery, reproducibility and limit of detection. The suitability of HR-ICP-MS as a reliable detection instrument at low pg ml<sup>-1</sup> levels was investigated by examining possible mass interferences with Rh, Pd and Pt. Laboratory experiments demonstrated the interaction and capability of forming complexes of humic substances with PGE, demonstrating the potential role of these ubiquitous natural substances in the mobilisation of PGE in the environment.

The use of internal standards combined with standard additions calibration for ICP-MS is discussed by Salin et al. [70]. Yttrium, rhodium, magnesium, cobalt, copper, nickel, silver, thallium, molybdenum and lead were analysed in solutions of known composition with a 500 mg ml<sup>-1</sup> Na matrix. Additionally, the Mg, Co, Y, Rh and Pb signals were used as internal standards for the other elements in the same matrix. Severe drift effects were simulated by drastically altering the liquid sample uptake rate. The signals were used to compare the results obtained using four different calibration methods: external stan-

dards, standard additions, internal standards and standard additions in combination with an internal standard. The average errors for external standards varied from 23 to 41% while the average errors for internal standards ranged from 1 to 71%. The error for standard additions was 45%. The use of standard additions with an internal standard produced an average error of 0.7–5%, suggesting that this is a powerful calibration technique.

The quantitative determination of platinum group metals from ore samples and industrial materials using inductively coupled plasma mass spectrometry (ICP-MS), inductively coupled plasma atomic emission spectrometry (ICP-OES), atomic absorption spectrometry (AAS) and X-ray fluorescence (XRF) techniques was conducted, and the performance of these techniques was compared [71]. The ICP-OES technique exhibited better accuracy than AAS but showed limitations in its application due to strong spectral interference in the presence of common matrix elements such as iron. The ICP-MS showed the lowest detection limit and less spectral interference than the previous two techniques. The XRF technique was also applied to examine the total amount of PGM from industrial materials.

Table 3 describes the details of other selected studies of rhodium and other metal ions. Also, the studies made to know the distribution of rhodium and other PGEs in the environment and its relation with the use of the auto-catalysts are very important. A summary of the carried out most significant investigations on this question, and that uses the technique of ICP-MS for the determination of these metals, takes shelter in Table 4.

#### 4. Conclusions

Rhodium and other PGEs (principally, platinum and palladium), mainly released by vehicle exhaust catalysts, have been significantly accumulated in environmental matrices over the past decades. Automobile catalyst emitted particles deposit on the roadside and can be transported to waterbodies through stormwater runoff.

Demands for trace level determination of PGEs for the purpose of exploration, biological evaluation and monitoring of environmental impact will stimulate the development of newer and more advanced analytical techniques. Extremely sensitive and selective methods are required for these determinations, particularly in complex environmental and geological matrices. Many research reports on determinations of rhodium (also Pt, Pd) have appeared recently.

ICP-OES has gained worldwide acceptance as a versatile analytical technique for many types of samples. The technique is characterized by low background emission hence superior detection limits, high temperature leading to few chemical interferences and wide linear response range. When all the PGEs are to be estimated NiS–FA and tellurium coprecipitation are employed. However, the limited use of ICP-OES in rhodium and other precious metal analysis, as evinced by the fewer publications, is mainly due to the large sample to volume ratio required.

The sensitivity and multi-element capability of ICP-MS has resulted in its adoption as an important instrumental technique. A limitation is the requirement of preparing sample solutions which are relatively free of elements whose polyatomic ions give rise to severe spectral interferences and which contain low concentrations of total dissolved solids.

SF-ICP-MS can alleviate some spectral interferences and reduce the necessity for prior chemical separations of analytes from complex matrices. Also, LA is an alternative means of sample introduction that does not involve preparations of sample solutions.

Many applications of ICP-MS to the determination of rhodium and other precious metals have been reported during the past 10 years. Lowering of cost and increased availability of instruments and never features such high resolution ICP-MS, time of flight mass spectrometry, laser ablation, etc., ensures ICP-MS of the leading role in the years ahead for PGEs analysis, including rhodium.

#### References

- [1] C. Bosch Ojeda, F. Sánchez Rojas, *Talanta* 67 (2005) 1.
- [2] C. Bosch Ojeda, F. Sánchez Rojas, *Talanta* 68 (2006) 1407.
- [3] R.K. Winge, V.A. Fassel, V.J. Peterson, M.A. Floyd, *Inductively Coupled Plasma Atomic Emission Spectroscopy. An Atlas of Spectral Information*, Elsevier, Amsterdam, 1993.
- [4] H. Watanabe, M. Aihara, M. Kiboku, *Bunseki Kagaku* 39 (1990) 61.
- [5] V.N. Mitkin, S.V. Zemskov, B.I. Zaksas, E.A. Petrova, A.N. Kurskii, *Zh. Anal. Khim.* 46 (1991) 2416.
- [6] M. Sun, J. Jain, M. Zhou, R. Kerrich, *Can. J. Appl. Spectrosc.* 38 (1993) 103.
- [7] S. Xie, M. Zhao, *Guijinshu* 13 (1992) 53.
- [8] X. Zhang, H. Li, Y. Yang, *Huaxue Fence* 29 (1993) 281.
- [9] S. Elinazarov, S. Rustamov, B.O. Khamidov, L.A. Egorova, V. Kompleksoobraz, *Rastvorakh, Tadzh. Gos. Un-t Dushanbe* (1991) 186.
- [10] X. Guang, F. Zhong, *ICP Inf. Newsl.* 23 (1998) 663.
- [11] M.L. Lee, E. Beinrohr, P. Tschöpel, G. Tölg, *Anal. Chim. Acta* 272 (1993) 193.
- [12] M. Etoh, H. Tokumori, *Bunseki Kagaku* 35 (1986) 39.
- [13] M. Etoh, *Bunseki Kagaku* 37 (1988) 11.
- [14] R. Gaita, S.J. Al-Bazi, *Talanta* 42 (1995) 249.
- [15] P. Hernández, *ICP Inf. Newsl.* 24 (1999) 671.
- [16] F.M. Pennebaker, M.B. Denton, *Appl. Spectrosc.* 55 (2001) 504.
- [17] R.K. Malhotra, K. Satyanarayana, G.V. Ramanaiah, *At. Spectrosc.* 20 (1999) 92.
- [18] H. Xu, J. Wang, G. Wang, M. Liu, B. Lu, Z. Lo, W. Feng, X. Chen, *Guangpuxue Yu Guangpu Fenxi* 19 (1999) 191.
- [19] Z. Fan, *Fenxi Huaxue* 30 (2002) 509.
- [20] Z. Fan, L. Du, X. Jin, *Guangpuxue Yu Guangpu Fenxi* 23 (2003) 365.
- [21] L. Li, J. Ma, L. Chen, *Gaodeng Xuexiao Huaxue Xuebao* 10 (1989) 531.
- [22] X. Chang, X. Luo, G. Zhan, Z. Su, *Talanta* 39 (1992) 937.
- [23] G. Xu, Z. Feng, *Guijinshu* 16 (1995) 51.
- [24] M. Etoh, H. Irokawa, *Bunseki Kagaku* 35 (1986) 849.
- [25] Y.S. Chung, R.M. Barnes, *J. Anal. At. Spectrom.* 3 (1988) 1079.
- [26] R. Vlasankova, V. Otruba, J. Bedl, M. Fiserá, V. Kanicky, *Talanta* 48 (1999) 839.
- [27] R. Komendova-Vlasankova, *Chemicke Listy* 95 (2001) 805.
- [28] Y. Duan, W. Li, Y. Xu, *Fénix Huaxue* 22 (1994) 366.
- [29] R.M. Barnes, A. Diallo, *Invited Lect. Int. Symp.* (1986) 3.
- [30] X. Zhang, H. Li, Y. Zhao, *Guijinshu* 18 (1997) 28.
- [31] A.R. Date, A.E. Davis, Y.Y. Cheung, *Analyst* 112 (1987) 1217.
- [32] S.E. Jackson, B.J. Fryer, W. Gosse, D.C. Healey, H.P. Longerich, D.F. Strong, *Chem. Geol.* 83 (1990) 119.
- [33] G.S. Reddi, C.R.M. Rao, T.A.S. Rao, S.V. Lakshmi, R.K. Prabhu, T.R. Mahalingam, *Fresenius J. Anal. Chem.* 348 (1994) 350.
- [34] R. Juvonen, E. Kallio, T. Lakomaa, *Analyst* 119 (1994) 617.
- [35] C.J.B. Gowing, P.J. Potts, *Analyst* 116 (1991) 773.
- [36] B.J. Perry, J.C. Van Loon, D.V. Speller, *J. Anal. At. Spectrom.* 7 (1992) 883.
- [37] B.J. Perry, D.V. Speller, R.R. Barefoot, J.C. Van Loon, *Can. J. Appl. Spectrosc.* 38 (1993) 131.
- [38] B.J. Perry, R.R. Barefoot, J.C. Van Loon, A.J. Naldrett, D.V. Speller, in: G. Holland, A.N. Eaton (Eds.), *Applications of Plasma Source Mass Spectrometry II*, The Royal Society of Chemistry, Cambridge, 1993, p. 91.
- [39] B.J. Perry, D.V. Speller, R.R. Barefoot, J.C. Van Loon, *Chem. Geol.* 124 (1995) 47.
- [40] M. Totland, I. Jarvis, K.E. Jarvis, *Chem. Geol.* 104 (1993) 175.
- [41] J. Godfrey, E.M. McCurdy, in: G. Holland, A.N. Eaton (Eds.), *Applications of Plasma Source Mass Spectrometry II*, The Royal Society of Chemistry, Cambridge, 1993, p. 64.
- [42] M. Totland, I. Jarvis, K.E. Jarvis, *Chem. Geol.* 124 (1995) 21.
- [43] I. Jarvis, M. Totland, K.E. Jarvis, *Chem. Geol.* 143 (1997) 27.
- [44] K.E. Jarvis, J.G. Williams, S.J. Parry, E. Bertalan, *Chem. Geol.* 124 (1995) 37.
- [45] E.S. Beary, P.J. Paulsen, *Anal. Chem.* 67 (1995) 3193.
- [46] C. Lüdke, E. Hoffmann, J. Skole, S. Artelt, *Fresenius J. Anal. Chem.* 355 (1996) 261.
- [47] J.P. Byrne, D.C. Grégoire, M.E. Benyounes, C.L. Chakrabarti, *Spectrochim. Acta Part B* 52 (1997) 1575.
- [48] R.L. Van Hoven, S.H. Nam, A. Montaser, M.W. Doughten, A.F. Dorzapf Jr., *Spectrochim. Acta Part B* 50B (1995) 549.
- [49] D.M. Wayne, *J. Anal. At. Spectrom.* 12 (1997) 1195.
- [50] T. Meisel, N. Fellner, J. Moser, *J. Anal. At. Spectrom.* 18 (2003) 720.
- [51] J. Schäfer, J.D. Eckhardt, Z.A. Berner, D. Stüben, *Environ. Sci. Technol.* 33 (1999) 3166.
- [52] C. Barbante, G. Cozzi, G. Capodaglio, K. Van de Velde, C. Ferrari, A. Veyssyere, C.F. Boutron, G. Scarponi, P. Cescon, *Anal. Chem.* 71 (1999) 4125.

- [53] K. Van de Velde, C. Barbante, G. Cozzi, I. Moret, T. Vellón, C. Ferrari, C. Boutron, *Atm. Environ.* 34 (2000) 3117.
- [54] G. Köllensperger, S. Hann, G. Stingeder, *J. Anal. At. Spectrom.* 15 (2000) 1553.
- [55] M. Motelica-Heino, S. Rauch, G.M. Morrison, O.F.X. Donard, *Anal. Chim. Acta* 436 (2001) 233.
- [56] H.G. Riepe, V. Loreti, R. García-Sánchez, C. Cámara, J. Bettmer, *Fresenius J. Anal. Chem.* 370 (2001) 488.
- [57] S. Rauch, G.M. Morrison, M. Moldovan, *Sci. Total Environ.* 286 (2002) 243.
- [58] M.A. McKibben, A.A. Williams, G.E.M. Hall, *Econ. Geol.* 85 (1990) 1926.
- [59] C. Turetta, G. Cozzi, A. Varga, C. Barbante, G. Capodaglio, P. Cescon, *J. Phys.* 107 (2003) 1321.
- [60] A. Varga, C. Barbante, G. Gozzi, I. Mantovan, G. Rampazzo, P. Cescon, *J. Phys.* 107 (2003) 1337.
- [61] R. Djingova, P. Kovacheva, G. Wagner, B. Markert, *Sci. Total Environ.* 308 (2003) 235.
- [62] R. Djingova, H. Heidenreich, P. Kovacheva, B. Markert, *Anal. Chim. Acta* 489 (2003) 245.
- [63] J. Begerow, L. Dunemann, *J. Anal. At. Spectrom.* 11 (1996) 303.
- [64] M. Krachler, A. Alimonti, F. Petrucci, K.J. Irgolic, F. Forastiere, S. Caroli, *Anal. Chim. Acta* 363 (1998) 1.
- [65] S. Caroli, A. Alimonti, F. Petrucci, B. Bocca, M. Krachler, F. Forastiere, M.T. Sacerdote, S. Mallote, *Spectrochim. Acta Part B* 56 (2001) 1241.
- [66] K. Benkhedda, B. Dimitrova, H.G. Infante, E. Ivanova, F.C. Adams, *J. Anal. At. Spectrom.* 18 (2003) 1019.
- [67] K.H. Jensen, S. Rauch, G.M. Morrison, P. Lindberg, *Arch. Environ. Contam. Toxicol.* 42 (2002) 338.
- [68] K.H. Ek, S. Rauch, G.M. Morrison, P. Lindberg, *Sci. Total Environ.* 334 (2004) 149.
- [69] C.M. Menzel, Z. Berner, D. Stuben, *Geostand. Newsl.* 25 (2001) 239.
- [70] E.D. Salin, M. Antler, G. Bort, *J. Anal. At. Spectrom.* 19 (2004) 1498.
- [71] H. Yoon, C. Yoon, C.S. Park, T. Ko, N.S. Kim, K.N. Han, *Miner. Metall. Process.* 22 (2005) 59.
- [72] H. Urban, F. Zereini, B. Skerstupp, M. Tarkian, *Fresenius J. Anal. Chem.* 352 (1995) 537.
- [73] A. Frimpong, B.J. Fryer, H.P. Longerich, Z. Chen, S.E. Jackson, *Analyst* 120 (1995) 1675.
- [74] M. Tredoux, I. McDonald, *Geostand. Newsl.* 20 (1996) 267.
- [75] Y. Sun, X. Guan, A. Du, *ICP Inf. Newsl.* 24 (1998) 114.
- [76] Y. Sun, X. Guan, A. Du, *Spectrochim. Acta Part B* 53 (1998) 1463.
- [77] P. Nowinski, V. Hodge, *At. Spectrosc.* 15 (1994) 109.
- [78] I. Jarvis, M. Totland, K.E. Jarvis, *Analyst* 122 (1997) 19.
- [79] A.G. Coedo, M.T. Dorado, D.I. Padilla, F.J. Alguacil, *Anal. Chim. Acta* 340 (1997) 31.
- [80] J. Amosse, *Geostand. Newsl.* 22 (1998) 93.
- [81] A.P.S. Jorge, J. Enzweiler, E.K. Shibuya, J.E.S. Sarkis, A.M.G. Figueiredo, *Geostand. Newsl.* 22 (1998) 47.
- [82] O.V. Borisov, D.M. Coleman, R.O. Carter, *J. Anal. At. Spectrom.* 12 (1997) 231.
- [83] O.V. Borisov, D.M. Coleman, K.A. Oudsema, R.O. Carter, *J. Anal. At. Spectrom.* 12 (1997) 239.
- [84] C. Li, C. Chai, X. Li, X. Mao, *Geostand. Newsl.* 22 (1998) 195.
- [85] E.K. Shibuya, J.E.S. Sarkis, J. Enzweiler, A.P.S. Jorge, A.M.G. Figueiredo, *J. Anal. At. Spectrom.* 13 (1998) 941.
- [86] P. Krystek, K.G. Heumann, *J. Anal. At. Spectrom.* 14 (1999) 1443.
- [87] M. Moldovan, M.M. Gómez, M.A. Palacios, *J. Anal. At. Spectrom.* 14 (1999) 1163.
- [88] L. Qi, J. Hu, *Yankuang Ceshi* 18 (1999) 267.
- [89] X. Jin, H. Zhu, *J. Anal. At. Spectrom.* 15 (2000) 747.
- [90] A.M.G. Figueiredo, J. Enzweiler, J.E.S. Sarkis, A.P.S. Jorge, E.K. Shibuya, *J. Radioanal. Nuc. Chem.* 244 (2000) 623.
- [91] A.E. Pillay, C. Punyadeera, *J. Trace, Microprobe Tech.* 19 (2001) 243.
- [92] X. Jin, H. Zhu, *Fenxi Huaxue* 29 (2001) 653.
- [93] H. He, C. Lu, Z. Zhou, S. Shi, B. Li, *Yankuang Ceshi* 20 (2001) 191.
- [94] M. Gros, J.P. Lorand, A. Luguët, *Chem. Geol.* 185 (2002) 179.
- [95] F. Petrucci, B. Bocca, A. Alimonti, S. Caroli, *J. Anal. At. Spectrom.* 15 (2000) 525.
- [96] M.B. Gómez, M.M. Gómez, M.A. Palacios, *Anal. Chim. Acta* 404 (2000) 285.
- [97] S. Rauch, M. Motelica-Heino, G.M. Morrison, O.F.X. Donard, *J. Anal. At. Spectrom.* 15 (2000) 329.
- [98] B. Gómez, M. Gómez, J.L. Sánchez, R. Fernández, M.A. Palacios, *Sci. Total Environ.* 269 (2001) 131.
- [99] C. Barbante, A. Veysseyre, C. Ferrari, K. Van de Velde, C. Morel, G. Capodaglio, P. Cescon, G. Scarponi, C. Boutron, *Environ. Sci. Technol.* 35 (2001) 835.
- [100] M.B. Gómez, M.M. Gómez, M.A. Palacios, *J. Anal. At. Spectrom.* 18 (2003) 80.
- [101] K. Kanitsar, G. Koellensperger, S. Hann, A. Limbeck, H. Puxbaum, G. Stingeder, *J. Anal. At. Spectrom.* 18 (2003) 239.
- [102] F. Zereini, F. Alt (Eds.), *Anthropog. Platinum-group Element Emission*, Springer-Verlag, Berlin, 2000.
- [103] L.A. Simpson, R. Hearn, T. Catterick, *J. Anal. At. Spectrom.* 19 (2004) 1244.
- [104] M. Suominen, E. Kontas, H. Niskavaara, *Geostand. Geoanal. Res.* 28 (2004) 131.
- [105] M. Niemela, P. Peramaki, J. Piispanen, J. Poikolainen, *Anal. Chim. Acta* 521 (2004) 137.
- [106] M. Niemela, H. Kola, P. Peramaki, J. Piispanen, J. Poikolainen, *Microchim. Acta* 150 (2005) 211.
- [107] F. Zereini, B. Skerstupp, F. Alt, E. Helmers, H. Urban, *Sci. Total Environ.* 206 (1997) 137.
- [108] J. Schafer, H. Puchelt, *J. Geochem. Explor.* 64 (1998) 307.
- [109] F. Zereini, F. Dirksen, B. Skerstupp, H. Urban, *Environ. Sci. Pollut. Res.* 5 (1998) 223.
- [110] K.E. Jarvis, S.J. Parry, J.M. Piper, *Environ. Sci. Technol.* 35 (2001) 1031.
- [111] O. Morton, H. Puchelt, E. Hernandez, E. Lounejeva, *J. Geochem. Explor.* 72 (2001) 223.
- [112] C.P.R. Morcelli, A.M.G. Figueiredo, J.E.S. Sarkis, J. Enzweiler, M. Kakazu, J.B. Sigolo, *Sci. Total Environ.* 345 (2005) 81.
- [113] J.D. Whiteley, *Water Air Soil Pollut.* 160 (2005) 77.
- [114] J.D. Whiteley, F. Murray, *Sci. Total Environ.* 341 (2005) 199.
- [115] F. Zereini, F. Alt, J. Messerschmidt, C. Wiseman, I. Feldmann, A. Von Bohlen, J. Muller, K. Liebl, W. Puttmann, *Environ. Sci. Technol.* 39 (2005) 2983.
- [116] B.A. Lesniewska, B. Godawska-Zylkiewicz, B. Bocca, S. Caimi, S. Caroli, A. Hulanicki, *Sci. Total Environ.* 321 (2004) 93.
- [117] M. Moldovan, M.A. Palacios, M.M. Gomez, G. Morrison, S. Rauch, C. McLeod, R. Ma, S. Caroli, A. Alimonti, F. Petrucci, B. Bocca, P. Schramel, M. Zischka, C. Pettersson, U. Wass, M. Luna, J.C. Saenz, J. Santamaria, *Sci. Total Environ.* 296 (2002) 199.
- [118] M.A. Palacios, M. Gomez, M. Moldovan, B. Gomez, *Microchem. J.* 67 (2000) 105.
- [119] J. Schafer, D. Hannker, J.D. Eckhardt, D. Stuben, *Sci. Total Environ.* 215 (1998) 59.
- [120] M. Moldovan, S. Rauch, M. Gomez, M.A. Palacios, G.M. Morrison, *Water Res.* 35 (2001) 4175.
- [121] K.H. Ek, G.M. Morrison, P. Lindberg, S. Rauch, *Arch. Environ. Contam. Toxicol.* 47 (2004) 259.
- [122] S. Zimmermann, J. Messerschmidt, A. Von Bohlen, B. Sures, *Environ. Res.* 98 (2005) 203.



## Determination of nitrate in mineral water and sausage samples by using a renewable in situ copper modified electrode

Thiago R.L.C. Paixão<sup>a</sup>, Juliana L. Cardoso<sup>b</sup>, Mauro Bertotti<sup>a,\*</sup>

<sup>a</sup> Instituto de Química, Universidade de São Paulo, São Paulo 05508-900, SP, Brazil

<sup>b</sup> Escola Politécnica, Universidade de São Paulo, São Paulo, SP, Brazil

Received 23 January 2006; received in revised form 21 March 2006; accepted 22 March 2006

Available online 9 May 2006

### Abstract

A new approach for in situ electrodeposition of a renewable copper layer onto a copper electrode is reported. The active surface was obtained by anodic dissolution of a copper electrode at an appropriate potential and further redeposition of copper ions still remaining at the diffusion layer. Under optimal experimental conditions the peak current response increases linearly with nitrate concentration over a range of 0.1–2.5 mmol L<sup>-1</sup>. The repeatability of measurements for nitrate was evaluated as 1.8% ( $N = 15$ ) and the limit of detection of the method was found to be 11 μmol L<sup>-1</sup> ( $S/N = 3$ ). Nitrate contents in two different samples (mineral water and sausages) compared well with those obtained from using the standard Griess protocol at a 95% of confidence level measured by the *t*-student test. The interference from chloride on the nitrate analysis and the possibility of simultaneous determination of nitrite were also examined.

© 2006 Elsevier B.V. All rights reserved.

**Keywords:** Nitrate; Freshly copper layer; Mineral water and sausage

### 1. Introduction

Nitrates have a large distribution on the nature. In food, nitrates are used for conservation of meat and in the agriculture its use as a fertilizer is widespread. However, there are concerns on contamination of water supplies [1] and a correlation between cancer in stomach and nitrate levels in potable water in UK has been suggested [2]. Similar studies were carried out in Italy [3] and authors have also found a strong correlation between high cancer levels and nitrate concentration above 4.5 mg L<sup>-1</sup>. Toxicological problems associated with nitrates and nitrites are related to the formation of endogenously *N*-nitros compounds (nitrosamines and nitrosamides), the carcinogenic activity of these species being well-known [3]. Hence, measurements of nitrate levels in potable water and other products that have a high consumption by humans, like conserving food, are increasingly relevant.

A review in literature [4] shows a large number of methods for the quantification of nitrate and most of them are based on

techniques such as spectrophotometry, electrochemistry or chromatography (liquid chromatography or capillary electrophoresis). It should be pointed out, additionally, that the majority of the procedures depend on a previous step involving the stoichiometric conversion of nitrate to nitrite by using convenient chemical reductors such as Cu/Cd.

The large number of studies in the electroanalytical field on the determination of nitrate can be classified in two main groups, voltammetric/ampereometric or potentiometric methods. The latter one involves the use of ion-selective electrodes, which are based on the selective passage of the analyte from the solution to another phase, the potential gradient being proportional to the concentration. Accordingly, the use of ion-selective electrodes is widespread for the analysis of nitrate [5–10] and several other anions [11–15]. On the other hand, voltammetric/ampereometric techniques depend on the electrochemical reduction of nitrate at electroodic surfaces and different materials have been used such as copper [16–23], cadmium [17,24,25], lead [26,27], silver [22,28] and boron-doped diamond [29–31]. However, the use of bare unmodified electrodes for the direct determination of nitrate is difficult owing to the slow kinetics of the charge transfer [32], methods based on the direct reduction of nitrate being characterised by low sensitivity and irreproducibility and asso-

\* Corresponding author. Tel.: +55 11 3091 3837; fax: +55 11 3815 5579.  
E-mail address: [mbertott@iq.usp.br](mailto:mbertott@iq.usp.br) (M. Bertotti).

ciated with surface passivation effects. Nevertheless, procedures to increase the sensitivity in direct electroanalytical determinations of nitrate are generally associated with activation of the electroodic surface, especially when copper cathodes are used. Accordingly, two different approaches are currently used: (1) Deposition of a fresh electroodic layer prior to each analysis by introduction of a copper salt into the sample medium. The measurement is performed by sweeping the potential to the negative direction after copper is electrolytically plated onto the electrode surface [33]. (2) Ex situ conditioning of the electrode surface by using a plating solution of defined composition and further transfer of the sensor to the sample solution [34]. This second approach avoids sample contamination, whereas the catalytic property of the freshly deposited layer is lost after a few analysis and the surface needs to be regenerated regularly [34]. Recently, a procedure for the electrode cleaning and activation by application of a 20 kHz ultrasound has been proposed, the use of copper electrodes for nitrate measurements being extended to complex matrices [35].

The aim of the present work is to show a new approach for the electroanalytical determination of nitrate at copper cathodes. The novelty of the proposed methodology is related to the continuous renovation of the electroodic surface by using a pre-treatment potential program that allows each determination to be performed at a new fresh and reproducible copper surface. This is accomplished by electrochemical dissolution and immediate cathodic reduction of copper ions present at the diffusion layer. The analytical applicability of the approach was examined by measuring the nitrate content in mineral water and sausage samples and the results show that this approach is very promising.

## 2. Experimental section

### 2.1. Chemicals and electrodes

All solid reagents were of analytical grade and were used without further purification. Solutions were prepared by dissolving the reagents in deionised water processed through a water purification system (Nanopure Infinity, Barnstead).  $\text{H}_2\text{SO}_4$ ,  $\text{Na}_2\text{SO}_4$  and  $\text{KNO}_3$  were obtained from Merck (Darmstadt, Germany). The supporting electrolyte for the differential pulse voltammetric experiments was a  $0.1 \text{ mol L}^{-1}$   $\text{Na}_2\text{SO}_4$  solution, pH 2.0 (adjusted with  $\text{H}_2\text{SO}_4$ ). Solutions were deoxygenated with argon for 5 min prior each experiment. The copper wire (purity 99.7% by atomic absorption spectrometry analysis) had a diameter of 3 mm and was embedded in a Teflon rod to fabricate the working electrode. Copper commercial wires (São Marco Indústria e Comércio LTDA) with nominal radius of  $60 \mu\text{m}$  were used to fabricate copper disc microelectrodes. The performance of the set of microelectrodes was evaluated by recording voltammetric curves in a standardized solution of  $[\text{Ru}(\text{NH}_3)_6]\text{Cl}_3$  obtained from Alfa Aesar (Ward Hill, Massachusetts). Then, limiting currents measured in voltammograms recorded at slow scan rates were compared with those calculated by using the equation that relates the steady-state current with the experimental parameters ( $I_L = 4nFDCr$ , where  $I_L$ ,  $n$ ,  $F$ ,  $D$ ,  $C$  and  $r$  are,

respectively, the steady-state current (A), number of electrons, Faraday constant ( $\text{C mol}^{-1}$ ), diffusion coefficient of the electroactive species ( $\text{cm}^2 \text{ s}^{-1}$ ), concentration of the electroactive species ( $\text{mol cm}^{-3}$ ) and radius of the electrode (cm)) [36].

All electroodic surfaces were polished with emery paper and alumina ( $1 \mu\text{m}$ ). Cleaning of the electrodes was accomplished rinsing thoroughly the surface with a direct stream of water. Then, the electrodes were rinsed with a (1:1) mixture of water and concentrated  $\text{HNO}_3$  to remove any oxide layer and rinsed again with copious amounts of deionised water. This procedure [37] was adopted every day to remove any oxide occasionally formed due to exposition of the electrode to atmospheric oxygen. A potential pulse sequence step was employed to obtain a renewable copper surface and to assure the repeatability of measurements. Accordingly, the copper electrode was polarized at 0.50 V for 10 s (copper dissolution) and then at  $-0.25 \text{ V}$  for 15 s (copper redeposition) before each voltammetric experiment.

### 2.2. Instrumentation

An Autolab PGSTAT 30 (Eco Chemie) bipotentiostat with data acquisition software made available by the manufacturer (GPES 4.8 version) was used for electrochemical measurements. Experiments were done in a conventional electrochemical cell, a Ag/AgCl (saturated KCl) electrode and a platinum wire being used as reference and counter electrodes, respectively.

Micrographs for morphological examination of the copper surfaces were obtained with a Cambridge microscope (Stereoscan 440). Experiments were carried out by using  $1 \text{ cm}^2$  copper sheets (Pertech<sup>®</sup> of Brazil) fabricated by copper electroplating in a substrate composed of paper and phenolic resin. Copper surfaces were conveniently pre-treated and stored in plastic bottles purged with argon to prevent the oxidation of copper from air oxygen prior to microscopic analysis.

### 2.3. Sample preparation

The extraction of nitrate from sausages (weight of sample taken = 83.4 g) was accomplished by leaving a certain amount of crushed samples in deionised water at  $70^\circ\text{C}$  under stirring for 10 min and further filtering of the remaining liquid [38]. No preparation was required for mineral water samples.

### 2.4. Spectrophotometric analysis

Results on the nitrate content in the analysed samples were compared with those obtained from quantitative reduction of nitrate to nitrite using a copperized cadmium reactor column and further determination of nitrite by the Griess protocol [34,39]. Griess reagent was prepared by mixing equal volumes of solutions of  $\alpha$ -naphthylamine (0.1 g dissolved in 100 mL of deionised water) and sulphanilamide (1 g of the reactant, 5.9 mL of concentrated phosphoric acid solution and dilution to 100 mL with deionised water). Absorbance measurements were performed at 534 nm in a CIBA-Corning 2800 Spectroscan using a 1.00 cm optical pathlength quartz cuvette.

### 3. Results and discussion

Even though a definitive explanation is not found in literature, a sensitivity enhancement in electroanalytical determinations of nitrate has been achieved by carrying out measurements with large and activated surface area copper cathodes [33–35]. These recent findings reinforce the proposed mechanism related to adsorption of both nitrate and hydrogen atoms produced by cathodic reduction of protons [40]. According to this mechanism, the transfer of an O-atom from nitrate to adsorbed hydrogen leads to the formation of water and nitrite. This latter species is then further reduced to other nitrogen compounds, the nature of them depending on the experimental conditions. Hence, electrocatalytic materials with high area surfaces and that facilitate the proton discharge and adsorption of hydrogen are candidates to be used as sensitive and reproducible sensors for nitrate determination. Indeed, a large decrease in activation energy for the nitrate electroreduction has been observed at rhodium surfaces activated by potential cycles in KCl alkaline electrolyte [41], morphological changes in the electrode surface being characterised by the existence of porous structures.

Our previous experience with copper electrodes for amperometric monitoring of the concentration of some organic molecules in various matrices [42–45] directed our efforts to investigate alternatives to activate the electrode surface. This was accomplished by using a procedure involving the anodic dissolution of copper followed by a subsequent cathodic reduction of copper ions present at the diffusion layer (i.e. still in the vicinity of the electrode surface). As mass transport to and from microelectrodes occurs at very high rates owing to radial diffusion, comparative experiments were performed with a conventional sized copper electrode ( $r = 1.5$  mm) and a copper microelectrode ( $r = 60$   $\mu\text{m}$ ). By analysing voltammograms shown in Fig. 1 it is possible to evaluate the effectiveness of the proposed method towards the cathodic reduction of nitrate. At no pre-treated surfaces no clear response related to a faradaic process involving the reduction of nitrate is seen for both copper electrodes (dashed lines in Fig. 1). On the other hand, a sharp peak is observed when the voltammogram was recorded after the proposed electrocatalytic pre-treatment (solid line, Fig. 1(B)). The small cathodic peak appearing at around  $-0.2$  V when a copper microelectrode is used (solid line, Fig. 1(A)) is an indication that copper ions

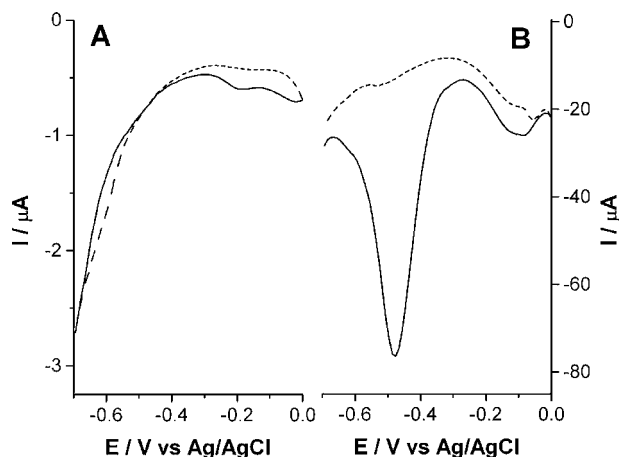
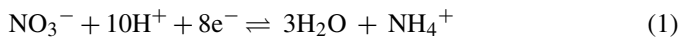


Fig. 1. Differential pulse voltammograms recorded in a  $0.1 \text{ mol L}^{-1} \text{ Na}_2\text{SO}_4 + 0.5 \text{ mmol L}^{-1} \text{ NO}_3^-$  solution (pH 2.0) using a copper microelectrode (A) and a copper electrode ( $d = 3$  mm) (B). Curves (---) and (—) represent experiments carried out with bare and modified copper electrodes, respectively. Scan rate:  $0.1 \text{ V s}^{-1}$  and potential amplitude:  $0.05 \text{ V}$ .

were not redeposited at the electrocatalytic surface after the anodic dissolution, hence a fresh copper layer is not available to facilitate the nitrate reduction process.

At sufficient acidic conditions nitrate is believed to be reduced to ammonium ions according to the following equation:



As shows Eq. (1), an acidic medium is required for the cathodic process. However, at very low pH values the onset of hydrogen evolution may interfere with the nitrate electroreduction as both processes occur at similar potentials. Carpenter and Pletcher [21] investigated the reduction of nitrate at copper cathodes in sulphuric medium by voltammetry with a rotating disc electrode and these authors indicated that the analytical applicability of copper electrodes for nitrate monitoring is possible at a very narrow pH range. At these optimal pH conditions, the electrocatalytic process is controlled by nitrate diffusion rather than by transport of protons and there is still a good potential separation between both reduction processes (nitrate and  $\text{H}^+$ ).

The morphology of the freshly copper layer prepared by the proposed procedure was examined by SEM and a porous mesh-like structure was observed, as shows Fig. 2(B). The different

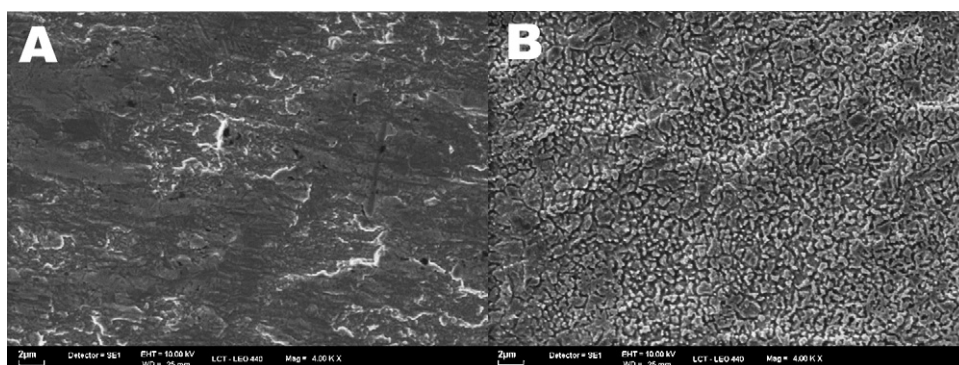


Fig. 2. SEM micrograph of two different layers of copper: bare copper electrode (A) and freshly copper layer (B).

aspect of this surface when compared with the polished copper substrate, Fig. 2(A), is clearly demonstrated and confirms the effectiveness of the copper dissolution/redeposition steps to promote the modification of the copper surface and to produce a freshly copper layer with an active role concerning the cathodic reduction process of nitrate [21,34].

The optimization of the parameters involving the pre-treatment potential program (dissolution and deposition processes) was further investigated as an attempt of enhancing the sensitivity of nitrate determinations. Fig. 3, curve (A), shows that no faradaic signal is obtained when copper dissolution is not promoted (i.e. bare copper electrode), a different situation being observed as the amount of copper ions generated during the anodic process increases. As expected, the nitrate reduction occurs at a higher extent as the deposition time following the anodic dissolution increases (Fig. 3, curve (B)). Optimal conditions were achieved by using 10 and 15 s, respectively, for the dissolution and redeposition steps, and this procedure was employed for the preparation of the copper electrode for analytical determinations.

The influence of the acidity of the supporting electrolyte on the current response was investigated to evaluate the best performance of the sensor. Taking into account the previous comments on the compromise between hydrogen evolution and the high proton consumption to nitrate electroreduction, experiments were performed at pH 2.0. Fig. 4 shows a calibration plot for consecutive additions of aliquots of a  $\text{NO}_3^-$  solution in supporting electrolyte ( $\text{Na}_2\text{SO}_4$  solution, pH 2.0). The plot of peak current values measured in the voltammograms as a function of nitrate concentration in the range of 0.1–2.5  $\text{mmol L}^{-1}$  yielded straight lines ( $-I_p (\mu\text{A}) = -1.9 + 143.5 [\text{NO}_3^- (\text{mmol L}^{-1})]$ ,  $R^2 = 0.99994$ ). The detection and quantification limits were estimated to be 11.6 (S/N = 3) and 38.7 (S/N = 10)  $\mu\text{mol L}^{-1}$ .

A previous work [35] investigated the influence of ultrasound on the structure of the copper deposit and the response to nitrate.

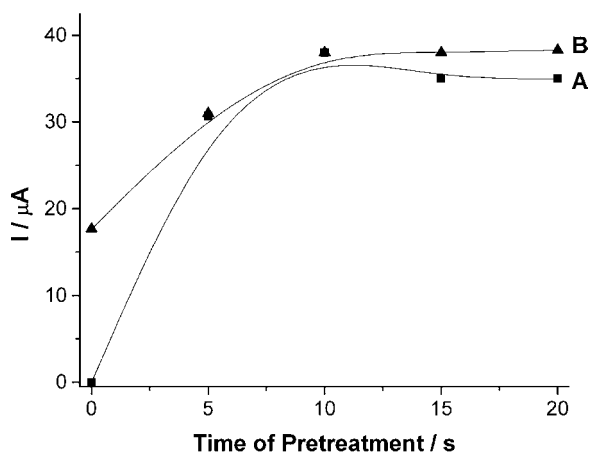


Fig. 3. Dependence of cathodic peak current values measured in differential pulse voltammograms recorded in a  $0.1 \text{ mol L}^{-1} \text{ Na}_2\text{SO}_4 + 0.5 \text{ mmol L}^{-1} \text{ NO}_3^-$  solution (pH 2.0) using a copper electrode ( $d = 3 \text{ mm}$ ) on the dissolution (A) and redeposition (B) time. The redeposition time was 15 s for experiments represented by curve (A) and the dissolution time was 10 s for experiments represented by curve (B). Scan rate:  $0.1 \text{ V s}^{-1}$  and amplitude potential: 0.05 V.

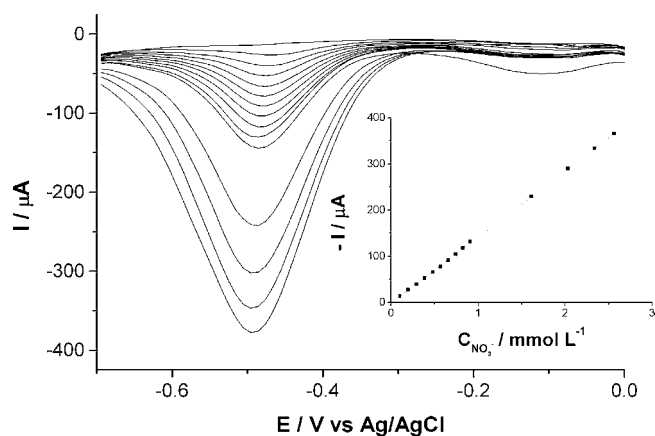


Fig. 4. Differential pulse voltammograms recorded in a  $0.1 \text{ mol L}^{-1} \text{ Na}_2\text{SO}_4$  solution (pH 2.0) before and after addition of nitrate to give final solution concentrations in the range  $0.1\text{--}2.5 \text{ mmol L}^{-1}$ . Scan rate:  $0.1 \text{ V s}^{-1}$  and amplitude potential: 0.05 V. The inset shows the calibration plot.

AFM images and voltammograms obtained demonstrated a significant loss of the deposited layer after the insonation period, indicating the mechanical fragility of the upper porous structure. This observation associated with our interest to use the modified copper electrode as a sensor for continuous monitoring of nitrate concentration directed our attention to evaluate the repeatability of determinations. Fig. 5 shows results of measurements performed in a  $0.5 \text{ mmol L}^{-1}$  nitrate solution by using two different protocols. In the first one (curve (A)), the proposed electrode pre-treatment was employed before each measurement and the continuous renovation of the electrode surface ensures a reproducible response, attested by the very low standard deviation (S.D. = 1.8%,  $N = 15$ ). On the other hand, determinations carried out with no periodic renewal of the electrodic surface (curve (B)) yielded a poor reproducibility, the continuous current decrease being likely originated by a passivation process.

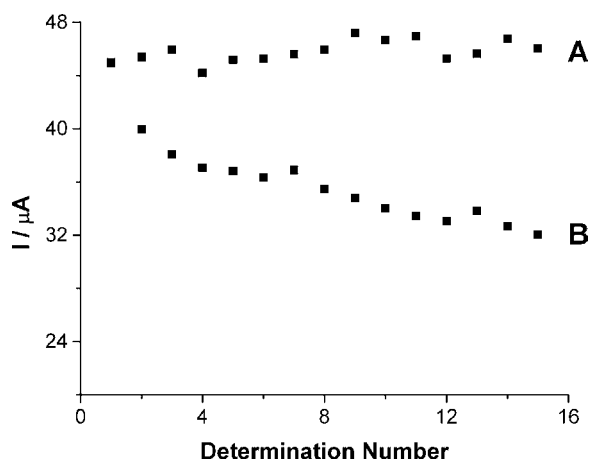


Fig. 5. Cathodic peak current values obtained from differential pulse voltammograms recorded in a  $0.1 \text{ mol L}^{-1} \text{ Na}_2\text{SO}_4 + 0.5 \text{ mmol L}^{-1} \text{ NO}_3^-$  solution (pH 2.0) using a copper electrode ( $d = 3 \text{ mm}$ ). Data shown in (A) were obtained by pre-treating the copper surface before each experiment and in (B) only in the beginning of the set. Scan rate:  $0.1 \text{ V s}^{-1}$  and amplitude potential: 0.05 V.



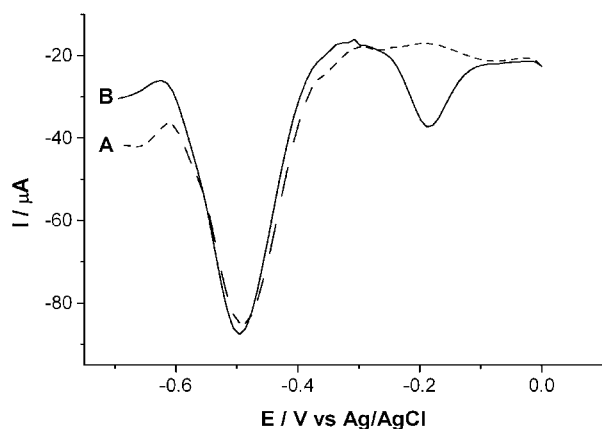


Fig. 6. Differential pulse voltammograms recorded in  $0.1 \text{ mol L}^{-1} \text{ Na}_2\text{SO}_4 + 0.5 \text{ mmol L}^{-1} \text{ NO}_3^-$  solution (pH 2.0) before (A) and after (B) addition of  $\text{NO}_2^-$  ( $0.5 \text{ mmol L}^{-1}$ ). Scan rate:  $0.1 \text{ V s}^{-1}$  and amplitude potential:  $0.05 \text{ V}$ .

The reduction of nitrite was also investigated at the modified copper surface in order to evaluate the possibility of simultaneous detection of nitrate and nitrite. Accordingly, Fig. 6 shows voltammetric curves recorded with the pre-treated copper electrode in solutions containing nitrate in the presence and absence of nitrite. The peak appearing at around  $-0.2 \text{ V}$  corresponds to the cathodic reduction of nitrite and it does not interfere in the nitrate peak at the established experimental conditions. The good resolution between both cathodic peaks makes it possible further studies involving speciation between nitrate and nitrite at some particular samples where the concentration of both ions is not very different (for instance, in saliva samples) [46].

Previous works in literature have commented on the influence of chloride on both the copper deposition step and the nitrate electroreduction [18,21,34]. The stabilization of Cu(I) species by chloride shifts the potential of the copper deposition towards more negative potentials and the electrode process occurs in two steps. On the other hand, the change in the electrochemistry of nitrate at copper surfaces in solutions not containing copper ions upon addition of halides can be explained by the competitive and inhibiting effect of co-adsorption [47]. For instance, Pletcher and Poorabedi [18] have demonstrated that the influence of halides on the electroreduction of nitrate at copper cathodes increases in the sequence iodide, bromide, chloride and fluoride, a possible explanation involving adsorption of the anionic species onto the electrodic surface [40]. In terms of sensitivity, it has been shown that at relatively low concentrations of chloride (at least  $1.2 \text{ mmol L}^{-1}$ ) the influence of the anion is not significant [34]. Similar conclusions on the potential shift (measured as  $100 \text{ mV}$  to the negative direction by changing the chloride concentration from  $0.1$  to  $1 \text{ mmol L}^{-1}$ ) and the response for nitrate were observed in this work in experiments carried out with the copper modified electrode in solutions containing different concentrations of chloride. Hence, the presence of chloride up to  $10 \text{ mmol L}^{-1}$  did not cause any change in the nitrate peak height and no subsequent investigations on this subject were done. As a matter of fact, it should be pointed out that there was no need to

Table 1  
Content of nitrate in real samples

Sample	Proposed method	Griess method
Mineral water ( $\text{mg L}^{-1}$ )	$14.7 \pm 0.3$	$14.3 \pm 0.6$
Sausage ( $\text{mg kg}^{-1}$ )	$26.4 \pm 0.5$	$25 \pm 1$

add deliberately chloride to the working solutions as the amount diffusing from the reference electrode was proved to be enough to give a reproducible signal.

The dynamic concentration range was sufficiently wide to be applicable to the analysis of the majority of samples containing nitrate. In order to confirm the reliability of the proposed voltammetric method, the nitrate content in two different samples was also determined by using an official method. The results are given in Table 1 and the standard addition method was used in determinations performed with the proposed electroanalytical procedure. The correlation between both methodologies was found to be  $0.9998$  and the good agreement at the  $95\%$  confidence level measured by the  $t$ -student test is an indication that the results are statistically comparable, confirming the absence of interfering species in the analysed samples. By analysing the potential peak in the voltammetric determinations it was noticed that both samples did not possess chloride at relatively high levels. For instance, the chloride content in the mineral water sample was  $1.02 \text{ mg mL}^{-1}$ . On the other hand, for samples containing significantly high chloride levels (i.e. sea water samples) the potential shift may be sufficiently high and signals for nitrate and hydrogen reduction may overlap. The use of the proposed electrochemical sensor at these experimental conditions requires a previous removal of chloride, some possible alternatives being reported in literature [48–51]. The influence of active-surface compounds in samples such as saliva may be alleviated by convenient dilution or by using ultrasound, as proposed by Compton and co-workers [35] for nitrate measurements in complex matrices.

#### 4. Conclusion

The reduction of nitrate at copper cathodes in acidic medium is facilitated at surfaces activated by deposition of fresh layers of metallic copper. Two typical procedures described in literature are based on in situ or ex situ deposition steps, both of them having drawbacks as the need to add copper ions to the solution and the loss of signal due to passivation of the generated surface, respectively. Taking these aspects into account, the proposed approach possesses two main advantages as the electrode substrate is very cheap (copper) and a plating solution is not required for the deposition of the catalytic layer.

#### Acknowledgements

Authors are thankful to FAPESP (Fundação de Amparo à Pesquisa do Estado de São Paulo) and CNPq (Conselho Nacional de Desenvolvimento Científico e Tecnológico) for the financial support.



**References**

- [1] D. Forman, *Cancer Surv.* 8 (1989) 443.
- [2] C.S. Bruning-Fann, J.B. Kaneene, *Vet. Hum. Toxicol.* 35 (1993) 521.
- [3] S.A. Kyrtopoulos, *Cancer Surv.* 8 (1989) 423.
- [4] M.J. Moorcroft, J. Davis, R.G. Compton, *Talanta* 54 (2001) 785.
- [5] A.R. Asghari, M.K. Amini, H.R. Mansour, M. Salavati-Niasari, *Talanta* 61 (2003) 557.
- [6] E. Santos, M.C.B.S.M. Montenegro, C. Couto, A.N. Araújo, M.F. Pimentel, V.L. da Silva, *Talanta* 63 (2004) 721.
- [7] J. Gallardo, S. Alegret, M. Del Valle, *Sens. Actuators B* 101 (2004) 72.
- [8] T.A. Bendikov, J. Kim, T.C. Harmon, *Sens. Actuators B* 106 (2005) 512.
- [9] P.K.T. Lin, A.N. Araujo, M.C.B.S.M. Montenegro, R. Perez-Olmos, *J. Agric. Food Chem.* 53 (2005) 211.
- [10] S.S.M. Hassan, S.A.M. Marzouk, H.E.M. Sayour, *Talanta* 59 (2003) 1237.
- [11] A.K. Jain, V.K. Gupta, J.R. Raison, *Talanta* 69 (2006) 1007.
- [12] V.K. Gupta, R. Ludwig, S. Agarwal, *Anal. Chim. Acta* 538 (2005) 213.
- [13] A.K. Jain, V.K. Gupta, L.P. Singh, P. Srivastava, J.R. Raison, *Talanta* 65 (2005) 716.
- [14] R. Prasad, V.K. Gupta, A. Kumar, *Anal. Chim. Acta* 508 (2004) 61.
- [15] V.K. Gupta, S. Agarwal, *Talanta* 65 (2005) 730.
- [16] A. Turrentine, *Trans. Am. Electrochem. Soc.* 10 (1896) 49.
- [17] S. Glasstone, A. Hickling, *Electrolytic Oxidation and Reduction: Inorganic and Organic*, Chapman Hall, London, 1934.
- [18] D. Pletcher, Z. Poorabedi, *Electrochim. Acta* 24 (1979) 1253.
- [19] M. Shibata, K. Yoshida, N. Furuya, *J. Electroanal. Chem.* 387 (1995) 143.
- [20] M. Shibata, K. Yoshida, N. Furuya, *J. Electrochem. Soc.* 145 (1998) 2348.
- [21] N.G. Carpenter, D. Pletcher, *Anal. Chim. Acta* 317 (1995) 287.
- [22] S. Cattarin, *J. Appl. Electrochem.* 22 (1992) 1077.
- [23] A.G. Fogg, S.P. Scullion, T.E. Edmonds, B.J. Birch, *Analyst* 116 (1991) 573.
- [24] R.J. Davenport, D.C. Johnson, *Anal. Chem.* 45 (1973) 1979.
- [25] M.E. Bodini, D. Sawyer, *Anal. Chem.* 49 (1977) 485.
- [26] J.D. Genders, D. Hartsough, D.T. Hobbs, *J. Appl. Electrochem.* 26 (1996) 1.
- [27] H.L. Li, J.Q. Chambers, D.T. Hobbs, *J. Appl. Electrochem.* 18 (1988) 454.
- [28] M. Fedurco, P. Kedzierzawski, J. Augustynski, *J. Electrochem. Soc.* 146 (1999) 2569.
- [29] F. Bouamrane, A. Tadjeddine, J.E. Butler, R. Tenne, C. Levy-Clement, *J. Electroanal. Chem.* 405 (1996) 95.
- [30] C. Reuben, E. Galun, H. Cohen, R. Tenne, R. Kalish, Y. Muraki, K. Hashimoto, A. Fujishima, J.M. Butler, C. Levy-Clement, *J. Electroanal. Chem.* 396 (1995) 233.
- [31] R. Tenne, K. Patel, K. Hashimoto, A. Fujishima, *J. Electroanal. Chem.* 347 (1993) 409.
- [32] Z. Zhao, X. Cai, *J. Electroanal. Chem.* 252 (1988) 361.
- [33] O.V. Kaminskaya, E.A. Zakharova, G.B. Slepchenko, *J. Anal. Chem.* 59 (2004) 1091.
- [34] J. Davis, M.J. Moorcroft, S.J. Wilkins, R.G. Compton, M.F. Cardosi, *Analyst* 125 (2000) 737.
- [35] J. Davis, M.J. Moorcroft, S.J. Wilkins, R.G. Compton, M.F. Cardosi, *Electroanalysis* 12 (2000) 1363.
- [36] A.J. Bard, L.R. Faulkner, *Electrochemistry Methods: Fundamentals and Applications*, 2nd ed., Wiley, New York, 2000, pp. 156–222.
- [37] A.M. Bond, Kh.Z. Brainina, M. Koppenol, *Electroanalysis* 6 (1994) 275.
- [38] AOAC, *Official Methods of Analysis of the Association of Official Analytical Chemists*, 16th ed., AOAC, Gaithersburg, 1997 (Method 984.18).
- [39] J.R.C. Rocha, L. Kosminsky, T.R.L.C. Paixão, M. Bertotti, *Electroanalysis* 13 (2001) 155.
- [40] B.K. Simpson, D.C. Johnson, *Electroanalysis* 16 (2004) 532.
- [41] P.M. Tucker, M.J. Waite, B.E. Hayden, *J. Appl. Electrochem.* 34 (2004) 781.
- [42] T.R.L.C. Paixão, D. Corbo, M. Bertotti, *Anal. Chim. Acta* 472 (2002) 123.
- [43] M.D.M. Quintino, D. Corbo, M. Bertotti, L. Angnes, *Talanta* 58 (2002) 943.
- [44] T.R.L.C. Paixão, R.C. Matos, M. Bertotti, *Electroanalysis* 15 (2003) 1884.
- [45] T.R.L.C. Paixão, M. Bertotti, *J. Electroanal. Chem.* 571 (2004) 101.
- [46] V. Mori, M. Bertotti, *Anal. Lett.* 32 (1999) 25.
- [47] G.E. Dima, A.C.A. de Vooy, M.T.M. Koper, *J. Electroanal. Chem.* 554 (2003) 15.
- [48] R.S. Gärtner, G.J. Witkamp, *Sep. Sci. Technol.* 40 (2005) 2391.
- [49] H.-J. Rapp, P.H. Pfromm, *J. Membr. Sci.* 146 (1998) 249.
- [50] K. Köhler, M. Nowak, A. Seubert, *Fresenius J. Anal. Chem.* 358 (1997) 551.
- [51] W. Shotyk, I. Immenhauser-Potthast, H.A. Vogel, *J. Chromatogr. A* 706 (1995) 209.

# Aminopolycarboxyl-modified Ag<sub>2</sub>S nanoparticles: Synthesis, characterization and resonance light scattering sensing for bovine serum albumin

Hongcheng Pan<sup>a</sup>, Xiancong Tao<sup>a</sup>, Changjie Mao<sup>a</sup>, Jun-Jie Zhu<sup>a,\*</sup>, Fupei Liang<sup>a,b,\*</sup>

<sup>a</sup> Key Laboratory of Analytical Chemistry for Life Science, School of Chemistry and Chemical Engineering, Nanjing University, Nanjing 210093, China

<sup>b</sup> School of Chemistry and Chemical Engineering, Guangxi Normal University, Guilin 541004, China

Received 29 December 2005; received in revised form 28 March 2006; accepted 30 March 2006

Available online 2 May 2006

## Abstract

A novel method was proposed to prepare a series of functionalized Ag<sub>2</sub>S nanoparticles capped with various aminopolycarboxylic acids. The as-prepared Ag<sub>2</sub>S nanoparticles were characterized by UV–vis, FTIR, resonance light scattering spectra (RLS) and transmission electron microscopy (TEM). Based on the RLS intensities enhanced by BSA-induced Ag<sub>2</sub>S nanoparticles aggregation, a sensitive RLS method for the detection BSA at nanogram levels was established. The detection limits for BSA are between 8.6 and 112.6 ng mL<sup>-1</sup>, depending on the different capping agents. The effects of various capping agents on the detection limits of BSA have been investigated. The detection limit is found to be dependent on the stability constant (log *K*<sub>MY</sub>) of the silver–aminopolycarboxyl complexes.

© 2006 Elsevier B.V. All rights reserved.

**Keywords:** Ag<sub>2</sub>S nanoparticles; Resonance light scattering; Bovine serum albumin

## 1. Introduction

The surface-modification of the nanoparticles has attracted special attention because it provides a strategy for selective tailoring the nanoparticles of different surface physical and chemical properties. It allows the functionalized nanoparticles extensive applications in different fields, ranging from biosensing to biolabeling. Oligonucleotide-modified nanoparticles and sequence-specific particle assembly events, induced by target DNA, were used to generate materials with unusual optical properties [1,2]. By using various ligands, some functionalized nanoparticles can be attached to special biomolecules such as sugars [3], peptides [4], proteins [5], and DNA [6].

Resonance light scattering technique (RLS), pioneered by Pasternack et al., has been used to investigate porphyrin assemblies on DNA [7]. As a new spectral technique, the resonance light scattering measurements are very simple and sensitive by using a common spectrofluorometer. Yguerabide and Yguerabide demonstrated the light scattering power of a 60-nm gold

particle is equivalent to about  $5 \times 10^5$  fluorescein molecules [8]. In the past decade, RLS spectroscopy, including total internal reflected RLS [9], has been successfully applied to detect DNA [7,10,11], protein [12–15], drugs [16], and inorganic substances [17]. Recently, the research interests have been focused on the enhancement of the light scattering signal based on biomolecule-induced nanoparticle aggregation. The nanoparticle-based RLS probes have advantages over conventional dye-based probes because they are chemically stable and do not suffer from photolysis. Bao et al. reported the application of 80-nm-diameter gold RLS particles coated with anti-biotin antibodies for detection of DNA hybridization on cDNA microarrays [18]. By measuring the ratio of scattered light intensities at 560 and 680 nm, Aslan et al. developed a glucose sensing platform by using modified gold colloids [19]. Polyhydroxylated fullerene (C<sub>60</sub>) derivative, polystyrene–acrylic acid and polyvinyl alcohol keto-derivative nanoparticles have been employed as RLS probes to detect protein [20–22]. Wang et al. prepared a series of mercaptoacetic acid functionalized metal sulfide nanoparticles such as PbS and HgS. A novel assay of  $\gamma$ -globulin, without separation of human serum albumin, is established on the basis of the measurement of enhanced RLS signals resulting from the interaction of protein and functionalized metal sulfide nanopar-

\* Corresponding authors. Tel.: +86 25 8359 4976; fax: +86 25 8359 4976.  
E-mail address: [jjzhu@nju.edu.cn](mailto:jjzhu@nju.edu.cn) (J.-J. Zhu).

ticles [23,24]. The surface-modification of the nanoparticles is currently under intensive research for development of sensitive RLS probes. However, few studies were focused on the influence of the capping molecules on the sensitivity (e.g. detection limits) of RLS technique.

In the present study we develop a novel RLS technique to detect bovine serum albumin (BSA) at nanogram levels, and investigate the effect of the capping agent on the detection limit. A series of functionalized Ag<sub>2</sub>S nanoparticles capped with various aminopolycarboxylic acids were prepared and characterized by UV–vis, FTIR, RLS and TEM. The scattering signals of aminopolycarboxyl-modified Ag<sub>2</sub>S nanoparticles have been strongly enhanced by the reactions between BSA and Ag<sub>2</sub>S nanoparticles. BSA was detected based on the proportional relationship between the enhanced RLS intensities at 468 nm and the concentration of BSA. The detection limits for BSA are between 8.6 and 112.6 ng mL<sup>-1</sup>, depending on the different capping agents. It was found that the detection limits (DL) for BSA strongly depended on the stability constant (log *K*<sub>MY</sub>) of the silver–aminopolycarboxyl complexes. To the best of our knowledge, this is the first description about the relationship between capping molecules and the detection limit (DL) for BSA. The results could be considered to be useful to design nanoparticle-based RLS probes with sufficient sensitivity.

## 2. Experimental

### 2.1. Reagents

Diethylenetriaminepentaacetic acid (DTPA, Beijing Chemical Plant, China), triethylenetetraaminehexaacetic acid (TTHA, Shanghai Chemical Reagent Co. Ltd., China), *trans*-1,2-diaminocyclohexanetetraacetic acid (DCTA, Fluka), Ethylenediamine tetraacetic acid (EDTA, Shanghai Chemical Reagent Co. Ltd., China), Ethylene glycol bis(aminoethylether) tetraacetic acid (EGTA, Huzhou Chemical Plant, China), Hydroxyethylethylenediaminetriacetic acid (HEDTA, Shanghai Chemical Reagent Co. Ltd., China), Nitritotriacetic acid (NTA, Beijing Chemical Plant, China), AgNO<sub>3</sub> (Shanghai Chemical Reagent Co. Ltd., China), and Na<sub>2</sub>S·12H<sub>2</sub>O (Shanghai Chemical Reagent Co. Ltd., China) were all used as received. Bovine serum albumin (BSA, Sigma) was directly dissolved in water to prepare stock solutions of 50 μg mL<sup>-1</sup> and stored at 4 °C. The working solutions were obtained by diluting the stock solutions with water just before use. NaAc–HAc buffer solution was used to adjust the acidity of the aqueous system. All reagents were of analytical grade and used without further purification. Doubly distilled water was used throughout.

### 2.2. Synthesis

Various aminopolycarboxyl-modified Ag<sub>2</sub>S nanoparticles were prepared as follows. In a typical synthesis, 0.2 mmol of aminopolycarboxylic acid (DTPA, TTHA, DCTA, EDTA, EGTA, HEDTA, or NTA) was dissolved in 30 mL solution and the solution was adjusted to pH 9 with 1 M NaOH. Subsequently, 5 mL of 0.04 M (0.02 mmol) AgNO<sub>3</sub> was added under stirring,

followed the pH was adjusted by 1 M NaOH solution to 9. Afterward, a 10 mL freshly prepared Na<sub>2</sub>S solution (0.02 mmol) was injected into the reaction solution while the mixture continued to stir rapidly. The solution rapidly changed to brown and was left for 10 h at room temperature under stirring. The colloidal solution was purified through centrifugation at 5000 rpm for 5 min to remove the large particles and dialysis for 30 h to remove any residual reagents. Then the solution was diluted to 100 mL with doubly distilled water. The as-prepared Ag<sub>2</sub>S solutions can be stored for months at room temperature without aggregation. These different aminopolycarboxyl-modified Ag<sub>2</sub>S nanoparticles are referred to Ag<sub>2</sub>S–DTPA, Ag<sub>2</sub>S–TTHA, Ag<sub>2</sub>S–DCTA, Ag<sub>2</sub>S–EDTA, Ag<sub>2</sub>S–EGTA, Ag<sub>2</sub>S–HEDTA and Ag<sub>2</sub>S–NTA, according to their capping molecules; the size of the Ag<sub>2</sub>S nanoparticles are 19, 17, 20, 23, 16, 24 and 18 nm, respectively.

### 2.3. Apparatus and measurements

UV–vis absorption spectra were measured on a Shimadzu UV-240 spectrophotometer. The transmission electron microscopy (TEM) sample was prepared by depositing a droplet of solution onto a carbon film supported by copper grids. The TEM images were taken on a JEOL JEM-200CX transmission electron microscope, using an accelerating voltage of 200 kV. Fourier transform infrared (FTIR) spectra were recorded with an FTS 165 Bio-Rad FTIR spectrophotometer in the range 4000–400 cm<sup>-1</sup> on KBr pellets.

The RLS spectra were obtained by synchronously scanning the excitation and emission monochromators (namely, Δλ = 0.0 nm) of Hitachi 850 Fluorescence spectrophotometer (Kyoto, Japan) in the wavelength region from 300 to 700 nm. The intensity of light scattering was measured at the wavelength where the maximum scattering peak is located. Both the intensity measurement and the spectrum scanning of the resonance light scattering were made by keeping the bandpass of the excitation and the emission of the spectrofluorometer at 5.0 nm.

Appropriate amounts of HAC–NaAc buffer solution were mixed with the aminopolycarboxyl-modified Ag<sub>2</sub>S solution. Subsequently, an appropriate volume of bovine serum albumin solution was added. The mixture was diluted with doubly distilled water to 5.0 mL and mixed thoroughly. Then, it is allowed to stand for 5 min, before RLS spectra and the enhancement of light scattering intensity at maximum wavelength were measured. The enhancement of light scattering intensity is represented as Δ*I* = *I* – *I*<sub>0</sub>, where *I* and *I*<sub>0</sub> are the intensity at maximum wavelength of RLS spectra with and without proteins, respectively.

## 3. Results and discussion

### 3.1. Absorption spectra

Fig. 1 shows the absorption spectra of the modified Ag<sub>2</sub>S nanoparticles. According to the literature, the band gap of bulk silver sulfide is 1 eV (1240 nm), the apparent large blue shift

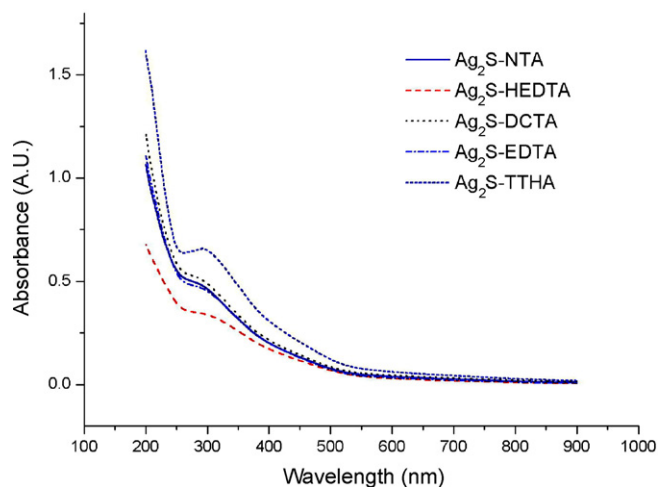


Fig. 1. Absorption spectra of aminopolycarboxyl-modified  $\text{Ag}_2\text{S}$  nanoparticles.

indicates that the nanoparticles are within the quantum confinement regime [25].

### 3.2. FTIR spectra

To better understand the adsorption mechanism of aminopolycarboxylic acids on the surface of  $\text{Ag}_2\text{S}$  nanoparticles, Fourier transform infrared (FTIR) measurements were carried out. Fig. 2(A) represents the typical IR spectrum of the  $\text{Ag}_2\text{S}$  nanoparticles. Fig. 2(B) reveals that the IR spectrum obtained from the  $\text{Ag}_2\text{S}$  nanoparticles coated with EDTA and others aminopolycarboxyl-modified  $\text{Ag}_2\text{S}$  nanoparticles have the similar IR spectra. It is noted that the  $\text{C}=\text{O}$  stretch band of the carboxyl group located at about  $1700\text{ cm}^{-1}$ , is absent in the spectrum of the  $\text{Ag}_2\text{S}$  nanoparticles coated with EDTA. Instead, two new bands at  $1560$  and  $1412\text{ cm}^{-1}$  are characteristic of the asymmetric  $\nu_{\text{as}}(\text{COO}^-)$  and the symmetric  $\nu_{\text{s}}(\text{COO}^-)$  stretch. According to the previous investigations, when carboxylic acids adsorb from solution to the metal surface, there may exist two different bonding types of carboxylate groups to the metal, i.e.

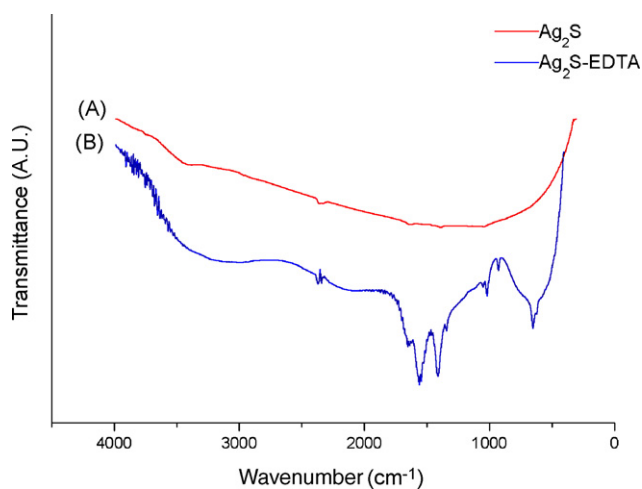


Fig. 2. Representative FTIR spectra of  $\text{Ag}_2\text{S}$  nanoparticles modified with and without EDTA. (A)  $\text{Ag}_2\text{S}$  nanoparticles; (B)  $\text{Ag}_2\text{S}$  nanoparticles modified with EDTA.

either a bidentate bond or a monodentate bond [26,27]. In case of the monodentate bond, the  $\text{C}=\text{O}$  bond, which displays a strong band at about  $1700\text{ cm}^{-1}$ , is still present and the metal atoms substitute the acid hydrogen. In the present study, the absence of IR band at  $1700\text{ cm}^{-1}$  and two new bands at  $1560$  and  $1412\text{ cm}^{-1}$  demonstrate that EDTA is chemisorbed as a carboxylate onto the surface of  $\text{Ag}_2\text{S}$  nanoparticles. And the two oxygen atoms in the carboxylate are coordinated symmetrically to the Ag atoms.

### 3.3. TEM images

The typical TEM images for the aminopolycarboxyl-modified  $\text{Ag}_2\text{S}$  nanoparticles are shown in Figs. 3(A) and (C) and 4(A) and (C). It is observed that the particles are well dispersed with a narrow size distribution. TEM images of the aminopolycarboxyl-modified  $\text{Ag}_2\text{S}$  nanoparticles after the addition of appropriate amounts of BSA are shown in Figs. 3(B) and (D) and 4(B) and (D). It is observed that  $\text{Ag}_2\text{S}$  nanoparticles can change from dispersion to aggregation. This indicates the interaction between BSA and the  $\text{Ag}_2\text{S}$  nanoparticles.

### 3.4. RLS spectral characteristics

Under optimal conditions, both the RLS spectra of aminopolycarboxyl-modified  $\text{Ag}_2\text{S}$  nanoparticles in the absence and presence of BSA have similar features and presented two peaks at  $410$  and  $468\text{ nm}$ . The scattering signals of  $\text{Ag}_2\text{S}$  nanoparticles have been strongly enhanced after adding BSA and these RLS signals increased with the increase the concentration of BSA. As reported in the literature, BSA has a rather weak RLS signal even if its concentration is higher than  $20\text{ }\mu\text{g mL}^{-1}$  [28]. Therefore, the enhancement of the RLS signal suggested that there are the interactions between BSA and the functionalized  $\text{Ag}_2\text{S}$  nanoparticles. The enhancement of the signal can be attributed to the aggregation induced by reaction between carboxyl groups of functionalized  $\text{Ag}_2\text{S}$  nanoparticles and BSA [Ref.]. When surface capped with carbonyl and carboxyl, nanoparticles can bond with the remaining  $\text{NH}_2$ -groups in proteins. The hydrophobic carbon-carbon skeletal chain of capping molecules can also bond with the hydrophobic amino acid residues. The presence of large aggregation for  $\text{Ag}_2\text{S}$  particles can clearly be observed in the TEM images (Figs. 3 and 4) and thus the inferences can be confirmed. At room temperature, the reactions between functionalized  $\text{Ag}_2\text{S}$  nanoparticles and BSA occur immediately and the time of equilibrium takes only about  $5\text{ min}$ . The scattering intensity is stable for at least  $40\text{ min}$ . The maximum wavelength at  $468\text{ nm}$  was selected as the optimum for the detection of BSA with high sensitivity. The RLS intensities of functionalized  $\text{Ag}_2\text{S}$  nanoparticles-BSA were found to be proportional to the concentration of BSA, indicating that the detection of BSA with the functionalized  $\text{Ag}_2\text{S}$  nanoparticles is possible.

### 3.5. Optimization of the general procedures

The optimal conditions such as the effects of pH, concentration of NaAc-HAc buffer solution and  $\text{Ag}_2\text{S}$  nanoparticles

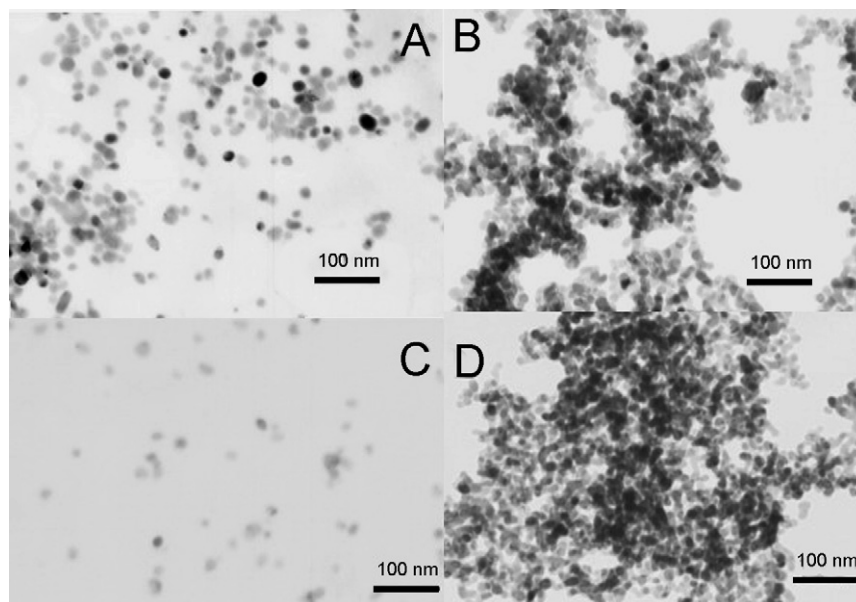


Fig. 3. TEM images:  $\text{Ag}_2\text{S}$  nanoparticles modified with TTHA in the absence (A) and presence (B) of BSA;  $\text{Ag}_2\text{S}$  nanoparticles modified with DCTA in the absence (C) and presence (D) of BSA.

on RLS intensity were investigated. All the optimal conditions are listed in Table 1. Under optimal conditions, BSA was detected based on the proportional relationship between the enhanced RLS intensities at 468 nm and the concentration of BSA. The detection limit is calculated following the equation:  $DL = K S_b / S$ , where  $K$  is a constant related to the confidence level, according to the suggestion of IUPAC,  $K = 3$ ;  $S_b$  is the standard deviation of 10 blank measurements, and  $S$  is the slope of the calibration curve. As listed in Table 1, the detection limits for BSA are  $8.6 \text{ ng mL}^{-1}$  for  $\text{Ag}_2\text{S}$ -DTPA,  $11.8 \text{ ng mL}^{-1}$  for  $\text{Ag}_2\text{S}$ -TTHA,  $11.2 \text{ ng mL}^{-1}$  for  $\text{Ag}_2\text{S}$ -DCTA,  $15.7 \text{ ng mL}^{-1}$

for  $\text{Ag}_2\text{S}$ -EDTA,  $34.2 \text{ ng mL}^{-1}$  for  $\text{Ag}_2\text{S}$ -EGTA,  $38.5 \text{ ng mL}^{-1}$  for  $\text{Ag}_2\text{S}$ -HEDTA and  $112.6 \text{ ng mL}^{-1}$  for  $\text{Ag}_2\text{S}$ -NTA, respectively.

### 3.6. Interferences of coexisting substances and sample determinations

The experiments on the effect of coexisting substances were carried out and the results are shown in Table 2. The results indicated that the method is free from interference from most of amino acids, common metal ions, nucleic acids and glucose. The

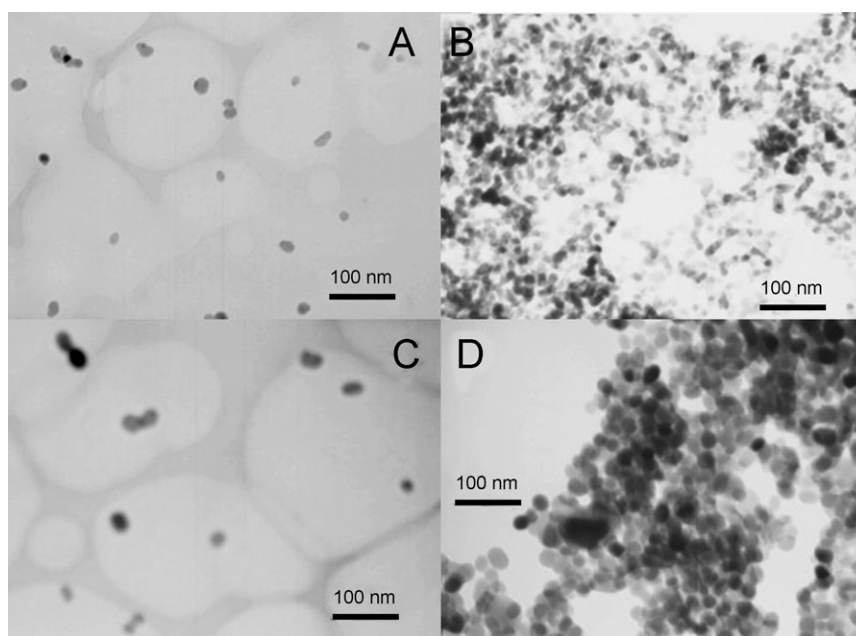


Fig. 4. TEM images:  $\text{Ag}_2\text{S}$  nanoparticles modified with NTA in the absence (A) and presence (B) of BSA;  $\text{Ag}_2\text{S}$  nanoparticles modified with EDTA in the absence (C) and presence (D) of BSA.



Table 1  
Optimal conditions of detection BSA using functionalized Ag<sub>2</sub>S nanoparticles

	Linear range ( $\mu\text{g mL}^{-1}$ )	Detection limit $3\sigma$ (ng mL <sup>-1</sup> )	Linear regression equation (ng mL <sup>-1</sup> )	pH	Concentration of buffer (M)	C <sub>Ag<sub>2</sub>S</sub> (M)	<i>r</i>
Ag <sub>2</sub> S–DTPA	0.01–0.12	8.6	$\Delta I = 0.1402C + 7.3302$	4.6	0.05	$2 \times 10^{-4}$	0.9935
Ag <sub>2</sub> S–TTHA	0.02–0.26	11.8	$\Delta I = 0.031C + 2.5586$	4.6	0.04	$4 \times 10^{-4}$	0.9988
Ag <sub>2</sub> S–DCTA	0.03–0.15	11.2	$\Delta I = 0.1791C + 1.3166$	4.6	0.04	$2 \times 10^{-4}$	0.9935
Ag <sub>2</sub> S–EDTA	0.05–0.3	15.7	$\Delta I = 0.1134C + 0.9724$	4.2	0.03	$3.2 \times 10^{-4}$	0.9834
Ag <sub>2</sub> S–EGTA	0.04–0.24	34.2	$\Delta I = 0.0462C + 4.4324$	4.6	0.04	$1.2 \times 10^{-4}$	0.9847
Ag <sub>2</sub> S–HEDTA	0.05–0.5	38.5	$\Delta I = 0.0257C + 4.9394$	4.6	0.04	$1.2 \times 10^{-4}$	0.9817
Ag <sub>2</sub> S–NTA	0.15–0.7	112.6	$\Delta I = 0.0308C + 3.1792$	4	0.03	$2 \times 10^{-4}$	0.9876

Table 2  
Interference of coexisting substances<sup>a</sup>

Coexisting substances	Concentration (ng mL <sup>-1</sup> )	Change of $\Delta I_{468 \text{ nm}}$ (%)	Coexisting substances	Concentration (ng mL <sup>-1</sup> )	Change of $\Delta I_{468 \text{ nm}}$ (%)
Glucose	1000	5.6	Na(I), Cl <sup>-1</sup>	500	1.7
L-tryptophan	500	4.4	K(I), Cl <sup>-1</sup>	500	3.2
L-cysteine	300	-3.7	Ca(II), Cl <sup>-1</sup>	300	-5.3
L-phenylalanine	500	5.8	Zn(II), Cl <sup>-1</sup>	300	-2.8
L-leucine	500	3.2	Mg(II), Cl <sup>-1</sup>	300	3.3
L-glycine	200	6.7	Pb(II), NO <sub>3</sub> <sup>-</sup>	100	6.4
fsDNA	500	4.3	Co(II), SO <sub>4</sub> <sup>2-</sup>	100	-3.9

<sup>a</sup> BSA 30 ng mL<sup>-1</sup>; Ag<sub>2</sub>S–DTPA nanoparticles  $2 \times 10^{-4}$  M; pH 4.6.

Table 3  
Analytical results for the diluted cow milk sample<sup>a</sup>

Samples	Content of protein (mg mL <sup>-1</sup> )		Recovery <i>n</i> = 6 (%)	R.S.D. (%)
	This method	The CBB G-250 method		
Cow milk 1	25.3	23.9	96.5	3.1
Cow milk 2	28.7	29.6	103.1	2.5
Cow milk 3	27.2	28.8	104.6	4.7

<sup>a</sup> Ag<sub>2</sub>S–DTPA nanoparticles  $2 \times 10^{-4}$  M; pH 4.6.

real sample determinations were also performed. Table 3 lists the results for the detection of three diluted cow milk samples with the present method. It can be seen that the recovery and relative standard deviation (R.S.D.) are satisfactory and the results are identical to the reference method of CBB G-250 [29].

### 3.7. Discussion of mechanism

We attribute the enhanced RLS intensities to the aggregation of nanoparticles which was induced by reactions between BSA and aminopolycarboxyl-modified Ag<sub>2</sub>S nanoparticles. It was in accordance with the TEM results. In our experiments, BSA (PEI 4.7–4.9) carries a positive charge in the aqueous medium with pH range from 4.0 to 4.6, while the surface of Ag<sub>2</sub>S nanoparticles carries negative charges, due to chemisorbed carboxyl groups. The negative charged Ag<sub>2</sub>S nanoparticles surface and counterions form an electrostatic double layer that provides a repulsive force enable Ag<sub>2</sub>S nanoparticles stable in solution. When aminopolycarboxyl-modified Ag<sub>2</sub>S nanoparticles mixed with BSA, positive charged BSA would compress the diffuse double layer around the negative charged Ag<sub>2</sub>S nanoparticles,

allowing the particles to densely aggregate, thus increasing RLS intensities. No corresponding relationship was found between the size of the as-prepared Ag<sub>2</sub>S nanoparticles and the detection limits for BSA. However, we observed the dependence of capping molecules of Ag<sub>2</sub>S nanoparticles on the detection limits of BSA. According to the data given by literature, the log  $K_{MY}$  of the silver–aminopolycarboxyl complexes are 5.16 for Ag<sub>2</sub>S–NTA, 6.71 for Ag<sub>2</sub>S–HEDTA, 7.06 for Ag<sub>2</sub>S–EGTA, 7.32 for Ag<sub>2</sub>S–EDTA, 8.7 for Ag<sub>2</sub>S–TTHA, 8.67 for DTPA, respectively [30]. Compared with the corresponding data for DL, a decline trend of DL with the increase of log  $K_{MY}$  was observed. With a high log  $K_{MY}$  value, the bonding of the aminopolycarboxylic acid and the surface of Ag<sub>2</sub>S nanoparticles becomes more stable. As a result the Ag<sub>2</sub>S nanoparticles can carry more negative charges. The functionalized Ag<sub>2</sub>S nanoparticles with dense negative charges are easily to react with BSA molecules, resulting in the increase of sensitivity in the detection of BSA.

## 4. Conclusions

In the present study, a novel method to prepare a series of functionalized Ag<sub>2</sub>S nanoparticles capped with various aminopolycarboxylic acids was proposed. The as-prepared Ag<sub>2</sub>S nanoparticles could be used as RLS probes in response to BSA. Based on the RLS intensities enhanced by BSA-induced Ag<sub>2</sub>S nanoparticles aggregation, a sensitive RLS method to detect BSA at nanogram levels was established. The detection limits for BSA are between 8.6 and 112.6 ng mL<sup>-1</sup>, depending on the different capping agents. It was found that the dependence of the detection limits for BSA on the stability constant (log  $K_{MY}$ ) of the silver–aminopolycarboxyl complexes. Although the relationship between capping molecules and detec-

tion limits for BSA is still under study, it is undoubted that the stability of silver–aminopolycarboxyl complexes strongly affects on the detection limits of Ag<sub>2</sub>S nanoparticles-based RLS probes.

### Acknowledgements

We greatly appreciate the support of the National Natural Science Foundation of China (Grant nos. 20325516, 90206037). This work is also supported by NSFC for Creative Research Group (20521503).

### References

- [1] C.A. Mirkin, R.L. Letsinger, R.C. Mucic, J.J. Storhoff, *Nature* 382 (1996) 607.
- [2] R. Elghanian, J.J. Storhoff, R.C. Mucic, R.L. Letsinger, C.A. Mirkin, *Science* 277 (1997) 1078.
- [3] T.C. Rojas, J.M. de la Fuente, A.G. Barrientos, S. Penadés, L. Ponsoonnet, A. Fernández, *Adv. Mater.* 14 (2002) 585.
- [4] S.R. Whaley, D.S. English, E.L. Hu, P.F. Barbara, A.M. Belcher, *Nature* 405 (2000) 665.
- [5] H. Mattoussi, J.M. Mauro, E.R. Goldman, G.P. Anderson, V.C. Sunder, F.V. Mikulec, M.G. Bawendi, *J. Am. Chem. Soc.* 122 (2000) 12142.
- [6] S.J. Park, A.A. Lazarides, C.A. Mirkin, R.L. Letsinger, *Angew. Chem. Int. Ed.* 40 (2001) 2909.
- [7] R.F. Pasternack, C. Bustamante, P.J. Collings, A. Giannetto, E.J. Gibbs, *J. Am. Chem. Soc.* 115 (1993) 5393.
- [8] J. Yguerabide, E.E. Yguerabide, *Anal. Biochem.* 262 (1998) 137.
- [9] P. Feng, W.Q. Shu, C.Z. Huang, Y.F. Li, *Anal. Chem.* 73 (2001) 4307.
- [10] R. Liu, J. Yang, C. Sun, L. Li, X. Wu, Z. Li, C. Qi, *Chem. Phys. Lett.* 376 (2003) 108.
- [11] X. Long, Q. Miao, S. Bi, D. Li, C. Zhang, H. Zhao, *Talanta* 64 (2004) 366.
- [12] C.Z. Huang, Y. Liu, Y.H. Wang, H.P. Guo, *Anal. Biochem.* 321 (2003) 236.
- [13] R. Jia, H. Zhai, Y. Shen, X. Chen, Z. Hu, *Talanta* 64 (2004) 355.
- [14] H. Zhong, N. Li, F. Zhao, K.A. Li, *Talanta* 62 (2004) 37.
- [15] Y.J. Chen, J.H. Yang, X. Wu, T. Wu, Y.X. Luan, *Talanta* 58 (2002) 869.
- [16] N.B. Li, H.Q. Luo, S.P. Liu, *Talanta* 66 (2005) 495.
- [17] A.H. Liang, Z.L. Jiang, B.M. Zhang, Q.Y. Liu, J. Lan, X. Lu, *Anal. Chim. Acta* 530 (2005) 131.
- [18] P. Bao, A.G. Frutos, C. Greef, J. Lahiri, U. Muller, T.C. Peterson, L. Warden, X. Xie, *Anal. Chem.* 74 (2002) 1792.
- [19] K. Aslan, J.R. Lakowicz, C.D. Geddes, *Anal. Chem.* 77 (2005) 2007.
- [20] G.C. Zhao, P. Zhang, X.W. Wei, Z.S. Yang, *Anal. Biochem.* 334 (2004) 297.
- [21] L.Y. Wang, H.Q. Chen, L. Li, T.T. Xia, L. Dong, L. Wang, *Spectrochim. Acta. Part A* 60 (2004) 747.
- [22] Y. Zhou, S. She, L. Zhang, Q. Lu, *Microchim. Acta* 149 (2005) 151.
- [23] L.Y. Wang, L. Wang, H.Q. Chen, L. Li, L. Dong, T.T. Xia, F.Z. Dong, Z.Q. Xu, *Anal. Chim. Acta* 493 (2003) 179.
- [24] L.Y. Wang, L. Wang, L. Dong, Y.L. Hu, T.T. Xia, H.Q. Chen, L. Li, C.Q. Zhu, *Talanta* 62 (2004) 237.
- [25] M.C. Brelle, J.Z. Zhang, L. Nguyen, R.K. Mehra, *J. Phys. Chem. A* 103 (1999) 10194.
- [26] L.H. Dubois, B.R. Zegarski, R.G. Nuzzo, *Langmuir* 2 (1986) 412.
- [27] N.Q. Wu, L. Fu, M. Su, M. Aslam, K.C. Wong, V.P. Dravid, *NanoLetters* 4 (2004) 383.
- [28] Y.F. Li, C.Z. Huang, X.H. Huang, M. Li, *Anal. Sci.* 16 (2000) 1249.
- [29] D.A. Zhang, *Experimental Handbook of Biological Molecules*, Jilin University Press, Changchun, China, 1991, p. 327.
- [30] L.S. Shen, *Handbook of Chemical Analyses and Computation*, China Water Power Press, Beijing, China, 1992, p. 227.

# Development of a one-step immunochromatographic strip test for the rapid detection of nevirapine (NVP), a commonly used antiretroviral drug for the treatment of HIV/AIDS

M. Pattarawarapan<sup>a</sup>, S. Nangola<sup>b,c</sup>, T.R. Cressey<sup>d,e</sup>, C. Tayapiwatana<sup>b,\*</sup>

<sup>a</sup> Department of Chemistry, Faculty of Sciences, Chiang Mai University, Thailand

<sup>b</sup> Division of Clinical Immunology, Department of Medical Technology, Faculty of Associated Medical Sciences, Chiang Mai University, Chiang Mai 50200, Thailand

<sup>c</sup> Research and development Unit, i+MED LABORATORIES, Bangkok, Thailand

<sup>d</sup> Harvard School of Public Health, Harvard University, Boston, MA, USA

<sup>e</sup> Institut de Recherche pour le Développement (IRD), UR 174, Program for HIV Prevention and Treatment, Chiang Mai University, Thailand

Received 27 March 2006; received in revised form 16 May 2006; accepted 17 May 2006

Available online 30 June 2006

## Abstract

Currently, high-performance liquid chromatographic (HPLC) methods are mainly used to measure antiretroviral plasma concentrations in HIV-infected patients. Although the utility of routine therapeutic drug monitoring (TDM) as an additional tool to optimize long-term antiretroviral therapy is unclear, if TDM is to be widely used, the availability of simple, cheap and reliable methods for the measurement of antiretroviral drug levels are needed, particularly in resource-limited settings. In this study, an immunochromatographic (IC) strip test to detect the presence of nevirapine (NVP) in body fluids has been developed. Antiserum to NVP was first raised in rabbits by immunization against NVP chemically conjugated with bovine serum albumin, and subsequently validated by Western immunoblotting and competitive indirect ELISA. The partially purified anti-NVP antibodies were conjugated with colloidal gold particles. The conjugation of the colloidal gold and polyclonal antibodies was monitored by UV–vis spectroscopy, while transmission electron microscopy images were used to characterize the particle size and shape of the conjugates. The resulting colloidal gold conjugates were used for the production of an IC strip test to detect nevirapine in human plasma. Preliminary assessment suggests no-cross reactivity of the NVP polyclonal antibodies but assessment of plasma samples from HIV-infected patients receiving HAART needs to be conducted. This assay could potentially be used for drug monitoring as part of the clinical care of HIV infected patients.

© 2006 Elsevier B.V. All rights reserved.

**Keywords:** NVP; Immunochromatographic strip test; Colloidal gold; Immunoassay

## 1. Introduction

Nevirapine (NVP), 11-cyclopropyl-5,11-dihydro-4-methyl-6H-dipyrido-[3,2-b:2',3'-e], is a non-nucleoside reverse transcriptase inhibitors (NNRTI) which is widely used as a part of highly active antiretroviral therapy (HAART) for the treatment of HIV/AIDS, and as a single dose prophylactic intervention during labor for the prevention of mother-to-child transmission of HIV (PMTCT) [1,2].

NVP inhibits HIV-1 replication by binding directly to the HIV-1 reverse transcriptase enzyme and disrupting its catalytic site. Unfortunately, NVP viral drug resistance can result from a specific single mutation, such as the K103N, in the viral reverse transcriptase gene and these mutations confer cross resistant to the other NNRTIs in the drug class [3]. A relationship between plasma NVP levels and efficacy has been reported [4]; therefore, maintaining sufficient NVP plasma drug levels is critical to reduce the risk for selecting NNRTI resistance viruses. For the majority of antiretroviral drugs, a similar relationship has been demonstrated and it has been proposed that individualization of drug dosing, guided by the measurement of drug levels (i.e., therapeutic drug monitoring (TDM)) could help optimize

\* Corresponding author. Tel.: +66 18845141; fax: +66 53946042.

E-mail address: [asimi002@chiangmai.ac.th](mailto:asimi002@chiangmai.ac.th) (C. Tayapiwatana).

therapeutic outcome and prevent adverse effects [5]. Furthermore, TDM has also been suggested to be an additional tool to the standard methods of questionnaires and pill counts to help monitor drug adherence [6].

For the quantitative analysis of NVP in plasma, high-performance liquid chromatography (HPLC) with UV detection has been primarily used [7]. Recently, LC/MS methods have also been developed, these methods can simultaneously detect up to nine antiretroviral drugs in the same plasma sample [8]. However, since the majority of HIV-infected patients are living in rural areas, simpler and cheaper methods of NVP detection are needed to facilitate the assessment of TDM of antiretrovirals. Indeed, for plasma nevirapine levels, a qualitative thin-layer chromatography (TLC) method as well as a quantitative ELISA method has been reported [9,10].

Immunochemical strip tests are simple, rapid and cheap assays which have been developed for the qualitative measurement of many biological markers [11–15]. These assays rely on the transport of a labeled antibody (or antigen) probe to its specific antigen (or antibody) binding partner immobilized on the surface of a membrane. Among the different labeled test systems, colloidal gold appears to be the most attractive as unlike fluorescence or enzyme tags, gold probes are more stable and do not require time-consuming procedures such as incubations, washing steps and enzymatic reactions to generate a signal [16,17]. Due to the accumulation of colloidal gold, a red-purple color can be rapidly observed visually. These characteristics significantly shorten the analysis time and make it a very convenience to assay on-site.

In this study, we described the preparation and characterization of anti-NVP polyclonal antibodies and an antibody–colloidal gold probe. These reagents were used to develop a one-step immunochemical strip test for the rapid detection of NVP.

## 2. Experimental

### 2.1. Reagents

All chemicals were purchased from commercial suppliers and used as received. Chloroauric acid ( $\text{HAuCl}_4 \cdot 3\text{H}_2\text{O}$ ), methyl-5-bromovalerate, 4-(dimethylamino)pyridine (DMAP), anhydrous *N,N*-dimethylformamide (DMF), *N*-hydroxy succinimide (NHS), and 1,3-diisopropylcarbodiimide (DIC) were purchased from Fluka, USA. Bovine serum albumin (BSA) was obtained from Sigma, USA. NVP was obtained as a gift from the Government Pharmaceutical Organization (GPO) of Thailand.

### 2.2. Instruments

Solid-phase EIA was performed in 96-well microtiter plates (Nunc, Denmark), and optical density (O.D.) was measured with an automatic plate reader (Tecan, Austria). NMR spectra were recorded on a Bruker AVANCE<sup>TM</sup> NMR spectrometer (400 MHz for <sup>1</sup>H). Chloroform-*d* ( $\text{CDCl}_3$ ) was used as the sol-

vent. Chemical shift values ( $\delta$ ) are reported in ppm relative to internal tetramethylsilane. Coupling constants (*J*) are expressed in Hz. Transmission electron microscopy (TEM) images were recorded on a transmission electron microscope equipped with energy dispersive spectrometer (EDS) (JEOL JEM-2010, Japan).

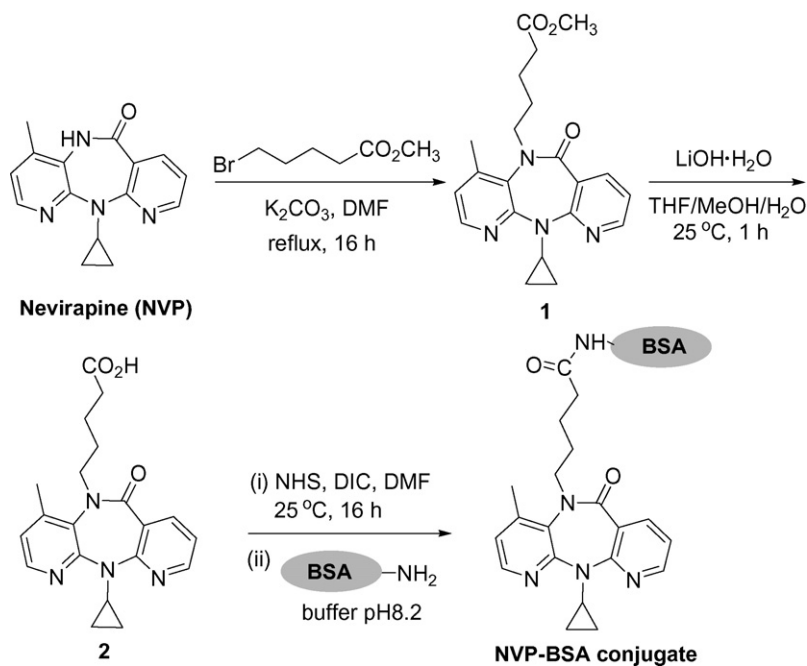
### 2.3. Preparation of NVP–BSA antigen

The immunogen (NVP–BSA conjugate) was synthesized according to Azoulay et al. [10], except that the carrier protein was changed to BSA instead of keyhole limpet hemocyanin (KLH) because the cost of immunogen production was significantly lower and it was presumed that the immunogenicity would not be affected.

*NVP linked methyl ester* (compound **1**; see Scheme 1): A solution of methyl 5-bromovalerate (60  $\mu\text{l}$ , 0.36 mmol) in DMF (1.5 ml) was added to a mixture of NVP (100 mg, 0.36 mmol) and potassium carbonate (149.3 mg, 1.08 mmol) in DMF (1.5 ml). The resulting mixture was refluxed for 16 h, and then the solvent removed in vacuo. The crude residue was purified by chromatography on a silica gel (hexane-ethyl acetate 60/40,  $R_f = 0.37$ ) to generate NVP linked methyl ester (**1**) as a yellow oil (78.1 mg, 52%). The following <sup>1</sup>H NMR (400 MHz,  $\text{CDCl}_3$ ) was produced:  $\delta$  8.49 (dd, *J* = 2, 4.8 Hz, 1H), 8.05 (d, *J* = 4.8 Hz, 1H), 7.75 (dd, *J* = 2, 7.6 Hz, 1H), 6.97 (dd, *J* = 7.6, 4.8 Hz, 1H), 6.92 (d, *J* = 5.2, 1H), 4.38 (t, 2H), 3.66 (s, 3H), 3.65 (m, 1H), 2.42 (t, 2H), 2.34 (s, 3H), 1.87 (m, 4H), 0.96 (m, 2H), 0.47 (m, 2H). <sup>13</sup>C NMR (100 MHz,  $\text{CDCl}_3$ )  $\delta$  173.7, 162.9, 159.0, 152.8, 151.3, 143.8, 143.5, 137.3, 132.7, 122.0, 119.6, 118.4, 51.5, 33.7, 29.0, 28.2, 21.7, 18.0, 8.7, 8.6.

*NVP linked carboxylic acid* (compound **2**): Compound **1** (78.1 mg, 0.20 mmol) was dissolved in a solution of THF/MeOH/H<sub>2</sub>O 3:2:1 (2 ml). LiOH·H<sub>2</sub>O (16.7 mg, 0.40 mmol) was then added and the mixture was stirred for 1 h at 25 °C. After concentration of the mixture in vacuo, the crude residue was diluted with water and neutralized with 1 M HCl. The resulting solution was extracted with 2 ml × 2 ml EtOAc, dried with anhydrous Na<sub>2</sub>SO<sub>4</sub> and concentrated in vacuo to yield compound **2** as yellow oil (62.3 mg, 85%). The following <sup>1</sup>H NMR (400 MHz,  $\text{CDCl}_3$ ) was produced:  $\delta$  8.49 (dd, *J* = 2, 4.8 Hz, 1H), 8.10 (d, *J* = 4.8 Hz, 1H), 7.78 (dd, *J* = 2, 7.6 Hz, 1H), 6.99 (dd, *J* = 7.6, 4.8 Hz, 1H), 6.90 (d, *J* = 5.2 Hz, 1H), 4.40 (t, 2H), 3.66 (m, 1H), 2.42 (t, 2H), 2.32 (s, 3H), 1.87 (m, 4H), 0.96 (m, 2H), 0.47 (m, 2H). <sup>13</sup>C NMR (100 MHz,  $\text{CDCl}_3$ )  $\delta$  177.9, 162.8, 159.0, 152.6, 151.4, 144.0, 143.7, 137.4, 132.8, 122.0, 119.6, 118.5, 33.6, 29.0, 28.1, 21.0, 18.1, 14.1, 8.9, 8.7.

*NVP–BSA conjugate*: Compound **2** (33 mg; 0.087 mmol) was reacted with NHS (12.0 mg; 0.1 mmol) in the presence of 1,3-diisopropylcarbodiimide (23.4 mg; 0.11 mmol) in anhydrous DMF (3.6 ml) for 16 h at 25 °C. The mixture was then added dropwise to a stirred solution of BSA in 5 ml of 0.05 M carbonate/bicarbonate buffer pH 8.2 at 0 °C. The solution was stirred for a further hour at 25 °C and then for 24 h at 4 °C. The synthesized immunogen was then dialyzed with 0.1 M phosphate buffer saline (pH 7.4). The resulting solution was kept frozen at –20 °C until it was used.



Scheme 1. Synthesis of the NVP-BSA conjugate.

#### 2.4. Preparation of polyclonal antibodies

An albino New Zealand rabbit was immunized with 1.0 mg of NVP-BSA antigen in complete Freund's adjuvant. The rabbit preimmunized serum was collected before subcutaneous multi-site injections. Booster injections of 1.0 mg of antigen in incomplete Freund's adjuvant were given 1 week post-immunization, followed by three additional boosters at 2-week intervals. The hyperimmune serum obtained 2 weeks after the last immunization was collected and precipitated with saturated  $(\text{NH}_4)_2 \text{SO}_4$  and dialyzed against 5 mM sodium borax buffer pH 9.0.

#### 2.5. Validation of polyclonal antibodies

##### 2.5.1. Western immunoblotting

SDS-PAGE was performed according to the technique described by Laemmli [18]. Reduced forms of NVP-BSA and unconjugated BSA were electrophoretically separated on a 12% polyacrylamide gel. Samples were prepared in 2-mercaptoethanol and SDS under heat denaturing conditions. The separated polypeptides were transferred to a PVDF membrane as described by Towbin et al. [19]. The membrane was blocked with 5% skimmed milk in PBS for 1 h. Subsequently, the NVP-BSA immunized rabbit serum (1:2000 with 2% BSA in PBS) was applied to the blocked membrane. After 1 h incubation, excess polyclonal antibodies were washed out and HRP-swine anti-rabbit immunoglobulins conjugate (DAKO, Germany) diluted 1:5000 was added. The TMB/ $\text{H}_2\text{O}_2$  immunoblotting substrate solution (Fermentas, Lithuania) was used to visualize bound antibodies on the membrane. The molecular size of each reactive band was calculated relative to standard proteins.

##### 2.5.2. Competitive indirect ELISA

A competitive indirect ELISA was used to test the NVP-BSA immunized rabbit serum reactivity with other antiretroviral drugs. The drugs tested were: nucleoside reverse transcriptase inhibitor (NRTI); zidovudine (AZT), lamivudine (3TC), didanosine (ddI), abacavir (ABC) and stavudine (d4T); the non-nucleoside reverse transcriptase inhibitor (NNRTI); efavirenz (EFV); and the protease inhibitors (PIs), indinavir (IDV), saquinavir (SQV), amprenavir (APV), ritonavir (RTV), nelfinavir (NFV), NFV metabolite (M8) and lopinavir (LPV). For antiretroviral drugs, although the therapeutic ranges vary the plasma concentrations achieved during a dosing interval following oral administration are commonly within 0.10–12  $\mu\text{g}/\text{ml}$  [20]. For the competitive ELISA high concentrations of 10  $\mu\text{g}/\text{ml}$  were used to mimic those concentrations which can be achieved in plasma. NVP-BSA antigen (50  $\mu\text{l}$ ) at a concentration of 10  $\mu\text{g}/\text{ml}$  in carbonate buffer pH 9.6 was added to polystyrene wells and allowed to passively adsorb for 16 h at 4 °C. Subsequently, 200  $\mu\text{l}$  of 2% skimmed milk in PBS was added to each well and incubated for 2 h at RT. The blocking solution was removed by washing three times with 0.05% TWEEN in PBS. A 1:8000 dilution of rabbit serum was mixed with a fix drug concentration (10  $\mu\text{g}/\text{ml}$ ) and incubated for 1 h at 37 °C. The mixture (50  $\mu\text{l}$ ) was applied into an individual NVP-BSA coated well. After washing the wells, 50  $\mu\text{l}$  of HRP-swine anti-rabbit immunoglobulin conjugate diluted 1:3000 was added, incubated for 1 h and washed. TMB/ $\text{H}_2\text{O}_2$  substrate solution (100  $\mu\text{l}$ ) was added for 15 min. The enzymatic reaction was stopped by adding 100  $\mu\text{l}$  of 1 M HCl. The O.D. was measured at 450 nm. The O.D. value was used to compare the ability of each drug to compete with the anti-NVP polyclonal antibodies in the rabbit hyperimmune serum.



## 2.6. Synthesis and characterization of colloidal gold

Colloidal gold was synthesized according to the procedure described by Turkevich et al. [21] using a reduced scale. An aqueous solution of chloroauric acid (5 mM  $\text{HAuCl}_4 \cdot 3\text{H}_2\text{O}$ , 5 ml) was diluted with 90 ml of deionized water. This solution was stirred and heated until boiling and then reduced with 0.5% sodium citrate solution (5 ml). Heating was continued until the solution color changed to a red-purple color.

## 2.7. Formation of gold conjugate

Polyclonal antibodies were diluted in 5 ml of 5 mM sodium borate buffer pH 9.0 in order to obtain 2.5 mg/ml of immunoglobulins. This solution was then added dropwise to a stirred solution of colloidal gold 0.25 mM, 100 ml. The pH of the colloidal gold solution was pre-adjusted to 7.0 by addition of 0.01 M  $\text{Na}_2\text{CO}_3$ . The mixture was stirred for 30 min and 5 ml of 5% BSA in 5 mM NaCl solution was added. After 5 min, the solution was centrifuged at 4 °C 14,000 rpm for 30 min to

remove unconjugated antibodies from the solution. The pellet was subsequently resuspended in Phosphate Gold Diluent buffer (1% BSA in 49 mM  $\text{Na}_2\text{HPO}_4$ ) to obtain an antibody–colloidal gold conjugate solution which had an O.D. of 40 at  $\lambda$  580 nm.

## 2.8. Characterization of colloidal gold conjugates

### 2.8.1. Transmission electron microscopy (TEM)

The size and shape of colloidal gold with and without conjugated antibodies bound were compared using TEM measurements. The TEM samples were prepared by placing a drop of the colloidal gold in acetone/ $\text{H}_2\text{O}$  mixture onto a carbon-coated TEM copper grid. The resulting film was allowed to dry overnight and then used for TEM imaging. TEM microscope was operated at an acceleration voltage of 120 kV and at a magnification of 80,000. The size distributions of the particles from enlarged photographs of the TEM images were measured using at least 150 counts of the particles. A selected area diffraction (SAD) pattern of a colloidal gold particle containing antibodies was taken directly from the corresponding TEM image and the resulting diffraction pattern was indexed according to a standard procedure [22].

### 2.8.2. UV–vis spectroscopic studies

The formation of antibody–colloidal gold conjugates was monitored by UV–vis spectroscopy using a double beam spectrophotometer. The UV absorption of the colloidal gold and antibody–colloidal gold solution (0.5 mM in aqueous) were monitored immediately after preparation at  $\lambda$  200–700 nm.

## 2.9. Preparation of an immunochromatographic (IC) strip test

An IC test strip was developed using rabbit anti-NVP polyclonal antibodies conjugated with colloidal gold particles (anti-NVP–CGC). A lateral flow test strip was constructed as follows:

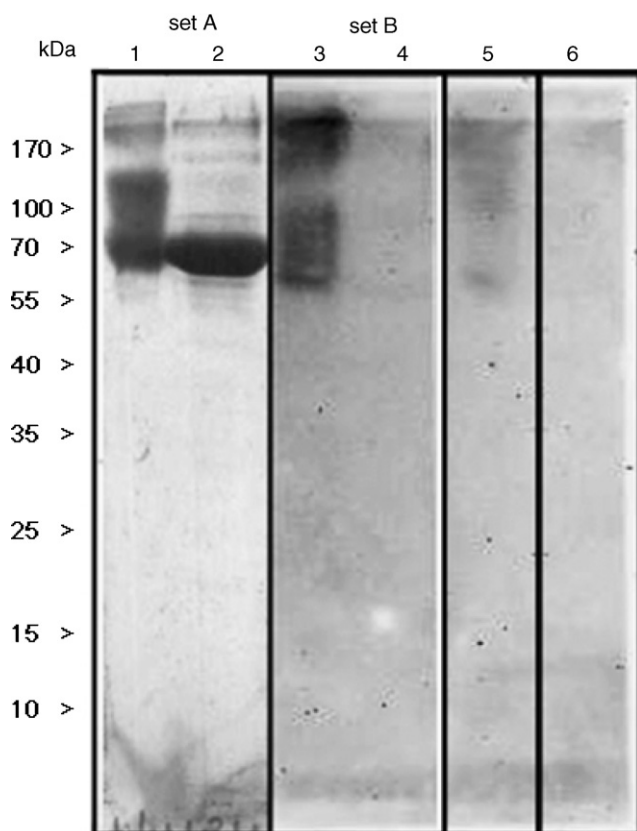


Fig. 1. Western immunoblotting analysis of NVP–BSA and BSA alone using the rabbit hyperimmune serum. Lanes 1, 3, 5 and 6 were NVP–BSA separated under denaturing condition. Lanes 2 and 4 were unconjugated BSA separated under denaturing condition. Set A was stained with Amido black B for protein detection on blotting membrane. Set B was reacted with rabbit serum (dilution 1:2000). Lane 5 was probed with rabbit serum mixed with NVP (10  $\mu\text{g}/\text{ml}$  final concentration). No rabbit serum was added to lane 6. The HRP–swine anti-rabbit immunoglobulin conjugate was applied to all lanes. Molecular weight markers (in kilodaltons) are indicated.

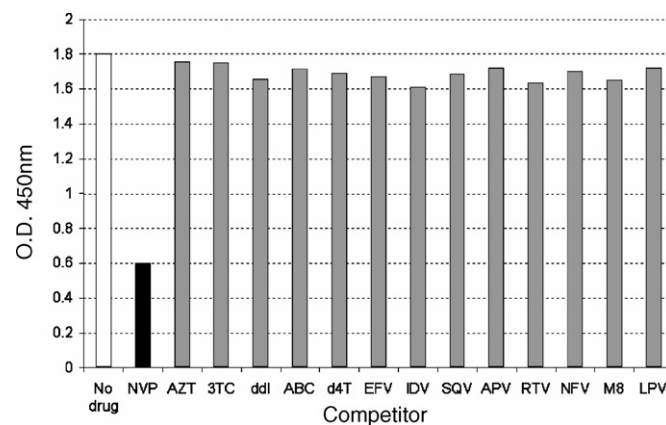


Fig. 2. Assessment of the rabbit anti-NVP polyclonal antibodies by competitive indirect ELISA with various anti-HIV drugs at 10  $\mu\text{g}/\text{ml}$ . This experiment was performed in triplicate and a similar absorbance pattern was observed (see Section 2.5.2 for drug names).

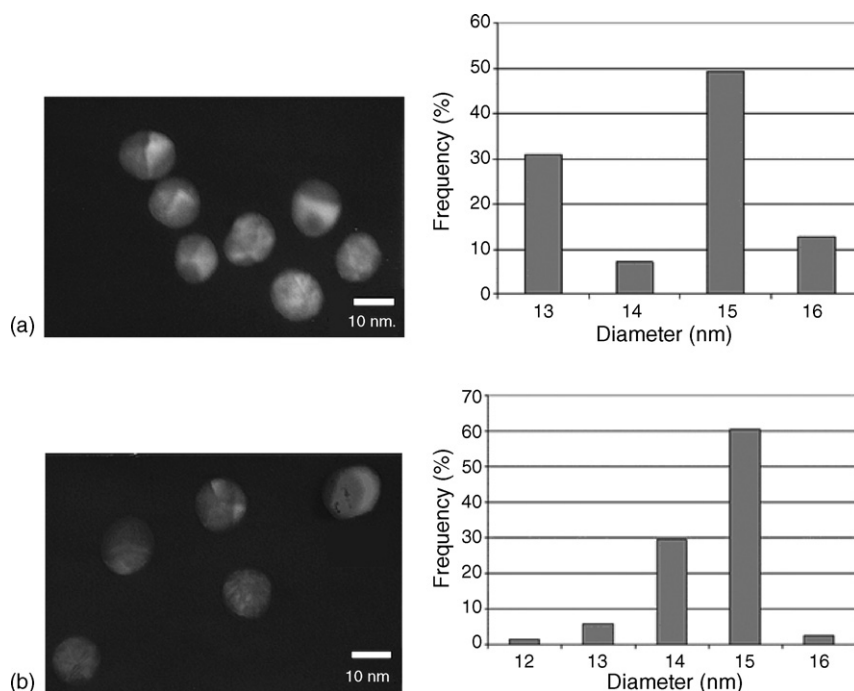


Fig. 3. TEM images and size distribution of (a) unconjugated colloidal gold particles (b) conjugated antibody-colloidal gold particles. For particle size comparison, the 10-nm-scale marker is indicated.

anti-NVP-CGC (O.D. of 40 at  $\lambda$  580 nm) was jetted onto a glass fiber (conjugate pad) by an isoflow dispenser (Imagene Technology, USA). The nitrocellulose membrane (Scheicher and Schuell, Germany) was laminated on a plastic support by a Precision Laminator (Zeta Corporation, Korea). NVP-BSA at 1.0 mg/ml and goat anti-rabbit IgG (KPL, USA) at 0.5 mg/ml in PBS were jetted onto a laminated nitrocellulose membrane at two separate zones; test line and control line, respectively. Subsequently, the conjugate pad and jetted membrane were incubated for 2 h at 37 °C and then dried in a desiccator at room temperature. After drying, the components of strip, i.e., sample

application pad, anti-NVP-CGC sprayed conjugate pad, jetted nitrocellulose membrane and absorbent pad were assembled and then cut into individual strips (3.5 mm/strip), using a strip cutter (INDEX CUTTER, USA).

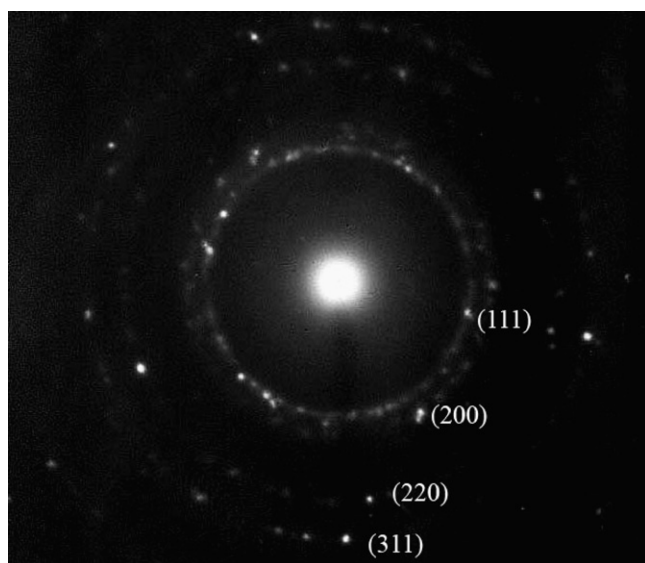


Fig. 4. Selected area diffraction (SAD) pattern derived from a conjugated antibody-colloidal gold particle.

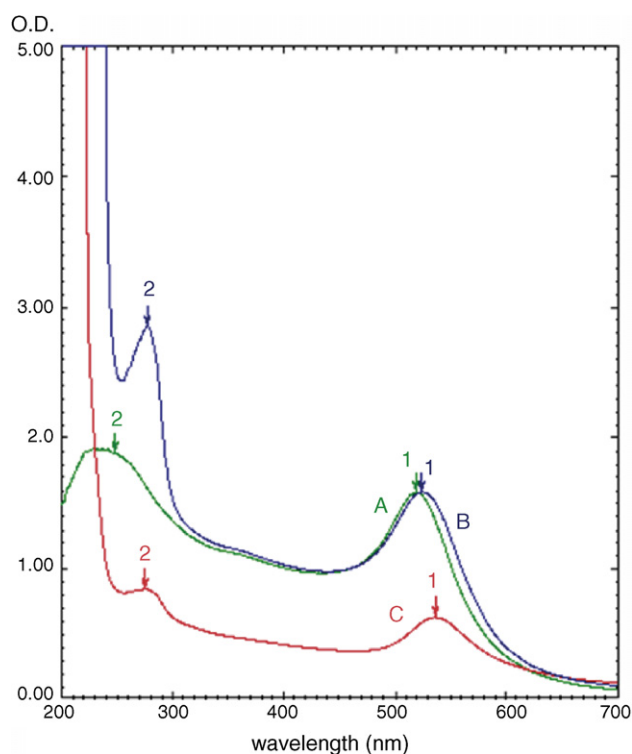


Fig. 5. UV-vis spectra of colloidal gold and antibody-colloidal gold conjugates. Curve A, colloidal gold solution; curve B, anti-NVP-CGC immediately after addition of antibody to gold solution; Curve C, anti-NVP-CGC after centrifugation to remove the unbound antibodies.

### 2.10. Detection of NVP by the Immunochromatographic strip test

Analysis of NVP by the IC strip test was performed by dipping the strip into standard solutions of NVP in PBS buffer pH 7.4 at 0, 0.1, 0.5, 1.0 and 3.0  $\mu\text{g/ml}$ . The result was interpreted after a red-purple color appeared at the control line. At the test line, the presence of a red-purple color suggested no NVP was present in the sample and vice versa.

### 2.11. Cross-reactivity of the NVP immunochromatographic test strip

The procedure was performed as described in Section 2.10 excepted that the IC strip test was dipped into NVP and a set of commonly coadministered antiretroviral drugs in PBS buffer pH 7.4. A high drug concentration of 10  $\mu\text{g/ml}$ , which is near the maximum concentration achieved in plasma for many of the antiretroviral drugs, was used. The drugs tested are described in Section 2.5.2. To evaluate the potential influence of the plasma matrix on the strip, human plasma spiked with 5.0  $\mu\text{g/ml}$  of NVP was tested along with blank human plasma.

## 3. Results and discussion

### 3.1. Synthesis of NVP–BSA conjugate

NVP–BSA conjugate was synthesized according to Scheme 1 and the structures of the NVP linked methyl ester (compound 1) and the NVP linked carboxylic acid (compound 2) were confirmed by NMR (see Section 2.3).

### 3.2. Validation of polyclonal antibodies

Western immunoblotting in Fig. 1 showed immunoreactive bands of the synthesized NVP–BSA (lanes 1, 3, 5 and 6) in comparison with unconjugated BSA (lanes 2 and 4). NVP–BSA and BSA protein bands were observed in lanes 1 and 2 (set A) by Amido black B staining. The major protein band of BSA was located at 66 kDa. The proteins with higher molecular weight were regarded as impurities from the partially purified BSA fraction. Following incubation with rabbit serum (dilution 1:2000, Set B), the presence of polyclonal anti-NVP antibodies in the serum was demonstrated by the positive signal observed with NVP–BSA (lane 3). No signal was observed with BSA alone (lane 4). This result suggested that anti-BSA antibodies present

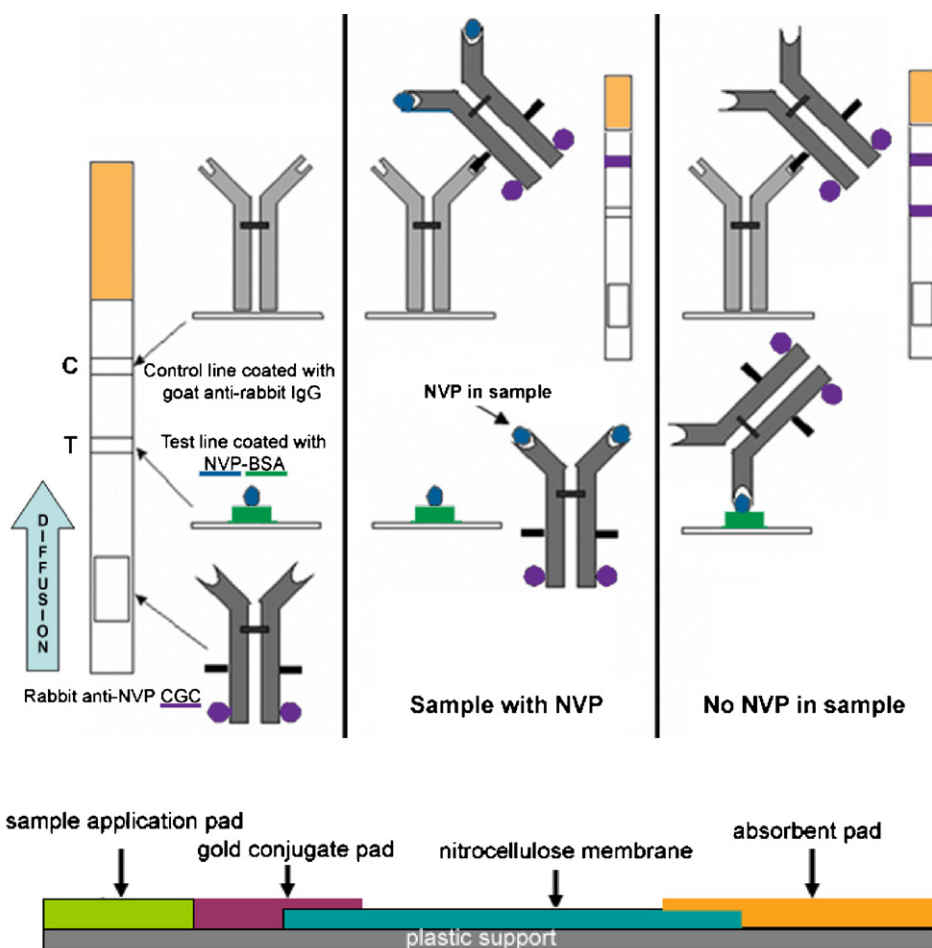


Fig. 6. Configuration of the IC NVP strip test. The schematic diagram shows the areas where rabbit anti-NVP–CGC, NVP–BSA and goat anti-rabbit IgG are immobilized (left panel). The reactions which occur on the IC strip in the presence of NVP (middle panel), and in the absence of NVP (right panel) are shown. A red-purple color appears at the test and/or control lines depending on the presence of NVP.



in the hyperimmune serum were neutralized by BSA in the serum diluting buffer. Furthermore, mixing the hyperimmune serum with 10  $\mu\text{g/ml}$  NVP reduced the intensity of the 66 kDa band and the higher molecular weight proteins (lane 5) confirming the presence of polyclonal anti-NVP antibodies.

The specificity of antibodies was analyzed by competitive indirect ELISA (Fig. 2). Several commonly administered anti-HIV drugs (AZT, 3TC, ddI, ABC, d4T, EFV, IDV, SQV, APV, RTV, NFV (plus NFV metabolite, M8) and LPV) were tested. The O.D. of the well containing NVP as the competitor was significantly lower than that obtained in the control well (no drug). In contrast, the O.D. of the wells with the other antiretroviral drugs was similar to the control well. This data suggested that the anti-NVP antibodies produced were highly specific to NVP.

### 3.3. Characterization of the colloidal gold particles and antibody–gold conjugates

#### 3.3.1. TEM imaging

The TEM images of gold colloid and anti-NVP–CGC are shown in Fig. 3(a and b). Both forms of gold particles were homogeneous in size and shape, and there was no marked difference in the size distribution of colloidal gold before and after conjugation. The gold particles obtained showed narrow size distribution with a mean diameter of  $15.0 \pm 3.05$  nm and this is within the typical range of colloidal gold used in IC assays (10–20 nm) [23]. The selected area diffraction (SAD) pattern taken from an antibody gold particle (Fig. 4) shows the central intense direct beam and an array of diffraction spots from different atomic planes. These spots were assigned to the 1 1 1, 2 0 0, 2 2 0 and 3 1 1 planes of a face centered cubic (fcc) lattice of gold, according to JCPDS File No. 4-784 [24]. This result confirms that colloidal gold was successfully produced.

#### 3.3.2. UV–vis spectra

The presence of antibody on the gold surface was characterized using UV–vis spectroscopy. Spectra of the colloidal gold solution were recorded without antibody and immediately after the addition of antibody (Fig. 5a and b). A peak at  $\sim 519$  nm in curve A was due to surface plasmon resonance of colloidal gold. Immediately following the addition of antibody (curve B), red shift of this band occurred as a result of antibody–colloidal gold interaction and a new band appeared at  $\sim 280$  nm which corresponded to a protein absorption band. After centrifugation and removal of unbound antibody from antibody–colloidal gold conjugate (curve C) showed two absorption bands at  $\sim 510$  and 280 nm indicating that antibody was presented on the gold surface. The absorption band at 510 nm was much lower for the antibody–colloidal gold conjugate than for the unbound colloidal gold as some gold particles were lost during the washing step to remove unbound antibodies.

### 3.4. Construction of Immunochromatographic strip test system using anti-NVP–CGC

A schematic diagram showing the areas where the components are immobilized on the IC-test strip is illustrated in Fig. 6.

Dipping the strip into a test solution will cause the liquid to move upward by capillary action and dissolve the dried rabbit anti-NVP–CGC on the conjugate pad. The anti-NVP–CGC complex subsequently migrates up the surface of nitrocellulose membrane. If no NVP is present in the sample, rabbit anti-NVP–CGC will bind to NVP–BSA streaked at the test line (T). The immobilized anti-NVP–CGC generates a red-purple color line caused by colloidal gold particle accumulation. In contrast, if the sample contains NVP, rabbit anti-NVP–CGC will be neutralized by free NVP. Consequently, the intensity of the red-purple color observed will be reduced. For the control line (C), a red-purple color will appear independently of the presence of NVP in the test sample since the amount of rabbit anti-NVP–CGC is in excess. When the rabbit anti-NVP–CGC reaches C, it will be captured by the goat anti-rabbit IgG. The control line is used to monitor whether the anti-NVP–CGC has passed over the test line and the result can be interpreted.

### 3.5. Analysis of NVP standards with the IC test strips

Results from the IC strip assessing NVP in PBS are shown in Fig. 7. In the absence of NVP, the binding of anti-NVP–CGC with the solid-phase NVP–BSA produced an intense red-purple



Fig. 7. IC strip test results at NVP concentrations of 0, 0.1, 0.5, 1.0 and 3.0  $\mu\text{g/ml}$  in PBS pH 7.4. C, control line; T, test line.

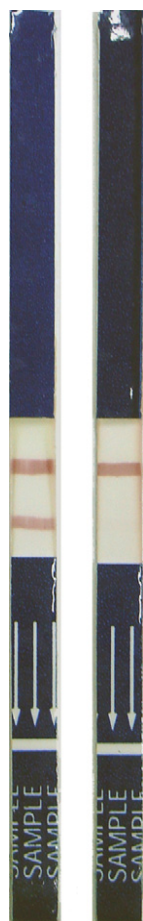


Fig. 8. Evaluation of IC strip with blank human plasma (left strip) and human plasma and spiked with NVP at a concentration of 5.0 µg/ml (right strip).

band at the test line. The intensity of the color faded when the concentrations of NVP were increased. At NVP concentrations of 1.0 and 3.0 µg/ml, no color was observed at the test line. The limit of NVP detection in PBS using the IC strip test was 1.0 µg/ml. The results of the IC strip test could be read within 10 min.

To determine if components in the plasma matrix could interfere with the IC strip test result, human plasma spiked with NVP at a therapeutic drug concentration of 5.0 µg/ml, in addition to blank human plasma were tested. The results showed that NVP could be detected and no interference of the plasma matrix in blank samples was observed (Fig. 8); however, clearly assessment of the strip in plasma samples from HIV-infected patients receiving HAART needs to be conducted.

### 3.6. Cross reactivity test of the IC strip test

To study the effect of other commonly administered anti-HIV drugs on the IC strip test, twelve other HIV drugs (AZT, 3TC, ddI, ABC, d4T, EFV, IDV, SQV, APV, RTV, NFV and LPV) were tested. A high drug concentration of 10 µg/ml, which is near the maximum concentration achieved in plasma for many of the antiretroviral drugs, was used. The intensity of red-purple color at test line was as the similar to that observed in the absence of NVP (data not shown). This suggested that the presence of

these antiretroviral drugs in a test sample will not interfere with the detection of NVP.

## 4. Conclusion

Herein, we have successfully developed an IC strip test for the rapid detection of NVP. Preliminary results show that it was possible to detect the presence of NVP at a concentration as low as 1.0 µg/ml in PBS, and no cross-reactivity from other commonly administered HIV drugs or components in the human plasma was observed. Following the standard nevirapine 200 mg twice daily dose, plasma nevirapine concentrations range between 3.0 and 10.0 µg/ml, thus the IC test strip should be able to detect NVP concentrations in patients using a NVP based HAART regimen. The established assay is simple and easy to interpret without requirement of any sophisticated instruments. This low cost method could be routinely used in developing countries for drug adherence purposes (potentially including urine specimens) and TDM, and could be extended to other anti-HIV drugs, in particular the protease inhibitors where high interpatient variability has been reported and the use of TDM has been suggested [5]. Overall, this report describes the construction and preliminary assessment of the first immunochromatographic strip test for nevirapine but detailed assessment of this IC strip in plasma samples from HIV-infected patients receiving HAART is needed.

## Acknowledgements

This work was supported by the Institut de Recherche pour le Développement (IRD), UR 174, Program for HIV Prevention and Treatment (PHPT), *i*+MED LABORATORIES, Thailand, and The Thailand Research Fund.

## References

- [1] F. van Leth, P. Phanuphak, K. Ruxrungtham, et al., *Lancet* 363 (2004) 1253.
- [2] M. Lallemand, G. Jourdain, S. Le Coeur, et al., *N. Eng. J. Med.* 351 (2004) 217.
- [3] D.D. Richman, D. Havlir, J. Corbeil J, et al., *J. Virol.* 68 (1994) 1660.
- [4] A.I. Veldkamp, G.J. Weverling, J.M. Lange, et al., *AIDS* 15 (2001) 1089.
- [5] D. Back, G. Gatti, C. Fletcher, et al., *AIDS* 16 (Suppl. 1) (2002) 5.
- [6] P.W. Hugen, D.M. Burger, R.E. Aarnoutse, et al., *Ther. Drug Monit.* 24 (2002) 579.
- [7] B.S. Kappelhoff, H. Rosing, A.D. Huitema, J.H. Beijnen, *J. Chromatogr. B Analyt. Technol. Biomed. Life Sci.* 792 (2003) 353.
- [8] W. Egge-Jacobsen, M. Unger, C.U. Niemann, et al., *Ther. Drug Monit.* 26 (2004) 546.
- [9] J.G. Dubuisson, J.R. King, J.S.A. Stringer, M.L. Turner, C. Bennetto, E.P. Acosta, J. Acquir. Immune Defic. Syndr. 35 (2004) 155.
- [10] S. Azoulay, M.C. Nevers, C. Créminon, *Antimicrob. Agents Chemother.* 48 (2004) 104.
- [11] S.H. Paek, C.W. Lee, S.H. Yook, O.H. Kwon, Y.N. Park, *Anal. Lett.* 32 (1999) 335.
- [12] S.H. Paek, S.H. Lee, J.H. Cho, *Methods* 22 (2000) 53.
- [13] D.J. Chiao, R.H. Shyu, C.S. Hu, H.Y. Chiang, S.S. Tang, *J. Chromatogr. B Analyt. Technol. Biomed. Life Sci.* 809 (2004) 37.
- [14] Y.J. Cho, D.H. Lee, D.O. Kim, W.K. Min, K.T. Bong, G.G. Lee, J.H. Seo, *J. Agric. Food Chem.* 53 (2005) 8447.



- [15] I.A. Liubavina, A.A. Zinchenko, I.S. Salomatina, A.V. Zherdev, B.B. Dzantiev, *Bioorg. Khim.* 30 (2004) 201.
- [16] B. Johne, K. Hansen, E. Mark, J. Holtlund, *J. Immunol. Methods* 183 (1995) 167.
- [17] W.P. Faulk, G.M. Taylor, *Immunochemistry* 8 (1971) 1081.
- [18] U.K. Laemmli, *Nature* 227 (1970) 680.
- [19] H. Tawbin, T. Stachelin, J. Gordon, *Proc. Nat. Acad. Sci.* 76 (1979) 4350.
- [20] E.P. Acosta, J.R. King, *Clin. Infect. Dis.* 36 (2003) 373.
- [21] M. Turkevich, P.L. Stevenson, J. Hillier, *Discuss. Faraday Soc.* 11 (1951) 55.
- [22] D.B. Williams, C.B. Carter, *Transmission Electron Microsc. Diffraction II* N.Y. (1996) 265–287.
- [23] X. Sun, X. Zhao, J. Tang, Z. Jun, F.S. Chu, *Int. J. Food Microbiol.* 99 (2005) 185.
- [24] JCPDS Powder Diffraction File: Inorganic Phases, International Centre for Diffraction Data, Swarthmore, Pennsylvania, 1985.

## Complementarity of XRFS and LIBS for corrosion studies

J.A. Pérez-Serradilla, A. Jurado-López, M.D. Luque de Castro\*

*Department of Analytical Chemistry, Annex C-3, Campus of Rabanales, E-14071 Córdoba, Spain*

Received 30 January 2006; received in revised form 3 March 2006; accepted 10 March 2006

Available online 27 April 2006

### Abstract

A study of ancient coins with different corrosion degrees and the same or different composition has been carried out by using energy-dispersive X-ray fluorescence spectrometry (XRFS) and laser-induced break-down spectroscopy (LIBS). The results obtained show the complementarity of both techniques: XRFS provides information about the superficial composition which is used for the assignation of atomic lines in LIBS, and this provides in-depth and tomographic information. Thus, some very superficial impurities such as Ag, Cl, Au, Sr and Sb are only detected by XRFS, while highly corroded coins of iron-based alloy provided no iron signal by XRFS but increased concentration of this element up to constant composition by LIBS by increasing the shot number. The average of the same laser-shot number for all sampling positions of a sampling zone produces a significant improvement of the signal-to-noise ratio (SNR) in the detriment of punctual information as that obtained by single-position kinetic series.

© 2006 Published by Elsevier B.V.

*Keywords:* XRFS; LIBS; Screening; Corrosion

### 1. Introduction

The required analytical information from a target sample may not be provided by a single technique owing to the complexity of the sample and/or the nature of the demanded information. These cases make mandatory the combined use of two or more complementary techniques to fulfil the analytical requirements.

Laser-induced breakdown spectroscopy (LIBS) is a well-known atomic emission spectroscopic technique for elemental analysis of materials, which provides qualitative, semi-quantitative, and even quantitative information if appropriate standards are available [1]. Recently published reviews on this technique show the diversity of its analytical applications, a consequence of LIBS characteristics, namely: (1) capability for multi-elemental analysis; (2) nil or minimal sample preparation; (3) applicability to solid samples (nevertheless, gasses [2] and liquids [3] can also be analysed); (4) small amount of sample; (5) negligible sample damage, practically invisible to the naked eye; (6) surface and in-depth information with spatial resolution across the surface nearly to microscopic [4–6]. Nevertheless, the sensitivity of LIBS makes necessary the use of powerful lasers –

which in turn can deteriorate seriously the sample, especially if this possesses a soft surface and several shots are delivered in the same position – for low concentrated analytes; its poor precision and the lack of standards – this last a shortcoming characteristic of direct analysis of solids – restrict LIBS applicability.

X-ray fluorescence spectrometry (XRFS) can complement LIBS thanks to its non-destructive character, minimal or none sample preparation required and capacity to provide screening information of the sample surface without necessity for standards. Despite lateral spatial resolution of XRFS is rather poor (between 1 and 5 mm), and in-depth analysis is limited to a very thin surface layer because scant penetration depth (scarcely 100  $\mu\text{m}$ ) of X-rays [1], this technique is usually adequate for the accurate analysis of homogeneous and coated samples, when coatings range from 0.1 to a few  $\mu\text{m}$ . In these cases both the coating thickness and chemical composition of the underneath material can be determined. However, corroded samples yield erroneous results.

There are a number of analysis areas (namely, jewellery industry, art, archaeological [7], coating and corrosion studies) where distinction between surface and bulk composition is of paramount importance. The use of XRFS in these fields makes mandatory polishing the superficial layer after surface analysis for subsequent in-depth analysis, which can cause a significant or dramatic damage to the sample.

\* Corresponding author. Tel.: +34 957 218615; fax: +34 957 218615.  
E-mail address: [qa1lucam@uco.es](mailto:qa1lucam@uco.es) (M.D. Luque de Castro).

The joint use of XRFS and LIBS can be complementary as the former provides screening information of the sample surface and the latter in-depth and spatial resolution. The complementarity of these techniques can be of special interest in corrosion studies, as is the case with ancient coins, which often exhibit different corrosion degree depending on the alloy, the conditions to which the coin has been subjected and its age. Coins of historical value must not be polished; thus, alloy composition of the coin bulk cannot be determined by XRFS; on the other hand, LIBS can provide in-depth resolution of the corroded zone, but low-power laser-shots may be used in order to obtain the required shot-to-shot information of this soft zone, but sensitivity cannot be enough, particularly in the most external, more corroded layer.

This research has been aimed at demonstrating the complementary use of LIBS and XRFS for corrosion studies, for which six ancient coins with different corrosion degree have been used.

## 2. Experimental

### 2.1. Instrumentation

#### 2.1.1. LIBS

The experimental set-up to carry out the laser-induced breakdown spectrometric method is depicted in Fig. 1, and was as follows: a Minilite II pulsed Nd:YAG laser (Continuum; Santa Clara, CA, USA) was used as excitation source, operating at the first harmonic, wavelength 532 nm, and at 1 Hz repetition frequency. As the laser module does not permit to change the beam energy, it was modified by the joint use of (a) a pin-hole (70 mm diameter) at the output of the resonance chamber; (b) a 33 mm focal length plane-convex lens (Oriel; Stratford, USA), 36 mm outside diameter, 2–36 mm aperture range to disperse the beam (ca. 3 mm size at the output); and (c) an iris diaphragm set on its lowest aperture (2.5 mm i.d.) to control the beam size; thus, the beam energy was 1.3 mJ. The pulse energy was measured with a ED-200L pyroelectric joulemeter (Gentec, Palo Alto,

CA, USA), nominal sensitivity of  $9.86 \text{ V J}^{-1}$ , coupled to a TDS 380 digital real-time oscilloscope (Tektronix, Wilsonville, OR, USA). The beam was guided to the sample with a flat aluminised mirror (Oriel, 50 mm  $\times$  50 mm, coated with aluminium and over coated with  $\text{MgF}_2$ ) and focused at normal incidence on the target by a 135 mm focal length plane-convex lens (Melles-Griot, 25 mm in diameter). Under these experimental conditions, the irradiance on the target was  $1.7 \text{ W cm}^{-2}$ . The radiation emitted by the plasma was collected and transmitted by an Oriel 77564 fused silica fiber optic to an Oriel 77400 Czerny-Turner 1/8 m MS125 spectrograph, equipped with an Oriel 77220 entrance slit of 25  $\mu\text{m}$  and an Oriel 77420 grating of 2400 grooves  $\text{mm}^{-1}$ . The spectrograph resolution was 0.2 nm. The linear dispersion was 3.5 nm  $\text{mm}^{-1}$ . The detector was an Andor-Oriel, Instaspec IV, 78430-V charge-coupled device, which consists of 1024  $\times$  128 elements and a total photoactive area of 26  $\mu\text{m}^2$ , connected via a 16-bit ISA card to a Pentium II microprocessor computer. Calibration of the detector was carried out with a laser-induced emission spectrum of tin. A multiple I/O box (Oriel, IO-140) allowed the connection between the Instaspec card and the laser power supply in order to synchronise the Q-switch with data acquisition. The plasma emission signal was integrated using an acquisition time of 17 ms and corrected by subtraction of the dark signal. Interference of the continuum radiation emitted at the earliest stage of laser-induced plasma was decreased by baseline correction. The sample was placed in a manual X-Y-Z translation stage (Oriel, Model 16921), which made possible sample manipulation as required. A 13.5 mm longitudinal movement could be achieved for the three axes with a mechanical resolution of 10  $\mu\text{m}$ . An M5L/50 optical distance laser sensor (Mikroelektronik, Germany) was used for reproducible positioning of the sample based on the triangulation principle.

Andor CCD software (Andor Technology, version 2.0) was used for management of the detection system. Each LIBS spectrum was displayed on the computer screen and stored for subsequent data handling. Data treatment was carried out by Microsoft Excel (version 2003).

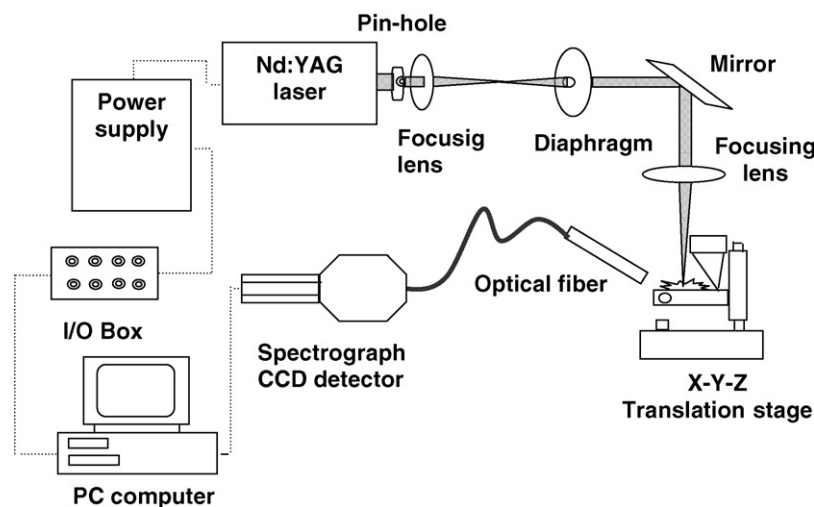


Fig. 1. Experimental set-up for LIBS.

### 2.1.2. XRFS

An energy-dispersive Fischerscope X-ray XAN spectrometer (Helmut Fischer GmbH+Co. KG, Sindelfingen, Germany) was used in this study. It consists of an X-ray tube with a tungsten anode (50 kV/0.8 mA) and a silicon semiconductor detector (Peltier cooling at  $-30^{\circ}\text{C}$ ; energy resolution 200 eV). The chamber dimensions ( $H \times W \times D = 90 \text{ mm} \times 320 \text{ mm} \times 460 \text{ mm}$ ) enable the analysis of moderate large samples. A colour video microscope allows the selection and view of the irradiated area with up to  $25\times$  magnification. The spectrometer is equipped with two primary filters, one of aluminium and the other of nickel.

Helmut Fischer software (WinFTM XAN, version 6.05-PDM) was used for management of the detection system.

The samples were analysed using an algorithm based on Fundamental Parameters.

### 2.2. Samples

Six XVIIIth century ancient coins provided by the Archaeological Museum of Montilla (Spain) were used for this research and subjected to the analytical procedure. These samples were split into two groups, each corresponding to a coin series with identical or very similar composition but different corrosion degree; namely, coin series I, made up of coins 1, 2 and 3; coin series II, made up of coins 4, 5 and 6.

### 2.3. Analytical procedure

#### 2.3.1. XRFS data acquisition and treatment

The first step was collection for 60 s of the XRFS spectrum within a 2 mm diameter circumference for each coin in a sampling zone at the centre of the coin.

Semiquantitative XRFS data treatment was carried out by the fundamental parameters method, an atomic physics algorithm that theoretically describes the interaction between the instrument and the analytes. It basically interprets the processed X-ray spectra into elemental composition, taking into account the physical parameters of the spectrometer (namely, generation of primary X-rays from the X-ray tube, secondary fluorescent X-ray production in the sample, inter-element matrix effects and detection of the emitted X-rays) [8].

#### 2.3.2. LIBS data acquisition and treatment

Each sampling zone was divided into 36 sampling positions with  $250 \mu\text{m}$  separation between them, as can be seen in Fig. 2. Thirty-six kinetic series, composed by 59 spectra each, were

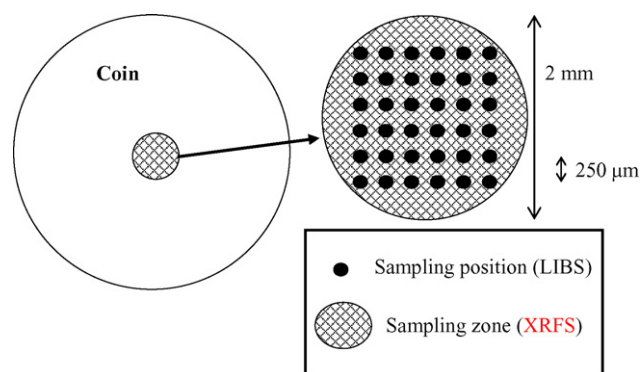


Fig. 2. Distribution of sampling positions within a sampling zone.

obtained by delivering 60 laser shots at each sampling position and deleting the spectrum from the first shot, which was not reproducible. The spectral region selected for collecting plasma emission measurements was 255–332 nm. The analytical signals were used after background correction of the raw spectroscopic data. The plasma emission lines from each element were compared with those from tabulated data to carry out both qualitative analysis and in-depth characterisation [9,10].

After the 36 kinetic series, each composed by 59 spectra, were obtained from the 36 sampling positions, the spectrum from a given shot number in a sampling position was averaged with all spectra from the same shot number in the other kinetic series. In other words, 2124 spectra (59 spectra from each of the 36 sampling positions) were averaged in order to achieve 59 spectra which made up new kinetic series as layer average from the 36 original kinetic series. The data treatment results in these new kinetic series, which will be named as *layer averaged kinetic series*. Contrarily to the widely reported single-shot spectra accumulation [11–15], in which a number of spectra obtained from a given sampling position are accumulated in order to increase the signal-to-noise ratio (SNR) at the expenses of in-depth information, the spectra from different sampling positions are shot-to-shot averaged in *layer averaged kinetic series* so that the in-depth information is retained and the SNR is improved at the expenses of in layer information as the overall sampling zone is layered as a whole.

## 3. Results and discussion

### 3.1. XRFS studies

All samples were analysed by XRFS following the procedure as described in Section 2 and the results obtained are shown in

Table 1  
Element composition obtained by XRFS analysis of the samples

Sample	Cu (%)	Zn (%)	Fe (%)	As (%)	Pb (%)	Ca (%)	Ag (%)	Au (%)	Sr (%)	Sb (%)	Cl (%)
Coin 1	81		1	3	3	10	<1	< 1	< 1	1	
Coin 2	91			1	<1	7	<1			<1	
Coin 3	86		<1	6		<1	<1			<1	6
Coin 4	78	18		<1	3	<1	<1				
Coin 5	62	31	<1	<1	2	4	<1				
Coin 6	78	7	<1	<1	3	3	<1				8

**Table 1.** Oxygen and sulphur have not been taken in this table as XRF does not provide information about them.

### 3.2. LIBS studies

#### 3.2.1. Preliminary experiments

Owing to both the low-laser energy used in order to obtain in-depth resolution and the high corrosion degree of the samples, the lines of the LIBS spectra showed poor SNR, making identification of the lines attributable to impurities very difficult. For this reason, the *layer averaged kinetic series* approach was designed taking into account the randomized nature of noise, which makes the different noise spectra cancel each other by spectra averaging, whereas the atomic lines do not suffer cancellation as their appearance in the spectrum is not randomized, thus improving the SNR (this parameter was calculated from the noise within a spectral zone where the atomic lines are absent [16,17]) by the *layer averaged kinetic series* with respect to the best SNR from the spectrum from a single sample position.

The *layer averaged kinetic series* provide layer-by-layer information about the overall sampling zone; thus, as the impurities distribution can vary from sampling position to sampling position, the atomic lines from impurities appeared in a *layer averaged kinetic series* are not necessarily present on the whole sampling zone layer.

#### 3.2.2. Study of the variables influencing LIBS

The three main parameters influencing plasma formation (namely, laser wavelength, laser energy and working distance) were studied.

**3.2.2.1. Selection of laser wavelength.** Between the four wavelengths available from the Nd:YAG laser (namely, 1064, 532, 355 and 266 nm), that at 532 nm was selected for present study since the optical elements required by the system are of lower cost than those required in the UV region; furthermore, the beam trajectory is easily observed, thus decreasing safety problems.

**3.2.2.2. Selection of laser energy.** The dissociation and excitation of the ablated mass, and therefore, the spectral emission intensity, are dependent on the plasma temperature. This temperature is significantly increased by increasing laser energy; consequently, higher laser energy improves sensitivity [18], decreases in-depth-resolution and produces higher sample deterioration. As in-depth resolution is of crucial importance in corrosion evaluation, the rough and porous nature of the corrosion film made convenient to reduce the laser energy to 1.3 mJ, which was made by using a pin-hole, a lens and an iris diaphragm due to the absence of an energy selector in the laser device [19]. This energy is appropriate to achieve in-depth resolution in the target samples. Usually, this energy is not enough to obtain measurable atomic lines when oxidized samples are involved owing to the low relative concentration of metals in oxidized layers as compared with unaltered samples; but both the LIBS data treatment used in this research and the information from the XRF spectra (from which the search for low-intensity lines in the LIBS spectra was carried out) makes possible to obtain suitable

information from very damaged samples using very low laser energy.

**3.2.2.3. Selection of the working distance.** The distance between the focusing lens and the sample surface – known as working distance (WD) – dramatically influences the shape of the ablation crater, which, for a given energy per pulse, is significantly deeper when the WD coincides with the focal length than when the beam is defocused. As for a better in-depth resolution a defocused beam is needed, a WD = +2 mm was selected, which was easily reproduced by using a distance sensor.

#### 3.2.3. Tomographic studies

The spectral lines selected for the tomographic study of components distribution were 324.85 nm for Cu, 330.35 nm for Zn, 260.02 nm for Fe, 318.03 nm for Ca, 288.53 nm for As and 283.30 nm for Pb, which were simultaneously monitored as a function of the laser shot. Nevertheless, some other elements such as Ag, Au, Cl, Sr and Sb, identified in the coins by XRF, were not detected by LIBS.

LIBS sampling required a lateral displacement of 250  $\mu\text{m}$  (see Fig. 2) between adjacent craters to avoid contamination from sampling-to-sampling positions during ablation, as well as to obtain a representative sampling area of the target with enough lateral resolution.

General restrictions of LIBS owing to the strong dependence of the ablation process on certain physico-chemical properties of the sample (to be taken into account in this study) are as follows:

- The ablation of targets with different elements proportion produce variations in the amount of material ablated by each laser shot; so the number of laser shots required to penetrate each corrosion layer can be considered only as approximately indicative of its thickness.
- Standards of known composition and matrix similar to that of the samples (which are difficult to obtain) are required for quantitative studies.

**3.2.3.1. Determination of coin composition.** In-depth profiles (plots of signal intensity versus shot number) were carried out using the *layer averaged kinetic series* for each element detected by LIBS, namely: Cu, Zn, Fe, Ca, As and Pb. Representative examples of the profiles of the main components in both coin series (namely, Cu and Fe in coin series I and Cu, Fe and Zn in coin series II) appear in Fig. 3.

In-depth profiles were quite similar in both groups of samples, possibly due to the fact that the six coins were found in the same site and belonged to the same century (according to the information provided by the Archaeological Museum of Montilla, Spain) and, therefore, affected by similar corrosion processes.

Fig. 3 shows that the atomic line monitored for Cu reaches a maximum at 10–15 shots and then decreases slightly, meanwhile the atomic lines monitored for Fe (in the two coins series) and Zn (only present in coin series II) increase up to the shot 15–30 and levelled off for higher shot number. The first increase in the atomic lines of the three elements may be ascribed to decreased corrosion as the depth of the crater increases. The subsequent



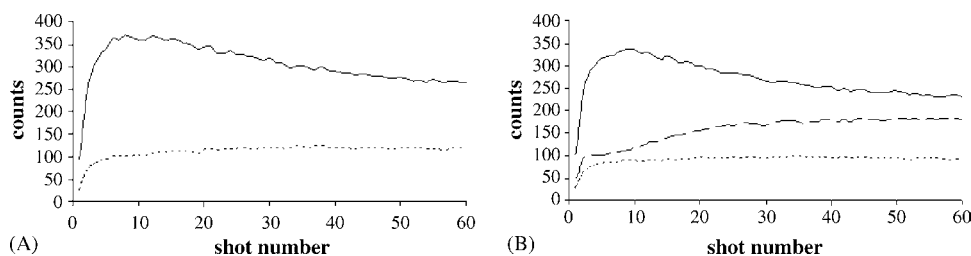


Fig. 3. In-depth profiles of the main elements in the coins: (—) copper, (· · ·) iron, (---) Zn. Profiles in (A) correspond to coin 2, and those in (B) to coin 4.

decrease for copper and the increase for Fe and Zn lines can be explained as an oxidation effect which produces a surface enrichment in the most noble metals; phenomenon reported for several ancient alloys [20,21].

Iron was either detected at very low concentration or not detected in the XRFS screening of both coin series. Monitoring the atomic line of Fe by LIBS (promoted by XRFS screening), enabled assessment of Fe as an alloy component; this was confirmed by the differences of its in-depth profile with respect to a typical element of the corrosion layer, as shown in Fig. 4 for Pb. *Layer averaged kinetic series* also helped to assess the presence of Fe in the sample by increasing SNR and thus making easier identification of its atomic line for subsequent monitoring. Moreover, the in-depth profiles obtained by *layer averaged kinetic series* from a coin are much better defined than those corresponding to single kinetic series (obtained from a sampling position), thus allowing an easier characterisation of in-depth profiles for the two types of profiles of a copper-based coin, as can be seen in Fig. 5.

**3.2.3.2. Distribution of impurities.** A study of the surface and in-depth distribution of impurities has also been carried out for As, Pb and Ca. In addition, other impurities such as Ag, Au, Cl, Sr and Sb were identified by XRFS screening, but any atomic LIBS line could be assigned to them under the working conditions. The information on coin composition provided by XRFS screening made the assignation of atomic lines to As, Pb and Ca easier, as it allowed the search for atomic lines for each element in a database; then, a search of these atomic lines in the spectra was carried out.

The shot number at which the atomic line chosen for each element disappears (the disappearance shot number, dsn) was col-

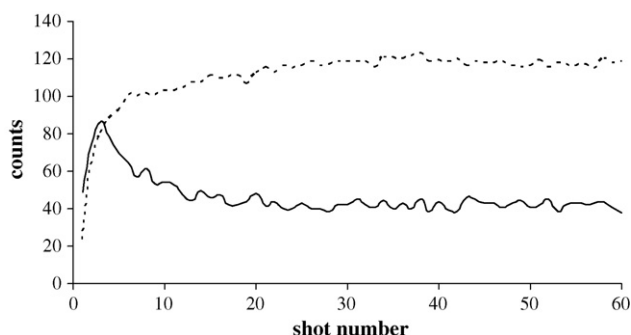


Fig. 4. In-depth profiles of Fe, major component (---), and Pb, impurity (—), in coin 2.

lected at each sampling position. This parameter varies largely depending on both the element and the coin, even within a given series. In some sampling positions, the dsn takes the extreme values: zero (which means that the element is not present in that sampling position) and higher than 60 (which indicates that the corrosion layer has not been surpassed by the 60 shots delivered).

The dsn for a given element at each sampling position, as three-dimensionally plotted in Fig. 6, provides information about how the element is distributed both on the surface and in-depth in a sampling zone.

In the two series of samples analysed the impurities are distributed heterogeneously, with remarkable differences from sampling position to sampling position.

#### 3.2.4. Corrosion degree

The relationship between intensity of LIBS lines and corrosion degree of the sample is based on the following facts: (a) the increase of corrosion decreases the height of the atomic lines; (b) the intensity of a given atomic line increases by increasing the shot number as a consequence of corrosion decrease. These facts enabled development of a methodology to assess the corrosion degree which consists of: (1) selection, within the *layer averaged kinetic series*, of the layer where the atomic line of the element under study reaches the maximum intensity; (2) subtraction of the intensity of the given atomic line in the layer corresponding to the second shot (the first one was rejected due to lack of reproducibility) from that obtained in (1). It has been checked that the magnitude thus obtained is directly related to

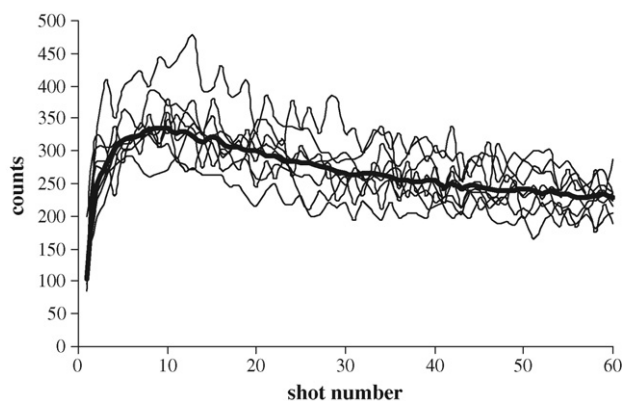


Fig. 5. In-depth profile of copper from *layer averaged kinetic series* (thick line) and single kinetic series (thin lines). For better comprehension, only nine of the 36 single kinetic series making up a *layer averaged kinetic series* are shown.

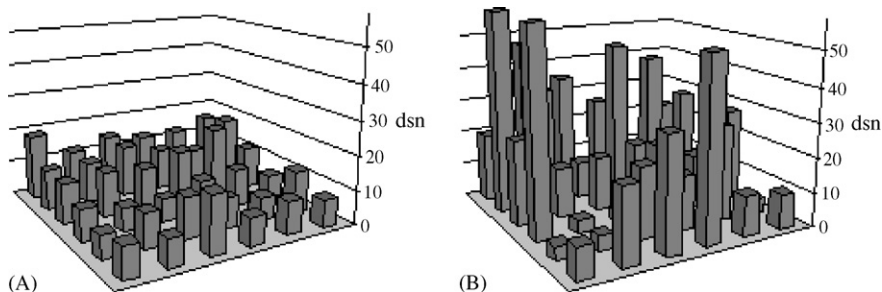


Fig. 6. Distribution of Ca (coin 6) and Pb (coin 4) are plotted in (A) and (B), respectively, vs. the disappearance shot number for the 36 sampling positions of each sampling zone.

the corrosion degree of the sampling zone. Applied to the three coins making up coin series I, the results are as follows: at the more deteriorated coin (coin 1) the value of this parameter is 2814 counts, and that of the less deteriorated coin (coin 2) is 442 counts. This value is 1042 counts for coin 3, which corresponds to an intermediate corrosion degree, as foreseeable. Similar results were obtained from the second coin series, thus confirming the validity of the proposed approach.

Another way to evaluate the corrosion degree in metallic alloys is by the *layer averaged kinetic series* SNR. The SNR improvement from the use of *layer averaged kinetic series* with respect to the SNR obtained from a single spectrum is proportional to the corrosion degree. Thus, improvements ranging between 90 and 300%, depending on the selected coin, were found; the higher improvement corresponded to the more corroded samples and vice versa. The corrosion sequences thus obtained coincided with those provided by visual examination.

#### 4. Conclusions

Complementary aspects of the two atomic techniques used for the corrosion study here presented are as follows:

- (1) Sample screening by XRFS prior to LIBS studies facilitates assigning of atomic lines in the spectrum from the latter.
- (2) Semi-quantitative information of superficial elements provided by XRFS is absent in LIBS information.
- (3) In-depth lateral and tomographic information characteristic of LIBS cannot be obtained by XRFS.
- (4) Examples of complementarity of both atomic techniques in the present research are (a) the detection of impurities such as Ag, Cl, Au, Sr and Sb by XRFS, which did not appear in LIBS spectra, thus demonstrating both their very superficial location and low concentration; (b) the absence of iron in the XRFS screening, despite this element was a major component in the alloy, as demonstrated by LIBS.

In addition, the *layer averaged kinetic series* here proposed have shown to be useful for enhancing the SNR in homogenous corrosion by facilitating layer-by-layer study in the detriment of one-sampling position information. Nevertheless, only elemental composition is provided by both techniques, in contrast to the combination of techniques such as synchrotron radiation-X

ray diffraction (SR-XRD) which provides information on the mineralogy of the compounds involved.

#### Acknowledgements

The authors are grateful to the Spanish Comisión Interministerial de Ciencia y Tecnología and the EU for financial support (project 95-0714.OP.01.02) and to the Archaeological Museum of Montilla (Spain) for providing the samples.

#### References

- [1] A. Demetrios, *Appl. Spectrosc.* 55 (2001) 186–205.
- [2] A.J. Ball, V. Hohreiter, D.W. Hahn, *Appl. Spectrosc.* 59 (2005) 348–353.
- [3] H. Hotokezaka, N. Aoyagi, Y. Kawahara, N. Yamaguchi, S. Nagasaki, K. Sasaki, S. Tanaka, *Microsyst. Technol.* 11 (2005) 974–979.
- [4] I.B. Gornushkin, B.W. Smith, H. Nasajpour, J.D. Winefordner, *Anal. Chem.* 71 (1999) 5157.
- [5] T. Kim, C.T. Lin, Y. Yoon, *J. Phys. Chem.* 102 (1998) 4284.
- [6] D. Romero, J.J. Laserna, *J. Anal. At. Spectrom.* 13 (1998) 557.
- [7] A. Jurado-López, M.D. Luque de Castro, *Spectrochim. Acta Part B*, in press.
- [8] D. Kloos, *Precious Met.* 24 (2001) 17–38.
- [9] W.L. Wiese, M.W. Smith, B.M. Glennon, *Atomic Transition Probabilities, National Standard Reference Data Series, National Bureau of Standards 4 (US), vol. 1–2, 1966.*
- [10] W.G. Mallard, G.R. Dalton, and J.W. Gallagher, *NIST Spectroscopic Properties of Atoms and Atomic Ions Database, NIST Standard Reference Database 38 (US), 1992.*
- [11] B.C. Castle, K. Talabardon, B.W. Smith, J.D. Winefordner, *Appl. Spectrosc.* 52 (1998) 649–657.
- [12] R. Wisbrun, I. Schechter, R. Niessner, H. Schroder, K. Kompa, *Anal. Chem.* 66 (1994) 2964–2975.
- [13] C. Aragón, J.A. Aguilera, F. Peñalba, *Appl. Spectrosc.* 53 (1999) 2964–2975.
- [14] L. Dudragne, P. Adam, J. Amouroux, *Appl. Spectrosc.* 52 (1998) 1321–1327.
- [15] E. Tognoni, V. Palleschi, M. Corsi, G. Cristoforetti, *Spectrochim. Acta, Part B* 57 (2002) 1115–1130.
- [16] J. Sijbeks, P. Scheunders, N. Bonnet, D. Van Dyck, E. Raman, *Magn. Reson. Imaging* 14 (1996) 1157–1163.
- [17] R.M. Henklemen, *Med. Phys.* 12 (1985) 232–233.
- [18] R.E. Russo, X.L. Mao, in: M.C. Miller (Ed.), *Laser Ablation and Desorption*, Academic Press, San Diego, 1998, pp. 375–412.
- [19] M. Mantler, M. Schreiner, *X-Ray Spectrom.* 29 (2000) 3–17.
- [20] Z. Sándor, S. Tölgyesi, I. Gresits, Z. Kasztovszky, *J. Radioanal. Nucl. Chem.* 254 (2002) 283–288.
- [21] I. Brissaud, P. Chevallier, C. Dardenne, N. Deschamps, J.P. Frontiere, K. Gruelf, A. Taccoeng, A. Tarrats, T.X. Wangd, *Nucl. Instrum. Methods Phys. Res., Sect. B* 49 (1990) 305–308.

# Simple and versatile operational fractionation of Fe and Zn in dietary products by solid phase extraction on ion exchange resins

P. Pohl\*, B. Prusisz

*Faculty of Chemistry, Wrocław University of Technology, Wybrzeże Stanisława Wyspiańskiego 27, 50-370 Wrocław, Poland*

Received 21 December 2005; received in revised form 3 April 2006; accepted 13 April 2006

Available online 23 May 2006

## Abstract

A simple and versatile protocol, based on use of solid phase extraction on strong ion exchangers and off-line detection by flame atomic absorption spectrometry, was devised to fractionate iron and zinc in common dietary food and beverages products, i.e., bee honeys, fruit juices and tea infusions. In the procedure proposed, cation exchanger Dowex 50Wx4 and anion exchanger Dowex 1x4 were used separately for distinguishing broadly meant the cationic metal fraction and the fraction of stable anionic metal complexes, respectively, after retention of metal species and their exhaustive elution by means of a  $4.0 \text{ mol l}^{-1}$  HCl solution. The third fraction, referred to the residual metal species, was retrieved by difference between total soluble metal contents and sum of metal quantities in separated cationic and anionic fractions. The fractionation pattern observed for both metals was described and discussed.

© 2006 Elsevier B.V. All rights reserved.

**Keywords:** Fractionation; Solid phase extraction; Iron; Zinc; Food; Beverages; Flame atomic absorption spectrometry

## 1. Introduction

Solid phase extraction (SPE) on ion exchange sorbents is a very useful technique for the enrichment of metal ions present in liquid samples at levels lower than the detection range of commonly applied in laboratories such instrumental method of detection as flame atomic absorption spectrometry (FAAS) [1–3]. In relation to liquid-liquid extraction, application of packed columns or cartridges prior to concentration of metals from sample solutions by their sorption on solid phase of sorbents and subsequent quantitative recovery by solvent elution, indeed reduces analysis time, costs and labor, and provides, in addition, reasonably high pre-concentration factors. The technique is convenient as well for cleaning up the samples or separation of interfering matrix components, usually disturbing the detection of metals [3].

Another impressive capacity of SPE on ion exchangers or adsorbents lies in the possibility for distinguishing and selective isolation of different metal groupings of comparable chemical characteristics. Such property offers the opportunity for frac-

tionation of metals into different groups of compounds and can be valuable for study of metal bioavailability or prediction of their effect on living organisms existing in natural waters [4].

The protocol in which metals species are classified according to their size association by filtration through a defined pore size filter, and then, further differentiation of metals compounds occurring in the separated soluble fraction is performed owing to their affinity, charge, hydrophobicity, solubility or lability using SPE and different sorbent–metal interaction mechanisms has been established so far for water researches. This approach is accepted nowadays to be much better in the assessment of bioavailability and toxic effect of metals than detailed speciation analysis aiming the exact definition of molecular forms of metals and structure of ligands complexing the metal ions [4]. Such method is cheaper, simpler and more versatile in comparison to the speciation analysis by means of hyphenated techniques, which is impractical and even impossible to carry out in many cases due to a large number of the individual metals species occurring in water samples.

There is a growing evidence that the operationally defined fractionation protocol based on use of SPE, except for water samples, might be used to determine the distribution of metals amongst the defined chemical species in dietary food and beverages, yielding useful knowledge on nutritional value, safety

\* Corresponding author. Tel.: +48 71 3203445; fax: +48 71 3284330.  
E-mail address: [pawel.pohl@pwr.wroc.pl](mailto:pawel.pohl@pwr.wroc.pl) (P. Pohl).

or authenticity of analyzed products. Previously, different anion and cation exchange resins as well as chelating and adsorbing media were applied to fractionation of metals in that sort of samples, e.g., Cu and Mn in milk [5]; Al and Mn in tea infusions [6–8]; Cu, Fe and Zn in wines [9]; or Cd, Co, Cu, Fe, Mn, Ni and Zn in beers [10,11], providing valuable information on charge of metal species or their distribution.

To the best of our knowledge there are no published reports concerning the fractionation of metals, including such essential and nutritional microelements as iron and zinc, in honeys and juices; usually total contents of these metals are measured and reported [12–16]. Direct experimental evidence on classification of Fe and Zn groupings in tea infusions is occasional too [17]. Therefore, in the present study, the protocol of operational fractionation of Fe and Zn in bee honeys, fruit juices and tea infusions was developed to retrieve the information on charge and distribution of these metal species. It was based on solid phase extraction of distinct metal fractions on strong cation exchanger Dowex 50Wx4 and strong anion exchanger Dowex 1x4 used separately. In terms of usefulness of other sorbents for retention of cationic species of metals in question, weak cation exchanger Diaion WT01S and chelating resin Duolite GT73, differed from Dowex 50Wx4 with regard to the type of interactions between specific functional groups of the resins and metal cations, were also examined. The concentrations of Fe and Zn were determined using flame atomic absorption spectrometry (FAAS).

## 2. Experimental

### 2.1. Instrumentation

A flame (air–acetylene) atomic absorption spectrometer Perkin Elmer 1100B (Germany) with deuterium background correction was used for all experiments. The absorbance was measured at 248.3 and 213.9 nm using ordinary hollow cathode lamps operated at 15 and 8 mA, respectively for Fe and Zn. Other working conditions applied to the instrument were those recommended by the manufacturer, i.e., acetylene flow rate  $-2.51 \text{ min}^{-1}$ , air flow rate  $-8.01 \text{ min}^{-1}$ , sample aspiration rate  $-2.0 \text{ ml min}^{-1}$ , spectral bandwidths  $-0.20$  and  $0.70 \text{ nm}$ , respectively for Fe and Zn. The signal-processing selected for measurements was a “hold” mode with an integration time of 1 s and a three-read cycle. The calibration was based on five reference analyte solutions and performed using two-coefficient equations.

A digital pH-meter PM1 (TMS Electronics, Poland) with a combined electrode was applied for measuring the pH of sample solutions.

### 2.2. Materials and reagents

The resins used in this work, i.e., strong acidic, gel-type cation exchanger Dowex 50Wx4 (200–400 mesh, sulfonic acid); weak acidic, highly porous cation exchanger Diaion WT01S (100–200 mesh, carboxylic acid); chelating, macroporous resin Duolite GT73 (16–50 mesh, thiol); strong basic, gel-type anion

exchanger Dowex 1x4 (100–200 mesh, trimethylbenzyl ammonium), were supplied by Supelco (USA).

Glassware employed throughout the experiments was made from Pyrex. Before use, it was soaked for 24 h in a 28% (m/v) solution of  $\text{HNO}_3$  and then, rinsed thoroughly with doubly distilled water.

All reagents applied were of analytical grade. Doubly distilled water was used throughout. Stock standard solutions of Fe(III) and Zn(II) at concentrations of  $1000 \mu\text{g ml}^{-1}$  were purchased from Merck (Germany). Other chemicals, that is concentrated nitric acid ( $\text{HNO}_3$ ), concentrated hydrochloric acid (HCl), 30% (m/v) solution of hydrogen peroxide ( $\text{H}_2\text{O}_2$ ), sodium hydroxide (NaOH), potassium dihydrogen phosphate ( $\text{KH}_2\text{PO}_4$ ), potassium hydrogen phthalate ( $\text{C}_8\text{H}_5\text{KO}_4$ ) and dipotassium salt of ethylenediaminetetraacetic acid ( $\text{C}_{10}\text{H}_{14}\text{N}_2\text{K}_2\text{O}_8 \cdot 2\text{H}_2\text{O}$ , EDTA) were obtained from POCH (Poland).

Mixed, 100-ml working solutions, containing metals of interest at concentrations of 1.0 and  $0.20 \mu\text{g ml}^{-1}$ , respectively for Fe and Zn, were prepared daily by dilution of stock solutions with water. Before topping up with water, the solutions were adjusted to appropriate pH by addition of 10 ml of two-component buffers, i.e.,  $0.05 \text{ mol l}^{-1}$  solution of  $\text{C}_8\text{H}_5\text{KO}_4$  containing NaOH at concentration of 1.3, 8.7, 23 and  $37 \text{ mmol l}^{-1}$ , correspondingly, for pH of 4.0, 4.5, 5.0 and 5.5;  $0.05 \text{ mol l}^{-1}$  solution of  $\text{KH}_2\text{PO}_4$  comprising NaOH at concentration of 5.6 and  $14 \text{ mmol l}^{-1}$  for pH of 6.0 and 6.5, respectively. Mixed, 100-ml solutions of anionic complexes of Fe ( $1.0 \mu\text{g ml}^{-1}$ ) and Zn ( $0.20 \mu\text{g ml}^{-1}$ ) with EDTA were prepared using 10 ml of a  $0.10 \text{ mol l}^{-1}$  solution of EDTA. For buffering, 10 ml of appropriate two-component buffering solutions were added. After mixing and topping up with water, the solutions were heated to about  $70^\circ\text{C}$  and let to equilibrate for 48 h.

### 2.3. Column operation

For solid phase extraction, Supelco glass columns (1.0 cm in diameter) ended with frits and stopcocks were packed with resins as received (approximately 1.2 g) using slurry method. Before use, resin beds of cation exchangers were pre-conditioned. At first, rinsing with 25 ml of water was proceeded, followed by 10 ml of a  $2.0 \text{ mol l}^{-1}$  solution of HCl. After that, the resin beds were washed with 25–75 ml of water, dependently on the resin type used, and next, rinsed with 10 ml of a  $1.0 \text{ mol l}^{-1}$  solution of NaOH. Finally, successive washing with water was carried on. The conditioning treatment of anion exchange resin Dowex 1x4 included rinsing with 25 ml of water, followed by 10 ml of  $2.0 \text{ mol l}^{-1}$  HCl solution, and then, washing with 25 ml portion of water.

Each experiment relating to study of sorption and desorption properties of Fe and Zn on the sorbents applied was repeated three times. The procedural column blanks were performed and considered in calculations. The flow rates of the solutions and the eluents passed through the columns were controlled by a two-channel peristaltic pump.

To evaluate the influence of the flow rate with which the solutions were propelled through the resin beds on the retention

efficiency of Fe and Zn on ion exchange resins, working solutions of metals under consideration, adjusted to pH of 5.0, were driven through the columns with the flow rate of 1.0, 2.0 and 4.0 ml min<sup>-1</sup>, correspondingly. The effect of the solution pH on the retention of metals on the resins was investigated by passing the working solutions of Fe and Zn, adjusted to pH values equal to 4.0, 4.5, 5.0, 5.5, 6.0 and 6.5, through the columns with the flow rate of 1.0 ml min<sup>-1</sup>. In all cases above, about 20 ml portions of column effluents were collected and next analyzed on the content of Fe and Zn using FAAS. In order to determine the amounts of metals retained by the resins as percentage retention efficiencies, metal quantities found in the effluents were compared to their concentrations in loaded solutions.

The desorption of Fe and Zn from the resins was studied by elution with HCl and HNO<sub>3</sub> solutions corresponded to the concentrations of 1.0, 2.0 and 4.0 mol l<sup>-1</sup>. Accordingly, after passing 100-ml two-component working solutions of Fe and Zn (pH 5.0) through the columns at the flow rate of 1.0 ml min<sup>-1</sup>, 10 ml of the selected eluents were driven through them at the same flow rate and portions of the eluates (10 ml) were collected prior to the analysis by the FAAS method. To evaluate the percentage recovery efficiencies for Fe and Zn, metal concentrations determined were compared to their initial concentrations in the solutions loaded onto the columns.

In addition, the influence of matrix constituents, that is Ca and Mg, present in analyte solutions at concentrations of 20, 50 and 100 µg ml<sup>-1</sup>, respectively, was researched on retention efficiencies of Fe and Zn on Dowex 50Wx4 and Dowex 1x4. For that purpose, 100-ml working solutions of Fe (1.0 µg ml<sup>-1</sup>) and Zn (0.20 µg ml<sup>-1</sup>), buffered to pH 5.0, were passed through the columns at the flow rate of 1.0 ml min<sup>-1</sup>. To recover the metals from the resin beds, 10 ml of 4.0 ml l<sup>-1</sup> HCl solution were used.

#### 2.4. Sample treatment and analysis

Acacia, multi-flower and mixed flower-honeydew honeys, apple juice, black currant nectar, green China leaf tea Loyd and black India granulated tea were analyzed. All the samples were available on the market in Poland. Before analysis they were kept in the laboratory in the original packing.

Honeys (2.5 g sample portions) were dissolved in water obtaining sample solutions of volume of 100 ml. Resulted honey solutions as well as juices after opening (500 ml) were filtered through 0.45 µm pore size Nylon 66 filters (Supelco, USA). Filters were digested in the mixture of concentrated HNO<sub>3</sub> and 30% (m/v) H<sub>2</sub>O<sub>2</sub> by heating on a hot plate in glass beakers covered with watch glasses. For that purpose, two 5-ml portions of HNO<sub>3</sub> were added until no solid residues were observed. After that, the solutions were let to cool and 5 ml of H<sub>2</sub>O<sub>2</sub> were added subsequently. Heating was carried on to evaporate the solutions nearly to dryness. The aliquots left were quantitatively transferred to 25 ml volumetric flasks and taken up with water to volume. The resulting sample solutions were subjected to analysis by FAAS.

Total concentrations of Fe and Zn in the filtrates (dissolved fraction) of honey solutions and juices were determined directly by FAAS. Before measurements, samples were acidified with concentrated HNO<sub>3</sub> to final concentration of 5% (m/v).

Tea infusions were prepared by pouring 5.0 g portions of tea leaves or granulates with 500 ml portions of boiling doubly distilled water. After 10 min of brewing, the infusions were separated from the grounds by filtration using 3W paper filters (Filtrak, Germany). Total contents of Fe and Zn in the infusions were measured by the FAAS method directly in the samples acidified only with HNO<sub>3</sub> to final concentration of 5% (m/v).

Total amounts of Fe and Zn in teas analyzed were determined after complete digestion of the samples in the mixture of concentrated HNO<sub>3</sub> and 30% (m/v) H<sub>2</sub>O<sub>2</sub>. Tea leaves and granulates were initially grounded in an agate mortar. Portions of resulting powders of mass of 0.5 g were placed in glass beakers and poured with 5 ml of HNO<sub>3</sub>. The beakers were covered with watch glasses and left overnight. Afterwards, another 5-ml portions of HNO<sub>3</sub> were added and the beakers were heated on a hot plate until no fumes of nitrogen oxide were observed. After cooling, 5 ml of H<sub>2</sub>O<sub>2</sub> were added and heating was continued. After evaporation almost to dryness, aliquots were taken up with water to 50 ml and filtered through quantitative 3H paper filters (Filtrak, Germany) prior to measurement by means of FAAS.

For each sample preparation procedure, three independent experiments were performed; the respective blind samples were prepared as well.

#### 2.5. Recovery test

The quality of direct measurements of Fe and Zn in honey solutions, juices and tea infusions, as well as determinations of these metals in digests, was verified by performance of recovery tests. For that purpose, samples were spiked with Fe and Zn in quantities being very close to analyte concentrations in the samples, *i.e.*, from 0.15 to 2.0 µg ml<sup>-1</sup> for Fe and from 0.040 to 0.35 µg ml<sup>-1</sup> for Zn. The recoveries of Fe and Zn determined after accomplishment of the respective procedures and analyses, were in the range from 93.0 ± 0.4 to 101 ± 1% what indicated that matrix components of analyzed samples had insignificant influence on measurements of both metals studied in this contribution.

#### 2.6. Fractionation scheme

For fractionation of Fe and Zn, filtrates of honey solutions (100 ml), juices (50 ml) and tea infusions (50 ml) were passed with the flow rate of 1.0 ml min<sup>-1</sup> through the columns packed with strong cation exchanger Dowex 50Wx4 and strong anion exchanger Dowex 1x4 prior to sorption of distinct metal groupings. After that, metal species retained on the columns were eluted using 10 ml of a 4.0 mol l<sup>-1</sup> HCl solution. For that aim, the eluent was passed through the resin beds at the flow rate of 1.0 ml min<sup>-1</sup>. The respective eluates collected were subjected to analysis by means of FAAS in order to determine the concentrations of the fractions separated by solid phase extraction.

Metal groupings classified through that protocol were the cationic fraction (B) comprising free cations of Fe and Zn, stable cationic complexes of both metals with inorganic and organic ligands as well as labile metal species of different charge (cationic, anionic and/or neutral) that might dissociate on the



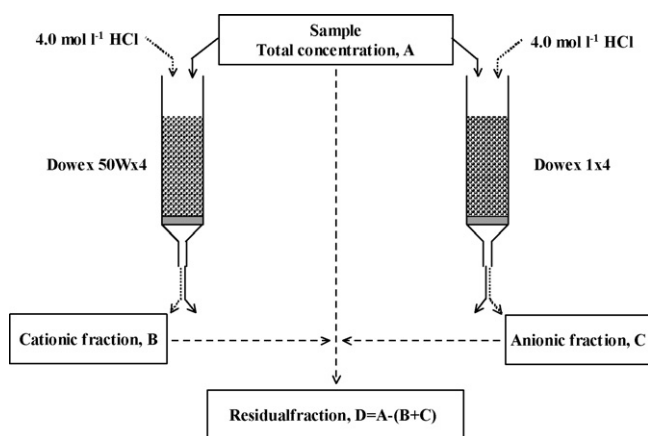


Fig. 1. Scheme of Fe and Zn fractionation procedure based on solid phase extraction using Dowex 50Wx4 and Dowex 1x4 resins.

column of the cation exchanger, and the anionic fraction (C) containing stable anionic complexes of Fe and Zn with inorganic and organic ligands. Additionally, the third, residual metal fraction (D) was distinguished by subtraction of the sum of metal concentrations in the cationic and the anionic fractions from their total contents (A) in the samples. Schematic flowchart showing the procedure applied to the fractionation of Fe and Zn is given in Fig. 1.

### 3. Results and discussion

At the outset, the sorption properties of Fe(III) and Zn(II) cations toward the selected cation exchangers, that is Dowex 50Wx4, Diaion WT01S and Duolite GT73, in addition to retention behavior of anionic complexes of Fe(III) and Zn(II) with EDTA on anion exchanger Dowex 1x4 were investigated under various experimental conditions referred to the flow rate at which the solutions were passed through the resin beds and the pH of the solutions loaded onto the columns.

#### 3.1. Sorption properties of Fe and Zn ions toward different exchangers

The influence of the flow rate of the solutions through the columns on the sorption efficiency of Fe and Zn for the resins applied was investigated for three different settings, i.e., 1.0, 2.0 and 4.0 ml min<sup>-1</sup>. The standard deviations of single retention efficiencies determined for three independent replicates under particular conditions were in the range from 0.3 to 1%.

It was found that among the cation exchangers studied, the flow rate had no significant effect on the retention behavior of Fe and Zn on finer particle size resins, that is 200–400 mesh size Dowex 50Wx4 and 100–200 mesh size Diaion WT01S. In case of Dowex 50Wx4, the average retention efficiency, estimated as mean value for the individual retention efficiencies obtained under the flow rates examined, was equal to 99.6 and 100%, respectively for Fe and Zn. For Diaion WT01S resin, the respective average retention efficiencies were corresponded to 99.0% for Fe and 100% for Zn. The metal uptake by Duolite GT73 resin was determined to decrease successively with the

Table 1  
Percentage retention efficiencies<sup>a</sup> of Fe and Zn vs. solution pH

Resins	pH					
	4.0	4.5	5.0	5.5	6.0	6.5
<b>Fe</b>						
Dowex 50Wx4	100	99.8	99.8	99.5	99.5	99.6
Diaion WT01S	99.8	99.8	99.8	99.4	98.8	97.6
Duolite GT73	99.1	99.1	99.0	97.2	99.0	98.2
Dowex 1x4	99.8	99.8	99.6	99.2	99.5	99.4
<b>Zn</b>						
Dowex 50Wx4	100	100	100	100	100	100
Diaion WT01S	100	100	99.9	100	99.2	99.7
Duolite GT73	100	99.9	100	100	99.6	99.2
Dowex 1x4	100	100	100	100	100	100

<sup>a</sup> Mean values for three independent replicates.

increase of the flow rate, most likely due to the particle size of the resin beads (15–60 mesh) [18]. Consequently, passing the solution through the resin beds at the flow rate of 1.0 ml min<sup>-1</sup>, it was assessed that the retention of Fe and Zn was 98.1 ± 0.7 and 98.3 ± 0.5%, correspondingly. At the flow rate of 4.0 ml min<sup>-1</sup>, it was diminished just to 81.6 ± 1.0% for Fe and 78.8 ± 0.7% for Zn. In case of anion exchange resin Dowex 1x4 (100–200 mesh size), the average retention efficiency established for the flow rates investigated was quantitative for both metals in question, i.e., 99.0% for Fe and 99.8% for Zn.

The percentage of Fe and Zn bound by the resins versus pH of the solutions was investigated for the conditions matching the acidity of analyzed bromatological samples, i.e., in the range from 4.0 to 6.5. The results for the resins studied are given in Table 1. Standard deviation of a single retention efficiency assessed for three replicates reached maximally 1.5%.

It was found that for strong acidic cation exchanger Dowex 50Wx4 and strong basic anion exchanger Dowex 1x4, both possessing active ion exchange sites at any pH value due to nearly complete dissociation of their functional groups [3,18], the retention of cations of Fe(III) and Zn(II) and negatively charged complexes of these metals with EDTA, occurred through ion exchange interactions and was exhaustive in the whole studied pH range. The average retention efficiencies for Fe and Zn, calculated as mean values of individual retention efficiencies attained for distinct pH value, were equal to 99.8 and 100% in the case of Dowex 50Wx4 and 99.6% and 100% for Dowex 1x4, respectively.

For weak cation exchanger Diaion WT01S containing carboxylic acid functional group, which complete dissociation occurs at pHs greater than pK<sub>a</sub> value equal to about 4.8, the retention of metal cations through ionic interactions [19] and possibly via metal-donor oxygen atom attractions [3] was also quantitative at each solution pH studied. The average retention efficiency for Fe and Zn for that resin was established to be 99.2 and 99.8%, correspondingly.

The complete retention of Fe and Zn cations (the average retention efficiency was calculated to be 98.7 and 99.8%, respectively) observed for Duolite GT73 resin of functionality provided by thiol group, likely took place by chelation of Fe<sup>3+</sup> and

Table 2  
Percentage recovery efficiencies of Fe and Zn for cation exchange resins obtained using HCl and HNO<sub>3</sub> solutions (10 ml)

Eluent	Recovery efficiency <sup>a</sup> (%)					
	Dowex 50Wx4		Diaion WT01S		Duolite GT73	
	Fe	Zn	Fe	Zn	Fe	Zn
1.0 mol l <sup>-1</sup> HCl	17.6 ± 1.9	9.2 ± 0.5	75.4 ± 1.3	103 ± 2	65.1 ± 2.0	67.9 ± 2.7
2.0 mol l <sup>-1</sup> HCl	94.0 ± 0.7	97.5 ± 2.2	80.2 ± 1.2	99.5 ± 4.4	81.4 ± 3.2	84.2 ± 2.0
4.0 mol l <sup>-1</sup> HCl	97.3 ± 1.2	101 ± 2	86.0 ± 1.2	98.0 ± 2.2	106 ± 4	91.8 ± 6.2
1.0 mol l <sup>-1</sup> HNO <sub>3</sub>	1.9 ± 0.4	4.9 ± 0.8	63.3 ± 1.2	98.4 ± 2.0	65.2 ± 2.2	89.9 ± 3.8
2.0 mol l <sup>-1</sup> HNO <sub>3</sub>	69.9 ± 0.6	91.0 ± 2.3	70.4 ± 1.1	98.4 ± 2.0	76.9 ± 3.0	94.2 ± 1.8
4.0 mol l <sup>-1</sup> HNO <sub>3</sub>	83.6 ± 3.0	95.7 ± 4.4	67.2 ± 9.4	90.4 ± 3.3	82.3 ± 2.0	102 ± 3

<sup>a</sup> Mean value ± 1S.E. for three independent replicates.

Zn<sup>2+</sup> as both metal cations exhibit high affinity toward donor sulfur atom containing groups [3,20].

### 3.2. Elution conditions

With respect to interactions ascribed to the retention of Fe and Zn, for the elution of metals from cation exchange resins (Dowex 50Wx4, Diaion WT01S, Duolite GT73), moderately concentrated (1.0, 2.0 and 4.0 mol l<sup>-1</sup>) solutions of HCl and HNO<sub>3</sub>, commonly used for stripping of transition metals [18], were applied. The percentage recoveries of Fe and Zn obtained using 10 ml portions of the eluent solutions employed are given in Table 2.

It was ascertained that moderately concentrated solutions of HCl, capable of forming positively charged complexes of Fe(III) and Zn(II), were more convenient for desorption of both metals from the resin beds than HNO<sub>3</sub> solutions. And thus, the application of 10 ml portions of HCl solutions at concentrations corresponded to 2.0 or 4.0 mol l<sup>-1</sup> led to complete retrieval of Fe and Zn from Dowex 50Wx4. For Diaion WT01S, all HCl solutions used in quantity of 10 ml were suitable for quantitative recovery of Zn. Usage of HNO<sub>3</sub> solution produced the same effect. Stripping of Fe from the resin under these conditions did not exceed 86%. Only usage of 20 ml portion of a 4.0 mol l<sup>-1</sup> HCl solution facilitated the complete recovery of that metal. In case of Duolite GT73, the application of 4.0 mol l<sup>-1</sup> solution of HCl led to obtain quantitative desorption of Fe and Zn as well.

For strong anion exchanger Dowex 1x4, similarly as for the strong cation exchanger, usage of 10 ml of 2.0 or 4.0 mol l<sup>-1</sup> solutions of HCl was appropriate for quantitative recovery of Fe and Zn; the recovery efficiencies determined were from 95.0 to 100% on average.

Considering sorption and desorption properties of studied resins, for the fractionation analysis of Fe and Zn in dietary products under discussion, strong cation exchanger Dowex 50Wx4 and strong anion exchanger Dowex 1x4 were chosen for solid phase extraction of distinct species of these metals. Diaion WT01S and Duolite GT73 resins were rejected due to difficulties in elution and susceptibility to solution flow rate.

In addition, for selected resins, the influence of the concentration of matrix elements on the retention efficiency of Fe and Zn was examined. According to the mineral composition and typical amount of macrocomponents reported in the literature

for honeys, juices and teas [12–16,21,22], calcium and magnesium were chosen as the main matrix constituents for that examination. Their final concentration corresponded to 20, 50 and 100 µg ml<sup>-1</sup>.

It was determined that the presence of both alkaline earth metals had no effect on sorption of Fe and Zn by Dowex 50Wx4 and Dowex 1x4. The recoveries found using 10 ml 4.0 mol l<sup>-1</sup> HCl were varied from 98.7 ± 4.3 to 101 ± 6% for Fe and from 97.2 ± 1.7 to 104 ± 1 for Zn for both resins.

### 3.3. Determination and fractionation of Fe and Zn

Total concentrations of Fe and Zn determined in the analyzed samples (column A) as well as distribution of fractions separated by the developed fractionation protocol, i.e., cationic fraction (column B), anionic fraction (column C) and residual fraction (column D), are given in Tables 3 and 4.

#### 3.3.1. Honeys

It was ascertained that iron and zinc were present in solutions of honeys in the form of the dissolved fraction (<0.45 µm); the concentrations of both metals in the solutions of digests of the filters were below the detection limit of FAAS established for Fe and Zn as 0.005 and 0.002 µg ml<sup>-1</sup> (2σ criterion), respectively. In Polish honeys, distinguished fractions of Fe were very equally abounded. The percentage contribution of broadly meant cationic fraction, comprising free cations, stable cationic complexes, as well as labile metal species of different charge that dissociate on the column, was within 25–40% in relation to the total dissolved metal concentration. The contribution of the anionic fraction amounted to 31–40% comparing to the total metal content while the fraction of residual Fe species ranged from 29 to 42%.

In case of zinc, the predominant metal groupings were the cationic species as the percentage content of that fraction varied from 85 to nearly 100%. The contributions of anionic and residual fractions were minor and did not exceed more than 8%. In Polish honeys, the donations of these two fractions for Zn were very comparable.

For honey being the mixture of honeys from different countries of European Union, the fractionation pattern of iron and zinc was quite different from that observed for Polish honeys. Consequently, the predominant class of Fe species was the

Table 3  
Fractionation analysis of Fe in solutions of honeys, fruit juices and tea infusions

Sample	Origin	pH	A	B	C	D <sup>a</sup> = A – (B + C)
Honeys (in $\mu\text{g g}^{-1}$ )						
Acacia	Poland	4.8	3.70 ± 0.07	24.6 ± 7.6	33.2 ± 10.0	42.2 ± 12.7
Multi-flower	Poland	5.0	6.16 ± 0.10	40.1 ± 3.9	30.8 ± 3.4	29.1 ± 5.4
Multi-flower	UE countries	4.6	9.53 ± 0.58	14.9 ± 1.2	12.5 ± 0.9	72.6 ± 6.3
Honeydew	Poland	4.8	5.20 ± 0.02	25.2 ± 3.5	40.2 ± 0.2	34.6 ± 3.5
Fruit juices (in $\mu\text{g ml}^{-1}$ )						
Apple	Poland	3.8	0.570 ± 0.040	22.8 ± 0.7	55.1 ± 0.4	22.1 ± 7.0
Black currant	Poland	4.0	1.92 ± 0.09	59.4 ± 0.5	39.5 ± 0.2	1.1 ± 4.7
Tea infusions (in $\mu\text{g ml}^{-1}$ )						
Green <sup>b</sup>	China	5.2	0.138 ± 0.039	52.2 ± 12.3	39.1 ± 10.1	8.7 ± 32.6
Black <sup>c</sup>	India	5.2	0.157 ± 0.017	40.8 ± 4.4	28.0 ± 4.4	31.2 ± 12.7

A, total concentration; B, percent contribution of cationic fraction; C, percent contribution of anionic fraction; D, percent contribution of residual fraction. Error terms denote 1S.D. for three independent replicates.

<sup>a</sup> Propagated S.D. is given.

<sup>b</sup> Total content equal to  $194 \pm 8 \mu\text{g g}^{-1}$ .

<sup>c</sup> Total content equal to  $223 \pm 13 \mu\text{g g}^{-1}$ .

residual fraction which contributed to almost 73% of the total dissolved metal quantity. The percentage content of cationic and anionic fractions was equal to 15 and 12%, respectively. For zinc, the main fraction was also that containing residual inert species (50%) but the donation of the cationic fraction was comparable (41%).

### 3.3.2. Fruit juices

For samples of apple juice and black currant nectar, the concentration of Fe in the separated particulate fraction ( $>0.45 \mu\text{m}$ ) was found to be 0.010 and  $0.004 \mu\text{g ml}^{-1}$ , respectively. The concentration of that fraction for Zn in apple juice and black currant nectar was equal to 0.003 and  $0.001 \mu\text{g ml}^{-1}$ , correspondingly.

In the soluble fraction ( $<0.45 \mu\text{m}$ ) of apple juice, the main groupings of Fe species were stable anionic complexes; the percentage contribution of the anionic fraction was equal to 55% in relation to the total dissolved metal concentration. The percentage contents of cationic and residual fractions of iron were very

corresponding, i.e., 23 and 22%, respectively. In black currant nectar, the most abounded fractions of Fe species were cationic (59%) and anionic (40%) ones.

The predominant grouping of Zn species in both analyzed juices was the cationic fraction; more than 90% on average in relation to the total dissolved metal content. The percentage donation of anionic and residual fractions was less than 8%.

### 3.3.3. Tea infusions

The efficiency of extraction of studied metals from teas, expressed as amount of soluble metals in the infusions related to their total concentrations, was established to be 7.1% for Fe and 34% for Zn in green leaf tea, and 7.0% for Fe and 27% for Zn in black granulated tea. These results were consistent with those in Ref. [17] and the contributions quoted therein and reporting low extractabilities for Fe and reasonably high for Zn.

In case of iron, dominating metal fraction in the infusions was the cationic fraction; its percentage contribution was determined

Table 4  
Fractionation analysis of Zn in solutions of honeys, fruit juices and tea infusions

Sample	Origin	pH	A	B	C	D <sup>a</sup> = A – (B + C)
Honeys (in $\mu\text{g g}^{-1}$ )						
Acacia	Poland	4.8	0.830 ± 0.088	85.3 ± 3.5	7.2 ± 2.8	7.5 ± 11.4
Multi-flower	Poland	5.0	11.5 ± 0.1	100 ± 1	1.6 ± 0.1	–
Multi-flower	UE countries	4.6	3.31 ± 0.47	41.4 ± 1.5	8.4 ± 4.0	50.2 ± 14.8
Honeydew	Poland	4.8	2.79 ± 0.02	90.3 ± 0.4	4.8 ± 1.2	4.9 ± 1.5
Fruit juices (in $\mu\text{g ml}^{-1}$ )						
Apple	Poland	3.8	0.130 ± 0.005	95.4 ± 1.5	<0.3	<4.3
Black currant	Poland	4.0	0.340 ± 0.001	89.1 ± 1.2	2.9 ± 0.3	8.0 ± 1.2
Tea infusions (in $\mu\text{g ml}^{-1}$ )						
Green <sup>b</sup>	China	5.2	0.108 ± 0.018	79.6 ± 3.7	6.5 ± 2.8	13.9 ± 17.6
Black <sup>c</sup>	India	5.2	0.079 ± 0.012	62.0 ± 12.6	8.9 ± 3.8	29.1 ± 20.2

A, total concentration; B, percent contribution of cationic fraction; C, percent contribution of anionic fraction; D, percent contribution of residual fraction. Error terms denote 1S.D. for three independent replicates.

<sup>a</sup> Propagated S.D. is given.

<sup>b</sup> Total content equal to  $31.6 \pm 1.7 \mu\text{g g}^{-1}$ .

<sup>c</sup> Total content equal to  $29.4 \pm 2.4 \mu\text{g g}^{-1}$ .

to be 52 and 41%, respectively for green tea and black tea. For both teas, the amount of anionic species fraction was lower about 13% than that for cationic one.

This disproportion between these two fractions was observed to be much greater for zinc. Accordingly, the cationic fraction of that metal, contributed to 80 and 62% in relation to the total dissolved metal concentration, respectively for green tea and black tea, was higher about 88% on average than the anionic fraction.

#### 3.3.4. Metal-binding association and bioavailability

Considering the composition of the analyzed samples [22] as well as recent studies devoted to the complexing properties of natural macromolecules in food and beverages [23–27], it was expected that the cationic fraction of Fe and Zn included hydrated cations of these metals, hydroxycations, and partially metal complexes of different charge dissociating on the cation exchanger due to their lability (labile metal species). These metal species are recognized as the most bioavailable to human body through gastric digestion.

Anionic metal fraction presumably contained stable anionic complexes of Fe and Zn with relatively low molecular alpha-hydroxy organic acids namely tartaric, citric, oxalic and malic. This kind of chelates were documented lately to increase the solubility of both metals as well as metal absorption by human body [25]. The presence of chloride or fluoride anionic complexes in this fraction could not be excluded.

Both metals were also assumed to be associated with high molecular endogenous metal-binding food constituents, that is polyphenolic and flavonoid compounds which contents in honey, fruit juices and especially in tea infusions may reach even several percents [22]. To this group of natural macromolecular ligands belongs mostly phenolic acids (phytic, gallic, tannic, salicylic, vanillic, dihydroxybenzoic and shikimic) and flavonoids such as rutins, quercetins, myricetins, anthocyanins, catechins and tannins. All these compounds have been established to bind Fe and Zn cations strongly and to form high molecular hydrophobic and inert species what considerably reduces the bioavailability of both metals and impairs their absorption [23–26]. It was also supposed that polysaccharides containing hydroxyl, carboxyl and sulfate groups and indicating a large extent of metal-binding might interact with both metal cations giving rise to mentioned nonpolar inert species [27].

In terms of possible associations of iron and zinc with endogenous metal-binding sample constituents, it can be considered that the cationic fraction contains the most bioavailable metal species. Whereas, the anionic species may be regarded as less bioavailable and finally the residual fraction should contain the species inert to human body. On the account of these statements, the bioavailability of the analytes can be estimated by the summarizing cationic and anionic metal fractions. It can be seen (Tables 3 and 4) that, although the analyzed food samples and beverages are rich in iron and zinc, the bioavailable shares of Fe and Zn can be as low as 30 and 50%, respectively, in multi-flower honey being mixture of various honeys from UE countries. Significant source of bioavailable iron can be black current nectar and green tea infusion for which the sum of cationic and anionic

species is higher than 90% of the total metal concentration. Zinc may be readily available to humans through daily diet from Polish honeys and fruit juices (the sum of cationic and anionic fractions in this case is ranged from 92 to 100%).

## 4. Conclusions

This work was attained to develop a simple and versatile procedure of fractionation of iron and zinc in samples of common dietary products. The devised protocol, based on solid phase extraction on ion exchange resins, is low-cost, easy in operation and does not require a sophisticated measurement device. The metal fractions distinguished are operationally defined and relate to sorption behavior of Fe and Zn species toward strong cation and strong anion exchangers applied. The applicability of the protocol in classification of groupings of both metals in honeys, fruit juices and tea infusions has been demonstrated. Compared to the total content analysis, the fractionation procedure described provides useful information about bioavailability of metals in view of possible metal association with endogenous ligands occurring in the samples and found distribution of cationic, anionic and residual fractions.

In terms of adulteration and identification of botanical or geographical origin, the proposed method might be helpful for more inclusive evaluation of quality and authenticity of food and beverages of natural origin or supplemented with substances changing sample integrity and fractionation pattern of metals.

## Acknowledgement

The technical assistance of Eng. J. Skornowicz is gratefully acknowledged.

## References

- [1] B.B. Kebbekus, in: S. Mitra (Ed.), *Sample Preparation Techniques in Analytical Chemistry*, John Wiley and Sons, Hoboken, New Jersey, 2003 (Chapter 5).
- [2] M. de Godoi Pereira, M.A.Z. Arruda, *Microchim. Acta* 141 (2003) 115.
- [3] V. Camel, *Spectrochim. Acta Part B* 58 (2003) 1177.
- [4] O.E. Troccoli, in: R.A. Meyers (Ed.), *Encyclopaedia of Analytical Chemistry, Theory and Instrumentation*, vol. 3, John Wiley and Sons, Chichester, West Sussex, 2000.
- [5] O. Abollino, M. Aceto, M.C. Bruzzoniti, E. Mentasti, C. Sarzanini, *Anal. Chim. Acta* 375 (1998) 299.
- [6] S.B. Erdemoglu, K. Pyrzynska, S. Gucer, *Anal. Chim. Acta* 411 (2000) 81.
- [7] A. Ruszczynska, K. Pyrzynska, E. Bulska, *Chem. Anal. (Warsaw)* 49 (2004) 19.
- [8] Y. Ozdemir, S. Gucer, *Food Chem.* 61 (1998) 313.
- [9] I. Karadjova, B. Izgi, S. Gucer, *Spectrochim. Acta Part B* 57 (2002) 581.
- [10] P. Pohl, B. Prusisz, *Anal. Chim. Acta* 502 (2004) 83.
- [11] R. Svendsen, W. Lund, *Analyst* 125 (2000) 1933.
- [12] M.N. Rashed, M.E. Soltan, *J. Food Comp. Anal.* 17 (2004) 725.
- [13] H. Yilmaz, O. Yavuz, *Food Chem.* 65 (1999) 475.
- [14] M.J. Latorre, R. Pena, C. Pita, A. Botana, S. Garcia, C. Herrero, *Food Chem.* 66 (1999) 263.
- [15] W.A. Simpkins, H. Louie, M. Wu, M. Harrison, D. Goldberg, *Food Chem.* 71 (2000) 423.
- [16] P.L. Fernandez, F. Pablos, M.J. Martin, A.G. Gonzalez, *Food Chem.* 76 (2002) 483.
- [17] K.E. Odegard, W. Lund, *J. Anal. At. Spectrom.* 12 (1997) 403.

- [18] O. Samuelson, *Ion Exchange Separations in Analytical Chemistry*, John Wiley and Sons, New York, 1963.
- [19] M. Pesavento, R. Biesuz, J.L. Cortina, *Anal. Chim. Acta* 298 (1994) 225.
- [20] C. Kantipuly, S. Katragadda, A. Chow, H.D. Gesser, *Talanta* 37 (1990) 491.
- [21] A. Marcosa, A. Fishera, G. Reab, S.J. Hill, *J. Anal. At. Spectrom.* 13 (1998) 521.
- [22] R.S. Singhal, P.R. Kulkarni, D.V. Rege, *Handbook of Indices of Food Quality and Authenticity*, Woodhead Publishing, Cambridge, 1997.
- [23] S. Khokhar, R.K. Owusu Aparenten, *Food Chem.* 81 (2003) 133.
- [24] M. O’Coinceanainn, S. Bonnely, B. Baderschneider, M.J. Hynes, *J. Inorg. Biochem.* 98 (2004) 657.
- [25] P.K. South, D.D. Miller, *Food Chem.* 63 (1998) 167.
- [26] M. Umata, C.E. West, H. Futa, *J. Food Comps. Anal.* 18 (2005) 803.
- [27] S.J.J. Debon, R.F. Tester, *Food Chem.* 73 (2001) 401.



## Statistical validation of sulfate quantification methods used for analysis of acid mine drainage

David J. Reisman<sup>a</sup>, Vijayakumar Sundaram<sup>b</sup>, Souhail R. Al-Abed<sup>a,\*</sup>, Derrick Allen<sup>a</sup>

<sup>a</sup> National Risk Management Research Laboratory, Office of Research and Development, U.S. Environmental Protection Agency, 26 W. Martin Luther King Dr., Cincinnati, OH 45268, USA

<sup>b</sup> Pegasus Technical Services, 46 E. Hollister Street, Cincinnati, OH 45219, USA

Received 16 February 2006; received in revised form 3 April 2006; accepted 4 April 2006

Available online 15 May 2006

### Abstract

Turbidimetric method (TM), ion chromatography (IC) and inductively coupled plasma atomic emission spectrometry (ICP-AES) with and without acid digestion have been compared and validated for the determination of sulfate in mining wastewater. Analytical methods were chosen to compare the performance of a portable field turbidimetric instrument and to validate the underlying assumption utilized in conversion of total sulfur to sulfate during ICP-AES analysis. Accuracy and precision of analytical techniques were compared to one another using control and field samples collected from a mine site using the Bonferroni multiple comparison test. Effects of sample dilution, filter pore size and acidification on sulfate quantification were also studied. The results showed that IC and ICP-AES with and without acid digestion provided excellent recoveries in the case of control samples (within 90–110%). These analytical methods also showed lower relative standard deviation for both control and field samples. On the other hand, performance of the turbidimetric method was severely affected by sample dilution and acidification, and also revealed poor sulfate recoveries for control samples ranging from 0 to 83.5%. Analysis of variance (ANOVA) was used to evaluate the response (sulfate concentration) obtained from factorial design. Analytical method had significant effect ( $P < 0.0001$ ) on the sulfate quantification. The interaction between determination method and sample dilution was more significant than other two-way interactions.

Published by Elsevier B.V.

**Keywords:** Sulfate; Mine water; Turbidimetric method; Ion chromatography; ICP-AES; Acid digestion; AMD; ARD

### 1. Introduction

Sulfate ions are present in natural, ground and surface waters. Measurement of sulfate is a crucial step in environmental monitoring, regulatory inspection and compliance, especially in the treatment of mining-influenced waters. Determination of sulfate is useful in assessing the redox state of the system because sulfur is a critical element in controlling the fate and solubility of polluting elements in the aquatic environment [1]. Performance of industrial treatment units and contaminated site remediation are evaluated by measuring sulfate in the field. Acid mine drainage (AMD) generated mostly by pyrite oxidation from abandoned mine sites contain significant concentrations of heavy metals and sulfate [2]. Performance of AMD treatment technologies using

sulfate reducing bio-reactors (SRBR) are evaluated based on the concentration of residual sulfate as a measure of the sulfate-reducing activity in the bioreactors [3]. The Code of Federal Regulation within the United States specifies that the safe discharge limit for sulfate should not exceed 250 mg/L [4].

Sulfate ions are measured using many direct and indirect analytical principles including ion chromatography (IC) [5,6], inductively coupled plasma absorption spectrophotometry (ICP-AES) [7], turbidimetric [8,9], colorimetric [10] and gravimetric methods [11]. Gravimetric and colorimetric techniques are not widely used as they require more time and skill in determining the end point of the analysis. IC and turbidimetric methods are widely used laboratory and field techniques for sulfate quantification. ICP-AES is rarely used due to the underlying assumption of negligible sulfur species with lower oxidation states.

IC is a direct way of determining the concentration of sulfate. Anions present in the sample are separated on the basis of their relative affinities and detected by measuring suppressed

\* Corresponding author. Tel.: +1 513 569 7849; fax: +1 513 569 7879.  
E-mail address: [al-abed.souhail@epa.gov](mailto:al-abed.souhail@epa.gov) (S.R. Al-Abed).

conductivity. A review on suppressed ion chromatographic analysis of anions in environmental waters reported that performance should be validated by another established method [12].

ICP-AES is an indirect way of measuring sulfate concentration in wastewaters that may cause interference to other sulfate determination methods. This method has been proven to be robust in terms of analyzing a high amount of sulfate in wastewater containing other anions and cations at low pH. However, the output from the instrument is concentration of total sulfur. Sulfur element concentration is then converted to sulfate concentration. Concentration of sulfate and other species in acid mine drainage primarily depend on pH and redox potential. In oxidizing conditions, sulfur compounds have a tendency to oxidize to sulfate. The stoichiometric conversion factor of 2.996 is used in indirect sulfate determination, and is based on the assumption that concentrations of non-sulfate sulfur species (sulfides and sulfites) are negligible.

Conversion of sulfur concentration to sulfate:

$$\begin{aligned} 1 \text{ mg/L of S} &= \left( \frac{96.056}{32.06} \right) \text{ mg/L of SO}_4^{-2} \\ &= 2.996 \text{ mg/L of SO}_4^{-2} \end{aligned}$$

Pritchard and Lee have reported the quantification of sulfur using ICP-AES in biological and soil mixtures [13]. Miles and Cook employed this technique to quantify the sulfate in natural waters [14]. Calcium and hydrochloric acid provided major interferences during the ICP-AES sulfate quantification [14]. However, ICP-AES sulfate quantification has not been utilized widely in analysis of mine influenced water. Since high concentrations of sulfates and sulfides exist in mine water, it is necessary to validate the assumption involving lower oxidation sulfur species while using ICP-AES for sulfate determination in mine water analysis. Chirstensen et al. have reported the usage of ICP-AES for sulfate analysis; however the validation of sulfur to sulfate conversion was not reviewed [7].

The turbidimetric method is a well-known sulfate quantification technique based on precipitation of sulfate ions as insoluble barium sulfates [15–21]. Sheen et al. proposed the application of the Tyndall effect for the turbidimetric determination of sulfates [15]. To improve the stability of barium sulfate suspension, different stabilizing agents including thymol and gelatine, Tween 80 [18] and polyvinyl alcohol [19] have been employed. Baban et al. used EDTA in the barium sulfate turbidimetric method to reduce the interference from metal ions [17].

In this study we used SulfaVer 4 turbidimetric kit developed by HACH company based on HACH Method 8051 [22]. Method 8051, equivalent to US EPA Method 375.4, was chosen in this study to simulate field determination steps followed by several regulatory agencies in the United States. SulfaVer 4 is also used frequently in sulfate field-testing during waste and mine site remediation activities [23]. Barium chloride, an active constituent present in the kit, reacts with soluble sulfate ions to form an insoluble barium sulfate precipitate. Citric acid present in the kit acts as a stabilizing agent, and enables accurate photometric quantification by forming finely divided barium sulfate turbid-

ity. Interferences listed in HACH Method 8051 were calcium over 20,000 mg/L as CaCO<sub>3</sub>, magnesium over 10,000 mg/L as CaCO<sub>3</sub>, chloride over 40,000 mg/L and silica over 500 mg/L as CaCO<sub>3</sub> [22]. Filtration is recommended for highly colored and turbid samples to avoid any interference. A literature review on sulfate analysis on mining water did not produce studies validating the widely used SulfaVer 4 kit for mine water testing.

Turbidimetric analysis is a commercial method available for measurement of sulfate in the field; however, the performance of sulfate kits in terms of accuracy and precision in quantifying sulfate ions in mine-affected water is unknown. Furthermore, as passive treatment using SRBRs become more prevalent worldwide, sulfate reduction and the ability to meet discharge requirements is one important measurement of the success of the treatment system. The primary objective of the present investigation was to determine the precision and accuracy, and to validate the turbidimetric method by comparing results from different well-established analytical methods for measuring sulfate concentrations. Indirect ICP-AES sulfate analysis is versatile in the case of AMD but the underlying assumption of sulfur to sulfate conversion requires validation. The secondary objective was to resolve the uncertainties regarding the validity of assumptions involved in ICP-AES analysis of sulfate present in mining water.

Both intentional and unintentional sample preparation steps practiced in sulfate quantification are acidification and filtration. The presence of suspended particles in the sample may affect the performance of instruments due to interference and blocking. Addition of acid creates a greater possibility of interference in IC analysis, whereas in ICP-AES, acidification helps in mobilizing the metals. Filtration and acidification are chosen as candidate factors in this study to investigate the effects of sample preparation steps. Also, most of the sulfate determination methods have a limited range of quantification. Widely used sulfate methods require several dilution steps prior to the analysis. To investigate the linear ranges of analytical methods, dilution of samples was investigated. In addition, effects of sample matrix and sample preparation technique including dilution, filter pore-size and acidification on the performance of different analytical approaches employed in sulfate quantification were studied.

## 2. Experimental

### 2.1. Reagents and solutions

Sulfate stock solution containing 1000 mg/L of sulfate was purchased from Absolute Standards, Inc., and used as control sample in all the analysis and in matrix spike and interference check standards. Samples from the Golinsky Mine (California) site were collected and shipped to the U.S. EPA Laboratory in Cincinnati, Ohio. High purity deionized water (Millipore Systems, MA, 18 MΩ) was used during the dilution of samples and standards. All the samples were filtered through 0.2 or 0.45 μM filters prior to the analysis, since 0.2 μM is commonly used in the United Kingdom and other European Nations, while 0.45 μM is used in most U.S. methods.

Table 1  
Instrumentation details

IC	
Ion-chromatographic unit	Dionex ICS-2000 Reagent-Free™ ion chromatography (RFIC)
Pump	GP50 gradient pump
Guard column	IonPac® AG-18 Guard, 4 mm
Column	IonPac® AS-18 Analytical, 4 mm
Column temperature	30 °C
Suppressor	ASRS Ultra II 4 mm
Suppressor current	57 mA
Eluent	23 mM KOH
Eluent source	Dionex EluGen® EGC-KOH cartridge
Eluent accessories	Dionex continuously regenerated-anion trap column (CR-ATC)
Flow-rate	1 mL/min
Detector	Dionex CD20 conductance detector
Cell temperature	35 °C
Injection volume	25 mL
Run time	15 min
Background conductance	≈0.7 mS
Back pressure	≈2000 psi
Data management	Chromeleon® 6.5 chromatography workstation
Auto sampler	AS-40
Additional conditions	Separation under isocratic conditions
ICP-AES	
Instrumentation	IRIS Intrepid Spectrometer Simultaneous ICP-AES
Generator	0.8–1.1 kW
Wavelength	182.034 nm
Readout	ppm
Frequency	50/60 Hz
Forward power	RF Power 1150 W
Nebulizer	Concentric Pneumatic Burgener
Internal standard	Yttrium
Sample volume	15 mL
Auxiliary coolant	Liquid Argon
Auxiliary coolant flow rate	15 L/min
Auxiliary gas	0.5 L/min
Liquid uptake rate	1.5 mL/min
Carrier gas rate	80 psi
Nebulizer pressure flow	28 psi
Turbidimetric	
Spectrophotometer	Hach DR-890 portable data logging colorimeter
Wavelength	420 nm
Reagent	SulfaVer® 4 powder pillow
Program number	91
Sample volume	10 mL
Reaction time	5 min

## 2.2. Analytical methods

Analytical instrumentation used for TM, IC and ICP-AES and determinations of sulfate ions in controls and field samples is reported in Table 1.

### 2.2.1. Turbidimetric method

The turbidimetric analysis was conducted using a portable colorimeter (Model No: DR/890, HACH Co.) to quantify the presence of sulfate. The procedure described in the HACH Method—Sulfate 8051 was followed during the analysis. A pre-stored sulfate program was chosen in the colorimeter and the instrument was zeroed using the zero vial containing deionized water. The 10 mL sample was added to the vial followed by the addition of SulfaVer 4 powder pillows. Vials were shaken for 5 min and placed in the colorimeter. A mid-point standard

check was analyzed during start-up, after every 10 samples and at the end of analytical set.

### 2.2.2. Ion chromatography

Dionex ICS 2000 Ion Chromatograph was used for IC analysis. The procedure described in U.S. EPA SW-846 Method 300.0 was followed during the analysis [24]. Samples were injected onto the IC column after dilution and filtration. One laboratory reagent blank (LRB) and laboratory-fortified blank (LFB) were analyzed for every batch of samples. A calibration blank was analyzed immediately following calibration, after every 10 samples, and at the end of sample run.

### 2.2.3. ICP-AES

Sulfate emission intensities were monitored at the suggested analytical wavelength 182.037 nm [25]. Quality checks

described in U.S. EPA SW-846 Method 6010B were followed during the analysis [26]. Samples to be analyzed on the ICP-AES were split. A part of the sample was injected directly (with and without concentrated  $\text{HNO}_3$ ) and the rest of the sample was digested in a microwave acid digester. The digestate was analyzed by ICP-AES. Comparison of the split sample results was used to evaluate the effect of acid digestion on sulfate determination. A method blank (MB) was analyzed for every 10 samples to determine if contamination or any memory effects are occurring. The concentration of analyte in method blank was within three times the MDL, and the ICP-AES was calibrated prior to each analytical run. Calibration was verified with a continuing calibration verification (CCV) standard immediately following daily calibration, after every 10 samples, and at the end of an analytical run. If the concentration of CCV standard varied from the expected values by more than  $\pm 10\%$ , the test was repeated, using fresh calibration standards. Matrix spiked duplicate (MSD) samples were analyzed at a frequency of one per matrix batch. The MSD sample recovery was within  $\pm 25\%$  of the actual value. A post digestion spike addition was performed whenever a new sample matrix was encountered. The recovery of post digestion spike should be within 75–125% of the known value. An interference check standard (ICS), containing 1000 mg/L of calcium and 250 mg/L of sulfate with concentrated  $\text{HNO}_3$ , and without  $\text{HNO}_3$ , was analyzed at a frequency of one per batch.

#### 2.2.4. With acid digestion (ICPAD)

The sample container was placed on the shaker to obtain a homogeneous sample for analysis, with 45 mL of sample being digested in a microwave acid digester using concentrated nitric acid [27]. For each analytical batch of samples processed, analytical reagent blanks were carried throughout the entire sample preparation and analytical process. These blanks were useful in determining sample contamination. A post digestion spike was added whenever a new sample matrix was encountered. The recovery of the post digestion spike was within 75–125% of the known value.

#### 2.2.5. Without acid digestion (ICP)

The sample container was placed on the shaker to obtain a homogeneous sample for analysis, and 15 mL of sample was loaded in an injection vial for analysis. Concentrated nitric acid was used for acidification for analysis of samples with acid.

### 2.3. Procedure

Samples collected from the Golinsky mine site were received and stored at  $4 \pm 2^\circ\text{C}$ . In the ICP and turbidimetric samples requiring acidification, samples were acidified with conc.  $\text{HNO}_3$ , while samples for all other analyses were not acidified during storage time. Preserved samples were filtered using 0.2 and  $0.45 \mu\text{M}$  filters. Filtered samples were diluted to desired dilutions: 1:40, 1:80 and 1:100. For IC analysis, diluted samples were injected directly into the IC column. For turbidimetric analysis, samples were tested using sulfate kits. For ICP-AES, part of diluted samples was analyzed directly (ICP) and the rest were acid-digested prior to the analysis (ICPAD). Sulfate concentrations obtained from four different analyses were utilized for data analysis and method validation purposes.

## 3. Results and discussion

### 3.1. Factorial design

The variables affecting the sulfate measurement, namely determination method, sample matrix, dilution level, filter pore-size and acidification were included in the experimental design. The levels over which the variables were studied are listed in Table 2. Effect of acidification was not investigated in IC analysis due to major interferences of nitrate ions from nitric acid [24], and in ICP-AES with acid digestion analysis due to a presence of an excess amount of nitric acid added during the acid digestion step [27].

### 3.2. Sulfate determination methods

In order to evaluate effectiveness, each considered instrumental method was applied initially to the sulfate standard controls at different dilution levels in the absence of concentrated nitric acid. Subsequently, the same instrumental approaches were applied to field samples. Results obtained from control samples, along with expected certified values are presented in Table 3. Samples were filtered through standard  $0.45 \mu\text{M}$  filters prior to any analysis.

#### 3.2.1. Ion chromatography (IC)

The ion chromatography system was equilibrated for  $\approx 60$  min before sample analysis to attain a stable conductivity baseline. The instrument was calibrated using five sulfate

Table 2  
Factor levels in the factorial design

Factors	Levels			
	I	II	III	IV
Method	ICP without acid digestion (ICP)	ICP with acid digestion (ICPAD)	Turbidimetric (TM)	Ion chromatography (IC)
Matrix	Influent (INF)	Effluent (EFF)	Effluent-spike (EFF-SPK)	Control (CTL)
Dilution	40	80	100	–
Filter pore size ( $\mu\text{M}$ )	0.2	0.45	–	–
Acidification	Nitric	No acid	–	–

Table 3  
Sulfate values from control samples

Dilution level	IC		ICP		ICPAD		TM		Certified value (mg/L <sup>a</sup> )
	mg/L <sup>a</sup>	R.S.D. (%)	mg/L <sup>a</sup>	R.S.D. (%)	mg/L <sup>a</sup>	R.S.D. (%)	mg/L <sup>a</sup>	R.S.D. (%)	
40	991.9	0.28	1066.2	1.55	969.2	0.63	835.6	7.95	1000
80	985.4	0.38	1071.9	1.18	1006.84	2.48	595.6	3.48	1000
100	988	0.13	1060.9	1.54	993.07	1.85	477.8	3.35	1000

<sup>a</sup> Mean sulfate values (mg/L).

standards concentration ranging from 0.5 to 50 mg/L. The final calibration curve resulted in a 99.9% correlation coefficient. Instrument performance was validated by injecting a standard check at the start of the sequence, every two samples and at the end of the analysis. Standard deviations of standard checks were always within the 10% quality criterion. Each sample was injected three times into IC column to evaluate the precision of the instrument. A superQ water blank was injected after each sample to monitor the sulfate carryover. Sulfate peaks were below detection limit for all the blanks. Sulfate recoveries for the control sample were from 98.58 to 99.2%. Relative standard deviations (R.S.D.s) computed from 9 replicates (3-dilution replicates  $\times$  3-analytical replicates) were within 0.13–0.38%. Ion chromatography showed an exceptional accuracy and precision in the case of control samples. The suppressed conductivity detection method enabled a more precise and accurate sulfate concentration present in the sample.

### 3.2.2. ICP-AES

Inductively coupled plasma atomic emission spectrophotometry (ICP-AES) is a widely used analytical technique for quantifying metals. In this study, ICP-AES was utilized for sulfate determination. Total sulfur present in the sample was converted to sulfate using the previously illustrated conversion factor 2.996. Sulfate recoveries ranged from 106 to 107%. R.S.D.s were within 1.1–1.5%, comparable to the previously reported R.S.D. listed in Table 4.

Samples subjected to digestion prior to ICP-AES analysis (represented as ICPAD) showed recoveries from 96.9 to 100.6%. Relative standard deviations were within 0.6–2.4%. Lower precision noticed in ICPAD could be from the acid digestion step, which uses a microwave digester with PTFE vials. This acid digestion step reduced the over-estimation of sulfate and provided better recoveries of sulfate in control samples. More accurate result from ICPAD could be due to the presence of

nitric acid in acid digestion step. Mroczek et al. also observed the differences in sulfate intensities resulting from sample pre-treatment [28].

### 3.2.3. Turbidimetric method

Turbidimetric analysis provided sulfate recoveries from 47.8 to 83.5%. R.S.D.s ranged from 6.5 to 14%, and were higher than the precision values listed in Table 4. Accuracy and precision of the turbidimetric method dropped proportionally with an increase in sample dilution levels. Turbidimetric sulfate analysis was validated using standard checks ranging from 10 to 40 mg/L sulfate standards. Quality checks were analyzed at the start of the analysis, at every five samples and at the end of the analysis. Standard deviations of QC checks were within a quality criterion of 15%.

### 3.3. Field samples

Samples from the Golinsky mine site were analyzed for sulfate using a similar procedure as control samples. Redox potentials of the influent and effluent samples were +412 and +372 mV, respectively. pH of the influent and effluent samples was 2.69 and 6.92, respectively. Samples were stored at the room temperature with considerable headspace. Sulfate values obtained from influent and effluent samples are shown in Fig. 1. Each histogram represents an analytical technique. Sample labels indicate the sample preparation procedure.

#### 3.3.1. Reproducibility of sulfate values

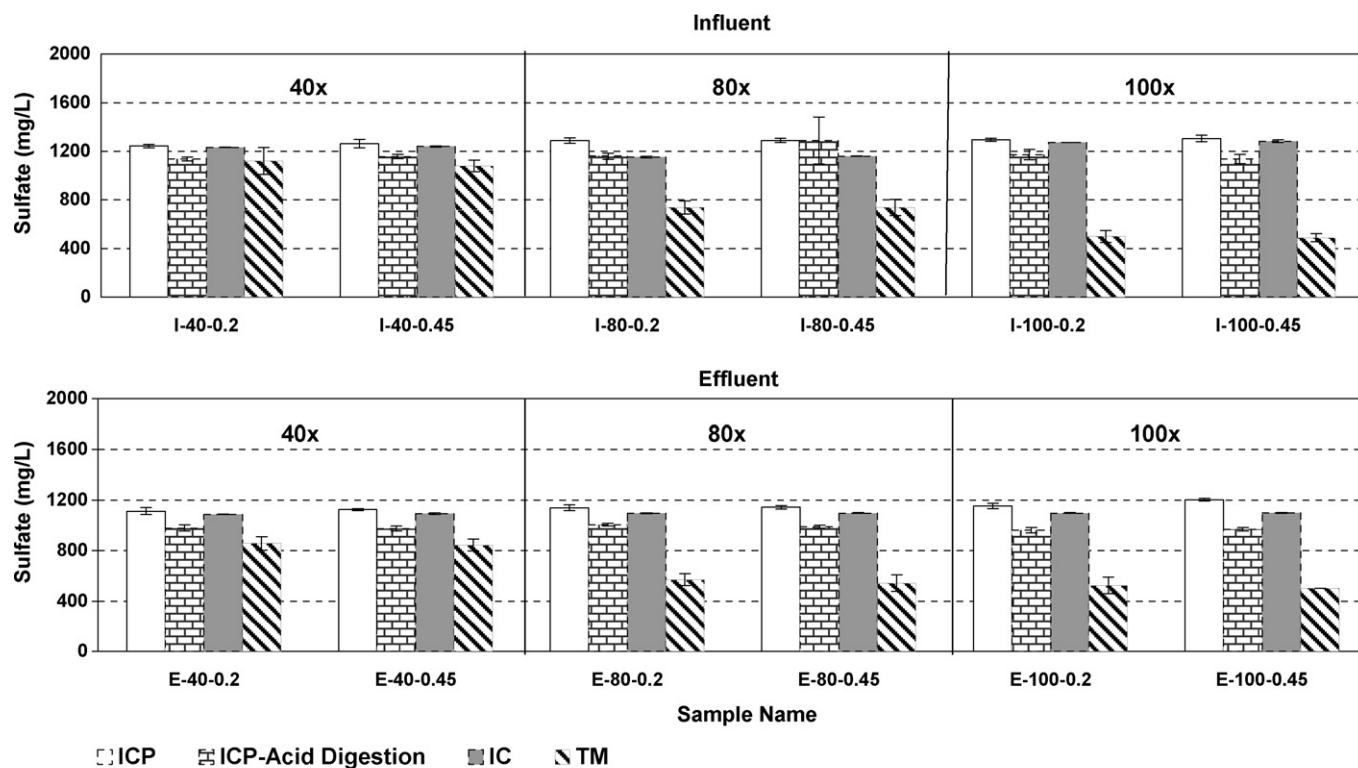
Sulfate values obtained from ICP-AES without acid digestion (represented as ICP) had R.S.D.s from 0.8 to 2.81%. Samples subjected to acid digestion showed R.S.D.s from 1.1 to 3.6% except in one sample with 15%. Results from the IC analysis had the lowest R.S.D.s from 0.1 to 0.86%. Field samples R.S.D.s from ICP, ICPAD were comparable to the reported

Table 4  
Summary of instrumental method parameters

Method	DL (mg/L <sup>a</sup> )	Dynamic range (mg/L <sup>a</sup> )	Precision	Interference	Method
IC [24]	0.02	–	3.2 mg/L S.D. (40 mg/L)	High concentration of cations, anions and suspended matters	300.0
TM [22]	4.9	0–70	$\pm$ 0.5 mg/L S.D.	Color, turbidity, and silica	8051
ICP-AES [14]	0.079	0.5–10000	0.81% R.S.D. (200 mg/L) 1.2% R.S.D. (2800 mg/L)	Hydrochloric acid and calcium	6010B

<sup>a</sup> For sulfate quantification.





Sample Name: I-40-0.2 represents Influent - 40x dilution - 0.2  $\mu$ M filter; E - Effluent

Fig. 1. Comparison of sulfate quantification methods on field samples.

R.S.D. in Table 4. It should be noted that precision of IC, ICP and ICPAD analysis were almost independent of sample matrix. Turbidimetric sulfate measurements from field samples showed R.S.D. values from 0 to 12.7%, and these are higher than R.S.D.s obtained from control samples and other previously reported R.S.D. values. Precision of the turbidimetric samples were seriously affected by the nature of the sample matrix, and appeared to be interference from other anions and cations present in the mine water samples.

### 3.3.2. Comparison of sulfate methods by sulfate values

In this study, the turbidimetric method provided a high underestimation of sulfate values by as much as 50% less than the sulfate measured using other analytical techniques. In comparison to the laboratory samples, the field turbidimetric techniques showed poor results when the samples were diluted prior to the analysis. Mean values of sulfate obtained from ICP were slightly higher than the values obtained from both IC and digested

ICPAD analysis. Digested samples analyzed in ICPAD also provided sulfate values lower than the IC and ICP.

More detailed comparison of sulfate values was performed using the Bonferroni multiple comparison test based on a 95% confidence limit. Expressions used for Bonferroni tests are discussed elsewhere [29]. A pair-wise comparison of treatment means was conducted by comparing the difference between two treatment means. A critical difference B was calculated for each sample based on number of replicates, level of significance, standard deviation and the total number of treatments. The difference among treatment means was compared with the critical difference (B). If the difference in mean is greater than critical difference, we can conclude that there is a significant difference in treatment means, while if the difference is lower than the critical difference, treatment means are not different. Sulfate means obtained from different analytical technique were compared for each sample containing nine replicates. The values obtained from 24 samples consisting of 216 independent sulfate values

Table 5  
Bonferroni multiple comparison test

Pair	Number of significantly different samples
Ion chromatography-inductively coupled plasma (IC-ICP)	16 out of 24 (67%)
Ion chromatography-inductively coupled plasma with acid digestion (IC-ICPAD)	11 out of 24 (46%)
Ion chromatography-turbidimetric method (IC-TM)	24 out of 24 (100%)
Inductively coupled plasma-inductively coupled plasma with acid digestion (ICP-ICPAD)	23 out of 24 (96%)
Inductively coupled plasma-turbidimetric method (ICP-TM)	24 out of 24 (100%)
Inductively coupled plasma with acid digestion-turbidimetric method (ICPAD-TM)	23 out of 24 (96%)

Table 6  
Spike concentration and recovery

Dilution	IC		ICP		ICPAD		TM	
	Spike conc. <sup>a</sup> (mg/L)	Spike rec. <sup>b</sup> (%)	Spike conc. <sup>a</sup> (mg/L)	Spike rec. <sup>b</sup> (%)	Spike conc. <sup>a</sup> (mg/L)	Spike rec. <sup>b</sup> (%)	Spike conc. <sup>a</sup> (mg/L)	Spike rec. <sup>b</sup> (%)
40	1567.2	94.9	1657.8	106.5	1520.4	109.2	1328.9	96.9
80	1556	91.7	1649.5	101.1	1541.5	110.6	906.7	72.9
100	1555.2	91.4	1698.1	98.9	1547.8	115.9	855.6	71.1

<sup>a</sup> Mean sulfate values in spiked sample (mg/L).

<sup>b</sup> Spike recovery (%).

were used for the comparison. Overall distribution of the test results obtained from 24 samples was considered for validation.

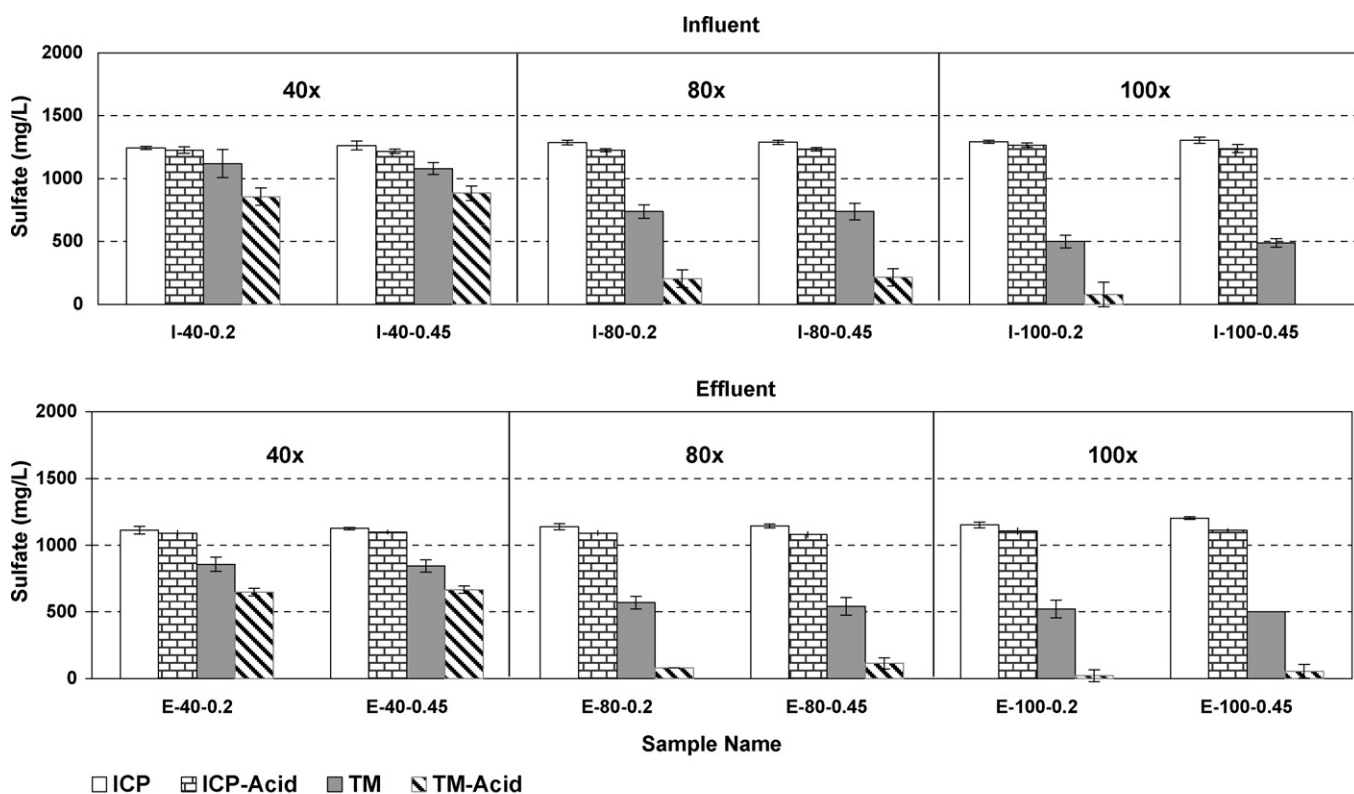
Results from Bonferroni test are listed in Table 5. Comparison of turbidimetric sulfate mean values with IC, ICP and ICPAD values showed that the means were different in most of the samples (96–100%), confirming the inaccuracy of turbidimetric method in determining the sulfate concentration. Results also showed that in 16 samples ( $\approx 67\%$ ), the mean sulfate values obtained from IC and ICP were different. Comparison of IC and ICPAD values showed relatively lower differences (46% of the 24 samples had the difference in means). Sulfate values obtained from sample with and without acid digestion showed a difference in most of the samples (96% of 24 samples had differences in mean). Differences between sulfate mean values seen in ICP and ICPAD can be attributed to presence of nitric acid in digested samples, which appears to enable better analysis free of interferences.

### 3.4. Spiked effluent samples

An effluent sample obtained from the Golinsky mine site was spiked with 500 mg/L of sulfate. The spiked effluent sample was analyzed in similar steps as control and unspiked samples. Results obtained from spiked samples are shown in Table 6. Spike recoveries calculated for IC, ICP and ICPAD samples were within 91–116% and 71–97% for turbidimetric analysis.

### 3.5. Effect of dilution

Effect of dilution on sulfate determination was investigated by analyzing samples diluted to desired dilution levels: 1:40, 1:80 and 1:100. Results from control samples listed in Table 3 show that the increasing sample dilutions (1:40–1:100) have pronounced effect on performance of the turbidimetric method reducing the recovery from 83.56 to 47.78%. Sulfate quantifica-



Sample Name: I-40-0.2 represents Influent - 40x dilution - 0.2 μM filter; E - Effluent

Fig. 2. Effect of acidification in field samples.

Table 7  
Effect of acidification in control samples

Dilution	Acid	ICP		TM		Certified value (mg/L)
		mg/L <sup>a</sup>	R.S.D. (%)	mg/L <sup>a</sup>	R.S.D. (%)	
40	Acid	1022.9	0.78	520	6.7	1000
80	Acid	1035.7	0.34	177.8	30	1000
100	Acid	1031.6	0.32	0	0	1000

<sup>a</sup> Mean sulfate values (mg/L).

tion of control samples was almost independent of dilution during the IC, ICP and ICPAD analyses. When spiked and unspiked field samples were analyzed, results depicted in Table 6 and Fig. 1 reveal that accuracy of turbidimetric method was affected severely by sample dilution. Performance of IC, ICP and ICPAD methods were unaffected by dilution of spiked and unspiked samples. When turbidimetric sulfate values obtained from samples subjected to different dilution levels were compared, effect of acidification was pronounced in the diluted samples as shown in Fig. 2.

### 3.6. Effect of acidification

Effect of sample acidification was determined by comparing the sulfate values with and without addition of nitric acid. Sample acidification was followed based on the procedure used in preservation of metal analysis samples. In the field, when other samples are taken and acidified for metal analyses in the laboratory, accidental acidification of the sulfate samples has been observed by the authors. Concentrated nitric acid (0.65 mL) was added to 50 mL sample to insure the pH was below 2. Acidified and non-acidified samples were analyzed by ICP and turbidimetric methods. Results from control samples were shown in Table 7. When comparing sulfate values obtained from acidified and non-acidified samples analyzed in ICP in this study, the effect of acidification was statistically insignificant. In the turbidimetric analysis a large drop in sulfate concentration was observed. The sulfate concentration dropped from 477.8 to 0 mg/L when the acidified samples were analyzed.

When sulfate values obtained from acidified field samples were compared with non-acidified mine samples depicted in Fig. 2, a similar trend was observed as in control samples. Effects of acidification on field samples were statistically insignificant in ICP analysis, whereas a considerable drop in sulfate concentration was observed when samples were acidified in the turbidimetric analysis. Baban et al. reported serious interference from a high concentration of nitrate during flow-injection turbidimetric sulfate analysis. Results from their study also showed a similar trend, sulfate concentration dropping to negligible levels when the nitrate concentration was increased. Bobtelsky and Eisenstadter confirmed the possibility of co-precipitation of nitrate ions as barium nitrate, thereby delaying the end point during the titration [30]. The reason for the drop in sulfate concentration in the case of acidified samples during the turbidimetric method might be due to the presence of an excessive amount of nitrate ions. In the case of turbidimetric analysis employed in this investigation, excessive nitrate ions might have acted as

Table 8  
Details of ANOVA procedure

Model information	
Dependent variable	Sulfate
Covariance structure	Compound symmetry
Subject effect	Matrix (method × dilution × filtration)
Estimation method	REML
Residual variable method	Profile
Fixed effects of SE method	Model-based
Degrees of freedom method	Satterthwide
Dimension	
Covariance parameters	2
Columns in X	36
Columns in Z	0
Subjects	96
Max observations per subject	9
Observations used	864
Additional information	Convergence criteria met. Types three tests are used for fixed effects

a competitive ion, thus increasing the solubility of barium ions in the solution. Investigators working on spectrometric determination of barium sulfate precipitate reported interferences from nitrate when it was present >100 mg/L [31].

### 3.7. ANOVA

Results obtained from non-acidified samples, including the replicate sulfate measurements, were subjected to analysis of variance (ANOVA) to quantify the main and interactions effects of factors considered in this study using Statistical Analysis Software (SAS 9). Table 8 provides the details of ANOVA procedure. ANOVA results presented in Table 9 were based on sulfate concentration as the dependent variable at 95% confidence limit. The probability statistic, *P*, is compared to chosen  $\alpha$  value 0.05 (95% confidence limit) to evaluate the main effect of factors on sulfate measurement. If the *P* value is less than

Table 9  
ANOVA results

Source of variation	Num DF	Den DF	F-value	P level
Main effects				
Method	2	78	1.56	<0.0001
Dilution	1	78	0	0.2169
Filter size	3	78	24.06	0.9644
Interaction effects				
Method × dilution	2	78	0	0.0531
Method × filter size	6	78	2.19	0.9999
Dilution × filter size	3	78	0	0.9964

0.05, we can conclude that the main effect is significant with 95% confidence. ANOVA results listed in Table 9 confirm that quantification method had a significant individual effect on sulfate quantification as the  $P$  value ( $<0.0001$ ) was less than the  $\alpha$  value (0.05). The  $P$  value of main effect of filter pore size alone was 0.9644, revealing the insignificant effect on sulfate determination. Even though dilution had a pronounced effect on turbidimetric analysis, the probability statistic ( $P=0.2169$ ) was greater than  $\alpha=0.05$ , implying that when all three quantification were considered the impact of dilution on sulfate quantification was not significant. This trend can be further explained by analyzing the interaction effects between dilution and quantification method.

ANOVA results listed in Table 9 show that the two-way interaction involving determination method and dilution (method–dilution) had a  $P$  value (0.0531) closer to  $\alpha$  value (0.05). A relatively significant interaction effect between determination method and dilution (method–dilution) was mainly attributed to the trends observed during turbidimetric method. Other two-way interaction  $P$  values (0.9999 and 0.9964) were closer to 1, confirming that the interactions were insignificant (method–filter pore size, and dilution–filter pore size).

#### 4. Conclusion

Results reported in this investigation indicate clearly that the widely used turbidimetric sulfate determination method is limited by its quantification range and suffers from interference of nitrate ions. Furthermore, sample dilution had a pronounced effect on the turbidimetric method, reducing measured sulfate concentration by nearly 50%. When 100 times diluted samples were acidified prior to the analysis, sulfate values dropped to 0 mg/L during turbidimetric analysis. Surprisingly, in the ICP without acid digestion analysis, recoveries of sulfate were improved from 106 to 103% when the sample was acidified. IC method showed higher precision in quantifying sulfate in controls and fields samples and performance is almost independent of sample dilution.

The underlying assumption of negligible non-sulfate sulfur species in ICP-AES analysis was found to be suitable mainly in the case of samples collected from oxidized conditions. Further studies elucidating the speciation of sulfur are required in the case of samples from reducing conditions. ICP-AES analysis provides a versatile indirect way of sulfate quantification with larger quantification and almost negligible matrix, dilution and acidification effects. In this study, acid digestion of samples prior to the analysis slightly decreased the precision and accuracy of the ICP-AES analysis. While the authors have completed this study under the best quality standards, because of the implication, further research should be conducted to validate these results. Until those studies are completed, analysis of field and laboratory samples for sulfate using the turbidimetric method should be verified using either the ICP or IC method. In field instances where the verification may be delayed, the data should be marked to denote which sulfate determination method was employed and what equipment was used.

#### Acknowledgments

This paper has not been subjected to internal policy review. Therefore, the research results presented herein do not, necessarily, reflect the views of the USEPA or its policy. Mention of trade names or commercial products does not constitute endorsement or recommendation for use.

#### References

- [1] A.G. Howard, Aquatic Environmental Chemistry Oxford Chemistry Primers, 57, Oxford University Press, Oxford, UK, 1998, p. 84.
- [2] D.B. Johnson, Water Air Soil Poll.: Focus 3 (2003) 47.
- [3] Å. Kolmert, P. Wikström, K.B. Hallberg, J. Microbiol. Meth. 41 (2000) 179.
- [4] U.S. Government CFR 40: Protection of environment 40 CFR Ch. 1 Pt 143.3 7-1-021979.
- [5] A.H. Kaksonen, P.D. Franzmann, J.A. Puhakka, Biodegradation 14 (2003) 207.
- [6] J.A. Morales, L.S. de Graterol, J. Mesa, J. Chromatogr. A 884 (2000) 185.
- [7] B. Christensen, M. Laake, T. Lien, Water Res. 30 (1996) 1617.
- [8] N.G. Elenkova, R.A. Tsoneva, T.K. Nedelcheva, Talanta 27 (1980) 67.
- [9] R. Raghavan, S. Raha, Talanta 38 (1991) 525.
- [10] R.J. Bertolacini, J.E. Barney, Anal. Chem. 29 (1957) 281.
- [11] APHA, Standard Methods for the Examination of Water and Wastewater, 16th ed., APHA, Washington, 1985.
- [12] R.P. Singh, N.M. Abbas, S.A. Smesko, J. Chromatogr. A 733 (1996) 73.
- [13] M.W. Pritchard, J. Lee, Anal. Chim. Acta 157 (1984) 313.
- [14] D.L. Miles, J.M. Cook, Anal. Chim. Acta 141 (1982) 207.
- [15] R.T. Sheen, H.L. Kahler, E.M. Ross, W.H. Betz, L.D. Betz, Ind. Eng. Chem. 7 (1935) 262.
- [16] R. Sidjerius, Anal. Chim. Acta 11 (1954) 28.
- [17] S. Baban, D. Beetlestone, D. Betteridge, P. Sweet, Anal. Chim. Acta 114 (1980) 319.
- [18] J.A. Vieira, J. Raimundo, M. Ivo, B.F. Reis, Anal. Chim. Acta 438 (2001) 75.
- [19] I.P.A. Morais, M.R.S. Souto, T.I.M.S. Lopes, A.O.S.S. Rangel, Water Res. 37 (2003) 4243.
- [20] R. Burakham, K. Higuchi, M. Oshima, K. Grudpan, S. Motomizu, Talanta 64 (2004) 1147.
- [21] J.F. van Staden, R.E. Taljaard, Anal. Chim. Acta 331 (1996) 271.
- [22] Hach Co., Water Analysis Handbook, Method 8051 2003.
- [23] S. Eberts, S.A. Jones, C.L. Braun, G.J. Harvey, Ground Water 43 (2005) 178.
- [24] U.S. EPA, SW 846, Test methods for evaluating solid waste physical/chemical methods, Method 300.0, Determination of inorganic anions by ion chromatography, 1999.
- [25] J. Nolte, ICP Emission Spectrometry: A Practical Guide, Wiley–VCH Verlag GmbH & Co., KgaA, Weinheim, 2003, p. 201.
- [26] U.S. EPA, SW 846 Test methods for evaluating solid waste physical/chemical methods, Method 6010B, Inductively coupled plasma atomic emission spectrometry, 1996.
- [27] U.S. EPA, SW 846, Test method for evaluating solid waste physical/chemical methods, Method 3051, Microwave assisted acid digestion of sediments, sludges, solids and oils, 1994.
- [28] A. Mroczek, G. Werner, R. Wennrich, W. Schrön, Fresen. J. Anal. Chem. 361 (1998) 34.
- [29] W. Medenhall, T. Sinsich, Statistics for Engineering and the Sciences, 4th ed., Prentice-Hall, Inc., New Jersey, USA, 1994, p. 895.
- [30] M. Bobtelsky, J. Eisenstadter, Anal. Chim. Acta 14 (1956) 186.
- [31] T.R. Crompton, Determination of Anions, Springer-Verlag Berlin Heidelberg, Germany, 1996, p. 305.



# Measurements of calcium with a fluorescent probe Rhod-5N: Influence of high ionic strength and pH

Anne-Cécile Ribou\*, Jean-Marie Salmon, Jean Vigo, Catherine Goyet

*University of Perpignan, BDSI Biophysics and dynamics of Integrated Systems, 52 av. Paul Alduy, 66860 Perpignan, France*

Received 25 November 2005; received in revised form 4 April 2006; accepted 14 April 2006

Available online 24 May 2006

## Abstract

We describe a new method for the spectroscopic determination of high calcium concentration using a fluorescent probe Rhod-5N. This method was investigated in order to be utilized in high ionic strength solution, such as seawater. The probe is fluorescent when bound to calcium, LM, but not as the free form L. The dissociation constant of the equilibrium (0.14 mM) was determined at several ionic strengths, i.e. in the absence and in the presence of additional ions (0.7 M NaCl). The influence of pH was studied. In order to correctly model the experimental data, we included a new fluorescent compound: LHM (calcium bound protonated probe). The first acidity constant (0.02  $\mu$ M) and the second dissociation constant (4.5 mM) were calculated. A useful range for the determination of calcium concentration is provided. Such a method is fast and easy to carry out. © 2006 Elsevier B.V. All rights reserved.

*Keywords:* Rhod-5N; Fluorescence; Probe; Calcium; Data analysis; Seawater

## 1. Introduction

Formation and dissolution of calcium carbonate in the ocean are important players in the global carbon cycle and are intimately related to the control of atmospheric CO<sub>2</sub>. This gas, one of the most abundant green house gases in the earth's atmosphere, is thought to be mostly absorbed by the oceans and ultimately neutralized by the reaction with CaCO<sub>3</sub> in marine sediments. The precipitation and dissolution of calcium carbonate are a function of [Ca<sup>2+</sup>] and [CO<sub>3</sub><sup>2-</sup>] concentrations as well as the calcite and aragonite solubility constants. In the open ocean, variations of Ca<sup>2+</sup> concentrations are rather small and related with salinity variations. However, a direct determination of [Ca<sup>2+</sup>] can help in the determination of CaCO<sub>3</sub> saturation state and in the understanding of the carbon cycle.

In 1976, Lebel and Poisson [1] proposed a potentiometric titration of magnesium and calcium ions in seawater. The method uses the differences between ethylenediaminetetraacetic acid (EDTA) and ethyleneglycol bis-( $\beta$ -aminoethyl ether)-*N*-*N'* tetraacetic acid (EGTA) dissociation constants. They obtain, in ideal conditions, a reproducibility of 1/1000. However, this

method is long and demanding. It requires stable environment to avoid erroneous measurements and it cannot be adapted for on board measurements, as a result, it is barely used. Recently, a number of teams attempted to develop new methods using electrophoresis [2], plasma atomic spectrometry [3,4] and near-infrared spectroscopy [5]. We make use of our knowledge of fluorescent probe to conceive new calcium measurements. Molecular probe, Inc. provides calcium probe with high dissociation constant, the highest belonging to Rhod-5N. Fluorescent measurements are fast and require small volume of seawater (<1 ml). Nowadays, companies can provide small spectrofluorimeter that can be easily brought on boat.

In this paper, we described the probe interaction with calcium and proton. We check the influence of high ionic strength on the measurement. We propose a methodology and a model to determine calcium quantity in high ionic strength solution, such as seawater. Finally, we test the reproducibility of the method and give a useful range of optimal utilization.

## 2. Experimental

### 2.1. Chemicals

CaCl<sub>2</sub>, NaCl, HgCl<sub>2</sub> and EDTA are of analytical grade and are used as received. A buffer solution of Titrisol at pH 8 is

\* Corresponding author. Tel.: +33 468662113; fax: +33 468662144.  
E-mail address: [ribou@univ-perp.fr](mailto:ribou@univ-perp.fr) (A.-C. Ribou).



used. No calcium concentration higher than residual calcium is detected in this solution. Addition of 10% of the buffer, give a stable pH ( $8.05 \pm 0.02$ ). Rhod-5N was purchased from Molecular Probe, Inc. Aliquots of 40  $\mu\text{l}$  Rhod-5N at 0.6 mM are kept at  $-20^\circ\text{C}$ . Before use, the solution is diluted to the final volume of 1 ml with de-ionized water. The final concentration is tested by recording a fluorescence spectrum for each new solution. Ultra-pure de-ionized water was generated by a MilliQ plus system (Millipore).

## 2.2. Fluorescence measurements

Emission fluorescence spectra are recorded with a spectrofluorimeter (Flx, SAFAS, Monte Carlo, Monaco) after excitation at 551 nm. At this wavelength and at the working concentration, the fluorescence intensity of the probe is more than thousand times higher than the combined intensities of the Raman band and the dissolved organic material in seawater samples. Residual calcium is found in the water used for the experiments. It has to be regularly checked that the residual concentration does not exceed 10  $\mu\text{M}$ . The glassware is washed with concentrated solution of acid (HCl) and rinsed with de-ionized water. If required, EDTA solution is used.

Three different experiments were performed for  $K_d$  determination, for pH variation and for reproducibility of  $\text{Ca}^{2+}$  determination.

### 2.2.1. $K_d$ determination

When the fluorescent spectra of the free probe L and the bound probe LM are different,  $K_d$  can be determined studying the evolution of the LM fluorescence spectra in presence of M. Knowing  $K_d$  the relation can be used to calculate the concentration of M. For these experiments, the concentration of probe L is chosen constant and we vary the concentration  $[\text{M}]_{\text{total}}$  of calcium. Two solutions are prepared: solution A containing Rhod-5N (0.3–0.6  $\mu\text{M}$ ), buffer at pH 8 (10%) and residual calcium, and solution B, containing specific calcium concentration in solution A. Varying concentrations of calcium are prepared by mixing different amounts of the two solutions A and B. If necessary, the pH is adjusted with micro-drop of NaOH. The fluorescence spectra are recorded for up to 14 calcium concentrations between 10  $\mu\text{M}$  and 20 mM.

### 2.2.2. pH variation

With calcium chelating dyes, protonated and non-protonated probes show two different fluorescent forms [6]. We study the evolution of the LM fluorescent spectra in presence of  $\text{H}^+$  proton. This was done in order to determine at which pH the non-protonated form exists alone. For these experiments, micro-volumes of NaOH or HCl are added to fresh solution B directly in the glass spectrocell. pH is measured with a pH-meter (PHN 81, Tacussel) with an accuracy of 0.01. The fluorescent spectra are recorded for 20 solutions ranging from 4 to 10.

### 2.2.3. Reproducibility

For  $\text{Ca}^{2+}$  determination experiments, the reproducibility of the results is checked preparing several solutions of the same

Table 1

Mean and standard deviation (S.D.) of Rhod-5N fluorescence intensities and calculated calcium concentrations for five identically prepared solutions

	Corrected <sup>a</sup> $I_{\text{LM}}$ (a.u.)	Corrected <sup>b</sup> $I_{\text{max}}$ (a.u.)	(Ca) <sup>c</sup> (M)	[Ca] <sup>d</sup> (M)
	7461	22699	$4.10 \times 10^{-4}$	$1.00 \times 10^{-3}$
	7414	22086	$4.23 \times 10^{-4}$	$1.04 \times 10^{-3}$
	7697	22738	$4.29 \times 10^{-4}$	$1.05 \times 10^{-3}$
	7471	22746	$4.10 \times 10^{-4}$	$1.00 \times 10^{-3}$
	7662	22777	$4.25 \times 10^{-4}$	$1.04 \times 10^{-3}$
Mean	7442	22600	$4.19 \times 10^{-4}$	$1.03 \times 10^{-3}$
S.D.	180	290	$0.08 \times 10^{-4}$	$0.02 \times 10^{-3}$

<sup>a</sup> Correction factor for LH: 1.090 (Section 3.3.3).

<sup>b</sup> After addition of 25  $\mu\text{l}$  Ca (4M) to the 1 ml solution. Correction factors: dilution factor (1.025/1) and probe saturation factor: 1.060 (Section 3.2.2).

<sup>c</sup>  $[\text{NaCl}] = 0.07 \text{ M}$ ,  $[\text{L}]_{\text{total}} = 0.48 \mu\text{M}$  and  $K_{\text{dLM}} = 1.4 \text{ mM}$ .

<sup>d</sup>  $\gamma_{\text{Ca}} = 0.409$ .

calcium concentrations with various NaCl concentrations. In Table 1, 20  $\mu\text{l}$  of the probe (24  $\mu\text{M}$ ), 10% of buffer (pH 8) and 100  $\mu\text{l}$  of NaCl (0.7 M) are mixed directly in the glass spectrocell with 100  $\mu\text{l}$  of calcium (10 mM). De-ionized water is added to obtain 1 ml final volume. After spectrum recording, 25  $\mu\text{l}$  of calcium (4 M) are added to the solution. This is done in order to check the variation of the total probe concentration  $[\text{L}]_{\text{total}}$ . The pH is increased with micro-drops of NaOH to a value between 8.5 and 10. The probe spectrum in the solution with an excess of calcium is then recorded. The temperature is regulated at  $25 \pm 0.1^\circ\text{C}$ .

## 2.3. Data analysis

Since LM is the only fluorescent form, LM concentration can be calculated from the experimental data obtained at constant volume:

$$[\text{LM}] = \frac{I_{\text{LM}}}{I_{\text{max}}} \times [\text{L}]_{\text{total}} \quad (1)$$

where  $[\text{L}]_{\text{total}}$  is the total probe concentration and  $[\text{LM}]$  is the calcium bound probe concentration.  $I_{\text{LM}}$  is the intensity of LM at the equilibrium and  $I_{\text{max}}$  is the intensity if the entire probe is bound to calcium. It was initially determined after addition of an excess of calcium. After analysis of the fluorescence spectra, we obtain an experimental curve of LM concentration as a function of the total calcium concentration (Fig. 1) or as a function of pH (Fig. 2). The total calcium concentration is calculated considering the calcium concentration of solution B and calcium residual in solution A.

## 2.4. Theoretical model

We created a theoretical model in order to model the experimental data. A system of equilibrium equations defines the binding model. Basic hypotheses about individual species involved in these interactions are made as follows.

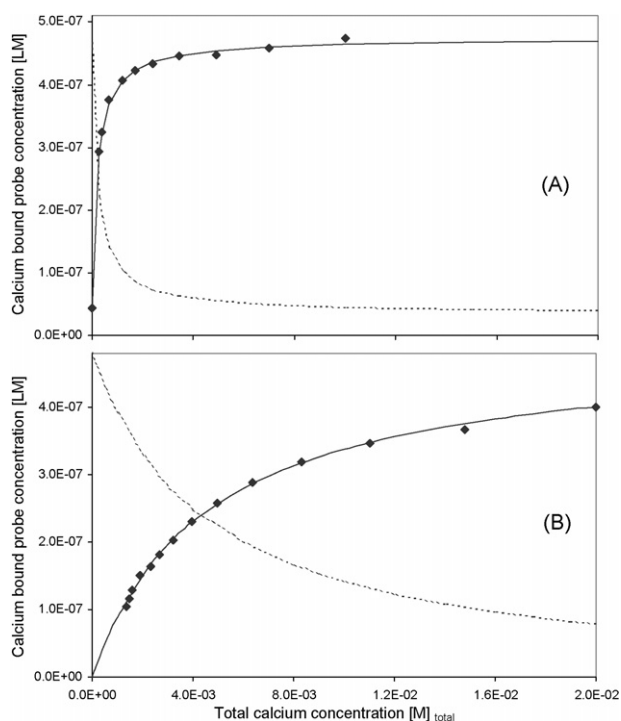


Fig. 1. Concentration of Rhod-5N bound to calcium vs. calcium concentration measured by fluorescence. The X-axis represents calcium concentration in the solution in mol per liter. The Y-axis represents LM concentration in mol per liter. Experimental data are shown as full symbols ( $\blacklozenge$ ), theoretical data obtained with Eq. (3) as full line. The dotted line corresponds to L concentration (free Rhod-5N). (A)  $[L]_{\text{total}} = 0.51 \mu\text{M}$ ,  $[\text{NaCl}] = 0 \text{ M}$  and (B)  $[L]_{\text{total}} = 0.48 \mu\text{M}$ ,  $[\text{NaCl}] = 0.7 \text{ M}$ .

#### 2.4.1. $K_d$ determination

pH was maintained to 8 in order to avoid the presence of protonated form of the probe. The environment is modeled by the classical equilibrium between M (the calcium) and L (the free probe). We obtain:

$$[L] = K_{dLM} \times \frac{\gamma_{LM}}{\gamma_L \times \gamma_M} \times \frac{[LM]}{[M]} \quad (2)$$

We find the theoretical Eq. (3) resulting from the conservation of the probe concentration at constant volume  $[L]_{\text{total}} = [L] + [LM]$ :

$$[LM] = \frac{[L]_{\text{total}}}{(1 + (K_{dLM}/[M]_{\text{total}}) \times (\gamma_{LM}/\gamma_L \times \gamma_M))} \quad (3)$$

The fluorescent probe concentration  $[LM]$  is connected to the total calcium concentration  $[M]_{\text{total}}$  and total probe concentration  $[L]_{\text{total}}$  with equilibrium constants  $K_{dLM}$  as variable. We assume that  $[M]$  is equal to  $[M]_{\text{total}}$  when  $[M]_{\text{total}} > 100[L]_{\text{total}}$ . In order to compare the experimental and the theoretical curves, the variables are computed with the solver of MS Excel [7].

#### 2.4.2. pH variation

The complex model, presented here, is used to correctly simulate the pH variation experiments. The complex equilibrium system of L, M, H, LM, LMH, LH, LH<sub>2</sub> species (L = Rhod-5N and M = calcium and H = proton), when the calcium M binds to

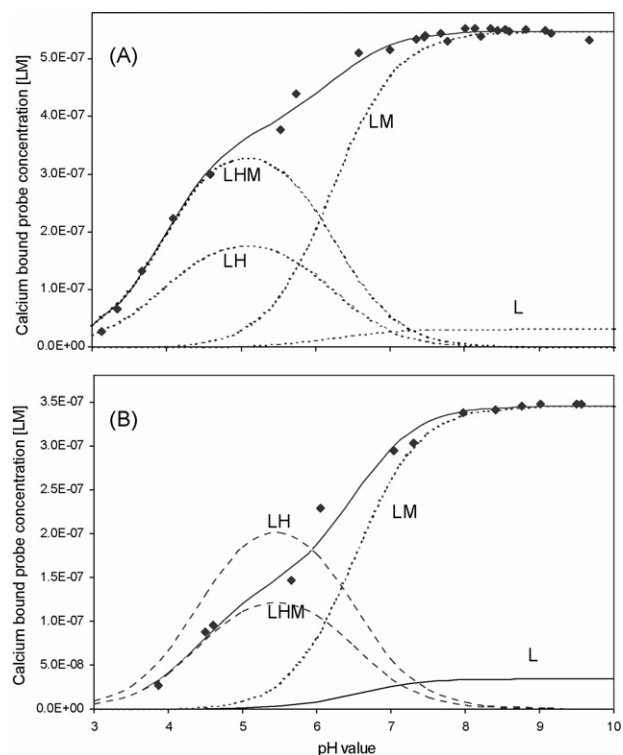


Fig. 2. Concentration of Rhod-5N bound to calcium vs. proton concentration measured by fluorescence. The X-axis represents pH value, corrected for the error of the pH-meter. The Y-axis represents LM concentration in mol per liter. Experimental data are shown as full symbols ( $\blacklozenge$ ), and theoretical data as full line (LM + LHM). The different component concentrations in solution calculated by the model are presented as dotted line. The compound name is given next to the respective curves: LM (Rhod-5N bound to calcium); LH (protonated Rhod-5N); LHM (protonated Rhod-5N bound to calcium); L (free probe). (A)  $[L]_{\text{total}} = 0.58 \mu\text{M}$ ,  $[M]_{\text{total}} = 0.1 \text{ M}$  and (B)  $[L]_{\text{total}} = 0.38 \mu\text{M}$ ,  $[M]_{\text{total}} = 0.01 \text{ M}$ .

L and to LH, is solved. Four equations for LM, LH, LHM and LH<sub>2</sub> have to be solved. We assume that LM and LHM are both fluorescent.

The mathematical resolution results from the conservation of the probe concentration  $[L]_{\text{total}} = [LM] + [L] + [LH] + [LHM] + [LH_2]$ , with  $[L]$  defined in Eq. (2)

$$[LH] = \frac{1}{K_{aLH}} \times \frac{\gamma_L}{\gamma_{LH}} \times (H) \times [L] \quad (4)$$

$$[LHM] = \frac{1}{K_{dLHM}} \times \frac{\gamma_{LH} \times \gamma_M}{\gamma_{LHM}} \times [LH] \times [M] \quad (5)$$

$$[LH_2] = \frac{1}{K_{aLH_2}} \times \frac{\gamma_{LH}}{\gamma_{LH_2}} \times (H) \times [LH] \quad (6)$$

Combining these equations, we obtain second-degree equation to calculate  $[LM]$ .  $[LM]$  is computed resolving this second-degree equation,  $[LHM]$  is computed with Eqs. (2), (4)–(6). Fluorescent probe concentration ( $[LM] + [LHM]$ ) is connected to proton activity (H), total calcium concentration  $[M]_{\text{total}}$  and total probe concentration  $[L]_{\text{total}}$  with equilibrium constants  $K_{dLM}$ ,  $K_{aLH}$ ,  $K_{dLHM}$ ,  $K_{aLH_2}$  as variables. The proton activity (H) is obtained from pH data.

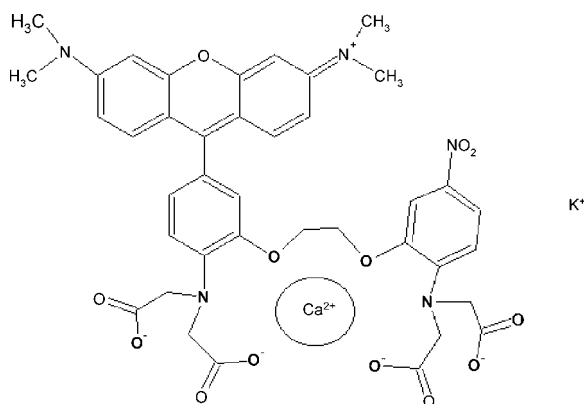


Fig. 3. Structure of calcium bound Rhod-5N: LM. Atoms in bold letters correspond to the crown ether structure. Global charge of the anion: 1, of the counter ion  $K^+$ : 1.

### 2.4.3. Activity coefficients

Activity coefficients of each ions in the prepared solutions are calculated from Davies formula (derived from Debye and Hückel theory) [8]:

$$\log(\gamma_M) = -A \times z_i^2 \left( \frac{\sqrt{I}}{1 + \sqrt{I}} - 0.3 \times I \right) \quad (7)$$

The coefficient  $A$  varies with temperature; at  $25^\circ\text{C}$  we take 0.509. Notice that the ionic strength change with the ion concentration  $C_i$  ( $I = 1/2 \sum c_i z_i^2$ ). As long as the calcium concentration is above 0.1 mM we neglect the probe and proton concentrations. Thus, calcium concentrations vary during  $K_d$  determination experiments but not for pH variation experiments. It is also true for the activity coefficient of each ion.  $z_i$  is the global charge of the ions. We assume that the global charge of the probe is equal to 3 for the free probe L, 1 for LM (Fig. 3), 2 for LH, 1 for LH<sub>2</sub> and 0 for LHM.

## 3. Results and discussion

The metal chelate LM is shown in Fig. 3. The probe forms a crown ether structure around the calcium ion, the two remaining carboxyl group positioning above and below the central structure. Complexation avoids possible interaction between carboxyl and amino groups due to electrostatic attraction. In the free probe L, the twist due to this interaction makes less favorable the delocalization in the rhodamine moiety. It certainly causes the quenching of the fluorescence of the free probe.

### 3.1. Rhod-5N emission

The probe is fluorescent when bound to calcium, i.e. LM, with an intensity maximum at 574.5 nm. The linearity of the response of the probe fluorescence is verified when totally bounded, within the range 0.1–0.8  $\mu\text{M}$  Rhod-5N. After EDTA addition, the probe solution, i.e. L, does not show fluorescence anymore. Without EDTA, in de-ionized water the residual calcium bounds partially to the probe. Increasing the calcium concentration increases the fluorescence intensity of LM, the

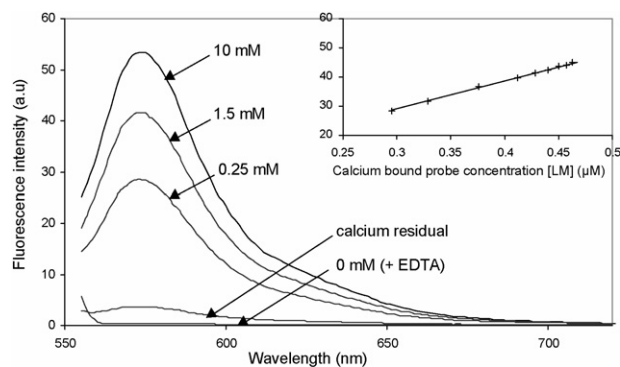


Fig. 4. Experimental spectra of Rhod-5N (0.51  $\mu\text{M}$ ) after excitation at 551 nm obtained for different calcium concentrations. The X-axis represents the emission wavelength in nanometer. The Y-axis represents the fluorescence intensity in arbitrary units. Five spectra were recorded separately and overlaid. The arrows pointed to the respective curves indicate the corresponding calcium concentration. *Insert*: The fluorescence intensity versus calcium bound probe concentration calculated from the corresponding calcium concentrations.

metal chelate. These results are shown in Fig. 4. The response of the fluorescence signal versus calcium bound probe, LM, concentration is linear (Fig. 4, insert) in all the range tested ( $[M] = 0.1\text{--}10\text{ mM}$ ). The fluorescence spectrum shape does not change up to 0.2 M. However, we observe a gradual red-shift when the calcium concentration becomes higher than 0.2 M due to a more complex behavior. It is already known that the fluorescence of the cation probe Mag-Indo-1 changes with increasing calcium concentration [9]. Here, we record spectra below this calcium concentration. Besides, since the unbound probe L is degraded under irradiation, we carefully avoid irradiation before recording the spectrum and reduce the recording-range between 560 and 630 nm. We do not notice any degradation of the calcium bound probe LM.

### 3.2. Determination of $K_d$

Fig. 1 shows the concentration of the calcium bound probe  $[LM]$  versus the total calcium concentration  $[M]_{\text{total}}$  in absence (Fig. 1A) and in presence (Fig. 1B) of sodium chloride. Experimentally, the calcium concentration is decreased and the pH is kept at 8.0 (see Section 2). Experimental  $[LM]$  is calculated (Eq. (1)) from the intensities and the total probe concentration  $[L]_{\text{total}}$ .

Eq. (3) gives the theoretical  $[LM]$ . In Fig. 1A, only calcium and Rhod-5N are present in solution. The equilibrium between L and LM depends on the equilibrium constant, with  $K_{dLM}$  the only variable in the equation to be computed with the solver of MS Excel. For each point,  $[M]_{\text{total}}$  is calculated using the calcium concentration of solution B and calcium residual in solution A. This concentration varies from one experiment to the other. It is calculated from the fluorescence intensity of solution A and we use it as an additional variable in the model. We compute the dissociation constant ( $0.14 \pm 0.03\text{ mM}$ ) and the residual calcium concentration.  $K_{dLM}$  is lower than the dissociation given by Molecular Probe (0.32 mM). The residual calcium (13  $\mu\text{M}$ ) was exceptionally high in our first experiment. The correction for residual calcium is not necessary in this case, but improved

the fit of experimental and modeled curves at lower calcium concentrations.

### 3.2.1. Addition of NaCl

Seawater is a complex medium. If the calcium is present at about 10 mM, the other ions increase the global ionic concentrations. Salinity 35 is equivalent to a sodium chloride concentration of 0.7 M. To confirm the validity of our model and to test  $K_{dLM}$  value, we decided to reproduce the experiments replacing the de-ionized water by a solution of 0.7 M NaCl. The experimental data and the model (Eq. (3)) is shown in Fig. 1B. The ionic strength of our solutions (0.69–0.72) is slightly higher than the limit recommended by Davies formula ( $I > 0.5$ ). However, we obtain a reasonable good similarity between the experimental and theoretical data with identical  $K_{dLM}$  value (0.14 mM) and residual calcium concentration of 1.2 mM. This high concentration is probably due to a calcium impurity in the commercially obtained NaCl. As expected, after NaCl addition, the probe binding is delayed. After addition of 20 mM of calcium the probe is not fully bound anymore.

### 3.2.2. $I_{max}$ calculation

To calculate the experimental [LM] with Eq. (1), we need to obtain  $I_{max}$ , the intensity when the entire probe is bound to calcium. Generally (Fig. 1), the employed calcium concentration is not sufficient to entirely bind the probe especially for high ionic strength solutions. We perform a correction to obtain a realistic value of  $I_{max}$ . Moreover, calcium concentration higher than 0.2 M cannot be used without changing the probe binding. From the theoretical model, we calculate  $I_{max}$ . For example, with initial  $[M]_{total} = 0.02$  M,  $[L]_{total} = 0.48$   $\mu$ M and  $[NaCl] = 0.7$   $\mu$ M (Fig. 1B) we used a probe saturation factor of 1.198 (4.800/4.006). After correction we obtained  $I_{max} = 22,300$  a.u., the intensity of the first recorded spectrum (higher calcium concentration) was only of 18,600 a.u.

### 3.3. pH variation

Accurate results require careful control of pH value since the binding equilibrium is strongly dependent on pH. Molecular Probes advises to work at pH above 6 [10]. LH is a non-fluorescent form of the probe. However, the fluorescent probe LM concentration will depend on LH deprotonation. To confirm that at pH 8 no LH is present, we perform pH variation experiments.

Fig. 2 shows the experimental data obtained for constant calcium concentrations,  $[M]_{total} = 0.1$  M (Fig. 2A) and for  $[M]_{total} = 0.01$  M (Fig. 2B). The latter concentration corresponds to the calcium concentration in seawater. At these concentrations even for high pH values, the probe is not totally bound to calcium (94% and 91%, respectively). The ionic strength ( $I = 0.3$  and 0.03, respectively) is not dependent on the proton concentration. Therefore, the ion activities are constant. To model these experimental data, the equilibrium of LM and LH alone cannot be used. The shape of the curve is too complex. To correctly model these data, we use the second-degree equation described in Section 2.

### 3.3.1. Model

We assume that calcium can bind LH. The new complex LHM is fluorescent and shows a spectrum identical to the one of LM. Since the structure of LHM is very similar to the one of LM (i.e. no interaction between carboxyl and amino groups) there is no reason for a spectral change. But, we expect the affinity of LH to calcium to be smaller than that of L since only three carboxyl groups are present. The new dissociation constant is  $K_{dLHM}$ . Thus, the addition of a fourth equilibrium (for the formation of  $LH_2$  in competition with LHM) with a second acidity constant ( $K_{aLH_2}$ ) is necessary. The addition of subsequent  $LH_3$  and  $LH_2M$  forms of the probe was not required as our model already correctly fit the experimental data. Moreover, the affinity of  $LH_2$  for calcium must be highly reduced. We were able to model the two sets of data with the same set of constants after a careful search for the global charge of the probe complexes. We make simple hypotheses as followed: carboxyl groups: four negative charges and amino group: one positive charge (global charge of L: 3). After addition of  $Ca^{2+}$ , the global charge of LM is 1 (Fig. 3). After reaction of one carboxyl group with a proton, the global charge of LH is 2 and that of LHM is 0.

### 3.3.2. Dissociation and acidity constants

The simulation of the experimental data with a model with four constants allows for many possible solutions for the four values. To obtain the new constants with reliability, we set  $K_{dLM}$  to 0.14 mM. This enabled us to find for the two experiments (Fig. 2A and B), the following set of constants: dissociation,  $K_{dLHM} = 4.5$  mM and acidity,  $K_{aLH} = 0.02$   $\mu$ M and  $K_{aLH_2} = 15$   $\mu$ M. The presence of a second calcium-probe equilibrium can explain the difference found between the dissociation constant given by Molecular Probe (0.32 mM) and our dissociation constants (0.14 and 4.5 mM). The value of  $pK_{aLH}$  is 7.7.

### 3.3.3. Working pH

In Fig. 2, we can observe that the protonated forms of the probe, LH and LHM; are present, among others, between pH 6 and 8. From the theoretical model established for the pH variation, we can extrapolate the pH value from which these two protonated forms disappeared. In Fig. 2B ( $[Ca^{2+}] = 0.01$  M), at pH 8, less than 2% of the probe are bound to proton. For  $[Ca^{2+}] = 0.001$  M, 9% of the probe are bound to protons. This will restrict the use of Eq. (3) for measurements of calcium at this pH and lower one. However, a mathematical correction of the probe concentration can be simply obtained from the theoretical model. This will allow working at a chosen pH.

### 3.4. Useful range of utilization and reproducibility

The method is tested for the determination of calcium concentration by multiple replicate measurements. Different manipulation conditions are tested and compared (replacement of titrisol solution by NaOH, pH 9). We have also tested the potential interactions of other cations with Rodh-5N to mimic the complexity of seawater. We have checked the effect of the addition of  $MgCl_2$  ( $Mg^{2+}$  being the main cation in seawater after  $Na^+$ ) and of the

addition of  $\text{HgCl}_2$  (1  $\mu\text{l}$ /1 ml, an inhibitor of biological development that is added to the sea sample for technical reason). We did not see changes of the spectrum shape or changes of fluorescence intensities after addition of  $\text{HgCl}_2$  or  $\text{MgCl}_2$ .

In order to obtain an optimal utilization range, we make the hypothesis that we obtain a reliable evaluation of calcium concentration between  $\text{p}K_d - 1$  and  $\text{p}K_d + 1$ . In this case the intensity ratio,  $I_{\text{LM}}/I_{\text{max}}$ , is between 0.1 and 0.9. In theory, this is related to a calcium concentration between 0.14  $\mu\text{M}$  and 1.4 mM. However, in this calcium concentration domain, the ionic strength effect is not negligible. If we calculate with our model the ionic strength effect due to calcium alone (i.e. without  $[\text{NaCl}]$ ), the domain ranges from  $[\text{Ca}] = 20 \mu\text{M}$  to 7 mM. Considering that domain and the calcium concentrations usually found in seawater, we should dilute a seawater sample tenfold. In this case, we have to consider the presence of other ions in the diluted sample. Thus, for  $\text{NaCl} = 0.07 \text{ M}$ , we obtain the domain for calcium concentrations ranging from 0.2 to 40 mM. With this approach, we will be able to adapt the domain of measurements depending upon the experimental conditions.

The results obtained for one set of measurements ( $[\text{Ca}] = 1 \text{ mM}$  and  $[\text{NaCl}] = 0.07 \text{ M}$ ) are shown in Table 1. The calcium activities are calculated from Eqs. (1) and (3) after correction of the presence of LH around pH 8. The correction factor for LH, 1.090 for pH 8.05 was obtained from the theoretical model. Within the variation range of pH ( $\pm 0.02$  after addition of 1/10 of the titrisol solution, pH 8), this correction factor varies only 1/1000th fold.  $\text{NaCl}$  concentration (0.07 M) was used to evaluate the ionic strength value using our model. We obtained after iterative calculation, a ionic strength of 0.073 for

the experimental solution, allowing us to calculate an activity coefficient of 0.409 for calcium. We obtained the mean calcium activity and the mean concentration of 0.419 and 1.03 mM, respectively (Table 1). The reproducibility is expressed as the standard deviation of the five samples (S.D. = 0.02 mM for calcium concentration). We are now testing if this accuracy (<2%) is sufficient to measure calcium concentration variations in seawater collections.

The spectroscopic determination of calcium concentrations in high ionic strength solutions constitutes a very rapid method. The new method described here was successfully tested on seawater collected from 3000 m depth to surface Pacific Ocean water and we intend to develop automated measurements. This will increase the accuracy of data acquisition and will allow us to perform the measurements directly on board oceanographic ships just after sampling.

## References

- [1] J. Lebel, A. Poisson, *Mar. Chem.* 4 (1976) 321.
- [2] T. Wang, H.L. Hian, S.F.Y. Li, *J. Liq. Chromatogr. R. T.* 21 (1998) 2485.
- [3] G. Abbasse, G. Ouddane, J.-C. Fischer, *J. Anal. Atom. Spectrom.* 17 (2002) 1354.
- [4] K. Mitko, M. Bebek, *Atom. Spectrosc.* 21 (2000) 77.
- [5] J.Y. Chen, R. Mastsunaga, K. Ishikawa, H. Zhang, *Appl. Spectrosc.* 57 (2003) 1399.
- [6] A.-C. Ribou, J. Vigo, P.M. Viallet, J.-M. Salmon, *Biophys. Chem.* 81 (2000) 179.
- [7] Microsoft Windows 98 Microsoft Excel 97 SR-2.
- [8] C.W. Davies, *Ion Dissociation*, Butterworths, London, 1962, p. 41.
- [9] J. Pesco, J.-M. Salmon, J. Vigo, P. Viallet, *Anal. Biochem.* 290 (2001) 221.
- [10] Molecular Probe, [www.probes.com/handbook](http://www.probes.com/handbook), section 20.3.



# New biosensing platforms based on the layer-by-layer self-assembling of polyelectrolytes on Nafion/carbon nanotubes-coated glassy carbon electrodes

Gustavo A. Rivas<sup>a,\*</sup>, Silvia A. Miscoria<sup>b</sup>, Jacques Desbrieres<sup>a,b,1</sup>, Gustavo D. Barrera<sup>b</sup>

<sup>a</sup> INFIQC, Departamento de Fisicoquímica, Facultad de Ciencias Químicas, Universidad Nacional de Córdoba, 5000 Córdoba, Argentina

<sup>b</sup> Departamento de Química, Universidad Nacional de la Patagonia San Juan Bosco, Ciudad Universitaria, Km 4, 9000 Comodoro Rivadavia, Argentina

Received 16 February 2006; received in revised form 29 March 2006; accepted 29 March 2006

Available online 9 May 2006

## Abstract

We are proposing for the first time the use of a Nafion/multi-walled carbon nanotubes dispersion deposited on glassy carbon electrodes (GCE) as a new platform for developing enzymatic biosensors based on the self-assembling of a chitosan derivative and different oxidases. The electrodes are obtained by deposition of a layer of Nafion/multi-wall carbon nanotubes dispersion on glassy carbon electrodes, followed by the adsorption of a chitosan derivative as polycation and glucose oxidase, L-aminoacid oxidase or polyphenol oxidase, as polyanions and biorecognition elements. The optimum configuration for glucose biosensors has allowed a highly sensitive (sensitivity =  $(0.28 \pm 0.02) \mu\text{A mM}^{-1}$ ,  $r = 0.997$ ), fast (4 s in reaching the maximum response), and highly selective (0% interference of ascorbic acid and uric acid at maximum physiological levels) glucose quantification at 0.700 V with detection and quantification limits of 0.035 and 0.107 mM, respectively. The repetitivity for 10 measurements was 5.5%, while the reproducibility was 8.4% for eight electrodes. The potentiality of the new platform was clearly demonstrated by using the carbon nanotubes/Nafion layer as a platform for the self-assembling of L-aminoacid oxidase and polyphenol oxidase. Therefore, the platform we are proposing here, that combines the advantages of nanostructured materials with those of the layer-by-layer self-assembling of polyelectrolytes, opens the doors to new and exciting possibilities for the development of enzymatic and affinity biosensors using different transduction modes.

© 2006 Elsevier B.V. All rights reserved.

**Keywords:** Carbon nanotubes; Layer-by-layer; Enzymatic biosensors; Nafion; Glassy carbon; Glucose oxidase; Polyphenol oxidase; L-aminoacid oxidase

## 1. Introduction

Carbon nanotubes (CNTs) represent an important group of nanomaterials with very unique electronic, chemical and mechanical properties [1–4]. The first application of CNTs for biosensors was proposed in 1996 by Britto et al. [5]. Since then, CNTs have been used for preparing biosensors employing different strategies: by dispersing them in acidic solutions [6,7], *N,N'*-dimethylformamide [8–10], Nafion [11,12] and chitosan [13–15] among others; by incorporating in composites matrices using different binders like Teflon [16,17], bromoform [18], mineral oil [19–24] and inks [25]; by immobilizing on pyrolytic

graphite electrodes [26,27]. Wang et al. [11] have demonstrated the ability of the perfluorosulfonated polymer Nafion to disperse single wall (SWCNTs) and multi-wall (MWCNTs) carbon nanotubes. They reported a dramatic decrease in the overvoltage for hydrogen peroxide oxidation and reduction as well as a highly selective glucose quantification after immobilization of glucose oxidase (GOx) by cross-linking with glutaraldehyde.

Here, we propose the use of MWCNTs dispersed in Nafion and deposited on a glassy carbon electrode (GCE) as a platform for building supramolecular architectures based on the self-assembling of polyelectrolytes. Since the pioneering work of Decher [28], there has been great interest in using the layer-by-layer immobilization of polyelectrolytes for the development of biosensors [29–31]. In this case we used a chitosan derivative called quaternized chitosan (CHIT) as polycation; and glucose oxidase (GOx), polyphenol oxidase (PPO) and L-aminoacid oxidase (L-AAOx) as polyanions and biorecognition elements.

\* Corresponding author. Tel.: +54 351 4334169/80; fax: +54 351 4334188.

E-mail address: [grivas@mail.fcq.unc.edu.ar](mailto:grivas@mail.fcq.unc.edu.ar) (G.A. Rivas).

<sup>1</sup> Permanent address: Laboratoire de Physico-Chimie des Polymères, UMR CNRS 5067, LRMP – Hélioparc Pau Pyrénées, 2 Av. du Président Angot, 64053 PAU Cedex 09, France.

In the following sections we report the analytical performance of the resulting supramolecular architectures for the highly sensitive determination of glucose, phenols, catechols and L-aminoacids.

## 2. Experimental

### 2.1. Reagents

Hydrogen peroxide (30% v/v aqueous solution) was purchased from Baker. Ascorbic acid (AA) was obtained from Fluka. Glucose oxidase (GOx) (Type X-S, *Aspergillus niger*, (EC 1.1.3.4), 210,000 Units/g of solid, Catalog number G-7141), polyphenol oxidase (PPO) (from mushroom, (EC 1.14.18.1), 4800 Units/mg of solid), L-aminoacid oxidase (L-AAOx) (Type I from crude dried venom from *Crotalus adamanteus*, (EC 1.4.3.2), 0.38 Units/mg of solid), dopamine, catechol, catechine, L-hystidine and L-phenylalanine were from Sigma. Uric acid (UA) and glucose were obtained from Merck. Nafion (Naf) (5% in alcoholic solution) was purchased from Aldrich. Other chemicals were reagent grade and used without further purification. Multi-wall carbon nanotubes 5–20  $\mu\text{m}$  long and 20–50 nm diameter were obtained from NanoLab (USA).

Chitosan is obtained by deacetylation of chitin and it can be considered as a copolymer of (1–4) linked *N*-acetyl- $\beta$ -D-glucosamine and  $\beta$ -D-glucosamine units. Original chitosan from Pronova (Norway) with molecular weight of 190,000 g/mol was used for preparing quaternized chitosan (CHIT). The degree of acetylation (DA) is the molar fraction of acetylated unit in the polymeric chain while the degree of substitution (DS) is the molar fraction of ammonium units in the macromolecular chain. In this case, DA is 12 mol% and DS is 40 mol%. Briefly, the quaternized chitosan (Scheme 1) was prepared in the following way. The purified chitosan was dispersed in *N*-methyl pyrrolidone containing methyl iodide, sodium iodide and 15% aqueous solution of sodium hydroxide. This dispersion was stirred at 60 °C for a given time. The counterion  $\text{I}^-$  is then exchanged by  $\text{Cl}^-$  by dissolving the quaternized polymer in a small quantity of water followed by the addition of HCl in ethanol. The average molecular weight was 52,750 g/mol.

All solutions were prepared with ultrapure water ( $\rho = 18 \text{ M}\Omega$ ) from a Millipore-Milli-Q system. A 0.050 M phosphate buffer solution pH 7.40 was employed as supporting electrolyte.

### 2.2. Apparatus

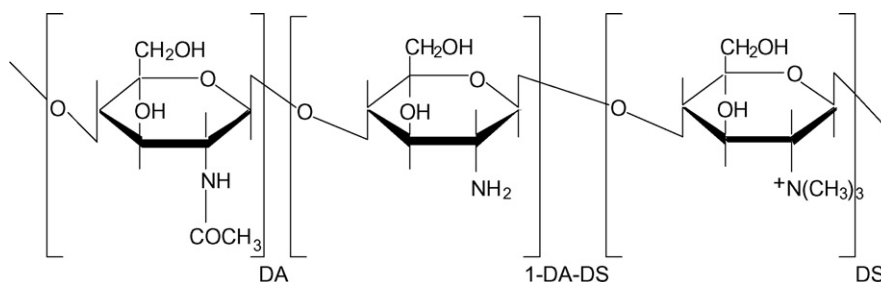
The measurements were performed with an EPSILON potentiostat (BAS). The electrodes were inserted into the cell (BAS, Model MF-1084) through holes in its Teflon cover. A platinum wire and Ag/AgCl, 3 M NaCl (BAS, Model RE-5B) were used as counter and reference electrodes, respectively. All potentials are referred to the latter. A magnetic stirrer provided the convective transport during the amperometric experiments.

#### 2.2.1. Preparation of the working electrode

Prior to surface modification, the glassy carbon electrodes (3 mm diameter, Model CHI104, CH Instruments) were cleaned by polishing with 1.0, 0.3 and 0.05  $\mu\text{m}$  alumina slurries, washed with water and finally sonicated in water for 1 min. After that, the electrodes were cycled 10 times between  $-0.300$  and  $0.800 \text{ V}$  in a phosphate buffer solution (0.050 M, pH 7.40) at  $0.050 \text{ s}^{-1}$ . The biosensors were prepared by casting the GCE with 20  $\mu\text{L}$  of a 2.0 mg/mL CNTs dispersion prepared in Nafion by sonicating for 5 min. The coating was allowed to dry for 2 h at room temperature. In the selected scheme for glucose biosensing, an additional casting of 20  $\mu\text{L}$  Nafion solution without CNTs was also done and it was allowed to dry for two more hours. After that, the electrodes were immersed in a solution of 1.0 mg/mL CHIT for 20 min, followed by an immersion in a GOx solution (1.0 mg/mL) for additional 20 min (both solutions prepared in 0.050 M phosphate buffer solution pH 7.40). Biosensors containing PPO or L-AAOx as biorecognition layers were prepared in a similar way by immobilizing the CNTs dispersed in a 2% v/v Nafion solution (in a phosphate buffer solution pH 7.40), followed by the alternate deposition of CHIT and PPO or L-AAOx (2.0 mg/mL). No additional Nafion layer was included in these cases. Supramolecular multistructures with higher number of CHIT/enzyme bilayers were obtained by alternate deposition of the polyelectrolytes.

### 2.3. Procedure

The amperometric experiments were carried out in a phosphate buffer solution (0.050 M, pH 7.40) by applying 0.700 V (glucose and L-aminoacids sensors) or  $-0.050 \text{ V}$  (catechols and phenols sensors) and allowing the transient current to decay to a steady-state value prior to the addition of the analyte and subsequent current monitoring. Cyclic voltammetric experiments



Scheme 1.

were performed using a 0.050 M phosphate buffer solution pH 7.40.

### 3. Results and discussion

In this work we used Nafion in two directions, for dispersion and further immobilization of CNTs on GCE, and as a precursor film for the self-assembling of CHIT and oxidases. Fig. 1 displays amperometric recordings at 0.700 V for GCE/(CNTs/Naf) (A) and for GCE/(CNTs/Naf)/CHIT/GOx (B) after successive additions of 2.5 mM glucose solution. As expected, no response is obtained at the electrode without the biocatalytic layer (A). On the contrary, a sensitive (sensitivity =  $(0.0869 \pm 0.0004) \mu\text{A mM}^{-1}$ ,  $r = 0.9996$ ), fast (4 s to reach the stationary current), and well-defined response is obtained once GOx was self-assembled on the GCE/(CNTs/Naf). These results are clear evidence that the Nafion layer containing CNTs behaves as a “precursor” film allowing the efficient self-assembling of CHIT and GOx. Analogous experiments using GCE/(Naf)/(CHIT/GOx) gave a sensitivity of  $(0.00098 \pm 0.00004) \mu\text{A mM}^{-1}$ , demonstrating the excellent catalytic effects of CNTs towards the oxidation of hydrogen peroxide.

The influence of the time for drying the CNT/Naf layer deposited on the glassy carbon surface on the analytical performance of the resulting electrodes was evaluated by preparing electrodes with different drying times (30, 60, 120 and 240 min). The comparison was made from the amperometric response of the hydrogen peroxide enzymatically generated after successive additions of glucose. The sensitivity increased with the drying time between 30 and 120 min, to remain constant thereafter (not shown). Therefore, the selected time was 120 min.

The influence of the number of CNTs/Naf layers on the response of the bioelectrode was also studied (not shown). Dif-

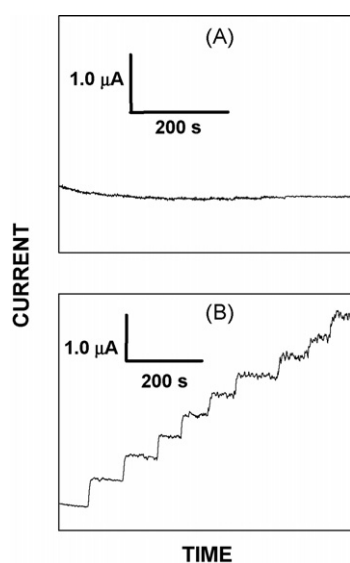


Fig. 1. Amperometric recordings obtained after successive additions of 2.5 mM glucose at GCE/(CNTs/Naf) (A) and at GCE/(CNTs/Naf)/CHIT/GOx (B). Working potential: 0.700 V. Supporting electrolyte: 0.050 M phosphate buffer solution pH 7.40.

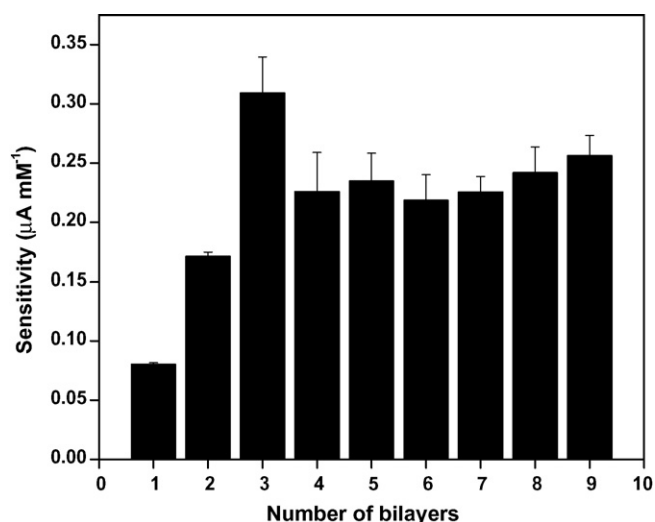


Fig. 2. Sensitivities for glucose determination obtained from amperometric recordings at 0.700 V as a function of the number of CHIT/GOx bilayers.

ferent electrodes were prepared by immobilizing successive layers of CNTs/Naf up to five. The response of the resulting electrodes was obtained from amperometric measurements at 0.700 V after successive additions of hydrogen peroxide. The sensitivity remained constant even after five CNTs/Naf layers. Sensitivities of 18.12, 20.03, 16.81, 17.47 and 17.75  $\mu\text{A mM}^{-1}$  were obtained for 1, 2, 3, 4 and 5 CNTs/Naf layers, respectively. Therefore, it is clear that CNTs located far away from the glassy carbon electrode are not connected each other and further developments include just one CNTs/Naf layer.

The number of biocatalytic layers in the supramolecular architecture is another very important variable in the analytical performance of biosensors prepared by self-assembled multilayers. Fig. 2 shows the effect of the number of CHIT/GOx bilayers on the sensitivity of the resulting bioelectrodes obtained from amperometric recordings at 0.700 V after successive additions of glucose. The sensitivity increases almost linearly with the number of CHIT/GOx bilayers up to the third one. After that, the response of the bioelectrode slightly decreases to remain almost constant even up to nine CHIT/GOx bilayers. Two can be the reasons for this behavior, either the occurrence of some disturbance in the assembling of additional CHIT/GOx bilayers after the third one, or the appearance of some problems associated with the diffusion of the hydrogen peroxide generated in the biocatalytic layers placed far away from the electrode surface. To evaluate these two possibilities, we carried out experiments similar to those performed with glucose (Fig. 2), but using hydrogen peroxide instead of glucose. After assembling one CHIT/GOx bilayer to GCE/(CNTs/Naf), the sensitivity for hydrogen peroxide decreased from 18.12 to 9.0  $\mu\text{A mM}^{-1}$ . No further changes in sensitivity were observed for bioelectrodes prepared by assembling additional CHIT/GOx bilayers. In fact, sensitivities of 8.3, 9.3, 9.1 and 9.5  $\mu\text{A mM}^{-1}$  were obtained for electrodes containing 2, 3, 4 and 5 bilayers, respectively. These results demonstrate that there are no problems with hydrogen peroxide diffusion to the glassy carbon electrode through the supramolecular multistructure, even for electrodes prepared

with five CHIT/GOx bilayers. The decrease in sensitivity observed when assembling the first CHIT/GOx bilayer can be attributed to the interaction of CHIT with CNTs/Naf film that generates some disturbance in the organization of this film and makes CNTs less accessible for hydrogen peroxide oxidation.

In order to evaluate the incidence of the interaction between CHIT and the Nafion layer that “supports” the CNTs on the analytical response of the electrode, we carried out analogous experiments using an extra layer of Nafion (without CNTs) placed between CNTs/Naf and CHIT/GOx layers (GCE/(CNTs/Naf)/Naf/(CHIT/GOx)). The sensitivity of the resulting bioelectrode for hydrogen peroxide was  $15.00 \mu\text{A mM}^{-1}$ , value close to the sensitivity obtained at GCE/(CNTs/Naf) ( $18.12 \mu\text{A mM}^{-1}$ ). In agreement with these results, the sensitivity to glucose also increased when an additional layer of Nafion was placed between the layers of CNTs/Naf and CHIT/GOx ( $0.080 \mu\text{A mM}^{-1}$  versus  $0.201 \mu\text{A mM}^{-1}$ ). Thus, the additional layer of Nafion avoids the interaction between the Nafion layer that “supports” CNTs and the CHIT layer, leaving the CNTs more accessible for hydrogen peroxide oxidation. Hence, the “no increase” in sensitivity towards glucose for electrodes prepared with several CHIT/GOx bilayers may be due to a non adequate charges screening that leads to a poor assembling of CHIT and GOx after the third CHIT/GOx bilayer.

Another important aspect to be considered when evaluating the analytical performance of an electrochemical glucose biosensor is the interference of easily oxidizable compounds such as ascorbic acid and uric acid. In the simplest scheme GCE/(CNTs/Naf)/(CHIT/GOx)<sub>n</sub>, the interference of these easily oxidizable compounds decreases as the number (*n*) of CHIT/GOx bilayers increases. For instance, the interference of AA in the oxidation signal for 5.0 mM glucose decreases from 389% to 27% for electrodes prepared with 1 and 5 bilayers, respectively. Considering that the scheme based on the use of an intermediate layer of Nafion gave better sensitivity for glucose, we evaluate the effect of such intermediate Nafion layer on the selectivity of the bioelectrode. The interference for the maximum physiological level of AA ( $1.0 \times 10^{-4}$  M), decreased from 389% to 12% at GCE/(CNTs/Naf)/Naf/(CHIT/GOx). Even

a more important decrease in the interference of AA and UA was obtained after assembling a second CHIT/GOx bilayer. Fig. 3 shows the amperometric response at 0.700 V of  $5.0 \times 10^{-3}$  M glucose followed by successive additions of  $5.2 \times 10^{-5}$  M UA (A) and  $2.5 \times 10^{-5}$  M AA (B). While a well defined glucose response is obtained, the maximum physiological levels of AA ( $1.0 \times 10^{-4}$  M) and UA ( $3.6 \times 10^{-4}$  M) results in negligible signals that gives a final interference of 0% in both cases.

Amperometric experiments at 0.700 V showed that GCE/(CNTs/Naf)/Naf/(CHIT/GOx)<sub>2</sub> responds rapidly to changes in the level of glucose, producing steady-state signals within 4 s accompanied by a low noise level. A linear relationship between current and glucose concentration was obtained up to 7.5 mM glucose with a sensitivity of  $(0.28 \pm 0.02) \mu\text{A mM}^{-1}$ ,  $r = 0.997$ , a detection limit of 0.035 mM (taken as  $3.3 \times S_0/m$  being  $S_0$  the signal obtained in the absence of the analyte and  $m$  the slope) and a quantification limit of 0.107 mM (taken as  $10 \times S_0/m$ ). The repetitivity for 10 calibrations was 5.5%, while the reproducibility was 8.4% for eight electrodes.

Therefore, since GCE/(CNTs/Naf)/Naf/(CHIT/GOx)<sub>2</sub> has allowed the best compromise between sensitivity, selectivity and preparation time, it was the selected scheme for the design of a sensitive and selective biosensing platform for glucose determination.

The potentiality of the new platform was evaluated in connection with the assembling of other enzymes like PPO and L-AAOx. PPO is an enzyme involved in the aerobic oxidation of phenols and catechols to the corresponding quinones. Fig. 4A shows the effect of the number of CHIT/PPO bilayers on the sensitivity of the bioelectrode towards catechol obtained at  $-0.050$  V from the reduction of the quinone enzymatically generated. The sensitivity increases linearly with the number of bilayers up to six due to the increase in the amount of the biocatalyst, to remain almost constant thereafter, probably due to some nonstability of the resulting supramolecular architecture. Fig. 4 also shows the amperometric recordings at  $-0.050$  V obtained after addition of different substrates, catechol (B) dopamine (C), and the polyphenol catechine (D). A very fast and sensitive response was observed in all cases, demonstrating the usefulness of the CNTs/Nafion layer as a precursor film for self-assembling of PPO. The sensitivities were  $(0.186 \pm 0.004)$ ,  $(0.123 \pm 0.004)$ ,

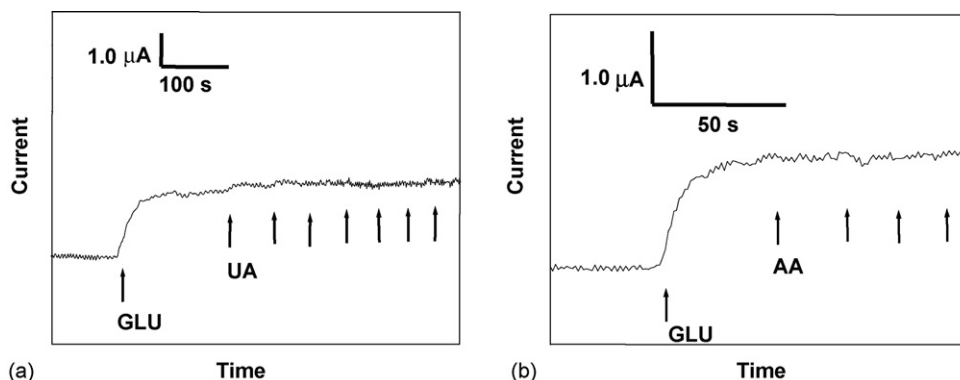


Fig. 3. Amperometric recordings for additions of 5.0 mM glucose followed by additions of  $5.2 \times 10^{-5}$  M UA (A) and  $2.5 \times 10^{-5}$  M AA (B). Working potential: 0.700 V.

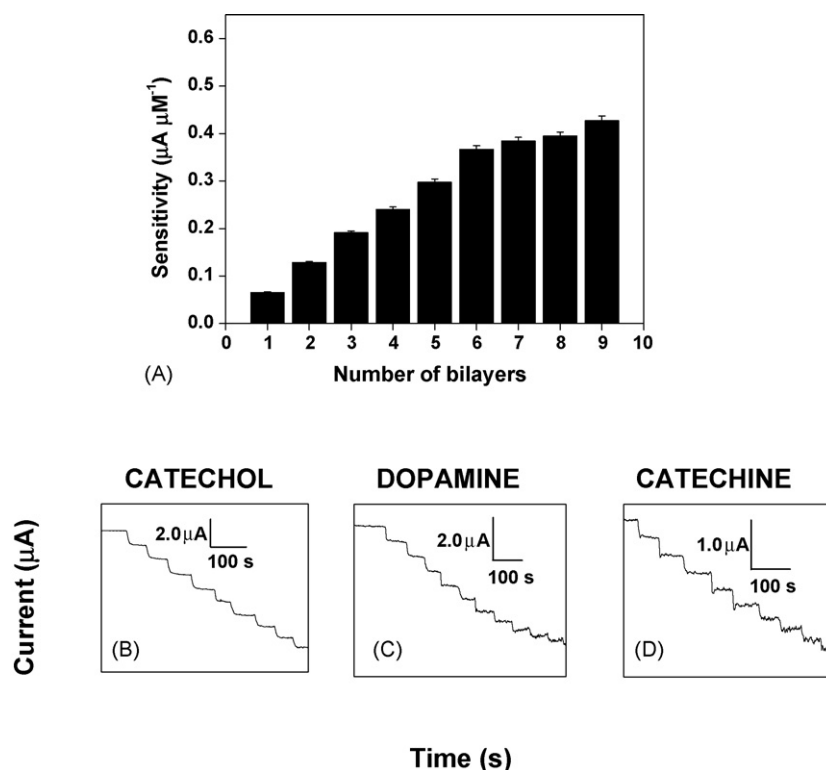


Fig. 4. (A) Sensitivities for catechol obtained from amperometric recordings as a function of the number of CHIT/PPO bilayers. Amperometric recordings for catechol (B), dopamine (C) and catechine (D). Working potential:  $-0.050$  V.

and  $(0.062 \pm 0.002) \mu\text{A } \mu\text{M}^{-1}$  for catechol, dopamine and catechine, respectively.

The new platform was also used for designing L-aminoacids biosensors by self-assembling of L-AAOx, enzyme that catalyzes the oxidation of L-aminoacids to  $\alpha$ -ketoacids, and produces hydrogen peroxide during its regeneration. The immobilization of L-AAOx demonstrated to be highly efficient. For instance, detection limits of 0.5 and 0.2  $\mu\text{M}$  were obtained for L-histidine and L-phenylalanine, respectively, using a GCE/(CNTs/Naf)/(CHIT/L-AAOx) (not shown).

#### 4. Conclusions

In summary, we are proposing for the first time the use of a dispersion of CNTs in Nafion deposited on GCE as a new platform for developing enzymatic biosensors based on the self-assembling of quaternized chitosan and different oxidases. This approach that combines the advantages of nanostructured materials like CNTs with those of the layer-by-layer self-assembling of polyelectrolytes, opens the doors to new and exciting possibilities for the development of enzymatic and affinity biosensors using different transduction modes. Our group is currently working on this direction.

#### Acknowledgments

The authors thank Fundación Antorchas, Consejo Nacional de Investigaciones Científicas y Técnicas de Argentina (CON-

ICET), Secretaría de Ciencia y Tecnología de la Universidad Nacional de Córdoba (SECyT-UNC), Agencia Nacional de Promoción Científica y Tecnológica and Asociación de Bioquímicos de la Provincia de Córdoba (ABC) for the financial support. The authors also want to thank Prof. Pierre Labbé for his help to get the quaternized chitosan samples.

#### References

- [1] H. Dai, Acc. Chem. Res. 35 (2002) 1035.
- [2] H. Dai, Surf. Sci. 500 (2002) 218.
- [3] G.G. Wildgoose, C.E. Banks, H.C. Leventis, R.G. Compton, Microchim. Acta 152 (2006) 187.
- [4] J. Wang, Electroanalysis 17 (2005) 7.
- [5] P. Britto, K. Santhanam, P. Ajayan, Bioelectrochem. Bioenergetics 41 (1996) 121.
- [6] M. Musameh, J. Wang, A. Merkoci, Y. Lin, Electrochem. Commun. 4 (2002) 743.
- [7] J. Wang, A. Kawde, M. Musameh, Analyst 128 (2003) 912.
- [8] J. Wang, M. Li, Z. Shi, N. Li, Z. Gu, Anal. Chem. 74 (2002) 1993.
- [9] J. Wang, M. Li, Z. Shi, N. Li, Z. Gu, Electrochim. Acta 47 (2001) 651.
- [10] X. Yan, D. Pang, Z. Lu, J. Li, H. Tong, Electroanal. Chem. 1 (2004) 47.
- [11] J. Wang, M. Musameh, Y. Lin, J. Am. Chem. Soc. 125 (2003) 2408.
- [12] K. Gong, Y. Dong, S. Xiong, Y. Chen, L. Mao, Biosens. Bioelectron. 20 (2004) 253.
- [13] M. Zhang, A. Smith, W. Gorski, Anal. Chem. 76 (2004) 5045.
- [14] Y. Liu, M. Wang, F. Zhao, Z. Xu, S. Dong, Biosens. Bioelectron. 21 (2005) 984.
- [15] X. Tan, M. Li, P. Cai, L. Luo, X. Zou, Anal. Biochem. 337 (2005) 111.
- [16] J. Wang, M. Musameh, Anal. Chem. 75 (2003) 2075.
- [17] J. Wang, M. Musameh, Anal. Lett. 36 (2003) 2041.



- [18] J. Davis, R. Coles, H. Hill, *Electroanal. Chem.* 440 (1997) 279.
- [19] M. Rubianes, G. Rivas, *Electrochem. Commun.* 5 (2003) 689.
- [20] M. Rubianes, G.A. Rivas, *Electroanalysis* 17 (2005) 73.
- [21] M. Pedano, G. Rivas, *Electrochem. Commun.* 6 (2004) 10.
- [22] M. Chicharro, A. Sánchez, E. Bermejo, A. Zapardiel, M. Rubianes, G. Rivas, *Anal. Chim. Acta* 543 (2005) 84.
- [23] M. Chicharro, E. Bermejo, M. Moreno, A. Sánchez, A. Zapardiel, G. Rivas, *Electroanalysis* 17 (2005) 476.
- [24] R. Antiochia, I. Lavagnini, F. Magno, *Anal. Lett.* 37 (2004) 1657.
- [25] J. Wang, Musameh, *Analyst* 129 (2004) 1.
- [26] M. Guo, J. Chen, D. Liu, L. Nie, S. Yao, *Bioelectrochemistry* 29 (2004) 29.
- [27] R. Moore, C. Banks, R. Compton, *Anal. Chem.* 76 (2004) 2677.
- [28] G. Decher, *Science* 277 (1997) 1232.
- [29] Narváez, G. Suárez, I. Popescu, I. Katakis, E. Domínguez, *Biosens. Bioelectron.* 15 (2004) 43.
- [30] E. Domínguez, O. Rincón, A. Narváez, *Anal. Chem.* 76 (2004) 3132.
- [31] M. Rodríguez, G. Rivas, *Electroanalysis* 16 (2004) 1717.

# A PVC-membrane bulk optode for gallium(III) ion determination

Afsaneh Safavi\*, Marzieh Sadeghi

*Department of Chemistry, Faculty of Sciences, Shiraz University, Shiraz 71454, Iran*

Received 6 December 2005; received in revised form 30 March 2006; accepted 6 April 2006

Available online 9 June 2006

## Abstract

An optical probe responsive to gallium(III) ion has been developed. The gallium sensing system was prepared by incorporating 4-(*p*-nitrophenyl azo)-pyrocatechol (NAP) as ionophore in a plasticized PVC membrane containing tributylphosphate (TBP) as plasticizer. The sensing membrane in contact with gallium ion at pH 3.5, changes color from yellow-brown to pink-brown. Under optimum conditions, the proposed membrane displayed a linear range of 5–83  $\mu\text{M}$  with a limit of detection of 4  $\mu\text{M}$ . The response time of the membrane was within 10–15 min depending on the concentration of  $\text{Ga}^{3+}$  ions. The selectivity of the probe towards gallium determination was found to be very good. Experimental results showed that the probe could be used as an effective tool in analyzing the gallium content of water samples.

© 2006 Elsevier B.V. All rights reserved.

**Keywords:** Gallium determination; 4-(*p*-Nitrophenyl azo)-pyrocatechol; PVC membrane

## 1. Introduction

Chemical sensor technology involves the key processes of chemical recognition of the analytes of interest and subsequent transduction of the analytical signal. In many optode systems the sensing element is a reagent that changes its optical properties in response to an analyte. The sensing reagent is frequently an indicator dye that has to be immobilized on or entrapped within a suitable matrix. The optical properties measured can be absorbance, reflectance, fluorescence, and refractive index [1,2]. Basic principle and the theoretical description of bulk optode membranes, which are based on the reversible mass transfer of analyte from the sample in the bulk of the sensing layer, have been well elucidated [3,4]. During the last decade optochemical sensors based on organic polymeric thin or thick films have been investigated [5–9].

Gallium is an indispensable rare metal in manufacture of electronic products. Electrothermal atomic absorption spectrometry for trace gallium determination has been developed. Solvent extraction [10,11], adsorption [12], ion exchange [13], membrane [14], coprecipitation [15], extraction and chromatographic techniques [16] have been used to preconcentrate gal-

lium prior to electrothermal atomic absorption spectrometric analysis in order to improve detection limit. A sensitive and selective flow injection time-based method for on-line preconcentration/separation and determination of gallium by flame atomic absorption spectrometry at trace levels has been reported [17]. Electrothermal atomic absorption spectrometry and flame atomic absorption spectrometry have good detection limits for gallium determination, but these instrumental methods need a preliminary step for separation and preconcentration of gallium.

A simple and sensitive spectrofluorimetric procedure for the analysis of microquantities of gallium in alloys was described. The method is based on the formation of Ga(III)–(calon-carboxylic acid) complex [18]. Other chromogenic reagents for gallium determination have also been reported such as rutin [19], carminic acid and hexadecylpyridinium chloride [20]. Although gallium is important for use in the semiconductor industry, gallium particles and gallium compounds such as gallium arsenide have been identified as potential health hazards. Therefore, from an environmental point of view, the need for sensitive and reliable methods for determining trace concentrations of gallium has become apparent in various fields. Although there are many reports on the development of optodes for metal ion determinations [21–25], to the best of our knowledge there has been no report on the use of optical sensor for gallium determination. Thus, sensitive and simple gallium optical sensor is still demanding.

\* Corresponding author. Tel.: +98 711 6305881; fax: +98 711 2286008.  
E-mail address: [safavi@chem.susc.ac.ir](mailto:safavi@chem.susc.ac.ir) (A. Safavi).

## 2. Experimental

### 2.1. Reagents

Standard gallium ion solutions were prepared daily by appropriate dilution of stock 0.01 M  $\text{Ga}(\text{NO}_3)_3 \cdot 8\text{H}_2\text{O}$  (Fluka). 4-(*p*-Nitrophenyl azo)-pyrocatechol (Fluka), dimethyl sebacate (DMS), *ortho*-nitrophenyl octyl ether (*o*-NPOE), dibutyl phthalate (DBP), diethyl sebacate (DES), dibutylsebacate (DBS), tributylphosphate (TBP), high molecular weight poly (vinyl chloride) (PVC), tetrahydrofuran (THF), all from Fluka or Merck Chemical Companies were used as received. All other chemicals were of reagent grade and were used without further purification. Direct-Q water was used throughout the experiments.

### 2.2. Apparatus

A Shimadzu 1601 PC UV–vis spectrophotometer with a 1 cm cell was used for recording all spectra and absorbance measurements. A Metrohm pH meter (model 780) with a combined double junction glass electrode, calibrated against two standard buffer solutions at pH 4.0 and 7.0, was used for monitoring pH values. All measurements were made in the absorbance mode. The pH of the solutions was kept constant by using 0.02 M glycine buffer at pH 3.5.

### 2.3. Membrane preparation

The membrane consisted appropriate amounts of active components. 50 mg of PVC (31.44%), 100 mg of tributylphosphate, (62.90%) as plasticizer and 9 mg of 4-(*p*-nitrophenyl azo)-pyrocatechol (NAP), (5.66%) were added in a glass vial and dissolved in 1.5 ml of THF. The solution was immediately shaken vigorously to achieve complete homogeneity. A glass plate was cleaned with pure THF to remove organic impurities and dust and then placed in the spin-on device. Sixty microliter of the above cocktail was injected with 100  $\mu\text{l}$  glass syringe to the glass plate. After 30 s spinning, at rotation frequency of 600 rpm, the membrane was located in ambient air and allowed to dry in air for few minutes. The glass-supported membrane was fixed in a 1-cm glass cell containing the test solution and was mounted in the spectrophotometer for absorbance measurements.

## 3. Results and discussion

### 3.1. Measuring principle

Measuring principle can be explained as follows:

The membrane response may be defined as the ratio of the concentration of the uncomplexed ligand  $[C]$  to the total amount present in the membrane  $[C_T]$ , i. e.  $\alpha = [C]/[C_T]$ . Then the  $\alpha$  value can be calculated by absorbance measurements at  $\lambda_{\text{max}}$  of complexed ligand as  $\alpha = (A_C - A)/(A_C - A_L)$ , where  $A_C$  is the absorbance value of the membrane for complete complexation (i.e. at  $\alpha = 0$ ),  $A_L$  is the absorbance value of the membrane for the free ligand (i. e. at  $\alpha = 1$ ) [26] and  $A$  is absorbance measured at any time during the titration procedure.

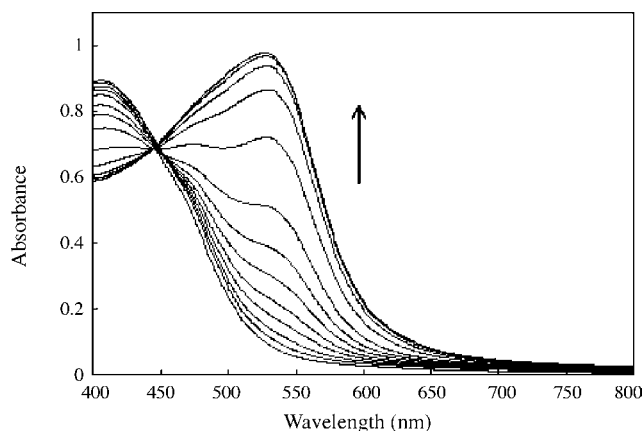


Fig. 1. Absorption spectra for the immobilized NAP in the presence of 0–150  $\mu\text{M}$  of gallium. Arrow indicates increase in gallium concentration.

### 3.2. Spectral characteristic

4-(*p*-Nitrophenyl azo)-pyrocatechol is a complexometric agent for some metal ions such as uranyl, thorium, and gallium ions [27]. Fig. 1 shows the absorption spectra of the membrane which were obtained after being equilibrated in glycine buffer solution (pH 3.5) containing different concentrations of  $\text{Ga}^{3+}$  ion. The spectral change (decrease in absorption band at 400 nm and increase in the absorption band at 526 nm) is a result of an increase in gallium ion concentration in the membrane.

### 3.3. Effect of membrane composition

The response characteristics and working concentration range of optical sensor depends significantly on the membrane composition, the nature of solvent mediator and the additive used [28].

Several solvent mediators such as *o*-NPOE, TBP, DES, DBP, DBS were tested as potential plasticizers for preparing the membrane. The absorbance measurements were made for 30  $\mu\text{M}$  gallium ion. The blank membrane (membrane in buffer solution without gallium ion) was taken as the reference. Plasticizers such as DES and DBS showed good sensitivity but membranes containing these plasticizers showed leakage of the reagent. The membranes containing TBP revealed best physical properties. A weight ratio of TBP to PVC of 2 provided the best physical properties with no leakage of reagent from the membrane. Thus, TBP was selected as an optimum plasticizer.

The effect of the amount of NAP on the response of the membrane is illustrated in Fig. 2. The absorbance measurements at 526 nm were made for 30  $\mu\text{M}$  gallium ion using membranes with different amounts of NAP. The blank membrane (membrane without NAP in the buffer solution) was taken as the reference. The absorbance measurements were expressed as absorbance difference, which was defined as the difference between the absorbance of the immobilized NAP alone and the absorbance of the  $\text{Ga}^{3+}$ -NAP complex at 526 nm. As can be seen from Fig. 2, increase in the amount of NAP results in an increase in absorbance. Membranes containing high amounts of NAP (more than 6%; 10 mg) showed leakage of NAP–gallium complex.

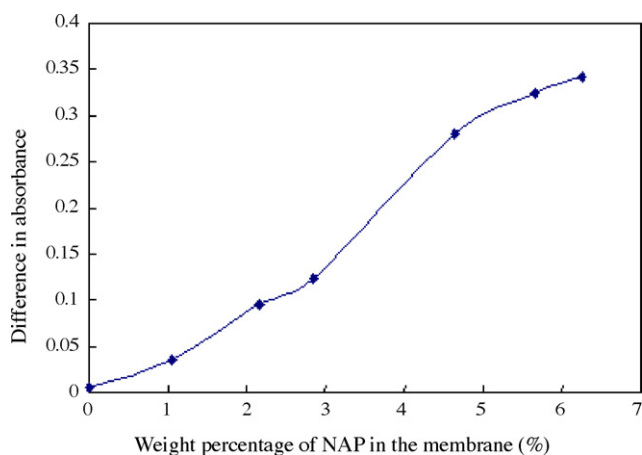


Fig. 2. Effect of the percentage of NAP in the membrane on response of the membrane toward  $30 \mu\text{M Ga}^{3+}$  at 526 nm.

In the proposed gallium selective membrane, the presence of lipophilic anionic additives such as KTpCIPB or NaTPB had no effect on the response of the membrane. This is due to the response mechanism of the membrane. In fact it is believed that the mechanism of the response of the proposed optode is based on complexation of NAP and gallium which is accompanied by deprotonation of NAP and release of proton in the solution. Thus, the electroneutrality is maintained through the membrane, without the need for the addition of any lipophilic anionic additive.

#### 3.4. Effect of pH and buffer type on response of the optode

Fig. 3 shows the effect of pH values on the absorbance intensity of the optode membrane. The absorbance measurements were made for  $30 \mu\text{M}$  gallium ion at different pH values at 526 nm. The blank membrane (membrane without NAP in buffer solution) was taken as the reference. The absorbance measurements were expressed as absorbance difference, which was defined as the difference between the absorbance of the immobilized NAP alone and the absorbance of the  $\text{Ga}^{3+}$ -NAP complex

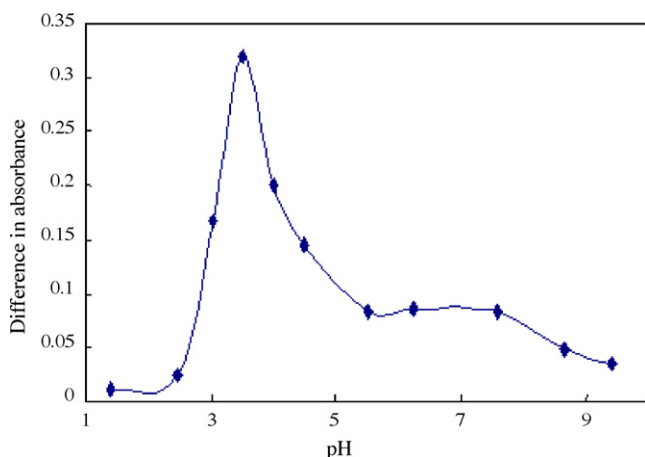


Fig. 3. Effect of pH on response of the membrane in the presence of  $30 \mu\text{M Ga}^{3+}$  at 526 nm.

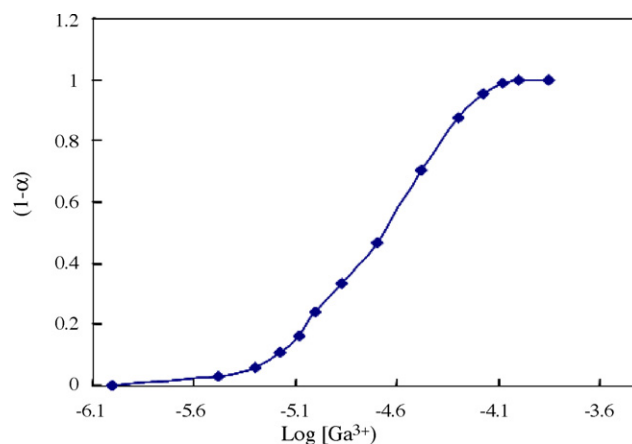


Fig. 4. Calibration curve at 526 nm.

at 526 nm. pH values were adjusted by the addition of NaOH (1 M) and HCl (1 M).

As pH increases from one to nine, the difference in absorbance reaches a maximum at pH 3.5, and then decreases sharply. This phenomenon might be due to the fact that at low pH values ( $\text{pH} < 3$ ), complexation is weak. At pH values higher than 3.5,  $\text{Ga}^{3+}$  forms different hydroxide species ( $\text{Ga}(\text{OH})_n^{-(n-3)}$ ) which make it unable to form complex with NAP ( $\alpha$  values for  $\text{Ga}^{3+}$  at pH 1, 3, 3.5, 4, are 0.99, 0.39, 0.11,  $1.9 \times 10^{-4}$ , respectively) [29]. Also at pH values higher than 3.5, the ligand has leakage from the membrane. Thus, pH 3.5 was selected for further studies. Response studies of this membrane to various buffer solutions including acetate, citrate, universal and glycine (pH 3.5 and 0.1 M) showed that it responded the best to glycine buffer. In glycine buffer the membrane optode showed better sensitivity and response time. Therefore, glycine buffer was selected as the optimum buffer for further studies.

#### 3.5. Dynamic range and response time

Fig. 4 shows the response of the optode membrane to various concentrations of  $\text{Ga}^{3+}$  ions under optimal experimental conditions. In this case  $150 \mu\text{M}$  was found as the concentration of  $\text{Ga}^{3+}$  ion that saturates the membrane optode. As can be seen from Fig. 4, the plot of  $(1 - \alpha)$  versus logarithm of gallium ion concentration (M) exhibited a linear range between 5 and  $83 \mu\text{M Ga}^{3+}$  with equation of  $Y = 0.8284X + 4.3961$  ( $R^2 = 0.9926$ ,  $R = 0.9963$ ) where  $Y$  is  $(1 - \alpha)$  and  $X$  is logarithm of gallium ion concentration (M).

The limit of detection estimated as the concentration of analyte producing an analytical signal equal to three times the standard deviation of the blank signal was  $4 \mu\text{M}$ .

An important analytical feature of any optode is its response time. The response time of the present optode is controlled by the time required for the analyte to diffuse from the bulk of the solution toward the membrane interface to associate with ligand. The response of the membrane was found to reach 90% of the total signal in 10–15 min depending on the concentration of  $\text{Ga}^{3+}$ . Fig. 5 shows the time course of the response of the membrane to a  $30 \mu\text{M}$  solution of Ga(III) ion. In general, the

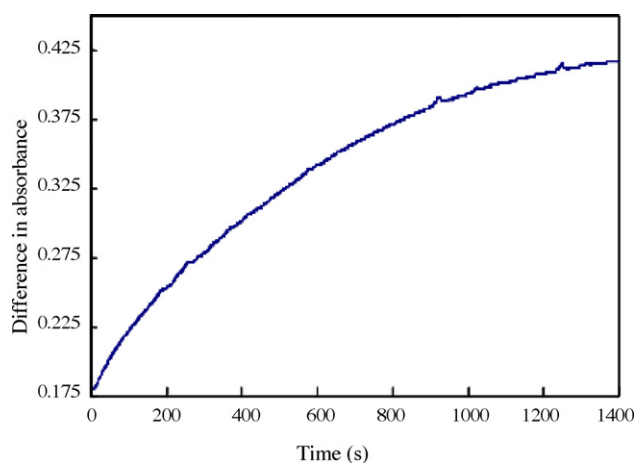


Fig. 5. Typical response curve of the membrane for 30  $\mu\text{M}$  of  $\text{Ga}^{3+}$  at 526 nm.

response time is more rapid when proceeding from dilute to concentrated solution.

### 3.6. Regeneration of optode membrane

Some reagents including HCl,  $\text{HNO}_3$ ,  $\text{H}_3\text{PO}_4$ , pyrogallol, bis (aminoethyl)-glycoether- $N,N,N',N'$ -tetra acetic acid (EGTA), citrate, nitrilotriacetic acid (NTA), EDTA, NaF, 5-sulfosalicylic acid (dihydrate) and different mixtures of them were studied as regenerating reagents. It was found that none of the above reagents or their mixtures could regenerate optode membrane completely and thus the membrane could be used as a probe for gallium ion determination.

### 3.7. Reproducibility, short-term stability and lifetime

To study the short-term stability of the optode membrane, the absorbance of optode in contact with 10  $\mu\text{M}$  solution of  $\text{Ga}^{3+}$  buffered at pH 3.5 was recorded over period of 5 h. During this period, there was no evidence of leakage of NAP from the membrane. When the membrane was exposed to light, no drift in signal was occurred and the optode was stable over the duration of the experiment with no leaching of the indicator. The membrane was stable over a period of 2 months when not in use (membrane was kept in air) and the signal value of the membrane did not change.

The difference in the response of individual membrane was evaluated by preparing seven membranes from the same mixture and the reproducibility was obtained by determining the signal of the membrane to 15  $\mu\text{M}$  solution of  $\text{Ga}^{3+}$ . The mean absorbance was found to be  $0.330 \pm 0.009$  (mean  $\pm$  2S.D.) with R.S.D% = 1.36%. The results show that the reproducibility is satisfactory.

### 3.8. Selectivity

The optical membrane selectivity, which reflects the relative response of the optode for primary ion over diverse ions present in solution, is perhaps the most important characteristic of an

Table 1  
Effect of foreign ions on the determination of 10  $\mu\text{M}$  gallium ion

Foreign ions	Tolerated molar ratio, [interference]/[ $\text{Ga}^{3+}$ ]
$\text{Ba}^{2+}$ , $\text{Fe}^{2+}$ , $\text{Ni}^{2+}$ , $\text{Mn}^{2+}$ , $\text{Co}^{2+}$ , $\text{Cu}^{2+}$ , $\text{Al}^{3+}$ , $\text{Mg}^{2+}$ , $\text{Ca}^{2+}$ , $\text{K}^+$ , $\text{Na}^+$ , $\text{Zn}^{2+}$ , $\text{Be}^{2+}$	500
$\text{Fe}^{3+a}$ , $\text{Zr}^{4+b}$ , $\text{UO}_2^{2+b}$ , $\text{Th}^{4+b}$ , $\text{Pb}^{2+}$ , $\text{Cd}^{2+}$ , $\text{Ti}^{4+}$ , $\text{Tl}^+$ , $\text{Tl}^{3+}$ , $\text{In}^{3+}$ , $\text{Ce}^{3+}$ , $\text{Se}^{4+}$ , $\text{As}^{3+}$ , $\text{Fe}^{2+}$ , $\text{La}^{3+}$ , $\text{Cr}^{3+}$ , $\text{Cr}_2\text{O}_7^{2-}$	100
$\text{VO}^{2+}$	4
$\text{Hg}^{2+}$ , $\text{Ag}^+$	Precipitated

<sup>a</sup> In the presence of salicylic acid (0.01 M).

<sup>b</sup> In the presence of NaF (0.01 M).

ion-selective optode. To determine the selectivity of the optode membrane, the membrane was tested for the determination of 10  $\mu\text{M}$  of  $\text{Ga}^{3+}$  ions in the presence of some metal ions including,  $\text{Pb}^{2+}$ ,  $\text{Ba}^{2+}$ ,  $\text{Ni}^{2+}$ ,  $\text{Mn}^{2+}$ ,  $\text{Co}^{2+}$ ,  $\text{Cu}^{2+}$ ,  $\text{Hg}^{2+}$ ,  $\text{Ag}^+$ ,  $\text{Al}^{3+}$ ,  $\text{UO}_2^{2+}$ ,  $\text{Th}^{4+}$ ,  $\text{Cd}^{2+}$ ,  $\text{Mg}^{2+}$ ,  $\text{Ca}^{2+}$ ,  $\text{K}^+$ ,  $\text{Na}^+$ ,  $\text{Ti}^{4+}$ ,  $\text{Tl}^+$ ,  $\text{Tl}^{3+}$ ,  $\text{In}^{3+}$ ,  $\text{Ce}^{3+}$ ,  $\text{Se}^{4+}$ ,  $\text{As}^{3+}$ ,  $\text{Fe}^{2+}$ ,  $\text{Fe}^{3+}$ ,  $\text{Zr}^{4+}$ ,  $\text{VO}^{2+}$ ,  $\text{La}^{3+}$ ,  $\text{Zn}^{2+}$ ,  $\text{Cr}^{3+}$ ,  $\text{Cr}_2\text{O}_7^{2-}$ . The tolerance limit was taken as the concentration causing an error of  $\pm 5\%$  in the analytical signal for determination of  $\text{Ga}^{3+}$ .

At the applied pH value, no interference was observed from even 100-fold excess of the above metal ions except  $\text{VO}^{2+}$ ,  $\text{Fe}^{3+}$ ,  $\text{Zr}^{4+}$ ,  $\text{UO}_2^{2+}$ , and  $\text{Th}^{4+}$ . Ions such as  $\text{Hg}^{2+}$  and  $\text{Ag}^+$  are precipitated at glycine buffer because of the presence of  $\text{Cl}^-$  anion.

In addition to gallium ion, the membrane produces a response to some other metal ions such as uranyl, and thorium ions that form complexes at pH 3.5.

Ions such as  $\text{Fe}^{3+}$ ,  $\text{VO}^{2+}$ ,  $\text{Th}^{4+}$ ,  $\text{UO}_2^{2+}$ ,  $\text{Zr}^{4+}$  show some levels of interferences. Trials to eliminate the effects of interfering ions were made using some masking agents such as EDTA, EGTA, and salicylic acid, NaF. The results are shown in Table 1.

Interference from  $\text{Fe}^{3+}$  can be omitted by using salicylic acid (0.01 M) as a masking agent.  $\text{UO}_2^{2+}$ ,  $\text{Th}^{4+}$ ,  $\text{Zr}^{4+}$  were masked by addition of NaF (0.01 M) in glycine buffer solution. However, the interfering effect of  $\text{V}^{4+}$  cannot be eliminated or reduced by using the above masking agents.

### 3.9. Determination of $\text{Ga}^{3+}$ in natural water

To test the practical application of the present sensor, some natural water samples (river water) spiked with different amounts of gallium ion were analyzed and the concentrations of gallium ion were measured by the proposed optode (Table 2).

Table 2  
Results of gallium (III) ion determination in spiked samples

Sample	Ga(III) Added ( $\mu\text{M}$ )	Ga(III) Found ( $\mu\text{M}$ ) <sup>a</sup>	Recovery (%)
Water 1	0	N.D. <sup>b</sup>	
	8	7.8 ( $\pm 0.16$ )	97.5
Water 2	0	N.D.	
	20	18.7 ( $\pm 0.12$ )	93.5
Water 3	0	N.D.	
	70	69.1 ( $\pm 0.3$ )	98.7

<sup>a</sup> Average of three determinations.

<sup>b</sup> Not detected.



pH of the water samples were adjusted by the addition of 5 ml of glycine buffer (pH 3.5) to 20 ml of water samples. The recoveries were all satisfactory (93.5–98.7%). These experimental results showed that the optode is an effective tool in analyzing the gallium content of water samples.

#### 4. Conclusion

The optode described in this work provides a simple means for determination of Ga(III) ions. A PVC based membrane with good optical and mechanical properties is used as a matrix for immobilization of the selective ligand for Ga(III) ion. The membrane responds to Ga(III) ion by changing color from yellow–brown to pink–brown. The proposed optode was successfully applied as a probe for determination of Ga(III) ion at micromolar concentration levels in water samples.

#### Acknowledgement

The authors wish to acknowledge the support of this work by Shiraz University Research Council.

#### References

- [1] C.K. Mahutte, *Biochemistry* 31 (1998) 119.
- [2] L. Zhang, M.E. Langmuir, M. Bai, W.R. Seitz, *Talanta* 44 (1997) 1691.
- [3] R. Seitz, in: O.S. Wolfbeis (Ed.), *Fiber Optic Chemical Sensors and Biosensors*, vol. 2, CRC Press, Boca Raton, 1991, pp. 1–19 (chapter 9).
- [4] K. Seiler, W. Simon, *Anal. Chim. Acta* 266 (1992) 73.
- [5] I. Murkovic, S.O. Wolfbeis, *Sens. Actuators B* 39 (1997) 246.
- [6] C. Sanchez-pedreno, J.A. Ortuno, M.I. Albero, M.S. Garcia, M.V. Valero, *Anal. Chim. Acta* 414 (2002) 195.
- [7] T. Werner, T. Mayer, *Analyst* 127 (2002) 248.
- [8] A. Safavi, M. Bagheri, *Sens. Actuators B* 90 (2003) 143.
- [9] A. Safavi, H.R. Abbdoullahi, *Anal. Chim. Acta* 367 (1998) 167.
- [10] N. Hirayama, Y. Horita, S. Oshima, K. Kubono, H. Kokusen, T. Honjo, *Talanta* 53 (2001) 857.
- [11] J. Jayachandran, P. Dhadke, *Hydrometallurgy* 50 (1998) 117.
- [12] A. Uzawa, H. Minamisawa, T. Okutani, *Anal. Sci.* 16 (2000) 1085.
- [13] L. Junshen, H.E. Zhengguang, C. Jun, C. Chunguang, Z. Baoxue, C. Weimin, *Rare Metals* 22 (2003) 235.
- [14] J. Shida, S. Matsuzaki, *Anal. Sci.* 13 (1997) 41.
- [15] H. Minamisawa, S. Iizima, M. Minamisawa, S. Tanaka, N. Arai, M. Shibukawa, *Anal. Sci.* 20 (2004) 683.
- [16] B. Gong, X. Li, F. Wang, X. Chang, *Talanta* 52 (2000) 217.
- [17] A.N. Antheraidis, G.A. Zachariadis, J.A. Stratis, *Talanta* 60 (2003) 929.
- [18] G. Jinzhang, T. Jianniao, Z. Yanchun, Y. Wu, D. Hualing, *Rare Metals* 22 (2003) 1.
- [19] H. Filik, M. Do.utan, E. Tütem, R. Apak, *Anal. Sci.* 18 (2002) 955.
- [20] H. Filik, E. Tütem, R. Apak, E. Erça, *Mikrochim. Acta* 129 (1998) 57.
- [21] N. Mahendra, P. Gangaiya, S. Sotheeswaran, R. Narayanaswamy, *Sens. Actuators B* 81 (2002) 196.
- [22] N. Mahendra, P. Gangaiya, S. Sotheeswaran, R. Narayanaswamy, *Sens. Actuators B* 90 (2003) 118.
- [23] A. Safavi, M. Bagheri, *Sens. Actuators B* 99 (2004) 608.
- [24] A. Safavi, M. Bagheri, *Anal. Chim. Acta* 530 (2005) 55.
- [25] A. Safavi, M. Bagheri, *Sens. Actuators B* 107 (2005) 53.
- [26] W.E. Morf, K. Seiler, P. Sorenson, W. Simon, in: E. Pungor (Ed.), *Ion-Selective Electrodes*, vol. 5, Akademia Kiado, Budapest, 1989, pp. 141–159.
- [27] E. Bishop, *Indicators*, First ed., Pergamon Press Ltd., Headington Hill Hall, Oxford, 1972.
- [28] E. Bakker, P. Büllmann, E. Pretsch, *Chem. Rev.* 97 (1997) 3083.
- [29] J. Lurie, *Handbook of Analytical Chemistry*, English translated by: N. Bobrov, Moscow, 1978.

Short communication

## CCD camera full range pH sensor array

A. Safavi\*, N. Maleki, A. Rostamzadeh, S. Maesum

*Department of Chemistry, Faculty of Sciences, Shiraz University, Shiraz 71454, Iran*

Received 28 November 2005; received in revised form 26 March 2006; accepted 6 April 2006

Available online 6 June 2006

### Abstract

Changes in colors of an array of optical sensors that responds in full pH range were recorded using a CCD camera. The data of the camera were transferred to the computer through a capture card. Simple software was written to read the specific color of each sensor. In order to associate sensor array responses with pH values, a number of different mathematics and chemometrics methods were investigated and compared. The results show that the use of “Microsoft Excel’s Solver” provides results which are in very good agreement with those obtained with chemometric methods such as artificial neural network (ANN) and partial least square (PLS) methods.

© 2006 Elsevier B.V. All rights reserved.

*Keywords:* CCD camera; pH sensor array; Full range

### 1. Introduction

Sensors have traditionally been considered to respond selectively to a component in a mixture. But only a few numbers of sensors are selective. Sensors with different selectivity coefficients are widely used in many areas for chemical analysis. Nonselectivity was once considered as their drawback. These sensors when used as arrays and when they have different responses toward different components can be used for multi-component analysis. In the course of calibration, arrays produce large amounts of data and thus quantitative and qualitative information are mixed up. This type of data can only be manipulated with mathematical and chemometrics methods [1]. Solid-state sensors used to detect gases are usually quartz crystal microbalance or metal oxide semiconductors sensors [2]. In the liquid state mostly different electrochemical methods are used [3]. The arrays which either detect the gaseous components (electronic nose) or components in aqueous form (electronic tongue) measure the electrical properties of the system under study.

Optodes, which fall in neither of the above categories, have been long used in practical cases such as clinical analysis, environmental analysis, and process control. They are suitable for sensing wide range of organic and inorganic materials. Several optodes have been designed to determine pH [4–8], but

all suffer from limited measuring range. Artificial neural networks (ANNs) have shown to be very successful in extending the response range of an optical pH sensor. The application of ANN enabled the extension of the useful pH response range of an optode from its narrow linear range (pH 5–7.25) to much wider range of pH (2.51–9.76) [9]. In another work multilayer feed-forward ANN was used to model the input–output data of an optical-fiber pH sensor at three different wavelengths. The resulting model was tested with 70 solutions of pH 1.60–10.17. The average prediction error was 0.2 pH units [10]. Recently we described the development of an optical pH sensor based on immobilization of a mixture of two dyes on a triacetylcellulose membrane [11]. The sensor has a useful pH range at low and high pH values, where glass electrodes show acidic and alkaline errors, respectively. Application of a back-propagation artificial neural network (ANN) model extended the measuring range of the proposed optode to the whole pH range. Another strategy in extending pH range using optodes is based on dynamic method of analysis [12].

Usually the quantitative and qualitative data of optodes are obtained photometrically [4]. CCD cameras can also obtain similar data. The color and intensity (power) data as obtained by the camera are usually 24 bit data. These are three colors red (R), green (G) and blue (B). The intensity of each color has 8 bits or 256 levels. In this color Scheme  $256 \times 256 \times 256 = 16777216$  colors are obtained and the value zero refers to black and 16777215 is pure white and other colors are in between, which has no resemblance to the white light spectrum. In harmony with

\* Corresponding author. Fax: +98 711 2286008.

E-mail address: [safavi@chem.susc.ac.ir](mailto:safavi@chem.susc.ac.ir) (A. Safavi).

the electronic tongue and nose, which relate to human sense of taste and olfaction, this system, which is related to human sense of sight, can be termed as an electronic eye. Although this term has previously been used to refer to a light intensity measurement device, it is also very suitable in this context. Also it should be noted that in contrast to conventional optodes, which are transmissive, this technique could also be reflective.

CCD camera detection system is used in many areas of science and industry and has been employed in many areas of chemical experimentation [13]. Lavigne et al. [14] analyzed the transmitted light through a series of polymer beads that were derivatized with some complexing agents in micromachined wells by a CCD camera. They determined species such as  $\text{Ca}^{2+}$ ,  $\text{Ce}^{3+}$ , and simple sugars at different pH values. Recently, we have reported the use of a CCD camera as a detection system for simultaneous determination of Al(III) and Fe(III) in alloys, using chromeazurol S (CAS) as the chromogenic reagent [15].

In an effort to extend the measuring range of pH optodes, in this communication we explain the design of an array of five partially selective reflective optodes for pH measurements. The responses of these optodes cover the whole pH range. Frames are taken by the CCD camera and are transferred to the computer. The frames were analyzed for red, green and blue components. The main superiority of this method compared to the previously reported methods for extending the pH range, such as chemometrics, is that by using CCD camera as the detection system, not only full range pH measurement is accessible but the use of digital images opens the possibility of increased usage of processing by computer software without the need for time-consuming analysis by conventional spectrophotometric techniques. Moreover, in this method the user friendly "Microsoft Excel's Solver" can be simply applied for data processing and it could provide results as good as those obtained by more sophisticated chemometric methods such as ANN or PLS.

## 2. Experimental

### 2.1. Reagents

Victoria blue (VB), solo chrome dark blue (SC) and congo red (CR) were supplied by BDH Laboratory Supplies (Poole, Dorset, UK), titan yellow GR (TY), and Nile blue hydrogen sulfate (NB) were from Merck (Darmstadt, Germany). Ethylene diamine (97%) and all other reagents were analytical grade (Merck, Darmstadt, Germany). Universal aqueous pH buffer solutions (pH 1.81–11.98) were prepared from acetic/phosphoric/boric acids (0.04 M, respectively). The final pH is adjusted by the addition of 0.2 M sodium hydroxide solutions. For lower and higher pH values,  $-\log[\text{H}^+]$  and  $-\log[\text{OH}^-]$  were used to calculate the pH values of the solutions.

### 2.2. Instrumentation

Optode array responses were recorded using a Sony CCD TR750E video Hi8 Handycam. Setting all controls to manual, its video output was connected to a PV-BT848 video capture card on an IBM compatible computer. Fig. 1 shows a schematic

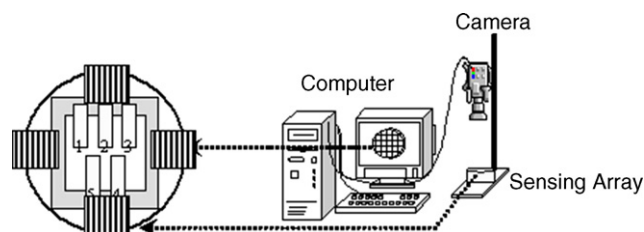


Fig. 1. Schematic representation of the sensing set-up system.

set-up diagram for the sensor system. Image analysis program was written in Visual Basic.

For comparison purposes spectrophotometric measurements were performed using a Jasco V-530 UV–vis spectrophotometer attached to an IBM compatible personal computer.

### 2.3. Optode preparation

The triacetylcellulose membranes were produced from waste photographic film tapes. These were previously treated with commercial sodium hypochlorite for several seconds in order to remove the colored gelatinous layers. The tapes simply were treated with a clear solution of indicators in ethylene diamine (about  $5 \times 10^{-3} \text{ g mL}^{-1}$ ) for 5 min at room temperature. Then, they were washed with water to remove ethylene diamine and loosely trapped dyes. These membranes were washed with hot ethanol for removing extra dyes. Finally, the membranes were washed with detergent solution and water, and kept under water when not in use.

### 2.4. Sensor array

Five different pH optodes were prepared by coating TY, VB, SC, CR, and, NB indicators on the membrane. The sensor array was formed from five membranes over a white background. The sensors were arranged randomly in a glass container. The system was stable over 40 successive pH measurements in the pH range of 0–14, after that a minor leaching of the dye materials was observed. Sensor array was kept under water when not in use.

### 2.5. RGB values

The response of the sensor array at each pH value was first obtained as a single frame taken by the CCD camera. The analytical data that a digital camera returns are a standard trichromatic response, with 8-bit red, green and blue channels, respectively. Hence, a value is returned to the user ranging from 0 to 255 for each channel. The data which were transferred to the computer were analyzed by a program written in Visual Basic and was then transported to Excel.

## 3. Results and discussion

### 3.1. Analytical signals

In this technique the three-dimensional RGB values of pixels of the pH optodes' pictures were taken as analytical signals,

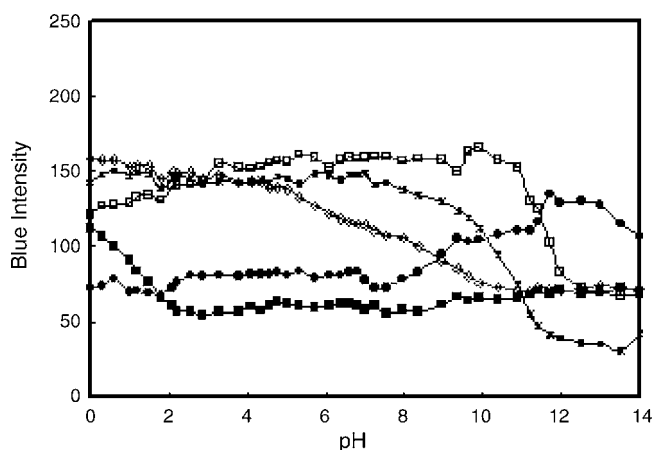


Fig. 2. Blue imaging signal for CR (■), NB (◇), SC (●), VB (\*), and TY (□) optodes.

instead of the one-dimensional absorbance values of the pH optodes (at their wavelength of maximum absorption). As an example, the response of blue component as a function of pH for the optode array is shown in Fig. 2.

Thus, for each pH, a series of 15 signals (3 colors  $\times$  5 optodes) were recorded. In order to correlate sensor array responses to pH values, the resulting patterns were analyzed using different mathematical or chemometrical methods. The data were randomly split into calibration and validation sets consisting of 29 and 14 frames for model definition and evaluation, respectively. For comparison, spectroscopic studies on TY, VB, SC, CR, and, NB pH optodes were performed at  $\lambda_{\max}$  of 510, 430, 650, 600, and, 645 nm, respectively (see Fig. 3). It is to be noted that spectrophotometric measurement with one wavelength per optode cannot cover the whole range of pH.

### 3.2. Measuring ranges

The two limiting activities at which the slope of the response function reduce to quarter of its maximum value have been used to quantify the practical pH measuring ranges of the pH optodes described herein (Fig. 3). Estimation of the best fitting curves on the curves of RGB light intensity values versus pH for slope calculation was performed by Table Curve windows software [16].

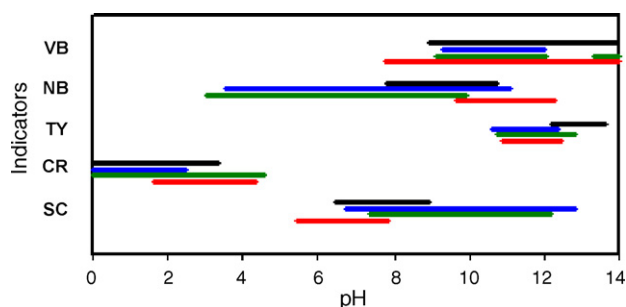


Fig. 3. The pH measuring range obtained for imaging (red, green, and blue light intensities) and spectrophotometric (absorbance at  $\lambda_{\max}$ ) results for different indicators. The black lines represent spectroscopic measuring range. The red, green, and blue components have been shown in their corresponding colors.

### 3.3. Calibration procedures

For the data set described above, different methods were used for processing the data in order to obtain the best results. The calibration set of data was used as the input for ANN, Microsoft Excel's Solver (generalized reduced gradient nonlinear optimization algorithm), and partial least squares (PLS).

The data obtained from the image were processed by ANN, which was trained with the back-propagation of errors learning algorithm. In this study, the calibration and prediction sets were prepared randomly. Twenty-nine solutions were selected as the calibration set and 14 were selected as the prediction set. The structure of network was comprised of three layers, an input, a hidden and an output layer. The parameters of the network were optimized based on the minimum error of prediction of the testing set. The optimum learning rate of 0.3 and momentum of 0.2 for two nodes in the hidden layer gave minimum error of prediction. Continued training up to 2000 iterations resulted in the best network's prediction performance.

A multi-linear model ( $Y = C_0 + C_1X_1 + C_2X_2 + \dots + C_{15}X_{15}$ ) estimates pH values ( $Y_i$ ) from RGB patterns ( $X_{i1} \dots X_{i15}$ ). Solver was used to optimize the values of coefficients ( $C_0$ – $C_{15}$ ) to obtain the best fit of the experimental pH values with the estimated pH values.

To select the number of factors in PLS and in order to model the system without over-fitting the pH data, a cross-validation method [17], leaving out one sample at a time, was used on the validation data. Nine factors gave the best performance.

Table 1, shows some results on prediction of pH values using different methods. This table shows that a very good correlation exists between true and predicted pH values using different chemometric and mathematical methods. Comparison of the correlation coefficients obtained between the true and predicted pH values using different methods reveals the suitability of the user friendly Excel's Solver for data analysis in here which in fact eliminates the need to use chemometrics methods for untrained experimentalists.

### 3.4. Interferences

The proposed immobilized indicators were tested in the appropriate buffer solutions for any possible interference from ions, which have been previously reported [18,19] to react with free indicators (Table 2).

No interference from the ions was observed when the indicators were immobilized on the proposed optodes.

Table 1  
Prediction results for pH data

Method	MSE <sup>a</sup>	Avg <sup>b</sup>	Corr <sup>c</sup>
ANN	0.03	0.09	0.9997
Solver	0.04	0.10	0.9997
PLS	0.05	0.17	0.9930

<sup>a</sup> Mean square errors computed for validation.

<sup>b</sup> The average prediction error of pH values.

<sup>c</sup> The correlation between predicted pH and true pH.

Table 2  
List of reported interferences for the free indicators

Indicator	Ions
NB	–
VB	–
TY	Mg <sup>2+</sup> (pH 12.5) [18]
CR	Hg <sup>2+</sup> (pH 5.5) [19]
SC	Ca <sup>2+</sup> , Cd <sup>2+</sup> (pH 11.5), Mg <sup>2+</sup> , Mn <sup>2+</sup> , Zn <sup>2+</sup> (pH 10) [19]

#### 4. Conclusions

Imaging pH measurements with the potential of simultaneous detection of many samples, not only yields wider measuring ranges, but it also offers other measuring ranges, which could not be obtained from spectrophotometric measurement (at a single wavelength) (see Fig. 3). One of the best features of such an optode array is its ability to measure pH values at high and low extremes of the pH range, where glass electrodes encounter alkaline and acid errors, respectively. The mathematical and chemometric models show good performance for association of three-dimensional imaging data to one-dimensional chemical data. The presented methodology allows rapid determination of pH values in a full pH range. The good correlation that exists between the true and predicted pH values warrants the applicability of the method to different samples.

#### Acknowledgement

The authors thank Shiraz University Research Council for the support of this work.

#### References

- [1] C.D. Natale, R. Paolesse, A. Macagnano, A. Mantini, A. D'Amico, A. Legin, L. Lvova, A. Rudnitskaya, Y. Vlasov, *Sens. Actuators B* 64 (2000) 15.
- [2] R.E. Baby, M. Cabezas, E.N. Walsoe de Reça, *Sens. Actuators B* 69 (2000) 214.
- [3] S. Winquist, C. Holmin, P. Krantz-Rülcker, I. Wide, Lundström, *Anal. Chim. Acta* 406 (2000) 147.
- [4] O.S. Wolfbeis, *Fiber Optic Chemical Sensors and Biosensors*, vol. 1, CRC Press, Inc, Boca Raton, 1991 (and references cited therein).
- [5] H. Hisamoto, M. Tsubuku, T. Enomoto, K. Watanabe, H. Kawaguchi, Y. Koike, K. Suzuki, *Anal. Chem.* 68 (1996) 3871.
- [6] Y. Kostov, S. Tzonkov, L. Yotova, M. Krysteva, *Anal. Chim. Acta* 280 (1993) 15.
- [7] A. Safavi, M. Pakniat, *Anal. Chim. Acta* 335 (1996) 227.
- [8] A. Safavi, H. Abdollahi, *Anal. Chim. Acta* 367 (1998) 167.
- [9] M.N. Taib, R. Andres, R. Narayanaswamy, *Anal. Chim. Acta* 330 (1996) 31.
- [10] M.N. Taib, R. Narayanaswamy, *Sens. Actuators B* 39 (1-3) (1997) 365.
- [11] A. Safavi, M. Bagheri, *Sens. Actuators B* 90 (2003) 143.
- [12] A. Safavi, A. Rostamzadeh, S. Maesum, *Talanta* 68 (5) (2006) 1469.
- [13] S. Borman, *Chem. Eng. News* 74 (1996) 33.
- [14] J.J. Lavigne, S. Savoy, M.B. Clevenger, J.E. Ritchie, B.S.J. McDoniel Yoo, E.V. Anslyn, J.T. McDevitt, J.B. Shear, D. Neikirk, *J. Am. Chem. Soc.* 120 (1998) 6429.
- [15] N. Maleki, A. Safavi, F. Sedaghatpour, *Talanta* 64 (2004) 830.
- [16] <http://www.systat.com/products/TableCurve3D>.
- [17] E.R. Malinowski, *Factor Analysis in Chemistry*, second ed., Wiley, New York, 1991.
- [18] R.J. Hall, G.A. Gray, L.R. Flynn, *Analyst* 91 (1966) 102.
- [19] E. Bishop, *Indicators*, Pergamon Press Ltd, 1972.



## A new ion-selective electrode for anionic surfactants

M<sup>a</sup> Jesús Seguí, Josefa Lizondo-Sabater, Angel Benito, Ramón Martínez-Máñez\*,  
Teresa Pardo, Félix Sancenón, Juan Soto\*

*Instituto de Investigación en Química Molecular Aplicada, Departamento de Química, Universidad Politécnica de Valencia,  
Camino de Vera s/n, 46022 Valencia, Spain*

Received 23 November 2005; received in revised form 27 March 2006; accepted 6 April 2006  
Available online 24 May 2006

### Abstract

The new ligand 7-methyl-7,13-di-octyl-1,4,10-trioxa-13-aza-7-azonia-cyclopentadecane ( $L^1$ ) has been designed, synthesised and used as ionophore in the development ion-selective electrodes for anionic surfactants. Different PVC-membrane anionic-surfactants-selective electrodes were prepared by using  $L^1$  as ionophore and bis(2-ethylhexyl)sebacate (BEHS), dibutyl phthalate (DBP) and nitrophenyl octyl ether (NPOE) as plasticizers. The PVC-membrane electrode containing  $L^1$  and NPOE (electrode E1) showed a Nernstian response to lauryl sulfate with a slope of  $-59.5$  mV per decade in a range of concentrations from  $1.3 \times 10^{-6}$  to  $6.8 \times 10^{-3}$  M and a detection limit of  $6.0 \times 10^{-7}$  M. The electrode E1 also showed a reasonable response to other alkyl sulfates and alkylbenzene sulfonates, whereas it does not respond to carboxylates and to cationic and non-ionic surfactants. A similar electrode to E1 but additionally containing the cationic additive *n*-octylammonium bromide was also prepared (electrode E2) and compared with the response of E1. Selectivity coefficients for different anions with respect to lauryl sulfate were determined by means of the fixed interference method considering lauryl sulfate as the principal anion and using a concentration of  $1.0 \times 10^{-2}$  mol dm<sup>-3</sup> for the corresponding interfering anion. The selectivity sequence found for the electrode E1 was:  $LS^- > SCN^- > ClO_4^- > CH_3COO^- > I^- > HCO_3^- > Br^- > NO_3^- > NO_2^- > Cl^- > IO_3^- > \text{phosphate} > SO_3^{2-} > C_2O_4^{2-} > SO_4^{2-}$ . Electrode E1 showed remarkably better selectivity coefficients than electrode E2. © 2006 Elsevier B.V. All rights reserved.

**Keywords:** Anionic surfactants; Ion selective electrodes; PVC membranes; Potentiometry

### 1. Introduction

The development of potentiometric ion-selective electrodes (ISEs) is an area of interest. They are used in a very wide range of applications for the determination of ions in aqueous environments [1–3]. When compared with other analytical methodologies, ion selective electrodes are simple, relatively inexpensive, robust, durable and ideal for their use in field environments. Some other advantages involve that they can be used very rapidly, are invaluable tools for continuous monitoring, they measure the activity rather than the concentration and are not affected by turbidity or sample colour. It is well known that ISE are one of the few techniques that can measure both positive and negative ions depending on the nature of the ionophore. In fact a number of ion-selective electrodes for target cations and

anions have been reported [4]. We are especially interested in the development of anion sensors [5,6]. Anions are known to display fundamental roles in a wide range of environmental and biological processes and the search of receptors and sensors for target anionic chemical species is a timely area of interest [7,8]. Among the wide number of environmentally important anions, opportune investigations have been developed for anionic surfactants. They are widely used in domestic and the industrial processes as washing agents. It is quite usual to find these anions in locations such as lakes, rivers, where they are cause of environmental concern. Because of this, it is of certain interest the development of methodologies for accurate determination of anionic surfactants in aqueous environments. In this sense, many known methods require somehow tedious procedures such as liquid and gas chromatography [9–11] and are not suitable for in situ quantitative determinations and continuous monitorization. As stated above, an attractive alternative for quantitative and pseudo-quantitative determinations is the use of ion selective electrodes and, at this respect, a certain number of electrodes for anionic surfactants have been described [12–14]. As an alternative we have recently

\* Corresponding authors. Tel.: +34 963877343; fax: +34 963879349.

E-mail addresses: [rmaez@qim.upv.es](mailto:rmaez@qim.upv.es) (R. Martínez-Máñez),  
[jsotoca@qim.upv.es](mailto:jsotoca@qim.upv.es) (J. Soto).

reported the use of aza-oxa cycloalkanes as active ionophores in ion-selective electrodes for anionic surfactants [15]. However some of these reported electrodes typically show problems related with reproducibility and stability and therefore the search of new ion-selective electrodes for anionic surfactant is still an area of interest. In most cases the carriers used are simple quaternary ammonium salts [16–18] that display electrostatic interactions with the anionic part of the surfactants and there are relatively few examples using more advanced hosts as suitable ionophores. Two recent reviews have been published covering the topic of surfactant ISEs [19,20]. Following our recent interest in the development of ion-selective electrodes for anionic and cationic species [21–27] we report here the synthesis of a new aza-oxa cycloalkane derivative and its use as active carrier for the development of PVC-based membrane ion-selective electrodes for anionic surfactants.

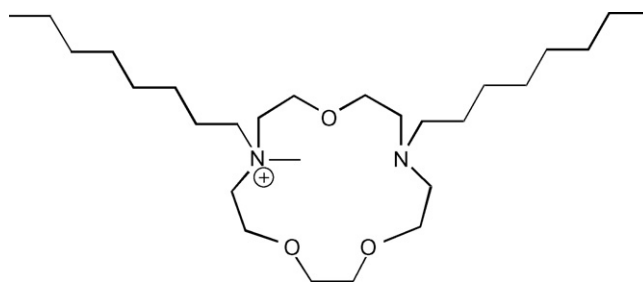
## 2. Experimental

### 2.1. Reagents and apparatus

Poly(vinyl chloride) of high molecular weight (PVC), 2-nitrophenyl octyl ether (NPOE) and *N*-2-hydroxyethyl-piperazine-*N'*-2-ethanesulfonic acid (HEPES) were purchased from Sigma–Aldrich. Tetrahydrofuran (THF), acetonitrile (CH<sub>3</sub>CN), tetra-*n*-octylammonium bromide, methyl iodide and dimethyl formamide were purchased from Merck. Sulfate, sulfite, thiocyanate, chloride, perchlorate, bromide, iodide, acetate, nitrate, nitrite, phosphate, oxalate, carbonate and iodate solutions were prepared from potassium salts purchased from Scharlau. Anionic surfactants, decyl sodium sulfate, tetradecyl sodium sulfate, 1-decanesulfonic acid sodium salt and isethionic acid sodium salt were purchased from Acros Organics. Cholic acid sodium salt, hexadecyltrimethylammonium bromide, *t*-octylphenoxypolyethoxyethanol (Triton-X-100) and *N*-tetradecyl-*N,N*-dimethyl-3-ammonio-1-propanesulfonate surfactants were purchased from Sigma–Aldrich. Lauryl sodium sulfate was purchased from Merck. Alkylbenzenesulfonate (NALAS), was obtained from Petresa. All the aqueous solutions and buffers were prepared with deionized distilled water (Milli-Q water purification system). Experiments were performed at 25 °C.

### 2.2. Synthesis of 7-methyl-7,13-di-octyl-1,4,10-trioxa-13-aza-7-azonia-cyclopentadecane (L<sup>1</sup>)

The macrocycle 7,13-bis(*n*-octyl)-1,4,10-trioxa-7,13-diazacyclopentadecane [15] (185.5 mg, 0.419 mmol) was dissolved in dry dimethyl formamide (40 mL) and the reaction mixture was stirred, heated to 50 °C and 0.125 g (55 μL) of methyl iodide added for 30 min. The mixture was stirred at room temperature for 24 h then diethyl ether was added and the solution kept at low temperature overnight. The precipitate obtained was filtered off and washed with diethyl ether and dried. Yield: 56.9 mg (0.297 mmol), 29.7%. FAB high resolution mass spectroscopy; found *m/z* 457.4329, calculated for C<sub>27</sub>H<sub>57</sub>N<sub>2</sub>O<sub>3</sub>, 457.4369 (Scheme 1).



Scheme 1.

### 2.3. Membrane preparation

The general procedure used to prepare the membrane was similar to that described in a previous work [15]. The PVC membranes were obtained by thoroughly mixing the ionophore, the poly(vinyl chloride) and the corresponding plasticizer. Some of the membranes prepared also contained the cationic additive tetra-*n*-octylammonium bromide. The mixtures were dissolved in 5 mL of THF and transferred into a glass dish 5 cm in diameter. The solvent was allowed to evaporate overnight and a yellow coloured transparent membrane was obtained. A 7 mm diameter piece was cut out with a Fluka punch for ion-selective membranes and incorporated into a Fluka electrode body ISE (ref. 45137) containing 0.01 M lauryl sodium sulfate at pH 7 and 0.01 M KCl as internal filling solution. The electrode was conditioned for 24 h by soaking in a 0.01 M lauryl sodium sulfate–HEPES pH 7 solution. When not in use the electrode was kept immersed in the same solution.

### 2.4. Emf measurements

The external reference electrode was Ag–AgCl (KCl 3 M) and an electrode body ISE of Fluka ref. 45137 was used for all emf measurements. Potentiometric measurements were obtained by using the following cell assembly: Ag/AgCl (KCl 3 M) | test solution | membrane | 0.01 M LS<sup>−</sup>, 0.01 M HEPES, 0.01 M KCl | Ag/AgCl. All potential measurements were carried out at pH 7 (0.01 M HEPES) on a GLP22 Crison pH/mV meter. Calibration curves were constructed by plotting the potential, *E* versus the logarithm of the sodium lauryl sulfate activity at pH 7.0 [28–30]. The detection limit was defined as the intersection of the extrapolated linear regions of the calibration graph. Potentiometric selectivity coefficients were determined according to the fixed interference method using 0.01 M solutions of the interfering ion. Activity coefficients were calculated according to the Debye–Hückel approximation.

## 3. Results and discussion

### 3.1. Synthesis and the emf response characteristics

The design of L<sup>1</sup>, and its use as ionophore in ion-selective electrodes, is based on the idea that sophisticated receptors might show enhanced interactions with anions in terms of selectivity when compared with simple commonly-used quaternary

ammonium salts. Thus, pre-organised receptors bearing multiple binding sites can display enhanced selectivity because of both enthalpic and entropic factors. Based on this general concept, the designed ionophore, ( $L^1$ ) is a polyazacycloalkane containing one tertiary amine and a quaternary ammonium group being part of a macrocycle also containing ether moieties. Additionally, from the two nitrogen atoms in the macrocyclic scaffolding, *n*-octyl alkyl chains have been anchored in order to enhance the lipophilicity of the final derivative. This design was based in our previous studies, where it was shown that polyazaoxacycloalkanes can form strong complexes in aqueous environments with anionic surfactants. Thus we have recently used the aza-oxa-cycloalkane 7,13-bis(*n*-octyl)-1,4,10-trioxa-7,13-diazacyclopentadecane as ionophore for the preparation of electrodes for anionic surfactants [15]. The difference between this ligand and  $L^1$  is one methyl group attached to one amine on the later that transform a tertiary amine in a quaternary ammonium group. Despite the similitude of both ligands, we found it interesting to prove the behaviour of  $L^1$  in PVC-based membranes and study the effect that minor changes in the ionophore structure might have on the electrode response.

As it has been reported the response of the ion-selective electrodes in terms of selectivity and sensitivity depends not only on the ionophore, but also on the final composition of the membrane ingredients, the plasticizer used and the presence or not of cationic or anionic additives. Because of this number of factor, in a first step several proportions of the membrane components (ionophore, plasticizer and PVC) were tested. Additionally, the membranes were prepared using three different plasticizers of different dielectric constant; specifically bis(2-ethylhexyl)sebacate (BEHS,  $\epsilon = 4$ ), dibutyl phthalate (DBP,  $\epsilon = 6.4$ ) and nitrophenyl octyl ether (NPOE,  $\epsilon = 24$ ). Also the membranes were prepared using proportions of the ionophore in the 1–10 wt.% range. All the membranes prepared were tested against lauryl sulfate. The best results, in terms of linear range, slope and detection limit were found for the membranes prepared with the plasticizer with larger permittivity (NPOE) and a proportion of 4 wt.% of ionophore. Based on these preliminary studies, the final membrane composition used for the experiments detailed below was 4 wt.% of ionophore, 41 wt.% PVC and 55 wt.% NPOE. This electrode was named as E1. For the sake of comparison, a similar membrane but containing additionally a 7 wt.% of tetra-*n*-octylammonium bromide as cationic additive was also prepared (electrode E2).

### 3.2. Effect of pH

The influence of pH on the potential response of the electrodes E1 and E2 was studied at a fixed concentration of lauryl sulfate of  $1 \times 10^{-4}$  mol dm<sup>-3</sup> over a pH range of 5–11. The pH was varied by potassium hydroxide and hydrochloric acid addition. The results observed for electrode E1 are shown in Fig. 1. As it can be seen, the potential is independent on the pH in the range of ca. 5–8. Thus, this range may be chosen as the working pH for the electrode assembly. Further potential changes were found at basic pH probably involving membrane response to OH<sup>-</sup>. A very close behaviour was found for elec-

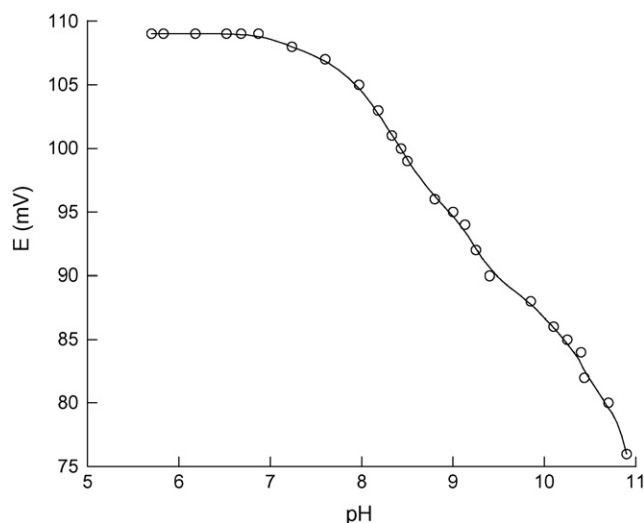


Fig. 1. The pH effect on the potential of the membrane electrode containing  $L^1$ , PVC and NPOE.

trode E2. Based on these data all the potentiometric measurements detailed below were carried out at pH 7.

### 3.3. Response of electrodes to anionic surfactants

The electrode containing  $L^1$  as ionophore and NPOE as plasticizer (electrode E1) showed a Nernstian potentiometric response of  $-59.5$  mV per decade in a range of lauryl sulfate concentration from  $1.3 \times 10^{-6}$  to  $6.8 \times 10^{-3}$  M with a detection limit of  $6.0 \times 10^{-7}$  M. A response time of ca. 2–3 s was found for electrode E1 measured as the time required for the membrane electrode to reach a potential within  $\pm 1$  mV of the final equilibrium when the measurements were performed alternatively in  $10^{-2}$  and  $10^{-4}$  mol dm<sup>-3</sup> solutions of lauryl sulfate. This electrode does not show appreciable decay of the slope for at least 20 days. The response of electrode E2 was similar to that found for E1, but showing in general slightly poorer figures. Thus, a slope  $-58.7$  mV per decade in a range of lauryl sulfate concentration from  $6.3 \times 10^{-6}$  to  $6.8 \times 10^{-3}$  M was found with a detection limit of  $1.9 \times 10^{-6}$  M for electrode E2. The response time for electrode E2 was of ca. 6–7 s. Table 1 shows a comparative between the response parameters of E1 and E2. For the sake of comparison, Table 1 also includes the response of the electrode in reference 15 (electrode E3) containing the cyclic aza-oxa-cycloalkane 7,13-bis(*n*-octyl)-1,4,10-trioxa-7,13-diazacyclopentadecane as ionophore. As it can be observed, sensitivities closer to theoretical values and a moderate improvement of the detection limit are found for electrode E1 when compared with E3.

Several studies on the response of electrode E1 were carried out. In a first step the response to lauryl sulfate and other inorganic anions as nitrate, perchlorate, carbonate, iodide, sulfate and thiocyanate was studied. The results are shown in Fig. 2. As it can be observed, E1 display a remarkable selective response to the anionic surfactant, whereas, display a poor response to perchlorate and a near negligible response to the remaining anions studied. The response of electrode E1 was also studied towards

Table 1  
Response parameters of prepared lauryl sulfate electrodes

Electrode	E1	E2	E3 <sup>a</sup>
Slope (mV per decade)	−59.5	−58.7	−57.7
Detection limit (mol dm <sup>−3</sup> )	$6.02 \times 10^{-7}$	$1.99 \times 10^{-6}$	$2.23 \times 10^{-6}$
Linear range (mol dm <sup>−3</sup> )	$1.26 \times 10^{-6}$ – $6.76 \times 10^{-3}$	$6.30 \times 10^{-6}$ – $6.76 \times 10^{-3}$	$3.31 \times 10^{-6}$ – $6.67 \times 10^{-3}$

<sup>a</sup> Data from Ref [15]. The membrane E3 contains 3.7 wt.% of the ionophore 7,13-bis(*n*-octyl)-1,4,10-trioxo-7,13-diazacyclopentadecane, 40.98 wt.% PVC and 55.17 wt.% NPOE.

different surfactants. Surfactants are traditionally divided in four types; anionic, cationic, non-ionic and zwitterionic [31,32] and the electrode E1 gave a quite different response to each of them. Hence, E1 responds linearly to lauryl sulfate (an alkylsulfate), whereas gave a no-linear response, especially at large concentrations, towards Na-LAS (an alkylbenzene sulfonate) (see Fig. 3) probably due to its lower critical micelle concentration value. Practically no response was observed for the alkylsulfonates 1-decanesulfonate acid sodium salt and the isethionic acid sodium salt. No response was neither found for the anionic surfactant cholic acid which is a surfactant bearing a carboxylate group. The electrode E1 gave a no well-defined cationic response in the presence of the cationic surfactants hexadecyltrimethylammonium bromide and in the presence of the zwitterion *N*-tetradecyl-*N,N*-dimethyl-3-ammonio-1-propanesulfonate. Finally, also a poor response was observed for E1 in the presence of non-ionic surfactants such as *t*-octylphenoxypolyethoxyethanol.

Additional studies were carried out with E1 and a family of alkyl sulfates of different length. These studies were carried out because it is well documented that the response of surfactants is in general a function of the length of the hydrophobic alkylic group. Electrode E1 gave a good response to the C10, C12 and C14 alkylsulfates, whereas the response is poorer with octylsulfate and quite weak in the presence of hexylsulfate. The best response was found for lauryl sulfate (see Fig. 4). These results were expected and are in quite good agreement with the

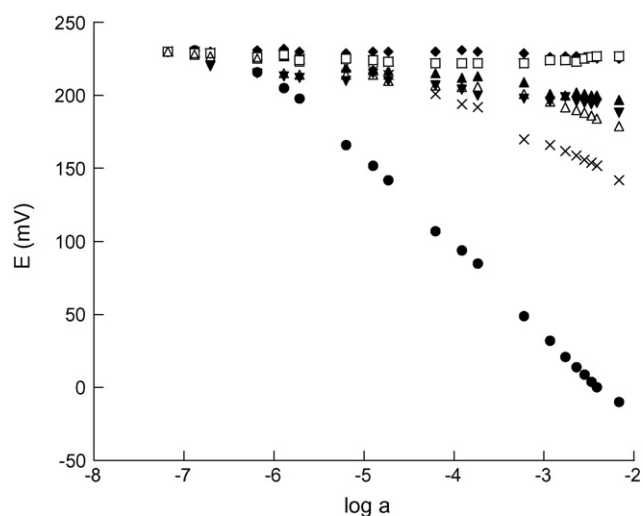


Fig. 2. Response of the PVC-based membrane E1 electrode at pH 7 in the presence of certain anions: (●) lauryl sulfate, (▼) nitrate, (×) perchlorate, (◆) bicarbonate, (▲) iodide, (□) sulfate, (△) thiocyanate.

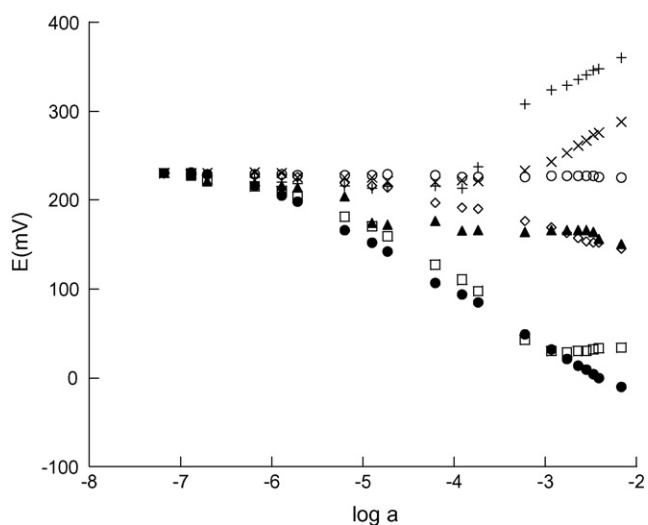


Fig. 3. Response of the PVC-based membrane E1 electrode at pH 7 in the presence of certain surfactants: (●) lauryl sodium sulfate, (◇) 1-decanesulfonic acid sodium salt, (▲) isethionic acid sodium salt, (□) Na-LAS, (○) cholic acid sodium salt, (×) *t*-octylphenoxypolyethoxyethanol, (+) *N*-tetradecyl-*N,N*-dimethyl-3-ammonio-1-propanesulfonate.

response found for other reported ion-selective electrodes for anionic surfactants [15].

In order to complete the work of characterization of the ion-selective electrodes E1 and E2 we have carried out stud-

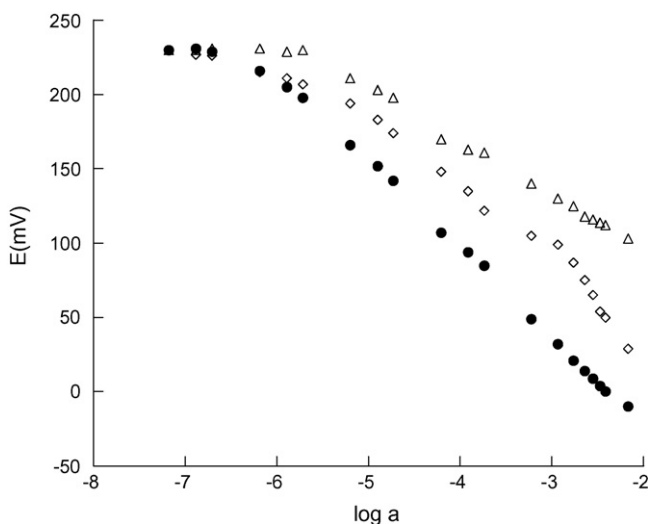


Fig. 4. Response of the PVC-based membrane E1 electrode at pH 7 in the presence of alkyl sulfate of different alkylic chain: (●) lauryl sodium sulfate, (△) decyl sodium sulfate, (◇) tetradecyl sodium sulfate.

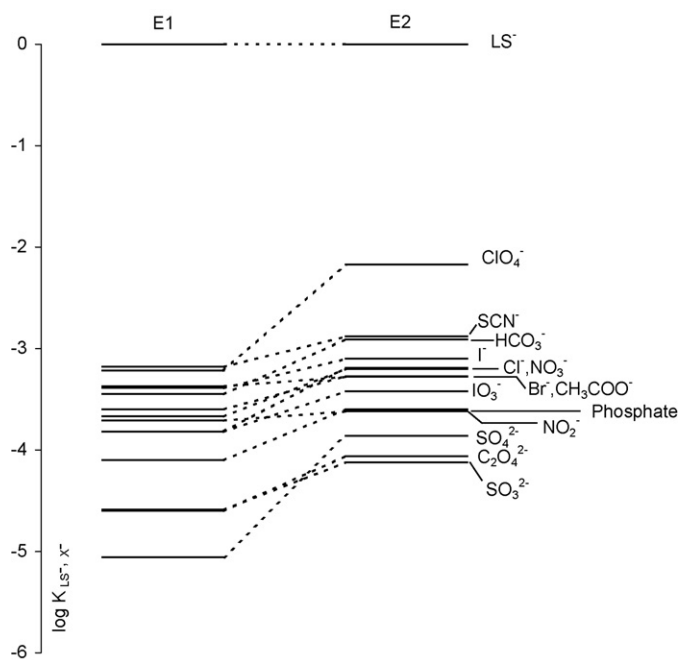


Fig. 5. Potentiometric anion selectivity coefficients of electrodes E1 and E2.

ies to determine selectivity coefficients. Selectivity is one of the most important characteristic of electrodes that gives an idea of their ability to distinguish a certain ion in a complex mixture. The potentiometric selectivity coefficients for electrodes E1 and E2 with respect to lauryl sulfate ( $K_{LS^-, X^-}^{pot}$ ) were calculated by means of the fixed interference method considering lauryl sulfate as the principal anion and using a concentration of  $1.0 \times 10^{-2} \text{ mol dm}^{-3}$  for the corresponding interfering anion. The observed selectivity coefficients for electrodes E1 and E2 are represented in Fig. 5. These coefficients clearly show that both E1 and E2 behave as selective electrodes to lauryl sulfate ( $LS^-$ ) over different anions tested.

The selectivity sequence found for the electrode E1 was:  $LS^- > SCN^- > ClO_4^- > CH_3COO^- > I^- > HCO_3^- > Br^- > NO_3^- > NO_2^- > Cl^- > IO_3^- > \text{phosphate} > SO_3^{2-} > C_2O_4^{2-} > SO_4^{2-}$ , whereas the selectivity sequence for electrode E2 was  $LS^- > ClO_4^- > SCN^- > HCO_3^- > I^- > Cl^- > NO_3^- > Br^- > CH_3COO^- > IO_3^- > \text{phosphate} > NO_2^- > SO_4^{2-} > C_2O_4^{2-} > SO_3^{2-}$  (see Table 2). Both electrodes respond preferentially to lauryl sulfate, although both selectivity sequences show some slight differences in the order of the response to anions. Additionally, both E1 and E2 electrodes show some deviations from the Hoffmeister series ( $ClO_4^- > SCN^- > I^- > NO_3^- > Br^- > Cl^- > HCO_3^- > CH_3COO^- > SO_4^{2-} > HPO_4^{2-}$ ). Although this deviation is not very important when compared with the remarkable response to lauryl sulfate, it is significant and most likely related to some kind of preferential coordination of certain anions with the ligand  $L^1$  in the PVC membrane.

As can be seen, for all of the diverse ions used, the logarithm of the selectivity coefficients for electrode E1 were lower than  $-3.3$  indicating that the studied anions would not significantly

Table 2

Potentiometric selectivity for lauryl sulfate ( $K_{LS^-, X^-}^{pot}$ ) in ion-selective PVC membranes

$X^-$	E1	E2	E3 <sup>a</sup>
$SCN^-$	-3.18	-2.88	-3.20
$ClO_4^-$	-3.22	-2.17	-2.43
$CH_3COO^-$	-3.37	-3.28	-3.94
$I^-$	-3.39	-3.10	-3.89
$HCO_3^-$	-3.45	-2.91	-4.10
$Br^-$	-3.60	-3.27	-3.76
$NO_3^-$	-3.67	-3.20	-4.06
$NO_2^-$	-3.71	-3.62	-
$Cl^-$	-3.82	-3.19	-3.97
$IO_3^-$	-3.82	-3.42	-4.00
Phosphate	-4.10	-3.60	-4.77
$SO_3^{2-}$	-4.59	-4.12	-
$C_2O_4^{2-}$	-4.60	-4.06	-5.14
$SO_4^{2-}$	-5.06	-3.86	-4.83

<sup>a</sup> Data from Ref. [15].

disturb the determination of lauryl sulfate. It is also evident from Fig. 5 that the selectivity coefficients obtained for E1 are better than those found for E2. The difference between these electrodes is that whereas E2 contains a mixture of the ionophore  $L^1$  and the cationic additive tetra-*n*-octylammonium bromide, E1 only contains the ionophore  $L^1$ . Thus, whereas in E2 both  $L^1$  and the cationic additive would act as carriers, in E1 only the ionophore  $L^1$  would display coordination with the anions. This is a remarkable result that suggests that the interaction of the prepared ligand with lauryl sulfate is more selective than the use, as ionophore, of a simple quaternary ammonium salt. For the sake of comparison the potentiometric anion-selective coefficients of electrode E3 are also included in Table 2. Similar values of  $K_{LS^-, X^-}^{pot}$  were found for E1 and E3 except for perchlorate for which a remarkable selectivity improvement with respect to lauryl sulfate was observed for electrode E1.

### 3.4. Analytical applications

The new electrode E1 in combination with an Ag/AgCl reference electrode has been used for the determination of lauryl sulfate in water by titration procedures with accurate and reproducible values. In a typical assay, 30 mL of a certain sample was placed in a beaker with 2.5 mL of methanol and 5 mL of buffered water (citrate/HCl) at pH 3. The electrode E1 was immersed in the cell and the solution titrated using  $0.004 \text{ mol dm}^{-3}$  of TEGOtrant A100 (1,3-didecyl-2-methylimidazolium chloride from Metrohm). These titration curves showed a characteristic sigmoidal shape from which the titration volume can be measured at the inflection point of the titration curve. It was found a very accurate determination of lauryl sulfate with similar results and response than those found when using the commercially available "ionic surfactant" electrode from Metrohm (i.e. real concentration of lauryl sulfate for a selected sample in water:  $3.24 \times 10^{-5} \text{ mol dm}^{-3}$ ; found  $3.29 \pm 0.06 \times 10^{-5} \text{ mol dm}^{-3}$  as averaged value from five independent determinations).



#### 4. Conclusions

A new polyazacycloalkane (L<sup>1</sup>) has been synthesized and used in the preparation of PVC membrane ion-selective electrodes for anionic surfactants. PVC membrane ion selective electrodes containing L<sup>1</sup> and NPOE as plasticizer displayed a Nernstian response in the presence of lauryl sulfate, a reasonable detection limit and response time. The electrode also showed a reasonable response to other alkyl sulfates and alkylbenzene sulfonates, whereas does not respond to carboxylates and non-ionic surfactants. A poorly defined cationic response to cationic and zwitterionic surfactants was observed for electrode E1. The selectivity sequence found for the electrode E1 was:  $LS^- > SCN^- > ClO_4^- > CH_3COO^- > I^- > HCO_3^- > Br^- > NO_3^- > NO_2^- > Cl^- > IO_3^- > \text{phosphate} > SO_3^{2-} > C_2O_4^{2-} > SO_4^{2-}$ . Additionally, the potentiometric anion-selectivity coefficients are lower than  $-3.3$  indicating that classical anions would show a very poor disturbance in the determination of lauryl sulfate. It was also remarkable that the electrode E1 showed a better response than that also containing a cationic additive indicating that L<sup>1</sup> and similar systems might be an attractive alternative to the commonly used quaternary ammonium salts as ionophores in ion-selective electrodes for anionic surfactants.

#### Acknowledgements

We would like to thank the Ministerio de Ciencia y Tecnología (projects MAT2003-08568-C03 and REN2002-04237-C02-01) and Generalitat Valenciana (GRUPOS03/035) for support. F.S. thanks the Ministerio de Educación y Ciencia for a Ramón y Cajal contract. M<sup>a</sup>.J.S. thanks the Universidad Politécnica de Valencia for a Doctoral Fellowship.

#### References

- [1] E. Bakker, P. Bühlmann, E. Pretsch, *Chem. Rev.* 97 (1997) 3083.  
 [2] E. Pungor, *Anal. Sci.* 14 (1998) 249.

- [3] E. Bakker, *Trends Anal. Chem.* 16 (1997) 252.  
 [4] P. Bühlmann, E. Pretsch, E. Bakker, *Chem. Rev.* 98 (1998) 1593.  
 [5] R. Martínez-Máñez, F. Sancenón, *Chem. Rev.* 103 (1993) 4419.  
 [6] R. Martínez-Máñez, F. Sancenón, *J. Fluoresc.* 15 (2005) 267.  
 [7] F.P. Schmidtchen, M. Berger, *Chem. Rev.* 97 (1997) 1609.  
 [8] P.D. Beer, P.A. Gale, *Angew. Chem. Int. Ed.* 40 (2001) 486.  
 [9] M. Petrovik, D. Barceló, *Anal. Chem.* 72 (2000) 4560.  
 [10] F. Smedes, J.C. Kraak, C.F. Werkhoven-Goewie, U.A.T. Brinkman, W.R. Frei, *J. Chromatogr.* 247 (1982) 123.  
 [11] H. Koenig, W. Stroebel, *Fresen. Z. Anal. Chem.* 314 (1983) 143.  
 [12] T. Tanaka, K. Hiirō, A. Kawahara, *Anal. Lett.* 7 (1974) 173.  
 [13] M. Gerlache, Z. Sentürk, J.C. Viré, J.M. Kauffmann, *Anal. Chim. Acta* 349 (1997) 59.  
 [14] J. Sánchez, M. del Valle, *Electroanalysis* 13 (2001) 471.  
 [15] M.J. Seguí, J. Lizondo-Sabater, R. Martínez-Máñez, T. Pardo, F. Sancenón, J. Soto, *Anal. Chim. Acta* 525 (2004) 83.  
 [16] J. Sánchez, A. Beltrán, J. Alonso, C. Jiménez, M. del Valle, *Anal. Chim. Acta* 382 (1999) 157.  
 [17] J. Baró-Romá, J. Sánchez, M. del Valle, J. Alonso, J. Bartroli, *Sens. Actuators B* 5 (1994) 179.  
 [18] S. Alegret, J. Alonso, J. Bartroli, J. Baró-Romá, J. Sánchez, M. del Valle, *Analyst* 119 (1994) 2319.  
 [19] M. Sak-Bosnar, Z. Grabaric, B.S. Grabaric, *Food Technol. Biotechnol.* 42 (2004) 197.  
 [20] J. Sánchez, M. del Valle, *Crit. Rev. Anal. Chem.* 35 (2005) 15.  
 [21] M.J. Seguí, J. Lizondo-Sabater, R. Martínez-Máñez, F. Sancenón, J. Soto, *Analyst* 127 (2002) 387.  
 [22] J. Lizondo-Sabater, R. Martínez-Máñez, F. Sancenón, M.J. Seguí, J. Soto, *Anal. Chim. Acta* 459 (2002) 229.  
 [23] J. Lizondo-Sabater, M.J. Seguí, J.M. Lloris, R. Martínez-Máñez, T. Pardo, F. Sancenón, J. Soto, *Sens. Actuators B* 101 (2004) 20.  
 [24] R. Martínez-Máñez, J. Soto, J. Lizondo-Sabater, E. García-Breijo, L. Gil, J. Ibáñez, I. Alcaina, S. Alvarez, *Sens. Actuators B* 101 (2004) 295.  
 [25] R. Martínez-Máñez, J. Soto, E. García-Breijo, L. Gil, J. Ibáñez, E. Llobet, *Sens. Actuators B* 104 (2005) 302.  
 [26] R. Martínez-Máñez, J. Soto, E. García-Breijo, L. Gil, J. Ibáñez, E. Gadea, *Sens. Actuators A* 120 (2005) 589.  
 [27] C. Coll, R.H. Labrador, R. Martínez-Máñez, J. Soto, F. Sancenón, M.J. Seguí, E. Sánchez, *Chem. Commun.* (2005) 3033.  
 [28] IUPAC, *Pure Appl. Chem.* 48 (1976) 127.  
 [29] IUPAC, *Pure Appl. Chem.* 67 (1995) 507.  
 [30] IUPAC, *Pure Appl. Chem.* 66 (1994) 2527.  
 [31] A. Pérez Dorado, *Detergentes*, UNED, 1996.  
 [32] J.-L. Salaguer, *Surfactantes, tipos y usos*, Cuaderno FIRP S300-A, 2002.

## Simultaneous determination of Cr(III) and Cr(VI) with prechelation of Cr(III) using phthalate by ion interaction chromatography with a C-18 column

Jirasak Threeprom<sup>a,b</sup>, Rattapol Meelapsom<sup>a</sup>, Waraporn Som-aum<sup>b</sup>, Jin-Ming Lin<sup>b,\*</sup>

<sup>a</sup> Department of Chemistry, Faculty of Science, Maharakham University, Maharakham 44150, Thailand

<sup>b</sup> Department of Chemistry, Tsinghua University, Beijing 100084, China

Received 17 January 2006; received in revised form 9 March 2006; accepted 11 March 2006

Available online 18 April 2006

### Abstract

Ion interaction chromatography has been successfully used for the simultaneous determination of Cr(III) and Cr(VI) in waste water. A C-18 column which had been dynamically coated with octylamine was used for the separation of Cr(III) and Cr(VI) based on anionic interaction. Cr(III) was chelated with potassium hydrogen phthalate (KHP) before injecting into the column since the Cr(III) did not exist in an anionic form like the Cr(VI) ( $\text{Cr}_2\text{O}_7^{2-}$ ) presented at the optimum condition. The analytes were detected at 200 nm and linear relationship between absorption with the concentration of Cr(III) or Cr(VI) was 0.1–50 mg/L. Most of the interested interferences including alkali metals, heavy metals and organic materials have no significant effect on Cr(III)–KHP complexation and Cr(VI) stability, only  $\text{NH}_4^+$  and ascorbic acid yielded the serious effect on the Cr(VI) stability. The relative standard deviations calculated from both of peak area and retention time were 0.75–2.20%. The sensitivity of the method at the level concentration of sub mg/L enabled the simultaneous determination of Cr(III) and Cr(VI) contents in waste water samples without any special sample preparation step.

© 2006 Elsevier B.V. All rights reserved.

**Keywords:** Ion interaction chromatography; Chromium; Potassium hydrogen phthalate; C-18 column

### 1. Introduction

It is well-known that the physiological effects of Cr(III) and Cr(VI) on the environment, including biological system, are totally opposite. Cr(III) appears to be essential while Cr(VI) is definitely a toxic form [1,2]. The most widely used techniques for the determination of chromium in various samples include graphite furnace atomic absorption spectrometry (GFAAS) [3,4], flame atomic absorption spectrophotometry (FAAS) [5] and electron capture detection gas chromatography (GC-ECD) [6]. Some of these methods involve the determination of one species and the calculation of the other by the difference between the total chromium concentration. This type of calculation may involve some uncertainty. High-performance liquid chromatography (HPLC) has also been used for the simultane-

ous determination of Cr(III) and Cr(VI). Cr(III) retention on a cationic column [7,8] and Cr(VI) on an anionic column [9,10], or both on paired anionic and cation columns have been reported [11,12]. Many HPLC studies involve the use of ion-pair chromatography on reversed phase columns, with either cation pairing reagents [13,14] or anion pairing reagents, and with Cr(III) eluting in the void peak [15]. Pre-column derivatization of Cr(III) species with lipophilic reagents for retention on reversed phase columns has also been reported [16,17]. Detections using visible spectrophotometry [18], post column derivatization [19], atomic emission spectrometry (AES) [14], inductively couple plasma-mass spectrometry (ICP-MS) [20], amperometry [21], conductivity [22] and chemiluminescence [23] have been described.

In our previous work [24], an ion interaction chromatography has been successfully employed to determine Cr(III) and Cr(VI) simultaneously using EDTA as the chelating agent for Cr(III)–EDTA anionic complexation. Although EDTA was suitable to be a chelating agent for Cr(III) and offered good characteristics for HPLC separation, but EDTA can also complex with

\* Corresponding author. Tel.: +86 10 62841953; fax: +86 10 62841953.

E-mail addresses: [jmlin@mail.tsinghua.edu.cn](mailto:jmlin@mail.tsinghua.edu.cn), [jmlin@mail.rcees.ac.cn](mailto:jmlin@mail.rcees.ac.cn) (J.-M. Lin).

the other metal ions. These metal–EDTA complexes could possibly interfere the separation and detection of Cr(III)–EDTA and Cr(VI). Therefore more selective complexing agent is desired for Cr(III) complexation. Posta et al. [14,23,25] reported the very selective complexing agent for Cr(III). They covered the C-18 column with potassium hydrogen phthalate (KHP), a special layer was formed which can bond Cr(III) quantitatively. The novel chromatographic phenomenon was utilized in the pre-concentration of Cr(III) before the analysis by flow flame emission spectrometry. Beside the availability of the chromatographic phenomenon presented by this group, the proposed HPLC–UV work should be the other alternative way for the simultaneous determination of Cr(III) and Cr(VI). Furthermore, HPLC–UV is well known as the conventional and common instrument in general laboratories.

In this work, therefore, the simultaneous determination of Cr(III) and Cr(VI) by ion interaction chromatography with UV detection was investigated. The separation of Cr(III) and Cr(VI) was based on anionic interaction. Since the Cr(III) did not exist in an anionic form like the Cr(VI) ( $\text{Cr}_2\text{O}_7^{2-}$ ) presented at the optimum condition, Cr(III) was pre-chelated with KHP before injecting into a C-18 column which had been dynamically coated with octylammonium. The optimum condition for complexation and elution were studied. The interference effects of the elements including alkali metals, heavy metals and organic compounds were also studied. Importantly, some reducing agents such as ascorbic acid and ammonium ions will be studied of their effects on the recovery of Cr(VI). Finally, the proposed work was applied to determine Cr(III) and Cr(VI) simultaneously in waste water.

## 2. Experimental

### 2.1. Apparatus

A high performance liquid chromatograph (Hewlett-Packard, HP1100) equipped with a G 1311 A pump and a 7125 Rheodyne injector with a 20- $\mu\text{L}$  loop was used to carry all of separation throughout this work. The chromatographic separation was achieved with a Nucleosil-100, C-18 (3  $\mu\text{m}$ , 60 mm  $\times$  4.6 mm) chromatographic column. The pH measurements were done by using the Denver Instrumental pH meter.

### 2.2. Reagents

All solutions and eluent were prepared in distilled deionized water. Stock standard solution of 500 mg/L Cr(III) and Cr(VI) were prepared from chromium(III) chloride and potassium dichromate (RDH, Aktiengesellschaft, Germany), respectively. Fresh working standard solutions of Cr(III) and Cr(VI) (single or mixed) were prepared by appropriate dilution of the stock solution with water. Potassium hydrogen phthalate solutions were prepared from the analytical reagent grade solid salt produced by Merck (Darmstadt, Germany). The eluents were prepared from HPLC grade methanol (Mallinkrodt, St. Louis, MO, USA), water and octylamine (Fluka, Switzer-

land). The mobile phase was finally adjusted to the desired pH with concentrated  $\text{H}_3\text{PO}_4$ . All eluents were filtered through a 0.45- $\mu\text{m}$  cellulose acetate membrane filter (Millipore, Bedford, MA, USA) and degassed ultrasonically before being used.

A mixed standard sample solutions containing Cr(III) and Cr(VI) was prepared. Before injecting into the HPLC system, an appropriate amount of KHP was added to the sample solution and the desired pH of the solution was adjusted with 0.1 M  $\text{H}_2\text{SO}_4$  or 0.1 M NaOH.

### 2.3. Chromatography

The chromatographic system was conditioned by passing the eluent through the column until a stable signal was obtained. Usually, about 2 h was necessary. Then, 20  $\mu\text{L}$  of a mixed standard of Cr(III)–KHP and Cr(VI) was injected into the chromatographic system with flow rate of 1.0 mL/min and the analytes were detected at 200 nm.

### 2.4. Method validation

The reliability of the determination can be checked by means of precision, accuracy and sensitivity. Precision in term of repeatability is indicated by percentage of relative standard deviation (R.S.D.) of retention time and peak area. The repeatability was studied by five consecutive injections of mixed standard solution of 5 mg/L Cr(III) and 10 mg/L Cr(VI). Accuracy is described by the mean of the % recovery. For % recovery, known amounts of pure standards (Cr(III)–KHP and Cr(VI)) were added to the sample (waste water). Each standard was added at three different concentrations and recoveries were calculated on the basis of the difference between the total amount determined in the spiked sample and the amount observed in the non-spiked samples. Sensitivity is described by the detection limit; it is defined in this work as the concentration that gave a signal three times that of the noise. External standards were used in the calibration curves and the data presented at the present study were the average of triplicate injections of samples or standard, unless stated otherwise.

### 2.5. Sample analysis

The optimum HPLC condition proposed by this work has been utilized for the simultaneous determination of Cr(III) and Cr(VI) in waste water. Three wastewater samples were collected from three sources of wastewater treatment plants nearby the Faculty of Science, Mahasarakham University, Thailand. This work was done successfully without any special sample preparation. Water sample was collected and kept in refrigerator ( $\sim 4^\circ\text{C}$ ) until the determination. It was filtered through 0.45- $\mu\text{m}$  cellulose acetate membrane filter before injecting into the HPLC system. Stock standard of KHP was added to the filtered water sample for the final concentration of 50 mg/L. In order to make sure the complete of the complexation, 5 min was needed in this step.

### 3. Results and discussion

To establish the optimum conditions for the simultaneous determination of Cr(III) and Cr(VI), factors affecting the formation of chelates and the retention behavior were studied. Various parameters affecting the formation of Cr(III)–KHP and stability of Cr(VI), namely the pH of sample solution, contact time and temperature, and KHP concentration were studied in detail. Meanwhile, the parameters affecting the retention behavior, i.e., concentration of octylamine, pH of mobile phase and % organic modifier were studied. Conversion of both chromium ions into species with similar charge is necessary for them to be retained simultaneously in a C-18 column, which had been coated by octylammonium. Cr(III) exists in the form of  $\text{Cr}(\text{H}_2\text{O})_6^{3+}$  in aqueous solution [25], hence a complexation reagent with higher complex forming ability than water is required to complex Cr(III). KHP was chosen to be the chelating agent used in this work. Being chelated with KHP, as  $[\text{Cr}(\text{III})\text{--KHP}]^-$ , Cr(III) will possibly be retained simultaneously with Cr(VI),  $\text{Cr}_2\text{O}_7^{2-}$ , on an anion-exchange C-18 column.

#### 3.1. Effect of pH on the chelation and stability of Cr(III)–KHP and Cr(VI)

The effect of pH on the chelation of Cr(III)–KHP and stability of Cr(VI) was studied by preparing the mixed standard solution of 5 mg/L Cr(III) (0.096 mM Cr(III)), 10 mg/L Cr(VI) and 50 mg/L KHP (0.245 mM KHP). Under this experimental condition the chelation of Cr(III)–KHP could be formed satisfactorily, more details will be discussed in Section 3.3. The pH of the medium ranging from 2 to 12 was adjusted by using 0.1 M  $\text{H}_2\text{SO}_4$  or 0.1 M NaOH, then the sample solutions were left for 5 min at room temperature before injecting into the HPLC system. The optimum HPLC conditions comprising of 5 mM octylammonium orthophosphate at pH 5.0 with 20% v/v MeOH, flow rate of 1.0 mL/min and detection at 200 nm were used in this section. The chelation ability and stability can be implied by the increase of peak areas of Cr(III)–KHP and Cr(VI). It was found that the formation ability of Cr(III)–KHP and stability of Cr(VI) did not depend on the pH of sample solution ranging from 2.0 to 12.0 (data did not show). These results were very strange that peak areas were independent on solution pH, as Cr(III), KHP and Cr(VI) have acid–base properties. However, it could have the theory and chemical mechanism that should probably be hypothesized to explain the experimental results. In the absence of complexing agents, other than  $\text{H}_2\text{O}$  or  $\text{OH}^-$ , Cr(III) exists as hexa-aquachromium(III) and its hydrolysis products [28].  $\text{Cr}(\text{H}_2\text{O})_6^{3+}$  is a moderately strong acid ( $\text{pK} \sim 4$ ). Its deprotonated forms formulated shortly as  $\text{CrOH}^{2+}$ .aq,  $\text{Cr}(\text{OH})_2^+$ .aq and  $\text{Cr}(\text{OH})_3$ .aq are dominating successively within pH 4–10.  $\text{Cr}(\text{OH})_4^-$  is the main form at pH higher than 10 [29,30]. When KHP ligand is added into the sample system, the Cr(III)–KHP complex could be taken place, as KHP is much more strong complexing reagent for Cr(III) than  $\text{H}_2\text{O}$  or  $\text{OH}^-$ . The similarity in term of peak areas obtained from injecting the Cr(III)–KHP complex into the HPLC system, indicating that the Cr(III)–KHP complex could be formed completely with regardless to the for-

mer Cr(III) complexes which occurred at individual pH medium. On the other hand, Cr(VI) also forms several species under different pH mediums.  $\text{H}_2\text{Cr}_2\text{O}_7$  belongs to the strong acids ( $\text{pH} < 1$ ), at within pH 1–7 its deprotonated forms are prevailing ( $\text{HCr}_2\text{O}_7^-$ ), and at above pH 7 only  $\text{Cr}_2\text{O}_7^{2-}$  ions existed in solution [31]. Therefore, the similarity of peak areas of Cr(VI) obtained from different pH mediums could be convinced that in HPLC system (mobile phase pH used was 5) all of those Cr(VI) forms would be changed to be the same one ( $\text{HCr}_2\text{O}_7^-$ ). Consequently, the pH of solution at 5.0 was chosen and used throughout this work, and it is also due to the original pH of Cr(III)–KHP solution including Cr(VI) was 5.0. It means, therefore, that the pH adjustment during Cr(III)–KHP formation could be negligible. This offered the more practical method when the real sample solution was studied.

#### 3.2. Effect of contact time and temperature

The contact times were studied in the range of 5–1500 min and the temperatures were taken account ranging from 20 to 100 °C. Then the mixed standard solution was injected into HPLC system under its optimum conditions. From the results obtained (data did not show), it was found that both of interested parameters did not play significant effect on the formation ability of Cr(III)–KHP and stability of Cr(VI). Therefore, 5 min and room temperature ( $25 \pm 1$  °C) were chosen and used throughout this work. These results showed more significant improvement of the proposed work than that of employed in previous work (30 min, 40 °C) [24].

#### 3.3. Effect of KHP concentration

The concentration of Cr(III) and Cr(VI) in sample solution were constant at 5 and 10 mg/L, respectively, meanwhile the KHP concentrations were studied in the range of 5.0–1250 mg/L. The complexation reactions were studied at pH 5, contact time of 5 min and at room temperature ( $25 \pm 1$  °C) before injecting the complex into the HPLC system under its optimum conditions. The dependence of the degree of complexation of Cr(III) on the concentration of KHP in the sample solutions is shown in Fig. 1. As shown in Fig. 1, peak areas of Cr(III)–KHP complex gives a saturation curve. In the presence of 5–100 mg/L KHP, about 90–95% of Cr(III)–KHP complex is taken place. However, to reach even better or complete complexation, higher concentration than 200 mg/L KHP would be necessary. To avoid this very high salt content we used 200 mg/L KHP (0.961 mM KHP) for the complexation step. Even though, according to the data obtained in this work, we did not know exactly whether what is the mole ratio of Cr(III)–KHP complex reaction. However, we had checked by the reversed electroosmotic flow (EOF) with capillary electrophoresis (CE)–UV detection and then found that the complex compound of Cr(III)–KHP represented the negative charge. In detail, negatively charged Cr(III)–KHP compound (1:10 mole ratio) moved to the anodic side (detection window) with higher mobility than that of the neutral EOF marker (acetone). Therefore, in order to make sure for the formation of an anionic complex prior to injecting into the chromatographic

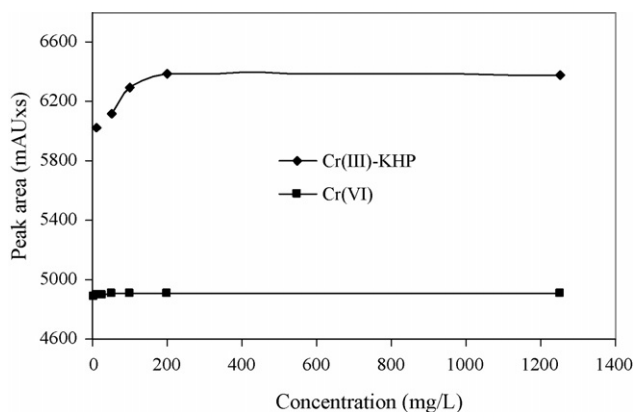


Fig. 1. Effect of KHP concentration on the formation ability of Cr(III)-KHP and stability of Cr(VI) during the sample preparation step.

HPLC system, 1:10 mole ratio of Cr(III):KHP was selected. Moreover, from the result obtained it was found that the stability of Cr(VI) is completely independent on KHP concentration even at the presence of high KHP concentration.

Under the optimum HPLC conditions and using the selected parameters comprising of pH 5.0 of sample medium,  $25 \pm 1$  °C room temperature and 5 min of contact time, the typical chromatogram of standard mixture 5 mg/L Cr(III)-KHP and 10 mg/L Cr(VI) is shown in Fig. 2. The chromatogram showed the good separation with short analysis time and acceptable resolution.

### 3.4. Effect of involving parameters on retention behavior

In order to optimize the chromatographic conditions for the simultaneous determination of Cr(III)-KHP and Cr(VI), the chromatographic parameters, such as the concentrations of octylamine and organic modifier and pH of mobile phase were investigated. The dependence of Cr(III)-KHP and Cr(VI) retention on the variation of the mobile phase pH is shown in Fig. 3. The retention time of both Cr(III)-KHP and Cr(VI) were constant

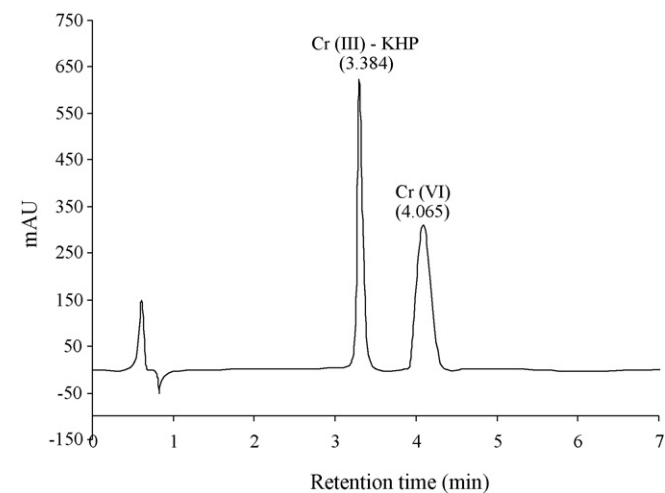


Fig. 2. Chromatogram of 5 mg/L Cr(III)-KHP and 10 mg/L Cr(VI). Chromatographic conditions: column, C-18 (Nucleosil-100, 3  $\mu$ m, 60 mm  $\times$  4.6 mm); eluent, 5 mM octylammonium orthophosphate at pH 5.0 with 20% MeOH (v/v); flow rate, 1.0 mL/min; detection at 200 nm.

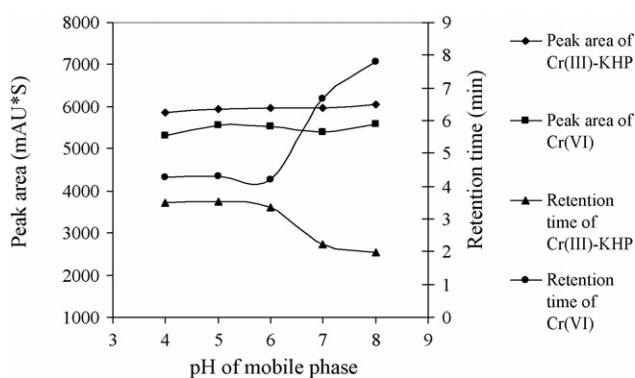


Fig. 3. Effect of pH of mobile phase on the retention time and peak areas of Cr(III)-KHP and Cr(VI). The chromatographic conditions were the same as those in Fig. 2, excepted pH of mobile phase was varied.

among the pH variation of 4–6. Then, the absolutely different behaviors were observed at pH ranging from 6–8, i.e. an increase of the retention time of Cr(VI) and the decrease of the retention time of Cr(III)-KHP. The increase of the retention time of Cr(VI) could be described by caused of a decrease of the amount of eluting anionic species (phosphate ion) leads to the increase in the retention time [27]. In addition,  $\text{Cr}_2\text{O}_7^{2-}$  is the main abundance of Cr(VI) species forming in this pH region [31], therefore longer retention was found since stronger interaction force between  $\text{Cr}_2\text{O}_7^{2-}$  and octylammonium ion taken place. Meanwhile, the decrease of the retention time of Cr(III) could probably be explained by caused of the interaction force between the cationic octylammonium ions modified on the C-18 stationary phase and the Cr(III)-KHP complex. It is due to when the pH of mobile phase increased, the abundance of active ammonium ions available on stationary phase surface were decreased, then resulting in the decrease of ion-ion interaction force. The lower interaction force taken place along with these pH variation (pH 6–8) leads to the decreasing in retention time of Cr(III). In addition, as can be seen in Fig. 3, it was also found that the variation of mobile phase pH did not influence the peak area of both types of chromium, which did not agree with other reported results [24,26]. As reported by these works, at mobile phase pH higher than 5.0, Cr(III) ion forms  $\text{Cr}(\text{OH})_3$  precipitation. Therefore, the mobile phase with a pH higher than 5.0 did not allow to be used for the simultaneous separation of Cr(III) and Cr(VI). Meanwhile, the result obtained by this work represented the high stability of Cr(III)-KHP even at pH higher than 5.0. This could be described by caused of a presence of KHP in the separation system. Since because KHP is too much more selective to Cr(III) than  $\text{OH}^-$ . Therefore, Cr(III)-KHP could remain stable even at high  $\text{OH}^-$  concentration presented in the system. The pH 5.0 was chosen to be the suitable mobile phase pH because of short analysis time and acceptable resolution for both of Cr(III)-KHP and Cr(VI).

The retention behavior of Cr(III)-KHP and Cr(VI) was depended on both octylamine concentration of the ion interaction reagent and MeOH concentration of organic modifier. The results obtained were similar fashions to those obtained in the previous work [24]. The retention mechanism could be described by using the same reasons, which had been explained in that



Table 1  
Recovery data of added 5 mg/L Cr(III) and 10 mg/L Cr(VI) from samples with high levels of salts and organic materials

Interfering species	Interfering species concentration (mg/L)	Recovery (%)	
		Cr(III)	Cr(VI)
Na <sup>+</sup>	1000	98.0	99.8
Ca <sup>2+</sup>	100	98.0	102.5
Mg <sup>2+</sup>	100	101.2	103.6
Al <sup>3+</sup>	500	89.6	95.9
NH <sub>4</sub> <sup>+</sup>	20	101.2	78.6
	200	100.8	18.7
	500	98.2	0
Fe <sup>3+</sup>	100	103.0	106.3
Mn <sup>2+</sup>	100	101.9	108.0
Co <sup>2+</sup>	500	96.2	93.4
Cu <sup>2+</sup>	500	98.7	90.2
Ni <sup>2+</sup>	500	100.9	102.2
Zn <sup>2+</sup>	500	102.9	90.6
EDTA	1000	106.9	105.7
Citric acid	1000	95.7	100.7
Tartaric acid	1000	108.2	104.2
Ascorbic acid	20	109.3	98.7
	50	111.2	75.0
	500	131.6	43.6
	1000	168.8	41.8

work [24]. To maintain the short analysis time with acceptable resolution of Cr(III) and Cr(VI) separation, 5 mM octylamine and 20% MeOH (v/v) were chosen.

### 3.5. Interferences

The study covered 14 selected interferences, including alkali metals, alkali-earth metals, transition metals and organic

materials. The recovery data of added Cr(III) and Cr(VI) from samples with high levels of interferences are shown in Table 1. It indicated that most interferences have no interference on the complex reaction of Cr(III)–KHP. These results agree well with the other works [14,23,25]. In addition, Cr(VI) showed great stability even at high levels of interferences. However, NH<sub>4</sub><sup>+</sup> and ascorbic acid shown the remarkable effects on the stability of Cr(VI) when their concentrations were over 20 and 50 mg/L in the mixture solution, respectively.

### 3.6. Method validation

The characteristics of the proposed method using the optimum chromatographic conditions is shown in Table 2. The reproducibilities calculated from peak area and retention time were satisfactory. The relative standard derivation is less than 2.2% ( $n=5$ ). Very good linearity ranges from 0.1 to 50.0 mg/L with an excellent correlation ( $r>0.99$ ) for both analytes were obtained. These results implied that those HPLC conditions were reliable for the determination of Cr(III) and Cr(VI). The limit of detection obtained were sensitive in level of sub mg/L allowing the applicability of the waste water analysis.

### 3.7. Determination of Cr(III) and Cr(VI) in waste water

Waste water collected from the developed treatment system was used as the real sample for this demonstration. The Cr(III) and Cr(VI) were found in the range of no detection (N.D.) to 0.30 mg/L Cr(III) and N.D. to 0.11 mg/L Cr(VI). The percentage recoveries and reproducibilities of Cr(III) and Cr(VI) which were proposed by this work are shown in Table 3, revealing acceptable accuracy and precision.

Table 2  
Characteristics of the method for the simultaneous determination of Cr(III) and Cr(VI)

Metal	Regression <sup>a</sup>	$r$	Range (mg/L)	Detection limit (mg/L, 3 $\sigma$ )	R.S.D. (% , $n=5$ )	
					Retention time	Peak area
Cr(III)–KHP	$Y=420.9X+324.3$	0.9997	0.1–50.0	0.01	0.93	2.20
Cr(VI)	$Y=121.0X+76.3$	0.9996	0.1–50.0	0.05	0.75	1.37

$r$ : correlation coefficient.

<sup>a</sup> Y, peak area (mAU s); X, metal concentration (mg/L).

Table 3  
Recoveries of Cr(III) and Cr(VI) from the waste water using the proposed method

Concentration of Cr in sample (mg/L)		Added (mg/L)		Found (mg/L)		Recovery $\pm$ S.D. <sup>a</sup> (%)	
Cr(III)	Cr(VI)	Cr(III)	Cr(VI)	Cr(III)	Cr(VI)	Cr(III)	Cr(VI)
0.30	0.11	1.00	1.00	1.36	1.07	104.3 $\pm$ 3.3	96.0 $\pm$ 2.0
0.30	0.11	3.00	3.00	3.48	2.84	105.6 $\pm$ 2.9	91.4 $\pm$ 1.3
0.30	0.11	5.00	5.00	5.78	5.07	109.1 $\pm$ 1.6	99.2 $\pm$ 1.6

On the basis of the Environmental Protection Agency (EPA) regulation, the maximum concentration level (MCL) of total chromium in ground water and drinking water is 0.1 mg/L.

<sup>a</sup> Standard deviation ( $n=3$ ).

#### 4. Conclusions

Simultaneous determination of Cr(III) and Cr(VI) with prechelation of Cr(III) using KHP by ion interaction chromatography was present. This work has been reported that KHP is a selective complexing agent for Cr(III). The highest formation ability of Cr(III)–KHP was found under the chosen conditions as follow: 1:10 mole ratio of Cr(III)–KHP; the pH of sample solution at 5.0;  $25 \pm 1$  °C room temperature and 5 min contact time. The optimum chromatographic conditions were found when the separating column used was a Nucleosil-100, C-18 (3  $\mu$ m, 60 mm  $\times$  4.6 mm), the mobile phase consisted of 5 mM octylammonium orthophosphate at pH 5.0 with 20% v/v MeOH, flow rate of 1.0 mL/min and detection at 200 nm. Under these conditions, the results obtained showed good characteristics for the simultaneous determination of Cr(III) and Cr(VI) in waste waters. Moreover, ion interaction chromatographic technique was flexible because many of parameters could be readily varied to obtain the good separation result. Importantly, this technique permits the use of the conventional HPLC instrumentation with C-18 column and UV detector.

#### Acknowledgements

The authors gratefully acknowledge financial support National Natural Science Foundation of China (Nos. 20437020, 20575008). Rattapol Meelapsom wishes to thank the financial supports from Faculty of Science, Mahasarakham University. Jirasak Threeprom wishes to thank the postdoctoral research scholar at Department of Chemistry, Tsinghua University.

#### References

[1] S.A. Katz, H. Salem (Eds.), *The Biological and Environmental Chemistry of Chromium*, VCH, New York, 1994.

- [2] T.M. Florence, G.E. Batley, *CRC Crit. Rev. Anal. Chem.* 92 (1980) 19.
- [3] N. Campillo, P. Vinas, I. Lopez-Garcia, M. Hernandez-Cordoba, *Talanta* 48 (1999) 905.
- [4] T.W. Lin, D.S. Wang, *Anal. Chem.* 73 (2001) 4319.
- [5] R. Rubio, A. Sahuquillo, G. Rauret, L. Garcia Beltran, P. Quevauviller, *Anal. Chim. Acta* 283 (1993) 207.
- [6] R.K. Mugo, K.J. Orians, *Anal. Chim. Acta* 271 (1993) 1.
- [7] B. Gammelgaard, O. Jons, B. Nielsen, *Analyst* 117 (1992) 637.
- [8] D.T. Gjerde, D.R. Wiederin, F.G. Smith, B.M. Mattson, *J. Chromatogr.* 640 (1993) 73.
- [9] M. Pansar-Kallio, P.K.G. Manninen, *J. Chromatogr. A* 750 (1996) 89.
- [10] M.J. Tomlinson, J.A. Caruso, *Anal. Chim. Acta* 322 (1996) 1.
- [11] M.J. Powell, D.W. Boomer, D.R. Wiederin, *Anal. Chem.* 67 (1995) 2474.
- [12] P.A. Sule, P.D. Ingle, *Anal. Chim. Acta* 326 (1996) 85.
- [13] K.E. La Freniere, V.A. Fassel, D.E. Eckels, *Anal. Chem.* 59 (1987) 879.
- [14] J. Posta, A. Gaspar, R. Toth, L. Ombodi, *Fresen. J. Anal. Chem.* 355 (1996) 719.
- [15] N. Jakubowski, B. Jebkens, D. Stuewer, H. Berndt, *J. Anal. Atom. Spectrom.* 9 (1994) 193.
- [16] X. Yao, J. Liu, J. Cheng, Y. Zeng, *Fresen. J. Anal. Chem.* 342 (1992) 702.
- [17] C.M. Andrie, J.A.C. Brockaert, *Fresen. J. Anal. Chem.* 346 (1993) 653.
- [18] A.M. Bond, G.G. Wallace, *Anal. Chim. Acta* 164 (1984) 233.
- [19] M. Trojanowicz, G. Pobozy, P.J. Worsfold, *Anal. Lett.* 25 (1992) 1373.
- [20] M. Pansar-Kallio, P.K.G. Manninen, *Anal. Chim. Acta* 318 (1996) 335.
- [21] A.M. Bond, G.G. Wallace, *Anal. Chem.* 54 (1982) 1706.
- [22] F.Y. Saleh, J.H. Huang, R.V. Lewis, *J. Chromatogr. Sci.* 27 (1989) 480.
- [23] J. Posta, A. Gaspar, R. Toth, L. Ombodi, *Microchem. J.* 54 (1996) 195.
- [24] J. Threeprom, S. Purachaka, L. Potipan, *J. Chromatogr. A* 1073 (2005) 291.
- [25] A. Gaspar, J. Posta, R. Toth, *J. Anal. Atom. Spectrom.* 11 (1996) 1067.
- [26] G.L. Ouyang, J.F. Jen, *Anal. Chim. Acta* 354 (1997) 107.
- [27] M.C. Gennaro, D. Giacosa, C. Abrigo, J. Liq. Chromatogr. 17 (1995) 4365.
- [28] D. Rai, B.M. Sass, D.A. Moor, *Inorg. Chem.* 26 (1987) 345.
- [29] J.W. Ball, D.K. Bordstrom, *J. Chem. Eng. Data* 43 (1998) 895.
- [30] F.C. Richard, A.C.M. Bourg, *Water Res.* 25 (1991) 807.
- [31] M. Sperling, S. Xu, B. Welz, *Anal. Chem.* 64 (1992) 3101.

## Chemiluminometric determination of vanillin in commercial vanillin products

Meropi Timotheou-Potamia\*, Antony C. Calokerinos

*University of Athens, Department of Chemistry, Laboratory of Analytical Chemistry,  
Panepistimiopolis, 157 71 Athens, Greece*

Received 1 November 2005; received in revised form 21 March 2006; accepted 23 March 2006  
Available online 19 June 2006

### Abstract

Vanillin, ethylvanillin and 4-hydroxy-3-methoxy-benzylalcohol have been found to chemiluminesce by the action of potassium permanganate in sulphuric or polyphosphoric acid media. Both acid media have been compared and sulphuric acid allows the sensitive determination of 0.15–10.0, 0.010–1.0 and 0.0030–0.30  $\mu\text{g mL}^{-1}$  of vanillin, ethylvanillin and 4-hydroxy-3-methoxy-benzylalcohol with limits of detection equal to 0.045, 0.0030 and 0.00090  $\mu\text{g mL}^{-1}$ , respectively. Recoveries of vanillin from commercial vanillin products are within the range of 95–109%. Comparison with results from the official method shows differences within the range of 0.5–3.0%. The chemiluminogenic reaction mechanism is also discussed. © 2006 Elsevier B.V. All rights reserved.

**Keywords:** Vanillin; Ethylvanillin; 4-Hydroxy-3-methoxy-benzylalcohol; Chemiluminescence; Potassium permanganate

### 1. Introduction

Vanillin (3-methoxy-4-hydroxy-benzaldehyde) and ethyl vanillin (3-ethoxy-4-hydroxy-benzaldehyde) (Fig. 1) are important food additives as flavor enhancers [1] and, hence, a plethora of analytical methods have been proposed for quantification of these analytes. Vanillin and ethylvanillin have been determined within the range of 1.0–20.0 mg/L and limits of detection equal to 0.49 and 0.38 mg/L, respectively by UV absorption spectrophotometry [2]. Vanillin (100–1400  $\mu\text{g/mL}$ ) has been measured amperometrically with limit of detection 44  $\mu\text{g/mL}$  [3], by reversed phase liquid chromatography in feeding stuffs [4], by gas chromatography in wine [5], by mixed micellar electrokinetic capillary chromatography in natural vanilla extracts and synthetic flavourings [6].

Limited information is available on the chemiluminogenic properties of vanillin. 5-Amino-4-sulfanylpthalhydrazide has been used for derivatization of aromatic aldehydes such as vanillin in the presence of sodium sulphite and disodium hydrogen phosphite in acidic medium at 100 °C to the corresponding

highly chemiluminescent 2-arylbenzothiazole derivatives. The resulting derivatives generated intense chemiluminescence by reaction with hydrogen peroxide and potassium hexacyanoferrate (III) in alkaline solution [7]. Vanillin enhances the CL from the luminol– $\text{H}_2\text{O}_2$ –horseradish peroxidase reaction [8]. Generation of CL in acid solution by the action of potassium permanganate on vanillin has been predicted and experimentally verified but not used analytically [9]. Vanillin was one of the phenolic compounds participating in the total phenolic content of wine monitored by acidic potassium permanganate CL [10]. No chemiluminogenic properties for ethylvanillin and 4-hydroxy-3-methoxy-benzylalcohol have been reported in the literature.

During the development of a CL procedure for the determination of reserpine, rescinnamine and yohimbine by the action of potassium permanganate in polyphosphoric acid [11], vanillin was found to interfere severely and also generated CL when injected alone into the reaction mixture. Since no application of direct CL for the determination of vanillin in commercial vanillin products has been reported, the chemiluminogenic reaction with permanganate in sulphuric and polyphosphoric acid was investigated in depth. The compounds investigated are vanillin, ethylvanillin and 4-hydroxy-3-methoxy-benzylalcohol (Fig. 1), which is the reduction product of vanillin.

\* Corresponding author. Tel.: +30 210 7274748.

E-mail address: [metimo@chem.uoa.gr](mailto:metimo@chem.uoa.gr) (M. Timotheou-Potamia).

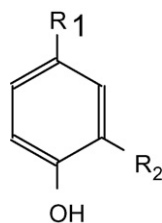


Fig. 1. Structure of vanillin ( $R_1 = -\text{CHO}$ ,  $R_2 = -\text{OCH}_3$ ), ethylvanillin ( $R_1 = -\text{CHO}$ ,  $R_2 = -\text{OCH}_2\text{CH}_3$ ), 4-hydroxy-3-methoxy-benzylalcohol ( $R_1 = -\text{CH}_2\text{OH}$ ,  $R_2 = -\text{OCH}_3$ ) and vanillic acid ( $R_1 = -\text{COOH}$ ,  $R_2 = -\text{OCH}_3$ ).

## 2. Experimental

### 2.1. Apparatus

The batch chemiluminometer used consisted of a reaction cell and a detector housing [12] (Fig. 2). The cylindrical glass cell (20 mm diameter, 70 mm height, 22 mL volume) was placed in front of the photomultiplier tube (PMT) at a distance of 45 mm from the photocathode. The solutions introduced into the cell were stirred continuously by means of a Teflon-coated magnetic bar. The PMT (EMI 9783B, S-5 response) and the cell were housed in a laboratory-made light-tight unit. With the use of a shutter, which shields the photocathode from ambient light, it was possible to wash the reaction cell, while the PMT was still under high voltage. The photocathode was operated at  $-750\text{ V}$  (cathode luminous sensitivity  $S = 95\ \mu\text{A lm}^{-1}$ ) supplied by a high voltage unit (Power Designs, Model 2K20). The output of the PMT was fed to a current-to-voltage (I/V) converter based on an RCA CA3140 operational amplifier. Damping was provided by inserting a RC circuit between the converter and the multi-speed variable-span recorder (Knauer).

### 2.2. Chemicals and solutions

All solutions were prepared from analytical reagent-grade or from the best commercially available grade material and deionised water.

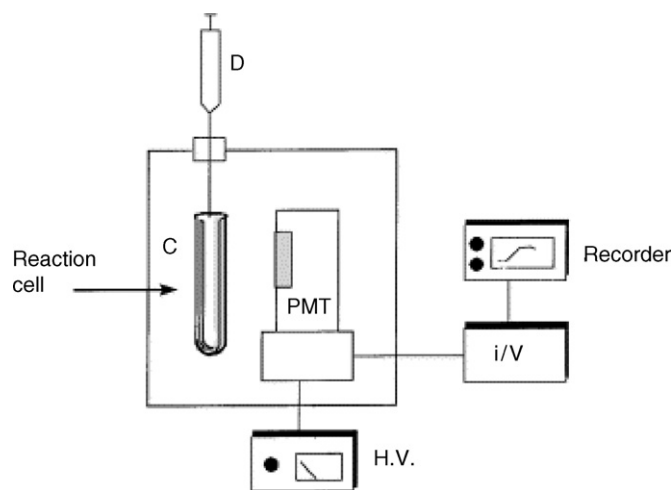


Fig. 2. Schematic diagram of batch chemiluminometer (D, injection syringe; C, reaction cell; PMT, photomultiplier; I/V: current-to-voltage converter; H.V., high voltage).

Stock solution (2000  $\mu\text{g/mL}$ ) of vanillin was prepared by dissolving 1.000 g of vanillin (Sigma) in water and diluting with water to 500 mL.

Stock solutions (200  $\mu\text{g/mL}$ ) of ethylvanillin or 4-hydroxy-3-methoxy-benzylalcohol were prepared by dissolving 0.100 g ethylvanillin or 4-hydroxy-3-methoxy-benzylalcohol (Sigma) in water and diluting with water to 500 mL.

Preliminary experiments were carried out by using 0.0100 M of vanillin or 0.00100 M of ethylvanillin or 4-hydroxy-3-methoxy-benzylalcohol, which were prepared by dissolving 1.521 or 0.166 or 0.154 g of vanillin or ethylvanillin or 4-hydroxy-3-methoxy-benzylalcohol (Sigma), respectively, in water and diluting with water to 1 L.

Potassium permanganate stock solution (0.0100 M) was prepared by dissolving 0.395 g of  $\text{KMnO}_4$  (Merck) in water and diluting with water to 250 mL. The solution was kept in amber-coloured bottles in the dark.

Polyphosphoric acid stock solution (6.0%, w/v) was prepared by dissolving 6.0 g of polyphosphoric acid (PPA) (Merck) in water and diluting with water to 100 mL.

More dilute solutions were prepared daily by the minimum number of dilution steps possible.

### 2.3. Procedure

A 5.00 mL aliquot of the oxidant solution followed by a 5.00 mL aliquot of acid or base solution were transferred into the reaction cell. Stirring of the solution at the highest possible rate without any effervescence was initiated. The shutter was then opened and after establishment of the base line, 100  $\mu\text{L}$  of analyte solution was injected into the reaction cell and the CL emission intensity ( $I$ ) was recorded.

A calibration graph of emission intensity ( $I$ , mV) as a function of concentration of analyte ( $\mu\text{g/mL}$ ) is constructed.

### 2.4. Determination of vanillin in commercial products

One gram of commercial vanilla was weighted accurately and diluted with water to 1 L. The solution was then diluted appropriately so that the final vanillin concentration is within the working range of the method.

## 3. Results and discussion

### 3.1. Preliminary experiments

The effect of potassium permanganate in acid and alkaline medium, cerium (IV) in acid medium and hydrogen peroxide in alkaline medium was investigated in order to establish the oxidant, which generates CL upon reaction with 0.0100 M of vanillin or 0.00100 M of ethylvanillin or 4-hydroxy-3-methoxy-benzylalcohol. No emission was recorded when 100  $\mu\text{L}$  of each analyte solution was injected into 0.0050 or 0.025 M of  $\text{Ce(IV)}$  acidified with 3.0 M  $\text{H}_2\text{SO}_4$  or 1.0 M  $\text{HClO}_4$  or 30% (v/v)  $\text{H}_2\text{O}_2$  or 0.00100 M  $\text{KMnO}_4$  in 4.0 M  $\text{NaOH}$ . Intense CL was noticed when 0.00100 M  $\text{KMnO}_4$  was used in 3.0 M  $\text{H}_2\text{SO}_4$  or 6.0% (w/v) PPA.

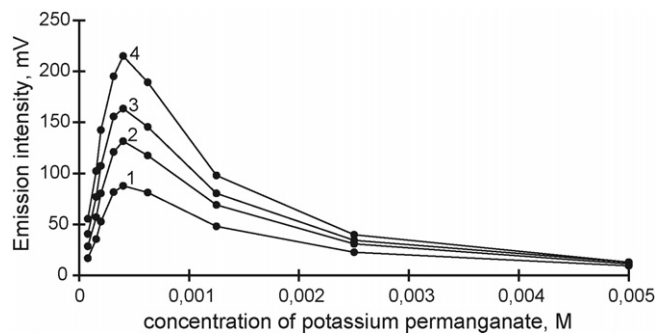


Fig. 3. Effect of concentration of potassium permanganate on the emission intensity from  $20.0 \mu\text{g mL}^{-1}$  vanillin in (1) 2.0, (2) 3.0, (3) 4.0 and (4) 5.0 M  $\text{H}_2\text{SO}_4$ .

It was decided to investigate extensively all parameters, which affect the CL from vanillin, ethylvanillin and 4-hydroxy-3-methoxy-benzylalcohol by the action of  $\text{KMnO}_4$  in sulphuric or PPA medium.

### 3.2. Effect of concentration of potassium permanganate and acid

The effect of concentration of potassium permanganate in sulphuric acid and PPA was investigated in order to establish the most sensitive analytical parameters for the measurement of vanillin, ethylvanillin and 4-hydroxy-3-methoxy-benzylalcohol. The effect of concentration of potassium permanganate in sulphuric acid and PPA medium on  $20 \mu\text{g mL}^{-1}$  of vanillin is shown in Figs. 3 and 4, respectively. Fig. 3 shows that the optimum concentration of potassium permanganate is  $4.0 \times 10^{-4}$  M but emission intensity increases with concentration of sulphuric acid. About 5.0 M  $\text{H}_2\text{SO}_4$  (2.5 M in the measuring cell) was chosen as the most concentrated which can be used. The optimum concentration of the oxidant in PPA was the same as with sulphuric acid and the emission intensity increases with concentration of polyphosphoric acid (Fig. 4). About 6.0% (w/v) of PPA was chosen for all further studies since the solubility of PPA hinders preparation of more concentrated solutions.

Table 2  
Analytical figures of merit for vanillin, ethylvanillin and 4-hydroxy-3-methoxy-benzylalcohol

	$\text{KMnO}_4$ (M) and 5.0 M $\text{H}_2\text{SO}_4$			$\text{KMnO}_4$ (M) and 6.0% (w/v) PPA		
	Vanillin ( $4.0 \times 10^{-4}$ )	Ethylvanillin ( $2.0 \times 10^{-4}$ )	4-Hydroxy-3-methoxy- benzylalcohol ( $6.0 \times 10^{-5}$ )	Vanillin ( $4.0 \times 10^{-4}$ )	Ethylvanillin ( $4.0 \times 10^{-5}$ )	4-Hydroxy-3-methoxy- benzylalcohol ( $1.0 \times 10^{-4}$ )
Linear range ( $\mu\text{g mL}^{-1}$ )	0.15–10.0	0.010–1.0	0.0030–0.30	1.00–10.0	0.10–1.0	0.20–1.00
Regression line <i>I</i> (mV) vs. <i>C</i> ( $\mu\text{g mL}^{-1}$ )	$I = 17.7C - 0.96$	$I = 16.0C + 0.22$	$I = 78.8C + 0.23$	$I = 1.76C - 0.12$	$I = 30.0C - 0.34$	$I = 33.4C - 1.33$
Limit of detection ( $\mu\text{g mL}^{-1}$ )	0.045	0.0030	0.00090	0.24	0.020	0.050
Limit of quantification ( $\mu\text{g mL}^{-1}$ )	0.15	0.010	0.0030	0.80	0.066	0.16
<i>r</i> (number of measurements)	0.9994 (8)	0.998 (9)	0.996 (8)	0.9993 (10)	0.9995 (9)	0.995 (10)
%R.S.D. ( $\mu\text{g mL}^{-1}$ , <i>n</i> = 8)	2.6 (0.82)	1.9 (0.35)	2.0 (0.19)	2.6 (3.50)	2.7 (0.20)	2.0 (0.35)

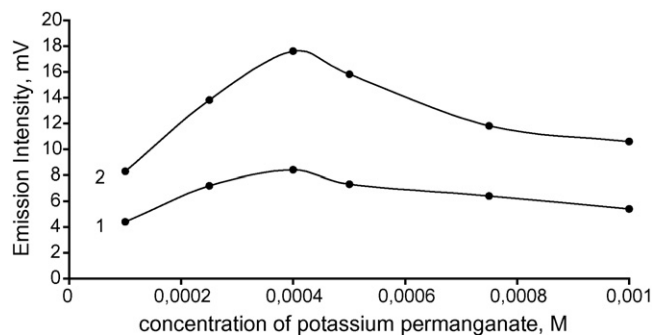


Fig. 4. Effect of concentration of potassium permanganate on the emission intensity from  $20.0 \mu\text{g mL}^{-1}$  vanillin in (1) 3.0 and (2) 6.0% (w/v) PPA.

Table 1  
Optimum concentrations of potassium permanganate and sulphuric or polyphosphoric acid for vanillin, ethylvanillin and 4-hydroxy-3-methoxy-benzylalcohol

Analyte	$\text{KMnO}_4$ (M)	
	5.0 M $\text{H}_2\text{SO}_4$	6.0% (w/v) PPA
Vanillin	$4.0 \times 10^{-4}$	$4.0 \times 10^{-4}$
Ethylvanillin	$2.0 \times 10^{-4}$	$4.0 \times 10^{-5}$
4-Hydroxy-3-methoxy-benzylalcohol	$6.0 \times 10^{-5}$	$1.0 \times 10^{-4}$

Optimum concentrations of oxidant and acid are summarized in Table 1.

### 3.3. Analytical figures of merit

The linearity of vanillin, ethylvanillin and 4-hydroxy-3-methoxy-benzylalcohol was investigated at the optimum concentration of potassium permanganate with 5.0 M sulphuric acid or 6.0% (w/v) PPA and the results are summarized in Table 2. From the results in Table 2, it is obvious that the permanganate chemiluminogenic reaction is more sensitive for vanillin, ethylvanillin and 4-hydroxy-3-methoxy-benzylalcohol in sulphuric acid medium than in PPA. The observation is verified by the results shown in Table 3.



Table 3  
Relative emission intensity from  $1.0$  and  $3.0 \times 10^{-6}$  M vanillin, ethylvanillin and 4-hydroxy-3-methoxy-benzylalcohol

Analyte	Relative emission intensity			
	5.0 M H <sub>2</sub> SO <sub>4</sub>		6.0% (w/v) PPA	
	$1.0 \times 10^{-6}$ M	$3.0 \times 10^{-6}$ M	$1.0 \times 10^{-6}$ M	$3.0 \times 10^{-6}$ M
Vanillin	4.7	19.4	0.5	1.9
Ethylvanillin	7.9	22.4	12.7	40.0
4-Hydroxy-3-methoxy-benzylalcohol	33.8	100	10.4	38.5

Table 4  
Recovery and determination of vanillin from solutions of commercial vanillin products

Product <sup>a</sup>	Vanillin ( $\mu\text{g mL}^{-1}$ )				% Difference ( $n=3$ )	% Recovery ( $n=3$ )
	Initially found	Expected <sup>b</sup>	Added	Recovered		
A	0.148	0.150			1.3	
	0.356	0.360	0.040	0.039	1.1	97.5
			0.040	0.038		95.0
		0.080	0.077		96.2	
B	0.195	0.200			2.5	
	0.485	0.500	0.040	0.042	3.0	105
			0.040	0.043		108
		0.080	0.086		108	
C	0.199	0.200			0.5	
			0.040	0.038		95.0
			0.080	0.087		109
			0.120	0.119		99.2
	0.492	0.500			1.6	
		0.040	0.039		97.5	
		0.080	0.078		97.5	

<sup>a</sup> Commercial vanillin products.

<sup>b</sup> Official method [15].

Recoveries of vanillin added to the solutions of commercial products are within the range of 95–109% (Table 4), which are considered satisfactory. Results by the proposed method and expected values are in good agreement (Table 4).

### 3.4. Mechanism of CL reaction

One of the most common reaction schemes for chemiluminescence is the formation of a fluorogenic product [12].

Typical example is the formation of the 3-aminophthalate ion by luminol chemiluminescence [13]. The reaction of vanillin with potassium permanganate leads to vanillic acid (Fig. 5), which is a known fluorogenic compound and this property has been extensively used for monitoring the analyte [14]. Hence, the reaction in Fig. 5 is the chemiluminogenic reaction of vanillin. Vanillic acid is also formed from 4-hydroxy-3-methoxy-benzylalcohol while ethylvanillin is oxidized to ethylvanillic acid.

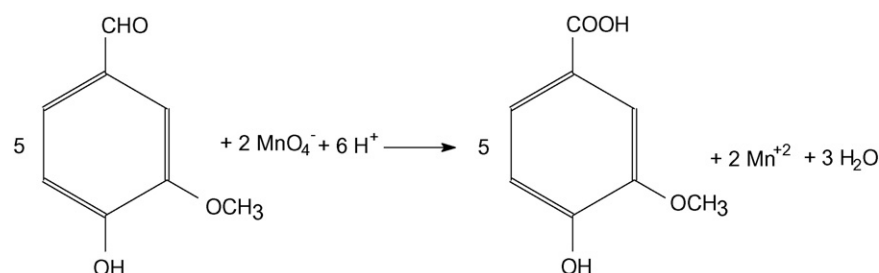


Fig. 5. Reaction scheme of vanillin with potassium permanganate to vanillic acid.

#### 4. Conclusions

The CL reaction of vanillin to vanillic acid by the action of potassium permanganate can be used successfully for the determination of vanillin in commercial products.

#### Acknowledgements

The authors wish to acknowledge Th. Theofylaktou and M. Kouloumbi for assistance with the optimisation procedure.

#### References

- [1] N.J. Walton, M.J. Mayer, A. Narbad, *Phytochemistry* 63 (2003) 505.
- [2] Y.N. Ni, G.W. Zhang, S. Kokot, *Food Chem.* 89 (2005) 465.
- [3] M. Luque, E. Luque-Perez, A. Rios, M. Valcarcel, *Anal. Chim. Acta* 410 (2000) 127.
- [4] J. de-Jong, B. Stoisser, K. Wagner, M. Tomassen, J. Driessen, P. Hofmann, H.A. Putzka, *JAOAC* 87 (2004) 1033.
- [5] D. Matejcek, B. Klejdus, O. Mikes, D. Sterbova, V. Kuban, *Anal. Bioanal. Chem.* 377 (2003) 340.
- [6] M.C. Boyce, P.R. Haddad, T. Sostaric, *Anal. Chim. Acta* 485 (2003) 179.
- [7] H. Yoshida, R. Nakao, H. Nohta, M. Yamaguchi, *J. Chromatogr. A* 898 (2000) 1.
- [8] F.G. Sánchez, A.N. Díaz, J.A.G. García, *J. Photochem. Photobiol.* 105 (1997) 11.
- [9] B.G.-T. Corominas, G.M.A. Fos, J.V.G. Mateo, L.L. Zamora, J.M. Calatayud, *Talanta* 60 (2003) 623.
- [10] J.W. Costin, N.W. Barnett, S.W. Lewis, D.J. McGillivray, *Anal. Chim. Acta* 499 (2003) 47.
- [11] N. Pinotsis, A.C. Calokerinos, W.R.G. Baeyens, *Analyst* 125 (2000) 1307.
- [12] L.P. Palilis, A.C. Calokerinos, *Anal. Chim. Acta* 413 (2000) 175.
- [13] E.H. White, M.M. Bursey, *JACS* 86 (1964) 941.
- [14] M.A. Rodriguez-Delgado, S. Malovana, J.P. Perez, T. Borges, F.J.G. Montelongo, *J. Chromatogr. A* 912 (2001) 249.
- [15] Commission Regulation EC 1459/98, *Official Journal of the European Communities*, 9-7-1998.

# Separation and speciation of selenium in food and water samples by the combination of magnesium hydroxide coprecipitation-graphite furnace atomic absorption spectrometric determination

M. Tuzen<sup>a</sup>, K.O. Saygi<sup>a</sup>, M. Soylak<sup>b,\*</sup>

<sup>a</sup> *Gaziosmanpasa University, Faculty of Science and Arts, Chemistry Department, 60250 Tokat, Turkey*

<sup>b</sup> *Erciyes University, Faculty of Science and Arts, Chemistry Department, 38039 Kayseri, Turkey*

Received 30 January 2006; received in revised form 3 April 2006; accepted 13 April 2006

Available online 22 May 2006

## Abstract

A simple and economic separation and speciation procedure for selenium in food and water samples have been presented prior to its graphite furnace atomic absorption spectrometry (GFAAS). Magnesium hydroxide coprecipitation system for selenium(IV) was applied to the separation and speciation of selenium ions. The influences of the various analytical parameters for the quantitative recoveries of selenium ions like pH, amounts of magnesium ions as carrier elements, etc. on were examined. The effects of the alkaline and earth alkaline metals, some transition metals and some anions on the recoveries of selenium(IV) were also investigated. The recoveries of analytes were found greater than 95%. No appreciable matrix effects were observed. The detection limit, defined as three times the blank standard deviation ( $3\sigma$ ), was  $0.030 \mu\text{g l}^{-1}$ . The preconcentration factor for the presented system was 25. The proposed method was applied to the speciation of selenium(IV), selenium(VI) and determination of total selenium in natural waters and microwave digested various food samples with satisfactory results. The procedure was validated with certified reference materials. The relative errors and relative standard deviations were below 6% and 10%, respectively.

© 2006 Elsevier B.V. All rights reserved.

**Keywords:** Selenium; Food; Preconcentration; Speciation; Graphite furnace atomic absorption spectrometry

## 1. Introduction

Due to essential and non-essential heavy metals play roles for living creature, researches on the heavy metal contents of foods are one of the main objects of the toxicology studies [1–4]. Selenium is an essential element for our body. Selenium is also an essential dietary constituent in mammals [5,6]. Se gives protection from several heart diseases, prevents heavy metal toxic effects and has anti-carcinogenic activity [7]. Selenium is promising as an anti-proliferative, anti-inflammatory, anti-viral and immune altering agent [8]. The inorganic selenium species most frequently found in waters and soils are selenite (Se(IV)) and selenate (Se(VI)). In this regard, a method for speciation is needed because selenium availability for plank-

ton uptake, mobility in soil and toxicity in biota depends on the oxidation state of this element [9]. Beside the total content of selenium, the chemical form in which selenium is present is also most important due to the differences in bioavailability and toxicity of the different forms [10–12]. The levels of the selenium in the food and water samples are generally lower than detection limits of instrumental techniques including spectrophotometry, atomic absorption spectrometry, etc. The influences of the matrix components of the real samples are another problem in the determinations of selenium [13–15]. Furthermore, it is not possible that to determine the level of the selenium species like Se(IV) and Se(VI). In order to solve these main problems in the determination selenium in environmental samples, the traditional preconcentration and separation methods for selenium like liquid–liquid extraction [16,17], solid phase extraction [18–20], and ion-exchange [21,22], etc. have been used. These preconcentration methods combined with instrumental analysis have frequently been used

\* Corresponding author. Fax: +90 352 4374933.

E-mail address: [soylak@erciyes.edu.tr](mailto:soylak@erciyes.edu.tr) (M. Soylak).

for the determination of selenium species in complex matrix samples.

Coprecipitation is also one of the important preconcentration-separation and speciation technique for the traces heavy metal ions [23–25]. The combination of a carrier element that is generally a metal ion and a precipitant that is organic or inorganic based have been used to coprecipitate traces metal ions in aqueous media [26–28]. Organic or inorganic coprecipitation procedures have been also preconcentration-speciation of selenium ions [29–32]. According to our literature survey, the application of hydroxide coprecipitation for selenium preconcentration and speciation is very limited. Rao et al. [29] has been presented a preconcentration work based on iron(III) hydroxide coprecipitation for selenium(IV). Selenium ions have been coprecipitated with using lanthanum hydroxide by Tang et al. [30].

In the presented work, a simple and fast coprecipitation study has been presented. The procedure based on the coprecipitation of selenium(IV) by the aid of magnesium hydroxide. After reduction of Se(VI) to Se(IV), total selenium in real samples were coprecipitated. The influences of the various analytical parameters including matrix effects have been investigated. Selenium determinations were performed by graphite furnace atomic absorption spectrometry.

## 2. Experimental

### 2.1. Instrument

A Perkin-Elmer analyst 700 atomic absorption spectrometer equipped with HGA graphite furnace and with deuterium background corrector was used. For graphite furnace measurements, argon was used as inert gas. The operating parameters for working element were set as recommended by the manufacturer given in Table 1. Perkin-Elmer pyrolytic-coated graphite tubes with a platform were used. Samples of 20  $\mu\text{l}$  + 10  $\mu\text{l}$  of mixture of 0.015 mg Pd + 0.010 mg  $\text{Mg}(\text{NO}_3)_2$  as matrix modifier during the study were injected into the furnace using Perkin-Elmer AS-800 autosampler. The signals were measured as peak areas. The range of the calibration standards for selenium was 0–50  $\mu\text{g l}^{-1}$ . The correlation coefficient of the calibration curves were generally 0.999.

Table 1  
Instrument settings and analytical conditions

Wavelength	196 nm
Slit width	2 nm
Argon flow	250 ml/min
Atomization site	Pyro/platform
Reading time	5 s
	Heating program temperature (°C (ramp time (s), hold time (s)))
Drying 1	100(5, 20)
Drying 2	140(15, 15)
Ashing	1100(10, 20)
Atomization	2100(0, 5)
Cleaning	2600(1, 3)

A pH meter, Sartorius pp-15 model glass-electrode was employed for measuring pH values in the aqueous phase. Nüve model NF 800 centrifuge was used to centrifuge of solutions. Milestone Ethos D closed vessel microwave system (maximum pressure 1450 psi, maximum temperature 300 °C) was used.

### 2.2. Reagents and solution

All chemicals were of analytical reagent grade and were used without further purification. Deionised water (Milli-Q Millipore 18.2  $\text{M}\Omega \text{ cm}^{-1}$  resistivity) was used for all dilutions. All the plastic and glassware were cleaned by soaking in dilute  $\text{HNO}_3$  (1 + 9) and were rinsed with distilled water prior to use. The standard solutions for Se(IV) and Se(VI) were from Sigma, St. Louis, USA. Stock solutions of diverse elements were prepared from high purity compounds. The calibration standards were not submitted to the preconcentration procedure.

NIST SRM 1573a tomato leaves, NIST SRM 1577b bovine liver, GBW 07605 tea and LGC 6010 hard drinking water, standard reference materials were used in the experiment.

### 2.3. Analytical procedure for Se(IV)

The coprecipitation method was tested firstly. One milliliter of 1% (w/v)  $\text{Mg}(\text{NO}_3)_2$  was added to 20 ml of solution containing 0.5  $\mu\text{g}$  of Se(IV). Then the pH of the solution was adjusted related pH by the addition of 1  $\text{mol l}^{-1}$  NaOH. After 10 min for the formation of magnesium hydroxide precipitate, the solution was centrifuged at 2750 rpm for 10 min. The supernatant was removed. The precipitate remained adhering to the tube was dissolved with 1 ml of 1  $\text{mol l}^{-1}$   $\text{HNO}_3$ . The last volume was completed to 2.0–10.0 ml with distilled water. The number of replicates for the test workings was three. The levels of selenium were determined by graphite furnace atomic absorption spectrometry.

### 2.4. Reduction of Se(VI) to Se(IV) and determination of total selenium

To reduction of Se(VI) to Se(IV), the reduction procedure given by Ferri et al. [33] was applied to model solutions and natural water samples. Appropriate amount of concentrated hydrochloric acid was added to the solutions to give 4  $\text{mol l}^{-1}$  as final acid concentration. Then the microwave program of 3 min for 250 W, 5 min for 450 W, 5 min for 650 W, vent: 8 min was performed. After reduction of Se(VI) to Se(IV), the method given in Section 2.3 was applied to the determination of the total selenium. The levels of selenium were determined by graphite furnace atomic absorption spectrometry. The level of Se(VI) is calculated by difference of total selenium and Se(IV) concentrations.

### 2.5. Analysis of the real samples

Digestion conditions for microwave system for the samples were applied as 2 min for 250 W, 2 min for 0 W, 6 min for 250 W, 5 min for 400 W, 8 min for 550 W, vent: 8 min [34,35].

Standard reference materials (250 mg) and food samples (1.0 g) were digested with 6.0 ml of HNO<sub>3</sub> (65%), 2.0 ml of H<sub>2</sub>O<sub>2</sub> (30%) in closed microwave digestion system and diluted to 15.0 ml with deionized water. The pHs of the solution were adjusted to 10.0 by the addition of 1 mol l<sup>-1</sup> NaOH. Then the preconcentration procedure given above was applied to the final solutions, which has 50 ml of total volume. A blank digest was carried out in the same way.

In order to digestion of milk, red wine and beer samples, 1.0 ml of sample was digested with 3.0 ml of concentrated HNO<sub>3</sub> and 1.0 ml of H<sub>2</sub>O<sub>2</sub> in microwave system. After digestion the samples, the volume of the digested sample was made up to 15.0 ml with distilled water. The blanks were prepared in the same way as the sample, but omitting the sample. The preconcentration procedure given above was applied to the samples.

A tap water from Tokat City, a mineral water from Sivas City, a bottled mineral water and LGC 6010 hard drinking water standard reference material were analyzed for their selenium concentrations. For this purpose, the pH of 20 ml of the samples was adjusted to 10.0 by the addition of 1 mol l<sup>-1</sup> NaOH. Then the procedure given above was applied to the samples. The levels of selenium in the final solution were determined by graphite furnace atomic absorption spectrometry.

### 3. Results and discussion

The effects of some analytical parameters such as pH, amount of magnesium, etc. on the recovery of selenium ions were investigated. The optimum conditions determined for the preconcentration procedure were as follows.

#### 3.1. Interference of magnesium ions on the absorbance of selenium

Increasing concentrations of magnesium(II) was added to aqueous solution containing selenium(VI) ions. These solutions were analyzed by GFAAS on the conditions given in Table 1 and Section 2.1 without any pre-treatment. The absorbances for selenium remained almost constant up to about 20 g l<sup>-1</sup> magnesium(II). This indicates that the concentration of magnesium ions in the final solution for the combination of coprecipitation method with GFAAS must to be exceeded 20 g l<sup>-1</sup>.

#### 3.2. Effects of pH

The influences of the pH of the aqueous solutions on the coprecipitation efficiency of selenium(IV) and selenium(VI) ions were investigated in the pH range of 8.0–13.0. The pH was adjusted by the addition of 1 mol l<sup>-1</sup> NaOH to the samples. The results were depicted in Fig. 1. Selenium(IV) was quantitatively recovered in the pH range of 10.0–11.0. Selenium(VI) was recovered lower than 5% at pH range of 8.0–13.0. This results show that the speciation of selenium(IV) and selenium(VI) is possible at the pH range of 10.0–11.0. For all subsequent coprecipitation works for selenium, pH 10.0 was used.

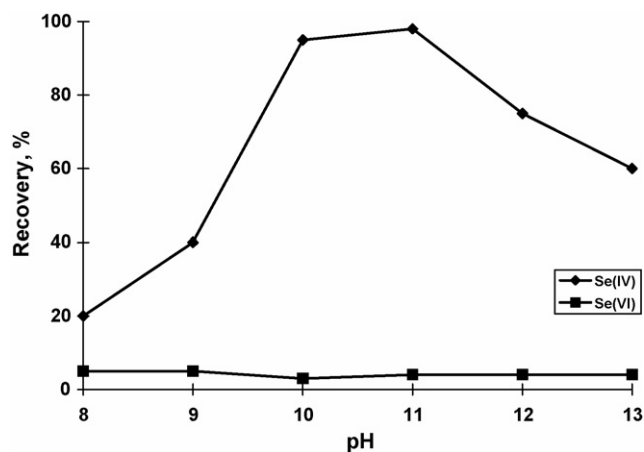


Fig. 1. Effects of pH on the coprecipitation efficiencies of Se(IV) and Se(VI) ( $N=4$ ).

#### 3.3. Influences of amounts of magnesium as carrier element

Magnesium(II) was selected as carrier element for the present work and the influences of magnesium(II) on the coprecipitation of selenium(IV) ions were investigated by using model solutions at pH 10.0. The influence of magnesium(II) was investigated in the range of 0–4.0 mg. The results were depicted in Fig. 2. The recoveries of selenium(IV) was 25% without any magnesium(II). Increasing recoveries for selenium(IV) were obtained increasing amounts of magnesium(II). After 1.0 mg of magnesium(II), the recoveries of selenium(IV) were kept constant and quantitative. For all further work, 1.0 mg of Mg<sup>2+</sup> was added to the model solutions.

#### 3.4. Effect of divers ions

In order to investigate the possibility of selective recovery of selenium(IV) in the presence of the metal ions and anions, the presented coprecipitation procedure has been performed with model solutions containing matrix ions. The amounts of selenium(IV) were 0.5 µg. The results are summarized in

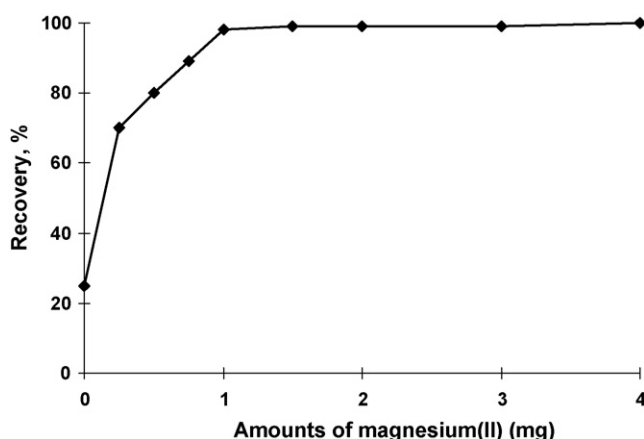


Fig. 2. Effects of magnesium amounts on the coprecipitation efficiency of Se(IV) ( $N=4$ ).



Table 2  
Effect of matrix components on coprecipitation efficiency of selenium(IV) ( $N=4$ )

Ions	Added as	Concentration of ions ( $\text{mg l}^{-1}$ )	Recovery of selenium(IV) <sup>a</sup> (%)
Na <sup>+</sup>	NaCl	20000	97 ± 3
K <sup>+</sup>	KCl	5000	96 ± 2
Ca <sup>2+</sup>	CaCl <sub>2</sub>	5000	97 ± 2
Cl <sup>-</sup>	NaCl	30000	96 ± 2
F <sup>-</sup>	NaF	1000	97 ± 3
SO <sub>4</sub> <sup>2-</sup>	Na <sub>2</sub> SO <sub>4</sub>	3000	96 ± 3
NO <sub>3</sub> <sup>-</sup>	KNO <sub>3</sub>	3000	98 ± 2
PO <sub>4</sub> <sup>3-</sup>	Na <sub>3</sub> PO <sub>4</sub>	1000	95 ± 3
Ag <sup>+</sup>	AgNO <sub>3</sub>	100	96 ± 2
Cu <sup>2+</sup>	CuSO <sub>4</sub>	100	98 ± 4
Ni <sup>2+</sup>	NiSO <sub>4</sub>	100	96 ± 3
Cd <sup>2+</sup>	Cd(NO <sub>3</sub> ) <sub>2</sub>	100	97 ± 2
Fe <sup>3+</sup>	FeCl <sub>3</sub>	100	99 ± 3
Mn <sup>2+</sup>	MnSO <sub>4</sub>	100	98 ± 3
Co <sup>2+</sup>	CoSO <sub>4</sub>	100	97 ± 2
Zn <sup>2+</sup>	ZnSO <sub>4</sub>	100	98 ± 3
Pb <sup>2+</sup>	Pb(NO <sub>3</sub> ) <sub>2</sub>	100	97 ± 2
Al <sup>3+</sup>	Al <sub>2</sub> (SO <sub>4</sub> ) <sub>3</sub>	100	95 ± 4

<sup>a</sup> Mean ± standard deviation.

**Table 2.** The tolerance limit is defined as the ion concentration causing a relative error smaller than ±5% related to the preconcentration and determination of analytes. The tolerable levels of the some heavy metal ions are suitable for the separation and preconcentration of selenium(IV) in the real samples examined present study, because of the levels of transition metals in these samples are lower than their interferic level. It can be seen that the major matrix ions in the food and natural waters show no obvious interference with the preconcentration of selenium(IV) ions.

The influences of the concentration of selenium(VI) as diverse ion on the recoveries of selenium(IV) were also investigated. The results were given in Table 3. The recoveries of Se(IV) were quantitative till 50  $\text{mg l}^{-1}$  of Se(VI). After 50  $\text{mg l}^{-1}$  of Se(VI), recovery values for Se(IV) were not quantitative.

### 3.5. Determination of total selenium

In order to determination of total selenium, test solutions that contain different amounts of selenium(IV) and selenium(VI)

Table 3  
Influences of Se(VI) ions on retentions of selenium(IV) ions ( $N=4$ ) (Se(VI) is added as Na<sub>2</sub>SeO<sub>4</sub>)

Concentration of Se <sup>6+</sup> ( $\text{mg l}^{-1}$ )	Recovery of selenium(IV) <sup>a</sup> (%)
10	96 ± 2
30	95 ± 3
50	96 ± 3
100	90 ± 2

<sup>a</sup> Mean ± standard deviation.

were prepared. Then reduction of selenium(VI) ions to selenium(IV) in the test solutions were performed by the procedure given by Ferri et al. [33]. Then the procedure given in Section 2.3 was applied to these solutions. The results are given in Table 4. Quantitative recovery values for selenium(IV) and total selenium were obtained these solutions. The results show that the proposed method could be applied for the determination of total selenium in aqueous solutions.

### 3.6. Figure of merits

The detection limit (LOD) of selenium(IV) for the present work was calculated under optimal experimental conditions. For this work, the preconcentration procedure given Section 2.3 was applied to the 50 ml of blank model solutions. The limit of detection for selenium(IV) based on three times the standard deviations of the blank ( $k=3$ ,  $N=21$ ) was 0.030  $\mu\text{g l}^{-1}$ . The precision of the determination of Se(IV) was evaluated under the optimum conditions mentioned Section 2.3. For this purpose, the procedure was repeated ten times for Se(IV) with model solutions containing 0.5  $\mu\text{g}$  of Se(IV). It was found that the recovery of Se(IV) was 99 ± 3 at 95% confidence level.

### 3.7. Application

The speciation procedure presented was applied to the speciation of Se(IV) and Se(VI) in natural water samples from a tap water from Tokat City, a mineral water form Sivas City and a bottled mineral water. Various amounts of selenium species were also spiked to these water samples. The results were given in Table 5. A good agreement was obtained between the added and measured analyte amounts. These results confirm the validity of the proposed method. The presented method could be applied

Table 4  
Total selenium determinations in spiked test solutions (volume: 50 ml,  $N=4$ )

Added ( $\mu\text{g l}^{-1}$ )		Found ( $\mu\text{g l}^{-1}$ )			Recovery (%) <sup>a</sup>		
Se(IV)	Se(VI)	Se(IV)	Se(VI)	Total Se	Se(IV)	Se(VI)	Total Se
0	10	–	9.8 ± 0.4	9.8 ± 0.4	–	98 ± 3	98 ± 3
3	7	2.9 ± 0.1	6.9 ± 0.3	9.8 ± 0.3	97 ± 2	99 ± 4	98 ± 3
7	3	6.8 ± 0.3	2.9 ± 0.4	9.7 ± 0.3	97 ± 3	97 ± 4	97 ± 3
5	5	4.8 ± 0.2	4.9 ± 0.3	9.7 ± 0.2	96 ± 2	98 ± 3	97 ± 2
10	0	9.9 ± 0.4	–	9.9 ± 0.4	99 ± 4	–	99 ± 4

<sup>a</sup> Mean ± standard deviation.

Table 5  
Speciation of Se(IV) and Se(VI) and total selenium in tap water and mineral waters<sup>a</sup> (N=4)

Samples	Added ( $\mu\text{g l}^{-1}$ )		Found ( $\mu\text{g l}^{-1}$ )			Recovery (%)			Relative error (%)		R.S.D. (%)	
	Se(IV)	Se(VI)	Se(IV)	Se(VI)	Total Se	Se(IV)	Se(VI)	Total Se	Se(IV)	Se(VI)	Se(IV)	Se(VI)
Tap water from Tokat City	–	–	0.11 ± 0.01	0.16 ± 0.01	0.27 ± 0.01	–	–	–	–	–	9.1	6.3
	0.3	1.0	0.40 ± 0.03	1.11 ± 0.10	1.51 ± 0.10	97 ± 2	95 ± 4	95 ± 3	–2.4	–4.3	7.5	6.3
	1.0	0.3	1.10 ± 0.07	0.45 ± 0.13	1.55 ± 0.11	99 ± 2	97 ± 4	98 ± 3	–0.9	–2.2	6.4	6.7
	1.0	1.0	1.09 ± 0.08	1.13 ± 0.16	2.22 ± 0.14	98 ± 3	97 ± 4	98 ± 3	–1.8	–2.6	7.3	5.3
Mineral water from Sivas City	–	–	0.07 ± 0.01	0.09 ± 0.01	0.16 ± 0.01	–	–	–	–	–	5.7	5.6
	0.2	1.0	0.27 ± 0.01	1.09 ± 0.09	1.35 ± 0.09	99 ± 1	100 ± 2	100 ± 2	–0.7	–0.4	4.1	4.9
	1.0	0.2	1.07 ± 0.10	0.29 ± 0.10	1.35 ± 0.01	100 ± 2	98 ± 2	99 ± 1	–0.5	–1.7	9.2	6.3
	1.0	1.0	1.06 ± 0.07	1.08 ± 0.15	2.14 ± 0.13	99 ± 2	99 ± 3	99 ± 2	–0.9	–0.8	6.6	8.0
Bottled mineral water	–	–	0.05 ± 0.01	0.09 ± 0.01	0.14 ± 0.01	–	–	–	–	–	4.0	4.7
	0.1	1.0	0.15 ± 0.01	1.08 ± 0.10	1.22 ± 0.10	96 ± 3	99 ± 4	99 ± 3	–2.7	–0.6	6.8	8.9
	1.0	0.1	1.05 ± 0.08	0.18 ± 0.08	1.23 ± 0.01	100 ± 1	96 ± 1	99 ± 1	–0.3	–2.2	7.5	7.9
	1.0	1.0	1.04 ± 0.09	1.07 ± 0.16	2.11 ± 0.13	99 ± 2	99 ± 4	99 ± 3	–0.6	–1.4	8.4	6.5

<sup>a</sup> Mean ± standard deviation.

Table 6  
The level of total selenium in the standard reference materials after application of the presented procedure (N=4)

Sample	Concentration	R.S.D. (%)	Certified value	Relative error (%)
NIST SRM 1573a tomato leaves	0.052 ± 0.003 $\mu\text{g g}^{-1}$	5.8	0.054 $\mu\text{g g}^{-1}$	–3.7
NIST SRM 1577b bovine liver	0.70 ± 0.05 $\mu\text{g g}^{-1}$	7.1	0.73 $\mu\text{g g}^{-1}$	–4.1
GBW 07605 tea	0.069 ± 0.006 $\mu\text{g g}^{-1}$	8.7	0.072 $\mu\text{g g}^{-1}$ <sup>a</sup>	–4.2
LGC 6010 hard drinking water	9.6 ± 0.6 $\mu\text{g l}^{-1}$	6.3	9.3 $\mu\text{g l}^{-1}$	+3.2

Uncertainty at 95% confidence limit.

<sup>a</sup> The value is not certified.

successfully for the separation, preconcentration and speciation of trace amounts of selenium in both spiked and water samples.

The coprecipitation procedure presented was applied to four different standard reference materials given in Table 6. The results are in good agreement with the certified values for selenium. The relative standard deviations for solid samples were in the range of 5.8–8.7%.

Because of the importance of the selenium consuming by the foods for a healthy life [2–5], the presented procedure was also applied to the various food samples. For this purpose, the samples given in Tables 7 and 8 were microwave digested then the procedure was applied.

Table 7  
The level of total selenium in cow milk, beer and red wine samples (N=4)

Sample	Added ( $\mu\text{g l}^{-1}$ )	Found ( $\mu\text{g l}^{-1}$ )	Recovery (%)
Cow milk	–	52 ± 5	–
	25	76 ± 6	99
	50	99 ± 8	97
Beer	–	29 ± 2	–
	10	37 ± 2	95
	50	76 ± 5	96
Red wine	–	35 ± 2	–
	10	42 ± 3	93
	50	82 ± 5	96

Table 8  
The level of total selenium in some real samples after application of the presented procedure (N=4)

Sample	Added ( $\mu\text{g kg}^{-1}$ )	Found ( $\mu\text{g kg}^{-1}$ )	Recovery (%)
Bread	–	144 ± 9	–
	50	189 ± 10	97
	100	237 ± 11	97
Tomato	–	14 ± 1	–
	10	24 ± 1	100
	20	33 ± 2	97
Onion	–	14 ± 1	–
	10	23 ± 1	96
	20	32 ± 2	94
Garlic	–	56 ± 3	–
	25	77 ± 4	95
	50	103 ± 8	97
Potato	–	17 ± 1	–
	10	26 ± 1	96
	20	35 ± 2	95
Black tea	–	68 ± 5	–
	25	90 ± 6	97
	50	116 ± 9	98
Cow's meat	–	165 ± 10	–
	100	260 ± 13	98
	200	351 ± 18	96
Honey	–	122 ± 7	–
	50	166 ± 10	97
	100	216 ± 9	97
Yogurt	–	30 ± 1	–
	10	39 ± 2	98
	30	58 ± 4	97

#### 4. Conclusion

The presented coprecipitation procedure was simple and rapid for speciation of Se(IV) and Se(VI). The time required for the coprecipitation and determination was approximately 30 min. The selenium ions can be sensitively determined by atomic absorption spectrometry without any influence of magnesium hydroxide. The preconcentration factor was 25 for 50 ml of sample volume and 2 ml of final volume. The contamination risk for analytes from the carrier element is very low.

#### Acknowledgements

The authors would like to thank the Scientific and Technological Research Council of Turkey (TUBITAK) for financial helps (project no: 104T448). The authors are also grateful for the financial support of the Unit of the Scientific Research Projects of Gaziosmanpasa University and the Unit of the Scientific Research Projects of Erciyes University. Miss E. Melek is thanked for helps in the experimental studies.

#### References

- [1] L.M.L. Nollet (Ed.), Handbook of Water Analysis (Food Science and Technology), Marcel Dekker, New York, 2000.
- [2] V.A. Lemos, D.R. Vieira, C.G. Novaes, M.E. Rocha, M.S. Santos, R.T. Yamaki, *Microchim. Acta* 153 (2006) 193.
- [3] L. Hussein, J. Bruggeman, *Food Chem.* 65 (1999) 527.
- [4] Z. Marczenko, M. Balcerzak, Separation, Preconcentration and Spectrophotometry in Inorganic Analysis (Analytical Spectroscopy Library 10), Elsevier, 2000.
- [5] A. Afkhami, T. Madrakian, *Talanta* 58 (2002) 311.
- [6] J.E. Huheey, *Inorganic Chemistry*, 3rd ed., Harper and Row, New York, 1983.
- [7] M. Ochsenkühn-Petropoulou, B. Michalke, D. Kavouras, P. Schramel, *Anal. Chim. Acta* 478 (2003) 219.
- [8] R. Van Cauwenbergh, H. Robberecht, V. Van Vlaslaer, H. Deelstra, *J. Trace Elem. Med. Biol.* 18 (2004) 99.
- [9] K. Pyrzynska, P. Drzewicz, M. Trojanowicz, *Anal. Chim. Acta* 363 (1998) 141.
- [10] W. Aeungmaitreprom, A. Hagege, Z. Asfari, L. Bennouna, J. Vicens, M. Leroy, *Tetrahedron Lett.* 40 (1999) 6389.
- [11] M.B. Melwanki, J. Seetharamappa, *Turk. J. Chem.* 24 (2000) 287.
- [12] P. Bermejo-Barrera, A. Moreda-ineiro, A. Bermejo-Barrera, *J. Anal. At. Spectrom.* 15 (2000) 121.
- [13] Y. Cai, M. Cabanas, J.L. Fernandezturriel, M. Abalos, J.M. Bayona, *Anal. Chim. Acta* 314 (1995) 183.
- [14] K. Pyrzynska, *Anal. Lett.* 31 (1998) 1777.
- [15] F.Z. Kucukbay, M. Demir, *Turk. J. Chem.* 25 (2001) 341.
- [16] M.N. Pathare, A.D. Sawant, *Anal. Lett.* 28 (1995) 317.
- [17] K. Suvardhan, L. Krishnaiah, K. Suresh Kumar, D. Rekha, B. Jayaraj, S. Ramanaiah, P. Chiranjeevi, *Chemosphere* 62 (2006) 899.
- [18] A. Larraya, M.G. Cobofernandez, M.A. Palacios, C. Camara, *Fresen. J. Anal. Chem.* 350 (1994) 667.
- [19] T. Ferri, P. Sangiorgio, *Anal. Chim. Acta* 321 (1996) 185.
- [20] S.X. Li, N.S. Deng, *Anal. Bioanal. Chem.* 374 (2002) 1341.
- [21] J.L. Gómez-Ariza, D. Sánchez-Rodas, M.A. Caro de la Torre, I. Giráldez, E. Morales, *J. Chromatogr. A* 889 (2000) 33.
- [22] P.E. Carrero, J.F. Tyson, *Spectrochim. Acta B* 53 (1998) 1931.
- [23] K.A. Uvarova, T.V. Poskrebysheva, S.M. Chumakova, M.A. Borozinets, *Ukrainskii Khimicheskii Zhurnal* 56 (1990) 458.
- [24] L. Elci, S. Saracoglu, *Talanta* 46 (1998) 1305.
- [25] S. Saracoglu, M. Soylak, L. Elci, *Trace Elem. Electr.* 18 (2001) 129.
- [26] L.K. Kurmanguzhina, R.M. Mineeva, I.N. Marov, G.A. Evtikova, A.A. Fakeev, *Zhurnal Neorganicheskoi Khimii* 37 (1992) 1004.
- [27] L.K. Kurmanguzhina, I.N. Marov, N.B. Kalinichenko, A.A. Fakeev, B.V. Zhadanov, *Zhurnal Neorganicheskoi Khimii* 36 (1991) 3077.
- [28] Y. Kashiwagi, E. Kokufuta, T. Kawashima, *Anal. Sci.* 13 (1997) 623.
- [29] T.P. Rao, M. Anbu, M.L.P. Reddy, C.S.P. Iyer, A.D. Damodaran, *Anal. Lett.* 29 (1996) 2563.
- [30] X. Tang, Z. Xu, J. Wang, *Spectrochim. Acta B* 60 (12) (2005) 1580.
- [31] Y.C. Sun, J.Y. Yang, *Anal. Chim. Acta* 395 (1999) 293.
- [32] Y. Kashiwagi, E. Kokufuta, T. Kawashima, *Bunseki Kagaku* 44 (1995) 1033.
- [33] T. Ferri, S. Rossi, P. Sangiorgio, *Anal. Chim. Acta* 361 (1998) 113.
- [34] M. Tuzen, M. Soylak, L. Elci, *Anal. Chim. Acta* 548 (2005) 101.
- [35] M. Tuzen, K. Parlar, M. Soylak, *J. Hazard. Mater.* 121 (2005) 79.

# 4-[[2-Hydroxyphenyl]imino]methyl]-1,2-benzenediol (HIMB) anchored Amberlite XAD-16: Preparation and applications as metal extractants

Gopalan Venkatesh, Ajai K. Singh\*

*Department of Chemistry, Indian Institute of Technology, New Delhi 110016, India*

Received 10 March 2006; received in revised form 30 March 2006; accepted 30 March 2006

Available online 9 May 2006

## Abstract

Amberlite XAD-16 was loaded with 4-[[2-hydroxyphenyl]imino]methyl]-1,2-benzenediol (HIMB) via azo linker and the resulting resin AXAD-16-HIMB explored for enrichment of Zn(II), Mn(II), Ni(II), Pb(II), Cd(II), Cu(II), Fe(III) and Co(II) in the pH range 5.0–8.0. The sorption capacity was found between 56 and 415  $\mu\text{mol g}^{-1}$  and the preconcentration factors from 150 to 300. Tolerance limits for foreign species are reported. The kinetics of sorption is not slow, as  $t_{1/2}$  is  $\leq 15$  min. The chelating resin can be reused for seventy cycles of sorption–desorption without any significant change (<2.0%) in the sorption capacity. The limit of detection values (blank + 3 s) are 1.72, 1.30, 2.56, 2.10, 0.44, 2.93, 2.45 and 3.23  $\mu\text{g l}^{-1}$  for Zn, Mn, Ni, Pb, Cd, Cu, Fe and Co, respectively. The enrichment on AXAD-16-HIMB coupled with flame atomic absorption spectrometry (FAAS) monitoring is used to determine the metal ion ions in river and synthetic water samples, Co in vitamin tablets and Zn in powdered milk samples. © 2006 Elsevier B.V. All rights reserved.

**Keywords:** 4-[[2-Hydroxyphenyl]imino]methyl]-1,2-benzenediol (HIMB); Amberlite XAD-16; Metal ions; Chelating resin; Enrichment; Flame atomic absorption spectrometry; Determination

## 1. Introduction

The interest in ligand immobilized solid phases like silica gel, organic polymer or copolymer and cellulose [1], which have good sorption capacity, continues because solid phase extraction (SPE) is an important metal enrichment technique [2] and the ligand anchored solids are important for designing new catalysts [3] as well as heterogenization of homogeneous catalysts [4]. Enrichment of metal ions by SPE makes possible the use of cheap and commonly available analytical techniques such as flame atomic absorption spectrometry (FAAS) for the determination at micro/trace level of metallic species in environmental samples, high purity materials, biological samples and other complex matrices. The advantages of SPE over ion exchange and solvent extraction are selectivity, eco-friendliness, reusability and high preconcentration factor [4]. Amberlite XAD-2 has been found to be a good support to design chelating resins for SPE [5–15]. In comparison to silica gel and cellulose, the kinetics of sorption is faster on Amberlite

XAD-2 based extractors. It has been reported recently that Amberlite XAD-16 [polystyrene-divinylbenzene copolymer] marketed by Aldrich (USA) recently on ligand immobilization gives chelating resins of better sorption capacities than those based on Amberlite XAD-2 [16–19]. This is due to higher surface area of Amberlite XAD-16 in comparison to Amberlite XAD-2 [20,21]. To obtain a matrix of good sorption capacity, it was therefore thought worthwhile to anchor tetradentate ligand 4-[[2-hydroxyphenyl]imino]methyl]-1,2-benzenediol (HIMB) on Amberlite XAD-16. The resulting chelating resin is used to enrich Zn(II), Mn(II), Ni(II), Pb(II), Cd(II), Cu(II), Fe(III) and Co(II) before their determination by FAAS. The method is applied to water, vitamin (Co) and milk samples (Zn). The results of these investigations are reported in this paper.

## 2. Experimental

### 2.1. Instruments

A flame atomic absorption spectrometer (FAAS) of Perkin-Elmer Instruments, Shelton, USA, model Analyst 100 equipped with air–acetylene flame was used for metal ion determination. The wavelengths used for monitoring Zn, Mn, Ni, Pb, Cd, Cu,

\* Corresponding author. Tel.: +91 11 2659 1379; fax: +91 11 2658 1037.  
E-mail addresses: [aksingh@chemistry.iitd.ac.in](mailto:aksingh@chemistry.iitd.ac.in), [ajai57@hotmail.com](mailto:ajai57@hotmail.com) (A.K. Singh).

Fe and Co are 213.9, 279.8, 231.1, 217.0, 228.8, 324.8, 248.8 and 240.7 nm, respectively. A Nicolet (Madison, USA) FT-IR spectrometer, model Protégé 460, was used to record IR spectra (in KBr) in the range 400–4000  $\text{cm}^{-1}$ . The pH was measured with digital pH meter (Toshniwal Instruments, Ajmer, India). Thermogravimetric analysis (TGA) was carried out on a Dupont (Wilmington, DE, USA) 2100 thermal analyzer and Perkin-Elmer (Rotkreuz, Switzerland) elemental analyzer, model 240C, was used for elemental analyses. The flow of solution through the column was controlled using peristaltic pump (Watson–Marlow Model 101/U/R, Falmouth, UK). The sorption and desorption studies of the metal ions on the chelating matrix were generally carried out on columns (Pharmacia, Bromma, Sweden) of size 1 cm  $\times$  10 cm [diameter  $\times$  length] equipped with adjustable frits. A mechanical shaker equipped with an incubator (Hindustan Scientific, New Delhi, India) with a speed of 200 strokes  $\text{min}^{-1}$  was used for batch equilibration.

## 2.2. Reagents

Non-ionic Amberlite XAD-16 (specific area 800  $\text{m}^2 \text{g}^{-1}$  and bead size, 20–60 mesh) was procured from Aldrich (Milwaukee, USA). 3,4-Dihydroxybenzaldehyde obtained from ACROS ORGANICS (New Jersey, USA) and 2-aminophenol obtained from Merck, Germany were used as received. The stock solutions of metal ions (1000  $\mu\text{g ml}^{-1}$ ) were prepared from analytical reagent-grade metal salts as described earlier [8–11]. They were standardized [22] and working solutions of the metal ions were made by suitable dilution of the stock solutions with doubly distilled water. The 0.1 M HCl and NaOH (pH 2 and 3), 0.1 M acetic acid–acetate buffer (pH 4 and 5), 0.1 M phosphate buffer (pH 6 and 7) and 0.1 M ammonia–ammonium chloride buffer (pH 8 and 9) were used to adjust the pH of the solutions, wherever suitable. Water samples from the Ganges river (Haridwar, India), and tap water (New Delhi, India) were collected, acidified with 2%  $\text{HNO}_3$ , filtered and stored in glass bottles. All glassware were washed with chromic acid and soaked in 5%  $\text{HNO}_3$  overnight and cleaned with doubly distilled water before use.

## 2.3. Synthesis of 4-[[2-(2-hydroxyphenyl)imino]methyl]-1,2-benzenediol (HIMB) and HIMB loaded Amberlite XAD-16 (AXAD-16-HIMB)

3,4-Dihydroxybenzaldehyde (0.138 g, 2 mmol) and 2-aminophenol (0.137 g, 1 mmol) were refluxed in methanol for 3 h. The solvent was removed on a rotary evaporator to give brown coloured Schiff's base HIMB. Analyses: Found C, 68.08; H, 4.85; N, 5.87%; Calc. for  $\text{C}_{13}\text{H}_{11}\text{NO}_3$ : C, 68.12; H, 4.80; N, 6.11%.

The published procedure [8,9] for Amberlite XAD-2 was used to prepare the nitrated beads of Amberlite XAD-16 also. The nitrated beads were reduced to amino resin by the method [8,9] reported for Amberlite XAD-2. The amino resin was suspended in 200 mL of ice-cold water and treated with an equimolar mixture of 1 M HCl and  $\text{NaNO}_2$  solution at  $-5^\circ\text{C}$  for diazotization until the reaction mixture started to change the colour of starch-iodide paper to violet. The diazotized Amber-

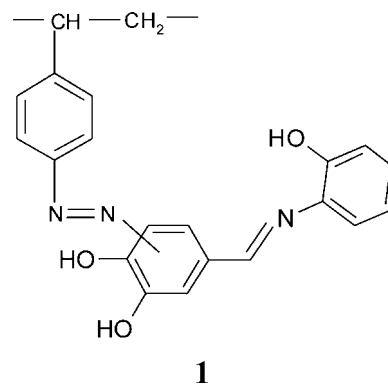
lite XAD-16 was filtered at  $-5$  to  $0^\circ\text{C}$  to avoid its disintegration at higher temperature and treated with HIMB (10 g taken in a mixture of 400 ml of water and 75 ml of 4% sodium hydroxide) at  $0-5^\circ\text{C}$  for 24 h. The resulting dark brownish crimson coloured beads were filtered, washed with 4 M HCl and doubly distilled water successively and finally air-dried. Analyses: AXAD-16-HIMB: Found C, 62.50; H, 5.40; N, 9.80%; Calc. for  $\text{C}_{21}\text{H}_{18}\text{O}_3\text{N}_3 \cdot 2\text{H}_2\text{O}$ : C, 63.63; H, 5.55; N, 10.60%.

## 2.4. Recommended column method for preconcentration and determination of metal ions

Amberlite XAD-16 loaded with HIMB (1.0 g) was swollen in water for 24 h, packed in a glass column C10/10 (Pharmacia, 10 cm  $\times$  10 mm), between frits, using the method recommended by the manufacturer [23]. The column was treated with 4 M HCl or  $\text{HNO}_3$  (50 ml) and washed with doubly distilled water until free from acid. A suitable aliquot of the sample solution containing Zn(II), Mn(II), Ni(II), Pb(II), Cd(II), Cu(II), Fe(III) or Co(II) in the concentration range 0.0060–1.0  $\mu\text{g ml}^{-1}$  was passed through the column after adjusting its pH to the optimum value (6.0) at a flow rate of 1.0–5.0  $\text{ml min}^{-1}$ , controlled with a peristaltic pump. The column was washed with distilled water to remove free metal ions. The bound metal ions were stripped from the column with 1.5 M HCl or  $\text{HNO}_3$  (10–25 ml) passed at flow rate 4.0  $\text{ml min}^{-1}$ . The concentration of the metal ion in the eluates was determined by FAAS, standardized previously. Dilution with double distilled water was performed before aspiration when the eluates were sufficiently concentrated to exceed the working range of FAAS.

## 2.5. Recommended batch method for preconcentration and determination of metal ions

A sample solution (100 ml) containing 0.1–26.39  $\mu\text{g ml}^{-1}$  of Zn(II), Mn(II), Ni(II), Pb(II), Cd(II), Cu(II), Fe(III) or Co(II) was placed in a glass stoppered bottle (250 ml) after adjusting its pH to the optimum value (6.0). The HIMB loaded Amberlite XAD-16 (0.1 g) was added. The bottle was stoppered and shaken for 30 min. The resin was filtered and the metal ions from the resin were desorbed by shaking the resin beads with 1.5 M HCl or  $\text{HNO}_3$  (25 ml) The resin was filtered off and the filtrate was aspirated into the flame of pre-standardized FAAS, after suitable dilution, if required.





### 3. Results and discussion

#### 3.1. Synthesis and characterization of the Amberlite XAD-16 loaded with HIMB

The elemental analyses and TGA of AXAD-16-HIMB (donor sites shown in structure 1) are consistent with the presence of nearly two water molecules per repeat unit. FT-IR spectrum of HIMB is characteristic and has bands at 1649, 1384 and 1238  $\text{cm}^{-1}$  due to  $\nu_{\text{sy}}(\text{C}=\text{N})$ , O–H (bending) and  $\nu(\text{C}-\text{O})$ , respectively. The presence of bands at 1655, 1540, 1342 and 1265  $\text{cm}^{-1}$  due to  $\nu_{\text{sy}}(\text{C}=\text{N})$ ,  $\nu(\text{N}=\text{N})$ , O–H bending and  $\nu(\text{C}-\text{O})$ , respectively, in FT-IR spectrum of AXAD-16-HIMB supports the loading of HIMB onto Amberlite XAD-16. The surface area of AXAD-16-HIMB was found to be 395.8  $\text{m}^2 \text{g}^{-1}$  by BET method.

#### 3.2. Optimum conditions for sorption and desorption

The multivariate approach was used to optimize sorption of Zn(II), Mn(II), Ni(II), Pb(II), Cd(II), Cu(II), Fe(III) and Co(II) on the column packed with AXAD-16-HIMB. Each optimum condition was established by varying one of them and following the recommended column procedure. It was rechecked after standardizing the remaining ones. A typical process for optimization of pH for Cu is as follows. A set of solutions (volume: 100 ml), containing 0.25  $\mu\text{g ml}^{-1}$  of Cu was taken. The pH of the solutions of the set was adjusted to different values in the range 2.0–9.0. The enrichment of the metal ion from these solutions was studied by the recommended column procedure. The optimum pH ranges for maximum recovery (97.6%) are 5.0–7.0, 5.5–6.5, 5.5–7.5, 5.0–7.0, 6.0–8.0, 4.0–6.0 and 6.0–8.0, respectively for Zn, Mn, Ni, Pb, Cd, Cu, Fe, and Co (pH profiles are shown in Fig. 1). The effect of pH on sorption was also studied by using the recommended batch method and the results are found to be consistent with those of the column method. The use of 5–10 ml of acetate, phosphate and ammonia buffer to adjust the pH does not affect

the sorption behavior. The metal ions are not significantly desorbed (<2%) by distilled water; therefore chelation contributes predominantly to the retention of metal ions. The average recoveries [for 0.25  $\mu\text{g ml}^{-1}$  of each metal ion (0.5  $\mu\text{g ml}^{-1}$  for Pb)] under optimum conditions are: 98.7, 99.4, 99.2, 97.8, 98.4, 99.0, 99.8, 97.6% for Zn, Mn, Ni, Pb, Cd, Cu, Fe, and Co, respectively. For five determinations of 0.25  $\mu\text{g ml}^{-1}$  of each metal ion (0.5  $\mu\text{g ml}^{-1}$  for Pb) under optimum conditions the standard deviations were found between 0.012 and 0.081 and corresponding R.S.D. 1.170–5.420%.

#### 3.3. Effect of flow rate and eluent

The metal ion sorption on AXAD-16-HIMB (1 g) packed column was studied at various flow rates of the metal ion solutions controlled with a peristaltic pump. The optimum flow rate for loading Zn, Cd, and Fe onto AXAD-16-HIMB was found to be between 1.0 and 5.0  $\text{ml min}^{-1}$ . For Cu and Ni it was 1.0–4.0  $\text{ml min}^{-1}$  and for Mn, Pb, and Co 2.0–5.0, 1.0–6.0 and 2.0–4.0  $\text{ml min}^{-1}$ , respectively. A flow rate <1.0  $\text{ml min}^{-1}$  was not employed to avoid the longer time of analysis. The decrease in the percentage of sorption at flow rate >5.0  $\text{ml min}^{-1}$ , is probably because the metal ions do not equilibrate sufficiently with the matrix. For stripping off bound Zn, Mn, Ni, Cd, Cu, Fe, and Co the optimum concentrations of HCl (maximum instant recovery >97.6%) needed are 1.5–3.5, 1.0–4.0, 1.0–2.5, 1.5–2.0, 1.0–4.0, 1.0–3.0, 1.0–2.0 M, respectively. The Pb, was eluted best with 0.5–1.5 M  $\text{HNO}_3$ . The flow rates between 2.0–5.0  $\text{ml min}^{-1}$  were found most effective for stripping the metal ions from the matrix.

#### 3.4. Kinetics of metal sorption

The kinetics of sorption was studied by batch method. AXAD-16-HIMB (0.5 g) was shaken with 50 ml of solution containing 40  $\mu\text{g ml}^{-1}$  of one of the eight metal ions for different equilibration times (2, 5, 10, 15, 20, 25, 30, 40 min and 5 h) under optimum conditions. The concentration of metal ions sorbed on the matrix as well as present in the supernatant solution was determined with FAAS using recommended batch method for the former. The sorption as a function of time for all the metal ions is shown in Fig. 2. Shaking for 2–15 min was required for 50% sorption.

#### 3.5. Effects of electrolytes and cations

The effects of NaCl, NaBr,  $\text{NaNO}_3$ ,  $\text{Na}_2\text{SO}_4$ ,  $\text{Na}_3\text{PO}_4$ , NaI and other foreign species on the sorption efficiency of Zn(II), Mn(II), Ni(II), Pb(II), Cd(II), Cu(II), Fe(III) and Co(II) (25  $\mu\text{g}$  each) on AXAD-16-HIMB were studied using the recommended column method. The tolerance limits of various foreign species in the sorption of the eight metal ions are given in Table 1. The criterion for interference was lowering of recovery by more than 3%. Each reported tolerance/interference is in the preconcentration and not in the determination by FAAS, as checked with the help of reagent matched standard solutions.

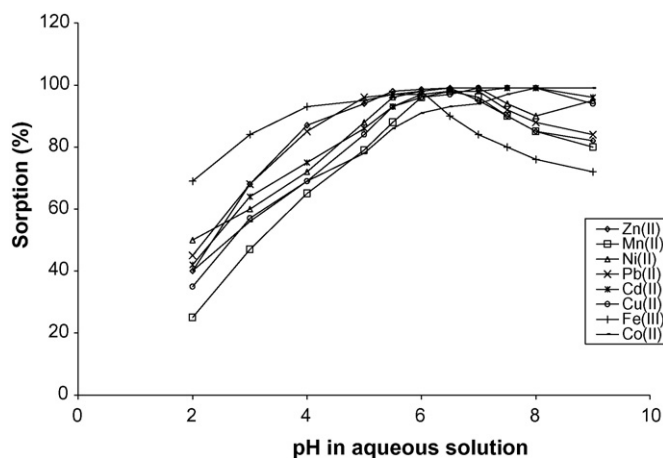


Fig. 1. Effect of pH on sorption of Zn(II), Mn(II), Ni(II), Pb(II), Cd(II), Cu(II), Fe(III) and Co(II) onto HIMB loaded Amberlite XAD-16.

Table 1  
Tolerance limit of electrolytes, cations Ca(II) and Mg(II) and other foreign species

Electrolyte	Metal ion							
	Zn(II)	Mn(II)	Ni(II)	Pb(II)	Cd(II)	Cu(II)	Fe(III)	Co(II)
NaNO <sub>3</sub> (mol l <sup>-1</sup> )	0.5	0.25	0.20	0.23	0.40	0.65	0.28	0.20
NaCl (mol l <sup>-1</sup> )	0.4	0.12	0.35	0.72	0.35	0.80	0.45	0.23
NaBr (mol l <sup>-1</sup> )	0.01	0.08	0.20	0.001	0.02	0.10	0.04	0.06
Na <sub>3</sub> PO <sub>4</sub> (mol l <sup>-1</sup> )	I	0.30	0.06	I	0.12	0.03	0.07	0.15
Na <sub>2</sub> SO <sub>4</sub> (mol l <sup>-1</sup> )	0.22	0.35	0.75	0.28	0.40	1.2	0.25	0.65
NaI (mol l <sup>-1</sup> )	0.07	0.19	0.30	0.02	0.05	0.20	0.35	0.5
Humic acid (μg ml <sup>-1</sup> )	15	20	20	18	5	30	35	12
Ascorbic acid (mmol l <sup>-1</sup> )	0.5	0.40	0.70	0.20	1.0	1.2	1.4	0.44
Citric acid (mmol l <sup>-1</sup> )	0.02	0.15	0.25	0.80	0.60	2.7	1.1	1.2
EDTA (mmol l <sup>-1</sup> )	0.003	0.001	0.004	0.001	0.003	0.006	0.019	0.022
Tartaric acid (mmol l <sup>-1</sup> )	0.44	0.60	0.55	0.80	1.0	0.85	0.70	0.35
Ca(II) (mol l <sup>-1</sup> )	0.20	0.27	0.12	0.50	0.30	1.4	0.05	0.65
Mg(II) (mol l <sup>-1</sup> )	0.30	0.45	0.25	0.05	0.15	0.60	0.90	0.40

I, interferes.

### 3.6. Sorption capacity

The sorption capacities of AXAD-16-HIMB for the eight metal ions were determined by batch method. The resin (0.1 g) was saturated with a metal ion solution (concentration: 50 μg ml<sup>-1</sup>) by equilibration on a mechanical shaker under optimum conditions. The solid matrix was filtered, washed with distilled water and subjected to recommended batch procedure. The filtrate was diluted suitably and also subjected to FAAS determination. The sorption capacities for Zn, Mn, Ni, Pb, Cd, Cu, Fe, and Co (μmol g<sup>-1</sup>) are 168, 111, 225, 105, 56, 415, 340 and 246, respectively (highest for Cu). The sorption capacity values determined by column method were consistent with the batch method values (variation <1.2%).

### 3.7. Resin stability and reusability

The stability of HIMB-loaded Amberlite XAD-16 was studied in 1.0–6.0 M HCl/HNO<sub>3</sub>). It was shaken with acid of varying

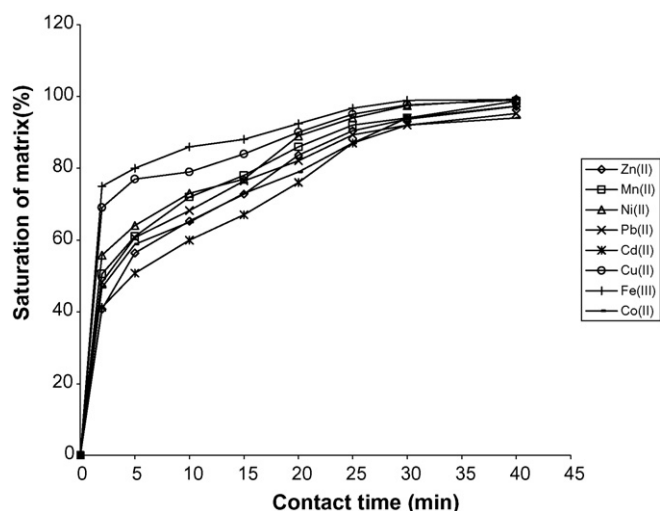


Fig. 2. Kinetics of the sorption of metal ions on HIMB loaded Amberlite XAD-16.

concentrations for 5 h and filtered. The solid was washed with distilled water until free from acid and air-dried. The sorption capacity of the acid treated resin determined by batch method was found to vary <2.4% than that of the untreated one. Thus the present resin can withstand acid concentration up to 6 M. It can be reused for 70 cycles of sorption–desorption without any significant change in the sorption capacity (<2.0%).

### 3.8. Preconcentration and recovery of metal ions

Enrichment factors for column method were determined by increasing the dilution of metal ion solution while keeping the total amount of loaded metal ion fixed at 15 μg for Mn, Cd or Co, 20 μg for Zn, Ni or Cu and 25 μg for Pb or Fe and applying the recommended column procedure. These were guided by middle concentration value of calibration curve of each metal ion, as it should be available in the final eluate so that error is least. The feed volume and preconcentration factors are given in Table 2. The recoveries reported in Table 2 are at the lowest concentrations. The limit of detection values (defined as (blank + 3 s) where s is standard deviation of the blank determination) for the FAAS are 1.72, 1.30, 2.56, 2.10, 0.44, 2.93, 2.45 and 3.23 μg l<sup>-1</sup> for Zn(II), Mn(II), Ni(II), Pb(II), Cd(II), Cu(II), Fe(III) and Co(II), respectively and corresponding limit of quantification (blank + 10 s) values are 3.28, 3.10, 4.78, 4.30, 2.03, 4.85, 5.01 and 5.65 μg l<sup>-1</sup>, respectively.

## 4. Applications of the method

Solid phase extraction with AXAD-16-HIMB coupled with FAAS determination was applied to determine the eight metal ions in water samples, cobalt in vitamin tablets, Zn in milk samples and Cu and Fe in water standards (synthetic).

### 4.1. Determination of metal ions in water samples

The estimations of Zn, Mn, Ni, Pb, Cd, Cu, Fe, and Co in water samples collected from the Ganges (Haridwar) and municipality taps (New Delhi) were made with and without (referred as

Table 2  
Enrichment factors and enrichment limits of metal ions

Metal ion	Total volume (ml)	Concentration (ng ml <sup>-1</sup> )	Final volume (ml)	Recovery (%)	Preconcentration factor
Zn(II)	2000	10	10	99.0	200
Mn(II)	2500	6	10	97.7	250
Ni(II)	3000	6.6	10	96.0	300
Pb(II)	2000	12.5	10	98.7	200
Cd(II)	1500	10	10	96.7	150
Cu(II)	2500	8	10	99.7	250
Fe(III)	3000	8.3	10	97.7	300
Co(II)	2500	6	10	98.3	250

direct determination) standard addition by subjecting 1000 ml of water sample (spiked with 50–100 µg of each of the eight metal ions in case of standard addition method) to recommended column method. The closeness of results of direct and SA method (Table 3) indicates the reliability of present method for metal analyses in water samples.

#### 4.2. Determination of Co in vitamin tablets and zinc in milk powder

Ten tablets (weighing 3.25 g) of Polybion (Merck, Mumbai, India) were digested in a beaker containing 25 ml of concentrated HNO<sub>3</sub> and brought into solution as reported earlier [25]. The pH of the solution was adjusted to optimum value and the concentration of cobalt was estimated by the recommended column procedure using FAAS. The average (four determinations) amount of cobalt was found to be 1.95 µg g<sup>-1</sup> of tablet with an R.S.D. of 3.25%. The reported value of cobalt in the tablet is 1.99 µg g<sup>-1</sup> of tablet.

A sample of powdered milk (1.0 g) was heated in a beaker containing mixture of concentrated sulphuric acid (20 ml) and nitric acid (8 ml) and brought into solution as reported earlier [25]. The pH was adjusted to optimum value (6.0) and the volume was made up to 1000 ml. Thereafter recommended column procedure was applied. The average (four determinations) amount of zinc was found to be 37.40 µg g<sup>-1</sup> of sample with a R.S.D. of 4.86%. The reported value of zinc in the milk sample is 38 µg g<sup>-1</sup>.

#### 4.3. Analysis of synthetic water samples

The recommended column procedure was applied to determine Cu and Fe content in synthetic water samples (1000 ml)

Table 3  
Determination of metal ions in water samples

Origin of sample	Method	Metal ion (µg l <sup>-1</sup> ) (R.S.D.)							
		Zn	Mn	Ni	Pb	Cd	Fe	Cu	Co
Ganges river, Haridwar	Direct	–	5.9 (6.3)	4.6 (3.1)	2.9 (8.1)	–	50.6 (1.5)	17.9 (1.4)	11.6 (2.8)
	S.A.	–	5.6 (3.1)	4.4 (4.4)	3.0 (4.0)	–	49.8 (1.5)	17.6 (1.4)	11.9 (1.4)
Tap water, New Delhi	Direct	12.3 (2.7)	18.7 (1.2)	4.9 (6.5)	19.8 (2.8)	–	55.4 (1.1)	34.5 (1.4)	22.3 (3.7)
	S.A.	12.2 (1.9)	18.8 (2.4)	4.8 (3.2)	19.7 (3.6)	–	55.6 (1.4)	34.4 (1.1)	22.0 (4.5)

Direct: Recommended procedure is directly applied. S.A.: standard addition method; the values are obtained by subtracting the amount of metal added for spiking from the total metal recovered. R.S.Ds. for four determinations.

having composition similar to certified water samples SLRS-4 (National Research Council, Ottawa, Ontario, Canada). The averages of four determinations of Cu and Fe were found to be 1.7 (R.S.D. 3.73%) and 101.8 µg l<sup>-1</sup> (R.S.D. 3.94%), respectively. Their quantities (µg l<sup>-1</sup>) taken were Cu, 1.81 and Fe, 103.

#### 5. Comparison with other chelating matrices

In comparison to thiosalicylic acid [11], chromotropic acid [8,15] pyrocatechol [12,15], *o*-aminophenol [9], tiron [10], pyrogallo l[14] quinalizarin [13] and 1-(2-pyridylazo)-2-naphthol [24] loaded Amberlite XAD-2, HIMB loaded Amberlite XAD-16 exhibits higher sorption capacities. However, present matrix and resacetophenone [26] and 5-formyl-8-hydroxyquinoline [27] loaded silica gel show comparable capacities to sorb several metal ions. 5-Formyl-8-hydroxyquinoline loaded silica gel exhibits better sorption capacities for Cu, Fe and Pb than the present matrix. Similarly sorption capacities of the cellulose loaded with 2,3-DHP [28], pyrocatechol [29], 8-hydroxyquinoline [30] and pyrogallo [31] are generally comparable with those of Amberlite XAD-16-HIMB except for few metals (Zn, Cu, Pb) particularly when ligands loaded are 2,3-DHP and 8-hydroxyquinoline. 2-[[1-(3,4-Dihydroxyphenyl)methylidene]-amino]benzoic acid anchored Amberlite XAD-16 [25] has somewhat higher sorption capacities (except for Ni, Co and Cu), but preconcentration factors of the present matrix for Mn, Ni and Co are better. The sorption capacities reported for N-(3,4-dihydroxy)benzyl-4-amino,3-hydroxynaphthalene-1-sulphonic acid [21] anchored Amberlite XAD-16 are exceptionally high (760–2050 µmol g<sup>-1</sup>), whereas preconcentration factors are not. The preconcentration factors for the present matrix are gen-

erally better than Amberlite XAD-2 based matrices mentioned above, but comparable to silica gel and cellulose based systems. However, the kinetics of sorption on the present matrix is faster than that of silica gel ones. The reusability of the present matrix is also higher than that of Amberlite XAD-16 loaded with 2- $\{[1-(3,4\text{-dihydroxyphenyl)methylidene}] \text{ amino}\}$  benzoic acid.

### Acknowledgement

Authors thank Department of Science and Technology, New Delhi (India) for giving research grant no. SR/S1/IC-16/2002.

### References

- [1] P.K. Jal, S. Patel, B.K. Mishra, *Talanta* 62 (2004) 1005.
- [2] N.J.K. Simpson, *Solid Phase Extraction, Principles, Techniques and Applications*, first ed., Marcel Dekker, Inc., New York, 2000.
- [3] M.H. Valkenberg, W.F. Holderich, *Catal. Rev.* 44 (2002) 321.
- [4] P.M. Price, J.H. Clark, D.J. Macquarrie, *J. Chem. Soc. Dalton Trans.* (2000) 101.
- [5] R. Saxena, A.K. Singh, S.S. Sami, *Anal. Chim. Acta* 295 (1994) 199.
- [6] R. Saxena, A.K. Singh, *Analyst* 120 (1995) 403.
- [7] R. Saxena, A.K. Singh, *Anal. Chim. Acta* 340 (1997) 285.
- [8] P.K. Tewari, A.K. Singh, *Analyst* 124 (1999) 1847.
- [9] M. Kumar, D.P.S. Rathore, A.K. Singh, *Talanta* 51 (2000) 1187.
- [10] M. Kumar, D.P.S. Rathore, A.K. Singh, *Analyst* 125 (2000) 1221.
- [11] P.K. Tewari, A.K. Singh, *Analyst* 125 (2000) 2350.
- [12] P.K. Tewari, A.K. Singh, *Talanta* 53 (2001) 823.
- [13] M. Kumar, D.P.S. Rathore, A.K. Singh, *Fresenius J. Anal. Chem.* 370 (2001) 377.
- [14] M. Kumar, D.P.S. Rathore, A.K. Singh, *Mikrochim. Acta* 137 (2001) 137.
- [15] P.K. Tewari, A.K. Singh, *Talanta* 56 (2002) 735.
- [16] I. Narin, M. Soylak, K. Kayakirilmaz, L. Elci, M. Dogan, *Anal. Lett.* 36 (2003) 641.
- [17] R.G. Wuilloud, H.A. Avedo, F.A. Vazquez, L.D. Martinez, *Anal. Lett.* 35 (2002) 1649.
- [18] S. Tokalioglu, S. Kartal, L. Elci, *Anal. Sci.* 16 (2000) 1169.
- [19] L. Elci, M. Soylak, A. Uzun, E. Buyukpatir, M. Dogan, *Fresenius J. Anal. Chem.* 368 (2000) 358.
- [20] D. Prabhakaran, M.S. Subramanian, *Anal. Bioanal. Chem.* 379 (2004) 519.
- [21] D. Prabhakaran, M.S. Subramanian, *Talanta* 61 (2003) 431.
- [22] A.I. Vogel, *Quantitative Inorganic Analysis*, third ed., Longman, London, 1961, p. 56.
- [23] *Gel filtration-Theory and Practice, A Manual of Pharmacia*, Pharmacia Co, Brama, Sweden, 1994, p. 14.
- [24] P.B. Barrera, M.A. Nancy, D.L. Cristina, B.B. Adela, *Mikrochim. Acta* 142 (2003) 107.
- [25] G. Venkatesh, A.K. Singh, *Talanta* 67 (2005) 187.
- [26] A. Goswami, A.K. Singh, *Anal. Chim. Acta* 454 (2002) 229.
- [27] A. Goswami, A.K. Singh, B. Venkataramani, *Talanta* 60 (2003) 1141.
- [28] V. Gurnani, A.K. Singh, B. Venkataramani, *Anal. Bioanal. Chem.* 377 (2003) 1079.
- [29] V. Gurnani, A.K. Singh, B. Venkataramani, *Talanta* 61 (2003) 889.
- [30] V. Gurnani, A.K. Singh, B. Venkataramani, *Anal. Chim. Acta* 485 (2003) 221.
- [31] V. Gurnani, A.K. Singh, *Ind. Eng. Chem. Res.* 43 (2004) 2302.

## Radical scavenging ability of polyphenolic compounds towards DPPH free radical

D. Villaño<sup>a</sup>, M.S. Fernández-Pachón<sup>a</sup>, M.L. Moyá<sup>b</sup>, A.M. Troncoso<sup>a</sup>, M.C. García-Parrilla<sup>a,\*</sup>

<sup>a</sup> Food Science and Nutrition Unit, Department of Biochemistry, Food Science, Toxicology and Legal Medicine, Faculty of Pharmacy, University of Seville, Seville, Spain

<sup>b</sup> Department of Physical Chemistry, Faculty of Chemistry, University of Seville, c/ Profesor García González 2, E-41012 Seville, Spain

Received 22 November 2005; received in revised form 22 March 2006; accepted 23 March 2006

Available online 2 May 2006

### Abstract

Free radical scavenging activity of different polyphenolic compounds commonly present in wine has been evaluated using DPPH method. The experiments were performed with different amounts of phenols within the linear interval of response and with an excess of DPPH• in all cases. In these conditions, for most of the compounds tested, the reaction was biphasic. Total stoichiometry values *n* confirm the implication of more than one step in the process. Flavan-3-ol compounds showed the highest values, especially procyanidins B1 (9.8) and B2 (9.1). In this family, *n* values coincide with the number of hydroxyl groups available. EC<sub>50</sub> and TEC<sub>50</sub> parameters have been calculated. EC<sub>50</sub> values are extremely diverse, being the procyanidins B1 and B2 the most potent scavenging compounds and resveratrol the less one. TEC<sub>50</sub> considers the rate of reaction towards the free radical. (+)-Catechin and (–)-epicatechin are the phenolic compounds that need more time to react. In contrast, caftaric and caffeic acids are the phenolic acids that react more rapidly. Antioxidant efficacy (AE) is a parameter that combines both factors. Compounds as kaempferol, with a high EC<sub>50</sub> value, could be considered as an antioxidant with low relevance, but instead shows the highest AE value of the phenolic compounds tested, due to its fast rate of reaction, what is of great biological importance.

© 2006 Elsevier B.V. All rights reserved.

**Keywords:** Polyphenols; Antioxidant; DPPH; Stoichiometry; Reaction rates; EC<sub>50</sub>; TEC<sub>50</sub>

### 1. Introduction

Nowadays it is well known that phenolic compounds are highly responsible of the health effects derived from consumption of plant origin food [1,2]. They play a key role as antioxidants due to the presence of hydroxyl substituents and their aromatic structure, which enables them to scavenge free radicals [3–5].

A wide variety of in vitro methods to assess radical scavenging ability have been set up. Different artificial species have been used such as 2,2'-azinobis-3-ethylbenzothiazoline-6-sulfonic acid (ABTS) [6], 1,1'-diphenyl-2-picrylhydrazyl (DPPH) [7], and *N,N*-dimethyl-*p*-phenylenediamine (DMPD) [8]. Conditions may vary from one to another (i.e. pH, solvents, wavelength of measurement), yielding different results [9]. As they are artificial radicals they do not reproduce in vivo situation, which is

a main drawback. However, they are useful to rank antioxidant activity of substances and food containing them. They may serve to evaluate if an elaboration process influences on food antioxidant activity and can be an indicator of the antioxidant potential prior to their consumption.

In the present paper, DPPH method has been applied to the phenolic compounds commonly present in wine. The spectrophotometric technique employs the 1,1-diphenyl-2-picrylhydrazyl free radical (DPPH•), which shows a characteristic UV–vis spectrum with a maximum of absorbance close to 515 nm in methanol. The addition of an antioxidant results on a decrease of absorbance proportional to the concentration and antioxidant activity of the compound itself [7]. This method presents the advantage of using a stable and commercially available free radical and has been extensively applied on the study of antioxidant activity of food items, such as olive oil, fruits, juices and wines [10–15]. It is easy to perform, highly reproducible and comparable with other methods such as ABTS, reduction of superoxide anion and inhibition of lipid peroxidation [16,17].

\* Corresponding author. Tel.: +34 954 55 67 60; fax: +34 954 23 37 65.  
E-mail address: [mcparrilla@us.es](mailto:mcparrilla@us.es) (M.C. García-Parrilla).



There are different forms to express results. One of the most commonly used is the TEAC index (Trolox Equivalent Antioxidant Capacity), firstly designed for ABTS method [18] where the antioxidant capacity of a given substance is compared to that of the standard antioxidant Trolox, an analogous hydrosoluble of Vitamin E. In particular, DPPH• free radical has been used to assess the ability of phenolic compounds to transfer labile H atoms to radicals [19]. Total H atom donating capacities are evaluated in the EC<sub>50</sub> index, defined as the concentration needed to reduce 50% of DPPH•. Time needed to reach the steady state at the concentration EC<sub>50</sub> is named TEC<sub>50</sub>, which considers the rate of reaction towards the free radical. Antioxidant Efficacy (AE) is a parameter that combines both factors [20].

The knowledge of the kinetics of atom transfer is important because free radicals in the organism are short-lived species, what implies that the impact of a substance as an antioxidant depends on its fast reactivity towards free radicals.

Studies have been conducted to evaluate antioxidant activity of different polyphenolic compounds [7], such as flavonoids [21], but the number of species studied is scarce. In this sense, we have included a large number of phenolic compounds, all of them present in wines and in other vegetable products. The objective of the present work is to compare the radical scavenging ability of the different polyphenolic compounds characteristic of wines towards DPPH• free radical. Besides, the reaction rates and stoichiometry have been explored.

## 2. Experimental

### 2.1. Chemicals

1,1-Diphenyl-2-picrylhydrazyl (DPPH•) as free radical form (90% purity) and 6-hydroxy-2,5,7,8 tetramethylchroman-2-carboxylic acid (Trolox) were obtained from Sigma–Aldrich Quimica (Alcobendas, Spain). A total of 19 standard phenolic compounds were purchased from Chromadex, Sigma, Aldrich and Merck, and were selected for their usual occurrence in wines and their availability as commercial standards. Certain phenolic compounds not usually present in wine, such as rutin and morin, were included for comparison purposes. All substances had a grade of purity higher than 99%. Methanol and ethanol were provided by Merck (Mollet del Vallés, Spain). All reagents were of analytical grade. Double distilled water (Millipore Co.) was used throughout.

### 2.2. Instrumental

Absorbance measurements were recorded on a Hitachi UV-2800<sup>®</sup> spectrophotometer thermostated with a Peltier system at 25 °C.

### 2.3. DPPH Method

A methanolic solution (25 mg L<sup>-1</sup>) of the radical DPPH• was prepared daily and protected from light. Absorbance was recorded to check the stability of the radical throughout the

time of analysis. Five different concentrations of DPPH• radical, comprising from 63 and 13 μM, were also prepared every day and a linear relationship between radical concentration and absorbance was established.

The effect of phenolic compounds on the DPPH• absorbance was estimated by using the procedure described by Sánchez-Moreno et al. [20]. 0.1 mL of different phenol concentrations dissolved in 15% ethanol in water were added to 3.9 mL of DPPH• methanolic solution. Absorbance at 515 nm was recorded at different time intervals until the reaction reached an equilibrium. The initial absorbance was close to 0.700 in all cases. The blank reference cuvette contained methanol. All measurements were performed in duplicate. Six different concentrations of each phenolic compound studied have been assayed in order to check the linearity of response and to establish the antioxidant activity values in the adequate linear range.

All phenolic compounds were properly dissolved in an aqueous solution with 15% ethanol, to mimic wine medium, making possible to fully compare the most representative families of polyphenols with wines themselves. Ethanol was tested against DPPH• radical and this resulted in nule effect on the absorbance at 515 nm.

### 2.4. Data analysis

Reaction kinetics of polyphenols with DPPH• were registered for each antioxidant concentration tested (see Fig. 1). From these plots, the percentage of DPPH• remaining at the steady state (DPPH• rem) was determined as

$$\%DPPH^{\bullet} \text{ rem} = \left( \frac{A_f}{A_0} \right) \times 100 \quad (1)$$

$A_0$  and  $A_f$  correspond to the absorbances at 515 nm of the radical at the beginning and at steady state, respectively. Time at steady state was used in order to ensure that reaction did not progress further. Concentrations of the phenolic compounds in the reaction medium were plotted against the percentages of the remanent DPPH• at the end of the reaction in order to obtain the EC<sub>50</sub> index, defined as the amount of antioxidant needed to decrease the initial DPPH• concentration by 50% (see Fig. 2). The time needed to reach the steady state at EC<sub>50</sub> concentration (TEC<sub>50</sub>) was also calculated graphically. Both factors can be combined in the anti-radical efficiency parameter ( $AE = 1/EC_{50} \times TEC_{50}$ ).

The total stoichiometry of the reaction was calculated employing the formula:

$$n = \frac{A_0 - A_f}{\varepsilon} c_0 l \quad (2)$$

where  $c_0$  is the initial concentration of phenolic compound (M);  $A_0$  the absorbance at 515 nm of the radical at  $t=0$ ;  $A_f$  the absorbance at 515 nm of the radical at steady state;  $\varepsilon$  the molar extinction coefficient for DPPH• radical (M<sup>-1</sup> cm<sup>-1</sup>) and  $l$  is the optical path of cuvette (cm).

As the molar extinction coefficient of DPPH• depends on the solvent [19,22],  $\varepsilon$  was estimated under our working conditions. A calibration curve was obtained measuring the absorbance at 515 nm at different DPPH• concentrations using

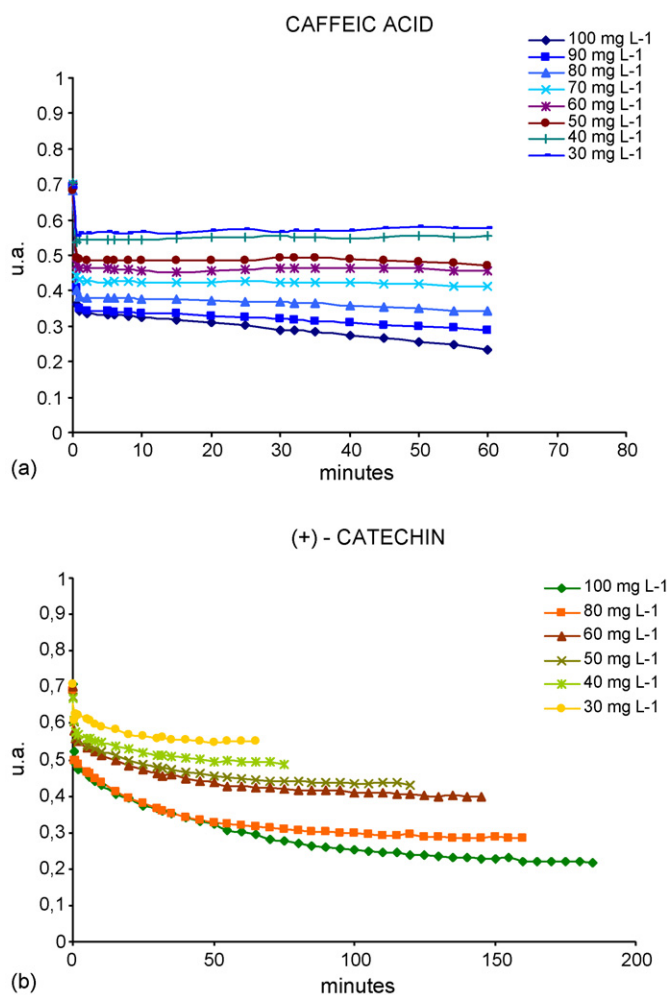


Fig. 1. Reaction curves between  $63 \mu\text{M}$  DPPH $^{\bullet}$  and different solutions of phenolic compounds: (a) caffeic acid; (b) (+)-catechin. 0.1 mL of each solution were added to 3.9 mL of DPPH radical.

the same reaction medium composed of methanol, ethanol and double distilled water in the right proportions. This gave an  $\varepsilon = 11\,563 \text{ M}^{-1} \text{ cm}^{-1}$ .

Analysis of variance and linear correlations tests were performed using the STATISTICA $^{\text{®}}$ 99 version software package.

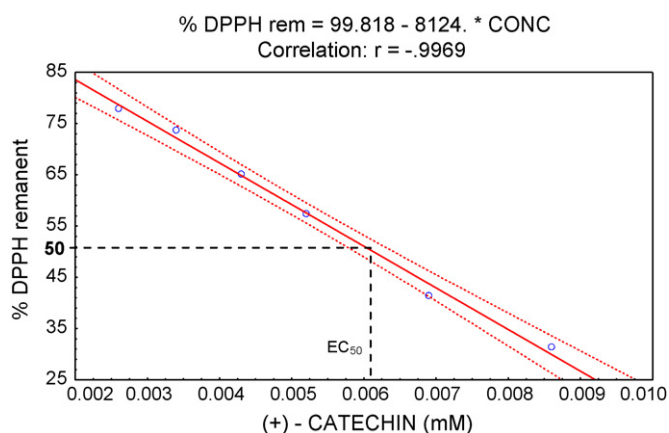


Fig. 2. Calculations of  $\text{EC}_{50}$  value of (+)-catechin towards DPPH $^{\bullet}$  free radical.

### 3. Results and discussion

The experiments were performed in an excess of DPPH $^{\bullet}$  radical (DPPH $^{\bullet}$ -antioxidant molar ratios ranging from 1.3 to 71) in order to exhaust the H-donating capacity of polyphenols. The final concentration of DPPH $^{\bullet}$  in the cuvette was  $0.063 \text{ mM}$ , while the phenols were added in the range  $0.011\text{--}0.0048 \text{ mM}$  (f.c.). These phenolic concentrations were selected from the linear interval of the dose–response curve [23].

For most of the compounds tested, the reaction is biphasic, with a fast decay in absorbance in the first minutes, followed by a slower step in which degradation products are involved, until equilibrium is reached (Fig. 1).

It is interesting to note that some phenolic compounds did not react against DPPH $^{\bullet}$  radical, such as vanillic acid and its aldehyde vanillin, siringaldehyde, *p*-hydroxybenzaldehyde, *p*-coumaric acid, tyrosol and the stilbenes piceid and pterostilbene.

#### 3.1. Stoichiometry of reaction

Compounds can be characterized by their antioxidant stoichiometry, which means the number of oxidant molecules reduced by one molecule of antioxidant [24] and can be calculated by using Eq. (2). Values obtained are shown in Table 1 and

Table 1  
Total stoichiometric values  $n$  of phenolic compounds classified by chemical structure

Compound	$n_{\text{tot1}}^{\text{a}}$	$n_{\text{tot2}}^{\text{b}}$	Number of –OH groups available
<b>Phenolic acids</b>			
Gallic acid	$5.6 \pm 0.2$	$6.1 \pm 0.2$	3
Protocatechuic acid	$2.8 \pm 0.1$	$2.8 \pm 0.4$	2
Gentisic acid	$3.5 \pm 0.4$	$4.1 \pm 0.3$	2
Siringic acid	$2.7 \pm 0.0$	$2.5 \pm 0.4$	1
Caffeic acid	$2.3 \pm 0.1$	$2.6 \pm 0.4$	2
Caftaric acid	$1.6 \pm 0.0$	$1.5 \pm 0.7$	2
Ferulic acid	$1.3 \pm 0.0$	$1.3 \pm 0.8$	1
<b>Flavan-3-ols</b>			
(+)-Catechin	$4.5 \pm 0.3$	$5.1 \pm 0.2$	5
(–)-Epicatechin	$6.6 \pm 0.7$	$6.8 \pm 0.2$	5
(–)-Epigallocatechin	$5.4 \pm 0.4$	$6.1 \pm 0.2$	6
(–)-Epicatechin gallate	$7.3 \pm 0.6$	$7.4 \pm 0.1$	7
(–)-Epigallocatechin gallate	$7.9 \pm 0.9$	$8.7 \pm 0.1$	8
Procyanidin B1	$7.6 \pm 2.3$	$9.8 \pm 0.1$	10
Procyanidin B2	$7.4 \pm 1.6$	$9.1 \pm 0.1$	10
<b>Flavonols</b>			
Kaempferol	$1.8 \pm 0.1$	$1.6 \pm 0.6$	4
Quercetin	$5.2 \pm 0.5$	$5.7 \pm 0.2$	5
Myricetin	$7.6 \pm 0.9$	$8.6 \pm 0.1$	6
Morin	$1.8 \pm 0.0$	$1.9 \pm 0.5$	5
Rutin	$5.8 \pm 0.2$	$5.8 \pm 0.2$	4
<b>Stilbenes</b>			
Resveratrol	$1.0 \pm 0.0$	$1.0 \pm 0.1$	3
<b>Antioxidants of reference</b>			
Ascorbic acid	$2.3 \pm 0.2$	$2.6 \pm 0.4$	2
Trolox	$2.0 \pm 0.4$	$2.2 \pm 0.5$	1

<sup>a</sup> Calculated as  $n = (A_0 - A_f) / \varepsilon c_0 l$ .

<sup>b</sup> Calculated as  $n = 1 / (\text{EC}_{50} \times 2)$ .

they are determined by the structure of the antioxidant and the reaction mechanism. The number of hydroxyl groups available and the reaction products such as dimers or quinones, capable of further reacting with DPPH• radical, influence the stoichiometry by increasing it. At this point, it is interesting to indicate that different stoichiometric values have been reported and their meaning must be carefully examined.

*Total stoichiometry* can be determined from the overall amplitude of the reaction, while *kinetic stoichiometry* is established from the curve fitting of the kinetic traces featuring the decay of absorbance during the first part of the reaction, according to a simple model in which the antioxidant is a source of  $n$  H atoms that are transferred to DPPH• free radical. This kinetic stoichiometry has also been defined as *stoichiometric factor* [22]. This implies that, in the total stoichiometry, reaction products may contribute in the  $n$ -value, while in the kinetic stoichiometry do not. For compounds with a fast reaction kinetics, implication of reaction products is minor, and both values are almost identical.

On the other hand,  $n$  values can be obtained by different forms. Some authors have obtained the stoichiometry by multiplying the EC<sub>50</sub> of each antioxidant by 2, which gives the theoretical efficient concentration of each antioxidant needed to reduce 100% of the DPPH•. Their inverse values represent the number of DPPH• moles reduced by 1 mol of antioxidant [7]. In our experiments we obtained total stoichiometric values of the reaction by both manners and, as can be seen in Table 1, values are quite similar. The figures confirm the implication of more than one step in the process.

Particularly, total stoichiometric values observed for (+)-catechin and (–)-epicatechin (4.5 and 5.1) were higher than those reported by Goupy et al. [19] (3.4 and 3.6), who examined the behaviour of flavanols with a final time point of 15 min. Under our working conditions, steady state is achieved later and this affects the total stoichiometric values obtained. The highest values observed were those of procyanidin B1 and B2 (9.8 and 9.1), nearly followed by that of (–)-epigallocatechin gallate (8.7). Procyanidins display stoichiometries higher than the corresponding monomers. In flavan-3-ol family  $n$  values coincide with the number of hydroxyl groups available. Flavonols show a different behaviour. Those with only one hydroxyl group on the B ring have a low  $n$ , as it occurs with kaempferol and morin. Instead, myricetin possess a high  $n_{\text{tot}}$  (8.6).

It can be observed that structures possessing hydroxyl groups in *ortho* position have a higher  $n$ -value. Gallic acid has three –OH groups in the B ring and the  $n$ -value is 6. Phenolic compounds that possess a similar structure as gallic acid also demonstrate high activity, as (–)-epigallocatechin gallate or myricetin. A possible explanation is the hydrogen bonds formed inside the phenol molecule between hydroxyl groups next to each other. These interactions are stronger than those with solvent and stabilize the phenolic structure.

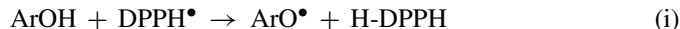
Medium is an important factor influencing the reaction of polyphenols with DPPH• and this makes difficult to compare results in the bibliography. The alcohol molecule can regenerate the catechol structure of the phenol by a nucleophilic attack to the corresponding *o*-quinones, which can transfer additional

H atoms to DPPH• [24]. This mechanism accounts well for the higher scavenging activity of compounds towards DPPH• radical in the presence of protic solvents, such as methanol, compared acetone nitrile [25] or ethyl acetate [21].

In the present paper, a mixture of methanol, ethanol and water was used as reaction medium, most of it being methanol (see Section 2). In conclusion, when evaluating the stoichiometry of the reaction, time point of measurement and solvent effects must be considered.

### 3.2. Study of the fast initiate step of DPPH• and polyphenols reaction

Nitrogen centered radicals such as DPPH• react with phenols (ArOH) via two different mechanisms: (i) a direct abstraction of phenol H-atom (HAT reactions) and (ii) an electron transfer process from ArOH or its phenoxide anion (ArO<sup>–</sup>) to DPPH• (ET reactions) [22]. The contribution of one or the other pathway depends on the nature of the solvent and/or the redox potentials of the species involved. Generally in apolar solvents the HAT mechanism is predominant, but in polar solvents such as methanol or ethanol, capable of forming strong hydrogen bonds with the ArOH molecules, the ET mechanism becomes important. One can see in Fig. 1 that the absorbance versus time plots show a fast initial decrease of the DPPH• absorbance followed by a slow subsequent disappearance of DPPH•. The initial tract was attributed to reactions (i) and (ii)



while the subsequent decay was attributed to secondary slow reactions from the products of dimerization (or disproportionation) of ArO• or from the products of reaction (ii). From the decrease of absorbance versus time in the first seconds of the reactions information about the rate constants of reaction (i) can be acquired. The rate of reaction (i) was defined as

$$-\frac{d[\text{DPPH}\bullet]}{dt} = nk_1[\text{DPPH}\bullet][\text{ArOH}] \quad (3)$$

where  $n$  is the stoichiometric factor of ArOH. In order to calculate  $k_1$ , the absorbance changes observed for reagents concentrations equal or close to 63 and 6.6 μM for DPPH• and phenols, respectively, in the reaction medium were considered. Under these working conditions, the DPPH• concentration was in large enough excess in respect to that of phenols as to be under pseudo-first-order conditions and, therefore, one can write:

$$\ln A = \ln A_0 - k_1 t \quad (4)$$

Here  $A$  represents the DPPH• absorbance,  $t$  the time and  $A_0$  the DPPH• absorbance at  $t=0$ .  $k_1$  values were calculated from the slopes of  $\ln A$  versus time plots (see Eq. (4)) and by considering the average value of the stoichiometric factors listed in Table 1, which are summarized in Table 2. It is interesting to note that the values corresponding to caffeic and ferulic acids are in agreement with those obtained by Foti et al. [22].

Table 2  
Rate constants,  $k_1$  ( $M^{-1} s^{-1}$ ), and stoichiometric factors  $n$ , for the reactions of 63  $\mu M$  DPPH• with 6.6  $\mu M$  of phenolic compounds at 25 °C

Compound	$k_1$ ( $M^{-1} s^{-1}$ )	$n$
Phenolic acids		
Gallic acid	519	5.5
Protocatechuic acid	95	2.8
Gentisic acid	459	3.7
Siringic acid	204	2.6
Caffeic acid	532	2.4
Caftaric acid	750	1.6
Ferulic acid	118	1.3
Flavan-3-ols		
(+)-Catechin	229	4.8
(-)-Epicatechin	297	6.7
(-)-Epigallocatechin	616	5.7
(-)-Epicatechin gallate	455	7.3
(-)-Epigallocatechin gallate	428	8.3
Procyanidin B1	104	8.7
Procyanidin B2	314	8.2
Flavonols		
Kaempferol	715	1.7
Quercetin	264	5.5
Myricetin	314	8.1
Morin	500	1.8
Rutin	266	5.8
Other antioxidants		
Resveratrol	138	1.0
Ascorbic acid	330	2.4
Trolox	306	2.1

$n$  is the mean value of  $n_1$  and  $n_2$  (Table 1).  $K_1 = K_{obs}/n$ .

Table 3  
Radical scavenging parameters of phenolic compounds:  $EC_{50}$ ,  $TEC_{50}$  and antioxidant efficacy AE values

Compound	$EC_{50}$ ( $10^{-6} M$ )	Time (min) of steady state	$TEC_{50}$ (min)	AE ( $\times 10^{-3}$ )
Phenolic acids				
Gallic acid	5.1 $\pm$ 0.1	20–75	53 $\pm$ 2	3.7 $\pm$ 0.2
Protocatechuic acid	11.1 $\pm$ 0.0	50–60	59 $\pm$ 0	1.5 $\pm$ 0.0
Gentisic acid	7.6 $\pm$ 0.2	30–50	41 $\pm$ 2	3.3 $\pm$ 0.2
Siringic acid	12.3 $\pm$ 0.0	40–60	56 $\pm$ 1	1.4 $\pm$ 0.0
Caffeic acid	12.1 $\pm$ 0.2	3–45	35 $\pm$ 5	2.4 $\pm$ 0.4
Caftaric acid	20.4 $\pm$ 0.4	5–15	11 $\pm$ 0	4.3 $\pm$ 0.0
Ferulic acid	24.7 $\pm$ 0.4	40–70	53 $\pm$ 0	0.8 $\pm$ 0.0
Flavan-3-ols				
(+)-Catechin	6.0 $\pm$ 0.2	55–140	120 $\pm$ 2	1.4 $\pm$ 0.0
(-)-Epicatechin	4.5 $\pm$ 0.2	40–155	180 $\pm$ 0	1.2 $\pm$ 0.1
(-)-Epigallocatechin	5.1 $\pm$ 0.1	60–110	95 $\pm$ 1	2.1 $\pm$ 0.1
(-)-Epicatechin gallate	4.2 $\pm$ 0.1	6–61	60 $\pm$ 0	4.0 $\pm$ 0.0
(-)-Epigallocatechin gallate	3.6 $\pm$ 0.0	7–120	67 $\pm$ 1	4.2 $\pm$ 0.1
Procyanidin B1	3.2 $\pm$ 0.0	12–60	50 $\pm$ 2	6.4 $\pm$ 0.2
Procyanidin B2	3.4 $\pm$ 0.4	8–60	44 $\pm$ 3	6.8 $\pm$ 1.3
Flavonols				
Kaempferol	18.8 $\pm$ 0.0	5–10	6.0 $\pm$ 0.1	8.9 $\pm$ 0.1
Quercetin	5.5 $\pm$ 0.0	15–60	66 $\pm$ 5	2.8 $\pm$ 0.2
Myricetin	3.6 $\pm$ 0.1	30–90	67 $\pm$ 1	4.2 $\pm$ 0.2
Morin	16.5 $\pm$ 0.4	8–40	24 $\pm$ 1	2.5 $\pm$ 0.1
Rutin	5.3 $\pm$ 0.1	35–70	52 $\pm$ 1	3.6 $\pm$ 0.1
Other compounds				
Resveratrol	31.4 $\pm$ 0.3	20–75	50 $\pm$ 1	0.5 $\pm$ 0.0
Ascorbic acid	11.8 $\pm$ 0.2	1–3	1.0 $\pm$ 0.0	28.4 $\pm$ 0.5
Trolox	14.1 $\pm$ 0.0	5–10	6.0 $\pm$ 0.2	10.9 $\pm$ 0.1

Nonetheless, taking into account the complexity of the reactions studied and the differences in the stoichiometric factors reported in the literature for the same phenolic compounds,  $k_1$  values listed in Table 2 have to be considered as approximated. From these values, it can be supposed that gallic acid and caffeic acid have the same rate of reaction towards DPPH• free radical. Instead, it must be considered  $n$  values of each compound (5.5 and 2.4, respectively).  $k_1$  constants refer to the rate of reaction of each –OH group on each molecule towards DPPH•. So, the  $k_{obs}$  for gallic acid is two-fold higher than that of caffeic acid.

### 3.3. $EC_{50}$

$EC_{50}$  is inversely related to the antioxidant capacity of a compound, as it expresses the amount of antioxidant needed to decrease the radical concentration by 50%. The lower  $EC_{50}$ , the higher the antioxidant activity of a compound is. An example of calculation can be seen in Fig. 2. As can be seen in Table 3,  $EC_{50}$  values are extremely diverse, being the procyanidins B1 and B2 the most potent scavenging compounds and resveratrol the less one. Chemical structure of flavan-3-ol family shows generally a good antioxidant response towards DPPH• radical. Phenolic acids have the same order of reactivity as reported by literature [7]: gallic acid ( $5.05 \times 10^{-6} M$ ) < gentisic acid ( $7.61 \times 10^{-6} M$ ) < caffeic acid ( $12.12 \times 10^{-6} M$ ) < ferulic acid ( $24.69 \times 10^{-6} M$ ). In the case of caffeic acid, values obtained are in accordance with some authors [26].



### 3.4. $TEC_{50}$

Some compounds react in a fast manner with DPPH<sup>•</sup>, examples are ascorbic acid, kaempferol, caftaric acid and Trolox. However, for most of the compounds tested, reactions are quite slow and complex mechanisms are involved. This makes advisable to select the equilibrium state as time of measure, which ensures that reaction does not progress further. Time at equilibrium state depends on the reactivity of antioxidants and the concentrations used. So, for comparison purposes, it has been defined the  $TEC_{50}$  parameter, as the time at equilibrium reached with a concentration of antioxidant equal to  $EC_{50}$ .

(+)-Catechin and (–)-epicatechin are the phenolic compounds that need more time to react, 120 and 180 min, respectively (Table 3). In contrast, caftaric and caffeic acids are the phenolic acids that react more rapidly, as the ascorbic acid. This behaviour has also been reported by other authors [20,27].

Times of reaction for flavonols differ greatly from one to another.  $TEC_{50}$  for kaempferol is only 6 min, while myricetin needs 66 min to decrease radical concentration by 50%.

### 3.5. Antioxidant efficacy

As previously seen, DPPH method permits to evaluate not only the electron- or hydrogen atom-donating properties of antioxidants, but also the rate of their reaction towards the free radicals. In this sense, a new parameter has been defined, the Antioxidant Efficacy (AE), which comprises these two aspects in order to characterize easily the behaviour of a substance as antioxidant. In Table 3 we can observe that compounds such as kaempferol, with an  $EC_{50}$  value of  $18.81 \times 10^{-6}$  M, could be considered as an antioxidant with low relevance, but instead shows the highest AE value ( $8.92 \times 10^{-3}$ ) of the phenolic compounds tested, due to its fast rate of reaction (Table 2). This characteristic is of great importance in biological systems, as free radicals have very short half-lives [28]. It is followed, in order of magnitude, by procyanidins B1 and B2. In contrast, ferulic acid and resveratrol show the lowest AE values. Gallic acid seems to play a key role in antioxidant activity of gallate esters of flavanols, as it increases their antioxidant efficacy four-fold compared to their respective free aglicon forms.  $EC_{50}$  values of gallic acid and (–)-epicatechin are quite similar, however gallic acid shows a  $TEC_{50}$  almost four-fold lower than (–)-epicatechin, which confers it a higher AE.

## 4. Conclusions

Polyphenolic compounds have shown a different behaviour towards DPPH<sup>•</sup> free radical, both in terms of capacity and rate of scavenging. The highest stoichiometric values found were those of flavan-3-ol family, especially in the case of procyanidins B1 and B2, due to the number of hydroxyl groups available. Gallic acid-like structures seem to be important for efficacy towards DPPH<sup>•</sup> radical. Rates of reaction must be compared taking into account  $n$  values.  $EC_{50}$  and  $TEC_{50}$  values greatly differ between

polyphenolic compounds and, in this sense, antioxidant efficacy seems to be a more appropriate parameter to better define a compound as good antioxidant.

## Acknowledgements

This study received financial support from the Spanish Government (Ministerio de Ciencia y Tecnología, Research project 2001-2368) and the Regional Government of Andalucía, Spain (Research Grant) to whom the authors are grateful.

## References

- [1] D.A. Bazzano, J. He, L.G. Ogden, *Am. J. Clin. Nutr.* 76 (2002) 93.
- [2] L.L. Marchand, S.P. Murphy, J.H. Hankin, L.R. Wilkens, L.N. Kolonel, *J. Natl. Cancer Inst.* 92 (2000) 154.
- [3] P. Kefalas, S. Kallithraka, I. Parejo, D.P. Makris, *Food Sci. Technol. Int.* 9 (2003) 383.
- [4] A. Rigo, F. Vianello, G. Clement, *J. Agric. Food Chem.* 48 (2000) 1996.
- [5] J.V. Verhagen, G.R.M.M. Haenen, A. Bast, *J. Agric. Food Chem.* 44 (1996) 3733.
- [6] N.J. Miller, C.A. Rice-Evans, M.J. Davies, V. Gopinathan, A. Milner, *Clin. Sci.* 84 (1993) 407.
- [7] W. Brand-Williams, M.E. Cuvelier, C. Berset, *Food Sci. Technol.* 28 (1995) 25.
- [8] V. Fogliano, V. Verde, G. Randazzo, A. Ritieni, *J. Agric. Food Chem.* 47 (1999) 1035.
- [9] M. Antolovich, P.D. Prenzler, E. Patsalides, S. Mc Donald, K. Robards, *Analyst* 127 (2002) 183.
- [10] A. Arnous, D.P. Makris, P. Kefalas, *J. Agric. Food Chem.* 49 (2001) 5736.
- [11] C. Da Porto, S. Calligaris, E. Celotti, M.C. Nicoli, *J. Agric. Food Chem.* 48 (2000) 4241.
- [12] S. Gorinstein, O. Martin-Belloso, E. Katrich, A. Lojek, M. Ciz, N. Gligelmo-Miguel, R. Haruénkit, Y.-S. Park, S.-T. Jung, S. Trakhtenberg, *J. Nutr. Biochem.* 14 (2003) 154.
- [13] I.M. Heinonen, P.J. Lehtonen, A.I. Hopia, *J. Agric. Food Chem.* 46 (1998) 25.
- [14] R. Llorach, J.C. Espín, F.A. Tomás-Barberán, F. Ferreres, *J. Agric. Food Chem.* 51 (2003) 2181.
- [15] C. Sánchez-Moreno, L. Plaza, B. De Ancos, M.P. Cano, *J. Sci. Food Agric.* 83 (2003) 430.
- [16] M.I. Gil, F.A. Tomás-Barberán, B. Hess-Pierce, D.M. Holcroft, A.A. Kader, *J. Agric. Food Chem.* 48 (2000) 4581.
- [17] Y. Lu, L.Y. Foo, *Food Chem.* 68 (2000) 81.
- [18] C.A. Rice-Evans, N.J. Miller, *Meth. Enzymol.* 234 (1994) 279.
- [19] P. Goupy, C. Dufour, M. Loonis, O. Dangles, *J. Agric. Food Chem.* 51 (2003) 615.
- [20] C. Sánchez-Moreno, J.A. Larrauri, F. Saura-Calixto, *J. Sci. Food Agric.* 76 (1998) 270.
- [21] D.I. Tsimogiannis, V. Oreopoulou, *Innovative Food Sci. Emerging Technol.* 5 (2004) 523.
- [22] M.C. Foti, C. Daquino, C. Geraci, *J. Org. Chem.* 69 (2004) 2309.
- [23] D. Villaño, M.S. Fernández-Pachón, A.M. Troncoso, M.C. García-Parrilla, *Anal. Chim. Acta* 538 (2005) 391.
- [24] O. Dangles, G. Fargeix, C. Dufour, *J. Chem. Soc., Perkin Trans. 2* (2000) 1653.
- [25] S. Saito, J. Kawabata, *J. Agric. Food Chem.* 52 (2004) 8163.
- [26] I. Gülçin, *Toxicology* 217 (2006) 213.
- [27] A. Dávalos, B. Bartolomé, C. Gómez-Cordovés, *J. Sci. Food Agric.* 84 (2004) 631.
- [28] A.T. Diplock, J.L. Charleux, G. Crozier, F.J. Kok, C.A. Rice-Evans, M. Roberfroid, W. Stahl, J. Viña-Ribes, *Br. J. Nutr.* 80 (1998) s77.



# One step fabrication of nanoelectrode ensembles formed via amphiphilic block copolymers self-assembly and selective voltammetric detection of uric acid in the presence of high ascorbic acid content

Chengyin Wang<sup>a,b,\*</sup>, Qingxiu Liu<sup>a</sup>, Xiaoqi Shao<sup>a</sup>, Gongjun Yang<sup>a,b</sup>,  
Huaiguo Xue<sup>a</sup>, Xiaoya Hu<sup>a,b,\*\*</sup>

<sup>a</sup> Department of Chemistry and Chemical Engineering, Yangzhou University, Yangzhou 225002, China

<sup>b</sup> Jiangsu Key Laboratory of Environmental Engineering and Monitoring, Yangzhou 225002, China

Received 6 January 2006; received in revised form 12 March 2006; accepted 21 March 2006

Available online 9 May 2006

## Abstract

A novel one-step approach to glassy carbon nanoelectrode ensembles (NEEs) with the pores of 20–120 nm in radii has been developed using an amphiphilic block copolymer [polystyrene-block-poly (acrylic acid)] self-assembly. This procedure is simple and fast, and requires only conventional, inexpensive electrochemical instrumentation. Electrochemical methods were used to characterize the NEEs prepared using this new procedure. The NEEs drastically suppressed the response of ascorbic acid (AA) and resolved the overlapping voltammetric response of uric acid (UA) and AA into two well-defined peaks with a large anodic peak difference ( $\Delta E_{pa}$ ) of about 310 mV. The peak current obtained from differential pulse voltammetry (DPV) was linearly dependent on the UA concentration in the range of 0.25–50  $\mu\text{M}$  at neutral pH (PBS, pH 6.86) with a correlation coefficient of 0.999, and the detection limit was 0.04  $\mu\text{M}$  (S/N = 3). The NEEs has also been demonstrated to be applicable in the detection of UA in serum and urine samples with excellent sensitivity and selectivity. The NEEs will hopefully be of good application for further sensor development. © 2006 Elsevier B.V. All rights reserved.

**Keywords:** Nanoelectrode ensembles; Block copolymer; Glassy carbon electrode; Uric acid; Ascorbic acid

## 1. Introduction

Ultrasmall electrodes offer a number of advantages when employed in electrochemical studies and applications [1–4]. However, an obvious challenge to successful exploration of the above benefits of individual nanoscale electrodes is their fabrication and handling; another is that single nanoelectrode generates low current, which is hardly detectable with the conventional electrochemical technique. This instrumentation problem can be circumvented by the use of nanoelectrode arrays or ensembles, whereby the individual electrodes in the array operate in parallel thus amplifying the signal while retaining the beneficial characteristics of the nanoelectrodes [5,6].

Martin and co-workers have prepared disk arrays by the electrodeposition of metals within the micrometre- and

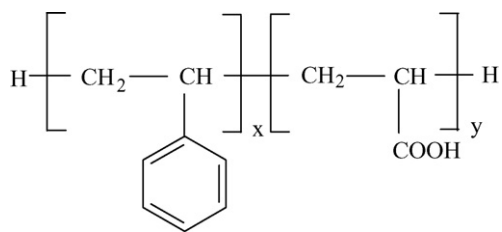
sub-micrometre-sized pores of polycarbonate porous membranes, referred to the template synthesis method [7,8]. Other approaches are based on exploiting as NEEs the defects generated in self-assembled monolayers [9–11]. The fabrication of NEEs with carbon-nanotubes (CNTs) offers opportunities for exploration of analytical/sensor applications in a number of areas [12,13]. Recently, Jeoung et al. who used the planar electrode coated with insulator approach, used block copolymer polystyrene (PS)/polymethylmethacrylate (PMMA) self-assembly to produce ordered arrays of pores on the electrode surface under an electric field and UV treatment [14]. However, this approach is complex, multiplex and time-consuming. A reliable method to mass-produce well-controlled NEEs at a reasonable cost is still lacking [15].

Uric acid (UA) measurements in human physiological fluids are used in the diagnosis and treatment of numerous renal and metabolic disorders, including renal failure, gout, leukemia, psoriasis, starvation, or other wasting conditions and in the treatment of patients receiving cytotoxic drugs. Enzyme-based methods are useful due to their high selectivity [16]. But these methods

\* Corresponding author. Tel.: +86 514 7975587; fax: +86 514 7975244.

\*\* Co-corresponding author.

E-mail addresses: [yzswcy@yzcn.net](mailto:yzswcy@yzcn.net) (C. Wang), [xyhu@yzu.edu.cn](mailto:xyhu@yzu.edu.cn) (X. Hu).



Scheme 1. Structure of PS-*b*-PAA, *x* and *y* are respectively the numbers of PS block and PAA block.

inherently lack stability and are very expensive and can only achieve a relative high detection limit of about 1 mM [17]. UA can be determined with electrochemical methods because of its electrochemical activity. However, one of the major problems frequently encountered in the electrochemical detection of UA is the serious interference caused by AA, which exists in body fluids in relatively high concentrations. Several approaches, based on polymer-modified electrodes [18], Nafion-modified electrodes [19], nanomaterial-modified electrodes [20] and self-assembled monolayers [21] have been made to eliminate AA interference for the determination of UA. All these electrochemical sensors use the concept of charge-based repulsion to achieve selectivity. The drawback associated with this method is that it is restricted to a pH range of 4.2–5.4. Both UA and AA exist as anions beyond pH 5.4 in the alkaline range ( $pK_a$  of AA and UA are 4.17 and 5.4, respectively). Hence, it is necessary to develop a method for the selective determination of UA in the presence of AA at neutral pH. By now, there were very few literatures reported to detect UA at neutral pH, such as an exfoliated graphite electrode [22].

In this paper, we firstly described a simple, facile, one-step approach to fabricate nanoelectrode ensembles formed by controlled nanopores polymeric thin film of an amphiphilic diblock copolymer, polystyrene-block-poly (acrylic acid) (PS-*b*-PAA, Scheme 1), on a glassy carbon electrode. The NEEs was applied to the voltammetric selective and sensitive detection of UA in the presence of high concentration of AA, owing to UA weak adsorption and fast electrochemical kinetics under the high mass transport and radial diffusion at the NEEs and in their specific micro-environment of the nanopores. The findings showed that the NEEs drastically suppressed the response of AA and resolved the overlapping voltammetric response of UA and AA into two well-defined peaks with a large anodic peak difference.

## 2. Experimental

### 2.1. Apparatus

Cyclic voltammetry (CV) and differential pulse voltammetry (DPV) experiments were carried out at CHI 660B electrochemical workstation (Chenhua Instruments, China). SEM images were obtained from XL-30E scanning electron microscopy (Philips, The Netherlands). Enzyme coupling colorimetric experiment was performed on an auto clinical chemical analyzer (Human Autohumalzer 900s plus, Germany). All

electrochemical experiments employed a conventional three-electrode system with a PS-*b*-PAA coated glassy carbon electrode (3.0 mm in diameter) as working electrode, a platinum wire as auxiliary electrode and a saturated calomel electrode (SCE) as reference electrode. All the potentials reported in this paper were referenced to the SCE. All the experiments were carried out at 25 °C.

### 2.2. Chemicals and solutions

Uric acid was purchased from Sigma (the USA). Ascorbic acid was obtained from Chemical Reagent Company of Shanghai (Shanghai, China). PS-*b*-PAA was obtained from Rohm and Hass Electronic Materials Company (Shanghai Branch, the block ratio of PS to PAA is 2:1, molecular weight is 12,500 g mol<sup>-1</sup>). They were used as received without further purification. All the other reagents used were of analytical grade. Doubly distilled water was obtained by purification through a Millipore water system and was used throughout. UA and AA were prepared with doubly distilled water immediately prior to each experiment. 0.10 M phosphate buffer solution (PBS) at various pH values was used as a kind of supporting electrolytes for the determination of UA and AA. UA KIT (KEHUA DONGLING® 20051122) was obtained from Shanghai KEHUA DONGLING® Diagnostic products Co., Ltd. Uric Acid Standard (Human® LOT 098B) and Quality control serum for clinical chemistry (SERODOS® LOT 6869A) were obtained from Human GmbH, Germany.

### 2.3. Fabrication of the NEEs

The glassy carbon electrode was polished before each experiment with 1, 0.3 and 0.05 μm α-alumina powder, respectively, rinsed thoroughly with doubly distilled water between each polishing step, sonicated in 1:1 nitric acid, acetone and doubly distilled water successively. Finally, it was dried with a stream of high-purity nitrogen immediately before use. PS-*b*-PAA was dissolved in tetrahydrofuran (THF), with a typical concentration in solution 0.1% by weight. A drop of PS-*b*-PAA/THF solution was spin-cast onto the polished glassy carbon electrode surface in a humid atmosphere (about 50% r.h.) with air flow across the surface. After several seconds the whole surface of the electrode was covered with translucent layer. The SEM images (Fig. 1(A and B)) show that the thin film consists of a 1 μm thick film with the pores of about 20–120 nm in radii.

## 3. Results and discussions

### 3.1. Mechanism and control of fabrication of the polymer film

Francois et al. firstly discovered that regular porous films were obtained, without the use of a template, when a solution of CS<sub>2</sub> and polystyrene-block-polyparaphenylene (PS-*b*-PPP) was cast under humid conditions [23]. The formation process of this ordered morphology and its formation mechanisms have been widely investigated. The mechanism of formation of this

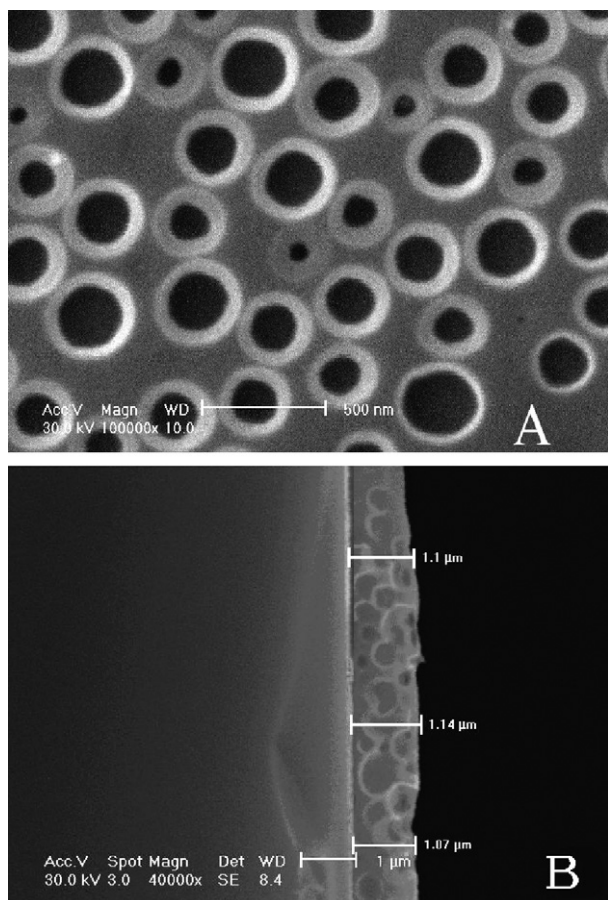


Fig. 1. SEM images of PS-*b*-PAA nanopores ((A) top view and (B) side view on a microscope slide).

new regular morphology involves a combination of complicated thermodynamics and transport phenomena [24]. After placing a drop of PS-*b*-PAA/THF solution on the substrate, the THF starts to evaporate. This leads to a decrease in solution temperature, and water droplets start to condense onto the solution surface. The stabilized water droplets will self-organize into a pores array before the polymer precipitates around them. The precipitation of the polymer at the solution–water interface prevents droplet coagulation. When the solvent and water have evaporated, an ordered pores packed polymeric structure will remain. The water droplets act as a sacrificial template for the ordered film [25]. The pore size can be tailored by changing the rate of the applied air flow, concentration of the cast solution, and humidity [26]. When the surface is completely covered with water droplets, the temperature difference between the surface and the droplets eventually dissipates, and if the droplets are denser than the solvent, they sink into the solution. When a solvent less dense than water is used, such as THF, the pores array propagates through the film. In the above mentioned example, the essential characteristics of the pores structure, such as film thickness, distance between the pores, and pore diameter, can be controlled by concentration of the polymer in the casting solution and humidity. Higher concentrations lead to larger pores and thicker film, whereas higher humidity leads to larger pore diameters. In general, a porous

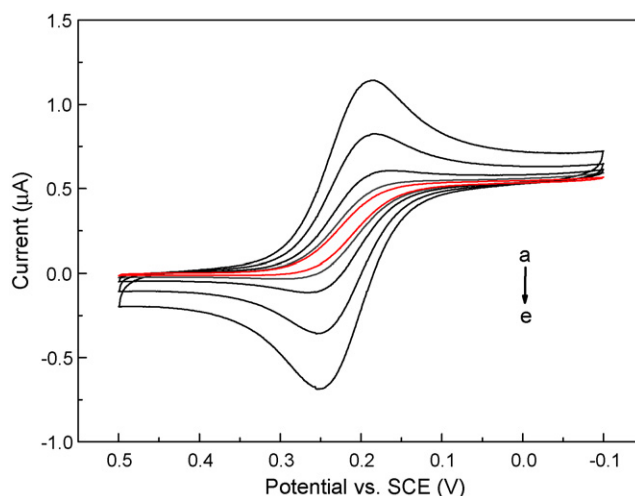


Fig. 2. Cyclic voltammograms of the NEEs in the solution of 6 mM  $\text{K}_3\text{Fe}(\text{CN})_6$  and 1 M  $\text{KNO}_3$  at different scan rates: (a) red line, 5, (b) 10, (c) 20, (d) 50, and (e)  $100 \text{ mV s}^{-1}$ . (For interpretation of the references to color in this figure legend, the reader is referred to the web version of the article.)

structure with pore diameters of  $200 \text{ nm} \sim 1 \mu\text{m}$  and a film thickness of  $800 \text{ nm} \sim 5 \mu\text{m}$  can be prepared. We attempted to prepare ordered pore morphology from PS-*b*-PAA in toluene solvents under other identical conditions but it was still unsuccessful.

Fig. 2 showed the cyclic voltammograms (CVs) of a PS-*b*-PAA coated the glassy carbon electrode in a solution containing 6 mM  $\text{K}_3\text{Fe}(\text{CN})_6$  and 1 M  $\text{KNO}_3$ . The redox current of  $\text{Fe}(\text{CN})_6^{3-}/\text{Fe}(\text{CN})_6^{4-}$  was observed when a PS-*b*-PAA coated the glassy carbon electrode was used. A peak-shaped waveform was observed at the scan rate of  $50 \text{ mV s}^{-1}$  (Fig. 2(d)), which indicated that the redox reaction of potassium ferricyanide ( $\text{K}_3\text{Fe}(\text{CN})_6$ ) was controlled by a linear diffusion under this condition. And the waveform can be attributed to the planar diffusion through each PS-*b*-PAA nanopores to the electrode surface. When the scan rate of CV decreased, the shape of the curves began to change. At the lower scan rate such as  $5 \text{ mV s}^{-1}$  (Fig. 2(a)), the CV became sigmoidal with the characterization of an ultramicroelectrode, which indicated that the redox reaction of  $\text{Fe}(\text{CN})_6^{3-}/\text{Fe}(\text{CN})_6^{4-}$  was controlled by a radial diffusion [27].

### 3.2. Cyclic voltammetric behavior of UA and AA at the NEEs

It is widely known that carbon-based electrodes are suitable substrates for exploring the adsorption properties of various compounds. The adsorption of UA on carbon-based electrodes has been reported earlier [22,28,29] and has been explained to be due to hydrogen bonding. The cyclic voltammograms of 0.50 mM UA and 1 mM AA at the bare glassy carbon electrode (Fig. 3(A)) showed that the voltammetric response of UA and AA was overlapped. The direct redox of the two substances at bare electrodes takes place at very similar potentials and often suffers from a pronounced fouling effect, which results in rather poor selectivity and reproducibility [30].

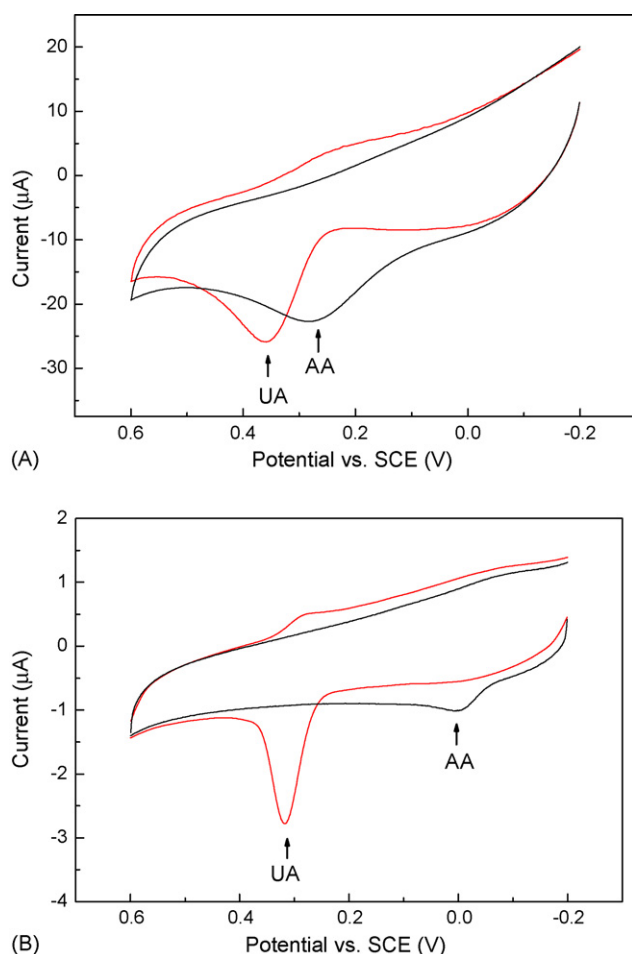


Fig. 3. Cyclic voltammograms of 1 mM AA (black line) and 0.5 mM UA (red line) on the glassy carbon electrode (A) and 1 mM AA (black line) and 0.05 mM UA (red line) at the NEEs (B) in 0.10 M PBS (pH 6.86). Scan rate:  $50 \text{ mV s}^{-1}$ . (For interpretation of the references to color in this figure legend, the reader is referred to the web version of the article.)

From the cyclic voltammograms of the NEEs in 0.10 M PBS (pH 6.86), we found no redox peak in the potential range from  $-0.20$  to  $1.20 \text{ V}$ . Thus, the NEEs provided a broad potential window to investigate the voltammetric behavior of UA and AA. Fig. 3(B) showed the cyclic voltammetric behavior of 0.05 mM UA and 1 mM AA at the NEEs in 0.10 M PBS (pH 6.86). At the bare glassy carbon electrode, UA showed irreversible electrochemical behavior with  $\Delta E_p$ , the difference between the anodic peak potential ( $E_{pa}$ ) and the cathodic peak potential ( $E_{pc}$ ),  $137 \text{ mV}$  at a scan rate of  $50 \text{ mV s}^{-1}$ . However, under the same condition, a pair of well-defined redox waves of UA was observed at the NEEs with  $\Delta E_p$  of  $37 \text{ mV}$ , thus the reversibility of UA redox at the NEEs was significantly improved. The oxidation peak of AA was broad and irreversible at about  $+0.282 \text{ V}$  at the bare glassy carbon electrode. In contrast, the peak potential shifted negatively to  $+0.009 \text{ V}$  at the NEEs. One possible reason why the NEEs effectively suppressed the response of AA is that the UA weakly adsorbs on the NEEs and undergoes a fast electron transfer reaction,  $k_s = 54 \text{ s}^{-1}$  [31]. And the voltammogram of UA (relatively fast electron transfer reaction) in the presence of AA (relatively slow electron transfer reaction) can

be resolved because of the kinetic differences in the response of the two substances [31–33]. Another possible reason is assigned to the carboxylic functional groups in the micropores. The carboxylic functional groups were introduced into walls of the pores during the fabrication of the NEEs. It is well-known that asymmetric, amphiphilic diblock copolymers can self-assemble to form aggregates in selective solvents [34]. The PS-*b*-PAA amphiphilic block copolymer has a hydrophobic PS block and a hydrophilic PAA block. These amphiphilic block copolymer molecules form micelles with a hydrophilic core (PAA) and a hydrophobic corona (PS) in the low polar media (THF), while aggregates with the opposite composition are present in solvents of high polarity (water). When water droplets condense onto the solution surface after THF evaporates, there is a process of phase inversion because PS-*b*-PAA contacts with the polar phase and the hydrophilic blocks remain extended to the walls of the pores. Therefore, the pores of the NEEs were inside full of carboxylic functional groups  $-\text{COO}^-$  ( $\text{p}K_a$  of PAA = 4.75 [35]). These functional groups can participate in charge-based interactions depending on the neutral pH of the electrolyte. And one possible chemical interaction could be the hydrogen bonding between the more acidic  $-\text{H}$  of the UA and the carboxyl group present in the nanopores [19].

The scan rate dependence on peak currents in the mixture of 0.05 mM UA and 0.5 mM AA was also studied at the NEEs. As the scan rate increased, the anodic peak current of UA increased and the anodic peak potential shifted slightly in the positive direction. A good linearity between the anodic peak current ( $i_{pa}$ ) of UA and the square root of scan rate ( $v^{1/2}$ ) was obtained over the range of  $50\text{--}1000 \text{ mV s}^{-1}$ , which demonstrated that the electrode reaction of UA was a diffusion-controlled process [36]. More evidences for the diffusion behavior of UA were demonstrated by the following experiments: when the NEEs was transferred into the 0.10 M PBS containing no UA after being used in the mixture of UA and AA, no peak signals were observed at all.

### 3.3. Effect of pH on the voltammetric response of UA and AA at the NEEs

The pH value of the base solution has a significant influence on the oxidation of UA and AA at the NEEs, by altering both the peak current and the peak potential. The effect of pH of the base solution on the peak current and potential was examined by recording differential pulse voltammograms (DPV) of UA and AA binary mixture in a series of PBS buffers of varying pH in the range of 1.3–13. The results were shown in Fig. 4. In general, both analytes gave higher response at more acidic solutions. For UA, there was a very interesting phenomenon. When pH varied between 1.3 and 5, the peak current decreased monotonically. But when pH was higher than 5, the peak response increased, and when pH was up to 7, it then sharply decreased. The similar pH response pattern was observed for AA. The peak current decreased monotonically between 1 and 8. When pH passed 8, it remained ascending, and when pH was up to 11, it then sharply decreased. If we calculated a relative ratio of the UA to AA currents as a function of pH, it exhibited a maximum around



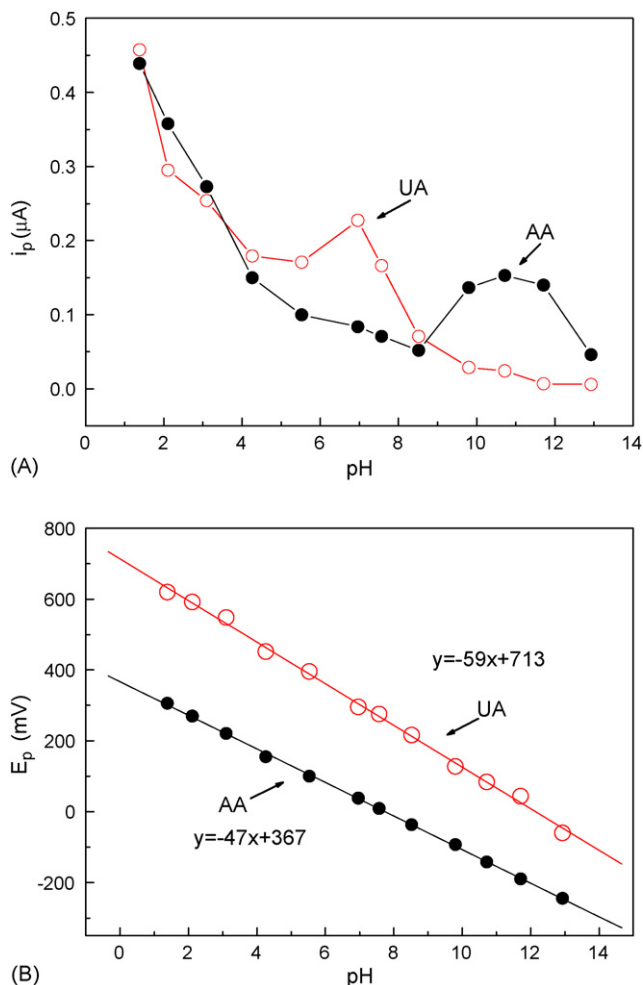


Fig. 4. Effect of pH on DPV peak current (A) and potential (B) of  $10\ \mu\text{M}$  UA and  $0.5\ \text{mM}$  AA on the NEEs. DPV was recorded with scan rate of  $5\ \text{mV s}^{-1}$ , pulse amplitude of  $50\ \text{mV}$ , pulse width of  $50\ \text{s}$  and pulse period of  $200\ \text{ms}$ .

neutral pH. This was a very important factor for the real sample analysis which must be performed at physiological pH.

In many cases, the reported  $i_p$ -pH dependencies were explained in terms of electrostatic interaction between ionic solution analytes and ionizable surface groups [18,37]. Hence, some gradual changes in peak currents were apparent at pHs close to characteristic  $\text{p}K_a$  values [37,38]. However, such effects were not apparent for the electrode studied in this work, which indicated that the interactions between the analyte and the electrode were different from those of electrostatic nature. And Milczarek and Ciszewski have also discovered above interesting phenomenon [37]. One possible reason is that the redox reactions of UA and AA take place in the different micro-environment in the presence of the carboxylic functional groups in the nanopores which affected the pH on the surface of the electrode. Fig. 4(B) showed that the oxidation peak potentials of UA and AA were linearly dependent on pH and the  $E_{\text{pa}}$  of them shifted to less positive potentials with the increasing pH from 1.3 to 13. And for UA, the slope of the  $E_p$ -pH dependence was  $-58.7\ \text{mV pH}^{-1}$ , which indicated that the total number of electrons and protons involved in the UA oxidation mechanism

was the same. As the oxidation of UA was a two-electron process, the number of protons involved was also predicted to be two [39].

### 3.4. Effect of accumulation time and accumulation potential on the voltammetric response of UA

The effect of accumulation potential and accumulation time on the DPV response for UA was studied. The accumulation step proceeded in constantly stirred solution and the voltage scanning step was performed after  $60\ \text{s}$  of quiet time. The peak current of UA increased very rapidly with the increasing accumulation time, which indicated that UA at the NEEs surface was rapid adsorption. After  $5\ \text{min}$ , further increase in the accumulation time did not increase the amount of UA on the electrode owing to surface saturation and the peak current remained almost constant. So,  $5\ \text{min}$  was selected as the accumulation time in this work. The effect of accumulation potential on the peak current of UA during the accumulation process was also examined. The peak current of UA was the highest at  $-0.2\ \text{V}$  as the accumulation potential. An accumulation potential of  $-0.2\ \text{V}$  was therefore chosen in all the subsequent work.

### 3.5. Calibration curve and detection limit

Fig. 5 showed the DPV responses of UA at the NEEs in  $0.10\ \text{M}$  PBS (pH 6.86) with different concentrations varied from  $1.5$  to  $60\ \mu\text{M}$ . Under the optimum detection conditions, the anodic peak currents were proportional to UA concentrations in the range of  $0.25$ – $50\ \mu\text{M}$  with the detection limit of  $0.04\ \mu\text{M}$  (three times the ratio of signal to noise). The linear equation was  $i_p\ (\mu\text{A}) = 0.0188c\ (\mu\text{M}) + 0.0122$  with the correlation coefficient of  $0.999$ . When the concentration of UA was higher than  $50\ \mu\text{M}$ , the current response decreased gradually and a plateau was observed, it was attributed to the saturation of UA at the NEEs.

### 3.6. Reproducibility

The lifetime of the NEEs was examined, and it demonstrated that the NEEs retained  $95.2\%$  of its initial response after 4 months of storage in pH 6.86 PBS. The lifetime of the electrode using serum samples was also investigated by experiment. After detecting the levels of UA in every five serum samples, the electrode was washed in pH 6.86 PBS under stirring and then transferred into a standard solution of  $10\ \mu\text{M}$  UA to record its oxidation peak current. The average current was  $0.198\ \mu\text{A}$  with the relative standard deviation (R.S.D.) of  $1.85\%$  ( $n = 5$ ). Such stability seemed to be acceptable for most practical applications. Because of the pores structure, UA and AA could easily penetrate into the interfacial layer that would affect the subsequent measurements. But it was found that the renewal of the electrode surface was easily accomplished by soaking the NEEs in pH 6.86 PBS and cycling its potential between  $-0.3$  and  $0.8\ \text{V}$  about 10 cycles under stirring. A quality control chart (X-chart) has been constructed. Fig. 6 showed the X-chart for the data of the anodic peak current of  $10\ \mu\text{M}$  UA applying the proposed



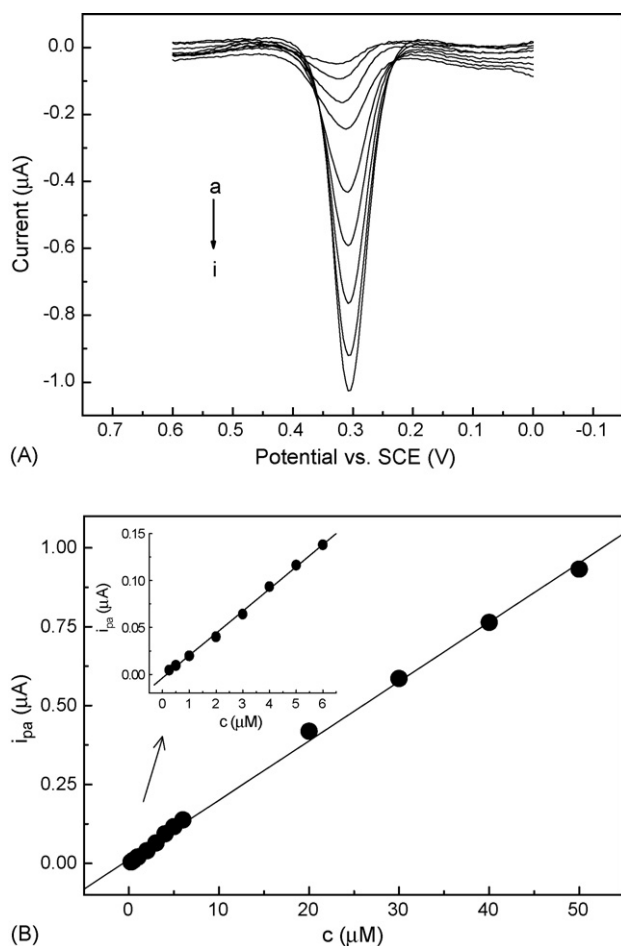


Fig. 5. (A) DPV responses of UA at the NEEs in 0.10 M PBS (pH 6.86). The concentration of UA: (a) 1.5, (b) 4, (c) 8, (d) 12, (e) 20, (f) 30, (g) 40, (h) 50, and (i) 60  $\mu\text{M}$ . (B) Plot of the anodic peak current vs. the concentration of UA.

method, where the X-axis represented the number of analyses while the Y-axis represented the anodic current of UA. There was a series of 15 points over the average score and all of them fell within the upper control limit (UCL) and the lower control limit (LCL), which indicated that the analysis progress was under the statistical control.

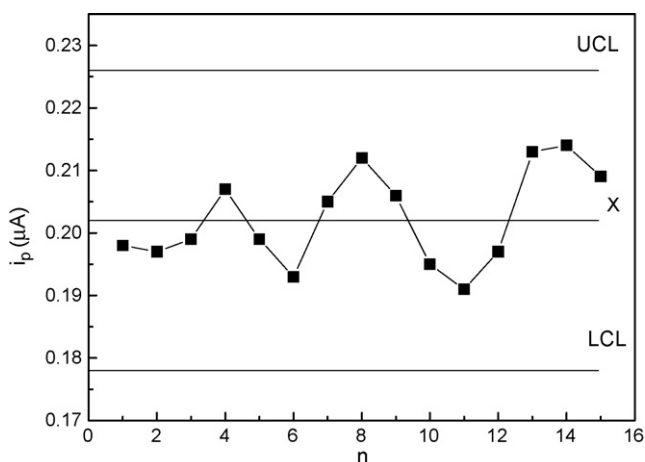


Fig. 6. Quality control chart (X-chart) for the anodic peak current of 10  $\mu\text{M}$  UA.

Table 1

The influence of the potential interferences on the voltammetric response of 5  $\mu\text{M}$  UA

Interferent	Concentration (mM)	Signal change ( $i_{\text{UA}} = 100\%$ ) (%)
AA	1.00	-0.83
AA	3.00	-2.55
AA	5.00	-3.62
Urea	0.05	-2.13
Glucose	5.00	+1.67
Levulose	2.50	-1.16
Cysteine	1.00	-2.92
DL-Tyrosine	1.00	+2.25
Oxalic acid	0.10	+0.49
Caffeine	1.00	-1.74
Purine	0.10	-2.29
NaCl	5.00	+1.32
KNO <sub>3</sub>	5.00	-0.71
Ca(NO <sub>3</sub> ) <sub>2</sub>	5.00	+3.43

### 3.7. Interference

For the follow special detection in the body fluid, a few possible interfering substances were examined for their influence on the voltammetric determination of 5  $\mu\text{M}$  UA. As AA is a serious interferent, its effect was investigated in detail previously. Other possible interferent substances, such as urea, glucose, levulose, cysteine, DL-tyrosine, oxalic acid, caffeine and purine were also examined. The effect of some inorganic compounds, such as NaCl, KNO<sub>3</sub>, Ca(NO<sub>3</sub>)<sub>2</sub> and so on was investigated, too. The results obtained were summarized in Table 1. As could be seen, most of these species did not interfere with the determination of UA.

### 3.8. Detection of UA in human urine and serum samples

Three human urine samples from volunteers were determined at the NEEs. To fit into the linear range and reduce the matrix effect, the urine samples were diluted 500 times with the 0.10 M PBS (pH 6.86) before analysis without further pretreatments. Standard addition method was employed in this test. A very sharp anodic peak was observed at +0.300 V when the urine sample was added into the PBS base solution. And the height of the peak quantitatively increased after the addition of a standard UA solution, which indicated conclusively that the anodic peak was caused by UA in the urine sample. The results obtained were listed in Table 2. And the recovery determined by spiking the urine samples with an amount of the standard UA solution was ranged from 97.9% to 101.3%. After multiplying by the dilution factor, the level of UA in the practical samples was ranged from 2.61 to 3.04 mM, which could be comparable with the results obtained previously by other research groups [37,40]. The determination of UA in human serum samples was also studied. The operating process was the same as that in the determination of UA in urine samples. The results obtained were listed in Table 2. In order to compare with the obtained results, uric acid has been determined in the same samples of human serum and urine by the standard enzyme coupling colorimetric method based on a

Table 2  
Determination of UA in urine and serum samples ( $n = 5$ ) with the NEEs<sup>a</sup>

Sample	Urine 1	Urine 2	Urine 3	Serum 1	Serum 2	Serum 3
Detected ( $\mu\text{M}$ )	$5.22 \pm 0.10$	$6.07 \pm 0.15$	$5.46 \pm 0.11$	$15.04 \pm 0.38$	$19.52 \pm 0.54$	$11.95 \pm 0.27$
Spike ( $\mu\text{M}$ )	10	10	10	10	10	10
Found ( $\mu\text{M}$ )	$15.42 \pm 0.39$	$15.73 \pm 0.49$	$15.24 \pm 0.30$	$23.86 \pm 0.65$	$30.64 \pm 0.92$	$21.75 \pm 0.53$
Average recovery (%)	101.3	97.9	98.6	95.3	103.8	99.1
Total value <sup>b</sup> (mM)	$2.61 \pm 0.05$	$3.04 \pm 0.07$	$2.73 \pm 0.07$	$0.301 \pm 0.007$	$0.391 \pm 0.012$	$0.239 \pm 0.005$
Enzyme coupling colorimetric method (mM)	2.39	3.20	2.97	0.309	0.381	0.247

<sup>a</sup> The level of confidence is 95%.

<sup>b</sup> Total value was obtained by multiplying the detected value and the dilution factor.

Table 3  
Results obtained in the UA analysis in three certified reference materials (CRMs)

CRMs sample	Number of analysis	Measured value (mM)	Certified value (mM)
KEHUA DONGLING <sup>®</sup> UA KIT 20051122	5	$0.586 \pm 0.029$	0.590
Human <sup>®</sup> UA Standard LOT 098B	5	$0.471 \pm 0.031$	0.476
SERODOS <sup>®</sup> Quality control serum, LOT 6869A	5	$0.269 \pm 0.020$	0.250

certified, clinical chemistry fully automated analyzer (Human Autohumalzer 900s plus, Germany) in the hospital center of Yangzhou University. The fully automated analyzer was operated by an analyst with well-documented inspection procedures. The enzyme coupling colorimetric method has been regarded as a most reliable, convenient and trouble-free method for the clinical determination of UA in plasma, serum or diluted urine samples [41–43]. The method involves the use of 4-aminoantipyrene as a color coupler with sulphonated dichlorophenol for detection of the hydrogen peroxide, which was produced by the uricase-catalyzed oxidation of uric acid. The hydrogen peroxidase and peroxidase are used for the coupling of 4-aminoantipyrene and sulphonated dichlorophenol to form a red quinoneimine dye. The red quinoneimine dye has the maximum absorbance at 520 nm [44,45]. The change in absorbance is directly proportional to the concentration of uric acid in the sample. The experimental results from the proposed method are coincident with those obtained from the enzyme coupling colorimetric method. Additionally, in order to properly validate the proposed procedure, some commercially available certified reference materials (CRMs) were determined by the proposed method. The results for the three CRMs were given in Table 3, indicating the measured values were in excellent agreement with the certified values.

#### 4. Conclusions

We firstly described a simple, facile, one-step approach to fabricate nanoelectrode ensembles formed by controlled nanopores polymeric thin film of an amphiphilic diblock copolymer, polystyrene-block-poly (acrylic acid). This procedure is simple

and fast, and requires only conventional, inexpensive electrochemical instrumentation. Electrochemical methods were used to characterize the NEEs prepared using this new procedure. The NEEs drastically suppressed the response of AA and resolved the overlapping voltammetric response of UA and AA into two well-defined peaks with a large anodic peak difference ( $\Delta E_{pa}$ ) of about 310 mV. The peak current obtained from DPV was linearly dependent on the UA concentration in the range of 0.25–50  $\mu\text{M}$  in 0.10 M PBS (pH 6.86) with a correlation coefficient of 0.999, and the detection limit was 0.04  $\mu\text{M}$  (S/N = 3). The assay method is simple, precise, relatively inexpensive, and rapid. The NEEs has also been demonstrated to be applicable in the detection of UA in serum and urine samples with excellent sensitivity and selectivity. The NEEs will hopefully be of good application for further sensor development.

#### Acknowledgements

This work was supported by the National Natural Science Foundation of China (no. 20375034) and the Novel Foundation of Jiangsu Provincial Education Department for Doctors (2005). We thank Hailin Ge (the hospital centre of Yangzhou University) for technical assistance.

#### References

- [1] C.G. Zoski, *Electroanalysis* 14 (2002) 1041.
- [2] C.Y. Wang, X.Y. Hu, *Talanta* 68 (2006) 1322.
- [3] E. Bakker, *Anal. Chem.* 76 (2004) 3285.
- [4] C.R. Yonzon, D.A. Stuart, X.Y. Zhang, A.D. McFarland, C.L. Haynes, R.P. Van Duyne, *Talanta* 67 (2005) 438.
- [5] D.W.M. Arrigan, *Analyst* 129 (2004) 1157.
- [6] A.A. Karyakin, E.A. Puganova, I.A. Budashov, I.N. Kurochkin, E.E. Karyakina, V.A. Levchenko, V.N. Matveyenko, S.D. Varfolomeyev, *Anal. Chem.* 76 (2004) 474.
- [7] R.M. Penner, C.R. Martin, *Anal. Chem.* 59 (1987) 2625.
- [8] V.P. Menon, C.R. Martin, *Anal. Chem.* 67 (1995) 1920.
- [9] W.L. Cheng, S.J. Dong, E.K. Wang, *Anal. Chem.* 74 (2002) 3599.
- [10] W.S. Baker, R.M. Crooks, *J. Phys. Chem.* 102 (1998) 10041.
- [11] S.E. Creager, P.T. Radford, *J. Electroanal. Chem.* 500 (2001) 21.
- [12] J. Koehne, J. Li, A.M. Cassell, H. Chen, Q. Ye, H.T. Ng, J. Han, M. Meyyappan, *J. Mater. Chem.* 14 (2004) 676.
- [13] Y.H. Lin, F. Lu, Y. Tu, Z.F. Ren, *Nano Lett.* 4 (2004) 191.
- [14] E. Jeoung, T.H. Galow, J. Schotter, M. Bal, A. Ursache, M.T. Tuominen, C.M. Stafford, T.P. Russell, V.M. Rotello, *Langmuir* 17 (2001) 6396.
- [15] J. Li, J.E. Koehne, A.M. Cassell, H. Chen, H.T. Ng, Q. Ye, W. Fan, J. Han, M. Meyyappan, *Electroanalysis* 17 (2005) 15.

- [16] T. Nakaminami, S. Ito, S. Kuwabata, H. Yoneyama, *Anal. Chem.* 71 (1999) 4278.
- [17] T. Hoshi, H. Saiki, J. Anzai, *Talanta* 61 (2003) 363.
- [18] P.R. Roy, T. Okajima, T. Ohsaka, *J. Electroanal. Chem.* 561 (2004) 75.
- [19] J.M. Zen, J.J. Jou, G. Ilangovan, *Analyst* 123 (1998) 1345.
- [20] Z.H. Wang, Y.M. Wang, G.A. Luo, *Analyst* 127 (2002) 1353.
- [21] C.R. Raj, T. Ohsaka, *J. Electroanal. Chem.* 540 (2003) 69.
- [22] P. Ramesh, S. Sampath, *Electroanalysis* 16 (2004) 866.
- [23] G. Widawski, M. Rawiso, B. Francois, *Nature* 369 (1994) 387.
- [24] O. Karthaus, N. Maruyama, X. Cieren, M. Shimomura, H. Hasegawa, T. Hashimoto, *Langmuir* 16 (2000) 6071.
- [25] O. Pitois, B. Francois, *Eur. Phys. J. B* 8 (1999) 225.
- [26] M. Srinivasarao, D. Collings, A. Philips, S. Patel, *Science* 292 (2001) 79.
- [27] K. Hirota, K. Tajima, K. Hashimoto, *Langmuir* 21 (2005) 11592.
- [28] X. Cai, K. Kalcher, C. Neuhold, B. Ogorevc, *Talanta* 41 (1994) 407.
- [29] E. Gonzalez, F. Pariente, E. Lorenzo, L. Hernandez, *Anal. Chim. Acta* 242 (1991) 267.
- [30] Z.Q. Gao, H. Huang, *Chem. Commun.* 19 (1998) 2107.
- [31] R. Bravo, C.C. Hsueh, A. Jaramillo, A. Brajter-Toth, *Analyst* 123 (1998) 1625.
- [32] A. Brajter-Toth, K.A. El-Nour, E.T. Cavaleiro, R. Bravo, *Anal. Chem.* 72 (2000) 1576.
- [33] C.C. Hsueh, A. Brajter-Toth, *Anal. Chem.* 65 (1993) 1570.
- [34] S.E. Burke, A. Eisenberg, *Langmuir* 17 (2001) 6705.
- [35] M.K. Chun, C.S. Cho, H.K. Choi, *J. Appl. Polym. Sci.* 94 (2004) 2390.
- [36] E. Laviron, *J. Electroanal. Chem.* 101 (1979) 19.
- [37] G. Milczarek, A. Ciszewski, *Electroanalysis* 16 (2004) 1977.
- [38] A. Ciszewski, G. Milczarek, *Anal. Chem.* 71 (1999) 1055.
- [39] L. Zhang, X.Q. Lin, *Analyst* 126 (2001) 367.
- [40] J.M. Zen, Y.J. Chen, C.T. Hsu, Y.S. Ting, *Electroanalysis* 9 (1997) 1009.
- [41] P. Trinder, *Ann. Clin. Biochem.* 6 (1969) 24.
- [42] N.W. Tietz, *Clinical Guide to Laboratory Tests*, 2nd ed., Saunders Co., 1991.
- [43] D.S. Young, *Effects of Drugs on Clinical Laboratory Tests*, 4th ed., AACC Press, 1995.
- [44] P. Fossati, L. Prencipe, G. Berti, *Clin. Chem.* 26 (1980) 227.
- [45] G.T.B. Sanders, A.J. Pasman, F.J. Hoek, *Clin. Chim. Acta* 101 (1980) 299.

# Flow injection determination of thyroxine in pharmaceutical preparations using tris(2,2'-bipyridyl)ruthenium(III)–NADH chemiluminescence detection

Amir Waseem, Mohammad Yaqoob, Abdul Nabi \*

*Department of Chemistry, University of Balochistan, Quetta, Pakistan*

Received 5 January 2006; received in revised form 6 March 2006; accepted 6 March 2006

Available online 18 April 2006

## Abstract

A flow injection (FI) method is reported for the determination of thyroxine based on its enhancement of chemiluminescence (CL) from the Ru(bpy)<sub>3</sub><sup>3+</sup>–NADH system. The calibration graph was linear over the range 2.0–10 × 10<sup>−8</sup> mol L<sup>−1</sup> (*r*<sup>2</sup> = 0.9989) with relative standard deviations (R.S.D.) in the range 2.0–4.5% (*n* = 4). The limit of detection (3σ blank) was 1.0 × 10<sup>−9</sup> mol L<sup>−1</sup> with sample throughput of 120 h<sup>−1</sup>. The effect of some organic compounds, anions and cations were studied for L-thyroxine determination. The method was applied to pharmaceutical preparations and the results obtained were in reasonable agreement with the amount labeled. The method was statistically compared with the results obtained by RIA; no significant disagreement at 95% confidence limit was observed. A calibration graph of NADH over the range 1.3 × 10<sup>−8</sup>–1.3 × 10<sup>−6</sup> mol L<sup>−1</sup> was also established (*r*<sup>2</sup> = 0.9992) with R.S.D. in the range 1.0–3.5% (*n* = 4). The limit of detection (3σ) was 1.0 × 10<sup>−10</sup> mol L<sup>−1</sup> NADH.

© 2006 Elsevier B.V. All rights reserved.

**Keywords:** Flow injection analysis; Chemiluminescence; Thyroxine; NADH; Pharmaceuticals

## 1. Introduction

Thyroxine hormones (3,5,3',5'-tetraiodothyronine, T4, & 3,5,3'-triiodothyronine, T3) secreted by the pituitary gland are compounds of major biological role as they are critically important for the normal development of the central nervous system in infants, the skeletal growth and the maturation in children as well as for the normal function of multiple organ systems in adults. These important hormones produced by the thyroid gland are synthesized from L-tyrosine residues in thyroglobulin, a dimeric glycoprotein that constitutes the bulk of the thyroid follicles [1,2]. Tetraiodothyronine and triiodothyronine also acts as a metabolic stimulant on respiring cells in vitro; it uncouples oxidative phosphorylation, i.e. increase oxygen consumption without generation adenosine 5'-triphosphate. Thyroid dysfunction is reflected by hypo- and hyper-thyroidism [3].

Chemiluminescence (CL) is the emission of electromagnetic radiation (ultraviolet, visible or infrared) as consequence of

chemical reactions at room temperature and observed in gas, liquid and gas phases. Two primary requirements for this emission are involved (i) the emission of energy released should be higher than that of the electronically excited product or intermediate molecule and (ii) the product must be a fluorescent molecule so that the transformation of the excited molecule to the ground state is accompanied by visible light emission or the reaction mixture has to include energy acceptor molecules with fluorescent properties [4]. The use of CL as a detection system relates to its high sensitivity and the simple instrumentation. No light source is required for CL as compared to absorption techniques and fluorimetry. Its rapid development is reflected to great numbers of publications devoted entirely to the discussion of CL [5–7].

Tris(2,2'-bipyridyl)ruthenium(II) [Ru(bpy)<sub>3</sub><sup>2+</sup>] in acidic solution has been observed to produce a bright orange emission [8] oxidised by solid lead dioxide and subsequently coupled with hydroxide/hydrazine which in turn producing [Ru(bpy)<sub>3</sub><sup>2+</sup>]\* excited state for the light emission at 610 nm [9]. Since then, Ru(bpy)<sub>3</sub><sup>3+</sup> chemiluminescence (CL) has emerged as a versatile detection method for flow injection analysis [10–12] and liquid chromatography [13–15]. A comprehensive and critical review

\* Corresponding author. Tel.: +92 81 9211266; fax: +92 81 9211277.

E-mail address: [nabiabdul@hotmail.com](mailto:nabiabdul@hotmail.com) (A. Nabi).

of the analytical applications of  $\text{Ru}(\text{bpy})_3^{3+}$  as a CL reagent has been published [16].

Various methods have been reported for the determination of thyroxine in pharmaceutical preparations and body fluids. These include; immunoassays [17–19], electrochemical [20,21], HPLC [22,23], GC–MS [24], fluorescence [25], bioluminescence [26] and electrochemiluminescence [27,28]. However, some of these methods involve several minutes per assay cycle with an incubation time of 20–25 min, lengthy procedure of column preparation, use of radioactive materials, enzymes and fluorophores, preparation of working electrodes, expensive instrumentation, complicated operation and low sample throughput.

FI-spectrophotometric method has been reported for the determination of thyroxine to be an inhibitor of glutamate dehydrogenase [29]. The change in NADH absorbance at 340 nm in the presence of the enzyme and thyroxine is measured on-line related to the percent inhibition. The relative standard deviation for  $8.0 \times 10^{-6} \text{ mol L}^{-1}$  thyroxine is 1.8% ( $n=7$ ) with limit of detection ( $3\sigma$ )  $9.0 \times 10^{-7} \text{ mol L}^{-1}$  thyroxine. Another flow injection-CL method based on the catalytic effect of cobalt(II) on CL reaction between luminol and hydrogen peroxide and the quenching of the emission intensity by thyroxine has been reported [30]. The limits of detection ( $3s$ ) are  $3.04 \times 10^{-5}$  and  $2.6 \times 10^{-5} \text{ mol L}^{-1}$  for D- and L-thyroxine, respectively with sample throughput of  $<30 \text{ h}^{-1}$ . These inhibition methods have poor detection limits, low sample throughput and limited linearity. Table 1, reports comparison of various methods for determination of L-thyroxine in terms of sample matrix, limit of detection and sampling rate.

The production of NADH through appropriate dehydrogenases has been used for a variety of analytes, e.g., glucose, ethanol, L-lactate and cholesterol based on ECL detection system [31,32]. In the present study a simple and rapid method is reported for the determination thyroxine by its enhancement effect on  $\text{Ru}(\text{bpy})_3^{3+}$ -NADH CL reaction.  $\text{Ru}(\text{bpy})_3^{2+}$  is chemically oxidized to  $\text{Ru}(\text{bpy})_3^{3+}$  by using lead dioxide column. The proposed method has the limit of

detection ( $3\sigma$ )  $1.0 \times 10^{-9} \text{ mol L}^{-1}$  with sample throughput of  $120 \text{ h}^{-1}$ .

## 2. Experimental

### 2.1. Reagents

All glass ware used during the experiments and for storage of reagents and standards was pre-cleaned with 30% HCl for 48 h, thoroughly rinsed with ultra high purity (UHP) deionized water ( $18.2 \text{ M}\Omega \text{ cm}^{-1}$ , Elgastat, Maxima, UK), stored in plastic bags to prevent contamination and used as required. All reagents were of analytical grade, supplied by Merck BDH, unless stated otherwise and solutions were prepared in ultra high purity (UHP) deionised water.

Tris(2,2'-bipyridyl)ruthenium(II) chloride stock solution ( $1.0 \times 10^{-3} \text{ mol L}^{-1}$ ) was prepared by dissolving 0.064 g of  $\text{Ru}(\text{bpy})_3^{2+}$  (Sigma) in aqueous solution of sulfuric acid ( $1.5 \times 10^{-2} \text{ mol L}^{-1}$ ). A working  $\text{Ru}(\text{bpy})_3^{2+}$  solution ( $1.0 \times 10^{-4} \text{ mol L}^{-1}$ ) was prepared by diluting 10.0 mL of the stock solution to 100 mL with aqueous solution of sulfuric acid ( $1.5 \times 10^{-2} \text{ mol L}^{-1}$ ).  $\beta$ -Nicotinamide adenine dinucleotide (NADH, Sigma) stock solution ( $1.0 \times 10^{-3} \text{ mol L}^{-1}$ ) was prepared by dissolving 0.071 g of NADH in 100 mL of phosphate buffer ( $5.0 \times 10^{-3} \text{ mol L}^{-1}$ , pH 8.0). A working solution ( $1.0 \times 10^{-6} \text{ mol L}^{-1}$ ) was prepared by diluting the required volume of the stock in 100 mL of phosphate buffer ( $5.0 \times 10^{-3} \text{ mol L}^{-1}$ , pH 8.0). L- and D-thyroxine (3,5,3',5'-tetraiodothyronine, sodium salt, Fluka) stock solutions ( $1.0 \times 10^{-3} \text{ mol L}^{-1}$ ) were prepared by dissolving the required amount of each separately in 100 mL of sodium hydroxide ( $0.01 \text{ mol L}^{-1}$ ), ultrasonicated at room temperature for 10 min and working standards were prepared by suitable dilution in phosphate buffer ( $5.0 \times 10^{-3} \text{ mol L}^{-1}$ , pH 8.0) as required. Stock solutions ( $1.0 \times 10^{-3} \text{ mol L}^{-1}$  and 0.1%) of organic compounds, anions and cations were prepared in UHP water and various working solutions were prepared from these stocks for interference studies. All solutions were protected from light and stored at  $4^\circ\text{C}$  and used whenever required.

Table 1  
Comparison of various methods with the reported method for determination of L-thyroxine

Detection technique	Matrix	Limit of detection ( $\text{mol L}^{-1}$ )	Sampling rate ( $\text{h}^{-1}$ )	Reference
HPLC/CL	Standard solutions	$1.0 \times 10^{-11}$	40	[18]
SIA/CL	Plasma	$5.4 \times 10^{-11}$	12	[19]
Electrochemical	Drugs	$6.5 \times 10^{-9}$	12	[20]
SIA/electrochemical	Pharmaceutical formulations	$1.1 \times 10^{-11}$	20	[21]
Ion chromatography	Urine	N/G	15	[22]
HPLC/UV	Pharmaceutical and biological samples	$2.25 \times 10^{-5}$	<03	[23]
GC/MS	Plasma	$5.62 \times 10^{-8}$	08	[24]
Fluorometry	Serum	$\sim 1.07 \times 10^{-12}$	N/G	[25]
Bioluminescence	Mutant photoprotein	$5.0 \times 10^{-12}$	N/G	[26]
ECL	Serum	$<3.0 \times 10^{-13}$	<04	[28]
FIA/spectrophotometry	Standard solutions	$9.0 \times 10^{-7}$	N/G	[29]
FIA/CL	Standard solutions	$2.58 \times 10^{-5}$	<30	[30]
FIA/CL	Pharmaceutical preparations	$1.0 \times 10^{-9}$	120	Reported method

N/G = not given; CL = chemiluminescence; SIA = sequential injection analysis; EC = electrochemical; ECL = electrochemiluminescence.



Thyroxine tablets were obtained from (Glaxo-Wellcome, Pakistan), eltroxin (Glaxo-Wellcome, New Zealand), synthroid (Abbott Laboratories, USA) and thyro-4 tablets (Faran, Greece), labeled to contain 50  $\mu\text{g}$  of levothyroxine sodium salt (L-thyroxine sodium) per tablet respectively.

## 2.2. Lead dioxide column

An acid washed glass column (10 mm  $\times$  4.0 mm, i.d.) was packed with solid lead dioxide plugged with cleaned cotton wool at both ends and connected to the flow injection manifold with silicone tubing. The packed tube was washed with a stream of water for 30 min and incorporated in-line within the FI-CL system for  $\text{Ru}(\text{bpy})_3^{2+}$  oxidation as reported previously [33].

## 2.3. Instrumentation

The flow injection-chemiluminescence manifold used for this work is shown in Fig. 1. A peristaltic pump (Ismatec Reglo 100, four-channels, Switzerland) was used to deliver the sample carrier and reagent solutions at a flow rate of 1.6  $\text{mL min}^{-1}$ . A rotary injection valve (Rheodyne 5020, Anachem, Luton, UK) was used to inject thyroxine standards (120  $\mu\text{L}$ ) into phosphate buffer (5.0  $\times 10^{-3}$   $\text{mol L}^{-1}$ , pH 8.0) stream and merged with a stream of NADH (1.0  $\times 10^{-6}$   $\text{mol L}^{-1}$  prepared in phosphate buffer 5.0  $\times 10^{-3}$   $\text{mol L}^{-1}$ , pH 8.0). This stream was then merged at a T-piece with an other reagent stream of  $\text{Ru}(\text{bpy})_3^{3+}$  chemiluminescence obtained by passing  $\text{Ru}(\text{bpy})_3^{2+}$  through a solid lead dioxide column (10 mm  $\times$  4.0 mm i.d.) used for the oxidation. The merged stream traveled 3.0 cm before passing through a glass coil spiral flow cell (1.1 mm i.d., 130  $\mu\text{L}$  internal volume) placed directly in front of an end window photomultiplier tube (PMT, 9798B, Electron Tubes, Ruislip, UK). The PMT, glass coil and T-piece were enclosed in a light tight housing [34]. The PMT was maintained at an operating voltage of 1020 V using Burle High Voltage Power Supply (2 kV, Type PF 1053, USA). The PMT output was recorded using a chart recorder (Kipp & Zonen BD 40, Switzerland).

The same manifold (Fig. 1) was used for the determination of NADH except that L-thyroxine solution (5.6  $\times 10^{-7}$   $\text{mol L}^{-1}$ ) prepared in phosphate buffer (5.0  $\times 10^{-3}$   $\text{mol L}^{-1}$ , pH 8.0)

was used as a stream, while NADH standard solutions were injected.

## 3. Results and discussions

### 3.1. Optimisation of the FI manifold

In order to establish optimal conditions for the lowest possible detection limit of thyroxine, the effect of various parameters was investigated. These were the phosphate buffer pH (6.5–8.5), NADH,  $\text{Ru}(\text{bpy})_3^{2+}$  and sulphuric acid concentrations, sample volume (30–180  $\mu\text{L}$ ), flow rate (0.35–2.3  $\text{mL min}^{-1}$ ) and solid lead dioxide column length (5.0–20 mm  $\times$  4.0 mm, i.d.). All of these studies were performed with a 5.6  $\times 10^{-7}$   $\text{mol L}^{-1}$  L-thyroxine standard solution and a detector (PMT) voltage of 1020 V.

The effect of  $\text{Ru}(\text{bpy})_3^{2+}$  concentration on the determination of thyroxine was studied over the range 5.0  $\times 10^{-6}$ –1.0  $\times 10^{-3}$   $\text{mol L}^{-1}$ . The CL intensity increased up to 1.0  $\times 10^{-4}$   $\text{mol L}^{-1}$ , above this noisy and irreproducible signals were observed. A  $\text{Ru}(\text{bpy})_3^{2+}$  concentration of 1.0  $\times 10^{-4}$   $\text{mol L}^{-1}$  was therefore used for all subsequent experiments. Similarly, the effect of sulfuric acid was investigated in the range 1.0  $\times 10^{-3}$ –2.0  $\times 10^{-2}$   $\text{mol L}^{-1}$  as shown in Fig. 2a and 1.5  $\times 10^{-2}$   $\text{mol L}^{-1}$  gave maximum CL response which was used for all further studies. In the proposed FI-CL system, the effect of phosphate buffer pH in the range 6.5–8.5 and concentration 1.0  $\times 10^{-3}$ –5.0  $\times 10^{-2}$   $\text{mol L}^{-1}$  was investigated in the sample and NADH carrier streams. Maximum CL responses was observed at pH 8.0 and concentration of 5.0  $\times 10^{-3}$   $\text{mol L}^{-1}$  as shown in Fig. 2(b and c) and were used for all subsequent studies. The effect of NADH concentration was studied over the range 1.0  $\times 10^{-7}$ –2.6  $\times 10^{-6}$   $\text{mol L}^{-1}$  prepared in phosphate buffer (5.0  $\times 10^{-3}$   $\text{mol L}^{-1}$ , pH 8). There was an increase in CL signal with increase in NADH concentration up to 1.0  $\times 10^{-6}$   $\text{mol L}^{-1}$  with a stable base line and was used for further studies.

The effect of flow rate and sample volume on the CL response was calibrated in terms of sensitivity, speed and reagent consumption. Flow rates for each of the three channels were simultaneously studied over the range 0.35–2.3  $\text{mL min}^{-1}$ . Maximum CL response was observed at a flow rate of 1.6  $\text{mL min}^{-1}$  with a steady baseline and reproducible peak height (R.S.D. < 2.0%;  $n = 4$ ). The optimum flow rate (1.6  $\text{mL min}^{-1}$ ) depends on the distance from the T-piece to glass coil placed in the front of PMT which in this case is 3.0 cm. The effect of sample injection volume on the sensitivity of the flow system was studied in range 30–180  $\mu\text{L}$ . Maximum CL signal was observed at 120  $\mu\text{L}$  and was used for further studies.

The in-line conversion of  $\text{Ru}(\text{bpy})_3^{2+}$  to  $\text{Ru}(\text{bpy})_3^{3+}$  was achieved chemically by using solid lead dioxide column. The effect of column length in the range (5.0–20 mm  $\times$  4.0 mm, i.d.) was investigated for continuous conversion of  $\text{Ru}(\text{bpy})_3^{2+}$  to  $\text{Ru}(\text{bpy})_3^{3+}$  for the determination of thyroxine. Maximum CL response was achieved by using a column (10 mm  $\times$  4.0 mm, i.d.) of solid lead dioxide. Approximately, 4 L of  $\text{Ru}(\text{bpy})_3^{2+}$  solution was passed through this column and no significant

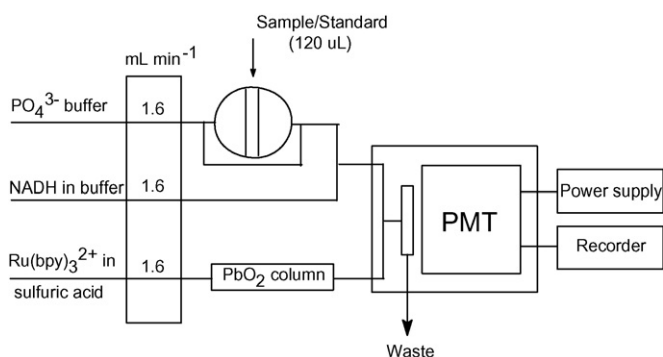


Fig. 1. Flow injection-chemiluminescence (FI-CL) manifold for the determination of thyroxine.

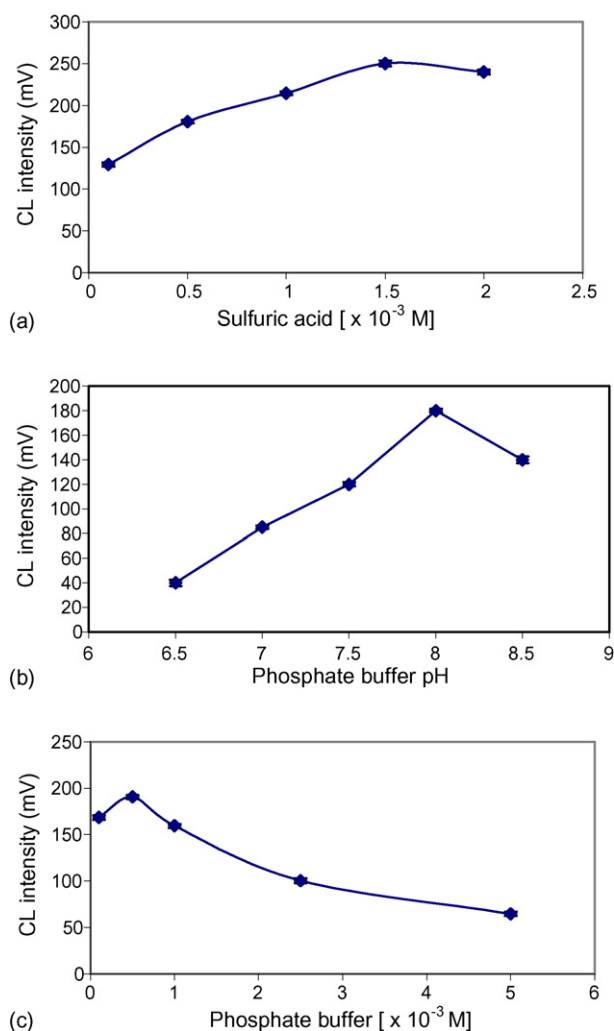


Fig. 2. Variation of CL intensity with: (a) concentration of sulfuric acid, (b) phosphate buffer pH and (c) concentration. For optimizing each parameter the optimized conditions for all other parameters were used, i.e., flow rates  $1.6 \text{ mL min}^{-1}$  for all the three channels; sample volume  $120 \mu\text{L}$ ; concentrations of  $\text{Ru}(\text{bpy})_3^{2+}$  ( $1.0 \times 10^{-4} \text{ mol L}^{-1}$ ); NADH ( $1.0 \times 10^{-6} \text{ mol L}^{-1}$ ) and phosphate buffer ( $5.0 \times 10^{-3} \text{ mol L}^{-1}$ , pH 8.0).

decrease in CL response was observed in the conversion process.

### 3.2. Analytical figures of merit

The calibration graph of CL intensity versus concentration of L-thyroxine over the range  $2.0\text{--}10 \times 10^{-8} \text{ mol L}^{-1}$  was obtained ( $r^2 = 0.9989$ ;  $n = 5$ ) with regression equation  $y = 6.65x - 0.7$ , ( $y = \text{CL response (mV)}$ ,  $x = \text{concentration (M)}$ , L-thyroxine). The relative standard deviation (R.S.D.) was 2.0–4.5% ( $n = 4$ ) over the range studied and the limit of detection ( $3\sigma$ ) was  $1.0 \times 10^{-9} \text{ mol L}^{-1}$  D- and L-thyroxine with a sample throughput of  $120 \text{ h}^{-1}$ .

A linear calibration graph of CL intensity versus concentration of NADH over the range  $1.3 \times 10^{-8}\text{--}1.3 \times 10^{-6} \text{ mol L}^{-1}$  was also obtained ( $r^2 = 0.9992$ ;  $n = 6$ ). The R.S.D. was 1.0–3.5% ( $n = 4$ ) over the range studied and the limit

of detection ( $3\sigma$ ) was  $1.0 \times 10^{-10} \text{ mol L}^{-1}$ . L-Thyroxine solution ( $5.6 \times 10^{-7} \text{ mol L}^{-1}$ ) prepared in phosphate buffer ( $5.0 \times 10^{-3} \text{ mol L}^{-1}$ , pH 8.0) was used as a stream in place of NADH (see Fig. 1).

### 3.3. Interference studies

The effect of various organic compounds, anions and cations on the blank signal (in the absence of thyroxine) and on the determination of L-thyroxine ( $2.0 \times 10^{-8} \text{ mol L}^{-1}$ ) is given in Table 2. Fructose, urea and pyruvate had no significant effect. Ascorbic acid and sucrose have slight enhancing effect on blank signal. Lactose, uric acid, starch, gum acacia and cellulose had significant enhancing effect on both the CL signal blank and on the thyroxine response, possibly due to the use of high concentrations of these interferents. Cations including potassium, calcium, magnesium, iron(II), zinc(II), and copper(II) had no significant effect while lead(II); ( $4.8 \times 10^{-6} \text{ mol L}^{-1}$ ) slightly enhanced CL signals with and without thyroxine. Anions such as sulfate, chloride and fluoride has no significant effect while iodide cause serious interference at low concentrations. Iodide could be removed by using on-line anion exchange column.

### 3.4. Application to pharmaceutical preparations

The proposed method was applied to commercially available L-thyroxine tablets; thyroxine (Glaxo-wellcome Pakistan), eltroxin (Glaxo-wellcome, New Zealand), synthroid (Abbott laboratories, USA) and thyro-4 tablets (Faran, Greece). The sample was prepared by dissolving each tablet in 50 mL of sodium hydroxide ( $0.01 \text{ mol L}^{-1}$ ), sonicated for 10 min at room temperature, undissolved particles were removed by filtration, diluted 10 times with phosphate buffer ( $5.0 \times 10^{-3} \text{ mol L}^{-1}$ , pH 8), and directly used for injection. The results obtained (in the range  $48.8 \pm 2.5$  to  $52.2 \pm 1.5 \mu\text{g}$  L-thyroxine per tablet) were in reasonable agreement with the amount labeled. Thyroxine tablet (Glaxo-wellcome, Pakistan) was analysed in another laboratory by RIA method and the result is compared statistically with the proposed method as shown in Table 3. No significant difference was found between the results of the two methods at 95% confidence limit.

### 3.5. Possible reaction mechanism

$\text{Ru}(\text{bpy})_3^{3+}$  solution was generated off-line by adding lead dioxide (0.2 g) to  $\text{Ru}(\text{bpy})_3^{2+}$  (30 mL) followed by vigorous mixing as reported previously [33]. The resultant suspension was allowed to settle prior to filtering through Whatman filter paper No. 41. The CL spectra of  $\text{Ru}(\text{bpy})_3^{3+}$ –NADH reaction in the presence and absence of thyroxine were scanned using a fluorescence spectrophotometer (RF-1501, Shimadzu, Japan) as shown in Fig. 3. Both spectra had same maximum emission wavelength at 595 nm, which suggested that they had same emitter  $\text{Ru}(\text{bpy})_3^{2+}$  [32]. The detailed reaction mechanism between NADH and  $\text{Ru}(\text{bpy})_3^{3+}$  may involve the production of active intermediate  $\text{NAD}^\bullet$  [35]. Thyroxine may increase the rate of this

Table 2  
Effect of various organic compounds, anions and cations on the blank signal (in the absence of L-thyroxine) and on the determination of L-thyroxine ( $n=4$ )

Compound/anions/cations	Concentration (mol L <sup>-1</sup> )	Response without L-thyroxine (mV)	Response with L-thyroxine ( $2.0 \times 10^{-8}$ mol L <sup>-1</sup> ) (mV)
Blank (buffer)	$5.0 \times 10^{-3}$	$0.2 \pm 0.02$	$10.2 \pm 0.23$
Ascorbic acid	$1.0 \times 10^{-6}$	$2.3 \pm 0.18$	$9.7 \pm 0.74$
Fructose	$5.0 \times 10^{-4}$	$1.0 \pm 0.12$	$10.0 \pm 0.22$
Sucrose	$3.0 \times 10^{-4}$	$2.3 \pm 0.30$	$9.0 \pm 0.41$
Pyruvate	$1.0 \times 10^{-6}$	$0.4 \pm 0.10$	$9.0 \pm 0.22$
Urea	$1.0 \times 10^{-4}$	$0.35 \pm 0.17$	$9.7 \pm 0.30$
Uric acid	$1.0 \times 10^{-6}$	$19.5 \pm 0.56$	$23.0 \pm 0.45$
Lactose	$3.0 \times 10^{-4}$	$10.2 \pm 0.23$	$14.3 \pm 0.34$
Starch	0.01%	$10.8 \pm 0.66$	$15.6 \pm 0.60$
Gum acacia	0.01%	$10.1 \pm 0.40$	$14.1 \pm 0.43$
Cellulose	0.01%	$4.3 \pm 0.32$	$14.4 \pm 0.45$
Potassium	$6.4 \times 10^{-4}$	$1.0 \pm 0.17$	$11.3 \pm 0.33$
Calcium	$2.5 \times 10^{-4}$	$0.6 \pm 0.01$	$11.0 \pm 0.32$
Magnesium	$1.0 \times 10^{-3}$	$1.0 \pm 0.28$	$10.6 \pm 0.23$
Iron(II)	$1.8 \times 10^{-5}$	$1.0 \pm 0.18$	$11.4 \pm 0.25$
Zinc(II)	$1.5 \times 10^{-5}$	$2.0 \pm 0.13$	$11.5 \pm 0.56$
Copper(II)	$1.6 \times 10^{-5}$	$1.1 \pm 0.20$	$11.0 \pm 0.28$
Lead(II)	$4.8 \times 10^{-6}$	$1.75 \pm 0.28$	$13.6 \pm 0.42$
Sulfate	$5.2 \times 10^{-4}$	$1.0 \pm 0.22$	$10.6 \pm 0.60$
Chloride	$9.9 \times 10^{-4}$	$1.3 \pm 0.23$	$10.5 \pm 0.56$
Fluoride	$5.3 \times 10^{-5}$	$1.0 \pm 0.18$	$10.2 \pm 0.32$
Iodide	$1.0 \times 10^{-8}$	$8.5 \pm 0.56$	$19.6 \pm 0.60$

Table 3  
FI–CL determination of L-thyroxine in four pharmaceutical preparations (L-thyroxine sodium) ( $n=5$ )

Sample	L-Thyroxine labeled ( $\mu\text{g}/\text{tablet}$ )	Proposed method L-thyroxine found ( $\mu\text{g}/\text{tablet}$ ) <sup>a</sup>	RIA method <sup>d</sup> L-thyroxine found ( $\mu\text{g}/\text{tablet}$ )
1	50	$52.2 \pm 1.5$	$49.5 \pm 0.8$
2	50	$49.5 \pm 2.0$	–
3	50	$48.8 \pm 2.5$	–
4	50	$51.5 \pm 1.1$	–

<sup>a</sup> IMMUNOTECH (Beckman Coulter Company, Czech Republic).

active mediate which enhanced CL response. However, mechanism of thyroxine effect enhancing CL is still unclear, possibly thyroxine facilitating the co-reactant Ru(bpy)<sub>3</sub><sup>3+</sup>–NADH oxidation and leading to increased CL efficiency.

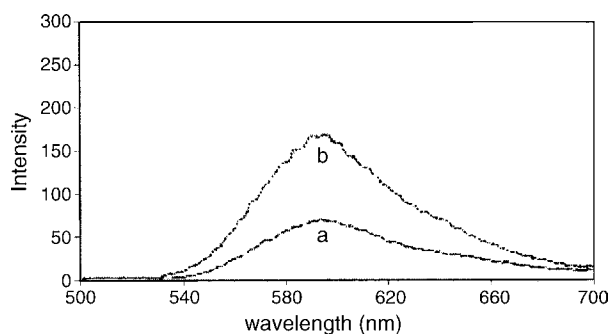


Fig. 3. CL spectra of the reactions; (a) Ru(bpy)<sub>3</sub><sup>3+</sup> ( $1.0 \times 10^{-5}$  mol/L in H<sub>2</sub>SO<sub>4</sub>,  $5.0 \times 10^{-3}$  mol L<sup>-1</sup>) + NADH ( $1.0 \times 10^{-6}$  mol L<sup>-1</sup> in phosphate buffer,  $5.0 \times 10^{-3}$  mol L<sup>-1</sup>, pH 8). (b) Ru(bpy)<sub>3</sub><sup>3+</sup> ( $1.0 \times 10^{-5}$  mol/L in H<sub>2</sub>SO<sub>4</sub>,  $5.0 \times 10^{-3}$  mol L<sup>-1</sup>) + NADH ( $1.0 \times 10^{-6}$  mol L<sup>-1</sup> in phosphate buffer,  $5.0 \times 10^{-3}$  mol L<sup>-1</sup>, pH 8) + thyroxine ( $1.0 \times 10^{-5}$  mol L<sup>-1</sup> in phosphate buffer,  $5.0 \times 10^{-3}$  mol L<sup>-1</sup>, pH 8).

## 4. Conclusion

The proposed flow injection-chemiluminescence method is simple, rapid (120 h<sup>-1</sup> sample throughput) with a limit of detection of  $1.0 \times 10^{-9}$  mol L<sup>-1</sup> L-thyroxine. The method was applied to commercially available thyroxine tablets and the results are in reasonable agreement with the amount of L-thyroxine labeled and RIA method. The method can be applied to total thyroxine (free and protein bound) in biological samples after performing extraction or dialysis process. The enhancement effect of thyroxine on Ru(bpy)<sub>3</sub><sup>3+</sup>–NADH CL system can further extend its applications to NAD<sup>+</sup>–NADH converting enzymes and their substrates.

## Acknowledgments

The authors are grateful to Higher Education Commission, Pakistan for financial support in the form of Indigenous PhD Scholarship program (IQC-03600101) and Pakistan Science Foundation (R&D/B-BU/Chem (252)).

## References

- [1] M. Breder, T. Scott (Eds.), Concise Encyclopedia of Biochemistry, de Gruyter, New York, 1983, p. 461.
- [2] H. Gika, M. Lammerhofer, I. Papadoyannis, W. Lindner, J. Chromatogr. B 800 (2004) 193.
- [3] H.R. Schroeder, F.M. Yeager, R.C. Boguslaski, P.O. Vogelhut, J. Immunol. Methods 25 (1979) 275.
- [4] D.R. Vij, Luminescence of Solids, Plenum Press, New York, USA, 1998, P. 391.
- [5] A.R. Bowie, M.G. Sanders, P.J. Worsfold, J. Biolumin. Chemilumin. 11 (1996) 61.
- [6] J.-M. Lin, M. Yamada, Pure Appl. Anal. Chem. 1 (1998) 133.

- [7] A. Roda, M. Pazzagli, L.J. Kricka, P.E. Stanley (Eds.), *Bioluminescence & Chemiluminescence Perspectives for the 21st Century*, John Wiley & Sons, Chichester, UK, 1999.
- [8] D.M. Hercules, F.E. Lytle, *J. Am. Chem. Soc.* 88 (1966) 4745.
- [9] F.E. Lytle, D.M. Hercules, *J. Am. Chem. Soc.* 91 (1969) 253.
- [10] T.M. Downey, T.A. Nieman, *Anal. Chem.* 64 (1992) 261.
- [11] N.W. Barnett, T.A. Bowser, R.D. Gerardi, B. Smith, *Anal. Chim. Acta.* 318 (1996) 309.
- [12] A.W. Knight, G.M. Greenway, *Anal. Commun.* 23 (1996) 171.
- [13] W.Y. Lee, T.A. Nieman, *J. Chromatogr. A* 659 (1994) 111.
- [14] S. Yamazaki, K. Ozaki, K. Saito, T. Tanimura, *J. High Resolut. Chromatogr.* 18 (1995) 68.
- [15] J.S. Ridlen, G.J. Klopff, T.A. Nieman, *Anal. Chim. Acta* 341 (1997) 195.
- [16] R.D. Gerardi, N.W. Barnett, S.W. Lewis, *Anal. Chim. Acta* 378 (1999) 1.
- [17] R. Sapin, *Clin. Biochem.* 34 (2001) 367.
- [18] M.R. Oates, W. Clarke, A. Zimlich II., D.S. Hage, *Anal. Chim. Acta* 470 (2002) 37.
- [19] H. Silvaieh, R. Wintersteiger, M.G. Schmid, O. Hofstetter, V. Schurig, G. Gubitz, *Anal. Chim. Acta* 463 (2002) 5.
- [20] C. Hu, Q. He, Q. Li, S. Hu, *Anal. Sci.* 20 (2004) 1049.
- [21] R.I. Stefan, J.F.V. Staden, H.Y. Aboul-Enein, *Talanta* 64 (2004) 151.
- [22] L. Bhavana, V.J. Ajimon, S.L. Radhika, M. Sindhu, C.S.P. Iyer, *J. Chromatogr. B* 803 (2004) 363.
- [23] H.G. Gika, V.F. Samanidou, I.N. Papadoyannis, *J. Chromatogr. B* 814 (2005) 163.
- [24] A.L. Hantson, M.D. Meyer, N. Guerit, *J. Chromatogr. B* 807 (2004) 185–192.
- [25] F.B. Wu, S.Q. Han, C. Zhang, Y.F. He, *Anal. Chem.* 74 (2002) 5882.
- [26] J.C. Lewis, S. Daunert, *Anal. Chem.* 73 (2001) 3227.
- [27] P.B. Lippa, S. Reutemann, U. Huber, R. Hoermann, S. Poertl, S. Kraiss, S. von Bulow, D. Neumeier, *Clin. Chem. Lab. Med.* 36 (1998) 789.
- [28] M. Sanchez-Carbayo, M. Mauri, R. Alfayate, C. Miralles, F. Soria, *Clin. Biochem.* 32 (1999) 395.
- [29] T. Ghous, A. Townshend, *Anal. Chim. Acta* 411 (2000) 45.
- [30] E. Gok, S. Ates, *Anal. Chim. Acta* 505 (2004) 125.
- [31] F. Jameison, R.I. Sanchez, L. Dong, J.K. Leland, D. Yost, M.T. Martin, *Anal. Chem.* 68 (1996) 1298.
- [32] A.F. Martin, T.A. Nieman, *Biosens. Bioelectron.* 12 (1997) 479.
- [33] R.D. Gerardi, N.W. Barnett, P. Jones, *Anal. Chim. Acta* 388 (1999) 1.
- [34] M. Yaqoob, A. Nabi, M. Masoom-Yasinzai, *J. Biolumin. Chemilumin.* 12 (1997) 1.
- [35] W. Miao, J.-P. Choi, A.J. Bard, *J. Am. Chem. Soc.* 124 (2002) 14478.

## Iron isotope fractionation between liquid and vapor phases of iron pentacarbonyl

René A. Wiesli<sup>a</sup>, Brian L. Beard<sup>a,\*</sup>, Paul S. Braterman<sup>b</sup>, Clark M. Johnson<sup>a</sup>,  
Susanta K. Saha<sup>b</sup>, Mahadeva P. Sinha<sup>c</sup>

<sup>a</sup> Department of Geology and Geophysics, University of Wisconsin, Madison, WI 53706, USA

<sup>b</sup> Department of Chemistry, University of North Texas, PO Box 305070, Denton, TX 76203, USA

<sup>c</sup> Jet Propulsion Laboratory, California Institute of Technology, Pasadena, CA 91109, USA

Received 2 December 2005; received in revised form 9 March 2006; accepted 10 March 2006

Available online 18 April 2006

### Abstract

Iron isotope fractionation between liquid and vapor iron pentacarbonyl was measured in a closed system at  $\sim 0$  and  $\sim 21$  °C to determine if Fe isotope analysis of iron pentacarbonyl vapor is viable using electron-impact, gas-source mass spectrometry. At the  $2\sigma$  level, there is no significant Fe isotope fractionation between vapor and liquid under conditions thought to reflect equilibrium. Experiments at  $\sim 0$  °C indicate iron pentacarbonyl vapor is  $\sim 0.05$  per mil (‰) greater in  $^{56}\text{Fe}/^{54}\text{Fe}$  than liquid iron pentacarbonyl, which is just resolvable at the  $1\sigma$  level. Partial decomposition of iron pentacarbonyl vapor or liquid to an iron oxide or iron metal shows that significant isotopic fractionation occurs, where the decomposed product has a lower  $^{56}\text{Fe}/^{54}\text{Fe}$  ratio as compared to the starting iron pentacarbonyl. It follows that methods to decompose iron pentacarbonyl must be quantitative to obtain accurate isotope values.

© 2006 Elsevier B.V. All rights reserved.

**Keywords:** Fe isotopes; Iron pentacarbonyl; Isotope fractionation; Electron impact ionization mass spectrometry

### 1. Introduction

The field of Fe isotope research has tremendously grown since the first high-precision Fe isotope ratio measurements were reported in 1999. There are currently over 20 laboratories pursuing Fe isotope studies and over 60 peer-reviewed papers have been published on mass-dependent fractionation of Fe isotopes [1]. Several observations have spurred Fe isotope research including (1) significant mass-dependent fractionation of Fe isotopes occur during oxidation or reduction, suggesting that Fe isotopes may be used to infer paleo-redox conditions and redox cycling of metals in different environments [2]; (2) mass-dependent fractionation of Fe isotopes may occur during high-temperature processes such as vaporization, indicating that Fe isotopes may be used in cosmochemistry to gain a better

understanding of the formation of planetary bodies [3,4]; (3) Fe is an important metabolic element and is fractionated by biological processes during bacterially catalyzed redox cycling of Fe or nutritional uptake of Fe by humans [5,6].

High-precision iron isotope ratio measurements ( $\pm 0.05\%$  for the  $^{56}\text{Fe}/^{54}\text{Fe}$  ratio) for these studies have been primarily made using multi-collector inductively coupled plasma mass spectrometry with correction for instrumental mass bias through correction to bracketing Fe standards or normalization to an element of similar mass such as Ni or Cu [7]. Iron isotope measurements have also been made using thermal ionization mass spectrometry and a double-spike to correct for instrumental mass bias [8], although these are less precise than analyses by MC-ICP-MS. A cursory study has been conducted to evaluate the feasibility of using a gas-source electron-impact ionization mass spectrometer to make Fe isotope measurements [9]. Such instrumentation is ideal for measurements of isotope ratios that preserve naturally occurring, mass-dependent fractionation because of the ability to use a dual inlet system to make comparison between sample and standard, thus removing the effects of instrumental mass bias. This type of instrumentation has made

\* Corresponding author. University of Wisconsin, Department of Geology and Geophysics, Lewis G. Weeks Hall, 1215 W. Dayton Street, Madison, WI 53706, USA. Tel.: +1 608 262 1806; fax: +1 608 262 0693.

E-mail address: [beardb@geology.wisc.edu](mailto:beardb@geology.wisc.edu) (B.L. Beard).



the traditional stable isotopes such as H, C, N, O, and S widely available to a host of scientific disciplines. However, because most Fe compounds have low vapor pressures, it is difficult to introduce Fe into an electron-impact ionization mass spectrometer. An initial study made use of the compound  $\text{Fe}(\text{PF}_3)_5$ , which is highly volatile (sublimation occurs at 22 °C) [9]. The synthesis of  $\text{Fe}(\text{PF}_3)_5$  is time consuming and handling of the compound is difficult because hydrolysis produces HF. Ionization of  $\text{Fe}(\text{PF}_3)_5$  in an electron-impact ionization mass spectrometer yields a mass spectrum that is dominated by  $\text{Fe}^+$  ions [9], providing a simple mass spectra.

Iron pentacarbonyl ( $\text{Fe}(\text{CO})_5$ ) is an orange–yellow liquid at room temperature and has a vapor pressure of  $\sim 2933$  Pa at 20 °C [10,11]. Thus,  $\text{Fe}(\text{CO})_5$  is suitable for introduction into a gas-source electron-impact ionization mass spectrometer. Like  $\text{Fe}(\text{PF}_3)_5$ , ionization of  $\text{Fe}(\text{CO})_5$  yields a mass spectrum dominated by  $\text{Fe}^+$  ions [12,13], and hence corrections need not be made for the isotopic composition of C or O. In a separate contribution we will report on a novel methodology for measurement of Fe and O isotope compositions in hematite [14], and this method depends on understanding the isotope fractionations produced by reactions involving  $\text{Fe}(\text{CO})_5$ , the subject of this report. The method of Saha et al. [14] is based on reduction of  $\text{Fe}_2\text{O}_3$  with  $\text{H}_2$  at  $\sim 390$  °C, followed by conversion of the resulting Fe to  $\text{Fe}(\text{CO})_5$  by reaction with CO. The carbonylation reaction is carried out at mild temperature and pressure conditions (110 °C,  $< 620$  kPa pressure of CO). Because of the high vapor pressure and production of Fe as the base peak in its mass spectrum,  $\text{Fe}(\text{CO})_5$  could be an excellent compound for conducting Fe isotope analysis by electron impact ionization mass spectrometry. Here, we report on a series of experiments to evaluate the Fe isotope fractionation factor between liquid and vapor  $\text{Fe}(\text{CO})_5$  at  $\sim 0$  and  $\sim 21$  °C. An additional set of experiments have been conducted to document the range of Fe isotope compositions that can be produced during partial thermal decomposition of liquid and vapor  $\text{Fe}(\text{CO})_5$  to hematite or Fe metal. These experiments are a critical first look at the feasibility of using  $\text{Fe}(\text{CO})_5$  as a compound for Fe isotope analysis. Moreover, because  $\text{Fe}(\text{CO})_5$  is a byproduct of possible pre-biotic reactions during the synthesis of organic molecules associated with reactions between iron sulfides and CO gas [15], the Fe isotope composition of possible pre-biotic reactants and Fe carbonyl decomposition products may be useful in evaluating the role Fe carbonyl played in the assembly of some organic compounds.

## 2. Experimental setup and procedure

The experimental apparatus consisted of a 250 mL European style flask (Ace Glass<sup>TM</sup>, # 6961) with 5 ports. Two of the three larger ports were connected via three-way, high-vacuum stopcocks (Ace Glass<sup>TM</sup>, # 8196) to 25 mL Equilibrium flasks (Ace Glass<sup>TM</sup>, # 7408). The center neck contained a rubber septum for sampling with a syringe. One of the two smaller threaded necks was hooked up to a hand vacuum pump, the other one was closed with a solid glass rod. Two batches of  $\text{Fe}(\text{CO})_5$  liquid were used in these experiments. One batch was purchased from Strem Chemicals, Inc. and was 99.5% pure. The other batch was

obtained from Aldrich Chemicals and was 99.999% pure. Fortuitously, the Fe isotope compositions of the reagent  $\text{Fe}(\text{CO})_5$  from both manufacturers were the same (Table 1). The  $\text{Fe}(\text{CO})_5$  from Strem Chemicals was used in experiments 1, 2, and 4 and in the partial decomposition of liquid experiment. The Aldrich Chemicals  $\text{Fe}(\text{CO})_5$  was used in experiments 3 and 5 and in the partial decomposition of vapor experiments.

Experiments were conducted at  $\sim 21$  and  $\sim 0$  °C to evaluate possible temperature effects on the isotope fractionation between liquid and vapor iron pentacarbonyl. The room temperature experiments were conducted indoors; the 0 °C experiments were performed outside on mild Wisconsin winter days when the temperature was stable. All reagents and the experimental apparatus were allowed to come to thermal equilibrium with the surrounding air by letting all items sit for two hours before assembling the experimental apparatus. Before introduction of liquid  $\text{Fe}(\text{CO})_5$ , the entire apparatus was purged with Argon gas with the following procedure: initially Ar was flushed through the apparatus for 5 min, then all outer valves were closed and the Ar–air mixture was evacuated with a hand vacuum pump to  $\sim 15\,340$  Pa (absolute). Argon was then bled into the apparatus and it was allowed to equilibrate under  $\sim 100$  kPa of laboratory-grade Ar. This purging procedure was repeated four times. In addition, during the last purging cycle, the stopcocks of the two 25 mL Equilibrium flasks were closed to keep them under vacuum ( $\sim 15\,340$  Pa absolute). For a typical experimental run, about 27 mL of liquid iron pentacarbonyl was introduced into the Ar-purged flask with a syringe through the rubber septum. The gas-exposed surface area of the  $\text{Fe}(\text{CO})_5$  liquid was  $\sim 56$  cm<sup>2</sup>. The liquid–gas system was allowed to equilibrate for a predetermined time before sampling. Sampling of the vapor phase utilized the pressure difference between the main flask and the previously evacuated Equilibrium flask and was accomplished by opening the proper valve for 5 s and then closing it. The  $\text{Fe}(\text{CO})_5$  vapor in the 25 mL Equilibrium flask was quantitatively decomposed to iron using a heat gun. In all experiments the amount of vapor removed relative to the volume of  $\text{Fe}(\text{CO})_5$  liquid was infinitesimally small with respect to the mass balance of Fe in the system.

In a different set of experiments we investigated the Fe isotope fractionation associated with partial decomposition of liquid and vapor  $\text{Fe}(\text{CO})_5$ . The isotope fractionation between vapor and Fe metal due to incomplete decomposition was tested by filling a 25 mL Equilibrium flask with  $\text{Fe}(\text{CO})_5$  vapor (see procedure above) and stopping decomposition as soon as Fe metal deposition on the flask wall was noticed. The Equilibrium flask was hooked up to a vacuum line and the remaining  $\text{Fe}(\text{CO})_5$  vapor was condensed using liquid nitrogen into a clean evacuated Equilibrium flask, which was then completely decomposed thermally. Iron isotope fractionation related to partial decomposition of liquid iron pentacarbonyl was also tested because non-quantitative decomposition might produce kinetic Fe isotope fractionation. For non-quantitative decomposition in air, a small amount ( $\sim 20$   $\mu\text{L}$ ) was extracted with a syringe from a stock vial and transferred to a Savillex<sup>TM</sup> beaker. The beaker was immediately capped and heated with a heat gun until the reaction between  $\text{Fe}(\text{CO})_5$  and air was

Table 1  
Experimental data

Experiment	<i>T</i> (°C)	Time (min)	$\delta^{56}\text{Fe}^a$ (‰)	$\delta^{57}\text{Fe}^a$ (‰)	<i>n</i>	Fe <sup>b</sup> (μg)	Yield <sup>c</sup> (%)
1	21	4	0.02 ± 0.05	0.01 ± 0.03		1106.4	62.3
1	21	6	0.06 ± 0.06	0.08 ± 0.04		922.2	51.9
1	21	64	−0.02 ± 0.04	−0.07 ± 0.06	2	1889.1	106.4
1	21	66	0.09 ± 0.04	0.06 ± 0.18	2	1647.9	92.4
1	21	125	0.03 ± 0.06	0.07 ± 0.03		1537.2	86.6
2	20	5	−0.01 ± 0.04	−0.01 ± 0.16	2	1105.8	65.6
2	20	10	0.05 ± 0.00	0.00 ± 0.08	2	1109.4	65.8
2	20	20	0.20 ± 0.06	0.22 ± 0.10	2	1375.8	81.7
2	20	40	0.03 ± 0.14	0.07 ± 0.02	2	1364.4	81.0
3	21	19	0.03 ± 0.04	0.00 ± 0.03		1359.3	76.6
3	21	21	0.00 ± 0.03	0.01 ± 0.02		1372.2	77.3
3	21	49	0.11 ± 0.03	0.12 ± 0.02		1444.5	81.3
3	21	51	0.12 ± 0.03	0.18 ± 0.03		1452.0	81.8
3	21	80	0.10 ± 0.03	0.21 ± 0.03		1557.6	87.7
4	0	19	0.08 ± 0.06	0.16 ± 0.06	2	413.4	76.4
4	0	21	0.04 ± 0.02	0.10 ± 0.12	2	396.0	73.1
4	0	49	0.23 ± 0.06	0.38 ± 0.10	3	609.9	112.6
4	0	51	0.23 ± 0.12	0.42 ± 0.16	2	538.8	99.5
4	0	79	0.22 ± 0.00	0.37 ± 0.08	3	560.1	103.5
5	−3	22	0.09 ± 0.03	0.20 ± 0.03		390.3	86.8
5	−3	18	0.13 ± 0.03	0.14 ± 0.02		357.0	79.4
5	−3	48	0.18 ± 0.04	0.30 ± 0.04		408.0	90.7
5	−3	52	0.23 ± 0.03	0.26 ± 0.04		319.2	71.0
5	−3	81	0.22 ± 0.03	0.24 ± 0.03		393.0	87.4
Partial Decomposition Vapor							
Partial decomposition vapor	21	20	−1.11 ± 0.03	−1.66 ± 0.03		551.1	74.0 <sup>d</sup>
Remaining vapor	21		0.77 ± 0.03	1.15 ± 0.02		763.5	
Partial decomposition vapor	21	20	−1.56 ± 0.02	−2.35 ± 0.03		501.0	81.1 <sup>d</sup>
Remaining vapor	21		0.78 ± 0.04	1.16 ± 0.03		939.0	
Partial decomposition liquid <sup>e</sup>							
	21		−1.25 ± 0.04	−1.95 ± 0.03		3211.5	37.8
	21		−0.36 ± 0.08	−0.53 ± 0.04	2	4229.4	49.8
	21		−2.57 ± 0.05	−3.78 ± 0.04		144.0	1.70
Fe(CO) <sub>5</sub> reagents <sup>f</sup>							
Fe(CO) <sub>5</sub> Strem Chemicals			0.09 ± 0.10	0.14 ± 0.12	7		
Fe(CO) <sub>5</sub> Aldrich Chemicals			0.08 ± 0.04	0.12 ± 0.08	6		

<sup>a</sup> Errors are 2 standard errors (S.E.) from in-run statistics or where *n* is given, the errors are 2 standard deviations (S.D.) external, calculated from the average of up to seven mass spectrometry analyses.

<sup>b</sup> Amount of Fe recovered from decomposition of extracted vapor, as determined from *Ferrozine* analyses.

<sup>c</sup> Yields are calculated from recovered Fe and the theoretical yields inferred from Fe pentacarbonyl vapor pressure data.

<sup>d</sup> Yield is based on sum of decomposed vapor and remaining vapor.

<sup>e</sup> The escaping vapor phase has not been collected.

<sup>f</sup> Averages of initial and final compositions of reagents; all processed throughout the entire analytical procedure.

complete. The product was a brown–orange, fine-grained iron oxide powder, which we believe is mostly hematite [16]. In addition, to establish a baseline for the isotopic composition of the extracted vapor and for quality control, aliquots (~4 μL) of Fe(CO)<sub>5</sub> liquid from the beginning and end of an experiment were transferred into 5 mL sample tubes (Ace Glass<sup>TM</sup>, # 7410) and quantitatively decomposed (in air) using a heat gun. The Fe metal/iron oxide deposited in the Equilibrium flasks and Savillex<sup>TM</sup> beakers was dissolved in double-distilled 7 M HCl and transferred to clean Savillex<sup>TM</sup> beakers. Iron concentrations and yields of Fe(CO)<sub>5</sub> decompositions were determined by *Ferrozine* assays [17]. Theoretical yields were calculated assuming Fe(CO)<sub>5</sub> behaved as an ideal gas ( $PV = nRT$ ) and using the formula  $\log_{10} P$  (Pa) =  $-(2092.4 K/T) + 10.605$  to adjust the vapor

pressure of Fe(CO)<sub>5</sub> [10] to the relevant temperature of the experiment.

Decomposition of liquid and vapor Fe(CO)<sub>5</sub> was conducted by heating the vessel with a 1200 W heat gun (Heat Gun<sup>TM</sup> model HC1001). This heating method produces a maximum temperature of ~140 °C on the surface of the sample vessel, in approximately 2 min. To ensure complete decomposition, samples were typically heated for 10 min.

### 3. Mass spectrometry and nomenclature

Mass spectrometry for iron isotopes was performed with the University of Wisconsin–Madison *IsoProbe*, a single-focusing, multi-collector, inductively coupled plasma-mass spectrometer

(MC-ICP-MS) that is equipped with a collision cell to eliminate or minimize argide isobar interferences such as  $^{40}\text{Ar}^{16}\text{O}$ ,  $^{40}\text{Ar}^{14}\text{N}$ , and  $^{40}\text{Ar}^{16}\text{OH}$  that interfere with  $^{56}\text{Fe}$ ,  $^{54}\text{Fe}$ , and  $^{57}\text{Fe}$ , respectively. Chemical separation and mass analysis procedures followed the methods reported in Skulan et al. [18] and Beard et al. [19].

Iron isotope analyses are reported using standard  $\delta$  notation in units of per mil (‰):

$$\delta^{56}\text{Fe} = \left( \left[ \frac{^{56}\text{Fe}/^{54}\text{Fe}}{\text{Sample}} / \left[ \frac{^{56}\text{Fe}/^{54}\text{Fe}}{\text{Standard}} \right] - 1 \right) \times 10^3$$

and  $\delta^{57}\text{Fe} = \left( \left[ \frac{^{57}\text{Fe}/^{54}\text{Fe}}{\text{Sample}} / \left[ \frac{^{57}\text{Fe}/^{54}\text{Fe}}{\text{Standard}} \right] - 1 \right) \times 10^3.$

$\delta^{56}\text{Fe}$  and  $\delta^{57}\text{Fe}$  values are calculated using the average of terrestrial igneous rocks as a standard reference reservoir [19]. On this scale, the measured Fe isotope composition of the IRMM-014 Fe isotope standard was  $\delta^{56}\text{Fe} = -0.09 \pm 0.10\text{‰}$  and  $\delta^{57}\text{Fe} = -0.11 \pm 0.14\text{‰}$  (2 standard deviations, S.D.). The external precision (2 S.D.) of  $^{56}\text{Fe}/^{54}\text{Fe}$  and  $^{57}\text{Fe}/^{54}\text{Fe}$  ratio is  $\pm 0.10$  and  $\pm 0.14\text{‰}$ , respectively, based on 99 analyses of standards during the study.

#### 4. Results

Yields of all vapor extractions were determined using *Ferrozine* assays, and these were compared to calculated yields using published vapor pressure relations for iron pentacarbonyl. The low yield of samples from earlier time measurements (Fig. 1) reflects the time required to establish equilibrium conditions, and can be explained by a concentration gradient caused by diffusion of iron pentacarbonyl vapor through a stagnant Argon atmosphere towards the Equilibrium flasks. Initially, before introduction of liquid Fe pentacarbonyl, the entire apparatus

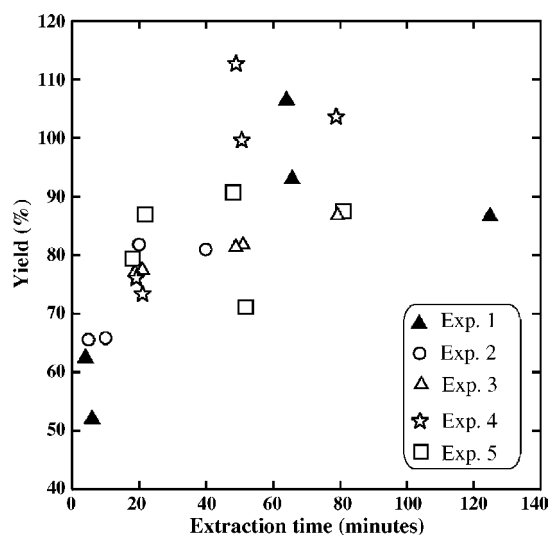


Fig. 1. Plot of vapor extraction time vs. yield in percent. The yield has been calculated by using Fe concentration measurements of the extracted vapor and comparing it to theoretical yields obtained from the ideal gas law and published vapor pressure data for iron pentacarbonyl.

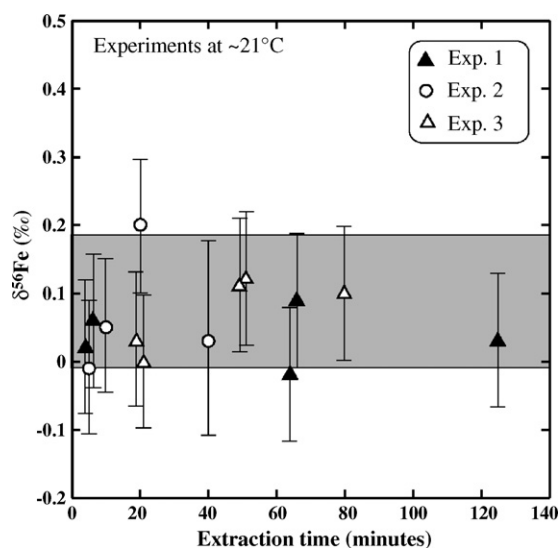


Fig. 2. Plot of vapor extraction time vs.  $\delta^{56}\text{Fe}$  of the extracted vapor for experiments conducted at  $\sim 21^\circ\text{C}$ . The iron pentacarbonyl vapor samples were completely dissociated in each experiment. Error bars are 2 S.D. ( $\pm 0.10\text{‰}$ ) external. The gray shaded area indicates the error envelope of the average of the initial and final reagent (2 S.D.).

has an Argon atmosphere (except the Equilibrium flasks, which were partially evacuated). Evaporation of Fe pentacarbonyl and subsequent diffusion of the vapor results in a concentration gradient in the reaction vessel and glass tubes. The concentration of  $\text{Fe}(\text{CO})_5$  becomes constant with time after  $\sim 20$  min.

##### 4.1. Complete decomposition at $\sim 21$ and $\sim 0^\circ\text{C}$

The isotopic results for the  $\sim 21^\circ\text{C}$  experiments are given in Fig. 2 and Table 1. The variations in  $\delta^{56}\text{Fe}$  for the extracted iron pentacarbonyl vapor ranged from  $-0.02$  to  $+0.20\text{‰}$ . If the  $0.20\text{‰}$  point is omitted, the average of all vapor extractions at  $\sim 21^\circ\text{C}$  is  $\delta^{56}\text{Fe} = 0.05 \pm 0.10\text{‰}$  (2 S.D.,  $n = 13$ ). The initial and final isotope compositions of the liquid iron pentacarbonyl were determined for each experiment, resulting in an average  $\delta^{56}\text{Fe}$  value of  $0.09 \pm 0.10\text{‰}$  (2 S.D.,  $n = 6$ ).

Isotopic data for the  $\sim 0^\circ\text{C}$  experiments are presented in Fig. 3 and Table 1 and show a similar range ( $\delta^{56}\text{Fe} = 0.04\text{--}0.23\text{‰}$ ) in vapor iron pentacarbonyl isotope composition as measured in the  $\sim 21^\circ\text{C}$  experiments. However, unlike the  $\sim 21^\circ\text{C}$  experiments, the later sampled vapor consistently has a greater  $\delta^{56}\text{Fe}$  value ( $0.22 \pm 0.04\text{‰}$ ; 2 S.D.,  $n = 6$ ) for vapor extracted at  $\sim 50$  and  $\sim 80$  min as compared to vapor extracted at  $\sim 20$  min ( $\delta^{56}\text{Fe} = 0.09 \pm 0.08$ ; 2 S.D.,  $n = 4$ ). The average combined initial and final  $\delta^{56}\text{Fe}$  values of the liquid iron pentacarbonyl for the  $0^\circ\text{C}$  experiments was determined as  $0.07 \pm 0.08\text{‰}$  (2 S.D.,  $n = 4$ ). Although it is uncertain if the experiments were conducted for a time period long enough to achieve Fe isotope equilibrium between liquid and vapor  $\text{Fe}(\text{CO})_5$ , the fact that the Fe isotope compositions of the  $\text{Fe}(\text{CO})_5$  vapor at 80 and 50 min are identical (Table 1) we conclude that isotopic equilibrium was achieved.

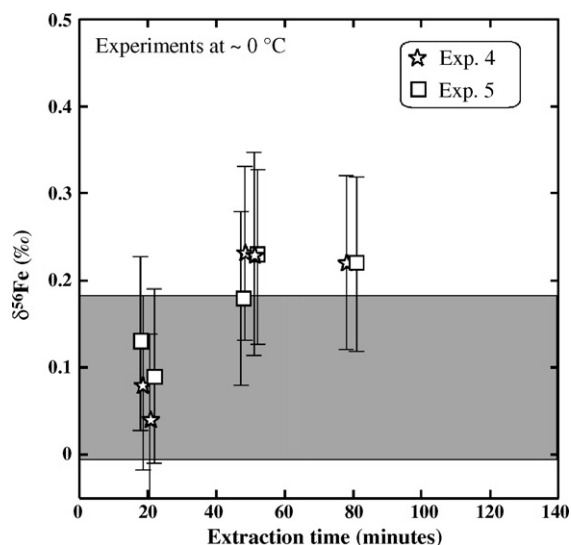


Fig. 3. Plot of vapor extraction time vs.  $\delta^{56}\text{Fe}$  measured after complete dissociation of the extracted vapor. The experiments were conducted at  $\sim 0^\circ\text{C}$ . Error bars are 2 S.D. ( $\pm 0.10\text{‰}$ ) external. The gray shaded area indicates the error envelope of the average of the initial and final reagent (2 S.D.).

#### 4.2. Partial decomposition at $\sim 21^\circ\text{C}$

The isotopic results for partial decomposition of iron pentacarbonyl vapor are given in Fig. 4 and Table 1. The partially decomposed iron pentacarbonyl vapor had  $\delta^{56}\text{Fe}$  values of  $-1.56$  and  $-1.11\text{‰}$  for decompositions of 35 and 42% of the total vapor phase in the 25 mL Equilibrium flask, respectively. The residual decomposed vapor had  $\delta^{56}\text{Fe}$  values of 0.78 and 0.77‰, respectively. Mass balance calculations using  $\delta^{56}\text{Fe}_{\text{System}} = f \delta^{56}\text{Fe}_{\text{Partial, Decomp.}} + (1-f) \delta^{56}\text{Fe}_{\text{Residue}}$ , where  $f$  is the fraction of vapor decomposed, result in calculated  $\delta^{56}\text{Fe}_{\text{System}}$  values of  $-0.03$  and  $-0.02\text{‰}$ , which lies within

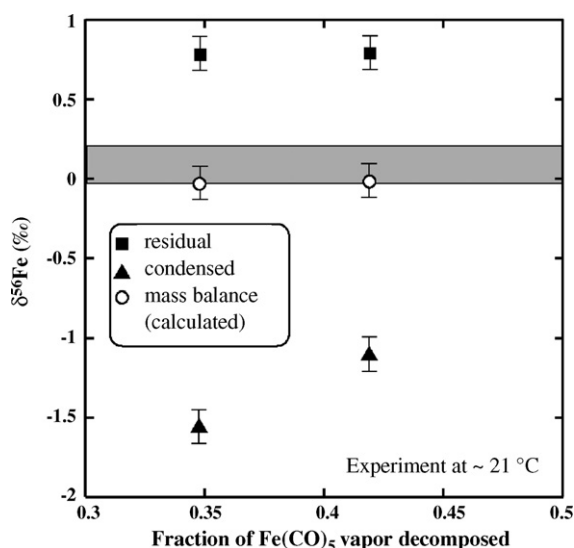


Fig. 4. Plot of the fraction of  $\text{Fe}(\text{CO})_5$  decomposed vs.  $\delta^{56}\text{Fe}$  of the partially condensed and residual vapor for the partial decomposition experiment performed at  $\sim 21^\circ\text{C}$ . Error bars are 2 S.D. ( $\pm 0.10\text{‰}$ ) external. The gray shaded area indicates the error envelope for the average of the initial and final reagent (2 S.D.). Circles indicate the results of the calculated isotope mass balance.

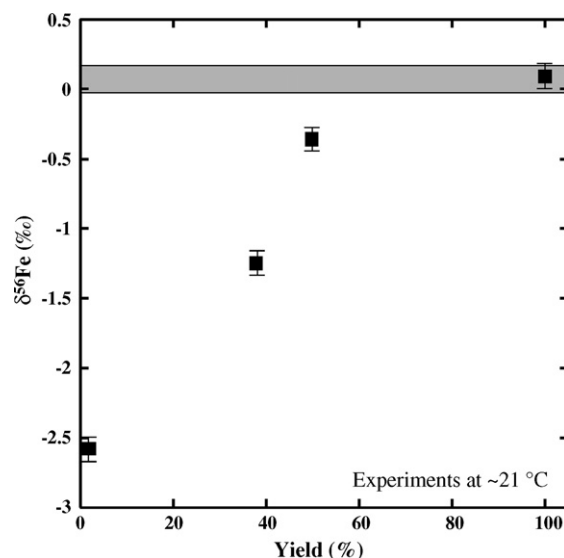


Fig. 5. Plot of yield in percent vs.  $\delta^{56}\text{Fe}$  of the partially decomposed iron pentacarbonyl liquid (hematite). Error bars are 2 S.D. ( $\pm 0.10\text{‰}$ ) external. The gray shaded area indicates the error envelope of the average of the initial and final reagent that has been quantitatively decomposed (2 S.D.).

the uncertainty of the isotope composition of the initial iron pentacarbonyl liquid ( $\delta^{56}\text{Fe} = 0.08 \pm 0.10\text{‰}$ ; 2 S.D.,  $n = 6$ ).

Iron isotope data for non-quantitative decomposition of liquid Fe pentacarbonyl in air to iron oxide is given in Fig. 5 and Table 1. The  $\delta^{56}\text{Fe}$  values for iron oxide are all strongly negative, from  $-2.57$  to  $-0.36\text{‰}$ . Similar to the partial vapor decomposition, higher yields correspond to  $\delta^{56}\text{Fe}$  values that are higher and more closely match those expected for equilibrium conditions or complete reactions. Mass-balance calculations indicate that the escaped phase during decomposition must have had high  $\delta^{56}\text{Fe}$  values. In both experiments, the rapidly condensed solid phase has a lower  $\delta^{56}\text{Fe}$  values as compared to the uncondensed liquid or vapor.

## 5. Discussion and conclusion

Theoretical calculations predict that molecules containing light isotopes, in general, have higher vapor pressures and are more volatile than the same compounds that contain heavier isotopes [20]. Thus the vapor of a compound tends to have an “isotopically light” composition as compared to its liquid. There are exceptions to such generalizations, where, for example, Grootes et al. [21] found that during evaporation of  $\text{CO}_2$ , the  $^{13}\text{C}^{16}\text{O}_2$  species is more volatile than the  $^{12}\text{C}^{16}\text{O}_2$  species, with the consequence that  $^{13}\text{C}^{16}\text{O}_2$  is enriched in the vapor phase. The higher vapor pressures of the isotopically heavier compound may be related to the effect of intra-molecular vibrations on binding energies [21].

The magnitude of isotopic fractionation between liquid and vapor can be affected by a number of parameters. For example, in the well studied case of oxygen isotope fractionation between steam and water, the oxygen isotope composition of steam is dependent upon evaporation in closed or open systems, the relative humidity during evaporation, the surface temperature of



the liquid, and the existence of any stagnant gaseous boundary layers at the surface and/or adsorbed monolayers at the liquid surface [22–25]. Similar parameters could effect the Fe isotope composition of Fe in vapor  $\text{Fe}(\text{CO})_5$ . In our experimental setup, the  $\sim 27$  mL of liquid iron pentacarbonyl represents an infinite reservoir with respect to the amount of vapor removed, thus the Fe isotope composition of the liquid will remain constant during the experiment and our experimental system is effectively a closed system. In all of our experiments, vapor was extracted at different times following the injection of liquid  $\text{Fe}(\text{CO})_5$  into the Ar-filled apparatus, which allows us to partially evaluate the effects of the changing vapor pressure of iron pentacarbonyl on the Fe isotope composition of  $\text{Fe}(\text{CO})_5$  vapor. For example, initially there was no iron pentacarbonyl vapor, and based on theoretical Fe yields, our experiments did not reach saturation until the liquid had been in the apparatus for at least 20 min (Fig. 1). Because there are no significant differences in the Fe isotope composition of Fe vapor sampled between 4 and 125 min after introduction of Fe liquid, it would appear that different partial pressures of iron pentacarbonyl vapor and/or diffusion through the Ar atmosphere had no effect on the Fe isotope composition of the  $\text{Fe}(\text{CO})_5$  vapor, at least under our experimental conditions. Additionally, although our experiments were performed at constant temperatures, initial evaporation leads to cooling of the iron pentacarbonyl liquid surface [26], thereby lowering the vapor pressure and possibly enhancing isotope effects. Over the time scales of this experiment, no Fe isotope effect has been noted. Similarly, diffusion through a stagnant gaseous layer or through an adsorbed monolayer at the liquid–gas interface will slow the evaporation rate, but we have not observed an Fe isotope effect over the duration of our experiment. Thus, although we cannot rigorously demonstrate if we have achieved equilibrium Fe isotope exchange between liquid and vapor, we can document that over a span of temperature conditions and changing partial pressures of iron pentacarbonyl, there is no Fe isotope fractionation between iron pentacarbonyl liquid and vapor. Because the Fe isotope fractionation between liquid and vapor iron pentacarbonyl is not a function of temperature or partial pressure conditions, Fe isotope analysis of Fe carbonyl by a gas-source electron-impact mass spectrometer will be able to easily relate the measured vapor Fe isotope composition to the Fe isotope composition of the iron pentacarbonyl liquid.

The partial thermal decomposition experiments indicate that the product of thermal decomposition (Fe metal or iron oxide) from either vapor or liquid  $\text{Fe}(\text{CO})_5$  has a  $\delta^{56}\text{Fe}$  value that is less than the  $\text{Fe}(\text{CO})_5$  reactant. Moreover, there is a positive correlation between Fe isotope composition of the partially decomposed product and the amount of decomposition (Figs. 4 and 5). The Fe isotope fractionation factors that can be inferred from these experiments are variable. For example, for partial decomposition of liquid  $\text{Fe}(\text{CO})_5$  to iron oxides, the  $\delta^{56}\text{Fe}$  values of the decomposed iron oxide product can be modeled using an open-system Rayleigh fractionation model, and the iron isotope fractionation factors between the  $\text{Fe}(\text{CO})_5$  liquid and iron oxide that can be inferred for this experiment, range from 1.35 to 0.65‰. For the closed system partial decomposition experiment between  $\text{Fe}(\text{CO})_5$  vapor and Fe metal, the measured fractiona-

tion factor between vapor and metal are 1.88 and 2.34‰. In general the Fe isotope fractionation associated with these partial decomposition experiments appears to be a result of a unidirectional kinetic process, whereby the product of  $\text{Fe}(\text{CO})_5$  thermal decomposition is isotopically light, as predicted by theory [27]. The wide range in observed fractionation factors is probably a result of the complicated pathway of  $\text{Fe}(\text{CO})_5$  decomposition that includes formation of intermediary species of  $\text{Fe}(\text{CO})_4$  and  $\text{Fe}(\text{CO})_3$  during formation of iron metal or iron oxide [28,29], which may allow for variable amounts of isotope exchange between the intermediate species. Moreover, the range in temperatures that the reaction vessel experienced during thermal decomposition was likely to enhance variable amounts of isotope exchange between different Fe species as well as effect the magnitude of the fractionation factor. Additionally, the larger Fe isotope fractionation factors associated with partial decomposition of  $\text{Fe}(\text{CO})_5$  to Fe metal as compared to iron oxide may be a result of differences in decomposition product. Calculated Fe isotope fractionation factors from Mössbauer spectroscopy data tend to predict that Fe metal will have a lower  $^{56}\text{Fe}/^{54}\text{Fe}$  ratio as compared to ferric Fe-bearing minerals [30]. The smaller fractionation factor observed between  $\text{Fe}(\text{CO})_5$ –iron oxide as compared to  $\text{Fe}(\text{CO})_5$ –Fe metal is consistent with the trends in calculated Fe isotope fractionation factors.

Overall, there is no measurable Fe isotope fractionation at  $\sim 0$  and  $\sim 21$  °C at the  $2\sigma$  level between liquid iron pentacarbonyl and its vapor when decompositions are done quantitatively. However, a closer look at the isotope data from the  $\sim 0$  °C experiments indicates that the isotope composition of vapor extracted at  $\sim 50$  and  $\sim 80$  min has a slightly greater  $\delta^{56}\text{Fe}$  value compared to the liquid. There are reported cases where the isotopically heavy species of compounds are preferentially incorporated into the vapor phase [21,31–33]. The higher vapor pressure of isotopically heavier compounds are possibly related to quantum mechanical effects, i.e., the effect of intra-molecular vibrations on binding energies [21]. A similar mechanism may be invoked to explain a possible “inverse” isotopic effect for the iron pentacarbonyl system, i.e., that the vapor phase is isotopically heavier than the remaining liquid, although the magnitude of this fractionation is not resolvable at the  $2\sigma$  level.

## Acknowledgements

We thank Mike Spicuzza for letting us use his vacuum line for the partial decomposition experiment. This research was supported by NASA Astrobiology Science and Technology Instrument Development under JPL subcontract 1244716. Paul Braterman would like to thank the Welch Foundation, Grant B-1445, for partial support of the effort by UNT personnel. We thank an anonymous reviewer for helpful comments.

## References

- [1] C.M. Johnson, B.L. Beard, *Science* 309 (2005) 1025.
- [2] B.L. Beard, C.M. Johnson, in: C.M. Johnson, B.L. Beard, F. Albarède (Eds.), *Geochemistry of Non-traditional Stable Isotopes*, Mineralogical



- Society of America and Geochemical Society, Washington, DC, 2004, pp. 319–357.
- [3] K. Kehm, E.H. Hauri, C.M.O.D. Alexander, R.W. Carlson, *Geochim. Cosmochim. Acta* 67 (2003) 2879.
- [4] F. Poitrasson, A.N. Halliday, D.-C. Lee, S. Levasseur, N. Teutsch, *Earth Planet. Sci. Lett.* 223 (2004) 253.
- [5] C.M. Johnson, B.L. Beard, E.E. Roden, D. Newman, K.H. Nealson, in: C.M. Johnson, B.L. Beard, F. Albarède (Eds.), *Geochemistry of Non-traditional Stable Isotopes*, Mineralogical Society of America and Geochemical Society, Washington, DC, 2004, pp. 359–408.
- [6] T. Walczyk, F. Von Blanckenburg, *Int. J. Mass Spectromet.* 242 (2005) 117.
- [7] F. Albarède, B.L. Beard, in: C.M. Johnson, B.L. Beard, F. Albarède (Eds.), *Geochemistry of Non-traditional Stable Isotopes*, Mineralogical Society of America and Geochemical Society, Washington, DC, 2004, pp. 113–152.
- [8] C.M. Johnson, B.L. Beard, *Int. J. Mass Spectromet.* 193 (1999) 87.
- [9] P.D.P. Taylor, S. Valkiers, P. De Bièvre, U. Flegel, T. Kruck, *Anal. Chem.* 65 (1993) 3166.
- [10] A.G. Gilbert, K.G.P. Sulzmann, *J. Electrochem. Soc.* 121 (1974) 832.
- [11] D.F. Shriver, K.H. Whitmire, in: G. Wilkinson, F.G.A. Stone, E.W. Abel (Eds.), *Comprehensive Organometallic Chemistry*, Pergamon Press, Oxford, 1982, pp. 243–329.
- [12] R.E. Winters, R.W. Kiser, *Inorg. Chem.* 3 (1964) 699.
- [13] D.R. Bidinosti, N.S. McIntyre, *Can. J. Chem.* 45 (1967) 641.
- [14] S.K. Saha, P.S. Braterman, M.P. Sinha, B.L. Beard, R.A. Wiesli, C.M. Johnson (2006) unpublished data.
- [15] G.D. Cody, N.Z. Boctor, T.R. Filley, R.M. Hazen, J.H. Scott, A. Sharma, H.S.J. Yoder, *Science* 289 (2000) 1337.
- [16] J.B. MacChesney, P.B. O'Connor, M.V. Sullivan, *J. Electrochem. Soc.* 118 (1971) 776.
- [17] M. Dawson, S. Lyle, *Talanta* 37 (1990) 1189.
- [18] J.L. Skulan, B.L. Beard, C.M. Johnson, *Geochim. Cosmochim. Acta* 66 (2002) 2995.
- [19] B.L. Beard, C.M. Johnson, J.L. Skulan, K.H. Nealson, L. Cox, H. Sun, *Chem. Geol.* 195 (2003) 87.
- [20] H.C. Urey, *J. Chem. Soc.* (1947) 562.
- [21] P.M. Grootes, W.G. Mook, J.G. Vogel, *Zeitschr. Phys.* 221 (1969) 257.
- [22] G.T. Barnes, *Coll. Surf. A: Physicochem. Eng. Asp.* 126 (1997) 149.
- [23] T.K. Sherwood, R.L. Pigford, C.R. Wilke, *Mass Transfer*, McGraw-Hill, New York, 1975, p. 677.
- [24] J.R. Welty, C.E. Wicks, R.E. Wilson, *Fundamentals of Momentum, Heat, and Mass Transfer*, John Wiley & Sons, New York, 1984.
- [25] R.E. Criss, *Principles of Stable Isotope Distribution*, Oxford University Press, Oxford, 1999, p. 254.
- [26] C.D. Cappa, M.B. Hendricks, D.J. DePaolo, R.C. Cohen, *J. Geophys. Res.* 108 (D16) (2003) 4525.
- [27] J. Bigeleisen, *Science* 147 (1965) 463.
- [28] M. Xu, F. Zaera, *J. Vac. Sci. Technol.* 14 (2) (1996) 415.
- [29] F. Zaera, *Surf. Sci.* 255 (3) (1991) 280.
- [30] V.B. Polyakov, S.D. Mineev, *Geochim. Cosmochim. Acta* 64 (5) (2000) 849.
- [31] P. Baertschi, W. Kuhn, *Helv. Chim. Acta* 40 (1957) 1084.
- [32] G. Jansco, W.A. Van Hook, *Chem. Rev.* 74 (1974) 689.
- [33] S.R. Poulson, J.I. Drever, *Environ. Sci. Technol.* 33 (1999) 3689.

## Partial filling multiple injection affinity capillary electrophoresis (PFMIACE) to estimate binding constants of receptors to ligands

Jose Zavaleta<sup>a</sup>, Dinora B. Chinchilla<sup>a</sup>, Alejandra Ramirez<sup>a</sup>, Amaris Pao<sup>a</sup>, Karla Martinez<sup>a</sup>, Sanjay Nilapwar<sup>b</sup>, John E. Ladbury<sup>b</sup>, Sanku Mallik<sup>c</sup>, Frank A. Gomez<sup>a,\*</sup>

<sup>a</sup> Department of Chemistry and Biochemistry, California State University, Los Angeles, 5151 State University Drive, Los Angeles, CA 90032-8202, USA

<sup>b</sup> Department of Biochemistry and Molecular Biology, University College London, Gower Street, London WC1E 6BT, United Kingdom

<sup>c</sup> Department of Biochemistry and Molecular Biology, University of Central Florida, 4000 Central Florida Blvd., Orlando, FL 32816, USA

Received 2 March 2006; received in revised form 22 March 2006; accepted 22 March 2006

Available online 15 May 2006

### Abstract

Partial filling multiple injection affinity capillary electrophoresis (PFMIACE) is used to determine binding constants between vancomycin (Van) from *Streptomyces orientalis*, teicoplanin (Teic) from *Actinoplanes teicomyceticus* and ristocetin (Rist) from *Nocardia lurida* to D-Ala-D-Ala terminus peptides and carbonic anhydrase B (CAB, E.C.4.2.1.1) to arylsulfonamides. Two variations of PFMIACE are described herein. In the first technique, the capillary is partially filled with ligand at increasing concentrations, a non-interacting standard, three or four separate plugs of receptor each separated by small plugs of buffer, a plug containing a second non-interacting standard, and then electrophoresed in buffer. Upon continued electrophoresis, equilibrium is established between the ligand and receptors causing a shift in the migration time of the receptors with respect to the non-interacting standards. This change in migration time is utilized for estimating multiple binding constants ( $K_b$ ) for the same interaction. In the second technique, separate plugs of sample containing non-interacting standards, peptide one, buffer, and peptide two, were injected into the capillary column. The capillary is partially filled with a series of buffers containing an antibiotic at increasing concentrations and electrophoresed. Peptides migrate through the column at similar electrophoretic mobilities since their charge-to-mass ratios are approximately the same but remain as distinct zones due to the buffer plug between peptides. Upon electrophoresis, the plug of antibiotic flows into the peptide plugs affecting a shift in the migration time of the peptides with respect to the non-interacting standards occurs due to formation of the of the antibiotic–peptide complex. The shift in the migration time of the peptides upon binding to the antibiotic is used for the Scatchard analysis and measurement of a  $K_b$ . The PFMIACE technique expands the functionality and potential of ACE as an analytical tool to examine receptor–ligand interactions. In PFMIACE, a smaller amount of sample is required in the assay compared to both conventional ACE and MIACE. Furthermore, a wide array of data is obtained from a single experiment, thus, expediting the assay of biological species.

© 2006 Elsevier B.V. All rights reserved.

**Keywords:** Partial filling multiple-injection affinity capillary electrophoresis; Vancomycin; Teicoplanin; Ristocetin; Carbonic anhydrase B; Binding constants; Scatchard plot

### 1. Introduction

Interactions between biological species are key to life and play a direct role in many of the enzyme-based reactions involved in cell division, cell death, and cell transformations [1]. It fol-

lows then that biological interactions are important in the initiation, progression, and harmful effects of human disease including Parkinson's, Alzheimer's, AIDS-HIV, and cancer. With the advancement of molecular biological tools has come the discovery of a huge array of biological interactions focusing foremost on receptor–ligand interactions. Parallel to this development has been the great strides in combinatorial chemical techniques that has allowed for the synthesis of many millions of potential drug targets and precursors. In combination, these two areas

\* Corresponding author. Tel.: +1 323 343 2368; fax: +1 323 343 6490.

E-mail address: [fgomez2@calstatela.edu](mailto:fgomez2@calstatela.edu) (F.A. Gomez).

of research have made the development of new analytical techniques an important area of research.

At present there are several analytical techniques currently available to measure affinity parameters of noncovalent interactions including radioimmunoassays, fluorescence quenching, ammonium sulfate precipitation, and slab gel electrophoresis techniques [1]. These techniques frequently require the separation and quantitation of free or complexed molecules in an equilibrium mixture. If the amount of bound and free ligand in solution can be distinguished, these techniques can provide reasonable estimates of binding constants ( $K_b$ ) for the interaction in question.

Since the first papers in 1992 [2–6] documenting the use of affinity capillary electrophoresis (ACE) to measure affinity parameters between biological species, its use in probing a variety of receptor–ligand interactions has greatly expanded to include protein–drug, protein–DNA, peptide–peptide, peptide–carbohydrate, carbohydrate–drug, and antibody–antigen [7–36]. For example, Kaddis et al. has used ACE to estimate binding constants for the substrate and activator of *Rhodobacter sphaeroides* adenosine 5'-diphosphate-glucose pyrophosphorylase [7]. Li et al. used capillary isoelectric focusing (CIEF) and ACE to determine binding constants between antibodies to the prion protein [8]. Finally, Lewis et al. described the screening of antimicrobial targets using ACE [9]. In a typical form of ACE a sample of receptor and non-interacting standard(s) is exposed to an increasing concentration of ligand in the running buffer causing a change in the migration time of the receptor relative to the standard(s). It is this change in the migration time that is used in the Scatchard analysis to obtain a value for  $K_b$ .

ACE affords a number of advantages over other techniques to study biological interactions. One, only small quantities of receptor and ligand are required. Two, purification of the sample is not required as long as CE can distinguish the impurities from the analyte of interest. Three, radiolabelling of the molecules is not necessary. Four, automated CE instrumentation is widely available. Five, data is reproducible and expeditiously obtained. Finally, a wide range of molecular interactions can be characterized in free solution.

We recently described the use of multiple injection ACE (MIACE) to examine the binding of receptors to ligands [1]. In this technique, multiple samples of receptor (or ligand) are injected into the capillary column and electrophoresed in an increasing concentration of ligand (or receptor). Multiple binding constants for the same interaction are subsequently obtained, thereby, shortening the ACE experiment. In earlier work we described the use of partial-filling ACE (PFACE) techniques to determine binding constants between receptors and ligands that utilizes less material than in standard ACE techniques [15–18]. Here, the capillary is partially filled with ligand (or receptor) and sample plug of receptor (or ligand) is introduced into the capillary and electrophoresed. During electrophoresis the zones of samples overlap within the capillary where an equilibrium is established prior to the point of detection.

When limited quantities of material are available for use in standard ACE due to expense, synthetic difficulty, and/or time constraints, there is a need for either alternative assay techniques

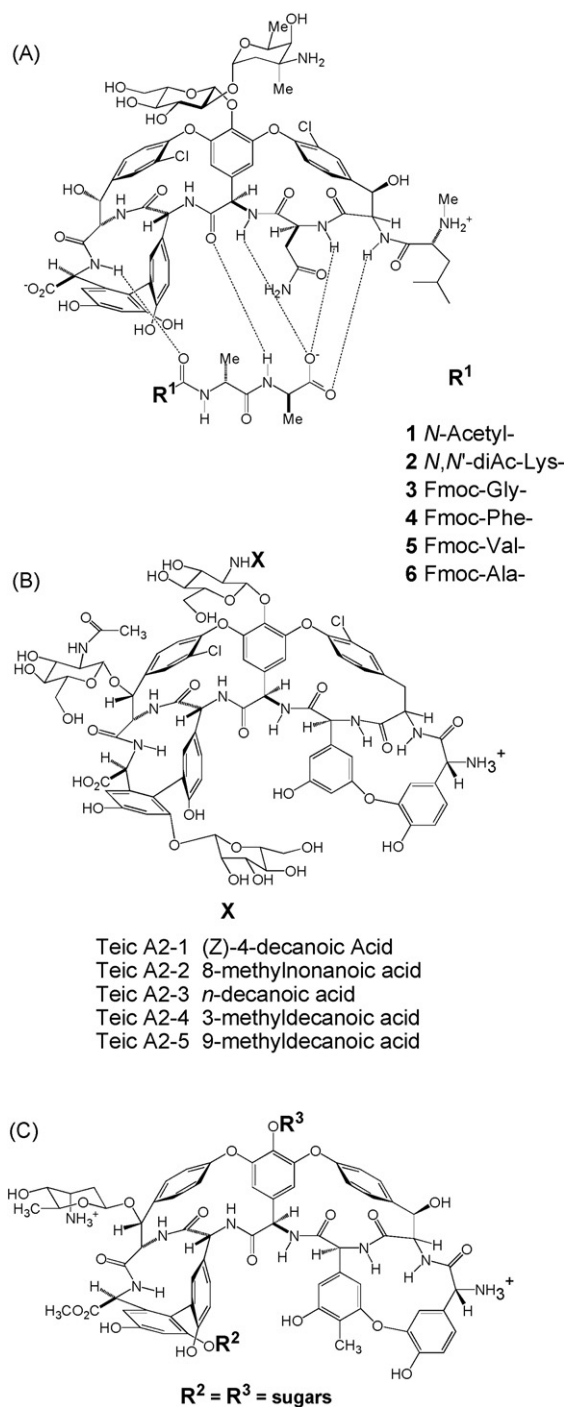


Fig. 1. Structures of (A) vancomycin, (B) teicoplanin, (C) ristocetin, and D-Ala-D-Ala ligands 1–6 used in this study.

or a variation in the ACE technique. Herein, we describe the use of partial filling multiple injection ACE (PFMIACE) for examining receptor–ligand interactions using as model systems the glycopeptide antibiotics vancomycin (Van), teicoplanin (Teic) and ristocetin (Rist) (Fig. 1) and the enzyme carbonic anhydrase B (CAB, E.C.4.2.1.1.). Two variations of PFMIACE are detailed that demonstrate the versatility of the technique for evaluating binding interactions between receptors and ligands.

## 2. Materials and methods

### 2.1. Chemicals and reagents

All chemicals were analytical grade. Vancomycin, D-Ala-D-Ala, *N*-acetyl-D-Ala-D-Ala (**1**), *N,N'*-diacetyl-Lys-D-Ala-D-Ala (**2**), carbonic anhydrase B (CAB, E.C.4.2.1.1), horseheart myoglobin (HHM), nicotinamide adenine dinucleotide (NAD), and nicotinamide adenine dinucleotide, reduced form (NADH) were purchased from Sigma Chemical Company (St. Louis, MO, USA) and were used without further purification. Teicoplanin-HCl was purchased from Advanced Separation Technologies Inc. (Whippany, NJ, USA) and was used without further purification. Fmoc-Gly-NHS, Fmoc-Ala-NHS, Fmoc-Phe-NHS, and Fmoc-Val-NHS were purchased from

Bachem California Inc. (Torrance, CA, USA). Mesityl oxide (MO) was purchased from Calbiochem (San Diego, CA, USA). Ristocetin was obtained from BioData Corporation (Horsham, PA, USA) and was used without further purification. Compounds **7–11** (Fig. 2) were synthesized based on literature procedures [24].

#### 2.1.1. Receptor PFMIACE

Stock solutions of Van (0.2 mg/mL), Teic (0.2 mg/mL), and HHM (1 mg/mL) were each prepared by dissolving in buffer (192 mM glycine–25 mM Tris; pH 8.3). Stock solutions of the *N*-protected amino acids (4 mM) were prepared by dissolving the compounds in buffer. Fmoc-Gly-D-Ala-D-Ala (**3**), Fmoc-Phe-D-Ala-D-Ala (**4**), Fmoc-Ala-D-Ala-D-Ala and Fmoc-Val-D-Ala-D-Ala (**5**) were prepared based

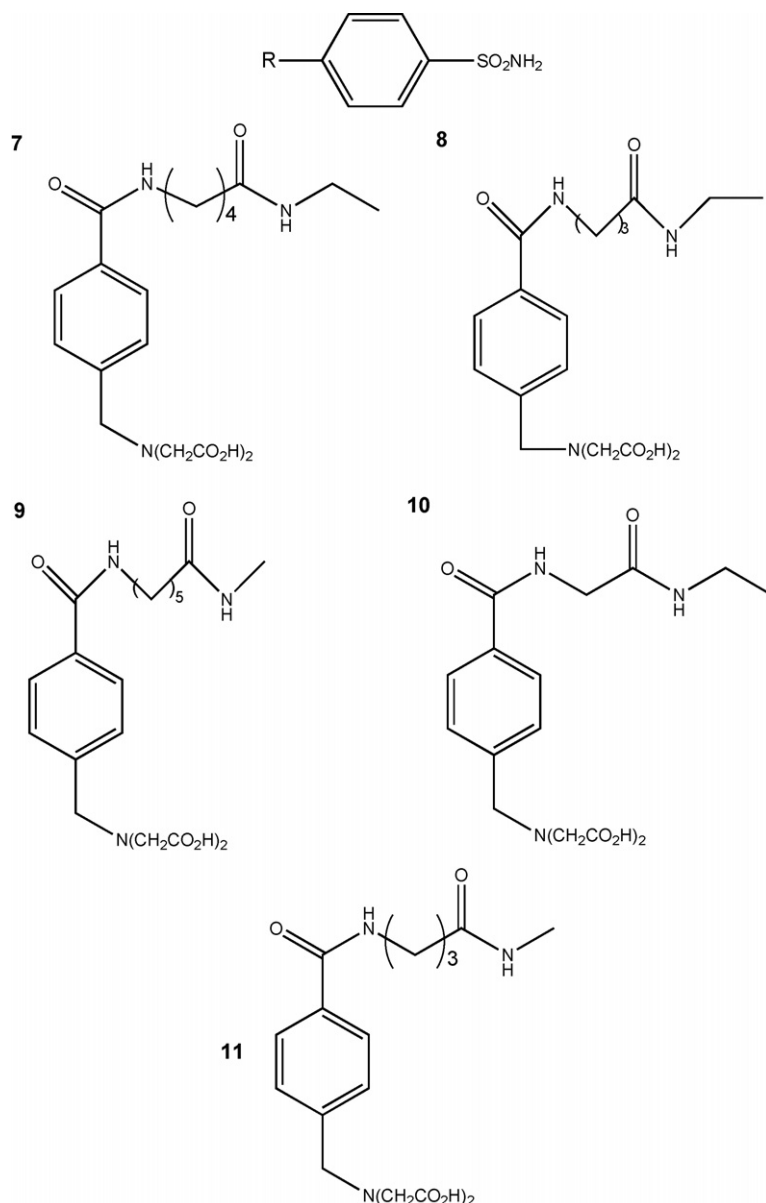


Fig. 2. Ligands **7–11** used in this study.

on literature procedures [22]. For CAB, stock solutions of CAB (1 mg/mL), HHM (2 mg/mL), MO (100/1000  $\mu$ L buffer) were each prepared by dissolving in buffer (192 mM glycine–25 mM Tris; pH 8.3). Stock solutions of ligands 7–11 (1 mg/mL) were prepared by dissolving the compounds in buffer.

### 2.1.2. Peptide PFMIACE

Stock solutions of Van (0.2 mg/mL), Teic (1.0 mg/mL), Rist (1.0 mg/mL), NAD (0.2 mg/mL), and NADH (0.2 mg/mL), were each prepared by dissolving in buffer (192 mM glycine–25 mM Tris; pH 8.3). Stock solutions of the *N*-protected amino acids (4 mM) were prepared by dissolving the compounds in buffer. Fmoc–Gly–D-Ala–D-Ala (**3**), Fmoc–Ala–D-Ala–D-Ala (**6**), Fmoc–Val–D-Ala–D-Ala (**5**), and Fmoc–Phe–D-Ala–D-Ala (**4**) were prepared based on literature procedures [22].

## 2.2. Apparatus

### 2.2.1. Receptor PFMIACE

The capillary electrophoresis (CE) system used in this study was a Beckman Model P/ACE 5510 (Fullerton, CA, USA). The capillary tubing (Polymicro Technology, Inc., Phoenix, AZ, USA) used for the experiment was uncoated fused silica with an internal diameter of 50  $\mu$ m, length from inlet to detector of 40.5 cm and a length from detector to outlet of 6.5 cm. The conditions used in CE were as follows: for Van and Teic, voltage, 25 kV; current, 6.7  $\mu$ A for Van, 7.9  $\mu$ A for Teic; detection, 200 nm; temperature, 23.0  $\pm$  0.1  $^{\circ}$ C; for CAB, voltage, 25 kV; current, 8.0  $\mu$ A; detection, 200 nm; temperature, 23.0  $\pm$  0.1  $^{\circ}$ C. Data were collected and analyzed with Beckman System Gold software.

### 2.2.2. Peptide PFMIACE

The CE system used in this study was a BeckmanCoulter MDQ (Fullerton, CA, USA). The capillary tubing (Polymicro Technology, Inc., Phoenix, AZ, USA) used for the experiment was uncoated fused silica with an internal diameter of 50  $\mu$ m, length from inlet to detector of 50.0 cm and a length from detector to outlet of 11 cm. The conditions used in CE were as follows: for Van, Teic, and Rist, voltage, 25 kV; current, 7.8  $\mu$ A for Van, 7.9  $\mu$ A for Teic and Rist; detection, 200 nm; temperature, 23.0  $\pm$  0.1  $^{\circ}$ C. Data were collected and analyzed with Beckman-Coulter 32 Karat software.

## 2.3. Procedures

### 2.3.1. Receptor PFMIACE

For Van, the capillary was first equilibrated with buffer (192 mM glycine–25 mM Tris; pH 8.3) for 0.5 min. A 0.12 min buffer plug is then introduced containing a concentration of peptide (0–300  $\mu$ M). Separate plugs of sample solution (5 s injections each, 6 nL [at 0.5 psi, 1 s injection equals 1.2 nL]) containing the marker MO, four plugs of Van, and the second marker (HHM) were introduced by pressure injection each separated by a plug of buffer (36 s injection). The electrophoresis was carried out using Tris–glycine buffer containing no ligand

at 25 kV for 8.0 min to complete the detection of all species. The sequence was repeated for increasing concentrations of peptide. Experimental conditions for Teic were similar except that three injections of Teic were used each separated by a 18 s plug of buffer.

### 2.3.2. Peptide PFMIACE

For analysis of **1** and **2**, separate plugs of solution (3.6 nL) containing the marker (MO), **2**, buffer (18.0 nL), and **1** were introduced by pressure injection followed by an injection of antibiotic (96 s at 0.7 psi) and electrophoresed at a concentration of antibiotic (0–60  $\mu$ M). The electrophoresis was carried out using Tris–glycine buffer at 25 kV for 7.0 min to complete the detection of all species. The sequence was repeated for increasing concentrations of antibiotic. For Rist and Teic NADH was used as the non-interacting standard. For CAB, separate plugs of solution of ligand (0.12 min at high pressure), markers (MO and HHM), buffer, CAB, buffer, CAB, buffer, and CAB, were electrophoresed at increasing concentrations of ligand. The electrophoresis was carried out using Tris–glycine buffer at 25 kV for 8.0 min to complete the detection of all species.

### 2.3.3. Microcalorimetric studies

All the titration experiments were performed using the VP-ITC system (MicroCal Inc., MA). In each experiments 20 aliquots of 15  $\mu$ L of **4** (1.30 mM), Fmoc–Val–DADA (1.20 mM) and **4** (1.31 mM) were injected into 1.463 mL of Rist (0.108 mM in 192 mM glycine–25 mM Tris Buffer, pH 8.3) at 25  $^{\circ}$ C. Resulting data was fitted after subtracting the heats of dilution. Heats of dilution were determined in separate experiments from addition of **4**, **5** and **6** into buffer. Titration data was fitted using a nonlinear least-squares curve fitting algorithm with three floating variables: stoichiometry, binding constant ( $K_b = 1/K_d$ ) and change of enthalpy of interaction ( $\Delta H^{\circ}$ ).

## 2.4. Forms of analysis

We employed two forms of analysis to estimate  $K_b$ . The first form of analysis (Eq. (1)) used electrophoretic mobilities ( $\mu$ ) as the basis of the analysis; the second (Eq. (2)), termed the relative migration time ratio (RMTR), utilized two markers [14] (an extended discussion of these two forms of analysis can be found in this reference). The use of either forms of analysis allowed for the estimation of  $K_b$  via a Scatchard plot. We have found that the use of Eq. (2) best compensates for variations in electroosmotic flow (EOF) caused by Joule heating and other changes in the constitution of the capillary. If minimal changes in EOF exist either equation can be successfully used for ACE analysis:

$$\frac{\Delta\mu_{P,A}}{[A]} = K_b\Delta\mu_{P,A}^{\max} - K_b\Delta\mu_{P,A} \quad (1)$$

$$\frac{\Delta\text{RMTR}_{P,A}}{[L]} = K_b\Delta\text{RMTR}_{P,A}^{\max} - K_b\Delta\text{RMTR}_{P,A} \quad (2)$$



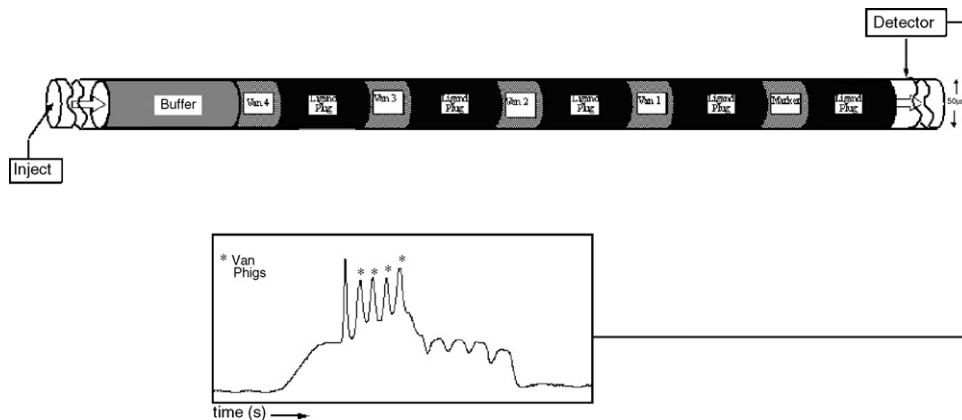


Fig. 3. Schematic of partial-filling multiple injection affinity capillary electrophoresis (PFMIACE) experiments (A) receptor in sample and (B) ligands in sample.

### 3. Results and discussion

#### 3.1. PFMIACE: receptor as sample

In our first series of experiments we examined the binding of **3** to Van. Van-group antibiotics kill bacterial cells by inhibiting peptidoglycan biosynthesis by binding to the D-Ala D-Ala terminus of the bacterial cell wall precursors [37–42]. Within the past two decades there has been an increase in Van resistant enterococci (VRE), thereby, making it increasingly important to develop new Van-group antibiotics. Using the PFMIACE technique, a buffer plug of **3** was introduced at a given concentration of ligand (0.5 psi at 7.2 s) followed by a sample plug (0.5 psi at 3 s) containing the non-interacting standard MO, ligand plug, and then four plugs (0.5 psi at 3 s) of sample containing Van (Fig. 3). Between each injection of Van was placed a small plug (0.5 psi at 36 s) of buffer to aid in the separation of the Van zones of solution. Upon application of a voltage the individual plugs of sample migrate through the capillary and into the zone of **3**. The injection sequence was then repeated at increasing concentration of ligand.

Fig. 4 shows a representative series of electropherograms of Van in a capillary partially filled with increasing concentrations of **3**. The height of the ligand plateaus present in the electropherograms increase as a result of the increasing concentration of **3** partially filled in the capillary. As the concentration of **3** in the capillary increases the peak for the Van species shift to a greater migration time due to complexation and the formation of Van-**3** which is more negatively charged than Van alone. The inverted peaks are a result of the dilution of **3** in the ligand plug upon complexation to Van. This effect is commonly observed in ACE studies and is more pronounced when the ligand is highly chromophoric.

Fig. 5 details the Scatchard plots of the data for the Van peaks according to Eq. (1). As can be seen the first three plugs of Van result in similar Scatchard plots. The last Van peak does not give a reliable Scatchard plot possibly due to the broadness of the peak. In our earlier work on PFACE we found that if the inverted peak(s) migrated too close to the peak of interest a Scatchard plot with poor correlation coefficient ( $R^2$ ) was realized [15]. Methods of decreasing the likelihood of this occurring include the

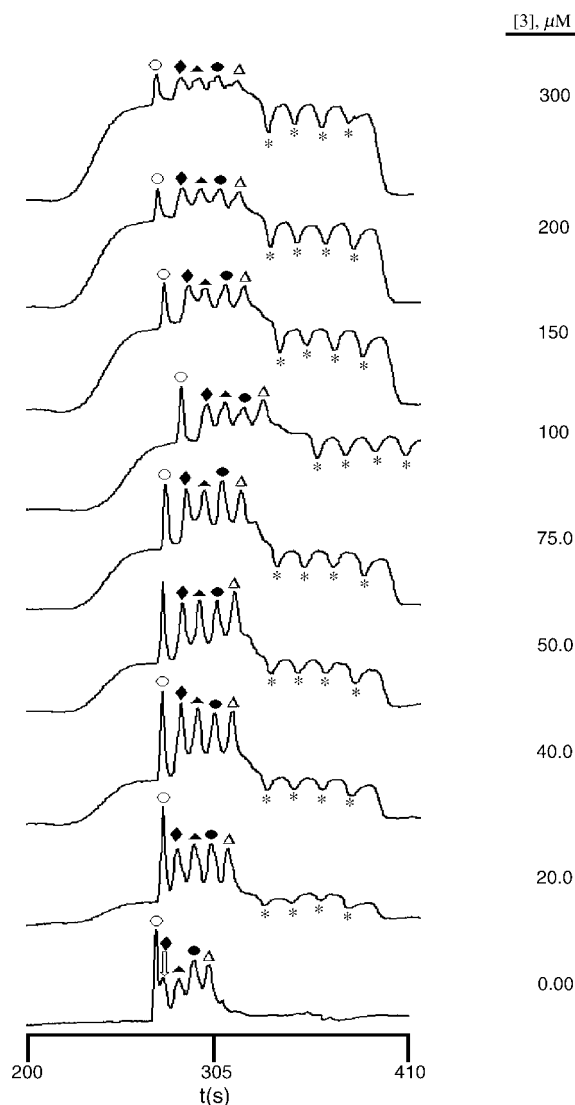


Fig. 4. A representative set of electropherograms of Van (darkened diamond, triangle, circle, and open triangle) in 192 mM glycine–25 mM Tris buffer (pH 8.3) containing various concentrations of **3** using the partial filling multiple injection affinity capillary electrophoresis (PFMIACE) technique. The total analysis time in each experiment was 8.0 min at 25 kV (current 6.7  $\mu$ A) using a 40.5 cm (inlet to detector), 50  $\mu$ m ID open, uncoated quartz capillary. MO (open circle) was used as an internal standard. The asterisks are explained in the text.

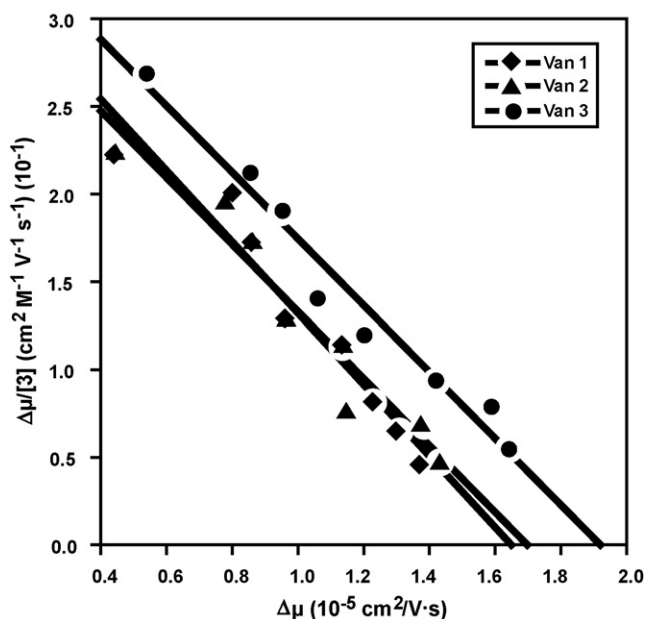


Fig. 5. Scatchard plots of the data for Van and 3 according to Eq. (1).

use of a longer capillary, different voltage, and/or modification in buffer pH. Still, it is not always possible to completely eradicate the effects of the negative peak(s) on peak migration times as the electrophoretic mobility ( $\mu$ ) of a species is dependent on many variables some of which are out of control of the operator. The migration time of the Van plugs did not allow for the placement of a marker between the first Van plug and marker MO and the initial Van peak. In addition, we were unable to use a second marker that migrated after the last plug of Van because the two markers used (NAD and 4-carboxybenzenesulfonamide [CBSA]) migrated at similar migration times as the inverted peaks. Hence, Eq. (1) was used for the analysis instead of Eq. (2).

Table 1 summarizes the binding data obtained for Van and ligand 3. The average binding constant was determined to be  $19.5 \times 10^3 \text{ M}^{-1}$ . In our previous work using MIACE we determined a value for  $K_b$  of  $22.3 \times 10^3 \text{ M}^{-1}$  [1]. Note, that this study was conducted at a different pH so it is difficult to compare the values for  $K_b$  between the two techniques. At present, we are examining the two techniques under the same experimental conditions to determine which method best realizes accurate binding constant data. Now that the proof of concept for PFMIACE was demonstrated we then examined several other ligands. Table 2 lists the values for  $K_b$  obtained for peptides 1, 4, and 5. The values for  $K_b$  for ligand 1 and 4 were approximately 2.0 and 2.5 times as large using PFMIACE than MIACE. On the other hand 5 was slightly smaller than that found for MIACE. We have

Table 1  
Experimental values of binding constants  $K_b$  ( $10^3 \text{ M}^{-1}$ ) of ligand 3 to Van obtained by Eq. (1)

Van peak	$K_b$ ( $10^3 \text{ M}^{-1}$ )	$R^2$
1	20.3	0.937
2	19.1	0.934
3	19.0	0.967

Table 2

Experimental values of binding constants  $K_b$  ( $10^3 \text{ M}^{-1}$ ) of ligands 1–6 to Van and Teic obtained by Eqs. (1) and (2)

Antibiotic	Ligand	$K_b$ ( $10^3 \text{ M}^{-1}$ )
Van	1	7.2 <sup>a</sup>
Teic	1	24.9 <sup>b</sup>
Teic	2	78.1
Teic	4	62.4 <sup>c</sup>
Van	4	102.4 <sup>d</sup>
Teic	5	122.3 <sup>e</sup>
Van	5	19.1 <sup>f</sup>

<sup>a</sup> Previous estimates [1]:  $K_b = 3.7 \times 10^3 \text{ M}^{-1}$ .

<sup>b</sup> Previous estimates [1]:  $K_b = 20.7 \times 10^3 \text{ M}^{-1}$ .

<sup>c</sup> Previous estimates [1]:  $K_b = 15.5 \times 10^3 \text{ M}^{-1}$ .

<sup>d</sup> Previous estimates [1]:  $K_b = 40.0 \times 10^3 \text{ M}^{-1}$ .

<sup>e</sup> Previous estimates [1]:  $K_b = 21.5 \times 10^3 \text{ M}^{-1}$ .

<sup>f</sup> Previous estimates [1]:  $K_b = 25.9 \times 10^3 \text{ M}^{-1}$ .

found that variable values for binding constants can be obtained based on differences in voltage, buffer strength, capillary length, and receptor concentration.

We then examined the binding of Teic to ligands 1, 2, 4, and 5. Like Van, teicoplanin (Teic) inhibits cell wall synthesis by impeding the action of transglycosylases and transpeptidases. It has a linear heptapeptide structure which is cross-linked between residues 1–4, and 4 and 6 by diphenyl ether bridges. It is cross-linked by a biphenyl bridge between residues 5 and 7. Teic is composed of a mixture of smaller analogue forms termed T-A<sub>1-1</sub> through T-A<sub>1-5</sub> [20]. The analogues differ by about 20 g/mol due to the variation in the carbon chain and the substituent groups of the hydrophobic acyl side chain.

A similar injection sequence was used for analysis of Teic and the ligands. Table 2 summarizes the binding data for these ligands to Teic. The value obtained for the  $K_b$  for ligand 1 was comparable for both PFMIACE and MIACE. For ligands 4 and 5 the values obtained for PFMIACE were 4 and 6 times larger than for MIACE. We are unable to explain the difference in binding constants but studies are continuing to determine optimal assay conditions for the PFMIACE technique [1].

One of the major advantages of PFMIACE over MIACE and other ACE techniques is the quantity of sample used in the experiment. Whereas in MIACE multiple zones of Van, migrate through a constant flow of solution containing ligand, in PFMIACE the capillary is only partially filled with ligand. The amount of ligand used in PFMIACE analysis for Van and Teic is 170 and 89 pmol, respectively; in MIACE 592 pmol. Hence, there is a clear advantage in using PFMIACE over MIACE especially when limited quantities of ligand are available as is common in the pharmaceutical industry and in combinatorial chemistry practices.

We then wanted to prove that another receptor–ligand combination could be accurately assessed using the PFMIACE technique. Here, we examined the binding of arylsulfonamides to the enzyme CAB. CAB is a zinc protein of the lyase class that catalyzes the equilibration of dissolved carbon dioxide and carbonic acid. It is strongly inhibited by sulfonamide-containing molecules. We chose the CAB system for several reasons: (1) it does not absorb to the walls of the uncoated capillaries; (2)

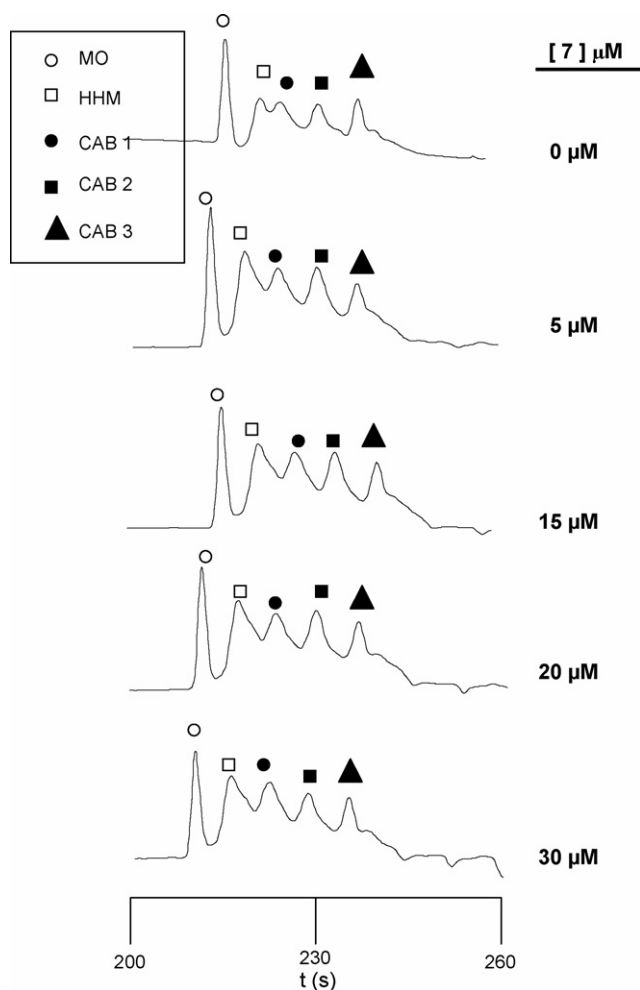


Fig. 6. A representative set of electropherograms of CAB (darkened diamond, square, triangle) in 192 mM glycine–25 mM Tris buffer (pH 8.3) containing various concentrations of **7** using the PFMIACE technique. The total analysis time in each experiment was 8.0 min at 25 kV (current 8.0  $\mu$ A) using a 40.5 cm (inlet to detector), 50  $\mu$ m ID open, uncoated quartz capillary. MO (open circles) and HHM (open squares) were used as internal standards.

we have data describing its electrophoretic behavior in other circumstances; (3) it is commercially available and inexpensive; (4) ligands for it can be easily synthesized, and; (5) many ligands bind to it with values of  $K_b$  between  $10^5$  and  $10^9$   $M^{-1}$ .

Using a similar series of injections as that used for the Van studies, three samples of CAB were injected onto the capillary column and their binding to ligand **7** examined (Fig. 2). Fig. 6 shows a representative series of electropherograms of CAB in a capillary partially filled with increasing concentrations of **7**

Table 3

Experimental values of binding constants  $K_b$  ( $10^6$   $M^{-1}$ ) of ligands **7–11** to CAB obtained by Eq. (2) and values for the correlation coefficient ( $R^2$ )

Ligand	$K_b$ ( $10^6$ $M^{-1}$ ) ( $R^2$ )
<b>7</b>	0.19 (0.996)
<b>8</b>	0.46 (0.961)
<b>9</b>	0.59 (0.956)
<b>10</b>	2.48 (0.945)
<b>11</b>	0.19 (0.973)

at 200 nm. Compound **7** is negatively charged and when bound to CAB shifts the migration time of the CAB-**7** complex to a greater migration time. Table 3 lists the values for  $K_b$  for ligands **7–11** binding to CAB. The small negative peaks to the right of the final CAB peak represent the dilution of ligand in the electrophoresis buffer upon binding to CAB. The voids are common in ACE techniques and are more pronounced when the ligand (or receptor) in the running buffer is highly chromophoric.

### 3.2. PFMIACE: ligand as sample

ACE can exploit either changes in migration time of a receptor on complexation to a ligand or vice versa. As long as there is a change in charge and significant change in mass between uncoupled and coupled species (and as long as  $K_{on}$  and  $K_{off}$  are appreciably fast) then a shift in migration time will occur and a binding constant elucidated. When exploring the binding simultaneously of two or more species in a sample criteria for the assay is that both species either have different charges or a significant difference in molecular weight. From previous work, we established that ligands **3** and **6** failed to separate using conventional CE as both have the same charge and varied in molecular weight by only 14 g/mol. We, though, were able to successfully separate both ligands using the MIACE technique. To further expand on the MIACE technique we chose to couple it to partial filling techniques.

Fig. 7 shows a schematic representation of the injection plug sequence. In this technique, separate plugs of sample solution (3.6 nL) containing the marker (MO), second marker (NADH), **6**, buffer (18.0 nL), and **3** (18.0 nL) were introduced via pressure injection followed by partially filling the capillary with an antibiotic. Upon electrophoresis, the plug of antibiotic migrates into the zones of the two ligands due to it having a greater electrophoretic mobility. There is sufficient time during electrophoresis for equilibrium to be established. The ligand–antibiotic complex is then detected by UV–vis absorption. Analysis of the change in the migration time of the ligands

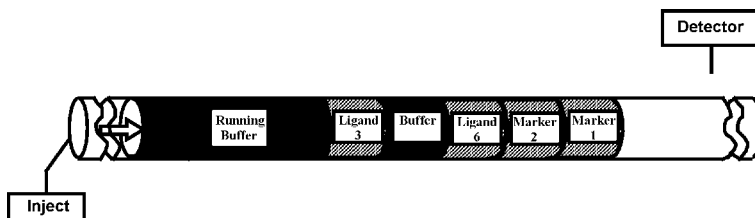


Fig. 7. A schematic representation of the sample injection sequence using the partial filling multiple injection technique to estimate binding interactions of **3** and **6** to Van, Rist, and Teic.

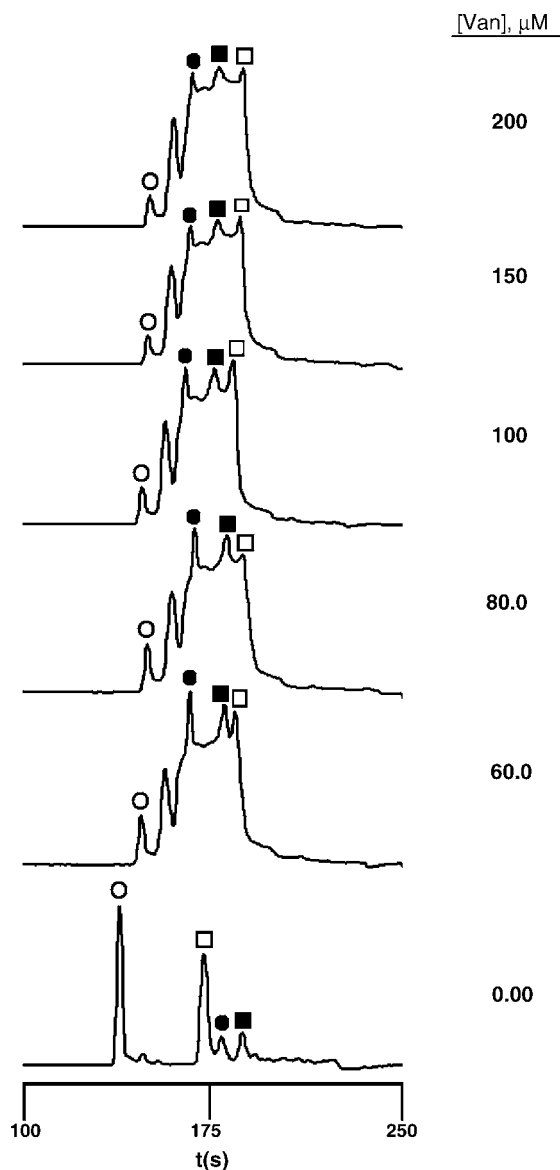


Fig. 8. A representative set of electropherograms of ligands **3** (darkened square) and **6** (darkened circle) in 192 mM glycine–25 mM Tris buffer (pH 8.3) containing various concentrations of Van using the partial filling multiple-injection affinity capillary electrophoresis (PFMIACE) technique. The total analysis time in each experiment was 7.0 min at 25 kV (current 8–12  $\mu$ A) using a 50 cm (inlet to detector), 50  $\mu$ m ID open, uncoated quartz capillary. MO (open circle) and NAD (open square) were used as internal standards.

relative to the standards, as a function of the concentration of the antibiotic yields a value for the  $K_b$ . In the present study we examined four peptides and their binding to Van, Rist, and Teic. Fig. 8 illustrates a representative series of electropherograms of **3**, **6**, and increasing concentrations of Van partially filled in the capillary column. Upon increasing the concentration of Van a shift in the migration time of **3** and **6** is observed. The newly formed Van-**3** and Van-**6** complexes have different charge-to-mass ratios than the unbound species causing a shift to less migration time relative to the standards. The two markers (MO and NAD) are unaffected during the experiment.

Increasing concentrations of Van can be seen as a height increase of the Van plateaus. The distinctive box-like shape

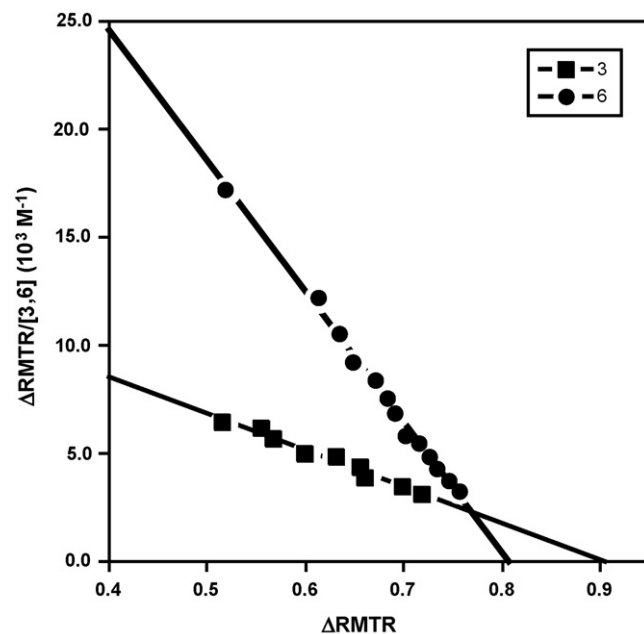


Fig. 9. Scatchard plots of the data for ligands **3** and **6** and Van according to Eq. (2).

represents the peak corresponding to the Van zone. The near-horizontal box is proof of a uniform injection of antibiotic and a stable concentration of Van in the capillary column. Further proof of binding interaction is the negative peaks indicating dilution of Van upon complexation with the ligands. At the zero concentration of Van, the peaks are base-line resolved clearly showing the separation between ligands **3** and **6**. At  $[\text{Van}] = 60 \mu\text{M}$  the peaks for **3** and **6** have completely shifted to the left of the NAD marker. Further increasing the concentration of Van shifts the Van-**3** and Van-**6** complexes to even shorter elution times. The extra peak between MO and **6** is excess D-Ala-D-Ala peptide from the reaction. Only six electropherograms were reproduced in order to grant clarity to Fig. 8 although more concentrations were used to obtain the  $K_b$ .

The dual marker form of analysis was used to calculate  $K_b$ . Fig. 9 are the Scatchard plots for ligands **3** and **6** binding to Van. The data illustrates that ligand **6** binds stronger to Van than ligand **3** with similar magnitude. Previous work using MIACE observed that the  $K_b$  is smaller for ligands **3** and **6** ( $9.8$  and  $11.4 \times 10^3 \text{ M}^{-1}$ , respectively) [1]. Table 4 lists the values obtained using the PFMIACE technique. Ligands **4** and **5** were also studied with Van. The data suggests that ligand **5** is a much stronger binder to Van than ligand **4** ( $273.1$  and  $81.5 \times 10^3 \text{ M}^{-1}$ , respectively). Our results show that different binding constants are obtained for **3–6** to Van contrary to previous studies that have shown that modification at the N-terminus does not significantly affect binding. It is possible that upon complexation to Van, the side group of the amino acid alpha to the D-Ala-D-Ala terminus peptide might cause a structural change to the binding pocket and changing the proximity of the five key hydrogen bonds, hence, giving either a favorable or unfavorable interaction. Moreover, interactions such as hydrophilic, hydrophobic, esteric, and others might also play a role in the different binding affinities.

Table 4

Experimental values of binding constants  $K_b$  ( $10^3 \text{ M}^{-1}$ ) of ligands 3–6 to Van, Rist, and Teic obtained by Eq. (2) and values for the correlation coefficient ( $R^2$ )

Ligand	$K_b$		
	Van	Rist	Teic
3	16.9 (0.977) <sup>a</sup>	16.6 (0.907) <sup>b</sup>	68.3 (0.938) <sup>c</sup>
4	81.5 (0.959)	35.4 (0.972) <sup>d</sup> 46.9 (ITC)	108.8 (0.930)
5	273.1 (0.935)	25.7 (0.920) <sup>e</sup> 40.0 (ITC)	13.5 (0.950)
6	60.5 (0.995) <sup>f</sup>	16.0 (0.916) <sup>g</sup> 29.3 (ITC)	68.5 (0.887) <sup>h</sup>

<sup>a</sup> Previous estimates [21]:  $K_b = 41.6 \times 10^3 \text{ M}^{-1}$  (pH 7.5).

<sup>b</sup> Previous estimates [1,21]:  $K_b = 41.4 \times 10^3 \text{ M}^{-1}$  (pH 8.3),  $K_b = 8.2 \times 10^3 \text{ M}^{-1}$  (pH 7.5).

<sup>c</sup> Previous estimates [21]:  $K_b = 21.8 \times 10^3 \text{ M}^{-1}$  (pH 7.5).

<sup>d</sup> Previous estimates [1]:  $K_b = 16.4 \times 10^3 \text{ M}^{-1}$  (pH 8.3).

<sup>e</sup> Previous estimates [1]:  $K_b = 25.3 \times 10^3 \text{ M}^{-1}$  (pH 8.3).

<sup>f</sup> Previous estimates [21]:  $K_b = 174.5 \times 10^3 \text{ M}^{-1}$  (pH 7.5).

<sup>g</sup> Previous estimates [1,21]:  $K_b = 9.1 \times 10^3 \text{ M}^{-1}$  (pH 8.3),  $K_b = 52.4 \times 10^3 \text{ M}^{-1}$  (pH 7.5).

<sup>h</sup> Previous estimates [21]:  $K_b = 185.1 \times 10^3 \text{ M}^{-1}$  (pH 7.5).

A series of experiments were also conducted with Rist. Like Van, Rist is a glycopeptide antibiotic which inhibits cell wall peptidoglycan biosynthesis in susceptible bacteria by binding to key peptidoglycan intermediates. Table 4 illustrates the data afforded by the PFMIACE technique.

We used isothermal titration calorimetry (ITC) to examine the binding of peptides 4–6 to Rist [43]. Fig. 10 is the ITC sample data for the titration of 4 to Rist. The data for the ITC studies are found in Table 4. As can be seen there is close agreement between the data from ACE and ITC. It was also determined that ligands 4–6 bind to Rist with stoichiometry of 1. Binding studies of ligands 3–6 to Teic were also examined. The data obtained is listed in Table 4.

The PFMIACE technique affords numerous advantages: one, even smaller quantities of sample are required than in traditional ACE assays. Two, the capillary need only be partially filled with receptor/ligand. An important point when nominal quantities of material are available. Three, like the MIACE technique, it is possible to obtain multiple binding constants for different species, thus shortening the time required to conduct the experiment. Table 5 is a general comparison between PFMIACE, standard ACE, and MIACE. In standard ACE a single plug of receptor is injected into the capillary column in increasing concentration of ligand in the electrophoresis buffer. A shift in migration time of the receptor on change of ligand concentration is used for the analysis of a binding constant. Due to variations in EOF multiple experimental runs are conducted which lengthens the time of the binding assay. As can be seen the amount of ligand used in PFMIACE is much smaller than in standard ACE techniques and is almost one order of magnitude smaller than in the original MIACE method. The length of the time for the PFMIACE method (and MIACE technique) is variable depending on the length of the capillary column, voltage, buffer ionicity, etc. but, overall, it is less than 30% the time required for standard ACE. In turn, a higher throughput of samples is possi-

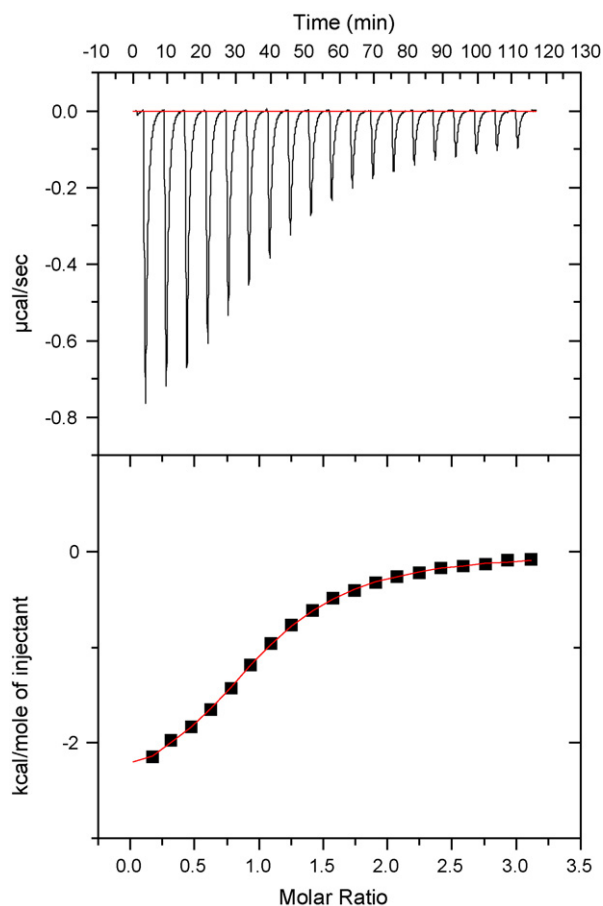


Fig. 10. Sample raw data for the titration of 4 into Rist at 25 °C. In the top panel, the peaks in the lower data set show a heat produced by 15  $\mu\text{L}$  serial injections of 1.16 mM 4 into 1.463 mL of 0.108 mM Rist contained in the sample cell of the calorimeter. Integration of these peaks produces the binding isotherm shown in bottom panel (solid squares). The points are fitted to a model for a single independent binding site.

ble with PFMIACE than with typical ACE techniques. Finally, there can be some improvement in reproducibility since only one electrophoretic run is required per concentration of ligand thereby lessening the potential for instrument and technician error although we saw little variance in our statistical analysis.

Table 5

Comparison between receptor PFMIACE, standard ACE, and MIACE for a typical binding assay

Variable	PFMIACE	Standard ACE <sup>a</sup>	MIACE
Volume of receptor	43.2 nL	43.2 nL	43.2 nL
Moles of receptor	5.82 pmol	5.82 pmol	5.82 pmol
Volume of ligand	2.77 $\mu\text{L}$	116.26 $\mu\text{L}$	23.25 $\mu\text{L}$
Moles of ligand	0.32 nmol	13.58 nmol	2.72 nmol
Time for assay	54–72 min <sup>b,c</sup>	270 min <sup>b,c</sup>	54–72 min <sup>b,c</sup>

<sup>a</sup> Based on five repetitions for each ligand concentration.

<sup>b</sup> The length of the experiment is dependent on the number of ligand concentrations utilized in the assay and in the experimental conditions including, for example, length of capillary column, voltage, and buffer. In this comparison, nine different electrophoretic runs are assumed and a similar duration of electrophoresis was assumed. The buffer conditions are comparable.

<sup>c</sup> Time noted is the amount of time for electrophoresis. Excludes time between each electrophoresis run, change of sample, and buffer wash.



#### 4. Conclusion

We have demonstrated the development of partial filling multiple injection ACE (PFMIACE) using as model systems the glycopeptide antibiotics vancomycin, teicoplanin and ristocetin and carbonic anhydrase B. In PFMIACE, partial filling and multiple injection techniques are coupled to each other. Two techniques are described. In the first, multiple plugs of receptor are injected into the capillary column which migrate with equal electrophoretic mobility into a zone of ligand where a dynamic equilibrium is established prior to detection. Multiple binding constants are subsequently determined for the same biological interaction which are similar in agreement to those obtained via other ACE techniques. In the second, separate plugs of sample containing non-interacting standards, peptides, and buffer are injected into the capillary column and electrophoresed. Peptides migrate through the column at similar electrophoretic mobilities since their charge-to-mass ratios are approximately the same but remain as distinct zones due to the buffer plugs between peptides. The electrophoresis is then carried out in an increasing concentration of antibiotic in the running buffer. The shift in the migration time of the peptides upon binding to the antibiotic is used for the Scatchard analysis and measurement of a  $K_b$ .

PFMIACE offers a number of advantages over other ACE techniques. Specifically, a typical binding assay utilizes less receptor and ligand than that used in other ACE methods. Additionally, since only electrophoretic run needs to be conducted per concentration of ligand thereby yielding multiple binding constants for the same interaction concurrently, the technique is faster than other ACE techniques. Finally, a single electrophoretic can lessen the propensity of instrument error and/or variability in peak migration times that can lead to a poor analysis of the data although we did not see any marked improvement in reproducibility when comparing PFMIACE and standard ACE. Future work is focused on expanding the technique to other systems and in further modifying the technique for use with even smaller sample volumes.

#### Acknowledgment

The authors gratefully acknowledge financial support for this research by grants from the National Science Foundation (CHE-0136724, CHE-0515363 and DMR-0351848), and the National Institutes of Health (1R15 AI055515-01, 1R15AI65468-01, and GM54939).

#### References

- [1] D. Chinchilla, J. Zavaleta, K.M. Martinez, F.A. Gomez, *Anal. Bioanal. Chem.* 383 (2005) 625.
- [2] J.C. Kraak, S. Busch, H. Poppe, *J. Chromatogr.* 608 (1992) 257.
- [3] Y.-H. Chu, G.M. Whitesides, *J. Org. Chem.* 57 (1992) 3524.
- [4] Y.-H. Chu, L.Z. Avila, H.A. Biebuyck, G.M. Whitesides, *J. Med. Chem.* 35 (1992) 2915.
- [5] N.H.H. Heegaard, F.A. Robey, *Anal. Chem.* 64 (1992) 2479.
- [6] Y. Baba, M. Tsuhako, M. Sawa, M. Akashi, E. Yashima, *Anal. Chem.* 64 (1992) 1920.
- [7] J. Kaddis, C. Zurita, J. Moran, M. Borra, N. Polder, C.R. Meyer, F.A. Gomez, *Anal. Biochem.* 327 (2004) 252.
- [8] G. Li, X. Zhou, Y. Wang, A. El-Shafey, N.H. Chiu, I.S. Krull, *J. Chromatogr. A* 1053 (2004) 253.
- [9] L.M. Lewis, L.J. Engle, W.E. Pierceall, D.E. Hughes, K.J. Shaw, *J. Biomol. Screen.* 9 (2004) 303.
- [10] F. Progent, M. Taverna, I. Le Potier, F. Gopee, D. Ferrier, *Electrophoresis* 23 (2002) 938.
- [11] A. Varenne, P. Gareil, S. Collic-Jouault, R. Daniel, *Anal. Biochem.* 315 (2003) 152.
- [12] C.F. Silverio, M. Azad, F.A. Gomez, *Electrophoresis* 24 (2003) 808.
- [13] M. Azad, L. Hernandez, A. Plazas, M. Rudolph, F.A. Gomez, *Chromatographia* 57 (2003) 339.
- [14] E. Mito, Y. Zhang, S. Esquivel, F.A. Gomez, *Anal. Biochem.* 280 (2000) 209.
- [15] J. Heintz, M. Hernandez, F.A. Gomez, *J. Chromatogr. A* 840 (1999) 261.
- [16] M. Azad, C. Silverio, Y. Zhang, V. Villareal, F.A. Gomez, *J. Chromatogr. A* 1027 (2004) 193.
- [17] C. Schou, N.H.H. Heegaard, *Electrophoresis* 27 (2006) 44.
- [18] M. Cirri, F. Maestrelli, S. Orlandini, S. Furlanetto, S. Pinzauti, P. Mura, *J. Pharm. Biomed. Anal.* 37 (2005) 995.
- [19] V. Villareal, A. Brown, A. Gomez, C. Silverio, F.A. Gomez, *Chromatographia* 60 (2004) 73.
- [20] M. Azad, A. Brown, I. Silva, F.A. Gomez, *Anal. Bioanal. Chem.* 379 (2004) 149.
- [21] M.A. Azad, J. Kaddis, V. Villareal, L. Hernandez, C. Silverio, F.A. Gomez, M. Strege, A.L. Lagu (Eds.), *Capillary Electrophoresis of Proteins and Peptides*, Humana Press, Totowa, NJ, 2004, pp. 153–168.
- [22] A.R. Stettler, M.A. Schwarz, *J. Chromatogr. A* 1063 (2005) 217.
- [23] K. Sato, A. Inoue, K. Hosokawa, M. Maeda, *Electrophoresis* 26 (2005) 3076.
- [24] A. Brown, R. Desharnais, B.C. Roy, S. Malik, F.A. Gomez, *Anal. Chim. Acta* 540 (2005) 403.
- [25] X.-H. Qian, K.B. Tomer, *Electrophoresis* 19 (1998) 415.
- [26] J.J. Colton, J.D. Carbeck, J. Rao, G.M. Whitesides, *Electrophoresis* 19 (1998) 367.
- [27] K.L. Rundlett, D.W. Armstrong, *Electrophoresis* 18 (1997) 2194.
- [28] H. Meisel, C. Olieran, *Anal. Chim. Acta* 372 (1998) 291.
- [29] J.K. Abler, K.R. Reddy, C.S. Lee, *J. Chromatogr. A* 759 (1997) 139.
- [30] A. Taga, Y. Yamamoto, R. Maruyama, S. Honda, *Electrophoresis* 25 (2004) 876.
- [31] S. Kiessig, H. Bang, F. Thuncke, *J. Chromatogr. A* 853 (1999) 469.
- [32] C. Karakasyan, M. Taverna, M.-C. Millot, *J. Chromatogr. A* 1032 (2004) 159.
- [33] M. Castagnola, D.V. Rossetti, R. Inzitari, A. Lupi, C. Zuppi, T. Cabras, M.B. Fadda, G. Onnis, R. Petruzzelli, B. Giardina, I. Messina, *Electrophoresis* 25 (2004) 846.
- [34] D.D. Buchanan, E.E. Jameson, J. Perlette, A. Malik, R.T. Kennedy, *Electrophoresis* 24 (2004) 1375.
- [35] J. Liu, K.J. Volk, M.S. Lee, M. Pucci, S. Handwerker, *Anal. Chem.* 66 (1994) 2412.
- [36] Y.-H. Chu, Y.M. Dunayevskiy, D.P. Kirby, P. Vouros, B.L. Karger, *J. Am. Chem. Soc.* 118 (1996) 7827.
- [37] A.J.R. Heck, P.J. Bonnici, E. Breukink, D. Morris, M. Wills, *Chem. Eur. J.* 7 (2001) 910.
- [38] J.H. Griffin, M.S. Linsell, M.B. Nodwell, Q. Chen, J.L. Pace, K.L. Quast, K.M. Krause, L. Farrington, T.X. Wu, D.L. Higgins, T.E. Jenkins, B.G. Chirstensen, J.K. Judice, *J. Am. Chem. Soc.* 125 (2003) 6517.
- [39] N.E. Allen, D.L. LeTourneau, J.N. Hobbs Jr., *Antimicrobial. Agents Chemother.* 41 (1997) 66.
- [40] G. Chiosis, I.G. Boneca, *Science* 293 (2001) 1484.
- [41] H. Arimoto, K. Nishimura, T. Kinumi, I. Hayakawa, D. Uemura, *Chem. Commun.* (1999) 1361.
- [42] R. Kerns, S.D. Dong, S. Fukuzawa, J. Carbeck, J. Kohler, L. Silver, D. Kahne, *J. Am. Chem. Soc.* 122 (2000) 12608.
- [43] J.E. Ladbury, B.Z. Chowdhry, *Chem. Biol.* 3 (1996) 791.

# A fluorescent chemical sensor for Fe<sup>3+</sup> based on blocking of intramolecular proton transfer of a quinazolinone derivative

Xiao-Bing Zhang<sup>a,\*</sup>, Guo Cheng<sup>a</sup>, Wei-Jun Zhang<sup>a,b</sup>, Guo-Li Shen<sup>a</sup>, Ru-Qin Yu<sup>a,\*</sup>

<sup>a</sup> State Key Laboratory of Chemo/Biosensing and Chemometrics, College of Chemistry & Chemical Engineering, Hunan University, Changsha 410082, PR China

<sup>b</sup> Hunan University of Science and Engineering, Yongzhou, Hunan 425000, PR China

Received 18 November 2005; received in revised form 20 March 2006; accepted 20 March 2006

Available online 2 May 2006

## Abstract

In this paper, 2-(2'-hydroxy-phenyl)-4(3H)-quinazolinone (HPQ), a typical compound that exhibits excited state intramolecular proton transfer (ESIPT) reaction and possesses good photophysical properties, is synthesized and used as fluoroionophore for Fe<sup>3+</sup> sensitive optochemical sensor. The decrease of fluorescence intensity of HPQ membrane upon the addition of Fe<sup>3+</sup> was attributed to the blocking of ESIPT reactions of HPQ and quenching its fluorescence. The effect of the composition of the sensing membrane was studied, and experimental conditions were optimized. The sensor shows a linear response toward Fe<sup>3+</sup> in the concentration range of  $7.1 \times 10^{-7}$  M to  $1.4 \times 10^{-4}$  M with a limit of detection of  $8.0 \times 10^{-8}$  M, and a working pH range from 2.5 to 4.5. It shows excellent selectivity for Fe<sup>3+</sup> over a large number of cations such as alkali, alkaline earth and transitional metal ions. The proposed sensor is applied to the determination of the content of iron ions in pharmaceutical preparations samples with satisfactory results.

© 2006 Elsevier B.V. All rights reserved.

**Keywords:** Intramolecular proton transfer; Fluorescent chemical sensor; Iron(III) ion; Quinazolinone derivative

## 1. Introduction

Iron is widely distributed in nature and is one of the most important elements in biological systems, which plays a crucial role in many biochemical processes at the cellular level. It is an essential element for the formation of hemoglobin of red cells and plays an important role in the storage and transport of oxygen to tissues. Iron is indispensable for most organisms, and both its deficiency and overload can induce various disorders. Iron metabolism disorders have been reported to cause anemia as well as the liver and kidney damage (hemochromatosis) which might ultimately cause liver cancer, liver cirrhosis, arthritis, diabetes or heart failure [1]. Recent studies have linked neurodegenerative disorders such as Parkinson's disease to elevated iron levels [2]. Iron also plays a key role in some important infectious diseases such as malaria [3].

The development of reliable sensing methods for iron ions is, therefore, of considerable importance for environment and human health. Several techniques such as spectrophotometry [4–6], atomic absorption spectroscopy [7], chemiluminescence [8] and voltammetry [9] have been used for iron assay in various samples. Some techniques necessitate the use of sophisticated instrumentation and require complicated pretreatment procedures, not suitable for on-line or in-field monitoring. The sensor technology is much simpler in instrumental implementation and sample preparation. Owing to the advantages of simple, rapid and non-destructive characteristics, many potentiometric sensors for iron-selective assay have been reported in the past decades [10–13]. However, this kind of sensor faced a problem related to the low response slopes due to a charge of analyzed ions (a theoretical Nernstian slope towards Fe<sup>3+</sup> ion should be about 20 mV/decade, which is relatively low and sometimes lays in a range of sensor absolute error). The development of fluorescent chemical sensors for physiologically relevant alkali, alkaline earth metal ions, as well as heavy and transition metal ions has attracted considerable attention in recent years [14–17], as such sensors can offer advantages in terms of size, electrical

\* Corresponding authors.

E-mail addresses: [xiaobingzhang89@hotmail.com](mailto:xiaobingzhang89@hotmail.com) (X.-B. Zhang), [rquyu@hnu.cn](mailto:rquyu@hnu.cn) (R.-Q. Yu).

Table 1  
Compare of proposed sensor with reported fluorescent chemical sensors

Fluorophore	Limit of detection (M)	Working range (M)	Response time	Interference of other metal ions
HPQ (this work)	$8.0 \times 10^{-8}$	$7.1 \times 10^{-7}$ to $1.4 \times 10^{-4}$	1 min	No interference at 0.1 mM
Pyoverdin [18]	$6.0 \times 10^{-8}$	$6.0 \times 10^{-8}$ to $3.6 \times 10^{-6}$	2 min	Fe <sup>2+</sup> interference
Calix[4]arene [19]	ND	ND	ND	Cu <sup>2+</sup> interference
NN525 [20]	$6.24 \times 10^{-8}$	$6.24 \times 10^{-8}$ to $1.5 \times 10^{-7}$	ND	Fe <sup>2+</sup> and Co <sup>2+</sup> interference
Functionalized lipid membrane [21]	ND	$1.0 \times 10^{-6}$ to $1.0 \times 10^{-4}$	ND	Fe <sup>2+</sup> , Cr <sup>3+</sup> , Cu <sup>2+</sup> interference
Alexa fluor 488 [22]	$1.8 \times 10^{-7}$	$2.0 \times 10^{-7}$ to $1.5 \times 10^{-5}$	3 min	Cu <sup>2+</sup> interference at 1 $\mu$ M

ND: not discussed.

safety, costs, not requiring a reference element, and the fact that the analytical signal is free of the influence of an electromagnetic field and easy to transmit over a long distance. The fluorescent chemical sensors for Fe<sup>3+</sup> ions have been the subject of a series of investigations [18–22], though sensors for Fe<sup>3+</sup> reported so far usually have interference problems caused by other transition metals cations such as Cu<sup>2+</sup> or Co<sup>2+</sup> (Table 1). Besides intense fluorescence, searching for new fluorophores for iron ions with high selectivity, excellent photostability and large Stokes shifts is still a challenge for analytical chemistry research. Examples of recent advances along this line have been the synthesis of some new Fe<sup>3+</sup> carriers including a tailor-made dithia-azoxa macrocycle linked boron dipyrromethene type dye [23], 1,8-bis(4,4'-diisopropyl-9,9'-diacridyl)naphthalene [24] or anti-1,8-bis(2,2'-diisopropyl-4, 4'-diquinoly)naphthalene [25].

Fluorescent dyes that exhibit excited state intramolecular proton transfer (ESIPT) reactions have attracted great interest for several decades because such compounds show good photophysical properties such as intense luminescence, large Stokes shifts and significant photostability [26–28]. Several fluorescent chemical sensors for various analytes based on compounds undergoing ESIPT reactions have been reported in the past decade [29–32]. 2-(2'-Hydroxy-phenyl)-4(3H)-quinazolinone (HPQ), a typical compound exhibiting ESIPT reaction with a mechanism similar to that of 2-(2'-hydroxyphenyl)benzothiazole [26] (Scheme 1), had been reported to show good photophysical properties, and be applied

in the preparation of fluorescent compositions of inks and enamels, as well as fluorescent precipitating substrates for various enzymes [33–35]. Up to date, HPQ derivatives are scarcely reported as sensing materials for chemical sensors in analytical chemistry. In the context of our long-term interests in searching for novel carriers for sensors [36–38], we try to use HPQ derivatives as fluoroionophores of optochemical sensors for metal ions. Such compounds are generally insoluble in water and highly fluorescent in the solid state, displaying a large Stokes shift and significant photostability due to ESIPT reactions. After selectively binding with some metal ions, ESIPT reactions of HPQ might be blocked and its fluorescence quenched. Herein we report the use of several compounds with ESIPT reactions as sensing materials for the preparation of Fe<sup>3+</sup> sensitive optochemical sensors. An optode based on HPQ as a fluoroionophore shows fluorescent response toward Fe<sup>3+</sup> with a wide linear concentration range, high selectivity and fast response time. The sensor is preliminary applied in determination of the content of iron ions in pharmaceutical preparations with satisfied results.

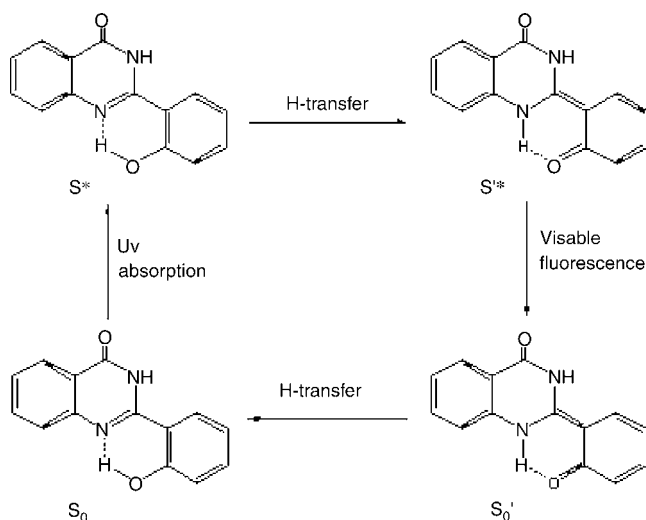
## 2. Experimental

### 2.1. Reagents

High molecular weight poly(vinyl chloride) (PVC), bis(2-ethylhexyl) phthalate (DIOP), dibutyl phthalate (DBP), bis(2-ethylhexyl) sebacate (DOS) and sodium tetraphenylboron (NaTPB) were purchased from Shanghai Chemical Reagents (Shanghai) and used as received. 2-(2-Hydroxyphenyl)benzoxazole (HPBO) and 2,3-dichloro-5,6-dicyano-1,4-benzoquinone (DDQ) were obtained from Sigma–Aldrich. Before used, anhydrous ethanol was subjected to simple distillation from MgSO<sub>4</sub>. Except when specified, other chemicals were of analytical reagent grade and used without further purification. Doubly distilled water was used throughout all experiments.

### 2.2. Synthesis of HPQ

HPQ was synthesized by a modified procedure of literature [34]. In a 100 ml three-necked flask, anthranilamide (1.36 g, 10 mmol) and salicylaldehyde (1.22 g, 10 mmol) were added in anhydrous ethanol (60 ml) and refluxed for 50 min. Then *p*-toluenesulfonic acid (0.04 g, 0.21 mmol) was added and the reaction mixture was allowed to reflux for another 2 h. The reaction solution was cooled to room temperature, and DDQ (2.28 g, 10 mmol) was added. The mixture was stirred at room



Scheme 1. Basic mechanism for ESIPT reaction of HPQ.

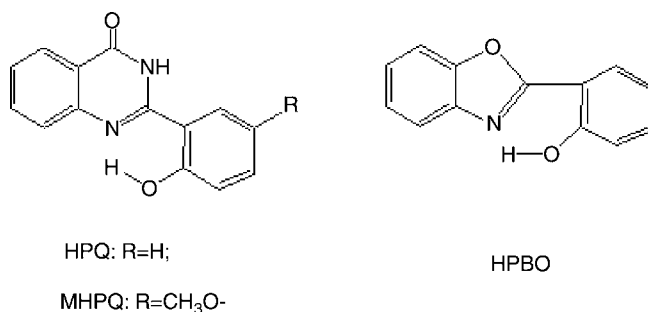


Fig. 1. Structure of HPQ, MHPQ and HPBO.

temperature for 2 h, and filtered to collect the brown solid. After simple purification by washing with cold ethanol ( $3 \times 10$  ml), HPQ (1.98 g, 83%) was obtained as a pale yellow solid. <sup>1</sup>H NMR (DMSO-*d*<sub>6</sub>)  $\delta$  8.24–8.12 (2H, m, ArH), 7.85–7.73 (2H, m, ArH) 7.57–7.41 (2H, m, ArH) 7.01–6.91 (2H, m, ArH). Melt point: 301 °C (literature: 297–298 °C).

### 2.3. Synthesis of

#### 2-(2'-hydroxy-5'-methoxy-phenyl)-4(3H)-quinazolinone (MHPQ)

MHPQ (shown in Fig. 1) was synthesized by the reaction of anthranilamide with 2-hydroxy-5-methoxybenzaldehyde following the similar procedure of HPQ. Spectroscopic and physical properties concur with published data [34].

### 2.4. Apparatus

All fluorescence measurements were carried out on a Perkin-Elmer LS55 luminescence spectrometer with excitation slit set at 5 nm and emission slit at 10 nm. A home-made poly(tetrafluoroethylene) flow-cell described elsewhere [38] and a bifurcated optical fiber (30 + 30 quartz fibers, diameter 6 mm and length 1 m) were used for the Fe<sup>3+</sup> measurements. The excitation light was carried to the cell through one arm of the bifurcated optical fiber and the emission light collected through the other. A glass plate (diameter 10 mm) covered with sensing membrane was fixed on the top of the flow chamber by the mounting screw nut with the membrane contacted with the sample solution.

The standard solution of Fe<sup>3+</sup> was obtained by serial dilution of  $1.0 \times 10^{-2}$  M FeCl<sub>3</sub> solution and buffered with NaOAc–HOAc (pH 3.96). The pH measurements were carried out on a Mettler-Toledo Delta 320 pH meter.

### 2.5. Preparation of optode membrane

The optode membrane solution was prepared by dissolving a mixture of 3.1 mg of HPQ, appropriate amount of sodium tetraphenylborate, 50 mg of PVC, and 100 mg of plasticizer in 1 ml of freshly distilled THF. A glass plate (diameter 10 mm) was mounted on a spinning device and then rotated at a frequency of 800 rpm. Using an asyringe, 0.1 ml of the membrane solution was sprayed to the center of the plate. A membrane of

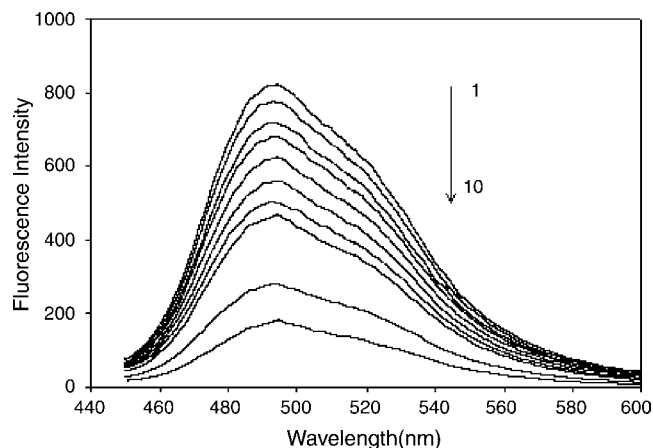


Fig. 2. Fluorescence emission spectra of the HPQ sensing membrane in the presence of different concentration of Fe<sup>3+</sup>: (1) blank solution; (2)  $5.0 \times 10^{-7}$  M; (3)  $2.0 \times 10^{-6}$  M; (4)  $5.0 \times 10^{-6}$  M; (5)  $1.0 \times 10^{-5}$  M; (6)  $5.0 \times 10^{-5}$  M; (7)  $1.0 \times 10^{-4}$  M; (8)  $5.0 \times 10^{-4}$  M; (9)  $1.0 \times 10^{-3}$  M. (10)  $5.0 \times 10^{-3}$  M.

about 4  $\mu$ m thickness was then coated on the glass slides and dried in ambient air at room temperature for 24 h before used.

### 2.6. Measurement procedure

Two arms of the bifurcated optical fiber were fixed in the detecting chamber of the spectrofluorometer to carry the excitation and emission light. The fluorescence intensity was measured with the maximal excitation wavelength of 364 nm and at the maximal emission wavelength of 492.5 nm. The sample solution was driven through the flow-cell by a peristaltic pump (Guokang Instruments, Zhejiang, China) at a flow rate of  $1.4 \text{ ml min}^{-1}$ . After each measurement, the flow-cell was washed with a NaOAc–HOAc buffer solution (pH 3.96) until the fluorescence intensity of the optode reached the original blank value.

### 2.7. Sample preparation

After carefully peeling off the coat, the multi-vitamin tablets were ground into powder. A 10 mg of powder was then dissolved in 1 ml of aquaregia first and heated to dryness to oxidize Fe<sup>2+</sup> to Fe<sup>3+</sup>. After being cooled, it was transferred into a calibrated flask and diluted to 10 ml with NaOAc–HOAc (0.1 M, pH 3.96) buffer solution and then filtered for analytical determination.

## 3. Results and discussion

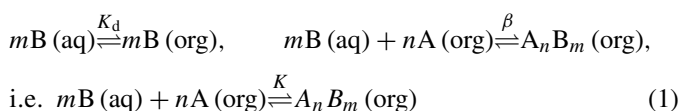
### 3.1. Fluorescence quenching of optode by Fe<sup>3+</sup>

HPQ is a typical compound exhibiting ESIPT reactions with excellent photophysical properties. In this paper, we use HPQ derivatives as fluoroionophores of optochemical sensors for Fe<sup>3+</sup>. Fig. 2 shows the fluorescence spectra of HPQ-based optode membrane exposed to a solution containing different concentrations of Fe<sup>3+</sup>, which are recorded at  $\lambda_{\text{ex}} = 364$  nm,  $\lambda_{\text{em}} = 450$ –600 nm. Owing to its ESIPT reactions, HPQ exhibits an intensive fluorescence emission at 492.5 nm with a large

Stokes shift (128.5 nm) when excited by the radiation of 364 nm. After selectively binding with  $\text{Fe}^{3+}$ , ESIPT reactions of HPQ was blocked and its fluorescence quenched. From Fig. 2, one can see that the fluorescence intensities of the optode membrane decrease with the increase of  $\text{Fe}^{3+}$  concentration, which constitutes the basis for the determination of  $\text{Fe}^{3+}$  with the optical fiber sensor proposed in this paper.

### 3.2. Principle of operation

While contacting with HPQ-based optode,  $\text{Fe}^{3+}$  in aqueous sample solution was extracted into the membrane phase and interacted with HPQ. Suppose a complexation equilibrium between  $\text{Fe}^{3+}$  (B) in the aqueous sample solution and HPQ (A) in the organic membrane phase is established with formation of a complex with a complexing ratio of  $m:n$ , one has [37,38]:



Here  $K_d$ ,  $\beta$ , and  $K$  are the distribution coefficient, the apparent complex formation constant of  $\text{A}_n\text{B}_m$ , and the over-all equilibrium constant of the reaction, respectively. When the difference between the activity and concentration is neglected for simplification, the corresponding equilibrium constant  $K$  can be expressed by the law of mass action:

$$K = K_d\beta = \frac{[\text{A}_n\text{B}_m]_{(\text{org})}}{[\text{A}]_{(\text{org})}^n [\text{B}]_{(\text{aq})}^m} \quad (2)$$

When the concentrations of  $\text{Fe}^{3+}$  and HPQ inclusion complex in membrane are low, the observed fluorescence intensity of the membrane is a sum of several contributions:

$$F_0 = K_A C_{\text{A}(\text{org})} \quad (3)$$

$$F = K_A [\text{A}]_{(\text{org})} + K_B [\text{B}]_{(\text{org})} + K_{\text{A}_n\text{B}_m} [\text{A}_n\text{B}_m]_{(\text{org})} \quad (4)$$

where  $F_0$  is the fluorescence intensity of the HPQ complex sensing membrane when it is exposed to blank solution,  $F$  the fluorescence intensity of the HPQ complex sensing membrane when exposed to  $\text{Fe}^{3+}$  solution and  $C_{\text{A}(\text{org})}$  is the total concentration of HPQ in the membrane.

To indicate the degree of association between HPQ inclusion complex and  $\text{Fe}^{3+}$  in the optode membrane, a response parameter,  $\alpha$ , needs to be introduced and defined as follows:

$$\alpha = \frac{C_{\text{A}(\text{org})} - [\text{A}]_{(\text{org})}}{C_{\text{A}(\text{org})}} = \frac{n[\text{A}_n\text{B}_m]_{(\text{org})}}{C_{\text{A}(\text{org})}} \quad (5)$$

It can be derived from Eqs. (3) to (5) that

$$\alpha = \frac{F - F_1}{F_0 - F_1} \quad (6)$$

where  $F_1$  represents the fluorescence intensity of the HPQ membrane when HPQ is completely complexed with  $\text{Fe}^{3+}$ . Combining Eqs. (2) and (5), the relationship between the  $\alpha$  and  $\text{Fe}^{3+}$

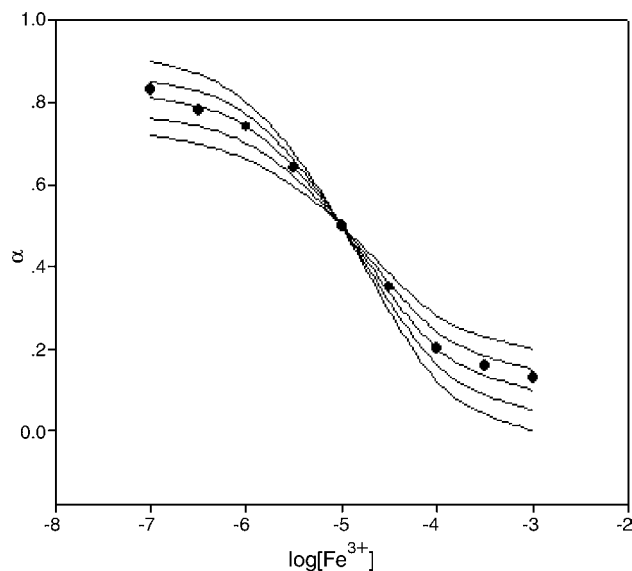


Fig. 3. Relative fluorescence intensity  $\alpha$  as a function of  $\log[\text{Fe}^{3+}]$ . The curves fitting the experimental data were calculated from Eq. (1)  $m:n=3:1$ ,  $K=6.17 \times 10^4$ ; Eq. (2)  $m:n=2:1$ ,  $K=5.42 \times 10^5$ ; Eq. (3)  $m:n=1:1$ ,  $K=7.12 \times 10^6$ ; Eq. (4)  $m:n=1:2$ ,  $K=5.64 \times 10^8$ ; Eq. (5)  $m:n=1:3$ ,  $K=2.37 \times 10^{11}$ . The dots are obtained from the experiment.

concentration  $[\text{B}]_{(\text{aq})}$  can be represented as

$$\frac{\alpha^n}{1 - \alpha} = \frac{1}{nK C_{\text{A}(\text{org})}^{n-1} [\text{B}]_{(\text{aq})}^m} \quad (7)$$

From Eq. (7), it can be seen that when the stoichiometric ratio of complex changes, the relative fluorescence intensity value  $\alpha$  with the various concentration of  $\text{Fe}^{3+}$  exhibits different functional relationships.

According to Eq. (7), the experimental data were fitted by altering the ratio of  $m-n$  and the equilibrium constant  $K$ . Fig. 3 shows the fitted curve for the determination of  $\text{Fe}^{3+}$ . The curve of the 1:1 complex ratio and  $K=7.12 \times 10^6$  was in agreement with the experimental data, which can serve as the calibration curve. A linear range for  $\text{Fe}^{3+}$  covered from  $7.1 \times 10^{-7}$  M to  $1.4 \times 10^{-4}$  M.

### 3.3. Optimization of membrane compositions

Several optode membranes were prepared using different sensitive materials including HPQ, HPBO, MHPQ with DOS as plasticizer to study the effect of sensing materials. The results are shown in Table 2.

Table 2  
The effect of sensing materials on the response behaviors of optodes

Optode	Sensing material	Working concentration range (M)
1	HPQ	$3.6 \times 10^{-6}$ to $2.1 \times 10^{-4}$
2	MHPQ	$6.7 \times 10^{-6}$ to $3.2 \times 10^{-4}$
3	HPBO	$8.9 \times 10^{-4}$ to $4.2 \times 10^{-2}$

Membrane composition for each optode was: 2% sensing material, 65% DOS and 33% PVC (w:w).



Table 3  
The effect of NaTPB on the response behaviors of optodes

Optode	Content of NaTPB	Working concentration range (M)
1	0	$3.6 \times 10^{-6}$ to $2.1 \times 10^{-4}$
2	1%	$9.8 \times 10^{-7}$ to $3.6 \times 10^{-4}$
3	2%	$8.7 \times 10^{-7}$ to $3.9 \times 10^{-4}$
4	3%	$7.1 \times 10^{-7}$ to $1.4 \times 10^{-4}$
5	4%	$4.1 \times 10^{-6}$ to $6.3 \times 10^{-4}$

From Table 2 one can see that the optode of HPQ shows obviously better response characteristics towards  $\text{Fe}^{3+}$  than that of MHPQ in terms of working concentration range, while the optode based on HPBO shows responses toward  $\text{Fe}^{3+}$  only in high concentration. The effect of the structure of the sensing materials to the optode response is obvious. From aforementioned discussion one can see that the fluorescence response of HPQ derivatives toward  $\text{Fe}^{3+}$  is associated with the blocking of ESIPT reactions of HPQ by  $\text{Fe}^{3+}$ . The difference of structures between HPQ and MHPQ is that MHPQ possesses a methoxy group on the 5' position of the phenolic group, while HPQ has no functional group on this position (Fig. 1). The methoxy group is an electron-donating group, which locates on the *para*-position of the hydroxy group of the phenolic group in MHPQ and cause the decrease of polarity of the O–H band by conjugation effect. The ESIPT reaction in MHPQ is, therefore, weaker than that of HPQ. Meanwhile, the binding capability of MHPQ towards  $\text{Fe}^{3+}$  is also weaker and shows worse response than that of HPQ. The structure of HPBO is obviously different from HPQ and seems not favorable for the  $\text{Fe}^{3+}$  binding.

Optodes with different plasticizers, DIOP, DBP, and DOS were also prepared using HPQ as the sensing membrane component. The optode with DOS as the plasticizer gave the best response for  $\text{Fe}^{3+}$ . In the experiment, we also find that, with the addition of lipophilic ion, sodium tetraphenylborate (NaTPB), the response characteristics of the optode membrane are improved. The results are shown in Table 3.

From Table 3 one can see that the response concentration range of the optode membrane becomes wider as the amount of NaTPB in the optode membrane increases, which might be caused by the increasing hydrophilicity owing to the addition of NaTPB. This seems favorable for the  $\text{Fe}^{3+}$  approaching the solution/membrane interface and undergoing the reversible coordination/dissociation processes. Moreover, with the pH value of sample solution fixing at 3.96, HPQ in the optode membrane was expectable existing at a neutral form rather than a negative charge form with proton removed from the phenol. As discussed in literature [39], lipophilic anionic sites (NaTPB) will enhance response of neutral carrier (HPQ)-based sensor towards cations ( $\text{Fe}^{3+}$ ). However, the response concentration range of the optode membrane becomes narrower when the content of NaTPB is larger than 3%, which results in decreasing basic fluorescence intensity of the optode membrane. The experimental results show that the optode membrane composition consisting of 2% HPQ, 3% NaTPB, 63% DOS, and 32% PVC (w/w) could provide the best response for  $\text{Fe}^{3+}$ , which is chosen for further experiments.

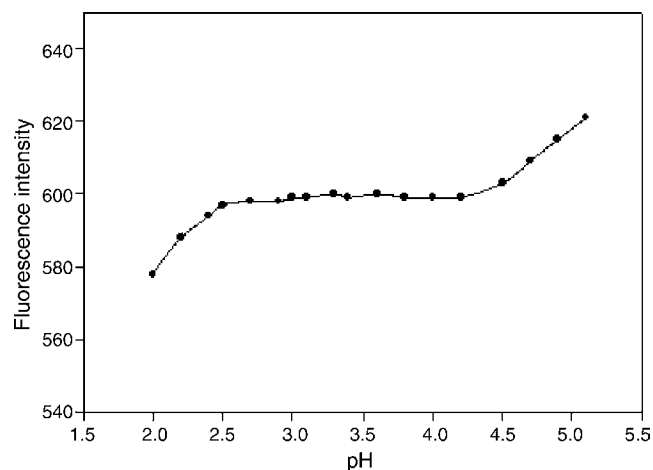


Fig. 4. Effect of pH on the determination of  $\text{Fe}^{3+}$  with proposed optode (the concentration of  $\text{Fe}^{3+}$  was fixed at  $1.0 \times 10^{-5}$  M).

### 3.4. Effect of pH

The fluorescence intensity versus pH plot for the HPQ optode shown in Fig. 4 was obtained by changing the solution pH with different NaOAc–HOAc buffer solutions and fixing the  $\text{Fe}^{3+}$  concentration at  $1.0 \times 10^{-5}$  M. Considering the low acid condition, a solution of a high concentration of  $\text{Fe}^{3+}$  might cause precipitation of  $\text{Fe}(\text{OH})_3$ , so the experiment of the effect of pH on the response of the optode was carried out at a pH range from 2.0 to 5.5. It can be seen that, in the section of lower pH value, the fluorescence intensity of the optode decreased with decreasing pH value. This phenomenon might be caused by extraction of  $\text{H}^+$  from aqueous solution into the optode membrane at high acidity, which causes the protonation of the nitrogen atom on HPQ and blocks its ESIPT reaction. In the section of higher pH value,

Table 4  
Interference of different species to the fluorescence determination of  $\text{Fe}^{3+}$  with the proposed optode

Interferant	Concentration <sup>a</sup> (M)	Fluorescence ( $\Delta F = F - F_0$ ) <sup>b</sup>	Relative error% ( $\Delta F/F_0$ ) $\times 100$
$\text{Na}^+$	$1.0 \times 10^{-1}$	$3.21 \pm 0.36$	0.53
$\text{Li}^+$	$1.0 \times 10^{-1}$	$5.82 \pm 0.41$	0.97
$\text{K}^+$	$1.0 \times 10^{-1}$	$6.41 \pm 0.64$	1.07
$\text{Mn}^{2+}$	$1.0 \times 10^{-2}$	$4.37 \pm 0.32$	0.73
$\text{Mg}^{2+}$	$1.0 \times 10^{-2}$	$-9.78 \pm 0.67$	-1.63
$\text{Ca}^{2+}$	$1.0 \times 10^{-2}$	$8.61 \pm 0.41$	1.44
$\text{Al}^{3+}$	$1.0 \times 10^{-2}$	$9.64 \pm 0.55$	1.61
$\text{Ag}^+$	$1.0 \times 10^{-3}$	$4.36 \pm 0.38$	0.73
$\text{Cd}^{2+}$	$1.0 \times 10^{-3}$	$7.61 \pm 0.62$	1.27
$\text{Hg}^{2+}$	$1.0 \times 10^{-3}$	$-4.57 \pm 0.54$	-0.76
$\text{Zn}^{2+}$	$1.0 \times 10^{-3}$	$-9.94 \pm 0.68$	-1.66
$\text{Ni}^{2+}$	$1.0 \times 10^{-3}$	$8.53 \pm 0.51$	1.42
$\text{Pb}^{2+}$	$1.0 \times 10^{-3}$	$-10.79 \pm 0.73$	-1.80
$\text{Cu}^{2+}$	$1.0 \times 10^{-3}$	$-9.53 \pm 0.46$	-1.59
$\text{Co}^{2+}$	$1.0 \times 10^{-4}$	$-6.87 \pm 0.39$	-1.15
$\text{Fe}^{2+}$	$1.0 \times 10^{-4}$	$-13.66 \pm 0.58$	-2.29

<sup>a</sup> The concentration of  $\text{Fe}^{3+}$  is fixed at  $1.0 \times 10^{-5}$  M (pH 3.96).

<sup>b</sup>  $F$  and  $F_0$  are the fluorescence intensities of the optode contacting with  $1.0 \times 10^{-5}$  M  $\text{Fe}^{3+}$  solution with and without adding the interferant ( $F_0 = 598.74$ ); relative standard deviations were calculated with  $n = 3$ .

Table 5  
Determination of iron ion in vitamin samples using HPQ-based sensor

Sample	Content of the sample (mg/100 mg)	Found by the HPQ sensor (mg/100 mg) <sup>a</sup>	Relative error (%)
1	5.62	5.68 ± 0.08	1.06
2	4.71	4.62 ± 0.02	-1.91
3	3.85	3.92 ± 0.05	1.81

<sup>a</sup> Relative standard deviations were calculated with  $n=3$ .

the increase of fluorescence intensity of the optode seems to be caused by the partial precipitation of  $\text{Fe}^{3+}$  to  $\text{Fe}(\text{OH})_3$ , which decrease the actual concentration of  $\text{Fe}^{3+}$  in the sample solution. From Fig. 4 one can see that, with the  $\text{Fe}^{3+}$  concentration fixing at  $1.0 \times 10^{-5}$  M, acidity does not affect the fluorescence intensity of the proposed optode in a range of pH from 2.5 to 4.5. Our further investigations show that a pH 3.96 NaOAc–HOAc buffer solution provided a lowest limit of detection. It was selected, therefore, in subsequent experiments.

### 3.5. Response characteristics of the optode

The response curve of HPQ-based optode as shown in Fig. 3 (dots) shows a linear response range covers from  $7.1 \times 10^{-7}$  M to  $1.4 \times 10^{-4}$  M of  $\text{Fe}^{3+}$  in a pH 3.96 NaOAc–HOAc buffer solution. The limit of detection for  $\text{Fe}^{3+}$  is  $8.0 \times 10^{-8}$  M calculated as three times the standard deviation of the blank. The response time for  $\text{Fe}^{3+}$  concentration of  $5.0 \times 10^{-5}$  M is less than 1 min. The short-time stability of the optode was tested by recording the fluorescence intensity of  $5.0 \times 10^{-5}$  M  $\text{Fe}^{3+}$  over a period of 12 h for 20 measurements. A relative standard deviation of fluorescence reading of 1.8% was recorded. Meanwhile, during the continuous measurements of sample solutions for 4 weeks, the fluorescence intensity of the optode was dropped by 11.5%. Apparently, the lifetime of the optical membrane sensor is acceptable for continuous analytical applications.

The reproducibility of the optode membranes preparation is one of their important characteristics feature. This parameter was evaluated by performing five measurement cycles with five membranes with the same composition (sensing of  $5.0 \times 10^{-5}$  M  $\text{Fe}^{3+}$  and regeneration with blank buffer solution). A relative standard deviation of fluorescence reading of 4.2% for these optode membranes was recorded. The optode membranes are stored in buffer solution in the dark when not in use. No detectable change of the intensity of fluorescence signal is found after 1 month, implying that the HPQ used is stable in a membrane contacting with water.

The interference for a number of common species of the fluorescence determination of  $\text{Fe}^{3+}$  was investigated. The experiments were carried out by fixing the concentration of  $\text{Fe}^{3+}$  at  $1.0 \times 10^{-5}$  M and then recording the change of the fluorescence intensity before and after adding the interference into the  $\text{Fe}^{3+}$  solution buffered with a NaOAc–HOAc solution (pH 3.96). Many common anions, such as  $\text{Cl}^-$ ,  $\text{SO}_4^{2-}$ , and  $\text{NO}_3^-$ , which might co-exist with  $\text{Fe}^{3+}$ , were investigated for their effect on the determination of  $\text{Fe}^{3+}$ . No observable effects were found in the interference studied. Some other anions, such as  $\text{S}^{2-}$ ,  $\text{PO}_4^{3-}$  and  $\text{OH}^-$ , which might react with  $\text{Fe}^{3+}$  and produce precipitate, showed expectable obvious interfering effects on the  $\text{Fe}^{3+}$  assay.

However, these effects could be eliminated by pretreatment of the sample solution with appropriate masking agents. The experimental results for common metal cations presented in Table 4 reveal that most alkali, and alkaline earth metal cations, and some transition metal cations including  $\text{Mn}^{2+}$  and  $\text{Al}^{3+}$  existing in a concentration of  $1.0 \times 10^{-2}$  M do not show significant interfering effect on the  $\text{Fe}^{3+}$  assay with relative error less than  $\pm 5\%$ . Many other transition metal cations such as  $\text{Ag}^+$ ,  $\text{Hg}^{2+}$ ,  $\text{Cd}^{2+}$ ,  $\text{Zn}^{2+}$ ,  $\text{Ni}^{2+}$ ,  $\text{Pb}^{2+}$  and  $\text{Cu}^{2+}$  presenting in a concentration less than  $1.0 \times 10^{-3}$  M do not show appreciable interfering effect on the  $\text{Fe}^{3+}$  assay. However,  $\text{Co}^{2+}$  and  $\text{Fe}^{2+}$  existing in the same concentration show slight interfering effect on the  $\text{Fe}^{3+}$  assay. Further research shows that  $\text{Co}^{2+}$  and  $\text{Fe}^{2+}$  present in a concentration less than  $1.0 \times 10^{-4}$  M can be tolerated with relative error less than  $\pm 5\%$ .

### 3.6. Preliminary analytical application

The proposed sensor was applied to the determination of three kinds of multi-vitamin tablets. In these samples iron is in the form of  $\text{Fe}^{2+}$ . It needs to be oxidized to  $\text{Fe}^{3+}$  first. A 1 ml of the sample solution prepared as described in the experimental section was diluted with the NaOAc–HOAc (0.1 M, pH 3.96) buffer solution to 50 ml and then analyzed using the proposed sensor. Results are shown in Table 5.

It can be seen that the content of iron ions as determined by the HPQ optical fiber sensor was in good agreement with the nominated content in multi-vitamin tablets with the relative error less than 2%. The present sensor seems useful for the determination of iron ions in real samples.

### Acknowledgements

Financial support from the National Natural Science Foundation of China (Grants 20435003 and 20505008) is gratefully acknowledged.

### References

- [1] C. Brugnara, Clin. Chem. 49 (2003) 1573.
- [2] J. Beard, J. Nutr. 133 (2003) 1468S.
- [3] T.J. Egan, R. Hunter, C.H. Kaschula, H.M. Marques, A. Misplon, J. Walden, J. Med. Chem. 43 (2000) 283.
- [4] Z.O. Tesfaldet, J.F. van Staden, R.I. Stefan, Talanta 64 (2004) 1189.
- [5] D.M.C. Gomes, M.A. Segundo, J.L.F.C. Lima, A.O.S.S. Rangel, Talanta 66 (2005) 703.
- [6] S. Lunvongsa, M. Oshima, S. Motomizu, Talanta 68 (2006) 969.
- [7] A. Ohashi, H. Ito, C. Kanai, H. Imura, K. Ohashi, Talanta 65 (2005) 525.
- [8] W. Qin, Z.J. Zhang, F.C. Wang, Fresenius J. Anal. Chem. 360 (1998) 130.

- [9] A. Bobrowski, K. Nowak, J. Zarebski, *Anal. Bioanal. Chem.* 382 (2005) 1691.
- [10] P. Buhlmann, E. Pretsch, E. Bakker, *Chem. Rev.* 98 (1998) 1593.
- [11] B. Pejčić, R. De Marco, C.E. Buckley, C.F. Maitland, R. Knott, *Talanta* 63 (2004) 149.
- [12] M.H. Mashhadizadeh, I.S. Shoaie, N. Monadi, *Talanta* 64 (2004) 1048.
- [13] A. Sil, V.S. Ijeri, A.K. Srivastava, *Sens. Actuators B* 106 (2005) 648.
- [14] A.P. de Silva, H.Q.N. Gunaratne, T. Gunnlaugsson, A.J.M. Huxley, C.P. McCoy, J.T. Rademacher, T.E. Rice, *Chem. Rev.* 97 (1997) 1515.
- [15] E. Kimura, T. Koike, *Chem. Soc. Rev.* 27 (1998) 179.
- [16] K. Kikuchi, K. Komatsu, T. Nagano, *Curr. Opin. Chem. Biol.* 8 (2004) 182.
- [17] N.C. Lim, H.C. Freake, C. Bruckner, *Chem. Eur. J.* 11 (2005) 38.
- [18] P. Pulido-Tofino, J.M. Barrero-Moreno, M.C. Pérez-Conde, *Talanta* 51 (2000) 537.
- [19] J.M. Liu, Q.Y. Zheng, J.L. Yang, C.F. Chen, Z.T. Huang, *Tetrahedron Lett.* 43 (2002) 9209.
- [20] L. Tarazi, N. Narayanan, J. Sowell, G. Patonay, L. Streckowski, *Spectrochim. Acta Part A* 58 (2002) 257.
- [21] J.L. Pincus, C. Jin, W. Huang, H.K. Jacobs, A.S. Gopalan, Y. Song, J.A. Shelnut, D.Y. Sasaki, *J. Mater. Chem.* 15 (2005) 2938.
- [22] J.P. Sumner, R. Kopelman, *Analyst* 130 (2005) 528.
- [23] J.L. Bricks, A. Kovalchuk, C. Trieflinger, M. Nofz, M. Buschel, A.I. Tolmachev, J. Daub, K. Rurack, *J. Am. Chem. Soc.* 127 (2005) 13522.
- [24] C. Wolf, X. Mei, H.K. Rokadia, *Tetrahedron Lett.* 45 (2004) 7867.
- [25] G.E. Tumambac, C.M. Rosencrance, C. Wolf, *Tetrahedron* 60 (2004) 11293.
- [26] D.L. Williams, A. Heller, *J. Phys. Chem.* 74 (1970) 4473.
- [27] J. Catalán, F. Fabero, M.S. Guijarro, R.M. Claramunt, M.D.S. Maria, M.C. Foces-Foces, F.H. Cano, J. Elguero, R. Sastre, *J. Am. Chem. Soc.* 112 (1990) 747.
- [28] L.M. Tolbert, K.M. Solntsev, *Acc. Chem. Res.* 35 (2002) 19.
- [29] K. Choi, A.D. Hamilton, *Angew. Chem. Int. Ed.* 40 (2001) 3912.
- [30] A.S. Klymchenko, A.P. Demchenko, *J. Am. Chem. Soc.* 124 (2002) 12372.
- [31] X. Zhang, L. Guo, F.Y. Wu, Y.B. Jiang, *Org. Lett.* 5 (2003) 2667.
- [32] M.M. Henary, Y. Wu, C.J. Fahrni, *Chem. Eur. J.* 10 (2004) 3015.
- [33] J.L. Rodgers, J.P. Milionis, *US Patent* 63,169,129 (1965).
- [34] J.J. Naleway, C.M.J. Fox, D. Robinhold, E. Terpetschnig, N.A. Olson, R.P. Haugland, *Tetrahedron Lett.* 35 (1994) 8569.
- [35] Z. Diwu, Y. Lu, R.H. Upson, M. Zhou, D.H. Klaubert, R.P. Haugland, *Tetrahedron* 53 (1997) 7159.
- [36] X.B. Zhang, C.C. Guo, J.B. Xu, G.L. Shen, R.Q. Yu, *Analyst* 125 (2000) 867.
- [37] X.B. Zhang, Z.Z. Li, C.C. Guo, S.H. Chen, G.L. Shen, R.Q. Yu, *Anal. Chim. Acta* 439 (2001) 65.
- [38] X.B. Zhang, C.C. Guo, Z.Z. Li, G.L. Shen, R.Q. Yu, *Anal. Chem.* 74 (2002) 821.
- [39] M.M. Ardakani, H. Dehghani, M. Jalayer, H.R. Zare, *Anal. Sci.* 20 (2004) 1667.

# Anodic voltammetric behavior of resveratrol and its electroanalytical determination in pharmaceutical dosage form and urine

Hongfang Zhang, Lifeng Xu, Jianbin Zheng\*

*Institute of Analytical Science, Shaanxi Provincial Key Laboratory of Electroanalytical Chemistry, Northwest University, 710069 Xi'an, China*

Received 4 October 2005; received in revised form 24 February 2006; accepted 3 March 2006

Available online 18 April 2006

## Abstract

The anodic voltammetric behavior of resveratrol was studied using cyclic and square wave voltammetric techniques. The oxidation of resveratrol is irreversible and exhibits an adsorption controlled process which is of pH dependence. The oxidation mechanism was proposed in this work. The dependence of the current on pH, the concentration and nature of buffer, and scan rate was investigated to optimize the experimental conditions for the determination of resveratrol. It was found that the optimum buffer for the determination of resveratrol is  $1.0 \times 10^{-3}$  M KCl + 0.1 M HNO<sub>3</sub> solution with the pH of 1.0. In the range of  $5.00 \times 10^{-9}$  to  $1.65 \times 10^{-7}$  M, the current measured by square wave voltammetry presents a good linear property as a function of the concentration of resveratrol. In addition, the reproducibility, precision and accuracy of the method were checked as well. The method was applied for the determination of resveratrol in Chinese patent medicine and diluted urine.

© 2006 Elsevier B.V. All rights reserved.

**Keywords:** Resveratrol; Square wave voltammetry; Tablet; Urine; HPLC

## 1. Introduction

Resveratrol (3,5,4'-*trans*-trihydroxystilbene), a natural phytoalexin used by plants to defend themselves from fungal and other forms of aggression, has been proved to possess a variety of biological activities including antiinflammatory, anticarcinogenic, and antioxidative activities [1,2]. The latest experiments of Cengiz et al. [3] demonstrated that resveratrol may be useful in the preservation of liver function in cholestasis. With the understanding of its biological activities, a Chinese medicinal herb, *Polygonum cuspidatum* (Huzhang in Chinese), has drawn much attention from researchers for the fact that it contains hundreds of times more resveratrol than wines [4]. In China the roots of the *P. cuspidatum* have been used as herbal folk remedies for the treatment of atherosclerosis and for other therapeutic purposes for centuries [5,6]. Park et al. [6] investigated the pharmacological effects of *P. cuspidatum* water extract (PCWE) on lipid biosynthesis in cultured human hepatocyte HepG2 cells (HepG2 cells have been widely used as in vitro models of human hepatocytes for lipid metabolism research). The results confirmed

that PCWE, in a dose dependent manner, remarkably inhibits acyl-coenzyme A-cholesterol acyltransferase (ACAT) activity. Among the main active chemicals of *P. cuspidatum*, resveratrol decreased ACAT activity in a dose-dependent manner from the level of  $10^{-3}$  M. ACTA catalyzes the formation of cholesteryl esters from cholesterol and long-chain fatty acyl-coenzyme A, and the elevation of the serum cholesterol concentration is well known to increase the risk of coronary artery disease. Therefore, the results strongly suggest that resveratrol might, at least in part, be responsible for the ACAT inhibition of PCWE. Recently, *P. cuspidatum* has been produced as capsules or tablets for healthy or therapeutic purpose. Fufang Huzhang tablets, pharmaceutical dosage form of the mixture of the extraction of *P. cuspidatum*, *Caulis mahoniae* and leaves of *Eriobotrya japonica*, has been used as a cure for chronic bronchitis.

A number of investigations on the determination of resveratrol in grape-derived products such as wines have been conducted. High performance liquid chromatography (HPLC) [7–10] or capillary electrophoresis (CE) [4,11–13] techniques were often used due to their separation ability, but complicated preconcentration or multisolvent extraction techniques are also coupled with these separation techniques due to the complexity of the real samples and the low concentration of the analyte. Orea et al. [14] reported the analysis of resveratrol content in

\* Corresponding author. Tel.: +86 29 88303448; fax: +86 29 88373025.  
E-mail address: [zhengjb@nwu.edu.cn](mailto:zhengjb@nwu.edu.cn) (J. Zheng).

vine leaves and grape skin by laser desorption coupled with resonant ionization spectrometry, but few institutes possess this kind of instrument. For the analysis of resveratrol in *P. cuspidatum* or its related products, only a few reports were available. Moreover, the techniques were still using HPLC or EC, which is extremely time exhausted and equipment costly [4,15]. To our knowledge, only three papers using electroanalytical techniques to determine resveratrol have been published. Cyclic voltammetry was applied to examine the extraction of phenolic compounds during vinification of Pinot Noir wine [16]. Cyclic voltammetry produced a semi-quantitative measure of the level of galloyl and catechol groups, which correlated well with other total phenol measures. Similarly, cyclic voltammograms in a model wine solution at a glassy carbon electrode were used to determine the total phenol content in three red and two white Croatian wines, and the concentration was expressed in catechin equivalents [17]. Linear sweep voltammetry, based on its redox properties at a silver electrode, was employed to the determination of resveratrol in our laboratory [18]. After 2 min accumulation, the method was sensitive enough to determine resveratrol in wines, but the linear range was too narrow ( $2.0 \times 10^{-9}$  to  $1.0 \times 10^{-8}$  M and  $1.0 \times 10^{-8}$  to  $9.0 \times 10^{-8}$  M) to determine the real resveratrol samples. Also as well known, the silver working electrode is easy to be oxidized and then displays small useful potential range.

Electrochemical methods, especially differential pulse voltammetry (DPV) and square wave voltammetry (SWV), make it possible to decrease the analysis time as compared to the time exhausted chromatographic methods [19,20]. The advantages of SWV over other electroanalytical techniques are greater speed of analysis, lower consumption of electroactive species in relation to the other electroanalytical techniques and less problems with blocking of the electrode surface. A new electrocatalytic mechanism for the oxidation of resveratrol (in the presence of methanol) on the surface of a Pt electrode was suggested. The proposed mechanism is based on the formation of a film of Pt oxide/hydroxides onto which the phenol and the products of its electrochemical oxidation are further deposited [21]. The mechanism for resveratrol oxidation on the surface of a carbon electrode is quite different from the noble metal electrodes. Carbon paste electrodes are often used as a working electrode for voltammetric and amperometric measurements because of their attractive properties [22,23]. From an analytical point of view, these electrodes exhibit rather low background currents over a large range of potentials compared with other solid electrodes.

The purpose of this work is to develop a sensitive, simple, rapid and selective voltammetric method for the determination of resveratrol and real samples like the pharmaceuticals and urine. In the proposed method, there is no time-consuming sample preparation step prior to drug assay. Our aim of this study was also to establish the experimental conditions, to investigate the voltammetric behavior and oxidation mechanism of resveratrol on carbon paste electrode (CPE) using cyclic and square wave voltammetric techniques. In this study, SWV was proposed as an alternative method to the HPLC techniques in therapeutic drug monitoring.

## 2. Experimental

### 2.1. Apparatus

A Model CHI660A Electrochemistry Workstation (Chenhua Instruments in Shanghai, China) was employed for all the electrochemical techniques. A three-electrode system was used, where a standard saturated calomel electrode (SCE) served as reference electrode, a platinum wire electrode as the auxiliary electrode, and a hand-made CPE as the working electrode. A DL-180 ultrasonic apparatus (ShiPuTian Electronic Apparatus Company, Xiangshan, Zhejiang, China) was used to completely dissolve resveratrol. All the pH measurements were made with an Orion Model SA 720 digital ionizer.

The HPLC system is Agilent 1100 series (Agilent Technologies, USA), including a quaternary solvent delivery pump, a thermostat column compartment, a diode array detector (DAD) and a manual sample injection valve with a 20  $\mu$ L loop. Chromatographic separation was carried out using a Zorbax Eclipse XDB-C<sub>8</sub> (150 mm  $\times$  4.6 mm i.d., 5  $\mu$ m) column [8].

The carbon paste was prepared (in the usual way) by hand-mixing 1.0 g of graphite powder and 0.6 mL paraffin oil [22–24]. Subsequently, this mixture was homogenized in a glass mortar for at least 5 min. The resulting carbon paste was packed tightly into a Teflon tube. Electric contact was established by inserting a copper wire into an appropriate depth of the carbon paste (0.1–0.3 cm to the electrode surface).

### 2.2. Reagents

Fufang Huzhang tablets (Batch No: 050101, HeFeng, pharmaceutical Ltd. Company, GuangXi, China) were purchased from the local drugstore. Stock solution of resveratrol ( $5.00 \times 10^{-3}$  M) was prepared by dissolving an accurate amount of resveratrol (Sigma Corporation, USA) in ethanol, and then the above solution was diluted to a 50 mL volumetric flask with distilled water. The stock solution of resveratrol was kept in dark before use [8]. Diluted working standard solutions were prepared from stock solution with distilled water.

All reagents are of analytical grade and the water used is from a Milli-QG (Millipore Corp., USA) water-purification system.

### 2.3. Working voltammetric procedure

About 10 mL of the electrolyte solution containing appropriate amount of resveratrol standard solution or sample were added to the electrolytic cell. Then the electrodes were immersed and cyclic voltammogram or square wave voltammogram were recorded between 0.2 and 1.0 V or between 0.5 and 0.9 V, respectively. The surface of the CPE was renewed mechanically by smoothing some paste off with a piece of graph paper [22], and four times scan from  $-0.4$  to 1.2 V in supporting electrolyte solution was applied to obtain a stable voltammogram [25].

### 2.4. Working chromatographic procedure

Standard samples of resveratrol were made by taking an appropriate volume of stock solution and dissolving in a suitable



quantity of the mobile phase. The HPLC separation was carried out by isocratic elution with a mobile phase of methanol/water (35:65) at a flow rate of  $1.0 \text{ mL min}^{-1}$ . Detection by diode array was performed at 306 nm [8]. Each sample was injected in triplicate and the height of peak was used for quantitative determination.

### 2.5. Tablets assay procedure

The sample powder was obtained by grinding 10 Fufang Huzhang tablets after sugar-coats were removed carefully. Accurate amount of the powder (about 2.7 g) was weighed and extracted with 20 mL ethanol for 30 min in an ultrasonic bath. Then the solution was filtered into a 50 mL volumetric flask through an ordinary filtration paper, and then the solution was diluted to the exact volume with distilled water. Sample solution was stored in the dark [8]. Just before each measurement, the sample solution was diluted quantitatively with the supporting electrolyte. This solution was then transferred into a voltammetric cell and square wave voltammograms were recorded.

### 2.6. Urine analysis procedure

Spiked urine samples were obtained by treating 1.0 mL aliquots of urine with  $10 \mu\text{L}$  resveratrol standard solutions ( $1.00 \times 10^{-3} \text{ M}$ ) to obtain  $10.0 \mu\text{M}$  resveratrol. A  $20 \mu\text{L}$  aliquot of spiked urine was diluted with 10 mL of 0.1 M  $\text{HNO}_3$  containing  $1.0 \times 10^{-3} \text{ M}$  KCl, without any pre-treatment, and transferred into the voltammetric cell. The square wave voltammograms were recorded under optimized conditions [25].

## 3. Results and discussion

The electrochemical behavior of resveratrol was investigated in 0.1 M HCl,  $\text{HNO}_3$ ,  $\text{H}_2\text{SO}_4$ ,  $\text{H}_3\text{PO}_4$ , B-R (pH 4.7), HAc–NaAc,  $\text{KNO}_3$ , KCl, KI, KBr, NaCl,  $\text{NH}_4\text{Cl}$ ,  $\text{Na}_2\text{CO}_3$ , sodium tartrate,  $\text{Na}_2\text{B}_4\text{O}_7$ , and NaOH solution, respectively. In strong acidic media, only one oxidative peak of resveratrol was observed. Compared with the peak in HCl and  $\text{HNO}_3$ , the peak in  $\text{H}_2\text{SO}_4$  was not pronounced and not well-defined. The effect of pH of  $\text{HNO}_3$  solution on the peak current of resveratrol was displayed in Fig. 1. From Fig. 1, 0.1 M  $\text{HNO}_3$  (pH 1.0) was chosen as the supporting electrolyte in this experiment to investigate the electrochemical behavior in detail.

It was found that  $\text{Cl}^-$  could enhance the oxidative peak of resveratrol at CPE (Fig. 2). This may be due to the adsorption of  $\text{Cl}^-$  at the CPE, ameliorating the characteristic of electrode surface and facilitating the electron transfer rate [18]. The peak current of resveratrol increased after certain amount of KCl or NaCl was added to the  $\text{HNO}_3$  solution. The biggest peak current of resveratrol was obtained when  $\text{Cl}^-$  reaches  $1.0 \times 10^{-3} \text{ M}$ . So, the final supporting electrolyte was  $1.0 \times 10^{-3} \text{ M}$  KCl + 0.1 M  $\text{HNO}_3$ .

To elucidate the electrode reaction of resveratrol, the repetitive cyclic voltammograms of resveratrol in  $1.0 \times 10^{-3} \text{ M}$  KCl + 0.1 M  $\text{HNO}_3$  supporting electrolyte were recorded. The

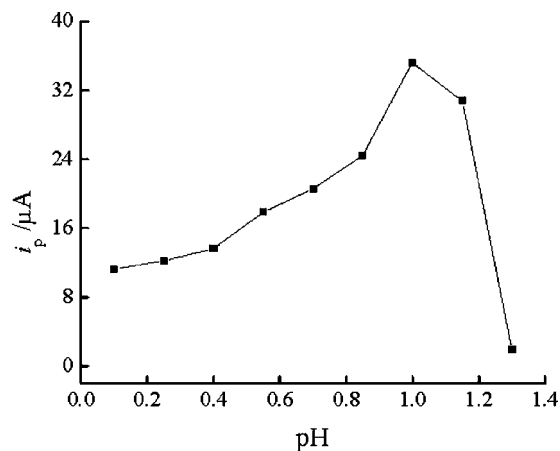


Fig. 1. Effect of pH on the peak current of resveratrol on cyclic voltammograms. Supporting electrolyte:  $\text{HNO}_3$ . Conditions:  $c_{\text{res}} = 1.05 \times 10^{-7} \text{ M}$ ;  $\nu = 100 \text{ mV s}^{-1}$ .

cyclic voltammogram of resveratrol exhibits only one anodic peak, with no peak on the reverse scan, indicating the totally irreversible nature of the electrode reaction. In addition, the peak currents decrease with succeeding potential scan. This phenomenon may be partly attributed to the consumption of adsorbed resveratrol on the electrode surface [19].

A further evidence of the adsorption of resveratrol at the surface of CPE is the restraint effect of surfactant on the peak current because competitive adsorption would happen at the surface of electrode [18,26]. In  $1.0 \times 10^{-3} \text{ M}$  KCl + 0.1 M  $\text{HNO}_3$  solution containing  $1.05 \times 10^{-7} \text{ M}$  resveratrol, a small quantity of polyvinyl alcohol (PVA), diphenylguanidine, sodium dodecyl sulfonate (SDS), hexadecyl pyridine bromide (HPB), cetyl trimethyl ammonium bromide (CTAB), were added into the solution, respectively. As expected for an adsorption-controlled process, all these surfactants decreased the peak current of resveratrol in different degree [27].

The oxidation process of resveratrol was proved to be irreversible. For an irreversible oxidation process, the peak potential  $E_p$  shifts to less negative values with the increase of scan

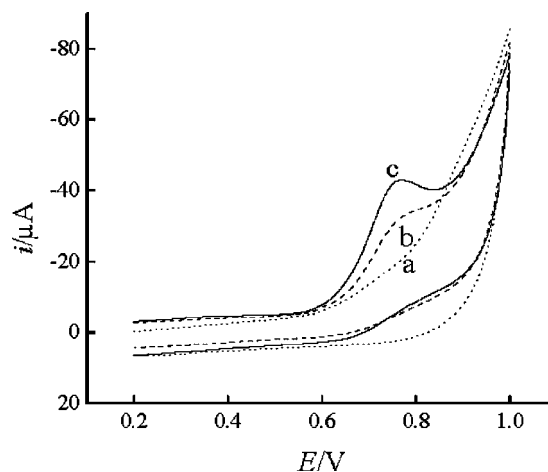


Fig. 2. Cyclic voltammograms of resveratrol in solution of: (a) 0.1 M  $\text{HNO}_3$ ; (b) a +  $1.05 \times 10^{-7} \text{ M}$  resveratrol; (c) b +  $1.0 \times 10^{-3} \text{ M}$  KCl,  $\nu = 100 \text{ mV s}^{-1}$ .

rate  $\nu$  according to the equation [10]:  $E_p = E^0 + RT/(1 - \alpha)nF \{ \ln(k_s/D^{1/2}) - 0.5 \ln[(1 - \alpha)nF\nu/RT] - 0.78 \}$ , where  $E^0$  is the standard electrode potential,  $D$  is the diffusion coefficient,  $\nu$  is the scan rate,  $F$  is the Faraday constant,  $R$  is the gas constant and  $T$  is the room temperature (298 K). The variation of peak potential with scan rate  $\nu$  from 5 to 300 mV is represented by a linear equation  $E_p = -0.0209 \ln \nu + 0.6654$  ( $R = 0.999$ ). From the slope  $0.51RT[(1 - \alpha)nF]^{-1}$ ,  $(1 - \alpha)n = 0.63$  can be obtained and the electron participated in the electrode reaction process can be calculated to be 1, when assuming  $\alpha$  is 0.5.

From the repetitive cyclic voltammograms recorded in different pH solutions, the peak potentials shifted to less negative values with the increase of pH, following the linear equation  $E_p = 0.8073 - 0.093\text{pH}$ , ( $R = 0.998$ ). According to Nernst equation,  $E_p = E^0 - 2.303RTmpH[(1 - \alpha)nF]^{-1}$  ( $m$  is the proton number of electrode reaction), the proton number participated in electrode reaction can be calculated to be 1 from the slope of  $E_p$ -pH equation [20]. The standard electrode potential  $E^0$ , which resveratrol was oxidized at CPE in  $1.0 \times 10^{-3}$  M KCl+0.1 M HNO<sub>3</sub> solution, can also be calculated to be 0.807 V from the intercept of  $E_p$ -pH equation.

Resveratrol has similar chemical structure with flavonoids. They are all derived from phenylalanine and contain an aromatic ring with a reactive hydroxyl group. The oxidation of flavonoids is related mainly with the hydroxyl in its B ring, and the resorcinol group in ring A presents less electroactive [27,28], suggesting that the oxidative peak detected in this experiment should correspond to the oxidation of 4'-hydroxyl of resveratrol.

SWV was used to the determination of resveratrol, and corresponding parameters were optimized. Effects of accumulation time and potential on the peak current were investigated. The peak current of  $1.05 \times 10^{-7}$  M resveratrol increased with the increasing of accumulation time  $t_{\text{acc}}$  and then reached a maximum when  $t_{\text{acc}}$  is above 140 s. So the accumulation time of 140 s was used for further studies. The accumulation potential has little effect on peak current of  $1.05 \times 10^{-7}$  M resveratrol in the range of 0.2–0.5 V. To reduce scanning time, 0.5 V was selected as the accumulation potential in this experiment.

The influence of the square wave parameters such as amplitude and frequency on the peak current was investigated. The peak current  $i_p$  increased with the increasing of square wave amplitude from 5 to 75 mV or square wave frequency in the range of 5–55 Hz, but the peak potential shifted to less negative values and the peak changed unshapely. So 35 mV was chosen as the optimum amplitude and 15 Hz was chosen as the optimum frequency.

### 3.1. Analytical applications and methods validation

Under optimized experimental conditions, a linear relationship between the peak current of resveratrol at CPE and concentration can be established in the range of  $5.00 \times 10^{-9}$  to  $1.65 \times 10^{-7}$  M (Fig. 3). Linear regression equation was  $i_p$  ( $\mu\text{A}$ ) =  $(0.924 \pm 0.102) + (4.917 \pm 0.091) \times 10^{-8}c$  (M);  $r = 0.999$ . And the detection limit was estimated from calibration curve as  $3S_{y,x}/b$  [25], was  $2 \times 10^{-9}$  M.

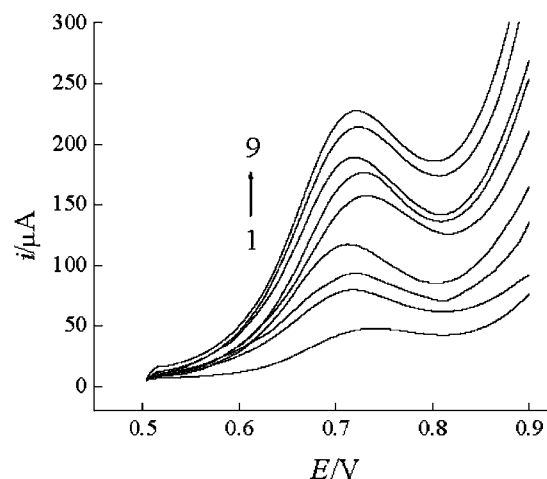


Fig. 3. Variation of peak current on square wave voltammograms with concentration of resveratrol in  $1.0 \times 10^{-3}$  M KCl+0.1 M HNO<sub>3</sub> solution, conditions:  $t_{\text{acc}} = 140$  s,  $f = 15$  Hz,  $w = 35$  mV, 1–9 concentration ( $10^{-8}$  M): 0.50, 4.5, 5.5, 9.5, 10.5, 12.5, 14.5, 15.5, 16.5.

To estimate the repeatability of the proposed method, the R.S.D. of six times successful measurement of peak current of  $2.0 \times 10^{-8}$  and  $1.05 \times 10^{-7}$  M resveratrol on a CPE was calculated to be 3.2% and 0.48%, respectively, which demonstrate the good repeatability of the method. The electrode-to-electrode reproducibility of the SWV method was examined on three CPEs constructed individually, the R.S.D. of the three average peak current of  $2.0 \times 10^{-8}$  M and  $1.05 \times 10^{-7}$  M resveratrol was calculated to be 5.8% and 2.7%, respectively.

For the possible analytical application of the proposed method, the effect of some common excipients used in pharmaceutical preparations was studied by analyzing sample solutions containing a fixed amount of resveratrol ( $1.05 \times 10^{-7}$  M) spiked with various excess amount of each excipient under the same experimental conditions. Some tested excipients, such as glucose and sucrose, were tolerated in 100-fold excess M/M over resveratrol. The results show that no serious interference occurred from the classical additives tested. The influence of ascorbic acid, which is a potentially interfering compound present in biological samples, was investigated. It was found that an equimolar concentration or even at higher molar excess (100:1) of ascorbic acid had no distinct effect on the peak response of resveratrol. Also interference of some metal ions was tested under the same conditions. It was observed that 1000-fold excess of Al(III), Cu(II), Fe(II), Cd(II), Pb(II), Zn(II), Mg(II), and Tl(I) metal ions had no effects on resveratrol determination. Therefore, the proposed method can be used as a selective method.

### 3.2. Determination of resveratrol in Fufang Huzhang tablets

The content of the tablet was usually determined by standard addition method [23]. In this paper, we found that if proper amount of sample solution was used, the content of resveratrol in cell could be obtained through calculating from the linear regression equation of the standard solution. The resveratrol content in

Table 1  
Determination results of resveratrol in tablets by SWV and HPLC<sup>a</sup>

SWV ( <i>n</i> = 6)						HPLC ( <i>n</i> = 3)	
Amount found (mg g <sup>-1</sup> )	R.S.D. (%)	Standard added (mg g <sup>-1</sup> )	Total found (mg g <sup>-1</sup> )	Recovery (%)	R.S.D. of recovery (%)	Amount found (mg g <sup>-1</sup> )	R.S.D. (%)
0.694	1.7	1.110	1.805	100.1	1.3	0.705	3.0

<sup>a</sup> The *t*-test (1.03) value was less than the theoretical value (2.36) at 95% confidence limit for seven degree of freedom.

Table 2  
Application of the SWV method to the determination of resveratrol in spiked urine sample

Resveratrol added ( $\times 10^{-7}$ M)	Resveratrol found <sup>a</sup> ( $\times 10^{-7}$ M)	Average recovery (%)	R.S.D. of recovery (%)
0.50	0.493	98.6	5.7
0.80	0.824	103.0	4.0
1.20	1.152	96.0	3.6
1.50	1.588	105.9	3.1

<sup>a</sup> Average of five determinations.

the Fufang Huzhang tablets was calculated and compared statistically by Student's *t*-test for accuracy with the result obtained by HPLC method (Table 1) at the 95% confidence level with seven degrees of freedom [23]. The result showed that the *t*-test value was less than the critical value, indicating that there was no significant difference between the proposed and the HPLC methods. Because the proposed method was more simple and time-saving than the HPLC method, it can be recommended for the resveratrol analysis of the tablet. The recovery of SWV was also conducted to evaluate the accuracy of the method, and the results are also listed in Table 1. From Table 1, the average recovery of six independent experiments was calculated to be 100.1% when 1.110 mg g<sup>-1</sup> of resveratrol was added into the sample.

### 3.3. Determination of resveratrol in spiked urine

The applicability of the SWV to the determination of resveratrol in spiked urine was investigated. The direct determination of resveratrol in urine was found to be possible by

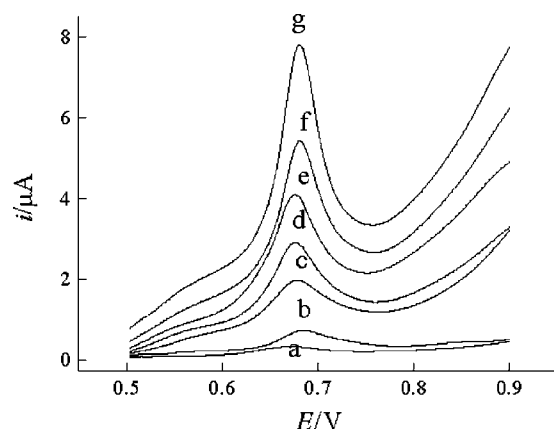


Fig. 4. Square wave voltammograms of resveratrol in spiked urine sample in  $1.0 \times 10^{-3}$  M KCl + 0.1 M HNO<sub>3</sub> solution. Other parameters as in Fig. 3: (a) sample of urine; (b)  $2.0 \times 10^{-8}$  mol L<sup>-1</sup>; (c)  $5.0 \times 10^{-8}$  mol L<sup>-1</sup>; (d)  $8.0 \times 10^{-8}$  mol L<sup>-1</sup>; (e)  $1.2 \times 10^{-7}$  mol L<sup>-1</sup>; (f)  $1.5 \times 10^{-7}$  mol L<sup>-1</sup>; (g)  $2.5 \times 10^{-7}$  mol L<sup>-1</sup> of resveratrol.

employing a high dilution of the sample with the supporting electrolyte [25]. Fig. 4 shows square wave voltammograms obtained with 140 s accumulation of a blank urine sample (20 μL in 10 mL of base solution) (line a) together with urine sample containing different concentration of resveratrol (line b–g). Successive additions of resveratrol to a blank urine sample gave rise to a linear range from  $2.00 \times 10^{-8}$  to  $2.50 \times 10^{-7}$  M of resveratrol in urine with a typical regression equation:  $i_p$  (μA) =  $(0.134 \pm 0.061) + (1.979 \pm 0.048) \times 10^{-7} c$  (M);  $r = 0.998$ . The repeatability of total analytical process was determined from multiple measurements at each of the urine samples (Table 2). An average deviation of 3.6% was obtained.

### 4. Conclusions

A simple, sensitive and selective SWV method for the quantitative determination of resveratrol based on the oxidation of resveratrol at CPE has been established. In the presence of Cl<sup>-</sup>, the oxidation current was further increased. The method can be used successfully to assay the drug in dosage form as well as in spiked urine samples. Compared with HPLC, the proposed method did not require time-consuming extraction or pre-treatment steps prior to the drug assays.

### Acknowledgements

The authors gratefully acknowledge the financial support of the National Natural Science Foundation of China (no. 20275030) and the Natural Science Foundation of Shaanxi Province in China (no. 2004B20).

### References

- [1] M. Nielsen, R.J. Ruch, O. Vang, Biochem. Biophys. Res. Commun. 275 (2000) 804.
- [2] P. Signorelli, R. Ghidoni, J. Nutr. Biochem. 16 (2005) 449.
- [3] A. Cengiz, K. Hale, K.B. Aysun, C. Sacit, A. Selma, H. Murat, K. Vedat, Y. Sezai, J. Surg. Res. 127 (2005) 112.

- [4] L.Y. Gao, Q.C. Chu, J.N. Ye, *Food Chem.* 78 (2002) 255.
- [5] Y.S. Kim, C.S. Hwang, D.H. Shin, *Food Microbiol.* 22 (2005) 139.
- [6] C.S. Park, Y.C. Lee, J.D. Kim, H.M. Kim, C.H. Kim, *Vasc. Pharmacol.* 40 (2004) 279.
- [7] I. Kolouchová-Hanzlíková, K. Melzoch, V. Filip, J. Šmidrkal, *Food Chem.* 87 (2004) 151.
- [8] J. Zhou, H. Cui, G.H. Wan, H. Xu, Y.Q. Pang, C.F. Duan, *Food Chem.* 88 (2004) 613.
- [9] M.C. Pascual-Martí, A. Salvador, A. Chafer, A. Berna, *Talanta* 54 (2001) 735.
- [10] H. Long, Y.X. Zhu, P.T. Kissinger, *Chin. J. Anal. Chem.* 30 (2003) 631.
- [11] X.L. Gu, Q.Y. Chu, M. O'Dwyer, M. Zeece, *J. Chromatogr. A* 881 (2000) 471.
- [12] L. Arce, M.T. Tena, A. Rios, M. Valcárcel, *Anal. Chim. Acta* 359 (1998) 27.
- [13] Ö. Tokuşoğlu, M.K. Ünal, F. Yemiş, *J. Agric. Food Chem.* 53 (2005) 5003.
- [14] J.M. Orea, C. Montero, J.B. Jiménez, A.G. Uren, *Anal. Chem.* 73 (2001) 5921.
- [15] B. Zhang, *Chin. Tradit. Herbal Drugs* 32 (2001) 35.
- [16] H.L. Zou, P.A. Kilmartin, M.J. Inglis, A. Frost, *Aust. J. Grape Wine R.* 8 (2002) 163.
- [17] J. Piljac, S. Martinez, T. Stipèviæ, E. Petroviæ, M. Metiko-Hukoviæ, *Am. J. Enol. Viticult.* 55 (2004) 417.
- [18] S.Y. Dong, J.B. Zheng, H. Gao, *Chem. J. Chin. Universities* 24 (2003) 428.
- [19] A. Golcu, B. Dogan, S.A. Ozkanb, *Talanta* 67 (2005) 703.
- [20] N. Erk, *Anal. Bioanal. Chem.* 378 (2004) 1351.
- [21] S. Andreescu, D. Andreescu, O.A. Sadik, *Electrochem. Commun.* 5 (2003) 681.
- [22] H. Guo, Y. Li, P. Xiao, N. He, *Anal. Chim. Acta* 534 (2005) 143.
- [23] O.A.E.M. Farghaly, N.A.L. Mohamed, *Talanta* 62 (2004) 531.
- [24] M.F.S. Teixeira, G. Marino, E.R. Dockal, É.T.G. Cavalheiro, *Anal. Chim. Acta* 508 (2004) 79.
- [25] A. Radi, Z. El-Sherif, *Talanta* 58 (2002) 319.
- [26] A.P. dos Reis, C.R.T. Tarley, N. Maniasso, L.T. Kubota, *Talanta* 67 (2005) 829.
- [27] X.Q. Xu, J. You, G.N. Chen, *J. Fuzhou University (Nat. Sci.)* 31 (2003) 485.
- [28] P. Janeiro, A.M.O. Brett, *Anal. Chim. Acta* 518 (2004) 109.